# THEORETICAL FUNDAMENTALS OF RADAR

V. E. Dulevich, et al

Foreign Technology Division
Wright-Patterson Air Force Base, Ohio

22 November 1967

FTD-HT-67-192

# FOREIGN TECHNOLOGY DIVISION


## THEORETICAL FUNDAMENTALS OF RADAR

by

V. Ye. Dulevich, A. A. Korostelev et al.

This translation was made to provide the users with the basic essentials of the original document in the shortest possible time. It has not been edited to refine or improve the grammatical accuracy, syntax or technical terminology.

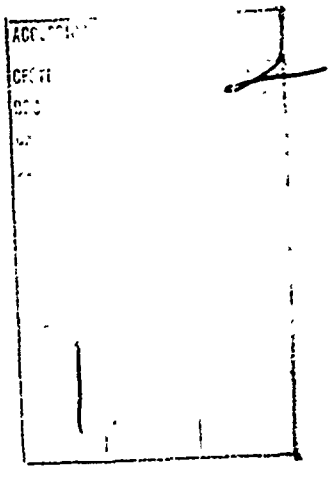

FTD-HT- 67-192

# UNEDITED ROUGH DRAFT TRANSLATION

THEORETICAL FUNDAMENTALS OF RADAR

By: V. Ye. Dulevich, A. A. Korostelev et al.

English pages: 962

Translated under: Contract AF33(657)-16408

TM7001875

| | |
|---|---|
| THIS TRANSLATION IS A RENDITION OF THE ORIGINAL FOREIGN TEXT WITHOUT ANY ANALYTICAL OR EDITORIAL COMMENT. STATEMENTS OR THEORIES ADVOCATED OR IMPLIED ARE THOSE OF THE SOURCE AND DO NOT NECESSARILY REFLECT THE POSITION OR OPINION OF THE FOREIGN TECHNOLOGY DIVISION. | PREPARED BY:<br><br>TRANSLATION DIVISION<br>FOREIGN TECHNOLOGY DIVISION<br>WP-AFB, OHIO. |

V. Ye. Dulevich, A. A. Korostelev, Yu. A. Melnik,
N. I. Burenin, A. V. Petrov, A. A. Veretyagin,
N. G Bandurko

# TEORETICHESKIYE OSNOVY RADIOLOKATSII

Pod Redaktsiyey
V. Ye. Dulevicha

Izdatel'stvo "Sovetskoye Radio"
Moskva — 1964

732 pages

FTD-HT-67-192

ITIS INDEX CONTROL FORM

| 01 Acc Nr | 68 Translation Nr | 65 X Ref Acc Nr | 76 Reel/Frame Nr |
|---|---|---|---|
| TM7001875 | HT6700192 | AM5001448 | 1881 1798 |

| 91 Header Clas | 63 Clas | 64 Control Markings | 94 Expansion | 40 Ctry Info |
|---|---|---|---|---|
| UNCL | UNCL, O | O | | UR |

| 02 Ctry | 03 Ref | 04 Yr | 05 Vol | 06 Iss | 07 B. Pg. | 45 E. Pg. | 10 Date |
|---|---|---|---|---|---|---|---|
| UR | 0000 | 64 | 000 | 000 | 0001 | 0732 | NONE |

Transliterated Title

SEE SOURCE

09 English Title

THEORETICAL FUNDAMENTALS OF RADAR

43 Source

TEORETICHESKIYE OSNOVY RADIOLOKATSII (RUSSIAN)


42 Author

DULEVICH, V. YE.

16 Co-Author

KOROSTELEV, A. A.

16 Co-Author

MEL'NIK, YU. A.

16 Co-Author

BURENIN, N. I.

16 Co-Author

PETROV, A. V.


98 Document Location

47 Subject Codes

17

39 Topic Tags: target discrimination, radio engineering, radar interference, radar scanning, radio wave, wave propagation, radar target


ABSTRACT : This book is intended for students in the radio engineering faculties of higher technical educational institutions and can serve as an aid to engineers and graduate students specializing in radar. The book examines the principles of radar, methods of coordinate measurement and scanning and circuits for radar stations of three types: with an operator, a continuous computer installation and a digital computer. It presents the characteristics of radar signals with a consideration of the statistical regularities that occur in the reflection of radio waves their propagation, and the presence of noise on the signal. The book describes methods of building optimal and near optimal receivers considering statistical, spatial and frequency time characteristics of the signal and interference. The book estimates the maximum capacities of radar in detecting and measuring target coordinates. It gives a statistical evaluation of target position or trajectory on the basis of radar measurement data. In conclusion, the book describes methods of combating various types of interference and the operating principles of passive radar systems. All of the factual and numerical material is taken from the open domestic and foreign press.
English translation: 962 pages.


TABLE OF CONTENTS (abridged)

TABLE OF CONTENTS

*This book is designed for students and auditors of the radio departments of institutes of higher technical education and may serve as a textbook for engineers and graduate students specializing in the field of radar.*

*This book examines the principles of radar, methods of measuring coordinates and of scanning, and also gives block diagrams of radar-station design for three types of observers: an operator, an analog computer, a digital computer. The characteristics of radar signals are given, taking into account the statistical laws of the reflection and propagation of radio waves and of the application of noises to the signal.*

*Optimal and nearly optimal methods of designing receivers are described, based on the statistical, spatial, and frequency-time characteristics of the signal itself and of interferences.*

*An estimate is given of the limitations of radar stations in detecting and measuring target coordinates. A statistical evaluation is given of the target position or of its trajectory on the basis of the radar measurement data.*

*In conclusion a description is given of techniques of combating various types of interference and also of the principles of operation of passive radar systems.*

*All of the factual and mathematical material is taken from unclassified Soviet and foreign literature.*

FOREWORD

In recent years the fruitful application of the methods of information theory and mathematical statistics have led to the creation of a harmonious theory of radar. This theory makes it possible to evaluate the potential of a radar system and to determine the most appropriate lines of its development. The intensive development of a series of trends in contemporary radioelectronics, and the use in radar systems of automation and digital computers, have also contributed to the rapid progress of radar.

All of these circumstances required a substantial alteration in the program of the "Foundations of Radar" course which is standard for a whole series of the country's institutes of higher technical education, and a corresponding revision of the textbooks.

The present textbook is the result of the authors' many years of experience teaching radar courses and of their work on a series of textbooks and textual materials. The authors have endeavored to illuminate, in a form accessible to students of institutes of higher technical education, contemporary concepts dealing with the theory of the reception of radar signals, the principles of design of automatic and non-automatic radar systems, and also with the estimation of target position or trajectory on the basis of the data of radar observation. Since part of the readers are more familiar with the older concepts of radar, the book's material is so arranged as to make it possible to integrate with newer concepts of the technique of processing radar signals.

Chapters 1, 3, and 4 were written by V.Ye. Dulevich; Chapters 2, 5, and 6 (except for §6.8), 7 (except for §§7.9, 7.10, 7.11, 7.13, and 7.14), 8 (except for §§8.1, 8.7, 8.8, and 8.10) were written by A.A. Korostelev; §§6.8, 7.13, 7.14, 8.1, and 8.10 by Yu.A. Mel'nik; Chapter 11 and §§7.9, 7.10, 7.11, 8.7, and 8.8 by N.I. Burenin; Chapters 9 and 10 by A.V. Petrov, Chapter 12 by A.A. Veretyagin; Chapter 13 by N.G. Bandurko; §2.9 was written jointly by V.Ye. Dulevich, N.I. Burenin, and A.A. Korostelev.

In their work on this manuscript the authors made continual use of the valuable advice and recommendations of Ye.K. Aukhimovich, N.I. Klyuyev, N.F. Klyuyev, N.M. Sedyakin, L.A. Serebrov, I.V. Shitov, I.V. Smirnov, B.M. Stepanov, and other comrades, and would like to express their sincerest gratitude to them.

The critical comments and important recommendations expressed, after reading the manuscript, by V.V. Vasin, O.V. Vlasov, V.V. Grigorin-Ryabov, P.I. Dudnik, S.D. Sil'vestrov, S.K. Khokhlov, and other comrades were of great assistance to the authors.

The authors will be grateful to all persons or groups for their comments or recommendations, or for pointing out the inevitable errors which arise in writing educational materials as a result of the rapid development of this area of technology.

# Chapter 1

# GENERAL INFORMATION ON RADAR DEVICES AND METHODS OF RADAR OBSERVATION

## §1.1. RADAR AND ITS AREAS OF APPLICATION

*Radar* is the name for that area of radio technology which uses reflections, retransmissions, or the electromagnetic radiation of the object itself to detect various objects and to measure their coordinates and the parameters of their motion.

We will use the term, radar observation, for the process of detection of objects, of determining their positions, and of measuring the parameters of their motion using radio methods; and the device which fulfills these functions we will call the radar station (RLS).

Information on the objects of observation (radar targets) is carried by radar signals. The latter may be formed in different ways. Three types of radar observation may be distinguished on the basis of how the radar signals are formed.

*The first type* is based upon the reflection from the object (target) of the outcoming or direct signal emitted by the radar transmitter (Fig. 1.1a). With this method the characteristic of the observed objects is the distinction between their reflective properties and the reflective properties of the surrounding medium. In other words the observed objects must possess radar contrast.

The reflected radar signal carries information on the parameters of the position (coordinates) and movement (velocity, acceleration) of the object, and also on its physical characteristics (dimensions,

shape, electrical properties, etc.).

A very important property of this type of radar observation is that it makes possible the detection of objects which are not in themselves the sources of radio radiation. Therefore it has been most widely used in solving various problems of a military or non-military character.

*The second type* of radar observation is based upon the retransmission of the radar-station signals by a special transponder located on the object (Fig. 1.1b).

At large ranges or with small target contrast it is difficult to distinguish the reflected signals from the background of external interferences and fluctuating receiver noises and thus to derive useful information from them. For this reason some objects may be equipped with transponders which, in the process of retransmission, develop answering signals of adequate intensity. Here the radar station itself works in the same way as in the first case. Furthermore, one and the same radar station may observe targets equipped with transponders and those without them at the same time.

Such a method of observation is sometimes called active radar, and the corresponding system – a radar system with active response. In practice, the method of active radar is used in observation of airplanes, rockets, satellites, and also in air and sea navigation. It permits a considerable extension of the range of a radar station and improves the reliability of the reception of information. And, since the object is equipped with an apparatus which can receive and transmit signals, supplementary information, including information irrelevant to the radar observation itself, may be transmitted from the transponder to the radar station.

Active radar methods have also been widely used for recognition

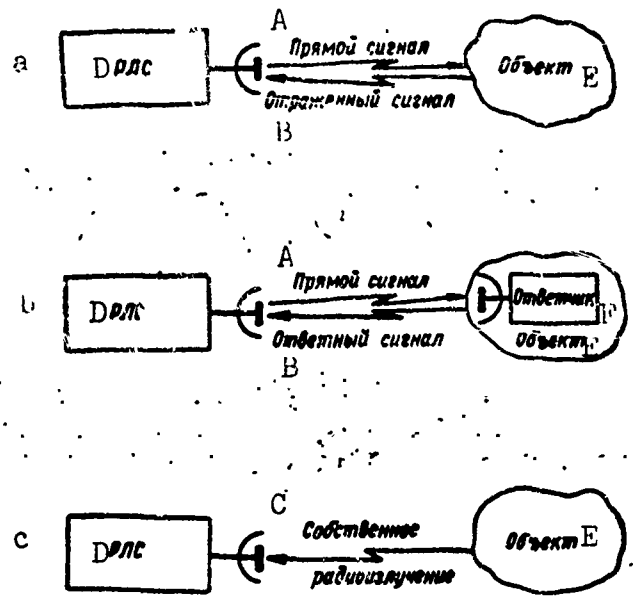


Fig. 1.1. Signal formation with various types of radar observation: a) using a reflected signal; b) system with active response; c) passive radar system. A) Direct signal; B) reflected signal; C) radiation from the object; D) radar station; E) object; F) transponder.

of the nationality of various objects. Special interrogators, usually located in radar stations, send out interrogation signals which are received by the transponders located on airplanes, ships, and other objects. Under the stimulation of the interrogation signal, the transponder radiates a coded response signal which indicates its nationality.

*A third type* of radar observation is called passive radar. It is based upon the reception of the signals of the object's own radiation (Fig. 1.1c). Such types of radiation may include:

– thermal radiation of bodies in the millimeter and centimeter ranges, such as infrared radiation;

– long-wave radiation emitted by rocket engines, nuclear reactions, and lightning flashes;

– the radiation of various radio devices which may be located on objects.

Passive radar is applied in radio astronomy, in scanning the earth's surface, in radio navigation, in systems for reconnoitering radar, radio-navigational, and other radio systems, and for observation of thunderstorms, etc.

Radar methods are widely used in the navigational problems associated with the spatial orientation of moving objects (airplanes, ships, etc.).

Radio navigation is in substance one of the trends of contemporary radar based upon the scientific and technical principles which are identical for all radar. However, because of the specific nature of the application of radar navigation systems, the latter is usually studied as an independent discipline.

In its early years radar technology was used fundamentally for military purposes. The first radar stations were set up for detecting airplanes in flight, since, because of the technical growth of aviation, the old acoustical and optical methods of anti-aircraft defense were no longer satisfactory.

As radar devices were improved, and as increasing experience in their practical application was accumulated, ever newer uses were found for them, both military and non-military. At the present time the field of application of radar methods has become exceptionally broad.

Radar systems can solve such problems as:

1) detection of airplanes, ships, pilotless missiles, and other targets;

2) guidance of airplanes, winged and ballistic missiles;

3) interception of airplanes and pilotless missiles of the opponent;

4) bombing when the target is not optically visible;

5) guiding artillery fire (on land, on ships, on airplanes, etc.);

6) the detection of airplanes, ships, and other objects of the opponent with searchlights;

7) controlling the detonators of artillery shells, air-borne bombs, mines, and torpedoes;

8) warning airplane and ship crews of the danger of collision with moving objects and obstacles;

9) the detection of tank columns, individual tanks, self-propelled artillery, and mortar batteries;

10) guiding the trajectories of moving objects;

11) the navigation of airplanes, ships, and space devices;

12) weather investigation and storm warning;

13) geodesic measurements;

14) astrophysical research, etc.

Radar techniques of target detection and of the measurement of the parameters characterizing its position and movement, are based upon the virtual constancy of the propagation velocity of electromagnetic waves ($c \approx 3 \cdot 10^8$ m/sec) and upon the linearity of the propagation of electromagnetic waves in a homogeneous medium.

The constant velocity and linear propagation of electromagnetic waves makes it possible to determine the target range through direct or indirect measurement of the time taken by the wave to traverse the distance from the radar station to the target and back. If this time is $\tau$, then with linear propagation of the radio waves at velocity $c$, the target range will be

$$R = c\tau/2. \qquad (1.1)$$

Because of the linear propagation and the constant velocity of electromagnetic waves, the use of a receiver with spatially dispersed antenna elements provides for determining the target direction –

through measurement of its angular coordinates (target bearing determination).

The relative delay of the signals received by the various antenna elements is a function of the target direction. With change in the latter the phase relations of these signals also change, and, consequently, the amplitude of the resultant signal at the antenna output. By using the dependence of the phase relations of the signals or of their resultant amplitude upon the direction of arrival of the electromagnetic wave, it is possible to determine the target's angular coordinates.

With a moving target the delay time of the reflected or retransmitted signals changes from observation cycle to the other. This leads to a change in the phase shift of the received signals over the radiated ones, which is equivalent to a frequency shift between them (Doppler effect). By measuring the magnitude of the frequency shift it is possible to determine the radial velocity of the target relative to the radar station.

Furthermore, the different Doppler frequencies of the signals received by the dispersed antenna make it possible to measure the angular velocities of the target.

Despite the comparative simplicity of the principles of radar observation, several decades were required before they could be applied in practice. The modern achievements of radar technology are the result of the theoretical research and practical elaborations of the scientists and engineers of many countries. A prominent contribution to the development of radar was made by Soviet physicists and radio specialists. Even before the Great Fatherland War they had created radar devices with high tactical and technical performance characteristics. In 1941 scientists of the Physical-Technical Institute, Yu.B.

Kobzarev, A.P. Pogorelko, and N.Ya. Chernetsov, were awarded the State Prize "for inventing a device for detecting airplanes."

In subsequent years the efforts of Soviet scientists, engineers, designers, and industrial workers were directed at the further improvement of radar technology and at the creation of new types of radar devices.

As has been noted above, radar methods are used in the solution of many problems. Therefore there exists a large variety of types of radar stations and devices. They may be classified according to their position, purpose, techniques of developing the radar information, and other characteristics.

## §1.2. TRANSMISSION OF INFORMATION IN THE RADAR CHANNEL AND METHODS OF DETERMINING TARGET POSITION

Radar observation is a means of obtaining information on targets lying within the scanning area of the radar station. The actual carrier of information on the position, movement, and properties of the object is the electromagnetic wave coming from it to the radar station.

In contrast to the usual communications or telemetry channels, the oscillations emitted by the radar-station transmitter, even though they may be modulated in amplitude, phase, or frequency, are still not radar signals. In their propagation from the station they bear no radar information about the target, and therefore the frequently used terms, "outcoming" or "direct" signals, are to some extent conventional. In fact, these signals may carry some useful information and may be points of reference for calculating the parameters of the coordinates and movement of the observed objects.

In their propagation through the area surrounding the radar station the emitted electromagnetic waves encounter objects and are reflected from them. In the process of reflection the electromagnetic

waves are transformed into a radar signal which carries information about the target. This information is imprinted on the changes in the parameters of the reflected electromagnetic wave in comparison with the wave emitted by the radar station.

In systems with active response the signal retransmitted by the transponder plays the role of the reflected signal. In addition to pure radar information the response signal may be used also to transmit supplementary data from the object upon which the transponder is located. In passive systems the radiation of the object itself constitutes the useful signal.

The radar-station transmitter may work in a continuous or a pulse mode. The type of radiated selected determines to a considerable extent the volume of the information which can be derived from the signal arriving from the target. At the present time the following types of direct signals are utilized:

- amplitude-modulated oscillations;
- frequency-modulated oscillations;
- undamped oscillations.

And of these the most commonly used signal up until recent times has been a particular form of amplitude modulation known as pulse-amplitude manipulation of the radiated signals.

The electromagnetic wave reaching the radar station from the target is characterized by:

- amplitude;
- phase;
- frequency;
- polarization;
- direction of propagation.

Modern radar stations emit signals with linear (horizontal or

vertical) polarization and sometimes with circular polarization. The polarization of the signal may be altered upon reflection from the target, that is, it becomes depolarized. Therefore one may generally consider that the reflected wave has an elliptical polarization. Such a wave may be conveniently represented as the sum of two orthogonal linearly polarized waves of the same frequency: horizontally polarized wave $E_x$ and vertically polarized wave $E_y$ (Fig. 1.2a). These waves will differ from one another in amplitude and phase

$$E_x = E_{Mx}\cos\left[\omega\left(t-\frac{2R}{c}\right)-\varphi_1\right],$$
$$E_y = E_{My}\cos\left[\omega\left(t-\frac{2R}{c}\right)-\varphi_2\right], \qquad (1.2)$$

where $E_{Mx}$ is the amplitude of the electric field strength of the horizontally polarized wave; $E_{My}$ is the amplitude of the electric field strength of the vertically polarized wave; $\omega$ is the circular frequency of the oscillations; $R$ is the distance from the radar station to the target; $\varphi_1$ and $\varphi_2$ are the phase shifts, taking into account the initial phase of the oscillations and the shift of the phases of the orthogonal components.

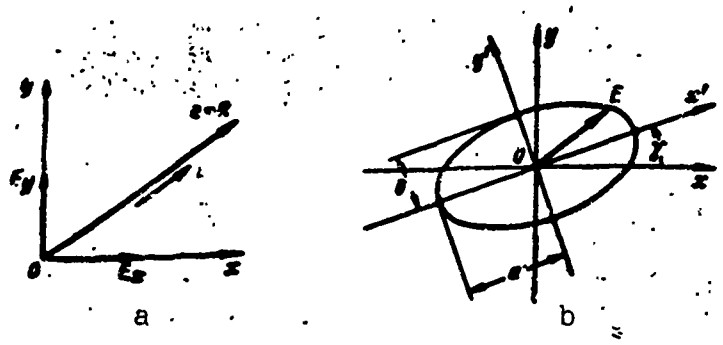


Fig. 1.2. Coordinate system for an elliptically polarized wave (a) and polarization ellipse (b).

The values of the amplitude and phase shifts of the orthogonal waves fully determine the character of the polarization of the re-

flected signal. However, it is more convenient to characterize the polarization of the wave by the direction of rotation of the resultant electrical field vector and by the parameters of the polarization ellipse: the eccentricity $k$, which [illegible] the ratio between the minor and major semiaxes of the ellipse, and the tilt angle $\gamma$ between the major axis of the ellipse and the horizontal axis $x$ (Fig. 1.2b).

The character of the depolarization depends upon the form of the object and upon the relations among its dimensions. Therefore the polarization parameters of the reflected wave carry certain information on the target and may be used in evaluating its properties. However, as a rule, radar-station antennas emit and receive signals of the same polarization. For that reason, in the case of an antenna with linear polarization, one of the orthogonal components of the reflected signal is not received at all. As a result of this, all of the target information contained in the polarization parameters of the radar signal is lost by such stations.

All parameters of the electromagnetic wave may carry information on target position and motion.

The signal amplitude contains information on the physical properties, dimensions, movement, and range of the target. It is practically impossible to derive information on target range from an analysis of the magnitude of the signal amplitude, however, since the latter depends very strongly upon the propagation conditions of the electromagnetic waves, and, for targets of complex shape, may vary sharply depending upon the direction from which it is beamed. Nonetheless, an examination of the statistical laws of signal amplitude fluctuation makes it possible to determine the character and dimensions of the target and sometimes the characteristics of its motion.

In active response systems the amplitude of the response signal

contains little information on the character of the target. And in active response systems information on target range cannot be derived from analysis of the magnitude of the amplitude, since the propagation conditions are unknown, and at the point of the signal's reception the radiation power of the transponder is unknown. In contrast to the reflected signal, the retransmitted signal may be amplitude-modulated in the transponder in order to transmit supplementary information from the object to the radar station.

In passive radar observation the amplitude of the received signal enables one to judge, primarily, only the properties of the observed object.

The phase of the reflected or of the coherently retransmitted signal is connected with the delay time $\tau$ of the incoming wave relative to the transmitted one. Delay time is determined by target range $= 2R/c$. Thus, the phase of the received signal $\varphi = \omega \times \left(t - \frac{2R}{c}\right) - \varphi_1$ depends upon target range and may be utilized to measure the latter.

It should also be borne in mind that if the amplitude or frequency of the signal emitted by the radar station is modulated according to a definite law, the phase of the modulation of the reflected signal will be determined by target range. Therefore, information on target range may be derived from a comparison of the phases of the received and emitted signals or of the phases of their modulation. Phase fluctuations of the signals coming from the target depend upon the structure of the target itself and upon its displacement relative to the radar station; they may in principle be used to obtain such information.

The frequency of the reflected or retransmitted signal carries information on the radial velocity of the target. Because of the Doppler effect the signal coming from the target possesses carrier fre-

quency (Fig. 1.3)

$$f=f_0+F_д,$$

where $f_0$ is the carrier frequency of the outcoming signal; $F_д$ is the Doppler shift of the carrier frequency of the radar signal as determined by target movement.

Doppler frequency $F_d$ is proportional to radial velocity $v_R$ of the observed object relative to the radar station. Thus, by measuring value $F_d$, we can establish the value of the target's radial velocity.

The direction of propagation of the electromagnetic wave reaching the radar station is the opposite of the direction from the radar station to the target. The basis of the determination of the direction of propagation of electromagnetic waves is the measurement of the angular coordinates (bearing-determination) of the target through reception of signals on a spatially dispersed antenna system and the subsequent analysis of their amplitude or phase.

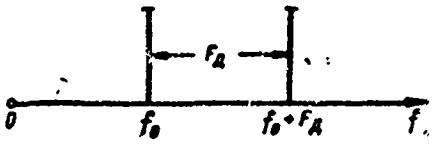


Fig. 1.3. Frequency diagram of direct and reflected signals in monochromatic radiation.

The radar channel, like other types of radio channels, is subject to the influence of externally and internally derived interferences (Fig. 1.4). Interferences reduce the effectiveness with which the radar signals are processed and lead to the derivation of erroneous information on the target. Some target signals are omitted, and the existence of some targets is indicated where they do not in fact exist. In addition, interference leads to an imprecise measurement of the parameters characterizing target position and movement.

The reception of target signals should be free of all unwanted information caused by external and internal interference, and the useful information on the target should be isolated. Furthermore, the

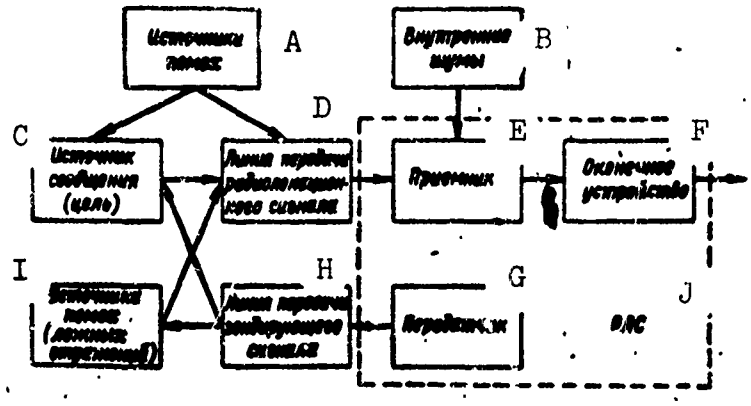


Fig. 1.4. Block diagram of a radar channel. A) Sources of interference; B) internal noises; C) source of information (target); D) transmission line of radar signal; E) receiver; F) end device; G) transmitter; H) transmission line of outcoming signal; I) sources of interference (false reflections); J) radar station.

useful information should be presented in a form convenient for the user.

One must bear in mind that in the radar channel the primary source of information is the target. Therefore the properties of the target and its performance characteristics must be borne in mind in approaching the problem of its observation by radar. In particular, one must bear in mind that every moving target has its own trajectory and that this expresses more fully the distinguishing characteristics of the target than do the instantaneous values of its current coordinates and velocity.

Radar observation means the derivation of information on the current parameters of the target – its coordinates and their derivatives. Depending upon the task to be solved by the radar station, the conditions of observation, and the principles of design of the radar set, various coordinate systems may be used to determine the spatial position of the target. Thus, for example, a spherical coordinate system is very commonly used to determine target position. In this case, as follows from Fig. 1.5, the position of the target in space is fully

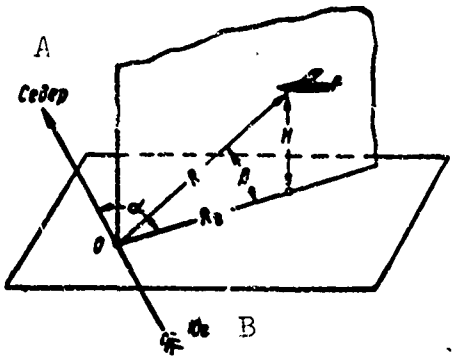


Fig. 1.5. Systems for reading off coordinates. A) North; B) south.

determined by:

- range $R$,
- azimuth $\alpha$,
- elevation angle $\beta$.

Sometimes, for example, in guiding the interception of enemy airplanes or in landing an airplane, one must know the altitude of the target and its horizontal range. In such cases, it is convenient to utilize a coordinate system in which the spatial position of the target is characterized by:

- horizontal range $R_g$,
- azimuth $\alpha$, and
- altitude $H$.

It is in principle possible to construct a radar system capable of analyzing all signal parameters and of deriving the greatest possible amount of information about the target. However, because of technical difficulties and the characteristics of the problems to be resolved, the radar stations used in practice usually measure a limited number of target position and movement parameters.

In general, the geometrical locus of the points in space for which the parameter measured by the radar station is constant is a surface, henceforth called the *position surface*. If the problem is viewed in a plane, the geometrical location of the points of the constantly measured parameter will represent the *position line*. For example, in the case of a radar station measuring only target range $R$, the geometrical location of the points at which $R$ is constant is a sphere of radius $R$ with its center at the radar station. In a plane surface this will be a circumference of radius $R$. In a system which

determines direction, the geometrical location of the points at which the measured parameters have constant values will represent a straight line passing through the radar station.

The target location may be defined as the point of intersection of the position lines or position surfaces corresponding to the values of the measured parameters. Depending upon which position parameters (coordinates) are measured by the radar system, various methods of determining the target position are possible. In practice, the following methods have been used most widely.

*The range and angular measurement method* is used when the radar station measures all three target coordinates: range $R$, azimuth $\alpha$, and elevation angle $\beta$. Then the target position is found as the point of intersection of a sphere of radius $R$ and the straight line corresponding to the direction of the target. This method is fundamental for radar observation since it makes possible a unique definition of the position of the target when the target is observed from the point of the location of the radar station. If the observation is done in a plane, the target position corresponds to the point of intersection of circumference $R$ = const and the bearing line (point $C$ in Fig. 1.6a).

*The range-measuring method* is used when the radar device measures only one target coordinate – range $R$. Here the target position is defined as the intersection of the spheres or the circles corresponding to the ranges measured and having their centers at the locations of the radar stations (Fig. 1.6b). To avoid major errors in determining target position, the distance between the points from which range is measured should be commensurable with the presumed target range.

The range-measuring method can be applied in both navigational and in pure radar systems. It is advisable to use it in the latter

case, if substantial errors enter into the measurement of angular coordinates by radar.

*The method of bearing determination (angular measurement)* is used when measuring systems located at various points are used to determine just the direction of the target. Then, in terms of a plane surface, the target position is found as the point of intersection of two bearing lines (Fig. 1.6c).

Because of its simple design, the method of bearing-determination is utilized very widely. It is applied specially frequently in radio navigation. In radar this method is used in passive systems utilizing observation of a radiating object. In addition, this method may also be useful in ordinary radar when interference disturbs the operation of the range-measuring channels of the radar station, and the target can be observed only through determination of its bearing.

*The differential range-measuring method* is based upon measurement of distances $R_1$ and $R_2$ of the target from two fixed points and determination of the difference between these two distances (Fig. 1.6d). The position line for which the difference between $R_1$ and $R_2$ is constant is a hyperbola passing through target point $C$. Here points $A$ and $B$ are foci of hyperbolas. The position of the target is defined as the point of intersection of hyperbolas $R_1 - R_2 = \text{const}$ and $R_3 - R_4 = \text{const}$, these being derived from different bases ($AB$ and $AD$).

This method has been most widely used in navigation.

*The summary range-measuring method* consists in the measurement of the sum of the distances from two points of reference (Fig. 1.6e). The position line for which $R_1 + R_2 = \text{const}$ is an ellipse in the foci of which the radar units are located. The various values of the sum of $R_1 + R_2$ yield a family of ellipses. In this case the position of the object is defined as the point of intersection of two ellipses belong-

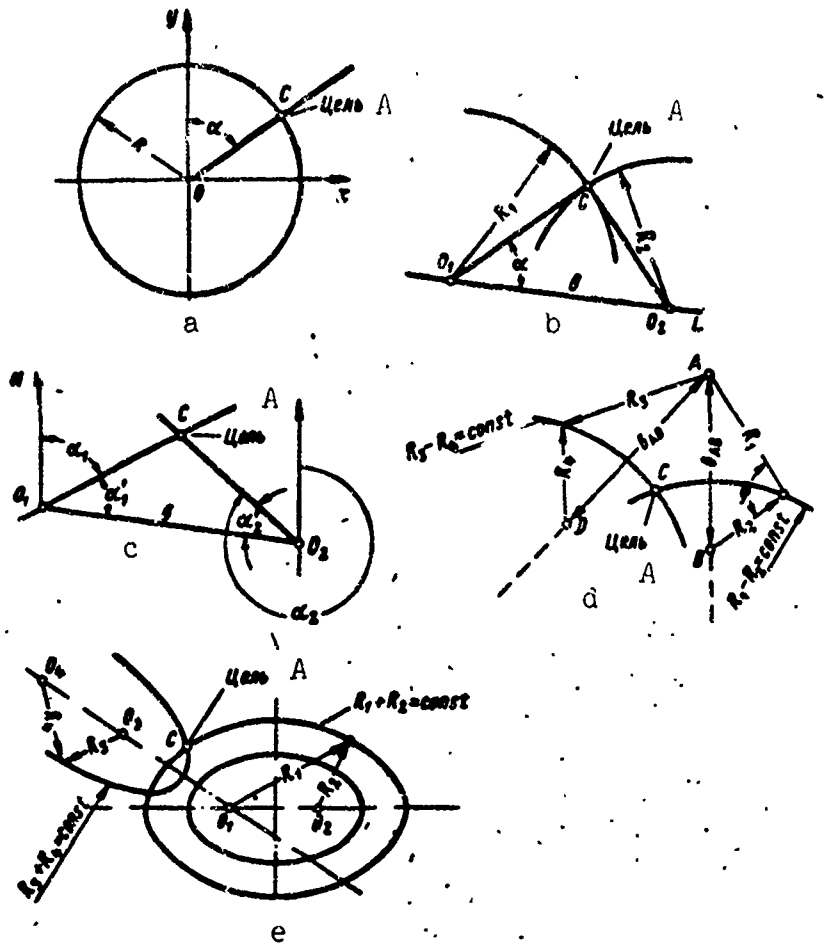


Fig. 1.6. Methods of determining target position: a) measurement of range and angle; b) measurement of range; c) bearing method (angular measurement); d) differential range measurement; e) summary range measurement. A) Target.

ing to two reference systems.

## §1.3. TACTICAL AND TECHNICAL CHARACTERISTICS OF RADAR STATIONS

By tactical data of a radar station we mean the parameters characterizing its possible military uses.

The basic tactical characteristics of a radar station are:

– the station's operating zone or scanning area,

– the coordinates which can be determined and their measurement accuracy,

– its resolution capacity,

– its noise resistance,

– its scanning time,

– its reliability.

*Operating zone of a station.* The spatial area in which a station can conduct uninterrupted radar observation of targets is commonly as its operating zone. The boundaries of the operating zone are defined by the station's maximum and minimum observation ranges and by the scanning range in azimuth and elevation.

The extent of the operating zone depends upon the function of the radar station. Thus, for example, a ground station for long-range detection of intercontinental ballistic missiles must have an operating zone with a range of thousands of kilometers, while devices for protecting the tail of an airplane require zones of only a couple of kilometers. A station used for detection and aiming must have circular scan, while an airplane's radar station for interception and aiming only needs to scan within the limits of a part of the forward hemisphere.

*The coordinates to be determined and their measurement accuracy.* The practical utilization of a radar station depends upon the coordinates which it can define and the accuracy with which they can be measured. Thus, for example, in determining the location of targets on land and on water only two coordinates need be measured: range and azimuth, while the observation of targets in the air requires the measurement of all three coordinates. For guidance of weapons or of pilotless objects, velocity and acceleration must be measured in addition to the coordinates of the object's position.

The degree of accuracy within which the coordinates must be measured is determined by the tactical function of the station. Such accuracy must be very high, especially in the case of stations used for

automatic guidance of weapons. Stations used for aiming weapons measure range with an accuracy of the order of tens of meters and angular coordinates with an accuracy of hundredths of a degree. In stations used for long-range detection, the accuracy of the coordinates is, naturally, lower. In the latter case, range-measurement error may be as great as several hundred meters, while errors in measurement of angular coordinates may be as high as several degrees.

*Resolution.* A station's resolution is its capacity to distinguish among targets which are close to one another. Since targets may be displaced with reference to one another in range and in direction, a distinction is made between range resolution and direction or angular resolution.

Range resolution is characterized numerically by minimum distance $\delta R$ between two targets displaced radially relative to the radar station and which can be ultimately distinguished on the radar screen. When the distance between the targets is less than $\delta R$, it is impossible to distinguish between these two targets by radar.

Angular resolution is characterized numerically by the minimum angle between two targets equidistant from the radar station at which the targets can be distinguished from one another on the radar screen. In the plane of the azimuth such an angle will be denoted by $\delta\alpha$, and in the vertical plane by $\delta\beta$.

*Noise protection.* The operation of the radar station may be affected by various types of interference, both natural interference and interference deliberately created by the enemy. Interference may be divided into internal and external depending upon its point of origin.

In the ultrahigh-frequency range the basic sources of external noises are the noises of the atmosphere, the galaxy, and the sun,

and of internal noises – the fluctuating noises of various elements of the receiver. The relation between the intensities of the external and internal noises depends upon a series of factors and, principally, upon the noise characteristics of the radio receiver.

Radar operations may be interfered with by passive noises, the signals reflected from various objects in the space around the radar station (buildings and structures, trees, hills, mountains, etc.). In the case of stations operating in the centimeter and millimeter ranges supplementary sources of reflection are hydrometeors (raindrops, snowflakes, hail). It is also possible that the enemy will use special reflectors which hamper the normal work of the radar station.

Active interference is very dangerous for radar operation. In this class we find, above all, such organized active interference as electromagnetic waves emitted in order to suppress or complicate the work of the radar station.

It is possible to interfere effectively with the operation of a radar station if its fundamental parameters, primarily, its carrier frequency and other characteristics of the radiated signals, are known. Whether or not these parameters can be determined depends upon the *concealment* of the radar. The greater the concealment of the radar station, the more difficult it is to observe its operation, to measure the characteristics of its signals, and to create the necessary interference.

In addition to deliberately created noises, the operation of the radar station may be hampered by radiation from other radio devices, in particular, the operation of other radar stations located nearby and operating in the same frequency range.

Noises act on the receiving system and the end devices of the radar station. When interference is very intense the radar station can-

not operate normally. Comparatively weak interferences hinder observation of the target spots on the station's indicator screen, lead to measurement errors, and distort the functioning of various automatic devices.

We will characterize the radar station's capacity to fulfill its functions in the presence of external interference by the term *noise resistance*. One of the major effects of external noises is the reduction in the radar station's range. Here we mean by range the distance at which target detection is accomplished with the required trustworthiness and at which it maintains the assigned accuracy in measurement of coordinates and in resolution. Since range is the main tactical characteristic of the radar station, its noise resistance may be quantitatively defined as the reduction in the observation range caused by noise.

Noise protection is the characteristic which takes into account both secrecy and the radar station's noise resistance.

*Scanning time* $T_0$. In time $T_0$ the antenna beam accomplishes a single scan of the whole assigned space. The value of $T_0$ selected depends upon the speed of the target and its maneuverability. The greater the velocity and maneuverability, the shorter the scanning time must be. Otherwise target displacement in a single scanning cycle would become so great as to make continuous observation impossible.

*Reliability*. By reliability we mean the station's ability to maintain its tactical and technical characteristics within the assigned limits under the assigned operating conditions.

Modern radar stations consist of a large number of interconnected elements, and each of them must be in proper working condition for the whole system to operate efficiently. The failure of any element will put an end to the normal operation of the radar station and prevent it

from fulfilling its assigned task.

In order to evaluate the possibilities of use of a radar station it is necessary to know its reliability. Reliability is characterized quantitatively by the probability of uninterrupted operation during a determined number of hours, or by the average period of uninterrupted operation of the station, frequency of breakdown, etc.

The technical parameters of the radar station are indissolubly connected with its tactical characteristics. The basic technical parameters of the radar station include:

- the carrier frequency of the oscillations $f$ or wavelength $\lambda$;
- the method of measuring range and the fundamental characteristics of the emitted signal;
- radiation power;
- the method of measuring angular coordinates;
- the shape and width of the coverage diagram of the antenna system and the antenna's coefficient of directivity;
- the scanning method and scanning speed;
- the sensitivity of the receiver;
- the dimensions and weight of the device;
- the feed-power required;
- the end device type.

Technical characteristics of a radar station are selected so as to satisfy the tactical demands made upon the station.

Since any radar station is a complex device, subject to the influence of various noises and unstable operating conditions, its technical and tactical parameters are usually statistical in character.

| Manuscript Page No. | [Transliterated Symbols] |
|---|---|
| 15 | д = d = doppler = Doppler |
| 17 | г = g = gorizontal'nyy = horizontal |

## Chapter 2

## METHODS OF SPACE SCANNING AND OF MEASUREMENT OF COORDINATES

### §2.1. PRINCIPLES AND METHODS OF MEASURING RANGE AND RADIAL VELOCITY

Two of the properties of radio waves are used for measuring range by radio methods: their constant propagation velocity and their linearity of propagation in a homogeneous medium. In practice, the medium is not homogeneous, and therefore these properties are displayed only with a certain degree of accuracy.

Radio waves are propagated at the speed of light, which, according to the most recent measurements, is $c$ = 299,792 ± 0.4 km/sec in a vacuum, or, if rounded off, $c = 3 \cdot 10^8$ m/sec. A radio wave traverses a distance $R$ in a time

$$\tau = R/c. \qquad (2.1)$$

This formula is customarily used to measure the difference between intervals. The value of $R$ = 300 m corresponds to delay $\tau$ = 1 μsec.

In measuring an absolute range value using radio methods, the delay time of the reflected or retransmitted signal is usually measured by comparison with the transmitted signal. Since here the radio waves travel along two paths, the delay time

$$\tau = 2R/c \qquad (2.2)$$

leaving out of the calculations signal delay in the circuits of the interrogator and the transponder. The obtained relationship is fundamental for radio range-measurement. A distance of $R$ = 150 m is equivalent to delay $\tau$ = 1 μsec.

Thus, to measure range it is necessary to note the moment of radiation and the moment of reception of the answering signal. Measured time interval $\tau$ corresponds uniquely to this range. There are various methods of noting the moment of radiation and of reception and of measuring time intervals.

1. Phase Method

Measurement of range by the phase method is based upon the proportional relationship between phase shift $\Delta\varphi$ and signal delay time $\tau = 2R/c$.

Let us assume that the transmitter is radiating an unmodulated sinusoidal oscillation of frequency $\omega_0$, whose initial phase we will assume equal to zero. If the target is stationary the received signal frequency is also equal to $\omega_0$. The current phase of the radiated oscillation is equal to $\omega_0 t$, and that of the received signal is $\omega_0\left(t-\frac{2R}{c}\right)$. The constant phase shift between the received and the emitted oscillation

$$\Delta\varphi=\omega_0\frac{2R}{c} \quad \text{or} \quad \Delta\varphi=2\pi\frac{R}{\frac{\lambda}{2}} \qquad (2.3)$$

is proportional to range.

As follows from the derived formula, target range in the UKV range can be measured with great accuracy using the phase method, but the resulting value is not uniquely defined since a phase shift which is a multiple of whole number $2\pi$ cannot be measured. A uniquely defined reading for range, within the limits of interval $2\pi$, may be obtained using the phase method according to Formula (2.3) under condition $R_{maks} = \lambda/2$, corresponding to an operating wavelength at least twice as great as the operational range of the RLS. Since $R_{maks}$ is at least several tens or hundreds of kilometers, not only would such a wavelength

be unsuitable for radar use, but it could not even be effectively radiated.

In addition to the lack of a unique definition, measurement of range from the phase of a sinusoidal oscillation is also made difficult by the fact that the phase shift occurring when the signal is reflected from the target is unknown.

In the case of a moving target, received signal frequency $\omega_{pr}$ is different from the frequency of the radiated oscillations. In fact, if we differentiate received signal phase $\omega_0[t - [2R/c)]$ over time, we obtain

$$\omega_{np} = \omega_0 - \omega_0 \frac{2V_R}{c},$$

where $V_R = dR/dt$ is the target radial velocity.

As has already been pointed out, the difference between the frequencies of the received and the radiated oscillations

$$F_д = \frac{\omega_0}{2\pi} \cdot \frac{2V_R}{c} = \frac{2V_R}{\lambda}, \qquad (2.4)$$

is proportional to target radial velocity and is called the Doppler frequency.

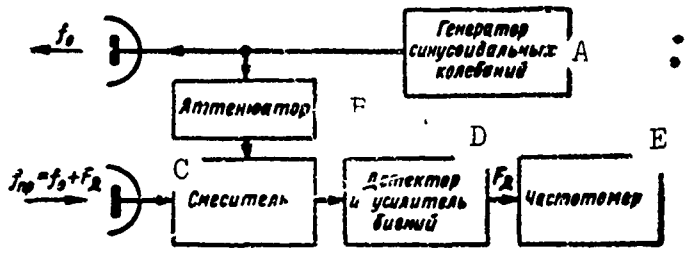


Fig. 2.1. Block diagram of a continuous-wave RLS for measuring velocity. A) Sinusoidal generator; B) attenuator; C) mixer; D) Detector and beat amplifier; E) frequency meter.

Figure 2.1 gives a block diagram of a continuous-wave RLS used for measuring radial velocity. The emitted oscillations enter the receiver through the attenuator and in the mixer form a beat with the received

signal. The beat frequency is equal to Doppler frequency $F_d$. At the mixer output there is a detector and an amplifier which develop oscillation frequency $F_d$ which is then measured by a frequency meter. The scale of the frequency meter can be directly graduated in units of velocity.

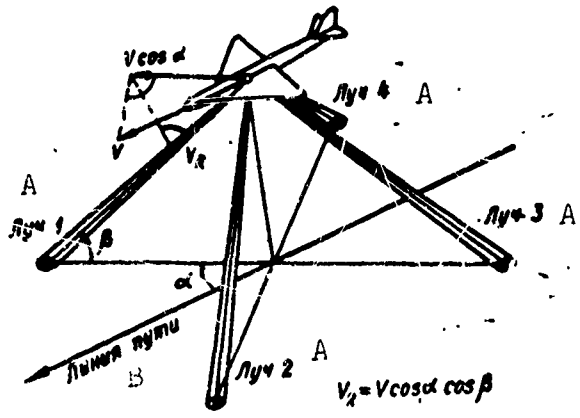


Fig. 2.2. Airborne multibeam RLS for measuring ground speed vector. A) Beam; B) line of flight.

An analogous principle underlies airborne multibeam RLS used for measuring the ground speed vector of a flying device (Fig. 2.2).

The RLS antenna forms four symmetrical antenna beams 1, 2, 3, and 4 which are displaced by azimuth angle $\alpha$ and elevation angle $\beta$ relative to the longitudinal axis of the flying device. Since $V_R = V \cos\alpha \cos\beta$, the radial component of velocity vector $V_R$ along one of the narrow beams is proportional to the absolute value of velocity $V$.

The RLS receiver contains two mixers. One of these mixers receives the signals of the first and third beams as reflected from the earth, and the second — the second and fourth. In the absence of wind, the symmetricity of the beams means that the Doppler shift of the frequencies of the first and third signals, and of the second and fourth, are equal in magnitude and opposite in sign. Therefore the beat frequencies at the outputs of both mixers are equal to double the Doppler frequency

and are identical. The value of the doubled frequency is proportional to the absolute value of the ground speed of the device.

If there is a sideways drift due to wind, the beat frequencies at the outputs of the first and second mixers will differ. Using these frequencies a special computer determines the absolute value of the velocity and of the drift angle – the two values which characterize the ground-speed vector.

Thus, by using the unmodulated carrier type of radiation, a sufficiently accurate determination of target radial velocity may be obtained – a derivative of range – but not range itself.

This difficulty in determining target range by using the phase method is overcome in various ways. One way is to emit oscillations of two frequencies: $\omega_1 = \omega_0$ and $\omega_2 = \omega_0 + \omega_d$, possessing very low difference frequency $\omega_d << \omega_0$. Since frequencies $\omega_1$ and $\omega_2$ are so close, the conditions for propagation and reflection of radiowaves at these frequencies are identical. If the initial phases of the emitted oscillations are assumed equal to zero, the current phases of the received oscillations will, correspondingly, be equal to

$$\omega_0\left(t-\frac{2R}{c}\right)=\omega_0 t-\omega_0\frac{2R}{c}$$

and

$$(\omega_0+\omega_d)\left(t-\frac{2R}{c}\right)=(\omega_0+\omega_d)t-(\omega_0+\omega_d)\frac{2R}{c}. \qquad (2.5)$$

The constant phase shift between the two received signals

$$\Delta\varphi=\omega_d\frac{2R}{c} \quad \text{or} \quad \Delta\varphi=2\pi\frac{R}{\frac{\lambda_d}{2}}, \qquad (2.6)$$

where $\lambda_d$ is the wavelength corresponding to differential frequency $\omega_d$.

We then differentiate the phases of received signals

$$\omega_{1\,пр} = \omega_0 - \omega_0 \frac{2V_R}{c}$$

and

$$\omega_{2\,пр} = (\omega_0 + \omega_d) - (\omega_0 + \omega_d) \frac{2V_R}{c}.$$

Here the second items are the Doppler frequencies, and the second items in Expression (2.5) are the phases of the Doppler frequencies. Therefore Formula (2.6) expresses the difference between the phases of the Doppler frequencies of the two received sinusoidal oscillations as a function of target range.

Difference frequency $\omega_d$ in Formula (2.6), in contrast to working frequency $\omega_0$ in Expression (2.3), may be assumed to be rather small so as to satisfy the condition that range be uniquely defined

$$R_{макс} \leqslant \frac{\lambda_d}{2}.$$

Thus, for a unique determination of range, the outcoming signal must consist of at least two sinusoidal oscillations. If range measurement accuracy turns out to be unsatisfactory, a method using several scales may be used: a third oscillation is emitted, yielding a second difference frequency larger than the first. The first difference frequency ensures a crude uniquely determined reading, the second – a highly accurate one. The first difference frequency may be likened to the hour hand, the second – to the minute hand. In case of need a "second hand" – a third difference frequency – may be employed, etc.

There is another method for unique definition of phase measurements: modulation of the carrier by a low frequency sinusoid whose phase shift is proportional to range. In this case the minimum number of frequencies is three: one carrier frequency and two side frequencies.

The phase method of measuring range is associated with a whole se-

ries of difficulties which cause it to be inadequate.

In the first place, during reception it is necessary to suppress direct passage of oscillations from the transmitter. Even when different antennas are used for reception and transmission these oscillations enter the receiver and form, together with the received signal, a total signal from whose phase range cannot be determined. By using rejector filters tuned to the frequencies of emission, direct passage of these oscillations may be suppressed. As a result of this, it is possible to detect and measure the range of moving targets only, since the signal frequencies of stationary targets are equal to the frequencies of the emitted oscillation.

Targets with radial velocities equal to zero are not detected by this type of phase RLS, which is both its merit and its drawback. Its merit consists in the fact that the reflections from local objects and from all targets except moving targets are automatically eliminated. At the same time, the loss of moving targets whose radio velocities are, with respect to the RLS, accidentally equal to zero is a drawback of the phase method.

A second drawback of the phase method is the absence of range resolution. The sinusoidal signals of two targets located at different ranges but possessing identical radial velocities form a total signal which cannot be distinguished. This drawback can to some extent be compensated by a technique of velocity selection of targets using filters tuned to various Doppler frequencies.

A third drawback of the phase method is, finally, the need for accurate phasemeters.

When the corresponding phase meters are available, the phase method is very accurate. When observation is deliberately limited to a single target, the apparatus may be of rather simple design.

2. TV Keying Method

Range may also be uniquely defined, and a distinction made between direct and reflected signals, if one of the parameters of the emitted oscillation: amplitude, frequency, phase, or polarization, is sharply altered from time to time. Then the received and the emitted oscillations will differ with respect to this parameter during delay time $\tau = 2R/c$.

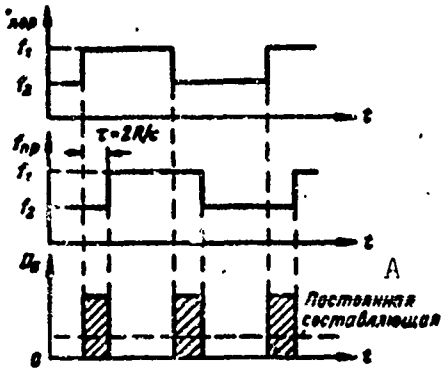


Fig. 2.3. Range measurement by frequency keying. A) Constant component.

Figure 2.3 gives the processes of emission and reception in frequency keying. By measuring time interval $\tau$ during which the keyed parameters of the direct and reflected signals differ, target range may be determined.

Frequency keying differs from the phase method, involving the simultaneous emission of two frequencies, in that oscillation first of one and then of another frequency are emitted sequentially. During time period $\tau = 2R/c$ for each half cycle of keying, there will appear at the receiver output beats whose frequency is equal to the difference between the two frequencies. After amplitude clipping the detected beat pulses may be fed into a smoothing filter. The constant component derived is proportional to target range.

By making the apparatus more complicated, it is possible to determine separately the range and velocity of a moving target and also to select targets according to their velocities.

The frequency keying method possesses approximately the same drawbacks as the phase method.

However, it does not require special procedures for distinguishing between direct and reflected signals and, therefore, it may be used to

measure the range of a stationary target.

Another type of keying is the amplitude method in which the RLS transmits during half of a cycle and during half of the cycle does not transmit. This method has also been called the *small reciprocal duty factor* method.*

Like the phase method, the keying method is applied when range resolution is not needed. The oscillations have a narrow frequency spectrum which prevents a sufficiently large volume of information from being superimposed upon them; in particular, the signals of several targets cannot be transmitted separately.

An improved method is the one in which the reflected target signals of various ranges are distinguished either in time or in frequency. The first condition is satisfied in the pulse method of operation, the second condition in the frequency method.

3. The Pulse Method

The pulse may be represented in the form of an infinitely large number of harmonic components in such defined relationships with cer-

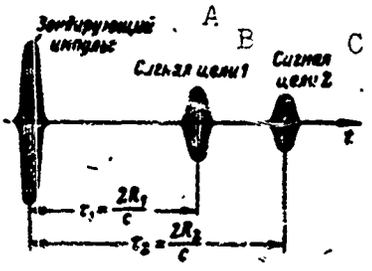


Fig. 2.4. Bunching of target signals according to range in the pulse method. A) Outcoming pulse: B) target signal 1; C) target signal 2.

tain mutual phase shifts that they are summed at pulse length interval $\tau_i$ and extinguish one another over the whole remaining time interval. These components are propagated in free space after emission, and return to the receiver after reflection, in the same mutual phase relationship as during emission, since the relative width of the signal

spectrum is small and the propagation conditions of the various spectrum components are practically identical. The phase shift of the signal is converted into a group delay which will be greater as the target is further away. At the receiver input these components again form short pulses some of which appear earlier and others later (Fig. 2.4).

The time distribution of the received pulses relative to the moment of emission of the upcoming pulse depends upon target range. Because of this, the signals of two targets of different ranges are received separately, if the targets are not too close to one another. It follows from what has been said that such a division is possible because of the broad frequency spectrum of the emitted oscillation. One or several of the harmonic components utilized in the phase method can not be bunched in time in such a way as to cancel one another during a certain time interval and thus to leave a place for the signals of other targets. Precisely because of this, the phase method does not possess range resolution.

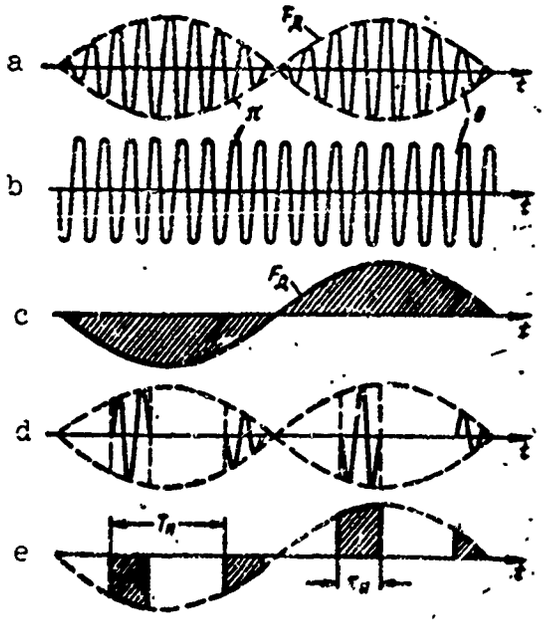


Fig. 2.5. Beat detection: a) beats of continuous signals; b) reference voltage of phase detector; c) output voltage of phase detector during a continuous signal; d) beats of received signal pulse with coherent voltage; e) output voltage of phase detector in pulse signal.

Because of its merit the pulse radar method has become the predominant one at the present time. In the first place, it makes possible a simple measurement of range – by time delay. It is only necessary to note two moments in time: the moment of emission and the moment of return of the reflected signal. Another merit of the pulse method is the comparatively simple way in which it distinguishes between direct and reflected oscillations: during emission the receiver is closed by using an antenna switch, and during reception the transmitter does not operate.

Together with this the pulse method also possesses certain drawbacks. One of them is the need for large transmitting power which involves the danger of arcing and requires application of cumbersome pulse modulators. Furthermore, very short ranges cannot be measured because of the paralysis of the receiver during recovery of the antenna switch discharger after emission.

A major disadvantage of the pulse method is that the Doppler method cannot be used for a unique determination of target radial velocity. We will understand this disadvantage if we examine the processes taking place during production of beat frequencies in the continuous and in the pulse modes of operation (Fig. 2.5).

During continuous operation the received and emitted oscillations form beats whose envelope changes with differential Doppler frequency $F_d$ (a). A phase detector which is fed with reference voltage (b) is used to produce frequency $F_d$. The phase detector output yields sinusoidal oscillation (c) of frequency $F_d$ which is measured to determine radial velocity.

The received pulse signals may be represented in the form of slices of continuous oscillation; pulse length is $\tau_i$, and the repetition period is $T_p = 1/F_p$. After the output of the mixer (d) and of the phase

detector (e) these signals form pulses whose amplitudes change with the frequency of the beat. By observing the change in the amplitude of the pulses the frequency of the beat may be determined.

With a continuous signal the beat frequency produced is always equal to the Doppler frequency. In the case of a pulse signal, beat frequency $F_b$ of the high-frequency direct and reflected oscillations coincide with Doppler frequency $F_d$ only when condition $F_d << F_p/2$ is fulfilled. In other cases the beat frequency derived is not a uniquely defined function of the Doppler frequency; this is one of the manifestations of the stroboscopic effect and is explained in Fig. 2.6.

The pulses given in drawings a and b follow sufficiently closely upon one another for it to be possible to depict Doppler frequency in the form of a modulation of their amplitude. With the increase in frequency $F_d > F_p/2$ (drawings c, d, e) the rate of arrival of pulses becomes too low to represent all of the changes of the modulating function. During pulse repeat period $T_p$ all cycles of the changes of the modulating function are completely lost to the observer. In particular, the derived beat frequency $F_b$ is zero when the Doppler frequency is a multiple of the frequency of the packages (drawings d and e). The case $F_d = F_p/2$ (drawing b) is the boundary case. The case in which frequency $F_d$ is not a multiple of whole number $F_p$ (drawing c) is transitional.

The stroboscopic effect occurs until the point at which the Doppler frequency becomes large enough so that, within the limits of the length of a pulse, there is not less than a single Doppler frequency cycle. As a result of this the Doppler frequency may be discovered from the change in amplitude within the limits of a single pulse. For frequencies $F_d = 1/\tau_i$ and higher quality $F_b = F_d$ again applies, and target radial velocity may again be uniquely defined. However, because of the short pulse length, this phenomenon obtains at excessively high veloci-

ties, and, for the time being, has no practical meaning.

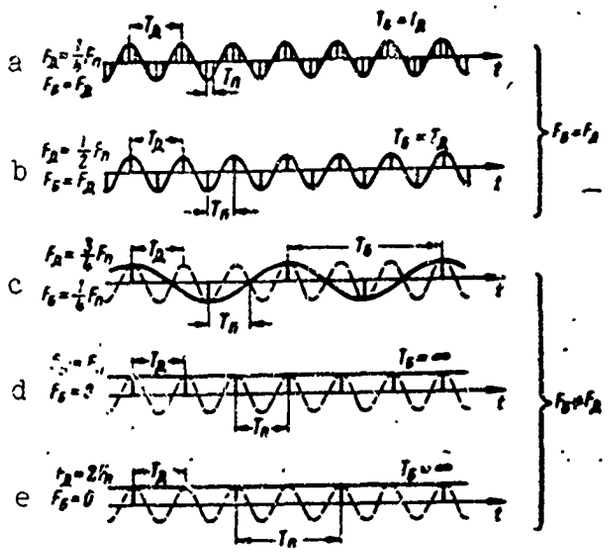


Fig. 2.6. Stroboscopic effect: a, b) absence of stroboscopic effect; c, d, e) presence of stroboscopic effect.

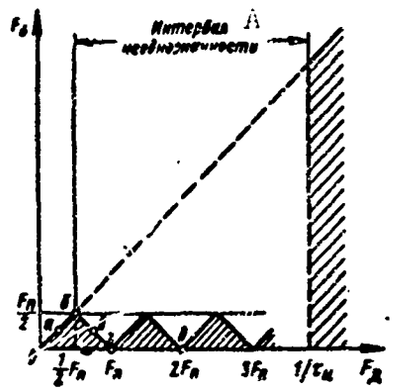


Fig. 2.7. Dependence of beat frequency upon Doppler frequency and upon the frequency of pulse packages. A) Interval within which values are not uniquely defined.

The dependence of $F_b$ and $F_d$ is given in Fig. 2.7, which sets forth, in the circular dots and the corresponding letters, the relationships given in Fig. 2.6. The interval within which radial velocity cannot be uniquely defined using the pulse method extends from $F_d = F_p/2$ to $F_d = 1/\tau_i$. A uniquely defined reading over the whole interval of Doppler frequencies is possible only if both limits coincide, that is,

in continuous operation.

The pulse-package method of operation is often used to measure radial velocity: during a given time period a pulse package is emitted at a sufficiently high frequency, and then emission is stopped for an extended interval. This method is used in order to eliminate the inconveniences associated with the use of continuous emission.

Furthermore, it should be pointed out that during pulse operation the emitted signal is usually cut off during reception. Therefore, a special coherent oscillation is produced using a rather complex circuit and used as a reference voltage in order to form a beat with the received signal.

4. Frequency Method

The continuous method of operation with frequency modulation can also be used to maintain range resolution and to measure velocity. In

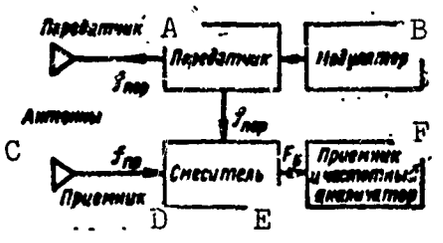


Fig. 2.8. Simplified block diagram of a continuous RLS with frequency modulation. A) Transmitter; B) modulator; C) antenna; D) receiver; E) mixer; F) receiver and frequency analyzer.

describing the principle of operation of an RLS with frequency modulation we will assume that frequency changes rather slowly; this makes possible the comparison of instantaneous frequencies.

Figure 2.8 gives a block diagram of a frequency RLS, and Fig. 2.9 illustrates its operation.

The transmitter emits continuous oscillations which are frequency modulated according to the sawtooth law (continuous broken line). The signals from a stationary target, which are delayed by time $\tau$ with ref-

erence to the emitted signal (dashed line) are fed into the mixer. A weakened direct signal is also fed to the mixer. A beat frequency $F_b = F_R$, is formed, which is proportional to target range.

Actually, if we denote the frequency deviation by $\Delta f$, and the modulation period by $T_m = 1/F_m$, we obtain, in accordance with Fig. 2.9

$$F_6 = F_R = \frac{df}{dt}\tau; \quad \frac{df}{dt} = \frac{\Delta f}{\frac{T_м}{2}} = 2\Delta f F_м, \quad \tau = \frac{2R}{c},$$

whence

$$F_R = \frac{4}{c}\Delta f F_м R. \qquad (2.7)$$

A modulation period $T_m$ is selected such that it is many times greater than the maximum delay time. Otherwise the time of the transitional processes would play a noticeable role in the beat signal (see Fig. 2.9), and the linear dependence between range and beat frequency would be violated.

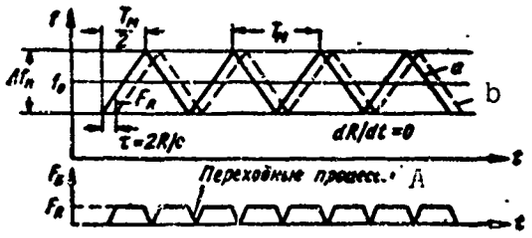


Fig. 2.9. Measuring the range of a stationary target: a) frequency of emitted oscillations; b) frequency of received signals. A) Transitional processes.

After amplification, the beat signal enters the frequency analyzer (frequency meter), which is directly graduated in units of range.

Two types of frequency analyzers exist: the sequential and the parallel.

The sequential analyzer consists of a narrow-band filter whose frequency is periodically retuned. During the retuning process the filter is tuned to the beat frequency during a small part of the period of

retuning, and this beat frequency corresponds to target range; a signal appears at the receiver output. Target range is determined by the frequency to which the filter is tuned at the moment of appearance of a target signal. During the greater part of the period of tuning of the filter, there is no target signal at the receiver output even though there is one at the receiver input. Because of this the greater part of the energy of the received signal is lost, and the operational range of an RLS with a sequential frequency analyzer is several times smaller than that of a pulse RLS.

An analyzer of the parallel type, which consists of a large selection of narrow-band filters covering the whole range of the beat frequencies, does not possess this drawback. The whole energy of the signal reflected from the target passes through one of the analyzer filters to the receiver output. Target range is determined by the number of this filter. Radar stations with parallel analyzers possess the same operational range as pulse RLS if the average power is the same and other conditions are equal.

The continuous method of operation with frequency modulation, like the pulse method, possesses good range resolution thanks to the presence of a broad spectrum of frequencies. The difference is in the principle of bunching of the signals of targets of different ranges. In the pulse method target signals are bunched in pulses which are disbursed over time and, consequentially, over range. In the frequency method, target signals at the mixer output are bunched into "pulses" of the beat spectrum whose frequencies are disbursed according to target range (Fig. 2.10). Signals from targets of different ranges are differentiated according to beat frequency if the targets are not too close together.

The greater the deviation $\Delta f$, the broader the signal spectrum. In

accordance with Formula (2.7) an increase in $\Delta f$ causes an increase in the beat frequency at the same target range. As a result of this the signals of targets which are close to one another differ by larger in-

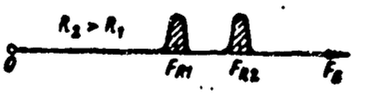


Fig. 2.10. Bunching of target signals by range in the frequency method.

tervals in their beat frequency and that can be effectively distinguished. Consequently, expansion of the signal spectrum also heightens resolution in the frequency method.

Target signals are grouped according to range in a very similar way in the pulse and frequency method. However, these two methods differ very greatly in their technical implementation. The pulse method has a range scale available — current time, during which the delay time is established by noting the time of emission and that of reception. The frequency method does not have available such a scale but must create one by using a frequency analyzer. As has already been noted, the sequential analyzer involves inacceptable energy losses, while the parallel analyzer is very complex and cumbersome. This drawback of the frequency method is one of the principal factors which have led to the broad application of the pulse method at the expense of the continuous method.

A second major drawback of the continuous method is that it is difficult to distinguish effectively between the emitted and the received oscillations. The ferrite dividing devices which have appeared in recent years have made this task much easier but have not yet solved it completely. There also remains the problem of reducing the level of the transmitter noises which pass through the mixer into the receiver.

A third drawback is the stiff requirement for linearity of the

change of frequency in order to obtain a uniquely determined reading of range in RLS of high resolution.

The frequency radar method has a number of advantages over the pulse method, and this explains why people strive to use it.

In the first place, with the frequency method very short ranges can be measured. This is why the frequency method is used in low-altitude radio altimeters where the presence of only one target – the earth's surface – makes it possible to do without the filter array, altitude being measured by counting the number of beats per unit of time.

A second merit of the continuous method is the low radiating power required – several hundreds or thousands of times lower than the peak radiating power of a pulse RLS with the same range. Already pulse RLS are operating at the pulse radiation limit determined by the danger of arcing, and this prevents their range from being increased. The weight and dimensions of the transmitter are also reduced in the frequency method.

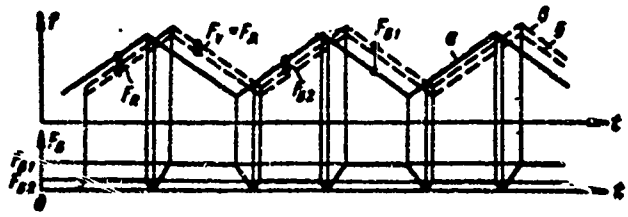

Fig. 2.11. Measurement of target range and radial velocity using the frequency method: a) frequency of emitted oscillations; b) frequency of received signals from stationary target; c) frequency of received signals from moving target.

An important advantage of the continous method is the possibility of a uniquely determined measurement of target velocity. Figure 2.11 illustrates the processes occurring in a station when target radial velocity is not equal to zero. In this case beat frequency $F_b$ is determined not only by frequency $F_R$ which is proportional to range, but also

by Doppler frequency $F_d = F_V$, which is proportional to velocity. Because of this, the beat frequency for one modulation half-period is greater by quantity $F_V$ than frequency $F_R$, and for the other – less by the same quantity, that is, $F_{61} = F_R + F_V$, $F_{62} = F_R - F_V$, , and, consequently,

$$F_R = \frac{F_{61} + F_{62}}{2}; \qquad F_V = \frac{F_{61} - F_{62}}{2}. \tag{2.8}$$

Thus the determination of range is reduced to a measurement of the half-total of the beat frequencies for two half-periods, and the determination of target radial velocity – to measurement of the half-difference. Here it is assumed that condition $F_{V\text{maks}} \leq F_{R\text{min}}$ is fulfilled.

When a filter array is available, signals may be selected not only for range, but also for velocity, which heightens the noise defense of the RLS. However, the technical implementation of all of these merits is complex and is still in the stage of development.

## §2.2. PRINCIPLES AND METHODS OF MEASURING ANGULAR COORDINATES AND ANGULAR VELOCITIES

The measurement of target angular coordinates (direction-finding) uses the same properties of radiowaves as the measurement of range: constant velocity and linear propagation, together with reception of the target signal on spatially dispersed points of reception. The dispersed reception points form an antenna system at whose output the signals received by its various elements are compared. The result of the comparison depends upon the direction of arrival of the signal and can therefore be used to determine the direction of the target.

Depending upon the manner in which the signals are compared, two basic methods of direction-finding are to be distinguished: the phase method and the amplitude method.

### 1. The Phase Method

Let us now take up the case of target direction-finding in a sin-

gle plane using the simplest antenna system in the form of two nondirection vibrators (Fig. 2.12). The space between the vibrators is called the *base* and is denoted by $b_a$. The target direction is read off from a line perpendicular to the center of the base, which is often called the equisignal direction.

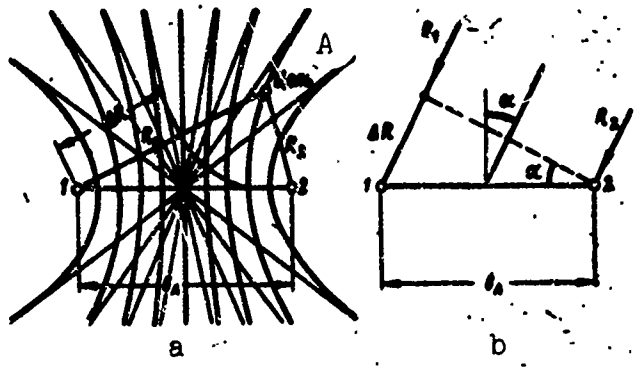


Fig. 2.12. Target direction finding with two dispersed antennas (phase method): a) adjacent zone; b) distance zone. A) Target.

The principle of direction finding consists in the measurement, by two vibrators, of the difference in the times of reception of the target signals. As the target deviates from the equisignal direction, there arises a difference in the signal traces $\Delta R = R_1 - R_2$. Because of constant velocity and linearity of propagation of radiowaves, relative signal delay is proportional to trace difference

$$\tau = \frac{\Delta R}{c}. \qquad (2.9)$$

Systems using this principle are called *differential-range* systems. In these systems the difference in times of signal reception depend, generally speaking, not only upon target direction, but also upon the distance between the target and the center of the base. On a plane surface the lines corresponding to an identical difference in distances have the form of hyperbolas (Fig. 2.12a).

However, at large distances from the center of the base, when $P >> b_a$, the hyperbolas in practice coincide with their asymptotes, in

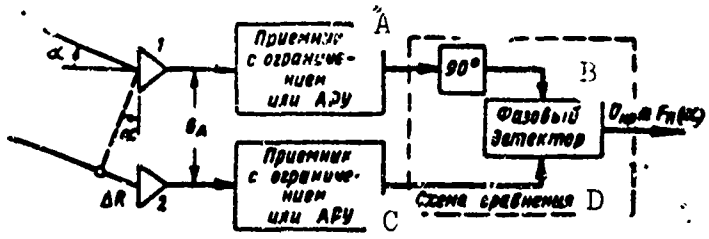


Fig. 2.13. Block diagram of phase direction finder. A) Receiver with limiter or ARU; B) phase detector; C) receiver with limiter or ARU; D) comparison circuit.

the form of beams radiating out from the center of the base. Differential-range systems are converted into angular systems. Actually, in this case beams $P_1$ and $R_2$ may be assumed parallel (Fig. 2.12b), and when the target is deflected by angle $\alpha$, trace difference

$$\Delta R = b_a \sin\alpha,$$

arises which, with the given base dimensions, depends only upon the direction of reception. The relative signal delay

$$\tau = \frac{b_a}{c}\sin\alpha \qquad (2.10)$$

is also determined only by angle $\alpha$.

Time interval $\tau$ may be measured by any of the methods examined above: phase, pulse, or frequency. However, in practice only the phase method is used since it is the most accurate, delay being measured from the difference of the phases of the very carrier frequency $f_0$ itself.

The basic reasons limiting the use of the phase method in measuring range no longer apply. In the first place, a phase difference is measured and not the absolute value of a target signal phase containing some unknown initial phase. In the second place, the difference of distances $\Delta R$ is small – does not exceed base dimensions $b_a$ – and therefore

the nonunique definition of the angular reading is also small and is comparatively easily eliminated.

The pulse and frequency methods are considerably less accurate, and they are therefore used only in differential-range systems with a relatively large base. In direction-finding systems these methods may be used to eliminate the phase method's lack of unique definition.

Figure 2.13 shows a block diagram of a phase direction-finding system in a single plane. In order to determine target direction simultaneously in two planes, a second identical direction-finding system in the other plane is required. No transmitter is shown in the circuit since, in contrast to the measurement of range, it is in principle not needed: direction may be determined with equal success from one's own reflected signals as well as from outside signals of the same frequency. The circuit does not show the frequency converters and the local heterodyne which is common to the two receivers, since the phase relations among the signals are maintained during frequency conversion.

The phase difference of the received signals, determined by their relative delay $\tau = \frac{b_0}{c}\sin\alpha$, is

$$\Delta\varphi = 2\pi f_0 \tau = 2\pi \frac{f_0}{c} b_0 \sin\alpha$$

or

$$\Delta\varphi = 2\pi \frac{b_0}{\lambda}\sin\alpha. \qquad (2.11)$$

The sensitive (comparison) element in the system is the phase detector. If signals to be compared, possessing amplitude $U_1$ and phase difference $\Delta\varphi$, are fed directly to the inputs of the phase detector, the output is the obtained voltage

$$U = kU_1^2 \cos\Delta\varphi = kU_1^2 \cos\left(2\pi \frac{b_0}{\lambda}\sin\alpha\right).$$

It is not yet possible to determine angle $\alpha$ of signal arrival from

the magnitude of this voltage. In the first place, amplitude $U_1$ of the received signals is unknown. To eliminate unknown quantity $U_1$ either the signal is sharply limited down to a constant amplitude or automatic gain control (ARU) changing the receiver gain factors in inverse proportion to the received signal amplitude, is used. In the second place, function $\cos [2\pi(b_a/\lambda) \sin \alpha]$ does not depend upon the direction of deviation ($+\alpha$ or $-\alpha$) and is quadratic, that is, weakly dependent upon the angle, when $\alpha$ is small. Therefore the phase of one of the signals is shifted by $\pi/2$.

As a result of these measures mismatch voltage

$$U_{mp} = U_m \sin\left(2\pi \frac{b_a}{\lambda} \sin\alpha\right), \qquad (2.12)$$

is obtained from the phase detector. This voltage depends only upon angle $\alpha$, since factor $U_m$ is a constant obtained as a result of the limiting or of the operation of the ARU.

At small angles $\alpha$ the dependence of mismatch voltage

$$U_{mp} \approx U_m 2\pi \frac{b_a}{\lambda} \alpha$$

upon the direction of reception is linear and changes its polarity (sign) with change in the direction of deflection, which is convenient for direction finding.

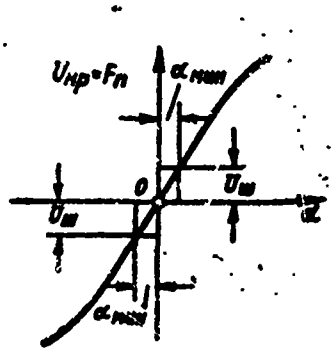


Fig. 2.14. Direction-finding characteristic of a phase direction finder.

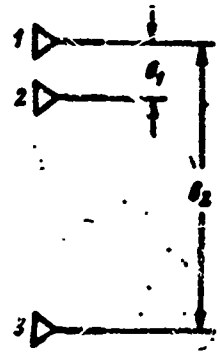


Fig. 2.15. The phase method of expanding a nonunique angular reading.

Because of imperfections in the equipment, equipment errors arise in the system. Thus, different phase shifts of the signals in the two receiver circuits cause displacement of the equisignal direction. When clipping is not perfect or when the ARU circuit is not operating correctly, the mismatch voltage depends not only upon the angle, but also upon the dimensions, target range, etc. This is the basic cause of difficulty in designing phase direction-finding systems.

The dependence of the relative mismatch voltage value $F_{pkh} = U_{nr}/U_m$ is called the *direction-finding characteristic* and is depicted in Fig. 2.14. The steepness of the direction-finding characteristic in the equisignal direction

$$S_\phi = \left| \frac{dF_{nr}}{d\alpha} \right|_{\alpha=0} = \frac{2\pi b_a}{\lambda}$$

is determined by the relative base size $b_a$. The steeper the direction-finding characteristic, the smaller insensitivity angle $\alpha_{min}$ at the assigned noise level $U_m$, and the better the system's direction-finding sensitivity.

Consequently, increasing the relative size of the base by increasing the spacing of the waves or by reducing their length heightens the direction-finding sensitivity of the system. However, at the same time the nonuniqueness of the angular reading from the value of the mismatch voltage also increases. As follows from Formula (2.12), as the target deviates from the equisignal direction, mismatch voltage $U_{nr}$ again becomes equal to zero, and its phase is altered by whole number $\pm\pi$. The number of transits through zero (cycles of nonuniqueness) $N = 2(b_a/\lambda)$ is also determined by the relative size of the base.

To obtain high accuracy and a uniquely determined reading at the same time, several scales are used. Figure 2.15 gives an antenna system with two bases $b_1$ and $b_2$ formed by three antennas. Small base $b_1$

yields a crude but uniquely determined angular reading; large base $b_2$ provides high accuracy. When the accuracy of the reading from the second scale is inadequate, another antenna with a still larger base can be added etc., if a single crude scale is not enough fully to eliminate the nonuniqueness of the most accurate scale.

The decisive role in direction-finding is played not by the absolute size $b_a$ of the base, but by relative size $b_a/\lambda$. Therefore the same base may be used for several scales by employing several signals of different wavelength.

It follows from what has been said that there is a complete analogy between the phase method of measuring range using system $\omega_d = 2\pi f_d$ of different frequencies and the phase method of measuring angles using the system of relative bases $b_a/\lambda = (b_a/c)f_0$.

The phase systems in the form presented do not possess resolution. Two targets located in different directions create in space a total signal which in the antenna system forms a phase difference corresponding to some false direction which, generally speaking, does not coincide with the direction of one or the other target. For high directional resolution and a long operational range the antennas must possess sufficiently sharp amplitude directivity characteristics.

Continuing the analogy between the range and angular phase systems, we may note one further common property. Just as the range phase system can be used for accurate and unique measurements of radial velocity, angular phase systems may be used to measure target angular velocities.

Actually, the phase difference of the compared signals is proportional to the distance differential between the target and two points of reception

$$\Delta\varphi = \frac{2\pi}{\lambda}(R_1 - R_2) \approx \frac{2\pi b_a}{\lambda}\sin\alpha;$$

the derivative of the phase difference, and also differential frequency

$$F_{\dot{\alpha}} = \frac{1}{2\pi}\frac{d}{dt}\Delta\varphi = \frac{\dot{R}_1}{\lambda} - \frac{\dot{R}_2}{\lambda} = \dot{\alpha}\frac{b_a}{\lambda}\cos\alpha \qquad (2.13)$$

are proportional to target angular velocity $\dot{\alpha}$. Near the equisignal direction $F_{\dot{\alpha}} \approx (b_a/\lambda)\dot{\alpha}$. The antenna system sensitivity to angular velocity increases with an increase in the relative size of the base as well as during measurement of the angles themselves.

Frequency $F_{\dot{\alpha}}$ is the difference between Doppler frequencies $F_{d1} = \dot{R}_1/\lambda$ and $F_{d2} = \dot{R}_2/\lambda$, which are proportional to the corresponding target radial velocities $\dot{R}_1$ and $\dot{R}_2$ relative to both points of reception. Two ways of measuring target angular velocity are possible: measuring the Doppler frequencies at dispersed reception points and then subtracting them or the direct measurement of the differential Doppler frequency obtained using a mixer. The latter method is better, since, with the same relative error in measuring the frequency, the absolute error in measuring the frequency difference is less. In the first case the absolute error is proportional to the Doppler frequency itself, and in the second – to the difference of the Doppler frequencies which is several orders lower than the Doppler frequency.

2. The Amplitude Method

The phase relation among signals received by a dispersed antenna may be converted into a dependence of the amplitude of the antenna output signal upon the angle of arrival.

In the simplest antenna system, one consisting of two vibrators, the two signals are summed. The amplitudes $U_1$ of these signals may be considered equal, since the difference in the traces $\Delta R \ll R$. If the phases of the signals are read off relative to the phase of the wave in the center of the base, one of these signals arrives with phase advance $\Delta\varphi/2$ and the other with phase delay $-\Delta\varphi/2$, where $\Delta\varphi = 2\pi(b_a/\lambda)$.

·cos α is the difference in the signal phases. After addition we obtain a total signal with amplitude

$$U_{cc}=U_1\left(e^{j\frac{\Delta\varphi}{2}}+e^{-j\frac{\Delta\varphi}{2}}\right)=2U_1\cos\left(\pi\frac{b_a}{\lambda}\sin\alpha\right).$$

The obtained dependence of the total signal upon angle enables us in principle to determine target direction according to the signal maximum. However, direction finding involves a series of drawbacks. In the first place, at small α the dependence of amplitude on angle is quadratic, and the direction-finding sensitivity is low. In the second place, the direction of the deviation is not determined, since the result is identical when the target deviates by angle +α and −α. In the third place, the total signal depends not only upon the direction of arrival, but also upon the unknown amplitude $U_1$ of the received signal.

The first two drawbacks are eliminated if the signals are not summed but subtracted. At low α, different signal amplitude

$$U_{pc}=2U_1\sin\left(\pi\frac{b_a}{\lambda}\sin\alpha\right)$$

is proportional to the angle, and the direction of deviation may in principle be determined from the sign (phase) of the voltage. The obtained dependence is used in frame antennas where the electromotive forces of the two opposed sides of the frame are connected in such a way as to be opposed. Target direction is determined from the position of a line perpendicular to the plane of the frame at the moment when signal $U_{rs}$ at the frame output is zero. From this the direction-finding method has gotten the name of *minimum method* or, more accurately, *zero method.*

The drawback of the minimum method is that during direction-finding the antenna must be keyed so as to ensure that the signal vanishes, while at the moment of the direction finding it is impossible to measure target range or even to reach a confident judgment as to its pres-

ence, since the signal is equal to zero. Furthermore, the difference signal cannot be used to determine the amount of the deviation since it contains unknown factor $U_1$. Nor is there any reference voltage for determining the direction of deviation according to the signal sign (phase).

These drawbacks are eliminated when the difference and the total signal are used at the same time. For this the antenna output should be equipped with adding and subtracting devices whose signals are then fed into the two receiver circuits. The relation between the difference signal and the total signal

$$F_{\text{пл}} = \frac{U_{\text{рс}}}{U_{\text{сс}}} = \text{tg}\left(\pi \frac{b_a}{\lambda} \sin\alpha\right) \qquad (2.14)$$

depend only upon the direction of reception and is called the direction-finding characteristic. This function may be obtained by automatic gain control of the difference signal by the total signal. The correlation between the phase of the total signal and of the difference signal is used to determine the direction of deviation with a phase detector. Furthermore, the total signal may be used to discover the target and to measure its range by the delay time.

It should be noted that such devices are rather complex and are usually combined with highly directional antenna systems. Therefore, their more detailed description will be postponed to a somewhat later stage.

The direction-finding sensitivity of the amplitude system is defined by the steepness of the direction-finding characteristic in the equisignal direction

$$S_a = \left|\frac{dF_{\text{пл}}}{d\alpha}\right|_{\alpha=0} = \frac{\pi b_a}{\lambda}$$

and increases with the increase in the relative size of the base $b_a/\lambda$.

The very simple, two-vibrator, phase and amplitude direction-find-

ing systems examined above are based on quite identical principles and therefore, in principle, possess identical properties and capacities.

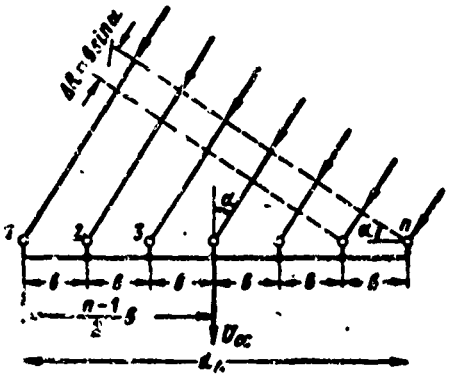

Fig. 2.16. Principle of shaping of directivity diagram of cophasal antenna grid.

To the general disadvantages of the very simple systems examined above should be added the absence of resolution and the fact that when the base is large the angular reading is not uniquely defined. Both of these disadvantages are eliminated in complex antenna systems with small or large bases; they can be used to obtain angular readings which are both uniquely determined and highly accurate, and they are also highly directional which makes possible a high degree of resolution and a long operating range. These properties are characteristic of multivibrator cophasal grids and continuous aperture antennas.

Let us examine a cophasal antenna grid consisting of $n$ nondirectional vibrators spaced at intervals $b$ (Fig. 2.16). In all vibrators signal amplitudes $U_1$ are identical while the relative phase shift increases evenly by quantity $\Delta\varphi = 2\pi(b_a/\lambda)\sin\alpha$, from vibrator to vibrator, the signal phase in the vibrator on the far left being equal to $-[(n-1)/2]\Delta\varphi$, if phase is read from the middle of the antenna grid. Then the amplitude of the total signal at the output of the antenna grid

$$U_\alpha = U_1\left(e^{-j\frac{n-1}{2}\Delta\varphi} + e^{-j\frac{n-3}{2}\Delta\varphi} + \ldots + e^{j\frac{n-1}{2}\Delta\varphi}\right) =$$

$$= U_1\frac{e^{-j\frac{n-1}{2}\Delta\varphi}\left(e^{jn\Delta\varphi}-1\right)}{e^{j\Delta\varphi}-1} = U_1\frac{e^{j\frac{n}{2}\Delta\varphi}-e^{-j\frac{n}{2}\Delta\varphi}}{e^{j\frac{1}{2}\Delta\varphi}-e^{-j\frac{1}{2}\Delta\varphi}}$$

as the sum of $n$ members of a geometrical progression with initial

ber $a_1 = e^{-j\frac{n-1}{2}\Delta\varphi}$ and denominator $q = e^{j\Delta\varphi}$. If the last expression undergoes an Euler transfo mation, we finally obtain

$$U_{cc} = U_1 \frac{\sin\left(\frac{n}{2}\Delta\varphi\right)}{\sin\left(\frac{1}{2}\Delta\varphi\right)}.$$

At $U_{ss}$ the maximum value of $\Delta\Phi \to 0$ is $nU_1$. Therefore the standardized directivity characteristic of a grid consisting of $n$ vibrators

$$F_E(\alpha) = \frac{\sin\left(n\pi\frac{b}{\lambda}\sin\alpha\right)}{n\sin\left(\pi\frac{b}{\lambda}\sin\alpha\right)}. \qquad (2.15)$$

A cophasal antenna with continuous aperture $d_a$ and even field distribution may be represented as a multivibrator antenna at $n \to \infty$, with $d_a = nb$, $b = d_a/n$, and, therefore, the function of the sinus in the denominator of Formula (2.15) may be replaced by the argument. Then the directivity characteristic of a continuous antenna with aperture $d_a$ and even distribution of the field across the aperture

$$F_E(\alpha) = \frac{\sin\left(\pi\frac{d_a}{\lambda}\sin\alpha\right)}{\pi\frac{d_a}{\lambda}\sin\alpha} \qquad (2.16)$$

has the form $\sin x/x$ (Fig. 2.17).

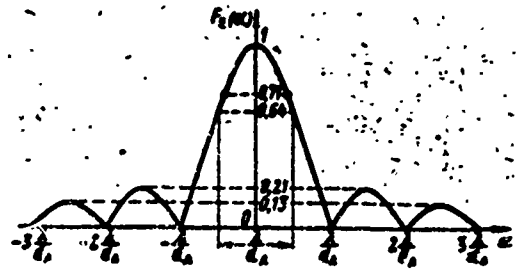

Fig. 2.17. Directivity diagram of the type $\sin x/x$, formed by a cophasal antenna with even field distribution across the aperture.

The first zero of the characteristic appears at $\alpha_0 \approx \sin\alpha_0 = \frac{\lambda}{d_a}$ and the aperture of the directivity characteristic at the zero level $\theta_0 = 2\lambda/d_a$. If the angle is read at level $2/\pi \approx 0.63$, which corresponds

approximately to the generally accepted level for reading at half power, an aperture angle of the directivity diagram, expressed in radians,

$$\theta = \frac{\lambda}{d_a}. \qquad (2.17)$$

is obtained.

In actual antennas the aperture field is not usually distributed evenly, but falls to zero at the edges. Therefore part of the aperture has no effect, and the directivity diagram is somewhat wider (to 20%).

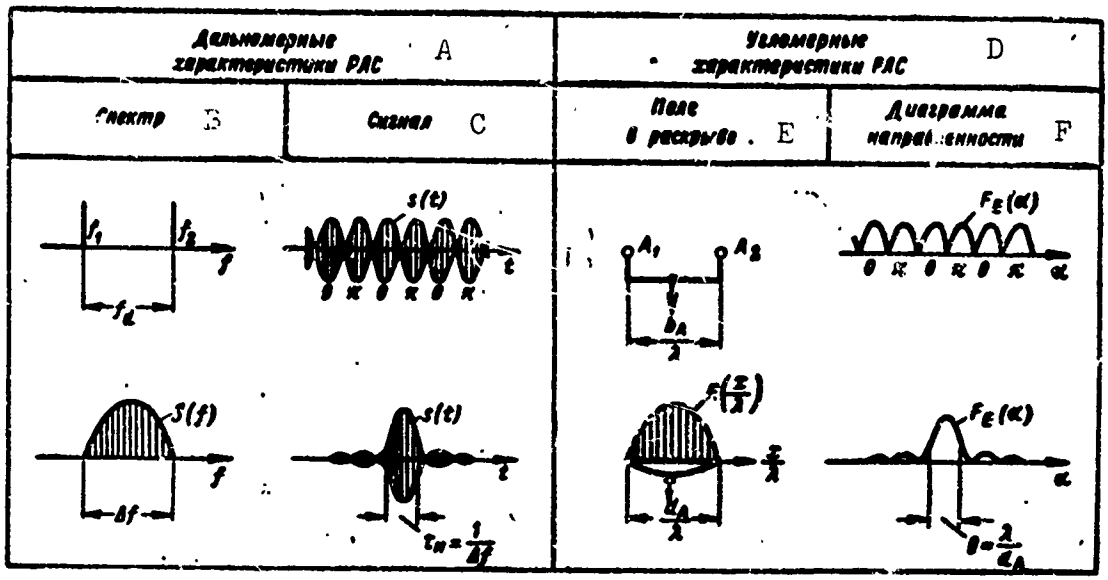


Fig. 2.18. Analogy between RLS range and angular characteristics: upper diagrams – accurate measurement of coordinates, absence of resolution; lower diagrams – simultaneous measurement accuracy and resolution. A) RLS range characteristics; B) spectrum; C) signal; D) RLS angular characteristics; E) aperture field; F) directivity diagram.

Target signals which do not fall within the limits of the aperture angle of directivity diagram $\theta$ are not received by the antenna; this is the basis of directional resolution. Thus, directional resolution in each of the two planes is determined by the relative antenna aperture $d_a/\lambda$ in the corresponding plane and increases with an increase in the latter.

There is a direct analogy between signal spectrum width $\Delta f$ and relative antenna aperture $d_a/\lambda$. Range resolution and range accuracy in-

crease with an increase in spectrum width $\Delta f$; with an increase in the relative aperture $d_a/\lambda$ the width of the directivity diagram is reduced thanks to which directional resolution and direction-finding accuracy are heightened. In an analogous manner, use of two sinusoidal oscillations widely spaced along frequency $f_d$ ensures highly accurate measurement of range but not range resolution; in precisely the same way, large relative spacing $b_a/\lambda$ of two nondirectional antennas makes it possible to determine target direction precisely but does not ensure directional resolution. The full signal section is needed for range resolution, and directional resolution is obtained by using continuous or nearly continuous antennas. These propositions are illustrated in Fig. 2.18.

3. Radar Direction-Finding Systems

Let us examine the characteristic of amplitude direction-finding methods using complex (directional) antennas which are not only accurate but possess high directional resolution and long range.

At the output of a directional antenna is obtained a signal whose amplitude depends upon direction of arrival

$$U_c(\alpha) = U_{s0}F(\alpha),$$

where $U_{s0}$ is the signal amplitude in the direction of the maximum, while $F(\alpha)$ is the antenna directivity characteristic. When a direct signal is received, $F(\alpha)$ is replaced by $F_E(\alpha)$ – the field strength directivity characteristic. In the case of a reflected signal $F_r(\alpha) = F_E^2(\alpha)$ is substituted for $F(\alpha)$, since signal amplitude is twice multiplied by the directivity characteristic: during transmission and reception.

It is still not possible directly to judge the direction of signal arrival and to determine target direction by the amplitude of the received signal, since this depends upon unknown quantity $U_{s0}$.

To obtain the angle from voltage $U_s(\alpha)$ it is necessary to eliminate the dependence upon $U_{s0}$. Such exclusion is done using one of the following methods.

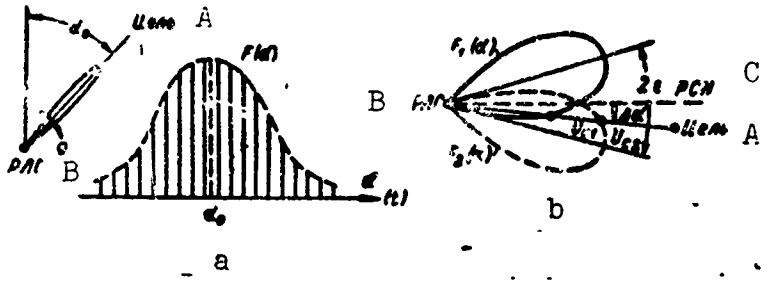


Fig. 2.19. Amplitude direction finding: a) method of envelope analysis (by the maximum); b) comparison method. A) Target; B) RLS; C) equisignal direction.

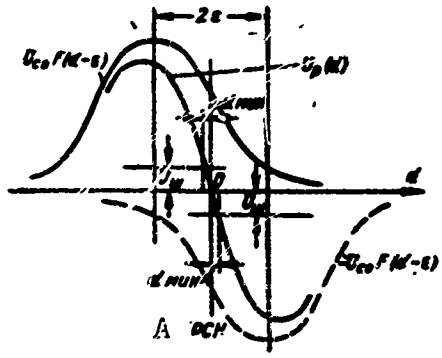


Fig. 2.20. Differential characteristic of amplitude direction finder operating by the comparison method. A) Equisignal direction.

1. A highly focused directivity diagram is shifted relative to the target at a certain angular velocity (Fig. 2.19a). If quantity $U_{s0}$ does not change substantially during the time of irradiation of the target, the amplitude envelope of the received signals may be considered to repeat directivity diagrams $F(\alpha)$. In analyzing the envelope target direction $\alpha_0$ is determined from the position of the antenna at the moment when the envelope passes through the maximum. Hence this method has been called the *envelope analysis method* or the method of the maximum.

2. Two intersecting directivity diagrams may be employed and there corresponding signals $U_{s1}$ and $U_{s2}$, compared (Fig. 2.19b). If the re-

ceived signals are equal, the target may be considered to lie in the equisignal direction where the directivity diagrams intersect. Hence this method has received the name of *comparison method.*

*The envelope analysis method* combines well with sequential phase scanning but may be used to measure only one angular coordinate. In the simplest case the operator clamps the maximum at the highest point of the signal in amplitude indicators or at the brightest point in brightness indicators.

The sharper the directivity characteristic, the more precise is the maximum of the envelope and the lower the direction-finding error. Consequently, by using the envelope analysis method direction-finding accuracy is determined by relative antenna aperture $d_a/\lambda$.

*The comparison method* employs subtraction of the signals corresponding to two identical directivity diagrams, whose maximums are symmetrically displaced by bias angles $\varepsilon$ from the equisignal direction (Fig. 2.20). The directivity diagrams are usually biased by moving the radiators from the focal axis of the antenna's parabolic mirror.

The signal obtained after subtraction is described by differential characteristic

$$U_p(\alpha) = U_{c0}[F(\alpha+\varepsilon) - F(\alpha-\varepsilon)],$$

which is linear at small angles and changes sign in the equisignal direction. Therefore the comparison method is broadly used in target direction autotrack systems.

In the equisignal direction the steepness of the differential characteristic

$$S = \left|\frac{dU_p}{d\alpha}\right|_{\alpha=0} = U_{c0}\left[\frac{d}{d\alpha}F(\varepsilon) - \frac{d}{d\alpha}F(-\varepsilon)\right] = 2U_{c0}\frac{d}{d\alpha}F(\varepsilon), \quad (2.18)$$

since $[d/d\alpha]F(\alpha) = -[d/d\alpha]F(-\alpha)$. The directivity diagram is a function of the relative value of angle $\alpha/\theta$, therefore

$$\frac{d}{d\alpha} F\left(\frac{\alpha}{\theta}\right) = \frac{1}{\theta} F'(\alpha)$$

and the steepness will increase as aperture angle $\theta$ of the directivity diagram decreases. Therefore in the comparison method also, direction-finding accuracy is determined by the relative antenna aperture $d_a/\lambda$.

Consequently, in principle the method of the envelope maximum and the comparison method are equally accurate. However, in practice the method of the maximum in scanning systems often takes into account the behavior of the envelope only near the maximum itself and ignores sharp declines at the edges, as a result of which direction-finding accuracy is substantially reduced.

The equisignal direction may be clamped with sufficient accuracy from different signal $U_r(\alpha)$; however, because of the presence of factor $U_{s0}$ this signal may not yet be used to determine the value of the deviation. Therefore, for direction finding, the relation between the difference signal and the total signal

$$F_{nz}(\alpha) = \frac{F(\alpha+\varepsilon) - F(\alpha-\varepsilon)}{F(\alpha+\varepsilon) + F(\alpha-\varepsilon)}, \qquad (2.19)$$

which depends only upon the angle and is called the direction-finding characteristic, is used.

The difference signal is divided by the total signal in the receiver device by changing the gain factor in inverse proportion to the amplitude of the total signal (ARU). At the output of the receiver device is obtained mismatch voltage $U_{rr}$ which is proportional to $F_{pkh}$.

Direction finders using the comparison method are of two kinds: single-circuit (sequential) and multicircuit (parallel).

In *single-circuit* comparison, the signal is received through a common receiver with the directivity diagram first in one position and then in the other (Fig. 2.21a). The received signals are fed one by one, in synchronization with the antenna commutation, into an inertial

comparison circuit with different signs. Therefore, from the output of the comparison circuit is obtained the value of the difference of the

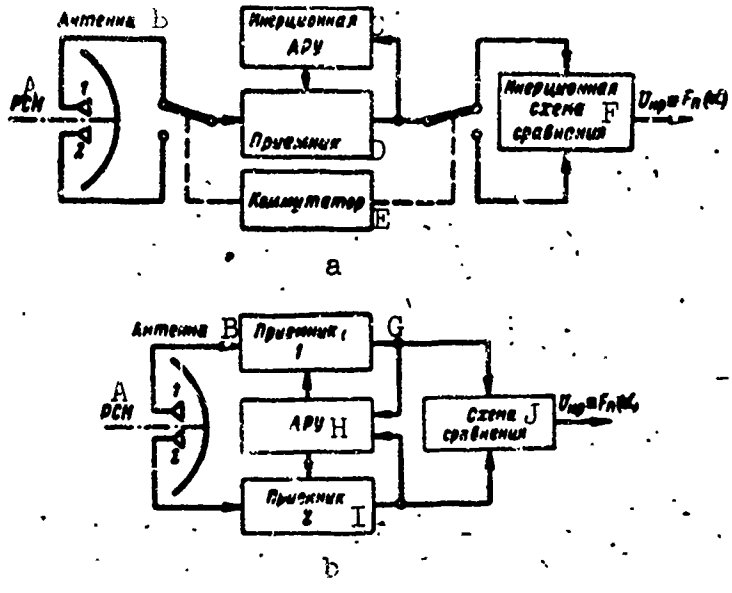


Fig. 2.21. Block diagram of amplitude direction finder operating by the comparison method: a) single-circuit (sequential); b) multicircuit (monopulse). A) RSN; B) antenna; C) inertial ARU; D) receiver; E) commutator; F) inertial comparison circuit; G) receiver 1; H) ARU; I) receiver 2; J) comparison circuit.

signals of one or the other sign, averaged over both half-periods of commutation. The signals of both half-periods are fed with the same sign into an inertial ARU, thanks to which the gain factor of the receiver changes in inverse proportion to the average value (sum) of the signals for both half-periods.

In *multicircuit* comparison the signals which have passed through different receiver circuits are compared at the same time (Fig. 2.21b). An ARU to which the total signal is fed acts upon the receivers. Signals may in principle be compared in a parallel circuit through reception of a single target pulse; hence such systems are called monopulse systems.

The merit of single-circuit comparison lies in the simplicity of

the device and the rather low demands upon it. One receiver will suffice even for finding the direction of a target in two planes. Antenna commutation is achieved by rotating a radiator, which has been displaced from its focus, around the focal axis of the antenna mirror, as a result of which the directivity diagram describes a cone in space, occupying the right, upper, left, and lower positions in sequence. Hence such a method of commutation is called conical scanning (rotation) of the beam and has been very widely employed.

The basic drawback of the single-circuit system is the presence of additional direction-finding errors: a change in the target-signal intensity during the commutation period yields a false mismatch voltage. Interference whose amplitude changes with the frequency of commutation may completely upset the operation of the system. Therefore, at the present time efforts are being made everywhere to change to multicircuit comparison.

Multicircuit (monopulse) comparison lacks these drawbacks. Any change in the power of the received signal is reflected equally in both of the signals being compared and has no effect on the system. Therefore, in monopulse direction-finding, it is impossible to create an effective angular interference from the same point in space at which the target itself is located. In principle, a multicircuit system is capable of distinguishing among the direction of several targets falling within the limits of its directivity diagram; this is impossible in single circuit systems.

However, the design of multicircuit comparison systems is difficult because of the complexity of the apparatus, the stiff requirements on identity of the circuits, and on the stability of their operation.

When target direction is determined in two planes, 4 radiators together with their separate feeder lines are placed in the antenna, and

not less than three receiver channels are used, whose characteristics should be identical.

A difference in the receiver gain factors leads to a shift of the equisignal direction; less than perfect operation of the ARU leads to an incorrect determination of the magnitude of the deflection. In some systems the signals are subtracted directly at the antenna output before amplification, and for that reason there is no displacement of the equisignal direction.

We may note in conclusion that, in contrast to amplitude systems, phase direction-finding systems using highly directional antennas in no way differ in principle from the simplest systems. This is because directivity is reflected in signal amplitude, while phase systems react to phase, the latter depending only upon the extent of the dispersion of the reception points.

## §2.3. CLASSIFICATION OF SCANNING METHODS

In radar systems range scanning is done naturally – on the basis of the propagation of radiowaves at constant velocity from the RLS to the target and back. No special operations are required. Because of the high velocity of propagation of radiowaves, the delay time of signals from even the most distant targets in the regions of space near the earth is very small and does not depend upon the design of the RLS itself. Therefore scanning of the whole range interval is practically instantaneous.

On the other hand, scanning along angular coordinates depends to a great extent upon the structure of the RLS and also upon the number of elements to be resolved within the limits of the scanning zone.

Radar stations may employ either a single beam or multiple beams. The element whose angular coordinates are to be resolved corresponds to the angular dimensions of the RLS antenna beam and is selected on the

condition that the assigned direction-finding accuracy and directional resolution are assured. The number of resolvable elements depends upon the dimensions of the resolvable element and also upon the dimensions of the scanning zone as determined by the purpose for which the RLS is used.

The space scanning method is conditioned by the correlation between the number of RLS beams and the number of elements whose angles are to be resolved within the scanning zone.

If the number of resolvable elements is equal to the number of RLS beams, and these cover the whole scanning zone, scanning is instantaneous, its length being equal to the largest delay time of the ranging signals.

If the total number of beams is less than the number of resolvable elements, and they do not cover the whole scanning zone, it is necessary to employ sequential spacing by means of a sweeping movement of the antenna beams within the limits of the scanning zone. During sweeping each direction within the RLS scanning zone is viewed during the course of a certain time interval $\tau_{obl}$, known as the target irradiation time. The interval $T_0$ between the periodically repeated emission in a given direction is, as is known, known as the scanning time.

Thus, in sequential scanning, targets are detected and their coordinates are measured only during the moment of irradiation, that is, discretely, at time intervals $T_0$.

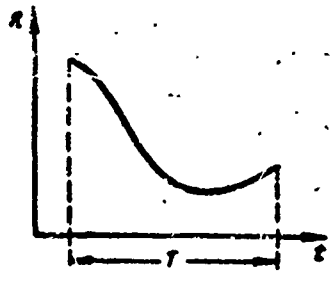


Fig. 2.22. Change in range of a target passing by RLS during time $T$.

For undistorted reproduction of a target trajectory on the basis of the data of a discrete reading of its coordinates, the scanning time must satisfy the Kotel'nikov reading theorem

$$T_0 \leqslant \frac{1}{2F_m}, \qquad (2.20)$$

where $F_m$ is the maximum frequency in the spectrum of the target coordinates as functions of time.

To determine the maximum frequency $F_m$ of the spectrum difficult target trajectories are selected and target coordinates are represented as functions of time. Figure 2.22 shows as an example the change $R(t)$ in the range of a target passing along a given trajectory to the side of the RLS. Then by using Fourier transformations the spectrum of these coordinates may be found according to Formula

$$R(F) = \int_0^T R(t) e^{-j2\pi Ft} dt,$$

where $T$ is the observation time.

The spectra of all free coordinates for various target trajectories obtained according to this formula are compared with one another. The spectrum with the widest band is selected. Then at some conventional level, sufficiently close to zero, the largest frequency $F_m$ is read off (cut-off frequency). The scanning time obtained by substituting this frequency in Formula (2.20) makes possible an undistorted determination of target trajectory from discrete data of observation, if coordinate measurement error is not considered.

During radar observation of rapidly moving targets, using sequential scanning, Condition (2.20) is usually not satisfied in practice, and as a result the accuracy of determination of the trajectories of radar targets may turn out to be low, despite the fact that the coordinates were measured with sufficient accuracy. Ignorance of the precise

character of the target trajectory may, for example, lead to an inaccurate conception of its later course and may hinder interception of this target. Therefore maximum efforts are made to reduce the scanning time.

It should be pointed out that when not only the target coordinates are measured, but also the $\mu$ of their first derivatives, the requirement as regards the maximum permissible scanning time may be lowered by $\mu + 1$ times, according to the reading theorem

$$T_0 \leqslant \frac{1+\mu}{2F_m}. \qquad (2.21)$$

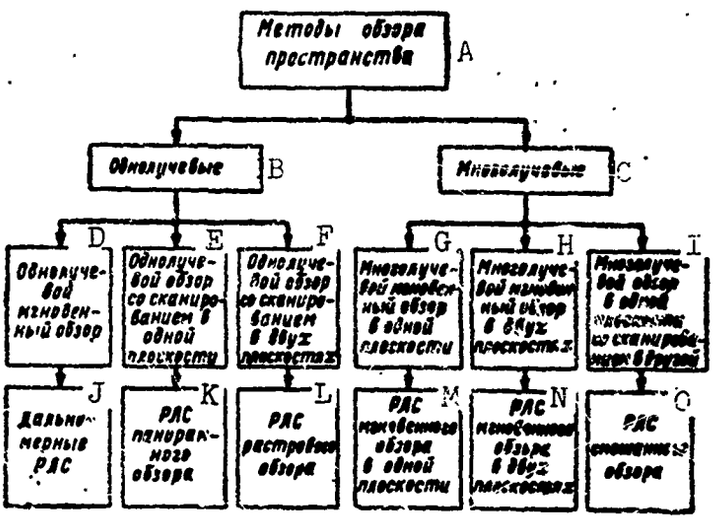


Fig. 2.23. Classification of scanning methods. A) Methods of space scanning; B) single-beam; C) multibeam; D) single-beam instantaneous scan; E) single-beam scan with sweeping in one plane; F) single-beam scan with sweep in two planes; G) multibeam instantaneous scan in one plane; H) multibeam instantaneous scan in two planes; I) multibeam scan in one plane with sweep in the other; J) ranging RLS; K) RLS with panoramic scan; L) RLS with raster scan; M) RLS with instantaneous scan in one plane; N) RLS with instantaneous scan in two planes; O) RLS with mixed scan.

Measurement of the derivatives increases the volume of information, reduces the errors involved in determining the target trajectory, but on one indispensable condition; data relating to the coordinates and their derivatives must be determined independently.

For example, using the Doppler effect to determine velocity and

measuring range from echo-signal delay are independent measurements. On the contrary, determining velocity by differentiating the measured range values over time is not making an independent measurement and does not yield any supplementary information on the target trajectory.

In line with these considerations a classification of space scanning methods is given below (Fig. 2.23), and a short comparative description is given.

Instantaneous scan using single-beam RLS is only possible when the antenna beam covers the whole scanning zone (one resolvable element). Stations utilizing this method are called ranging stations.

If the scanning zone contains one resolvable element alone one angular coordinate and several resolvable elements along the other, the single-beam RLS sweeps in one plane (panoramic RLS). When there are a large number of resolvable elements along both angular coordinates, the antenna beam sweeps in both planes according to a complex law (raster scan).

Multibeam RLS can accomplish instantaneous space scan in the presence of a large number of resolvable elements both in one plane and in two planes. There are also mixed scan multibeam RLS which in one plane cover the whole scanning zone by using a selection of beams, and in the other plane sweep in a manner similar to single-beam panoramic RLS.

Single-beam RLS are much simpler than multibeam but involve a long scanning time, especially when sweeping in two planes. The actual scanning time is equal to the time of irradiation of the target multiplied by the number of elements of resolution and by a certain coefficient characterizing the supplementary time losses. Since the condition of effective discovery of the target and of accurate measurement of coordinates requires that the time of irradiation not be very small, the actual sweep time, in the presence of a large number of elements of re-

solution, turns out to be much greater than is necessary, as determined by Formulas (2.20) and (2.21). This circumstance can lead to overlooking targets, to an inaccurate conception of their actual trajectories, to data delay, etc.

It should be noted that the contradiction between the required and the actual sweep time is manifested with particular acuteness in single-beam RLS with nigh-performance technical characteristics, where a broad scanning area together with extreme accuracy of measurement of coordinates is required, tnat is, where there are a large number of elements of resclution.

Multibeam RLS with instantaneous scan do not possess this defect. They have the additional merit of being able to accomplish direction-finding with great accuracy by comparing the signals received on several beams. The drawback of these stations is that they are complicated to build and operate, especially when there are a large number of elements of resolution along both angular coordinates. Mixed scanning systems which sweep in two planes have appeared as a compromise between the complexity of the multibeam system and a large actual scanning time of the single-beam RLS.

## §2.4. RANGING RADAR STATIONS

Radar stations accomplishing instantaneous scan with a stationary beam measure only one target coordinate – range. In many practical instances this is quite sufficient. Thus, radio altimeters are designed to measure just the true altitude of flight – the distance to the earth's surface. Radio rangefinders measure target distance and automatically introduce this information into a computerized sighting device with an optical sight. Ranging stations are also used for special purposes: to give warning of the danger of collision at sea or in the air, to measure the altitude of meteor formations, etc.

A station of this type has a stationary beam which must be broad enough to cover the whole scanning zone.

In radio altimeters the width of the beam is determined by the maximum healing angle $\gamma$: $\theta = 2\gamma_{maks}$. The figure 2 takes into account healing in both directions from the vertical (Fig. 2.24a). If this condition is not met, the altitude reading is incorrect.

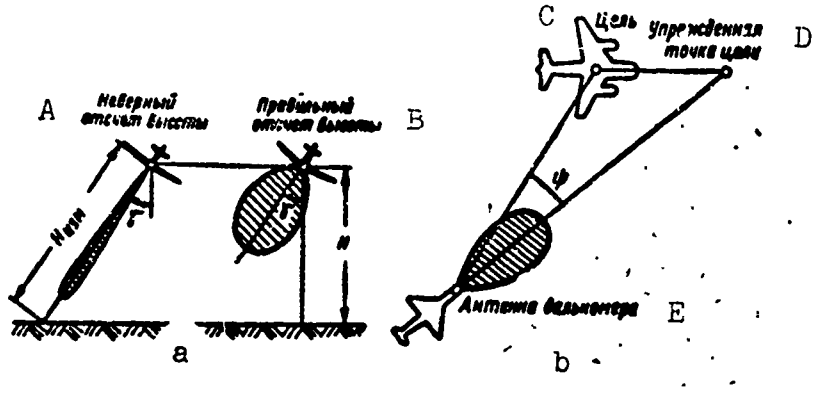


Fig. 2.24. Requirements on width of directivity diagram: a) radio altimeter; b) radio rangefinder of a gunsight. A) Incorrect altitude reading; B) correct altitude reading; C) target; D) interception point of target; E) rangefinder antenna.

The gunsight radar rangefinder has an immovable antenna whose directivity characteristic is oriented along the axis of the pursuit plane. The width of the characteristic should be such that when the airplane width and immovable weapon turns to its maximum interception angle $\psi_{maks}$ relative to the target, the target should remain within the limits of the antenna beam. This requirement is met at condition $\theta = 2\psi_{maks}$ (Fig. 2.24b). Analogous requirements are imposed upon the directivity diagram in other cases as well, for example, in the radio rangefinders of movable artillery installations, where the angle of drift has also to be taken into account.

Range-finding stations utilize the simplest kind of amplitude indicator or automatic range measurement system. The immobile weakly di-

rectional antennas are small and do not require rotating mechanisms or any energy losses to drive them. Nor do they require any rotating articulated waveguides or systems for transmitting the angle of rotation to the indicator. The whole station becomes extremely simple as is explained by the limited nature of the tasks to be accomplished. Another merit of an RLS with a motionless beam is that scanning is continuous.

The disadvantages of ranging RLS are the result of the weak directivity of the antenna, as determined by the requirement of a wide scanning zone. Because of this, the energy relations deteriorate, there is no angular resolution, and the station's noise-protection is lowered. The reason for the low noise-protection is that, with such a broad directivity diagram, intense noises can enter from various directions.

The deterioration of the energy relations is to some extent compensated for by scanning continuously, which makes it possible to receive and integrate a large number of target pulses. Very often, as in the case of altimeters, the absence of directional resolution is not a drawback.

## §2.5. PANORAMIC RADAR STATIONS

Single-beam radar stations which scan by sweeping the beam in one plane are used to measure two coordinates: range and azimuth. In many

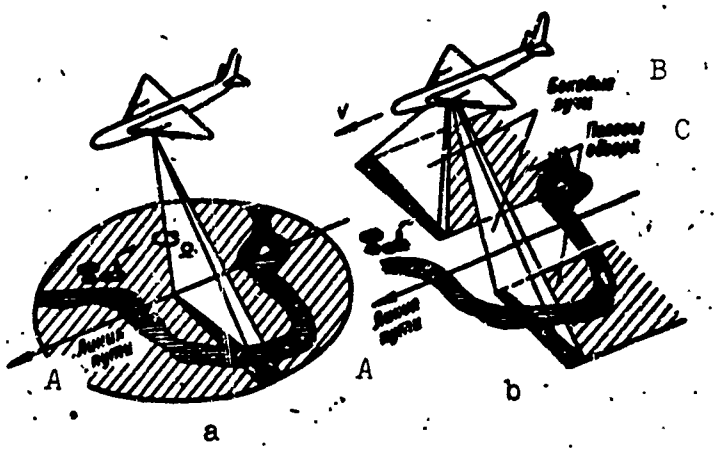


Fig. 2.25. Airborne RLS for scanning the earth's surface: a) circular scan RLS; b) lateral scan RLS. A) Flight path; B) lateral beams; C) scanning belts.

cases knowledge of two coordinates is quite enough for determining target position. This is the case, in particular, with airborne radar stations for scanning the earth's surface during flight over a flat surface or over water, and also with sure-based and ship-borne stations for spotting targets on water. Knowledge of two target coordinates is enough to establish its position in one plane. Sometimes these types of stations are also used for scanning the sky from the earth or from a ship if the altitude of flight of the target is of no interest or can be established by some other radar station.

The most widespread radar stations of this type are the airborne RLS for scanning the earth's surface which are used by airplanes and other flying devices. These stations may be subdivided into two types: circular scan RLS and lateral scan RLS.

Airborne circular scan RLS have a fan-shaped antenna beam which rotates around the vertical axis with constant angular velocity $\Omega$ or which sweeps back and forth within the limits of the assigned sector (Fig. 2.25a). Circular scan stations use brightness indicators; these are usually circular scan indicators (IKO). A two-coordinate image is well reproduced on the flat screen of the indicator. The picture on these screens closely resembles a geographical map of the area.

For a detailed representation of the earth's surface the station must possess good resolution. Radial resolution is obtained by employing short ranging pulses, and azimuth resolution – through a sufficiently large horizontal antenna aperture. During scan the antenna rotates or rocks (if a sector is being examined); a special system transmits the angenna rotation angle to the indicator for representation of angular sweep. (In land-based circular scan RLS the control room and the transmit-receive apparatus often rotates with the antenna in order to avoid the employment of rotating waveguides at high levels of radi-

ated power).

Despite their broad application and their simplicity, airborne circular scan RLS are beginning gradually to yield to other types of stations because of a number of limitations which increase with increase in the velocity of flight of the device on which this station is mounted.

In the first place, the large rotating antenna is covered by a bubble which, projecting outside the fuselage, degrades the aerodynamic characteristics of the flying device. As a result, the antenna must be sharply reduced in size, and this prevents improvement of the azimuth resolution. Furthermore, a substantial portion of the energy consumed by the station is used to rotate the antenna.

In the second place, circular scan does not fit in well with the forward movement of the flying device itself. The portral of the area is undistorted only when the movement of the device during the time of a single antenna rotation may be neglected. At high flight speed this condition is not satisfied. That being the case, it is difficult to obtain a continuous radar map of the area along the flight path of the flying device.

These disadvantages are completely eliminated by the use of airborne lateral scan RLS (Fig. 2.25b). In contrast to the preceding, in lateral scan RLS the forward movement of the flying device plays a useful role: it makes it possible to sweep with a stationary beam. Two stationary cophasal antennas are stretched out along the fuselage of the airplane. Because of their large dimensions the antennas form highly directional fan-shaped beams which "look" to the left and the right of the fuselage.

When pulse signals are emitted, narrow strips of ground across the flight path are irradiated. A cathode-ray tube with range sweep regis-

ters the signal crosswise on phototape. With the movement of the flying device the tape is stretched, relative to the tube, in proportion to the velocity of flight; the result is that after many irradiations, the tape will register a continuous radar map of the area along the flight path. Usually two lateral strips are examined; the area immediately under the flying device is not viewed because of the poor range resolution and the steep sighting angles. (By the same token, in circular scan stations the center of the indicator screen is completely light.)

Among the merits of the lateral scan may be included the successful arrangement of the antenna. The antennas are stationary and, being located along the aircraft, may cover the whole length of the fuselage. The result is a comparatively high resolution along the flight path (analogous to the azimuth resolution in circular scan RLS) and no energy is wasted on antenna rotation.

The antennas may be arranged in the form of of slots in the body of the fuselage or they may be suspended below the airplane in a cigar-shaped container. The first arrangement is very advantageous from the point of view of the size and weight of the antenna system; the second arrangement yields better antenna electrical characteristics.

The disadvantage of the lateral scan system is the absence of forward radar visibility, the relative complexity of the antenna feed device for eliminating electrical oscillation and distortion of the antenna beam during creep of the transmitter frequency, temperature changes, and vibration.

1. Requirements on the Shape of the Directivity Diagram

As has already been noted, panoramic stations use a fan-shaped beam which is narrow in the scanning plane and wide in the second plane. In the narrow section the beam width is selected so as to yield the assigned direction-finding accuracy using the method of the maximum

and so as to possess resolution in the direction-finding plane. The diagram selected in the second plane is wide enough to cover the whole scanning zone in this plane. Thus, in an airborne RLS for scanning the earth's surface, the vertical dimensions of the zone are defined by the maximum operational range and by flight altitude $\varphi_{\text{об}} = \arccos\left(\frac{H_{\text{макс}}}{R_{\text{макс}}}\right)$ (Fig. 2.26). Beam width in this plane should also be the same.

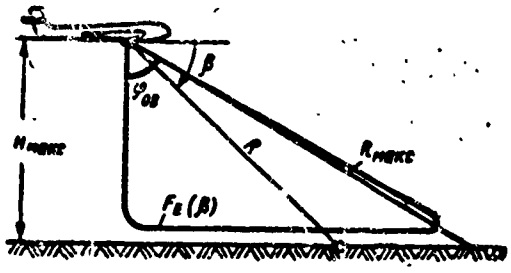


Fig. 2.26. Width and shape of flat antenna beam of airborne RLS in the vertical plane.

The shape of the directivity diagram in the vertical plane is selected so that the point targets on the earth's surface with equal in intensity of reflection should yield the signals of identical force at the receiver input or of identical brightness on the indicator screen

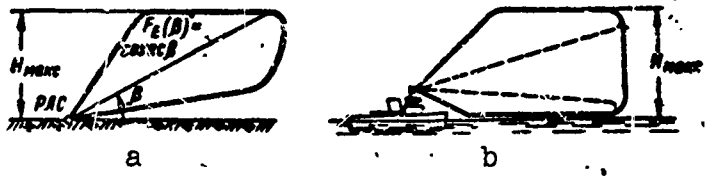


a b

Fig. 2.27. Selection of the shape of the directivity diagram: a) inverted cosecant beam of ground RLS; b) bicosecant beam of ship-borne RLS.

regardless of their range.

In circular panoramic scan with constant antenna rotation velocity, Ω number of pulses are constantly being received from targets of different ranges. Therefore, for all targets to register with the same brightness and with an identical dispersion area, the intensity $P_{\text{pr}}$ of the received signals should not depend upon their range.

It is known that, because the signal moves in the direct and re-

verse directions, the amplitude of the reflected signal at the point of reception is proportional to the square of the antenna directivity characteristic for the field voltage, and power – to the fourth degree. Furthermore, the power of the received signal is inversely proportional to the fourth degree of distance $R$, since during propagation in both directions the power flux density decays proportionately to the square of the distance.

In accordance with this, in surface scanning stations, received signal power

$$P_{пр} = \frac{k_1}{R^4} F_E^4(\beta),$$

where $k_1$ is the proportionality factor, and $F_E(\beta)$ is the directivity characteristic for field voltage in the vertical plane.

If we replace $R$ by $H$ cosec $\beta$, we obtain

$$P_{пр} = k_2 \frac{F_E^4(\beta)}{\operatorname{cosec}^4 \beta},$$

where $k_2 = k_1/H_4$ is a constant factor.

It is obvious that received signal power $P_{pr}$ will not depend upon range if

$$F_E(\beta) = \operatorname{cosec} \beta$$

or

$$F_p(\beta) = \operatorname{cosec}^2 \beta. \qquad (2.22)$$

An antenna beam with such a characteristic is called a *cosecant* beam and has the shape shown in Fig. 2.26.

Calculations show that the directivity characteristic should also have approximately the same form in order to obtain an evenly bright background formed by the reflections from homogeneous targets distributed on the surface.

The cosecant beam has also been broadly employed in ground and ship-borne radar stations. In ground RLS used for discovering airborne

targets up to altitude $H_{maks}$, an inverted cosecant beam is used (Fig. 2.27a). Such a shape of the beam is economical, since it distributes the emitted power in the most suitable way. Some ship-borne stations are used for scanning both the air and the surface of the water. These operating conditions are satisfied by a bicosecant beam, consisting as it were of direct and inverted cosecant beams (Fig. 2.27b).

In lateral scan the number of pulses received from targets located at different distances from the flight path varies and is proportional to target range $n = k_3 R$, since, at constant velocity of flight $V$, the linear dimensions of the antenna beam and the time of irradiation of the target increase with increasing range, while the frequency of the packages is constant.

The energy of a single pulse is proportional to received signal power $P_{pr}$, while the energy of $n$ pulses is proportional to the product

$$P_{np} n = P_{np} k_3 R = \frac{k_1}{R^4} F_E^4(\beta) k_3 R.$$

To make this independent of $R$, if we proceed analogously to the preceding, we obtain

$$F_E(\beta) = \operatorname{cosec}^{\frac{3}{4}}\beta \qquad (2.23)$$

or

$$F_p(\beta) = \operatorname{cosec}^{\frac{3}{2}}\beta.$$

In lateral scan, consequently, a less stretched-out directivity diagram than the cosecant diagram is required, and therefore it is easier to shape.

2. Time Correlations in Circular Scan

We will assume that during scanning a series (package) of pulses of constant amplitude is received from the target, that is, the antenna directivity diagram is replaced by its right-angle equivalent with aperture angle $\theta_e$. At antenna angular velocity $\Omega$ the time of irradia-

tion of the target

$$\tau_{обл} = \frac{\theta_э}{\Omega}. \qquad (2.24)$$

At repetition frequency $F_p$ the number of pulses received per second of irradiation is

$$n = F_п \tau_{обл} = \frac{\theta_э F_п}{\Omega} \qquad (2.25)$$

Usually the number $n$ of pulses is assigned beforehand (on the condition of certain disclosure of the target against the background of noise), while the frequency $F_p$ of the packages is limited by the condition that the range reading should be uniquely determined. Pulse width $\theta_e$ is selected on the basis of the requirement for resolution and for precision of the angular reading. Then the angular velocity of displacement of the antenna beam is uniquely determined from Formula (2.25)

$$\Omega = \frac{\theta_э F_п}{n}.$$

Let us assume that the station is effecting *circular* scan, that is, the scanning zone in the horizontal plane $\varphi_{og} = 2\pi$. Then scanning time $T_0$ is equivalent to the time required for the antenna to make one rotation

$$T_0 = \frac{2\pi}{\Omega}. \qquad (2.26)$$

It should be noted that at assigned values of $n$, $F_p$, and $\theta_e$ this time is the minimum possible

$$T_0 = T_{0\,мин} = \frac{2\pi n}{\theta_э F_п}. \qquad (2.27)$$

In *sector* scanning $\varphi_{og} < 2\pi$ and the minimum scanning time

$$T_{0\,мин} = \frac{\varphi_{or}}{\Omega} = \frac{\varphi_{or} n}{\theta_э F_п}, \qquad (2.28)$$

while the actual scanning time

$$T_0 = \psi T_{0\,мин}. \qquad (2.29)$$

Coefficient $\psi$, which accounts for time losses in excess of the

minimum necessary ones, is known as the coefficient of the use of scanning time. In stations using mechanical rocking of the antenna beam, supplementary time is required for reversing when the beam reaches the boundary of the scanning sector or for running unloaded outside the scanning zone. Coefficient $\psi$ characterizes the degree of development of scanning methods. The closer it is to unity, the more perfect the method.

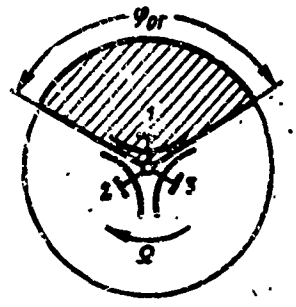


Fig. 2.28. Sequential irradiation of the scanning zone by several antennas. Antenna I is radiating.

In scanning using the rocking method, velocity decreases to zero at the moment of reversing, and then, changing to its opposite, accelerates. Targets near the sector boundary are irradiated for a longer time, and therefore

$$\psi = \psi_n = 1{,}2 \div 1{,}6;$$

where the lower value corresponds to low velocities and small antennas, and the higher – to large $\Omega$ and massive antennas. Subscript n next to $\psi$ means that the time losses are due to the unequal irradiation velocity.

In sector scanning ($\varphi_{og} < 2\pi$) it is sometimes advisable to rotate the antenna all the way around, even though outside sector $\varphi_{og}$ the antenna is not radiating. Then the scanning time will be equal to time of rotation: $T_0 = 2\pi/\Omega$, and the time losses during no-load operation are evaluated by coefficient

$$\psi = \psi_x = \frac{2\pi}{\varphi_{or}}.$$

If $\varphi_{og} \leq 2\pi/k$, where $k$ is a whole number, scanning time may be reduced by using the $k$ of alternately radiating antennas rotating as a single unit around a common axis (Fig. 2.28, where $k = 3$). In each moment of time only the antenna whose beam lies within the boundaries $\varphi_{og}$ of the sector is emitting. Here time losses during no-load operation are evaluated by

$$\psi = \frac{2\pi - k\varphi_{or}}{k\varphi_{or}},$$

and are practically absent when $\varphi_{og} = 2\pi/k$. The drawback of such systems is the need for commutation, which involves serious difficulties at high radiating powers.*

In a circular scanning station with a large operating range time $T_0$ is significant, since the frequency of the package cannot be high, the beam is narrow, and therefore the rotational velocity of the antenna is low. Short-range stations have a comparatively short scannint time, thus satisfying the requirements of the theorem of readings. In lateral scan stations the very concept of scanning time is absent, since no area of the surface is swept by the antenna beam more than once.

A drawback of the stations examined is the presence of a broad directivity diagram in the vertical plane. This reduces the noise-protection of a RLS, and, if they are used in aerial scanning systems, there is no angular resolution in the vertical plane. Therefore these kinds of stations satisfy their requirements best only when used in airplanes or ships for panoramic scan of the earth's surface.

## 52.6. RASTER RADAR STATIONS WITH MECHANICAL SWEEP

A radar station whose antenna beam is displaced in two planes views the whole scanning zone sequentially according to a complex law (a raster). Stations of this type use a sharp, needle-like beam whose

width in both planes is determined by the assigned accuracy of measurement of the angular coordinates and by the angular resolution.

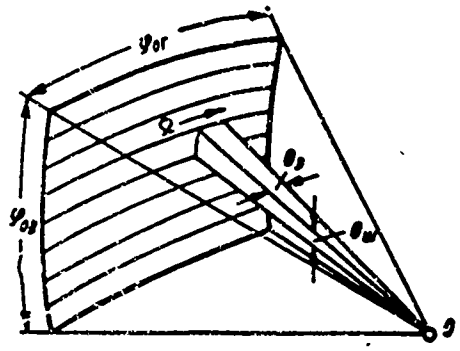

Fig. 2.29. Line or screw raster.

There are many types of rasters. In stations with mechanical sweep the principle constraint upon them is that time losses over the minimum necessary ones defined by coefficient $\psi$ be as low as possible. The importance of this constraint derives from the fact that the time required for a narrow beam to scan the assigned zone, which is already large enough, increases with the transitions from line to line and with reversing at the boundaries of the scanning zone. The type of raster selected is also determined by the scanning zone shape required as well as, in some cases, by the convenience of switching to conical scan autotrack.

*Line or screw raster.* Let the assigned vertical and horizontal dimensions of the scanning zone be $\varphi_{0v}$ and $\varphi_{0g}$, the effective beam width along the line be $\theta_e$, and the width of the line, or the scanning space, be $\theta_{sh}$ (Fig. 2.29).* The beam illuminates the whole scanning zone line by line, moving along the line with angular velocity $\Omega=\frac{\theta_e F_n}{n}$, making possible the reception of assigned number of pulses $n$ from the target.

The vertical dimension $\varphi_{0v}$ of the zone is usually small and, therefore, all the lines of the raster can be considered approximately equal in length. Scanning along each line is equivalent to sector scanning in one plane, and therefore the minimum scanning time of a single line

$$T_{\text{стр мин}}=\frac{\varphi_{0g} n}{\theta_e F_n}.$$

At constant spacing $\theta_{sh}$ within the limits $\varphi_{0v}$ of the whole zone the number of lines $z = \varphi_{0v}/\theta_{sh}$, and then the minimum scanning time of the whole zone

$$T_{0\,min} = zT_{str\,min} = \frac{\varphi_{0v}\varphi_{0g}\Omega}{\theta_{sh}\theta_{ah}F_n}. \qquad (2.30)$$

Further time losses are determined by the manner of passage from one line to the other. If horizontal scanning is circular ($\varphi_{0g} = 2\pi$), the passage from line to line is accomplished by gradually raising the beam, during the time of a single line $T_{str} = 2\pi/\Omega$, by one space $\theta_{sh}$ at velocity

$$\Omega_v = \frac{\theta_{sh}}{T_{str}} = \Omega\frac{\theta_{sh}}{2\pi}.$$

The beam trajectory has the form of a spiral. As the vertical boundaries of the scanning zone are approached, $\Omega_v$ reduces to zero and changes its sign. In this part of the lines are superimposed upon one another. Since the vertical velocity is small, additional time losses due to overlay of the lines do not exceed 20% and, consequently,

$$\psi = \psi_n \approx 1{,}2.$$

Maintaining the spiral at $\varphi_{0g} < 2\pi$ yields the additional losses due to no-load operation. Then the total increase in scanning time is

$$\psi = \psi_n\psi_x = 1{,}2\frac{2\pi}{\varphi_{0g}}.$$

For the case of $\varphi_{0g} \leq 2\pi/k$ using $k$ antennas rotating as a single unit around a common axis, the coefficient $\psi_{kh}$ may be equal to unity. The vertical reverse and the passage from one line to the other may be accomplished when each antenna is operating loaded. Therefore $\psi_p = 1$, and the scanning time is reduced to its minimum possible value.

If, at $\varphi_{0g} < 2\pi$, horizontal rocking of the antenna is employed instead of circular rotation, to avoid dynamic shocks during rocking at high velocities, this rocking should be accomplished according to the

harmonic law, which yields a ($\psi_m = \pi/2$)-fold increase in the scanning time. Furthermore, vertical rocking causes losses $\psi_p = 1.2$ due to superposition of the lines. Here the over-all times losses may be evaluated by factor $\psi = \psi_p\psi_n \approx 1.9$.

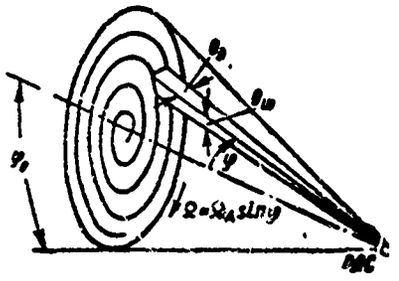

Fig. 2.30. Spiral raster.

A comparison of all the ways of effecting the linear method demonstrates that a scanning time close to the minimum possible value may be obtained if the antenna is moved circularly, and not rocked, in the horizontal direction. Furthermore, a less powerful drive is required for even rotation of the antenna than for rocking.

Another advantage of the linear method is that the most practically convenient scanning zone shape can be obtained with it, one which is wide in the horizontal plane and narrow in the vertical plane. A disadvantage of the linear method is the complexity of the transition to conical scanning when the station is switched to target autotrack. In direction finding using the method of simultaneous signal comparison (instead of sequential) this disadvantage disappears, but the station itself ceases to be a single-circuit station.

*A spiral raster* is formed by rapid rotation of the beam around an axis forming the center of the scanning zone, with gradual displacement of the beam along angle $\varphi$ from 0 to $\varphi_0$ (Fig. 2.30). The lines of the raster are the spires of a spiral. The number of lines $z = \varphi_0/\theta_{sh}$.

The linear displacement of the beam at distance $R$ from the RLS $L_{str} = 2\pi R \sin\varphi$ is a function of angle $\varphi$. The angular displacement of the beam along the line $\Phi(\varphi) = L_{str}/R = 2\pi \sin\varphi$ is also a function of $\varphi$. When the dimensions of the scanning zone, as is usually the case, are small ($\varphi_0 \leq 30^\circ$), $\Phi(\varphi) \approx 2\pi\varphi$ may be assumed as an approximation. If

$\Omega = \theta_e F_p / n$ is assigned as the constant angular velocity of the movement of the beam along the line, one assuring even irradiation of all targets, the minimum scanning time of one line

$$T_{\text{стр мин}} = \frac{\Phi(\varphi)}{\Omega} \simeq \frac{2\pi n}{\theta_e F_n} \varphi$$

will be a linear function of angle $\varphi$. Since $\varphi$ changes from 0 to $\varphi_0$, the average minimum time of a line is $T_{\text{str min}}$ at $\varphi = \varphi_0/2$

$$(T_{\text{стр мин}})_{\text{ср}} = \frac{\pi n \varphi_0}{\theta_e F_n}. \qquad (2.31)$$

Then minimum scanning time

$$T_{0\,\text{мин}} = z(T_{\text{стр мин}})_{\text{ср}} = \frac{\pi \varphi_0^2 n}{\theta_e \theta_{\text{ш}} F_n}. \qquad (2.32)$$

However, because of technical considerations, stations with mechanical sweep do not retain $\Omega$ as the constant value, but rather time $T_{\text{str}}$ during which the beam traverses the line and returns. Here the angular velocity of the antenna beam

$$\Omega(\varphi) = \frac{\Phi(\varphi)}{T_{\text{стр}}} = \frac{2\pi}{T_{\text{стр}}} \varphi$$

increases with an increase in angle $\varphi$ and is maximum at $\varphi = \varphi_0$. Here the number of target pulses is minimum. If the minimum number of target pulses is required to be equal to the rated number, the maximum velocity should satisfy the condition

$$\Omega_{\text{макс}} = \frac{2\pi\varphi_0}{T_{\text{стр}}} = \frac{\theta_e F_n}{n}.$$

Then the actual scanning time of any line

$$T_{\text{стр}} = \frac{2\pi n \varphi_0}{\theta_e F_n} \qquad (2.33)$$

will be twice as great as the average line time in Formula (2.31) during even irradiation. Consequently, time losses due to unevenness of irradiation are determined by quantity $\psi_n = 2$. If it considered that time losses due to superposition of lines in rocking at the edge of the scanning zone $\psi_n = 1.2$, the time use factor in spiral scanning $\psi =$

$= \psi_n \psi_p = 2.4$.

Thus, from the point of view of time losses, spiral scanning is not advantageous. Furthermore, the very shape of the scanning zone is inconvenient. Thus, in airborne RLS for space scanning, the large vertical dimensions of the scanning zone cause powerful reflections from the earth to be received, not to mention the fact that a certain amount of time is lost on scanning an unnecessary part of the zone.

An advantage of the spiral method is that it lends itself readily to the transition to conical scan autotrack: the beam is at angle $\varphi$, equivalent to displacement angle $\varepsilon$, relative to the axis of the zone.

*Cycloidal raster.* If the beam is moved so that its trajectory has the form of a sliding cycloid, the result is a scanning zone of convenient shape, narrow in the vertical and wide in the horizontal planes, and also a simplified transition to conical scan autotrack (Fig. 2.31). A cycloidal raster is obtained by rapid rotation of the antenna beam around the horizontal axis, the beam being displaced relative to this axis by angle $\varphi = \varphi_0/2$, and by slowly turning the whole antenna system in the horizontal plane.

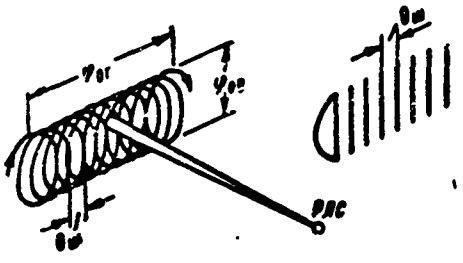

Fig. 2.31. Cycloidal raster.

Within the limits of the scanning zone the vertical density of the raster is uneven. In the center of the scanning zone, where the lines are most distant from one another, their relative displacement is equal to the width $6_{sh}$ of the line.

Near the upper and lower boundaries of the zone the lines are superimposed. If the horizontal beam was moving along the vertical, and not in a semicircle (right-hand side of Fig. 2.31), there would be no superposition and the beam would cover

the line $\pi/2$ times more rapidly.

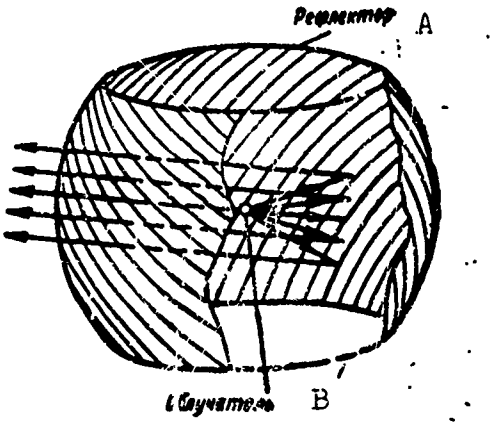


Fig. 2.32. Sweep of long-range RLS beam using a specially designed antenna system. A) Reflector; B) radiator.

If a factor of the order of 1.2 is used to cover additional losses due to overlapping of the lines during reversal, the scanning time use factor in the cycloidal method will be $\psi = \psi_p = 1.2\pi/2 = 1.9$.

As regards time loss, the cycloidal method is inferior to the linear method but more economical than the spiral method. Its drawback is that the pulse packet is broken up, since any target is irradiated twice while being scanned: on the ascending branch of one line and on the descending branch of the other line.

There exist other types of rasters than the ones enumerated above. Each of them may be evaluated in accordance with this method.

Raster space-scanning radar stations are the most complicated to design. The antenna must be very large in both planes in other to emit a narrow antenna beam. Rocking the antenna in two planes requires a complicated and cumbersome antenna drive, one consuming a considerable amount of power. The remote transmission system must transmit to the indicator the antenna position in two planes for purposes of angular scanning. The plane screen of the indicator cannot be satisfactorily used to reproduce all three target coordinates. Therefore the third co-

ordinate is either given conventionally by using some special notation, or it is reproduced on a second indicator screen. In either method the reading of coordinates is difficult in the presence of many targets. No practical result has yet been obtained from attempts to design three-dimensional indicators.

If a single-channel receiver is used, the accuracy of the measurement of angular coordinates at right angles to the line is low. The angle is read from the position of the line upon which the target is discovered. This yields an error of the order of $0.5\theta_{sh} = 0.3\theta$, while along the line measurement error using the method of the maximum is as low as $0.1\theta$.

The basic defect of raster methods is the very large scanning time. As follows from a comparison of Formulas (2.28) and (2.30) the scanning time in the raster method is at least $z$ times greater, in terms of the number of lines, than in the circular or sector scanning method. As a result of this, in long-range stations where the frequency of the packages is low and a very narrow antenna beam is selected so as to obtain a long range and a uniquely defined reading, the scanning time is excessively long. For this reason the raster scanning method finds a limited application in long-range stations.

Another limitation of the raster method in long-range stations is the complexity of mechanical sweeping when antennas are large, reaching hundreds of meters, and when the radiation power is great – tens and hundreds of megawatts. Antennas must be specially designed in order to eliminate this drawback, or else electrical sweeping is used.

An example of such a specially designed antenna system is given in Fig. 2.32. The reflector is a spherical radum of large dimension constructed to very close specifications from radio-transparent material. The radum is covered with a network of metallic bands laid on at a 45°

angle to the vertical. An antenna radiator with a movable head, located in the center of the sphere, irradiates a part of the inner surface of the radum with a wave of plane polarization whose field is parallel to the band. As a result the irradiated sector of the radum acts as a continuous metallic reflector and forms a narrow beam. The metallic strips on the opposite wall of the radum are at a 90° angle to the field vector and thus do not hinder the passage of the radiowaves. There is no limitation on azimuth scanning with an antenna of this design.

## §2.7. RADAR STATIONS WITH ELECTRICAL SWEEP

Inertialess electrical sweep requires no additional time losses ($\psi = 1$) and may follow any law. Furthermore, no cumbersome antenna drive is needed, upon whose rotation as much as 50% of the energy consumed by the station is sometimes expended. Therefore radar stations with electrical sweep are the most advanced.

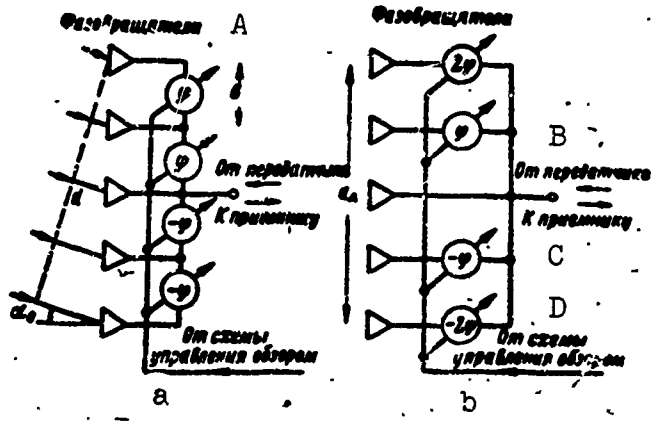


Fig. 2.33. The principle of electrical sweep using a phased antenna array. A) Phase shifters; B) from the transmitter; C) to the receiver; D) from the scanning control circuit.

However, up until recently the development of such stations was delayed by the absence of practicable devices for rocking the beam. With the development of ferrite phase shifters and other elements of antenna-waveguide technology, the era of the RLS with electrical sweeping of the antenna beam arrived.

Figure 2.33 explains the principle of sweeping in one plane using a phased antenna array. To simplify the explanation only 5 vibrators are shown in the figure; actually there are several dozens and hundreds of them in a row.

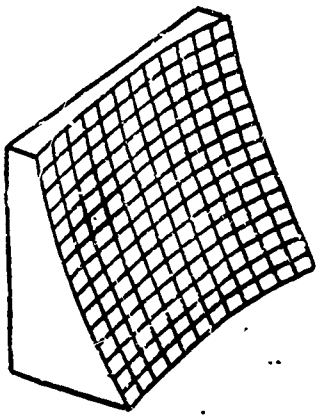

Fig. 2.34. Antenna array for electrical sweeping in two planes.

The operating principle of the phase array consists in the following.

By using ferrites inserted in waveguide sections of the antenna array and controlled by a special circuit, a supplementary mutual phase shift $\varphi$ is applied to the transmitted and received signals of the vibrators. Linear growth of the phase shift along the array may be obtained either in series or in parallel (see circuits a and b in Fig. 2.33).

Then the maximum received signal will correspond to direction $\alpha_0$, satisfying condition

$$\varphi = \frac{2\pi b}{\lambda} \sin \alpha_0, \qquad (2.34)$$

where $b$ is the space between the vibrators, since target signals received from this direction by the individual vibrators will have their

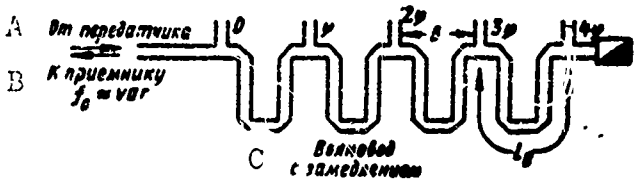


Fig. 2.35. Electrical sweeping through changing the frequency of the emitted oscillations. A) From the transmitter; B) to the receiver; C) waveguide with delay.

phases summed. In an analogous manner, the transmitted oscillations will create maximum field strength in this direction.

Thus direction $\alpha_0$ is the direction of the maximum of the directiv-

ity diagram formed by the antenna array during noncophasal feed. The directivity diagram aperture is determined by array aperture $d_a$. A change in the control current from the scanning control circuit causes the beam of the antenna array to rock within the limits of the assigned sector through variable shift of phases $\varphi$.

As the antenna directivity maximum is deflected by angle $\alpha_0$, the antenna dimensions $d$ visible from the direction of the maximum diminish: $d = d_A \cos \alpha_0$. The antenna beam widens accordingly. Thus, at $\alpha_0 = 60°$ the aperture angle of the antenna beam is doubled. Therefore electrical sweeping is always done in a comparatively narrow sector (of the order of $\varphi_0 = 60°$), whose dimensions are determined by the allowable broadening of the beam and reduction of the directional gain.

In order to shape and rock a narrow beam in two planes, the phase antenna array takes the form of a curtain whose height and width are both large (Fig. 2.34). Here there may be as many as several thousand phase vibrators.

In some RLS each vibrator is connected to its transmitter and receiver, thanks to which very long-range operation is achieved with the radiating power of each individual transmitter being kept limited. The signals received by each receiver are summed after being amplified, which is equivalent to summing the vibrator signals at the input of a common receiver if the receivers of all circuits are cophased. The whole device is rather complex, but it consists of a large number of identical elements which is technologically convenient.

Another technique for electrical sweeping of the antenna beam is retuning the signal frequency by feeding one end of the antenna array from a waveguide delay line (Fig. 2.35).

The phase jump from one vibrator to the other

$$\varphi = 2\pi \frac{l_v}{\lambda_v}, \qquad (2.35)$$

where $l_v$ is the length of a section of the waveguide feed between adjacent vibrators, and $\lambda_v$ is the wavelength in the waveguide. Through change in the transmitter frequency $\lambda_v$ and $\varphi$ also change, thanks to which the beam sweeps at $\alpha_0$ in accordance with Formula (2.34).

To obtain a sufficiently large phase shift $\varphi$ with a limited frequency deviation, the length of waveguide sections $l_v$ must be large, and to this purpose the waveguide is specially looped.

Sweeping the beam by changing frequency resembles the deflection which a beam of monochromatic light of various frequencies (colors) undergoes when passing through a prism: the beams of the red light are deflected in the prism by a greater angle than those of the blue or violet light. An even change of the wavelength of light on the red to the violet is obtained by rocking the light beam in a given sector.

## §2.8. MULTIBEAM INSTANTANEOUS AND MIXED SCANNING SYSTEMS

*Multibeam systems* of instantaneous scanning make it possible to measure all target coordinates at the same time. Because of this the antenna beam may remain stationary and still effect continuous space scanning. The basic drawback of the sequential method – a large scanning time – disappears.

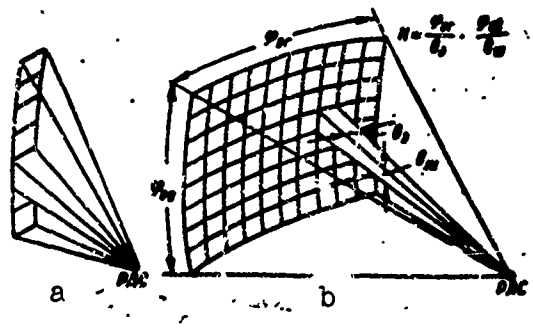


Fig. 2.36. Instantaneous multibeam scanning: a) in one plane; b) in two planes.

In order to possess exactly the same range and resolution as stations with narrow beam sequential reception, multichannel systems must employ a large number of narrow reception beams covering the whole

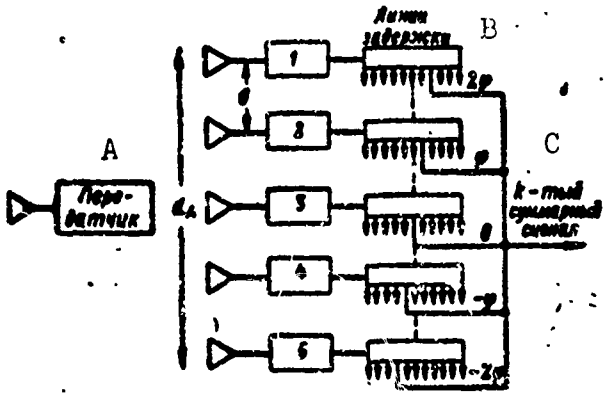


Fig. 2.37. Block diagram of multibeam instantaneous-scan RLS. A) Transmitter; B) delay line; C) kth total signal.

scanning zone. Each beam must be connected to a separate multichannel receiver; this ensures high direction-finding accuracy through comparison.

The multibeam stations used for instantaneous space scanning in one plane must, at scanning zone width $\varphi_0$ and with effective antenna beam width $\theta_e$, in principle possess $N = \varphi_0/\theta_e$ receiver antenna beams, each of which is connected to a multichannel receiver (Fig. 2.36a).

Multichannel RLS for instantaneous scan in two planes, whose scanning zone dimensions are $\varphi_{og}$ and $\varphi_{ov}$ and whose beams have, correspondingly, effective dimension $\theta_e$ and $\theta_{sh}$, must possess

$$N = \frac{\varphi_{or}}{\theta_e} \frac{\varphi_{ov}}{\theta_{sh}}$$

receiver beams (Fig. 2.36b). According to classic principles of station design the signal from each of these beams should enter a three-channel receiver device which can be used to determine all three target coordi-

nates at the same time. Thus the total number of receiver circuits is $3N$.

However, multichannel systems cannot be suitable designed according to this principle. By following another design principle, the total number of receiver channels can be substantially reduced and the difficulties associated with shaping a large number of highly directional antenna beams using a single antenna are avoided.

The new principle of designing multichannel systems is based on the use of the phased antenna arrays examined above. The difference consists in the fact that only the receiver device is multichannel, while the common transmitter possesses a separate antenna (Fig. 2.37).

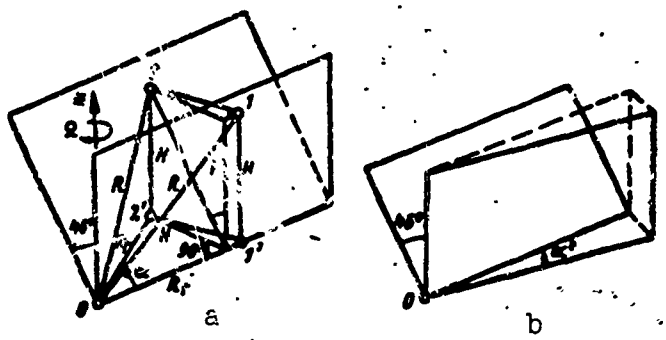


Fig. 2.38. $V$-beam method: a) dependence of target altitude on the rotation angle $\alpha$; b) additional turn of beams through angle $\alpha_0$.

The directivity diagrams of the transmitting antenna and of all receiving antennas are identical and cover the whole scanning zone. Therefore all targets within the limits of the scanning zone are irradiated during transmission. The signals from each target are received by all receivers, but their phase relations differ depending upon the condition of the target. After amplification the signals enter delay lines with a large number of turns.

The supplementary phase shift imparted to the high-frequency sig-

nal depends upon the number of the turn. By combining the signals of all channels in such a way that the supplementary phase shift increases linearly from channel to channel, the $k$th total signal is obtained. This signal is maximum when the target is located at direction $\alpha_{0k}$ determined by formula

$$\Delta\varphi_k = \frac{2\pi}{\lambda} b \sin \alpha_{0k},$$

where $\Delta\varphi_k$ is the phase jump between two adjacent channels.

As the target deviates from direction $\alpha_{0k}$ the total signal declines rapidly. This corresponds to reception of the signal by an imaginary narrow beam formed by an antenna array with aperture $d_e$, whose maximum is at direction $\alpha_{0k}$.

In other words the summing of signals at the output of the receivers is equivalent to the summing of signals by the antenna array examined above at the input of a common receiver.

If we combine the signals with the other phase shifts as determined by the combination of taps from the delay line channels, we obtain a signal corresponding to reception and an imaginary narrow beam, but from the other direction. If we then proceed further in the same manner we will form a large number of output channels. Target direction is determined by the number of the channel in which the maximum signal is discovered, and target range – by the delay time. The antenna array must be two-dimensional for direction finding in two planes.

Thanks to this system design, the whole zone may be examined during the time it takes for the signal to return from the most distant target, as in range-finding RLS, that is, practically instantaneously.

Multibeam systems are extremely complex to produce and operate. They are presently in the developmental stage. However, it must be borne in mind that multibeam systems are capable of replacing many

of the single-beam RLS presently in operation, and in many cases their application promises large economic and technical advantages.

Since three-coordinate multibeam systems are extremely complex, and single-beam systems involve excessively large standing times, multibeam mixed scanning systems have been widely employed in space scanning as a compromise solution.

*The V-beam method* is the simplest of the mixed scanning methods (Fig. 2.38). This method can be used to measure all three target coordinates: range, azimuth, and altitude, the beam being displaced in only one plane. The essence of the *V*-beam method consists in the following.

The complex antenna beams consist of two plane beams, one vertical and one inclined, which together form a figure in the form of the letter *V* (Fig. 2.38a). Both beams emanating from point *O* where the radar station is located, are conventionally depicted in the form of plane. The beams are formed by two antennas on a common base, as a result of which both beams rotate around the vertical axis as a single unit, the vertical beam contacting the target first and the inclined beam second.

Each beam is connected with its receiver. Target range and azimuth are determined from the signal received by the vertical channel, the time interval between the moments of reception of target signals in the vertical and inclined channels is a function of altitude. The greater altitude *H*, the greater this interval, and the greater is the antenna rotation angle $\alpha$ between the moments of irradiation of the target by both beams.

To find the relation between *H* and $\alpha$ we again turn to Fig. 2.38a.

Let the vertical beam intersect the target at point *1*, and the inclined beam at point *2*. The inclination angle of the inclined beam is 45°, as a result of which the distance from point *2* to the plane of the vertical beam is equal to flight altitude *H*. From triangle 01'2', in

$H = R_g \sin \alpha$, where $R_g = \sqrt{R^2 - H^2}$ is the horizontal projection of range $R$. By solving equation $H = \sqrt{R^2 - H^2} \sin \alpha$ for $H$ we obtain

$$H = \frac{R \sin \alpha}{\sqrt{1 + \sin^2 \alpha}}. \qquad (2.36)$$

This function is what is used to determine the flight altitude of the target.

It should, however, be pointed out that with this mutual arrange-

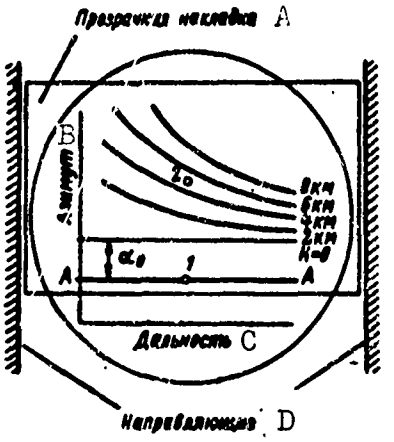


Fig. 2.39. Indirect reading of altitude on the indicator using the $V$-beam method. A) Transparent cover; B) azimuth; C) range; D) guide rails.

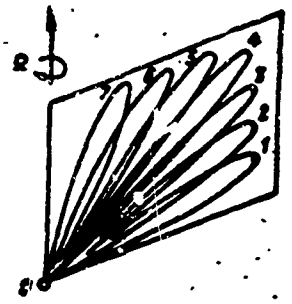

Fig. 2.40. The method of partial diagrams.

ment of the beams it is difficult to determine the altitude of low-flying targets since the two beams come together and form a single signal. To eliminate this drawback the beams are further separated in the horizontal plane, by angle $\alpha_0 \approx$ $\approx 10°$ (Fig. 2.38b). Then the moments of reception of signals of low-flying targets in the two channels are distinguished. The angle of rotation between the moments of reception is $\alpha_0$ at $H = 0$ and $\alpha_0 + \alpha$ at $H \neq 0$.

The target's altitude of flight, as determined by Formula (2.36), may be read directly from an altitude indicator whose screen is fitted with a special transparent cover (Fig. 2.39).

Target range is laid out along the axis of the abscissa, and azimuth along the axis of the ordinate. Target signals received in different channels produce two bright spots at the same range but at different azimuths. Spot *1* represents the signal of the vertical channel. The azimuth of spot *2*, representing the signal of the inclined channel, lags behind that of spot *1* by the magnitude $\alpha_0 + \alpha$.

The transparent cover may be moved vertically along the indicator screen. Horizontal base line *AA* is plotted on the lower edge of the cover, and above it are laid out the lines of equal altitude as calculated from Formula (2.36). The line of zero altitude is located at angle $\alpha_0$ away from the base line. All other lines of equal altitude take the form of curves which diverge at $R \to 0$, since, according to Formula (2.36), if $H$ = const and range $R$ is reduced, angle $\alpha$ must increase.

To determine altitude the radar station operator moves the transparent cover up or down in such a way as to superpose base line *AA* on the first target blip. Then the altitude of flight is read off along the line of equal altitudes upon which the second target blip falls. If the target blip falls in the space between lines of equal altitude, the operator uses interpolation to determine altitude precisely.

The merit of the *V*-beam method lies in the comparative simplicity of the equipment needed. By using the vertical and inclined beams target direction may be found from the method of the maximum, which imposes no serious demands on the receivers. However, the *V*-beam method possesses serious drawbacks.

This method is strictly correct only for a stationary target, since the derived relationships were based on the assumption that target position does not change between the moment when the target is irradiated by both beams. Methodological errors arise in determining the altitude of supersonic and hypersonic targets.

Another drawback of the *V*-beam method is that the accuracy of measuring altitude is comparatively low and changeable. At long ranges angle $\alpha$ is weakly dependent upon altitude.

Furthermore, in the process of reading altitude on the indicator, if there is more than one target at the given range it is difficult to determine which pair of blips refers to one target and which to the other. Reading the altitude of any target also requires manipulation of the transparent cover, which reduces the carrying capacity of the station. Finally, angular resolution is very low in the plane of each of the beams.

*The method of partial lobes* is an improved form of mixed scan.

The RLS antenna creates a vertical beam in space, consisting of a large number of needle-shaped beams in the form of a fan (Fig. 2.40). By rotating the fan-shaped beam in the horizontal plane, scanning is accomplished, and azimuth and range are measured, in all channels at the same time. The signals received by the individual beams (lobes) enter their respective receivers. Elevation angle is crudely determined by the number of the lobe upon which the signal is received. Within the limits of the lobe the elevation angle is refined through a comparison of phases or amplitude.

In this more advanced method of reception all the drawbacks associated with the *V*-beam method disappear. Accuracy and angular resolution are heightened.

The drawback of the partial lobes method lies in the complexity of the equipment required. This complexity is due, in the first place, to the use of comparison for precise reading of the elevation angle: special devices are needed to compare amplitudes, phases, or the length of pulse packages in contiguous lobes, and also to eliminate the influence of interfering factors on angular reading (standardization).

Other drawbacks of the method are the need for a large number of receiver channels and the difficulty of fitting a large number of reflectors in the aperture of the common antenna mirror. However, by comparison with the *V*-beam method the increase in the equipment is not as great as may at first appear. The reason is that in the *V*-beam method each of the two beams usually consists of several narrow beams connected to their receiver (and transmitter). These beams are arranged in approximately the same way as in systems utilizing the method of partial lobes.

At the present time, long-range ground stations are gradually changing over from the *V*-beam method to the more advanced method of partial lobes.

## §2.9. BLOCK DIAGRAMS OF TYPICAL RADAR STATIONS

Radar systems utilizing the pulse method are the most widespread at the present time.

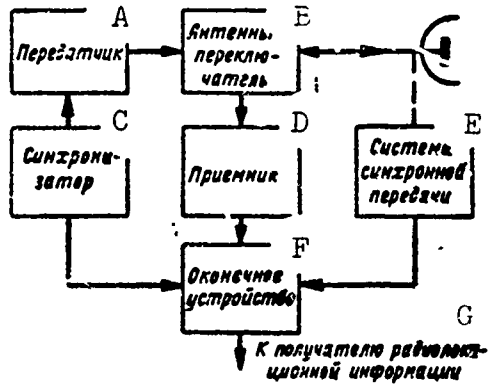


Fig. 2.41. Simplified block diagram of pulse RLS. A) Transmitter; B) antenna switch; C) synchronizer; D) receiver; E) synchronous transmission system; F) terminal device; G) to the receiver of radar information.

The pulse radar station periodically transmits short pulses, of length $\tau_1$, of high-frequency oscillations. The reflected signals are received in the time intervals between the periodic emissions. In the

simplest cases, when the targets are isolated objects of small dimensions, the received signals are in the form of high-frequency pulses of very low intensity and of approximately the same shape and length as the transmitted pulses. Each target yields its own signal. The time shift between the emitted (direct or outcoming) and reflected pulses is

$$\tau = \frac{2R}{c}.$$

When there are several targets, the signals reflected from them will be displaced in time relative to the moment of transmission in accordance with target range.

A simplified block diagram of a pulse radar station is given in Fig. 2.41. Basic elements of the radar station include: a synchronizer, a transmitter, an antenna-feeder device with an antenna switch, a system for synchronous transmission of the antenna rotation angle, a receiver, and a terminal device.

The terminal device is an extremely important element of a radar station. At the receiver output there are always interferences of various origins as well as the internal noises of the receiver device itself, as well as the useful reflected signals. Therefore, the signal must be cleansed of its noise before the radar information can be converted into a form suitable for the user. The terminal device should solve two tasks: in the first place, distinguish the signal against the background of noise and preserve all its useful parameters bearing various information on the target, and, in the second place, measure the target coordinates and the characteristics of its motion from the parameters of the derived signals.

Various types of terminal devices may be employed depending upon who is to utilize the radar information.

If the user of the radar information is the operator, a cathode-

ray indicator is, as a rule, employed as the terminal device of contemporary radar stations. This is a very effective way of transmitting radar information and is the reason for the broad application of visual indicators employing cathode-ray tubes.

The user of the radar information may be a computer or a continuously and directly acting mechanism. In this case the radar station terminal device should be a system for automatic tracking of the target. Such a system usually gives information on target range in the form of voltage, and information on target angular coordinates in the form of rotation angles of the antenna axes.

In complex guidance systems, for example, the radar station may be one of the sources of information. In order to make such systems automatic, the information arriving may be introduced into a digital computer which develops the guidance commands.

A digital computer is a discretely acting device. It deals with quantities presented in the form of numbers. Therefore, if the receiver of the radar information is a digital computer, the terminal device should feed all target data derived from the received radar signal into the input of the computer in the form of a binary code. The terminal device for filling this sort of function is called a device for the instrumental registration of data.

1. The Radar Station with Cathode-Ray Indicator

Let us in the first place examine the operation of a pulse radar station utilizing a cathode-ray indicator as its terminal device. Figure 2.42 gives the time diagrams explaining the interaction of its elements.

Using periodically repeated control pulses (Fig. 2.42a), the synchronizer coordinates over time the operation of all elements of the radar station. To each synchronizer pulse there corresponds one cycle

of work of the station, whose length $T_p$ is customarily called the pulse repetition period. The quantity which is the inverse of $T_p$ is the pulse repetition frequency $F_p$.

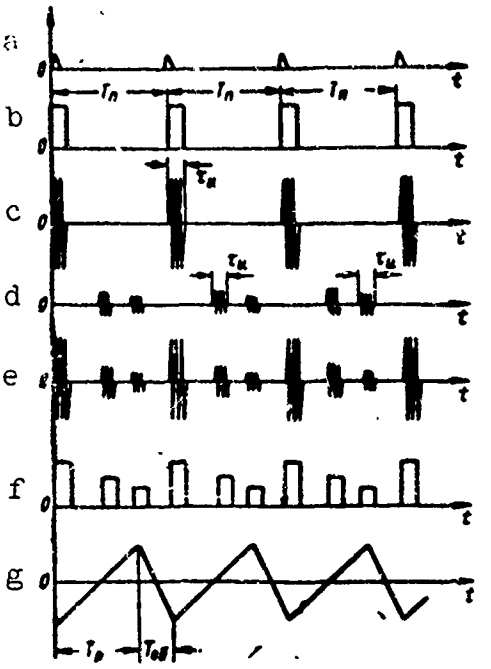


Fig. 2.42. Time diagram explaining the operation of a pulse radar station utilizing a cathode-ray indicator: a) synchronizer control pulses; b) modulator pulses; c) outcoming transmitter pulses; d) signals reflected from target; e) signals at receiver input; f) signals at receiver output; g) indicator range scan voltage.

The transmitter consists of a modulator and a high-frequency generator. The modulator is usually triggered by the synchronizer and shaped pulses of a determined shape and length (Fig. 2.42b). Stimulated by the modulator pulses, the generator develops pulses of high-frequency oscillations (Fig. 2.42c). Their length $\tau_i$ is determined principally by the length of the modulator pulses.

Most radar stations use the same antenna for emitting electromagnetic oscillations and for receiving signals. During emission of the outcoming pulses the antenna-feeder device is connected to the transmitter and disconnected from the receiver. This is necessary in order

to avoid damage to the input circuits of the receiver by the powerful transmitter pulses. During reception, on the contrary, the receiver should be connected to the antenna-feeder device, while the transmitter is disconnected from it. Disconnecting the transmitter makes it possible to avoid losing part of the energy of the received signals in its output circuits. These switching operations are accomplished by a low inertia antenna switch.

As the antenna rotates the intensity of the received signals changes in accordance with a definite law, achieving its greatest value each time the maximum of the directivity diagram coincides with the target direction. This circumstance is utilized for target direction finding (determination of angular coordinates) by simply reading off the antenna rotation angles corresponding to the maximum value of the reflected signals.

The high-frequency signals (Fig. 2.42d) reflected from the target and received by the antenna pass through the feeder system and the antenna switch into the receiver where they undergo the necessary amplification and are rectified into video pulses.

Despite all these measures, the antenna switch cannot completely disconnect the receiver from the antenna-feeder device during operation of the transmitter. For that reason outcoming transmitter pulses (Fig. 2.42e) leak through the antenna switch, although in a considerably weakened form, and appear at the receiver input together with the reflected signals. The amplitude of these leaked pulses is considerably greater than that of the pulses reflected from the target.

The amplified and rectified signals pass from the receiver output to the RLS indicator (Fig. 2.42f).

Two types of indicators are utilized in radar stations: amplitude and brightness indicators. The simplest pulse radar indicator is the

range indicator using a cathode-ray tube with electrostatic drive and amplitude marking.

Range sweep is accomplished by feeding voltage from a sweep generator which is triggered at the same time as the transmitter by the synchronizer pulses, to the horizontally deflecting plates of the cathode-ray tube. The sweep generator develops voltage which causes the light spot to move across the screen along the line of sweep from the extreme left position, corresponding to zero range, to the extreme right position, corresponding to the maximum observed range. The movement of the spot from left to right is the working stroke of the sweep. During the working stroke the voltage increases linearly over time (Fig. 2.42g). Because of this, the movement of the light spot from the beginning of the sweep line is proportional to the time elapsing from the beginning of the radiation of the direct pulse. During the return stroke the sweep voltage rapidly returns to its initial value. The electron beam must move from the extreme right position to the extreme left position. As a rule, the return stroke of sweep is not viewed on the screen since the cathode-ray tube is switched off during this operation.

Signals reflected from the target and received and amplified in the receiver are fed to the vertically deflecting plates of the cathode-ray tube. These move the light spot in the vertical direction. Over the sweep line appear blips whose shape corresponds to the reflected signals – target amplitude blips (Fig. 2.43a).

The space between the beginning of the sweep and the target blip is proportional to the time interval between emission of the outcoming pulse and arrival of the reflected signal and, consequently, is proportional to range. Therefore a scale graduated in units of range may be laid out along the sweep line, its point of origin coinciding with the beginning of the sweep. A direct transmitter pulse is usually applied

to the beginning of the indicator range scale.

Range blips may be observed on the indicator screen, and range may be read off, only for those targets which at the given time are located in the direction of radiation of the antenna system. When it is necessary to observe the positions of all targets in the surrounding space at the same time and to read off their ranges and azimuths rapidly, a circular sweep indicator with radial-circular scan and brightness mark-

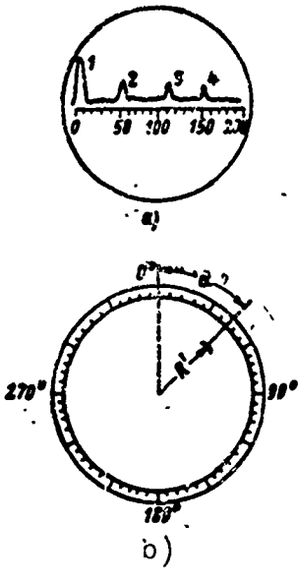


a)

b)

Fig. 2.43. Types of radar indicator screens: a) range indicator; b) circular scan indicator; 1) outcoming transmitter pulse blip; 2,3,4) target blips.

ing is utilized. The center of the screen is, as a rule, used as the beginning of such a sweep and as the point of zero range (Fig. 2.43b). During the working stroke the bright spot moves along the radius from the center of the screen to its periphery, thus accomplishing range sweep, and during the return stroke it returns to its initial position. After completing the return stroke the bright spot begins to move along the next radius, one which is displaced relative to the preceding radius by an angle equal to the angle in the azimuth plane through which the antenna has moved during the pulse repetition period.

Thus it may be considered that radial sweep is accomplished by movement of the bright spot along the radius with the velocity of the range sweep and of the rotation (synchronous with the antenna rotation) of this radius. A definite position of the radius of the sweep on the cathode-ray tube screen corresponds to each position of the antenna-beam axis in the azimuthal plane.

The voltage at the receiver output is fed to the control electrode of the cathode-ray tube. When the reflected signals arrive, the brightness of the luminescence on the screen increases — the presence of the target is indicated by a brightness marking in the form of a small lighted arc which is brighter in the middle. The length of the arc of a point target is determined fundamentally by the aperture angle of the antenna directivity diagram in the azimuthal plane. Distance $R'$ of the blip from the center of the screen is proportional to target range, while the rotation angle of the radius of the sweep, at which the center of the arc is located, is equal to target azimuth $\alpha$ relative to the initial position (Fig. 2.43b).

Circular scan indicators utilize cathode-ray tubes whose screens possess considerable afterglow. Because of the afterglow the image on the screen is retained through one rotation of the antenna, as a result of which it is possible to observe at the same time the blips of targets located at various points in the space around the radar station.

Only two types of radar station indicators have been examined as examples. Because of the variety of tasks which must be solved in the practice of radar, various types of indicators are employed. However, the general principles of design and operation of the RLS remain analogous to those examined above.

Information is usually taken directly from the indicator screen by the operator. His possibilities, however, are very limited, and, there-

fore, special registering devices are employed when it is necessary to effect detailed processing and analysis of the obtained data, especially during observation of objects traveling at high speed. Their component is the ordinary cathode-ray indicator with amplitude or brightness marking. The image on the indicator screen is photographed with an inary photograph or movie camera. The radar image which has been registered in this way can be subjected to detailed analysis at a later stage in order to derive the information of interest.

2. Radar Station with Target Autotrack

Target autotrack systems may be employed in airborne stations for interception and sighting, in radar stations for tracking objects in space, in stations for sighting weapons, and in devices for the sighting and self-sighting of rockets and guided missiles.

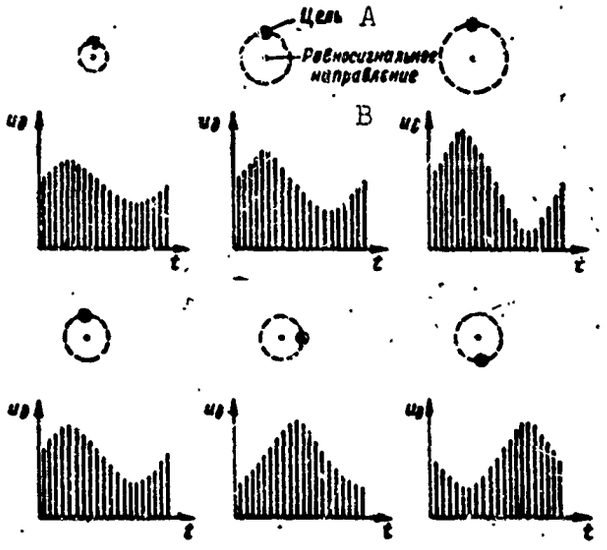


Fig. 2.44. Dependence of the amplitude and phase of the received signal envelope upon the extent and direction of target movement. A) Target; B) equisignal direction.

The RLS with conical rotation of the antenna beam may serve as an example of a radar station with target autotrack. For automatic deter-

mination of angular coordinates this station uses the method of comparison of the amplitudes of signals received in a single-channel receiver.

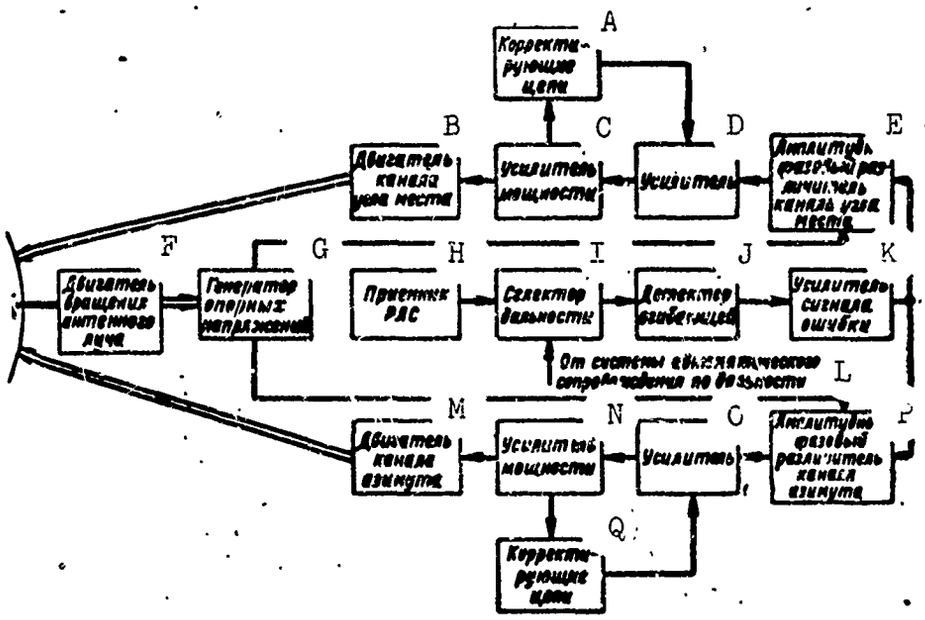


Fig. 2.45. Block diagram of target autotrack system with conical rotation of the antenna beam. A) Correcting circuits; B) elevation channel motor; C) power amplifier; D) amplifier; E) amplitude-phase discriminator of elevation channel; F) antenna beam rotation motor; G) reference voltage generator; H) RLS receiver; I) range selector; J) envelope rectifier; K) error-signal amplifier; L) from the range autotrack system; M) azimuth channel motor; N) power amplifier; O) amplifier; P) amplitude-phase discriminator of the azimuth channel; Q) correcting circuits.

The axis of the antenna directivity diagram is displaced relative to the antenna optical axis by displacing the radiator from the focal point of the mirror. As the radiator rotates the axis of the radio beam describes a conical surface in space. The power of the emitted and received signals does not change in the direction of the axis of rotation. This direction is called the equisignal direction. If the target is located in the equisignal direction, the reflected signal received by the RLS will consist of a sequence of pulses of identical magnitude. But if the target is located at some angle relative to the rotation axis, the reflected pulses are amplitude-modulated with the frequency of

the antenna's rotation, the extent of the modulation being proportional to the size of the angular displacement of the target relative to the equisignal direction and the phase of the envelope being determined by the direction of displacement of the target in space relative to some direction accepted for purposes of computation.

Figure 2.44 demonstrates the time diagrams of signals at the output of the receiver detector for various target positions relative to the equisignal zone. The upper drawing shows the change in the amplitude of the received signals over one rotation period at various deviations of the target from the equisignal zone. The lower drawing shows the change in the phase of the envelope at identical target displacement from the axis of rotation, but for various positions of the target in space. The drawings show that the envelope amplitude characterizes the extent of target deviation, and the phase — the direction of this deviation.

The voltage of the envelope may be utilized to guide an antenna system and to bring the axis of rotation automatically in line with the target direction. Since, generally speaking, the target may be displaced relative to the equisignal zone both in elevation and in azimuth, autotrack should employ two tracking systems, one for tracking in the vertical plane, and the other in the horizontal plane.

Each of the tracking systems consists of an amplitude-phase discriminator, a reference voltage generator (usually common to both channels), voltage and power amplifiers, and a driving motor for changing the antenna position (Fig. 2.45). The tracking systems of both channels function in an absolutely identical manner.

The target signals enter a detector which isolates the voltage of the envelope of the target pulses. The amplified voltage, which is usually called the error signal, is a harmonic oscillation whose amplitude

characterizes the extent of target deviation relative to the antenna axis, and whose phase characterizes the direction of this deviation. The error signal voltage is fed to two amplitude-phase discriminators in which the error voltage is resolved into its components which are proportional to displacement of the target in azimuth and in elevation. The error signal is resolved thus using the reference voltages developed by a special generator. The latter, whose rotation is synchronous with that of the radiator, creates two harmonic oscillations of a frequency $\Omega$ and whose phases are shifted by 90°. These voltages are usually transformed into rectangular oscillations and in that form fed to the corresponding phase discriminators. As a result of the combined action of the error signal and the reference voltage, at the output of each phase discriminator is developed a control signal which is proportional to target deviation in the corresponding plane. The control voltages of each channel are amplified and fed to the azimuth and elevation motors. The angular tracking device includes directing circuits which improve the dynamic qualities of the system and eliminate the possibility that autooscillations will arise in it.

Direct-current motors, operating together with amplidynes, are most frequently used to drive the antenna. It is also possible to employ biphase asynchronous motors with magnetic amplifiers. The drive motors turn the antenna in azimuth and elevation in a direction which reduces the error signal, that is, in a direction which reduces the mismatch between the target direction and the equisignal zone.

Thus the antenna axis coincides accurately with the target direction unless there is error in the autotrack. The position of the antenna axis uniquely defines the target angular coordinates.

Obviously, automatic directional tracking is possible only when signals from only one target enter the envelope detector. This is pro-

vided by gating the receiver with a selector pulse generated by the target range autotrack system (ACD).

A typical block diagram of an ACD system is given in Fig. 2.46.

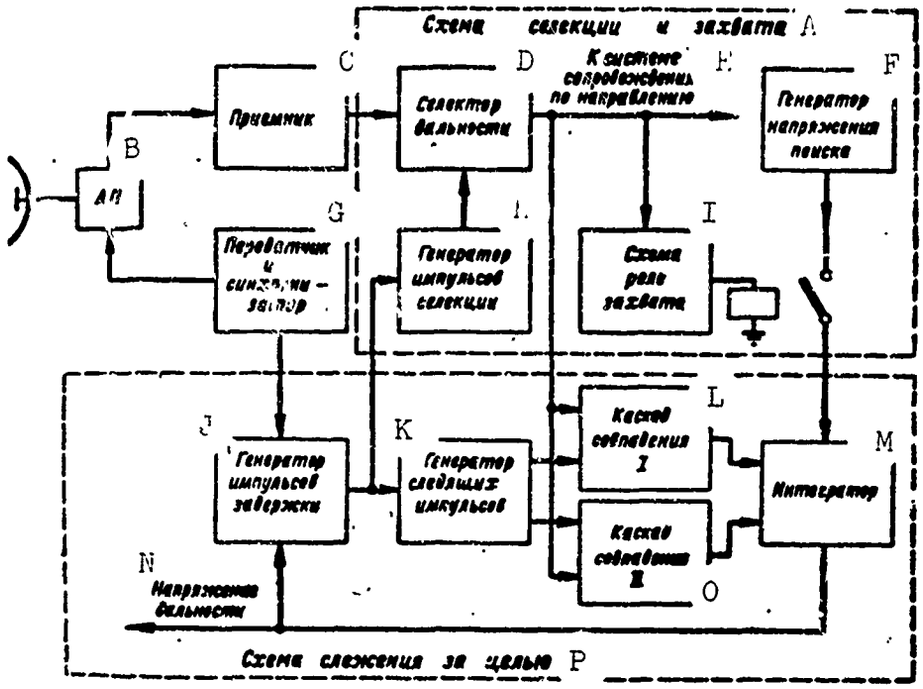


Fig. 2.46. Block diagram of range autotrack system. A) Selection and locking circuit; B) AP; C) receiver; D) range selector; E) to the direction tracking system; F) search voltage generator; G) transmitter and synchronizer; H) gate generator; I) locking relay circuit; J) delay pulse generator; K) tracking pulse generator; L) coincidence cascade I; M) integrator; N) range voltage; O) coincidence cascade II; P) target tracking circuit.

The ACD system consists of a selection and locking circuit and a target tracking circuit. The selection and locking circuit is for automatic discovery (interception) of the target and for supplying the pulse of the target selected to the autotrack circuit. The target is intercepted jointly by the search voltage generator, the locking relay circuit, and the range selector. During search of the target a voltage from the search generator which periodically charges and discharges the integrator capacitor linearly, is fed to the generator. The sawtooth voltage of the integrator causes the delay pulse generator (for example, a

phantastron), which is triggered by the synchronization pulse, to develop pulses whose length is proportional to the instantaneous value of the search voltage. Because of this, the selection pulses triggered at the moment of termination of the daly pulse will be periodically shifted first in the direction of an increase in range, then in the direction of a decrease in range. When the selectropulse coincides with the target signal the latter passes through the selector into the locking relay circuit.

The locking relay circuit includes a simple storage device (for example, a capacitor) and a relay. Target pulses are accumulated synchronously in the range selector; all interference which do not coincide in time and in tracking frequency with the target pulse are suppressed. Since the range of the selectropulse is slowly being retuned, several target pulses pass through the selector, and the capacitor is tuned to the value necessary to trigger the relay. The relay disconnects the search voltage generator from the integrator, and the range autotrack system switches over to tracking.

In the tracking regime the tracking pulse generator, which develops two short pulses following right upon one another, the length of each of them being equal to half of the selectropulse, is triggered at the same time as the selectropulse generator. Because of this the back side of the first tracking pulse and the front of the second tracking pulse coincide in time with the middle of the selectropulse.

The tracking pulses open the two coincidence cascades one after the other, and the target pulse passes partially through the first coincidence cascade and partially through the second. At the output of the coincidence cascades is a capacitor which is discharged by the output current of the first coincidence cascade and charged by the current of the second cascade.

If the middle of the reflected signal is somewhat delayed relative to the dividing line of the tracking pulses, the capacitor at the output of the coincidence cascades will be discharged less than it is charged, and the voltage at the integrator output will increase. This increased voltage compels the pulse delay generator to shift the tracking pulses in such a way that their dividing line coincides with the middle of the reflected signal. But if the middle of the target pulse is somewhat in advance of the dividing line of the tracking pulses, the capacitor is discharged more than it is charged. Range voltage is reduced, and the tracking pulses are shifted in the reverse direction.

Thus, the tracking pulses always accompany the target signals. And here the output voltage of the integrator is proportional to target range at any moment in time. This is how target range autotrack is accomplished and target range converted into voltage.

3. Radar Station with Digital Data Output

Only a discretely acting computer device – a digital computer (TsVM) – is capable of automatic analysis of the scanning zones of one or several RLS, taking into account the relative positions and displacements of several targets at the same time. Therefore in automated scanning and guidance complexes the radar stations are connected to a digital computer.

In contrast to analog computers, discretely acting computers possess high carrying capacity and run very fast. They consist of many comparatively simple standardized elements and, consequently, are suitable for mass automated production. Because of its universality and high speed, one digital computer replaces a large number of analog computers.

Computation by digital computers is of practically unlimited accuracy. Accuracy is determined only by the number of series in the arith-

Computation by digital computers is of practically unlimited accuracy. Accuracy is determined only by the number of series in the arithmetical device of the computer, also by mistakes in rounding off, and have nothing to do with the precision with which the individual elements are manufactured. The elements of the analog computer, even when manufactured with the greatest precision and individually fitted, possess a limited, and in some cases inadequate, accuracy.

Digital computers may vary the order of the problem's solution depending upon the results of intermediate calculations. This property, which is known as self-tuning, gives this computer a flexibility which is unattainable by analog computers.

The drawback of the digital computer is the need to transform all the input data into digits, and the output data – from the form of digits back into the continuous electrical signals which drive the executive mechanisms. The reason for the reverse transformation is that the digits cannot be directly used to drive these mechanisms. Since the quantity of input and output data may be very great, the device which links the TsVM with the rest of the control system at the input and output may be very cumbersome.

Of the discrete computers the most widespread are those using the binary system of numbering as opposed to the generally accepted decimal system of numbering. The binary system of numbering is based on the number 2; each unit of any series contains two units of the preceding series. Any number may be transmitted by using the two digits 0 and 1.

The binary system is the most convenient for digital computers principally because most electronic circuits for registering and transmitting numbers (triggers, relays, etc.) may take two sharply opposed stable positions: open and shut, connected and disconnected, charged and discharged (*yes* and *no*). The value 1 is ascribed to one position,

the value 0 to the other. Each binary series may be transmitted by one of these elements taking one of the two possible positions.

Another important merit of the binary system is that it is economical: to register and reproduce any number in the binary system one-third as many elements is required as in the decimal system.

When operating jointly with a radar station the digital computer fulfills the functions of the operator, while the terminal device of a RLS, instead of being an indicator, is a device for the instrumental registration of data (Fig. 2.47). The device for instrumental registration solves two basic tasks.

The first task is the suppression of noises and isolation of the useful target signal. The operation of noise suppression is known as the primary processing of the signal and is executed by a preliminary selection element, i.e., the preselector. The ultimate suppression of noise is done in the computer itself. The preselector only accomplishes preliminary isolation of the signal, hence its name.

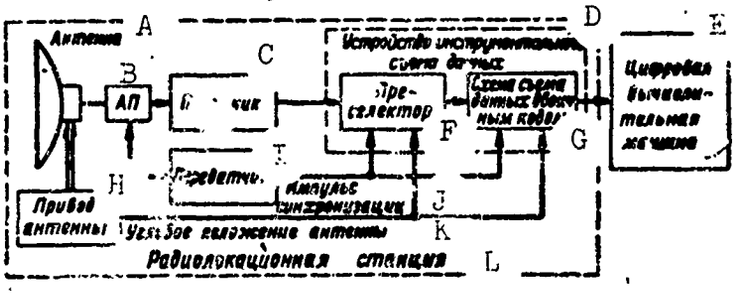


Fig. 2.47. Coupling of RLS and TsVM. A) Antenna; B) AP; C) receiver; D) device for instrumental registration of data; E) digital computer; F) preselector; G) circuit for registration of data in a binary code; H) antanna drive; I) transmitter; J) synchronization pulse; K) angular position of antenna; L) radar station.

The second task is the representation of target coordinates in the form of binary numbers, and this is accomplished by a circuit which delivers data in binary code.

Data on target coordinates are already contained in the received

signals. Thus the delay time of the echo pulse relative to the synchronization pulse determines target range. To measure delay time, target pulses and trigger pulses must be fed to the data delivery circuit.

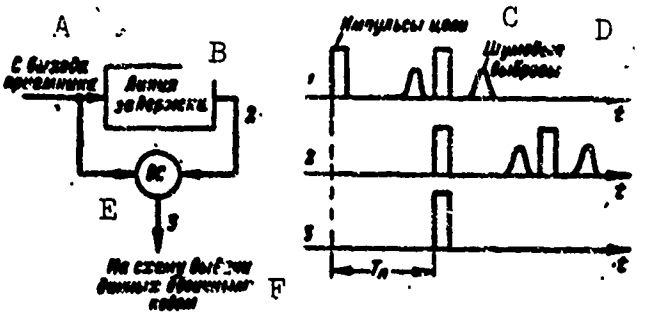


Fig. 2.48. Principal of noise suppression in preselector. A) From receiver output; B) delay line; C) target pulses; D) noise blips; E) VS; F) to the circuit for binary delivery of data.

The angular coordinates of the target are determined from the direction of the RLS antenna axis at the moment of arrival of the echo signal. For this data on the antenna angular position are fed from the antenna drive to the data delivery circuit. All calculated values for target coordinates enter the memory element of the digital computer in the form of binary numbers. This operation resembles the calculation of target coordinates by the operator from a scale on the indicator screen.

Furthermore, it must be borne in mind that even the primary processing of signals (noise suppression) is accomplished through registering and preservation of data on target coordinates. Therefore to the preselector are also fed data on the time of triggering the transmitter and on the antenna angular position.

As is known, in visual observation the operator himself plays an active role. In observing the position of blips on the indicator screen from one scanning cycle to another, the operator distinguishes false signals from genuine ones. The digital computer performs an analogous

task. To this end, the TsVM, in analyzing changes in the target coordinates, establishes the regularities in these changes from one cycle to another for each target individually. Because of this the computer can discard false targets caused by leakage of interference through the preselector, since there is usually no regularity in their changes.

This operation is called secondary processing of radar data and is accomplished by remembering target data over several scanning cycles.

Thus the following sequence of operations is performed when the RLS and TsVM are coupled: primary processing – registration of data in a primary code – secondary processing. We will analyze each of these operations using the simplest possible example, devoting greater attention to secondary processing, since the first two operations will be analyzed in detail in subsequent chapters.

The simplest principle of noise suppression during primary processing of signals is selection according to repetition frequency. Target pulses are spaced at repetition period $T_p$, while noise blips are sporadic. If the receiver output signal is delayed for a repetition period, and then the delayed and undelayed signals are fed to a coincidence valve (VS), at the output of the valve is obtained only the target pulse, the noise blip whose intervals are sporadic having been suppressed (Fig. 2.48).

Part of the noise nonetheless reaches the output of the circuit and there forms a false target which can be discarded during secondary processing.

We may also note that the pulse at the circuit output coincides in time with one of the target input pulses, and therefore retains information on range. If, furthermore, the largest pulse of the package is isolated, from its position the angular position of the target can also be read.

Let us examine the functioning of the binary data output circuit from the point of view of its transformation into a number representing the target range and angular position.

The principle of the registration of range in the form of a number is the following (Fig. 2.49). The pulse counter counts the number of counter pulses arriving at high frequency from a special generator during the echo-signal delay time $\tau = 2R/c$. Interval $\tau$ during which the counter pulses reach the counter is assigned by a control circuit consisting of a coincidence valve (VS) and a trigger.

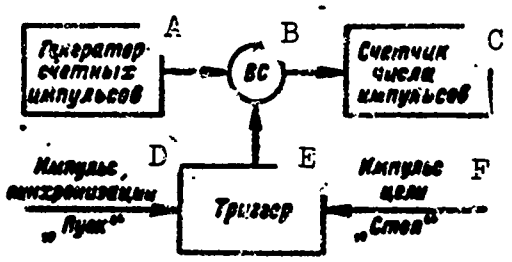


Fig. 2.49. Principle of registration of range in the form of a binary number. A) Generator of counter pulses, B) VS; C) counter of the number of pulses; D) "stop" and synchronization pulse; E) trigger; F) "stop" target pulse.

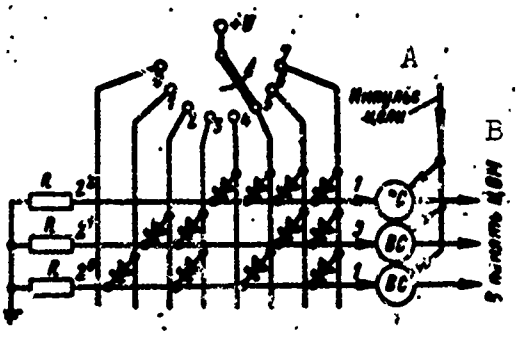


Fig. 2.50. Principle of binary registration of angular coordinates. A) Target pulse; B) to the TsVM memory.

The synchronization pulse which clamps the moment of emission of the transmitter pulse is given by the control trigger. Starting at this moment the trigger feeds a positive voltage to the coincidence valve, opening it. Upon arrival of the target pulse from the preselector, the trigger again returns to its initial stage. As a result, the coincidence valve is open during time interval $\tau = 2R/c$. The number of counter pulses entering the counter through the coincidence valve during this time interval is proportional to range.

The device which transforms target angular coordinates into a binary code should solve two tasks: it should represent any antenna position in the form of a binary number and, at the moment of arrival of the target pulse from the preselector, should feed this number to the TsVM memory.

Figure 2.50 explains the principle of operation of this device. A mechanical switch which is rigidly attached to the antenna axis and rotates together with it closes one of the contacts on the immovable base of the antenna.

Here, closure of one of the contacts of the "positive source - ground" circuit correspond to one of the eight values of the angle of rotation. For the number of the contact to be received at the output in binary form a matrix network of semiconductor diodes and resistances

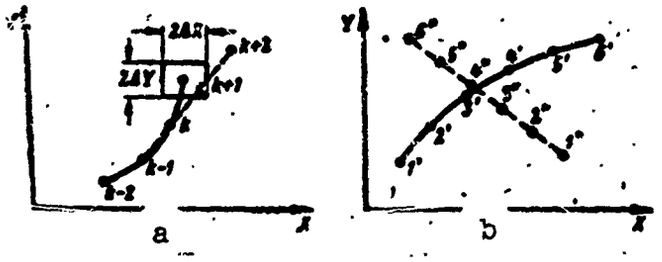


Fig. 2.51. Principle of secondary processing of data: a) extrapolation and identification; b) isolation of data on several targets.

is employed. Thus, when the switch is in position 5, current passes through the resistances of series $2^2$ and $2^0$. The appearance of voltage in resistors $R$ corresponds to a binary unit, and therefore the figure 101 (5) appears in the form of voltage at the inputs of the coincidence valves.

At the moment of arrival of the target pulse from the preselector to the TsVM memory, pulses (units) are registered only in those coincidence valves at whose inputs there are voltages. This number corre-

sponds to the target angular position.

In the memory element of the TsVM are concentrated data on the coordinates of all targets, including false targets, for each scanning cycle of the RLS. On the basis of these data the TsVM accomplishes secondary processing of the signals, the essence of this process consisting of the following.

After, in a given scanning cycle, obtaining numbers expressing the target coordinates, the computer must determine that these numbers emanate from some particular target which is either known or unknown depending upon the previous scanning cycle. This task is known as target identification. To solve this problem the digital computer must, on the basis of the data of preceding cycles, independently determine, with regard to each successive scanning cycle, in what area of space the appearance of the target is to be anticipated, that is, it must extrapolate the coordinates.

Let us assume that on the basis of the data of three preceding scanning cycles it is necessary to determine at what point on plane $XY$ the target will be located at the $k + 1$ scanning cycle (Fig. 2.51a). Let us take the three last actual positions of the target (the black dots $k - 2$, $k - 1$ and $k$) and formulate a hypothesis on target movement. It would be a natural assumption that the target will continue to move along the same trajectory and with the same velocity as in preceding cycles. On this basis we may extrapolate the target trajectory (in the figure it is the arc of the circle expressed by the continuous curve) and plot on it a section equal to the path traversed by the target between the two last cycles. We thus obtain the point at which the appearance of the target is to be expected at the $k + 1$ irradiation cycle; this is denoted in the figure by the little circle.

This is just the task which the computer is to solve, that is,

calculation of the target coordinates to be anticipated at the $k + 1$ scanning cycle

$$X^{\circ}_{k+1} \text{ and } Y^{\circ}_{k+1}.$$

The TsVM must at the same time determine the extent of the possible deviation of the target from the computed position $\Delta X$ and $\Delta Y$. This deviation is determined both by the radar station's inaccuracy in determining the coordinates and by target maneuvering, that is, by deviation of the actual movement of the target from that accepted as the hypothesis of the extrapolation.

In the $k + 1$ scanning cycle the RLS gives the actual target coordinates $X_{k+1}$ and $Y_{k+1}$ (black dot). The task of the computer is to compare the actual and the anticipated (computed) coordinates, and as a result of this the target is identified.

If the condition is satisfied that the actual coordinates of the target do not differ from the calculated coordinates by more than $\Delta X$ and $\Delta Y$

$$\begin{aligned} |X^{\circ}_{k+1} - X_{k+1}| &< \Delta X, \\ |Y^{\circ}_{k+1} - Y_{k+1}| &< \Delta Y, \end{aligned} \qquad (2.37)$$

the target is considered to be *the same*, and the actual target coordinates are substituted for the anticipated coordinates in the memory element of the computer. The computer then immediately sets out to compute the anticipated coordinates for the $k + 2$ scanning cycle for which the coordinate of the $k - 2$ scanning cycle are discarded and only the data of the $k - 1$, $k$, and $k + 1$ cycles are considered (Fig. 2.51a, dotted curve). This process continues to be repeated as long as the target remains within the RLS scanning zone.

If Condition (2.37) is not satisfied, the computer compares the measured coordinates with the anticipated data of other targets pre-

served in other memory cells. Upon coincidence (with deviation by not more than $\Delta X$ and $\Delta Y$) of the measured data with the anticipated data for some target, new coordinates are attributed to that target. If Condition (2.37) is not satisfied for all targets, the target is considered a new one, and its data are introduced into a new memory cell.

Here there are three points of extrapolation. Depending upon the concrete situation other types of extrapolation may also be used.

By continuous calculation of anticipated coordinates and comparison of them with actual coordinates, the TsVM accomplishes continuous observation of each individual target. The coordinates of one target cannot be confused with those of another target since their trajectories are what is being analyzed. As can be seen from Fig. 2.51b, the coordinates of two targets (one stroke and two stroke, respectively) are distinguished, despite the fact that the targets occupy the same positions both on $X$ and on $Y$ during 6 scanning cycles.

What is more, accidental vanishing of a target in a given standing cycle does not interrupt the tracking process. In this case the anticipated coordinates of the preceding cycle are used instead of the actual coordinates to calculate the anticipated coordinates of the subsequent cycle. The computer, as it were, "restores" the target when it accidentally vanishes for a short time.

On the other hand, if the passage of noise through the preselector causes false target coordinates to be delivered, they are rejected through the operations of extrapolation and comparison in subsequent scanning cycles, since there is no regularity in the "behavior" of false targets from one cycle to another: the trajectory is unreal and confused.

Thus the process of extrapolation and identification makes it possible to track target trajectories, to determine their velocities and

directions, and also to reduce noise interference: to restore the target signal if it vanishes for a short time, and to discard false targets caused by noise. Secondary processing, as it were, cleans out the "flaws" arising during primary processing of the signal in the preselector. The designer's task is to distribute the function of noise suppression in the best possible way as between the preselector and the computer.

Error in extrapolation of $\Delta X$ and $\Delta Y$ reduces the resolution of the RLS-TsVM system, especially during the first scanning cycle (after appearance of the target) when the target trajectory is still insufficiently clear. During subsequent cycles the law of the target's motion becomes more clear, and the device automatically narrows down the area of indeterminateness $\Delta X$ and $\Delta Y$ (self-tuning). The area of indeterminateness is ultimately determined only by imprecise delineation of the target trajectory because of coordinate measurement errors or because of possible maneuvers of the target during a scanning cycle. Consequently the RLS resolution may be heightened by improving the coordinate measurement accuracy and by reducing the scanning time.

Manuscript Page No.

[Footnotes]

35 The *reciprocal duty factor* means the ratio between the repetition period and the length of the repeated signals.

80 Systems consisting of several antennas are also used in panoramic circular-scan RLS to increase the data delivery rate.

81 The ratio between antenna beam width $\theta$ and quantities $\theta_e$ and $\theta_{sh}$ will be examined in Chapter 5.

| Manuscript Page No. | [Transliterated Symbols] |
|---|---|
| 28 | УКВ = UKV = ul'trakorotkiye volny = ultrashort waves |
| 28 | макс = maks = maksimum = maximum |
| 29 | пр = pr - prinimayemyy signal = received signal |
| 29 | Д = d = Doppler - Doppler |
| 34 | пер = per = peredavayemyy = transmitted |
| 34 | б = b = biyeniye = beat |
| 35 | и = i = interval = interval |
| 37 | п = p = period = period |
| 41 | м = m = modulyatsiya = modulation |
| 45 | мин = min = minimal'nyy = minimum |
| 47 | АРУ = ARU = avtomaticheskaya regulirovka usileniya = automatic gain control |
| 47 | нр = nr = naprezheniye rassoglasovaniya = mismatch voltage |
| 49 | ш = sh = shum = noise |
| 50 | пх = pkh = pelengatsionnaya kharakteristika = direction-finding characteristic |
| 53 | сс = ss = summarnyy signal = total signal |
| 53 | рс = rs = raznostnyy signal = difference signal |
| 58 | с = s = signal = signal |
| 62 | р = r = otrazhennyy = reflected |
| 64 | РЛС = RLS = radiolokatsionnaya stantsiya = radar station |
| 59 | РСН = RSN = ravnosignalnoye napravleneniye = equisignal direction |
| 60 | р = r = raznostnyy = differential |
| 65 | обл = obl = oblucheniye = irradiation |
| 72 | НКО = IKO = indikator krugovogo obzora = circular scan indicator |

Manu-
script
Page
No.

78 обл = obl = oblucheniye = irradiation

78 п = p = povtoreniye = repetition

78 мин = min = minimal'nyy = minimum

78 г = g = gorizontal'nyy = horizontal

79 н = n = neravnomernyy = nonuniform

79 х = kh = kholostoy = no-load

81 в = v = vertikal'nyy = vertical

81 ш = sh = shirina = width

81 стр = str = stroka = line

91 в = v = volnovód = waveguide

99 и = i = impul's = pulse

102 п = p = povtoreniye = repetition

111 АП = AP = avtomaticheskiy povtoritel' = automatic repeater

111 АСД = ASD = avtomaticheskoye soprovozhdeniye tseli po dal'nosti = target range autotrack system

116 ВС = VS = ventil' sovpadeniy = coincidence valve

## Chapter 3

## RADAR TARGETS AND CHARACTERISTICS OF REFLECTED SIGNALS

### §3.1. GENERAL INFORMATION ON RADAR TARGETS

An electromagnetic wave striking a material body provokes, regardless of the nature of the body, forced oscillations of free and bound charges which are synchronous with the oscillations of the applied field. The forced oscillations of the charges create a secondary field inside and outside of the body. As a result of this, the energy of the electromagnetic wave striking the target is dissipated in all directions, including the direction of the radar station. The retransmitted wave returning back to the radar station forms the reflected signal of the target.

The character of the secondary emission or reflection of the electromagnetic waves depends upon the shape of the object located in the path of the propagation of the electromagnetic wave, upon its dimensions and electrical properties, and also upon the length of the wave and its polarization.

It is customary to distinguish among specular, diffuse, and resonance reflections. If the linear dimensions of the reflecting surface are much greater than the wavelength, and the surface itself is smooth, the reflection is specular. The angle of incidence of the radio beam is equal to the angle of reflection, and the wave of secondary emission does not return to the radar station (unless the wave strikes the surface perpendicularly).

If the linear dimensions of the object's surface are large as com-

pared with the wavelength, and the surface itself is rough, reflection is diffuse. Because of the different orientations of the surface elements, the electromagnetic waves are here reflected in different directions, including the direction of the radar station. The so-called "resonance reflection" is equally favorable for radar observation. This type of reflection is observed when the linear dimensions of the reflecting object or their elements are equal to an odd number of half-waves. In contrast to diffuse reflection, secondary resonance emission usually possesses high intensity and sharply defined directivity, depending upon the construction and orientation of the reflecting element. The intensity of reflection will depend substantially upon the angle between the electrical field intensity vector and the axis of the element.

When the wavelength of the radar station is large in comparison with the linear dimensions of the target, the incident wave envelops the target and the intensity of the reflected wave is insignificantly small.

From the point of view of the shaping of the structure of signals during reflection, a number of different types of objects (targets) are encountered in radar practice. In this connection one may first of all isolate individual objects of the simplest geometrical form whose dimensions are small in comparison with the transverse dimensions of the antenna beam and with quantity $c\tau_1/2$ (dimensions of the volume to be resolved). The reflective properties of such objects may, as a rule, be determined theoretically and foretold accurately for each relative position of the target being viewed and the radar station.

Under actual conditions of radar observation targets of the simplest type are encountered rather rarely. More frequently one encounters either objects of complex shape consisting of a whole series of

reflective elements which are tightly bound to one another, or with a group of objects arbitrarily distributed in a particular area of space. As examples of targets of complex shape may be given airplanes, ships, various structures, etc. Representative targets of the second type are targets which are distributed with regard either to volume or to surface. Typical complex targets and elementary objects of the simplest shape occupy an insignificant part of the volume of resolution when they are at great distances from the RLS. For this reason they are viewed as point-shaped. The concept of the point-shaped target is derived from purely geometrical considerations and has nothing to do with the question of the shape of the reflected signal, which is determined by the physical properties of the object and by the relation between its dimensions and the wavelength.

A volume-distributed target represents a collection of a number of reflective elements which are relatively close to one another and occupy a comparatively large area of space. The dimensions of this area may greatly surpass the dimensions of the antenna beam and minimum range-resolution distance ($c\tau_1/2$). Volume-distributed targets include various hydrometeors, clouds of dipole reflectors, etc.

A particular case of the volume-distributed target is the group target. This consists of several isolated objects the distances between which are less than the resolvable distances. Such group targets may include airplane formations, ship formations, etc.

Individual reflective elements may combine into one comparatively thinner layer which thus forms a surface-distributed target. Such types of targets are encountered during radar scanning of the surface of the earth or sea.

The components of complex or spatially distributed targets are sources of the reflected waves which are summed at the input of the ra-

dar station receiver. The amplitudes of the electromagnetic waves reflected from the individual elements differ from one another, since the elements themselves may possess different reflective properties. And because of the differences between the distances from the radar station to each of the elements, the phases of the reflected waves will also differ from one another.

Because of the arbitrary relative positions of the station and the irradiated target, the relations between the amplitudes and phases of the waves of individual elements will generally be accidental. However, for each fixed position of the RLS and the reflecting objects, the amplitudes and phases of the reflected waves are completely determined quantities. Therefore, in principle, a resultant total reflected signal may be determined for each concrete relative position of the radar station and the target.

The relative position of the target and station usually changes during the process of radar observation. The reasons for such changes may be movement of the radar station together with its carrier, target movement (airplanes, ships), movement of the reflecting elements which form the target (drops of rain, snow, leaves and branches of trees, stubble). Because of the relative displacement of the radar station and the target, the amplitudes and phases of individual reflected waves change continuously, and this gives rise to accidental fluctuations in the intensity of the resultant reflected signals.

## §3.2. THE EFFECTIVE SCATTERING CROSS-SECTION OF THE TARGET (EPR)

Calculation of the range of radar observation requires a quantitative characteristic of the intensity of the reflected wave. The power of the reflected signal at the station receiver input depends upon a whole series of factors and, above all, upon the reflective properties of the target. Radar targets are usually characterized by effective

scattering cross sections $\sigma_{ts}$.

By effective scattering cross section of a target is meant quantity $\sigma_{ts}$ satisfying equation

$$\sigma_{ts}\Pi_1 = 4\pi R^2 \Pi_2,$$

where $\Pi_1$ is the power flux density of the direct wave at the location of the target, $\Pi_2$ is the power flux density of the wave reflected from the target at the radar station antenna, $R$ is the distance from the radar station to the target. It follows from this that the value of the effective scattering cross section may be calculated directly from formula

$$\sigma_{ts} = 4\pi R^2 \frac{\Pi_2}{\Pi_1}. \qquad (3.1)$$

As follows from Formula (3.1), the quantity $\sigma_{ts}$ has the dimensions of area. Therefore, it may be viewed provisionally as a certain plane surface $\sigma_{ts}$, perpendicular to the radio beam and equivalent to the target, which, scattering evenly in all directions all the power incident upon it from the RLS, creates at the point of reception the same power flux density $\Pi_2$ as the actual target.

If the effective scattering cross section $\sigma_{ts}$ of the target is assigned, for known $\Pi_1$ and $R$ the power flux density of the reflected wave

$$\Pi_2 = \frac{\sigma_{ts}\Pi_1}{4\pi R^2},$$

may be calculated, and then, by determining the power of the received signal, the operational range of the radar station may be estimated. Thus, quantity $\sigma_{ts}$ is a quantitative characteristic of the target's reflective properties in the direction of the radar station.

The obtained relation for $\sigma_{ts}$ includes quantities characterizing the field intensities at the target and at the radar station antenna, and also the distance between these points. Quantity $\sigma_{ts}$ does not depend either upon the intensity of the emitted wave or upon the distance

between the target and the station. Actually, any increase in $\Pi_1$ leads to a proportional increase of $\Pi_2$, and their ratio does not change. With change in the distance between the radar station and the target, ratio $\Pi_2/\Pi_1$ changes in inverse proportion to $R^2$, and quantity $\sigma_{ts}$ here remains unchanged. Thus, the effective cross section of the target depends only upon the latter's reflective properties.

Equation (3.1) may be expressed in terms of the electrical field intensity

$$\sigma_{ts} = 4\pi R^2 \frac{E_2^2}{E_1^2}, \qquad (3.2)$$

where $E_1$ is the electrical field intensity of the direct wave at the target; $E_2$ is the electrical field intensity of the reflected wave at the radar station.

It follows from Formulas (3.1) and (3.2) that to determine the magnitude of the target's effective scattering cross section, one must know the field intensity of the direct wave at the target and also the intensity of the reflected wave at the radar station antenna. The task of finding the intensities of the direct and reflected wave may be solved either by calculation or experimentally. The analytical determination of the direct wave field does not usually involve any particular difficulties. However, data on the reflected wave field and quantity $\sigma_{ts}$ may be found theoretically only for targets of the simplest shape.

In principle the effective scattering cross section of targets of complex shape may also be discovered analytically. However, this involves great difficulties. Therefore, in the case of complex targets like the great majority of the actual objects of radar observation, quantity $\sigma_{ts}$ is defined experimentally.

In the case of objects of the simplest shape (sphere, cylinder, a

flat plate, etc.) the size of the effective scattering cross section and its dependence upon the direction of irradiation are sufficiently complete characteristics of the reflective properties of these objects.

In the case of complex and spatially distributed targets, when the resultant signal is shaped as the outcome of the combining of signals of separate reflectors, the effective scattering cross section is subject to fluctuations and is an accidental value. In order to characterize it one must resort to the methods of probability theory and mathematical statistics.

## §3.3. THE LINEAR VIBRATOR

Our examination of the problem of the effective scattering cross section of bodies of the simplest shape will begin with the linear vibrator.

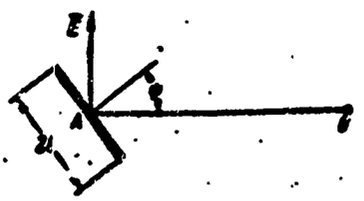

Fig. 3.1. Determining the effective scattering cross section of a linear vibrator.

Let us assume that at some point $A$, where the electrical field strength of a direct wave is $E_1$, there is a linear vibrator of length $2l$, the perpendicular to which forms angle $\psi$ with the direction of the radar station (Fig. 3.1).

It is obvious that in the vibrator will be induced, e.m.f.

$$e = E_1 h_д \cos\psi,$$

where $h_д$ is the effective height of the vibrator.

If the vibrator input impedance is $Z_a$, the e.m.f. will cause current to flow in it

$$I = \frac{E_1 h_д \cos\psi}{Z_a}.$$

The current flow gives rise to a secondary ignition whose electrical field strength in a distant zone at distance $R$ will be

$$E_2 = 60\pi \frac{Ih_д \cos\psi}{R\lambda} = 60\pi \frac{E_1 h_д^2 \cos^2\psi}{\lambda R Z_в},$$

where $\lambda$ is the wavelength.

Knowing field strength $E_1$ and $E_2$, we can determine the effective scattering cross section of the vibrator

$$\sigma_д = 4\pi R^2 \left(\frac{E_2}{E_1}\right)^2 = 4\pi^3 \frac{3600 h_д^4 \cos^4\psi}{\lambda^2 Z_в^2}. \qquad (3.3)$$

In radar practice one encounters electromagnetic wave reflections from bodies whose shapes are similar to that of the vibrator. Such vibrators are very often much shorter than $\lambda$.

In the case of an elementary vibrator for which $2l << \lambda$, the effective height $h_д = l$.

Furthermore, it may be considered that the resistance $R_a$ of the vibrator is approximately equal to its radiation resistance $R_\Sigma$, while the latter is significantly less than the reactance $R_a$. Then the input impedance

$$Z_в = \sqrt{R_в^2 + X_в^2} \approx \sqrt{R_в^2 + X_в^2} \approx X_в = \frac{Z_0}{\operatorname{tg}\frac{2\pi}{\lambda} l},$$

where $Z_0$ is the wave impedance of the vibrator, which is about 1000 ohms for relatively thin, and about 400 ohms for relatively thick vibrators.

Since $l << \lambda$ and $\tan(2\pi/\lambda)l \approx (2\pi/\lambda)l$, it may be considered that quantity

$$Z_в \approx \frac{Z_0 \lambda}{2\pi l}.$$

After subsitution of value $Z_a$ in Expression (3.3) we finally find that the effective scattering cross section

$$\sigma_д \approx 5{,}76 \cdot 10^4 \cdot \frac{\pi^6}{Z_0^2} \frac{l^6}{\lambda^6} \cos^4\psi. \qquad (3.4)$$

As is seen from the formula, quantity $\sigma_{ts}$ is proportional to ratio $l^6/\lambda^4$. This sort of dependence is characteristic both for a small vi-

brator and for other bodies whose dimensions are much smaller than the wavelength. Furthermore, for the vibrator the intensity of reflection is strongly dependent upon the direction of irradiation (polarization of the incident wave).

Another characteristic case is that of reflection of electromagnetic waves from a half-wave vibrator. Dipole reflectors, elements of ships, airplanes, etc. may have properties similar to this.

As is known, the effective height of a half-wave vibrator $h_д = \lambda/\pi$, and its input impedance

$$Z_a = R_a = 73{,}1 \text{ ohms}$$

By substituting values $h_д$ and $Z_a$ in Formula (3.3), we obtain a relationship for calculating the effective scattering cross section of a half-wave vibrator

$$\sigma_д = 0{,}86\lambda^2 \cos^4 \psi. \qquad (3.5)$$

If the half-wave vibrator is parallel to vector $\dot{E}_1$, the intensity of the reflected wave is maximum, and the effective surface of the vibrator,

$$\sigma_{д\,макс} = 0{,}86\lambda^2.$$

On the other hand, when the vibrator is perpendicular to vector $\dot{E}_1$, its effective scattering cross section is equal to zero.

## §3.4. THE METALLIC PLATE

At a sufficient distance from the RLS the wave front near the target may be considered flat. Because of this, calculation of the effective scattering cross section of the target in free space is reduced to an investigation of scattering of a flat wave by the target. Such a problem may be precisely solved only for a sphere, and approximately solved for some bodies of very simple shape.

Let us assume that a flat electromagnetic wave falls perpendicularly upon a metallic plate with a mirror surface whose dimensions are

much greater than the wavelength. The power of the incident wave will be $\Pi_1 S$, where $\Pi_1$ is the power flux density of the incident electromagnetic wave at the plate, and $S$ is the cross section of the metallic plate.

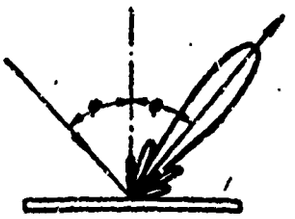

Fig. 3.2. Diagram of reflection from a flat metallic plate.

The effect of the incident wave is to cause build-up of currents in the plate which coincide in phase and amplitude at any point of the plate. Thus, the field of the plate's secondary emission will be equivalent to the field of a cophased antenna with gain factor

$$G=4\pi\frac{S}{\lambda^2}.$$

The power flux density of the reflected wave at the radar station

$$\Pi_2=\frac{\Pi_1 S}{4\pi R^2}G,$$

or, after substitution of value $G$,

$$\Pi_2=\frac{\Pi_1 S^2}{\lambda^2 R^2}.$$

On the basis of Formula (3.1) the effective scattering cross section of a metallic plate perpendicular to the direction of the radar station

$$\sigma_n=4\pi\frac{S^2}{\lambda^2}. \qquad (3.6)$$

The value of the $\sigma_{ts}$ of a metallic plate at normal incident of a wave is proportional to the square of its cross section. This can be explained physically by the fact that with increase in $S$, in the first place, the power of the reflected wave grows, and, in the second place, the directivity of the secondary emission also increases. As the direction of incidence of the wave deviates from the perpendicular, the value $\sigma_{ts}$ alters sharply, and the diagram of secondary ratiation (scattering) of the plate becomes globe shaped.

The greater part of the power of the reflected wave is contained in the major lobe, and only a small part goes into the side lobes. If the direct wave forms angle $\psi$ with the direction perpendicular to the plane of the plate, the axis of the major lobe of the diagram of secondary emission will also be displaced by angle $\psi$ to the opposite side of the perpendicular (Fig. 3.2).

## §3.5. METALLIC AND DIELECTRIC SPHERES

A body in the form of a sphere is a very characteristic object of radar observation. Elements of various targets, exploratory balloons, hydrometeors, etc. may take this shape.

The character of electromagnetic reflection from a sphere depends upon the relationship between its diameter and the wavelength of the oscillations, and also upon the material of which it is constructed.

Let us first examine a sphere whose diameter $d_{sh}$ is much smaller than wavelength $\lambda$. Such a sphere behaves like an electrical vibrator of small dimensions. Just as in the case of the vibrating element, the effective scattering cross section of a small sphere is proportional to ratio $d^6_{sh}/\lambda^4$.

The effective scattering surface of a metallic sphere of small diameter is determined by formula

$$\sigma_{\text{м}} = 690 \frac{d^6_{\text{ш}}}{\lambda^4}. \qquad (3.7)$$

And in the case of a dielectric sphere of small dimensions

$$\sigma_{\text{м}} = 306 \frac{d^6_{\text{ш}}}{\lambda^4} \left( \frac{\varepsilon' - 1}{\varepsilon' + 2} \right)^2. \qquad (3.8)$$

If the small sphere is a drop of water, its relative specific inductive capacitance $\varepsilon' \approx 80 \gg 1$ and, consequently

$$\sigma_{\text{м}} \approx 306 \frac{d^6_{\text{ш}}}{\lambda^4}. \qquad (3.9)$$

Let us now examine the reflection of electromagnetic waves by a

sphere whose diameter is much greater than the wavelength. In this case analysis is based upon the methods of geometrical optics.

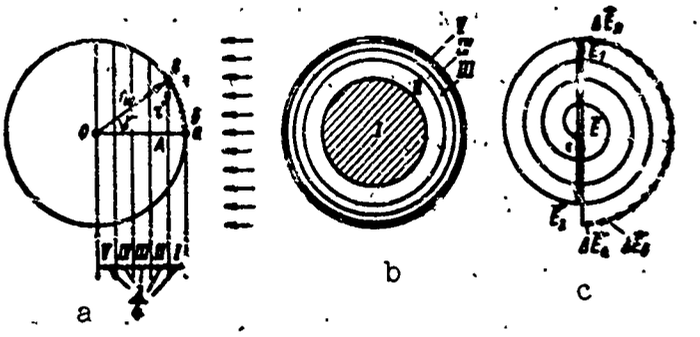


Fig. 3.3. Analysis of the reflection of electromagnetic waves from a sphere of large dimensions: a and b) Fresnel zones on the surface of the sphere; c) determining the resultant electrical field strength.

Let us assume that a flat electromagnetic wave of length $\lambda$ is incident upon an ideally conducting sphere of radius $r_{sh}$. Let us divide the surface of the sphere into Fresnel zones (Fig. 3.3a). The depth of each zone in the direction of incidence of the electromagnetic wave must be $\lambda/4$. The difference in the traces of the beams to the edges of each zone and back will be $\lambda/2$, and the corresponding difference between the phases of the reflected oscillations will equal to $\pi$.

Field strength $E$ of the reflected wave is equal to the sum of the field strength of the component waves reflected from the various Fresnel zones. Considering that the phases of the waves reflected from adjacent Fresnel zones are shifted by $\pi$, the following equality may be written for the resultant electrical field strength

$$E = E_1 - E_2 + E_3 - E_4 + \ldots,$$

where $E_1$, $E_2$, ... are the component field produced by the action of the corresponding Fresnel zones.

Despite the fact that the cross sections of the Fresnel zones are

equal, being surfaces of spherical belts of identical altitude, the intensities of the waves reflected from them will differ. This is due to the different slopes of the zone surfaces relative to the direction of incidence of the wave. The larger the number of the Fresnel zone, the smaller the strength of the wave reflected from it, that is,

$$E_1 > E_2 > E_3 > E_4 > \ldots > E_n.$$

Considering what has been written above we may write that

$$E = E_1 - (E_2 - E_3) - (E_4 - E_5) - \ldots - (E_{n-1} - E_n). \qquad (3.10)$$

In Relationship (3.10) all the differences enclosed in parentheses are positive. Therefore the strength of resultant field $E$ will be less than the field $E_1$ created by the reflection from one first Fresnel zone.

In order to conduct a quantitative evaluation of the field strength of the reflected wave we add the field intensities produced by various sections of the surface of the sphere, taking into account the phase difference. To do this the whole surface of the sphere is broken up into very small sections – spherical belts (Fig. 3.3a). Each of these sections creates a reflected wave whose intensity and phase will be characterized by the length and direction of the elementary vector $\Delta\dot{E}_i$ (Fig. 3.3c). Thus, vector $\Delta\dot{E}_a$ corresponds to lower section "a" of the first Fresnel zone, to section "b" corresponds $\Delta\dot{E}_b$ which is turned through a rather small angle relative to vector $\Delta\dot{E}_a$, etc. Vector $\Delta\dot{E}_{ya}$, corresponding to the upper element of the first Fresnel zone, point in the opposite direction to vector $\Delta\dot{E}_a$.

By summing elementary vectors $\Delta\dot{E}_i$, we find the strength of field $\dot{E}_1$, created by the first zone. Here, in the case of elements of infinitely small value, the broken line is transformed into an arc resting upon vector $\dot{E}_1$.

If we add up the field determined by the elements of the second

zone, we obtain vector $\dot{E}_2$, which is shorter than vector $\dot{E}_1$. After summing the fields of the elements of all the Fresnel zones we obtain a diagram (Fig. 3.3c) from which it is seen that the resultant field strength is equal to half the field strength of the wave formed during reflection from only one first zone

$$E = \frac{1}{2} E_1.$$

The field strength of the wave reflected from the first Fresnel zone, with a spherical surface, is $\pi/2$ times smaller than the strength of electrical field $E_{1\ vid}$, which arises when the wave is reflected from a flat plate with the same apparent cross section $S_{1\ vid}$ (Fig. 3.3b) as in the first zone:

$$E_1 = \frac{E_{1\ vid}}{\left(\frac{\pi}{2}\right)}.$$

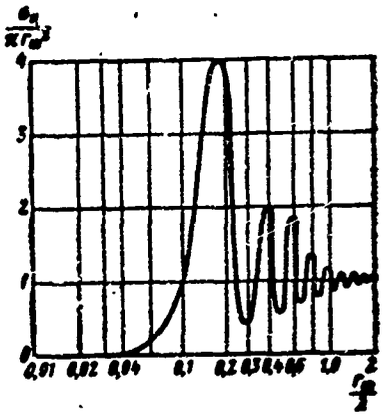


Fig. 3.4. Dependence of the effective scattering cross section of a sphere upon the relationship between its radius and the wavelength.

Correspondingly, for the voltage of the resultant field of a wave reflected from a sphere,

$$E = \frac{1}{2} E_1 = \frac{E_{1\ vid}}{\pi}.$$

Since the effective cross sections of objects are related as the

squares of the voltages of the waves reflected from the objects, between value $\sigma_{ts}$ of a sphere and the effective surface of scattering $\sigma_{1\ vid}$ of plane surface $S_{1\ vid}$ there exists the relationship

$$\sigma_{\text{п}} = \frac{1}{\pi^2}\sigma_{1\ \text{вид}}.$$

The apparent cross section of the first Fresnel zone

$$S_{1\ \text{вид}} = \pi(r')^2.$$

It follows from triangle *OAB* (see Fig. 3.3a) that at $r_{sh} >> \lambda$

$$r' = r_{\text{м}}\sqrt{1-\left(1-\frac{\lambda}{4r_{\text{м}}}\right)^2} \approx \sqrt{\frac{r_{\text{м}}\lambda}{2}}.$$

Consequently, the apparent cross section of the first zone

$$S_{1\ \text{вид}} = \pi r_{\text{м}}\frac{\lambda}{2}.$$

The effective scattering cross section of plane surface $S_{1\ vid}$ will, in accordance with Formula (3.6), be

$$\sigma_{1\ \text{вид}} = \pi^2 r_{\text{м}}^2.$$

Hence the effective scattering cross section of a large sphere

$$\sigma_{\text{п}} = \frac{1}{\pi^2}\sigma_{1\ \text{вид}} = \pi r_{\text{м}}^2. \qquad (3.11)$$

Thus, the effective scattering surface of a sphere of large dimension is the same as its apparent cross section.

From the example of a sphere it becomes quite apparent that the character of the reflection of electromagnetic waves changes as a function of the relationship between the dimensions of the body and the wavelength (Fig. 3.4).

At $r_{sh} << \lambda$ diffraction phenomena predominate, and the sphere acts like an elementary electrical vibrator. The intensity of the reflections is small, and the effective scattering cross section changes in proportion to ratio $r^6_{sh}/\lambda^4$. As ratio $r_{sh}/\lambda$ increases, $\sigma_{ts}$ increases monotonously until the point at which the dimensions of the sphere become commensurable with the wavelength, as a result of which resonance

phenomena occur during reflection. If $r_{sh} = \lambda/4$, the reflected wave is shaped by only first Fresnel zone, and therefore the ratio $\sigma_{sh}/\pi r^2_{sh}$ reaches its maximum possible value, approximately equal to four.

Further increase in ratio $r_{sh}/\lambda$ leads to the appearance, within the limits of the sphere, of an area corresponding to the second Fresnel zone. Because of this, as ratio $r_{sh}/\lambda$ grows, $\sigma_{ts}$ will decline. Then, with the appearance of sections corresponding to the third zone, $\sigma_{ts}$ will begin to grow, etc. Thus, the change in ratio $\sigma_{ts}/\pi r^2_{sh}$ with those of $r_{sh}/\lambda$ is oscillatory. And with the increase in $r_{sh}/\lambda$ the sweep of the oscillations is reduced (Fig. 3.4), and at $r_{sh}/\lambda \approx 1.6$ the value of the effective scattering cross section becomss practically equivalent to the cross section of a transverse section of the sphere.

Reflection from a sphere is a particular case of scattering of electromagnetic waves by a curvilinear surface. In general, in the case of an ideal reflecting surface whose dimensions are considerably greater than the wavelength, the effective scattering cross section is determined by expression

$$\sigma_{\text{э}} = \pi r_1 r_2, \qquad (3.12)$$

where $r_1$ and $r_2$ are the principal radii of the curve.

In the particular case of a spherical surface for which $r_1 = r_2$, Formula (3.12) becomes Formula (3.11).

## §3.6. ARTIFICIAL REFLECTORS

It is very often necessary to employ artificial devices which, under irradiation from various directions, form intensive reflected signals. Such devices may be corner reflectors and dielectric reflectors.

Corner reflectors are broadly applied in practice. They are used for radar orientation and may also be used for radar camouflage. Corner reflectors are a combination of three mutually perpendicular specular reflecting facets.

The most important property of corner reflectors is their ability intensively to reflect waves incident from various directions. At various angles of incidence of the electromagnetic wave the corner reflectors act like a flat plate which is perpendicular to the direction of the RLS.

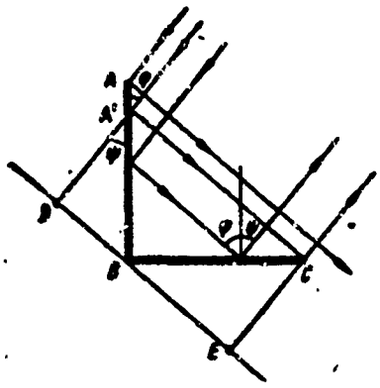

Fig. 3.5. Path of beam in a two-facet corner reflector.

The process of shaping a reflected wave may be most simply examined from the example of a corner reflector made up of two mutually perpendicular facets (Fig. 3.5).

We will consider that the direction of propagation of the incident electromagnetic wave is perpendicular to the rib of the two-facet reflector. Since the dimensions of the corner reflector must be much greater than the wavelength, we may utilize the methods of geometrical optics. Then determining the effective scattering cross section of a corner reflector for each possible direction of arrival of a radio beam is reduced to discovery of the equivalent flat plate perpendicular to the beam.

a b

Fig. 3.6. Path of beams in three-facet corner reflectors.

Analysis of the possible trajectories of radio beams perpendicular to the rib of the reflector leads to the conclusion that not all the beams which are captured by the corner reflector are actually reflected from its two facets and returned. As can be seen from Fig. 3.5, at angle of incidence $\psi$ only those beams are reflected back which strike the facets within the limits of sections $A'B$ and $BC$. Beams striking section $AA'$ are reflected only from facet $AB$ and do not return. Thus, the trace of the plane surface equivalent to

the corner reflector and perpendicular to the incident beams is given in the plane of the drawing by *DE* (Fig. 3.5).

On the basis of the designs given in Fig. 3.5 the cross section of an equivalent plate, with facet cross section $S_{gr}$, is determined by expression

$$S_э = 2S_{гр} \sin\varphi.$$

The effective scattering cross section of the equivalent plate and of the whole corner reflector

$$\sigma_{ц} = 4\pi \frac{S_э^2}{\lambda^2} = 16\pi \frac{S_{гр}^2}{\lambda^2} \sin^2\varphi. \qquad (3.13)$$

The obtained correlation is true for angles $\psi < 45°$. At angle $\psi > 45°$ the factor $\sin\psi$ should be replaced in Formula (3.13) by $\cos\psi$. Maximum values of $S_e$ and $\sigma_{ts}$ occur at $\psi = 45°$, that is, when the incident beams are parallel to the bisector of the reflector angle. In this case all the beams captured by the reflector are returned, and formulas

$$S_{э\,макс} = \sqrt{2} \cdot S_{гр},$$

$$\sigma_{ц\,макс} = 8\pi \frac{S_{гр}^2}{\lambda^2}.$$

are true.

The two-facet corner reflector is not very effective since, if the incident beam deviates from the plane perpendicular to the rib, the reflected beam does not return to the radar station. For return of the beam regardless of the direction of incidence of the wave, it is generally necessary to employ triple reflection from three mutually perpendicular planes. For this reason, three-facet corner reflectors are used in practice (Fig. 3.6).

The formula for the effective scattering cross section of a three-facet corner reflector is also found by determining the cross section of an equivalent flat plate. The cross section of an equivalent flat

plate reaches its maximum value when the direction of incidence of the wave coincides with the direction of the axis of symmetry of the corner reflector. In this case the effective cross section of a corner reflector with triangular facets

$$\sigma_{\text{ц}} = \frac{4}{3}\pi\frac{l^4}{\lambda^2}, \qquad (3.14)$$

and, for a reflector with square facets

$$\sigma_{\text{ц}} = 12\pi\frac{l^4}{\lambda^2}, \qquad (3.15)$$

here $l$ is the length of the reflector rib.

A comparison of Formulas (3.14) and (3.15) indicates that, with ribs of identical length, the effective cross section of a corner reflector with square facets is nine times greater than that of a triangular reflector. However, reflectors with triangular facets have been most widely used in practice. This is because they have a broader diagram of reflection than reflectors with rectangular facets, and their facets are more rigid. The latter circumstance is extremely important since the effectiveness of a reflector depends very greatly upon the ability of its corner facets to retain their strict perpendicularity.

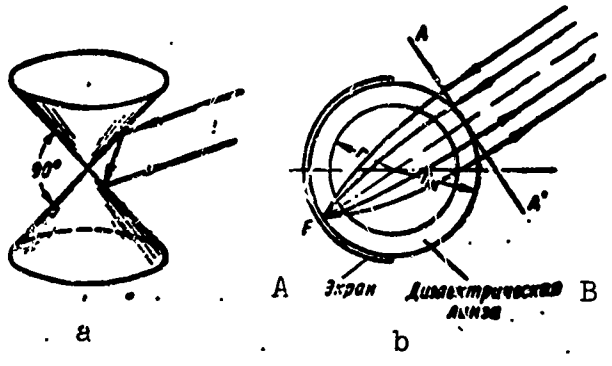


Fig. 3.7. Biconic reflector (a) and dielectric Luneberg lens (b). A) Screen; B) dielectric lens.

The corner reflects electromagnetic waves within the limits of one

quadrant. However, it is sometimes necessary to install an artificial reflector with broad diagrams of secondary emission in the horizontal and vertical planes. This task is usually solved by grouping several reflectors together. The result is a system yielding a sufficiently even reflection when beamed from several directions.

In radar practice cases are encountered when the elements of artificial structures form angular reflectors. The most frequently encountered formations are of the two-facet reflector types. The consequence of this is an increase in the observation range of railroad and road embankments, excavations, and also certain industrial structures.

In addition to corners, biconic reflectors (Fig. 3.7a) may be used as artificial reflectors. In reflectors of this type the path of the beam is analogous to the path of the beam in the two-facet corner reflector. However, in this case a change in the direction of arrival of the wave in the plane parallel to the bases of the cones causes no variation in the effectiveness of the reflector. Because they are complex to manufacture, biconic reflectors have not yet seen widespread use.

Another type of artificial reflector is the Luneberg dielectric lens, which is spherical in shape (Fig. 3.7b). Depending upon the distance to the center of the lens, the diffraction factor of the lens dielectric should vary according to the law

$$n(r)=\sqrt{2-\left(\frac{r}{r_{sh}}\right)^2},$$

where $r_{sh}$ is the radius of the lens. Half of the lens is covered with a metallic screen.

Parallel beams striking such a lens are focused at a point on the external surface of the sphere. This focal point $F$ is diametrically opposed to the point at which the flat front of the incident wave contacts the lens.

The beams which collect at the focal point are reflected from the screen and, after passing again through the dielectric sphere, form a bunch of parallel beams heading in the direction of the RLS. Thus, the Luneberg lens very effectively reflects back the waves which strike it at various angles. Because they are complicated to manufacture and expensive, such reflectors have as yet found limited practical application.

## §3.7. DENSITY OF AMPLITUDE DISTRIBUTION OF THE SIGNALS OF FLUCTUATING TARGETS

Before passing to an examination of the characteristics of the reflection of electromagnetic waves from the fundamental types of complex and spatially distributed targets, let us discuss the statistical characteristics of signals of such objects and their effective scattering cross section.

Since the signals and the effective scattering cross sections of complex and distributed targets are subject to random fluctuations, they may be characterized by using the methods of probability theory. In this way the statistical properties of signals of the effective cross sections of targets may be adequately described:

- by the laws of distribution,
- by the spectrum of fluctuation (autocorrelation function).

In this paragraph we will discuss the density of amplitude distribution of the signals of fluctuating units.

Let us assume that a complex or distributed target consists of a large number of arbitrarily distributed elements. The target contains an element (shining or bright spot, stable target) giving off a stable reflected signal whose amplitude exceeds the sum of the amplitudes of all other elements. In contrast to the shining spot, the amplitudes and phases of the signals of other elements undergo random variations dur-

ing relative displacements of the target and the RLS.

Such conditions may be fulfilled during observation of single intensively and steadily deflecting objects on a background of a spatially distributed target (hydrometeors, dipole noises, earth's surface). Furthermore, one may encounter cases in which the complex target (a ship, airplane, structure) contains an intensively and steadily reflecting element (bright spot).

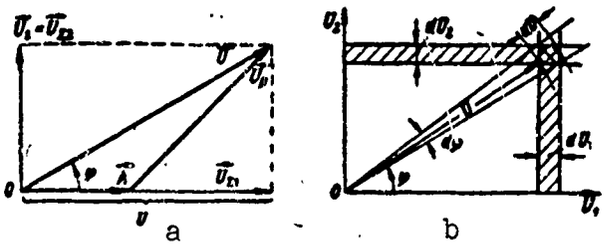

Fig. 3.8. Derivation of the distribution function of the resultant signal amplitude: a) vector representation of the signal; b) calculation of the probability that a random vector will strike an elementary section.

Taking into account the accepted conditions for the strength of the resultant signal, we may write

$$u = A\cos\omega t + \sum_{k=1}^{n} U_k \cos(\omega t - \varphi_k), \qquad (3.16)$$

where $A$ is the signal amplitude of a target or a bright spot; $U_k$ is the signal amplitude of the $k$th element; $\varphi_k$ is the phase shift of the signal of the $k$th element.

If the resultant amplitude of the sum of random elementary signals is denoted by $U_\Sigma$, and the phase by $\varphi_\Sigma$, Expression (3.16) takes the form

$$u = A\cos\omega t + U_\Sigma \cos(\omega t - \varphi_\Sigma). \qquad (3.17)$$

We expand oscillation

$$u_\Sigma = U_\Sigma \cos(\omega t - \varphi_\Sigma)$$

into its two orthogonal components of which the cosinusoidal component coincides in phase with the signal of the stable target (bright spot):

$$
\left.
\begin{aligned}
&u_\Sigma = U_{\Sigma 1}\cos\omega t + U_{\Sigma 2}\sin\omega t,\\
&\text{where}\\
&U_{\Sigma 1} = U_\Sigma\cos\varphi_\Sigma = \sum_{k=1}^{n} U_k\cos\varphi_k,\\
&U_{\Sigma 2} = U_\Sigma\sin\varphi_\Sigma = \sum_{k=1}^{n} U_k\sin\varphi_k,\\
&U_\Sigma = \sqrt{U_{\Sigma 1}^2 + U_{\Sigma 2}^2},\\
&\operatorname{tg}\varphi_\Sigma = \frac{U_{\Sigma 2}}{U_{\Sigma 1}}.
\end{aligned}
\right\} \qquad (3.18')
$$

Representing oscillations with amplitudes $A$, $U_{\Sigma 1}$, $U_{\Sigma 2}$ by vectors, we may show their interaction by diagram (Fig. 3.8a).

The cosinusoidal component of random signal $U_\Sigma$, together with the signal of the bright spot which is constant in value and coincident in phase, yields resultant vector

$$\vec{U}_1 = \vec{A} + \vec{U}_{\Sigma 1}.$$

The sinusoidal component of the random signal is accordingly represented by vector

$$\vec{U}_2 = \vec{U}_{\Sigma 2},$$

which is orthogonal to vector $\vec{U}_1$.

It is obvious that the amplitudes of orthogonal components $U_1$ and $U_2$ are independent quantities - variation of one has no influence on variation of the other.

Vector $\vec{U}$ (Fig. 3.8a), which is equal to the geometrical sum of the orthogonal components $\vec{U}_1$ and $\vec{U}_2$, represent the resultant signal

$$u = U\cos(\omega t - \varphi) = A\cos\omega t + U_\Sigma\cos(\omega t - \varphi_\Sigma), \qquad (3.19)$$

whose amplitude $U$ and phase $\varphi$ are random quantities.

We are interested, above all, in variations of the amplitude $U$ of the random total signal. To find the law of the probability distribution of this random quantity, we proceed in the following way.

With variations in the relative positions of the radar station and the target, the distances to the elementary reflectors and the effective scattering cross sections of the latter will also vary. This caus-

es random variation in the phases and amplitudes of the reflected signals. Consequently, the amplitudes of components $U_{\Sigma 1}$ and $U_{\Sigma 2}$ will also vary in a random manner.

Each of these components is the result of the addition of a large number of elementary signals for which the central limiting theorem of probability theory is true. It may therefore be considered that random amplitudes $U_{\Sigma 1}$ and $U_{\Sigma 2}$ of the orthogonal component are subordinated to the normal distribution law

$$\left.\begin{aligned} W(U_{\Sigma 1}) &= \frac{1}{\sqrt{2\pi}\cdot\sigma_1}\exp\left[-\frac{U_{\Sigma 1}^2}{2\sigma_1^2}\right], \\ W(U_{\Sigma 2}) &= \frac{1}{\sqrt{2\pi}\cdot\sigma_2}\exp\left[-\frac{U_{\Sigma 2}^2}{2\sigma_2^2}\right], \end{aligned}\right\} \qquad (3.20)$$

where $\sigma_1^2$ and $\sigma_2^2$ are the amplitude dispersions of the orthogonal components.

Considering the physical symmetry of the expansion of the random resultant strength into its orthogonal components, it can be maintained that dispersions $\sigma_1^2$ and $\sigma_2^2$ are equal, that is

$$\sigma_1^2 = \overline{U}_{\Sigma 1}^2 = \sigma_2^2 = \overline{U}_{\Sigma 2}^2 = \sigma^2.$$

When the laws of distribution of random amplitudes $U_{\Sigma 1}$ and $U_{\Sigma 2}$ are known, the laws of distribution for the amplitudes of orthogonal components $U_1$ and $U_2$ can be determined. The average values of these components are, accordingly,

$$\begin{aligned} \overline{U}_1 &= A, \\ \overline{U}_2 &= 0. \end{aligned}$$

Quantities $U_1$ and $U_2$ themselves undergo, relative to their average values, random oscillations in accordance with the normal law of distribution

$$\left.\begin{aligned} W(U_1) &= \frac{1}{\sqrt{2\pi}\cdot\sigma}\exp\left[-\frac{(U_1-A)^2}{2\sigma^2}\right], \\ W(U_2) &= \frac{1}{\sqrt{2\pi}\cdot\sigma}\exp\left[-\frac{U_2^2}{2\sigma^2}\right]. \end{aligned}\right\} \qquad (3.21)$$

Orthogonal components $U_1$ and $U_2$ are statistically independent. Therefore the two-dimensional density of the probability of random quantities $U_1$ and $U_2$ is equal to product

$$W(U_1, U_2) = W(U_1)\,W(U_2) = \frac{1}{2\pi\sigma^2}\exp\left[-\frac{(U_1 - A)^2 + U_2^2}{2\sigma^2}\right]. \quad (3.22)$$

In this case we are interested in the one-dimensional law of probability distribution of resultant amplitude $U$. We will find this distribution by using Relationship (3.22) for which we turn to Fig. 3.8b.

The probabilities that quantities $U_1$ and $U_2$ will be found within the limits of elements $dU_1$ and $dU_2$ are, accordingly, $W(U_1)dU_1$ and $W(U_2)dU_2$. Consequently, the probability that resultant amplitude $U$ will be located within the limits of rectangular element $dU_1dU_2$ shaded in Fig. 3.8b is

$$W(U_1, U_2)\,dU_1dU_2 = W(U_1)\,W(U_2)\,dU_1dU_2. \quad (3.23)$$

Amplitude $U$ and phase $\varphi$ of the resultant reflected signal are random polar coordinates of the point which we were examining in the coordinate system $U_1$, $U_2$. We will therefore go on to the law of distribution of probability density in polar coordinates $U$ and $\varphi$. Inasmuch as the form of the elementary section plays no role in transformation of the coordinates, we may write

$$dU_1dU_2 = UdUd\varphi.$$

Here, for corresponding elements of probability, the equation

$$W(U_1, U_2)\,dU_1dU_2 = W(U, \varphi)\,dUd\varphi. \quad (3.24)$$

applies.

From an examination of Fig. 3.8a it follows that in the numerator of the exponent of Formula (3.22) there is an expression for the square of the quantity of vector $U_p$ which, from the theorem of cosines,

$$U_p^2 = U^2 + A^2 - 2UA\cos\varphi. \quad (3.25)$$

Then, taking into account Relationships (3.24) and (3.25) we may write

$$W(U,\varphi)\,dU\,d\varphi=\frac{U\,dU\,d\varphi}{2\pi\sigma^2}\exp\left[-\frac{U^2+A^2-2AU\cos\varphi}{2\sigma^2}\right].$$

Whence the two-dimensional distribution of probability

(3.26)

We find the probability density of random resultant amplitude $U$ by averaging the two-dimensional distribution $W(U,\varphi)$ through integration over all possible values of phase $\varphi$ from 0 to $2\pi$:

$$W(U)=\int_0^{2\pi}W(U,\varphi)\,d\varphi=$$
$$=\frac{U}{\sigma^2}\exp\left[-\frac{U^2+A^2}{2\sigma^2}\right]\frac{1}{2\pi}\int_0^{2\pi}\exp\left[\frac{AU}{\sigma^2}\cos\varphi\right]d\varphi. \qquad (3.27)$$

It is well known that the integral written above

$$\frac{1}{2\pi}\int_0^{2\pi}\exp\left[\frac{AU\cos\varphi}{\sigma^2}\right]d\varphi=I_0\left(\frac{AU}{\sigma^2}\right), \qquad (3.28)$$

where $I_0(AU/\sigma^2)$ is the Bessel function of the null order from the imaginary argument.

Substituting Relationship (3.28) in Formula (3.27), we come to the expression for the probability density of the amplitude of the resultant signal

$$W(U)=\frac{U}{\sigma^2}\exp\left[-\frac{U^2+A^2}{2\sigma^2}\right]I_0\left(\frac{AU}{\sigma^2}\right), \qquad (3.29)$$

which is called the generalized Relay distribution.

In the absence of a stable signal component $A = 0$ and $I_0(AU/\sigma) = I_0(0) = 1$. As a result of this the probability density of the resultant amplitude of the signals of random reflectors will be determined by the simple Relay law

$$W(U)=\frac{U}{\sigma^2}\exp\left[-\frac{U^2}{2\sigma^2}\right]. \qquad (3.30)$$

Distributions (3.29) and (3.30) may be written in a more general form by introducing relative quantities

$$a=\frac{A}{\sigma},\quad v=\frac{U}{\sigma},\quad dv=\frac{dU}{\sigma}. \tag{3.31}$$

After transformations, we pass from Distributions (3.29) and (3.30) to the distributions for the relative quantity $v$

$$W(v)=v\exp\left[-\frac{v^2+a^2}{2}\right]I_0(av), \tag{3.32}$$

$$W(v)=v\exp\left[-\frac{v^2}{2}\right]. \tag{3.33}$$

Figure 3.9 gives the distribution curves (3.32) and (3.33) constructed for various values of relative quantity $a$ of the amplitude of the stable component. It follows from the curves that when the stable component is large, the law of distribution is normalized.

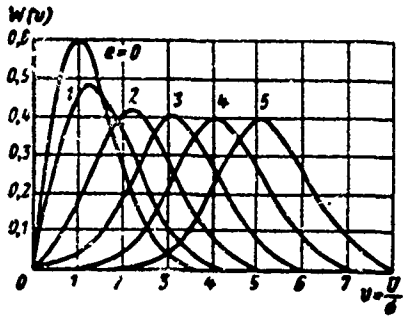


Fig. 3.9. Distribution curves of resultant amplitudes of signals.

In the absence of a stable component the total signal is formed by addition of only the signals of random reflectors. The average relative value of the amplitude of this signal

$$\bar{v}=\int_0^\infty v\exp\left[-\frac{v^2}{2}\right]dv=\sqrt{\frac{\pi}{2}},$$

and the dispersion of the relative amplitude

$$\overline{(v-\bar{v})^2}=\frac{4-\pi}{2}.$$

For a complete characteristic of the total received signal it is still necessary to examine the distribution law of resultant phase $\varphi$. To this end we write two-dimensional distribution $W(v, \varphi)$, taking into consideration initial expression (3.26) and introduce designations:

$$W(v, \varphi)=\frac{v}{2\pi}\exp\left[-\frac{v^2+a^2}{2}\right]\exp(av\cos\varphi). \tag{3.34}$$

By averaging (3.34) over all possible values of $v$ from zero to in-

finity, we obtain a distribution for the resultant phase of the total signal

$$W(\varphi) = \frac{1}{2\pi} \exp\left[-\frac{a^2}{2}\right] + \frac{a\cos\varphi}{\sqrt{2\pi}} \Phi(a\cos\varphi) \exp\left[-\frac{a^2\sin^2\varphi}{2}\right], \quad (3.35)$$

where the Laplace function is designated

$$\Phi(z) = \frac{1}{2\pi} \int_{-\infty}^{z} e^{-\frac{t^2}{2}} dt.$$

The obtained distribution is shown on Fig. 3.10. In the absence of a stable component ($a = 0$) the total signal is formed from the addition of random components, and all phases are equally probable. As the amplitude of stable component $a$ increases, the phase of the resultant signal differs less and less from the phase of this component.

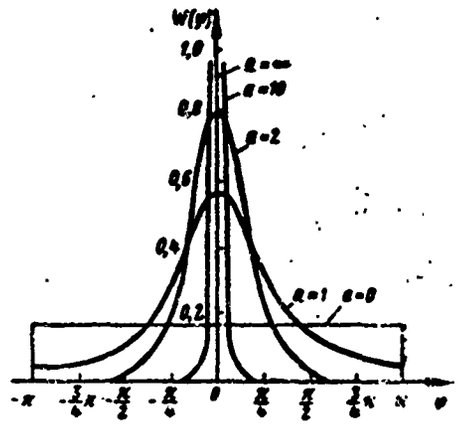


Fig. 3.10. Distribution of the probability density of the phase of the resultant signal.

## §3.8. DISTRIBUTIONS OF SIGNAL POWER AND OF THE TARGET EFFECTIVE SCATTERING CROSS-SECTION

In analyzing the range of radar observation we will be interested in the problem of the power of the reflected signal and the laws of its fluctuation. In this section, utilizing the generalized Relay distribution for amplitudes (3.29), we will establish the distribution law of probability density for the resultant signal power.

As a preliminary step let us explain the physical meaning of dispersion $\sigma^2$ in Expression (3.29). According to the definition given before, one may write

$$\sigma^2 = \overline{U_{\Sigma 1}^2} = \overline{U_{\Sigma 2}^2} = \frac{\overline{U_\Sigma^2}}{2},$$

where $U_\Sigma$ is the resultant amplitude of the sum of random elementary signals. However, $\overline{U_\Sigma^2}/2$ is the average value of the power $P_\Sigma$ of the sum of random reflector signals, which is derived from a resistance of one ohm. Thus, dispersion is equal to the average value of the power of the total signal of the random reflectors.

The power of the resultant signal, obtained on a one ohm resistance, $P = U^2/2$ and, accordingly, $dP = UdU$. In an analogous manner, the power of the stable component of the signal $P_0 = A^2/2$ and $UA = 2\sqrt{PP_0}$.

On the basis of the equality of probability elements which correspond to one another $W(P)dP = W(U)dU$ and utilizing Distribution (3.29), we may write

$$W(P)\,dP = \frac{UdU}{\sigma^2}\exp\left[-\frac{U^2+A^2}{2\sigma^2}\right] I_0\left(\frac{UA}{\sigma^2}\right) =$$
$$= \frac{dP}{\sigma^2}\exp\left[-\frac{P+P_0}{\sigma^2}\right] I_0\left(\frac{2\sqrt{PP_0}}{\sigma^2}\right).$$

Hence the probability density of the resultant signal power

$$W(P) = \frac{1}{\sigma^2}\exp\left[-\frac{P+P_0}{\sigma^2}\right] I_0\left(\frac{2\sqrt{PP_0}}{\sigma^2}\right). \qquad (3.36)$$

We denote by the letter $m$ the ratio of the power of the stable signal component to the average power of the total signal of random reflectors

$$m = \frac{P_0}{\sigma^2} = \frac{a^2}{2}. \qquad (3.37)$$

Here the average power of the received resultant signal

$$\overline{P} = \sigma^2 + P_0. \qquad (3.38)$$

Utilizing Relationships (3.37) and (3.38) we may write that

$$\sigma^2 = \frac{\overline{P}}{1+m} = \frac{\overline{P}}{1+\frac{a^2}{2}}. \qquad (3.39)$$

Then Distribution (3.36) takes the form

$$W(P) = \frac{1+m}{\overline{P}} \exp\left[-m-(1+m)\frac{P}{\overline{P}}\right] I_0\left[2\sqrt{m(1+m)\frac{P}{\overline{P}}}\right]. \qquad (3.40)$$

If the stable component is absent, $m = 0$ and the power of the resultant signal is distributed according to the exponential law

$$W(P) = \frac{1}{\overline{P}} \exp\left[-\frac{P}{\overline{P}}\right]. \qquad (3.41)$$

The effective target scattering cross-section $\sigma_{ts}$ is proportional to the power of the reflected signal. Taking this circumstance into account and utilizing Formulas (3.40) and (3.41), we obtain the laws of distribution of the effective scattering cross section

$$W(\sigma_{\Sigma}) = \frac{1+m}{\overline{\sigma}_{\Sigma}} \exp\left[-m-(1+m)\frac{\sigma_{\Sigma}}{\overline{\sigma}_{\Sigma}}\right] \times \\ \times I_0\left[2\sqrt{m(1+m)\frac{\sigma_{\Sigma}}{\overline{\sigma}_{\Sigma}}}\right], \qquad (3.42)$$

$$W(\sigma_{\Sigma}) = \frac{1}{\overline{\sigma}_{\Sigma}} \exp\left[-\frac{\sigma_{\Sigma}}{\overline{\sigma}_{\Sigma}}\right], \qquad (3.43)$$

where $\sigma_{ts}$ is the resultant effective scattering cross section of the target; $\overline{\sigma}_{ts}$ is the average value of the resultant effective scattering cross section of the target.

Here parameter

$$m = \frac{a^2}{2} = \frac{1}{2}\frac{A^2}{\sigma^2} = \frac{P_0}{\sigma^2} = \frac{P_0}{\overline{P}_{\Sigma}} = \frac{\sigma_{\Sigma 0}}{\overline{\sigma}_{\Sigma\Sigma}}$$

may also be viewed as the ratio of effective scattering cross section $\sigma_{ts}0$ of a stable reflecting element to the average value of the effective scattering cross section $\overline{\sigma}_{ts\Sigma}$ of all random reflectors.

For relative effective scattering cross section $\sigma_{ts}/\overline{\sigma}_{ts}$ Distributions (3.42) and (3.43) take the form

$$W\left(\frac{\sigma_{\Sigma}}{\overline{\sigma}_{\Sigma}}\right) = (1+m) \exp\left[-m-(1+m)\frac{\sigma_{\Sigma}}{\overline{\sigma}_{\Sigma}}\right] \times$$

$$\times I_0\left[2\sqrt{m(1+m)\frac{\sigma_{ц}}{\bar{\sigma}_{ц}}}\right], \qquad (3.44)$$

$$W\left(\frac{\sigma_{ц}}{\bar{\sigma}_{ц}}\right)=\exp\left[-\frac{\sigma_{ц}}{\bar{\sigma}_{ц}}\right]. \qquad (3.45)$$

Figure 3.11 gives the distribution curves $W(\sigma_{ts}/\bar{\sigma}_{ts})$ for several values of parameter $m$.

In the absence of a stable reflecting element ($m$ = 0) the effective scattering cross section of a number of random reflectors is distributed exponentially. The most probable value of $\sigma_{ts}/\bar{\sigma}_{ts}$ is zero, the probability that $\sigma_{ts}/\bar{\sigma}_{ts} > 1$ is 0.37, while the averaged value of $\sigma/\bar{\sigma}_{ts}$ is about 0.7.

For $m \leq 1$ distribution (3.44) differs from the simple exponential function by very little. As quantity $m$ increases, the maximum appears on the curve $W(\sigma_{ts}/\bar{\sigma}_{ts})$, and the influence of the stable signal component begins to prevail. When $m$ becomes significantly greater than unity, the curve $W(\sigma_{ts}/\bar{\sigma}_{ts})$ approaches the normal law of distribution with maximum at $\sigma_{ts}/\bar{\sigma}_{ts} = 1$.

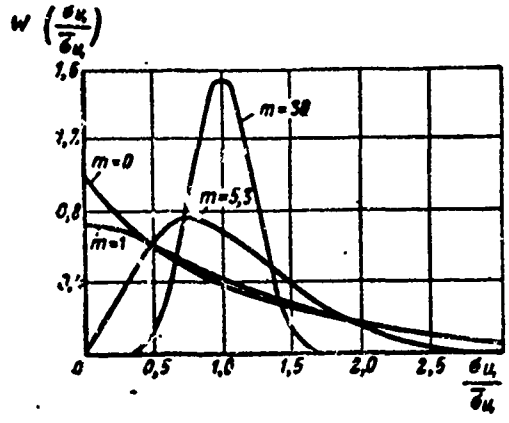


Fig. 3.11. Distribution of effective scattering cross section of a spatially distributed or complex target.

At $m >> 1$ the signal of the stable reflecting element becomes predominant. It considerably exceeds the total signal of the random reflectors and determines the target's effective scattering cross sec-

tion.

## §3.9. THE AUTOCORRELATION FUNCTION AND THE SPECTRUM OF FLUCTUATION OF REFLECTED SIGNALS

In the preceding section we examined the laws of intensity distribution of signals and of the effective scattering cross sections of a number of reflectors taken together. The characteristics obtained make it possible to evaluate the probability of appearance of a given value for amplitude, power, or effective scattering cross section. However, the question still remains unclear how rapidly the fluctuations in these quantities occur. To characterize random changes in signals over time it is advisable to employ the autocorrelation function or the signal spectrum.

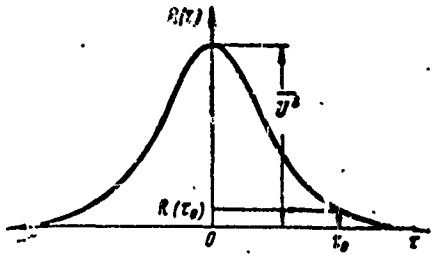

Fig. 3.12. Autocorrelation function.

The statistical connection between the adjacent values of fluctuating strength $U$, separated by time interval $\tau$, may be evaluated using the autocorrelation function

$$R(\tau)=\lim_{T\to\infty}\frac{1}{T}\int_0^T U(t)\,U(t+\tau)\,dt. \qquad (3.46)$$

For a stationary random process the autocorrelation function does not depend upon time $t$ but is a function only of quantity $\tau$.

The maximum connection between the values of the signal, and, accordingly, the largest value for the autocorrelation function, occurs at $\tau = 0$, namely:

$$R(0)=\lim_{T\to\infty}\frac{1}{T}\int_0^T U^2dt=\overline{U^2}.$$

As can be seen, in this case the autocorrelation function equals the average value of the square of the fluctuating strength. As interval $\tau$

increases, the connection between the values of the random strength decreases. These values become increasingly independent statistically, while the autocorrelation function here approaches zero at the limit

$$\lim_{\tau\to\infty} R(\tau)=0.$$

The approach of the autocorrelation function to zero with the increase in the quantity $\tau$ may be both monotonous and oscillatory.

Time interval $\tau = \tau_0$ during which the auto orrelation function reduces to a determined, sufficiently low value, is called the correlation time (Fig. 3.12). The values of the fluctuating strength, separated by interval $\tau > \tau_0$, are considered independent. Sometimes the correlation time is determined as the base of the quadrilateral with altitude $R(0)$ and a cross section equal to the cross section under the curve of the autocorrelation function at $\tau > 0$, that is

$$\tau_0=\frac{\int_0^\infty R(\tau)\,d\tau}{R(0)}.$$

During investigation of the reflected signals of complex and distributed targets the autocorrelation function is usually determined by a tested method. The changes over time of the amplitude or envelope of the reflected signal are written down on film or on paper by a registering device. From the obtained oscillogram a certain section, of length $T$, is selected so as to contain all the most characteristic fluctuations of the quantity investigated. Then, after assigning various values to $\tau$, a special instrument – the correlometer – which performs operation (3.46) is used to calculate the value of the autocorrelation function $R(\tau)$.

In many cases it is more convenient to use the standardized value of the correlation function

$$\rho(\tau)=\frac{R(\tau)}{R(0)}=\frac{R(\tau)}{U^2}.$$

The autocorrelation function is closely connected to the fluctuation spectrum of the signal. While the changes in the amplitude of the fluctuating signal represent a stationary random process $U(t)$, limited by time interval $-T \leq t \leq T$, the current spectrum of amplitude fluctuations is determined by relationship

$$S(f)=\int_{-T}^{T} U(t)\,e^{-j2\pi ft}\,dt.$$

Here the spectral density of fluctuations

$$G(f)=\lim \frac{1}{2T}|S(f)|^2.$$

Quantity $G(f)$ has the dimensionality of the power per unit of band and represents the spectral density of the average power of the process. Here $G(f)df$ is the average power of the signal fluctuations within the limits of infinitely small frequency band $df$.

In accordance with the Khinchin theorem, between the autocorrelation function of the viewed signal and its spectrum there exists a connection described by Fourier transformations

$$\left.\begin{aligned} R(\tau)&=\int_0^\infty G(f)\cos 2\pi f\tau\,df,\\ G(f)&=4\int_0^\infty R(\tau)\cos 2\pi f\tau\,d\tau. \end{aligned}\right\} \qquad (3.47)$$

The presence of this connection results from the fact that both one and the other characteristic describe the viewed process from the point of view of the velocity with which it transpires. A broad spectrum of fluctuations corresponds to a weak statistical connection. On the contrary, when there is a strong statistical connection, the spectrum is narrow. In accordance with this one must bear in mind that correlation time $\tau_0$ is connected to the width of the fluctuation spectrum in an inversely proportional dependence.

Now let us dwell briefly upon the basic factors determining the

spectral and correlational characteristics of the signals of moving targets composed of many reflecting elements. For objects of this sort the fundamental reasons for fluctuations of reflected signals will be:

1. Displacement, relative to the RLS, of the elementary reflectors representing the target; this displacement is caused by the movement of the target or of the vehicle carrying the radar station.

2. The mutual displacement of the individual elementary reflectors of the target (movement of branches and leaves of trees, rotation of the helicopter propeller, etc.).

3. Variation in the composition of the elementary reflectors forming the signal as a result of the sweeping movement of the antenna beam.

When the target or the vehicle carrying the RLS is moving at high velocity, the width of the spectrum of the fluctuations is determined principally by the mutual displacement of the RLS and the target. For this reason let us examine the influence of the first factor in greater

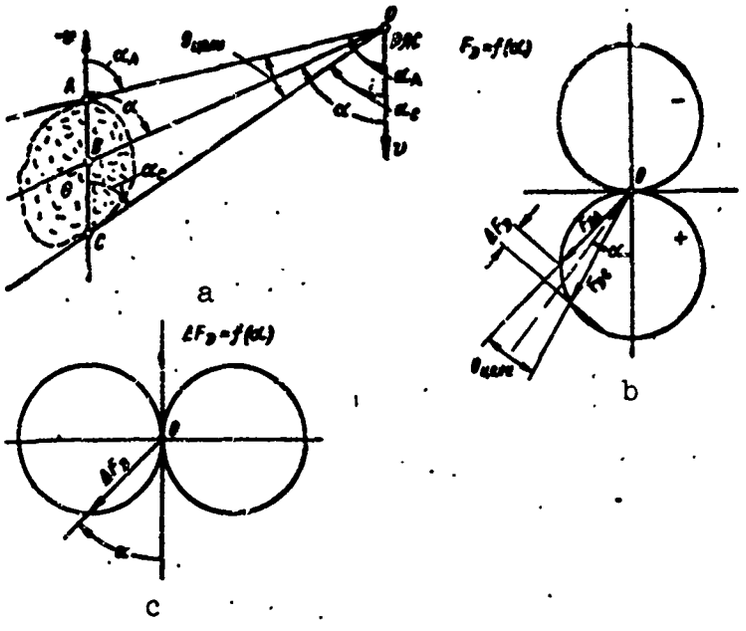


Fig. 3.13. Determining the spectrum of Doppler frequencies.

detail. In addition, for the sake of simplicity let us examine the case of a target of limited size. The results obtained in this case may be employed for a qualitative evaluation of the signal characteristics of distributed targets occupying large areas of space.

Let us assume that the radar station is moving relative to the target $Q$, consisting of many reflectors distributed at random, at velocity $v$ (Fig. 3.13a), the midpoint of the target is located at course angle $\alpha$. Then the course angles of the outside elements of the target, determining its dimensions, are, accordingly, equal to

$$\alpha_A = \alpha + \frac{\theta_{цели}}{2},$$

$$\alpha_C = \alpha - \frac{\theta_{цели}}{2}.$$

As a result of this the Doppler shifts of the carrier frequency of the signals reflected from elements $A$ and $C$ will differ

$$F_{дA} = \frac{2v}{c} f_0 \cos\left(\alpha + \frac{\theta_{цели}}{2}\right),$$

$$F_{дC} = \frac{2v}{c} f_0 \cos\left(\alpha - \frac{\theta_{цели}}{2}\right),$$

where $f_0$ is the carrier frequency of the radar station.

The remaining elements of the target will yield reflected signals whose carrier frequencies will have Doppler shifts lying between $F_{dA}$ and $F_{dC}$. Thus, the carrier frequencies of the signals reflected from individual elements of the target occupy the frequency spectrum from $f_0 + F_{dA}$ to $f_0 + F_{dC}$ with width

$$\Delta F_д = F_{дC} - F_{дA} = \frac{2v}{c} f_0 \left[\cos\left(\alpha - \frac{\theta_{цели}}{2}\right) - \cos\left(\alpha + \frac{\theta_{цели}}{2}\right)\right] = \frac{4v}{c} f_0 \sin\alpha \cdot \sin\frac{\theta_{цели}}{2}. \quad (3.48)$$

In the case of observation of an individual complex target (airplane, shift, bridge, isolated structure) angle $\theta_{tseli}$ may be very small, and $\sin(\theta_{tseli}/2) \approx (\theta_{tseli}/2)$. Therefore the spectrum of Doppler frequencies of the carrier for such a target will be

$$\Delta F_{\text{д}} \approx \frac{2v}{c} f_0 \theta_{\text{изл}} \sin\alpha. \qquad (3.49)$$

The diagrams illustrating the character of the dependences of Doppler shift of frequency $f_d$ and of the spectrum of Doppler frequencies $\Delta F_d$ upon the target course angle are given, respectively, in Fig. 3.13b and c.

Transformation of carrier frequency $f_0$ of the radar signal into a spectrum with width $\Delta F_d$ is the result of the fact that the target consists of many reflecting elements which are distribted in space and are moving at different velocities relative to the station. The presence of frequency band $\Delta F_d$ in the reflected signal spectrum is evident that the resultant signal varies according to a more complex law than the emitted signal. In the final analysis this indicates fluctuation of the resultant signal.

If the radar station emits a continuous monochromatic signal of frequency $f_0$, the discovered quantity $\Delta F_d$ fully characterizes the width of the spectrum of the reflected signal fluctuations. Most radar devices in fact operate in the pulse mode. In this mode the outcoming signals occupy a broad frequency band $\Delta f$. After reflection of such a signal, all of its frequency components undergo transformation in accordance with law (3.48).

Inasmuch as in this paragraph we have set ourselves the task of conducting a qualitative analysis of the phenomena, we may for purposes of simplification limit ourselves only to an examination of the spectrum of fluctuations occurring during reflection of a monochromatic signal. The regularities elucidated as a result of such an analysis will also appear in the case of signals of more complex shape, although the quantitative relationships between the basic parameters, of course, will change and will become more complicated.

It follows from Formulas (3.48) and (3.49) that the width of the spectrum of the fluctuations is proportional to carrier frequency $f_0$ and is heavily dependent upon course angle $\alpha$, upon the target dimension (angle $\theta_{tseli}$) and upon the velocity of its displacement relative to the radar station.

When we know the width of the spectrum of fluctuations $\Delta F_д$, we can determine the connection between this quantity and the correlation time of the signal. Here for purposes of simplification we will consider that within the limits of band $\Delta F_д$ the spectrum is continuous and even. Then, in accordance with Transformations (3.47) the auto correlation function

$$R(\tau)=\int_0^\infty G(f)\cos 2\pi f\tau df=C\int_0^{\Delta F_д}\cos 2\pi f df=C\frac{\sin 2\pi\Delta F_д\tau}{2\pi\Delta F_д\tau},$$

where $G(f)$, as agreed, is equal to constant quantity $C$.

From the obtained expression it is seen that the autocorrelation function changes in accordance with a law of the form $\sin x/x$. Therefore, during the correlation time we will accept interval $\tau_0$ corresponding to the first interception of curves $R(\tau)$ and the axis of abscissi.

It is obvious that $R(\tau_0) = 0$ under condition $2\pi\Delta F_д\tau_0=\pi$. Consequently, correlation time

$$\tau_0\approx\frac{1}{2\Delta F_д}. \qquad (3.50)$$

Analysis of Formulas (3.48), (3.49), (3.50) enables us to conclude that the spectrum of fluctuations and the correlation time depend upon the velocity of the relative displacement, target dimensions, and the target position relative to the radar station. It is characteristic that with increase in the dimensions (larger than $\theta_{tseli}$) the spectrum of fluctuations increases and the correlation time decreases. This reg-

ularity may be explained by the fact that in the case of an increase in the target dimensions a larger number of reflectors participate in shaping the resultant signal. Therefore, with the same displacements, there is a redistribution of the phases and amplitudes of a larger number of signals, which lead to an acceleration in the fluctuation of the resultant amplitude.

The connection between the spectrum of fluctuations and the dimensions of the target may be utilized to determine the latter's dimensions. For this it is necessary to possess data on the station's movement, the distance to the target, and the target's course angle, and also to measure the correlation time or the spectrum of fluctuations, after which, using Correlations (3.49) and (3.50) or similar ones, the dimensions of the target can be calculated.

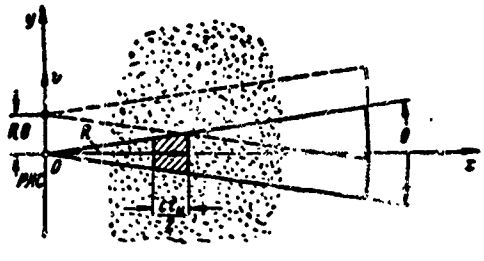

Fig. 3.14. Determining correlation time in lateral scan.

As has been noted above, the mutual displacement of the reflectors forming the target is also a source of fluctuations of reflected signals. The mutual displacement of reflectors (branches, leaves, trunks of trees, drops of rain, etc.) usually occurs at low velocity. For this reason the width of the spectrum of the corresponding fluctuations is comparatively small.

During the process of sweeping the antenna beam there is a change in the composition of the reflectors falling within the limits of the volume of resolution during scanning of distributed targets. This circumstance, in turn, leads to fluctuations of the reflected signals. The correlation time of such fluctuations may be determined by establishing the time during which the composition of the reflectors which shape the

signal changes completely.

As an example let us find the correlation time of the signals of a distributed target; this time is determined only by the shift in the reflectors in lateral scan when the axis of the antenna beam is perpendicular to the trajectory of the vehicle carrying the RLS (Fig. 3.14).

There is a complete shift of the reflectors when the linear displacement of the vehicle carrying the RLS along axis $y$ is $R\theta$, where $R$ is the distance to the part of the locality under observation. For this to occur at velocity $v$ of the vehicle carrying the radar station, time $\tau_0 \approx R\theta/v$, which may be viewed as the signal correlation time, is required. Thus, if $R$ = 100 km, $\theta = 0.5°$, then at $v$ = 2000 m/sec correlation time $\tau_0 \approx 0.5$ sec and $\Delta F \approx 2$ cps.

Thus, in a lateral scan RLS the width of the spectrum of fluctuation determined by a shift of the reflectors is small. The fundamental role is played by the spectrum of Doppler frequencies whose width is determined by Formula (3.49) at $\theta_{tseli} = \theta$ and $\alpha = 90°$.

## §3.10. COMPLEX AND GROUP TARGETS

Earlier we examined the reflection of electromagnetic waves from individual objects of the simplest shape. Most actual radar targets are complex condemnations of reflectors of various types. In the process of radar observation of such targets one encounters a signal which is the result of the interference of several signals reflected from different elements of the target.

In irradiation of a complex object (airplane, ship, tank, etc.) the character of the reflections from its various elements depends strongly upon their orientation. In some positions certain parts of the airplane or ship may yield extremely intense signals, while in other positions the intensity of the reflected signals may fall to zero. Furthermore, during change of the position of the object relative to

the radar station there is a change in the phase relationships of the signals reflected from the various elements. As a result of this fluctuations occur in the resultant signal.

There are other possible reasons for changes in the intensity of reflected signals. Thus, for example, in the case of an airplane there may be variation of the conductance of the contacts between its various elements. One of the causes of this is the vibration caused by the engine. Because of the variations in the conductance of the contacts, there is a change in the distribution of the current induced on the surface of the airplane and in the intensity of the reflected signals. In propeller driven airplanes a supplementary source of variation in the intensity of the reflections is the rotation of the propellers (propeller modulation).

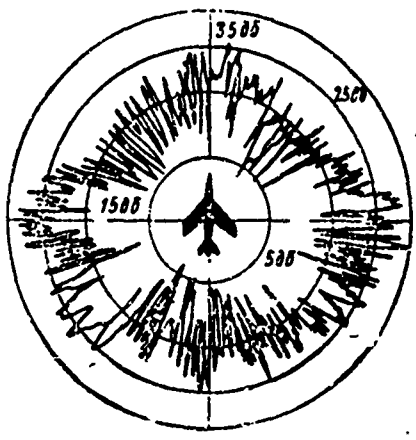


Fig. 3.15. Reflection diagram of an airplane ($\lambda$ = 10 cm).

Figure 3.15 gives an experimental diagram of the intensity of reflection from an airplane in the horizontal plane for $\lambda$ = 10 cm. It is seen from the diagram that insignificant reflections of the direction of beaming cause sharp variations in the power of the reflected signal, up to 30-35 db.

Figure 3.16 gives as another example the variation in the effective scattering cross section of the second Soviet earth satellite. This curve was obtained by processing the recordings of reflected signals on a wave 69 cm long.

In the process of radar observation the mutual positions of the airplane (a ship, satellite) and the RLS are continually changing due to the motion of the former. The result of this is fluctuation of the reflected signal and corresponding variation in effective scattering

cross section $\sigma_{ts}$.

The laws of the probability distribution of the target effective scattering cross section, and the character of the variation of this quantity over time are usually determined experimentally. For this the intensity of the reflected signals is recorded and, after processing of the recording, the statistical characteristics of the signals and of quantities $\sigma_{ts}$ are found.

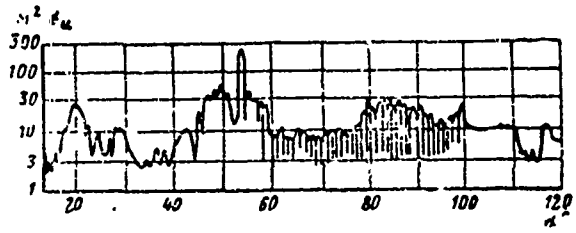


Fig. 3.16. Dependence of effective scattering cross section of the second Soviet artificial earth satellite upon the direction of beaming.

TABLE 3.1

| 1 Тип радиолокационной цели | Эффективная площадь цели, м² 2 |
|---|---|
| 3 Истребитель | 3—5 |
| 4 Средний бомбардировщик | 7—10 |
| 5 Дальний бомбардировщик | 15—20 |
| 6 Транспортный самолет | 16 До 50 |
| 7 Крейсер | 14 000 |
| 8 Транспорт малого тоннажа | 150 |
| 9 Транспорт среднего тоннажа | 7500 |
| 10 Транспорт большого тоннажа | 15 000 |
| 11 Траулер | 750 |
| 12 Малая подводная лодка в надводном состоянии | 140 |
| 13 Катер | 100 |
| 14 Рубка подводной лодки | 1 |
| 15 Человек | 0,8 |

1) Type of radar target; 2) effective target cross section, $m^2$; 3) pursuit plane; 4) medium bomber; 5) long-range bomber; 6) transport plane; 7) cruiser; 8) small cargo ship; 9) medium cargo ship; 10) large cargo ship; 11) trawler; 12) small submarine on the surface; 13) launch; 14) submarine conning tower; 15) person; 16) upto.

As much research has shown, for fluctuations of the $\sigma_{ts}$ of airplane the exponential law of distribution

$$W(\sigma_{\text{п}}) = \frac{1}{\bar{\sigma}_{\text{п}}} e^{-\frac{\sigma_{\text{п}}}{\bar{\sigma}_{\text{п}}}}.$$

applies with sufficient accuracy.

The diagram of the reradiation of a ship has a more subtly lobe-shaped structure than that of an airplane, which is due to the significantly greater dimensions and more complex construction of the ship The reflective elements of a ship are numerous and variagated. Therefore the ship must also be viewed as a group of elements whose reflections have random phases. Experimental research shows that fluctuations in the effective scattering cross section of a ship may also be approximately described by the exponential law of distribution.

On the basis of recordings of amplitudes of complex target signals (airplanes, ships satellites, etc.) it is possible to determine the autocorrelation function of signals and also the spectrum of their amplitude fluctuations.

Data on the laws of distribution of signal amplitudes or of effective scattering cross sections are necessary for calculating the operational range of a radar station and as a basis for the method of processing the signals. Information on the autocorrelation function and on the spectrum of fluctuations, furthermore, is important for determining the accuracy of measurement of coordinates.

The average value of the effective scattering cross section $\bar{\sigma}_{ts}$ is usually employed in the practical evaluation of a radar station's operational range. This quantity may be derived by averaging the values of $\sigma_{ts}$ for various directions of incidence of the irradiating wave.

Table 3.1 gives the average values of the effective cross sections of various real targets as obtained by generalizing a large number of measurements on waves in the centimeter range.

By using these quantities the average values of the range of de-

tection of various targets may be calculated.

The effective scattering cross sections of actual targets are usually determined experimentally.

In practice various methods of measuring the target's effective scattering cross section are applied. Above all, quantity $\sigma_{ts}$ may be determined by measuring electrical field strength $E_1$ and $E_2$. This method is convenient in the laboratory or under test conditions, but is not applicable in practice for investigation of such targets as airplanes or ships.

In some cases it is convenient to find the effective scattering cross section $\sigma_{ts}$ by measuring the intensities of waves reflected from standard targets under test conditions. If the effective cross section of a standard target is $\sigma_0$, and the field strength of the wave reflected from it is $E_0$, then $\sigma_{ts}$ is found from formula

$$\sigma_{\text{п}} = \sigma_0 \frac{E_{\text{п}}^2}{E_0^2}, \qquad (3.51)$$

where $E_{ts}$ is the field strength of the wave reflected from the target under investigation.

The use of Relationship (3.51) assumes identity of the conditions in which quantities $E_{ts}$ and $E_0$ were measured.

The most suitable standard target is a metallic sphere, since its reflective properties are identical during irradiation from various directions, and its effective scattering cross sections can be calculated accurately.

It is also possible to determine the effective cross section of a target by comparing the free-space range of standard target $R_0$ and the free-space range of test targets $R_{ts}$. It is obvious that, if there are no losses,

$$\sigma_{\text{п}} = \sigma_0 \frac{R_{\text{п}}^4}{R_0^4}.$$

The effective cross section of a target, which cannot be investigated using the methods examined above, is found by measuring the maximum range of its detection by a radar station and by calculating ts

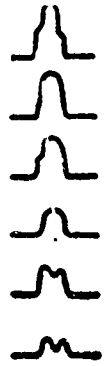

Fig. 3.17. Pulsations of a signal from a group target.

using the equation of the range of radar observation.

In radar observation the case is often encountered of a group target several of whose isolated objects are located at distances which are less than resolvable distances. This means that they fall within the antenna beam of the station and, as regards range, are located within the limits of a section which does not exceed $c\tau_i/2$.

The phase relationship among signals of individual targets are determined by their mutual positions and by the frequency of the transmitter. Relative displacements of individual targets, as well as frequency creep, are always encountered in practice. Because of this, variations in intensity – fluctuations of the resultant signal over time – are observed. On an indicator screen with amplitude marking, for example, this dependence is displayed in a continuous signal pulsation, change of its shape, and the appearance of gaps in the middle of the resultant pulse (Fig. 3.17).

Let us assume that a group target consists of $n$ objects. Let the signals reflected from them be characterized by electrical field

strengths $E_1$, $E_2$, ..., $E_n$. If the phase relationships are favorable, the strength of the resultant electrical field attains its maximum

$$E_{макс} = E_1 + E_2 + E_3 + \ldots + E_n.$$

Such phase relationships are also possible in which the electrical field strength is minimum and equal to zero: $E_{min} = 0$. In this case the signals reflected from the various objects cancel out one another.

In view of the fact that the effective scattering cross section of a target is proportional to the square of the electrical field strength, its maximum value may be written as

$$(\sigma_ц)_{макс} = (\sqrt{\sigma_{ц1}} + \sqrt{\sigma_{ц2}} + \ldots + \sqrt{\sigma_{цn}})^2. \qquad (3.52a)$$

Taking into account the arithmetical adding of the powers of signals, the average value of the effective scattering cross section will, accordingly, be

$$\bar{\sigma} = \sigma_1 + \sigma_2 + \ldots + \sigma_n. \qquad (3.52b)$$

If the objects forming a group of targets are complex in shape and themselves consist of a number of elements, variations in the effective scattering cross sections of the individual objects may be a supplementary source of fluctuation of the resultant signals. A skilled observer can usually distinguish the blips of group and individual targets from the appearance of the blip on the indicator screen.

3.11. VOLUME-DISTRIBUTED TARGET

Above we have examined targets whose dimensions are small by comparison with the transverse dimensions of the antenna beam and with

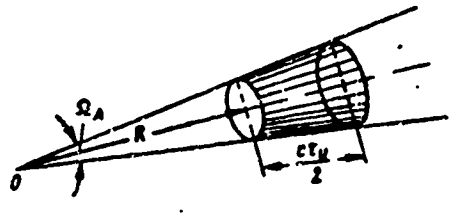


Fig. 3.18. Calculating the effective scattering cross section of a volume-distributed target.

quantity $c\tau_i/2$. Targets such as these may usually be viewed as point shaped.

In radar practice one very often encounters reflections from volume-distributed targets consisting of a large number of reflecting elements which are located relatively close to one another and take up a considerable amount of space.

Characteristic of three-dimensional targets is the fact that the elementary reflectors of which they are composed, as a rule, are in a state of continuous movement under the influence of the forces of gravity and wind. Because of this their relative positions and orientations change, which leads to continuous variation in the phase and amplitude relationships between the elementary signals. In this case the instantaneous value of the total signal at the receiver input will be random quantity

$$U=\sum_{k=1}^{n} U_k \cos(\omega t-\varphi_k).$$

By analogy with Formula (3.52b) the average value of the effective cross section of a volume-distributed target will be

$$\bar{\sigma}_{\Sigma}=\sum_{k=1}^{n}\sigma_k,$$

where $\sigma_k$ is the effective scattering cross section of an elementary reflector.

The elementary reflectors which participate in the shaping of the total signal are distributed within the limits of some volume $V$ (reflecting volume). The boundaries of volume $V$ are determined by the angular and range resolution of the radar station (Fig. 3.18). The inequality

$$R\gg\frac{c\tau_{\Sigma}}{2},$$

where $R$ is the distance to the reflecting volume, is in practice always

true.

It may therefore be accepted as an approximation that the observed volume has the shape of a cylinder with base $\Omega_A R^2$ and altitude $c\tau_1/2$, that is

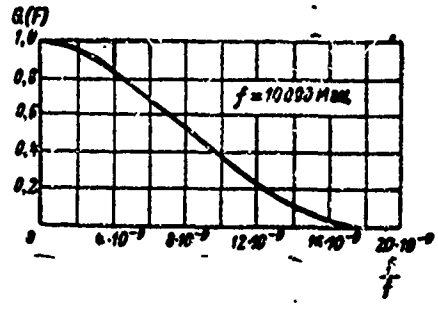


Fig. 3.19. Standardized spectrum of fluctuations of radar signals reflected from metallized strips.

$$V=\Omega_A R^2 \frac{c\tau_u}{2},$$

where $\Omega_A$ is the solid angle of the antenna beam.

Solid angle $\Omega_A$ is expressed by effective cross section $A$ or the antenna directive gain $D$

$$\Omega_A=\frac{\lambda^2}{A}=\frac{4\pi}{D}.$$

and, consequently, the reflecting volume

$$V=4\pi\frac{R^2}{D}\cdot\frac{c\tau_u}{2}. \qquad (3.53)$$

It is rather difficult to determine the effective cross section of a volume-distributed target on the assumption that its elementary reflectors possess different $\sigma_k$. Therefore we will consider that the elementary reflectors in volume $V$ possess identical effective scattering cross sections, that is

$$\sigma_1=\sigma_2=\ldots=\sigma_k=\sigma_0=\text{const},$$

where $\sigma_0$ is the average value of the effective cross section of the reflectors

Let us assume that the elementary reflectors are evenly distribu-

ted in space at density $n_0$. Then the volume will contain $N = n_0 V$ reflectors, and their average effective cross section

$$\bar{\sigma}_{\text{э}} = n_0 \sigma_0 V. \qquad (3.54)$$

By substituting Expression (3.53) in (3.54), we obtain a formula for calculating the average effective cross section of a volume-distributed target

$$\bar{\sigma}_{\text{э}} = 4\pi c_0 n_0 \frac{R^2}{D} \cdot \frac{c\tau_{\text{и}}}{2}. \qquad (3.55)$$

It can be seen from Formula (3.55) that the characteristic of volume-distributed targets is the dependence of the effective cross section upon radar station parameters $\tau_1$ and $D$, and also upon the distance between the station and the target.

The obtained relationships make it possible to evaluate the average power value of the resultant signal of a volume-distributed target. The amplitude of the resultant signal changes, since the individual reflectors are always changing the position relative to one another. Therefore the resultant signal received by the radar station receiver in consecutive repetition periods fluctuates over time in a random manner.

Experimental study of the reflections from a cloud of metallized strips and from hydrometeors has shown* that the actual laws of the distribution of amplitude probabilities and of effective scattering cross sections correspond well with the laws examined above which were developed theoretically. And in particular, the Relay distribution

$$W(U) = \frac{U}{\sigma^2} e^{-\frac{U^2}{2\sigma^2}},$$

is true for amplitude fluctuations, while the exponential law

$$W(\sigma_{\text{э}}) = \frac{1}{\bar{\sigma}_{\text{э}}} e^{-\frac{\sigma_{\text{э}}}{\bar{\sigma}_{\text{э}}}},$$

is true for the effective scattering cross section.

The velocity of the observed fluctuations is not great. It is determined by the time required for regrouping of the elementary reflectors in the reflecting volume and is therefore considerably lower than the velocity of noise fluctuations. The regrouping time of reflectors is usually so great that during it several pulses are reflected.

The shapes of the frequency spectrum of the fluctuations of signals reflected from metallized strips resemble the error curve which is symmetrical relative to the origin of the coordinate. The spectrum width depends strongly upon the relative velocity of displacement of the strips. The influence of the horizontal component of the scattering velocity, which is determined by the speed and gustiness of the wind, is particularly strong. It may be accepted as an approximation that the width of the spectrum of fluctuations is proportional to the average wind speed and to the frequency of the radar station.

Figure 3.19 gives, as an illustration, the frequency spectrum of the fluctuations of radar signals reflected from metallized bands.

It should also be borne in mind that the length of the signal reflected from a volume-distributed target may be significantly in excess of the length of the emitted pulse. This length is determined by the radial extension of the volumetric target. As the emitted pulse is propagated further, new reflections are given off by new areas of the volume-distributed target.

If some sort of object (for example, an airplane) is located within a volume filled with distributed reflectors, radar observation of this object is made difficult. In this case the reflections from the volume-distributed target constitute an interference which can mask the useful signal. The conditions of observation of a useful signal may be characterized by the ratio of signal power to noise. The size of the ratio of the power of the signal reflected from the target to the aver-

TABLE 3.2

| Вид гидрометеорного образования 1 | Диаметр капель, мм 2 | Среднее расстояние между каплями, мм 3 | Интенсивность осадка, мм/час 4 | Водность, г/м³ 5 |
|---|---|---|---|---|
| 6 Облака | 0,005—0,007 | 1—1,6 | — | 0,2—1,0 |
| 7 Туман | 0,01 | 4,3 | — | 0,006 |
| 8 Густой туман | 0,10 | 21 | 0,05 | 0,057 |
| 9 Мелкий дождь | 0,20 | 36 | 0,25 | 0,093 |
| 10 Легкий дождь | 0,45 | 70 | 1,00 | 0,14 |
| 11 Умеренный дождь | 1,00 | 123 | 4,00 | 0,28 |
| 12 Сильный дождь | 1,50 | 130 | 15,00 | 0,83 |
| 13 Очень сильный дождь | 2,10 | 138 | 40,00 | 1,8 |
| 14 Ливень | 3—5 | 137 | 100,00 | 5,4 |

1) Type of hydrometeor formation; 2) drop diameter, mm; 3) average space between drops, mm; 4) intensity of precipitation, mm/hour; 5) water content, g/m$^3$, 6) clouds; 7) fog; 8) thick fog; 9) fine rain; 10) light rain; 11) moderate rain; 12) heavy rain; 13) very heavy rain; 14) cloud burst.

age power of the signal from the volume-distributed reflectors is equal to the ratio of their effective cross sections, that is

$$\frac{P_{пр}}{P_{пр\,пом}} = \frac{1}{4\pi}\frac{\sigma_{ц}}{\sigma_0}\cdot\frac{D}{n_0 R^2\frac{c\tau_и}{2}}. \qquad (3.56)$$

It follows from Formula (3.56) that the effective discrimination of useful signals against the background of reflections from a volume-distributed target may be heightened by shortening the pulse length and narrowing the directivity diagram of the antenna.

Reflections from hydrometeors are those encountered most frequently in radar practice. In the case of rain of drop diameter $d_0$, quantity

$$\sigma_ц \approx 300\frac{d_0^6}{\lambda^4}$$

and signal/noise ratio

$$\frac{P_{пр}}{P_{пр\,пом}} = \frac{1}{1250\pi}\sigma_ц\frac{D\lambda^4}{n_0 d_0^6 R^2\frac{c\tau_и}{2}}. \qquad (3.57)$$

The reflection of electromagnetic waves from hydrometeors may be utilized for meteorological purposes. In such a case the reflections from hydrometeors are the useful signals. They can be used to determine

the locations of atmospheric formations, their intensities, and sometimes even their direction of movement.

For a preliminary estimate of the effective cross sections of rain the averaged data given in Table 3.2 may be used. In fact, the dimensions of rain drops may differ from one to the other. As follows from Formula (3.9), small oscillations in the distribution of drop diameters may cause substantial changes in the instantaneous values of the reflected signals.

Atmospheric hydrometeors in the hard phase (hail, snow) possess relative specific inductive capacitance $\varepsilon' \approx 3.0$ at temperatures from 0° to −50° C. For this reason the factor $[(\varepsilon' - 1)/(\varepsilon' + 2)]^2$ in Formula (3.8) is approximately 0.165, and not unity, and therefore the intensity of reflections from hail is considerably lower than from rain. The situation with regard to snow flakes and ice crystals is analogous.

When there is precipitation from clouds of ice particles at a certain height, the temperature being sufficiently high, the ice may begin to melt (a zero isotherm layer). The ice crystals become covered with water, and their effective scattering cross section increases sharply. It is characteristic that, because of their large dimensions and the characteristics of their shape, the $\sigma_{ts}$ of such particles is larger than for drops of water of the same mass. Because of this the zero isotherm layer gives rise to a reflection of maximum intensity. Furthermore, when the ice crystals turn into drops of water, their effective cross section is slightly reduced, and the intensity of the reflected signal declines.

Other hard particles suspended in the atmosphere (sand, dust) can also cause reflection of electromagnetic waves. The dimensions of sand particles are commensurable with the dimensions of rain drops. Therefore, sand storms create reflections of considerable intensity. Parti-

cles of dust or smoke are much smaller in size. According to experimental investigations, for particles of dust to remain suspended in the air for a long time their diameters must not exceed 10μ. It is obvious that the reflection from a cloud of such particles must be very weak.

In conclusion it should be noted that intense reflections from hydrometeors and hard particles can be observed only with waves in the centimeter and millimeter ranges.

## §3.12. SURFACE-DISTRIBUTED TARGETS

Examples of surface-distributed targets are: grass cover, forest, bushes, fields, waves on the surface of the water. In this case, in contrast to volume-distributed targets, it is difficult to distinguish the individual reflecting elements. Being distributed in a random manner, they form a continuous surface layer which gives off a scattered reflection of electromagnetic waves.

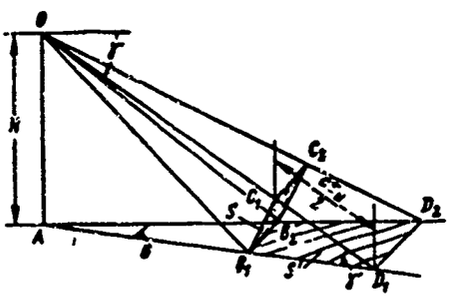

Fig. 3.20. Determining the effective scattering cross section of a surface-distributed target.

Let us assume that at point $O$ (Fig. 3.20), at altitude $H$ above the earth's surface, there is an airplane. In the horizontal plane its antenna beam has width $\theta$ and irradiates sector $AD_1D_2$ on the earth's surface.

We will consider that the radar station emits pulses of length $\tau_1$. Even when the antenna is not moving, irradiation of the surface in sector $AD_1D_2$ is not simultaneous. The first reflected signal returns in


Fig. 3.21. Time diagram of voltage at the receiver output of a surface-scan radar station. A) Noises.

time $\tau = 2H/c$ after the outcoming pulse (Fig. 3.21). Furthermore, despite the pulse-like character of the emission, reflected signals are continuously entering the input of the radar station receiver. The reason for this is that, as the emitted wave spreads, the reflected wave returns from ever further sections of the surface. Since the surface is continuous, the signal at the receiver output will also be continuous.

At each given moment in time, the signal at the receiver input will be the result of the addition of the signals reflected from the elementary reflectors distributed in a random manner within the resolvable area of the surface.

The resolvable area is limited in azimuth by the width of the directivity diagrams. In range the boundaries of the resolvable area depend upon pulse length $\tau_i$ and upon sighting angle $\gamma$. Thus, in our case

$$B_1 D_1 = \frac{c\tau_u}{2} \cdot \frac{1}{\cos\gamma}.$$

The size of the effective scattering cross section, in the case of a homogeneous surface with random distribution of irregularities, is proportional to cross section $S'$ which at the given moment shapes the reflected signal.

To determine quantity $\sigma_{ts}$ we examine area $S$ perpendicular to the direction of incidence of the wave. All the energy reflected from resolvable area $S'$ passes through its surface.

The resolvable area on the surface of the earth has cross section

$$S' = R\theta \frac{c\tau_u}{2} \cdot \frac{1}{\cos\gamma}.$$

Consequently, the cross section of surface $S$ perpendicular to the sighting line

$$S = S' \sin\gamma = R\theta \frac{c\tau_u}{2} \operatorname{tg}\gamma.$$

Knowing $S$, one can determine quantity $\sigma_{ts}$ if coefficient $\rho$ which

takes into account the influence of the reflective properties of the earth's surface:

$$\sigma_{\text{п}} = \rho R\theta \frac{c\tau_{\text{и}}}{2} \operatorname{tg} \gamma. \qquad (3.58)$$

is introduced.

Characteristic of the surface-distributed target is the dependence of the effective scattering surface $\sigma_{ts}$ upon the parameters $\tau_i$ and $\theta$ of the radar station, and also upon the distance to the area observed and the angle at which it is sighted. In this respect the properties of the surface-distributed target are close to those of the volume-distributed target.

As is seen from Formula (3.58), the reflective properties of the surface-distributed target depend upon quantity $\rho$. Knowing this quantity and the other parameters characterizing the scanning conditions one can determine the effective scattering cross section and proceed to a calculation of the intensity of the reflected signal.

In many cases the reflective properties of a surface-distributed target are conveniently characterized by a standardized value for the effective scattering cross section, one equal to the ratio of $\sigma_{ts}$ to the cross section of the corresponding area of the earth's surface

$$\sigma'_{\text{п}} = \frac{\sigma_{\text{п}}}{S'} = \frac{\sigma_{\text{п}}}{R\theta \frac{c\tau_{\text{и}}}{2} \cdot \frac{1}{\cos \gamma}} = \rho \sin \gamma.$$

TABLE 3.3

| Скорость ветра, км/час 1 | $m$ | $\Delta F$ на уровне 0,1 от максимума 2 |
|---|---|---|
| 17 | 1,3 | 1,5 |
| 22 | 1,0 | 6,0 |
| 30 | 0,2 | 10,0 |
| 50 | 0,0 | 15,0 |

1) Wind velocity, km/hour; 2) $\Delta F$ at a level 0.1 from the maximum, cycles.

The reflective properties of the surface and, consequently, quan-

tity $\sigma_{ts}$, are influenced by:

- surface irregularities,
- angle of incidence (angle of sighting) of the wave and the wave-

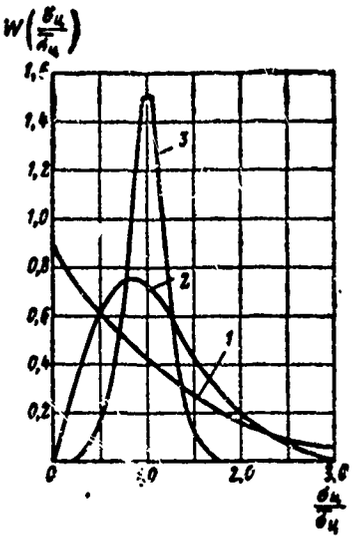


Fig. 3.22. Distribution of effective scattering cross section of a hill covered with wood: 1) gusts of wind with a velocity of 40 km/hour; 2) wind at velocity of 16 km/hour; 3) for rocky part of the hill at a wind velocity of 16 km/hour.

length,

- polarization of the wave,
- the specific inductive capacity of the soil.

All the earth covers encountered in practice may, roughly speaking, be divided into smooth and rough. Smooth surfaces include asphalt and concrete roads, etc. For them the intensity of the reflected signal drops rapidly with reduction in the sighting angle and depends upon the polarization of the incident wave.

In the case of uneven surfaces the roughness considerably exceeds the wavelength in value. Sections of land overgrown with grass, sewn areas, bushy patches, forest, etc. all have this character. Investigations demonstrate that the value of $\rho$ depends very little upon sighting angle $\gamma$ and upon polarization in the case of actual rough surfaces. For

each type of surface the values of $\rho$ and $\sigma'_{ts}$ usually fall within definite limits. Because of this, for example, the general character of the area from which the signals are reflected may be judged by the value of $\sigma'_{ts}$.

Radar reflections from a surface covered with plants undergo seasonal changes which are a function of the change in the water content of the plant. In addition, the character of the reflection of electromagnetic waves from all surfaces depends strongly upon their moisture content and upon the presence or absence of snow.

During observation of surfaces covered with plants the reflection comes from many random reflectors (leaves, stalks, branches). These reflectors are moved by the wind. The stronger the wind the more intensive their movement. In addition to moving reflectors there are various randomly dispersed but immovable reflectors (rocks, trunks of trees). The resultant signal is the sum of the signals of the first and second types of reflectors.

If the radar station is stationary, the reflections from moving elements yield a fluctuating signal component, while the reflections from stationary elements yield a stable component.

The law of distribution of the effective scattering cross section of this sort of target depends upon ratio $m$ of the powers of the stable and fluctuating components of the resultant signal.

Figure 3.22 gives an example of the variation in the character of the distribution of effective scattering cross sections $\sigma_{ts}$ of a heavily wooded hill. When the wind blows in gusts at velocity of about 40 km/hour, $m \approx 0.8$ and the distribution is almost exponential (*1*). In the case of a weaker wind at velocity of 16 km/hour, the noticeable stable signal component prevails, $m \approx 5$ and a clearly expressed maximum is formed in the distribution curve (*2*).

Figure 3.22 (*3*) also gives the distribution curve for the rocky part of the hill with sparse plant coverage at the same wind velocity of 16 km/hour. In this case $m \approx 30$, and the distribution law approaches the normal.

Comparison of Fig. 3.22 and Fig. 3.11 enables us to conclude that the distribution laws for effective scattering cross sections obtained experimentally coincide well with the same laws as predicted on theoretical grounds.

The width of the spectrum of signal fluctuations of the examined surfaces depends upon the latter's properties and upon wind velocity. Table 3.3 shows the dependence of quantity $m$ upon the width of the spectrum of the fluctuations of reflections from a wooded area in waves of the 10-centimeter range.

In observation of surface-distributed targets from flying devices the character of the signal fluctuations will be determined principally by the movement of the radar station itself. The width of the spectrum of fluctuations and the correlation time will depend upon the flight mode and upon the target dimensions in accordance with Formulas (3.49) and (3.50).

Manuscript Page No.

[Footnotes]

174 See [19] in Chapter 3.

| Manuscript Page No. | [Transliterated Symbols] |
|---|---|
| 130 | ц = ts = tsel' = target |
| 131 | цели = tseli = target |
| 134 | РЛС = RLS = radiolokatsionnaya stantsiya = radar station |
| 161 | д = d = doppler = Doppler |
| 168 | мин = min = minimal'nyy = minimum |
| 176 | пр = pr = ploshchad' rasseyaniya = effective scattering cross section |
| 176 | пом = pom = pomekha = noise |

## Chapter 4

## RADAR OBSERVATION RANGE

### §4.1. THE FREE-SPACE OBSERVATION RANGE

The task of radar observation is to detect targets and to measure the parameters of their position and movement. Target detection is an operation involving the discrimination of signals reflected from the target against a background of external interferences and fluctuating receiver noises. Characteristic of this operation is the statistical character of its results as determined by the random law of change of the interference voltages and by fluctuation in the size of the effective target cross sections. The useful signal may be discriminated with a certain degree of reliability, such reliability being characterized by the probability of detecting the target. Thus, a strict approach to the question of determining the maximum range of radar observation requires that it be viewed as a statistical task.

Radar observation range depends not only upon the random processes noted above, but also upon a series of completely determined factors: emission power, antenna directivity, atmospheric damping of electromagnetic waves, etc. The influence of these factors is very substantial and should be the first thing considered. However, this can be done only if the question of the operating range of a radar station is viewed from the standpoint of the power relationships which take into consideration the averaged conditions of radar observation.

To establish the fundamental functions determining the range of radar observation, we begin with the simplest case of target detec-

tion in free space. The analysis will be based the assumption that the atmosphere is homogeneous and that there is no damping of electromagnetic waves.

Let us assume that at some point in space, at distance $R$ from the radar station, there is a target with effective scattering cross section $\sigma_{ts}$. At a sufficient distance, the electromagnetic wave radiated by the transmitting antenna of the station possesses a spherical front which is limited by the limits of the directivity diagram. Hence the power flux density of the outcoming electromagnetic wave at the target

$$\Pi_1 = \frac{P_\Sigma D_{prd}}{4\pi R^2},$$

where $P_\Sigma$ is the power of the emitted oscillations; $D_{prd}$ is the directive gain of the transmitting antenna.

According to the definition of the effective cross-section of the target the power of the scattered oscillations

$$\sigma_{ts}\Pi_1 = \frac{P_\Sigma D_{prd}\sigma_{ts}}{4\pi R^2}.$$

It follows from this that the power flux density of the reflected wave at the receiving antenna of the radar station

$$\Pi_2 = \frac{P_\Sigma D_{prd}\sigma_{ts}}{(4\pi)^2 R^4}.$$

If we multiply quantity $\Pi_2$ by effective cross section $A_{pr}$ of the received antenna, we find the power of the reflected signal at the input of a matched receiver,

$$P_{np} = \Pi_2 A_{np} = \frac{P_\Sigma D_{prd}\sigma_{ts} A_{np}}{(4\pi)^2 R^4}. \qquad (4.1)$$

It is known from antenna theory that dependence

$$A_{np} = \frac{\lambda^2}{4\pi} G_{np}, \qquad (4.2)$$

which exists between the effective cross section $A_{pr}$ of an antenna and

its power gain factor $G_{pr}$, is true for any direction in the zone of emission and reception of the particular antenna.

Quantity $A_{pr}$ is proportional to antenna aperture cross section $S_a$

$$A_{пр} = K_S S_a.$$

The cross-section utilization factor $K_S$ depends upon the distribution of the field in the antenna aperture. If the field is identical in phase and in intensity over the whole aperture, factor $K_S$ is unity. For most radar antennas $K_S$ = 0.4-0.7.

Taking into account Formula (4.2) the expression for the power of the received signal

$$P_{пр} = \frac{P_{т} D_{пр.а} G_{пр} \lambda^2 \sigma_{ц}}{(4\pi)^3 R^4}.$$

This expression may be written differently if one takes into account the fact that the directive gain $D_{pr}$ and the received antenna gain factor $G_{pr}$ are in the relationship

$$G_{пр} = \eta D_{пр},$$

where $\eta$ is the efficiency of the antenna.

As a rule, $\eta$ = 0.9-0.95 for radar antennas, and it may be assumed that $G_{pr} \approx D_{pr}$. Then the power of the received signal

$$P_{пр} = \frac{P_{т} D_{пр.а} D_{пр} \lambda^2 \sigma_{ц}}{(4\pi)^3 R^4}. \qquad (4.3)$$

As distance $R$ increases, power $P_{pr}$ of the received signals rapidly diminishes. At a certain value of $R$ quantity $P_{pr}$ drops so far that the target signal cannot be distinguished by the terminal device with the assigned degree of reliability against the background of fluctuating noises.

The target range at which power $P_{pr}$ is reduced to the threshold value $P_{pr\ min}$ is the maximum operating range $R_{sv\ maks}$ of the radar station for the given target. It follows from Relationship (4.3) that the maximum range

$$R_{\text{св макс}} = \sqrt[4]{\frac{P_{\text{и}}}{P_{\text{пр мин}}} \frac{D_{\text{прд}} D_{\text{пр}} \lambda^2 \sigma_{\text{ц}}}{(4\pi)^3}}. \qquad (4.4)$$

Equation (4.4) is applicable both in the case of stations with separate antennas for transmission and reception and for stations with common antennas.

In pulse radar stations one and the same antenna are usually employed for reception and transmission, that is, $D_{prd} = D_{pr} = D$. Then Eq. (4.4) takes the form

$$R_{\text{св макс}} = \sqrt[4]{\frac{P_{\text{и}}}{P_{\text{пр мин}}} \frac{D^2 \lambda^2 \sigma_{\text{ц}}}{(4\pi)^3}}. \qquad (4.5)$$

If $D$ is expressed in terms of effective antenna cross section $A$, another variant of the range equation is obtained:

$$R_{\text{св макс}} = \sqrt[4]{\frac{P_{\text{и}}}{P_{\text{пр мин}}} \frac{A^2 \sigma_{\text{ц}}}{4\pi\lambda^2}}. \qquad (4.6)$$

Analysis of the obtained expressions leads to the following conclusions:

1. The radar observation range increases rather weakly with growth in the emission power. Thus the emitted power would have to be increased by 16 times to increase the station's operating range 2 times.

2. The range of radar observation also depends comparatively little upon receiver sensitivity. The effect of an increase in receiver sensitivity (reduction of $P_{pr\ min}$) is equivalent to a corresponding growth in the power of the radar station transmitter.

3. The operating range of a radar station depends to a great extent upon antenna directivity. Thus, for example, $D$ would have to be increased 4 times to increase the range of radar observation 2 times, other conditions being equal.

4. Change in the value of the effective scattering cross section of the target has comparatively little influence on the range of radar observation. As a result of this, there may be comparatively little

difference in the range of detection of targets whose dimensions differ considerably.

Wavelength $\lambda$ enters into the expression for $R_{sv\ maks}$. It should be borne in mind that in fact all quantities in Eqs. (4.4), (4.5) and (4.6) are functions of the wavelength. However, these dependences were not brought out in the obtained equations, and quantity $\lambda$ was introduced into the formulas only to take into account the influence of the antenna's directional properties. Because of this, the influence of $\lambda$ upon $R_{sv\ maks}$ may be examined in the present case only by considering this circumstance and by realizing that all other quantities entering into the equations remain unchanged. Thus, for example, at assigned $D$ (see Eq. (4.5)) as wave $\lambda$ becomes shorter there is a reduction in the range of radar observation, since at $D$ = const a reduction in $\lambda$ is accompanied by a reduction in quantity $A$ and, consequently, also in the power at the receiver input. On the contrary, if the condition $A$ = = const is accepted (see Eq. (4.6)), as $\lambda$ becomes shorter the observation range increases. This is explained by the fact that with unchanged antenna dimension, reduction in $\lambda$ leads to an increase in the directive gain and, consequently, to an increase in the power flux density of the wave going to the target.

The range equations obtained above may be used to evaluate various types of radar systems, since, when they were derived, no limiting assumptions were made regarding the method of operation used.

In examining pulse systems, emitted pulse power $P_i$ should be substituted instead of $P_\Sigma$ in the range equations. This circumstance may be the cause of mistaken conclusions to the effect that pulse radar systems possess greater operating ranges than continuous emission systems, since a large amount of power can be obtained more easily during pulse operation.

Actually, increase in the power emitted in the pulse leads to an increase in the power of the received reflected signal $P_{pr}$. However, the sensitivity of the receiver depends above all upon the noise level, that is, is determined by the relationship between the received signal power $P_{pr}$ and the noise power $P_{pr\ pom}$. If there are no external noises, the sensitivity of the station is limited by the internal fluctuating noises of the receiver and is determined by ratio

$$\text{signal/noise} = P_{pr}/P_{sh}.$$

In order to discriminate reflected signals in the terminal device with a reliability no lower than that assigned, it is necessary that the signal/noise ratio at the receiver input be not less than some fully determined quantity $m_r$, that is

$$\frac{P_{пр}}{P_ш} \geqslant m_r, \qquad (4.7)$$

where the equality corresponds to the threshold condition.

Quantity $m_r$ is called the discrimination factor. It shows how many times greater the power of the minimum received signals must be than the power of the internal noises of the receiver, as reduced to the input of a radio device, for the target signals to be discriminated with the assigned reliability.*

The power of the internal noises of the receiver, reduced to its input,

$$P_ш = kNT\Delta f,$$

where $k = 1.38 \cdot 10^{-23}$ w-deg/Hz is Boltzmann's constant, which characterizes the increase in noise power per unit of passband with a one-degree increase in temperature; $N$ is the receiver noise factor; $T$ is the absolute temperature; $\Delta f$ is the receiver passband.

At a certain noise power and an assigned value of the discrimination factor, the threshold value of the received signal power

$$P_{пр\ мин} = n_p P_{ш} = m_p kNT\Delta f. \qquad (4.8)$$

The largest signal/noise ratio at the output of the receiver channel of a pulse system occurs at the optimum value of the receiver path and

$$\Delta_{f\ опт} = \frac{\xi}{\tau_и}.$$

where $\xi$ is a constant dimensionless factor depending upon the pulse shape and with a value close to unity.

We substitute value $P_{pr\ min}$ in range equation (4.5), assuming that the optimum receiver band has been selected:

$$R_{ср\ макс} = \sqrt[4]{P_и \tau_и \frac{D^2 \lambda^2 \sigma_ц}{(4\pi)^3 m_p kNT\xi}}. \qquad (4.9)$$

It follows from Expression (4.9) that target detection range is determined by the pulse energy. This important circumstance must be taken into account in selecting the transmitter power of a radar station and the length of the emitted pulses.

We express power $P_1$ emitted in the pulse by the average emission power $P_{sr}$ during pulse repetition period $T_p$

$$P_и = P_{ср} \frac{T_и}{\tau_и} = P_{ср} \frac{1}{\tau_и F_и}. \qquad (4.10)$$

By substituting Relationship (4.10) in Eq. (4.9) we obtain

$$R_{ср\ макс} = \sqrt[4]{P_{ср} \frac{D^2 \lambda^2 \sigma_ц}{(4\pi)^3 m_p kNTF_и \xi}}. \qquad (4.11)$$

The second factor in Expression (4.11) under the radical is a quantity which is constant for the given radar station and target. Thus, if the receiver passband is selected in accordance with the optimum shape and length of the signals, the radar observation range is determined by the average emitted power.

With very long pulses, the optimum band may be so narrow that the frequency instability of the transmitter and the receiver heterodyne may cause interruption of the reception of reflected signals. For this

reason the receiver band must be broadened beyond the necessary point, which leads to a reduction in the radar observation range with the same emitted power. An analogous difficulty arises in the case of radar systems with continuous emission.

The desire to increase the range of radar observation leads to the use in RLS receiver devices of low-noise high-frequency parametric and quantum amplifiers. Here the role of the external fluctuating noises from the surrounding space increases, since their power may be commensurable with the power of the receiver's own noises. Thus, the effect of external noises must be taken into account in calculating the sensitivity of a radar receiver with a high-frequency low-noise amplifier. Furthermore, under these conditions the noises introduced by elements of the feeder channel connecting the receiver and the antenna must be taken into consideration.

In calculating the range of radar observation in the expression for the threshold signal power

$$P_{\text{пр мин}} = m_p P_{\text{ш}}$$

the full value of the noise power as determined by all sources acting upon the receiver channel of the station must, in general, be accepted as quantity $P_{sh}$.

Noise power $P_{sh}$ may be expressed as effective noise temperature $T_{sh}$

$$P_{\text{ш}} = k\Delta f T_{\text{ш}}. \qquad (4.12)$$

The radar station noise temperature is made up of antenna noise temperature $T_a$ and the noise temperature of the reception channel $T_{pt}$, that is

$$T_{\text{ш}} = T_{\text{а}} + T_{\text{пт}}.$$

As is known, the noise temperature of the reception channel

$$T_{\text{пт}} = (N_{\text{ф}} N - 1)\,290°,$$

where $N$ is the receiver noise factor; $N_f$ is the feeder system noise factor. Then the equivalent noise power, reduced to the input of the receiver device

$$P_{ш} = k\Delta f T_{ш} = k\Delta f [T_a + (N_\phi N - 1) 290^\circ]. \qquad (4.13)$$

When Expression (4.13) is taken into account, range equation (4.5) takes the form

$$R_{св.макс} = \sqrt[4]{\frac{P_и D^2 \lambda^2 \sigma_и}{(4\pi)^3 m_p k \Delta f [T_a + (N_\phi N - 1) 290^\circ]}}. \qquad (4.14)$$

This is a more general form of the range equation for radar observation in free space. It takes into account not only the fluctuation noises of the receiver itself, but also noises captured by the antenna and also the noises of the feeder channel.

All of the formulas examined above for range of radar observation were obtained on the assumption that when electromagnetic waves are reflected from the target, their polarization is maintained. Under actual conditions, the polarization of an electromagnetic wave may be changed by reflection from a target – it becomes depolarized. The character of the depolarization depends upon the particular configuration and structure of the observed object. Here the polarization of the field of the reflected wave will no longer coincide with the antenna polarization, leading to a reduction in the signal power at the RLS receiver input.

The influence of change in the polarization of the reflected signal may be taken into account quantitatively by a corresponding reduction in the effective cross section of the RLS antenna. This is effected by introducing factor $\gamma \leq 1$ into the numerator of the expression under the radical sign in range equation (4.14). The size of this coefficient may be determined if the RLS antenna polarization and the polarization of the reflected wave are known.

## §4.2. RADAR OBSERVATION RANGE WITH ACTIVE RESPONSE

We will take up the question of radar observation range in free space with active response. We will consider that a responder is installed on the object which is being observed. It receives RLS signals and emits response signals at the same frequency. Usually the same antenna is used in the responder for transmission and reception.

The power of the RLS signals at the responder reception input

$$P_{\text{пр отв}} = \frac{P_{\Sigma}}{4\pi R^2} DA_{\text{отв}}, \qquad (4.15)$$

where $R$ is the distance from the RLS to the responder; $P_{\Sigma}$ is the RLS emissive power; $D$ is the directive gain of the RLS antenna; $A_{\text{otv}}$ is the effective cross section of the responder antenna.

If $A_{\text{otv}}$ is expressed in terms of the antenna directive gain $D_{\text{otv}}$, Relationship (4.15) may be presented in the form

$$P_{\text{пр отв}} = \frac{P_{\Sigma}\lambda^2}{(4\pi R)^2} DD_{\text{отв}}. \qquad (4.16)$$

The power of the response signal received by the RLS may be expressed analogously

$$P_{\text{пр}} = \frac{P_{\Sigma\,\text{отв}}\lambda^2}{(4\pi R)^2} DD_{\text{отв}}, \qquad (4.17)$$

where $P_{\Sigma\ \text{otv}}$ is the power of the signal emitted by the responder.

The operating range of a radar system with active response is determined both by the length of the connection between the RLS and the responder and by the length of the connection between the responder and the RLS. If the reception sensitivity of the responder is $P_{\text{pr otv min}}$, the length of the connection between the RLS and the responder

$$R_{1\,\text{макс}} = \sqrt{\frac{P_{\Sigma}}{P_{\text{пр отв мин}}} \frac{\lambda^2}{(4\pi)^2} DD_{\text{отв}}}. \qquad (4.18)$$

And accordingly, the length of the connection between the responder and the RLS will be determined by formula

$$R_{2\,макс} = \sqrt{\frac{P_{\Sigma\,отв}}{P_{пр\,мин}} \frac{\lambda^2}{(4\pi)^2} DD_{отв}}, \qquad (4.19)$$

where $P_{pr\ min}$ is the RLS receiver sensitivity.

At $R > R_{1\ maks}$ the RLS signals cannot trigger the transmitter of the responder, and in case $R > R_{2\ maks}$ the response signal will not be distinguished by the RLS terminal device against the background of fluctuating noises.

In designing a radar system with active response it is advisable to seek to obtain equality of the communication range between the RLS and the responder and between the responder and the RLS, when

$$R_{1\,макс} = R_{2\,макс} = R_{макс}. \qquad (4.20)$$

Such a system is the most economical from the power point of view.

By equating Expressions (4.18) and (4.19) with one another, we obtain the condition at which Relationship (4.20) is satisfied

$$P_з P_{пр\,мин} = P_{\Sigma\,отв} P_{пр\,отв\,мин}. \qquad (4.21)$$

Equation (4.21) makes it possible correctly to select the transmitter power and the receiver sensitivity of the responder.

In cases where Condition (4.21) is not satisfied, the operating range of a radar system with active response is determined by the lowest value for communication range obtained by calculating according to Formulas (4.18) and (4.19). In practice, the range from the responder to the RLS is somewhat larger, since RLS receivers operating under stationary conditions have better parameters than the responder receivers which are located on moving objects.

As has already been pointed out, recognition systems are a variety of the radar system with active response. In such systems the connection with the responder is often through a special interrogator which operates on a frequency different from the RLS frequency. In this case, the parameters of the interrogator are to be introduced into the above

formulas instead of the RLS parameters for calculating recognition range.

## §4.3. INFLUENCE OF THE REFLECTION OF ELECTROMAGNETIC WAVES FROM THE EARTH'S SURFACE UPON THE RANGE OF RADAR OBSERVATION

### 1. Some Characteristics of the Reflection of Electromagnetic Waves from the Earth's Surface

One of our assumptions in deriving the equation for range of radar observation was that the earth's influence could be neglected.

Emission and reception of lectromagnetic waves by a radar station

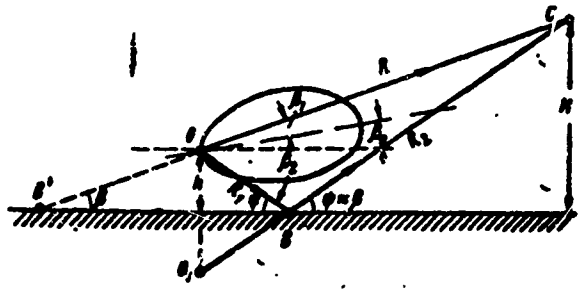

Fig. 4.1. Analysis of the problem of the range of radar observation.

antenna occur within some solid angle. Therefore, as the result of the reflection of electromagnetic waves from the earth's surface, there appears a supplementary path for propagation of electromagnetic waves from the radar station to the target and back. Because of this, the electrical field strength at the target will be determined by the vector sum of the strength of the direct wave and that of the wave arriving as a result of reflection from the earth's surface.

The electrical field strength $\dot{E}_1$ of the direct wave and the strength $\dot{E}_2$ of the reflected wave differ in amplitude and phase from one another. This difference is conditioned:

1) by the influence of the antenna directivity diagram, which has different gain factors for the target direction and for the direction

to the point of reflection from the earth's surface (Fig. 4.1);

2) by change in the amplitude and phase of the wave during reflection from the earth's surface;

3) by the geometrical difference in the traces of the direct and reflected waves.

If the surface of the earth at the point of impact of the electromagnetic wave is smooth (the height of roughness is small in comparison with the wavelength), reflection is specular. Here the reflected beam is in the plane of the incident beam and perpendicular to the reflective surface at the point of incidence, and the angle of reflection is equal to the angle of incidence. The change in amplitude and phase during reflection is characterized quantitatively by reflection factor $\dot{p} = pe^{-j\varphi}$. Quantity $\dot{p}$ depends upon the parameters of the soil, the polarization of the emitted wave, slip angle $\psi$, and the wavelength. In horizontal polarization the reflection factor

$$\dot{p}_{гор} = \frac{\sin\psi - \sqrt{\varepsilon' - \cos^2\psi}}{\sin\psi + \sqrt{\varepsilon' - \cos^2\psi}},$$

and in vertical reflection

$$\dot{p}_{вер} = \frac{\varepsilon' \sin\psi - \sqrt{\varepsilon' - \cos^2\psi}}{\varepsilon' \sin\psi + \sqrt{\varepsilon' - \cos^2\psi}}.$$

In these formulas $\varepsilon'$ is the relative dielectric permeability of the earth's surface in the area of reflection.

Distance $R$ to the target is usually much greater than altitude $h$ of the radar station antenna or altitude $H$ of the target itself. Because of this, beams $OC$ and $BC$ (Fig. 4.1) are practically parallel, slip angle $\psi$ may be considered equal to elevation $\beta$. Consequently, the reflection factor for a wave coming to the target along the path $OBC$ is a function of elevation.

If the target is viewed at small elevation, the size of the reflection factor is practically independent of the parameters of the

earth's surface, polarization, and wavelength. In this case

$$\dot{p}_{\text{гор}} \approx \dot{p}_{\text{вер}} \approx -1,$$

$$p_{\text{гор}} \approx p_{\text{вер}} \approx 1,$$

$$\varphi_{\text{гор}} \approx \varphi_{\text{вер}} \approx 180^{\circ}.$$

Thus, regardless of polarization the amplitude of the reflected wave is equivalent to that of the incident wave, and its phase differs by 180°.

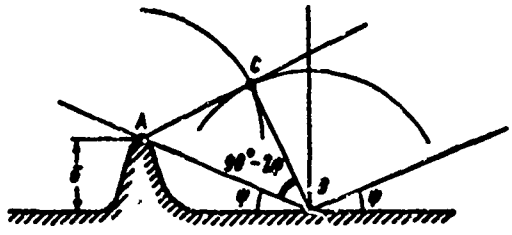

Fig. 4.2. Deriving the criterion of specular reflection.

The examined relationships for reflection factors are true for cases where the air-earth interface is smooth and there is specular reflection of the incident wave. However, under actual conditions the earth's surface has irregularities which can provoke a change in the character of reflection of the electromagnetic waves.

To establish the limits of the conditions in which there is specular reflection, we assume that a flat electromagnetic wave of length $\lambda$ (Fig. 4.2) is incident upon a surface with irregularities of height $\delta$. According to the Huygens principle each element of the front of a propagated wave may be viewed as the source of secondary elementary waves. Therefore, points *A* and *B* on the earth's surface will be viewed as sources of secondary emission.

If there were no irregularities, all the elementary sources of emissions on the earth's surface would form a flat reflected wave as the result of interference. One of the positions of the front of this wave would be the equiphase surface denoted by line *BC* in the plane of the drawing.

Because of the irregularities of altitude $\delta$, reflective elements *A* and *B* form fields which are shifted in phase at points *B* and *C* by a

quantity which depends upon the difference in traces

$$\Delta R = AB - AC = \frac{h}{\sin\psi}(1 - \cos 2\psi) = 2h\sin\psi,$$

to which correspond phase difference

$$\Delta\varphi = \frac{4\pi}{\lambda} h\sin\psi.$$

The phase shift between the oscillations at points $B$ and $C$ indicate that, due to the influence of the irregularities of the earth's surface, the front of the reflected wave is no longer flat. Because of this the waves are scattered in different directions upon reflection from a rough surface.

The influence of the irregularities will be smaller the smaller is the phase shift $\Delta\varphi$. For a surface of ideal smoothness $h = 0$ and $\Delta\varphi = 0$. In practice it may be considered that if the phase shift is small, the reflection is almost specular.

Similarly to the way this is done in optics, we assume that the phase shift may be neglected if $\Delta\varphi \leq \pi/4$. Then the height of the irregularities at which the earth's surface may be considered smooth,

$$h < \frac{\lambda}{16\sin\psi}. \qquad (4.22)$$

It follows from Formula (4.22) that the larger the wavelength and the smaller the slip angle $\psi$, the larger the permissible irregularities of the earth's surface.

As a rule, Condition (4.22) is satisfied with waves in the meter range. With waves in the decimeter range it is necessary to take into account the diffuse character of the reflection of electromagnetic waves, especially when targets are viewed at large elevations. In the centimeter range the earth's surface and the unquiet surface of the sea are almost always rough. Because of this the reflection is diffuse, and the intensity of the reflected waves falls to a very low value. The mod-

ulus of the reflection factor is tens or even hundreds of times smaller than in specular reflection. Therefore, in many cases only the direct wave need be examined in diffuse reflection.

## 2. Refining the Range Equation for Radar Observation Taking into Account Reflection of Electromagnetic Waves from the Earth's Surface

Assuming that the reflection of electromagnetic waves from the surface of the earth or water is specular, we examine the most general case when the antenna beam maximum is not directed at the target (Fig. 4.1).

Resultant electrical field strength $\dot{E}$ at the target represents the sum of the field strength of the direct wave $\dot{E}_1$ and the reflected wave $\dot{E}_2$

$$\dot{E}=\dot{E}_1+\dot{E}_2.$$

For strength $\dot{E}_1$ and $\dot{E}_2$ at the target, one may write

$$\dot{E}_1=\dot{E}_0\sqrt{D(\beta_1)},$$
$$\dot{E}_2=\dot{E}_0\sqrt{D(\beta_2)}\cdot pe^{-j(\varphi+\Delta\varphi)},$$

where $\dot{E}_0$ is the electrical field strength at the target created by a nondirectional antenna; $D(\beta_1)$ and $D(\beta_2)$ are the values of the antenna's directive gain in the corresponding directions (Fig. 4.1); $p$, $\varphi$ are, correspondingly, the modulus and the argument of the reflection factor; $\Delta\varphi=\frac{4\pi}{\lambda}h\sin\beta$ is the phase shift between the direct and reflected beams as conditioned by their trace difference.

Taking these relationships into account, the expression for electrical field strength may be written in the form

$$\dot{E}=\dot{E}_0\sqrt{D(\beta_1)}\left[1+\frac{\sqrt{D(\beta_2)}}{\sqrt{D(\beta_1)}}pe^{-j(\varphi+\Delta\varphi)}\right]=$$
$$=\dot{E}_1\cdot\left[1+\sqrt{\frac{D(\beta_2)}{D(\beta_1)}}pe^{-j(\varphi+\Delta\varphi)}\right]$$

or

$$\dot{E}=\dot{E}_1\left[1+p_{об}e^{-j(\varphi+\Delta\varphi)}\right]. \qquad (4.23)$$

Quantity

$$p_{об}=p\sqrt{\frac{D(\beta_2)}{D(\beta_1)}} \qquad (4.24)$$

will be called the *generalized reflection factor*. It shows the extent to which the amplitude of the wave reflected from the earth differs from the amplitude of the direct wave. Here the factor $p_{ob}$ takes into account not only the reflective properties of the earth's surface, but also the influence of the directivity diagram of the radar station antenna. In Expression (4.14) the latter is characterized by function $\sqrt{\frac{D(\beta_2)}{D(\beta_1)}}$.

We determine the amplitude value of the electrical field strength by multiplying Formula (4.24) by the conjugate complex expression

$$E_м^2=|\dot{E}|^2=\dot{E}\cdot\dot{E}^*=E_{м1}^2\left[1+p_{об}e^{-j(\varphi+\Delta\varphi)}\right]\left[1+p_{об}e^{j(\varphi+\Delta\varphi)}\right].$$

Whence the amplitude of the strength of the resultant field

$$E_м=E_{м1}\sqrt{1+p_{об}^2+2p_{об}\cos(\varphi+\Delta\varphi)}.$$

The analogous expression will be true also for the actual value of the electrical field strength

$$E=E_1\sqrt{1+p_{об}^2+2p_{об}\cos(\varphi+\Delta\varphi)} \qquad (4.25)$$

or

$$E=E_1\cdot\Phi(\beta), \qquad (4.26)$$

where

$$\Phi(\beta)=\sqrt{1+p_{об}^2+2p_{об}\cos(\varphi+\Delta\varphi)}. \qquad (4.27)$$

The function $\Phi(\beta)$ is called the *interference factor*.

In passing from the effective field strength values to the power flux density at the target, we may write

$$\Pi_c=\Pi_1\Phi^2(\beta),$$

where

$$\Pi_1=\frac{P_и D(\beta_1)}{4\pi R^2}.$$

The electromagnetic waves reflected from the target also return to the radar station by two paths, thanks to which at the RLS

$$П_{рлс}=\frac{П_{с\sigma_ц}}{4\pi R^2}\Phi^2(\beta)=\frac{P_1 D(\beta_1)\sigma_ц}{(4\pi)^2 R^4}\Phi^4(\beta)$$

and, consequently, for the power of the signals received by the radar station one may write

$$P_{пр}=P_{пр\,св}\Phi^4(\beta), \qquad (4.28)$$

where $P_{pr\ sv}$ is the power of the signals at the receiver input when the target is viewed in free space.

By comparing Expressions (4.3), (4.4) and (4.28) with one another, one reaches the conclusion that, taking into account reflection from the earth, radar observation range

$$R_{макс}=R_{св\,макс}\Phi(\beta), \qquad (4.29)$$

where $R_{sv\ maks}$ is the radar observation range in free space.

As is seen from Expression (4.27), the interference factor may, depending upon the target elevation $\beta$, vary between $\phi(\beta)_{min}=1-p_{ob}$ and $\phi(\beta)_{maks}=1+p_{ob}$. Thus, because of the reflection from the earth, the resultant characteristic of emission and reception even of a nondirectional antenna is lobe-shaped. Because of this the radar observation range will, depending upon target elevation, change from $(1-p_{об})R_{св\,макс}$ to $(1+p_{об})R_{св\,макс}$.

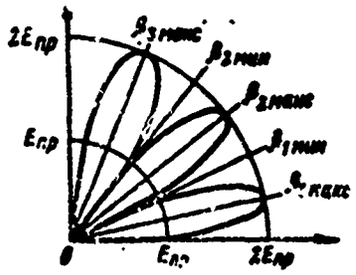


Fig. 4.3. Character of resultant directivity diagram in the vertical plane of a nondirectional antenna.

Let us examine several characteristic examples explaining the in-

fluence of the reflection of electromagnetic waves upon radar observation.

*First case.* The antenna is nondirectional in the vertical plane, that is, $D(\beta_1) = D(\beta_2)$. The polarization of the emitted electromagnetic waves is horizontal, and, consequently, at any elevation the modulus of the reflection factor $p \approx 1$, and the argument $\varphi \approx \pi$.

In this case the interference factor

$$\Phi(\beta) = 2\sin\left(\frac{2\pi}{\lambda} \cdot h\sin\beta\right). \qquad (4.30)$$

Relationship (4.30) is evidence that the resultant emission characteristic of a nondirectional antenna has become lobe-shaped because of the influence of the earth. Here $\Phi(\beta)_{min} = 0$, while $\Phi(\beta)_{maks} = 2$. In certain directions the radar observation range increases 2 times by comparison with $R_{sv\ maks}$. Together with this there is also a negative effect consisting in the fact that the power of the signals entering the receiver changes sharply with change in the target position, and there are directions in which the target cannot be viewed (Fig. 4.3).

It can be seen from Relationship (4.30) that for extremes of the resultant directivity diagram the condition applies

$$\frac{2\pi h}{\lambda}\sin\beta_n = n\frac{\pi}{2}, \qquad (4.31)$$

in which odd values of $n$ correspond to the directions of the maxima, while even values correspond to the minima.

We can use Condition (4.31) to derive the formula for determining elevations corresponding to the directions of the maxima and minima of the resultant directivity diagram

$$\sin\beta_n = \frac{n\lambda}{4h}. \qquad (4.32)$$

For small elevations it may be considered that

$$\sin\beta \approx \beta$$

and, consequently,

$$\beta_n \approx \frac{n\lambda}{4h}. \qquad (4.33)$$

On the basis of Formula (4.33) the tilt angle of the first lobe

$$\beta_{1\,\text{maks}} \approx \frac{\lambda}{4h}. \qquad (4.34)$$

Regardless of the altitude at which the target approaches the radar station, it will always pass through a zone in which it is observed at low elevations. If the target elevation $\beta << \beta_{1\,\text{maks}}$, that is, the direction of the target is much lower than the maximum of the first lobe, the discrimination of target signals will be made much more difficult. To improve the conditions of detection of targets at great distances or flying at low altitudes, it is necessary to increase the height of the antenna (see (4.34)). If this is done, the first lobe of the resultant directivity diagram hugs the surface of the earth, and the conditions of detection are improved. On the basis of Relationship (4.32) it is possible to determine the number of lobes of the resultant directivity diagram. Within the limits of elevation values from 0 to 90° the number of lobes of the directivity diagram is found from condition

$$\sin\beta_n = \frac{n\lambda}{4h} \leqslant 1.$$

Hence the number of maxima and minima of the directivity diagram is found from expression

$$n \leqslant \frac{4h}{\lambda}$$

as the nearest smaller whole number. The number of lobes $N_1$ is equal to the number of maxima, that is

$$N_1 = \frac{n}{2}$$

or

$$N_1 \leqslant \frac{2h}{\lambda}. \qquad (4.35)$$

Since $N_1$ is a whole number obtained from calculation according to Formula (4.35), the result must be rounded off to the nearest smaller whole number.

It is obvious that the number of lobes of the resultant diagram depends substantially upon the height of the antenna and upon the wavelength. As the wavelength is shortened and the station antenna is raised to a higher altitude, the number of lobes of the resultant directivity diagram is increased.

*Second case.* We will consider that the radar station antenna is directional in the vertical plane, while the emitted electromagnetic waves possess horizontal polarization. In this case the modulus of the reflection factor $p \approx 1$, the argument $\varphi \approx \pi$, while the generalized reflection factor for all cases when the tilt angle of the maximum of the directivity diagram $\beta_0 > 1$, will be

$$p_{об} = p\sqrt{\frac{D(\beta_2)}{D(\beta_1)}} < 1.$$

Consequently, the limiting values for the interference factor

$$\Phi(\beta)_{мин} = 1 - p_{об} > 0,$$
$$\Phi(\beta)_{макс} = 1 + p_{об} < 2.$$

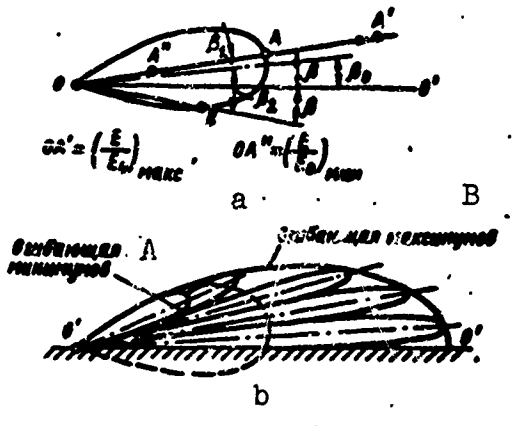


Fig. 4.4. Constructing the envelopes of the resultant directivity diagram. A) Envelope of the minima; B) envelope of the maxima.

The station's resultant directivity diagram in the vertical plane is lobe shaped as it was before. However, in the valleys of the diagram the intensity of the resultant field does not fall to zero, and in the maxima the field strength is not doubled.

The method of graphic construction of the envelopes of the maxima and minima of the diagram may be used for rapid evaluation of the resultant directivity characteristic of the radar station antenna.

As has been demonstrated, the resultant electrical field strength

$$\dot{E}=\dot{E}_0\sqrt{D(\beta_1)}+\dot{E}_0 p\sqrt{D(\beta_2)}\cdot e^{-j(\varphi+\Delta\varphi)}.$$

For the minima of the resultant directivity diagram

$$\varphi+\Delta\varphi=(2k+1)\pi,$$

and for the maxima of the lobe

$$\varphi+\Delta\varphi=k\cdot 2\pi,$$

where $k = 0, 1, 2, \ldots$

This means that the effective values of the field strength in the minima and maxima will be

$$E_{\min}=E_0\left[\sqrt{D(\beta_1)}-p\sqrt{D(\beta_2)}\right],$$
$$E_{\max}=E_0\left[\sqrt{D(\beta_1)}+p\sqrt{D(\beta_2)}\right],$$

where $E_0$ is the effective value of the field strength created by a non-directional antenna at the target.

Accordingly, we obtain in relative values

$$\left(\frac{E}{E_0}\right)_{\min}=\sqrt{D(\beta_1)}-p\sqrt{D(\beta_2)},$$
$$\left(\frac{E}{E_0}\right)_{\max}=\sqrt{D(\beta_1)}+p\sqrt{D(\beta_2)}. \qquad (4.36a)$$

If it is considered that in the case examined $p \approx 1$, then

$$\left(\frac{E}{E_0}\right)_{\min}=\sqrt{D(\beta_1)}-\sqrt{D(\beta_2)},$$
$$\left(\frac{E}{E_0}\right)_{\max}=\sqrt{D(\beta_1)}+\sqrt{D(\beta_2)}. \qquad (4.36b)$$

On the basis of Relationships (4.36) a first conception of the resultant directivity diagram may be obtained by using the antenna direc-

tivity diagram and data on the character of the reflection of electromagnetic waves from the earth's surface. For this an antenna directivity diagram must be constructed to a certain scale in the vertical plane (Fig. 4.4). Let the maximum of this diagram be directed at angle $\beta_0$ to the horizon. To find the point of the envelope of the diagram lobes from the origin of the coordinates we mark out beam *OA'* at some angle $\beta$ to the line of the horizon *OO'*. The beam intersects the diagram at point *A*. Radius vector *OA* characterizes in relative quantities the field of the direct wave. To determine the field of the reflected wave we project, starting from point *O*, beam *OB* which is displaced, also by angle $\beta$, down from the line of the horizon.

This beam intersects the diagram at point *B*. In the case under discussion, when $p \approx 1$, radius vector *OB* characterizes, in relative units, the field of the reflected wave. Then, by adding segment *OB* to *OA* we obtain point *A'* of the envelope of the maxima of the resultant diagram. Point *A"* of the envelope of the minima of the resultant diagram is, correspondingly, found by subtracting *OB* from *OA*. Other points of the envelopes of the maxima and minima of the resultant directivity diagram are found in an analogous manner. When the directions of the maxima and minima have been determined, they may be noted on the envelopes, and the lobes may be approximated.

If the target is flying at a constant altitude, as it draws nearer to the radar station it will fall within the lobes and the valleys of the resultant directivity diagram. Because of this there will occur changes in the character of the power $P_{pr}$ of the received signals (Fig. 4.5). In some range intervals quantity $P_{pr}$ will fall below the threshold value, and normal radar observation will be interrupted. The number of zones of this type, in wnich the target is not viewed, depends upon the number of lobes, which is determined by the relationship between $\lambda$

and λ. The smaller is λ, and the higher the radar station antenna, the more lobes there will be in the resultant diagram. During operation in the centimeter range the valleys in the observable zone are small. They are sources of supplementary fluctuation of the reflected signals when the target is moving. With longer, especially meter, waves, the number of lobes is small, and the valleys between them are so great that observation of the target may be interrupted.

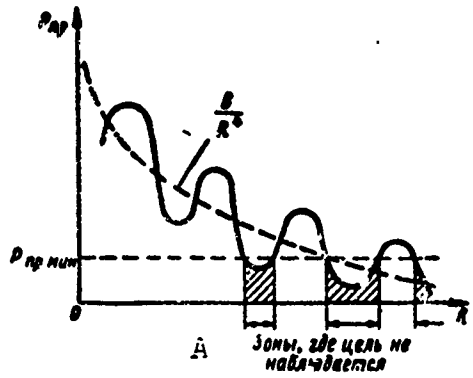


Fig. 4.5. Character of change of the power of a signal reflected from a target flying at constant altitude. A) Zones where target is not viewed.

*Third case.* The radar station antenna emits electromagnetic waves with vertical polarization. Here the modulus and argument of the reflection factor depend upon target elevation. In the general case $p < 1$, and, consequently,

$$\Phi(\beta)_{мин} = 1 - p_{об} > 0,$$
$$\Phi(\beta)_{макс} = 1 + p_{об} < 2.$$

The argument of the reflection factor $\psi < \pi$, and it approaches $\pi$ only for small elevations. This all means that the maxima and minima of the resultant directivity diagram, and their positions, will differ from the case of horizontal polarization.

At small elevations the size of the angular shift of the maxima is determined by relationship

$$\Delta\beta = \frac{\lambda}{h} \cdot \frac{\pi - \psi_0}{4\pi},$$

where $\varphi_v$ is the argument of the reflection factor for vertical polarization.

Inasmuch as $\varphi_v < \pi$, quantity $\Delta\beta_{maks} > 0$. Thus, with vertical polarization the lobes of the resultant directivity diagram are located somewhat higher than with horizontal polarization. This circumstance makes it difficult to detect targets observed at small elevations.

As was noted above, in the direction of the emission maxima the observation range increases considerably. For this reason the shaping of the maxima of the resultant diagram is of practical interest. For the maximum of the lower lobe to be shaped better, the area around the station within the limits of radius

$$r = 23\frac{h^2}{\lambda}$$

(first Fresnel zone) must provide specular reflection. If there are any irregularities or interfering objects, they must be smoothed and leveled off.

3. Detection Range of Low-Lying Targets

Low-lying targets are those whose sighting line is lower than the maximum of the first lobe. In this area, as a result of interference between the direct and reflected wave, there is a noticeable weakening in the strength of the resultant field, which leads to a sharp reduction in radar observation range.

Let us calculate the detection range of a low-lying target. To simplify the analysis without especially limiting the general validity of the obtained relationships, we will consider that the antenna used is nondirectional in the vertical plane.

If the accepted assumptions are taken into account, the interference factor

$$\Phi(\beta) = 2\sin\left(\frac{2\pi h}{\lambda}\sin\beta\right).$$

As an approximation it may be considered that sin β ≈ $H/R$ and, consequently,

$$\Phi(\beta) \approx 2\sin\left(\frac{2\pi Hh}{\lambda R}\right).$$

Since $H \ll R$, for low-lying targets, quantity $\sin\left(\frac{2\pi}{\lambda}\frac{Hh}{R}\right) \ll 1$ and the interference factor

$$\Phi(\beta) \approx 4\pi\frac{hH}{\lambda R}. \qquad (4.37)$$

Substituting Expression (4.37) into Formula (4.28) and considering that $P_{pr} = P_{pr\ min}$, we obtain the formula for the maximum range of radar observation of low-lying targets

$$R_{макс} = \sqrt[8]{\frac{P_s}{P_{пр\ мин}}\frac{4\pi D^2 H^4 h^4 \sigma_R}{\lambda^2}}. \qquad (4.38)$$

It is seen from Eq. (4.38) that the power of the reflected signals received from low-lying targets is inversely proportional to the eighth power of the distance. Such targets are detected only at comparatively small distances. To increase target detection range 2 times, the emission power would have to be increased by 256 times.

In accordance with the above derivation, the zone in which targets should be considered low lying is found from condition

$$\sin\left(\frac{2\pi}{\lambda}\cdot\frac{Hh}{R}\right) \approx \frac{2\pi}{\lambda}\cdot\frac{Hh}{R}.$$

It is satisfied if

$$\frac{2\pi}{\lambda}\cdot\frac{Hh}{R} < 0{,}2.$$

Hence the distance to the area in which the target is low lying

$$R_n = 10\pi\frac{Hh}{\lambda}. \qquad (4.39)$$

It follows from the latter formula that the higher the antenna, and the shorter the wave, the earlier the approaching target will be detected. On the contrary, if we are anxious to approach to within a minimum distance of the radar station without being detected, we should

fly at the minimum possible altitude.

## §4.4. THE INFLUENCE OF THE EARTH'S CURVATURE ON THE RANGE OF RADAR OBSERVATION

Hitherto we have been examining radar observation under conditions of propagation of electromagnetic waves over a flat earth. Such a way of viewing the task is correct when the target range is comparatively small. At large target distances from the radar station it is necessary to take into account the influence of the earth's curvature.

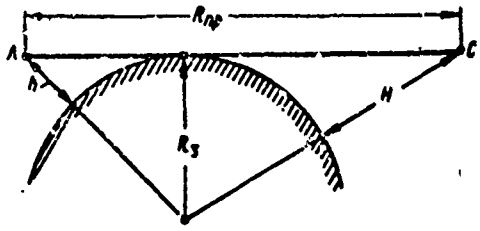


Fig. 4.6. Determining the range of direct visibility.

*Range of direct visibility.* The earth's curvature limits the range of radar observation to the range of direct visibility $R_{pr}$, which depends upon the altitude $h$ of the radar station antenna and upon target altitude $H$. Figure 4.6 shows the path

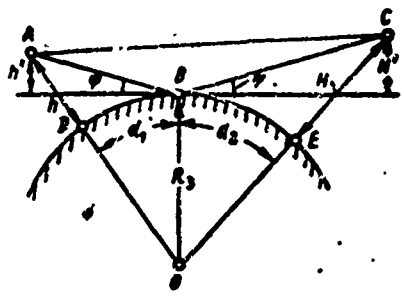


Fig. 4.7. Accounting for the influence of the earth's curvature.

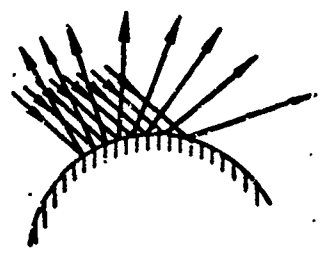

Spherical divergence of beams.

of beams in the limiting case of observation of a target at point $C$ located on a line tangential to the earth's surface. From the drawing it is seen that the range of direct visibility

$$R_{пр} = \sqrt{(R_з + H)^2 - R_з^2} + \\ + \sqrt{(R_з + h)^2 - R_з^2} \approx \sqrt{2R_з}(\sqrt{H} + \sqrt{h}), \qquad (4.40)$$

where $R_Z$ is the radius of the earth.

The case of propagation of electromagnetic waves within the limits of direct visibility must be distinguished from the case of their propagation outside the limits of $R_{pr}$. In the first case the field in the zone of radar observation is characterized by interference, and calculations may be carried out according to the formulas for reflection examined above, corrected to take into account the earth's curvature. In the second case the concept of interference cannot be used in reflection formulas.

*Taking the earth's curvature into account in determining the interference factor.* The formulas derived above for calculating the range of radar observation, which were obtained on the assumption that electromagnetic waves are reflected from the flat surface of the earth, become untrue for a spherical surface (Fig. 4.7). However, if a tangential plane is drawn through the point of reflection of electromagnetic waves from the earth's surface (point $B$), and the altitudes are calculated not from the surface of the earth but from this plane, the calculation procedure examined above can be used. For this it is sufficient to replace, in the appropriate formulas, the true altitudes of the target and antenna by their reduced altitudes $H'$ and $h'$. Such a substitution is justified because the slip angles of the beam relative to a spherical surface and relative to the plane of reduction are identical, both being equal to $\psi$.

On the basis of the constructions given in Fig. 4.7 one may write that the reduced altitudes*

$$h' = h - \frac{d_1^2}{2R_3},$$
$$H' = H - \frac{d_2^2}{2R_3}. \qquad (4.41)$$

Correspondingly, the elevation relative to the plane of reduction

$$\sin\beta' = \frac{n\lambda}{4h'}. \qquad (4.42)$$

It can be demonstrated by geometrical constructions that target elevation, as read off from the earth's surface

$$\beta=\beta'-\frac{d_1}{R_3}. \qquad (4.43)$$

We are usually interested in distant targets for which angles $\beta'$ are small and sin $\beta'$ can be replaced by its argument, whereupon

$$\beta=\frac{1}{4\left(h-\frac{d_1^2}{2R_3}\right)}\frac{n\lambda}{}-\frac{d_1}{R_3}. \qquad (4.44)$$

Using this formula the positions of the lobes of the resultant directivity diagram relating to the spherical surface of the earth are calculated.

In reflection of electromagnetic waves from a spherical surface there is divergence of the reflected beams. A bunch of parallel incident beams (Fig. 4.8) is transformed into a bunch of divergent reflected beams (spherical divergence) as a result of which the intensity of the reflected wave is reduced. This circumstance may be taken into account by reducing the coefficient of reflection from the spherical surface of the earth in comparison with the coefficient of reflection from a plane surface with the same parameters. Then the generalized coefficient of reflection

$$p_{об}=pD_p\sqrt{\frac{D(\beta_2)}{D(\beta_1)}}, \qquad (4.45)$$

where the coefficient of spherical divergence

$$D_p=\frac{1}{\sqrt{1+\frac{2H'h'}{R_3R_r\operatorname{tg}^2\beta}}}. \qquad (4.46)$$

In Formula (4.46) $R_g$ denotes the horizontal range of the observed target.

The coefficient of spherical divergence is minimum and equal to zero in slipping incidence of the beam upon the earth ($\beta = 0$). It reaches its maximum value, equal to unity, in perpendicular incidence

of the radio beam.

## §4.5. THE INFLUENCE OF ATMOSPHERIC REFRACTION UPON RADAR OBSERVATION RANGE

In analyzing the question of range it has been assumed up until now that the electromagnetic waves are propagated in a homogeneous atmosphere. In fact the atmosphere is a nonhomogeneous medium in which changes of the specific inductive capacitance cause changes in refraction factor $n = \sqrt{\varepsilon}$. As a result of this the trajectories of radio beams are bent – the electromagnetic waves are refracted.

The lower level of the atmosphere – the troposphere – has a substantial influence upon the RLS operating range. In the troposphere the specific inductive capacitance of air is a function of meteorological parameters: air pressure, temperature, and humidity. Being a function of meteorological parameters, the size of refraction factor $n$ is determined by formula

$$(n-1)10^6 \approx \frac{77,6}{T}\left(p_v + \frac{4810e}{T}\right), \qquad (4.47)$$

where $T$ is the absolute temperature of the air; $p_v$ is the total air pressure in millibars (1 mb = 0.75 mm col. merc.); $e$ is the partial pressure of water vapor in millibars (absolute humidity).

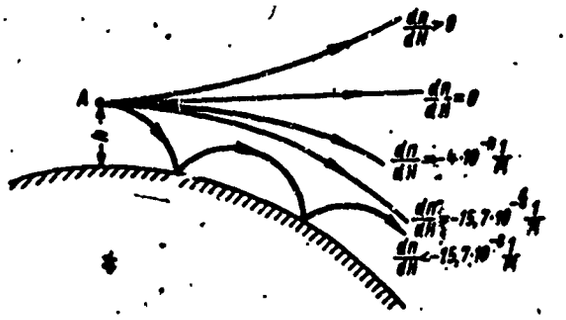


Fig. 4.9. Trajectories of outcoming horizontal radio beams with different kinds of refraction.

Relationship (4.47) does not depend upon frequency in the 100-

10,000 mc. It is considered to be true with an accuracy of up to 0.5% and for frequencies of up to 300,000 mc for usual values of pressure, humidity, and temperature.

When Formula (4.47) is used, a useful relationship may be that between the partial pressure $e$ of water vapor and the relative humidity $S_v$

$$e = \frac{S_v p_{vd}}{100}.$$

Here $p_{vd}$ is the pressure of water vapor in millibars at which, at the given temperature, there is saturation of the space.

The meteorological parameters of the atmosphere, and with them also the refraction factor, change with altitude. In this connection three characteristic cases of propagation of electromagnetic waves (Fig. 4.9) may be distinguished in function of the gradient of change of the refraction factor with altitude.

1. The case in which there is no refraction. Here $dn/dH = 0$ and electromagnetic waves are propagated rectilinearly.

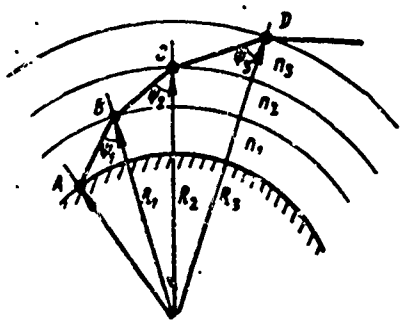


Fig. 4.10. Trajectory of a radio beam through stratified atmosphere.

2. Negative refraction occurs with increase in the refraction factor with altitude $dn/dH > 0$. In this case the radio beam is bulged downward, and the beam gradually moves away from the surface of the earth.

3. Positive refraction occurs when the refraction factor becomes weaker with altitude ($dn/dH < 0$). In this case the trajectory of the radio beam is bulged upwards. In contrast to negative refraction, positive refraction leads to an increase in the range of radar observation.

A quantitative evaluation of the influence of refraction on the range of radar observation requires in each concrete case a knowledge of the law of the change of the refraction factor with altitude. In practice, no general solution of this problem is possible because of the extreme variability of the atmosphere. Because of this, the influence of refraction on radar observation must, first of all, be evaluated for refraction in standard atmospheric conditions. The results obtained from such an analysis can be used, after the necessary adjustments have been made, for other cases as well.

For a standard atmosphere at the earth's surface the air pressure $p_v$ = 1015 mb, the temperature $T$ = 18°C, the relative humidity $S_z$ = 70%, and the relative specific inductive capacitance $\varepsilon'$ = 1.000676. Within the limits of the troposphere pressure, temperature, and humidity decrease with increase in altitude. Because of this quantity $\varepsilon'$ also decreases, tending toward unity as the air becomes thinner. In standard atmospheric conditions the gradient of the refraction factor is negative

$$\frac{dn}{dH} = -4 \cdot 10^{-8} \frac{1}{м}.$$

This comparatively slight change in the refraction factor with altitude causes the trajectory of the radio beam to bend toward the horizon, that is, there is positive refraction which in this case is known as normal refraction.

If the troposphere is viewed as consisting of a number of thin layers of air, differing in their refraction factor values $n$, the trajectory of a beam has the form shown in Fig. 4.10. For each layer the relationship is valid

$$n_i R_i \sin \psi_i = \text{const},$$

where $n_i$ is the refraction factor of the layer; $R_i$ is the distance from

the center of the earth to the layer; $\psi_i$ is the angle of incidence of the wave at the boundary of the layer.

The propagation of ultrashort waves over the spherical surface of the earth of radius $R_z$ in a nonhomogeneous troposphere with refraction factor $n$ decreasing with altitude, may be reduced to the case of propagation of electromagnetic waves in a homogeneous atmosphere with a constant refraction factor over the spherical surface of an earth of equivalent radius

$$R'_з = k_p R_з,$$

where $k_r$ is the refraction factor calculated from formula

$$k_p = \frac{1}{1 + R_з \frac{dn}{dH}}.$$

For standard atmospheric conditions in which $R_z$ = 6370 km the refraction factor $k_r$ = 1.33. The average value of $k_r$ changes with latitude: in arctic region $1.2 \leq k_r \leq 1.33$, and for the equatorial region $1.33 \leq k_r \leq 1.5$.

It should be pointed out that in the case of positive refraction $k_r > 1$ and $R'_z > R_z$, and, on the contrary, with negative refraction $k_r < 1$ and $R'_z < R$. It is obvious that in the absence of refraction $k_r = 1$ and $R'_z = R_z$.

One manifestation of atmospheric refraction is increase in the range of direct visibility. To take this increase into account, the equivalent radius of the earth for standard atmospheric conditions $R'_z = 1.33R_z \approx 8500$ km must be substituted in Formula (4.40). Then we find that

$$R_{пр} = 4{,}12(\sqrt{H} + \sqrt{h}),$$

where $R_{pr}$ is in kilometers, while quantities $H$ and $h$ are in meters.

Thus, under normal atmospheric conditions, refraction increases the range of direct visibility. However, refraction can also have an

undesired effect. Thus, curvature of the trajectory of the radio beam leads to mistakes in radar measurement.

Change in $\varepsilon'$ and in the refraction factor with altitude causes a change in the velocity of propagation of electromagnetic waves along the curvilinear trajectory of the radio beam. This, of course, should cause certain changes in the phase shifts of the direct and reflected wave heading toward the target. Analysis of the problem indicates that the influence of changes in the phase shift due to changing velocity is practical identical for the direct and the reflected beams. Therefore, in a first approximation, it may be considered that the influence of refraction is displayed only in change of the geometrical difference $\Delta R$ of the paths of the direct and reflected beams. Under usual conditions, when refraction factor $n$ decreases approximately linearly with altitude, this circumstance may be taken into account by replacing the radius of the earth by its equivalent value in the formulas examined above which were obtained on the basis of the interference concept.

The real atmospheric conditions are very often quite different from standard atmospheric conditions. In this connection let us examine some particular instances of positive refraction.

If the refraction factor of air changes with altitude in such a way that $dn/dH < -4 \cdot 10^{-8}$ m$^{-1}$, the curve in the radio beam trajectory increases in comparison with standard atmospheric conditions. *Critical refraction* occurs at $dn/dH = -1.57 \cdot 10^{-7}$ m$^{-1}$. Characteristic of this is transformation of the trajectories of radio beams, which were initially directed horizontally, into circles whose centers coincide with the center of the earth (see Fig. 4.9).

The conditions for critical refraction arise if the air temperature decreases by 1°C with each 9-10 m increase in altitude, or if the absolute humidity decreases by 1 mb with each 30 m increase in alti-

tude.

Conditions may arise in the troposphere in which $dn/dH < -1.57 \cdot 10^{-7}\ m^{-1}$. In such cases the curve of the radio beam trajectory becomes larger than the curve of the earth's surface, and there is superrefraction. In this case waveguide propagation of electromagnetic waves is possible (Fig. 4.9), when the trajectory of the radio beam lies completely within the limits of the lower layer of the troposphere – a waveguide channel.

The occurrence of a waveguide channel leads to a sharp increase in the limiting range of propagation of ultrashort-waves and causes a noticeable increase in the field strength.

If the altitude of the atmospheric waveguide above the earth's surface is such that the radar station antenna and the object are within this waveguide, the object may be viewed at distances many times exceeding the observation range under normal circumstances. Thus, for example, cases are known in which a station located at an altitude of 80 m above sea level detected ships which were more than 1120 km away, and detected the coast line at distances of up to 2500 km while the normal operating range was about 200 km.

Waveguide channels are formed when the temperature of the lower air layers increases with increase in altitude, while the specific humidity falls. With darkness the soil is cooled through radiation, causing supercooling in the lower layers of air. In the absence of wind the masses of air are not mixed, and, if the weather is clear, favorable conditions arise for the formation of a waveguide channel. Over the sea a low waveguide channel may arise in the region of the trade-winds where there is a sharp decrease in humidity with altitude. In addition, a waveguide channel is formed under the influence of the transfer of warm air from dry land to the cooler surface of the sea.

Superrefraction is an irregular phenomenon which it is hard to foresee and to utilize for radar observation. In practice, superrefraction leads to the appearance of signals from targets located at ranges in excess of the operating range of the station. Since the calibration of terminal devices and the selection of repetition period $T_p$ do not provide for the reception of signals from targets at ranges in excess of operating ranges, superrefraction is usually a source of supplementary interference in radar observation.

In observation of artificial earth satellites and space rockets the electromagnetic waves must pass through the ionosphere. This consists of a number of layers which differ from one another in the degree of concentration of free electrons $N$.

As is known, the refraction factor of a medium containing free electrons is determined by formula

$$n=\sqrt{1-\frac{4\pi Ne^2}{m\omega^2}}=\sqrt{1-80{,}8\frac{N}{f^2}}, \qquad (4.48)$$

where $N$ is the concentration of electrons in *electrons/cm*$^3$; $e$ is the electron charge, equivalent to $4.8\cdot10^{-10}$ electrostatic units; $m$ is the mass of the electron, equal to $9.1\cdot10^{-28}$ g; $f$ is the frequency of the incident wave.

It is obvious that for regions of the ionosphere in which the concentration of electrons increases with increase in altitude, $dn/dH < 0$ and there is positive refraction. On the contrary, in layers with $dn/dH > 0$ refraction is negative.

## §4.6. THE INFLUENCE OF ATMOSPHERIC ATTENUATION OF ELECTROMAGNETIC WAVES ON RADAR OBSERVATION RANGE

### 1. Atmospheric Attenuation of Electromagnetic Waves

During propagation in the troposphere ultrashort-waves are attenuated. The reason for attenuation are:

1) absorption of the energy of electromagnetic waves by atmospher-

ic gases, hydrometeors, and particles of dust and smoke;

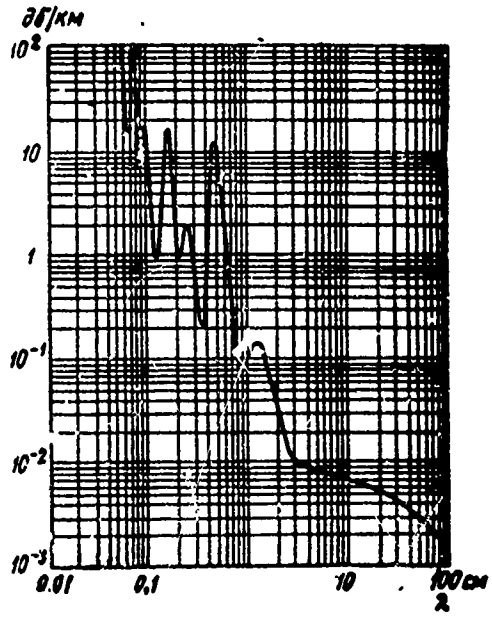


Fig. 4.11. Attenuation in the air as a function of wavelength.

2) scattering of electromagnetic waves by liquid and solid particles which lead to a reduction in the power flux density of the wave, that is, causes an effect analogous to energy absorption. The decrease in the power flux density of the electromagnetic wave with distance as a result of absorption and scattering is exponential. Therefore, an exponential weakening factor which accounts for attenuation of electromagnetic waves should be introduced into the formulas expressing the dependence of power flux density or the power at the receiver input upon distance $R$. If the signal power at the receiver input in the absence of attenuation is $P_{\text{pr sv}}$, in the presence of attenuation

$$P_{\text{пр}} = P_{\text{пр св}} e^{-\Gamma}, \qquad (4.49)$$

where $e^{-g}$ is the weakening factor; $\Gamma$ is the coefficient of total attenuation.

The size of the weakening coefficient depends upon the attenuation factor and upon target range. In the general case, when the intensity of attenuation of the electromagnetic wave changes along the trajectory of the radio beam

$$\Gamma = 2\int_0^R \alpha(R)\, dR, \qquad (4.50)$$

where $R$ is the distance from the radar station to the target; $\alpha(R)$ is the attenuation factor in an elementary section of the radio beam tra-

jectory.

For areas of homogeneous atmosphere characterized by constant attenuation, coefficient $\Gamma = 2\alpha R$, and the signal power at the receiver input

$$P_{пр} = P_{пр\,св} e^{-2\alpha R},$$

where $\alpha$ is the attenuation factor in napiers per kilometer, unchanged over the whole radio beam trajectory.

If attenuation factor $\alpha$ is expressed in decibels per kilometer, the obtained formula assumes the form

$$P_{пр} = P_{пр\,св} \cdot 10^{-0{,}4\alpha R}.$$

The size of the attenuation factor depends upon wavelength, atmospheric pressure, humidity, and temperature, and also upon the parameters of the particles causing scattering of the electromagnetic waves. If there are no hydrometeors or other particles in the atmosphere, attenuation is conditioned by energy absorption, principally by molecules of oxygen and water vapor. In accordance with what has been said, it may generally be considered that attenuation factor $\alpha$ is the sum of the items characterizing absorption of energy by molecules of oxygen – $\alpha_1$ and molecules of water vapor – $\alpha_2$, and also characterizing the influence of hydrometeors and other particles – $\alpha_3$, that is

$$\alpha = \alpha_1 + \alpha_2 + \alpha_3.$$

The absorption of ultrashort waves by water vapor is due to the fact that water molecules are polar and possess a constant electrical moment. The electrical field of the transient wave causes these molecules to oscillate. To each frequency of these oscillations there corresponds a particular energy level of the molecules. The number of these levels may be comparatively great. In the transition from the lower energy level to a higher one the gas molecules absorb energy from the electromagnetic wave. The opposite transition is accompanied by

emission of energy. However, this transition is disorderly and, as a result, the intensity of the transient wave is reduced. Collision among the molecules is a supplementary cause of energy losses by the wave.

Oxygen molecules possess constant magnetic momer ' 'nteract with the magnetic field of the transient wave, the result of which is also absorption of the wave's energy.

The absorption of energy by gas molecules depends upon the frequency of the electromagnetic wave There exist areas of resonance absorption where the absorption intensity increases sharply. The frequencies of resonance absorption are close to the frequencies of the transitions within the molecules themselves or coincide with them. On the whole, experimental research has demonstrated that the attenuation factor, as a rule, increases as the wave shortens.

Figure 4.11 shows the dependence of attenuation factor $\alpha = \alpha_1 + \alpha_2$ in the air at the earth's surface upon wavelength at a pressure of 760 mm col. merc., a temperature of 20°C, and with a water vapor content of 8 g per cubic meter of air. It is seen from the curves that there are peaks of resonance absorption in the centimeter and millimeter ranges. Theoretical and experimental research has demonstrated that the resonance absorption peaks at $\lambda \approx 0.5$ cm and $\lambda \approx 0.25$ cm are due to oxygen molecules, and at $\lambda \approx 0.18$ cm and $\lambda \approx 1.05$ cm — by water molecules. Furthermore, from an examination of the curves the conclusion may be drawn that absorption of the energy of electromagnetic waves by water vapor and oxygen in the air may be neglected for waves longer than 10 cm.

It should be borne in mind that absorption of the energy of electromagnetic waves by oxygen molecules varies in proportion to the square of the pressure ($\alpha_1 \equiv p_0^2$). Therefore, with increase in altitude

quantity $\alpha_1$ is reduced. At constant pressure absorption in oxygen varies in inverse proportion to temperature. The absorption of electromagnetic waves by water vapor is a function of humidity and temperature. Within the limits of the normal values of absolute humidity it may be considered that attenuation is proportional to humidity and, in the range $\lambda$ = 3-10 cm, inversely proportional to $(T)^{3/2}$.

TABLE 4.1

| Длина волны, см 1 | $\alpha_0$ |
|---|---|
| 1,0 | 0,20 |
| 2,0 | 0,075 |
| 3,0 | 0,032 |
| 4,0 | 0,014 |
| 5,0 | 0,007 |
| 6,0 | 0,0034 |
| 8,0 | 0,001 |
| 10,0 | $5 \cdot 10^{-4}$ |

1) Wavelength.

In many instances hydrometeors cause a very intense attenuation of electromagnetic waves. The size of the attenuation factor of a medium filled with hydrometeors depends upon the wavelength, the intensity of precipitation, the evenness of the distribution of particles, temperature, etc. A theoretical calculation of the influence of

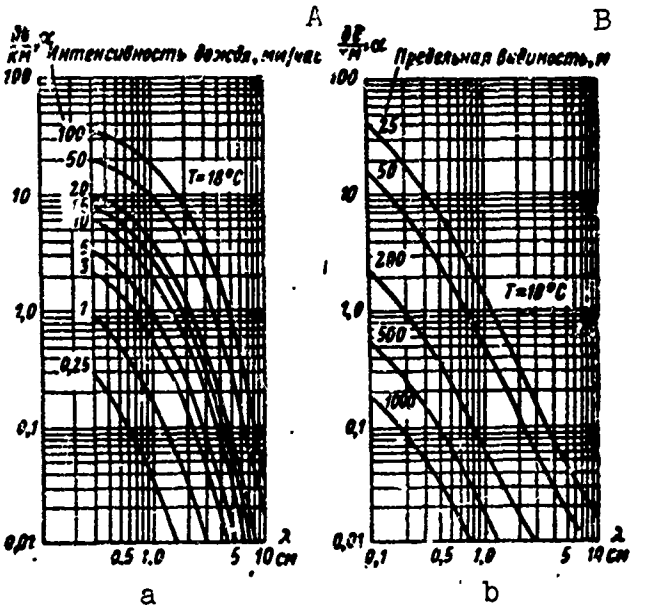


Fig. 4.12. Dependence of attenuation factor on wavelength at a temperature of 18°C: a) for various intensities of rain; b) for fog of various optical visibility. A) Rain intensity, mm/hour; B) limit of visibility, m.

all these factors is difficult. Consequently, in calculation either empirical expressions or experimental data are used for $\alpha_3$.

For an approximate evaluation of the average value of absorption factor $\alpha_3$, expressed in decibels per kilometer, one may employ the formula

$$\alpha_3 = \alpha_0 S_д,$$

where $\alpha_0$ is a coefficient depending upon the temperature and wavelength; $S_d$ is the intensity of precipitation, mm/hour.

Tables 3.2 and 4.1 give data characterizing the various kinds of hydrometeors and quantities $\alpha_0$ for rain at a temperature of 18°C and for various wavelengths.

For a more precise calculation of attenuation one may employ graphs of attenuation factor $\alpha_3$ which are constructed from data obtained theoretically and, in many instances, tested experimentally.

The graphs given in Fig. 4.12a are constructed for a temperature of 18°C. Therefore corrections must be introduced into these data for other temperatures.*

In the case of clouds and fog, when the drop diameter is small, the weakening of electromagnetic waves occurs principally through their absorption. Therefore, the average value of attenuation factor $\alpha_3$ depends not upon the drop diameter but upon the overall mass of water per unit of volume. For $\lambda$ = 0.5-10 cm an approximate value for the attenuation factor in clouds and fog may be determined from formula

$$\alpha_3 = 0{,}483 \frac{M}{\lambda^2},$$

where $\alpha_3$ is in db/km; $M$ is water content, g/m$^3$; $\lambda$ is in cm.

Electromagnetic waves are also attenuated when they pass through regions of hail. In the case of hail the size of the attenuation factor may be approximated by formula

$$\alpha_3 = \alpha_0' S_{гр},$$

where $\alpha_3$ is in db/km; $S_{gr}$ is the intensity of precipitation after melt-

ing, mm/hour; $\alpha_0'$ is a coefficient depending upon the temperature and wavelength.

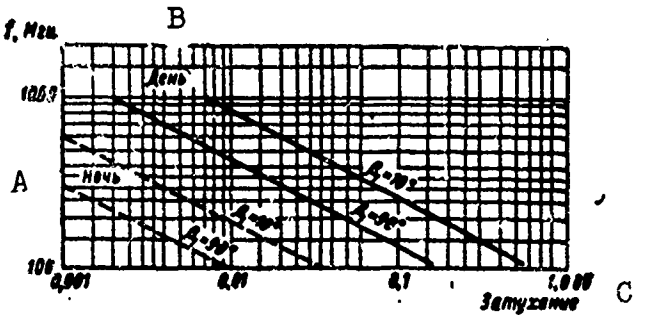


Fig. 4.13. Attenuation of electromagnetic waves in the ionosphere during propagation in one direction. Target altitude $H$ = 1000 km; $\beta_1$ is the beam elevation at the lower boundary of the atmosphere. A) Night; B) day; C) attenuation.

Values of $\alpha_0'$ for hail at $T°$ = 0°C and various values of $\lambda$ are given in Table 4.2.

TABLE 4.2

| Диаметр градин, см 1 | λ, см | | |
|---|---|---|---|
| | 1 | 3 | 8 |
| 0,25 | $2{,}7\cdot10^{-2}$ | $3{,}7\cdot10^{-4}$ | $2{,}2\cdot10^{-6}$ |
| 0,5 | $1{,}1\cdot10^{-1}$ | $1{,}5\cdot10^{-3}$ | $2{,}7\cdot10^{-5}$ |
| 1,0 | $7{,}3\cdot10^{-2}$ | $8{,}5\cdot10^{-3}$ | $7{,}5\cdot10^{-5}$ |
| 1,5 | $2{,}8\cdot10^{-2}$ | $1{,}7\cdot10^{-2}$ | $1{,}8\cdot10^{-4}$ |
| 2,0 | $1{,}0\cdot10^{-2}$ | $1{,}7\cdot10^{-2}$ | $3{,}6\cdot10^{-4}$ |

1) Diameter of hailstones, cm.

In radar observation of objects in the ionosphere and higher it is necessary to consider attenuation of electronic waves during passage through ionized media. The intensity of absorption of electromagnetic waves in the ionosphere is proportional to the electron concentration and the frequency of collisions of electrons with other particles.

Figure 4.13 gives graphs of the attenuation of electromagnetic waves in the ionosphere from which it may be concluded that under normal conditions and at frequencies higher than 100 Mhz attenuation in the ionosphere is comparatively slight.

## 2. Making the Radar Observation Range Equation More Precise by Introducing Attenuation of Electromagnetic Waves

It has been pointed out above that the attenuation of electromagnetic waves leads to an exponential decrease in the received signal power as a function of distance $R$ to the target. In the absence of attenuation, the received signal power is

$$P_{\text{прсв}} = \frac{B}{R^4},$$

where $B$ is a quantity whose value is determined by all the other parameters entering the range equation.

In the presence of attenuation

$$P_{\text{пр}} = \frac{B}{R^4} e^{-\Gamma}.$$

It is obvious that in the first case a longer range $R_{\text{sv maks}}$ corresponds to the threshold value of received signal power $P_{\text{pr min}}$ than in the second case. For threshold conditions

$$\frac{B}{R_{\text{св макс}}^4} = \frac{B}{R_{\text{макс}}^4} e^{-\Gamma}.$$

Hence the maximum range of radar observation in the case of attenuation

$$R_{\text{макс}} = R_{\text{св макс}} e^{-\frac{1}{4}\Gamma}. \qquad (4.51)$$

Substitution of the value of the coefficient of total attenuation (4.50) in Eq. (4.51) yield an expression for the general case

$$R_{\text{макс}} = R_{\text{св макс}} e^{-\frac{1}{2}\int_0^{R_{\text{макс}}} \alpha(R)\,dR}. \qquad (4.52)$$

If the trajectory of a radio beam can be broken down into a series of segments $\Delta R_i$ within the limits of each of which $\alpha = \alpha_i = \text{const}$, the coefficient of total attenuation

$$\Gamma = 2\sum_{i=1}^{k} \alpha_i \Delta R_i$$

and, consequently, the maximum range

$$R_{макс} = R_{св\ макс} e^{-\frac{1}{2}\sum_{i=1}^{k} \alpha_i \Delta R_i}, \qquad (4.53)$$

where

$$\sum_{i=1}^{k} \Delta R_i = R_{макс}. \qquad (4.54)$$

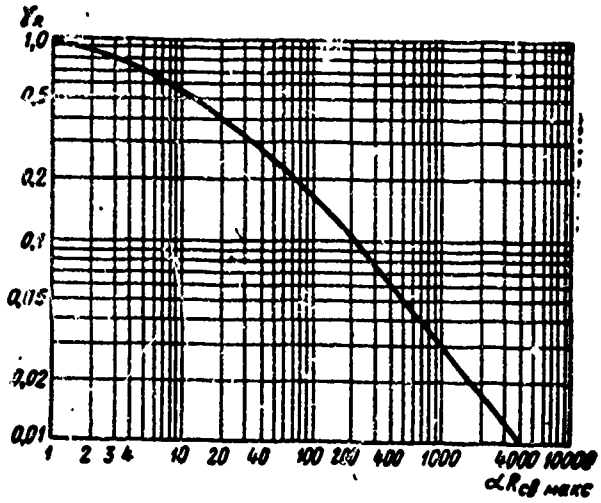


Fig. 4.14. Relative decrease in range as a function of atmospheric attenuation.

The solution of Eqs. (4.53) and (4.54) for $R_{maks}$ involves great difficulties. In practice, this sort of technical calculation is done through trial substitutions.

In many cases the medium through which the electromagnetic waves are being propagated is homogeneous, and in it attenuation is constant ($\alpha$ = const). It is sometimes possible to assume, as a preliminary estimate, that attenuation is constant along the whole trajectory of the radio beam, attenuation factor $\alpha$ being equal to some averaged quantity. Then Eq. (4.52) takes the form

$$R_{макс} = R_{св\ макс} e^{-\frac{1}{2}\alpha R_{макс}}, \qquad (4.55)$$

if $\alpha$ is expressed in nepers/km, and

$$R_{\text{макс}} = R_{\text{св макс}} e^{-0,115 \alpha R_{\text{макс}}},$$

when α is in db/km.

Although Eq. (4.55) is comparatively simple, it is impossible to obtain a general value for $R_{maks}$. This equation must either be solved graphically, which requires a large expenditure of time, or, making a rough approximation, the $R_{maks}$ in the index may be replaced by $R_{sv\ maks}$.

For a precise solution to the problem one may proceed as follows.

Transforming Eq. (4.55) into its logarithmic form, we obtain

$$\ln R_{\text{макс}} = \ln R_{\text{св макс}} - \frac{1}{2} \alpha R_{\text{макс}}$$

and after transformations

$$\alpha R_{\text{св макс}} = 2 \frac{R_{\text{св макс}}}{R_{\text{макс}}} \cdot \ln \frac{R_{\text{св макс}}}{R_{\text{макс}}}. \qquad (4.56)$$

The introduced quantity

$$\gamma_R = \frac{R_{\text{макс}}}{R_{\text{св макс}}},$$

which characterizes the relative decrease in radar observation ran e as a result of the attenuation of electromagnetic waves. When $\gamma_R$ is taken into consideration, Eq. (4.56) takes the form

$$\alpha R_{\text{св макс}} = 2 \frac{1}{\gamma_R} \ln \frac{1}{\gamma_R} = 4,6 \frac{1}{\gamma_R} \lg \frac{1}{\gamma_R}. \qquad (4.57)$$

Thus we have obtained a dependence of the type

$$\alpha R_{\text{св макс}} = f(\gamma_R).$$

This dependence is convenient for practical calculations because it can be used to determine the value of the relative decrease in range as a function of known quantities: observation range in free space without attenuation $R_{sv\ maks}$ and without attenuation factor α. Figure 4.14 gives the dependence curve

$$\gamma_R = \varphi(\alpha, R_{\text{св макс}}).$$

By using this curve we may determine the range of radar observation of

electromagnetic waves.*

An examination of Fig. 4.14 leads to the conclusion that the relative decrease in $R_{maks}$ increases with increase in the observation range and the attenuation. Radar practice shows that waves longer than 10 cm, even under the least favorable meteorological conditions, undergo little attenuation in the troposphere. Therefore, attenuations may be disregarded in calculating the $R_{maks}$ of radar stations in the decimeter and meter ranges. Waves in the centimeter and millimeter ranges undergo sensible attenuation in the atmosphere. For that reason they cannot be used in long-range stations. However, in short-range radar stations the centimeter and millimeter ranges may be quite suitable.

Ionospheric attenuation must be considered in the case of extra-long-range radar observation. During glancing impact of a radio beam on the ionosphere when the $F_2$ layer is very dense, even the shortest waves in the meter range undergo sensible absorption in the regular ionosphere. Ionized heterogenieties cause scattering of the electromagnetic waves, and the resultant attenuation may be noticeably heightened.

In the case of extra-long-range detection of objects it is desirable to initiate observation when they are still below the horizon. For this it is usually recommended to use waves shorter than 1-2 m. However, too short waves cannot be used, since they would be intensively attenuated in the troposphere.

## §4.7. DIAGRAM OF RADAR STATION VISIBILITY

From the point of view of the utilization of the radar station it is important in what zone of space the target will be observed. Visibility diagrams are used for visual representation of this zone.

The visibility diagram reproduces the geometrical locus of the space within which a target with an assigned $\sigma_{ts}$ would have a reflected signal power with the minimum acceptable value $P_{pr\ min}$. The visibility

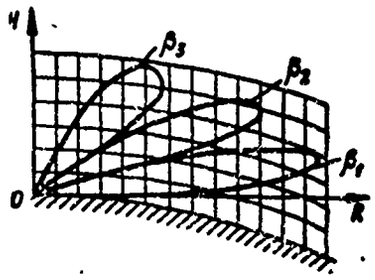


Fig. 4.15. Diagram of radar station visibility.

diagram divides all of space into two areas: the area in which targets with an assigned $\sigma_{ts}$ are detected and that in which these targets are not observed. To represent completely the zone of radar observation the visibility diagram would have to be constructed in a three-dimensional coordinate system. However, such a three-dimensional diagram is inconvenient to use in practice and difficult to construct. Therefore visibility diagrams are used which represent the radar observation zone in one plane – the vertical. Since the station antenna is usually scanning, the diagram is constructed for the plane of the antenna's maximum emission.

Visibility diagrams are most often constructed in the vertical plane. This is because in many types of stations the antenna beam is either motionless or practically so in the vertical plane, and a sweeping is accomplished through movement in azimuth.

The visibility diagram is usually constructed either in range – elevation coordinates $R = R(\beta)$, or range – altitude coordinate $R = R(H)$. In the latter case, reduced altitude $H'$ are laid out instead of true target altitudes $H$ so as to avoid introducing substantial errors due to the curvature of the earth's surface. The equation of the trace of the earth's surface in a plane passing through the center of the earth and the RLS takes the form

$$R^2 + (R_3 + H')^2 = R_3^2.$$

From this, removing the brackets and considering that $H' << R_3$, we obtain

$$H' \approx \frac{R^2}{2R_3}.$$

This relationship is the equation of a parabola. Thus, the lines of equal altitudes in the visibility diagram are a family of parabolas.

Fundamental for the construction of visibility diagrams is the equation

$$R_{макс}(\beta) = R_{св\ макс}(\beta)\,\Phi(\beta).$$

By assigning values for elevation, the corresponding values for observation range increases and for the interference factor are determined, $R_{maks}(\beta)$ is calculated, and the diagram is constructed (Fig. 4.15).

The initial data for calculating the diagrams are the station parameters, the effective target area, and data on the part of the earth's surface which participates in shaping the reflected beam. In cases, where surface reflection can be ignored, the visibility diagram is geometrically similar to the antenna directivity diagram with respect to strength.

It is difficult to calculate accurately all the factors determining the visibility diagram, especially the influence of the structure of the earth's surface. Therefore, the diagram which is calculated theoretically must be corrected by the results of observation of real targets (through test flights over the radar station).

Manuscript Page No.

[Footnotes]

190 In some work the factor $m_r$ is also called the observability or visibility factor.

212 These questions are treated more fully in the book by M.P. Dolukhanov "Rasprostraneniye radiovoln" [Propagation of Radio Waves], Svyaz'izdat [Communications Publishers], 1951.

225 See the book by A.G. Arenberg "Rasprostraneniye detsimetrovykh i santimetrovykh voln" [Propagation of Decimeter and Centimeter Waves], Izd-vo "Sovetskoye radio" [Soviet Radio Publish-

ers], 1957.

230 Such a method of calculating radar observation range was first proposed by N.I. Klyuyev.

| Manuscript Page No. | Transliterated Symbols |
|---|---|
| 186 | ц = ts = tsel' = target |
| 186 | прд = prd = peredacha = transmitting |
| 186 | пр = pr = priyemnyy = receiver |
| 187 | св = sv = svyaz' = link |
| 187 | мин = min = minimal'nyy = minimum |
| 187 | макс = maks = maksimal'nyy = maximum |
| 189 | и = i = impul'snyy = pulse |
| 190 | пом = pom = pomekha = noise |
| 190 | ш = sh = shum = noise |
| 190 | р = r = razlicheniye = discrimination |
| 191 | опт = opt = optimal'nyy = optimum |
| 191 | ср = sr = sredniy = average |
| 191 | п = p = povtoreniye = repetition |
| 192 | РЛС = RLS = radiolokatsionnaya stantsiya = radar |
| 192 | пт = pt = priyemnyy trakt = receiving channel |
| 192 | ф = f = fider = feeder |
| 194 | отв = otv = otvet = response |
| 197 | гор = gor = gorizontal'nyy = horizontal |
| 197 | вер = ver = vertikal'nyy = vertical |
| 201 | об = ob = obobshchennyy = generalized |
| 204 | л = l = lepestok = lobe |
| 208 | в = v = vertikal'nyy = vertical |
| 210 | н = n = nizkoletyashchiy = low-lying |
| 211 | з = z = zemlya = earth |
| 213 | р = r = raskhozhdeniye = divergence |
| 214 | в = v = vozdukh = air |
| 215 | вд = vd = voda = water |
| 217 | р = r = refraktsiya = refraction |
| 225 | д = d = dozhd' = rain |
| 225 | гр = gr = grad = hail |

## Chapter 5

## STATISTICAL EVALUATION OF RADAR SIGNAL OBSERVABILITY

### §5.1. RADAR SIGNAL RECEPTION AS A STATISTICAL TASK

Radar observation is accompanied by a whole series of factors which are not known to the observer and which cannot be calculated in any way other than statistically.

In the first case, the reflected signal of any real target itself undergoes fluctuation (this type of fluctuation is lacking in systems with active response).

In the second place, during propagation in a nonhomogeneous medium reflected or retransmitted signals undergo random fading due to interference by signals reaching the point of reception in various ways.

In the third place, upon the signal are superposed various types of interferences (noises) which are received by the antenna together with the signal from the surrounding space or are formed in the receiver itself.

As a result of the superposition of noises, the signal is distorted, and its intensity either increases or decreases.

In the fourth place, in nonautomatic systems where the observer is a person, radar observation is influenced by the operator's subjective qualities which do not lend themselves to accurate calculation: training, attentiveness, fatigue, the extent to which he is subject to external influence, etc. The influence of such factors is eliminated in fully automatic systems.

In view of the random statistical character of all of these factors,

the results of radar observation may be evaluated only by methods of the theory of probability and of random processes.

Chapter 3 gave a mathematical analysis of the statistical laws applying to the process of reflection of a signal from a complex target.

Signal fading during propagation may be viewed as the process of multiplication of the signal $u(t)$ by random factor $\mu(t)$ which changes slowly over time by comparison with the high-frequency duty ratio of the signal. Hence noises of the fading type are known as *multiplicative* noises from the Latin word multiplicatio.

In view of the fact that in defining the concept of effective scattering cross-section the reflected signal was evaluated not at the point of reflection but at the point of reception, the statistical laws examined above, which describe the processes associated with reflection, at the same time also cover the processes occurring during propagation. Therefore, there is no special need for examining multiplicative noises separately in describing the parameters of the received signal. This is even more true in that the phenomena of fading and interference of signals during reflection from a complex target have a similar physical nature.

However, knowledge of the statistical laws of fading should certainly not be regarded as devoid of interest. The law of fluctuation of the reflected signal is one of the characteristics bearing information on the properties of the target. Violation of this law through fading during propagation inhibits clarification of the true properties of the target. Therefore the statistical properties of multiplicative noises must be known in order to extract maximum information about the target.

The theory of optimum reception under conditions of multiplicative noises has not yet been developed. However, most contemporary RLS are not designed to distinguish targets on the basis of their fluctuation

law, and the statistical laws of the signal during fading need not be examined separately.

The influence of the operator upon the process of radar observation may be evaluated only experimentally, by extensive observation of the work of many operators under different conditions.

It only remains to evaluate the effect of noises upon the radar signal, which is what will be done in the following section. Inasmuch as, during their interaction with the useful signal, noises are superposed upon the signal, they have been called *additive* noises from the Latin word *additivus*.

The radar station's capacity to observe targets in the presence of noises is called the *observability of radar signals*. Together with the other RLS parameters, observability is determined by the statistical properties of the target signal itself and by the properties of the noise. Therefore, observability will be evaluated both for a nonfluctuating and for a fluctuating target. By noise is usually understood noise of natural origin. The capacity of the RLS to observe targets against the background of other noises is usually viewed as part of its noise-resistance, which will be examined in a separate chapter.

Observability is closely linked to receiver sensitivity. In the UKV range sensitivity is usually evaluated by the power of the minimum detectable signal at the receiver input $P_{\text{pr min}}$, which is introduced into the formula for calculating the RLS operating range.

As has been noted, sensitivity is limited by the average power of the receiver noise as calculated as its input:

$$P_ш = NkT^\circ \Delta f. \qquad (5.1)$$

The minimum detectable signal under assigned conditions of observation should stand out above the noises in a determined way; this is called the discrimination factor:

$$m_p = \frac{P_{\text{пр мин}}}{P_{\text{ш}}}. \qquad (5.2)$$

The discrimination factor is a quantitative measure of observability: the more effectively the receiver device discriminates the signal against the noise background of assigned intensity, the lower the discrimination factor, and the better the signal observability.

Let us move from power to energy. The energy in a pulse of a minimum detectable signal $E_{s1})_{\text{мин}} = P_{\text{пр мин}}\tau_и$. The noise energy opposing the signal over the length of a pulse in an optimum receiver passband $\Delta f \cong \frac{1}{\tau_и}$ is equal to the noise power per unit of band, $E_0 = P_ш\tau_и = \frac{P_ш}{\Delta f} = NkT^0$. Therefore, if we multiply the numerator and the denominator in Formula (5.2) by $\tau_1$, we will obtain

$$m_p = \left(\frac{E_{s1}}{E_0}\right)_{\text{мин}}. \qquad (5.3)$$

This latter expression shows that observability does not depend up n pulse length or upon the receiver passband when it is optimum, but is determined only by the ratio of the energy of the minimum detectable signal to the noise power per unit of band and does not depend upon the spectrum width. This means that if we artificially widen the spectrum of the pulse, maintaining its energy unchanged, in order to heighten accuracy and range resolution, the sensitivity and operating range of the RLS will remain unchanged. Therefore, Formula (5.3) is more general than Formula (5.2): it also applies to signals with pulse-wide modulation, in which $\Delta f = \frac{K}{\tau_и}$, where $K >> 1$. RLS sensitivity could be calculated for such signals from Formula (5.1) if $\Delta f$ is taken to mean not the actual width of the signal spectrum for the receiver passband, but $\Delta f' = \frac{1}{\tau_и}$*.

Thus, sensitivity is determined both by the noise level in the receiver and by the capacity of the RLS to distinguish the signal against a background of noise, that is, by observability. Observability is

evaluated quantitatively by the magnitude of the minimum detectable signal in comparison with noise. Sensitivity is evaluated by the absolute magnitude of the minimum detectable signal when the noise level is taken into account. Sensitivity is heightened both by reducing the noise level in the receiver strip and by using more effective methods and devices to improve signal observability against the noise background.

Reduction of the absolute noise level in the receiver strip is a purely technical task and is accomplished by using antinoise circuits and low-noise elements, by preamplification of the signals before the mixer, by the use of balance mixes, etc. Recently parametric and molecular amplifiers have come into use in receivers; these almost completely eliminate the influence of internal noises in the receiver. In this case the basic role is played by noises received by the antenna from space.

The task of the present chapter is to evaluate observability, that is, to determine the discrimination factor $m_r$ for an assigned noise level in the receiver input and also for certain assigned results of observation. This can be used to determine the receiver sensitivity and the RLS operating range. In detection the results of observation are evaluated by the probability of detecting target $D$ and the probability of false alarms $F$ (false detection) or, in other words, by the signal/noise ratio in the RLS output element when the coordinates are measured accurately. In addition, this chapter evaluates the influence of certain RLS parameters upon radar signal observability.

## §5.2. INTERACTION OF HIGH-FREQUENCY SIGNAL AND NOISE

Noise voltage at the receiver input (antenna noise) has a completely disorderly structure. Noise takes the form of sharp peaks of positive and negative polarity, which rise and fall very rapidly, practically instantaneously (Fig. 5.1a), relative to the average zero value. The

noise spectrum may be viewed as even all the way up to very high frequency (Fig. 5.2a). As a result, such noise is called "white noise" by analogy with light oscillations which possess a broad spectrum.

The structure of noise changes sharply at the output of the linear part of the receiver: from the whole broad spectrum there is detached only a narrow frequency band $\Delta f$ around resonance frequency $f_0$ of the UPCh band filter (Fig. 5.2b). At the output of a narrow-band filter noise oscillations can no longer vary arbitrarily. They take the form of almost sinusoidal oscillation with average frequency $f_0$, and the amplitude and phase of these oscillations can neither rise nor fall more rapidly than the filter passband permits. It is difficult to speed up or slow down a narrow-band, high-Q system, just as it is to bias the phase of the oscillations, and, therefore, the amplitude (envelope) and phase of high-frequency noise oscillations of frequency $f_0$ vary at comparatively low frequencies in the range from 0 to $\Delta f$ (Fig. 5.1b).

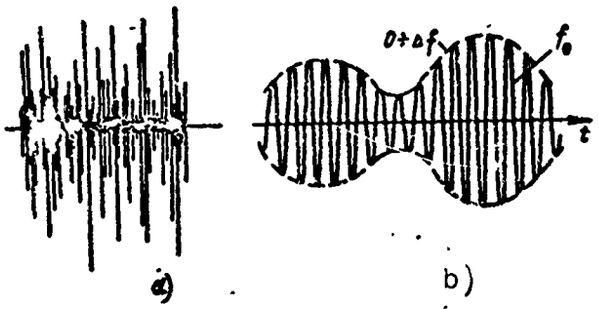


Fig. 5.1. Form of noise voltage: a) At the input of the linear part of the receiver; b) at the output of the linear part of the receiver.

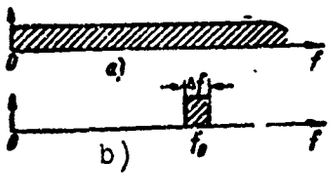


Fig. 5.2. Noise spectrum: a) At the receiver input; b) at the output of the linear part of the receiver.

The length of the shortest blip of the envelope of a high-frequency noise is of the order $\tau_ш \approx \frac{1}{\Delta f}$ ; within the limits of the time interval known as the correlation interval the amplitude and phase of the noise oscillations may be considered approximately unchanged.

When signal pulses of constant amplitude, with frequency $f_0$ and length $\tau_и = \frac{1}{\Delta f}$ , reach the receiver input, the high-frequency oscillations of the signal and the noise are added the result depending upon the relationship between the amplitude and the phases of these oscillations at each moment in time. Since frequencies are identical, and the length of the signal pulses and noise blips are approximately equal, the amplitude of the blips of the resultant oscillations (signal plus noise) will be equal to the sum of the amplitude of the signal and noise when the phases of their high-frequency duty ratios are equal and their amplitudes are different at a phase shift of 180°. In general, the amplitude of the resultant oscillations may have any value between the sum and the difference, depending upon the random phase relationships. In particular, if the amplitudes of the signal and the noise are accidentally equal, while the phases are opposed, the resultant amplitude is equal to zero, and the signal is lost.

As a result of the superposition of internal receiver noises upon the sequence of pulses of constant amplitude, there appears a sequence of signal (plus noise) pulses whose amplitude is a *random* quantity which can vary within broad limits from zero to the highest value possible in the receiver (formally – to infinity).

In addition, when the signal is absent, pure noise may yield large blips which are in no way to be distinguished from signal pulses.

The signal and noise may also interact in such a way as to be added together in one phase at the beginning of the signal pulse and in another at the end of the pulse, as a result of which the obtained to-

tal pulse may be biased. Since target range is judged from the pulse position, such a manifestation of the influence of noise upon signal leads to measurement error.

Thus, superposition of noise upon a regular signal may lead to the disappearance of the useful signal, to the appearance of a pulse signal and of measurement errors. The first two types of errors impose limits on sensitivity, the third type imposes limits on accuracy.

Noise voltage at the output of the linear part of the receiver may be represented in the form

$$n(t)=N(t)\cos[\omega_0 t-\varphi(t)], \qquad (5.4)$$

where amplitude $N(t)$ and phase $\varphi(t)$ are mutually independent random functions which change slowly by comparison with $\cos \omega_0 t$. Oscillation may be represented in the form of random vector $\vec{N}$. If we analyze vector $\vec{N}$ into its two orthogonal components in the rectangular coordinate system

$$N_1=N\cos\varphi \text{ and } N_2=N\sin\varphi,$$

representing oscillation

$$n_1(t)=N_1\cos\omega_0 t \text{ and } n_2(t)=N_2\sin\omega_0 t. \qquad (5.5)$$

In the first place, these two components are independent: the projection of one of them upon the other at any moment in time equals zero, and therefore variations in one projection have no influence upon the magnitude of the second (the property of being orthogonal).

In the second place, these two components are also functions which change slowly by comparison with $\cos \omega_0 t$ and $\sin \omega_0 t$.

In the third place, each of these components is distributed in accordance with normal law

$$W(N_{1,2})=\frac{1}{\sqrt{2\pi}\sigma_m}\exp\left[-\frac{N_{1,2}^2}{2\sigma_m^2}\right]$$

with average values $\overline{N}_1 = \overline{N}_{2sh} = 0$ and average squares $\overline{N}_1^2 = \overline{N}_2^2 = \sigma_{sh}^2$,

known as the noise dispersion or the noise power dissipated over a 1 ohm resistance.

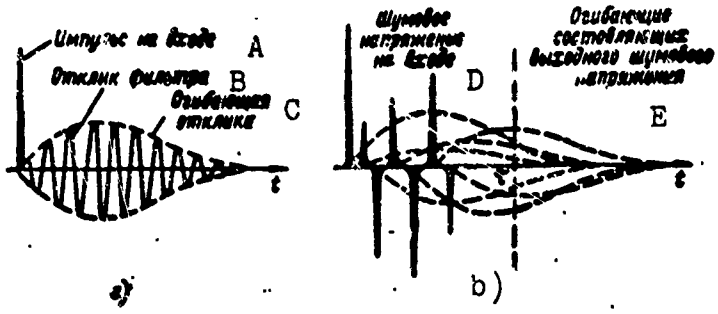


Fig. 5.3. Effect of independent disturbances upon a narrow-band system: a) Effect of single pulse; b) effect of noise voltage. A) Pulse at input; B) filter response; C) envelope of response; D) noise voltage at the input; E) envelopes of components of output noise voltage.

The normal distribution law is condition by the narrowness of the band of the receiver high-frequency filter and by the lack of dependence of the various noise blips, at the receiver input, upon one another. Actually, when a single noise blip acts upon the input of a narrow-band filter, at the output is obtained a high-frequency voltage, known as the response for the pulse characteristic of the filter (Fig. 5.3a). The input noise voltage takes the form of a sequence of spiked pulses, while the output voltage at any moment in time $\tau$ is equal to the sum of the filter responses for each pulse (Fig. 5.3b). In this case, in accordance with the central limiting theorem of probability theory, the output voltage, being at any moment in time the sum of a large number of independent random quantities (responses), is subject to the normal distribution law regardless of the law of distribution of each term.*

The normal law is even more applicable when the receiver itself possesses supplementary sources of noise (heat noises of the elements and shock noises of the tubes).

Let the signal at the receiver output take the form of a pulse of

sinusoidal oscillations of frequency $\omega_0$ with constant amplitude $A$

$$s(t) = A\cos\omega_0 t. \tag{5.6}$$

Here and below, quantities $x$, $s$, $X$, $A$ and $\sigma_{sh}$ will denote voltages across a 1 ohm resistance, numerically equal to the current.

We resolve (5.5) random vector $\vec{N}$ into two components: the phase $n_1(t)$ and the out-of-phase $n_2(t)$ in such a way that the phases of the signal $s(t)$ and of the noise component $n_1(t)$ coincide. Then, after adding the signal and the noise, we obtain two independent components $X_1 = A + N_1$ and $X_2 = N_2$, which are, as before, slowly changing random quantities which represent two oscillations

$$x_1(t) = X_1(t)\cos\omega_0 t \quad \text{and} \quad x_2(t) = X_2(t)\sin\omega_0 t.$$

Accordingly, the average values of these components are $\overline{X}_1 = A$ and $\overline{X}_2 = 0$, and quantities $X_1$ and $X_2$ themselves undergo random oscillations, according to the normal law, relative to their average values:

$$W(X_1) = \frac{1}{\sqrt{2\pi}\,\sigma_m}\exp\left[-\frac{(X_1 - A)^2}{2\sigma_m^2}\right] \tag{5.7}$$

and

$$W(X_2) = \frac{1}{\sqrt{2\pi}\,\sigma_m}\exp\left[-\frac{X_2^2}{2\sigma_m^2}\right].$$

Thus, we have obtained distribution for the two orthogonal components of the signal-plus-noise similar to those obtained in Chapter 3 for the two orthogonal components of the signal of a complex target.

By proceeding in the same way we can find the combined distribution of the probabilities of both orthogonal components $W(X_1, X_2)$ and then go on to the combined distribution of envelope (amplitude) $X$ and of phase $\varphi$ of the high-frequency signal at the detector input

$$W(X, \varphi) = \frac{1}{2\pi\sigma_m^2}\exp\left[-\frac{X^2 + A^2 - 2AX\cos\varphi}{2\sigma_m^2}\right]. \tag{5.8}$$

We introduce relative quantities

$$a=\frac{A}{\sigma_{ш}} \quad \text{and} \quad v=\frac{X}{\sigma_{ш}},$$

which do not depend upon the noise power. Then Formula (5.8) for the combined distribution of the normalized amplitude and phase takes the form

$$W(v,\ \varphi)=\frac{v}{2\pi}\exp\left[-\frac{v^2+a^2}{2}\right]\exp\left[av\cos\varphi\right]. \qquad (5.9)$$

If we eliminate phase by integrating Distribution (5.9) for all $\varphi$ from 0 to $2\pi$, we will obtain the probability distribution for the amplitude of the signal-plus-noise at the output of the linear part of the receiver

$$W(v)=v\exp\left[-\frac{v^2+a^2}{2}\right]I_0(av), \qquad (5.10)$$

where $I_0(av)$ is the Bessel function of the zero order from the imaginary argument, equal to 1 at $av = 0$.

If $a = 0$ in the last formula, we find the probability distribution for the envelope of a pure noise

$$W(v)=v\exp\left[-\frac{v^2}{2}\right]. \qquad (5.11)$$

As has been pointed out, such a distribution is called the Rayleigh distribution for the circular Gaussian distribution. Expression (5.10) is called the *generalized Rayleigh distribution.*

By integrating over all values of envelope $v$ from 0 to $\infty$, Formula (5.9) can also be made to yield the probability distribution for the phase of a high-frequency signal-plus-noise

$$W(\varphi)=\frac{1}{2\pi}\exp\left[-\frac{a^2}{2}\right]+\frac{a\cos\varphi}{\sqrt{2\pi}}\Phi(a\cos\varphi)\exp\left[-\frac{a^2\sin^2\varphi}{2}\right], \qquad (5.12)$$

where $\Phi(z)=\frac{1}{\sqrt{2\pi}}\int_{-\infty}^{z}e^{-\frac{t^2}{2}}dt$ is, as before, the Laplace function (probability integral).

The phase distribution for pulse noise

$$\dot{W}(\varphi)=\frac{1}{2\pi}. \qquad (5.13)$$

Formulas (5.10) and (5.12) for the amplitude and phase of a regular signal-plus-noise coincides fully with Formula (3.32) and (3.35) which describe the distribution of the amplitudes and phases of a reflected target signal. From the formulas and graphs given in Chapter 3 it is seen that as the signal intensity $a$ increases, the distribution of envelope $v$ of the signal-plus-noise approaches the symmetrical normal law. The law of the distribution of phase with the growth of $a$ also becomes normal, the probable values of the phase of oscillations concentrating near $\varphi = 0$. In the case of a very strong signal the phase of the resultant oscillation hardly differs from the phase of a pure signal ($\varphi = 0$) and, consequently, is stable.

The appearance of phase shift $\varphi \neq 0$ in the resultant oscillation is due to the presence of the out-of-phase noise component. The fact that the vector of a strong signal-plus-noise nearly coincides with the vector of a pure signal indicates, in this instance, the weak influence of the out-of-phase component. Therefore, elimination of the out-of-phase noise component, for example, to synchroncus detecting, will have a weak influence on the envelope of the strong signal. On the contrary, when the signal is very weak ($a < 1$), elimination of the out-of-phase noise component yields a significant improvement in the signal/noise ratio, by eliminating the effect of suppression of the relatively weak signal by noises. Thus, in synchronous detecting, when both amplitude and phase relationships are taken into consideration, noise will have an identical influence on the envelope of a weak and of a strong signal.

In ordinary detecting only amplitude relationships are taken into account, which lead to a loss of energy at small signal/noise ratios. Actually, the voltage at the output of the so-called linear detector is

proportional to the amplitude of the high-frequency signal at its input. Probability distribution for signal with noise and for a pure signal at the detector output are described by Formulas (5.10) and (5.11), respectively. When signals are weak ($a$ is small) the most probable and average signal values differ very little from the corresponding values for a pure noise because of the strong influence of the out-of-phase noise component.

Voltage at the output of a quadratic detector is proportional to the square of signal amplitude at the input. By substituting $w = v^2/2$ and $dw = 2vdv$ in Formula (5.10), we obtain a distribution density of signals at the output of the quadratic detector

$$W(w)=\exp\left[-w-\frac{a^2}{2}\right]I_0\left(a\sqrt{2w}\right) \qquad (5.14)$$

for the signal-plus-noise and

$$W(w)=\exp[-w] \qquad (5.15)$$

for pure noise.

The power of high-frequency signals is distributed according to the same laws. Actually, $w=\frac{v^2}{2}=\frac{X^2}{2\sigma_{ш}^2}$ is a relative value for the power of the signal-plus-noise, while $\frac{a^2}{2}=\frac{A^2}{2\sigma_{ш}^2}$ is the relative value of the power of the signal itself (across a 1 ohm resistance). Setting $P_{ш}=\sigma_{ш}^2$, $P=\frac{X^2}{2}$ and $P_c=\frac{A^2}{2}$, we will find the probability distributions for the power of the signal-plus-noise

$$W(P)=\frac{1}{P_{ш}}\exp\left[-\frac{P+P_c}{P_{ш}}\right]I_0\left(\frac{2\sqrt{PP_c}}{P_{ш}}\right) \qquad (5.16)$$

and for pure noise

$$W(P)=\frac{1}{P_{ш}}\exp\left[-\frac{P}{P_{ш}}\right]. \qquad (5.17)$$

Thus the receiver noise power is distributed exponentially, while the distribution law of the signal-plus-noise power is gradually normalized with increase in power $P_s$ of the signal itself.

## §5.3. PROBABILITY ESTIMATE OF THE RESULTS OF OBSERVATION AND CALCULATION OF THE DISCRIMINATION FACTOR

Distributions (5.10) and (5.11) characterize, respectively, the behavior of a signal with noise and of pure noise at the output of the so-called linear detector which reproduces without distortion the envelope of high-frequency oscillations.

The average relative value of noise at the output of a linear detector

$$\bar{v}=\int_0^\infty v W'(v)\,dv=\int_0^\infty v^2 e^{-\frac{v^2}{2}}dv=\sqrt{\frac{\pi}{2}}$$

is not zero. The absolute value of the average noise voltage

$$\bar{X}=\bar{v}\sigma_m=\sqrt{\frac{\pi}{2}}\sigma_m \qquad (5.18)$$

is proportional to the effective value, as is characteristic for the Rayleigh distribution.

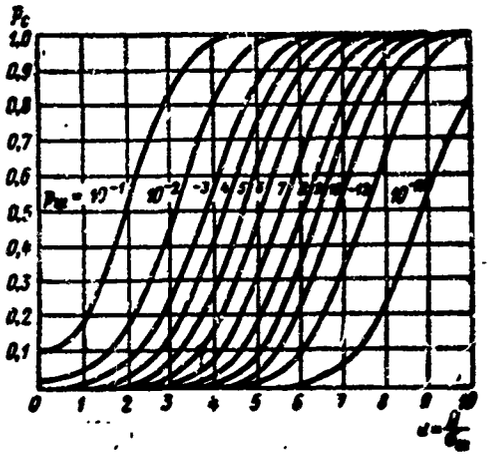


Fig. 5.4. The probability that target pulse $p_S$ will exceed some given level as a function of relative signal intensity $a$ at various values for the probability that noise voltage $p_{Sh}$ will exceed the indicated level.

The probability that noises will exceed some assigned level $v_0$

$$p_m=\int_{v_0}^\infty v e^{-\frac{v^2}{2}}dv=e^{-\frac{v_0^2}{2}}. \qquad (5.19)$$

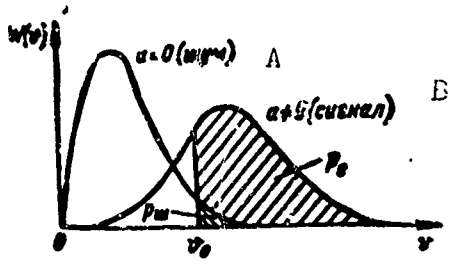


Fig. 5.5. Probability that pure noise ($a = 0$) and signal ($a \neq 0$) will exceed level $v_0$. A) Noise; B) signal.

To improve the conditions of observation of signals the noises are usually limited from below. For example, bias voltages applied to the control electrode of the indicator tube (hum cutoff). It is easy to evaluate the degree of choking of the screen by noise at various limiting levels. If limiting level $X_0 = 3\sigma_ш (v_0 = 3)$ is assigned, then $p_ш = e^{-\frac{3^2}{2}} = 0{,}01$. Thus, if 100 resolvable areas are laid out on the range sweep, corresponding to a noise blip length $\tau_ш \approx \frac{1}{\Delta f}$, an average of one noise blip may be anticipated during each range scanning period.

If we assign a probability for the appearance of noise blips $p_{sh}$, the required limiting threshold

$$v_0 = \sqrt{-2 \ln p_ш} \qquad (5.20)$$

is found logarithmically from Formula (5.19).

When the output voltage of the receiver is fed to the indicator, a limiting need not be used in principle, since the operator himself sets the "threshold" in his mind, by noting only the sufficiently bright blips among all the others which he perceives as background. But in automatic radar stations such limiting is required.

If noise blips exceed the threshold level, they may form a combination resembling the target blips. The appearance of such a combination is known as a false alarm. False alarms may not be completely eliminated regardless of the level of limiting, since the probability of noise blips of large amplitude is not equal to zero.

A second quantity of interest to the observer is the probability that the signal-plus-noise pulse will exceed the same threshold level. This probability may be determined as the integral

$$p_c = \int_{v_0}^{\infty} v \exp\left[-\frac{v^2+a^2}{2}\right] I_0(av)\, dv$$

or by taking into consideration (5.20)

$$p_c = \int_{\sqrt{-2\ln p_m}}^{\infty} v \exp\left[-\frac{v^2+a^2}{2}\right] I_0(av)\, dv. \qquad (5.21)$$

This integral may not be worked out analytically and may be calculated only through numerical integration. As follows from Formula (5.21), probability $p_s$ is a function of $p_{sh}$ and $a$. The results of the calculation of $p_s$ as a function of $a$, where $p_{sh}$ = const is a parameter, are given in Fig. 5.4. Thus, the graph reflects the mutual dependence of the three parameters: $p_s$, $p_{sh}$ and $a$.

Figure 5.5 demonstrates graphically the dependence of probabilities $p_{sh}$ and $p_s$ upon the level of limiting. Probability $p_{sh}$ is determined by the area under the curve $a = 0$ to the right of point $v_0$; probability $p_s$ is numerically equal to the area under the curve $a \neq 0$ to the right of point $v_0$. It can be seen from this drawing that reducing the probability of the appearance of noise through increasing level $v_0$ at an assigned value of $a$ leads simultaneously to a decreasing probability that signal $p_s$ will exceed this level. At the assigned value of $p_{sh}$ probability $p_s$ may be heightened only by shifting the curve $a \neq 0$ to the right, that is, by decreasing sensitivity, since $a$ is the relative amplitude of the signal itself.

The probability of correct detection of a target $D$, which depends also upon the number of pulses $n$ received from the target, as well as upon the design of the RLS terminal device, is found from quantity $p_s$. These functions will be examined in detail in the following chapter. Here we will limit ourselves to a calculation of a simplified model of the observer.

Let us assume that from the target are received $n$ pulses of identical amplitude, and it is considered as discovered as long as a single blip has appeared at the output of the limiter. The probability that any one of these pulses will exceed threshold $v_0$ is $p_s$. The probability that any pulse will not exceed threshold $v_0$ is $1 - p_s$. The probability that not one of $n$ pulses will exceed the threshold is equal to the product of the probabilities $(1 - p_s)^n$, since any time one of these pulses exceeds the threshold it is an independent event. The sum of the probability that at least one pulse will exceed the threshold, or that none of them will exceed it, is unity (full group of events). Therefore, the probability of detecting target $D$, that is, the probability that at least one pulse will exceed the threshold, is equal to unity less the probability that all $n$ pulses will not exceed the threshold:

$$D = 1 - (1 - p_c)^n. \qquad (5.22)$$

It should be pointed out that in the case of a sufficiently large number of pulses $n$, the probability that one pulse will detect target $D$ is sufficiently great even at a low probability of the appearance of each of the pulses. Thus, for $p_s = 0.1$ $D = 0.817$ at $n = 16$ and $D = 0.926$ at $n = 25$. In this consists the distinctiveness of the integration of signals.

The probability of false alarm $F$ at a given point in space may be determined analogously, if $p_{sh}$ is substituted in place of $p_s$ in Formula (5.22). However, probabilities $F$ and $p_{sh}$ are usually very small, and therefore $(1 - p_ш)^n \approx 1 - np_ш$ and

$$F = 1 - (1 - p_ш)^n \approx np_ш. \qquad (5.23)$$

On the basis of the results obtained it is possible to calculate the relative value of the amplitude of the minimum detectable signal $a_{min}$ and discrimination factor $m_r$ if at the assigned number of pulses

$n$ and the assigned probability of false alarms $F$ it is necessary to assure a probability of detection of the target of not less than $D$.

Actually, according to Formula (5.23), probability $p_{sh}$ is determined from assigned $F$ and $n$, while, in accordance with Formula (5.22), probability $p_s$ is found from $D$ and $n$. Knowing $p_{sh}$ and $p_s$, from the graph in Fig. 5.4 we find the point whose abscissa $a - a_{min}$. Since, in accordance with denotations $a = A/\sigma_{sh}$ introduced above, the discrimination factor

$$m_p = \frac{F_{пр\,мин}}{P_ш} = \frac{A^2_{мин}}{2\sigma^2_ш} = \frac{a^2_{мин}}{2}. \qquad (5.24)$$

If, in addition, we know the receiver noise power calculated at its input, it is possible to calculate the receiver sensitivity and, from its parameters, the RLS operating range for any value of the target effective scattering cross-section.

Example. On the basis of the method set forth above calculate discrimination factor $m_r$ if $F = 10^{-5}$, $D = 0.82$ and $n = 10$.

a) We determine $p_{sh}$ in accordance with Formula (5.23):

$$p_{ш} = \frac{F}{n} = \frac{10^{-5}}{10} = 10^{-6}.$$

b) We determine $p_s$ in accordance with Formula (5.22):

$$p_c = 1 - \sqrt[n]{1-D} = 1 - \sqrt[10]{1-0{,}82} = 0{,}1.$$

c) We find $a_{min}$ from the diagram in Fig. 5.4 at $p_s = 0.1$ and $p_{sh} = 10^{-6}$:

$$a_{мин} = 3{,}8.$$

d) We calculate discrimination factor $m_r$ from Formula (5.24):

$$m_p = \frac{a^2_{мин}}{2} \approx 15.$$

A statistical evaluation of the observability of signals of a nonfluctuating target against the background of internal noises has been given above. Most real targets yield a fluctuating echo-signal, and for

that reason a complete evaluation of observability must also take into account the statistics of these fluctuations.

To simplify this task we will consider at the outset that the signal fluctuations caused by noise are negligibly small by comparison with the fluctuations of the echo-signal itself.

Let us examine the case of a strongly fluctuating target where, among the elementary reflectors of the target, there is no bright spot. According to Formula (3.43) derived in Chapter 3, the density of the probability distribution of the effective scattering cross section (e.p.r.) of a strongly fluctuating target

$$W(\sigma_{\text{п}}) = \frac{1}{\bar{\sigma}_{\text{п}}} \exp\left[-\frac{\sigma_{\text{п}}}{\bar{\sigma}_{\text{п}}}\right],$$

whence we find the probability that the e.p.r. will exceed a given value of the $\sigma_{ts}$

$$p(\sigma_{\text{п}}) = \int_{\sigma_{\text{п}}}^{\infty} W(\sigma_{\text{п}})\, d\sigma_{\text{п}} = \exp\left[-\frac{\sigma_{\text{п}}}{\bar{\sigma}_{\text{п}}}\right], \qquad (5.25)$$

where $\bar{\sigma}_{ts}$ is the average value of $\sigma_{ts}$ corresponding to the probability $p(\bar{\sigma}_{ts}) = 0.37$.

Since the received signal power is proportional to $\sigma_{ts}$, if quantity $\sigma_{ts}$ exceeds a given level, this means that the received signal will also exceed the corresponding level at which the target will be detected in the absence of noise.

Consequently, probability $p(\sigma)$ is also the probability of detecting the target; we denote it by $p_{ts}$, distinguishing it from probability $D$ which takes into account the influence of noise.

We utilize range formula

$$R_{\max} = \sqrt[4]{\frac{P_{\text{и}} D^2(q) \lambda^2 \sigma_{\text{п}}}{(4\pi)^3 P_{\text{пр мин}}}} = \sqrt[4]{\frac{P_{\text{и}} D^2(q) \lambda^2 \bar{\sigma}_{\text{п}}}{(4\pi)^3 P_{\text{пр мин}}}} \sqrt[4]{\frac{\sigma_{\text{п}}}{\bar{\sigma}_{\text{п}}}} = R'_{\max} \sqrt[4]{\frac{\sigma_{\text{п}}}{\bar{\sigma}_{\text{п}}}}.$$

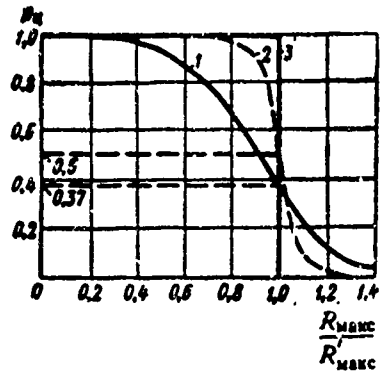


Fig. 5.6. Connection between detection range and probability of detection of a strongly fluctuating target (1), a weakly fluctuating target (2), a nonfluctuating target (3).

Whence

$$\left(\frac{R_{\text{макс}}}{R'_{\text{макс}}}\right)^4 = \frac{\sigma_{\text{ц}}}{\bar{\sigma}_{\text{ц}}}, \tag{5.26}$$

where

$$R'_{\text{макс}} = \sqrt[4]{\frac{P_{\text{и}} D^2 \eta \lambda^2 \bar{\sigma}_{\text{ц}}}{(4\pi)^3 P_{\text{пр мин}}}} \tag{5.27}$$

is the operating range of the RTS at $\sigma_{ts} = \bar{\sigma}_{ts}$. Substituting Expression (5.26) into Formula (5.25) and considering $p_{ts} = p(\sigma)$, we find that the probability of detecting a heavily fluctuating target is a function of normalized range $R_{maks}/R'_{maks}$

$$p_{\text{ц}} = \exp\left[-\left(\frac{R_{\text{макс}}}{R'_{\text{макс}}}\right)^4\right]. \tag{5.28}$$

This dependence is given in Fig. 5.6 (curve 1). The probability of detecting the target at range $R'_{maks}$, corresponding to $\sigma_{ts} = \bar{\sigma}_{ts}$, is 0.37.

Let us now take up the case of a weakly fluctuating target possessing, among its many reflectors, one strong reflector – a bright spot. Then the total target signal will contain a nonflickering constant

component which, against the background of the remaining elementary signals yielding a fluctuating component, may be viewed as a signal against a background of noises.

Probability $p_{ts}$ of a weakly fluctuating target may be obtained from Formula (3.42) in precisely the same way as for the case of a strongly fluctuating target. However, integration is not done analytically. Therefore, we will limit ourselves to a qualitative examination of the task for the case when the constant component of the reflected signal is sufficiently great in comparison with the fluctuating component, and the amplitude of the field strength of the reflected signal is distributed approximately normally around its average value. Since the RLS operating range is proportional to the field strength, the probability of detecting $p_{ts}$ as a function of normalized range $R_{maks}/R'_{maks}$ is determined by the integral function of the normal distribution (Fig. 5.6, curve). The probability of detecting a weakly fluctuating target at range $R'_{maks}(\sigma_{ts} = \bar{\sigma}_{ts})$ is 50%, since the normal law is symmetrical relative to its average value.

The function of $p_{ts}$ for a nonfluctuating target is shown in Fig. 5.6 (curve 3). Consequently, any law of the distribution of probabilities for $\sigma_{ts}$ may be described by a curve lying between two limits: curve 1 for a strongly fluctuating target and curve 3 for a nonfluctuating target. The actual curve for each complex target may be determined experimentally.

This analysis of the properties of the target effective scattering cross-section shows that it makes sense to speak of the target detection range only when it is indicated with what probability the target may be detected. That value for $\sigma_{ts}$ which corresponds to the assigned detection probability should be substituted in the range formula. For calculation it is necessary to know $\bar{\sigma}_{ts}$ for $\sigma_{ts}$, corresponding to any

other known detection probability, and also the character of the fluctuations.

Example. Determine the RLS operating range when the probability of detecting a strongly fluctuating target $p_{ts} = 0.5$ and $p_{ts} = 0.9$, if the operating range at $\sigma_{ts} = \bar{\sigma}_{ts}$ $R'_{maks} = 300$ km.

From curve 1 in Fig.5.6 we find:

$$\text{а) } p_{\text{д}} = 0{,}5 : \frac{R_{\text{макс}}}{R'_{\text{макс}}} = 0{,}9 \text{ and } R_{\text{макс}} = 0{,}9 \cdot 300 = 270 \text{ км}$$

$$\text{б) } p_{\text{д}} = 0{,}9 : \frac{R_{\text{макс}}}{R'_{\text{макс}}} = 0{,}55 \text{ and } R_{\text{макс}} = 0{,}55 \cdot 300 = 165 \text{ км}$$

In evaluating the combined set of target fluctuations and internal receiver noises upon the detection probability it is necessary to take into account not only the character of the fluctuations but also their velocity.

Most real targets, such as airplanes, fluctuate comparatively slowly. During the time of irradiation the echo-signal amplitude remains practically unchanged, changing only from one scanning period to another. Received signals of this type are called "a harmoniously fluctuating pulse packet." Probability $p_s$ for this case is calculated in the following manner.

We will assume that fluctuation law $\sigma_{ts}$ is known and, consequently, the distribution law $W(a)$ for the received signal amplitudes. Since $p_{sh}$ is known, and depends neither upon the intensity nor upon the velocity of the target fluctuations, we find particular probability $p'_s$ for a given fixed value of $a$ from Formula (5.21):

$$p'_c = \int_{\sqrt{-2\ln p_{\text{ш}}}}^{\infty} v \exp\left[-\frac{v^2 + a^2}{2}\right] I_0(av)\, dv.$$

Then, averaging particular probabilities $p'_s$ over all values of $a$ weighted by $W(a)$, we obtain the probability which we are seeking

$$p_c = \int_0^\infty W(a) \int_{\sqrt{-2\ln p_{ш}}}^\infty v \exp\left[-\frac{v^2+a^2}{2}\right] I_0(av)\, dv da. \qquad (5.29)$$

Unfortunately, calculating for all possible values of $p_{sh}$ and distribution laws $W(a)$ is excessively cumbersome [illegible] can be accomplished only by using high-speed digital computers.

When the radiation frequency changes from pulse to pulse, the amplitudes of the target pulses in the packet fluctuate independently, since the phase relationships among the elementary items of the total signal are added each time in a different way. The resultant signal is called a noise-like signal.

The calculation of probability $p_s$ in this case is rather simple. Let the target be fluctuating strongly and the dispersion of the fluctuation of the signal amplitude, which is $K^2$ times greater than the dispersion of the normalized noise $v = X/\sigma_{sh}$, be equal to 1. Then the amplitude of the noise-like signal will be distributed according to the Rayleigh law with resultant dispersion $1 + K^2$:

$$W(v) = \frac{v}{1+K^2} \exp\left[-\frac{v^2}{2(1+K^2)}\right] \qquad (5.30)$$

and the probability that the signal pulse will exceed a given level is determined by integral

$$p_c = \int_{v_0}^\infty W(v)\, dv = \left(e^{-\frac{v_0^2}{2}}\right)^{\frac{1}{1+K^2}}. \qquad (5.31)$$

Therefore the sought probability $p_s$ may be determined from Formula (5.31) taking into account Relationship (5.19) as

$$p_c = p_{ш}^{\frac{1}{1+K^2}}. \qquad (5.32)$$

Probability $p_s$ for a noise-like signal of a weakly fluctuating target may be calculated analogously.

We point out in conclusion that the probability of detecting a tar-

get with independently fluctuating pulses is somewhat higher than with harmoniously fluctuating pulses, since in the latter case the complete vanishing of all the pulses in the packet is more probable. However, the accuracy of determining the target angular position is lower, since the form of the pulse packet envelope is distorted to its maximum.

## §5.4. INFLUENCE OF INTEGRATION UPON OBSERVABILITY OF RADAR SIGNALS

The radar station usually receives from the target not one but several pulses. These pulses carry energy which can be accumudated (integrated) and used for better discrimination of the signal against the background of noise.

The integrated signal-plus-noise forms a target blip, and the integrated noise forms a noise hum. The target blip will stand out against the noise hum more reliably the greater is the difference among the average values $\bar{u}_{s+sh} - \bar{u}_{sh}$ of the integrated signal-plus-noise and the pure noise, respectively. However, the effectiveness with which the target signal is discriminated is determined not only by the absolute magnitude of the difference, but also by how great it is in comparison with the fluctuations of the noise hum, which are determined by the dispersion of the total noise $\bar{u}^2_{sh}$.

Therefore, the signal/noise ratio is introduced in order to evaluate observability

$$M = \frac{\bar{u}_{s+sh} - \bar{u}_{sh}}{\sqrt{\bar{u}^2_{sh}}}. \qquad (5.33)$$

When the number of integrated pulses $n$ is great, the distribution law of the resultant voltage approaches the normal. The normal law, as is known, is fully determined by the average value and by the dispersion. From the distribution law are found the detection probability $D$ and false alarm probability $F$, which yield a statistical evaluation of observability. The signal/noise ratio, as follows from (5.33), is also

determined by the average value and by the dispersion. Therefcre, with a normal distribution law, an evaluation of the quality of detection from the output signal/noise ratio $M$ is as effective as an evaluation from $F$ and $D$.

When the distribution law differs from the normal, the signal-noise ratio is no longer an effective evaluation. However, the normal law occurs in a very large number of situations, while evaluation of the quality of detection from quantity $M$ is rather simple and in many cases can be used to investigate important laws (for example, to compare the effectiveness of various systems of detection).

Let us examine the influence of integration upon signal/noise ratio $M$.

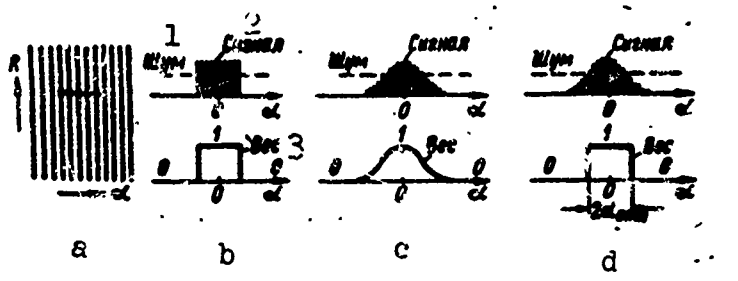


Fig. 5.7. Integration of pulses: a) Sweep and blips on indicator screen; b) optimum integration of pulses of constant amplitude; c) optimum integration of pulses of variable amplitude; d) equilibrium integration of pulses of variable amplitude. 1) Noise; 2) signal; 3) weight.

*Coherent integrations.* If integration includes phase relationships, for example, at high frequency, the signal amplitudes will be added. The average value of the amplitude of the resultant signal, in integration of $n$ pulses of identical amplitude $A$, will be

$$\bar{u}_{c+ш} = An,$$

while that of the resultant noise

$$\bar{u}_ш = 0,$$

since the average value of the sum is equal to the sum of the average values, while the average value of the noise is equal to zero.

The dispersion of the sum is equal to the sum of the dispersions of the items, and therefore

$$\bar{u}_{\Sigma}^2 = n\sigma_{ш}^2,$$

where $\sigma_{sh}^2$ is the noise dispersion before integration.

Then, in accordance with Formula (5.33), the signal/noise ratio with respect to voltage after coherent integration

$$\frac{nA}{\sqrt{n}\sigma_{ш}} = \sqrt{n}a, \qquad (5.34)$$

where $a = A/\sigma_{sh}$ is the signal/noise ratio with respect to voltage before detection.

The signal/noise ratio with respect to power increases in proportion to the number of pulses $n$. Consequently, coherent integration accumulates all the energy of the signal. However, to do this, it is necessary to maintain the required phase relationships among the items, which at the present time is an extremely difficult problem.

*Incoherent integration.* The integrator is usually the indicator or some other terminal device after the detector. When it is necessary to discriminate signals which are weaker than noise signals ($a < 1$), the detector is quadratic with respect to them. Then the signal/noise ratio with respect to *voltage* at the detector output is proportional to the signal/noise ratio with respect to *power* at its input.

As is known, the signal/noise ratio with respect to power before integration is $a^2/2$. In integrating voltage at the detector output which is proportional to the power at the input, we obtain a signal/noise ratio

$$M = \sqrt{n}\frac{a^2}{2}. \qquad (5.35)$$

Thus, as regards the power of a high-frequency signal, incoherent integration yields a loss of $\sqrt{n}$ in comparison with coherent integration.

The detection threshold of the RLS terminal device with respect to

the output signal/noise ratio $M_r$ is such that a signal exceeding it will be detected against the noise background. In accordance with Formula (5.35) the threshold ratio in each pulse before integration

$$m_p = \frac{a^2_{\text{кван}}}{2} = \frac{M_p}{\sqrt{n}} \qquad (5.36)$$

is the discrimination factor which we have already encountered. The greater the number of target pulses $n$ at the assigned terminal device threshold $M_r$, the smaller the discrimination factor, and the greater the sensitivity of the RLS receiver device.

Example. Let the signal on the indicator be definitely detectable when the signal/noise ratio upon the screen increases to quantity $M_r = 3$. With the number of pulses $n = 25$, the minimum signal/noise ratio in each pulse

$$m_p = \frac{M_p}{\sqrt{n}} = \frac{3}{\sqrt{25}} = 0{,}6.$$

The example indicates that the RLS will detect a signal which is lower than the average noise level, despite the fact that this signal becomes visible on the indicator only when it is three times in excess of the noises.

With signals which are very strong by comparison with the noise ($a \gg 1$) the detector acts linearly, taking the signal phase into consideration yields no additional advantage, and the integration after the detector is equivalent to coherent integration, that is, the signal/noise ratio with respect to power increases $n$ times. In the intermediate case ($a \approx 1$) the detector occupies an intermediate position between being linear and being quadratic.

In concluding this section we will examine how pulses should be integrated in the RLS terminal device.

Let a packet of target pulses of identical amplitude (Fig. 5.7a and b) be registered on an indicator with scanning of the azimuth –

range type. Then blips will be formed on $n$ adjacent range lines. If the range sweeps are sufficiently close to one another, the brightnesses of the blips are added together, and one spot of the screen is actually lighted. This is how the signal is integrated. The noise hum is integrated in the same way, but not as effectively, since the bright noise blips are distributed chaotically on the screen.

When the range sweeps are not sufficiently close together, only part of the target pulses will be integrated. If the sweeps are so close together that more than $n$ sweeps will be registered at each point on the screen, this just leads to an increase in the brightness of the noise hum. In both latter cases the signal/noise ratio will be low.

Consequently, for optimum integration of $n$ pulses of identical amplitude, range sweeps should be so distributed that the signals of exactly $n$ sweeps are integrated, while the signals of the remaining sweeps are not integrated. In other words, the signals of $n$ sweeps should be summed with weight 1, and those of the remaining sweeps with weight 0. The appearance of the weighting function is given in Fig. 5.7b: the weighting function reproduces the form of the envelope of the pulse packet.

In fact, the packet of target pulses possesses variable amplitude which is determined by the shape of the antenna directivity diagram. In this case also optimum integration must be done using weights corresponding to the form of the packet envelope (Fig. 5.7c). Actually, in this case signals which are strong in comparison with the noise are fully integrated, while the weaker signals in which the noise component is relatively great are integrated with a lower weight, while signals of pure noise are not integrated at all. Thereby the best signal/noise ratio after integration is ensured.

Not all integrators can total signals with different weights. There-

fore in many devices the pulses of variable amplitude are totaled with equal weight within the limits of a given angle near the directivity diagram maximum (Fig. 5.7d). If this angle is small, not all pulses will be integrated. A considerable increase in the angle leads to a reduction in the integration effect through accumulation of only one noise at those values of angles in which there is no signal. Therefore, there is an optimum integration angle $2\alpha_{opt}$ at which the signal-noise ratio becomes maximum after equilibrium integration. However, this maximum effect is nonetheless lower than at what is actually optimum integration with different weights (Fig. 5.7c).

## §5.5. EFFECTIVE ANTENNA BEAM WIDTH

Evaluation of the results of integration and of the probability of detecting signals is simple for a rectangular pulse packet, which does not exist in reality. In the case of a real pulse packet with variable

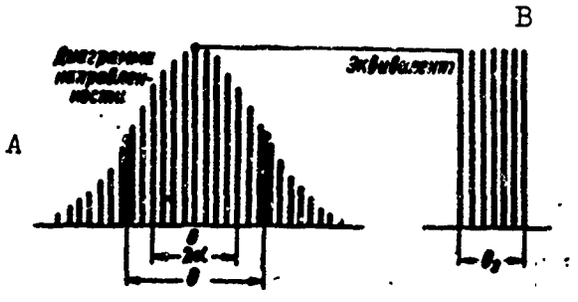


Fig. 5.8. Packet of target pulses of a real directivity diagram and of its rectangular equivalent. A) Directivity diagram; B) equivalent.

amplitude the difficulty of calculation increases many times. Therefore, to simplify the calculation, it is desirable to replace the real pulse packet by its rectangular equivalent; in this way the same integration effect is obtained and, consequently, the identical target detection range.

We will assume the amplitude of the pulses of the rectangular equivalent to be equal to maximum pulse amplitude $A_{v0}$ of the real packet (Fig. 5.8). Finding the equivalent is then the same thing as calculating

the angular size of rectangular packet $\theta_e$, known as the effective antenna beam width.

The amplitude envelope of high-frequency pulses reproduces the shape of the directivity diagram with respect to power, which can be approximated by a bell-shaped curve

$$F_p(\alpha) = \exp\left[-0{,}7\left(\frac{2\alpha}{\theta_\alpha}\right)^2\right],$$

where $\alpha$ is counted off to one side of the directivity diagram maximum, while $\theta_\alpha$ is the width of the directivity diagram at the half-power level, read off on both sides of the maximum.

Since integration is done after the detector, which acts quadratically for relatively weak signals, the amplitude of the integrated video pulses $A_v$ is proportional to the square of the pulses $A$ at the detector input, that is, to the square of the directivity diagram with respect to power $F_p(\alpha)$

$$A_v(\alpha) = A_{v0}\exp\left[-1{,}4\left(\frac{2\alpha}{\theta_\alpha}\right)^2\right].$$

We will introduce the concept of pulse density, equal to the number of received pulses per unit angle of the directivity diagram

$$n' = \frac{n_0}{\theta_\alpha},$$

where $n_0$ is the number of pulses arriving over the width of the directivity diagram $\theta_\alpha$. We will assume pulse density to be great, in order to have the right to use an integral representation of the summing of pulses.

Let us take elementary angle $d\alpha$. The amplitude of the pulses may be considered constant within the limits of this angle, the number of pulses is equal to $n'd\alpha$ and the result of integration of the amplitudes

$$A_v(\alpha)\,n'd\alpha = A_{v0}\exp\left[-1{,}4\left(\frac{2\alpha}{\theta_\alpha}\right)^2\right]n'd\alpha.$$

Integration of the amplitudes over the whole range α from 0 to ∞, on both sides of the maximum, with weighting $\exp\left[-1{,}4\left(\frac{2\alpha}{\theta_e}\right)^2\right]$ yields

$$2\int_0^\infty A_{s0}n'\exp\left[-1{,}4\left(\frac{2\alpha}{\theta_e}\right)^2\right]\exp\left[-1{,}4\left(\frac{2\alpha}{\theta_e}\right)^2\right]d\alpha = A_{s0}n'I, \qquad (5.37)$$

where

$$I = 2\int_0^\infty \exp\left[-2{,}8\left(\frac{2\alpha}{\theta_e}\right)^2\right]d\alpha = \theta_e\int_0^\infty \exp\left[-2{,}8\left(\frac{2\alpha}{\theta_e}\right)^2\right]d\frac{2\alpha}{\theta_e}. \qquad (5.38)$$

Since $\int_0^\infty e^{-z^2s^2}dz = \frac{\sqrt{\pi}}{2s}$, assuming $z = \frac{2\alpha}{\theta_e}$ and $s = \sqrt{2{,}8}$, we obtain

$$I = \theta_e\sqrt{\frac{\pi}{4\cdot 2{,}8}} = 0{,}53\theta_e. \qquad (5.39)$$

The result of the integration of the dispersion of video noises $\sigma^2_{vsh}$ over interval $d\alpha$, accordingly, is

$$\sigma^2_{sum}n'd\alpha,$$

while integration over the whole range α with weight $\exp\left[-2{,}8\left(\frac{2\alpha}{\theta_e}\right)^2\right]$ yields

$$2\int_0^\infty \sigma^2_{sum}n'\exp\left[-2{,}8\left(\frac{2\alpha}{\theta_e}\right)^2\right]d\alpha = \sigma^2_{sum}n'I. \qquad (5.40)$$

Here the weighting function is equal to the square of the weighting function for the amplitudes, since noises are summed according to their power (dispersion).

After integration, the signal/noise ratio is equal to the ratio of quantity (5.37) and the square root of Integral (5.40):

$$M = \frac{A_{s0}n'I}{\sigma_{sum}\sqrt{n'I}} = \frac{A_{s0}}{\sigma_{sum}}\sqrt{n'I} = \frac{A_{s0}}{\sigma_{sum}}\sqrt{n'0{,}53\theta_e}. \qquad (5.41)$$

A rectangular pulse packet contains $n'\theta_e$ pulses, with amplitude $A_{v0}$. Then the results of integration of the pulses of the equivalent packet

$$M = \frac{A_{s0}}{\sigma_{sum}}\sqrt{n'\theta_e}. \qquad (5.42)$$

By equating the results of integration according to Formulas (5.41)

and (5.42), we find the effective antenna beam width during optimum integration of the pulses

$$\theta_э = 0{,}53\theta_\alpha. \qquad (5.43)$$

In equilibrium integration within the limits of optimum angle ($2\alpha_{opt} = 0.84\theta_\alpha$), the effective width, as calculation demonstrates,

$$\theta_э = 0{,}47\theta_\alpha \qquad (5.44)$$

turns out to be somewhat smaller; this corresponds to the sensitivity loss of about 0.5 db.

In view of the slight difference between Formulas (5.43) and (5.44) if the factor is assumed equal to 0.5, the accuracy will be adequate for practical purposes. Then the effective number of integrated pulses

$$n = \frac{\theta_э F_п}{\Omega} = \frac{0{,}5\theta_\alpha F_п}{\Omega}, \qquad (5.45)$$

where $\Omega$ is the angular displacement velocity of the antenna beam during scanning. This is the number of pulses which should be utilized in calculation, considering that all pulses are identical and have an amplitude equal to the directivity diagram maximum.

During optimum integration relative to strong signals, when the detector's load characteristic may be considered linear, the effective width increases to $0.74\theta_\alpha$, and during equilibrium integration – to $0.67\theta_\alpha$ ($2\alpha_{opt} = 1.2\theta_\alpha$). However, as far as detection is concerned, this case of strong signals is of almost no practical interest.

## §5.6. SWEEP INTERVAL

Raster space scanning with an antenna beam is sequential, line by line. The angular displacement of the antenna beam during the transition from one line to another is called the sweep interval $\theta_{sh}$.

To determine the optimum size of the sweep interval it is necessary to examine the directivity diagram in two planes. We may also approximate the directivity diagram in two planes by a bell-shaped curve.

Then the amplitude of the relatively weak signals at the detector output, being proportional to the square of the directivity pattern, as a function of the angular displacement relative to the maximum assumes the form

$$A_s(\alpha, \beta) = A_{s0} \exp\left[-1{,}4\left(\frac{2\beta}{\theta_\beta}\right)^2\right] \exp\left[-1{,}4\left(\frac{2\alpha}{\theta_\alpha}\right)^2\right].$$

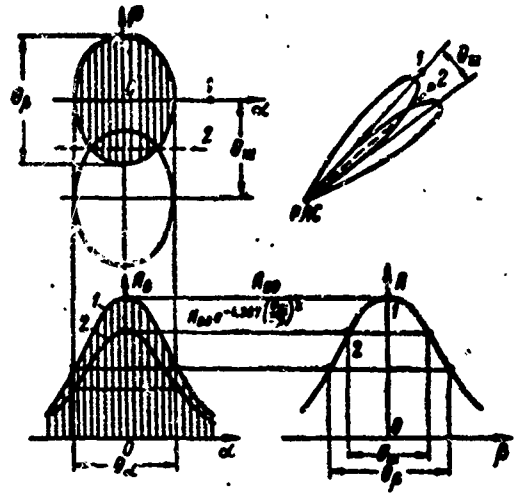

Fig. 5.9. Calculating the sweep interval.

Here $\alpha$ is the angle along the line, $\beta$ is the angle across the line, $A_{v0}$ is the amplitude in the diagram maximum. In general, the width of the directivity diagram is not the same with respect to $\alpha(\theta_\alpha)$ and with respect to $\beta(\theta_\beta)$.

Let us examine two targets: target 1 on the axis of the line and target 2 halfway between the axes of adjacent lines (Fig. 5.9).

As the antenna beam moves along $\alpha(\beta = 0)$ the amplitudes of the pulses of target 1 have their maximum possible value

$$A_{s1}(\alpha) = A_{s0} \exp\left[-1{,}4\left(\frac{2\alpha}{\theta_\alpha}\right)^2\right]. \qquad (5.46)$$

Target 2 is displaced relative to the axis of the line by angle

$\beta = \theta_{sh}/2$, and therefore the amplitudes of the pulses of target 2, as the beam is displaced along $\alpha$

$$A_{s2}(\alpha) = A_{s0}\exp\left[-1{,}4\left(\frac{\theta_m}{\theta_\beta}\right)^2\right]\exp\left[-1{,}4\left(\frac{2\alpha}{\theta_\beta}\right)^2\right] \qquad (5.47)$$

are $\exp\left[1{,}4\left(\frac{\theta_m}{\theta_\beta}\right)^2\right]$ times less than the corresponding amplitudes of the pulses of target 1. However, in contrast to target 1, target 2 is irradiated twice.* The dual irradiation may be treated as a doubling of pulse density $n'$.

The sweep interval is selected such that the observability conditions of targets 1 and 2 are identical, that is, the effect of integration of pulses of greater amplitude (5.46) received from target 1 should be equal to the effect of integrating the doubled number of pulses of target 2 with Amplitudes (5.47).

In accordance with Expression (5.40) we write the equality

$$\frac{A_{s0}}{\sigma_{пом}}\sqrt{n'l} = \frac{A_{s0}}{\sigma_{пом}}\exp\left[-1{,}4\left(\frac{\theta_m}{\theta_\beta}\right)^2\right]\sqrt{2n'l}.$$

or, after cancellation,

$$1 = \exp\left[-1{,}4\left(\frac{\theta_m}{\theta_\beta}\right)^2\right]\sqrt{2}.$$

From this we find the size of the sweep interval

$$\theta_m = 0{,}5\theta_\beta. \qquad (5.48)$$

If the corresponding calculations are done for relatively strong signals, we obtain

$$\theta_m = 0{,}7\theta_\beta. \qquad (5.49)$$

In general

$$\theta_m = (0{,}5 \div 0{,}7)\theta_\beta. \qquad (5.50)$$

For RLS of high sensitivity a sweep interval is selected closer to the lower limit, for RLS of low sensitivity – close to the upper limit. The sensitivity of an RLS employing raster space scanning is

usually not very high, lower than the sensitivity of stations employing circular or sector scanning, and therefore the upper limit is most frequently selected.

In stations measuring the second angular coordinate using the method of partial diagrams, the angular separation between neighboring lobes of the directivity diagram must also be selected in accordance with Formula (5.50).

It must be pointed out that the conditions of observability, and consequently, also the detection range of target 1 and 2, are equal only on the average, since, during the time between two irradiations of the target which are registered by two lines of the raster, its signal may change substantially due to flickering. The same applies to the method of partial diagrams if radiation is at different frequencies in the different lobes.

## §5.7. INFLUENCE OF SCANNING SPEED ON THE OBSERVABILITY OF RADAR SIGNALS

The effective number of target pulses [see (5.45)] depends upon angular velocity $\Omega$ of the displacement of the antenna beam during scanning. Therefore, the observability of radar signals as evaluated by discrimination factor (5.36) also depends upon the scanning speed.

In practice, real integrators cannot always effectively integrate all $n$ pulses as determined by Formula (5.45), since their effective integration time $T_1$ is finite.* Therefore, observability depends upon the relationship between effective integration time $T_1$, on one hand, and target irradiation time $\tau_{обл}=\frac{\theta_0}{\Omega}$, as well as the scanning period $T_0=\frac{2\pi}{\Omega}$, on the other hand (we limit ourselves to the case of circular scanning).

These relationships are determined by the speed of antenna rotation (Fig. 5.10).

At very low antenna rotation speed the target beaming time is

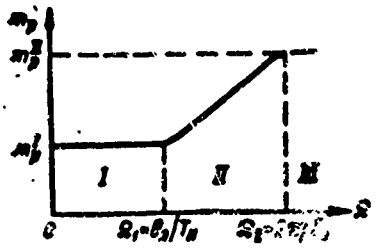


Fig. 5.10. Influence of scanning speed upon observability of radar signals.

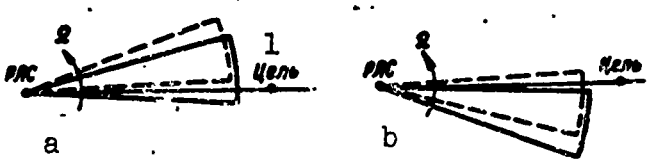


Fig. 5.11. Dynamic narrowing of antenna beam: a) Case of a trailing beam; b) case of a leading beam. 1) Target.

greater than the time of integration: $\tau_{обл}=\frac{\theta_р}{\Omega}>T_п$ (section I). At the assigned repetition frequency $n=F_пT_п$ the effective number of integrated pulses does not depend upon velocity Ω. Consequently, the discrimination factor also remains unchanged

$$m_р=m_р^1=\frac{M_р}{\sqrt{n}}=\frac{M_р}{\sqrt{F_пT_п}}. \qquad (5.51)$$

The second section in Fig. 5.10 corresponds to the condition

$$\tau_{обл}=\frac{\theta_р}{\Omega}<T_п<T_р=\frac{2\pi}{\Omega}.$$

It starts from the abscissa $\Omega_1=\frac{\theta_р}{T_п}$ at which the irradiation time is equal to the integration time. In this section the number of integrated pulses is determined by the irradiation time

$$n=F_п\tau_{обл}=\frac{F_п\theta_р}{\Omega}$$

and decreases with growth of Ω. The discrimination factor increases accordingly

$$m_p = \frac{M_p}{\sqrt{n}} = \frac{M_p}{\sqrt{F_n \theta_0}} \sqrt{\Omega} \qquad (5.52)$$

and observability deteriorates.

This continues up to velocity $\Omega_2 = \frac{2\pi}{T_n}$, at which the time of one rotation (scanning period $T_0$) is equal to the effective time of integration. Starting at this moment (section III) with growth of $\Omega$ the target irradiation time and the number of pulses received during one irradiation continue to decrease, but tne number of irradiations during the integration time increases in accordance. The effective number of integrated pulses is equal to the number of pulses during one irradiation $\left(n = \frac{F_n \theta_0}{\Omega}\right)$, multiplied by the number of irradiations of the target during tne integration time $\left(\frac{T_n}{T_0} = \frac{T_n \Omega}{2\pi}\right)$:

$$n = \frac{F_n \theta_0}{\Omega} \frac{T_n \Omega}{2\pi} = \frac{1}{2\pi} F_n \theta_0 T_n$$

and does not depend upon $\Omega$. The discrimination factor

$$m_p = m_p^{II} = \frac{M_p}{\sqrt{n}} = M_p \sqrt{\frac{2\pi}{F_n \theta_0 T_n}} \qquad (5.53)$$

also does not depend upon the velocity of antenna rotation, and its maximum quantity determines the limit of the deterioration of observability.

Actually, curve $m_r(\Omega)$ varies much more evenly than is indicated in Fig. 5.10, since the drop in the intensity of signals at the edges of the directivity diagram, and the drop in the effectiveness of integration over time, occur slowly.

Here two circumstances should be noted.

In the first place, for accurate measurement of azimuth a large enough number of pulses must be received from the target.

In the second place, the increase in velocity cannot continue infinitely, as would seem to be the case, at first glance, from the calculations given above. At high antenna velocities a *dynamic narrowing*

of the beam begins to take place. This effect is stronger as the target is more distant, that is, precisely where the task of detecting the target is solved. It is determined by the finite propagation time of radio waves.

To explain the dynamic narrowing effect we employ the rectangular equivalent of the directivity diagram, which in polar coordinates has the form of a sector (Fig. 5.11).

Let us first examine the case of a trailing beam (Fig. 5.11a). Let the antenna beam be still directed at the target and be irradiating it (solid line) at the moment of irradiation of the target, and, at the moment of return of the reflected signal, let the antenna beam have turned enough (dashed line) to prevent the signal from being received.

In the case of a trailing beam (Fig. 5.11b), on the contrary, the signal could be received (dashed line), but at the moment of irradiation the beam is still not directed at the target, and there is no reflected signal.

As a result of the influence of the dynamic narrowing effect, the number of pulses received from the target is no longer equal to the number of pulses sent out during the irradiation time, that is

$$n \neq \frac{F_{\text{п}} b_0}{\Omega},$$

and, therefore, Formula (5.53) ceases to be applicable. The dynamic narrowing of the beam begins to be prominent when velocity $\Omega$ is so great that the rated number of pulses approaches unity.

As a result of dynamic narrowing of the beam, section III in Fig 5.10 may be altogether absent if at $\Omega \leq \Omega_2$ the rated number of pulses is approximately equal to unity.

In selecting a scanning speed it is also necessary to take into account the fact that the detection of a target cannot be determined

with confidence from the blip obtained during a single scanning period, because of the influence of pulse noise blips. Confident detection of the target is possible only if two or more target blips are obtained in the given point on the screen during the observation time, and this is determined by the *overall probability of detection*.

The overall probability of detection depends both upon the number of irradiations of the target per unit of time and also upon the probability of detection for each irradiation. With increase in scanning speed $\Omega$ the number of irradiations per unit of time increases, but the probability of detection during each irradiation falls, since the number of received pulses decreases.

There exists an optimum scanning speed $\Omega_{opt}$, which yields a maximum overall probability of detection. However, in view of the complexity of the calculations, and also of the weakly expressed character of the optimum, these calculations are not done. Let us only note that the optimum velocity corresponds to a small number of pulses received from the target, which is in contradiction with the requirement of accuracy of measurement of the azimuth by the method of envelope analysis.

Manuscript Page No.

[Footnotes]

237 This problem will be examined in more detail in Chapter 7.

242 The only limitation is the requirement that any item be smaller than all the rest taken together.

267 Formally, both targets are irradiated many times, since a bell-shaped directivity diagram theoretically extends to infinity. In fact, irradiation is done through the side lobes, and these, because of their small size, need not be taken into account; this is even more true in view of the fact that the approximation of the bell-shaped curve is inaccurate outside the main lobe.

268 The integrating properties, in fact, fall gradually. The effective integration time is the time during which the integrating properties remain unchanged, and then drop suddenly to zero, giving rise to the same integration effect.

| Manuscript Page No. | Transliterated Symbols |
|---|---|
| 236 | ш = sh = shum = noise |
| 237 | р = r = razlicheniye = discrimination |
| 237 | пр = pr = priyem = reception |
| 237 | мин = min = minimal'nyy = minimum |
| 237 | и = i = impul's = pulse |
| 247 | с = s = signal = signal |
| 249 | РЛС = RLS = radiolokatsionnaya stantsiya = radar |
| 250 | мин = min = minimal'nyy = minimum |
| 252 | ц = ts = tsel' = target |
| 252 | макс = maks = maksimal'nyy = maximum |
| 263 | в = v = video = video |
| 265 | э = e = effektivnyy = effective |
| 265 | опт = opt = optimal'nyy = optimum |
| 268 | обл = obl = oblucheniye = beaming, irradiation |
| 268 | и = i = integrirovaniye = integration |
| 269 | п = p = povtoreniye = repetition |

# Chapter 6

# OPTIMUM RECEPTION AND DETECTION OF RADAR SIGNALS

## §6.1. ENTROPY AND INFORMATION

The transmission and reception of any communication may be viewed as the selection of one of all the many possible communications. From the point of view of the receiver this selection is accidental; to each of the possible communications could be ascribed the anticipated, or *a priori* probability of its transmission.

Consequently, until the signal is received the receiver is *uncertain* of the selection. After reception of the signal this uncertainty is either completely removed, if there is certainty that the signal has been received without distortions, or it is only reduced, if there is no such certainty. The latter case is the most characteristic for transmission of signals by radio because of the distortion of the signal by the inevitable noises. The reduction of indeterminacy after reception of the signal is precisely the role of the information received by the receiver.

To establish a basis for selecting a measure of indeterminacy we propose that one of two equally possible communications may be transmitted. The indeterminacy consists precisely in the possibility of selecting one of these two communications. Now assume that the number of equally possible communications has increased and become equal to some number $N$. It is felt intuitively that after this the indeterminacy of the situation has increased. Therefore, as a measure of the *a priori* indeterminacy may be taken the very number $N$ of equally possible com-

munications. However, this measure of indeterminacy is not very convenient.

In the first place, at $N = 1$ there is no indeterminacy, since there exists only one single situation, which is known to the receiver. Therefore, it is desirable that at $N = 1$ the measure of indeterminacy should be zero.

In the second place, it is desirable that the measure of indeterminacy, consisting of several particular indeterminacies, should be equal to the sum of their measures (should be additive). We will clarify this requirement with an example.

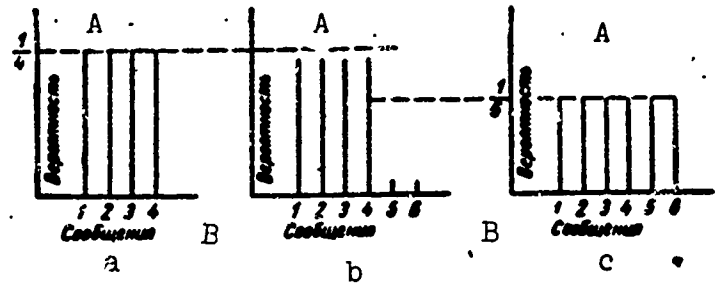


Fig. 6.1. Probabilities of reception: a) of four equally possible communications; b) of six unequally possible communications; c) of six equally possible communications. A) Probability; B) communications.

Let us assume that information on a certain signal is to be transmitted, this information comprising a complex communication consisting of two particulars. The first particular communication is the signal intensity: low (code 00), medium (01), high (10) and very high (11) -- in all, four equally possible situations. The second particular communication relates to signal polarity: positive (0) or negative (1) – two equally possible situations. We obtain a total of 8 equally possible communications.

| A Первое частное сообщение (интенсивность) | Второе частное сообщение (полярность) B | |
|---|---|---|
| | положительная | отрицательная |
| C малая | 000 | 001 |
| средняя D | 010 | 011 |
| E большая | 100 | 101 |
| весьма большая F | 110 | 111 |

G H

A) First particular communication (intensity); B) second particular communication (polarity); C) low; D) medium; E) high; F) very high; G) positive; H) negative.

If we simply take the number of equally possible communications $N$ as the measure of indeterminacy, the requirement of additiveness will not be satisfied: the sum of the first indeterminacy $N_1 = 4$ and the second indeterminacy $N_2 = 2$ is not equal to the total indeterminacy of the complex communication $N = 8$.

Therefore, as the measure of indeterminacy we take the logarithm of the number of equally possible communications $N$, whose probability of being transmitted is $p = 1/N$:

$$H = \log N = -\log \frac{1}{N} = -\log p. \qquad (6.1)$$

This measure satisfies the first and second requirements: $H = 0$ at $N = 1$ and $H = H_1 + H_2$.

In the above example, taking the logarithm to the base 2, we obtain $H_1 = \log_2 4 = 2$; $H_2 = \log_2 2 = 1$; $H = \log_2 8 = 3$.

Actually, any complex communication in this example may be transmitted with a unique meaning by three binary signs.

It is more complicated to calculate the measure of indeterminacy in the case of unequally possible communications. Figure 6.1 gives the probabilities for four equally possible communications, for six unequally possible communications, and for six equally possible communications. In this concrete case the second situation ($N = 6$) hardly differs from the first situation ($N = 4$), but at the same time it diverges substantially from the third situation, where $N = 6$.

As assumed from this example, the indeterminacy of the situation depends very strongly upon the relative weight of some communications with respect to others. Consequently, the overall uncertainty should be calculated taking into account the individual contribution of each separate communication, which is determined precisely by the probability of this communication. We use this to find the indeterminacy in the case of $N$ unequally possible communications.

If the $i$th communication were one of the equally possible communications with probability $p_i$, according to Formula (6.1) the indeterminacy of selection would be determined by quantity $-\log p_i$. In fact, this communication represents only the $p_i$th part of all possible communications, and, therefore, the indeterminacy of the situation, being conditioned by this one communication alone, is $-p_i \log p_i$. If we add up these particular indeterminacies with respect to all possible communications, we obtain a measure of indeterminacy of the selection of one of the unequally possible communications

$$H=-\sum_{i=1}^{N} p_i \log p_i. \qquad (6.2)$$

This quantity is known as the *entropy* of the discrete communications. In the case of equally possible communications $p_i=p=\frac{1}{N}$ and Formula (6.2) is transformed into Formula (6.1). From a comparison of Formulas (6.2) and (6.1), and also of the two last situations in Fig. 6.1, one will be convinced that at the assigned $N$ the entropy, or indeterminacy, will be maximum when all communications are equally possible.

If the communication is a continuously varying quantity $s$, which may assume an infinite number of meanings, its distribution is characterized by probability density $W(s)$, and the probability that it will fall within interval $s$, $s+\Delta s$ is $W(s)\Delta s$. By breaking down this whole interval of values $s$ into equal sections $\Delta s$, we obtain the calculated

number of values $s_i$ of this quantity. The entropy of the obtained aggregate of values $s_i$ is determined in accordance with Formula (6.2) by the dependence

$$H(s_i) = -\sum_i W(s_i)\,\Delta s \log [W(s_i)\,\Delta s].$$

The letter $i$ under the sign of the sum indicates that summing is for all $i$.

Since the logarithm of the product is equal to the sum of the logarithms of the factors and that, for decomposition into equal segments, $\log \Delta s$ does not depend upon the number $i$, we write

$$H(s_i) = -\sum_i W(s_i)\,\Delta s \log W(s_i) - \log \Delta s \sum_i W(s_i)\,\Delta s.$$

As $\Delta s$ tends toward zero, the sums at the limit turn into integrals, the second of them being equal to unity as the composite probability. The $\Delta s$ under the sign of the logarithm cannot tend to zero: noise and interference always limit the number of actually discernible levels. Therefore, at the assigned noise intensity, there exists a $\Delta s_{min}$ at which $-\log \Delta s_{min}$ is transformed into the constant $C$.

The expression for the entropy of continuously distributed communications assumes the form

$$H(s) = -\int_S W(s) \log W(s)\,ds + C, \qquad (6.3)$$

where the letter $S$ at the integral denotes summation for all values of $s$.

Maximum entropy corresponds to total ignorance of the situation. By employing the method of variational calculus it is possible to seek out those forms of distributions $W(s)$ yielding maximum entropy in the presence of certain limitations imposed upon random quantity $s$ by its physical nature.

The following distributions of continuous quantities possess maxi-

mum entropy:

– uniform distribution, if the quantity itself is limited from above and from below (for example, distribution of the phase over the interval $-\pi$, $\pi$);

– exponential distribution, if the quantity itself is limited only from one side (positive), and its average value is fixed (for example, the distribution of noise power or of random time intervals);

– normal, or gaussian, distribution, if the quantity itself is limited neither from above nor from below but the average square (power) of its fluctuations is fixed (for example, the distribution of noise voltage).

In the case of reception of radar signals we are in the presence of continuously varying quantities (voltage) representing a communication.

In accordance with Formula (6.3) the indeterminacy of the situation before reception is fully determined by *a priori* distribution $W(s)$. After signal $s$ has been transmitted (that is, has been reflected from the target), the receiver receives signal $x$ which is the sum of reflected signal $s$ and the noise. The indeterminacy of the situation relative to $s$ after reception of the signal

$$H_x(s) = -\int_s W_x(s) \log W_x(s) + C \qquad (6.4)$$

is completely determined by the *a posteriori* distribution of probabilities $W_x(s)$, that is, by the probability that some sort of $s$ was transmitted on the condition that $x$ was received. If there were no noises or interference, to each received $x$ there would correspond a completely determined $s$, and there would be no a posteriori indeterminacy.

In fact, because of the presence of the inevitable noise, after reception of signal $x$ the indeterminacy is not eliminated but is re-

duced. The reduction in indeterminacy, for entropy, after reception

$$J(s)=H(s)-H_x(s) \qquad (6.5)$$

is the quantity of information received by the receiver. The quantity of information is measured in the same units as is entropy. The logarithm to the base 2 is usually adopted, and one of the two equally possible communications is selected as the unit of information.

Consequently, reception amounts to receiving a posteriori distribution $W_x(s)$, which is determined by the second term in Formula (6.5), while the first term is considered to be known to the receiver before reception.

In conclusion, let us note the two following circumstances.

In the first place, entropy and the quantity of information are functions only of the probabilities of the communications, but not of the communications themselves. Therefore, only the statistical characteristics of communications are of interest for the transmission of information, and not the meaning or any other properties of the communications. Both an important and a completely senseless communication may bear identical quantities of information.

In the second place, although the entropy of a continuous quantity is an ambiguous quantity, information quantity $J$ is a completely determined quantity, since arbitrary constants $C$ in difference $H(s) - H_x(s)$ cancel each other out.

## §6.2. THE PROBABILITY FUNCTION AND THE ADEQUATE RECEIVER

The mutual correspondence between transmitted (reflected) signal $s$ and received signal $x$ is determined by the combined probability distribution $W(s, x)$. According to the multiplication theorem of probability theory

$$W(s, x)=W(s)\,W_s(x)=W(x)\,W_x(s),$$

whence is found a posteriori probability

$$W_x(s)=\frac{1}{W(x)}W(s)\,W_s(x).$$

If the latter expression is viewed as a function of $s$, it may be concluded that the first factor does not depend upon $s$ at all and can be replaced by constant factor $k$, which may be found from the condition of normalization of distribution $W_x(s)$

$$\int_S W_x(s)\,ds=1.$$

The second factor is the a priori distribution which, as before, is assumed to be known. The third factor is the conditional distribution of $x$ when $s$ is known. However, being a function of $s$ for the given received $x$, this factor is not a probability distribution but serves as a measure indicating to which $s$ received signal $x$ most probably corresponds. For this reason $W_s(s)$ as a function of $s$ is called the probability function (or the inverse probability function) and is denoted by $L(s)$.


Fig. 6.2. Received signal $x(t)$ over interval $T$.

Thus, discovery of the a posteriori probability

$$W_x(s)=kW(s)L(s) \qquad (6.6)$$

is reduced to discovery of the probability function. Consequently, the only operation which must be accomplished during reception is obtaining probability function $L(s)$ or its informational equivalent.

The concept of equivalence flows from the essence of reception. Reception may always be viewed as the destruction of the unnecessary information contained in the received signal. For example, the essence of radio reception consists in selection of the signal of the station which we need, using the tuned receiver filter, and suppressing the signals of other stations which are viewed as unnecessary information. Information may be destroyed only through irreversible operation: fil-

tering, integration, limiting. Reversible operations (amplification, raising to a power, taking the logarithm, etc.) do not destroy any information, since the initial quantity may easily be obtained by the reverse transformation or by suitable adjustment of the receiver output device. Therefore, from the informational point of view such operations are unessential.

The informational equivalent of the probability function is any function of the received signal which is obtained by performing, with respect to the signal, the same irreversible operations as during derivation of the probability function.

The *adequate* receiver is the one which performs all irreversible operations which are adequate for obtaining the probability function. In the informational sense the signal at the output of such a receiver is equivalent to the probability function and, consequently, contains *everything* that can be derived from received signal $x$ relative to transmitted signal $s$. No other operations on $x$ can heighten the information with respect to $s$ contained in $x$: unessential operations do not alter the quantity of information, while essential operations only destroy it.

To define the various tasks solved by the adequate radar receiver, we find probability function $L(s)$ for the case when gaussian noise $n(t)$ with dispersion $\sigma_{sh}^2$ is superimposed on the signal proper $s(t)$. We will assume that the target is punctiform and that the signal amplitude at the receiver input is known.* This enables us to assume that the signal amplitude is unchanging from the moment of emission to the moment of reception and is equal to the defacto amplitude of the signal proper $s(t)$ at the receiver input; the reflected signal is just delayed by time $\tau_0 = 2R/c$. After superposition of the noise we have, at the receiver input, a signal

$$x(t)=s(t-\tau_0)+n(t),$$

which exists during time $T$ (Fig. 6.2).

Furthermore, we will assume that target range $R$ is known. Then, since we know function $s(t)$ and assign to it a certain time shift $\tau$, we can form difference

$$x(t) - s(t-\tau) = n(t),$$

which is a pure noise upon the condition that time shift $\tau$ of function $s(\tau)$ is equal to the known delay time $\tau_0 = 2R/c$.

We select one of the values of received signal $x(t)$ at arbitrary moment in time $t_i$: $x_i = s_i + n_i$. The difference $n_i = x_i - s_i$ is subordinate to the normal distribution law

$$W_{s_i}(x_i) = \frac{1}{\sqrt{2\pi}\sigma_m} \exp\left[-\frac{n_i^2}{2\sigma_m^2}\right] = \frac{1}{\sqrt{2\pi}\sigma_m} \exp\left[-\frac{(x_i - s_i)^2}{2\sigma_m^2}\right].$$

The received signal, together with the noise, is usually limited along the frequency band from 0 to some frequency $F_m$. Then, according to the Kotel'nikov-Shannon theorem, function $n(t) = x(t) - s(t - \tau)$ on interval 0, $T$ is uniquely defined by $2F_mT$ of its values $n_i$ which are reckoned off at time intervals $\Delta T = 1/2F_m$ and are independent quantities.

By applying the theorem of multiplication of probabilities, we obtain the probability function in a discrete form for $2F_mT$ independent events

$$W'_s(x) = \prod_{i=1}^{2F_mT} W_{s_i}(x_i) = \left(\frac{1}{\sqrt{2\pi}\sigma_m}\right)^{2F_mT} \exp\left[-\frac{1}{2\sigma_m^2} \sum_{i=1}^{2F_mT} n_i^2\right]. \qquad (6.7)$$

Let us now turn again to the continuous representation of the signal. In accordance with the Shannon theorem, function $n(t)$ (Fig. 6.3) may be represented in the form of the sum

$$n(t) = \sum_{i=1}^{2F_mT} n_i \psi_i(t). \qquad (6.8)$$

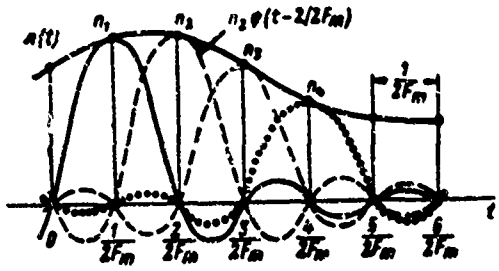

Fig. 6.3. Readings of function $n(t) = x(t) - x(t - \tau_0)$.

Here $n_i$ are the readings of function $n(t)$ at moments in time $t_i = i/2F_m$, while $\psi_i(t)$ are the orthogonal time functions of the form $\sin z/z$, differing from one another only by a time shift of a whole number of intervals $\Delta T = 1/2F_m$. For these functions the power relation obtained:

$$\int_0^T \psi^2(t)\,dt = \frac{1}{2F_m}. \qquad (6.9)$$

It follows from Fig. 6.3 that at the reference points all of the items of the sum in Equality (6.8) except for one, are equal to zero, which demonstrates the correctness of the equality for the reference points. Since the position of the reference points is arbitrary, it may be asserted that Equality (6.8) also obtains at the intermediate points.

In accordance with Formula (6.8) and the expansion of the square of the sum,

$$\int_0^T n^2(t)\,dt = \int_0^T \left[\sum_i n_i \psi_i(t)\right]^2 dt =$$

$$= \int_0^T \sum_i n_i^2 \psi_i^2(t)\,dt + \int_0^T \sum_{i,j} 2n_i n_j \psi_i(t)\,\psi_j(t)\,dt.$$

Since the functions $\psi_i(t)$ are orthogonal, the second term is equal to zero, and

$$\int_0^T n^2(t)\,dt = \int_0^T \sum_{i=1}^{2F_mT} n_i^2\psi_i^2(t)\,dt = \sum_{i=1}^{2F_mT} n_i^2 \int_0^T \psi_i^2(t)\,dt.$$

Since, in accordance with Formula (6.9) the latter integral is equal to $1/2F_m$,

$$\int_0^T n^2(t)\,dt = \frac{1}{2F_m}\sum_{i=1}^{2F_mT} n_i^2.$$

The physical content of the obtained equality will be more manifest if it is derived in another, less rigid, manner.

Within the limits of the $i$th interval, with length $\Delta T = 1/2F_m$, function $n(t)$ may be considered approximately unchanging and equal to $n_i$. Then signal energy $n(t)$ over this interval

$$\int_{(i-1)\Delta T}^{i\Delta T} n^2(t)\,dt = n_i^2\Delta T = \frac{n_i^2}{2F_m},$$

while the total energy over the whole interval $T$ is equal to the sum of the energies over all $2F_mT$ intervals

$$\int_0^T n^2(t)\,dt = \frac{1}{2F_m}\sum_{i=1}^{2F_mT} n_i^2.$$

Dividing both parts of the equality by the spectral noise density $E_0 = \frac{\sigma_m^2}{F_m}$, we obtain

$$\frac{1}{E_0}\int_0^T n^2(t)\,dt = \frac{1}{2\sigma_m^2}\sum_{i=1}^{2F_mT} n_i^2.$$

If, in Formula (6.7), we replace the sum by the integral according to the last equality, and consider that $n = x - s$, we ultimately obtain the probability function for a continuous signal

$$L(s) = W_s(x) = (2\pi\sigma_m^2)^{-F_mT}\exp\left[-\frac{1}{E_0}\int_0^T (x-s)^2\,dt\right]. \quad (6.10)$$

Since the integrand in Expression (6.10) is not negative, $L(s)$ reaches a maximum when, and only when the transmitted $(s)$ and the re-

ceived $(x)$ signals coincide to the greatest extent over the whole time interval $T$. The integral increases with increase in the divergence between $x$ and $s$, while $L(s)$ decreases. Thus, $L(s)$ actually characterizes the degree of correspondence between $x$ and $s$, and it is rightly known as the probability function. In reception the effort is made to maximize this function, that is, to ensure maximum probability.

From Formula (6.10) the conclusion may be drawn that with a normal distribution law the minimum of the mean-square deviation expressed by the integral corresponds to probability maximum $L(s)$. If the integral depended only upon difference $x - s$, and not upon the square of the difference, the function itself would no longer be a measure of the correspondence between $x$ and $s$, since even at large divergences between them the integral could accidentally turn out to be equal to zero due to summing of the deviations of $x - s$ with different signs. Integration of the difference $x - s$ is an optimum operation only when signal intensity is constant.

From the informational point of view the only essential operation in Formula (6.10) is expressed by integral

$$\frac{1}{E_0}\int_0^T [x(t)-s(t-\tau)]^2 dt,$$

where $x$ and $s$ are again given as functions of time. This integral is decomposed into three integrals

$$\frac{1}{E_0}\int_0^T x^2(t)\,dt-\frac{2}{E_0}\int_0^T x(t)s(t-\tau)\,dt+\frac{1}{E_0}\int_0^T s^2(t-\tau)\,dt.$$

The first integral is of no interest to the receiver, since it expresses an operation which is irreversible only with respect to received signal $x$ without reference to transmitted signal $s$. The latter integral is in no way an operation on the received signal. Both of these integrals are numbers characterizing, respectively, the energy of sig-

nals $x$ and $s$. The result of reception should be time function $\tau$ representing the connection between signals $x$ and $s$, this being precisely what is described by the mean integral.

Thus the only essential operation on received signal $x$, which reflects the latter's connection with the transmitted (reflected) signal $s$, is the calculation of integral

$$l(\tau)=\frac{2}{E_0}\int_0^T x(t)s(t-\tau)\,dt. \qquad (6.11)$$

This is just the operation which the adequate receiver should accomplish. In the informational sense, function $l(\tau)$ is the equivalent of the probability function $L(s)$, and therefore the adequate receiver derives all available information relative to $s$ which is contained in $x$. Depending upon the signal/noise relation, the quality of the derived information may be good or bad, but it is always the best that can be derived from the received signal at the disposal of the receiver.

If the a priori distribution $W(s)$ and the received signal strength are known, from the data of the adequate receiver $l(\tau)$ it is possible, by using unessential operations, to form the probability function $L(s)$, the a posteriori probability $W_x(s)$, and to calculate the quantity of information obtained during reception. In this way the task of reception is completely solved. The received signal is needed only in order to form function $l(\tau)$. All other operations are performed without reference to the received signal.

## §6.3. THE PROBABILITY RATIO AND THE OPTIMUM DETECTOR

The first task which the radar receiver must solve is detection of the target. The informational approach which serves as the basis for the adequate receiver is not suitable for evaluating the results of detection.

In the first place, it is necessary to know the a priori probabil-

ity, which is either unknown or has no meaning. For example, it is almost impossible to answer the question: what is the a priori probability that an airplane will be detected on such-and-such a day, at such-and-such a time, and at such-and-such a range, using the given RLS.

In the second place, in detection the observer must usually present, not the a posteriori probability distribution and not some quantity of information, but a well-grounded reply to the question of whether or not a target is present at a given point in the scanning zone.

In the third place, although the adequate receiver does ensure the best reception, detection may be reliable or unreliable depending upon the intensity of the received signal. But since the results of reception are not evaluated as a function of the relative signal intensity, the important concept of sensitivity, which determines one of the basic parameters of the radar station – its operating range, loses its meaning.

Therefore, a somewhat different approach, the *criterial approach*, is used in detecting radar signals. To clarify the essence of this approach let us examine two cases of signal reception.

1. There is no target. The received signal consists of pure noise ($s = 0$).

2. There is a target. The received signal is the sum of the reflected signal and the noise ($s \neq 0$).

These two cases differ in the statistical properties of the received signals, which are described by their distribution functions at $s = 0$ and $s \neq 0$, respectively.

The conditional probability of reception of signal $x$ in the presence of a target ($s \neq 0$) is already known to us from Formula (6.9)

$$W_s(x) = (2\pi\sigma_m^2)^{-F_m T} \exp\left[-\frac{1}{E_0}\int_0^T (x-s)^2\,dt\right].$$

We obtain the conditional probability of reception of signal $x$ in the absence of a target by substituting $s = 0$ into the preceding formula

$$W_0(x) = (2\pi\sigma_m^2)^{-\frac{1}{2}m^T} \exp\left[-\frac{1}{E_0}\int_0^T x^2 dt\right]. \qquad (6.12)$$

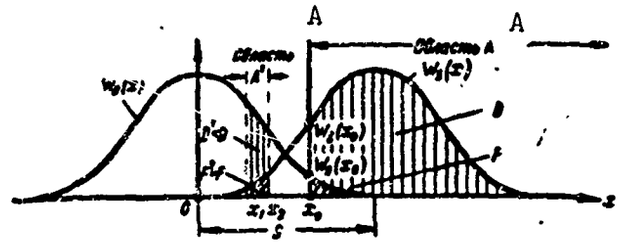


Fig. 6.4. Probabilities of detection and of false alarms at assigned threshold $\Lambda_0$. A) Region.

When $Ws(x)$ and $W_0(x)$ are known, it is possible to decide to which of the two groups, $s \neq 0$ or $s = 0$, received signal $x$ most probably refers. And this is just the way in which the problems of the presence of a target is solved.

*The ratio criterion*. There are a number of techniques or criteria used in reaching a decision as to which of the two groups received signal $x$ is to be referred. The best measurement technique for providing an answer to this question is the *probability ratio*

$$\Lambda(x) = \frac{W_s(x)}{W_0(x)}, \qquad (6.13)$$

which shows how much greater is the probability that received signal $x$ contains $s \neq 0$ as a gainst the probability of reception of $x$, consisting of pure noise. If ratio $\Lambda(x)$ is sufficiently large, that is, when

$$\Lambda(x) \geqslant \Lambda_0, \qquad (6.14)$$

the decision is that the target is present. In the opposed case it is

considered that the target is absent. Quantity $\Lambda_0$ is called the criterial threshold or criterial value.

Figure 6.4 gives distributions functions $W_0(x)$ and $W_s(x)$ at a certain value of signal $s$, from which it follows that threshold $\Lambda_0$ represents the ratio of $W_s(x)$ to $W_0(x)$ at point $x = x_0$

$$\Lambda_0 = \frac{W_s(x_0)}{W_0(x_0)}.$$

The area under the curves $W_0(x)$ and $W_s(x)$ to the right of $x_0$ determines, respectively, the probabilities that a noise or a signal-plus-noise will fall in region $A$ where condition $\Lambda(x) \geq \Lambda_0$ is satisfied.

The concept "region $A$" arose from the discrete representation of the signal. According to this representation, each concrete model (time function) of the received signal or of the pure noise may be represented in the form of a point in $2F_mT$-dimensional space. Readings $x_i$ of the time function are the coordinates of the describing point. The distance of this point from the origin of the coordinates is equal to the length of the radius-vector

$$\rho = \sqrt{\sum_{i=1}^{2F_mT} x_i^2}.$$

It is obvious that the describing points of pure noise are located mainly near the origin of the coordinates ($\rho$ is small). As a rule, $\rho$ of the signal-plus-noise is larger, since each reading of $x_i$ contains constant component $s$ which in noise is absent.

If the origin of the coordinates is surrounded by a closed surface, we may divide the whole space into two adjacent regions. The region inside the surface contains primarily pure noise; the outer region – region $A$ – most probably contains the signal. A boundary closed surface is selected such that condition $\Lambda(x) \geq \Lambda_0$ is satisfied for the given $s$.

Thus, with the criterial approach to the task of detection, probability ratio (6.13) must be obtained at the receiver output and tested at threshold $A_0$. These operations are performed by the *optimum detector*. It is called an optimum detector because it utilizes the optimum criteria, in this case – the ratio criterion.

To determine the structure of the optimum receiver we substitute Formulas (6.9) and (6.12) into (6.13). Then the probability ratio takes the form

$$A(x) = \exp\left[\frac{2}{E_0}\int_0^T xs\,dt - \frac{E_s}{E_0}\right], \qquad (6.15)$$

where

$$E_s = \int_0^T s^2\,dt$$

is the signal energy (across a 1 ohm resistance). When the signal intensity is known, ratio $E_s/E_0$ is a known quantity. Consequently, from the informational point of view Operation (6.15) is the equivalent of Operation (6.11), performed by the adequate receiver, since both include one and the same essential operation.

In addition to the adequate operation, the optimum detector performs one further essential operation – testing at the threshold $A_0$, or limiting. Introduction of a new essential operation in addition to the adequate operation, as has already been pointed out, leads to loss of information. However, this operation is *necessary* since the detecting receiver is required to yield one of two mutually exclusive answers: presence or absence of the target.

The loss of information is expressed by the fact that the adoption of a decision as to the presence of a target is accompanied by two kinds of errors.

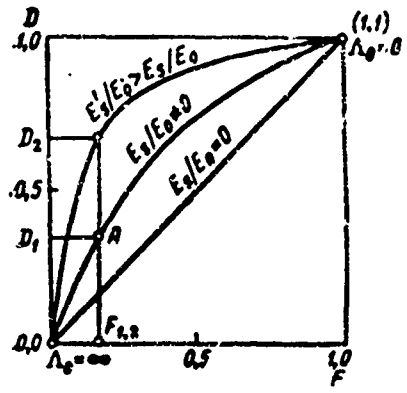


Fig. 6.5. Operating characteristics of the receiver (RKhP).

1. *False alarm* — the detection threshold is exceeded by pure noise, that is, signal $x$ taken from the aggregate $s = 0$ falls into region $A$. The probability of a false alarm

$$F=\int_A W_0(x)\,dx=\int_{x_0}^{\infty} W_0(x)\,dx \qquad (6.16a)$$

is determined by the area with slanted shading in Fig. 6.3.

2. *Failure to detect the target* — the signal-plus-noise reflected from the target fails to exceed the threshold of detection. In other words, signal $x$ from the aggregate $s \neq 0$ does not fall in region $A$. The probability that the target will not be detected $M = 1 - D$, where

$$D=\int_A W_s(x)\,dx=\int_{x_0}^{\infty} W_s(x)\,dx \qquad (6.16b)$$

is the probability of (correct) detection, which is numerically equal to the area with vertical shading (Fig. 6.3). The probability $M$ that the target will not be detected is represented by the area limited from above by curve $W_s(x)$, on the right by the ordinate $x = x_0$ and from below by the axis of the abscissa.

Probabilities $F$ and $D$ depend upon the size of the threshold. The dependence between $F$ and $D$ for all possible values of threshold $\Lambda_0$ is known as the *receiver operating characteristic* (RKhP). The operating characteristic is constructed in coordinates $F$ and $D$ in the form of a family of curves with parameter $E_s/E_0$ = const (Fig. 6.5). The RKhP curves used in practice are usually in a slightly different form, since only those sections are of interest for which $F$ is very small (of the order of $10^{-4}$-$10^{-7}$), while $D$ is close to unity.

According to Formulas (6.16a) and (6.16b) $W_0(x_0)=-\frac{dF}{dx_0}$; $W_s(x_0)=-\frac{dD}{dx_0}$.

Then for any point on the curve of the RKhP we find the threshold value $\Lambda_0$ as the tangent of the tilt angle at this point

$$\Lambda_0 = \frac{W_s(x_0)}{W_0(x_0)} = \left(\frac{dD}{dF}\right)_{x=x_0}.$$

It follows from this that selection of the operating regime for the receiver means selecting a point on the RKhP curve.

Since $\Lambda_0 \geqslant 0$, as the ratio of $W_s(x_0) \geqslant 0$ to $W_0(x_0) \geqslant 0$, the RKhP curves increase monotonically. With an infinitely large threshold ($\Lambda_0 = \infty$) neither the signal-plus-noise nor the pure noise can exceed this threshold, and $F = D = 0$ (the point of origin of all RKhP curves). When the threshold is zero ($\Lambda_0 = 0$), any signal can appear at the receiver output, and $F = D = 1$ (the point of convergence of all RKhP curves).

The more the signal energy exceeds the noises $E_s/E_0$ the higher the position of the curves. Consequently, different probabilities of $D$ for different levels of excess of the signal over noise $E_s/E_0$ (Fig. 6.5) correspond to one and the same region $A$, determined by the selection of $x_0$, with identical probability of false alarms $F$.

Together with the ratio criterion there exist other optimum criteria, that is, techniques for defining region $A$ for those values of signal $x$ at which it is decided that a target is present. We will show that all of these criteria are reduced to the ratio criterion which we have already examined.

*The weighted combination criterion.* The probability of a false alarm is usually assumed to be very small, and a one-percent change in it is not equivalent to a one-percent change in the probability of detection. Let us assume that there exist weighting factor $\beta$ which takes into account the importance of false alarm $F$ by comparison with correct detection $D$. In this case it is not advisable to include in region $A$

such values of $x$ which maximize the difference

$$D-\beta F \quad \text{or} \quad \int_A [W_s(x)-\beta W_0(x)]\,dx$$

since an increase in the probability of detection and (or) reduction in the probability of false alarm, is always desirable.

For the integral to be maximum it is necessary to assign to region $A$ only such values of $x$ for which the integrand is not negative, that is

$$W_s(x)-\beta W_0(x)\geqslant 0$$

or

$$\Lambda(x)=\frac{W_s(x)}{W_0(x)}\geqslant\beta.$$

Consequently, the weighted combination criterion is a ratio criterion with the threshold $\Lambda_0 = \beta$.

*The ideal observer criterion.* Let us assume that the observer knows the a priori probabilities of reception of target signal $p_s$ and of pure noise $p_0 (p_s + r_0 = 1)$. It is then desirable to select a region $A$ which will minimize the probability of overall error, this probability being equal to the weighted sum of the probability $M$ that a signal from aggregate $s \neq 0$ will fail to be detected, and of the probability of false alarm $F$ for a signal from the aggregate $s = 0$,

$$p_sM+p_0F=p_s(1-D)+p_0F=p_s-p_s\left(D-\frac{p_0}{p_s}F\right).$$

This is equivalent to obtaining the maximum from the difference

$$D-\frac{p_0}{p_s}F,$$

which is reduced to the requirement for a weighted combination criterion with weighting $\beta = p_0/p_s$. Consequently, the ideal observer criterion is also an optimum criterion, coinciding with a ratio criterion with threshold $\Lambda_0 = \beta = p_0/p_s$.

*The Neumann-Pearson criterion.* We assume that the probability of false alarms $F$ is assigned. Then from all regions $A$ with assigned $F$ it is advisable to select a region which will assure maximum probability of detection $D$.

We formulate the optimum weighted combination criterion with weighting $\beta$, for which $D = D(\beta)$ and $F = F(\beta)$. Inasmuch as this criterion is optimum, the weighted combination $D(\beta) - \beta F(\beta)$ utilizing this criterion is greater than or equal to the weighted combination $D - \beta F$ utilizing any other criterion at the assigned probability $F$, that is

$$D(\beta) - \beta F(\beta) \geqslant D - \beta F.$$

But since the probability of a false alarm has been assumed by us to be identical in both cases, and $F(\beta) = F$, we obtain from the latter inequality

$$D(\beta) \geqslant D,$$

which is what we should have obtained on the basis of the Neumann-Pearson criterion. Consequently, this criterion is also optimum and coincides with the ratio criterion at $\Lambda_0 = \beta$

In explanation of why the Neumann-Pearson criterion is optimum, Fig. 6.4 shows that with identical probability of false alarm, improper selection of region $A'$ leads to a considerable reduction in the probability of detection (for example, when region $A'$ includes only a small part of the space of the describing points).

A large number of other optimum criteria may be proposed; like the preceding, they also may be reduced to the ratio criterion. Of all the optimum criteria examined, the Neumann-Pearson criterion evidently correspond best to the conditions in which a RLS operates. For technical reasons it is usually required that the probability of false alarm not exceed some previously assigned quantity, since repeated false alarms lower confidence in the results of radar observation. At the same time,

it is desirable to maximize the probability of correct detection.

The selection of one or another optimum criterion, as determined by the mission and operating conditions of the RLS, represents rather a tactical than a technical task. From the point of view of the engineer, the properties of the optimum receiver are fully described by its operating characteristics and hold true for any criterion. Selection of a point on the RKhP curves in accordance with one of the optimum criteria determines the interconnected characteristics of the given receiver: the probability of false alarm $F$, the probability of correct detection $D$, and sensitivity $(E_s/E_0)_{min}$.

The output effect of the optimum receiver can be not only the probability ratio, but any monotonic function of it. It has turned out to be more convenient to use the logarithm of the probability ratio $l(x) = \ln \Lambda(x)$ for which, in accordance with Formula (6.15), we obtain

$$l(x)=\frac{2}{E_s}\int_0^T x(t)\,s(t-\tau)\,dt-\frac{E_s}{E_0}. \qquad (6.17)$$

Use of the logarithm is convenient because the result of successive stages of signal reception are usually not multiplied, but added. When the probability ratio is utilized, the result of $n$ successive stages of reception should be multiplied, since

$$W_s(x)=\prod_{k=1}^{n} W_{sk}(x), \quad W_0(x)=\prod_{k=1}^{n} W_{0k}(x)$$

and, consequently,

$$\Lambda(x)=\prod_{k=1}^{n}\Lambda_k(x).$$

Then

$$l(x)=\sum_{k=1}^{n} l_k(x),$$

which is what is required by the operating condition of the receiver ter-

minal device.

The logarithm of the probability ratio for the case of $n$ successive stages of signal reception

$$l(x)=\frac{2}{E_0}\sum_{k=1}^{n}\int_0^{T_k} x_k(t)\,s_k(t-\tau)\,dt-\frac{1}{E_0}\sum_{k=1}^{n}E_{sk}, \qquad (6.18)$$

where $\sum E_{sk}$ is the total energy of the received signal. When $F$ and $D$ are assigned, quantity $M_p=\frac{1}{E_0}\left(\sum E_{sk}\right)_{\min}$ characterizes the threshold signal/noise ratio at the output of the terminal device. The threshold signal/noise ratio in one central pulse $m_p=\left(\frac{E_{s1}}{E_0}\right)_{\min}$ is the discrimination factor which we have already encountered.

Replacement of $\Lambda(x)$ by $l(x)=\ln\Lambda(x)$ requires a corresponding substitution of the threshold: $l_0=\ln\Lambda_0$. Testing of Functions (6.17) or (6.18) at threshold $l_0$ is equivalent to testing of function

$$l(\tau)=\frac{2}{E_0}\int_0^{T} x(t)\,s(t-\tau)\,dt \qquad (6.11)$$

at threshold $l_0'=l_0+\frac{E_s}{E_0}$.

Thus, the optimum receiver reduces to the adequate receiver whose output function $l(\tau)$ is tested at threshold $l_0'$. Therefore, the optimum detector only differs from the optimum receiver yielding maximum information in that the detector possesses a threshold device at its output.

*The successive observer criterion.* There exists one further optimum criterion, differing from the preceding ones in that it not only defines the decision-making procedure and the size of the threshold, but also assigns the operating regime of the RLS itself. This is the successive observer criterion which has become particularly significant in connection with the development of inertialess antennas with electrical scanning.

In ordinary RLS the angular velocity of the antenna beam is constant, and the number of pulses received from the target is known beforehand. In the RLS utilizing the successive observer criterion the scanning velocity and the number of received pulses is not determined beforehand and depends upon the results of observation.

In space scanning the following procedure is used. The antenna beam is stationary and fixed in the assigned direction, and the RLS emits a single pulse. The resolving device at the receiver output has two thresholds: an upper one $A = D/F$ and a lower one $B = 1 - D/1 - F$. If $l(x) < B$, it is considered that a target is absent, while at $l(x) > A$ a target is considered to be detected. In both cases the antenna receives a command shifting the beam by one jump to scan the space in the other direction. But if the received signal has fallen in the region where $B < l(x) < A$, the beam continues to remain in the given direction, and pulses are emitted until one of the thresholds, $A$ or $B$, is exceeded. Then scanning continues in the other directions.

Thus, the time during which the beam remains in the given direction, and the number of pulses (received and emitted), depends upon the results of observation and is random for the observer. Such a procedure is known as the dynamic programing method of scanning.

In dynamic programing the receiver output signal $l(x)$ is defined by Formula (6.18); only the number of summing $n \geq 1$ is not constant, being equal to the test number $k$ at which one of the two thresholds is crossed. It has been discovered that under actual operating conditions of an RLS the average number of pulses $\bar{n}$ irradiating the target during dynamic programing may be several times smaller than the number of pulses $n$ when scanning velocity is constant. Accordingly, there is reduction in the energy expended during scan of the assigned zone. This is the merit of the successive observer criterion; it is more flexible.

The method of dynamic programing (sequential analysis) may also be utilized to solve other tasks, for example, in searching for a target using an automatic range-finder.

## §6.4. THE SYNTHESIS OF THE OPTIMUM RECEIVER

The structure of the optimum receiver is determined by the function

$$l(\tau)=\frac{2}{E_0}\int_0^T x(t)s(t-\tau)\,dt, \qquad (6.11)$$

which must be obtained at the receiver output when signal $x(t) = s(t - \tau_0) + n(t)$ is registered at its input. The output signal (6.11) may be viewed either as a function of the mutual correlation, or as a convolution, of functions $x(t)$ and $s(t)$. Thus there are two ways of designing the optimum receiver: the correlation method and the method of optimum filtration.

In principle these two methods are of equal value, since they are expressed mathematically by one and the same formula (6.11). However, in the synthesis of optimum receivers technical difficulties arise whose significance depends upon the design adopted and upon the signal shape $s(t)$.

### 1. Correlation Reception

Let us define the structure of the optimum correlation receiver for signal $s(t)$ in the form of a sinusoidal oscillation with an arbitrary modulation law. We will assume that the target is stationary and lies at distance $R_0$ from the RLS. Then the received signal has the form $x(t) = s(t - \tau_0) + n(t)$, where $\tau_0 = 2R_0/c$.

In order to form the correlation function, it is necessary to have reference voltage $s(t - \tau)$, in addition to signal $x(t)$; the former is obtained by passing the oscillations $s(t)$ emitted by the transmitter through a delay line. The integral is maximum at $\tau=\tau_0=\frac{2R_0}{c}$, and the delay time in the line is therefore taken equal to $\tau_0$.

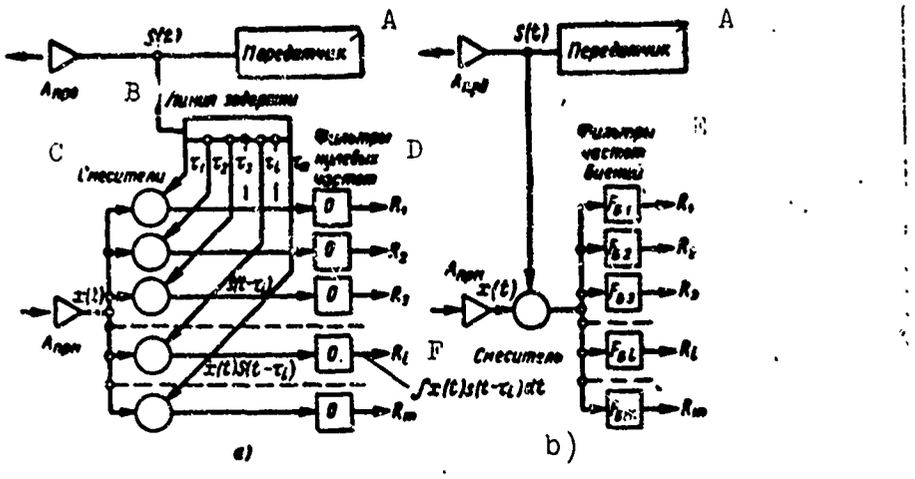


Fig. 6.6. Correlation reception: a) Block diagram of universal correlation receiver; b) block diagram of continuous-signal receiver with linear frequency modulation. A) Transmitter; B) delay line; C) mixers; D) zero-frequency filters; E) beat-frequency filters; F) mixer.

The functions $x(t)$ and $s(t-\tau_0)$ are multiplied in a mixer and integration within the limits of the length $T$ of the signal is accomplished by passing the multiplied signal through a low (zero) frequency filter with cutoff frequency $F_m = 1/T$.

The signal of the given target at the filter output

$$l(\tau_0)=\frac{1}{E_0}\int_0^T x(t)\,s(t-\tau_0)\,dt$$

has maximum amplitude, being a function of the correlation between $x(t) = s(t-\tau_0) + n(t)$ and $s(t-\tau_0)$ in the absence of a mutual time shift (the phase is assumed to be known).

The delay $\tau \neq \tau_0$, and the voltage at the filter output, of the signals of other targets is small or equal to zero. In particular, in the case of a continuous frequency-modulated signal at the mixer output, beats are formed which are not passed by the filter, since their frequency differs from zero. In pulsed emission the signal proper at the output is also equal to zero, if the shift between the signal and the reference voltage exceeds the pulse length, since the integrands do not

overlap.

That is how a target signal whose range is known is discriminated (detected). In order to receive signals from any range it is necessary to have a selection of receivers (channels) of the form examined above. Each channel is calculated for a given distance, and together they cover all the ranges.

Figure 6.6a gives a block diagram of a correlation receiver for target signals of arbitrary range. The reference voltage is tapped from the delay line and fed to the receiver mixers at different delay intervals $\tau_i$. The delay times from one channel to the next should differ by quantity $\delta\tau = 1/\Delta f$, where $\Delta f = 2F_m$ is the width of the spectrum of the high-frequency signal. At shift $\delta\tau = 1/\Delta f$ the signals in adjacent channels are considered as independent according to the Shannon theorem, and the targets are resolved with respect to range.

We should note that the resolvable distance $\delta R = \frac{c}{2}\delta\tau = \frac{c}{2\Delta f}$ is determined by the signal spectrum width $\Delta f$ regardless of its form.

To ensure continuous scan the signal modulation law is periodically repeated. The possibility of an ambiguous range reading is excluded by the fact that modulation period $T_m$ is selected on the basis of condition

$$T_м \geqslant \tau_m = \frac{2R_{макс}}{c},$$

where $\tau_m$ is the maximum delay time of the echo-signal and the delay in the line.

This correlation method is applicable for any modulation law. It is possible, in particular, to use noise modulation of the signal with respect to amplitude or frequency (phase).

Unfortunately, the practical design of a correlation receiver of the above form is beset with serious technical difficulties.

In the first place, when continuous emission is employed the strong transmitter signal penetrates into the receiver input, bypassing the delay line. As a result, intense parasite signals are formed in all the channels.

In the second place, the maximum delay required in the line, being proportional to the RLS operating range, may reach several milliseconds and more, which is difficult to achieve.

Because of this, a simpler method of correlation reception for continuous frequency-modulated signals, based upon beat-frequency analysis, is employed in practice.

Figure 6.6b gives a block diagram of a frequency RLS employing continuous emission and operating in accordance with the beat method. It is considerably simpler than the preceding method and utilizes the linear analogy between the delay time and the beat frequency, which is manifested only when the frequency varies linearly over time.

The operation of this type of RLS was examined in Chapter 2. We may only recall that in this design the transmitter signal is fed directly to the receiver input without delay. Thanks to this, the second inadequacy of the preceding design is eliminated. The beat frequency at the output of the only mixer is proportional to target range, the latter being measured by feeding the beats to a frequency analyzer which consists of a selection of filters each of which is tuned to its own frequency.

This design of the correlation receiver is approximately the same as the preceding with the following limitations:

a) frequency changes linearly over time;

b) modulation period $T_м \gg \frac{2R_{макс}}{c}$.

The latter condition is not satisfied, there is an increase in the

amount of time, of transient processes, when target range is not proportional to beat frequency. This causes range measurement error and reduction in sensitivity.

The remaining characteristics and limitations of this method, which have been examined above, are of no interest in the present case.

2. Optimum Filtering

Optimum reception

$$l(\tau)=\frac{2}{E_0}\int_0^T x(t)s(t-\tau)\,dt, \qquad (6.11)$$

viewed as the convolution of two time functions, may be accomplished simply by passing a signal $x(t)$ through a filter which is matched in a particular manner with the shape of the signal itself $s(t)$. Such a filter is called an optimum filter or a matched filter, and the operation itself is known as optimum filtering.

In radar the signal shape $s(t)$ is known beforehand (except for certain parameters), and it is therefore possible in principle to design an optimum filter. The principle of design of an optimum filter and the essence of optimum filtering are described below.

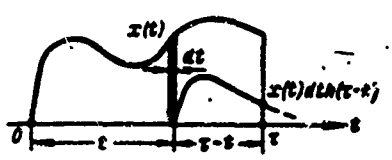


Fig. 6.7. Calculating the pulse characteristic of a filter.

It is known that the arrival of individual pulse $\delta(t)$ (delta-function) at the input of a linear filter yields response $h(t)$ at the output; this is known as the pulse characteristic of the filter. If the area of the pulse is equal not to unity, but to a certain number $A$, the filter response will be $Ah(t)$.

Let us feed voltage $x(t)$ to the input of this filter (Fig. 6.7) and break this voltage down into an infinitely large number of infinitely short pulses of length $dt$. The amplitude of a single pulse at arbi-

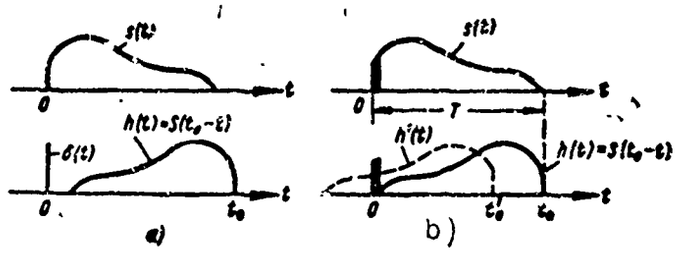


Fig. 6.8. The pulse characteristic of an optimum filter: a) Shape of signal and pulse characteristic; b) feasible $h(t)$ and unrealizable $h'(t)$ characteristics.

trary moment in time $t$ is $x(t)$, and the cross-section is $x(t)dt$. At the filter input this pulse will yield response $x(t)dth(t)$. At moment in time $\tau$ the voltage of the response will obtain magnitude $x(t)dth(\tau - t)$. The remaining pulses will produce analogous effects.

All the pulses comprising input voltage $x(t)$ at interval 0, $\tau$, will, as a result of the linearity of the system, form voltage $y(\tau)$ at the filter output, this being equal to the sum of the responses to each pulse

$$y(\tau)=\int_0^\tau x(t)h(\tau-t)dt.$$

The resultant function is known as the Duhamel convolution or integral. In the case where input voltage $x(t)$ terminates at moment in time $\tau = T$, the upper limit must be replaced by $T$.

If we take the latter circumstance into account and compare the obtained result with the function

$$l(\tau)=\frac{2}{E_0}\int_0^T x(t)s(t-\tau)dt, \qquad (6.11)$$

we will note that to accomplish optimum reception of signal $x(t) = s(t - \tau_0) + n(t)$ the latter need only be passed through a filter with a pulse characteristic of the form

(6.19)

and the value of theoutput signal is clamped at the moment $T$ of termination of the signal at its input (more accurately: at the moment $t_0 \geq T$).

Thus, the pulse characteristic of the optimum filter $h(t)$ represents, accurate to a constant factor, a "mirror image" in time of the signal proper $s(t)$ (Fig. 6.8a).

If we pass from a time description of the structure of the optimum filter to a frequency description, we find the complex transmission function $K(f)$ of the optimum filter as the Fourier transformation of this pulse characteristic $h(t) = s(-t)$, that is

$$K(f)=\int_{-\infty}^{\infty} s(-t)\,e^{-j2\pi ft}dt=\int_{-\infty}^{\infty} s(t')\,e^{j2\pi ft'}dt'.$$

The last integral was found by substituting $t' = -t$ and by a dual transposition of the limits of integration.

On the other hand, the signal frequency spectrum $s(t)$ is expressed by the dependence

$$S(f)=\int_{-\infty}^{\infty} s(t)\,e^{-j2\pi ft}dt.$$

By comparing the two last expressions we realize that the transmission function of the optimum filter is a complex conjugate function of the signal spectrum

$$K(f)=S^*(f). \qquad (6.20)$$

Conditions (6.19) and (6.20) are equivalent; however, the frequency approach makes possible a more graphic demonstration of the properties of the optimum filter.

The modulus of the transmission function of the optimum receiver reproduces the amplitude-frequency characteristic of the signal. Therefore, the optimum filter is the one which best passes those components of the signal spectrum which possess the greatest intensity in compari-

son with the noise spectrum, the signal spectrum being evenly distributed over the whole range of frequencies. The frequencies which are missing from the signal are not passed by the filter, since they are conditioned by noise alone. Thanks to this, the optimum filter assures the maximum possible signal/noise ratio at the output.

The complex association of the transmission function and the signal spectrum indicates that the mutual phase shift between the spectral components of the signal are compensated by the optimum filter when the signal has fully entered its input (moment of reckoning $T$). Thanks to this all of the signal spectrum components are added in phase at the moment of reckoning $T$, and the output signal is at the maximum determined by Expression (6.11).

The pulse characteristic of the optimum filter should be physically realizable, meaning that the response may not appear at the filter output before the input is acted upon.

Figure 6.8b (at the lower part of the illustration) depicts a realizable $h(t)$ and an unrealizable $h'(t)$ filter pulse characteristic. The short pulse of the forward front of the signal (shaded) acts first upon the filter, giving rise at the filter output to the response $h(t) = s(t_0 - t)$, which is a "mirror image" of signal $s(t)$. Since the response may not appear at the output earlier than moment $t = 0$, it is necessary to satisfy condition

$$t_0 > T, \qquad (6.21)$$

where $T$ is the signal length at the input. This is precisely the condition of physical realizability of a filter with pulse characteristic $h(t) = s(t_0 - t)$.

It should also be pointed out that the shortest possible impact at the input yields at the output of the optimum filter, response $h(t) = s(t_0 - t)$ whose length is $T$. Consequently, the optimum filter should

be able to remember during the length of the input signal.

It follows from what has been said that the design of the optimum filter is simplest for short signal-pulses. For a continuous signal a filter would be needed with an infinite or very long memory, which is physically unrealizable.

*Reception of a single pulse.* Let us examine the structure of the optimum filter for pulse radar signals. To avoid difficulties associated with ignorance of the initial phase, we will assume signal $s(t)$ to mean only its envelope (video signal), and we will assume the noise to be gaussian with an even spectrum. Such an assumption is permissible for a large signal/noise ratio and also for any signal, no matter how weak, if the out-of-phase noise component is suppressed by a phase detector. Questions connected with the phase of the high-frequency signal will be examined in the following sections.

As has already been noted, the moment of occurrence of the maximum output voltage of the optimum receiver, when it is equal to Integral (6.11), coincides with moment $t_0 \geq T = \tau_1$ after the termination of the input signal. Therefore it is convenient to refer the start of the reckoning of the echo-signal delay time $\tau$ to the moment in time when the transmitter pulse, leaking into the receiver input, reaches its maximum at the output of the optimum filter.

If the pulse has been emitted by the RLS at $\tau = 0$, the reflected signal of the target will reach its maximum at the output of the optimum filter (receiver) at moment $\tau_0 = 2R_0/c$, proportional to target range $R_0$. The crossing of threshold $l_0$ by output signal $l(\tau_0)$ establishes the fact that a target is present, and its range is reckoned from the quantity $\tau_0$. The output signals of several targets are distributed over time in proportion to range.

Two conclusions follow from this.

In the first place, when filtering is optimum, just as in correlation reception, target range may be measured just when the target is detected.

In the second place, optimum filtering differs from correlation reception in that processing consists in passing the signals of all targets successively through one and the same filter, which is much simpler. In view of this, optimum receivers of pulse signals have never been designed on the basis of the correlation principle.

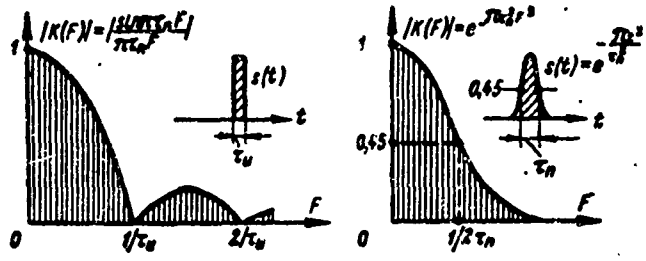


Fig. 6.9. Modulus of the transmission function of an optimum filter: a) For the envelope of a rectangular pulse; b) for the envelope of a bell-shaped pulse.

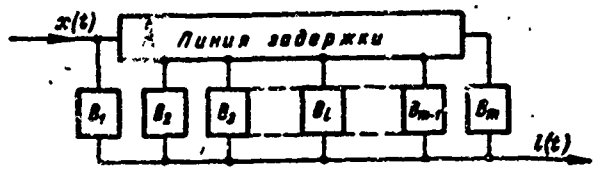


Fig. 6.10. The approximately optimum universal filter. A) Delay line.

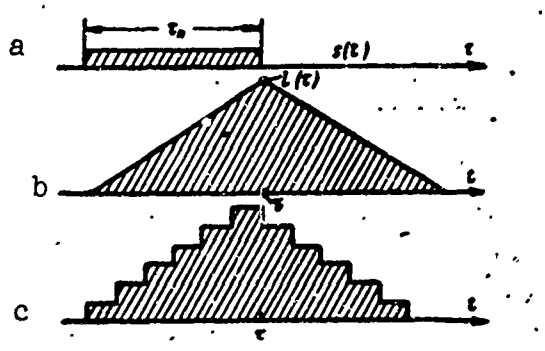


Fig. 6.11. Processes in filters: a) Signal at the input; b) signal at the output of an optimum filter; c) signal at the output of an approximately optimum universal filter.

In order to have an idea of the receiver parameters, Fig. 6.9 sets forth the frequency characteristics $|K(F)|$ for pulses with rectangular and bell-shaped envelopes.

In the case of pulses with a simple shape and evenly varying amplitude (for example, bell-shaped pulses), optimum filters are comparatively easily assembled out of $R$, $L$ and $C$ elements.

With respect to signals of complex shape and also pulses with steep fronts, it is either difficult or impossible to construct filters from such elements. As an example we may indicate a filter which is optimum for a pulse with rectangular envelope.

There is a universal way of designing optimum filters of any shape based upon the approximate replacement of Integral (6.11) by the sum. The universal filter consists of a delay line with taps (Fig. 6.10). The number of taps is equal to the number of terms in the sum replacing the integral; therefore, the filter is only an approximation of the optimum filter. With increase in the number of taps the result of summation approximates the required result which is determined by Integral (6.11). The signals from the taps are added in a certain proportion on a common load. For this they are first multiplied (in amplifiers or voltage dividers) by weighting factors $B_i \equiv S_i$, whose selection is governed by the signal shape (and by the amount of damping in the delay line).

By a suitable selection of maximum delay in the line, of the number and location of the taps, and also of the weighting factors, it is possible to design a filter approximating, with the assigned degree of accuracy, the optimum filter for a signal of practically any shape. Figure 6.11 shows, as an example, the shape of the voltage at the output of a filter with six taps and at the output of an optimum filter for a rectangular pulse (for such a signal the delay-line filter may be considerably simplified).

It is seen from the example that the optimum filter distorts the signal shape. This circumstance does not cause any loss of information, since in radar we are interested not in the signal shape (we know it), but in the target information which it carries (the fact of the presence of a target, its range, etc.). Earlier it was theoretically proven that the optimum filter is the best transmitter of information.

We note that some signals, for example the bell-shaped pulse, are in theory infinitely long, and therefore the output signal of the optimum receiver may generally be represented in the form

$$l(\tau)=\int_{-\infty}^{\infty} x(t)s(t-\tau)\,dt. \qquad (6.22)$$

*Reception of a pulse packet.* Usually not one, but several pulses, are received from the target, the shape of the envelope of their amplitudes reproducing the power of the antenna directivity diagram. For such a signal, known as the pulse packet, the optimum receiver may be designed in two ways.

*The first way* is to view the packet as a pulse of complex shape and to pass it through a filter *which is optimum for the whole pulse packet.*

Figure 6.12 gives the frequency characteristic $|K(F)|$ of an optimum filter for the rectangular pulse packet of rectangular shape which is depicted there. The filter should consist of a series of narrow-band filters which would be optimum for the "pulse" of the packet if it was continuous, while the envelope of the characteristics of these filters resembles the spectrum of a single pulse whose length is $\tau_1$.

The frequency characteristic of the filter

$$K(F)=\frac{\sin \pi F\tau_{\text{п}}}{\pi F\tau_{\text{п}}}\,\frac{\sin \pi FnT_{\text{п}}}{\sin \pi FT_{\text{п}}} \qquad (6.23)$$

is represented only by the first lobes of the functions $\sin x/x$ and $\sin nx/\sin x$, within the limits of which 90% of the signal energy is

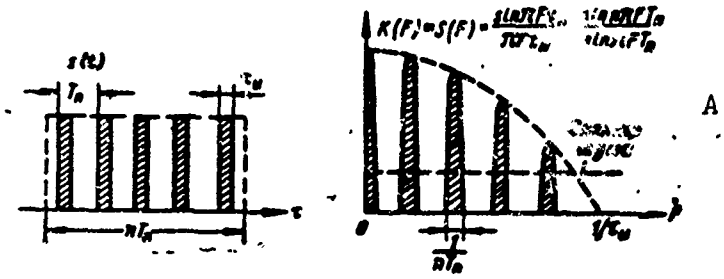


Fig. 6.12. Transmission function of a filter which is optimum for a packet of rectangular pulses of constant amplitude. A) Noise spectrum.

concentrated.

An optimum filter of this shape is known as a *comb filter*. The example of the comb filter graphically demonstrates the mechanism of noise suppression: the signal spectrum coincides with the filter transmittance bands while a considerable part of the noise spectrum, which is evenly distributed with respect to frequency, is not passed by the filter. That part of the noise spectrum which does not fall into the narrow transmittance band of the filter is delayed.

Let us make a crude estimate of the degree of suppression of noise by a comb filter (see Fig. 6.12). The width of the transmittance band of each narrow-band filter (except for the first) is $1/nT_p$, the number of filters in the array is $T_p/\tau_i$. The total transmittance band, consequently, $\frac{1}{nT_u}\cdot\frac{T_u}{\tau_u}=\frac{1}{n\tau_u}$, that is, $n$ times narrower than the band of the whole filter array, equal to $1/\tau_i$. The noise suppression coefficient is equal to the number of pulses $n$.

With increase in the number of pulses $n$ received from the target, it is necessary to narrow the transmittance band of each narrow-band filter. At the same time, the coefficient of noise suppression of the optimum filter increases.

Thus a comb filter integrates the pulses, the integrating properties being determined by the second factor in Formula (6.23) which de-

pends upon $n$ and makes the filter a "comb" filter.

When the data are those typical of many RLS: the number of pulses $n = 10$, the pulse length $\tau_i \approx 1$ μsec, and the pulse repetition period $T_p = 1000$ μsec, the width of the transmittance band of each filter is only 100 hz, and the number of filters in the ray is 1000 (!).

It can be seen from this example that to design a comb filter as an array of many narrow-band filters represents a complex technical task. The same result may be obtained more simply.

*The second method* of optimum reception of a pulse packet consists in examining each pulse and treating it as a separate signal, and then adding the results of the processing of the signal sequence. Actually, since Formula (6.18) has been utilized for a sequence of $n$ independent signals $x_k$, the optimum operation with respect to complex signal $x = \Sigma x_k(t - kT_p)$ may be expressed as a function of the probability ratio

$$l(\tau)=\frac{2}{E_0}\sum_{k=1}^{n}\int x_k(t)s_k(t-\tau)\,dt,\quad 0\leqslant\tau<T_n. \qquad (6.24)$$

From this we derive the rule for processing a pulse packet. The first step is optimum processing of individual pulses during each pulsing period $T_p$, as expressed by the integrals (intraperiod processing). Then the results for a given $\tau$ (of identical range and different period) are added (interperiod processing).

*Intraperiod processing* is accomplished by passing the signal through an optimum filter whose frequency characteristic $K_f(F)$ is determined only by the pulse shape. For a rectangular pulse $K_\phi(F)=\frac{\sin \pi F\tau_n}{\pi F\tau_n}$.

Interperiod processing is accomplished by a device which had signals corresponding to an identical range in different repetition periods (synchronous accumulation). This device is known as a *synchronous integrator*, but its characteristic $K_1(F)$ is determined only by the shape of the pulse packet envelope and by the repetition period $T_p$.

Thus, the optimum receiver for a pulse packet consists of a filter which is optimum for a single pulse and of a synchronous integrator (Fig. 6.13). The transmission function of the receiver

$$K(F)=K_{\phi}(F)K_{n}(F). \qquad (6.25)$$

To determine the structure of the synchronous integrator we utilize Formula (6.24) assuming $s_k$ and $x_k$ within the limits of a pulse length to be constant (rectangular pulses). Then

$$\int x_k(t)s_k(t-\tau)\,dt=\tau_n s_k x_k$$

and

$$l(\tau)=\frac{2\tau_n}{E_0}\sum_{k=1}^{n}s_k x_k=\frac{1}{\sigma_m^2}\sum_{k=1}^{n}B_k x_k, \qquad (6.26)$$

where $B_k = S_k$ are weighting factors proportional to the amplitudes of the pulses in the packet (to the antenna directivity diagram). Let us also note that the added signals are separated in time by a whole number of repetition periods $T_p$.

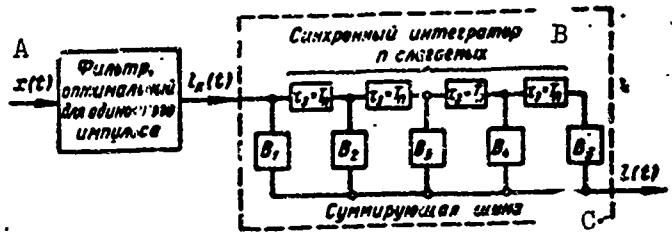


Fig. 6.13. Optimum receiver for a pulse packet with separate intraperiod and interperiod processing. A) Optimum filter for a single pulse; B) synchronous integrator for $n$ terms; C) summing bus.

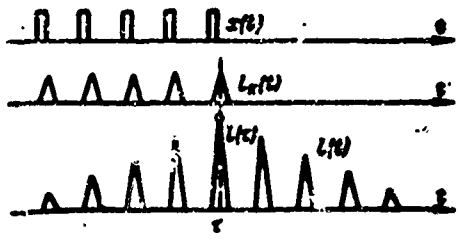


Fig. 6.14. Processes in an optimum receiver with separate processing.

Therefore a synchronous integrator takes, in general, the form of a series of delay lines, the delay time being $\tau_z = T_p$. From the taps of the lines signals enter the output summing bus through weighted amplifiers with gain factors $B_k$. Thus the target signals in consecutive repetition periods are summed at the output with weights $B_k = S_k$, as is required by Formula (6.26).

In general, when noise is not gaussian, $B_k = f(s_k)$. For a rectangular pulse packet $B_k = 1$.

The frequency characteristic of a synchronous integrator is comb-shaped, and in the case of a rectangular pulse packet the frequency characteristic has the form $K(F) = \frac{\sin \pi F n T_n}{\sin \pi F T_n}$, as follows from a comparison of Formulas (6.23) and (6.25). Therefore the synchronous integrator is often known as a comb (or integrating) filter.

Figure 6.14 gives as an example the processes at nodal points of an optimum receiver when a rectangular packet of rectangular pulses enters its input. The output signal maximum after interperiod processing, as determined by Formula (6.24), occurs at the moment of entry of the last pulse of the packet. Its angular position is determined from the envelope maximum at the moment of detection of the target. Thus, in the case of interperiod processing, the task of measuring the angular coordinates of the target may be solved at the same time as the target is detected. Let us recall that target range is measured during intraperiod processing of the pulse.

Integration may also be nonsynchronous, when the pulses are not selected with respect to range (their periodicity is not taken into account). Nonsynchronous integration is not an optimum operation and yields a loss in the signal/noise ratio.

At the end of the section we formulate the basic conclusions to be derived from this analysis.

In the first place, correlation reception and optimum filtering are of equal value and are both optimum operations.

In the second place, the pulse packet should be received in two stages: through intraperiod and interperiod processing.

Therefore, we will examine below the receiver of the most widespread pulse signals whose intraperiod processing is accomplished by filtering in the high-frequency strip, and whose interperiod processing is done by the RLS video frequency terminal device. Between these two devices there is a detector whose influence will vary depending upon whether or not the phase of the high-frequency signal is taken into account during the processing.

## §6.5. CHARACTERISTICS OF THE RECEPTION OF HIGH-FREQUENCY SIGNALS

Radar utilizes high-frequency signals possessing amplitude and phase. The outcoming pulse is an oscillation of frequency $f_0$ whose envelope we will denote by $A(t)$ and whose phase we will assume equal to zero.

$$s(t) = A(t)\cos 2\pi f_0 t.$$

If, in addition to the limitations introduced above, we add the condition that the target is motionless and that there is no Doppler shift of the frequencies, the received signal may be represented in the form

$$x(t) = X(t)\cos[2\pi f_0 t + \varphi(t)],$$

where $X(t)$ and $\varphi(t)$ are, respectively, the amplitude (envelope) and phase of the received signal, which are random time functions caused by noise. The frequency band occupied by the signal $\Delta f = 2F_m \ll f_0$, where $F_m$ is the largest frequency of the envelope spectrum and of the signal phase. Consequently, the signal amplitude and phase are time functions which change slowly by comparison with $2\pi f_0 t$.

The probability ratio

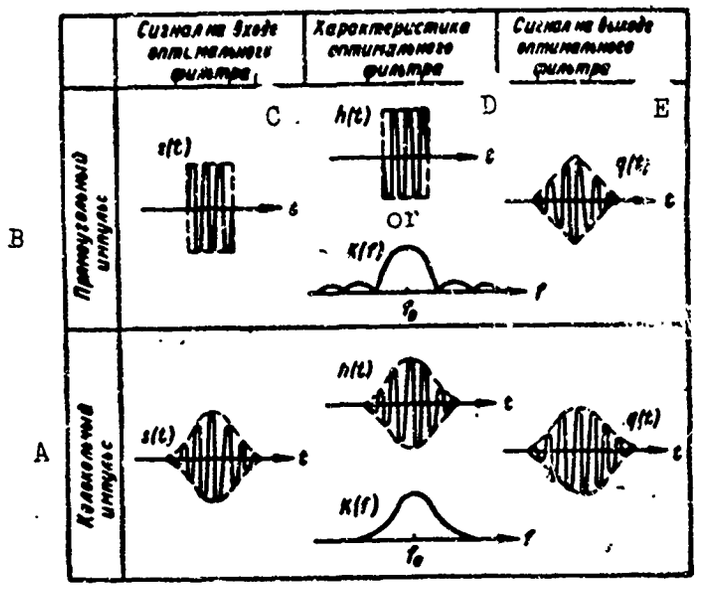


Fig. 6.15. Characteristics of the optimum filter and the signal shape at its output when its input consists of high-frequency rectangular and bell-shaped pulses. A) Bell-shaped pulse; B) rectangular pulse; C) signal at input of optimum filter; D) characteristic of optimum filter; E) signal at output of optimum filter.

$$\Lambda(x)=\exp\left[-\frac{E_s}{2_0}\right]\exp\left[\frac{2}{E_0}\int_0^T xsdt\right] \qquad (6.15)$$

for a high-frequency signal is also a high-frequency function, since the integral in the exponent of the second exponential curve, being a function of the mutual correlation of two functions of frequency $f_0$, is itself a function of the same frequency. The envelope of the probability ratio varies as slowly as the envelope of the signal itself.

Depending upon whether or not the high-frequency structure of function $\Lambda(x)$ is taken into account, the reception of radar signals may be divided, respectively, into coherent and noncoherent.

*Optimum filtering of a single pulse* is accomplished, as a rule, at intermediate frequency. The frequency converter exercises no influence on the processing itself, since, with respect to the intermediate-frequency signal, it is a linear element with a transmission factor of the order of unity.

Figure 6.15 depicts the shape of a signal at the input and output of an optimum filter for pulses of both shapes, and the time and frequency characteristics of the optimum filter are also given. It can be seen from the diagram that in the case of the most widespread bell-shaped pulse, the transmission function (frequency characteristic) of an optimum filter is also bell-shaped. This is precisely the frequency characteristic of the RLS intermediate frequency multistage amplifier with resonance circuits tuned to the signal frequency. Consequently, in the usual intermediate frequency amplifier with a matched passband there is practically optimum processing of each separate pulse.

Hence, there is no need to take into account the signal phase in optimum reception of a single pulse of the packet.* On the contrary, in the case of reception of several pulses the result of integration will depend upon whether or not we know the phase relations among them.

1. Coherent Reception

If the received signals are coherent (cophased) they may be integrated by adding their amplitudes, that is, in the most effective manner. Received signals will be coherent under the following two conditions:

a) if the phases of the reflected signals do not vary throughout the whole time of irradiation;

b) if the signals remain in phase in the receiver from one pulse to another, the first condition also being fulfilled.

The first condition is not satisfied in the case of signals of moving and fluctuating targets. Regular change in phase due to movement may in principle be offset if the target velocity is known. But coherent reception of the signals of a rapidly fluctuating target is completely impossible.

The signals in the receiver will be cophased if a coherent voltage

of identical phase with the emitted oscillations is fed into the mixer. In this case the signal phase at the mixer output does not depend upon the phase of the emission and remains constant from one pulse to another if the first condition is satisfied.

In an RLS whose transmitter follows the design: "master oscillator, pulse modulator, power amplifier," a coherent voltage is developed by the highly stable master oscillator. If the RLS transmitter includes a magnetron, coherent voltages developed by a special highly stable heterodyne which is brought into phase at the moment of emission from the magnetron. Similar circuits are examined in greater detail in Chapter 12.

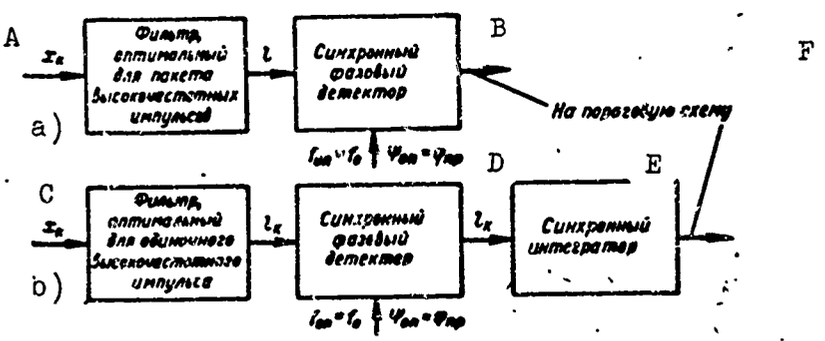


Fig. 6.16. Coherent receiver of signals with a known initial phase: a) With high-frequency processing; b) with video-frequency processing. A) Optimum filter for packet of high-frequency pulses; B) synchronous phase detector; C) optimum filter for single high-frequency pulse; D) synchronous phase detector; E) synchronous integrator; F) to the threshold circuit.

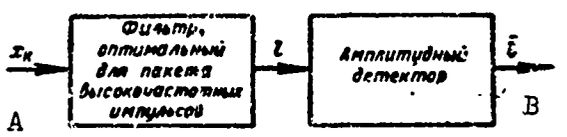


Fig. 6.17. Coherent receiver of signals of unknown phase with high-frequency processing (targets velocity unknown). A) Optimum filter for packet of high-frequency pulses; B) amplitude detector.

The result of coherent reception depends not only upon whether the signals are cophased but also upon whether or not the initial phase of

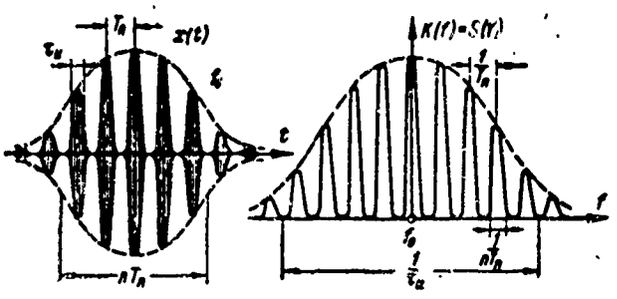

Fig. 6.18. Packet of high-frequency pulses and transmission function of comb filter.

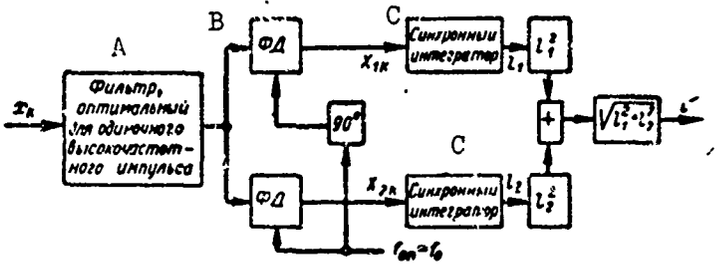


Fig. 6.19. Coherent receiver of signal of unknown phase with video-frequency processing (targets velocity unknown). A) Optimum filter for single high-frequency pulse; B) FD; C) synchronous integrator.

the signal is known.

*When the initial phase is known,* in the receiver may be placed a synchronous detector whose reference voltage coincides with the signal in frequency and in phase (Fig. 6.16). The out-of-phase noise component is eliminated, there is no suppression of weak signals by noise (the system is linear), and the receiver achieves a maximum sensitivity. The receiver itself may be assembled in two ways: a) with high-frequency processing of the pulse packet, and b) with breakdown of the processing into intraperiod (high-frequency filtering of the pulse) and interperiod (synchronous integration of the video pulses). Both designs are equivalent.

However, the initial phase is not known to the observer. The phase difference between the signal and the reference voltage is random and may lead to complete loss of the target signal if the latter is equal

to $\pi/2$. Therefore, maximum possible sensitivity may not be achieved in principle.

*When the initial phase of the signal is unknown,* both orthogonal noise components, possessing identical average power, are preserved, and this is equivalent to doubling the noise power with respect to reception of a signal whose initial phase is known. The signal/noise ratio at the output is reduced by one half.

Thus, real coherent receivers lose one half of their energy, that is, 3 decibels, by comparison with the theoretical limit.

The transition from optimum coherent reception of a signal of known initial phase to reception of a signal of unknown phase is very easily accomplished in a coherent receiver with high-frequency processing of the pulse packet: an amplitude detector is utilized instead of a phase detector (Fig. 6.17). What is detected here is the integrated signal whose signal/noise ratio must be large enough to ensure the assigned probabilities of $F$ and $D$. Therefore, there is no suppression of the signal by noise, and the sensitivity loss due to retention of the out-of-phase noise component is only 3 db by comparison with phase detection.

Unfortunately, such a coherent receiver design has not yet been utilized, since there is a high-frequency comb filter before the detector, and the characteristics of this filter must be matched with the spectrum of the pulse packet (Fig. 6.18). Such a filter is extremely complex to produce and operate.

In a coherent receiver with separate intraperiod and interperiod processing all difficulties are transferred from the high-frequency part of the circuit to the low-frequency part (Fig. 6.19). The high-frequency part of the receiver consists only of the filter of the intermediate-frequency amplifier whose production involves no particular difficulties.

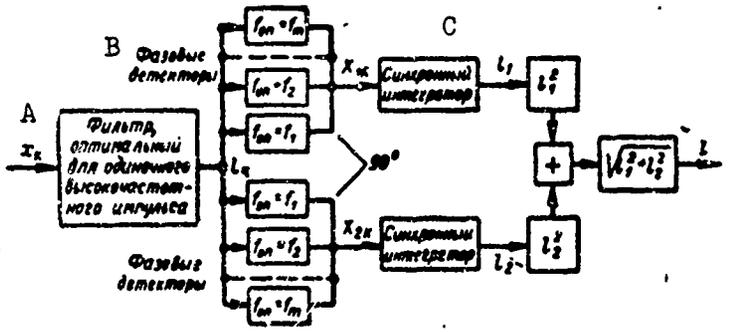


Fig. 6.20. Coherent receiver for signal of unknown phase with video-frequency processing (targets velocity unknown). A) Optimum filter for single high-frequency pulse; B) phase detectors; C) synchronous integrator.

In contrast to the receiver of the same design used for a signal of known initial phase, the output of the UPCh consists of not one but two phase detectors whose reference voltages are phase shifted by $\pi/2$. Because of this, ignorance of the initial phase does not lead to loss of the signal, since its phase may not shift simultaneously by $\pi/2$ toward the reference voltages of both phase detectors.

The high-frequency signal $X_k \cos(2\pi f_0 t - \varphi)$ is split up by the phase detectors into two quadrature components $X_{1k} = X_k \cos(\varphi - \psi)$ and $X_{2k} = X_k \sin(\varphi - \psi)$ where $\psi$ is the phase of the coherent reference voltage. Components $X_1$ and $X_2$ of all pulses of each target are summed individually by the two synchronous integrators. The summing is done with weights which are proportional to the envelope of the pulse packet, that is, optimally. Then the total components $l_1$ and $l_2$ are squared, put together, and passed through an amplifier with a nonlinear amplitude characteristic of the form $\sqrt{z}$.* As a result of this the output of the device yields the amplitude of the integrated signal

$$l = \sqrt{l_1^2 + l_2^2}.$$

Thus, this coherent receiver gives the same result as the receiver of the first shape (see Fig. 6.17). The only difference is that in the first instance the amplitude of the integrated signal was isolated di-

rectly by the amplitude detector, while in the second instance it is obtained by the method of quadrature components. In this case also, the energy loss due to ignorance of the initial phase is 3 db.

The essential difference between coherent receivers of the first and second types consists in the complexity of the apparatus. The requirements for manufacturing accuracy are much lower in the case of a synchronous video-signal integrator than in the case of a high-frequency integrator (comb filter), since in the latter case the accuracy with which the summed signals are accumulated does not exceed the phase of the high-frequency duty-factor.

A coherent receiver yields the desired result only if the frequencies of the reference voltage and the signal coincide, that is, if the target radial velocity is zero. In signals of moving targets the difference in frequencies will cause a phase lead from one pulse to another, and in integration of the pulses this may cause complete vanishing of the signal at the receiver output (when the velocity is known this lead may be offset).

The receiver device for signals of moving targets should consist of a number of the coherent receivers (channels) examined above, each of them tuned to its own frequency. Then, at the same time as the target is detected, its radial velocity is determined according to the number of the channel in which it is detected.*

In fact, the input circuit and the intermediate-frequency amplifier in the latter design may be generalized for all channels, since $|F_d| << \Delta f$ and a slight mistuning of the intermediate-frequency filter with respect to the signal of a moving target will not noticeably influence the effectiveness of the receiver.

In the case where the target radial velocity is of no interest to the observer, the design of a coherent receiver for target signals of

any radial velocity is even simpler (Fig. 6.20). Then only the set of phase detectors is multichannel; in it the number of pairs of phase detectors is equal to the number of channels. A reference voltage of determined frequency with a mutual phase shift of $\pi/2$ is fed to each pair of detectors.

A special coherent heterodyne unit, not indicated in the schematic, is used to create coherent reference voltages of various frequencies which are fed to the phase detectors.

In conclusion let us restate the fundamental characteristics of coherent reception.

In the first place, because the initial phase of the signal is not known, limiting sensitivity cannot be achieved, and the coherent receiver involves a 3 db energy loss with respect to this limiting sensitivity.

In the second place, a coherent receiver with video-frequency signal integration is much simpler than a receiver of equivalent efficiency using a high-frequency integrator. Even so, coherent receivers are rather complex devices and have therefore not yet been widely employed.

2. Noncoherent Reception

Hitherto the basic method of processing the high-frequency signal has been noncoherent reception which takes into account only the amplitude dependences and does not take into account the phase relations.

To determine how the probability ratio should appear when only amplitudes are taken into account, we may first represent $\Lambda(x)$ as a function of amplitudes and phases and then average the obtained result over all phases.

Utilizing the signal sampling theorem (see §6.2),

$$\frac{2}{c_0}\int_0^T xs\,dt=\frac{1}{\sigma^2}\sum_{i=1}^{2F_cT}x_is_i.$$

Viewing signals $s(t)$ and $x(t)$ as vectors $\vec{S}$ and $\vec{X}$ in $2F_mT$-dimensional space and basing ourselves on the scalar multiplication of vectors, we obtain

$$\vec{X}\vec{S}=\sum_i x_i s_i = XA\cos(\varphi-\omega_0\tau).$$

Here $x_i$ and $s_i$ are projections of vectors on the axis of a multidimensional coordinate system; $X$ and $A$ are vector moduli (amplitudes); $\varphi$ and $\omega_0\tau$ are their arguments (phases).

By successive substitution of the right sides of the two last equations in Formula (6.15) we obtain the probability ratio as a function of the amplitudes and phases

$$\Lambda(X,\varphi)=\exp\left[-\frac{E_s}{E_0}\right]\exp\left[\frac{XA}{\sigma_m^2}\cos(\varphi-\omega_0\tau)\right]. \qquad (6.27)$$

Ratio $E_s/E_0$ may also be expressed in terms of signal amplitude $A$ and noise dispersion $\sigma^2_{sh}$, dividing this ratio by $\Delta f\tau_u=1$. In the numerator we obtain the signal power (across a 1 ohm resistance) $\frac{E_s}{\tau_u}=\frac{A^2}{2}$, and in the denominator we obtain the noise dispersion $E_0\Delta f=\sigma_m^2$, whence, $\frac{E_s}{E_0}=\frac{A^2}{2\sigma_m^2}$.

To eliminate the phase it is necessary to average $\Lambda(X,\varphi)$ by integrating for all $\varphi$ over the integral from 0 to $2\pi$, i.e.,

$$\Lambda(X)=\frac{1}{2\pi}\int_0^{2\pi}\Lambda(X,\varphi)\,d\varphi.$$

As a result of integration we obtain the probability ratio for the case of noncoherent reception

$$\Lambda(X)=\exp\left[-\frac{A^2}{2\sigma_m^2}\right]\int_0^{2\pi}\frac{1}{2\pi}\exp\left[\frac{XA}{\sigma_m^2}\cos(\varphi-\omega_0\tau)\right]d\varphi= \\ =\exp\left[-\frac{A^2}{2\sigma_m^2}\right]I_0\left(\frac{XA}{\sigma_m^2}\right). \qquad (6.28)$$

A similar integral was already obtained in Chapter 3, Formula (3.32).

The logarithm of the probability ratio

$$l(X)=\ln I_0\left(\frac{XA}{\sigma_m^2}\right)-\frac{A^2}{2\sigma_m^2}.$$

If a packet of $n$ pulsing is received from the target, we then obtain, in accordance with Formula (6.18)

$$l(X)=\sum_{k=1}^{n}\ln I_0\left(\frac{X_kA_k}{\sigma_m^2}\right)+\frac{1}{2\sigma_m^2}\sum_{k=1}^{n}A_k^2. \qquad (6.29)$$

Thus, in noncoherent reception of radar signals, optimum processing of the pulse packet is reduced to the following operations:

a) optimum filtering of each pulse in the packet;

b) averaging the phase of the obtained signal and isolation of the envelope;

c) synchronous integration of the video-signals;

d) testing the total signal at the threshold.

The first operation is usually performed by an i-f filter, isolation of the envelope by an amplitude detector, and integration by a synchronous video-signal integrator. The parameters of all of these elements are examined below. The threshold device is characterized only by a limiting level.

The optimum filter for a single high-frequency pulse has the same shape as in the coherent receivers. In actual filters the band is usually selected somewhat wider than optimum, since the high-frequency generators in noncoherent RLS (magnetrons) possess low frequency stability, and the self-tuning frequency circuits do not completely eliminate mistuning. A certain widening of the passband beyond its optimum width does not lead to any noticeable energy loss.

The next operation is averaging the high-frequency correlation function obtained at the output of the UPCh for all phase values, that is, isolation of the envelope of the shape $\ln I_0\left(\frac{XA}{\sigma_m^2}\right)$. It is known that

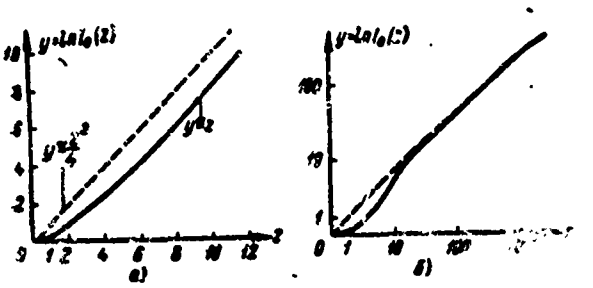

Fig. 6.21. Voltage at the output of a "linear" amplitude detector as a function of the relative signal intensity: a) Uniform scale; b) diminishing scale.

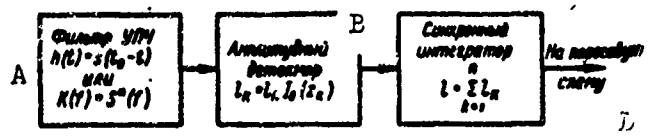

Fig. 6.22. Structure of optimum noncoherent receiver of radar signals. A) I-f filter; B) amplitude detector; C) synchronous integrator; D) to the threshold circuit.

$$\ln I_0(z) \approx \begin{cases} \frac{z^2}{4}, & z < 1, \\ z, & z \gg 1. \end{cases} \qquad (6.30)$$

The first instance corresponds to a weak signal ($z < 1$ is equivalent to $XA < \sigma_{sh}^2$); the second case represents a signal which is considerably stronger than the noise ($XA \gg \sigma_{sh}^2$). Consequently, the characteristic of the optimum device used to isolate the envelope must be quadratic for signals which are weak in comparison with the noise and linear for relatively strong signals (Fig. 6.21). The detector characteristic set forth on both axes in the diminishing scale particularly sharply emphasizes the dependence (6.30).

These are precisely the properties possessed by a "linear" amplitude detector whose static characteristic is linear for both weak and strong signals.

The structure of a synchronous integrator for relatively weak signals is determined by Formula (6.29) and by an asymptotic representation of function $\ln I_0(z)$ at $z < 1$ in accordance with Expression (6.30)

$$l(X) \approx \sum_{k=1}^{n} \frac{X_k^2 A_k^2}{4\sigma_{\text{ш}}^4} - \sum_{k=1}^{n} \frac{A_k^2}{2\sigma_{\text{ш}}^2} = \sum_{k=1}^{n} \frac{A_k^2}{2\sigma_{\text{ш}}^2}\left(\frac{X_k^2}{2\sigma_{\text{ш}}^2} - 1\right). \qquad (6.31)$$

The detector is quadratic with respect to a weak threshold signal, its output voltage in relative units being equal to

$$y_k = \frac{X_k^2}{2\sigma_{\text{ш}}^2}.$$

We also introduce a denotation for weighting factors

$$B_k = \frac{A_k^2}{2\sigma_{\text{ш}}^2}.$$

After substitution of quantities $y_k$ and $B_k$ in Formula (6.31), the structure of the synchronous integrator assumes the form

$$l(y) = \sum_{k=1}^{n} B_k y_k. \qquad (6.32)$$

The term $-1$ has been discarded by us since it may be taken into account in selecting the threshold quantity.

Consequently, each of the signal-plus-noise pulses $y_k$ should be summed with weight $B_k$ proportional to the square of the amplitude of the signal proper $A_k^2$ in the UPCh channel or to the square of the antenna directivity pattern with respect to power $F_p^2(\alpha)$.

In the case of strong signals ($XA \gg \sigma_{\text{ш}}^2$), in accordance with Formula (6.30) the structure of the optimum integrator should be different: the weighting factors are proportional to signal amplitude $A_k$ and to the antenna directivity pattern with respect to power $F_p(\alpha)$. In the intermediate case ($XA \approx \sigma_{\text{ш}}^2$) the weighting factors are proportional to $A_k^{\nu}$, where $2 \geq \nu \geq 1$. Consequently, the structure of the optimum synchronous integrator depends upon the signal intensity. However, it is sufficient in practice to make it optimum only for weak signals, as a stronger signal is in any case in considerably better condition than a weak signal.

Thus, a device consisting of a high- (intermediate-) frequency amp-

lifier with a matched band, of a "linear" detector, and of an optimum synchronous integrator is fully capable of performing all operations which may be required in noncoherent processing of the signal (Fig. 6.22).

This may all be accomplished rather simply in ordinary radar receiver devices if we disregard the difficulties associated with the design of optimum synchronous integrators.

Noncoherent reception may be distinguished from the reception of video signals in gaussian noises or from optimum coherent reception of radio signals in that it includes a supplementary essential operation — detection using an amplitude detector, which involves a loss of information.

As a result of isolating the envelope on a nonlinear element (detector), there is a change in the structure of the noise itself: instead of being gaussian it assumes a Rayleigh distribution. In accordance with Formula (6.30) there is also a deterioration of $a = A/\sigma_{sh}$ times ($a^2$ at the detector output instead of $a$ at the input at $a < 1$) in the signal/noise ratio for relatively weak signals due to the quadratic dependence, and a 50% deterioration due to the presence of an out-of-phase noise component. The overall reduction in the signal/noise ratio in decibels is $-20 \lg a + 3$. The energy losses are greater the weaker is the signal by comparison with the noise. That is why, in reception of very weak signals, an effort is made to accumulate them coherently before detection.

With increase in the signal intensity, losses in noncoherent receivers are reduced asymptotically to 3 db. Therefore, if the signals are sufficiently powerful, the coherent receiver has practically no advantages over the noncoherent receiver.

3. <u>The Signal Shape Required for Detection</u>

On the basis of this comparison of the two methods of receiving ra-

dar signals and of the obtained relations it is possible to pass to an evaluation of the influence of signal shape upon detection efficiency.

The properties of the optimum receiver are described by its operating characteristics (RKhP) which establish the interrelation of three parameters: $F$, $D$ and $E_s/E_0$. Thus, the assigned conditions of observability during optimum reception are determined by the probability of detection $D$ and the probability of false alarm $F$ and are satisfied by a particular ratio $E_s/E_0$ regardless of the signal shape.

From this we may draw the important conclusion: radar detection efficiency is completely determined by the ratio between the total energy of the signal and the spectral power of the noise $E_s/E_0$ and hardly depends upon the signal shape (pulse, continuous), *as long as optimum processing is actually used.**

Consequently, the first task confronting the engineer designing a radar station – that of ensuring the necessary operating range – has almost nothing to do with the shape of the outcoming signal.

However, one must not lose sight of the fact that everything which has been said above is true under one essential condition, that the optimum reception method is actually employed. This condition is often not satisfied: the overwhelming majority of radar stations employ noncoherent reception which is not optimum for a high-frequency signal. This leads to energy loss with some signal shapes.

In particular, if multipulse pulsing is employed, noncoherent processing of relatively weak signals involves a loss of $\sqrt{n}$, where $n$ is the number of pulses in the packet.

Actually, let $n$ pulses enter the receiver input, each of them bearing energy $E_{s1}$. The total energy of the received signal $E_s = E_{s1}n$ and the signal/noise energy ratio is $nE_{s1}/E_0$. The result of noncoherent processing of the weak pulse signals is a signal/noise ratio equal to

$\sqrt{n}E_{s1}/E_0$, which is the same as reducing the total energy of the signal by $\sqrt{n}$ times. Losses are also possible in a synchronous integrator if the summing of pulses is not ideal.

Thus, the dispersion of energy among several pulses when processing is less than optimum leads to energy loss. From this point of view it is more advantageous to reduce the number of pulses in the packet down to a single pulse, maintaining the total energy of the signal unchanged. From the point of view of the threshold relation, the only demand on the signal shape is that energy should not be dispersed during noncoherent reception. However, during scanning the target must be irradiated by not one but several pulses. This is dictated by the requirement that scanning be continuous, by the need for accuracy in measuring angular coordinates, and by the need to limit the peak power of emission.

## §6.6. INTEGRATING PROPERTIES OF RLS TERMINAL DEVICES

### 1. Storage Integrators

The operation of synchronous storage, or integration, is performed on radar station indicator screens of the range-sweep type. For example, on "azimuth-range" indicators, the range-sweep lines are traced from below upwards and with each pulsing period are displaced to the right by an amount corresponding to the antenna rotation angle during the pulsing period. Because the arrival of target pulses causes the indicator screen to light up synchronously with range sweep, light spots are produced on adjacent lines at identical distances from the origin of the range sweep. When the lines of the sweep are right next to one another, the light spots are formed in practically the same place, and therefore their brightnesses are summed.

Thus synchronous integration takes the form of accumulation of the excitation energy of the luminophor of the screen and not of the elec-

tric l signals themselves. The operator regards the brighter summed blips as indicating the presence of a target, and in this way he in fact fulfills the function of a threshold device.

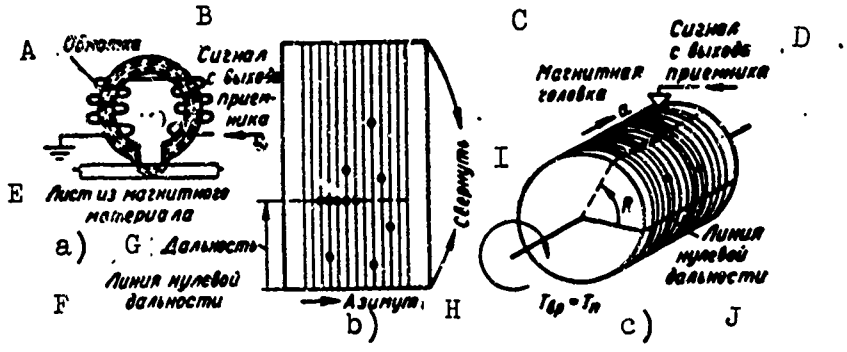


Fig. 6.23. Recording radar signals on a magnetic drum: a) Magnetic head; b) sheet of magnetic material with recorded signal; c) the same sheet wrapped around the drum, rotating at the pulsing frequency. A) Windings; B) signal from receiver output; C) magnetic head; D) signal from receiver output; E) sheet of magnetic material; F) line of zero range; G) range; H) azimuth; I) to be wound around the drum; J) line of zero range.

In indicators which do not possess range sweep, for example, in the "azimuth-elevation" directional type of indicator, there is nonsynchronous storage which, as has already been pointed out, is not an optimum operation for the reception of pulses signals. Since in such indicators it is impossible to isolate that part of the range in which the target is located, the signal should be strong enough to withstand the noise of the whole range spectrum. In indicators with range sweep, the signal must withstand the noise energy of only a small part of the range sweep, that corresponding to the length of a pulse. Therefore the discrimination factor in RLS with directional indicators is a whole order of magnitude greater than in RLS whose indicators employ range sweep.

The operation of synchronous storage may be accomplished not only in indicators but also in other memory devices: charge-storage tubes, magnetic drums (static memory) and supersonic delay lines (dynamic memory).

In charge-storage tubes the storage function is performed by a tar-

get. The target is a dielectric plate which may be viewed as an assembly of a very large number of elementary storage cells (condensers). On the target range and angular sweep are analogous to sweep on the indicator screen. When the scanning beam passes a number of times through a given point on the target, the charge of the small "condensers" at this point gradually accumulates. Where there is nothing but noise the accumulation of a charge is slow, since random noise blips appear at various points on the target. The accumulation of a signal is more rapid: when scanning is intense, signal pulses appear at practically one and the same spot on the target. The integrated signal is read from the charge-storage tube target by a special readout beam. The target pulse may be isolated from this signal by using a threshold circuit.

A synchronous integrator with a magnetic drum works in an analogous manner (Fig. 6.23). The signals are recorded by a magnetic head (Fig. 6.23a), consisting of a magnetic circuit (yoke) with a winding. The yoke has an air gap which creates a high resistance to the magnetic flux. Therefore, if a plate made of some magnetic material is placed near the open ends of the yoke, the magnetic flux caused by the signal current flowing through the winding bridges through the plate and magnetizes it. The stronger the signal the greater the magnetization of that part of the plate which is near the gap in the yoke.

The signal on the plate made of magnetically soft material may not only be recorded but also integrated: multiple recording increases the magnetization. In principle, the signal may be registered in accordance with its range and azimuth in precisely the same way as on an indicator screen or a charge-storage tube target (Fig. 6.23b).

An important distinction between the magnetic system and the indicator or the charge-storage tube is that the magnetic head cannot be displaced relative to the plate as rapidly as an inertialess electronic

beam. Therefore the plate is wound around a drum in such a way that the range lines turn with the drum, and the drum is then rotated at the pulsing frequency (Fig. 6.23c). The rotation angle of the drum, relative to some starting position, is proportional to target $R$, while the range lines themselves, because of the slow displacement of the head, are moved along the drum in accordance with the antenna rotation angle through azimuth $\alpha$. The pulses of each target, falling within different pulsing periods, are located on a single element of the cylinder.

The integrated signal is read by one or several readout heads and is passed to the threshold circuits. The design of the readout magnetic head is analogous to that of the recording head, but it works in the opposite way: the magnetized part of the drum, passing under the gap in the yoke, induces a current in the winding.

There are additional heads for erasing the recording. As a result the whole device is rather cumbersome. Furthermore, it requires large rotation velocities. For example, at a comparatively low pulsing frequency of 500 hz the drum should rotate at a velocity of 30,000 revolutions/minute. This imposes very severe requirements on the bearings, on alignment, and on rigidity of construction, since the gap between the surface of the drum and the magnetic head is very small.

Instead of a magnetic drum it is possible to use devices which register on magnetic tape (video tape recorders).

It is not difficult to note that the integrating processes in the indicator, the charge-storage tube, and the magnetic device are similar in many respects; but in the first the excitation energy of the luminophor of the screen is integrated, in the second – the electrical energy, and in the third – the magnetic energy. And they are all subject also to general limitations both of a theoretical and of a technical character.

Theoretical limitation consists in the fact that all target pulses located on adjacent sweep lines are summed on an identical basis -- balanced integration. At the same time it follows from Formula (6.26) that they should be summed with weights proportional to the intensity of the signal proper s. It is known that the pulse amplitudes of the signal proper in the packet are not identical and that, therefore, the synchronous storage methods examined are optimum only in the case of a rectangular pulse packet which does not exist in reality. However, this loss is insignificant, especially in indicators where it is reduced through participation by the operator who, without meaning it, attributes different weights to the pulses of the packet, concentrating on the middle of the target blip and hardly paying any attention to its edges.

The technical limitation consists in the fact that all of the devices examined above are more or less subject to saturation. Only a comparatively small number of pulses are effectively integrated. As the number of pulses increases, the contribution of each new pulse to the summed signal declines.

2. Integrating Filters

Integrators with a charge-storage tube and a magnetic drum may be made ideal, devoid of the drawbacks described above. For this a general technical procedure is utilized: breakdown of the problem solved by the

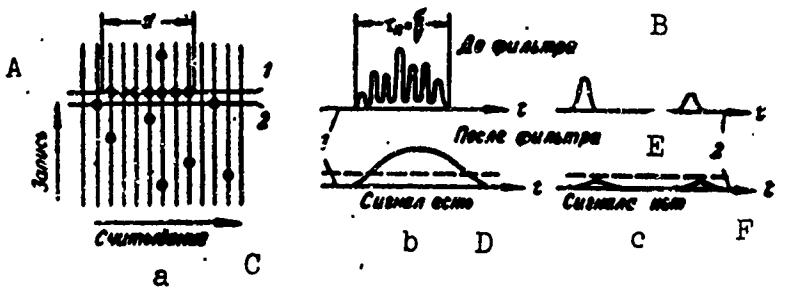


Fig. 6.24. Ideal integrator with a pulse-storage tube: a) Scanning and signals on the target; b) integration of the signal; c) integration of noise. A) Recording; B) before the filter; C) readout; D) there is a signal; E) after the filter; F) there is no signal.

integrator into the function of remembering the signal for $n$ period and the function of summing, these being accomplished by different elements. In ideal integrators the charge-storage tube, the delay line, or the magnetic drum only perform the memory function. Integration proper is done by a supplementary circuit, for example, the filter. The device as a whole has a comb-shaped frequency characteristic. Therefore it is often called a comb filter. However, this term has already been used by us for several devices, and we will introduce the concept of the integrating filter.

Let us examine the integrating filter with charge-storage tube (Fig. 6.24) developed by Yu.A. Mel'nik and Ye.G. Trubitsyn (see [13] in Chapter 6).

The signal is recorded on the charge-storage tube target by range lines separated by some distance so as to eliminate the integration effect, while readout is accomplished across the lines in sequence, starting from the zero range (Fig. 6.24a).

If line 1, upon which a series of target pulses of length $d$ had been recorded, is being read out, if the readout velocity is $v$, we obtain a packet of pulse which are very close to one another and whose overall length is $\tau_p = d/v$. The envelope of this packet (excluding noise) has the shape of the antenna directivity pattern and may be viewed as a pulse of length $\tau_p$. The readout signal is passed through a narrow-band filter which is optimum for the pulse packet envelope, and as a result the gaps between the individual pulses are smoothed over, and a wide target pulse is formed at the output (Fig. 6.24b).

Noise blips (line 2) which are isolated and short in length, are smoothed out when passed through the narrow-band filter (Fig. 6.24c). As a result of this the target signal, as before, may be separated from the noise by using a threshold circuit.

If the passband is narrowed, the filter may be made optimum for a practically unlimited number of pulses. If the form of the filter transmission function is selected so as to be optimum for the packet envelope, the signals are integrated with weights corresponding to their intensities. Thus both of the drawbacks inherent in the circuits examined earlier are eliminated.

Synchronous integration of the pulses passing through the optimum filter may also be accomplished in a memory device of the dynamic type - supersonic delay lines and a magnetic drum comprising a dynamic memory.

Figure 6.25 shows a device consisting of $n - 1$ identical delay lines ($\tau_z = T_p$), which perform the function of remembering the signal during $n$ pulsing periods. From the outputs (inputs) of the delay line the signals enter $n$ taps where they are multiplied by weighting factors $B_k = f(S_k)$ in amplifier stages and are then summed over a common load resistance. This device has already been examined by us above as the general type of synchronous integrator (see Fig. 6.13).

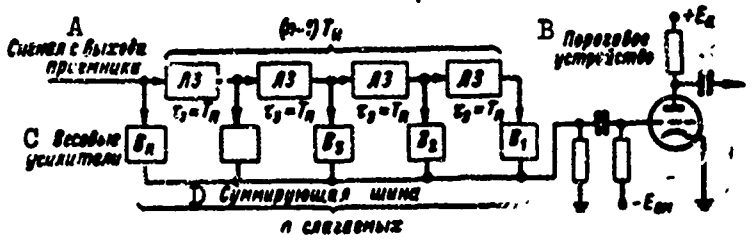


Fig. 6.25. Optimum integrating filter using delay lines. A) Signal from receiver output; B) threshold device; C) weighted amplifiers; D) summing bus of $n$ items.

At the output there is a threshold device in the form of a tube which is cut off by negative bias in the grid circuit. The detection threshold, i.e., the filter output voltage at which the tube is turned on, is established by adjusting the bias voltage.

Figure 6.26 represents an integrating filter with a magnetic drum.

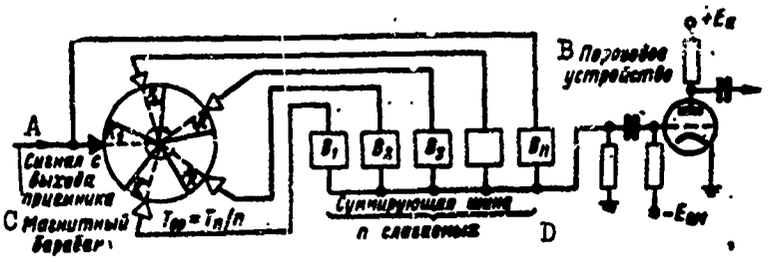

Fig. 6.26. Optimum integrating filter with a magnetic drum. A) Signal from receiver output; B) threshold device; C) magnetic drum; D) summing bus of $n$ items.

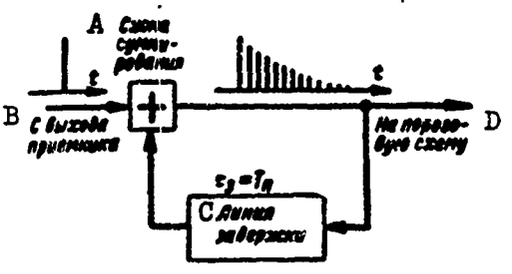

Fig. 6.27. Nonoptimum integrating filter with delay line. A) Summing circuit; B) from receiver output; C) delay line; D) to threshold circuit.

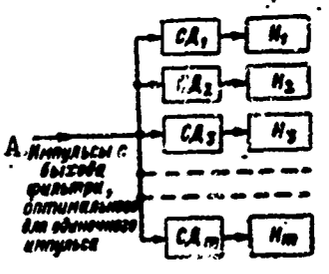

Fig. 6.28. Range selector of the parallel type. A) Pulses from output of a filter which is optimum for a single pulse.

In contrast to the device given in Fig. 6.24, here there is not one, but $n$, range scans around the drum. The drum itself rotates $n$ times more slowly. There is one recording head and $n - 1$ readout heads. All the heads are located at equal intervals from one another. Thus, regardless of the rotation angle of the drum, signals corresponding to the same range in $n$ pulsing periods are recorded and read out at the same time.

It is not difficult to see that the network in Fig. 6.25 and 6.26

are completely analogous in their working principle. In one case, however, dynamic memory is utilized with delay lines, and in the other, statistical memory with a magnetic drum which assumes the properties of a dynamic memory through the rotation of the drum relative to the recording heads synchronously with the arrival of signals.

Devices which assure optimum integration of dozens or hundreds of pulses in a packet become excessively complex. Nonoptimum integrating filters are much simpler.

Figure 6.27 shows a synchronous integrator with a single delay line ($\tau_z = T_p$). Integration is based on the use of a delayed positive feedback through a delay line and a summing device (+).

The reaction of the filter to the unitary pulse represents a passage of pulses with exponential attenuating amplitudes. Therefore, such a filter is not optimum for actual pulse packets. However, the actual loss is rather small if the time constant of the amplitude attenuation in the delay line is approximately equal to the length of a packet of integrated pulses.

A comparison of the various types of circuits for synchronous accumulation reveals one important characteristic: in all of them target signals are selected according to range.

In the statistical type of memory devices (indicators, charge-storage tubes) selection is accomplished in the following way: because of the repeating range sweep the target pulses fall in practically the same part of the screen or the target, one corresponding to the target range. This kind of synchronous integrating device may, therefore, be viewed as a multiple unit selection circuit for each of the elementary range zones (SD), terminating in storage elements (N) (Fig. 6.28). The target signal is distributed by an electronic beam among the various parallel range channels.

In memory devices of the dynamic type (in delay lines) range selection is accomplished directly on the basis of the delay time of the echo signal relative to cadence points (moments of emission). Thanks to this, no commutating device is required, and the signals of various pulsing periods are stored on an output load which is common for all of the range zones. Depending upon the circuit utilized magnetic drums may play the role of both static and of dynamic devices.

3. Integration of Signals of a Selected Target

The devices examined above select targets corresponding to all elementary range zones. However, there are terminal devices containing only one range selector and only one storage device (Fig. 6.29). In order to scan in all ranges the selector must be slowly retuned with respect to range.



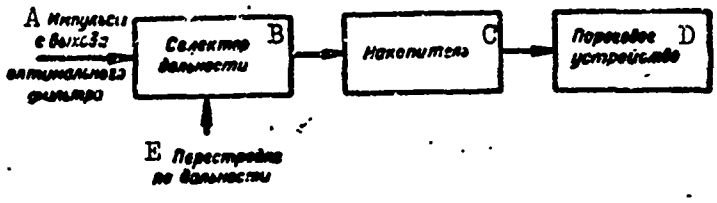


Fig. 6.29. Range selector of the sequential type. A) Pulses from the output of an optimum filter; B) range selector; C) storage device; D) threshold device; E) range returning.

Such selectors are utilized in target autotrack systems. The range selector is an amplifier which is usually shut off, but which is turned on by a special selector pulse for a time equal to approximately the length of a target pulse. The timing $\tau$ of the selector pulse relative to the moment of emission is determined by a special delay stage (for example, a phantastron) which is triggered by the synchronization pulse. Change in the voltage on the anode of the phantastron cause the selector to be retuned to a different range. If the selector is tuned to the target range, pulses will pass through it to the storage device (con-

denser). At the output of the storage device there is a threshold device which operates a locking relay which in turn signals the detection of the target.

The slow retuning of the range selector follows a definite law. When the timing of the selector pulse corresponds to the delay time, several pulses are received from the target and are integrated in the storage device, when the locking relay has been operated, the retuning of the range selector is usually shut off, and the system returns to the tracking mode. In order to search for a target at all possible ranges a considerable amount of time and energy are required, and this is a substantial drawback of this device by comparison with multiple unit devices.

To accelerate detection (locking) of the target nonsearch systems are also utilized in which there is no range selector, and the signals enter the storage device together with the noises from all range zones. Such systems are not optimum: there is an energy loss (nonsynchronous storage) since the influence of the noise is considerable, and the operating threshold of the locking relay must be rather high. The merits of such systems is that the circuitry is extremely simple, and locking is rapid, since there is no range search and no range selection.

4. Discrete Integrators

Up to now we have been examining terminal devices in which electrical signals in one form or another were integrated. All of these devices


Fig. 6.30. Multichannel discrete integrating system. A) Pulses from the output of an optimum filter; B) range selector; C) amplitude analyzer; D) standard pulse counters; E) resolver.

may be assigned to one class of analog storage devices. In contrast to the analog devices there also exist discrete integrators which utilize numbers representing the signal.

As is known, the distribution of pulse amplitudes at the output of an optimum filter for $n$ pulsing periods is different from the distribution of the amplitudes of the noise blips. Therefore, if the pulse amplitudes are measured, it is possible to establish, with a greater or lesser degree of error, whether the given combination of pulses is a target signal or pure noise.

In order to depict the pulse amplitude distribution function in a numerical form the whole range of possible signal amplitudes is broken down into a series of levels. The number of the highest level which is succeeded by the given pulse is a numerical measure of the amplitude of this pulse. The operation of breaking down signal amplitude into a series of levels is called *quantization*, and the device which performs this operation is called an amplitude analyzer.

The output of the amplitude analyzer is multichannel. Arrival of the signal causes the analyzer to send a standard pulse (unit) to the output bus whose number corresponds to the signal amplitude, the number of standard pulses in each channel is determined by using pulse counters. By estimating how many pulses out of $n$ have arrived in each channel it is possible to obtain the amplitude distribution function in a discrete form.

The number of channels $\nu$ is equal to the number of reading levels (including the zero level). However, since the total number ($n$) of pulses analyzed is known, there is no need to place a counter in one channel, since the number of pulses in this latter channel represents the difference between $n$ and all the other pulses counted. Therefore, $\nu - 1$ counting channels are utilized. The whole device together with the ampli-

tude analyzer is known as a *multichannel counting system*, and it performs numerical integration using the method of counting pulses.

Figure 6.30 gives a block-diagram of a discrete terminal device together with a resolving (threshold) device.

Signals from the output of the optimum filter enter the range selector which can be either single-channel or multi-channel. The signals of the corresponding range pass through the selector to the analyzer, and from the output busses of the latter they pass to the pulse counters. In the resolving device the obtained combination of counted numbers is compared with a known combination for pure noise, and the result is a decision as to the presence or absence of a target.

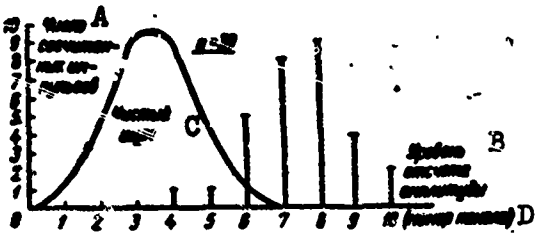


Fig. 6.31. Comparing the results of counting in the channels with the distribution for pure noise. A) Number of counted pulses; B) level of amplitude reading; C) pure noise; D) channel number.

Figure 6.31 gives the result of the processing of a packet of $n$ = = 30 pulses, the number of counting channels being $\nu - 1 = 10$. The levels of amplitude quantization are laid off on the axis of the abscissa, and on the axis of the ordinate are given the number of counted standard pulses in each channel, in the form of sections of vertical straight lines. The continuous line shows what shape the envelope of the counted numbers should have for pure noise.

From the situation given in Fig. 6.31 it is possible to conclude with a considerable degree of confidence that a signal has been received

and not noise. This last logical operation is just the one performed by the resolver which is guided by one of the optimum criteria.

Terminal devices utilizing multichannel counting systems are very complex. Thus, in scanning RLS employing multiple element range selection there should be a counting system at the output of each range selector element.

As a result of this, in practice devices are used in which the signal amplitude is subdivided into only two values: lower and higher than the limiting level ($\nu = 2$), and only one counting channel is used, one which takes into account the number of times the assigned level has been exceeded. When this level is exceeded, a standard pulse ("unit") is emitted, and if this level is not exceeded, no pulse is emitted ("zero"). The whole signal is a sequence of two figures: zeroes and units. Therefore, this sort of terminal device is known as a binary integrating device for a single-channel counting system.

The quantization of signals always involves a loss of information, and therefore even the best discrete processing of received signals is in principle inferior to the optimum methods of processing nonquantified signals. Information losses in quantization are lower as $\nu$ is larger. A nonquantified signal may be viewed as quantified at $\nu \to \infty$.

It should, however, be noted that the losses from quantization are very insignificant. Even in the case of the crudest binary quantization, the sensitivity loss does not exceed 2 decibels.

The circuit for single-channel processing of a signal (binary integrator) may be made much more simply than a multichannel circuit: it is only necessary to install after the range selector a single counter of the number of times the level is exceeded. The regulated level of operation of the counter acts as an amplitude analyzer. The counter itself may also act as a resolver, emitting a detection signal when the

number of times the level has been exceeded during $n$ pulsing periods is equal to a certain number $Y < n$.

There are also binary processing devices of a somewhat different type. Methods of designing devices for binary processing of quantified signals will be described in the following section.

Binary integration can be used as an example to demonstrate the similarity between counting systems and ordinary integrators. Let us assume that a packet of $n$ pulses of constant amplitude $A$ is being integrated in the absence of noise. Then the pulse counter emits a number $n$, while an ordinary integrator emits voltage $A_n = nA$: the integration effect of the ordinary integrator $A_n/A = n$ is equal to the reading on the counter.

## §6.7. EFFECIENCY OF AUTOMATED DETECTION DEVICES

### 1. Efficiency of Analog Integrators

In automated detection systems the threshold signal, characterized by discrimination factor $m_p = \frac{x^2_{min}}{2}$, may be calculated precisely. Here the number of pulses $n$ in the packet is assumed to be known, while probabilities $D$ and $F$ are assigned. We calculate the threshold signal for both coherent and noncoherent optimum devices.

*Coherent integration.* A coherent receiver is a linear system up to the detector; therefore the distribution of the signal and noise at the output of the amplitude detector follows the Rayleigh law. In calculation, the relative amplitude of the signal at the integrator output $a\sqrt{n}$ is considered large enough to ensure the assigned probabilities $D$ and $F$. Therefore the generalized Rayleigh distribution for the signal may be replaced by the normal law with the average value $a\sqrt{n}$.

Under these conditions the probability of correct detection

$$D=\frac{1}{\sqrt{2\pi}}\int_{v_0}^{\infty}e^{-\frac{(v-a\sqrt{n})^2}{2}}dv=\frac{1}{\sqrt{2\pi}}\int_{v_0-a\sqrt{n}}^{\infty}e^{-\frac{t^2}{2}}dt=$$
$$=\Phi(a\sqrt{n}-v_0), \qquad (6.33)$$

where $\Phi(z)=\frac{1}{\sqrt{2\pi}}\int_{-\infty}^{z}e^{-\frac{t^2}{2}}dt$ is the probability integral.*

The probability of false alarm with a Rayleigh distribution of noise

$$F=e^{-\frac{v_0^2}{2}},$$

therefore the threshold

$$v_0=\sqrt{2\ln\frac{1}{F}}.$$

The operating characteristic of a coherent receiver is found by substituting the derived threshold value $v_0$ into Formula (6.33):

$$D=\Phi\left(a\sqrt{n}-\sqrt{2\ln\frac{1}{F}}\right). \qquad (6.34)$$

From this one may determine the size of threshold signal $a$ by introducing function $z=\Phi^{-1}(Y)$, which is the reciprocal of probability integral $Y=\Phi(z)$ .** Values $\Phi^{-1}(Y)$ may be found by utilizing the tables or graphs of function $Y=\Phi(z)$; but they should be read backward: argument $z$ is found from the value of function $Y$.

When this is taken into account, from the latter formula we find

$$a\sqrt{n}-\sqrt{2\ln\frac{1}{F}}=\Phi^{-1}(D),$$

whence

$$a_{\text{мин}}=\frac{1}{\sqrt{n}}\left[\Phi^{-1}(D)+\sqrt{2\ln\frac{1}{F}}\right]$$

and

$$m_p=\frac{a^2_{\text{мин}}}{2}=\frac{1}{2n}\left[\Phi^{-1}(D)+\sqrt{2\ln\frac{1}{F}}\right]^2. \qquad (6.35)$$

And this is the relative value of the power of the threshold signal in coherent reception.

*Noncoherent integration.* In noncoherent integration of a large number $n$ of pulses, both signal and noise are normalized, inasmuch as the noise at the output of the amplitude detector also has a constant component $\left(\bar{y}=\frac{\overline{v^2}}{2}=1\right)$

Then the probability of false alarm

$$F=\frac{1}{\sqrt{2\pi}}\int_{y_0}^{\infty}e^{-\frac{(y-1)^2}{2}}dy=\frac{1}{\sqrt{2\pi}}\int_{y_0-1}^{\infty}e^{-\frac{t^2}{2}}dt=\Phi(1-y_0),$$

whence the detection threshold

$$y_0=\Phi^{-1}(1-F).$$

The constant component of the relative signal voltage at the integrator output is $\frac{a^2}{2}\sqrt{n}$.

Inasmuch as the law of signal distribution is normal, as in the case of coherent integration, by substituting the derived threshold values and the values of the constant components into Formula (6.33) we obtain the operating characteristics of a noncoherent receiver

$$D=\Phi\left[\frac{a^2}{2}\sqrt{n}-\Phi^{-1}(1-F)\right]. \qquad (6.36)$$

We recall that it is true for the case of a large number of pulses and a low signal/noise ratio within the pulse.

The value of the minimum detectable signal is easily found from the last formula

$$m_p=\frac{a^2_{min}}{2}=\frac{1}{\sqrt{n}}[\Phi^{-1}(D)+\Phi^{-1}(1-F)]. \qquad (6.37)$$

Example. Calculate the discrimination factor for coherent and noncoherent integration, when the following are assigned:

$$n=100;\ F=10^{-6},\ D=0{,}9.$$

1) Coherent integration.

From the table we find $\Phi^{-1}(0{,}9)=1{,}3$,

$$\sqrt{2\ln 10^6}=\sqrt{4{,}61\lg 10^6}=5{,}26.$$

Substituting the derived quantities into Formula (6.35) we obtain

$$m_p = \frac{(1,3+5,25)^2}{200} = 0,22.$$

2) Noncoherent integration.

From the table we find $\Phi^{-1}(0,9) = 1,3$; $\Phi^{-1}(1-10^{-4}) = 4,7$.

Substituting the derived values into Formula (6.37), we obtain

$$m_p = \frac{1,3+4,7}{\sqrt{100}} = 0,6.$$

2. Efficiency of Discrete Integrator

Specific detection devices are discrete integrators. The radical difference between these and analog integrators is the following. In principle, analog integrators make it possible to achieve the maximum achievable results, but there are losses due to the technical inadequacy of certain components. Discrete integrators involve losses in principle, and, therefore, their manufacture involves no further reduction of efficiency.

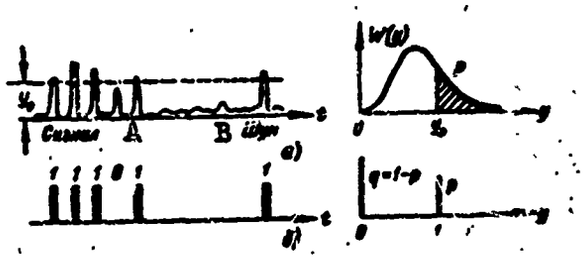

Fig. 6.32. Binary quantization of signals: a) Signal at receiver output and its distribution; b) standard pulses after quantization and the probability of their appearance or failure to appear. A) Signal; B) noise.

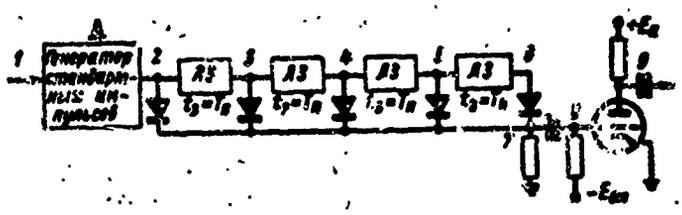

Fig. 6.33. Binary integrator with delay lines ($n = 5$). A) Generator of standard pulses.

Below we give a description of the design principles and an estimate of the efficiency of the simplest integrators of binary-quantified signals.

*Binary integration.* In noncoherent reception of weak signals the synchronous integrator yields the logarithm of the probability ratio for the pulse packet

$$l(y) \approx \sum_{k=1}^{n} B_k y_k, \quad a < 1, \tag{6.38}$$

which is then tested at threshold $l_0'$, calculated in accordance with the assigned probabilities of detection $D$ and of false alarm $F$. Here, as before, $y_k$ is the voltage at the detector output in the $k$th pulsing period, $B_k$ are the weighting factors used in summing voltages $y_k$, $a = \frac{A}{\sigma_m}$ is the signal/noise ratio for the voltage at the detector input.

Discrete integrating devices use signals which are quantified in amplitude. In binary quantization of the signal, $y_k$ are broken down into two groups: those exceeding and those failing to exceed a certain level $y_0$ known as the quantization level for the first threshold (Fig. 6.32a). Signals may be quantified, for example, using a standard pulse generator with an assigned operating threshold. If voltage $y_k$ exceeds the input threshold, the generator develops a standard pulse – "1," and in the case of failure to exceed this level – "0" (Fig. 6.32b) – nothing happens.

Thus signal $y_k$ becomes a series of units and zeroes, the probability of units $p$ (and the probability of zeroes $q = 1 - p$) being determined by the selection of the threshold quantity $y_0$ and depending upon parameter $a$.

The obtained signal is fed to the synchronous integrator. The structure of the optimum integrator, as before, is described by Formula (6.38), except that $y_k$ should be replaced either by "1" or "0." The syn-

chronous integrator is in no way simplified during the transition to binary-quantified signals: the number of summed pulses (memory size) is preserved, the weighted amplifiers are retained.

To simplify the circuit nonoptimum balanced integration within the limits of optimum angle $2\alpha_{opt} = 0.84$ is employed.* This leads to an extremely low energy loss, and the device itself is therefore considerably simplified by eliminating the weighting factors and reducing the size of the memory device, which is the most cumbersome unit in the integrator. In balanced integration $B_k = 1$ within the limits of the assigned interval, and Operation (6.38) is reduced to a simple calculation of the number of standard pulses (units). If the number of counted pulses out of $n$ possible pulses exceeds a certain number $K$, it is decided that the target is present. In the opposite case it is considered that a target is absent. The number $K$ is called the counting threshold, or the second threshold, and the method itself is known as the "$K$ out of $n$" method.

Figure 6.33 shows one of the possible binary integration (pulse counting) circuits using delay lines to detect according to the "$K$ out of $n$" method. A circuit utilizing a magnetic drum has a completely analogous appearance. An electron tube acts as a pulse counter and a threshold device. When the number of standard pulses forming the total pulse exceeds counting threshold $K$ in the grid circuit, the tube is turned on and emits a signal indicating the fact of detection. Counting threshold $K$ may be varied by selecting the bias value. The processes occurring in the circuit at $K = 3$ and $n = 5$ are explained in Fig. 6.34.

We calculate probabilities $F$ and $D$ for an equivalent rectangular packet of $n$ pulses in binary integration.

The probability that a single pulse will exceed the threshold is $p$, that it will not exceed the threshold $1 - p$. The probability that $k$ pulses will exceed the threshold is $p^k$, that $n - k$ pulses will not

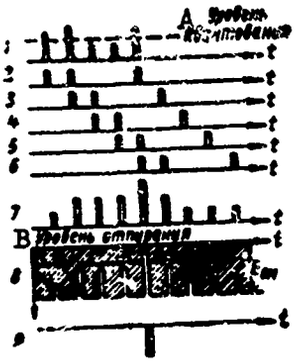

Fig. 6.34. Processes in a binary integrating circuit. A) Quantization level; B) triggering level.

exceed the threshold is $-(1-p)^{n-k}$. The probability that one combination of $k$ pulses out of $n$ will be formed is $p^k(1-p)^{n-k}$, $k$ pulses exceeded the threshold, and the remaining $n-k$ did not exceed the threshold. The number of possible combinations of this type is equal to the number of sets $C_n^k$. Then the probability of formation of any combination $k$ out of $n$ will be defined as $C_n^k p^k (1-p)^{n-k}$.

This probability may be considered the common term of the expansion of binomial $[p+(1-p)]^n$, and therefore the distribution itself had been called the binomial law. The sum

$$\sum_{k=0}^{n} C_n^k p^k (1-p)^{n-k} = [p+(1-p)]^n = 1$$

is the full probability.

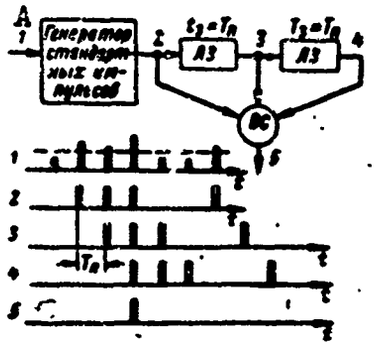

Fig. 6.35. Using the coincidence method to detect a target. A) Standard pulse generator.

The probability that the number of pulses is equal to or in excess of threshold $K$

$$D, F = \sum_{k=K}^{n} C_n^k p^k (1-p)^{n-k} \quad (6.39)$$

is the probability of detection or probability of false alarm depending upon whether $p = p_c$ or $p = p_{sh}$ are substituted into (6.39). The probabilities $p_s$ and $p_{sh}$ may be found from the formulas and graphs given in Chapter 5 and depend upon level $v_0$ which is in rigid functional dependence upon threshold $y_0 = \frac{v_0^2}{2}$. Therefore the type of detector characteristic, in the corresponding recalculation of the threshold, has no influence on probabilities $p_s$, $p_{sh}$, $D$ and $F$ in binary quan-

tization.

As follows from Formula (6.39) identical probabilities $D$ and $F$ may be obtained with different combinations of $k$ and $p_{sh} = f(y_0)$, i.e., with different combinations of the values of the first and second thresholds. However, identical $D$ and $F$ are obtained at different values of $a_{min}$. Therefore, one threshold is selected such as to satisfy the assigned false alarm probability $F$, while the second is selected so as to be optimum and to correspond to the least $a_{min}$ (to maximum sensitivity) at the assigned $F$ and $D$.

As the calculations demonstrate, the optimum threshold $y_0$ corresponds to $p_{sh} \approx 0.1$; the optimum counting threshold $K_{opt} \approx 1.5\sqrt{n}$. At the optimum $y_0$ the counting threshold $K$ should ensure the assigned $F$. If $K = K_{opt}$, to ensure the assigned $F$ it would be necessary to calculate the corresponding $y_0$ or $p_{sh}$.

Quantities $F$ and $D$ are easily found from Formula (6.39) for the assigned sensitivity ($a_{min}$) and thresholds $y_0$ and $K$. Unfortunately, a task which is more important for the calculations – determining the sensitivity and the value of one of the thresholds from the assigned $F$ and $D$ – cannot be resolved analytically from Formula (6.39). Therefore, one either uses a sampling method, substituting various $p_s$ and $p_{sh}$ into Formula (6.39) or previously compiled graphs may be used.

*The coincidence method.* The above circuit for integrating binary-quantified signals establishes the fact of detection using any $K$ pulses out of $n$. An easier device to build is one which records detection of a target from the arrival of $K$ pulses in a row, that is, $K$ pulses following at intervals of $T_p$.

This method has been called the "$K$ out of $K$" method, or the coincidence method, since it employs coincidence circuits; this device and its operating principle are explained for $K = 3$ in Fig. 6.35. If a gen-

erator of standard pulses located at the output of the RLS receiver sends three pulses at intervals of $T_p$, at a certain moment in time pulses will appear simultaneously in all three inputs of the coincidence valve (VS). The coincidence valve starts up and emits a pulse indicating that a target has been detected.

The optimum number of inputs of the coincidence circuit also corresponds to $K_{опт} \approx 1{,}5\sqrt{n}$. Since the memory capacity in a binary integrator is $(n-1)T_n$, while it is $(K-1)T_n$ in a coincidence circuit, the latter turns out to be a simpler device. At the same time, since the coincidence circuit is cruder, it has an additional sensitivity loss over that of the binary integrator; this loss increases with increase in $n$. Thus, at $D = 0.5$ and $F = 10^{-5}$ this loss attains 1.7 db, if $n = 10$, and 3 db if $n = 30$. Therefore, at large $n$ the coincidence method is unsuitable from the energy point of view.

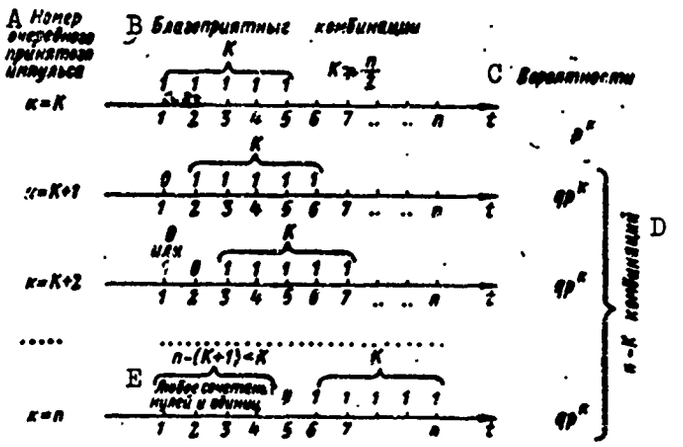


Fig. 6.36. Calculating the probability of detection by the coincidence method. A) Number of the regular received pulse; B) favorable combinations; C) probabilities; D) $n - k$ combinations.

Calculation of the probability of operation of the coincidence circuit is considerably more complicated than a calculation of the probability that the threshold will be exceeded in binary integration. Therefore we will derive the formula for the threshold of detection using $K$ pulses

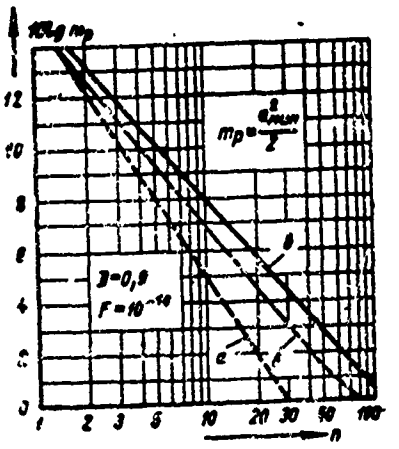


Fig. 6.37. Threshold signal as a function of the number of pulses: a) Coherent integration; b) noncoherent integration; c) processing by the coincidence method ($K \approx 1{,}5\sqrt{n}$).

in a row out of a series of $n$ pulsings only for the case when $K \geq n/2$. We will examine the pulses sequentially, in the order in which they arrive from the target.

It is obvious that a combination of $K$ pulses in a row is impossible before reception of the pulse with the number $k = K$. Upon reception of the $K$th pulse the coincidence circuit starts up if all $K$ pulses exceed the quantization level $y_0$. The probability of such an event is $p^k$ (Fig. 6.36).

With the arrival of each successive pulse, including the last, the probability of the formation of a detectable combination increases by the quantity $qp^K$, where $p = 1 - p$. This is the result of the fact that in order to form a new favorable combination, the last $K$ pulses must exceed the quantization level, while the pulse preceding them should not exceed it. Actually, if this pulse also exceeded the quantization level, a favorable combination would be formed one repetition period earlier, and the reception of a pulse in the current period cannot alter the fact that the coincidence circuit has operated nor the probability of

such an event.

Whether or not the quantization level is exceeded by the signals received before the pulse preceding the detectable combination of $K$ pulses does not affect operation of the coincidence circuit. Nor can these pulses form a favorable combination, since, with the limitation $\left(K \geqslant \frac{n}{2}\right)$ introduced by us above their number is $n-(K+1)<K$.

It follows from what has been said that the probability of formation of all favorable groups except for the first is identical and equal to $qp^K$. The number of such groups is $n - K$ (see Fig. 6.36).

Consequently, the probability that at least one pulse will appear at the output of the coincidence circuit over the course of $n$ pulsing periods is equal to the sum of the probabilities of formation of all incompatible favorable combinations: $p^K + (n-K)qp^K = p^K[1+(n-K)(1-p)]$.

At $p = p_s$ and $p = p_{sh}$, respectively, we obtained the probabilities of detection and of false alarm:

$$D,\ F = p^K[1+(n-K)(1-p)],\quad K \geqslant \frac{n}{2}. \tag{6.40}$$

at $K < n/2$ the calculation follows a more complex formula

$$D,\ F = p^K\left[1+\sum_{\nu=1}^{\nu_1}(-1)^\nu C^\nu_{n-K(\nu+1)}qp^K\right] - \sum_{\nu=1}^{\nu_2}(-1)^\nu C^\nu_{n-\nu K}qp^K \tag{6.41}$$

where $C^\nu_m$ is the number of combination; $\nu_1$ and $\nu_2$ are whole parts of numbers $n - 1/K + 1$ and $n/K + 1$ respectively.

It should be noted that for all $n \leq 10$ condition $K_{opt} \cong 1{,}5\sqrt{n} \geqslant \frac{n}{2}$ is satisfied, and Formula (6.40) may be utilized. The number of terms in Formula (6.41) $\nu_1 \cong \nu_2 \cong \frac{n}{K}$ at the condition $K = K_{opt} \cong 1.5\ \sqrt{n}$ is $0.9\sqrt{n}$. It may actually be taken equal to $0.3\sqrt{n}$, since the remaining terms make a negligible contribution. Then we may limit ourselves to two terms in sum at $n < 50$ and three terms at $n < 100$.

Unfortunately, as in the case of binary integration, the sensitivity

and level of one of the thresholds it may be calculated from the assigned $F$ and $D$ only using the sampling method or using previously compiled graphs. Figure 6.37 shows discrimination factor $m_r$ as a function of the number of pulses in the packet when the target is detected using the coincidence method ($K = K_{opt}$) in comparison with optimum coherent and noncoherent reception for certain concrete conditions.

## §6.8. CHARACTERISTICS OF THE DETECTION OF RADAR SIGNALS WHEN INDICATORS ARE USED

Visual radar observation has its specific characteristics which are determined by the properties of the indicator and by the physiological possibilities of the operator under the assigned observation conditions. Signals passing through the RLS receive strip and giving rise to target blips on the indicator are integrated by the screen and by the eye, giving rise to a certain imprint – trace – in the consciousness of the observer. The accumulation of traces and the analysis of their characteristics, as consciously performed by the operator, enable him to take a decision as to the presence or absence of a target.

Let us examine the influence of these factors on the efficiency of detection of radar signals.

### 1. Integrating Properties of Indicators

The indicator characteristics influence the process of radar observation in two ways: in the first place, the kind of marking (brightness or amplitude) and the type of indicator scan, and also certain properties of its screen determine the "quality" of the image reproduced – its brightness, clearness, stability over time, etc. As will be shown below, these factors have a substantial influence on the formation of the trace in the operator's consciousness. In the second place, the storage properties of the screen of the cathode-ray tube determine the efficiency of integration of radar signals, this being a process

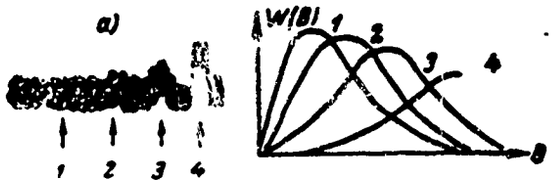


Fig.6.38. Observation of signals on an indicator with amplitude marking: a) Noise path in the absence and in the presence of a signal; b) brightness distribution of noise path.

which occurs without the participation of the operator's consciousness.

*The type of scan and character of the marking* substantially influence the sensitivity of the indicator. The indicator with amplitude marking is the most sensitive. To explain this characteristic we may examine the mechanism of detection of weak signals when amplitude marking is used.

During the course of one scanning cycle an oscillogram of the receiver output voltage is traced on the indicator screen; this is not enough for reliable selection of any individual blip as a useful signal. Visual inertia causes the scanning lines which are rapidly traced on the screen to create the impression of a broad bright band, the so-called noise path. The higher the pulsing frequency of the radar station the greater the number of oscillograms in the noise path and the less discernible is any individual blip.

The meaning of the brightness at each point in the noise path corresponds to the total time during which the bright spot remains at this point. Therefore, the brightness in a cross-section perpendicular to the scanning line changes in accordance with the distribution of the noise voltage, that is, according to the Rayleigh law (Fig. 6.38). In an analogous way for the part of the screen where the signal appears in each pulsing period, the distribution of brightness will correspond to a generalized Rayleigh law.

In the presence of a weak signal the section of the noise path possessing maximum brightness is slightly displaced upwards. This displacement is greater, the greater is the amplitude of the useful signal with respect to noise. The weakest signals are detected by a scarcely noticeable darkening in the lower part of the noise path. As signal intensity increases, a bright projection becomes visible above the scanning line; finally, powerful signals are depicted in the form of sharply defined pulses.

The possibility of detecting an extremely weak signal among the noise, the presence of this signal being ascertained from the scarcely noticeable darkening of the noise path, makes the amplitude indicator one of the most sensitive devices as regards detection thresholds. The discrimination factor of such indicators in the usual RLS operating regimes is of the order of unity. However, the amplitude indicator has practically no memory and does not give a sharp depiction of the target.

The mechanism of detection of weak signals on indicators with brightness markings and range sweep, as is known, consist of the following: establishing in his mind the limiting threshold with respect to brightness, the operator includes in his observation only those bright spots which exceed the threshold. The limiting level is close to the average noise level, which helps in the detection of weak signals. However, an indicator with brightness marking does not transmit amplitude relations well. The number of discriminable gradations on an ordinary screen with afterglow is 3-4; if it is necessary to detect a threshold signal which scarcely differs from the background, only one or two gradations are actually used. This type of amplitude quantization causes a reduction in the quantity of information transmitted by the blip and heightens the threshold signal. The discrimination factor of elevation-

range brightness indicators is considerably greater than that of amplitude indicators, comprising several units, usually from 3 to 10.

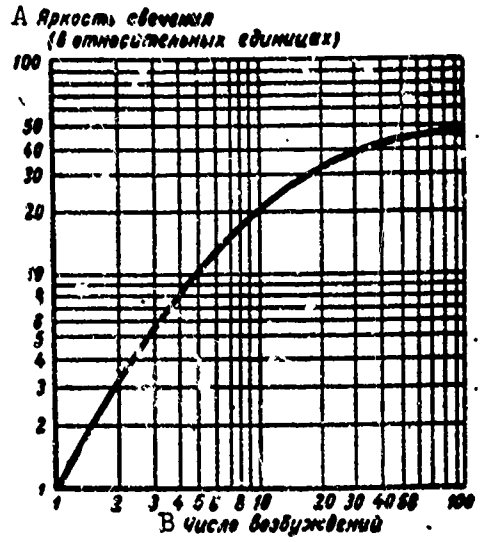


Fig. 6.39. The brightness of screen glow as a function of the number of repeated excitations. A) Brightness of glow (in relative units); B) number of excitations.

As has been pointed out earlier, directional indicators are nonsynchronous storage devices and therefore possess the lowest sensitivity. Their discrimination factor is 10-20 and more.

*The screens of indicator tubes* of the customary type are made of special substances — luminophors which glow when bombarded by electrons.

The afterglow of the luminophor is evaluated by the time it takes for the glow to reduce to 0.01 of its initial value. This quantity is conventionally called the afterglow time. Radar station indicator screens possess, essentially, three different values of afterglow time.

1. Screens with slight afterglow, measured in hundredths of a second. After the end of bombardment the glow intensity declines exponentially with a very low time constant. Such screens are utilized in almost all indicators with amplitude marking and in oscillographs.

2. Screens with average afterglow, measured in tenths of a second (more precisely, from 1/20 sec to about 2 sec), used to smooth out flicker when the repetition frequency of the images is less than the critical frequency as determined by the stroboscopic effect (about 1/10 sec).

3. Screens with considerable afterglow, several seconds and more, which are used to preserve the radar image on the brightness indicator during a complete scanning cycle.

Single-layer screens with extended afterglow work well with weak excitation: they assure considerable clarity of the image and a long afterglow. However, image brightness is inadequate. Image brightness cannot be substantially heightened by increasing the intensity of the electron flux without a deterioration in image quality. This is because excitation by an electron beam cannot penetrate to a considerable depth in the luminophor.

In contrast to the electron flux, light excitation penetrates to a considerably greater depth in the luminophor. This characteristic of photoluminescence (luminescence due to excitation by rays in the optical spectrum) is employed in the so-called cascade screens. Two different luminophors are applied in two layers to the surface of the glass of the screen. The layer which is subject to direct bombardment by electrons usually emits a blue or a light blue glow. Its afterglow time is insignificant. The glow of the first layer excites the second, so-called glass layer, which possesses extended afterglow.

A bright burst of blue light at the moment of excitation of the screen inhibits normal observation. By covering the screen with an orange light filter it is possible to eliminate almost completely the influence of the blue glow which passes through the second layer.

The brightness of the glow of cascade screens decreases over time

according to a law which is almost hyperbolic. The rapidity with which the brightness declines is slightly less at lesser values of the current density in the beam. Upon repeated excitation the afterglow declines more slowly.

*The integrating capacity of the screen* with extended afterglow, characterized by increase in brightness under the influence of repeated excitations, is illustrated by the experimental graph depicted in Fig. 6.39. Along the axis of the ordinates of the graph is laid out the brightness of the screen glow before each successive excitation, these being repeated every second. Brightness after the first excitation is taken as unity. Both axes follow identical logarithmic scales, and the linear function on the graph therefore takes the form of a straight line with a 45° slope angle.

It can be seen from this graph that initially the increase in the afterglow brightness is more rapid than the increase in the number of excitations (the slope angle of the initial sections of the curve is greater than 45°). Thus, for example, the second excitation increases the brightness of the blip not by two times, as might have been expected, but by three times. Such a nonlinear dependence (superproportionality) between the number of excitations and the increase in brightness which they produce occurs when excitation intensity is low.

The superproportionality phenomenon is connected with the presence of a certain energy threshold value which is needed for the occurrence of glow. Basically, this threshold is exceeded by the first excitation. Therefore, the glow brightness corresponding to it is less than the growth in brightness as determined by the subsequent pulses.

A superproportional increase in brightness occurs only for the first few initial excitations. Later the slope angle of the curve (Fig. 6.39) becomes lower than 45° and gradually decreases to zero. The glow

brightness increases noticeably up to about 20 excitations. A slight increase in brightness can be noted even up to 50, and in some instances to 200 excitations.

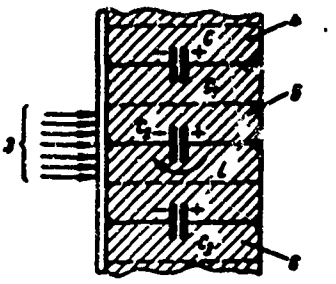

Fig. 6.40. Schematic depiction of elementary storage devices of a graphecon target: 1) Target dielectric; 2) signal plate; 3) high-voltage (recording) beam; 4, 5, 6) elementary storage devices for electrical charges; $C_1$, $C_2$, $C_3$) capacitances equivalent to elementary storage devices; $i$) discharge current of elementary storage device.

Thus, the typical screen with extended afterglow may be viewed as an ideal integrating device for 10-20 pulses, which corresponds approximately to the packet of reflected signals during customary RLS operating regimes.

As follows from what has been said, the luminescent screen of an ordinary cathode-ray indicator fulfills two basic functions: transformation of the electrical signals into brightness blips and remembering the image. However, these functions may be performed more successfully by separate elements. The charge-storage tube target is often utilized as a memory unit.

*The charge-storage tube* "remembers" the radar signals by transforming them into electrical charges which form on the dielectric target a peculiar sort of invisible radar image. The potential relief which may be maintained on the target without noticeable change for practically any length of time is then transformed into a bright visible image on the luminescent screen. These transformations are accomplished either

in the same cathode-ray device or a special television kinescope may be employed to obtain a visible image.

In the first case the potential relief registered on the target in the form of a finely structured grid governs the intensity of the broad electron beam which penetrates the target and excites the luminescence screen. Depending upon the depth of the potential relief, the holes in the grid let through a varying quantity of electrons of the reproducing beam and vary the velocity of their motion. The invisible image of the potential relief is transferred to the luminescent screen.

In the second case, various cathode-ray devices are utilized to remember the signal and reproduce the image. Recording is done by a charge-storage tube whose scan is synchronized with the antenna rotation and with the pulsing of the transmitter. The charge-storage tube output signal, which are obtained as a result of readout, are amplified and fed to a television kinescope. A television scan is used to read out the signals from the target and to reproduce the image on the kinescope.

Let us examine briefly the mechanism of formation of the potential relief of the target using as an example a charge-storage tube of the two-beam graphecon type.

In its first approximation the charge-storage tube target may be viewed as the totality of the elementary storage devices – condensers (Fig. 6.40). When they are being prepared for recording, all the elementary storage devices of the target are charged by a low-volt electron beam to an identical initial potential. Irradiation of part of the target by another, low-volt beam creates inside the dielectric layer free carriers of charges – electrons and holes. Their movement which is governed by the electrical field of the surface charge of the target forms a current of electron-excited conductance. The size of this current usually exceeds the current of the high-voltage beam and depends upon

its instantaneous intensity. The internal secondary electrons exiting to the surface of the target reduce the positive charge on the surface and give rise to potential relief. This process may be viewed as discharge of the target elementary storage devices by a current of excited conductance.

The recorded signals are fed to the modulator of the graphecon high-voltage projector. Change in the charge of the target elements is determined by the current of the recording beam, by the extent of the irradiation, and by the initial potential difference in the dielectric layer. The elementary storage device may be completely discharged by the current of excited conductance during one or several scanning cycles of the high-voltage beam, depending upon the recording conditions. When the current is low the elementary storage device is incompletely discharged during the time of existence of the packet of recorded pulses. Small changes in the target charge, determined by individual pulses, may be distorted by the internal noises of the charge-storage tube, and by various noises and babble in the apparatus. A high-intensity pulse completely discharges the target, and repeated pulses of the packet can no longer change the potential relief. Under optimum conditions only the last pulse of the recording packet completely discharges the target element and completes the formation of the potential relief.

Gradual increase in the potential relief with the arrival of additional recording pulses makes it possible to integrate the radar signals.

The integrating properties of indicators are sometimes mistakenly identified with memory time. Thus, for example, it might be assumed that when cathode-ray tubes with short afterglow are replaced by cascade screens with an afterglow time measured in seconds, the indicator sensitivity would increase substantially due to the possibility of ac-

cumulating a large number of pulses. It would seem that still greater possibilities are afforded by the charge-storage tube whose memory time for signals is practically unlimited. However, these assumptions are not justified.

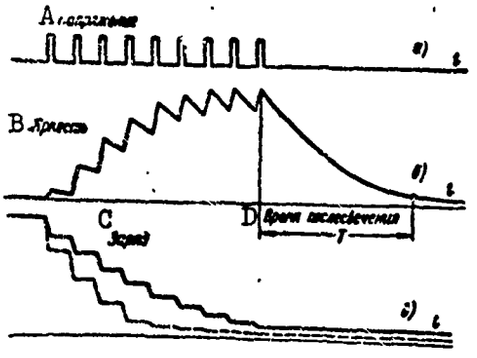


Fig. 6.41. Storage of pulse signals by a screen with afterglow and by a charge-storage tube target. A) Voltage; B) brightness; C) charge; D) afterglow time.

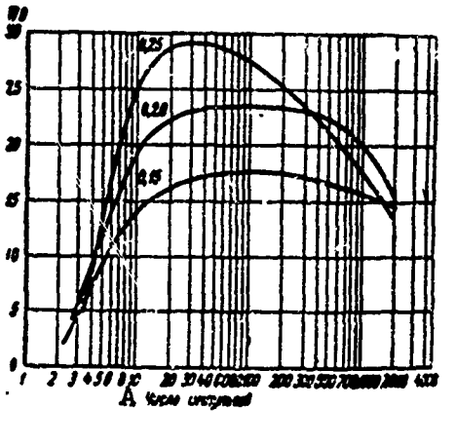


Fig. 6.42. Voltage of the read out signal of the graphecon as a function of the number of pulses recorded at one point. The figures under the curves give the collector current in microamperes. A) Number of pulses.

As follows from the mechanism of the formation of potential relief examined above, the integrating properties of the target are determined by its ability to alter its potential relief noticeably under the influence of repeated pulses (Fig. 6.41a and c), i.e., they are more amplitude than time characteristics. From the point of view of integration

the requirements on the memory are only that memory time be not less than the length of a series of accumulated pulses. This requirement is easily satisfied in the case of the charge-storage tube; the afterglow time of cascade screens (Fig. 6.41b) is also usually greater than the length of a pulse packet. Only in the case of screens with short afterglow is this relation often not satisfied.

From the point of view of the possibility of accumulating radar signals, cathode-ray tubes with ordinary screens possessing extended afterglow and charge-storage tubes are approximately equivalent. An experimental graph of signal intensity as recorded in a typical graphecon, as a function of the number of pulses in the packet (Fig. 6.42), shows that effective integration occurs up to about 10 pulses. After that the growth of the recorded signal slows down, and then the output signal may also decrease.

Readout, that is, the transformation of potential relief into electrical signals, is accomplished in the graphecon by secondary electron emission. In readout the target surface is irradiated by an electron beam of constant intensity. The accelerating voltage is selected low; therefore, the current of excited conductance is practically absent, and the target charge is formed as electrons are knocked off its surface.

When a low-voltage beam is run across the area of the target which has been discharged during recording, the charge is restored. The potential of this section increases toward the initial position, and a pulse of current arises in the target circuit. But if the readout beam irradidates a target element whose potential has not changed in the recording process, there is no restoration of the charge, and there is no current in the target circuit. Thus, the readout operation is accompanied by erasure of the potential relief created by the recording process, and the target is prepared for a new recording.

If the radar image is transformed into a television image, usually a readout current is established such that the potential relief is not disturbed essentially. Change in the readout current makes it possible to regulate the memory time within wide limits (to 10 min and more).

To summarize what has been said above, we note that from the point of view of the efficiency of integration of radar signals, this proces occurring without participation of human consciousness, a screen with extended afterglow and a charge-storage tube target are approximately equivalent and make possible the linear integration of 10-20 pulses. As regards afterglow time, brightness, and image stability, the afterglow law and other such indicator parameters, charge-storage tube systems are unquestionably superior. These parameters have a substantial influence upon the effectiveness of subsequent signal analysis in the operator's organs of sight and consciousness.

2. Influence of Physiological Factors

*The integrating capacity of vision* is determined by the photochemical reactions occurring in the sensitive elements of the eye. As is known, the sensitive elements of the eye are the cones and the rods forming a sort of mosaic – the retina. The molecules of the light-sensitive substance of the cones or the rods, decaying under the influence of light, create decay products which excite the visual nerve. This latter transmits the excitation to the brain. A certain time is required for the decomposition and restoration of the molecules of the light-sensitive substance. A pulse excitation which is repeated at time intervals of 0.1 sec or less is received by the eye as a continuous luminescence. This luminescence is accompanied by flicker, but at a frequency of excitation exceeding 50-60 hz this flicker becomes unnoticeable. According to Talbot's law the apparent brightness of a continuous luminescence is equal to its average brightness.

The increase in the effect of the sensation of light in the operator's eye, occurring automatically and without the participation of the consciousness, when excitation is repeated at short time intervals not exceeding the tenth part of a second, is called *visual accumulation.*

Light impulses arriving at larger time intervals are treated as new excitations and are not added to the preceding excitation in the operator's eye. The affect of such more widely spaced excitations may also be cumulative. In this case, the role of storage device is played by the operator's brain, which distinguishes among excitations with respect to certain characteristic signs. Such an accumulation of information occurring in the operator's consciousness is called visual correlation.

*Visual correlation* in radar observation is associated with a whole series of characteristics and signs of the target blip which may be detected by conscious analysis, and not automatically as in the case of visual accumulation. Such signs are: the appearance of the blip in successive scanning periods in a particular section of the screen, the increase in the size of the useful blip by comparison with noise, the formation of a trajectory of target movement by successive blips, and certain other factors.

If the trace which is left in the operator's consciousness may be viewed as the result of the primary processing of radar signals, then the process of visual correlation represents a secondary processing of these traces.

In the process of radar observation integration and visual correlation are not equally effective. As is known, in linear integration the threshold signal power is proportional to the square root of the number of integrated signals. This is also true for linear integration done by an indicator or by the operator's eye under normal RLS operating conditions. Since nearly linear integration occurs only in the

case of processes which are spaced at short time intervals (0.1 sec and less), its effectiveness is determined precisely by these rapid prcesses.

Thus, for example, a doubling of the number of pulses in the packet, when all other conditions are equal, usually leads to a lowering of the detection threshold by $\sqrt{2}$ times or by 1.5 db regardless of whether the indicator employs amplitude or brightness marking, or uses a tube with long or short screen afterglow. At the same time these factors have a substantial influence upon the effectiveness of visual correlation. The memory must be utilized in order to compare the various traces with one another. The memory power of the human mind may not be considered perfect, since the traces left in it are gradually lost. The effect of visual correlation may be achieved if the memory of the whole detection system is heightened by using an indicator device and if on the indicator there is a graphic image which is suitable for the comparison of traces.

An example of such an image could be registration on the tape of a chemical or photoelectric device connected to a range-measuring radar station. The fact that the tape is continuous makes it possible to register a practically unlimited number of traces. From the point of view of effectiveness of visual correlation, the indicator utilizing a charge-storage tube with an extended memory is also perfect. When rapidly moving objects are observed on such an indicator, what is detected is the group of traces forming the trajectory of motion of the blip.

In the examples examined above an increase in the number of traces is of maximum value for improving the observability. In particular, experiments with a chemical writing device have demonstrated that a doubling of the number of pulses leads to a 2.5 db reduction in the threshold signal.

Even though analogous images are viewed on an ordinary cathode-ray tube with afterglow of the order of several seconds, such a memory can no longer give substantial assistance to visual correlation. Here the operator's memory is called into play, and in it, as has been shown, old traces are gradually lost. Even if the number of traces is doubled, the operator in fact cannot handle this doubled quantity of traces, and he cannot reduce the threshold signal by 2.5 db as in the above experiment with a chemical writing device, but by approximately 2-2.2 db.

This all makes it possible to evaluate the degree of reduction of the detection threshold with change in the various RLS parameters.

3. The Influence of Observation Conditions

Contrast sensitivity is an important characteristic of sight, one which influences the process of radar observation. In radar the contrast sensitivity of the eye determines its capacity to note differences in the luminescence of two adjacent sections of the screen which are represented as being in contact with one another. As a measure of brightness ($K$) we use the difference in the brightness of the target blip ($B_0$) and the background ($B_f$), divided by the backgrcund process

$$K=\frac{B_0-B_\phi}{B_\phi}.$$

A number of experiments have established that the brightness contrast which can be detected on the indicator screen is approximately proportional to the signal power. Therefore, the graphs of contrast sensitivity given in this section characterize in their first approximation the change in the corresponding threshold signal.

Contrast sensitivity depends largely upon the view angle encompassing the blip (that is, upon its area), and upon the background brightness. Figure 6.43 is an experimental graph illustrating this function. The values of the view angle encompassing the blip are laid

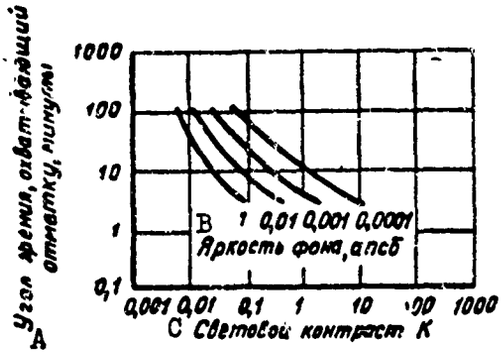


Fig. 6.43. Contrast sensitivity as a function of the angle of view (the angular area of the blip). The numbers on the curves indicate the background brightness in apostilbs. A) Angle of view encompassing the blip, min; B) background brightness, apsb; C) light contrast, $K$.

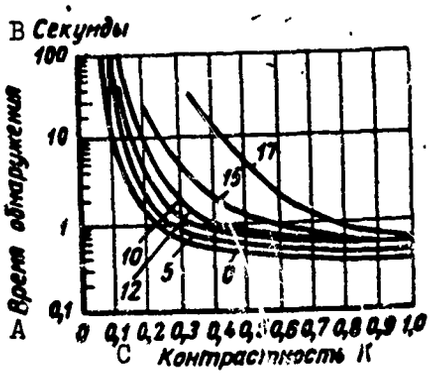


Fig. 6.44. The detection time of a blip as a function of contrast. The figures on the curves indicate the distance in centimeters between the blip and the point at which the operator looks. A) Detection time; B) second; C) contrast $K$.

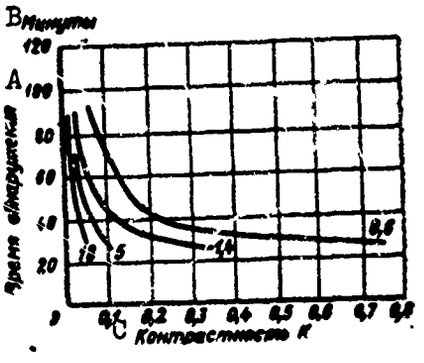


Fig. 6.45. Detection time after light adaptation as a function of blip contrast. Curves are given for the various values of the background brightness (in millilluxes). A) Detection time; B) minutes; C) contrast $K$.

out on the axis of the ordinate of the graph on a logarithmic scale; on the axis of the abscissa are laid out the threshold values of the contrast. Curves are given for the various brightnesses of the background – from dark (0.0001 apsb) to very bright (1 apostilb). The optimum value for background brightness of an indicator screen of a stationary radar station is about 0.01 apostilb.

The time during which the blip is detected is of substantial importance in characterizing the operating conditions of a radar-station operator. The relation between the time needed for detection and the brightness contrast of the blip relatied to the background is illustrated by the experimental curve in Fig. 6.44.

It is impossible to set up experiment in visual observations which exclude the operator's reaction and the delay involved in establishing the fact of detection. Therefore, the detection time laid out along the axis of the ordinate concerns a certain unknown and approximately constant quantity determined by the experimental conditions. However, indeterminacy in the position of origin of the coordinates of the graph do not prevent us from making practical use of it.

For example, let us take the case of observation of a target blip on the indicator screen of a stationary radar station. The operator's working conditions in this case are favorable for observation: in a quiet environment he can look around in the corresponding section of screen for several seconds. As follows from the graph, brightness contrast of the order of 0.1 may be detected in this case.

Let us take another extreme case, in which the operator of the radar station is a pilot.* Since he is operating the airplane, he can only glance at the screen, letting his eye rest on the blip for a fraction of a second. In this case the detectable contrast is approximately 0.3.

The light adaptation phenomenon preceding observation of the screen sharply reduces the contrast sensitivity of vision and causes a substantial deterioration in the observability of radar signals. In the case of stationary radar stations the harmful influence of adaptation may be practically eliminated by using external illumination, by employing tubes, etc.

On an airplane the radar station operator is the pilot or some other member of the crew who conducts visual observation of the air environment or of the earth's surface. In moving his eye from the brightly illuminated sky to the screen, the operator is for an extended period of time incapable of distinguishing the radar image.

Contrast sensitivity as a function of detection time in the presence of light adaptation is illustrated by the experimental graph of Fig. 6.45.* Prior to observation the operator looked for 120 sec at a source of illumination which was as bright as a sunlit sky. Curves are given for four constant background brightness values. A comparison of Fig. 6.44 and 6.45 shows that after light adaptation detection time increases by more than an order of magnitude. In this case the only way to heighten contrast sensitivity is to increase image brightness.

Manuscript Page No.

[Footnotes]

282 If the received-signal amplitude is not known, after reception the obtained results must be, as a supplementary operation, averaged over all amplitude values, with due account of their probabilities.

292 The derivative of the integral for the lower limit is equal to the integrand with the opposite sign.

317 If the problem is not one of detection with monopulse beaming.

321 Since finding the root is a nonessential operation, it is not obligatory; threshold $l_0$ may be replaced by $l_0^2$.

322 Here we do not take up the question of the ambiguity of the velocity reading in the pulse mode.

329 In fact, the energy requirement increases somewhat, although very slightly, with increase in the number of elements of resolution.

345* In many textbooks tables are given for the function $\Phi_1(z) = \frac{2}{\sqrt{2\pi}}\int_0^z e^{-\frac{t^2}{2}}dt$, which is connected with the above function by the dependence $\Phi(z) = \frac{1}{2}[1 + \Phi_1(z)]$.

345** Sometimes another notation is used for the reciprocal function: $\Phi^{-1}(y) = \arg\Phi(y)$.

349 See §5.5.

371 It is assumed that observation is done at night. Otherwise it is necessary to take into account the presence of light adaptation preceding observation, as is discussed below.

372 See [2] to Chapter 6.

## Transliterated Symbols

282 ш = sh = shum = noise

292 РХП = RKhP = rabochaya kharakteristika priyemnika = receiver operating characteristic

297 мин = min = minimal'nyy = minimum

297 РЛС = RLS = radiolokatsionnaya stantsiya = radar

300 прд = prd = peredacha = transmission

300 б = b = biyeniye = beat

300 прм = prm = priyem = reception

301 м = m = modulyatsiya = modulation

301 макс = maks = maksimal'nyy = maximum

310 и = i = impil's = pulse

310 п = p = paket = packet; povtoreniye = repetition

312 ф = f = fil'tr = filter

319 ФД = FD = fazovoy detektor = phase detector

320 оп = op = optimal'nyy = optimum

322 д = d = doppler = doppler

329 с = s = signal = signal

336 з = z = zaderzhka = delay

336 лд = LD = liniya zaderzhki = delay line

337 а = a = anod = plate

337 см = sm = smeshcheniye = bias

337 вр = vr = vrashcheniye = rotation

337 сд = SD = selektor dal'nosti = range selector

337 н = N = nakopitel' = store

369 ф = f = fon = background

## Chapter 7

# RESOLUTION, ACCURACY, AND UNIQUENESS OF THE READING IN MEASUREMENT OF RANGE AND VELOCITY

### §7.1. RANGE MEASUREMENT ERROR

The measurement of coordinates is one of the principal functions of radar devices. Measurement is inevitably accompanied by errors, and these provide a quantitative characterization of accuracy — one of the chief parameters of radar stations.

Errors may be divided into systematic and random.

Systematic error is the name given to the difference between the average value of a quantity obtained from numerous measurements, and its actual value. In principle, systematic errors may be offset by introducing corrections when calibrating the RLS or after the measurement has been made. The correction is equal to the systematic error with the opposite sign.

Random errors cannot be compensated, for their concrete value in each separate measurement is unknown. Therefore, random error is one of the determinants and limitations of measurement accuracy.

Range measurement accuracy is evaluated quantitatively by the mean square value of random error $\sigma_R$ or by dispersion $\sigma_R^2$, which is the average square of the difference between the measured value of the random quantity and its average value.

In practice, however, it is not always possible to determine and to compensate for systematic error. Therefore, in order to provide a complete description of accuracy, the RLS performance sheet often in-

BLANK PAGE

cludes, together with the $\sigma_R$, the limits of variation of the systematic error.

Range measurement errors are divided, with respect to their point of origin, into external and internal.

External errors include those due to unstable propagation conditions and errors introduced by the target itself. External errors do not depend upon the measurement method or upon the type of equipment used. Internal errors include those caused by noise in the particular range measurement method used (noise errors of the method) and instrumental errors.

*1. Propagation errors* ($\sigma_{R_r}$). Change in the conditions of propagation (the specific inductive capacitance of the medium) causes change in the velocity of propagation of radio waves $c$. The random error resulting from change in velocity $\Delta c$ is

$$\Delta R = \frac{\partial R}{\partial c} \Delta c.$$

If we make the substitution $\frac{\partial R}{\partial c} = \frac{R}{c}$ and replace the random quantities by their mean square value, we obtain

$$\sigma_{Rp} = R \frac{\sigma_c}{c}. \qquad (7.1)$$

It follows from this that the absolute value of the propagation error increases with increase in range.

The relative mean square value of the fluctuations of the propagation velocity $\sigma_s/c$ depend upon the state of the atmosphere and cannot be determined accurately, like the velocity itself. It can only be assumed as an approximation that it is of the order $\frac{\sigma_c}{c} = 10^{-6}$. Of approximately the same order of magnitude is the systematic (slowly changing) part of the error, which is not subject to being taken into account and offset. The question of propagation errors will be examined in more detail at the end of this chapter.

2. *Errors introduced by the target* ($\sigma_{Rts}$). Most real targets consist of a large number of elementary reflectors and have finite length $l_{ts}$ in the radial direction from the RLS. With relative displacement of the target or change in the RLS frequency the center of reflection of a complex target may be displaced within the limits of interval $l_{ts}$. Measurement errors will be most scattered relative to the center of the target when any position of the center of reflection $x$ within the limits of interval $l_{ts}$ is equally probable, that is, the distribution density

$$W(x)=\frac{1}{l_{\text{ц}}}.$$

Then

$$\sigma^2_{R\text{ц}}=\int_{-\frac{l_{\text{ц}}}{2}}^{\frac{l_{\text{ц}}}{2}} x^2 W(x)\,dx=\frac{2}{l_{\text{ц}}}\int_0^{\frac{l_{\text{ц}}}{2}} x^2 dx=\frac{l^2_{\text{ц}}}{12}$$

and the mean square value of the error introduced by the target will in all cases not exceed the quantity

$$\sigma_{R\text{ц}}=\frac{l_{\text{ц}}}{2\sqrt{3}}\approx 0{,}3 l_{\text{ц}}. \qquad (7.2)$$

Error introduced by the target has no particular significance for the measurement of range, since the center of reflection is not outside the target limits. However, range fluctuation of the center of reflection has a substantial impact upon the accuracy of measurement of target radial velocity.

In radar systems with active response no errors are introduced by the target. Instead of them, it is necessary to take into account errors $\sigma_{R0}=\frac{c}{2}\sigma_{\tau 0}$ determined by the scatter in the transponder triggering time $\sigma_{\tau 0}$.

3. *Noise errors of the method* ($\sigma_{Rm}$). With the given method of measuring range, errors due to noises are determined by the relative noise level, the signal shape, and the effectiveness with which the signal is processed. There is an optimum method of processing in which error $\sigma_{Rm}$

is minimum. This minimum error characterizes the potential possible measurement accuracy for the given signal shape and the assigned signal/ /noise ratio and is denoted by $\sigma_{Rp}$.

We introduce the relation

$$\sigma_{Rм} = K_м \sigma_{Rп}, \qquad (7.3)$$

where $K_m > 1$ is a factor characterizing the efficiency with which the signal is processed. The closer $K_m$ is to unity, the more efficient the processing method.

The calculation of quantity $\sigma_{Rp}$ and the optimum signal-processing procedure assuring achievement of the potential range measurement accuracy will be examined below.

*4. Instrumental errors ($\sigma_{Ri}$).* Instrumental measurement errors are determined by the inefficiency of the RLS as a technical device. These include errors in calibration and graduation, readout errors, errors of interpolation, etc. Instrumental errors entirely upon the particular station design employed. Very many of them may only be determined experimentally.

In conclusion let us note that systematic errors are added algebraically, while random errors are added geometrically. The total range-measurement error

$$\sigma_R = \sqrt{\sigma_{Rp}^2 + \sigma_{Rм}^2 + \sigma_{Rи}^2 + \sigma_{Rи}^2}. \qquad (7.4)$$

When the items are not equivalent, the total random error is determined by the largest of them; the smaller errors have only a slight effect. Thus, if a given error is half the size of all other errors together, the total error is increased by only 10% as a result. This should be borne in mind when apparatus is being designed, and the requirements on the apparatus should not be too severe if this will not lead to a perceptible reduction in the total error.

## §7.2. THE OPTIMUM RECEIVER FOR RANGE MEASUREMENT

Let us assume that signal $x(t)=s(t-\tau_0)+n(t)$ enters the input of a receiver (filter) with arbitrary pulse characteristics $h(t)$. The signal proper $s(t-\tau_0)$ reflected from a motionless punctiform target has the shape of the emitted signal $s(t)$, but is delayed with respect to the latter by time $\tau_0=\frac{2R}{c}$, while noise $n(t)$ is gaussian with a zero average value.

The signal at the receiver output

$$y(\tau)=\frac{2}{E_0}\int_{-\infty}^{\infty}x(t)h(\tau-t)\,dt=y_c(\tau)+y_m(\tau),$$

where

$$y_c(\tau)=\frac{2}{E_0}\int_{-\infty}^{\infty}s(t-\tau_0)h(\tau-t)\,dt; \qquad (7.5)$$

$$y_m(\tau)=\frac{2}{E_0}\int_{-\infty}^{\infty}n(t)h(\tau-t)\,dt$$

are the signal and noise output functions respectively. The signal function $y_s$ is regular: it is fully determined by the appearance of the signal and by the receiver characteristic. The noise function $y_{sh}$ is a random quantity with a gaussian distribution and a zero average value, since the normal distribution law is maintained when the signal passes through any linear system.

The signal function $y_s(\tau)$ is at a maximum at $\tau = \tau_0$. In the absence of a noise function at the receiver output during the moment of arrival of the signal maximum, the delay time of the echo signal $\tau_0$ and the target range $R=\frac{c\tau_0}{2}$ may be determined to any desired accuracy. However, the signal and the noise function may not be separated, and it is therefore possible to clamp only the moment $\hat{\tau}$ of arrival of the maximum of the total output signal $y(\tau)=y_c(\tau)+y_m(\tau)$. This moment is known as the *estimate* of the delay time. The presence of noise function $y_{sh}(\tau)$

causes estimate $\hat{\tau}$ to be biased relative to the true value $\tau_0$ by random quantity $\Delta\tau = \hat{\tau} - \tau_0$, which gives rise to range measurement error $\Delta R = \frac{c}{2}\Delta\tau$ (Fig. 7.1).

Range is usually measured for a sufficiently large signal/noise ratio $E_s/E_0$; otherwise it would no longer be a question of the accuracy of measuring the range of the true target, but rather of measuring the range of pulse targets from random blips of the noise function.

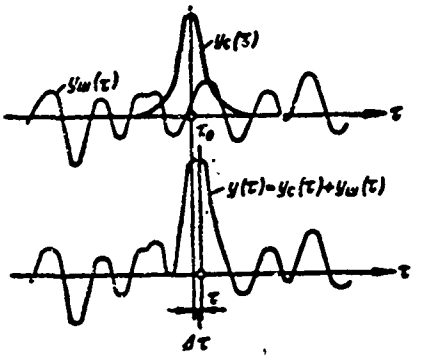


Fig. 7.1. Combined effect of the signal and the noise functions at the receiver output.

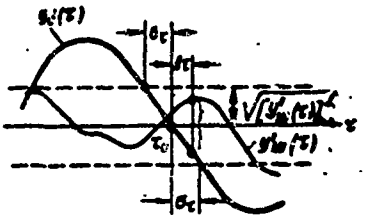


Fig. 7.2. Measurement errors as a function of the slope of function $y_s'(\tau)$ and the noise level.

When the signal/noise ratio is large, it may be considered that not only the high-frequency signal, but also its envelope and its video signal at the output of the linear detector are distributed normally. Therefore, without examining the precise structure of the high-frequency signal, we will understand signal $s(t)$ to mean the envelope or the video signal at the output of the linear detector. Although the high-frequency

structure can, in principle, be used to increase the accuracy of the reading off time on the carrier phase, in practice this accuracy cannot be achieved because of the extreme ambiguity within the limits of the pulse length.

In order to estimate the accuracy of measurement of delay time, we may examine the behavior of the derivative of function $y(\tau)=y_c(\tau)+y_ш(\tau)$ at the moment of reading. When the signal/noise ratio is large, the random errors are not large. Therefore, if we expand the derivative of signal function $y'_s(\tau)$ into a Taylor series in the vicinity of $\tau_0$ and limit outselves to the two first terms, we obtain

$$y'(\tau)\approx y'_c(\tau_0)+\Delta\tau y''_c(\tau_0)+y'_ш(\tau), \qquad (7.6)$$

where $y'_s(\tau_0)$ and $y''_s(\tau_0)$ are the derivatives of the signal function at the point $\tau=\tau_0$.

During the moment when the receiver output function $y(\tau)$ is passing through the maximum (moment of reading) its derivative is equal to zero:

$$y'(\tau_0)=y'_c(\tau_0)+\Delta\tau y''_c(\tau_0)+y'_ш(\tau_0)=0.$$

Since at point $\tau=\tau_0$ derivative $y'_s(\tau_0)=0$, the error

$$\Delta\tau=\hat{\tau}-\tau_0=-\frac{y'_ш(\tau)}{y''_c(\tau)_{\tau=\tau_0}}. \qquad (7.7)$$

The error dispersion in the vicinity of $\tau=\tau_0$

$$\sigma_\tau^2=\frac{\overline{[y'_ш(\tau)]^2}}{[y''_c(\tau)]^2_{\tau=\tau_0}}, \qquad (7.8)$$

where the line over the square of the noise function indicates that it is averaged.

The physical meaning of Formula (7.8) can be understood from Fig. 7.2, where the first derivatives of the signal and noise functions at the receiver output $y'_s(\tau)$ and $y'_{sh}(\tau)$ are given, being obtained by differentiating output signal $y(\tau)$. As follows from a comparison of the derivative of signal function $y'_s(\tau)$ and the mean square value of the

derivatives of the noise function $\sqrt{\overline{[y'_{ш}(\tau)]^2}}$, measurement error $\sigma_\tau$ becomes smaller as noise component $y'_{sh}(\tau)$ decreases and as function $y'_s(\tau)$ bedomes steeper, that is, as $y''_s(\tau)$, the second derivative of the signal function, becomes larger.

In accordance with Formulas (7.5) and the rules of differentiation under the sign of the integral, we may write

$$y'_{ш}(\tau) = \frac{2}{E_0}\int_{-\infty}^{\infty} n(t)\frac{d}{dt}h(\tau - t)\,dt,$$

$$y'_{c}(\tau) = \frac{2}{E_0}\int_{-\infty}^{\infty} \frac{d}{dt}s(t-\tau_0)\frac{d}{dt}h(\tau - t)\,dt.$$

Inasmuch as the integral depends only upon the relative shift of the integrand, only one of these has been differentiated, and the time position of the other has been clamped. In taking the second derivative the position first of one integrand, and then of the other, is clamped.

If we substitute the obtained values $y'_{sh}(\tau)$ and $y''_s(\tau)$ into Formula (7.8), we obtain

$$\sigma^2_{\tau m} = \frac{\overline{\left[\frac{2}{E_0}\int_{-\infty}^{\infty} n(t)\,h'(\tau - t)\,dt\right]^2}}{\left[\frac{2}{E_0}\int_{-\infty}^{\infty} s'(t-\tau_0)\,h'(\tau - t)\,dt\right]^2_{\tau=\tau_0}}. \qquad (7.9)$$

The error dispersion depends upon the signal shape and the receiver characteristic, that is, upon the method of measurement; therefore, it has the subscript "m." We find the receiver pulse characteristic $h(t)$ at which the measurement error dispersion is smallest. The receiver possessing such a characteristic is optimum from the point of view of range measurement and achieves the maximum potential measurement accuracy for the assigned signal shape.

The error dispersion $\sigma^2_{\tau m}$ is minimum when the integral in the denominator has its maximum possible value at $\tau = \tau_0$. This integral is the function of the mutual correlation of functions $s'(t - \tau_0)$ and $h'(\tau - t)$;

this function characterizes their mutual resemblance. It will be maximum when both functions are identical, that is

$$\frac{d}{dt}h(t)=\frac{d}{dt}s(t_0-t)$$

or

$$h(t)=s(t_0-t).$$

Thus, the pulse characteristics of the optimum receiver for range measurement coincides with the characteristic of the adequate receiver which best isolates any information, and with the characteristic of the optimum receiver-detector. The receiver for range measurement differs from the latter only in the procedure by which the results of reception are utilized: in detection the fact that the receiver output signal has exceeded a given threshold is clamped, while in measuring range the moment during which this signal passes through the maximum is clamped.

Let us direct our attention to the following important circumstance. As is known, the signal shape is changed substantially when it passes to an optimum filter. For example, a rectangular pulse becomes triangular. From the point of view of measurement of range we are interested not in the signal shape (it is known to us beforehand) but in the information borne by the reflected signal, in the given case – the delay time. The delay time may be clamped as accurately by the peak of a triangular pulse as by the front of the initial rectangular pulse. Therefore, if the receiver band is made broader than is optimum so as to make the wave front steeper, this only leads to a loss, since with widening of the band the steepness of the signal front increases more slowly than the noise level, and the error dispersion increases.

However, many textbooks recommend that accuracy be heightened by selecting a receiver passband which is 2-5 times broader than optimum. These recommendations are useful when the accuracy of range reading is

known to be lower than the potential accuracy and is limited by the instrumental measurement error which is lower as the pulse front is steeper.

As has already been noted, the output function of the optimum receiver is the logarithm of the probability ratio

$$l(\tau)=l_c(\tau)+l_{ш}(\tau),$$

where

$$l_c(\tau)=\frac{2}{E_0}\int s(t-\tau_0)s(t-\tau)\,dt \qquad (7.10)$$

is the signal function, while

$$l_{ш}(\tau)=\frac{2}{E_0}\int n(t)s(t-\tau)\,dt \qquad (7.11)$$

is the output noise function of the optimum receiver.

The probability ratio component, not depending upon $\tau$, has been eliminated since it has no influence upon range measurement, and is taken into account only in selecting a threshold quantity in receiver-detectors.

The value of the signal function at the point $\tau = \tau_0$ is numerically equal to the signal/noise energy ratio

$$l_c(\tau_0)=\frac{2}{E_0}\int s^2(t-\tau_0)\,dt=\frac{2E_s}{E_0}, \qquad (7.12)$$

where $E_s=\int s^2dt$ is the full signal energy. The factor 2 in Formula (7.12) is determined by the fact that comparison is made between the peak value of the signal and the effective value of the noise. In a sinusoidal signal the amplitude is $\sqrt{2}$ times greater than the effective value, and this yields a factor of 2 when converted to power (energy).

The dispersion of the noise component at the output of an optimum filter is also equal to this ratio. Actually,

$$\overline{l_{ш}^2(\tau_0)}=\overline{\left[\frac{2}{E_0}\int_0^T n(t)s(t-\tau_0)\,dt\right]^2}=\frac{4}{E_0^2(2F_m)^2}\overline{\left(\sum_i^{2F_mT} n_i s_i\right)^2}=$$

$$= \frac{1}{\sigma_ш^4} \sum_{i}^{2F_m T} \overline{n_i^2 s_i^2} = \frac{2}{E_0} \int_0^T s^2(t-\tau_0)\,dt = \frac{2E_s}{E_0}. \qquad (7.13)$$

Here we utilized discrete representations of the function and the relations known before:

$$E_0 F_m = \sigma_ш^2, \quad \overline{n_i^2} = \sigma_ш^2, \quad \int_0^T yz\,dt = \frac{1}{2F_m} \sum_{i}^{2F_m T} y_i z_i.$$

The ratio of the square of the signal function at moment $\tau = \tau_0$ to the dispersion of the noise function (signal/noise ratio at the receiver output with respect to power)

$$\frac{2P_{с вых}}{P_ш} = \frac{l_c^2(\tau_0)}{l_ш^2(\tau)} = \frac{2E_s}{E_0}$$

is also equal to the signal/noise energy ratio.

It follows from the relations given above that the optimum receiver possesses the following remarkable property: the signal at its output is concentrated at the moment of the maximum in such a way that the signal/noise ratio at this moment is numerically equal to the ratio of the whole energy of the received signal $2E_s$ to the spectral density of the noise $E_0$, regardless of how this energy is dispersed over time in the receiver input.

Inasmuch as, in accordance with Formula (7.10), the signal output function $l_s(\tau_0)$ is a function of the signal autocorrelation $s(t)$, the degree of concentration of the signal at the receiver output (compression) will be greater as the signal spectrum is wider. Consequently, accuracy and resolution increase with widening of the signal spectrum.

## §7.3. POTENTIAL ACCURACY OF RANGE MEASUREMENT

The dispersion of the error with which delay time is measured in an optimum receiver $\sigma_{тр}^2$ is found by substituting its pulse characteristic $h(t) = s(t_0 - t)$ into Formula (7.9):

$$\sigma^2_{\tau n} = \frac{\overline{\left[\frac{2}{E_0}\int n(t)\,s'(t-\tau)\,dt\right]^2}}{\left[\frac{2}{E_0}\int s'(t-\tau_0)\,s'(t-\tau)\,dt\right]^2_{\tau=\tau_0}}. \qquad (7.14)$$

We make use of the results of the derivation of Formula (7.13), substituting function $s'$ in place of $s$. Then

$$\overline{\left[\frac{2}{E_0}\int n(t)\,s'(t-\tau)\,dt\right]^2} = \frac{2}{E_0}\int [s'(t-\tau)]^2\,dt.$$

Replacing the numerator of Formula (7.14) by the right side of the latter equation, and assuming $\tau = \tau_0$, we find

$$\sigma^2_{\tau n} = \frac{1}{\frac{2}{E_0}\int [s'(t-\tau_0)]^2\,dt}. \qquad (7.15)$$

This formuda characterizes the dependence of the potential accuracy of measuring delay time (range) upon signal shape $s(t)$. Let us recall that it was obtained for a large signal/noise ratio when the distribution law of the signal envelope (amplitude) may be assumed normal. In this case the following relation applies

$$\overline{[l'(\tau)]^2_{\tau=\tau_0}} = \overline{[l'_c(\tau) + l'_{sn}(\tau)]^2_{\tau=\tau_0}} = [l'_c(\tau_0)]^2 +$$
$$+ 2l'_c(\tau_0)\,\overline{l'_{sn}(\tau_0)} + \overline{[l'_{sn}(\tau_0)]^2} = \overline{[l'_{sn}(\tau_0)]^2} = \frac{2}{E_0}\int [s'(t-\tau_0)]^2\,dt,$$

since $l'_s(\tau_0) = 0$ (point of the maximum) and only the third term remain, its value having been determined above. Thus, the denominator in Formula (7.15) is nothing other than the average value of the square of the derivative of the logarithm of the probability ratio with respect to the measured parameter at $\tau = \tau_0$, and the formula may be rewritten in the following form

$$\sigma^2_{\tau n} = \frac{1}{\left[\frac{d}{dt}\dot{l}(\tau)\right]^2_{\tau=\tau_0}}. \qquad (7.16)$$

We have obtained the fundamental relation establishing a connection between the potential accuracy of measurement and the output signal of the optimum receiver. This relation may be demonstrated to be universal.

In the first place, it is applicable for any law of probability distribution and for any signal/noise ratio. Formula (7.15) is a particular instance of Relation (7.16) and is applicable only for a normal distribution law, that is, when the signal/noise ratio is sufficiently large or the out-of-phase noise component is suppressed by a phase detector.

In the second place, Relation (7.16) characterizes the potential measurement accuracy of any signal parameter if the derivative is selected with respect to this parameter. From this we may formulate the general law for evaluating accuracy: the mean square value of the minimum measurement error is the reciprocal of the mean square value of the derivative of the output signal of an optimum receiver with respect to the measured parameter at the point of reading.

Let us return to Relation (7.15). If we multiply and divide the denominator by $E_s = \int s^2(t-\tau_0)\,dt$, we obtain

$$\sigma^2_{\tau m} = \frac{1}{\frac{2}{E_0}\int s^2(t-\tau_0)\,dt \dfrac{\int [s'(t-\tau_0)]^2\,dt}{\int s^2(t-\tau_0)\,dt}}.$$

The first factor in the denominator is the signal/noise ratio $2E_s/E_0$ which we already know. The second factor, which has the dimensionality of the square of the frequency, is denoted as

$$\Delta f_e^2 = \frac{\int [s'(t-\tau_0)]^2\,dt}{\int s^2(t-\tau_0)\,dt}. \qquad (7.17)$$

Quantity $\Delta f_e$ is known as the effective width of the signal spectrum.

The general formula for evaluating range-measurement accuracy ultimately takes the form

$$\sigma^2_{\tau m} = \frac{1}{\frac{2E_s}{E_0}\Delta f_e^2}. \qquad (7.18)$$

Thus, the potential accuracy of measuring delay time (range) is determined by the signal/noise energy ratio and by the effective spectral

band of the signal. Other signal parameters, in particular, length, play no role. It follows from this that pulse and continuous systems with frequency modulation are potentially of identical accuracy at identical $2E_s/E_0$ and $\Delta f_e$. Therefore, as will be demonstrated below, by artificially widening the spectrum it is possible to obtain a high degree of accuracy when using broad pulses.

In order to clarify the obtained result and the physical meaning of the effective width of the signal spectrum $\Delta f_e$, let us examine a pulse of the simplest shape – a bell-shaped pulse.

Actual radar signals are almost bell-shaped, and the passband of the filters of a multistage UPCh is nearly optimum for these pulses.

When the amplitude is unitary, the bell-shaped pulse (envelope) has the appearance

$$s(t)=e^{-\frac{\pi t^2}{\tau_u^2}},$$

where $\tau_1$ is the pulse length read at the level $e^{-\pi/4} \cong 0.45$ (approximately at the half-amplitude level).

The signal derivative with respect to time

$$s'(t)=-\frac{2\pi t}{\tau_u^2}e^{-\frac{\pi t^2}{\tau_u^2}}.$$

When calculating the effective band $\Delta f_e$ from Formula (7.17) we assume $\tau_0 = 0$, since the result is true at any $\tau_0$. In addition, we make use of tabular integrals

$$\int_0^\infty t^2 e^{-a^2t^2}dt=\frac{\sqrt{\pi}}{4a^3},\quad \int_0^\infty e^{-a^2t^2}dt=\frac{\sqrt{\pi}}{2a}.$$

Inasmuch as a bell-shaped pulse theoretically extends from $-\infty$ to $+\infty$, we substitute the limit given in Formula (7.17). After doing the necessary calculation (assuming $a^2 = 2\pi/\tau_1^2$) we obtain

$$\int_{-\infty}^{\infty} [s'(t)]^2 dt = \frac{8\pi^2}{\tau_u^4} \frac{\sqrt{\pi}}{4\left(\frac{2\pi}{\tau_u^2}\right)^{\frac{3}{2}}},$$

$$\int_{-\infty}^{\infty} s^2(t)\, dt = 2\frac{\sqrt{\pi}}{2\left(\frac{2\pi}{\tau_u^2}\right)^{\frac{1}{2}}},$$

$$\Delta f_e^2 = \frac{\pi}{\tau_u^2} \text{ and } \Delta f_e = \frac{\sqrt{\pi}}{\tau_u}. \qquad (7.19)$$

The spectrum of a bell-shaped pulse is also bell-shaped

$$S(f) = S_0 e^{-\frac{\pi f^2}{\Delta f^2}},$$

where $\Delta f = \frac{1}{\tau_u}$ is also measured at the level $e^{-\frac{\pi}{4}} \cong 0{,}45$ ; therefore $\Delta f_e = \sqrt{\pi}\Delta f \cong 1{,}8\Delta f$.

Thus, the effective spectral width of a bell-shaped pulse $\Delta f_e$ and its length $\tau_i$ are connected by the relation $\Delta f_e \tau_u = \sqrt{\pi}$ , if the reading is done at the 0.45 level with respect to amplitude. Similar results are obtained for pulses of any other very simple shape if the reading levels are selected in the appropriate way.

As has been pointed out, the signal/noise energy ratio at the point $\tau = \tau_0$ is

$$\frac{2E_s}{E_0} = a^2 n,$$

where $a$ is the ratio of the pulse amplitude to the mean square noise value, while $n$ is the number of effectively integrated pulses.

Substituting the values of $\Delta f_e$ and $2E_s/E_f$ into Formula (7.18), after extracting the root, we obtain

$$\sigma_{\tau u} = \frac{\tau_u}{\sqrt{\pi a^2}}. \qquad (7.20)$$

When pulses of very simple shape are used the obtained relation yields a result of trivial simplicity: the mean square range-measure-

ment error is proportional to the pulse length and inversely proportional to the signal/noise ratio with respect to voltage in the total signal. What is difficult is to define these quantities correctly. The obtained result is valid when the signal/noise ratio $a > 1$ is sufficiently large in a single pulse during noncoherent reception or when the signal/noise ratio $a\sqrt{n} > 1$ is large in the total signal during coherent reception.

In autotrack systems the number of pulses $n = F_p T_i$, where $F_p$ is the pulse repetition frequency, and $T_i$ is the time constant of the integrator. In scanning systems the number of effectively integrated pulses $n$ is determined from the known formulas (see Chapter 5).

The mean square value of the random error, determining the potential accuracy of range measurement is associated with time measurement errors by the well-known relation

$$\sigma_{\Delta R\Sigma} = \frac{c}{2}\sigma_{\Delta\tau\Sigma}. \qquad (7.21)$$

In range-differentiating systems measurement is made of the delay time between two received signals. If we denote the error dispersion of the measurement of the time of arrival of one signal by $\sigma^2_{\tau 1}$, and of the other by $\sigma^2_{\tau 2}$, the error involved in measuring the intervals between two independent signals is determined by the sum of the dispersion:

$$\sigma^2_{\Delta\tau\Sigma} = \sigma^2_{\tau 1} + \sigma^2_{\tau 2},$$

while the error involved in measuring the difference in distances, characterizing the potential accuracy of range-differentiating systems,

$$\sigma_{\Delta R\Sigma} = c\sigma_{\Delta\tau\Sigma}. \qquad (7.22)$$

The measurement error in the non-optimum method of signal reception may be found from Relation (7.9) if the actual form of the receiver function $h(t)$ is substituted into it.

## §7.4. SELECTION OF THE OPTIMUM SIGNAL SHAPE FOR MEASURING RANGE

In order to select a shape of the emitted oscillations which will ensure the highest accuracy of range measurement, it is convenient to represent the effective spectral width $\Delta f_e$ as a function of complex signal spectrum $S(f)$. We use the Parseval equality

$$\int_{-\infty}^{\infty} s^2(t)\,dt = \int_{-\infty}^{\infty} |S(f)|^2\,df,$$

where $|S(f)|^2 = S(f)S^*(f)$, and the Fourier transformation

$$S(f) = \int_{-\infty}^{\infty} s(t)\,e^{-j2\pi ft}\,dt.$$

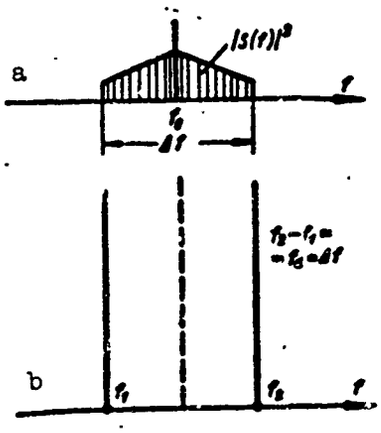


Fig. 7.3. Selection of the signal shape which will ensure maximum range-measurement accuracy: a) Signal spectrum of arbitrary shape; b) optimum signal spectrum.

By differentiating the last equality over time, we obtain

$$\frac{d}{dt}S(f) = \int_{-\infty}^{\infty} s'(t)\,e^{-j2\pi ft}\,dt - j2\pi f\int_{-\infty}^{\infty} s(t)\,e^{-j2\pi ft}\,dt = 0,$$

since $S(f)$ is not a function of time. The first integral expresses the spectrum of signal derivative $S'(f)$; the second integral expresses the spectrum of the signal itself $S(f)$. Thence

$$S'(f) = j2\pi f S(f),$$

and the Parseval equality for the signal derivative $s'(t)$ takes the form

$$\int_{-\infty}^{\infty} |s'(t)|^2 dt = (2\pi)^2 \int_{-\infty}^{\infty} f^2 |S(f)|^2 df.$$

By replacing the right side of the Parseval equality for a signal by its derivative in Formula (7.17), we obtain*

$$\Delta f_e^2 = (2\pi)^2 \frac{\int f^2 |S(f)|^2 df}{\int |S(f)|^2 df}. \qquad (7.23)$$

Inasmuch as the potential range-measurement accuracy increases with increase in $\Delta f_e$, it is necessary to search for a function $S(f)$ which will maximize the value of $\Delta f_e$ in the presence of certain limiting conditions. One such condition is that the signal spectrum $\Delta f$ should be full.

Figure 7.3a shows the square of the modulus of a certain spectral function of a signal with spectral width $\Delta f$. We may note in an analogy with mechanics that Formula (7.23) expresses the central moment of the inertia depicted on the drawing of the figure. As is known, the moment of inertia is maximum when the whole "mass" of the figure is concentrated at the edges of the assigned section, that is, when the signal consists of two harmonic components $f_1$ and $f_2$ separated by interval $f_d = \Delta f$ (Fig. 7.3b). We obtain phase systems of range measurement operating with two waves.

Single-wave phase systems may be visualized as two-wave systems in which the frequency of one component and, consequently, its phase lead, are equal to zero. Therefore, instead of measuring a phase difference, it is possible, in principle, to measure the phase of a single sinusoidal oscillation with frequency $f_0 = f_d$.

Thus, the phase method of measuring range examined in Chapter 2 possesses the greatest potential accuracy. As has been noted, this meth-

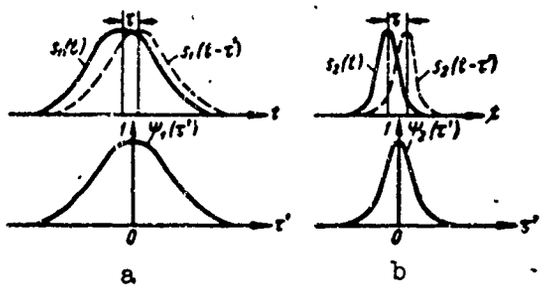

a b

Fig. 7.4. Signals of very simple shape and their correlation function, characterizing resolution and accuracy: a) Broad pulses (narrow spectrum); b) narrow pulses (broad spectrum).

od possesses certain drawbacks. In the first place, when the spacing of frequencies $f_d$ is sufficiently great, reading starts to be ambiguous, and part of the signal energy must therefore be expended on additional frequency components in order to form single-value scales, that is, a deviation from the optimum method. In the second place, there is no range resolution.

Therefore, the phase method of measuring range is the best for cases when observation is known to be limited to a single target, and ambiguity may be excluded (for example, by continuous tracking of a target from a known distance). When measuring the range of many targets it is necessary to provide range resolution.

Two targets are resolved with respect to range if their signals may be observed separately at the receiver output. The signals of two punctiform targets have the form of emitted oscillations $s(t)$ and differ from one another only in their amplitudes and time shifts $\tau'$, which are proportional to the distance between the targets. We are interested only in the time shift and therefore assume the amplitudes to be identical.

The degree of resemblance between two identical signals of the form $s(t)$, separated by interval $\tau'$, is evaluated, as is known, by the normalized autocorrelation function

$$\Psi(\tau') = \frac{1}{E_s} \int_{-\infty}^{\infty} s(t)\, s(t-\tau')\, dt, \qquad (7.24)$$

where $E_s$ is the value of the integral at $\tau' = 0$ (signal energy). In view of this $\Psi(0) = 1$, which indicates complete resemblance of both signals and the impossibility, in principle, of distinguishing them at $\tau' = 0$. With increase in $\tau'$ the function $\Psi(\tau')$ decreases, and a peak is therefore formed in the vicinity of $\tau' = 0$. The sharper this peak, the less the resemblance (correlation) between the signals at one and the same $\tau'$, and the easier it is to distinguish them (Fig. 7.4).

As follows from a comparison of Formulas (7.10) and (7.24), the signal proper at the output of an optimum receiver $z_s(\tau)$ coincide with accuracy up to a constant factor with the autocorrelation function $\Psi(\tau')$, if we assume $\tau_c - \tau = \tau'$. Consequently, the potential resolution is determined by the width of the signal peak at the output of the optimum receiver.

In the absence of noise one signal may in principle be distinguished from another regardless of how small the $\tau' \neq 0$ and with respect to any deviation of functions $\Psi(\tau')$ or $z_s(\tau)$ from the maximum value regardless of how small. Resolution is therefore limitless. In practice, noise is always present and limits it. Therefore resolution is a random quantity and depends upon the signal/noise energy ratio and also upon the rate of decline of function $\Psi(\tau')$ or $z_s(\tau)$.

The rate of decline of function $\Psi(\tau')$ increases, while the width of the peak (correlation time) declines, with broadening of signal spectrum $s(t)$, since the signal energy spectrum is a Fourier transformation of its autocorrelation function. Therefore, to heighten resolution it is necessary to broaden the signal spectrum. In the simplest case the signal spectrum is broadened by utilizing short pulses. In general, as will be demonstrated somewhat later, the spectrum may be broadened by

frequency (phase) modulation of the signal while its length is left unchanged.

Using Formula (7.23) it is easy to determine effective spectral width $\Delta f_e$ in the case of an even spectrum within the limits of the band $\Delta f$, assuming $S(f) = \text{const}$:

$$\Delta f_e^2 = (2\pi)^2 \frac{\frac{1}{3} f^3}{f} \Bigg|_{-\frac{\Delta f}{2}}^{\frac{\Delta f}{2}} = \frac{(2\pi)^2}{3} \frac{\Delta f^2}{4}.$$

Hence

$$\Delta f_e = \frac{\pi}{\sqrt{3}} \Delta f \approx 1{,}8 \Delta f.$$

The rate of decline of the output signal $l_s(\tau)$ or of the function $\Psi(\tau')$ also determines the accuracy of range measurement, since, when the peak is sharper, the position of its maximum is clamped more precisely. Actually, we differentiate Expression (7.24) twice; then

$$\Psi''(\tau') = \frac{1}{E_0} \int_{-\infty}^{\infty} s'(t) s'(t - \tau')\, dt.$$

By substituting this relation into Formula (7.15) we obtain

$$\sigma_{\tau\tau}^2 = \frac{1}{\frac{2\Sigma_0}{E_0} |\Psi''(0)|}. \qquad (7.25)$$

Consequently, increase in the resolution is accompanied by simultaneous increase in the accuracy of measurement. However, increase in the accuracy of measurement is not necessarily accompanied by a heightening of resolution; and this is the essential difference between them. Thus, the two-frequency phase method of measuring range examined above is not capable of resolution even though possessing high accuracy.

The reason for this is that, to obtain high resolution, the sharp peak of the output signal in the assigned range zone must be the only one. At the same time, to obtain a precise range reading it should also be sufficiently sharp but not necessarily the only one. Therefore, in

the first case the signal spectrum should be continuous, while in the second case it can be discrete. At the assigned spectral width the continuous spectrum is richer in harmonics and may carry more information. A discrete or discontinuous spectrum neither ensures an unambiguous reading at all times, nor, even less, does it ensure resolution.

Consequently, the requirement of a high degree of resolution is the most general requirement, and radar stations with a high degree of resolution are among the highest class of measuring systems.

Our general conclusion on the selection of a signal shape is as follows. If the ranges of a large number of targets are being measured, high measurement accuracy is achieved if the spectrum possesses a sufficiently large effective width $\Delta f_e$ and *is continuous*. To measure the range of an isolated target with the same accuracy the signal would have to have the same effective spectral width $\Delta f_e$; however, it may be discrete. In both cases as the signal/noise energy ratio $2E_s/E_0$ is considered to be identical.

Our final conclusion on the selection of a signal shape will be given in the analysis of the simultaneous measurement of range and radial velocity, since the frequency-time dependences in the signal are mutually dependent.

## §7.5. ACCURACY OF MEASURING RADIAL VELOCITY AND ANGULAR VELOCITIES

The measurement of target radial velocity $V_R = dR/dt$ may be reduced, as has been noted, to the measurement of the Doppler shift of the received signal frequency

$$F=\frac{2V_R}{c}f_0,$$

this being proportional to the emitted frequency $f_0$ (we eliminate the subscript $D$ of the letter $F$).

Having solved this formula for $V_R$, having differentiated it, and

converting to finite increments, we obtain the expression for the error in measuring radial velocity

$$\Delta V=\frac{\Delta cF}{2f_0}+\frac{c\Delta F}{2f_0}-\frac{cF}{2f_0^2}\Delta f.$$

The relative error

$$\frac{\Delta V}{V_R}=\frac{\Delta c}{c}+\frac{\Delta F}{F}-\frac{\Delta f}{f_0}.$$

Replacing the errors by the mean square values of σ and utilizing the law of their addition, we obtain

$$\left(\frac{\sigma_V}{V_R}\right)^2=\left(\frac{\sigma_c}{c}\right)^2+\left(\frac{\sigma_F}{F}\right)^2+\left(\frac{\sigma_f}{f_0}\right)^2. \qquad (7.26)$$

The first term in the right side of Equality (7.25) expresses the relative instability of the velocity of propagation; an evaluation of this has been given in the beginning of the chapter. The third term defines the relative instability of the frequency of the emitted oscillations; this is known for each individual RLS. The second term characterizes the mean square error of the measurement of the Doppler frequency, this being made up of instrumental error $\sigma_{Fi}$ and the error of the method of measuring $\sigma_{FM}$ ($\sigma_F^2=\sigma_{Fi}^2+\sigma_{FM}^2$). Both of these errors depend upon the degree of efficiency of the equipment.

In equipment which functions at a high degree of efficiency the instrumental error approaches zero, while the method error $\sigma_{Fm}$ approaches minimum quantity $\sigma_{Fp}$ characterizing the potential accuracy of measuring frequency.

In order to evaluate quantity $\sigma_{Fp}$ we may employ the relations obtained for $\sigma_{\tau p}$, establishing an analogy between frequency and time shift in the signal.

If we are not interested in the echo-signal delay, which is proportional to the target range, in the case of an emitted signal of the form $\cos 2\pi f_0 t$ the received signal may be represented as

$$\cos 2\pi t (f_0 - F).$$

If we are not interested in the frequency shift, which is proportional to the target radial velocity, the received signal takes the form

$$\cos 2\pi f (t - \tau),$$

where $\tau = 2R/c$ is the delay, while $f = f_0 - F$ is the frequency of the received signal.

A comparison of these two last dependences demonstrates the complete symmetry of the received signal relative to time and frequency. Therefore, all of the above conclusions relative to the accuracy of measuring time shift $\tau$ will also be valid for frequency shift $F$, if in the appropriate formulas the time and frequency characteristics are exchanged.

In accordance with this, the formula for the dispersion of the optimum measurement of the frequency shift, by analogy with Formula (7.17), takes the form

$$\sigma_{F_u}^2 = \frac{1}{\frac{2E_s}{E_0} T_e^2}. \qquad (7.27)$$

Here $T_e$ is the effective time of measurement, which may be determined, for example, by analogy with $\Delta f_e$ from Formula (7.23), as

$$T_e^2 = (2\pi)^2 \frac{\int s^2(t)\,dt}{\int s^2(t)\,dt}. \qquad (7.28)$$

where $s(t)$ is the envelope of the emitted signal. If the emitted oscillation is frequency modulated (complex modulation), it is necessary to take the absolute value of the square of the function $s(t)$. The obtained formulas, like the initial formulas, are valid for a sufficiently large signal/noise ratio.

These results yield the general properties of systems for measuring range and velocity.

Thus, the best signal shape for measuring the constant velocity of an isolated target during assigned observation time $T$ is a packet of two infinitely short pulses (delta-functions): one at thebeginning, the other at the end of interval $T$, with subsequent measurement of the difference in the times of their arrival. The spectrum of such pulses is continuous and, theoretically, infinitely wide. This signal may be compared with two sinusoids (two delta-functions on the frequency scale) of a phase range finder, which exists continuously during a theoretically infinite segment of time.

In practice what are used are not infinitely short, but simply short pulses, with length $\tau_i \ll T$. Velocity measurement consists of two measurements of range at interval $T$, that is, $V=\frac{(R_1-R_2)}{T}$. Then $\sigma_V = \frac{\sqrt{\sigma_{R_1}^2+\sigma_{R_2}^2}}{T}=\frac{\sqrt{2}\sigma_R}{T}$. Since $\sigma_R = \frac{c}{2}\sigma_\tau$, the mean square error when velocity is measured by the method of two fixes is

$$\sigma_{V_R}=\frac{c}{\sqrt{2}T}\sigma_\tau. \qquad (7.29)$$

However, this signal shape cannot be used to resolve two or more targets: the spectra of the signals of all of the targets overlap, and it is therefore impossible to separate them and measure the velocity of each target separately. In order to obtain high velocity resolution, high accuracy, and an unambiguous velocity reading the emitted signal should be continuous over the whole of observation interval $T$, just as a continuous spectrum over the whole of frequency interval $\Delta f$ was required for measuring range.

When a sinusoidal oscillation of constant intensity is emitted during interval $T$, the effective signal length, calculated from Formula (7.27), $T_e=\frac{\pi}{\sqrt{3}}T\cong 1{,}8T$. In the case of a bell-shaped pulse, we proceed by analogy with the conclusion of Formula (7.19) and also obtain

$$T_e = \frac{\sqrt{\pi}}{\Delta f} = \sqrt{\pi}\tau_u \approx 1{,}8\tau_u, \qquad (7.30)$$

where $\tau_i$ and $\Delta f$ are read at the 0.45 level of the maximum. The signal spectrum narrows with increase of $T_e$, and the accuracy of reading the Doppler frequency shift from the peak of the spectrum is therefore heightened, as well as the velocity resolution (with respect to frequency).

As regards the properties of the receiver for measuring velocity, they are to be radically distinguished from the properties of the range-measuring receiver.

It is known that the structure of the receiver does not have to be varied in order to receive a signal from different ranges. The range is read from the time at which the signal of the given target appears at the output of the common optimum filter.

It is in principle necessary to alter the structure of the optimum receiver (filter) in order to measure radial velocity. The resonance frequency to which the filter is tuned must coincide with the average frequency of the received signal, and this depends upon the Doppler velocity shift; otherwise the signal would fail wholly or partially to pass through the receiver output. The receiver must consist of an assembly of optimum filters, each tuned to its own Doppler frequency. Roughly speaking, velocity is read from the number of the filter at whose output the signal of the given target is detected.

In tracking only one filter need be used, and it is automatically tuned to the frequency of the received signal; target velocity is evaluated from the frequency to which it is tuned.

The potential accuracy with which target radial velocity is measured is determined by the error

$$\sigma_{V_R} = \frac{\lambda}{2}\sigma_{F_D}, \qquad (7.31)$$

since $F=\frac{2V_R}{\lambda}$ and $\Delta V_R=\frac{\lambda}{2}\Delta F$.

Velocity may also be measured in the video channel from the Doppler shift in the pulse repetition frequency

$$F=\frac{2V}{c}F_{\text{п}}.$$

Since $F$ is small in this case the velocity measurement accuracy is comparatively low.

We may, as an aside, briefly discuss the question of the potential accuracy of measurement of angular velocities.

As has been demonstrated in Chapter 2, target angular velocity is determined by the difference in the Doppler frequencies $F_{\text{д}} = F_1 - F_2$ of the target signals received on dispersed antennas. The dispersion of the measurement error of the frequency difference is equal to the sum of the dispersion of the measurement errors of each of the frequencies.

Consequently,

$$\sigma^2_{(F_1-F_2)\text{п}}=2\sigma^2_{F\text{п}},$$

where $\sigma^2_{Fp}$ is determined by Formula (7.27). Then, applying Formula (2.13) from Chapter 2, we find the mean square error

$$\sigma^2_{\text{ск}}=\frac{\sqrt{2}\sigma_{F\text{п}}}{\frac{b_A}{\lambda}\cos\varepsilon}, \qquad (7.32)$$

which determines the potential accuracy of the measurement of angular velocity.

The remaining types of velocity-measurement error, both external and those due to the equipment, may also be calculated by means of the corresponding frequency-measurement errors.

## §7.6. MEASURING THE RANGE AND RADIAL VELOCITY OF MOVING TARGETS. THE INDETERMINACY PRINCIPLE IN RADAR

In the observation of a moving target the echo-signal delay and

the Doppler shift of the frequency appear at the same time. Therefore, selection of the best signal shape must take into account the change in its parameters both with respect to range (from the time) and with respect to the velocity (from the frequency).

These dependences may not be considered separately. In the first place, the frequency and time relationships in the signal are interconnected. In the second place, measurement of range and measurement of velocity impose contradictory demands upon the signal. The resolution of these contradictions is precisely the task involved in the selection of a rational shape for the outcoming signal.

Let us examine the output signal of an optimum receiver in the presence of Doppler shift $F$ and in the absence of noise

$$l_c(\tau, F)=\frac{2}{E_0}\int_{-\infty}^{\infty} s(t)s^*(t-\tau)e^{-j2\pi Ft}dt, \qquad (7.33)$$

where the numerator $e^{-j2\pi Ft}$ takes into account frequency shift $F$ of signal $s(t)$, and the signal itself is generally assumed to be complex (modulated either in frequency or in phase). In the absence of a frequency or a time shift we obtain the maximum value of the output signal amplitude

$$l_c(0, 0)=\frac{2E_s}{E_0},$$

where $E_s$ is, as before, the full energy of the signal.

As has already been noted, the signal at the output of an optimum receiver may serve to characterize the range resolution, since it reproduces, with accuracy up to a constant factor, the autocorrelation function

$$\Psi(\tau', F')=\frac{1}{E_s}\int_{-\infty}^{\infty} s(t)s^*(t-\tau')e^{-j2\pi Ft}dt=$$

$$=\frac{1}{E_s}\int_{-\infty}^{\infty} S^*(f)S(f-F')e^{-j2\pi f\tau'}df. \qquad (7.34)$$

In general, this function is also complex. The second form of notation is derived from the first by using the Parseval theorem.

In the absence of a shift with respect to $\tau'$ and $F'$ function $\Psi(0.0) = 1$ is maximum, and in the presence of a time or frequency shift it decreases, forming a peak in the vicinity of the point 0.0 (Fig. 7.5). Thus, the function $\Psi(\tau', F')$ is a combined autocorrelation function of the signal with respect to time and frequency and may serve for simultaneous evaluation of resolution with respect to range and velocity. From it may be derived particular correlation functions with respect to time and frequency alone:

$$\Psi(\tau') \equiv \Psi(\tau', 0) = \frac{1}{E_s}\int_{-\infty}^{\infty} s(t)\,s^*(t-\tau')\,dt,$$

$$\Psi(F') \equiv \Psi(0, F') = \frac{1}{E_s}\int_{-\infty}^{\infty} S^*(f)\,S(f-F')\,df.$$

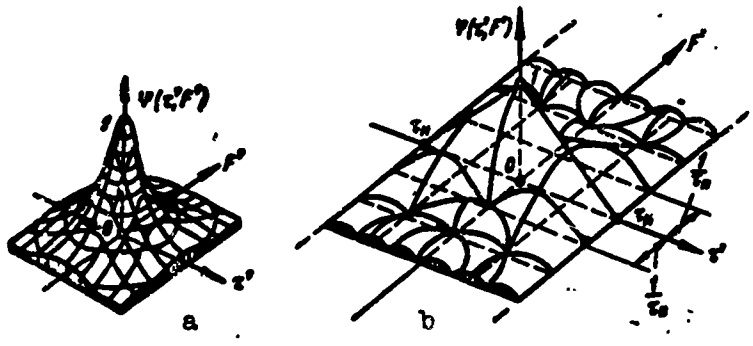


Fig. 7.5. Appearance of autocorrelation function with respect to time and frequency: a) Bell-shaped signals; b) rectangular signals.

The combined autocorrelation function $\Psi(\tau', F')$ also makes it possible to evaluate range-measurement accuracy using frequency detuning of an optimum receiver, as well as the accuracy of velocity measurement with a time shift relative to the moment of the maximum. Actually, by

employing formula (7.25) as well as the symmetry of function $\Psi(\tau', F')$ by comparison with $\tau'$ and $F'$, we obtain

$$\sigma_\tau^2 = \frac{1}{\frac{2E_s}{E_0}\frac{d^2}{d\tau^2}\Psi(0, F')}, \tag{7.35}$$

$$\sigma_F^2 = \frac{1}{\frac{2E_s}{E_0}\frac{d^2}{dF^2}\Psi(\tau', 0)}. \tag{7.36}$$

In the absence of detuning ($F' = 0$) and time shift ($\tau' = 0$) the above formulas characterize, respectively, the potential accuracy of measurement of range and velocity; in particular, at $F' = 0$, Formulas (7.25) and (7.35) coincide.

Finally, autocorrelation function $\Psi(\tau', F')$ is also convenient in that it can be used to discover the appearance of the envelope of the signal proper at the output of an optimum receiver for any frequency detuning. To do this it is necessary to pass the vertical plane $F' =$ = const, which is parallel to axis $\tau'$, through the figure depicted in Fig. 7.5. The trace of the section yields precisely the form of the signal envelope. Inthe figure it is demonstrated how the form of the output signal of matched filters changes due to action upon the input by bell-shaped and rectangular pulses from a frequency detuned filter.

As can be seen from the figure, the output signal has, in addition to a basic high correlation peak, an area of low correlation (the so-called side lobes) which may extend to infinity both in time and in frequency. The presence of side lobes inhibits observation of the signal of a second target close by, especially when this is weak by comparison with the signal of the first target.

To heighten measurement accuracy and range and velocity resolution, it is desirable to eliminate the side lobes, and to make the main signal (area of high correlation) as narrow as possible both with respect to $\tau'$ and with respect to $F'$. However, this cannot be done, since the

frequency and time characteristics of any signal are mutually dependent, and narrowing the signal in time is inevitably accompanied by a broadening of its spectrum.

The impossibility of heightening the potential resolution with respect to range and velocity at the same time is known as *the indeterminacy principle* in radar.

Before passing to a mathematical formulation of the indeterminacy principle let us examine the case where the signals of several targets whose side lobes overlap enter the receiver input. The areas of high correlation of the output signals form the target blips, and the side lobes, being added, form the hum. Inasmuch as the locations of the targets with respect to one another is arbitrary, the phase relations among the side lobes are random. Therefore, when there is a large number of targets, it may be considered that the average powers of the side lobes are summed, and not the amplitudes.

In this respect, it is advisable to examine how the signal power behaves at the output of an optimum receiver when there is a shift in time and frequency, that is, the function

$$|l_c(\tau, F)|^2 = l_c(t, f)\, l_c^*(t-\tau, f-F). \qquad (7.37)$$

If we multiply the integral expression (7.33) by a complex conjugate quantity, we obtain

$$|l_c(\tau, F)|^2 = \frac{4}{E_0^2}\int s(t)\, s^*(t-\tau)\, e^{-j2\pi Ft}dt \int s^*(t)\, s(t-\tau)\, e^{j2\pi Ft}dt^*.$$

We represent the obtained result as a compound integral with respect to $t_1$ and $t_2$; then the signal power at the receiver output

$$|l_c(\tau, F)|^2 = \frac{4}{E_0^2}\int\int s(t_1)\, s^*(t_1-\tau)\, s^*(t_2)\, s(t_2-\tau)\, e^{-j2\pi F(t_1-t_2)}dt_1 dt_2.$$

The obtained expression possesses one interesting property: its compound integral with respect to all values of $\tau$ and $F$ is equal to its

maximum value $l_s^2(0.0)$.

Actually

$$\iint |l_c(\tau, F)|^2 d\tau dF = \frac{4}{E_0^2} \iiint s(t_1) s^*(t_1 - \tau) s^*(t_2) \times$$
$$\times s(t_2 - \tau) e^{-j2\pi F(t_1 - t_2)} dt_1 dt_2 d\tau dF = \frac{4}{E_0^2} \iiint s(t_1) s^*(t_1 - \tau) \times$$
$$\times s^*(t_2) s(t_2 - \tau) \left[ \int e^{-j2\pi F(t_1 - t_2)} dF \right] dt_1 dt_2 d\tau.$$

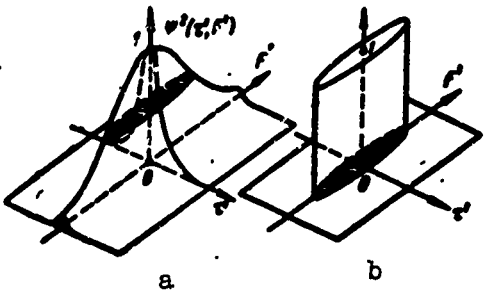

a b

Fig. 7.6. Solid of indeterminacy and its equivalent.

The inner integral is delta-function $\delta(t_1 - t_2)$, which is equal to zero at all values of $t_1$ and $t_2$ except for $t_1 = t_2$, when $\delta(0) = 1$. Therefore, integration with respect to $t_1$ and $t_2$ is reduced to integration only with respect to $t = t_1 = t_2$. Hence

$$\iint |l_c(\tau, F)|^2 d\tau dF = \frac{4}{E_0^2} \iint |s(t)|^2 |s(t - \tau)|^2 d\tau dt =$$
$$= \left| \frac{2}{E_0} \int |s(t)|^2 dt \right|^2 = l_c^2(0, 0), \qquad (7.38)$$

q.e.d.

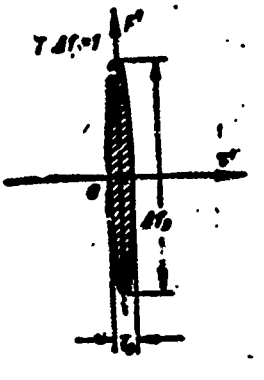

Fig. 7.7. Section of the solid (region of high correlation), equal in area to the volume of the solid of indeterminacy.

As has already been noted, the autocorrelation function $\Psi(\tau', F')$ of the input signal is similar to the output signal of the receiver $l_c(\tau, F)$, and, therefore, Relation (7.38) is also valid for it. If we denote the compound integral of the function $\Psi(\tau', F')$ with respect to all values of $\tau'$ and $F'$ as $V_{\Psi 2}$, we can write

$$V_{\Psi^2} = \int\int |\Psi(\tau', F')|^2 d\tau' dF' = \Psi^2(0, 0) = 1. \qquad (7.39)$$

And this is the fundamental mathematical formulation of the indeterminacy relation in radar.

From the point of view of the analysis of the indeterminacy relation it is convenient to use not the autocorrelation function $\Psi(\tau', F')$ but the indeterminacy function

$$\Psi^2(\tau', F') = \left| \int s(t) s^*(t - \tau') e^{-j2\pi F' t} dt \right|^2, \qquad (7.40)$$

which forms the spatial figure known as *the solid of indeterminacy* (Fig. 7.6). It is not hard to see that quantities $V_{\Psi 2} = 1$ is the volume of the solid of indeterminacy, which remains unchanged regardless of the signal shape $s(t)$. Change in the signal shape deforms the solid of indeterminacy without altering its volume. If we compress the solid in one direction, we inevitably expand it in the other; by improving the range parameters we cause the velocity parameters to deteriorate.

Thus the solid of indeterminacy is a graphic interpretation of the indeterminacy principle. The solid may be likened to a pile of sand the height of whose peak in the center is constant: regardless of how we deform it, the volume of the solid and the height of the peak remain unchanged.

A spatial figure is not suitable for graphic reproduction. Therefore, to depict the solid of indeterminacy we use the same technique as in representing relief on geographical maps – horizontal sections.

It is convenient to select a horizontal section of the figure such

that the product of the area of detection and the maximum altitude of the solid will be equal to its volume. In other words, the actual solid of indeterminacy is replaced by a cylinder of equal volume (Fig. 7.6b). Since the volume of the cylinder and its altitude are equal to unity, the area of the section is also equal to unity (area of indeterminacy).

Figure 7.7 is a graphic representation of the area of the section in the plane $\tau'F'$. The effective dimension of the area of indeterminacy with respect to the axis $\tau'$ is denoted by $T$, and with respect to the axis $F'$ by $\Delta f$. Since the area is equal to unity, while the effective linear dimensions of the figure, $T$ and $\Delta f$, are found by replacing the figure by a rectangle of the same size, we may write

$$T\Delta f=1. \tag{7.41}$$

And this is the mathematical formulation of the indeterminacy principle in radar for signals of very simple shape: a single pulse or a continuous oscillation without frequency (phase) modulation. When the pulses are short, the area of indeterminacy is extended along the axis $F'$, in the case of continuous emission – along the axis $\tau'$. Relation (7.41) characterizes the combined resolution, while the combined accuracy with respect to range and velocity is characterized, according to Formulas (7.19) and (7.30), by the product $\Delta f_{\text{э}}T_{\text{э}}=\pi\Delta fT=\pi$.

A rapid glance at Relation (7.41) could lead to the hasty conclusion that the selection of a signal shape is a trivial matter: if you want to improve range, reduce the pulse length, and in that way you widen its spectrum; if you want to improve velocity, narrow the spectrum by increasing the signal length. Naturally, in the case of signals of more complex shape, the solid of indeterminacy has new properties which, with certain sensible limitations, make possible an additional gain without violation of the general principle of indeterminacy.

Usually not one, but several pulses, are received from the target.

Let us examine a signal in the form of a bell-shaped pulse packet with length $\tau_1$ and repetition period $T_p$, the pulse amplitude envelope also being bell-shaped.

Under these conditions, the correlation function with respect to time $\Psi(\tau', 0)$ (signal at the output of an optimum receiver) will also look like the pulses of the same period, while the correlation function with respect to frequency $\Psi(0, F')$ (the signal spectrum at the output of an optimum receiver) takes the form of discrete bands separated by interval $F_p = 1/T_p$. The solid of indeterminacy will consist of a series of peaks (Fig.7.8).

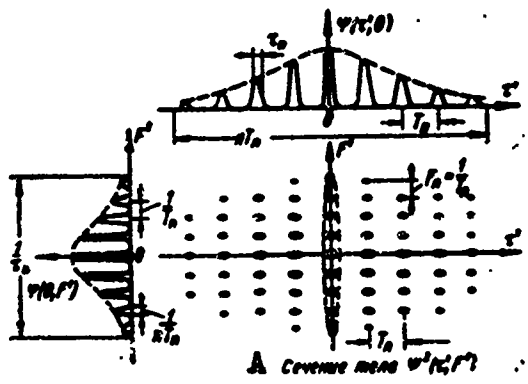

Fig. 7.8. Section of a solid of indeterminacy when the signal takes the form of a series of several pulses; appearance of the correlation functions along the main axes: A) Section of the solid.

The total volume of the solid of indeterminacy, and also the total area of its sections, remain equal to unity. For purposes of comparison, the dashed line in Fig. 7.8 encloses the sectional area of the solid of indeterminacy for a single pulse, which is equal to the sum of all of the shaded areas.

The effective width of the spectrum $\Delta f_e$ and, consequently, the accuracy of range measurement, remain unchanged during the transition from one pulse to several. However, effective signal length $T_e$ has increased substantially, and the accuracy of measurement of velocity has

therefore increased substantially: inthe case of a single pulse $T_{e1} \cong \sqrt{\tau_u}$ and in the case of $n$ pulses $T_{en} \cong \sqrt{nT_n}$ and the accuracy increases $T_{en}/T_{el} = nq$ times, where $q = T_p/\tau_i$ is the reciprocal duty factor.

Thus, the product $\Delta f_e T_e = \pi \Delta f n T_n \gg \pi$. The combined accuracy of measurement of range and velocity has increased substantially and may be heightened still further. However, the combined resolution has not changed, and the principle of indeterminacy is not violated, regardless of the fact that $\Delta f T = \Delta f n T_n \gg 1$.

We introduce the concept of the frequency extension $\Delta F_\Sigma$ and the time extension $T_\Sigma$. The frequency extension is the width of the discrete spectrum when all empty sections have been discarded. Accordingly, the time extension is equal to the signal length minus the empty sections.

From Fig. 7.8 it can be seen that the number of discrete bands of the spectrum separated by interval $F_n = \frac{1}{T_n}$ within the limits $\Delta f$ is $\Delta f : F_n = \Delta f T_n$. Since the width of one band is equal to $1/nT_p$, the frequency extension, equal to the total width of all bands

$$\Delta F_\Sigma = \frac{1}{nT_n} \Delta f T_n = \frac{\Delta f}{n}.$$

When the length of one pulse $\tau_u \cong \frac{1}{\Delta f}$ the time extension of the signal is equal to the total length of all $n$ pulses:

$$T_\Sigma = \frac{n}{\Delta f}.$$

Thus, in radar the indeterminacy relation for the compound signal

$$T_\Sigma \Delta f_\Sigma = 1 \qquad (7.42)$$

is formulated mathematically as follows: *the product of the frequency and time extensions of the signal is unity.*

Expansion of the solid of indeterminacy into discrete segments leads to a new phenomenon – ambiguity of the reading, which is a part of the concept of resolution. Thus, the signals of two targets separated

by single-value interval $T_p$ (or by whole number $T_p$) will not be distinguished, since they fall into discrete regions of ambiguity (see Fig. 7.8).

To eliminate ambiguity of the range reading the pulse repetition period $T_p$ is selected on the basis of the condition

$$T_n < \frac{2R_{max}}{c}, \qquad (7.43)$$

where $R_{max}$ is the operating range of the RLS. Under this condition the distance between any two targets within the scanning zone will be less than $R_{max}$, and the interval between their signals will be less than the single-value interval $T_p$.

The question of ambiguity with respect to velocity is resolved in an analogous manner. The only difference is that the Doppler shift of one target may be positive and of another – negative. Therefore, the single-value interval with respect to frequency is $\pm F_p/2$ and the uniquely measured Doppler frequency

$$|F_A| < \frac{F_n}{2} \qquad (7.44)$$

or

$$|V_R| < \frac{\lambda F_n}{4}.$$

In the presence of Limitations (7.43) and (7.44) with respect to range and velocity the total volume of the solid of indeterminacy, except for its central peak, plays no role. Therefore, the combined resolution is determined by the volume of the central peak alone, and this is considerably less than unity. It follows from this that when range and velocity are being measured at the same time a signal in the form of a pulse series is preferable to a single pulse.

However, Condition (7.44) is satisfied in practice only with respect to targets moving at very low velocities; therefore, the velocity of the remaining targets remains ambiguous. An additional velocity mea-

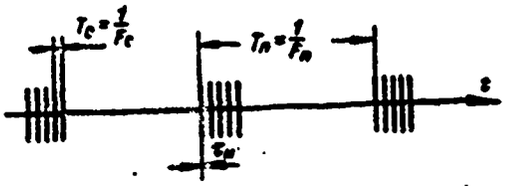

Fig. 7.9. The pulse-packet signal.

surement from the Doppler shift of the repetition frequency $F_d = \frac{V_R}{c} F_p$ can eliminate the ambiguity of velocity measurement; however, the resolution with respect to range and velocity remains unchanged.

To heighten the uniquely measured Doppler frequency at the assigned repetition period $T_p$, the pulse-packet method of operation is also employed: instead of single pulses, in each period pulse packets are emitted with a nigh repetition frequency $F_s$ of the pulses within the packet (Fig. 7.9). Then the single-value integral with respect to velocity $F_s/2$ increases substantially, since $F_s >> F_p$. In this case the resolution with respect to velocity also increases, but the resolution with respect to range decreases. The pulse-packet method has been applied in Doppler RLS for measuring ground speed where the only "target" is the earth's surface, and range resolution plays no role. It is important to separate the times of transmission and reception. With the pulse-packet method the solid of indeterminacy is broken up even further.

Let us recall that, together with the signal proper $l_s(\tau, F)$, there is a noise component $l_{sh}(\tau, F)$, at the output of the optimum receiver which hinders the resolution of signals of adjacent targets. Therefore, the potential resolution is a static characteristic of the signal, depending upon the signal/noise ratio $2E_s/E_0$.

In concluding this section let us note that the optimum coherent

receiver used to measure range and velocity, like the coherent receiver used for detecting moving targets, contains several channels tuned to different frequencies. Radio velocity is determined from the number of the channel, and range is determined from the delay time.*

The decision not to measure velocity does not simplify the structure of the optimum receiver. Only the resolving device is simplified: when velocity is measured this device is placed at the output of each channel, and when velocity is not measured, the outputs of the channels are combined and only a single resolver is employed (a detector and delay-time meter). In noncoherent reception velocity is not measured, and the receiver is practically as simple as in measuring the range of a stationary target.

## §7.7. THE EMPLOYMENT OF SIGNALS OF COMPLEX SHAPE. PULSE COMPRESSION

Up until now we have been examining signals of the most simple shape: continuous emission of a carrier, a single sinusoidal pulse signal, a packet of such pulses, etc. It was shown that within certain limitations it is possible to overcome the effect of the principle of indeterminacy but not to abolish it. The limitations applied for the maximum delay time and the Doppler frequency shift. Thanks to this a considerable part of the solid of indeterminacy turned out to be outside the limits of the indicated time-frequency region.

An analysis of the behavior of the indeterminacy function $\Psi^2(\tau; F')$ for various signals makes it possible to synthesize signals of complex shape which, with other acceptable limitations ensure a high combined range and velocity resolution, high accuracy ,and the absence of ambiguity in measurement. The employment of complex signals is also advisable when it is technically difficult to achieve the assigned RLS characteristics for signals of the most simple shape.

The general idea of shaping complex signals consists in artificial-

ly widening the spectrum $\Delta f$ of a pulse, when the assigned pulse length $\tau_n = T$; the product is then

$$\Delta f T = N \gg 1. \qquad (7.45)$$

The width of the signal spectrum with respect to the high frequency $\Delta f = 2F_m$, where $F_m$ is the maximum frequency in the spectrum of the video signal (the envelope). Hence $N = \Delta f T = 2F_m T$ is the number of independent readings in the signal, that is, the number of degrees of freedom.

Thus, signals in which the number of degrees of freedom $N >> 1$ are known as complex signals. Simple signals have one degree of freedom $N = \Delta f T = 1$. In the case of pulse signals $T = \tau_i$.

The spectrum is widened by modulating the signal within the limits of its length, mainly with respect to frequency for phase (complex signal). By selecting a sufficiently wide spectrum $\Delta f$ a high degree of measurement accuracy and a high degree of range resolution are assured; selection of signal length $T$ yields the necessary velocity measurement accuracy and the corresponding resolution.

A modulation law is selected such that the solid of indeterminacy has no supplementary peaks giving rise to ambiguity in the reading, and also such that it is convenient to form and generate a complex signal in the transmitter and process it in the receiver.

1. Frequency-Modulated Pulses

There is one way to change the shape of the solid of indeterminacy which is deserving of separate discussion. This involves the application of frequency-modulated pulses with a linear law of change of frequency. As pulse length is increased, a continuous frequency-modulated oscillation is obtained at the limit.

The effective length of frequency-modulated signal $T_e$ corresponds to pulse length $\tau_i$, while the effective spectral width $\Delta f_e$ during deep modulation is approximately equal to the frequency deviation $\Delta f$. By se-

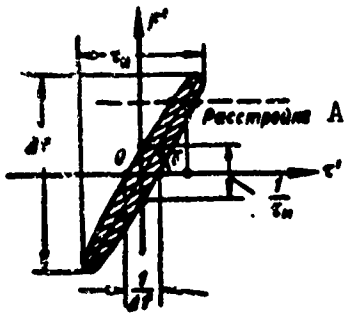


Fig. 7.10. Section of the solid of indeterminacy of frequency-modulated pulses. A) Detuning.

lecting a signal of sufficient length and with deep modulation ($\Delta f\tau_и \gg 1$) it is possible to obtain high range and velocity measurement accuracy at the same time. And the resolution increases in proportion.

To evaluate the limitations imposed by the indeterminacy principle upon optimum range and velocity measuring systems in the case of a signal of this shape, let us examine the section of a solid of indeterminacy which corresponds in shape with the output signal of a detuned optimum receiver. The solid looks like a mountain ridge turned by angle $\gamma$ toward axis $\tau'$, this angle characterizing the speed of frequency change (Fig. 7.10). The area of indeterminacy and the volume of the solid of indeterminacy remain, as

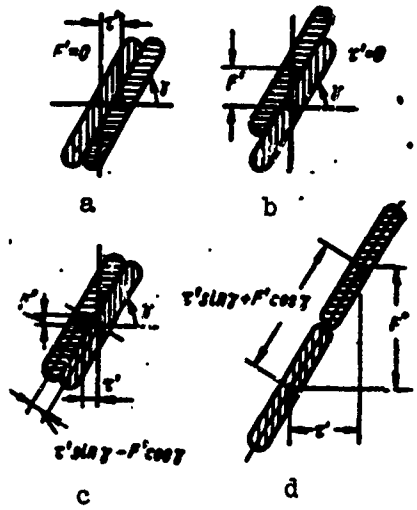


Fig. 7.11. Combined range and velocity resolution with a frequency-modulated pulse: a) Range resolution only; b) velocity resolution only; c) the best combined range and velocity resolution; d) the worst combined range and velocity resolution.

before, equal to unity.

If the solid of indeterminacy is turned by angle $\gamma$, this causes the

section of the solid of indeterminacy along each of the two axes to be narrow. The pulse length at the output of an optimum filter, equal to $1/\Delta f$, determines accuracy and resolution only with respect to range. Accordingly, the size of the solid along the coordinate $F'$, equal to $1/\tau_i$, characterizes accuracy and resolution only with respect to velocity.

The situation is more complicated when it comes to combined evaluation of accuracy and resolution with respect to both range and velocity. For this we refer to Fig. 7.11 which gives the various ways of resolving the signals of two targets. The upper part of the figure corresponds to the case already examined by us, of resolution only with respect to one of the parameters – either range or velocity.

The lower row shows two extreme instances of combined resolution with respect to range and velocity, where the relations between the differences of the two targets with respect to range and velocity are favorable and unfavorable. The least favorable case of resolution is displacement of the signals along the major axis of symmetry of the solid. It occurs when the difference in the ranges of the two targets $\Delta R$ and the difference of their velocity $\Delta V_R$ are found in the relation

$$\operatorname{arc\,ctg}\frac{\tau'}{F'} = \operatorname{arc\,ctg} f_0 \frac{\Delta R}{\Delta V_R} = \gamma.$$

The best case of combined resolution, displacement along the minor axis of symmetry, occurs when the relation is the inverse $\left(=\frac{1}{\gamma}\right)$.

In an analogous manner, the combined measurement accuracy will be the worst when range $R$ and velocity $V_R$ of the given target satisfy the relation $\operatorname{arc\,ctg} f_0 \frac{R}{V_R} = \gamma$.

Thus, the combined evaluation of range and velocity will be good if the comparatively rare cases of unfavorable relations among them are excluded, that is, if limitations are introduced.

Relative detuning of the optimum filter (through the Doppler ef-

fect) has hardly any influence on the mean square range measurement error. However, there does appear a systematic range error (displacement of the output signal maximum) which is proportional to velocity (see Fig. 7.10). This displacement may be ignored at low velocities. And the range velocity error may be eliminated at high velocity by using a signal with a symmetrical frequency-modulation law; the section of the solid of indeterminacy of such a signal is shown in Fig. 7.12.

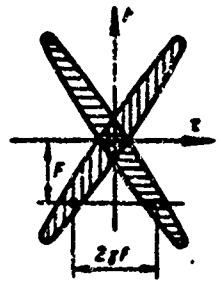


Fig.7.12. Section of the solid of indeterminacy of a signal with symmetrical linear frequency modulation.

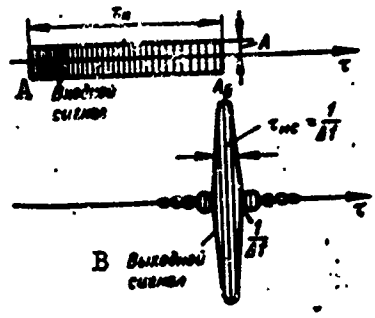


Fig. 7.13. Illustration of the process of compression of a frequency-modulated pulse in a universal filter on a delay line with taps. A) Input signal; B) output signal.

When the frequency of a symmetrically modulated signal is displaced relative to the tuning frequency of an optimum receiver due to the Doppler effect, two symmetrically displaced pulses are formed at the receiver output. The distance between the two pulses is proportional to velocity, and the position of the midpoint between them is proportional to the target range. The output of one receiver channel yields indepen-

dent information on range and velocity. However, when there is a large number of targets, it is difficult to determine which pair of pulses belongs to one target and which to another.

If we make a quantitative evaluation of the degree of compression of a frequency-modulated pulse with a rectangular envelope which is symmetrical relative to moment $t_0$

$$s(t)=\begin{cases} A \text{ for } t_0-\frac{\tau_u}{2}\leqslant t\leqslant t_0+\frac{\tau_u}{2}, \\ 0 \text{ for } t-t_0|>\frac{\tau_u}{2}. \end{cases}$$

When frequency modulation is linear $\left(\operatorname{tg}\gamma=\frac{\Delta f}{\tau_u}\right)$, frequency may be represented as a function of time in the form

$$f=f_0-\frac{\Delta f}{\tau_u}(t-t_0)$$

or

$$f-f_0=-\frac{\Delta f}{\tau_u}(t-t_0).$$

Thus, the frequency function coincides with the time function with accuracy up to a constant factor. Therefore, the spectrum $S(f)$ of a rectangular frequency-modulated pulse also has the appearance of a rectangular "pulse" with extension $\Delta f$ (valid on the condition $\Delta f\gg\frac{1}{\tau_u}$):

$$S(f)=\begin{cases} B \text{ for } f_0-\frac{\Delta f}{2}\leqslant f\leqslant f_0+\frac{\Delta f}{2}, \\ 0 \text{ for } |f-f_0|>\frac{\Delta f}{2}. \end{cases}$$

It should be taken into consideration that in frequency modulation the spectrum is a complex function

$$S(f)=|S(f)|\,e^{j\varphi_s(f)},$$

where $\varphi_s(f)$ is the phase-frequency characteristic of the signal (a squared phase dependence corresponds to the linear change in frequency). The transmission function of an optimum filter is a complex conjugate function of the spectrum

$$K(f)=S^*(f)=|S(f)|\,e^{-j\varphi_s(f)}.$$

Then the signal spectrum at the output of an optimum filter becomes a material quantity

$$L_s(f)=S(f)S^*(f)=|S(f)|^2=\begin{cases}B^2 \text{ for } f_0-\frac{\Delta f}{2}\leqslant f\leqslant f_0+\frac{\Delta f}{2},\\ 0 \text{ for } |f-f_0|>\frac{\Delta f}{2}.\end{cases}$$

We find the signal itself at the output of the optimum filter as a Fourier transformation of its spectrum:

$$l_s(\tau)=\int L_s(f)\,e^{j2\pi f\tau}df=B^2\int\limits_{f_0-\frac{\Delta f}{2}}^{f_0+\frac{\Delta f}{2}}e^{j2\pi f\tau}df=\frac{B^2}{\pi\tau}\frac{e^{j\pi\Delta f\tau}-e^{-j\pi\Delta f\tau}}{2j}.$$

According to the Euler formula the last factor is sin $\pi\Delta f\tau$. Then, assuming $B^2\Delta f = A_V$, we obtain the final expression for a signal at the output of an optimum compressing filter

$$l_s(\tau)=A_B\frac{\sin\pi\Delta f\tau}{\pi\Delta f\tau}.$$

The envelope of the compressed pulse has the form sin $x/x$ (see Fig. 7.13). Its length with respect to the first zeroes is $2/\Delta f$. The length of the compressed pulse is reckoned at the level $2/\pi \approx 0.64$, which corresponds approximately to the half-power level, we obtain

$$\tau_{sc}=\frac{1}{\Delta f}. \qquad (7.46)$$

The compression factor

$$\frac{\tau_N}{\tau_{sc}}=\tau_N\Delta f=N.$$

Since signal energy does not change when the pulse is compressed

$$A^2\tau_N=A_c^2\tau_{sc}=\frac{A_B^2}{\Delta f},$$

whence the increase in pulse amplitude during compression

$$\frac{A_B}{A}=\sqrt{\tau_N\Delta f}=\sqrt{N}.$$

Target range may be reckoned from a short output range pulse with high accuracy, determined by the pulse length $\tau_{sc}=\frac{1}{\Delta f}$.

Since the system is linear, the passage of thesignals of several

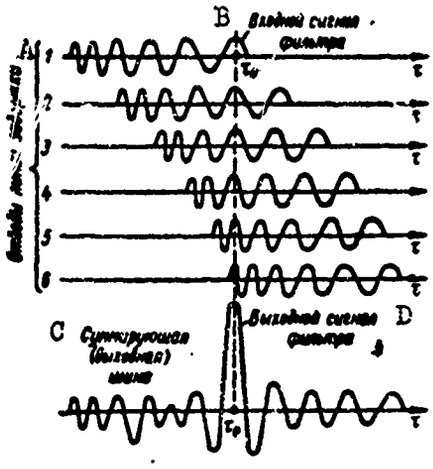


Fig. 7.14. Signals at the input and output of an optimum compression filter. A) Delay line tap; B) input signal of the filter; C) summing (output) bus; D) output signal of the filter.

targets through the filter may be examined independently. Therefore, in reception of broad overlapping pulses from several targets, at the filter output we will obtain short separating pulses if the distance between the targets exceeds the quantity $\delta R = \frac{c\tau_{ис}}{2} = \frac{c}{2\Delta f}$. A high resolution is obtained.

An optimum filter for frequency-modulated pulses may be designed in various ways, for example, in the form of the universal filter examined in Chapter 6 with several taps and a summing bus (see Fig. 6.10).

Figure 7.14 shows, as an illustration of the compression process, a simplified model of a frequency-modulated rectangular pulse in the input and the taps of an optimum filter and also the result of the summing of signals in the output bus of the filter. The taps are arranged in the filter in such a way that at moment in time $\tau_0$ the signals from all the taps are summed in phase. Before moment $\tau_0$ and after it the phases of the items diverge, since the frequency is not constant. As a result of this a short pulse of large amplitude forms in the vicinity of $\tau_0$, while in the remaining time interval of summing the amplitude is close to zero, inasmuch as the phase relations among the terms are un-

favorable. With increase in the depth of modulation the divergence among the phases of the summed signals with increasing distance from point $\tau_0$ will be more rapid. Therefore, the length of the compressed pulse will be less, the greater the frequency deviation $\Delta f$.

From the analysis in Fig. 7.14 it can be seen that with reduction in the signal frequency due to the Doppler effect the phase relations which are favorable for summing are displaced to the left of point $\tau_0$, that is, toward a point where the reduced instantaneous frequency value is equal to the instantaneous frequency value at point $\tau_0$ when there is no Doppler shift. This corresponds to a reduction in the reckoned range as against the true range. When there is positive increment in the frequency, the maximum of the output pulse shifts to the right. This is the explanation for velocity error with respect to range, proportional to the slope of the solid of indeterminacy tg$\gamma$. The amplitude of the output signal decreases simultaneously with the shift, since favorable phase relations do not occur at moment $\tau_0$ when the whole signal has entered the filter, but before or after this moment when either the whole signal has not yet been received or part of the signal has already left the filter.

There are two ways of forming frequency-modulated pulses – an active and a passive way. The active way consists in varying the transmitter frequency during the length of a pulse using, for example, a reactance tube. In the passive method the same optimally compressing filter is used in the transmitter, but in the reverse order: a short unmodulated pulse is fed to the filter input, and a long frequency-modulated pulse is obtained at the output.

The drawback of the active method is that any deviations in the law of variation of the frequency from the assigned value cause detuning of the signal relative to the optimum filter. The effectiveness of com-

pression decreases. In the passive method this inadequacy is automatically eliminated, since one and the same filter is used. However, the transmitter in this case should be designed in a particular way: "master oscillator – shaping filter – power amplifier" and, in addition, the shape of the outcoming pulse is not good enough.

The use of frequency-modulated pulses is a graphic illustration of the theoretical principle that resolution and potential range measurement accuracy are, in general, determined not by the signal length but by the width of its spectrum.

Let us now turn our attention to an extremely important circumstance.

Reception of a frequency-modulated pulse requires a considerably broader receiver passband than in the case of an unmodulated pulse of the same length. Here the noise power increases, but the peak power of the pulse after compression increases to the same extent. The same signal/noise ratio is maintained as in operation with unmodulated pulses with the same signal length and the same power of emission.

Consequently, the accuracy and resolution of frequency-modulated pulses are heightened without practically any reduction in the RLS operating range, which depends only upon the total signal energy $E_s$ and the noise power $E_0$ curve 1 hz (signal/noise ratio).

The use of frequency-modulated pulses makes it possible to increase the signal energy and the RLS operating range not through the peak power of emission but by lengthening the pulse. In this case a high range resolution is maintained by frequency modulation and pulse compression in the receiver.

With the RLS operating range unchanged, the irradiated power is reduced with increase in the pulse length and is least when emission is continuous. However, when the pulse is very long, the conditions of its

shaping and the design of the optimum filter become extremely complicated. Because of this the correlation (frequency) method of measuring range whose drawbacks have already been pointed out, is used with the continuous frequency-modulated signal, and not the method of optimum filtering. In addition, when emission is continuous it is difficult to separate the received and the emitted oscillations effectively.

Therefore, radar systems which use broad frequency-modulated or coded pulses are intermediate systems between pulse and continuous signal systems and embody a substantial part of the merits of both one and the other.

2. Noise-like Signals

One further change may be effected in the solid of indeterminacy of its basic colume, except for the sharp central peak, is spread out in the form of a thin layer covering the large area $\tau'F'$ (Fig. 7.15).

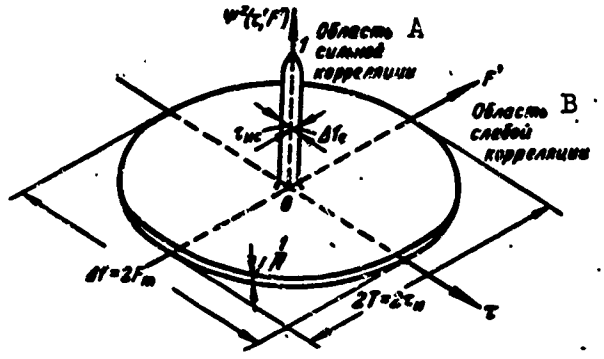


Fig. 7.15. Solid of indeterminacy of a noise-like signal. A) Region of strong correlation; B) region of weak correlation.

This is possible when the product of the signal spectrum and its length $N = \Delta f \tau_и \gg 1$.

The solid looks like a button. The altitude of the thin layer in which almost the whole volume of the field is concentrated

$$\frac{V_{ш1}}{\Delta f \tau_и} = \frac{1}{\Delta f \tau_и} = \frac{1}{N} \ll 1,$$

is much lower than the altitude of the central peak. Therefore, in an evaluation of accuracy and resolution the chief role is played by the narrow central peak, the area of whose section

$$\Delta f_c \tau_{иc} = \frac{1}{\Delta f \tau_и} \ll 1,$$

since the volume of the peak is $N = \Delta f \tau_и$ times less than the total volume $V_{ш} = 1$, while the output of the peak is 1.

Quantity $t_{is}$ is the pulse length at the output of a filter which is optimum for the given signal, while quantity $\pm \frac{\Delta f_c}{2}$ determines the limits of the Doppler shift of frequency when the signal at the filter output has a perceptible value. Thus the combined range and velocity resolution, and accuracy as well, increase without limitations with increase in the product $N = \Delta f \tau_и$.

However, the indeterminacy principle is not violated: these signal properties are manifested only with a limited number of targets. If the signals of a large number of targets are being received at the same time (and the number of targets increases with increase $N = \Delta f \tau_и$), the areas of low correlation (side lobes) of these signals overlap, their sum forming a hum which is commensurable with the signal of the given target (central peak). Thus, if the number of such targets (at the limit) is $N$, and their signals are of approximately equal intensity, the total power of the hum formed by the side lobes of all targets will become equal to the power of the signals of each target separately. The observation conditions deteriorate sharply.

In practice, however, in many cases the number of targets is known to be limited (scanning of the airspace) and the use of signals in which $\Delta f T \gg 1$ yields a positive result. In scanning the earth's surface the effectiveness of such signals decreases substantially.

Let us now take up the problem of the selection of a signal shape which will provide an indeterminacy function of the assigned form.

A signal of complex shape has $N=\Delta F\tau_и$ independent sections of length $1/\Delta f$ (Fig. 7.16a). Within the limits of each section (correlation interval) the signal phase is approximately constant, and it changes from section to section due to modulation.

Since the signal modulation law with respect to phase (frequency) is known beforehand, an optimum filter may be designed for it (Fig. 7.16b). The number of taps in the filter is $N$, and they are located on the delay line at intervals corresponding to $\tau_э=\frac{1}{\Delta f}$ . The signal phase is turned. The amount of the turn $-\Delta_i$ is selected such that at the moment $\tau_0$ when the signal has completely entered the filter (the initial section of the signal enters the final tap, and the final section enters the first tap of the filter) all the terms are in phase. The mutual phase shifts are compensated. Because of this at moment $\tau_0$ all the terms are summed with respect to amplitude in the output bus. Before moment $\tau_0$ and after it the amplitude of the output signal is considerably less. In the first place, not all components are summed: the signal has not yet entered the filter completely or has already left it in part. In the second place, and this is the main point, the phase relations among the terms are unfavorable.

As a result, at the optimum filter output there is formed a short pulse of length $\tau_и=\frac{1}{\Delta f}$ and side lobes at interval $2\tau_1$ (Fig. 7.16c). Consequently, with any modulation law a complex signal may be compressed $N = \Delta f\tau_1$ times – to the length of correlation interval $\tau_{1s} = 1/\Delta f$. Further compression is impossible, since the phase is constant within the limits of the correlation interval and one and the same filter may not be used to obtain favorable phase relations in one part of this interval an unfavorable phase relation at other moments in time: they will be

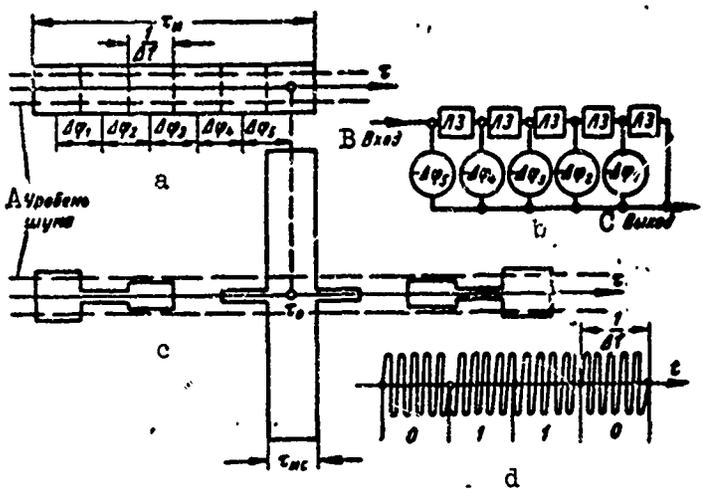


Fig. 7.16. Noise-like signals: a) Generalized complex signal at filter input; b) optimum filter; c) signal at filter output; d) phase-keyed signal. A) Noise level; B) input; C) output.

identical over the whole of interval $1/\Delta f$. Simple signals are also incompressible, since in them $\tau_1 = 1/\Delta f$

The signal modulation law must be selected such that side lobes yield no blips, and this corresponds to the thin even layer of the solid of indeterminacy. When we analyze a signal in the form of a periodic pulse sequence we saw that the solid of indeterminacy had, in addition to the narrow central peak, many additional peaks. When the periodicity of the pulses is violated these peaks are dissipated.

Consequently, a broad-band signal of great length, one least resembling a periodic signal, must be applied in order that an even thin layer be formed in the solid of indeterminacy instead of additional peaks. It is also necessary to eliminate the simple interdependence between frequency and time which is characteristic for pulses with linear frequency modulation. A certain chaotic state in the signal modulation law is essential.

These conditions are satisfied by a signal in the form of a section of noise with length $\tau_1 >> 1/\Delta f$. However, because of the sharp amplitude oscillations within the pulse, such a signal cannot be gener-

ated conveniently. The best way to obtain a noise-like signal is through nonlinear frequency modulation for phase keying of a pulse of constant amplitude.

The phase-keyed signal has constant frequency and amplitude, while its phase jumps at interval $1/\Delta f$ to take one of two opposite values: 0 or $\pi$, in a quasi-random series (Fig. 7.16d). One of two values of the binary code, 0 or 1, may be ascribed to each phase value. Then a random aperiodic law of the sequence of zeroes and units may be formulated under the rules of algebraic logic. An example of the aperiodic code on which the modulation law is based in the case of a noise-like signal at $N$ =31, is the binary number

00011100110111110100010010101l.

In addition to constant amplitude, phase-keyed signals have the merit of using simple filters for their shaping and processing: the phase is turned in the filter taps by feeding a signal to a summing bus in one or the other polarity

The noise-like signal may also be used in continuous emission if correlation reception is employed.

## §7.8. RESOLVING DEVICES FOR THE OPTIMUM RANGE-MEASURING RECEIVER

After the signal has passed through the receiver, the output signal maximum tests the bias relative to the input signal maximum. In a tuned optimum receiver this bias is identical for all targets, and it may

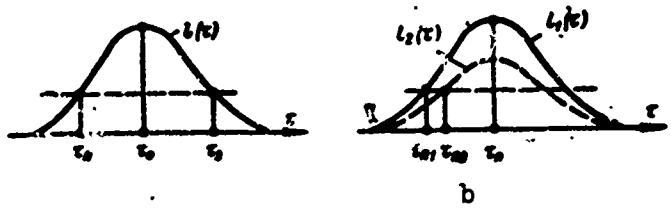

b

Fig. 7.17. Clamping the moments of the function maximum by testing it at the threshold: a) Reckoning from two moments of interception of the threshold; b) systematic error in fixing the maximum from the leading edge when signal intensity varies.

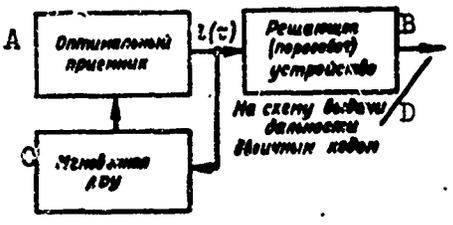


Fig. 7.18. Optimum resolving device for measuring range, clamping the maximum from the leading edge of the signal (first arrangement of the circuit). A) Optimum receiver; B) resolving (threshold) device; C) instantaneous ARU; D) to the circuit giving the range in binary code.

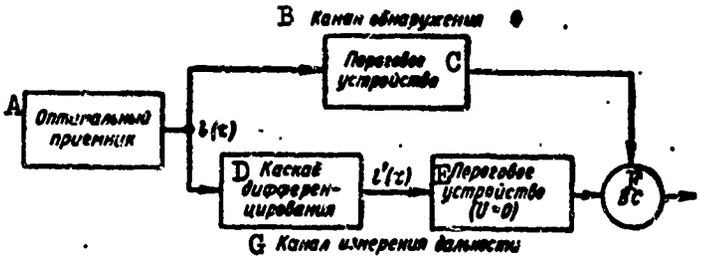


Fig. 7.19. Optimum resolving device for measuring range, clamping the function maximum from the moment at which its derivative passes through zero (second arrangement of the circuit). A) Optimum receiver; B) detection channel; C) threshold device; D) differentiation stage; E) threshold device; F) VS; G) range-measuring channel.

therefore be taken into account in calibration or it may be compensated. The simplest and most natural way of compensating systematic bias is by reckoning the delay time relative to the maximum of the transmitter outcoming pulse passing through the receiver.

The task of the reso ving device of an optimum range-measuring receiver is to register the moment when the receiver output signal $l(\tau)$ passes through its maximum.

This task is successfully resolved by the operator in visual registration of range. The operator's eye is a good analyzer of the signal shape and easily clamps the maximum. Then, by comparing the position of the maximum relative to the scale grid, the operator reads out the range value.

In automatic devices the signal-shape analyzer is much simpler if it clamps not the moment of the output signal maximum but the moment

when the signal exceeds a certain threshold level $U_0$.

There are two types of resolvers in stations with automatic data registration: the first design uses the output signal directly, the second requires it to be transformed.

*First design.* The output signal of the optimum receiver is fed to a threshold device which clamps the moment when the leading edge and the trailing edge of the signal, $\tau_p$ and $\tau_z$ (Fig. 7.17a) intersect assigned level $U_0$.

The actual position of the maximum is found as the mean value

$$\tau_0 = \frac{\tau_z + \tau_p}{2},$$

since the signal proper at the receiver output $l_s(\tau)$ is always symmetrical, being the autocorrelation function of the input signal $s(t)$.

It would be difficult to design a device which could clamp the moment at which the signal intersects the level $U_0$ from below upward and from above downward. Therefore, in order to clamp $\tau_0$ it is desirable to register only one moment $\tau_p$, and then introduce the correction $\tau_0 - \tau_p$. Unfortunately, the difference $\tau_0 - \tau_p$ varies with different signal intensities (Fig. 7.17b) and there appears a systematic error which cannot be known ahead of time. The systematic error may be eliminated if the signal level is maintained constant at the receiver output using an instantaneous ARU (normalization).

When normalization is employed the optimum resolver is extremely simple, and the threshold detection device as well. The moment of appearance of a pulse at the output of the threshold device relative to the nearest transmitter pulse represents the target range. This pulse enters a circuit which transforms the time interval into a number, and this circuit gives the range value in a numerical code.

Figure 7.18 shows an optimum receiver with a special device of this

type. Actually, it is impossible to design a receiver with instantaneous ARU, and this causes the appearance of small systematic errors depending upon the singal intensity.

*The second circuit.* The moment of the function maximum corrresponds to the moment when its derivative passes through zero. Therefore, in clamping the range the receiver output signal $l(\tau)$ is first differentiated and then its derivative $l'(\tau)$ is fed to a threshold device with the level $U_0 = 0$ (Fig. 7.19) At the moment in time when $l'(\tau) = 0$, a pulse appears at the output of the threshold circuit, and this may be used to reckon range.

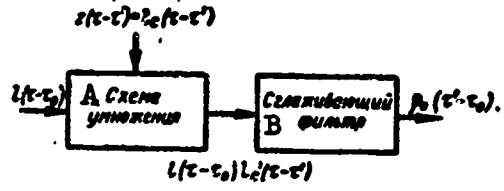


Fig. 7.20. Optimum correlator circuit. A) Multiplication circuit; B) smoothing filter.

However, function $l'(\tau)$ may also be equal to zero in the absence of a target. Therefore, the pulse from the threshold device output is fed to a coincidence valve (VS) which generates a reference range pulse only if the presence of a target has been clamped in the detection channel.

The reference pulse then passes to the transformation circuit which presents the target range in the form of a numerical code.

The resolver in range autotrack systems has a somewhat different appearance. These systems generate tracking function $s(\tau' - \tau)$, the time position of whose reference point $\tau'$ should coincide with time position $\tau_0$ of the output signal $l(\tau - \tau_0)$.

To clamp the maximum the time discriminator should form mutual cor-

relation function

$$\rho(\tau'-\tau_0)=\int_{-\infty}^{\infty} l(\tau-\tau_0)z(\tau-\tau')\,d\tau=\int_{-\infty}^{\infty} l_c(\tau-\tau_0)z(\tau-\tau')\,d\tau+$$

$$+\int_{-\infty}^{\infty} l_{sh}(\tau-\tau_0)z(\tau-\tau')\,d\tau=\rho_c(\tau'-\tau_0)+\rho_{sh}(\tau'-\tau_0).$$

Here $\rho_s(\tau' - \tau_0)$ is the regular part of the mutual correlation function, while $\rho_{sh}(\tau' - \tau_0)$ is the random component, distributed, like $l_{sh}(\tau)$, normally with a zero average value if the condition introduced above, that the signal/noise ratio is sufficiently great, is maintained.

Function

$$\rho_c(\tau'-\tau_0)=\int_{-\infty}^{\infty} l_c(\tau-\tau_0)z(\tau-\tau')\,d\tau$$

has a maximum at $\tau' = \tau_0$ and may therefore serve as a criterion of the coincidence in time of tracking function $z(t)$ and the output signal. The noise component $\rho_{sh}(\tau' - \tau_0)$ is the cause of the appearance of errors.

It is obvious that the function maximum $\rho_s(\tau' - \tau_0)$ will be clamped the more accurately the greater it is by comparison with noise component $\rho_{sh}(\tau' - \tau_0)$. Since $\rho_s(\tau' - \tau_0)$ is the mutual correlation function of functions $z(\tau)$ and $l_s(\tau)$, its maximum is largest when

$$z(\tau)=l_c(\tau)$$

with accuracy up to a constant factor.

In the optimum case the correlation function takes the form

$$\rho_0(\tau'-\tau_0)=\int_{-\infty}^{\infty} l(\tau-\tau_0)l_c(\tau-\tau')\,d\tau. \qquad (7.47)$$

As follows from Formula (7.35) the correlator consists of a device for multiplying functions $l(\tau - \tau_0)$ and $z = l_s(\tau - \tau')$ and a smoothing filter (Fig. 7.20).

However, the resolving device of a range autotrack system – a time discriminator – should not only clamp the moment of coincidence of func-

$z(\tau - \tau')$ and $l(\tau - \tau')$ but should also develop a mismatch signal $d(\tau' - \tau_0)$ which satisfy the condition

$$d(\tau' - \tau_0) \begin{cases} <0 & \text{for } \tau' < \tau_0, \\ =0 & \text{for } \tau' = \tau_0, \\ >0 & \text{for } \tau' > \tau_0. \end{cases}$$

When stimulated by this signal the control device of the autotrack system can automatically change shift $\tau'$ of function $z(\tau)$ so that it will coincide with signal $l(\tau)$, that is, accomplish tracking.

These conditions are satisfied by mismatch signal

$$d(\tau' - \tau_0) = \frac{d}{d\tau'} \rho(\tau' - \tau_0).$$

In accordance with Formula (7.47) and with the rules for differentiation under the sign of the integral, it is possible to obtain two equivalent descriptions of the structure of the optimum time discriminator:

$$d(\tau' - \tau_0) = \int_{-\infty}^{\infty} l(\tau - \tau_0) l_c'(\tau - \tau') d\tau \qquad (7.48a)$$

or

$$d(\tau' - \tau_0) = \int_{-\infty}^{\infty} l'(\tau - \tau_0) l_c(\tau - \tau') d\tau. \qquad (7.48b)$$

From this there follows the possibility of constructing the optimum time discriminator in two ways.

The first, according to Formula (7.48a), uses a signal directly from the output of the optimum receiver $l(\tau)$ while the tracking function $z(\tau) = l_s'(\tau)$ takes the form of a derivative of the signal proper (Fig. 7.21a).

The second design, in accordance with Formula (7.48) utilizes the derivative of the optimum receiver output signal $l'(\tau)$, while the tracking function takes the form of the signal proper at the optimum receiver output $l_s(\tau)$ (Fig. 7.21b).

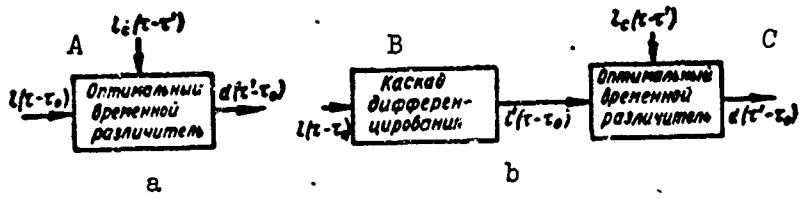


Fig. 7.21. Optimum time discriminator of a range autotrack system: a) First arrangement of the circuit; b) second arrangement of the circuit. A) Optimum time discriminator; B) differentiating stage; C) optimum time discriminator.

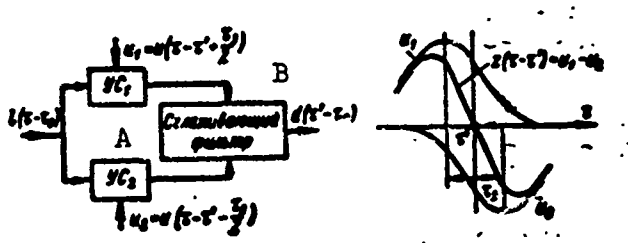


Fig. 7.22. Structure of a time discriminator. A) US; B) smoothing filter.

The first design of the time discriminator has proven more convenient in practice and has been utilized. It is designed in the following way (Fig. 7.22).

The signal enters two coincidence amplifiers (US). Pulse $u_1 = u\left(\tau' + \frac{\tau_3}{2}\right)$ is fed to the second input of the first amplifier, and pulse $u_2 = u\left(\tau' - \frac{\tau_3}{2}\right)$, which is delayed by $\tau_z$ relative to the first, is fed to the second input of the second amplifier. Both pulses are displaced in time as a single unit with reference to the control circuit. Initially signal $l(\tau)$ passes mainly through $US_1$, then through $US_2$. In the antiphase the output signals are fed to an averaging device (RC filter). The mismatch signals at the receiver output, obtained by averaging, is proportional to mismatch $\Delta\tau = \tau' - \tau_0$.

The resultant tracking function of the time discriminator

$$z(\tau - \tau') = u\left(\tau - \tau' + \frac{\tau_3}{2}\right) - u\left(\tau - \tau' + \frac{\tau_3}{2}\right)$$

may be made close to the optimum function by selection of the shape of

the selectro pulses $u(\tau)$ and of the shift $\tau_z$ between them.

## §7.9. TARGET RANGE AUTOTRACK

### 1. The Target Range Autotrack Principle in Pulse RLS

All range autotrack designs (ASD) may be divided into two fundamental types:

a) ASD systems with adjustable delay line;

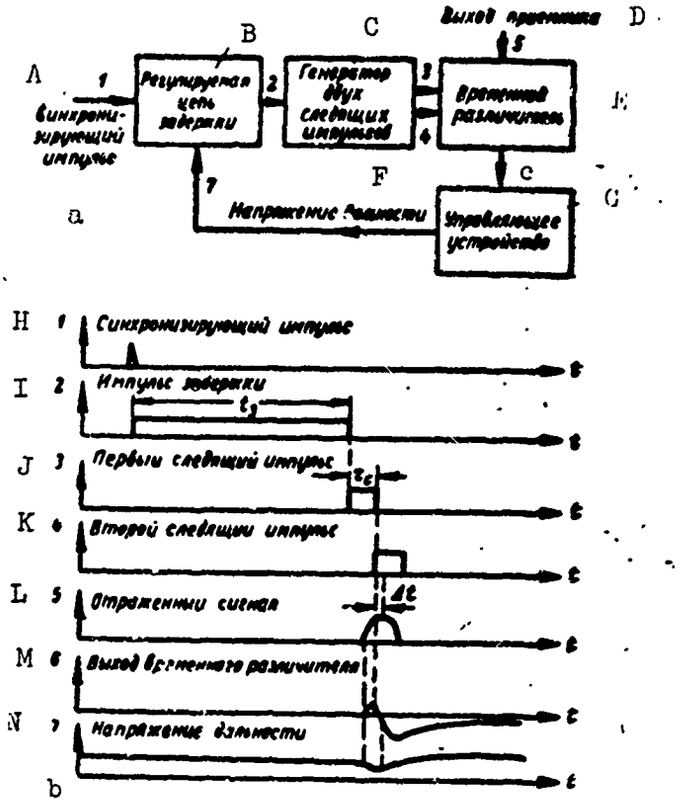


Fig. 7.23. Target range autotrack system: a) Block diagram of the system; b) time diagrams at various points. A) Synchronizing pulse; B) adjustable delay line; C) generator of two tracking pulses; D) receiver output; E) time discriminator; F) range voltage; G) control device; H) synchronizing pulse; I) delay pulse; J) first tracking pulse; K) second tracking pulse; L) reflected signal; M) time disciminator output; N) range voltage.

b) ASD systems with variable frequency generator.

Figure 7.23 gives a block diagram of a typical range autotrack system with an adjustable delay line; it also gives time diagrams characterizing the processes at key points in the circuit. As can be seen from

the diagram, the ASD system is a closed automatic control system consisting of four basic elements: a time discriminator (the sensitive element of the system), measuring the time mismatch between the reflected signal and the range pulses; circuits for shaping two range pulses or, as they are often called, tracking pulses; an actuating element – the adjustable delay line (RTsZ) which varies the time position of the tracking pulses in accordance with the size of the control signal, and, finally, a device which shapes the control signal and provides the assigned quality of control in the system.

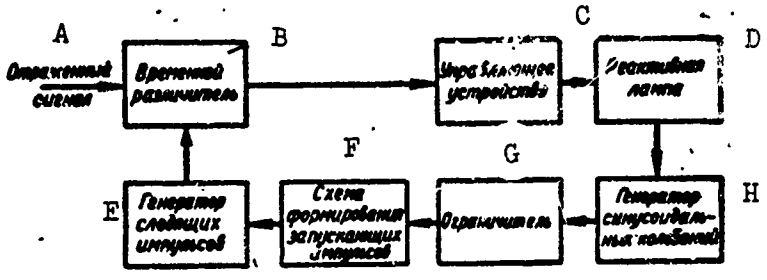


Fig. 7.24. Block diagram of ASD system with a controlled generator. A) Reflected signal; B) time discriminator; C) control device; D) reactance tube; E) tracking pulse generator; F) circuit for shaping trigger pulses; G) limiter; H) generator of sinusoidal oscillations.

The delay pulse generator which is triggered by RLS synchronization signals generate pulses whose length is proportional to the control voltage. The trailing edge of the delay pulse is differentiated, and the shape which is formed in this way triggers the tracking pulse generator. The pulses obtained pass to the time discriminator consisting of two coincidence stages and a comparison circuit. The range pulses in turn open the coincidence stages, and as a result part of the reflected signal passes through the first, and part through the second coincidence stage. At the output of the time discriminator there is a comparison circuit which generates an error voltage proportional to the deviation of the target signal from the middle of the range pulses, while the polarity of the voltage is determined by the direction of target devia-

tion. If the reflected pulse is situated symmetrically relative to the boundary between the tracking pulses, the error voltage is zero. If the target signal is somewhat delayed, a smaller part of the reflected pulse passes through the first coincidence stage and at the output of the comparison circuit there appears a positive voltage which, after transformation and amplification in the control device, causes the adjustable delay line to shift the range pulses in such a way that the target signal is located symmetrically relative to their center. If the echo-signal is leading the tracking pulses, a control voltage of the opposite sign is generated, and the delay in the range pulses is reduced.

As the target moves due to the constantly occurring mismatch between the time position of the reflected signal and the position of the center of the range pulses, there is a continuous change in the control voltage and, consequently, continuous displacement of the range pulses in the direction of a reduction of mismatch.

In this way target autotrack is accomplished, with a particular value of the control voltage corresponding to each position of the tracking pulses. Consequently, the magnitude of the control voltage is a uniquely determined function of target range.

Figure 7.24 gives a block diagram of an ASD system in which a tuned generator acts as the actuating device. The basic elements of the system are: a time discriminator, a control device, a tuned generator of sinusoidal oscillation, a circuit for shaping trigger pulses, and a tracking pulse generator.

The principle of operation of the system is as follows. From the sinusoidal voltage of the tuned generator are formed signals which trigger the range pulse generator. The moment of triggering of the range pulses is tightly linked to a particular phase of the sinusoidal voltage. The change in the frequency of the tuned generator leads to change in

the phase of the generated oscillation and, consequently, to displacement of the range pulses. If the reflected signal is located symmetrically relative to the middle of the tracking pulses, the output voltage of the time discriminator is equal to zero, and the tuned generator operates at its average frequency, which is a multiple of the RLS pulse repetition frequency. But if there is mismatch in the time position of the range pulses and the reflected signal, an error voltage will appear at the output of the time discriminator, the generator frequency will be deflected from its average value, and the tracking pulses will be displaced in a direction corresponding to reduction in the initial mismatch.

In contrast to a circuit with an adjustable delay line, the ASD system with a controlled generator does not require triggering, and its timing is not connected with devices shaping the radar station outcoming pulses. In the system there is no voltage proportional to the target range. Therefore, similar ASD systems are used when a radar station employs a digital computer as the device generating a stable reference pulse coinciding in time with the reflected target signal. In this case range is measured by transforming into binary code the time interval between the moment when the transmitter is triggered and the moment when the reference pulse appears.

2. Range Autotrack in RLS with Frequency Modulation

A simplified block diagram of a radar station with target autotrack is given in Fig. 7.25a. The ASD system includes a retuned range selector, a range measuring circuit, a comparison circuit, and an actuating motor with a range-setting potentiometer.

The range selector is usually a narrow-band filter, the average frequency of whose transparency band may be varied within the limits of the possible change in the beat frequency.

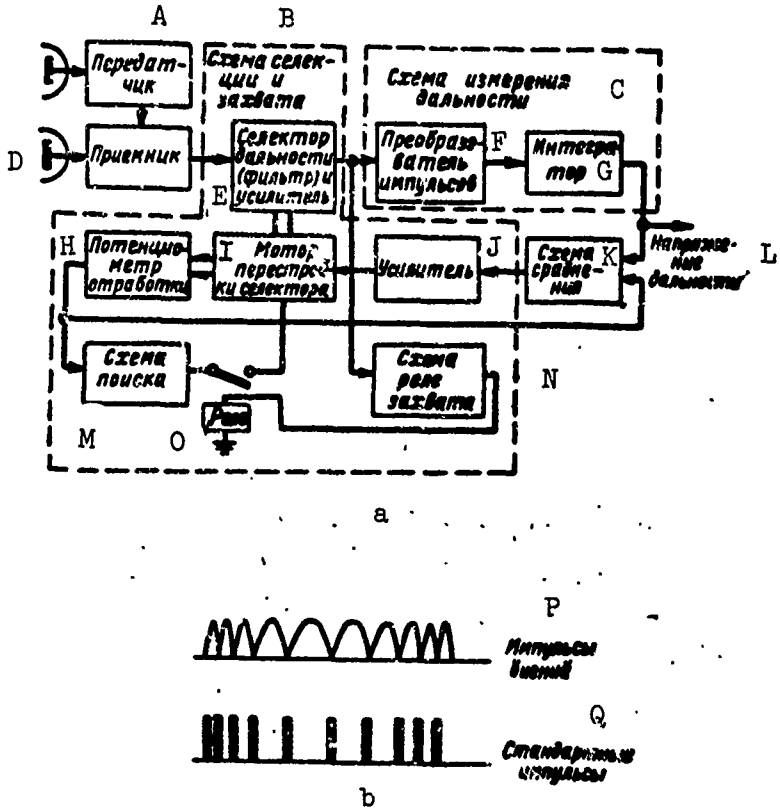


Fig. 7.25. RLS with frequency modulation: a) Block diagram of ASD system; b) transformation of the beating pulses. A) Transmitter; B) selection and locking circuit; C) range measuring circuit; D) receiver; E) range selector (filter) and amplifier; F) pulse transformer; G) integrator; H) range-setting potentiometer; I) motor for retuning the selector; J) amplifier; K) comparison circuit; L) range voltage; M) searching circuit; N) locking relay circuit; O) relay; P) beating pulses; Q) standard pulses.

Here it should be borne in mind that in a RLS with frequency modulation the beat frequency is proportional to target range. Consequently, the range of variation of the filter frequency is determined by the limits of the operating range of the autotrack system.

In searching for a target the filter frequency is retuned over the whole range by a special motor. The rapidity of search is limited by the width of the transparency band of the filter; the narrower the band the longer the time for build-up of the voltage at its output, and the slower must be the search.

When a target appears at some range, the filter at some moment in

time turns out to be tuned to the beat frequency corresponding to the range of this target. At the selector output there will appear a signal which operates the locking circuit and switches over the tuning motor from the searching mode to the autotrack mode. Starting at this moment in time, beat pulses from the selector output start entering the range measuring circuit. The latter consists of a beating pulse transformer and an integrator. The transformer converts beating pulses which differ both in shape and in length into standard pulses of constant amplitude and length (Fig. 7.25b). This sort of transformation is necessary in order that the output voltage of the range circuit be proportional only to the average pulse repetition frequency and not depend upon other parameters. The integrator isolates a constant component from the pulse series which it receives. And since, when pulse parameters are unchanging, their constant component is proportional to their frequency, the magnitude of the voltage at the integrator output is proportional to the target range.

From the integrator output the range voltage passes to a different circuit where it is compared with the voltage tap from the range-setting potentiometer. The latter is proportional to the range to which the selector is tuned. If the voltage of the target range is different from the set voltage, an error signal will appear at the output of the comparison circuit, proportional to the mismatch between the two voltages. The amplified error signal is fed to the actuating motor which varies the filter tuning in a direction opposed to the initial mismatch. The motor turns until the magnitude of the range voltage and of the set voltage become identical, that is, until the range selector is tuned to the zone in which the target is located. As the target moves the range voltage is continually varied and, consequently, the selector is continually being retuned. In this way the target is automatically select-

ed and tracked with respect to range, and the system continually emits a voltage proportional to the target range. The latter may be utilized in computers to solve various problems connected with sighting, interception, homing, etc.

The above ASD circuit functions sufficiently well only in the case of comparatively low relative target velocities when the Doppler frequency shift fits into the filter passband. Widening of the filter band is limited by deterioration of the RLS noiseproofness and by reduction of its operating range.

3. Elements of Pulse Systems for Range Automatic Tracking

The ASD systems of pulse radar stations are pulse control systems since the deflection of the position of the reflected signal from the middle of the tracking pulses is not measured continuously but only at the short moments of time when the target signal arrive. All the rest of the time information on target range is absent, and the autotrack system remains open. Therefore, the processes in the elements of the pulse ASD systems and the dynamic properties of the system as a whole are not described by differential equations but by difference equations. However, because the boundary frequency of the effective passband of the tracking system is always considerably lower than the signal repetition frequency, when ASD systems are analyzed it is possible in some cases to use the methods of the theory of continuous control as a first approximation.

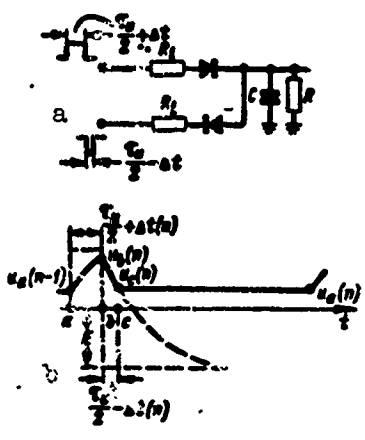


Fig. 7.26. Equivalent circuit of a time discriminator and voltage oscillograms at its output.

*Time discriminator.* As has already been pointed out above, time discriminators are destined for measuring the time mismatch between the re-

flected signal and the range pulses. In practice there are a large number of different time discriminator circuits; however, most have the same operating principle. This principle is that the reflected pulse used for autotrack is divided into two parts using two tracking pulses. The obtained parts are compared, and the difference of their areas is proportional to the range measurement error.

Figure 7.26a gives a simplified equivalent circuit of a discriminator. The capacitance of capacitor $C$ is selected such that the time constant of charging circuit $T_z$ is considerably larger than the length of the reflected signal $\tau_1$. In this case the comparison circuit will possess integrative properties, and the circuit output voltage will be proportional to the time mismatch $\Delta t$ of the target pulse relative to the center of the tracking pulses.

The voltage oscillograms at the output of the comparison circuit are depicted in Fig. 7.26b. As can be seen from the oscillograms the processes occurring in the time discriminator in the $n$th repetition period may be broken down into three characteristic parts. Assume that the target signal is displaced relative to the tracking pulses by quantity $\Delta t(n)$ in the direction of the first of them. Then, during the first time interval, equal to $\tau_1/2 + \Delta t(n)$, the capacitor is charged by the output pulse of the first coincidence stage. The voltage at the time discriminator output at the end of this time interval

$$u_a(n) = u_a(n-1) + [E - u_a(n-1)]\left[1 - e^{-\frac{\frac{\tau_1}{2} + \Delta t(n)}{T_z}}\right], \qquad (7.49)$$

where $E$ is the size of the charging pulse, equal to the amount by which the signal of the coincidence circuit exceeds the limiting threshold; $u_a(n-1)$ is the voltage on the capacitor at the moment of termination of the $(n-1)$th repetition period; $\Delta t(n)$ is the time mismatch between the middle of the echo signal and the center of the tracking pulses.

In the next time interval, equal to $\tau_1/2 - \Delta t(n)$, the capacitor is recharged by the pulse of the second coincidence amplifier. The time constant of the recharge remains $T_z$ under the condition that both coincidence circuits are identical. The significance of the output voltage of the comparison circuit at the end of the second time interval is determined by the relation

$$u_c(n) = u_s(n) - [E + u_s(n)]\left[1 - e^{-\frac{\frac{\tau_u}{2} - \Delta t(n)}{T_3}}\right]. \qquad (7.50)$$

In the last, third time interval the capacitor is discharged on the load resistance. The value of the output voltage at the end of the *n*th pulse repetition period will be approximately equal to

$$u_s(n) \approx u_c(n) e^{-\frac{T_u}{T_p}}, \qquad (7.51)$$

where $T_r = RC$ is the time constant of the capacitor discharge circuit; $T_p$ is the RLS pulse repetition period.

If Eqs. (7.49), (7.50) and (7.51) are solved jointly, one can obtain the difference equation of a time discriminator, one which ties together the value of its output voltages at moments in time which are spaced at intervals equal to the RLS operating period:

$$u_s(n) - e^{-\left(\frac{\tau_u}{T_3} + \frac{T_u}{T_p}\right)} u_s(n-1) = \left[2e^{-\frac{\frac{\tau_u}{2} - \Delta t(n)}{T_3}} - e^{-\frac{\tau_u}{T_3}} - 1\right] E e^{-\frac{T_u}{T_p}}. \qquad (7.52)$$

Considering that $e^{-\frac{\tau_u}{T_3}} \approx 1 - \frac{\tau_u}{T_3}$, Expression (7.52) may be simplified, and the equation of the processes in the time discriminator may be written in the following form

$$u_s(n) - A u_s(n-1) = \frac{2bE}{T_3} \Delta t(n), \qquad (7.53)$$

where $A = e^{-\left(\frac{\tau_u}{T_3} + \frac{T_u}{T_p}\right)}$; $b = e^{-\frac{T_u}{T_p}}$.

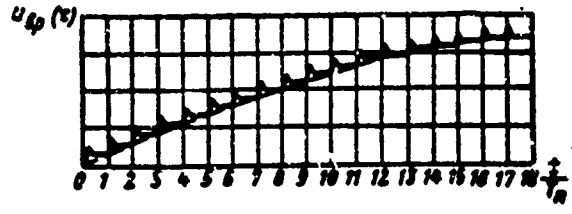

Fig. 7.27. Transient characteristic of a time discriminator.

We solve Eq. (7.53) for the case where mismatch $\Delta t(n)$ arises as a jump and then remains constant. We solve this by writing down values of $u_a(n)$ for several repetition periods, starting with $n = 1$:

$$\begin{aligned} u_a(1) &= \frac{2bE}{T_s}\Delta t, \\ u_a(2) &= (1+A)\frac{2bE}{T_s}\Delta t, \\ u_a(3) &= (1+A+A^2)\frac{2bE}{T_s}\Delta t, \\ &\cdots\cdots\cdots\cdots\cdots\cdots \\ u_a(n) &= (1+A+A^2+\ldots+A^{n-1})\frac{2bE}{T_s}\Delta t. \end{aligned} \qquad (7.54)$$

It is easy to see that Expression $(1 + A + A^2 + \ldots + A^{n-1})$ terms of a geometrical progression, and therefore Eq. (7.54) may be rewritten in the following form:

$$u_a(n) = \frac{2bE}{T_s}\frac{1-A^n}{1-A}\Delta t. \qquad (7.55)$$

The obtained solution of Eq. (7.55) determines the transient characteristic of the time discriminator as given in Fig. 7.27. The points of this characteristic lie on an exponential curve with a time constant equal to

$$T_{sp} = \frac{T_s}{\frac{T_s}{T_s} + \frac{T_s}{T_p}}. \qquad (7.56)$$

Consequently, the time discriminator as an element in an automatic control system is an aperiodic link whose time constant depends both upon the time constant of the charging circuit and upon the time constant

of the discharge of the comparison-circuit capacitor. With increase in $T_z$ and $T_r$ quantity $T_{vr}$ increases, and even in the absence of load resistance $R(T_r \to \infty)$, the time discriminator remains an aperiodic link with time constant

$$T_{sp} = \frac{T_z T_3}{\tau_u}$$

To design integrating time discriminators it is necessary to provide for constant charge-discharge currents regardless of the magnitude of the voltage at the output of the comparison circuit. In this case, when the mismatch is constant, the speed of change in the output voltage will be practically constant, and the dynamic properties of the time discriminator will approximate those of the integrating link.

Another parameter of a time discriminator is its transmission factor $k_{vr}$, which is equal to the ratio between the steady state output voltage and the size of the constant mismatch $\Delta t$. If we take into consideration the fact that the transient process terminates at $n \to \infty$ and that $\lim_{n \to \infty} A^n = 0$, from Formula (7.55) we obtain

$$k_{sp} = \frac{2bE}{T_3(1-A)}. \qquad (7.57)$$

Taking into account Expression (7.57), the difference equation of a time discriminator may be rewritten in the form

$$u_s(n) - Au(n-1) = k_{sp}(1-A)\Delta t(n).$$

In many cases, for example, when a time discriminator is used in ASD systems with a controlled generator, the element after the time discriminator do not react to the current value of the output voltage but to its average value over the period. With respect to such conditions, the difference equation of a time discriminator should link mismatch $\Delta t(n)$ and the average value of the output voltage $U(n)$.

Taking into consideration that $\tau_i \ll T_p$, the average value of the voltage may be calculated from Formula

$$U(n) \approx \frac{1}{T_n} \int_{(n-1)T_n}^{nT_n} u_c(n)\, e^{-\frac{t}{T_p}} dt.$$

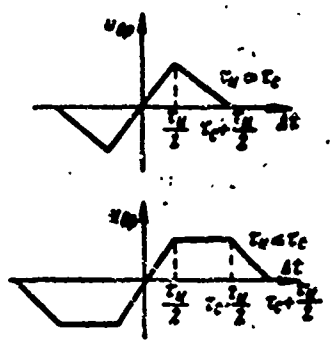

Fig. 7.28. Idealized static characteristic of a time discriminator.

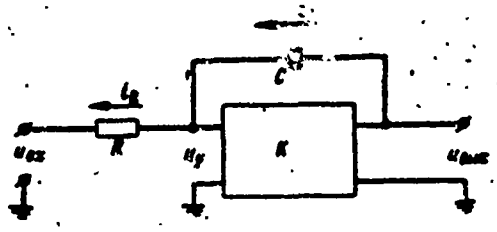

Fig. 7.29. Amplifier with capacitive negative feedback.

After integration, taking into consideration that $u_a(n) = u_c(n)\, e^{-\frac{T_n}{T_p}}$ and $b = e^{-\frac{T_n}{T_p}}$, we have

$$U(n) = \frac{T_p}{T_n} \cdot \frac{1-b}{b} u_a(n). \qquad (7.58)$$

Substituting the value of $u_a(n)$ from Formula (7.53) into Formula (7.58), we obtain a difference equation which associates the average values of the output voltage of the time discriminator in two adjacent periods,

$$U(n) - AU(n-1) = \frac{2E(1-b)}{T_n} \frac{T_p}{T_n} \Delta t(n). \qquad (7.59)$$

The transmission factor of the discriminator for the average value of the output voltage is equal to the ratio

$$k_{sp}=\frac{U(\infty)}{\Delta t}=\frac{2E(1-b)}{T_s(1-A)}\frac{T_y}{T_s}. \qquad (7.60)$$

Taking into consideration (7.60), the difference equation of the discriminator for average values of the output voltage may be written in the form

$$U(n)-AU(n-1)=k_{sp}(1-A)\Delta t(n). \qquad (7.61)$$

The complete idealized static characteristic of a time discriminator $U = f(\Delta t)$ has the form shown in Fig. 7.28. The linear region for which the expressions obtained above are valid has an extension equal to pulse length $\tau_i$. The size of the flat part of the discriminator curve depends upon the relation between the lengths of the reflected and the tracking pulses. The region of the characteristic with negative steepness is equal to the length of the received signal.

*Control devices.* The purpose of the control device is to shape a signal under whose effect the range pulses will be shifted. In most cases integrating circuits are used as control devices. The type of integrator used depends upon the kind of time discriminator and the type of actuating device. In the electronic circuit of an ASD integrating amplifier with capacitive negative feedback have been most widely employed. The equivalent circuit of an amplifier is given in Fig. 7.29. Since the input circuit of the amplifier has no grid current, $i_c = i_R$ and, consequently,

$$\frac{u_a-u_{ex}}{R}=\frac{d(u_{exit}-u_a)}{dt}C.$$

Considering that $u_{vykh} = Ku_d$, we obtain

$$(K+1)RC\frac{du_{exit}}{dt}+u_{exit}=-Ku_{ex}. \qquad (7.62)$$

By applying the Laplace transformation to Eqs. (7.62), it is easy to find the transmission function of an integrating amplifier

$$K_u(p)=\frac{k}{(K+1)RCp+1}=\frac{k_u}{p+\frac{1}{(K+1)RC}}, \qquad (7.63)$$

where $k_i = 1/RC$ is the transmission factor of an integrating amplifier.

As can be seen from Formula (7.63), from the point of view of its dynamic property an amplifier with capacitive negative feedback is an aperiodic link whose time constant $T_i$ increases $(K + 1)$ times by comparison with the time constant of an ordinary $RC$ circuit. With increase in $K$, $T_i$ increases, and the aperiodic length approximates an integrating link with respect to its dynamic properties. At sufficiently high values of $K$ the transmission function of an integrating amplifier may be written approximately in the form

$$K_u(p) \approx \frac{k_u}{p}.$$

From the point of view of principle such a substitution is incorrect; however, if the transient processes in the ASD system during a time interval which is significantly smaller than $T_i$, in the case of a quantitative evaluation of the control quality such an idealization yields negligible errors which may be ignored in the first approximation.

Another type of control device is the electromechanical integrator; a direct or alternating current motor may be used as such an integrator. The employment of an electric motor in such a device is based on the fact that the rotation angle of the motor axis is proportional to the integral of the voltage applied to the motor armature (in direct-current motors) or to the control winding (in two-phase induction motors). The motor equation has the form

$$\Delta\psi = \frac{K_{dv}}{D(T_{dv}D + 1)} U, \qquad (7.64)$$

where $\Delta\psi$ is the rotation angle of the motor axis; $U$ is the control voltage at the motor input; $T_{dv}$ is the electromechanical time constant; $K_{dv}$ is the transmission factor linking the steady-state speed of the motor with the voltage at its input; $D$ is a differentiation operator.

As can be seen from Expression (7.64) from the point of view of

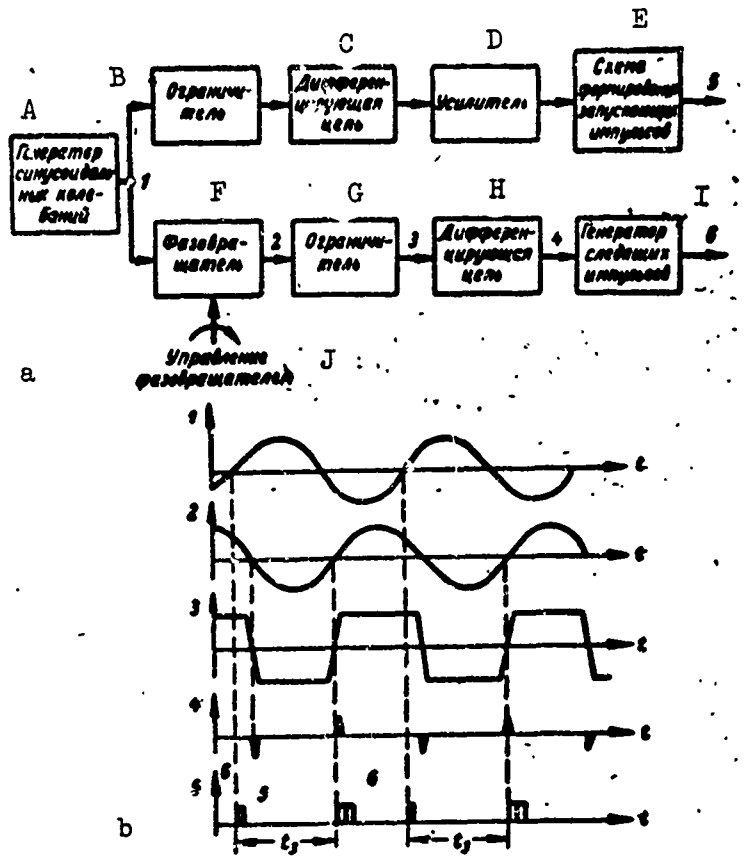


Fig. 7.30. Phasometric adjustable delay circuit: a) Block diagram; b) time diagrams. A) Sinusoidal generator; B) limiter; C) differentiating circuit; D) amplifier; E) circuit for shaping trigger pulses; F) phase shifter; G) limiter; H) differentiating circuit; I) tracking pulse generator; J) controlled by the phase shifter.

this dynamic property the engine is a series connection of an integrating and an aperiodic length. Electromechanical integrators are sometimes used in ASD systems with electronic adjustable delay line, but their basic application has been in phasometric autotrack systems. Electromechanical integrators may possess very high accuracy; however, their considerable inertia limits their application in high-speed ASD systems.

*Actuating devices.* As actuating devices ASD systems use circuits which vary the time position of the tracking pulses under the effect of a control voltage. In ASD systems with adjustable delay lines, RTsZ electronic circuits utilizing the voltage comparison method and devices employing the phasometric method have been the most widespread. The cir-

cuits of the first type are usually simpler; however, phasometric delay lines may be more accurate.

Electronic adjustable delay circuits include phantastrons, sanatrons, and similar circuits involving a linear discharge or charge of a capacitor.

In phantastron circuits the time delay error does not exceed one thousandth of the maximum pulse length. The static characteristic of a phantastron, expressing delay time $t_z$ as a function of the control voltage is very close to linear. The deviation from a straight line does not exceed tenths of a percent. However, this linear dependence obtains only after a certain minimum delay time, equal to about 2-4 μsec. This time interval determines the dead zone of an ASD system.

In accurate RTsZ electron circuits sanatrons are usually employed, functioning jointly with comparison circuits. The time delay accuracy of sanatrons is an order of magnitude higher than that of phantastron circuits, while their static characteristic possesses good linearity (deflection of the characteristic from a straight line does not exceed 0.05%).

From the point of view of their dynamic properties electronic time-delay devices are discontinuous circuits, since quantity $t_z$ can change only in jumps proportional to the change in the control voltage during one RLS operating period. However, because the change in the control voltage in the intervals between the outcoming pulses does not affect the amount of delay, from the point of view of the dynamics of control the RTsZ circuit may be considered an inertialess link with a transmission factor of $k_{rtsz}$.

Phasometric adjustable delay lines consist of a sinusoidal generator, a phase shifter, and a pulse-shaping circuit. The operating principle of an RTsZ is easily understood from examination of a block dia-

gram of the device and the voltage oscillograms at its various points (Fig. 7.30). The time delay of range pulses relative to RLS outcoming pulses is accomplished by a phase shifter. The magnitude of this delay is determined by the relation

$$t_з = \frac{\varphi}{2\pi} T_0,$$

where $T_0$ is the oscillation period of the sinusoidal generator; $\varphi$ is the phase shift of the oscillations in the phase shifter, in radians.

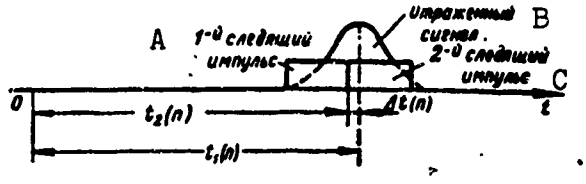


Fig. 7.31. Mutual positions of tracking and reflected pulses. A) First tracking pulse; B) reflected signal; C) second tracking pulse.

In most cases what are used are capacitive phase shifters in which the phase shift of the output signal is proportional to the rotation angle of the rotor. The axis of the phase shifter is rotated by an actuating electric motor. From the point of view of its dynamic properties the phasometric delay line may be considered inertialess if the rotation angle of the phase shifter $\varphi$ is viewed as an input signal, and if delay time $t_z$ is taken as the output quantity. On this assumption the RTsZ equation takes the form

$$t_з = K_{\text{рез}} \cdot \varphi.$$

When a controlled generator of harmonic oscillations is used as the actuating device, the tracking pulses are displaced relative to the reflected signal by retuning the frequency of this oscillator. The magnitude of the pulse shift during one period is proportional to the phase difference accumulated during time $T_p$ between the oscillations of the

control generator frequency and those of frequency $F_p$:

$$\delta t(n) = \frac{\Delta\varphi(n)}{2\pi} T_n = \frac{T_n}{2\pi} \int_{(n-1)T_n}^{nT_n} \Delta\omega(t)\,dt = \frac{1}{F_n} \int_{(n-1)T_n}^{nT_n} \Delta f(t)\,dt, \quad (7.65)$$

where $\delta t(n)$ is the shift of the tracking pulses relative to the reflected signal in the nth repetition period; $\Delta\Phi(n)$ is the phase difference in the nth repetition period; $\Delta f = f(t) - F_p$ is the current value of the frequency deviation of the controlled generator from frequency $F_p$.

The change in the frequency of the retuned generator follows practically instantaneously upon change in the control voltage

$$\Delta f(t) = k_r F_n u(t),$$

where $u(t)$ is the control voltage; $k_g$ is the frequency retuning factor.

Substituting the value of $\Delta f(t)$ into Eq. (7.65), we obtain

$$\delta t(n) = k_r \int_{(n-1)T_n}^{nT_n} u(t)\,dt. \quad (7.66)$$

The integral in the right part of (7.66) is a $T_p$ times increased average value of the control voltage in the nth repetition period. Therefore, Expression (7.66) may be rewritten in the form

$$\delta t(n) = k_r T_n U_y(n),$$

where $U_u(n)$ is the average value of the control voltage in the nth period.

If we assume that in the $(n-1)$th period the tracking pulses are delayed by time $t_2(n-1)$ relative to the outcoming pulses (Fig. 7.31), in the nth period after shift of the tracking pulses under the influence of the control voltage, the delay time will decrease by the quantity $\delta t(n-1)$, and

$$t_2(n) = t_2(n-1) - \delta t(n-1).$$

Since $\delta t(n-1) = k_r T_n U(n-1)$,

$$t_2(n) = t_2(n-1) - k_r T_n U(n-1)$$

or

$$t_2(n) - t_2(n-1) = -k_r T_n U(n-1). \qquad (7.67)$$

Expression (7.67) represents the difference equation of the controlled generator functioning as the actuating device of the ASD system. The minus sign in the right side of Eq. (7.67) indicates that value $t_2(n)$ must be reduced by comparison with $t_2(n-1)$ so as to eliminate the mismatch which has arisen.

To determine the dynamic properties of a controlled generator as a link in a control system we may find its transfer characteristic. We assume that the control voltage at moment $t = 0$ has jumped from zero to a certain value $U_0$ and henceforth remains constant. For the sake of simplicity we also assume that before the moment when the voltage is supplied the time shift $t_2 = 0$. Then, on the basis of (7.67) one can write the series

$$\begin{aligned} t_2(0) &= 0, \\ t_2(1) &= -k_r T_n U_0, \\ t_2(2) &= -2k_r T_n U_0, \\ &\cdots\cdots\cdots \\ t_2(n) &= -nk_r T_n U_0. \end{aligned} \qquad (7.68)$$

Expression (7.68) determines the transfer characteristic of the controlled generator when the type of jump is disturbed. The points of the transfer characteristic lie on a straight line which passes through the origin of the coordinate. The slope of the straight line is determined by the product $k_g T_p$. An integrator has such a transfer characteristic. Consequently, from the point of view of its dynamic properties, the controlled generator used as the actuating device of the ASD system is an ideal integrating link whose transmission factor is $k_1 = k_g T_p$.

## §7.10. THE DYNAMIC PROPERTIES AND ACCURACY OF PULSE RANGE AUTOTRACK SYSTEMS (ASD)

Range-measurement accuracy is determined by the size of the tracking error in the steady state. This latter depends both upon the charac-

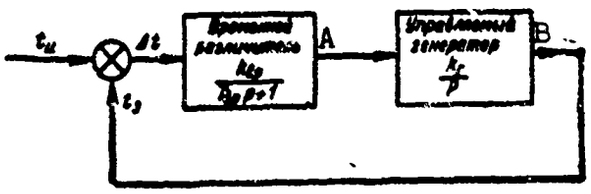


Fig. 7.32. Structural diagram of ASD system with one integrator. A) Time discriminator; B) controlled generator.

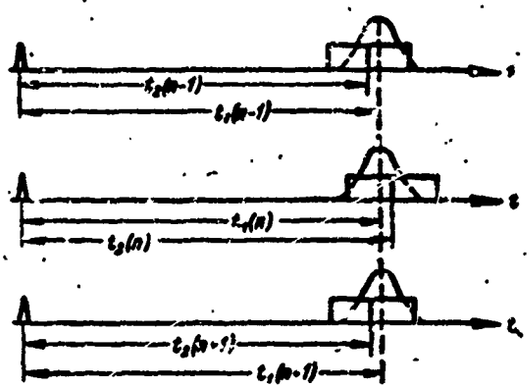

Fig. 7.33. Undamped oscillations in ASD system.

ter of the target's motion and upon the structural diagram of the system. The number of integrating links connected in series in the control circuit has a particularly strong influence upon the quality indicators of the ASD system. In practice, ASD systems are used with one or two integrators.

1. ASD Systems with One Integrator

A structural diagram of an ASD system with one ideal integrator is given in Fig. 7.32. A controlled generator acts as the integrator. In contrast to continuous systems which are described by a second order equation, the pulse ASD system may become unstable if its parameters have certain values. Let us define the conditions of stability of a pulse system. The processes in the system may be described using three difference equations:

1) The equation of the time discriminator

$$U(n) - AU(n-1) = k_s(1-A)\Delta t(n); \tag{7.69}$$

2) the equation of the controlled generator

$$t_2(n) - t_2(n-1) = -k_r T_n U(n-1); \tag{7.70}$$

3) the equation linking the tracking error $\Delta t(n)$ with the time position of the reflected signal and the range pulses (see Fig. 7.31),

$$\Delta t(n) = t_2(n) - t_1(n). \tag{7.71}$$

If the middle of the reflected signal is taken as the origin of the coordinates, the value of tracking error $\Delta t(n)$ will be equal to $t_2(n)$, and Eq. (7.70) will be rewritten in the form

$$\Delta t(n) - \Delta t(n-1) = -k_r T_n U(n-1). \tag{7.72}$$

The boundary stability of the system is determined by the moment at which sustained oscillations occur in it. The conditions for the occurrence of sustained oscillations are (Fig. 7.33)

$$\left.\begin{aligned} \Delta t(n) &= -\Delta t(n-1), \\ U(n) &= -U(n-1). \end{aligned}\right\} \tag{7.73}$$

At these boundary conditions the system of difference equations (7.69), (7.70) and (7.71) describing processes in the ASD circuit is converted into

$$\left.\begin{aligned} (1+A)U(n) &= k_s(1-A)\Delta t(n), \\ 2\Delta t(n) &= k_r T_n U(n). \end{aligned}\right\} \tag{7.74}$$

Simultaneous solution of Eq. (7.74) gives the condition for the generation of sustained oscillations in the system

$$2(1+A) = k_s k_r T_n (1-A).$$

Since the product $k_v k_g$ is the transmission factor of an open ASD system, the stability condition may be expressed by the following inequality:

$$K < K_{gr} = \frac{2}{T_n}\frac{1+A}{1-A}, \tag{7.75}$$

where $K_{gr}$ is the boundary transmission factor of an ASD system.

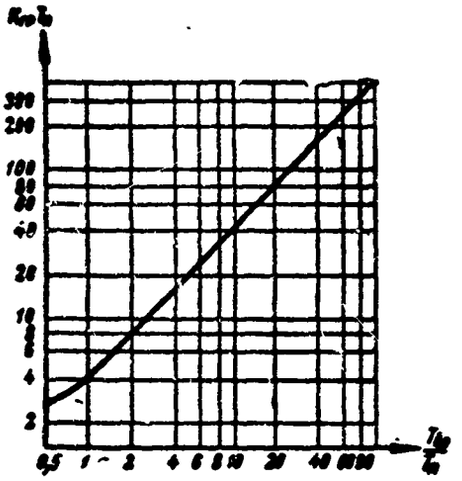

Fig. 7.34. The boundary transmission factor of an ASD system with one ideal integrator as a function of the time constant of the time discriminator.

If the time constant of the transfer characteristic of the time discriminator is much greater than the pulse repetition period ($T_{vr} >> T_p$), the following approximate expression may be used to determine the area of stability:

$$K < \frac{4T_{vr}}{T_u^2}.$$

Figure 7.34 is a graph representing the boundary transmission factor of the system as a function of the relative time constant of the transfer characteristic of the time discriminator. With increase in the ratio $T_{vr}/T_p$ the boundary transmission factor also increases. This may be explained by the fact that with increase in $T_{vr}/T_p$ the properties of the ASD system approach those of the linear systems of continuous control described by the second order equation, and they, as is known, are stable for any gain factor.

Range autotrack systems with a single integrating link possess first order astaticism. This means that if the ASD system measures the range of a target whose radial velocity relative to the RLS is constant and equal to $V_r$, the steady-state tracking error will be equal to a constant

quantity.

The physical presence of this error is explained by the fact that a certain constant voltage, varying the generator frequency, must be present at the output of the time discriminator in order to ensure movement of the tracking pulses with a velocity proportional to $V_r$. This voltage, in turn, may appear only if there is a constant tracking error.

In the case of a stationary target the repetition period of the reflected signals is equal to the pulsing period of the outcoming pulses. The repetition frequency of the tracking pulses should coincide with the frequency of the received signals. Since the rated frequency of a retuned generator is $F_p$, during tracking of a motionless target the control voltage is zero, and there is no error in the AFD system.

In the case of a moving target the repetition frequency of the received signals $F_{pr}$ differs from the repetition frequency of the emitted pulses by the magnitude of the Doppler frequency shift

$$F_{пр} = F_п\left(1 - \frac{2V_r}{c}\right).$$

For tracking a target it is necessary that the repetition frequency of the tracking pulses be $F_{pr}$. In the steady state this may be assured only by changing the frequency of the retuned generator by quantity $\Delta F = 2V_r/c\ F_p$. The frequency shift of the controlled generator is due to the presence of a constant voltage $U_{vr}$ at the output of the time discriminator. Since $\Delta F = k_g F_p U_{vr}$, the steady-state output voltage at the discriminator output is proportional to the radial velocity of the target's motion

$$U_{вр} = \frac{1}{k_г}\frac{2V_r}{c}. \qquad (7.76)$$

Constant voltage $U_{vr}$ is formed by mismatch $\Delta t$ between the time position of the reflected signal and the tracking pulses

$$\Delta t = \frac{2\Delta R}{c} = \frac{U_{вр}}{k_{вр}}, \qquad (7.77)$$

where $\Delta R$ is the target tracking error.

Substituting value $U_{vr}$ from Formula (7.76) into Formula (7.77) and solving the equation for the tracking error, we obtain

$$\Delta R = \frac{V_r}{K}.$$

The tracking error of a target which is moving at a constant radial velocity relative to the RLS is inversely proportional to the transmission factor of the ASD system.

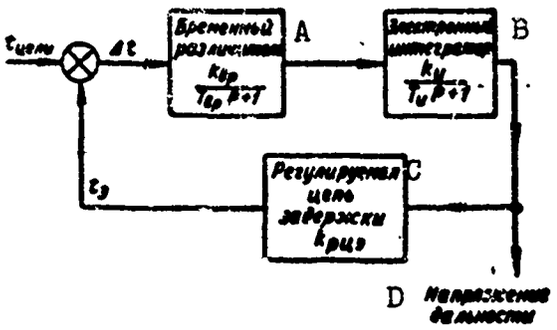


Fig. 7.35. Structural diagram of an ASD system with an electronic integrator. A) Time discriminator; B) electronic integrator; C) adjustable delay line; D) range voltage.

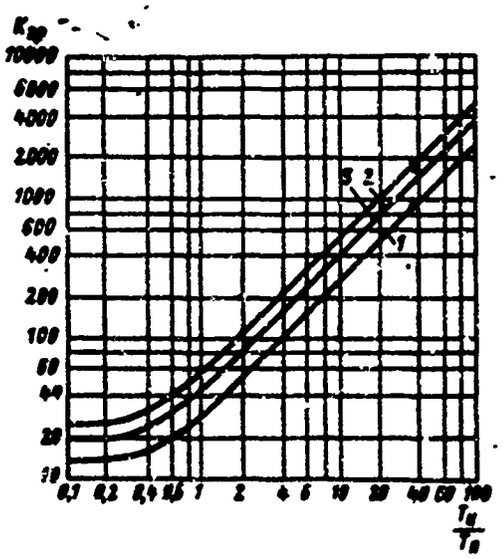


Fig. 7.36. The boundary transmission factor of an ASD system with one integrating amplifier as a function of the time constant of the integrator. Curves are given for three values of the time constant of the time discriminator filter: $1 - T_д = 40T_и$; $2 - T_д = 20T_и$; $3 - T_д = 10T_и$.

Electronic ASD systems with adjustable delay lines use as their integrating elements amplifiers with capacitive feedback. Figure 7.35 gives a structural diagram of an ASD system with an electronic integrator. It can be demonstrated by the stability condition of such a system is determined by the inequality

$$K < \frac{1+A}{1-A} \frac{1+e^{-\frac{T_{\text{д}}}{T_{\text{и}}}}}{1-e^{-\frac{T_{\text{д}}}{T_{\text{и}}}}},$$

where $K$ is the transmission factor of an open ASD system; $T_i$ is the time constant of an integrating amplifier.

Figure 7.36 is a graph representing the boundary gain factor as a function of the time constant of an integrating amplifier. With increase in $T_i$ the boundary transmission factor of the ASD system grows.

As was demonstrated above, such ASD systems cannot in principle be considered astatic, since the integrating amplifier is an aperiodic link with a large time constant. However, when the value of $T_i$ is many times greater than the time of the transient processes in the system, and with a large value of $K$ in the first approximation, conclusions relative to tracking errors in astatic ASD systems may also be utilized to evaluate systems with a single integrating operational amplifier.

Under actual conditions the signals reaching the autotrack circuit are not constant in amplitude but fluctuating, and sometimes the reflected pulse may disappear entirely for a certain time. When the target signal disappears, the control circuit is interrupted (there are no pulses at the output of the coincident stages of the time discriminator), and the voltage in the condenser of the comparison circuit of the time discrimirator begins gradually to be discharged with time constant $T_r$:

$$u_{\text{вр}} = u_{\text{вр}_0} e^{-\frac{t}{T_{\text{р}}}},$$

where $u_{vr_0}$ is the output voltage of the time discriminator at the moment when the reflected signal disappears.

Reduction of the voltage in the time discriminator leads to a decrease in the velocity of movement of the tracking pulses. The system continues to track the target; however, because the tracking speed is declining, the tracking error increases. If we assume that the target velocity remains unchanged during the time of disappearance of the signal, the tracking error at the moment of its appearance will be the quantity

$$\Delta R = V_c \left[\frac{1}{K} - \tau_з + T_р\left(1 - e^{-\frac{\tau_з}{T_р}}\right)\right],$$

where $\tau_z$ is the fading time of the signal.

If time $\tau_z << T_r$, the tracking error will hardly increase at all when the signal disappears, but if the fading time is large, the error may attain a value in excess of the length of the tracking pulse, and the ASD system loses the target.

Thus, the ASD system with one integrator can "remember" position, but its "memory" of velocity decreases over time. This is due to the inertia of the comparison circuit of the time discriminator.

2. <u>ASD Systems with Two Integrators</u>

The basic drawbacks of autotrack systems with a single integrator are the presence of considerable errors in the measurement of the range of rapidly moving objects and the possibility of losing the target when the reflected signal disappears for an extended time. ASD systems with two integrators are used to eliminate these drawbacks:

circuits with a retuned generator and an electronic integrator;

circuits with RTsZ and two integrating amplifiers;

electromechanical ASD systems with one electronic integrator.

It is known from the theory of automatic control that systems with

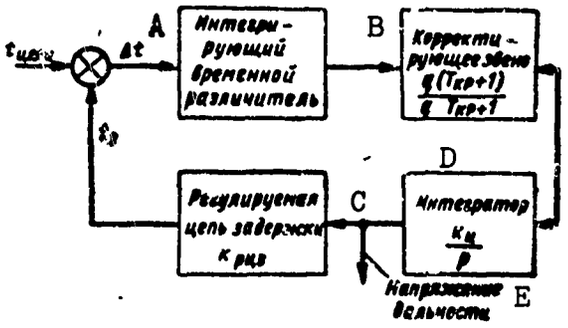


Fig. 7.37. Structural diagram of ASD system with two integrators. A) Integrating time discriminator; B) correcting link; C) adjustable delay line; D) integrator; E) range voltage.

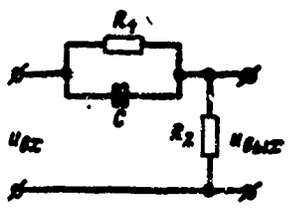

Fig. 7.38. Circuit of a correcting link.

two series connected integrating links are structurally unstable and that additional correcting links must be introduced to make them stable. Let us undertake an approximate analysis of the stability of systems with two integrators, assuming that both integrators are ideal and that the system is continuous.

Figure 7.37 gives one of the possible structural diagrams of a stabilized ASD system with two integrators. Stabilization is achieved by introducing into the control circuit a correcting link whose main circuit is given in Fig. 7.38. The transmission function of this link is

$$W_к(p)=\frac{q(T_к p+1)}{qT_к p+1}, \qquad (7.78)$$

where $q=\frac{R_2}{R_1+R_2}$; $T_к=R_1C$.

By taking into account Expression (7.78) it is easy to demonstrate that the transmission function of a stabilized ASD system with two integrators has the form

$$W(p)=\frac{1}{1+\frac{K}{p^2}\frac{q(T_к p+1)}{qT_к p+1}}=\frac{p^2(qT_к p+1)}{p^3T_к q+p^2+pqT_к K+qK}, \qquad (7.79)$$

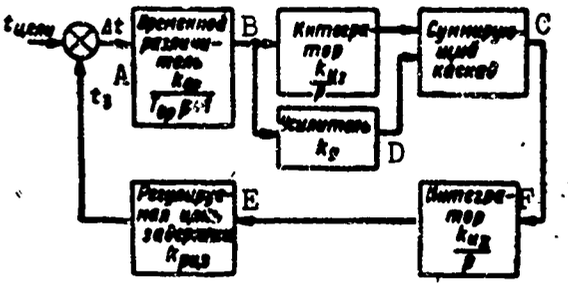

Fig. 7.39. Structural diagram of stabilized ASD system with two integrator. A) Time discriminator; B) integrator; C) summing stage; D) amplifier; E) adjustable delay line; F) integrator.

where $K=k_{ор}k_{рыз}k_{и}$.

It follows from Expression (7.79) that the condition of stability of an ASD system (on the basis of the Hurwitz criterion) is determined by the inequality

$$KT_{и}>KT_{з}q$$

or

$$q=\frac{R_2'}{R_1+R_2}<1. \qquad (7.80)$$

Inequality (7.80) shows that a stabilized system is stable regardless of the parameters of the correcting network. However, at values of $q$ close to unity the reserve of stability is small.

Another way to stabilize an ASD system with two integrators is to shape the controlling action from two voltages, one of the m proportional tc the unitary, and the other to the compound integral of the magnitude of the tracking error. Figure 7.39 gives a structural diagram of an ASD system which is stabilized in this way. Its transmission function has the form

$$W(p)=\frac{1}{1+\frac{k_{ор}k_{ин}k_{рыз}}{p(T_{ор}p+1)}\left(\frac{k_{и1}}{p}+k_{у}\right)}=$$
$$=\frac{p^2(T_{ор}p+1)}{p^3T_{ор}+p^2+k_{ор}k_{рыз}k_{ин}k_{ус}p+k_{ор}k_{рыз}k_{ин}k_{и1}}. \qquad (7.81)$$

On the basis of the Hurwitz criterion the condition of stability

of the ASD system with two integrators is determined by the inequality

$$k_{вр}k_{рид}k_{и2}k_{ус} > k_{вр}k_{рид}k_{и1}k_{и2}T_{вр}$$

or

$$k_{ус} > k_{и1}T_{вр}.$$

Stability of the system is ensured by appropriate selection of a gain factor for one of the branches of the summing device.

A simple way to stabilize ASD systems is to connect a correcting resistance directly into the feedback circuit of the integrating amplifier (Fig. 7.40). The transmission function of such an operational amplifier may be approximated in the following form:

$$W_{оу}(p) \approx -\frac{z_в(p)}{z_в(p)} = \frac{1}{pCR_в} + \frac{R_в}{R_в}.$$

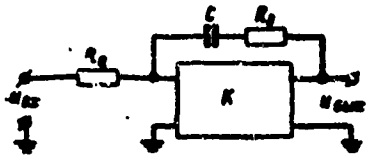


Fig. 7.40. Circuit of operational amplifier with capacitive-resistor feedback.

The output voltage of an operational amplifier consists of two components, one proportional to the input signal and the other to the integral of the input signal. It is obvious that this stabilization technique is completely equivalent to the preceding one. Therefore, in this case the condition of stability of an ASD system may be expressed by the inequality

$$\frac{R_в}{R_в} > k_{и1}T_{вр}. \qquad (7.82)$$

System stability is ensured by the selection of the resistances of the operational amplifier.

As can be seen from Expression (7.69) and (7.71) ASD systems with two integrators are second order astatic systems (inclusion of the correcting circuits does not lower the order of astaticism).

The range measurement error in the steady state depends upon the character of the target's motion. For example, let us assume that the target is moving at a constant acceleration, so that the range changes

in accordance with the law

$$R = R_0 + V_r t + \frac{1}{2} a t^2.$$

In this case the ASD system is influenced by control stimulus

$$t_R = \frac{2R_0}{c} + \frac{2V_r}{c} t + \frac{a}{c} t^2.$$

In the case of this sort of stimulus the error of an automatic rangefinder may be found by methods of operational calculus. The transform of the control stimulus has the form

$$t_R(p) = \frac{1}{p} \frac{2R_0}{c} + \frac{1}{p^2} \frac{2V_r}{c} + \frac{1}{p^3} \frac{a}{c}.$$

As is known, the transform of the tracking system error is equal to the product of the transmission function and the transform of the input stimulus:

$$\Delta t(p) = W(p)\, t_R(p) = \frac{p^2 (T_{\text{вр}} p + 1)\left[\frac{1}{p} \frac{2R_0}{c} + \frac{1}{p^2} \frac{2V_r}{c} + \frac{1}{p^3} \frac{a}{c}\right]}{p^2 T_{\text{вр}} + p^2 + k_{\text{вр}} k_{\text{рыз}} k_{\text{н1}} k_{\text{ус}} p + k_{\text{вр}} k_{\text{рыз}} k_{\text{н2}} k_{\text{н1}}}.$$

In accordance with the boundary value theorem the tracking error in the steady state

$$\Delta t_{\text{уст}} = \lim_{p \to 0} p W(p)\, t_R(p) = \frac{a}{c k_{\text{вр}} k_{\text{рыз}} k_{\text{н1}} k_{\text{ис}}}$$

or

$$\Delta R_{\text{уст}} = \frac{a}{k_{\text{вр}} k_{\text{рыз}} k_{\text{н1}} k_{\text{ис}}} = \frac{a}{K}.$$

If an automatic rangefinder with two integrators measures the range of a target moving with constant velocity relative to the RLS, the tracking error in the steady state will be zero. When the target is moving with a constant acceleration the range measurement error will be inversely proportional to the transmission factor of the ASD system. Thus, in order to reduce the errors caused by target movement it is necessary to strive to increase the transmission factor. However, the selection of quantity $K$ is affected by a series of other factors, fundamental ones

being the required stability reserve, length of the transient process, and random errors caused by fluctuating noise.

Temporary fading of the reflected signal does not suspend the operation of an autotrack system with two integrators. When the target pulses are lost, and the tracking pulses will continue to move out at their former velocity, equal to the target velocity at the moment when the signal was lost.

ASD systems with two integrators affect continuous automatic measurement not only of the target range, but also of its velocity. Actually, in the tracking mode the voltage at the output of the second integrator is proportional to target range at any moment in time, while the voltage at its input is proportional to the derivative of the range, that is, to the radial velocity of the target. In ASD systems with a retuned generator the generator itself is the second integrating link; therefore, the control voltage which is fed to the reactance tube is proportional to $V_r$. In autotrack systems with a phasometric adjustable delay line, the output integrating element is an electric motor the angle of rotation of whose shaft is proportional to the target range. Consequently, the angular velocity of he axis is linearly independent upon the radial velocity of the target.

Thus, all types of ASD systems with two integrators track the target not only with respect to range, but also with respect to velocity, generating data on the $V_r$ in the form of a voltage or of an angular rotation velocity of the axis of the actuating device.

3. Accuracy of ASD Systems when Acted upon by Random Noise

Above we have been examining the dynamic errors of ASD systems due to target movement. In addition to these regular errors there are also random errors due to the effect of internal and external noises. The effect of noise is to change the amplitude and shape of the useful sig-

nal. Random variations of the signal lead to an increase or a decrease in its area within these limits of each tracking pulse. A fluctuating error voltage, which is not linked with the target's position in space, appears at the output of the time discriminator. This voltage, which is a disturbing stimulus applied to the ASD system, causes random displacement of the target pulses.

Below we give an approximate evaluation of the random error of an ASD system due to internal receiver noises.

As has been demonstrated in §7.8, from the point of view of the least error in range reading, division of the pulse area into two equal parts is a very nearly optimum operation. Therefore, it may be considered that the mean square error of each measurement of range by the automatic rangefinder (when the signal/noise ratio is large) approaches the theoretical limit, equal to

$$\sigma_{R_1}=\frac{c}{2}\sqrt{\frac{\tau_u N_0}{4\Delta f E}},$$

where $E$ is the energy of the received signa; $N$ is the spectral density of the noise, $\Delta f$ is the passband of the receiver device.

The ASD system averages the random measurement error. The time needed for averaging is determined by the form of the frequency characteristic of the automatic rangefinder, mainly by the width of its effective passband $\Delta F_e$. As an approximation it may be considered that the ASD systems accumulate pulses during time $T_n=\frac{1}{\Delta F_e}$. The quantity of integrated pulses is

$$n=\frac{T_n}{T_u}=\frac{1}{\Delta F_e T_u}.$$

In accumulation the mean square error of range measurement is reduced $\sqrt{n}$ times. Consequently,

$$\sigma_R=\frac{c}{2}\sqrt{\frac{\tau_u N_0}{4\Delta f p_c \tau_u n}}=\frac{c}{4}\sqrt{\frac{N_0 T_u \Delta F_e}{p_c \Delta f}}. \qquad (7.83)$$

Formula (7.83) is valid for the case when the receiver device is open only during the time of the useful signal, that is, the total length of the tracking date is equal to the length of the reflected signal. In practice, the total length of the range pulses $2\tau_{str}$ is selected larger than the length of the receiver signal. This ensures a very steep discriminator characteristic, widens its working region, and makes it easier to lock into a useful search signal.

If $2\tau_{str} > \tau_i$, there is an increase in the energy of the noise acting upon the ASD system. Noise not only distorts the shape and changes the amplitude of the useful signal, but it also gives rise to separate voltage blips during the time when the reflected signal $(2\tau_{str} - \tau_i)$ is absent. As a result of this, increase in the length of the tracking pulses leads to increased dispersion in the tracking error. In this case, the magnitude of mean square error $\sigma_R$ may be evaluated from the approximate formula

$$\sigma_R \approx \frac{c}{4}\sqrt{\frac{N_0 T_n \Delta F_0}{p_c \Delta f}\left(\frac{4\tau_{стр}}{\tau_u} - 1\right)}.$$

It is often assumed that $\tau_{str} \approx \tau_i$ on the condition

$$\sigma_R \approx \frac{c}{4}\sqrt{\frac{3N_0 T_n \Delta F_0}{p_c \Delta f}}.$$

As can be seen from Formula (7.73) the mean square error in tracking a target with respect to range, caused by the presence of noise and by the spectral density of the noise, depends upon the width of the frequency characteristics of the ASD system. In turn, the frequency characteristic of the automatic rangefinder is determined by its transmission function (let us recall that the frequency characteristic is obtained from the transmission function by replacing $p$ by $j\omega$).

The frequency characteristic of an ASD system with one integrator has the form

$$\Phi(j\omega) = \frac{K}{K - \omega^2 T_{vr} + j\omega}, \qquad (7.84)$$

where $K$ is the transmission factor of the system; $T_{vr}$ is the equivalent time constant of the time discriminator.

The modulus of the frequency characteristic

$$|\Phi(j\omega)| = \frac{K}{\sqrt{(K - \omega^2 T_{vr})^2 + \omega^2}}.$$

Figure 7.41 gives graphs of the modulus of the frequency characteristic of an ASD system with one integrator for various relations between the system transmission factor and the discriminator time constant. Increase in the ratio $K/T_{vr}$ causes a broadening of the frequency characteristic and, consequently, increase in the fluctuation error of the ASD system. Analogous results may also be obtained for ASD systems with two integrators.

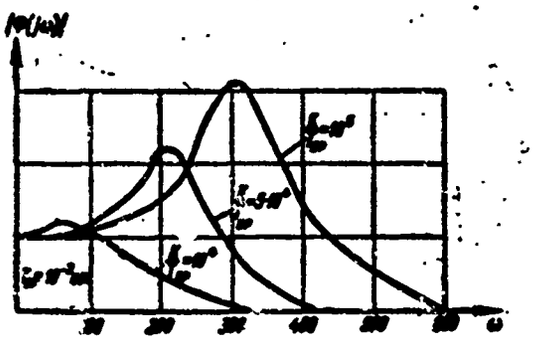

Fig. 7.41. Frequency characteristics of the ASD system.

Thus, increase in the transmission factor leads, on one hand, to a reduction in the dynamic errors caused by target motion and, on the other, to an increase in the errors caused by receiver noise. The optimum transmission factor should ensure a minimum value of the total autotrack error.

In addition to errors caused by receiver noise in ASD systems random errors may arise due to various circuit instabilities, principally

to instability of time delay (instability in the length of the phantastron pulse, phase instability of the controlled generator, etc.). The influence of the instability of time delay circuits upon the accuracy of range measurement depends upon the purpose of the autotrack system. If the automatic rangefinder yields information on the distance to the target in the form of a voltage tapped from the integrator output, rapid fluctuations of the delay time in the RTsZ circuit will have an insignicant influence upon the accuracy of range measurement. The reason for this is that between the source of the fluctuations and the system output there is a series of inertial and integrating links (the filter of the time discriminator and the integrators) which smooth out rapid variations in the error voltage. If target range is reckoned from the leading edge of the first tracking pulse (as is done in ASD systems with a controlled generator), rapid fluctuations in delay time leading to variation in the time position of the tracking pulses (for example, fluctuation of the controlled generator frequency) give rise to range measurement errors which are not averaged by the circuit of the automatic rangefinder. Slow variations in the generator frequency are eliminated by the tracking system and do not lead to range measurement errors.

## §7.11. SYSTEMS FOR AUTOMATIC VELOCITY TRACKING OF A TARGET

One of the possible methods of automatic velocity tracking of a target was examined in the description of ASD systems. This method is sufficiently simple and makes it possible to obtain data on target range and velocity at the same time. However, in many cases the accuracy of velocity measurements is inadequate. This is due to the fact that the basis of this method is the method of differentiation of range, velocity being determined as an increment in range between two pulse packets. These increments are small by comparison with the range itself,

and their measurements are therefore inaccurate; this leads to considerable fluctuations in the velocity voltage. The ASD system does not average the velocity data adequately, since the second integrating link does not participate in the averaging. This drawback may be eliminated by smoothing the obtained velocity data.

The mean square error of velocity measurement in smoothing may be calculated in the first approximation according to formula

$$\sigma_V^2 \approx \frac{\sqrt{3}\sigma_R^2}{T},$$

where $\sigma_R^2$ is the mean square error of range tracking of the target; $T$ is the time of averaging of the data.

An increase in time $T$ leads to reduction in the velocity measurement error; however, there is at the same time a delay in the output of information which in many instances may be acceptable. Wherever an extended time for smoothing the results of measurement is allowable, this method may yield satisfactory results.

The most accurate method of measuring target radial velocity is the one based on automatic tracking of the shift in the Doppler frequency of the received signal. Since the range of variation in Doppler frequency may be as high as hundreds of a percent of the carrier frequency $\left(\Delta F_д = \frac{2V_{r\,макс}}{c} f_0\right)$ in the case of rapidly flying objects, radar stations which track target velocity must possess a sufficiently wide passband (for example, at $V_{r\,макс}$ = 8 km/sec and $f_0$ = 10,000 Mhz the required receiver passband must exceed 1 Mhz).

This, in turn, means that the signal/noise ratio at the output of the receiver device may be very small, and the accuracy of velocity measurement will be low.

A substantial improvement in the signal/noise ratio may be obtained by connecting a narrow-band tracking filter into the receiver strip,

automatically tuned to the current value of the received signal frequency. Such a tracking filter can be connected because the frequency of the received signal varies comparatively slowly, while the automatic tracking radar station measures the coordinates of only a single target at one time.

There are two types of tracking filters – the frequency-tracking filter and the phase-synchronized tracking filter.

1. The Frequency-Tracking Filter

The automatic frequency-tracking filter is essentially a system of automatic frequency control of the heterodyne from the received signal. Figure 7.42a gives a block diagram of a frequency-tracking filter. Input signal $f_s$ is limited in amplitude and fed to a mixer which at the same time receives oscillations $f_n$ from a controlled heterodyne. An intermediate-frequency signal $f_p$, equal to the difference in the frequencies $f_n$ and $f_s$, is fed to a narrow-band quartz filter and to a frequency discriminator tuned to frequency $f_{po}$. In the case when the intermediate frequency differs from $f_{po}$, at the discriminator output is generated an error voltage whose magnitude and sign depend upon the size and direction of the deviation of the intermediate frequency. There is an integrating device at the discriminator output, which suppresses rapid fluctuation of the error voltage due to noise.

The control voltage from the integrator output is fed to a reactance tube which acts upon the heterodyne in such a way as to cause the intermediate frequency to approximate a value equal to $f_{po}$.

The heterodyne, the mixer, the discriminator, the integrating circuit, and the reactance tube form a closed automatic frequency control system (APCh). The band of the APCh system should be narrow, but at the same time it should ensure sufficiently accurate reproduction of the frequency variation caused by the Doppler effect. The transmission fac-

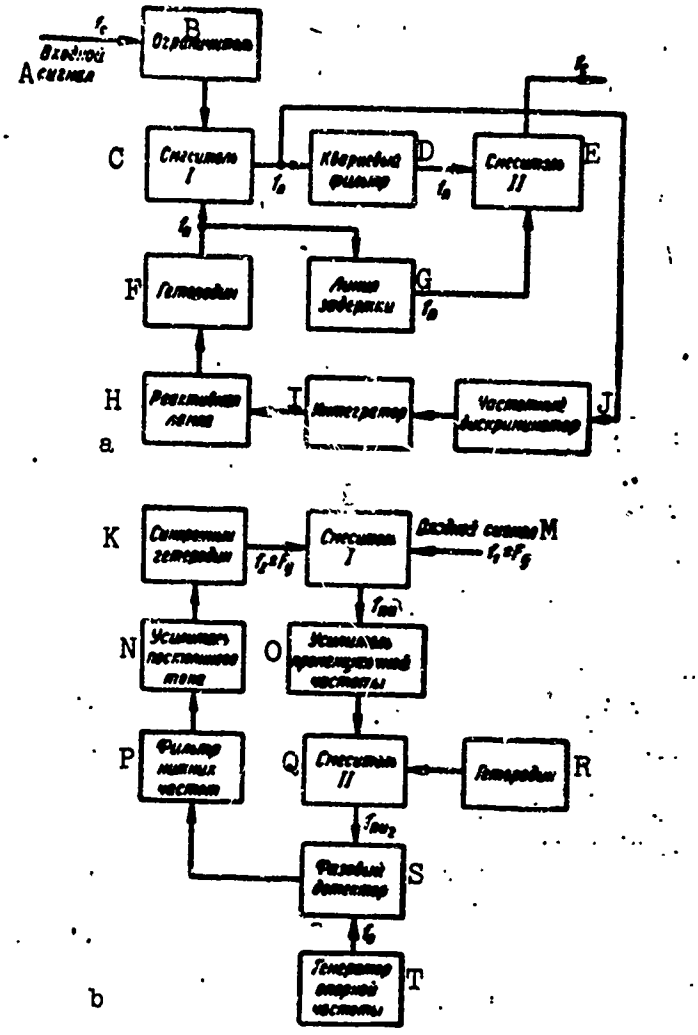


Fig. 7.42. Narrow-band tracking filters: a) Block diagram of frequency-tracking filter; b) block diagram of phase-synchronized tracking filter. A) Input signal; B) limiter; C) mixer I; D) quartz filter; E) mixer II; F) heterodyne; G) delay line; H) reactance tube; I) integrator; J) frequency discriminator; K) synchronous heterodyne; L) mixer I; M) input signal; N) direct current amplifier; O) intermediate-frequency amplifier; P) low-frequency filter; Q) mixer II; R) heterodyne; S) phase detector; T) generator of reference frequency.

tor of the system should be large enough so that the maximum static error of the system is several times smaller than the passband of the quartz filter. Thus, if the overall range of variation of the received signal frequency is $\Delta F_d$, while the passband of the quartz filter (for it is the effective passband of the frequency-tracking filter) is $\Delta F_e$, the transmission factor of the APCh system should be not less than

$(4-5)\Delta F_d/\Delta F_e$. Selection of such a transmission factor ensures that the circuit will operate in the linear section of the phase-frequency characteristic of the quartz filter.

The output signal of the quartz filter is mixed in the second mixer with the heterodyne oscillation delayed by time $t_z$, this being equivalent to the phase shift in the quartz filter. The mixer output yields a voltage which is free from noise, which is delayed relative to the received signal by time $t_z$, and which coincides with it in frequency with accuracy up to the error of the automatic frequency control system.

2. The Phase-Synchronized Tracking Filter

Figure 7.42b gives a block diagram of the phase-synchronized filter. Received signals of frequency $f_1 \pm F_d$ are transformed in the mixer into signals o the first intermediate frequency $f_p$. This transformation is accomplished by a synchronous generator with frequency $f_2 \pm F_d$. The oscillations of the first intermediate frequency are amplified and transformed in a local heterodyne into signals of the second intermediate frequency $f_{pch2}$. The phase of the oscillations of $f_{pch2}$ is compared in the phase detector with the phase of the oscillations of the reference heterodyne. The output voltage of the phase detector is proportional to the cosine of the phase difference of the compared oscillations. If the phase difference is 90°, the detector output voltage is zero. At an angle greater or less than 90°, the output signal has, respectively, a positive or a negative value. The low-frequency filter passes only the slow fluctuations of the phase detector output voltage. The rapid fluctuations due to noise are suppressed and do not reach the input of the direct current amplifier. The output voltage of the amplifier controls the generator in such a way that the phase difference between the received signal oscillations and the heterodyne voltage approaches close to zero.

If the input signal $f_1$ starts to vary due to the Doppler effect, these variations are fed to the input of the second mixer and cause a change in the phase of the signal fed to the input of the phase detector. These phase variations create an error voltage at the phase detector output, and this in turn changes the frequency of the synchronous heterodyne by the same quantity as the change in the received signal frequency. The phase error is again reduced to zero. The Doppler frequency reading which is thus obtained appears at the output of the synchronous heterodyne as a sinusoidal signal which is practically free of noise.

In determining the parameters of the tracking system it is necessary to take into account the following constraints: the passband of the phase-synchronized filter must be as small as possible, in order to achieve maximum suppression of noise, but it must be large enough so that the synchronous heterodyne can reproduce without distortion the frequency changes caused by the Doppler effect.

The advantage of the phase-synchronized tracking filter over the frequency-tracking filter is that it represents a phase automatic frequency control system and, consequently, does not have any static error.

## §7.12. BINARY READOUT OF RANGE AND RADIAL VELOCITY

The readout of range in binary code is based on counting the number of pulses $N_R$ arriving in interval $\tau = 2R/c$, if they are repeated at a sufficiently high and stable frequency $F$:

$$N_R = \frac{2F}{c} R. \tag{7.85}$$

Range is reckoned at discrete intervals

$$\Delta R = \frac{c}{2F}, \tag{7.86}$$

which decline with increase in frequency $F$.

The transformation of range into a binary number is accompanied by two kinds of instrumental errors. The first kind of error is due to

the fact that the reading is discrete and the repetition frequency of the counter pulses is unstable. Errors of the second kind are due to breakdown. Breakdown is an interruption of the normal operation of the transformation device at certain moments in time. It can lead to an incorrect range reading in any digit, that is, to the appearance of very large errors. Therefore, transformation circuits must be so designed that breakdown is unconditionally eliminated.

Below we give an estimate of instrumental error in range measurement due to reading discreteness $\Delta R$ and frequency instability $F$, and we also examine transformation circuits which eliminate breakdown.

Since the counted range value $N_R$ is proportional to frequency $F$, the relative range measurement error is equal to the relative frequency instability

$$\frac{\sigma_R}{R}=\frac{\sigma_F}{F},$$

where $\sigma_F$ is the mean square frequency deviation.

Consequently, the error due to instability in the repetition frequency of the counter pulses

$$\sigma_R=R\frac{\sigma_F}{F}$$

is proportional to range and is particularly great at large ranges. In order to reduce it, counter pulse generators are quartz stabilized.

The errors due to reading discreteness $\Delta R$ depend upon whether or not the position of the counter pulses is matched with the starting point of the range reckoning.

When the position of the counter pulses is coordinated with the starting-point of the range reading, the reckoned number $N_R$ remains unchanged as range varies within the limits $\Delta R$ (Fig. 7.43a). Since any true value of range in the interval $\Delta R$ is equally probable, the mean square measurement error

$$\sigma_R = \frac{\Delta R}{2\sqrt{3}} \approx 0{,}3\Delta R,$$

as may be found by analogy with Formula (7.2).

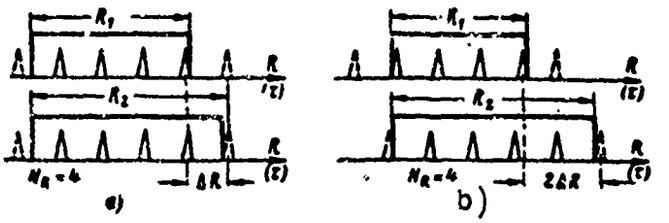


Fig. 7.43. Range measurement errors due to reading discreteness: a) When the position of the counter pulses is coordinated with the starting-point of the range reckoning; b) in the absence of such coordination.

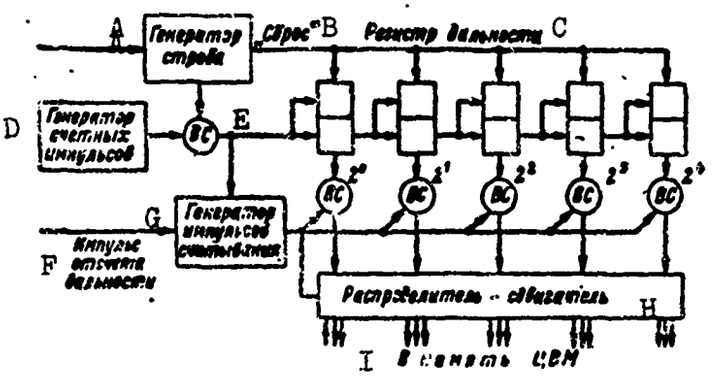


Fig. 7.44. Circuit for range readout in binary code. A) Gate generator; B) "drop to zero"; C) range register; D) counter pulse generator; E) VS; F) range-reading pulse; G) generator of readout pulses; H) distributor-shifter; I) to the memory of the TsVM.

When the position of the counter pulses is not coordinated with the starting-point of range reading, the indeterminacy interval is doubled (Fig. 7.43b), and the mean square value of the range error increases $\sqrt{2}$ times:

$$\sigma_R = \frac{\Delta R}{\sqrt{6}} \approx 0{,}45\Delta R.$$

Consequently, to reduce the error due to discreteness it is necessary not only to reduce the repetition frequency of the counter pulses but also to use a common master oscillator to shape the counter pulses

and the RLS synchronization pulses. In this case the total instrumental error of the circuit for digital reckoning of range is

$$\sigma_{RH} = \sqrt{\left(R\frac{c_p}{F}\right)^2 + \left(\frac{\Delta R}{2\sqrt{3}}\right)^2}. \qquad (7.87)$$

A circuit for reckoning range in the form of binary numbers must be capable of registering the range of a large number of targets without breakdown. One variation of such a circuit, given in Fig. 7.44, consists of a pulse counter (range register) with control stages, a readout device (readout valves VS and a generator of readout pulses), and a device for feeding range information to the memory of the TsVM (distributor-shifter).

With the arrival of a regular RLS synchronization pulse the gate generator (reactance trigger) generates a broad pulse which opens the coincidence valve *VS*. Because of this the pulses from the counter pulse generator pass to the counter. At the end of the current pulsing period the gate generator returns independently to its initial position. Therefore the counter pulses stop passing through the coincidence valve, and the counter readings drop to zero in order to prepare it for the following working cycle.

Each stage of the pulse counter (trigger) represents a binary digit. A high potential on the output side of the trigger corresponds to 1, a low potential to 0. With the arrival of the synchronization pulse the counter starts to reckon out the time (range), but these data from the counter do not go anywhere since a coincidence valve (readout valve) which is normally closed is connected to the output of the trigger of each digit.

Only when a range reckoning pulse arrives (through the counter pulse generator) the readout valves open momentarily and the counted number is fed to the memory of the digital computer. As has already been

noted, this number is proportional to the time which has elapsed since triggering of the transmitter, and consequently, to the target range. With arrival of a range reckoning pulse from another target, at a greater distance, a larger number will be fed to the TsVM memory through the readout valves. In this way the range of a practically unlimited number of targets may be measured, which is an important merit of this circuit.

The operation of the circuit is not disturbed by arrival from the preselector of a false target pulse. The false target coordinates will be screened out by the computer itself when the data are processed a second time.

*Range register.* Figure 7.45 shows the voltage oscillograms at nodal points in the circuit of Fig. 7.44 and at the output busses of the pulse counter triggers.

Each trigger of the range register has a counter input, that is, it operates with the arrival of each pulse. Let us call the switching of the trigger from position 0 to position 1 forward and from position 1 to position 0 reverse.

Negative counter pulses arrive at the input of the trigger of digit $2^0$. Each counter pulse switches the trigger in either the forward or the reverse direction. The result is that broad pulses are obtained, their number being half as great as the number of pulses at the input. The broad pulses are differentiated in the *RC* network which is connected to the output of each trigger. Short negative pulses whose repetition rate is half of the repetition frequency of the pulses at the stage input, are shaped at the *RC* network output during the switch to reverse. For the sake of simplicity the networks are not given in Fig. 7.44, nor are the negative pulses of the drop to zero given in Fig. 7.45.

The trigger of the next, $2^1$, digit is operated by each short nega-

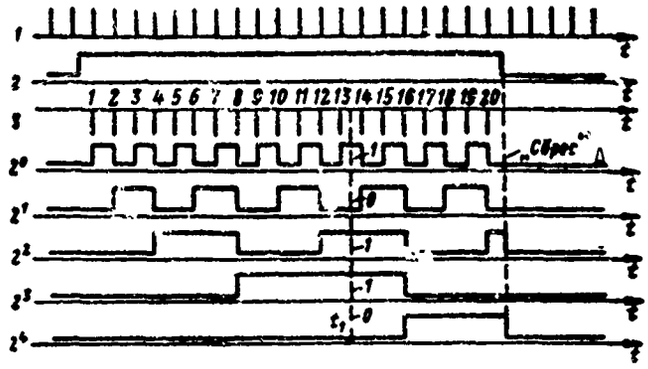


Fig. 7.45. Processes in the range register. A) "Drop to zero."

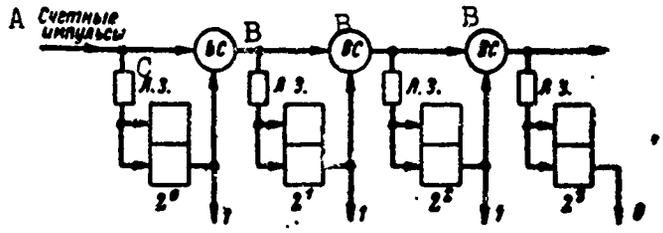


Fig. 7.46. Pulse counter with ripple-through carry of the higher digit. A) Counter pulses; B) VS; C) LZ.

tive pulse from the output of the trigger of the $2^0$ digit, that is, by each second counter pulse reaching the input of the range register. The number of short negative pulses at the output of this stage is also half as large as at the input; therefore, the trigger of the next $2^2$ digit is switched by each fourth counter pulse, the trigger of the $2^3$ digit by each eighth pulse, etc.

Thus, 1 at the output of the first trigger indicates the number of counted odd units, at the output of the second trigger – the number of odd twos, at the output of the third trigger – the number of odd fours, etc. An even number of units, twos, fours, etc., yields in each given digit 0 with carry-over of 1 to the higher digit. Consequently, the unit of each digital trigger has the value of its digit in the binary system: 1, 2, 4, 8 etc.

If we consider that a high potential exists on the output side of

digital trigger 1, and a low potential on the output side of trigger 0, we can read the number of counter pulses arriving at the input of the range register at a given moment in time. Thus, at moment in time $t_1$ after the beginning of counting (Fig. 7.45) the number 01101 (13) will appear in the register, and this, as may be easily seen, is equal to the number of counter pulses.

If a target pulse from the preselector enters the readout valve at this moment in time, pulses will be obtained at the output of only those valves to which a high potential has been fed from the counter (in the above case in the digit $2^3$, $2^2$, and $2^0$). The above number 01101, which is proportional to target range, will be counted and fed to the computer memory. If a signal arrives from a more distant target, a larger number will be fed to the computer memory.

For accurate range measurement the repetition frequency of the counter pulses must be sufficiently high, even up to several millions of pulses per second. At such a high frequency the pulse length and the time of the transient processes in the trigger occupy a considerable part of the repetition period of the counter pulses. At the same time, at some moment in time the transition from one binary number to the next number takes the form of a sequence of switching of the triggers of many digits. Thus, the transition from the number 1111 (15) to the number 10000 (16) is accompanied by the sequential switching of the triggers of five digits, and this means that the total time of the transient processes is several times greater than the time of the transient process of a single trigger (in this case it is approximately five times greater). When there is a large number of digits in the range register, the total time of the transient processes may be much greater than the repetition period of the counter pulses; as a result, the pulse counter can no longer operate normally, and there is a breakdown.

Breakdown is avoided by using more refined pulse counter circuits which either employ special devices to shorten the time of the transient processes while maintaining a sufficiently high pulse repetition frequency or reduce the repetition frequency of the counter pulses, maintaining the necessary reckoning accuracy by employing the nonius method.

An example of a device for shortening the time of the transient processes is the pulse counter with ripple-through carry of the higher digit, as depicted in Fig. 7.46. The characteristic of this counter circuit is that during the time of the transient process the triggers of several digits are not switched in sequence – in the order of growth of the number – but in all digits at the same time. Because of this the overall time of the transient process in the circuit is in all cases approximately equal to the time of the transient process of a single trigger.

The operating principle of a counter with ripple-through carry may be explained from the example of the transition from the number 0111 (7) to the number 1000 (8).

Let us assume that at the moment of arrival of a regular counter pulse at the counter input the number 0111 is recorded on the triggers, i.e., at the output busses of the triggers of the first three digits there is a "high" potential which is also fed to one of the inputs of the three coincidence valves. Thanks to this the regular counter pulse (unit) passes freely through the coincidence valves and enters the input of all four triggers, switching them at practically the same time. The trigger of the higher digit passes from position 0 to position 1, and the first three triggers – from position 1 to position 0. A new number 1000 is registered in the counter.

For normal operation of the circuit it is necessary to satisfy the condition that the triggers not be switched before the counter pulse has

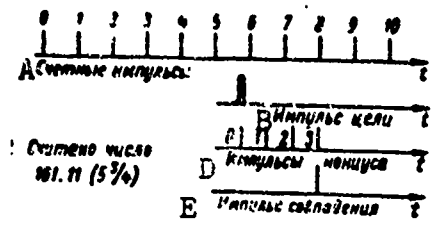

Fig. 7.47. Principle of the nonius. A) Counter pulses; B) target pulse; C) counted number; D) nonius pulses; E) coincident pulse.

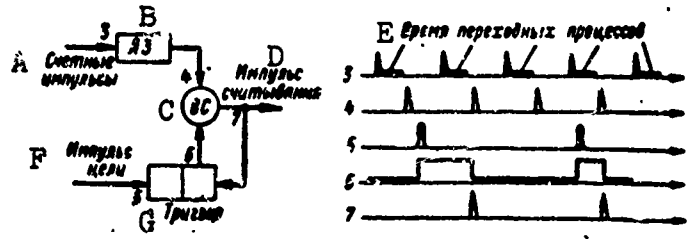

Fig. 7.48. Coordination of the moments of readout with the timing of the counter. A) Counter pulses; B) LZ; C) VS; D) readout pulse; E) time of transient processes; F) target pulse; G) trigger.

passed completely through the coincidence valves. This condition is satisfied by connecting into the input of each of the triggers small delay lines (LZ) consisting of several windings.

It is possible to obtain high range reading accuracy with a comparatively low repetition frequency of the counter pulses by utilizing the method of the nonius (interpolation) which is widely employed in micrometers and other measuring devices. Figure 7.47 gives the essence of this method as used to improve range reading accuracy.

Let the range reading pulse arrive between the fifth and the sixth counter pulses. Then, in accordance with the above technique, the number 101 (5) is registered in the range register. We assume that the obtained reading accuracy does not satisfy us and that it must be improved by $k$ orders of magnitude, that is, $2^k$ times. To accomplish this a special generator generates a series of $2^k$ pulses (nonius pulses) when the target pulse arrives. An impact excitation stage may be used as such a gen-

erator. The repetition period of these pulses is $1 + 1/2^k$ times smaller than the repetition period of the counter pulses. Consequently, the repetition frequency of the nonius pulses differs very slightly from the frequency of the counter pulses. In our case $k = 2$, and the reading accuracy is 4 times better.

Each of the $2^k$ nonius pulses is fed to a separate coincidence valve. Counter pulses are fed to the second inputs of these valves. The number of the coincidence valves (0, 1, 2, ..., $2k - 1$), in which any counter pulse has coincided with one nonius pulse will be a supplementary, refined, range reading. It only remains to transform the number of the coincidence valve into a binary number by using a special matrix circuit.

The length of the nonius pulses is selected to be $2^k$ times smaller than the repetition period of the counter pulses. Narrower nonius pulses will not ensure the necessary coincidence with one of the counter pulses, and wider nonius pulses will operate several coincidence valves at the same time (breakdown).

In our case one of the counter pulses coincide with nonius pulse 11 (3). We will consider the number 101 ($1 \cdot 2^2 + 0 \cdot 2^0 = 5$) obtained in the range register to be a whole number, and the result of the refinement 11 to be a fraction ($1 \cdot 2^{-1} + 1 \cdot 2^{-2} = 3/4$). We obtain the number 101,11, which is equal to $5\frac{3}{4}$, in the decimal system, and this corresponds to the condition in Fig. 7.47.

A drawback of the nonius method is reduction in range resolution, since the next range reading pulse from another target should not arrive before the last nonius pulse has terminated, that is, before $2k - 1$ period of the counter pulses.

*Readout pulse generator.* In order to avoid breakdown the passage of the number readout pulses from the range register to the TsVM memory

must be coordinated with the timing of the range register. This means that readout may be accomplished only at moments in time when the transient processes in the digital triggers have stopped after arrival of the regular counter pulse. Otherwise readout is accompanied by large errors as at the moment of switchover there is change in the status of more than one digit.

Actually, let us assume that readout occurs at precisely the moment of transition from the number 0111 (7) to the number 1000 (8), that is, at the moment when all units are changing to zeroes and zero is changing to unity. For example, in a counter with ripple-through carry either 0 or 1 may be read in each digit at this moment. The minimum readout number is zero (zeroes in all digits), and the maximum number is 15 (units are counted in all four digits). Instead of 7 or 8 an arbitrary number will appear somewhere between 0 and 15!

Coordination of the time of presentation of readout pulses with the timing of the range register is accomplished by a special readout-pulse generator, a variation of which is given in Fig. 7.48 together with explanatory oscillograms.

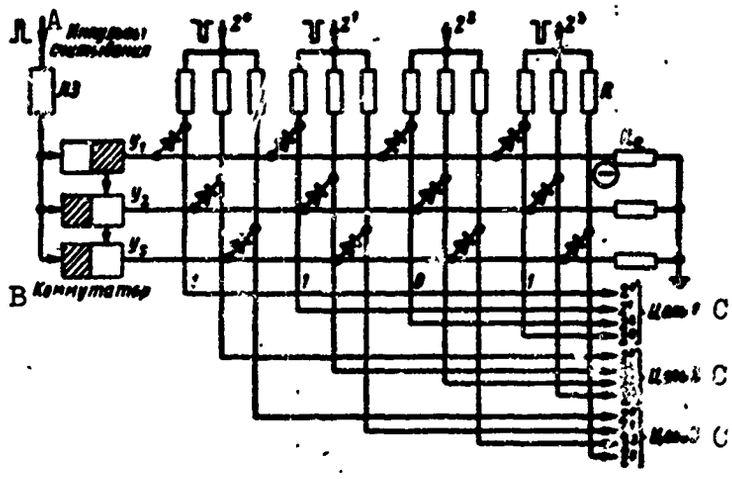


Fig. 7.49. Distributor-shifter. A) Readout pulses; B) commutator; C) target.

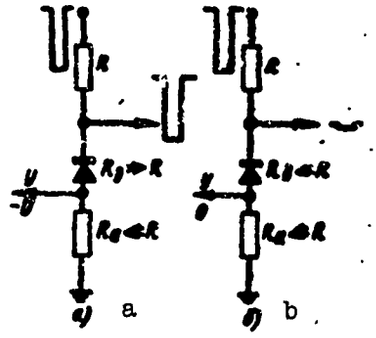

Fig. 7.50. Commutation of output busses of the distributor-shifter: a) The diode is shut (transmission; b) the diode is open (no transmission).

The beginning of the transient processes in the range register is determined by the times of arrival at its input of counter pulses 3. The number registered in the range register at the moment of arrival of a target pulse should be read out only at those moments in time when the transient processes have already terminated. These moments in time are determined by pulses 4 – which have been delayed in the delay line (LZ) for an appropriate time interval by the counter pulses. The arrival of target pulse 5 operates the trigger. At the output side of the trigger is formed a high potential 6, and the previously closed coincidence valve (VS) is now opened. The regular pulse 4 passes through the valve, forming readout pulse 7.

Thus a readout pulse is developed at the output of the valve only upon arrival of a target pulse, but the time of its appearance is coordinated with the termination of the transient process, and this is clamped by the moment of arrival of delayed counter pulse 4 at the second input of the coincidence valve. The readout pulse which has appeared at the circuit output passes to the readout valves and also to the second trigger input, returning the latter to its initial position. The circuit is prepared for the arrival of the next target pulse.

*The distributor-shifter.* The data from different targets tapped from the range register should be stored in different memory cells. The data read from the range register are distributed among the different cells by the distributor-shifter. Figure 7.49 depicts the matrix circuit of a distributor-shifter of a four-digit number among three memory cells corresponding to three targets.

Let us assume that from the output of the readout valves binary units are presented in the form of pulses of negative polarity. These pulses in any digit are distributed among the three branches. Each of the branches is a voltage divider consisting of a large resistance $R$, an internal diode resistance $R_d$, and a small resistance $R_a$ (Fig. 7.50). The anodes of the diodes are connected to the control busses $Y$, and the output voltage is tapped from the cathode through the output busses.

To one of the control busses there is fed a negative voltage whose absolute magnitude exceeds the amplitude of the incoming negative pulses; there is no voltage on all the remaining control busses ("ground"). The diodes which are connected by the anodes to the bus with a negative potential are closed to pulses of negative polarity. The internal resistance of the closed diode $R_d$ is considerably greater than resistance $R$, and the input pulses are tapped without distortion from the divider at the circuit output (see Fig. 7.50a). The diodes connected to busses with a zero potential are open. Their internal resistance $R_d$ plus resistance $R_a$ is considerably smaller than $R$, and the amplitudes of the output pulses are practically equal to zero (see Fig. 7.50b).

Figure 7.49 shows the case when a negative potential is fed to bus $Y_1$, which corresponds to the reception of data from the target which is first in order.

Let us assume that from the readout valves there arrives a number 1011, whose units are represented by negative pulses. The diodes which

are connected to the first bus are closed, and the number 1011 is fed to the memory cell of target 1. Nothing enters the remaining memory cells, since the diodes are open, and the whole voltage of the pulses falls over resistance $R$.

The supply of the negative voltage to the control busses of the distributor-shifter is governed by the commutator shown in the left part of Fig. 7.49. The commutator consists of triggers corresponding in number to the number of memory cells. Resistances $R_a$ in the circuit of the control busses of the distributor-shifter are located in the anodes of the output tubes of the triggers and are grounded. A negative feed voltage is supplied to the cathode of the trigger tubes.

Before arrival of the pulse from the first target cited the output tube of the first trigger is open, and the output tubes of the other triggers are closed. Because of this, the voltage taps from the resistance $R_a$ in the anode of the output tube of the first trigger is negative, and in the others it is equal to zero. The distributor shifter connects the output of the range register to the memory cell of the first target.

Upon arrival of the pulse from the first target the range is read and is fed through the distributor-shifter to the first memory cell. After a certain, adequate for readout and transmission of the number to the TsVM memory, this same target pulse, after passing through a short delay line (LZ), operates the commutator and switches over the output of the range register to the second memory cell.

The processes in the commutator occur in the following order. The positive delayed readout pulse enters the inputs of the trigger tubes. Inasmuch as all of the trigger input tubes except the first are open, the positive pulse only switches on the first stage, opening its input tubes. The short negative pulse arriving at the moment of switching the

first trigger closes the input tube and opens the output tube of the second stage. As a result of these processes the output bus of the first trigger acquires a zero potential, while the output bus $Y_2$ of the second trigger becomes negative due to the drop in voltage across resistance $R_a$. The outputs of the range register is connected to the memory cell of the second target. The commutator is prepared for operation by the pulse from the second target.

With arrival of the pulse from the second target all of the processes take place in an analogous way, except that in this case the third trigger is switched and the second trigger of the commutator is returned to its initial state.

In concluding this section we may note that the presentation of velocity in the form of binary numbers is analogous to the registration of range. The beats of the emitted and received oscillations, whose frequency $F_д$ is proportional to the target velocity, are fed to the counter through the coincidence tube during a measured time interval $\tau_m$. The number of beating blips counted by the target

$$N_V = \tau_м F_д = \tau_м \frac{2V_R}{\lambda}$$

is proportional to the target velocity.

## §7.13. THE USE OF INDICATOR DEVICES TO MEASURE RANGE

### 1. Range Measurement Accuracy

Indicator devices may be used to measure range by employing scale markings to create a range scale on the indicator screen or by matching a target blip and a special sighting line.

The accuracy of range measurement with scale markings is determined by the accuracy with which the operator's eye can reckon the target position relative to the neighboring scale markings and by the accuracy with which the scale markings are located on the radar image. Reading error depends upon the operator's experience and is 10-20% of the space between

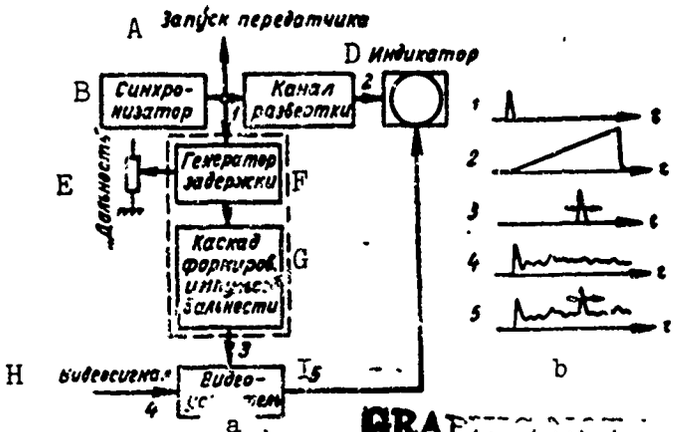


GRAPHIC NOT REPRODUCIBLE

GRAPHIC NOT REPRODUCIBLE

Fig. 7.51. Shaping range pulses so as to form a movable electronic sighting line: a) Functional diagram; b) simplified oscillograms. A) Start of transmission; B) synchronizer; C) scanning channel; D) indicator; E) "range"; F) delay generator; G) range-pulse shaping stage; H) video signal; I) video amplifier.

the scale markings. For the sake of a more convenient reading it is advisable that each range zone has its own scale marking, the total number not to exceed five. If distances can still not be determined with sufficient accuracy, it is possible to use a complex range scale in which each fifth or tenth scale marking stands out.

Range can be measured accurately by matching the target blip with an electronic sighting line or the so-called range marking. In indicators with amplitude markings the electronic sighting line may take the form of a pulse of one shape or another. Range markings in the form of a light or dark spot on the scanning line are also employed. In indicators with brightness marking the appearance of the electronic sighting line is determined by the character of the raster. In circular scan indicators the marking looks like a lighted ring, and in rectangular azimuth-range scan it takes the form of a straight line parallel to the axis of the azimuth.

The range-measuring device shaping the electronic sighting line (Fig. 7.51a) consists of a delay generator and pulse shaping stages

(Fig. 7.51b). The synchronizing pulses used to trigger the scan and which determine the moment of oscillation of the transmitter enter the delay generator. The delayed pulses are shaped in accordance with the required form of the electronic sighting line. The range pulses obtained at the output are fed to the video strip of the receiver and form an electronic sighting line on the indicator screen. With variation in the delay the electronic sighting line is displaced over the indicator screen and may be matched with the target pulse. In this case, the delay of the range pulse relative to the moment of oscillation of the transmitter is equal to the time taken for the radio signal to reach the target and return. The control device which varies the delay may be linked to a range measurement scale.

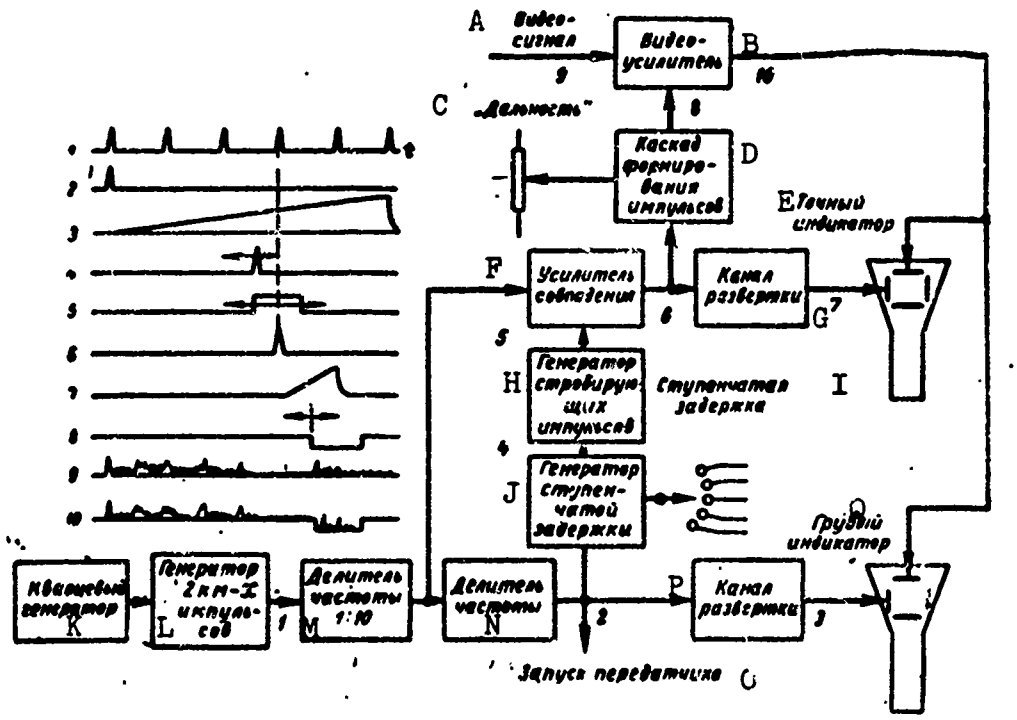


Fig. 7.52. A two-scale range measuring device. A) Video signal; B) video amplifier; C) "range"; D) pulse-shaping stage; E) precise indicator; F) coincidence amplifier; G) scanning channel; H) gate-pulse generator; I) step delay; J) step-delay generator; K) quartz master oscillator; L) generator of 2 km-x pulses; M) frequency divider;1:10; N) frequency divider; O) start of transmission; P) scanning channel; Q) crude indicator.

When an indicator device is used, range measurement error is determined by the error of the delay generator, by the instability of the parasitic delays in the circuits through which the pulses pass, and by the error involved in matching the target marking with the electronic sighting line.

*Delay-generator accuracy* has a considerable influence upon the error involved in measuring distance. When high accuracy is not required, a multivibrator with subsequent differentiation of the pulses is usually employed as the delay generator. The total time error of the multivibrator delay reaches several percent. However, this error may be considerably reduced by special stabilization measures and by careful selection of the circuit components. The most serious drawback of the multivibrator is the change in the delay when the tubes are replaced or grow old.

Phantastron circuits are broadly applied in indicators of average accuracy. The delay generator is often a cathode-coupled phantastron, which ensures a total time error of the order of 1% of the maximum delay. When a higher accuracy is required, complex devices consisting of a sawtooth voltage generator and a comparison circuit are used to delay the range pulses. Such devices ensure a time error of the order of tenths of a percent. For particularly high measurement accuracy circuits with phase shifters and quartz master oscillators, whose accuracy is 0.01-0.1%, are employed.

The measurement error due to error by the delay generator may be reduced to any desired point by the use of multiscale systems. The two-scale rangefinder (Fig. 7.52) contains two range measurement indicators - a crude one and a precise one. The range sweep of the crude indicator is triggered at the same time as the transmitter and makes it possible to view the target over the whole range accessible to the radar station. The precise indicator has a rapid scan which is delayed relative

to the transmitter pulse. The delay may be varied by steps corresponding to precise distances, for example, 20 km (Fig. 7.52). The range pulse may move about continuously within the limits of this interval.

The radar station pulsing frequency is assigned by a quartz master oscillator with frequency divider; the pulses from the output of the dividers pass to the step-delay generator. The step delay must be accurate. However, the maximum delay for which the system is rated is extremely significant, and a sufficiently low absolute delay cannot be obtained. Therefore, the delay is made more accurate in the subsequent stages by selection of 20-kilometer pulses (Fig. 7.52).

To this end the generator of rectangular gate pulses, which are used to unlock the coincidence amplifier, is triggered by the delayed pulses. During each pulsing period the coincidence amplifier passes one or another 20-kilometer pulse following upon dark-up of the transmitter, depending upon the size of the step delay. This technique almost entirely eliminates time error, as delay is in precise steps, each of which corresponds to 20 km.

The pulses from the step-delay channel are used to trigger the sweep of the precise indicator and the continuous delay channel. The latter does not differ in principle from the single-scale rangefinder examined above (Fig. 7.51); however, the position of the range marking formed by it may vary within comparatively small limits (up to 20 km).

During the measurement process the target marking on the crude indicator coincides with the sighting line which is moved in 20 km jumps by the step-delay switch. Further and more precise matching is accomplished in the precise indicator by the use of continuous delay.

Step delay is not convenient for continuous tracking of a target. This drawback is eliminated in special range-measuring devices which use phase shifters as delay generators.

Multiscale indicators can be used to obtain any accuracy which is practically required; if the noise level is low, accuracy is limited only by the accuracy of the quartz master oscillator.

The delay circuits used to measure range must be calibrated periodically.

*Calibration of range-measuring devices* is usually done by a special calibrating voltage in the form of pulses with a standard period. In the calibration process an electronic sighting line is matched on the indicator screen with the blip of calibration pulses which are introduced into received strip, and the correctness of the markings on the range scale is checked in this way. In the case of a divergence the voltage which controls the delay of the range-measuring marking is adjusted.

Methods of deriving a calibration voltage are determined by the synchronization system of the radar station which, in its turn, depends upon the type of keying device in the modulator. When an ionic keying device is used, the instability of the moment of its firing requires the operation of the whole station to be synchronized with the modulator pulses.* In this case the calibration voltage which should be rigidly synchronized with the transmitter pulses may be generated only by a generator with impact excitation.

When a keying device of the electronic type is used, the modulator is rigidly synchronized with the side pulses. These pulses may be derived by dividing the frequencyof the calibration voltage from the continuous wave generator.

Circuits with impact excitation ensure high accuracy of the time position of the pulses only if stabilization measures are employed: the use of stable elements with specially selected temperature coefficients, thermostats, etc. Therefore, when high range measurement accuracy is required, and a modulator of the electronic type can ensure the necessary

power, synchronization circuits are generally employed with division of the frequency of the quartz master oscillator. In such circuits the error is about $10^{-5}$ of the rated frequency value without employment of any special stabilization measures.

The fundamental demand imposed upon calibration pulses is that their frequency should be stable and standard. In calibration it is also necessary to know the extent to which the range scale formed by the calibration pulses is shifted relative to the true distance scale. This shift is due to parasitic delays of the synchronization pulses and the target signals.

*Parasitic delays* are caused by stretching of the edges and delay of the pulses in the stages containing the reactance elements. The finite steepness of the pulse front leads to delay in the operation of the triggering circuit, for example, the blocking oscillators and the frequency dividers. Considerable pulse delays occur in the receiver circuits due to the reactance element. The delay time depends substantially upon the amplitude of the input signals; powerful signals are delayed less. This is particularly true for the transmitter pulse which leaks through the antenna switch. Therefore, even accurate measurement of the time interval between the outcoming pulse and the target signal at the receiver output involves an error in range measurement, and this can be as large as ten meters.

Let us follow the course of the synchronizing and the calibration pulses, and also the signals, which form the target indication on the screen. In order to be definite we will assume that the station is synchronized by the pulses of a quartz master oscillator with frequency dividers (Fig. 7.53).

In each pulsing period one of the pulses forming the range calibration scale passes through the stages of the frequency dividers and trig-

gers the transmitter. This pulse (more accurately, a certain section of it, for example, its edge) determines the zero time reading of the calibration scale. However, the emission of high-frequency oscillations by the antenna is somewhat delayed relative to this moment in time. The received signal is subject to an additional delay in the feeder strip and the receiver circuits.

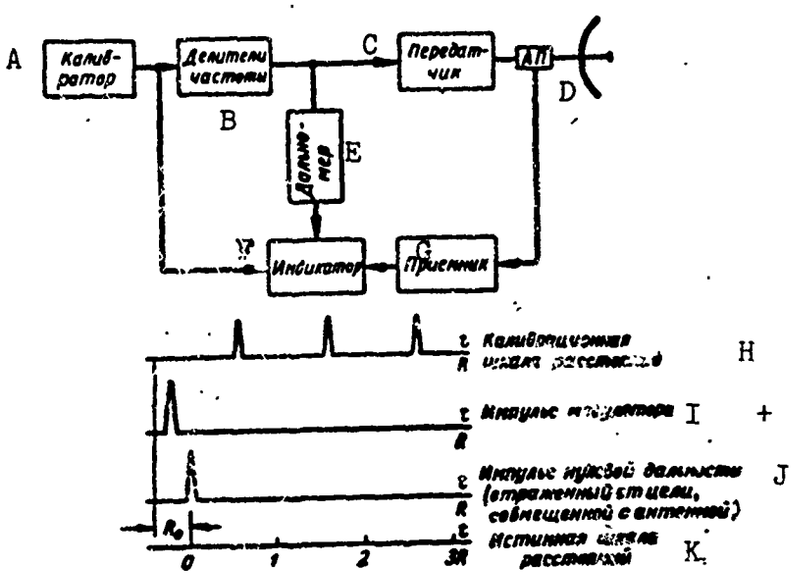


Fig. 7.53. Basic channels for passage of pulses in synchronization of the radar station by a quartz master oscillator (functional diagram and simplified oscillograms). A) Calibrator; B) frequency dividers; C) transmitter; D) AP; E) rangefinder; F) indicator; G) receiver; H) range-calibration scale; I) modulator pulse; J) zero-range pulse (reflected from the target, matched with the antenna); K) true range scale.

Time interval $\tau$ as reckoned from the calibration scale contains, in addition to the propagation time to the target and back $\tau_R$, the delay time $\tau_i$ in the circuits of the frequency divider and of the transmitter, in the feeder strip (manifested twice), and in the receiver. It is equal to

$$\tau = \tau_R + \sum \tau_i.$$

The whole calibration scale is shifted relative to the true zero range by the distance

$$R_0 = -\frac{c}{2}\sum \tau_i.$$

To eliminate this bias of the calibration scale (to establish the zero range), the pulses which shape this scale are usually delayed by additional quantity $2R_0/c$ in a small artificial long line. If such compensation for the shift in the calibration scale is not provided, it is necessary to take into account the fact that when the sighting line coincides with the $n$th calibration marking, the true indications of the scale of the range-measuring device should correspond to distance $n\frac{\tau_e c}{2} - R_0$, where $\tau_e$ is the period of the calibration voltage.

The correctness of the zero-range setting may be verified from a local object or an artificial target located at a precisely measured distance from the radar station. The reflected signal of such a target is coordinated with the electronic sighting line, and the range-marking scale should then indicate the required distance.

The zero on the range scale is in practice often established by matching the range marking with an outcoming pulse. Here it is necessary to bear in mind that the delay time of the outcoming pulse in the receiver circuits is less than that of a pulse reflected from a target.

The measurement errors due to parasitic delays are systematic and may be taken into account by special calibration. However, the variations in these delays are random, and it is therefore impossible to take them into account in practice in the operation of the station. The random measurement error due to parasitic delays is approximately equal to their absolute size.

To determine what are the circuit elements giving rise to parasitic delays which affect measurement, it is necessary to analyze in each concrete synchronization system the path followed by the target signals as well as that followed by the calibration and synchronization pulses. For

example, an examination of the circuit in Fig. 7.53 indicates that range measurement accuracy does not depend upon the parasitic delay in the frequency dividers. Actually, this delay has an equal influence upon the time position of the range pulse and upon that of the target signal. Its variation does not disturb the matching of the corresponding markings. At the same time, the instability of the delay in the transmitter or receiver circuits gives rise to a proportional error in range measurement.

To reduce errors an effort is made to reduce as far as possible the magnitude of the parasitic delays. To accomplish this pulses with large amplitude and steep fronts are employed. In the synchronization circuits which affect measurement special circuits are often employed, which eliminate delays in a train of series-connected stages. Such a circuit is utilized in the two-scale range-measuring device examined above (Fig. 7.52). The coincidence amplifier in the step-delay channel practically eliminates the parasitic delay of all preceding stages, starting from the generator of 20-kilometer pulses.

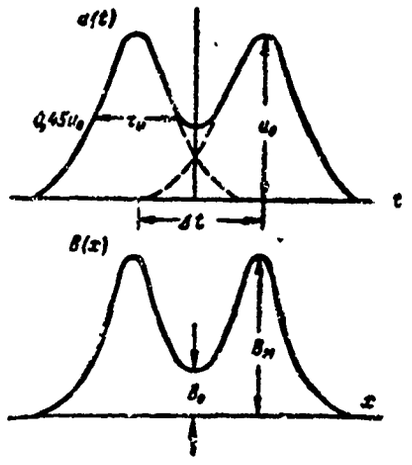


Fig. 7.54. Total voltage of target signal and range pulse.

*The accuracy with which the sighting line is matched with the target blip* results from a series of factors determined by the characteristics of the image of the blips and by the properties of vision:

1. The target blip and the electronic sighting line do not possess sharply expressed points from which it would be possible to match them.

2. The electron beam which traces the target blip and the sighting line has a finite diameter.

3. The noise voltage at the receiver output makes the trace of the

electronic blip unstable and makes it difficult to match them, especially in the case of signals of small magnitude.

4. When a mechanical sighting line is utilized, matching accuracy is reduced by parallax.

In the absence of noise the accuracy of matching the target amplitude blip and the sighting line is determined basically by the signal rise time. If the scanning velocity is sufficiently great, so that the pulse on the indicator screen is observed clearly, the matching error will be approximately 0.1 of the length of the front.

The brightness blip is matched with the electronic sighting line in such a way as to establish in the interval between them a definite brightness value relative to the maximum value. Various values for this relative brightness may be accepted; high accuracy of matching is assured if it is approximately 0.5.

There is a time shift between the pulses of the target and those of the electronic sighting line even when their respective blips have been accurately matched. In the accepted matching technique, where the brightness dip between the sighting line and the target blip is a constant quantity, this time shift depends upon the scanning velocity, the diameter of the spot, and the pulse length. We may determine this function, ignoring the influence of noise and assuming that the signal voltage and the range pulse are described by a bell-shaped curve

$$u(t) = u_0 e^{-\pi\left(\frac{t}{\tau_1}\right)^2}. \qquad (7.88)$$

The constant $\tau_1$ represents the pulse length at the 0.45 level of the maximum value $u_0$.

The equation for two matched pulses shifted by time interval $\Delta t$ (Fig. 7.54) will take the form

$$u(t)=u_0\left[e^{-\pi\left(\frac{t+0,5\Delta t}{\tau_u}\right)^2}+e^{-\pi\left(\frac{t-0,5\Delta t}{\tau_u}\right)^2}\right]. \qquad (7.89)$$

When scanning velocity $v$ is constant, voltage $u$ may be expressed as a function of the position of the center of spot $x$ on the scanning line. In this case we make the substitution $t=\frac{x}{v}$, $\Delta t=\frac{\Delta}{v}$, $\tau_u=\frac{r}{v}$ where $x$, $\Delta$ and $r$ are the distances traversed by the center of the spot during time $t$, $\Delta t$, and $\tau_i$ respectively,

$$u(x)=u_0\left[e^{-\pi\left(\frac{x+0,5\Delta}{r}\right)^2}+e^{-\pi\left(\frac{x-0,5\Delta}{r}\right)^2}\right]. \qquad (7.90)$$

We determine how the image orightness is distributed along the scanning line.

We assume that the current density in the pencil is distributed normally

$$j=j_0e^{-\left(\frac{x-\xi}{0,8d}\right)^2}, \qquad (7.91)$$

where $d$ is the diameter of the spot at the 0.1 level of the maximum value of the current density (or of the maximum value of the spot brightness); $x$ is the coordinate of the center of the spot; $\xi$ is the abscissa of the point at which the current density (or the brightness) is determined.

We consider the modulation characteristic of the tube to be quadratic and assume that the initial voltage on the control electrode coincides with the blanking voltage ($j_0 \equiv u^2$). Then the density of the charge at point $\xi$ and the brightness of luminescence $B(\xi)$ which is proportional to it at this point may be determined, without taking into account the constant factors, as

$$B(\xi)=\int_{-\infty}^{\infty}u^2(x)e^{-\left(\frac{x-\xi}{0,8d}\right)^2}dx. \qquad (7.92)$$

By substituting Expression (7.90) into Formula (7.92) and integrat-

ing, we obtain

$$B(\xi)=e^{-\frac{(2\xi+\Delta)^2}{d_e^2}}+e^{-\frac{(2\xi-\Delta)^2}{d_e^2}}+2e^{-\frac{4\xi^2+\Delta^2\left(1+0{,}6\frac{d^2}{r^2}\right)}{d_e^2}}. \qquad (7.93)$$

where

$$d_e=\sqrt{(0{,}8r)^2+(0{,}7d)^2}. \qquad (7.94)$$

We call quantity $d_e$ the equivalent diameter of the spot. The meaning of this definition will become obvious from the subsequent discussion.

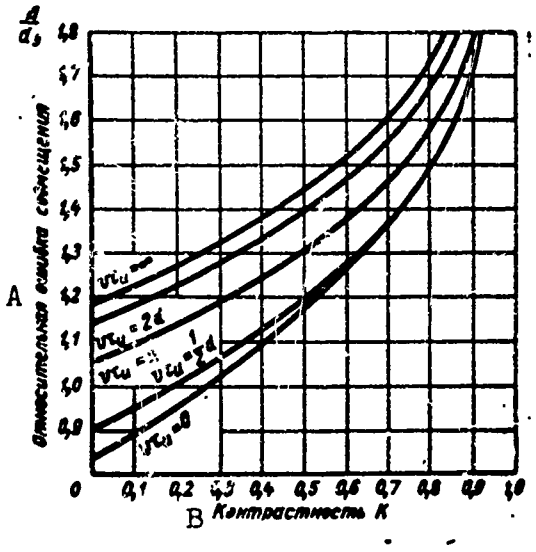


Fig. 7.55. The relative matching error as a function of the contrast of the brightness dip in the interval between the brightness blips. A) Relative matching error; B) contrast $K$.

To determine contrast we calculate maximum brightness $B_m$ and brightness $B_0$ in the space between the markings (Fig. 7.54b). We find quantity $B_m$ by assuming in Formula (7.9) that $\xi = 0.5\Delta$*

$$B_m=1+e^{-\left(\frac{2\Delta}{d_e}\right)^2}+2e^{-\left(\frac{2\Delta}{d_e}\right)^2\left(1+0{,}3\frac{d^2}{r^2}\right)}. \qquad (7.95)$$

As will be demonstrated below, ratio $\Delta/d_e$ is of the order of unity and more; therefore, even in the most unfavorable case, when $d \ll r$,

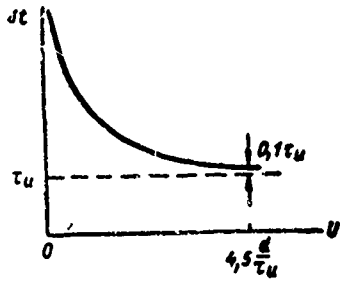


Fig. 7.56. The methodical matching error as a function of the scanning velocity.

the last terms of the expression are approximately 0.04. Consequently, it may be assumed with a sufficient degree of accuracy that the maximum relative brightness is equal to unity, that is, $B_m = 1$.

We determine the brightness in the space between the markings by assuming $\xi = 0$ in Formula (7.93),

$$B_0 = 2e^{-\left(\frac{\Delta}{d_e}\right)^2} + 2e^{-\left(\frac{\Delta}{d_e}\right)^2\left(1+0.6\frac{d^2}{l^2}\right)}. \qquad (7.96)$$

The contrast of the brightness dip is

$$K = \frac{B_м - B_0}{B_м} = 1 - 2e^{-\left(\frac{\Delta}{d_e}\right)^2} - 2e^{\left(\frac{\Delta}{d_e}\right)^2\left(1+0.6\frac{d^2}{l^2}\right)}. \qquad (7.97)$$

Equation (7.97) ties together the interval between the matched pulses, the pulse length, the pulse diameter, and the matching contrast. Inasmuch as the transcendental equation (7.97) cannot be solved in its general form, we resort to the graph in Fig. 7.55 which is constructed on the basis of this equation. The graph gives the values of the matching interval for the equivalent spot diameter. The family of curves is given for various quantities $v\tau_i$.

An examination of the graph reveals that for real values of $K$ and $d/v\tau_i$ quantity $\Delta/d_e$ varies comparatively little. The graph in Fig. 7.55 may be used to find averaged values of $\Delta/d_e$ for the accepted matching technique.

It has been pointed out above that the accuracy of matching is somewhat higher than in other cases when the operator establishes in the space between the pulses a brightness which is approximately equal to half the maximum value. In this case ($K = 0.5$), quantity $\Delta/d_e$ for the whole possible range of variations of scanning speed falls within the

limits 1.18 to 1.45. In all practical calculations it is perfectly permissible to ignore such variations of $\Delta/d_e$ and assume it to be, on the average, equal to 1.3. Then the sought value for the distance between the matched pulses may be described by the simple equation

$$\Delta = \sqrt{r^2 + 0{,}8d^2}. \qquad (7.98)$$

Thus, the distance between the matched pulses is a hyperbolic function of the scanning speed (Fig. 7.56). When the speed of movement of the spot is very low ($v\tau_i << d$), the blip is considerably larger than the distance over which the beam moves during the time of pulse length ($v\tau_i$). In this case the distribution of brightness in each marking along the scanning line corresponds to the distribution of brightness in a motionless spot. The distance between the matched markings comprises a definite part of the diameter of the spot, namely $\Delta = 0.9d$.

When scanning speed is great ($v\tau_i >> d$), the dimensions of the blips are determined basically by the pulse length and the scanning speed. The distance between the matched pulses is expressed by the asymptote of the hyperbola and is a definite part of the pulse extension on the screen, or, more accurately, of the extension of the pulse front (the length of the front of the bell-shaped pulse which we are using is $0.8\tau_i$ within the limits 0.1-0.9 of the maximum value).

The time interval corresponding to distance $\Delta$ on the screen

$$\Delta t = \frac{\Delta}{v} = \sqrt{\tau_u^2 + 0{,}8\frac{d^2}{v^2}}. \qquad (7.99)$$

It follows from Expression (7.99) that matching at different scanning speeds leads to a systematic error: between the matched pulses there is a time shift which depends essentially upon the scanning speed. This systematic error is reduced to a constant at high scanning speed.

Random matching errors are due to the operator's inaccurate of the assigned brightness dip. The graph (Fig. 7.55) may be used to evaluate

the magnitude of this error. If it is assumed that the contrast $K = 0.5$ may be spotted by the operator with an error of $\pm 0.1$, it follows from the graph that the corresponding change in $\Delta/d_e$ will be about $\pm 0.06$ for a large scanning speed and $\pm 0.08$ for a small scanning speed, that is, the average random matching error may be estimated as $\pm 0.07\Delta t$. The variation of the random error is the same as that of the systematic error.

2. Resolution

In radar observation using a brightness indicator range resolution is affected not only by pulse length but also by the spot diameter and the scanning speed. When the influence of these factors is combined, resolution may be evaluated by analogy to the way in which the accuracy

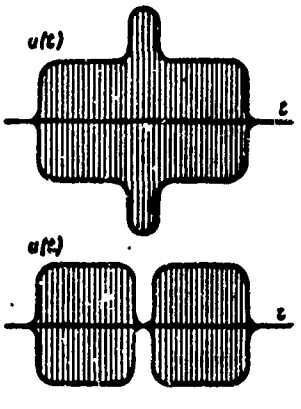


Fig. 7.57. Voltage in the linear part of the receiver, obtained from interference of the high-frequency signals of two punctiform targets.

of the matching of brightness blips was determined. However, these tasks differ somewhat in principle. The video frequency of the range-measurement pulse overlaps with that of the target signal, and in the time interval where they exist simultaneously the voltages are added arithmetically [see Expression (7.89)]. The high-frequency oscillations of two targets located close to one another are added directly with respect to the high frequency. The radar station antenna receives the high-frequency signal which results from the interference of these oscillations.

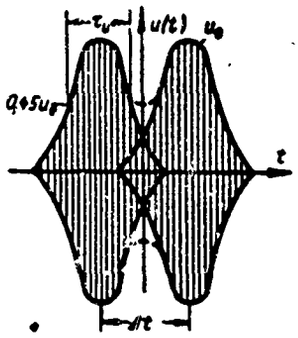

Fig. 7.58. Pulses of two targets in the linear strip of the receiver.

Even in the case of relatively motionless targets and a stationary radar station, there is always a variation, exceeding $\lambda/4$, of the difference of the distances between the targets.

The field strength resulting from the addition of identical signals with an arbitrary phase relation may vary from zero to a double value (Fig. 7.57). Thus the envelope of the signals of the two targets whose resolution we are discussing is an irregular quantity and varies in a random fashion from one pulsing period to the other even in the absence of noise.

However, with respect to the brightness of the blips, one may again speak of a definite value of the envelope due to the cumulative properties of the screen and to visual inertia. The resultant distribution of the brightness of the blips of the two targets determines the possibility of their resolution. If there is a noticeable dip in this curve, the operator may consider that the signal observed by him represents two targets. The minimum value of the discriminable brightness contrast, as will be demonstrated below, depends upon the observation conditions and is $K = 0.3$-$0.06$ of the maximum brightness value. The upper limit $K = 0.3$ applies to difficult observation conditions (for example, when the indicator is installed in the lighted cabin of an airplane). A brightness dip with a contrast of $K = 0.06$ may be detected if the background illumination is favorable, if the images of the targets themselves are clear, and if the blips can be observed for a long time. Under practical observation conditions, such a contrast value cannot usually be achieved. The minimum contrast noted by an operater without excessive effort is 0.1.

Thus we assume that in the linear part of the receiver the intermed-

iate-frequency signal for a single target is described by the expression

$$u(t)=f(t)\sin\omega t, \tag{7.100}$$

where $f(t)$ is the signal envelope.

We assume that the targets yield two pulses which are identical in amplitude, which are displaced by time interval $\Delta t$, and which have random phase shift $\Phi$ (Fig. 7.58):

$$u(t)=f\left(t+\frac{\Delta t}{2}\right)\sin\omega t+f\left(t-\frac{\Delta t}{2}\right)\sin(\omega t+\varphi). \tag{7.101}$$

This voltage may be expressed in the form of an envelope and a high-frequency duty factor

$$u(t)=\left[f^2\left(t+\frac{\Delta t}{2}\right)+f^2\left(t-\frac{\Delta t}{2}\right)+2f\left(t+\frac{\Delta t}{2}\right)\times\right.$$
$$\left.\times f\left(t-\frac{\Delta t}{2}\right)\cos\varphi\right]^{\frac{1}{2}}\sin(\omega t+\psi), \tag{7.102}$$

where $\psi$ is also the random phase shift depending upon angle $\varphi$ and upon the value of the functions $f\left(t+\frac{\Delta t}{2}\right)$ and $f\left(t-\frac{\Delta t}{2}\right)$.

We assume that signal $u(t)$ is detected by a linear detector since the signal/noise ratios under examination are large. After detection (and appropriate amplification) we obtain a voltage proportional to the envelope

$$U(t)=\left[f^2\left(t+\frac{\Delta t}{2}\right)+f^2\left(t-\frac{\Delta t}{2}\right)+2f\left(t-\frac{\Delta t}{2}\right)\times\right.$$
$$\left.\times f\left(t+\frac{\Delta t}{2}\right)\cos\varphi\right]^{\frac{1}{2}}. \tag{7.103}$$

This voltage is fed to the control electrode of the tube and is used to modulate the electron beam. When scanning speed $v$ is constant, the voltage may be viewed as a function of the movement of the center of the spot $x$ along the scanning line

$$U(x)=\left[f^2\left(\frac{x+\frac{\Delta}{2}}{v}\right)+f^2\left(\frac{x-\frac{\Delta}{2}}{v}\right)+2f\left(\frac{x+\frac{\Delta}{2}}{v}\right)\times\right.$$

$$\times f\left(\frac{x-\frac{\Delta}{2}}{v}\right)\cos\varphi\Big]^{\frac{1}{2}}. \qquad (7.104)$$

where $\Delta = \Delta t v$ is the distance on the screen corresponding to time interval $\Delta t$.

By utilizing Expression (7.92) we find the relative brightness value (leaving the constant factors out of consideration) at arbitrary point $\xi$ on the scanning line

$$B(\xi, \varphi) = \int_{-\infty}^{\infty}\left[f^2\left(\frac{x+\frac{\Delta}{2}}{v}\right)+f^2\left(\frac{x-\frac{\Delta}{2}}{v}\right)+2f\left(\frac{x+\frac{\Delta}{2}}{v}\right)\times\right.$$
$$\left.\times f\left(\frac{x-\frac{\Delta}{2}}{v}\right)\cos\varphi\right] e^{-\left(\frac{x-\xi}{0{,}3d}\right)^2} dx. \qquad (7.105)$$

In contrast to the case examined above, brightness is a function of two variables – the coordinate of point $\xi$ and the phase shift $\varphi$ between the high-frequency fillings of the pulses.

Each target blip is shaped during several successive pulsing periods and yield a certain total luminescent effect. Furthermore, in brightness indicators there is averaging of the brightness during successive scanning cycles as a result of screen afterglow. Therefore, the apparent brightness value registered by the operator may be found by averaging quantity $B(\xi, \varphi)$ for all possible values of phase angle $\varphi$ whose magnitude is evenly distributed within the limits 0 to $2\pi$:

$$\overline{B}(\xi) = \frac{1}{2\pi}\int_0^{2\pi}\int_{-\infty}^{\infty}\left[f^2\left(\frac{x+\frac{\Delta}{2}}{v}\right)+f^2\left(\frac{x-\frac{\Delta}{2}}{v}\right)+2f\left(\frac{x+\frac{\Delta}{2}}{v}\right)\times\right.$$
$$\left.\times f\left(\frac{x-\frac{\Delta}{2}}{v}\right)\cos\varphi\right] e^{-\left(\frac{x-\xi}{0{,}3d}\right)^2} dx d\varphi.. \qquad (7.106)$$

By integrating with respect to $\varphi$ we find

$$\overline{B}(\xi) = \frac{1}{\pi}\int_{-\infty}^{\infty}\left[f^2\left(\frac{x+\frac{\Delta}{2}}{v}\right)+f^2\left(\frac{x-\frac{\Delta}{2}}{v}\right)e^{-\left(\frac{x-\xi}{0{,}3d}\right)^2}\right] dx. \qquad (7.107)$$

As before, we examine the case where the envelope of the high-frequency pulse is expressed by a bell-shaped function (7.88).

After substituting $f(t) = u(t)$ from Formula (7.88), integration, and transformation, we obtain the expression for the brightness distribution

$$B(\xi) = e^{-\left(\frac{2\xi+\Delta}{d_0}\right)^2} + e^{-\left(\frac{2\xi-\Delta}{d_0}\right)^2}. \qquad (7.108)$$

The meaning of the definition adopted above (7.94) of the quantity $d_e = \sqrt{(0.8r)^2 + (0.7d)^2}$ – "the diameter of the equivalent spot" – becomes clear upon examination of Expression (7.108): the image may be considered as formed by two motionless spots which are displaced by distance $\Delta$ and have diameter $d_e$ (at the 0.37 level).

If we substitute $2\xi = \Delta$ and $\xi = 0$ into Formula (7.108) we obtain, respectively, the brightness value in the maximum

$$B_M = 1 - e^{-\left(\frac{2\Delta}{d_0}\right)^2} \approx 1 \qquad (7.109)$$

and in the space between the blips

$$B_0 = 2e^{-\left(\frac{\Delta}{d_0}\right)^2}. \qquad (7.110)$$

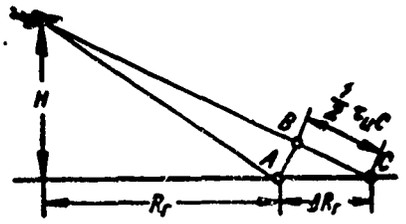


Fig. 7.59. The connection between horizontal range resolution and slant range resolution.

The contrast of the brightness dip is determined by expression

$$K \approx 1 - 2e^{-\left(\frac{\Delta}{d_e}\right)^2}. \qquad (7.111)$$

The curve for $v\tau_i = 0$ on the graph of Fig. 7.55 corresponds to Eq. (7.111).

Resolution may be determined from the value of the detectable contrast $K$ for the assigned observation conditions. Thus, to the detectable contrast 0.3 corresponds $\Delta/d_e \approx 1$ or

$$\Delta = \sqrt{(0{,}8r)^2 + (0{,}7d)^2}. \qquad (7.112)$$

We determine the resolved distance on the scale of the locality $\delta R$ by reference to the radial scale of the image, which is equal to the ratio of double the scanning speed and the speed of propagation of the radio waves

$$\delta R = \frac{c\Delta}{2v} = \sqrt{\left(0{,}8\,\frac{\tau_u c}{2}\right)^2 + \left(0{,}7\,\frac{dc}{2v}\right)^2}. \qquad (7.113)$$

The dependence of resolution upon scanning speed is of the same character as the matching error (Fig. 7.56). In order to heighten resolution it is desirable to increase the scanning speed. However, at a speed of $v = 4\frac{d}{\tau_u}$ the second term of the radicand increases the distance between the discriminable targets by only 10% over the limiting value of the resolution. It is obvious that further increase in the scanning speed does not yield a noticeable improvement in resolution.

In some cases, the first term under the radical in Expression (7.113) does not remain constant with variation in range, and for different distances the spot dimensions influence resolution in different ways. Thus, for example, a surface scanning station is mainly interested in horizontal range resolution. We can determine the minimum horizontal distance between targets ($\delta R_g$) at which their blips do not fuse. Targets $A$ and $C$ (Fig. 7.59) may be distinguished when the difference between their slant ranges exceeds the quantity $1/2\ \tau_i c$. If we view Fig.

$ABC$ as a right triangle, we can write

$$\frac{\delta R_r}{\delta R}=\frac{R}{R_r} \text{ or } \delta R_r=\delta R\sqrt{1+\left(\frac{H}{R_r}\right)^2}. \qquad (7.114)$$

As follows from Expression (7.114), at large distances ($H/R_g$ << 1) horizontal range resolution ($\delta R_g$) hardly differs from slant range resolution $\left(\delta R=\frac{1}{2}\tau_u c\right)$. However, at small target distances (by comparison with the altitude of flight) resolution deteriorates markedly. Expression (7.113) may be used to determine the horizontal range resolution taking into account the diameter of the spot, replacing in it $\delta R$ by the value of $\delta R_g$ found from Formula (7.114).

3. The Influence of Resolution of the Human Eye

The capacity of the eye to distinguish between two objects located close to one another is known in optics as acuteness of vision. Such objects, in particular, may be two lighted target blips on the indicator screen. Acuteness of vision is usually evaluated by the angle of resolution – the least angle between direction to points which are observed separately. Acuteness of vision is measured by a quantity which is the reciprocal of the angle of resolution, the unit of vision acuteness being a quantity which is the reciprocal of one angular minute. With a vision acuteness of 1 the distance between two sharply distinguishable points, as projected upon a grid, is approximately the size of a cone.

The acuteness of vision of the normal under favorable conditions of observation varies from several tenths to several units. Radar observation takes place under specific conditions: the brightness and contrast of the image are not great and vary during the antenna rotation period; the background is granular; the spectral composition of the light varies, etc. These factors have a substantial influence upon the acuteness of vision.

Below are given some experimental data on the resolution of human sight, obtained by imitating the observation conditions typical for the work of an operator. On the axis of the abscissa of the graph in Fig. 7.60 is laid out in logarithmic scale the contrast between the blip and the background. Values of the resolvable angle are laid out on the axis of the ordinate in minutes and the distances between the target blips on the indicator screen are shown. The five curves of the graph correspond to different values of the background brightness.

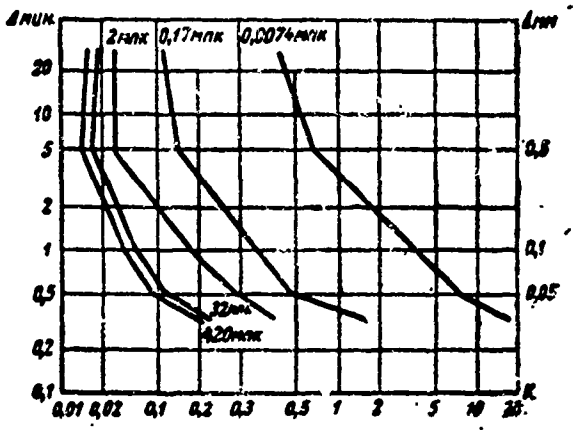


Fig. 7.60. Acuteness of vision in observing blips on an indicator screen. Curves are given for the various values of background brightness in milliluxes.

The graph has the same character as the dependences determining the sensitivity of sight examined in Chapter 6. With increase in contrast the curves of the graph decline rapidly, corresponding to an increase in resolution.

An exception is the path of the curve for extreme brightness in the area where the distance between the blips is approximately 0.5 mm. Here the blips are distinguished at minimum contrast values; in order to distinguish larger and smaller distances it is necessary to increase the contrast. A similar phenomenon is also encountered in discussing

the question of the observability of radar signals; there is a certain optimum blip size at which the operator's eye distinguishes it more easily against the noise background. This is connected with the limited dimensions of the field of vision. Evidently the optimum blip size utilizes the most sensitive part of the field of vision.

Another factor influencing resolution is the background brightness. With a blip of optimum size (0.5 mm) a $5.6 \cdot 10^4$ times change in the brightness background requires, in order that the blips be distinguished, threshold contrast differing by almost 50 times. Change in the background brightness has a substantial influence even though its values are small. When the brightness is considerable, the curves for which the brightness values differ 13 times practically coincide.

It is necessary to point out that the contrast values indicated in the graph are somewhat low, the reason being that the observation conditions are somewhat idealized: the influence of the noise background is absent, the blips appear at definite points on the screen, the adaptation conditions are extremely favorable.

## §7.14. RANGE AND VELOCITY MEASUREMENT ERRORS DUE TO RADIOWAVE PROPAGATION CONDITIONS

Two remarkable properties of radiowaves – constant velocity and rectilinear propagation – which underly the principle of range measurement, are violated in a heterogeneous real atmosphere. Deflection of the trajectory and change in the propagation velocity are infinitesimal by comparison with free space. However, when they accumulate over the long path between the target and the RLS, they may give rise to noticeable errors in range measurement.

Distortion in the propagation trajectory due to the phenomenon of atmospheric refraction leads to a lengthening of the path traversed by the radio wave by comparison with the straight distance between the RLS

and the target. On the other hand, the propagation time of the radar signal is usually determined by the group velocity of the radio waves, which is less than the speed of light in a vacuum. Both of these factors lead to an increase in the measured time interval over what would be necessary for propagation to the target in free space. The measured range values turn out to be slightly larger than the true one.

The phenomenon of atmospheric refraction, and the uneven velocity of propagation are due to atmospheric heterogeneity. The distinction is made between regular heterogeneity, whose law of variation is known, and random heterogeneity which can be described only statistically. In accordance with this, measurement errors due to atmospheric heterogeneity may be subdivided into systematic and random.

1. Regular Atmospheric Heterogeneity

In order to examine the errors due to regular atmospheric heterogeneity let us mention briefly the basic physical properties of the atmosphere's three layers - the troposphere, the stratosphere, and the ionosphere.

The lowest layer, the troposphere, which in the middle latitudes extends to an altitude of 10-12 km, contains about 80% of the mass and practically all of the moisture of the atmosphere. This determines one of its most important properties: being transparent to short wave solar radiation, it does not prevent the earth from heating up. At the same time the earth's radiation, which in accordance with Planck's law occurs at longer wavelengths, is absorbed by the atmosphere and is not dissipated into space. Thus the troposphere is not heated directly by the sun's rays, but by the earth's radiation. This, in particular, explains the reduction in air temperature with altitude.

The refractive properties of the troposphere were examined in Chapter 4. It was pointed out that the refractive index, which at the earth's

surface is on the average 1.000676, under normal conditions decreases with altitude at the rate $\frac{dn}{dH} = -4 \cdot 10^{-8} \frac{1}{м}$ due to the reduction in atmospheric pressure and moisture content. The value of the refractive index does not depend upon frequency over practically the whole ultrashortwave range.

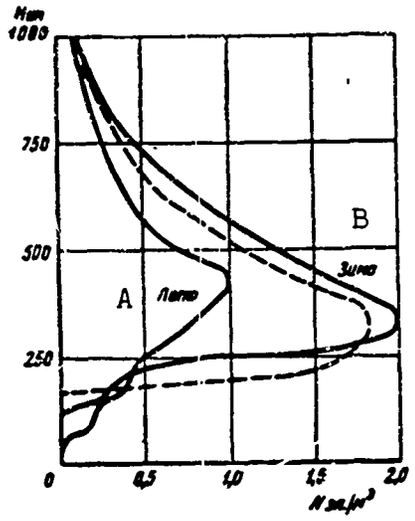


Fig. 7.61. Distribution of average electron concentration with altitude from experimental data and an approximate law (dashed line). A) Summer; B) winter.

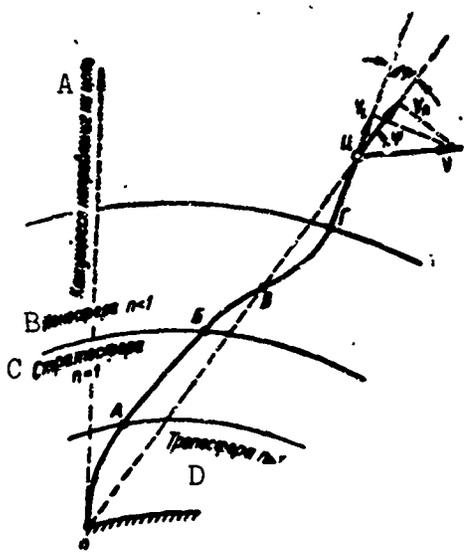


Fig. 7.62. Trajectory of propagation of target signals in the atmosphere. A) Apparent target direction; B) ionosphere; C) stratosphere; D) troposphere.

The next layer after the troposphere is the stratosphere; its upper boundary is at an altitude of about 80 km, and it contains about 20% of the mass of the atmosphere. The physical properties of the troposphere are determined by its considerable ozone content which absorbs the ultraviolet solar radiation. Maximum heating of the stratosphere occurs at an altitude of about 60 km; then the temperature again declines. From the point of view of its electrical properties the stratosphere represents a homogeneous medium with a refractive index equal to 1.

The most complex phenomena, and those most difficult to take into account, occur in the third atmospheric layer – the ionosphere, which contains only 0.5% of the mass of the atmosphere.

The specific properties of the ionosphere are determined by the action of the solar radiation (basically, the ultraviolet radiation), under whose influence gases are ionized. The concentration of electrons which are formed by ionization has its maximum value at altitudes of 300-400 km. At the upper boundary of the ionosphere (1100-1300 km) the electron concentration is small because of the low density of the gases; in the lower layers it declines with absorption of the sun's radiant energy which causes ionization.

Figure 7.61 gives averaged curves for the distribution of electron concentration by altitude. The electron concentration depends upon the time of day, the season of the year, and the intensity of solar activity. The latter, as is known, also has a periodic character. With increase in solar activity the electron concentration increases: as can be seen from Fig. 7.61, the maximum value of $N$ for the daytime differs by approximately 2 times from summer to winter.

The refractive index of a medium containing free electrons is determined by the formula (see Chapter 4)

$$n=\sqrt{1-\frac{80,8N}{f^2}}=\sqrt{1-\frac{f_0^2}{f^2}}, \qquad (7.115)$$

where $N$ is the number of electrons per cubic meter; $f$ is the oscillation frequency; $f_0 = \sqrt{80.8N}$ is a constant known as the plasma frequency.

The plasma frequency for the regular ionosphere may vary from 3 to 12 Mhz. A typical average value of the plasma frequency is 7 Mhz. Inasmuch as this is much lower than the carrier frequency values usually employed in radar, Formula (7.115) may be simplified by replacing its right side by the two first terms of the expansion into a series:

$$n=1-\frac{1}{2}\frac{f_0^2}{f^2}. \qquad (7.116)$$

As follows from Formulas (7.115) and (7.116), the refractive index of the ionosphere is a number less than unity. Its minimum value coincides with the area of greatest concentration of electrons. It is characteristic of the ionosphere that the refractive index depends upon frequency.

2. Deformation of the Radio Beam

Due to variation of the refractive index in the atmospheric layers the trajectory of propagation of radio waves is curvilinear. The RLS radio beam from point *O* on the earth's surface travels to the target not along the straight line *OTs*, but along the curve *OABVGTs* (Fig. 7.62); and the reflected target signal travels to the RLS along the same path.

The form of the curve is determined by the sign of the gradient of the refractive index. Under normal conditions the refractive index of the troposphere decreases with altitude. When the radio beam passes from an "optically dense" medium and enters a medium with a smaller refractive index, it is deflected downwards. In the stratosphere, where the refractive index remains constant, propagation is rectilinear (the *AB* section). With growth in the electron concentration in the ionosphere the refractive index becomes smaller, and the radio beam is again de-

flected downwards. The largest angular deflection of the beam relative to its initial direction occurs in the area of maximum concentration (point $V$). With further reduction in the electron concentration and increase in the refractive index the beam is distorted in the oppcsite direction (section $VG$).

Finally, leaving the ionosphere, the radio beam enters space (the so-called exosphere) where the refractive index is practically unity, and radiowaves are propagated without refraction.

Let us bear in mind that in examination of refractive phenomena and calculation of the coordinate measurement errors associated with them it is necessary to take into account the sphericity of the atmospheric layers.

3. Atmospheric Influence on Radio-Wave Propagation Velocity

The concept of the "velocity" of propagation of radio waves which we constantly employ in measuring distances by radar methods requires more precise definition.

If it is the troposphere, a medium in which propagation velocity does not depend upon frequency, the velocity of displacement of a certain clamp phase of the oscillations ($v_f$) and the speed of transport of electromagnetic energy in space ($v_{gr}$) are identical and are expressed as

$$v_{гр}=v_{ф}=\frac{c}{n}. \qquad (7.117)$$

The shape of complex electromagnetic oscillations, with a spectrum of practically any width, remains unchanged in the propagation process, since all of its harmonic components are displaced at identical velocity. It goes without saying that the shape of the oscillations remains unchanged in the stratosphere as well, where there is no refraction, and propagation is at the same velocity $c$ for all frequencies.

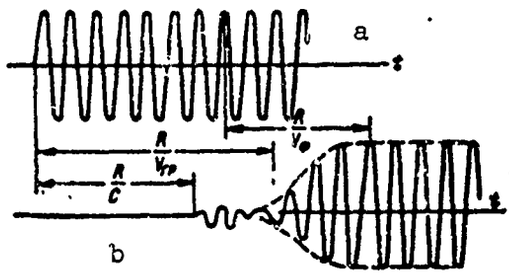


Fig. 7.63. Wave front when entering the ionosphere ($a$) and after propagation to distance $R$ ($b$).

The situation differs in the ionosphere where the refractive index is not the same for different frequencies (Formula 7.116). Inasmuch as the phase velocity of the harmonic components of a complex signal varies, their phase relations change in the propagation process, and this leads to deformation of the high-frequency pulse.

The value of the signal velocity now becomes indeterminate. However, the shape of the transmitted oscillations does not change instantaneously but only to the extent to which a noticeable phase shift accumulates among the harmonic components along the propagation path. In many cases the propagated signal may be considered unchanged. The displacement of the envelope of such a signal is characterized, and is known, by a group velocity. Between group ($v_{gr}$) and phase ($v_f$) velocity there exists the relation

$$v_\phi v_{гр} = c^2. \qquad (7.118)$$

Group velocity has meaning also in the case when the signal is completely distorted during propagation. It defines the speed of travel of the signal's electromagnetic energy.

Figure 7.63 illustrates the above by oscillograms of the transmitted oscillation and the oscillation received at distance $R$. It is assumed that signal delay and signal distortion are caused only by the propagation conditions of the radio waves. The first reaction to the

connection of high-frequency oscillations occurs at the point of reception at a time equal to $R/c$. However, the oscillations propagating at velocity $c$ (the so-called "predecessors") carry an infinitely small part of the energy of the transmitted wave and have no practical significance for radar. A substantial increase in power at the reception point begins at time $R/v_{gr}$. It goes without saying that since the shape of the transmitted oscillations differs from that of the received oscillations it is impossible to define the beginning of the wave front precisely.

The phase velocity characterizes the phase distribution of the field in the steady state. This quantity may be used to define the time interval $R/v_f$, at which any clamp phase value of the emitted oscillations will be repeated at the point of reception. According to Relation (7.118) the phase velocity in the ionosphere will be greater than that in free space, since the refractive index for the ionosphere is a number less than unity. However, this is not connected with the transport of energy and, being a group velocity, is not the signal transmission velocity. According to the postulate of the theory of relativity the latter cannot be greater than the speed of light in a vacuum.

The above considerations enable us to decide which velocity – the phase or the group velocity – to use for calculation when measuring the target range by radar:

1. If the measurement is being made in the presence of the modulation of high-frequency oscillations by their envelope, especially in pulse radar, range should be calculated using the group velocity. In this case the group and phase velocities coincide in the troposphere and stratosphere.

2. When range is measured by phasometric methods using unmodulated oscillations, distances are calculated using the phase velocity.

## 4. Distortion of Signal Shape in the Ionosphere

The distortion of signal shape due to the dependence between propagation velocity in the ionosphere and frequency imposes additional limitations upon the selection of the RLS wavelength. We may make an approximate evaluation of the acceptable distortions of signal shape and of their dependence upon the propagation conditions.

When an oscillation is propagated at frequency $f$ to distance $dl$ in a medium where the phase velocity is $v_f = c/n$, the phase shift may be expressed by the quantity

$$d\varphi = \frac{dl}{\lambda} 2\pi = \frac{2\pi f}{v_\phi} dl = \frac{2\pi f}{c} ndl.$$

The complete phase shift during propagation of radio waves between the RLS and the target

$$\varphi = \frac{2\pi f}{c} \int_L ndl, \qquad (7.119)$$

where integration is over the whole propagation path of the radio waves.

Substituting Expression (7.116) for $n$, we obtain

$$\varphi = \frac{2\pi f}{c} \int_L \left(1 - \frac{1}{2}\frac{f_0^2}{f^2}\right) dl = \frac{2\pi f 2R}{c} - \frac{\pi}{2cf} \int_L f_0^2 dl,$$

where $2R$ is the distance traveled by the direct and the reflected waves in the ionosphere.

The phase delay time of a harmonic oscillation with frequency $f$ may be expressed by the dependence

$$\tau = \frac{d\varphi}{d\omega} = \frac{1}{2\pi}\frac{d\varphi}{df} = \frac{2R}{c} + \frac{\pi}{2cf^2} \int_L f_0^2 dl.$$

The delay time difference for the harmonic components of a complex signal with maximum and minimum frequency $f_{maks}$ and $f_{min}$

$$\Delta\tau = \left(\frac{1}{f_{мин}^2} - \frac{1}{f_{макс}^2}\right) \frac{1}{2c} \int_L f_0^2 dl$$

or

$$\Delta\tau = \frac{(f_{макс} - f_{мин})(f_{макс} + f_{мин})}{2cf^2_{макс}f^2_{мин}} \int_L f_0^2 dl.$$

In the case before us, where the spectral width of the signal $\Delta f = f_{maks} - f_{min}$ is much less than the carrier and $f \approx f_{maks} \approx f_{min}$, we may write approximately

$$\Delta\tau = \frac{\Delta f}{cf^3} \int_L f_0^2 dl. \qquad (7.120)$$

Let us note that the highest harmonic components of the envelope of the transmitted oscillation, obtained after detection of a high-frequency signal, has frequency $\Delta f$. The acceptable time shift $\Delta\tau$ of this harmonic component should not lead to a noticeable shift of its phase. The condition of undistorted transmission of the signal envelope should be

$$\Delta\tau\Delta f \ll 1. \qquad (7.121)$$

At $\Delta\tau\Delta f = 1$ the harmonic component of the envelope of an oscillation transmitted at frequency $\Delta f$ will be shifted by a whole period during propagation.

For a preliminary evaluation of the distortions of the front we assume

$$\Delta\tau\Delta f \leqslant 0{,}1. \qquad (7.122)$$

The integral in Expression (7.120) is replaced by the expression

$$\int_L f_0^2 dl = \bar{f}_0^2 2R; \qquad (7.123)$$

where $\bar{f}_0^2$ is the average value of the square of the ionospheric plasma frequency.

Thus the lower carrier frequency value at which the envelope of a signal with a band $\Delta f$ can be transmitted without distortion is defined

by the expression

$$f \geqslant \sqrt[3]{20 \frac{R}{c} \Delta f \overline{f_c}} \qquad (7.124)$$

Let us examine an example. We assume that an earth satellite at low elevation is being observed by an RLS, the path traversed by the radio beam in the ionosphere being equal approximately to 2000 km. The average value of the plasma frequency is 7 Mhz, the width of the signal spectrum is 10 Mhz. According to Formula (7.124) the minimum carrier value which will ensure undistorted transmission is 870 Mhz ($\lambda$ = = 35 cm).

The above approximate estimate of ionospheric influence on distortion of the signal envelope is for an undisturbed ionosphere and solar activity of average intensity. In the period of maximum solar activity the group delay may increase many times and may cause considerable distortion of the signal in the decimeter wave range.

5. Systematic Range Measurement error

Returning now to the question of the error involved in measuring distances we may recall that this error is due to the curvilinearity

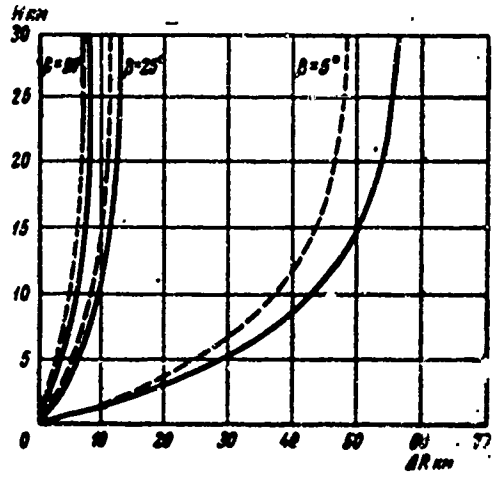


Fig. 7.64. Range measurement error in the troposphere at relative humidities of 100% (continuous lines) and 0 (dashed lines).

of the beam trajectory and to the variation in the propagation velocity.

The propagation time of radic waves in the troposphere along the curve *OTs* (Fig. 7.62) at velocity $v = c/n$

$$\tau_{изм} = \int_l \frac{dl}{v} \qquad (7.125)$$

differs from the value $\tau = 2R/c$ which would be measured in free space. In Expression (7.125) integration is over the whole curvilinear propagation trajectory of the radio beam in two directions. The distance measurement error will be

$$\Delta R = \frac{c(\tau_{изм} - \tau)}{2} = \int_l ndl - R. \qquad (7.126)$$

In calculation practice the troposphere is usually considered to consist of layers. Within the limits of each of the $m$ layers the value of the refractive index $(n_i)$ is assumed to be constant, and the integral in Expression (7.126) is replaced by the finite sum

$$\Delta R = \sum_{i=1}^{m} n_i R_i - R. \qquad (7.127)$$

The range measurement error values (Fig. 7.64) calculated using Formula (7.127) are not great, the maximum error not exceeding 60 m. However, in many cases, for example, in solving problems of controlling a missile trajectory, such errors have to be taken into account.

The size of the error is approximately proportional to the relative humidity, since with increase in the latter there is increase in the refractive index at the earth's surface and increase in its gradient of change with altitude. The target elevation is extremely significant, since at constant altitude it determines the length of the path traversed by the radio beam in the refractive medium.

As was indicated above, in the ionosphere the radar signal is pro-

pagated at the group velocity. In this case, the time of propagation to the target and back is

$$\tau_{изм}=2\int_L \frac{dl}{v_{гр}}=2c\int_L \frac{dl}{n}, \qquad (7.128)$$

while the measurement error is expressed by

$$\Delta R=\int_L \frac{dl}{n}-R. \qquad (7.129)$$

Calculations have been performed in accordance with Formula (7.129) for the law of distribution of the electron concentration with altitude; this law is approximated by a parabola with an exponent (dashed line in Fig. 7.61). The parameters of this curve have been made more accurate by measuring the time of radiorise and radioset of Soviet artificial earth satellites.

In Fig. 7.65 range-measurement error $\Delta R$ is expressed on the scale $f^2/f_0^2$ where $f_0$ is the average value of the plasma frequency and may be determined for any value of the RLS carrier frequency.

As can be seen, the curve resembles the shape of the beam trajectory in the ionosphere. The point where the curves bend corresponds to an altitude of 300 km at which the electron concentration is assumed to be maximum. As in the troposphere, the error increases with reduction in elevation, since this means an increase in the length of the path over which error is accumulated.

Other conditions being equal, measurement error is inversely proportional to the square of the frequency. Its values are negligible in the centimeter wave range. The error becomes noticeable in the decimeter range and very significant in the meter range.

In accordance with the conditions for which the curves of the concentration distribution were plotted, the data of the graph in Fig. 7.65 are for the maximum of solar activity which occurs during daylight hours

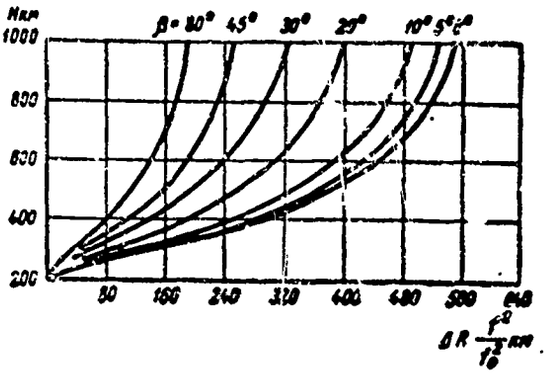

Fig. 7.65. Range-measurement error in the ionosphere.

in the autumn. These errors may be viewed as nearly limiting for the middle latitudes of the northern hemisphere.

6. The Systematic Velocity-Measurement Error

Distortion of the propagation trajectory of radio waves also leads to error in the radar measurement of velocity. Actually, the true value

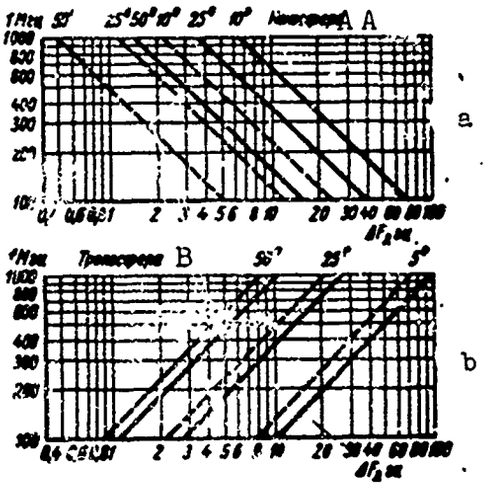

Fig. 7.66. Error in measuring Doppler frequency: a) For a target moving at a velocity of 6 km/sec at an altitude of 30 km at relative humidities of 100% (continuous line) and 0 (dashed lines); b) for a target moving at the same velocity at altitudes of 300 km in the daytime (continuous lines) and 250 km at night (dashed lines). A) Ionosphere; B) troposphere.

of the target radial velocity is a projection of velocity vector $V$ on the direction from the RLS to the target (see Fig. 7.62). However, be-

cause of refraction the radio beam arrives at the target from another direction at angle $\Delta\psi$ to the straight line $OTs$. The projection of the velocity on this direction will be $V_L$. The error in measuring radial velocity which, as follows from Fig. 7.62, may be expressed as

$$\Delta V = V_R - V_L = V \sin\psi \Delta\psi, \qquad (7.129')$$

is proportional to the tangential projection of the target velocity. Accordingly, the error in determining the Doppler frequency will be

$$\Delta F_{\text{д}} = \frac{2f}{c}\Delta V = \frac{2f}{c} V \sin\psi \Delta\psi. \qquad (7.130)$$

Angle $\Delta\psi$ between the true target direction and the radio beam trajectory at point $Ts$ is determined by the refractive index values at the RLS and the target and is practically independent of the intermediate values of $n$. Therefore, in contrast to the cases examined above, the error involved in measuring the radial component of the target velocity does not accumulate along the propagation path of the radio waves. The magnitude of the error may be calculated using Formula (7.130) from the values of the refractive index at the RLS and at the target taking into account the sphericity of the atmospheric layers.

Formula (7.130) has been used to calculate the errors (Fig. 7.66a and b) for a target (for example, a meteorite) moving at a velocity of 6 km/sec in the horizontal direction at an altitude of 30 km, and also in the ionosphere in the layers with the maximum electron concentration. As above, in both cases there is noted a substantial dependence between the error and the target elevation. According to Relation (7.130) the beam deflection angle increases with reduction in the target elevation. The moisture content is very significant for the troposphere, and, for the ionosphere, the significant factor is the electron concentration which depends, in particular, upon the time of day.

As follows from Formula (7.130), when the target is moving in the troposphere, the error in determining the Doppler shift is proportional

to the RLS carrier frequency. However, this dependence is of a different character for the ionosphere because of the reduction of the refractive index with frequency.

In concluding these sections devoted to the systematic errors involved in measuring range and velocity, we may note that the values of these errors were obtained for a certain definite state of the atmosphere. By using the methodology set forth above, error data may be made more precise for other conditions of radar observation by using the results of meteorological and ionospheric measurements. However, it is in practice impossible to obtain such data for the whole propagation path. Therefore, the systematic or slowly varying measurement errors may be taken into account only in part.

## 7. The Influence of Random Atmospheric Heterogeneities

Even greater difficulties are involved in a consideration of measurement errors due to random atmospheric heterogeneities. In this case it is quite impossible to take this error into account and compensate for it, and one can only estimate its size statistically.

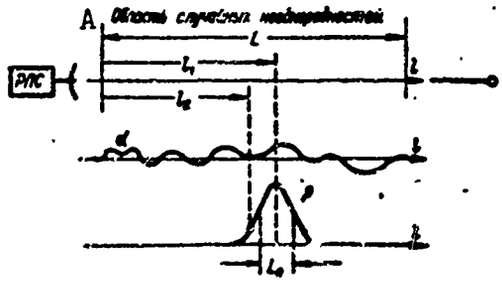


Fig. 7.67. Influence of random atmospheric heterogeneities: a) Path in heterogeneous atmosphere; b) fluctuations of refractive index; c) correlation coefficient of heterogeneities. A) Region of random heterogeneities.

Let us make such an evaluation for heterogeneities with large transverse dimensions.* In this case the atmospheric heterogeneity need be taken into account only in the direction of propagation, which simp-

lifies the task considerably.

The change in the r fractive index in a heterogeneous atmosphere may be conveniently characterized by quantity α, determined by equality

$$n=1+\alpha. \tag{7.131}$$

The average value of the refractive index is assumed equal to unity, and its fluctuations are assumed equal to α.

Utilizing Expression (7.131) we establish the link between the phase fluctuation φ of the incoming wave and the range-measurement error associated with the group velocity in unidirectional propagation.

The propagation time of radio waves with phase velocity along path $L$

$$t_\phi=\int_0^L\frac{dl}{v_\phi}=\frac{1}{c}\int_0^L ndl=\frac{1}{c}\int_0^L(1+\alpha)\,dl. \tag{7.132}$$

The propagation time of a signal with group velocity along the same path is

$$t_{rp}=\int_0^L\frac{dl}{v_{rp}}=\frac{1}{c}\int_0^L\frac{dl}{n}=\frac{1}{c}\int_0^L\frac{dl}{1+\alpha}$$

or, because α is small,

$$t_{rp}=\frac{1}{c}\int_0^L(1-\alpha)\,dl. \tag{7.133}$$

The absolute magnitude of the fluctuattions of propagation time $t_f$ and $t_{gr}$

$$\Delta t_\phi=\frac{1}{c}\int_0^L\alpha dl,\quad \Delta t_{rp}=-\frac{1}{c}\int_0^L\alpha dl$$

are equal and opposite in sign. Therefore

$$\Delta\varphi=-\frac{\omega}{c}\Delta R=\frac{\omega}{c}\int_0^L\alpha dl, \tag{7.134}$$

where $\Delta\varphi=\Delta t_\phi\omega$ is the phase fluctuation; $\Delta R=c\Delta t_{rp}$ is the range-measurement error.

In accordance with Expression (7.134) the absolute magnitude of the random range-measurement error is proportional to the phase fluctuation of the received wave and has the opposite sign.

We determine the magnitude of the mean square of the phase fluctuation and then the mean-square range-measurement error for propagation at range $L$ in a medium with large-scale heterogeneities.

By squaring quantity $\Delta\varphi$ from Expression (7.134) and averaging it over time, we may write

$$\overline{\Delta\varphi^2} = \frac{\omega^2}{c^2}\overline{\int_0^L \alpha dl \int_0^L \alpha dl},$$

whence

$$\overline{\Delta\varphi^2} = \frac{\omega^2}{c^2}\int_0^L\int_0^L \overline{\alpha_1\alpha_2}\, dl_1 dl_2.$$

The average size of the product $\overline{\alpha_1\alpha_2}$ of fluctuations $\alpha_1$ and $\alpha_2$ of the refractive index, taken at different points $l_1$ and $l_2$ of the trajectory (Fig. 7.67) may be expressed as the dispersion of the refractive index $\overline{\alpha}^2$ and the correlation coefficient $\rho$ which is a function of the distance between the points:

$$\overline{\alpha_1\alpha_2} = \overline{\alpha}^2\rho(l_1 - l_2). \qquad (7.135)$$

Then

$$\overline{\Delta\varphi^2} = \frac{\omega^2}{c^2}\overline{\alpha}^2\int_0^L\int_0^L \rho(l_1 - l_2)\, dl_1 dl_2. \qquad (7.136)$$

In meteorology the coefficient of correlation between values of the refractive index at points which are separated from one another by distance $r$ is often expressed by the function

$$\rho(r) = e^{-\left(\frac{r}{L_0}\right)^2} = e^{-\left(\frac{l_1-l_2}{L_0}\right)^2}. \qquad (7.137)$$

As is known, the values of this function decline rapidly at $r =$

$= l_1 - l_2 > L_0$: at the same time the heterogeneity dimensions characterized by quantity $L_0$ are many times smaller than the propagation path $L$ (Fig. 7.67). This makes it possible to replace the integration limits of function $\rho$ by the values $+\infty$ and $-\infty$ without any noticeable error; then

$$\overline{\Delta\varphi^2} = \frac{\omega^2}{c^2}\overline{\alpha^2}\int_0^L\int_{-\infty}^{\infty} e^{-\left(\frac{l_1-l_2}{L_0}\right)^2} dl_1 dl_2. \qquad (7.138)$$

After integration we obtain a final expression for the mean square of the phase fluctuations

$$\overline{\Delta\varphi^2} = \frac{\omega^2}{c^2}\overline{\alpha^2}\sqrt{\pi L L_0}. \qquad (7.139)$$

The mean square range-measurement error may be found from Expressions (7.134) and 97.139):

$$\sigma_R = \sqrt{\overline{\Delta R^2}} = 1{,}3\sqrt{\overline{\alpha^2} L L_0}. \qquad (7.140)$$

As is seen, this error is proportional to the square root of the dimension $L_0$ of the heterogenities, the path $L$ traversed by the wave in the heterogeneous medium, and the dispersion of the refractive index $\overline{\alpha}^2$. The order of magnitude of the error may be judged from the data of the following example: at $L$ = 600 km, $L_0$ = 200 m, $\overline{\alpha}^2 = 10^{-10}$ the mean square range-measurement error is only 15 cm. However, as will be demonstrated in Chapter 8, atmospheric heterogeneities lead to noticeable errors in the measurement of angular coordinates, and their influence may be assimilated to the above problem.

Manuscript Page No.

[Footnotes]

385 Both here and below integration is within the limits of the pulse length, in the general case from $-\infty$ to $+\infty$.

391 Formula (7.23) takes into account the so-called negative frequencies. If they are not considered, it is necessary to double the integral within the limits zero to infinity.

404 Both here and below the limits of integration extend from $-\infty$ to $+\infty$.

412 At the present time devices have been developed for combined measurement of range and velocity with a small number of channels [6]; in view of the complexity of their design principles they are not considered here.

491 An exception is the thyratron filled with hydrogen; its firing time may be determined by the synchronizer pulse.

498 Strictly speaking, the maximum brightness does not coincide with the brightness value at the point $\xi = 0.5\Delta$. However, the difference between them is negligibly small.

524 It is assumed that in a plane perpendicular to the propagation, within the limits of the first Fresnel zones, the parameters of the heterogeneities remain unchanged. We may recall that the Fresnel zones represent the geometrical locus of the point in space for which the RLS and target traces differ by not more than $\lambda/2$.

Transliterated Symbols

374 РЛС = RLS = radiolokatsionnaya stantsiya = radar

375 р = r = rasprostraneniye = propagation

375 с = s = sluchaynyy = random

376 ц = ts = tsel' = target

376 м = m = metod = method

377 и = i = instrument = instrument; impul's = pulse

378 с = s = signal = signal

378 ш = sh = shum = noise

384 вых = vykh = vykhod = output

384 п = p = priyemnik = receiver; povtoreniye = repetition

386 э = e = effektivnyy = effective

410 макс = maks = maksimal'nyy = maximum

410 д = d = doppler = doppler

416 с = s = szhatyy = compressed

425 ЛЗ = LZ = liniya zaderzhki = delay line

427 АРУ = ARU = avtomaticheskiy regulyator usileniya = automatic gain control

427 ВС = VS = ventil' sovpadeniya = coincidence valve

428 п = p = peredniy = leading

428 з = z = zadniy = trailing

432 УС = US = usilitel' = amplifier

433 АСД = ASD = avtomaticheskaya soprovozhdeniye po dal'nosti = = range autotrack

434 РЦЗ = RTsZ = reguliruyemaya tsep' zaderzhki = adjustable delay line

442 вр = vr = vremya = time

445 д = d = diskriminator = discriminator

445 вх = vkh = vkhod = input

455 и = i = integriruyushchiy = integrating

446 дв = dv = dvigatel' = motor

448 з = z = zaderzhka = delay

450 г = g = generator = generator, oscillator

450 у = u = upravleniye = control

454 р = r = radial'nyy = radial

455 п = p = perestraivayemyy = tunable

455 пр = pr = prinyatyy = received

456 цели = tseli = target

459 к = k = korrektiruyushchiy = compensating, correction

461 оу = ou = operatsionnyy usilitel' = operational amplifier

462 уст = ust = ustanovivshiysya = steady-state

465 стр = str = strobirovaniye = strobing

469 н = n = nesushchaya chastota = carrier frequency

469 п = p = promezhutochnaya chastota = i-f; also пч = pch

469 АПЧ = APCh = avtomaticheskaya podstroyka chastoty = automatic frequency control

481 ЦВМ = TsVM = tsifrovaya vychislitel'naya mashina = digital computer

484 д = d = diod = diode

484 а = a = anod = anode, plate

486 м = m = mernyy = measurement

493 АП = AP = antennyy pereklyuchatel' = TR switch

498 м = m = maksimal'nyy = maximum

514 гр = gr = gruppovoy = group

514 ф = f = fazovyy = phase

517 мин = min = minimal'nyy = minimum

517 макс = maks = maksimal'nyy = maximum

520 изм = izm = izmeryennyy = measured

## Chapter 8

## RESOLVING POWER, ACCURACY AND UNIQUENESS OF READINGS IN ANGULAR COORDINATES MEASUREMENTS

The accuracy of angular coordinates measurements is estimated by the errors of bearing originating from different elements of radio-locational tracts. Just as in the measurement of distance, errors can be divided into systematic and accidental ones. Systematic errors that arise from independent sources of disturbances add algebraically while accidental errors add geometrically.

For the sources of bearing errors, one can divide them into those of external sources introduced by target or propagation medium and those arising from the inadequecy of the apparatus and the imperfection of the measuring method. The minimum apparatus error in angle measurement determines the potential accuracy of the system of bearing: the system itself in this case becomes the optimum. Potential accuracy cannot be surpassed in any external conditions.

In distinction from errors in distance measurements, external angle errors introduced by target itself and effects of the earth, have their own features. Thus, while the center of reflection of an elongated object in distance does not go outside the outline of the actual target, in angle, the center of reflection may appear to be several target angular diameters away from the real one. The reason for this and several other errors is that during reflection from an elongated object (and also during reflection from the Earth), there is a complicated interference phenomenon which leads to local distortions of the phase front

of the waves.

This feature of angle error leaves a definite imprint on the structure of the bearing system and should be taken into account in the selection of a bearing system. Therefore, the problem of accuracy in angular coordinates measurements begins with an examination of the external sources of error.

## §8.1 EFFECT OF THE CONDITION OF RADIOWAVE PROPAGATION AND SIZE OF THE OBJECT ON THE ACCURACY OF ANGULAR COORDINATES MEASUREMENTS

The target, Earth and atmosphere are the sources of error in angular coordinates measurements. In the process of reflection from the object, which has finite dimensions and complex configurations, these distort the phase front of the reflected wave. Nonhomogeneous atmosphere causes the bending of the trajectory of radiowave propagation. Finally, reflection from the Earth creates further sources of radiation not in conformity with the RLS-target direction.

All these factors create errors in the bearing of the object which limit the ultimate accuracy of the measurement.

### 1. Effect of the Atmosphere

Errors dependent on the atmosphere can be systematic and accidental.

Systematic error of angular coordinates measurement is connected with regular atmospheric inhomogeneity. Since the variation of refractive index of the atmosphere may be considered only in the vertical direction, the systematic error dependent on it concerns the measurement of the angles of elevation. The reasons causing this error and the character of the deformation of the trajectory of radiowave propagation have been examined in sufficient detail in the previous chapter (see Fig. 7.62). It remains only to give them a quantitative evaluation.

The relationship between the values of refractive index and the angles of inclination of the beam for the atmosphere in the form of horizontal layers $n\cos\theta = \text{const}$ may serve as an initial expression for the determination of error. However, it is necessary to remember that the angle of incidence in each layer, is dependent not only on the variation of the refractive index in the preceding layers but also on the variation of the inclination of the layers relative to the trajectory.

The refraction of radiobeams in elementary layer of atmosphere during a change of refractive index by the increment $dn$ may be found from the equation

$$n\cos\theta = (n + dn)\cos(\theta + d\theta).$$

Reorganizing this expression and discarding the small second order values, we obtain

$$d\theta = \frac{dn}{n}\operatorname{ctg}\theta.$$

The elementary ray deflections built up in the path of propagation $L$, lead to a deflection of the trajectory by an angle

$$\Delta\theta = \int_L \frac{dn}{n}\operatorname{ctg}\theta. \qquad (8.1)$$

Calculations with Formula (8.1) are substantially simpler for not too small elevation angles (in the order of 10° and larger). Here the dependence of index of refraction on angle $\theta$ may be neglected and ctg $\theta$ may be considered as constant.

Bearing error $\Delta\beta$ may be found through the solution of a system of equations in which there are:

1) formula for bearing error

$$\Delta\beta = \Delta\theta + \theta - \varepsilon - \beta = \int_L \frac{dn}{n}\operatorname{ctg}\theta + \theta - \varepsilon - \beta, \qquad (8.2)$$

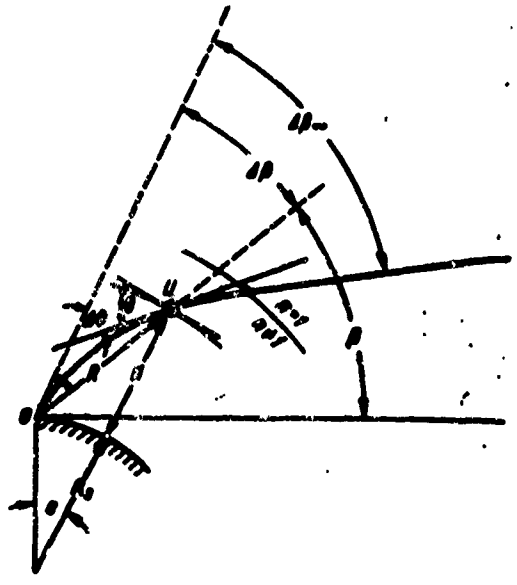

Fig. 8.1. Angular relationships during refraction of radiowaves over a spherical surface of the Earth.

expressed in the angle of the elevation of the object β and the geocentric angle ε (Fig. 8.1);

2) an expression connecting height $H$, distance $R$, radius of the Earth $R_z$ and the angle ε:

$$R=\sqrt{(R_3+H)^2+R_3^2-2R_3(R_3+H)\cos\varepsilon}. \qquad (8.3)$$

3) equation of the beam

$$\cos\theta\cdot n(R_3+H)=\cos\theta_0 n_0 R_3, \qquad (8.4)$$

where $\theta_0=\beta+\Delta\beta$.

4) expression for the actual value of the angle of elevation of the object, found through the theorem of sines from Fig. 8.1

$$\beta=\arccos\left(\frac{R_3+H}{R}\sin\varepsilon\right). \qquad (8.5)$$

The solution of these equations normally is done by graphical methods.

The calculation results for bearing error in the troposphere and

stratosphere are shown in Fig. 8.2:

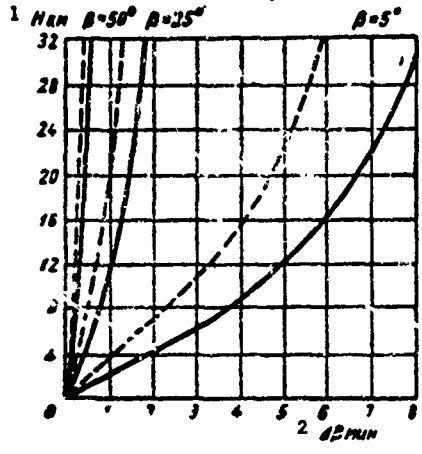


Fig. 8.2. Error of measurement of the angle of elevation in troposphere at 100% humidity and 0° (dotted line). 1) km; 2) min.

As can be seen, the magnitude of the error is substantially dependent on the inclination of the beam and the humidity of the atmosphere.

For the ionosphere (Fig. 8.3), owing to the dependence of the refractive index on the activity of the sun, the measurement error varies substantially from day (solid curves) to night (dotted curves). The largest error occurs at a position of height with a maximum concentration of electrons. The curves are given for a 400 megacycle frequency. The value of the error is proportional to the length of the waves and may be converted to other frequencies by the graph data.

There is certain interest in the cases where the object is located at a very large distance from the Earth. Then the direction of the waves past the limits of the atmosphere approximately coincides with the actual direction to the distant object from the point of observation (0 in Fig. 8.1). Bearing error for this case is designated as the angle of astronomical refraction $\Delta\beta_\infty$, which is equal to the bending of the radiobeam over the time of passing through the atmosphere

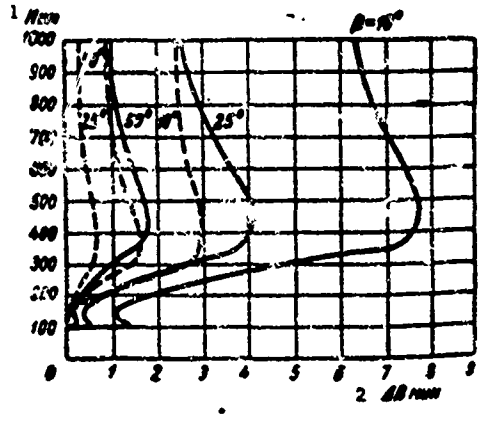


Fig. 8.3. Error of measurement of the angle of elevation in the ionosphere, daytime (solid lines); night (dotted lines). 1) km; 2) min.

($\Delta\theta$) and may be calculated by Formula (8.1). If we assume $n = 1$, which is completely satisfied by waves shorter than 30 cm, then a simple expression for the angle of astronomical refraction may be obtained

$$\Delta\beta_\infty = (n_0 - 1)\operatorname{ctg}\theta_0. \qquad (8.6)$$

As can be seen, bearing errors of objects outside the Earth are not dependent on the law of variation of refractive index but is determined by its initial ($n_0$) and final (1) values.

Accidental error of angular coordinates measurements, dependent on large scale nonhomogeneity of the atmosphere, may be evaluated by methods of geometrical optics.

The problem is formulated by the following example.

The vibration of a point radiowave source is received at points *A* and *B* equidistant from it (Fig. 8.4). Let us assume that the source of radiation *O* is located very far from the boundary of the area where there are zones of nonhomogeneity. Hence, for the portion of the trace with nonhomogeneity of the atmosphere ($L$), the beams *OA* and *OB* are considered parallel. Determine the inclination of the phase front within baseline *AB*, for which we find the difference in the phase of vibration received at points *A* and *B*.

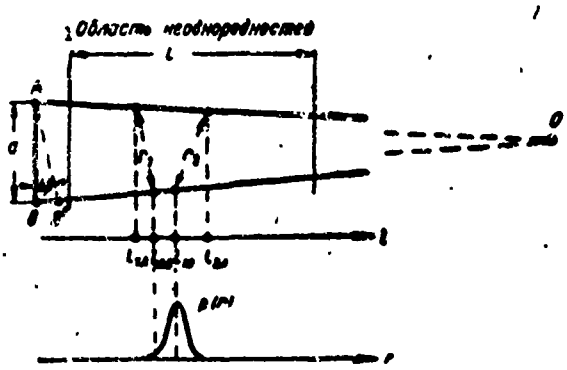

Fig. 8.4. Scheme of the trace with nonhomogeneous atmosphere during the evaluation of bearing error. 1) Area of nonhomogeneity.

According to Formula (7.134) obtained in Section 7.14, the absolute values of phase fluctuation at points $A$ and $B$ are expressed as

$$\Delta\varphi_A=\frac{\omega}{c}\int_0^L \alpha_A dl,\quad \Delta\varphi_B=\frac{\omega}{c}\int_0^L \alpha_B dl,$$

where $\alpha_A$ and $\alpha_B$ are fluctuations of refractive index along the beams $OA$ and $OB$. The phase difference at points $A$ and $B$

$$\Delta\varphi_{AB}=\Delta\varphi_A-\Delta\varphi_B=\frac{\omega}{c}\int_0^L(\alpha_A-\alpha_B)\,dl. \qquad (8.7)$$

Determine the mean square of this value similarly to what was given in §7.14

$$\overline{\Delta\varphi_{AB}^2}=\frac{\omega^2}{c^2}\overline{\int_0^L(\alpha_A-\alpha_B)\,dl\int_0^L(\alpha_A-\alpha_B)\,dl}=$$
$$=\frac{\omega^2}{c^2}\int_0^L\int_0^L\overline{(\alpha_{1A}-\alpha_{1B})(\alpha_{2A}-\alpha_{2B})}\,dl_1dl_2.$$

Here, $\alpha_{1A}$, $\alpha_{2A}$ and $\alpha_{1B}$, $\alpha_{2B}$ – values of fluctuation of refractive index in the current points on the beams $OA$ and $OB$. The corresponding coordinates of these points will be $l_{1A}$, $l_{2A}$ and $l_{1B}$, $l_{2B}$.

Multiplying the parentheses in the expression under the integral sign and substituting $\overline{\alpha_i\alpha_j}=\overline{\alpha^2}\rho(r)$, we obtain a double integral of

four terms

$$\overline{\Delta\varphi_{AB}^2} = \frac{\omega^2}{c^2}\overline{\alpha^2}\int_0^L\int_0^L [\rho(l_{1A}-l_{2A})+$$
$$+\rho(l_{1B}-l_{2B})-\rho(r_1)-\rho(r_2)]\,dl_1 dl_2. \qquad (8.8)$$

The integrals of the first two terms correspond completely to Expression (7.138) in the preceding chapter, and it is possible to write down for them the final result, which is twice the value of $\overline{\Delta\varphi^2}$ from Formula (7.139). Two other terms contain the coefficient of correlation connecting the value of $\alpha$ in points which are located on different beams. The distance between these points may be expressed as (Fig. 8.4)

$$r_1 = d^2+(l_{1A}-l_{2B})^2 \text{ and } r_2^2 = d^2+(l_{1B}-l_{2B})^2.$$

The formulas for the coefficient of correlation for these values of the argument

$$\rho(r_1)=e^{-\frac{d^2+(l_{1A}-l_{2B})^2}{L_0^2}} \text{ and } \rho(r_2)=e^{-\frac{d^2+(l_{1B}-l_{2A})^2}{L_0^2}}$$

differ from Expression (7.137) in the constant factor $e^{-\frac{d^2}{L_0^2}}$. Therefore, the result of integration of the last two terms of the Expression (8.8) also comes to $\overline{\Delta\varphi^2}$ from Formula (7.139) multiplied by $e^{-\frac{d^2}{L_0^2}}$.

Thus, the unknown phase difference at points $A$ and $B$ and the phase fluctuation at one point are related by the expression

$$\overline{\Delta\varphi_{AB}^2} = \overline{\Delta\varphi^2}2\left(1-e^{-\frac{d^2}{L_0^2}}\right). \qquad (8.9)$$

Dependent on the base of receiving points (or aperture of antenna) and the size of nonhomogeneity ($L_0$), the relationship between the shifts $\Delta\varphi_{AB}$ and $\Delta\varphi$ may be different. For long bases, larger than the nonhomogeneities ($d/L_0 >> 1$) vibrations received at points $A$ and $B$ propagate on paths with statistically independent inhomogeneities. Therefore, during the measurement of the phase difference, the mean square fluctuation is two times greater in comparison with the fluctua-

tions at one point

$$\overline{\Delta\varphi_{AB}^2}=2\overline{\Delta\varphi^2}. \qquad (8.10)$$

On the other hand, approaching the point of reception $\left(\frac{d}{L_0}\to 0\right)$, the paths of propagation become the same and the difference fluctuation approaches zero. The case when the aperture of the antenna system is smaller than the size of nonhomogeneity presents great interest. Expression (8.9) for it may be written in a still more simplified form if we expand $e^{-\frac{d^2}{L_0^2}}$ into a series and take the first two terms of the series:

$$\overline{\Delta\varphi_{AB}^2}=\overline{2\Delta\varphi^2}\frac{d^2}{L_0^2}. \qquad (8.11)$$

Or, substituting the value of $\overline{\Delta\varphi^2}$ from Formula (7.139), we obtain

$$\overline{\Delta\varphi_{AB}^2}=2\sqrt{\pi}\frac{\omega^2}{c^2}a^2d^2\frac{L}{L_0}. \qquad (8.12)$$

Now, owing to the accidental nonhomogeneity of the atmosphere, at points *A* and *B*, equidistant from the source, vibrations with phase shift $\Delta\varphi_{AB}$ are received. If there is phase $\varphi$ at point *A* then for the beam *OB* there will be at a certain point *B'*, a phase of similar value (see Fig. 8.4). Considering the wave front plane within the base, its angle of inclination may be expressed by

$$\Delta\beta=\frac{BB'}{d}=\frac{\Delta\varphi_{AB}\lambda}{2\pi d}. \qquad (8.13)$$

The accidental bearing error $\sigma_\beta$, which is dependent on the nonregular inhomogeneity of the atmosphere, may be determined by the root-mean-square value of this angle

$$\sigma_\beta=\sqrt{\overline{\Delta\beta^2}}=1{,}9\sigma_n\sqrt{\frac{L}{L_0}}. \qquad (8.14)$$

It can be seen that the accidental error of angular coordinate measurement is proportional to the fluctuation of refractive index $\sigma_n=\sqrt{\overline{n^2}}$ and the square root of the ratio of the extensive-

ness of the trace to the size of the nonhomogeneity. For the example in §7.12 ($L=600$ км, $L_0=10$ км, $\sigma_n=10^{-1}$), the mean square error comes to an appreciable value of $\sigma_\beta=30'$.

2. Effect of the Finite Dimensions of the Target

For any method of direction finding, the antenna system of a radar system responds to the variation of phase front of waves in its aperture. If there are no errors in the RLS itself, the object bearing indicates a direction normal to the phase front of the reflected wave. In an overwhelming majority of problems related to the propagation of electromagnetic waves, it is assumed that the wave front is spherical and the source of radiation, the target, is located in its center. However, if the object consists of two or more number of reflective points, the wave front is distorted and the normal to it may pass through very far beyond the boundary of the contour of the object.

For a clarification of the physical substance of this phenomenon, let us examine an object with two reflective points *I* and *II* separated from each other by a distance of $D_0$. We will consider these points to be radiating in all directions with a fixed phase shift $\varphi_0$ (Fig. 8.5).

At a distant point of space *O* with polar coordinates *R* and $\psi$, the radiators create the field strengths.

$$e_1=E_1\sin\left(\omega t-\frac{2\pi R}{\lambda}+\frac{2\pi}{\lambda}\frac{D_0}{2}\sin\psi\right),$$

$$e_2=E_2\sin\left(\omega t-\frac{2\pi R}{\lambda}-\frac{2\pi}{\lambda}\frac{D_0}{2}\sin\psi-\varphi_0\right).$$

The phase displacement between these waves is determined by the phase angle $\varphi_0$ and the path difference $D_0\sin\psi$ dependent on the direction $\psi$ to the receiving point.

The field of the resultant wave at a distance *R* from the center of the base $D_0$ may be presented as a vibration

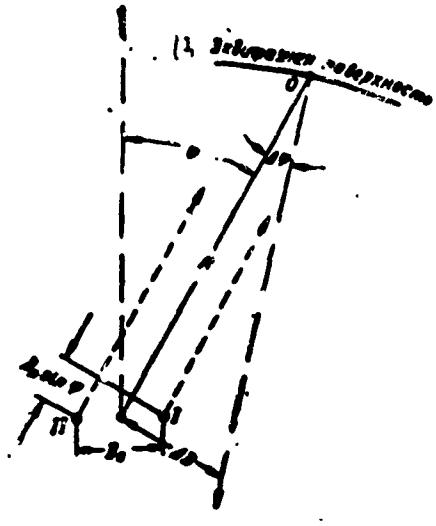

Fig. 8.5. Geometric relationship during the determination of phase front of the waves of two sources. 1) Equiphase surface.

$$e = E \sin\left(\omega t - \frac{2\pi R}{\lambda} + \Phi\right) \tag{8.15}$$

with amplitude

$$E = \sqrt{E_1^2 + E_2^2 + 2E_1E_2 \cos\left(\frac{2\pi D_0}{\lambda} \sin\psi + \varphi_0\right)} \tag{8.16}$$

and phase

$$\Phi = \operatorname{arctg} \frac{E_1 \sin\left(\frac{\pi D_0}{\lambda} \sin\psi\right) - E_2 \sin\left(\frac{\pi D_0}{\lambda} \sin\psi + \varphi_0\right)}{E_1 \cos\left(\frac{\pi D_0}{\lambda} \sin\psi\right) + E_2 \cos\left(\frac{\pi D_0}{\lambda} \sin\psi + \varphi_0\right)}. \tag{8.17}$$

As it is known, phase front of waves is described as the geometric locus of points in space with the same phases. For a fixed moment of time, assuming the phase in Expression (8.15) to be constant, it is possible to get a relationship between $R$ and $\psi$ in an equation of phase front in polar coordinates

$$\frac{2\pi R}{\lambda} = \Phi(\psi, \varphi_0). \tag{8.18}$$

The derivative $dR/d\psi$ at any point with coordinates $R$, $\psi_r$ found from this equation, determines the distortion of the wave front in comparison with the spherical surface which passes through the same point.

The error in determining direction to the center of the target, arising as a result of the distortion of the phase front, may be expressed as an angle $\Delta\psi$ between the normal to the equiphase surface and the radius vector $R$

$$\operatorname{tg}\Delta\psi=\frac{\frac{dR}{d\psi}}{R}. \tag{8.19}$$

This error may also be easily determined by the linear deviation of the apparent position of the object relative to its center

$$\Delta D=R\operatorname{tg}\Delta\psi=\frac{dR}{d\psi}=\frac{\lambda}{2\pi}\frac{d\Phi(\psi)}{d\psi}. \tag{8.20}$$

This deviation of the phase front normal from the target center, which may be found by the differentiating (8.17) (Fig. 8.5):

$$\Delta D=\frac{D_0\cos\psi}{2}\frac{E_1^2-E_2^2}{E_1^2+E_2^2+2E_1E_2\cos\left(\frac{2\pi D_0}{\lambda}\sin\psi+\varphi_0\right)}, \tag{8.21}$$

depends on the relationship between $E_1$ and $E_2$ and the phase difference $\varphi=\frac{2\pi}{\lambda}D_0\sin\psi+\varphi_0$. At $\varphi$ equal to an even multiple of $\pi$, the error

$$\Delta D_{\min}=\frac{D_0\cos\psi}{2}\frac{E_1-E_2}{E_1+E_2} \tag{8.22}$$

does not exceed the apparent dimensions of the object $\pm\frac{D_0\cos\psi}{2}$, but the field intensity (8.16) has its largest value. If the phase shift is equal to $\pi$ or any odd multiple of $\pi$, then the normal to the phase front deviates from the center of the object by an amount

$$\Delta D_{\max}=\frac{D_0\cos\psi}{2}\frac{E_1+E_2}{E_1-E_2}. \tag{8.23}$$

and may deviate beyond the boundary of the object. Large errors occur for closely similar values of $E_1$ and $E_2$. However, the resulting field strength will be small.

The reason for the error phenomenon is clearer, if we determine the form of phase front of the waves for the particular case

when the amplitudes and phases of the sources are the same: $E_1=E_2$, $\varphi_0=0$.

In the direction perpendicular to the object at a distance $R$ from its center the field strengths created by the sources are identical in phase. The resultant vector $E$ (Fig. 8.6) has the same phase. We shall find the equiphase surface for which the resultant vector $E$ in the phase plane remains unchanged.

Let us move a short distance to the right along a sphere of radius $R$ in the far zone. The point of observation (point 2 in Fig. 8.6) is now closer to the source *I* and as much farther from source *II*. Consequently, the vectors of the field strength $E_1$ and $E_2$ retaining identical amplitude, rotate by the same angle in opposite directions. The phase of the resulting vector will remain unchanged (see the vector diagram for point 2 in Fig. 8.6). This signifies that the spherical surface on which the point of observation is transposed, is an equiphase surface.

Transposing further along the wave front, we hit point 3 at which the phase vectors $E_1$ and $E_2$ are oppositely located. At further points on the same sphere (point 4) the resulting field changes phase by 180°. In order to continue the motion of the point of observation on the previous surface it is necessary to move over onto a sphere of radius $R \pm \lambda/2$, where the resultant vector $E$ again assumes a vertical position.

Repeating the above discussion, we are convinced again that this sphere remains an equiphase surface, until the phase shift reaches a value of $3\pi$. At this point, (point 5 in Fig. 8.6) a jumpwise shift of equiphase surface by $\lambda/2$ again occurs.

Under this condition, in the directions for which the phase between the sources of vibration amounts to $(2n + 1)$ where $n$ is an integer, the normal to the wave front rotates 90° relative to the di-

rection to the object. Taking the bearing from these directions one may expect an error of $\Delta\psi = 90°$ (or $\Delta D = \infty$). However, in the present case, such large errors do not occur since owing to the equality in the amplitudes of the vibrations $E_1$ and $E_2$, resulting fields do not exist at front discontinuities.

Let us examine what sort of shape does the equiphase surface take if the relation of the amplitudes of the source fields is somewhat modified.

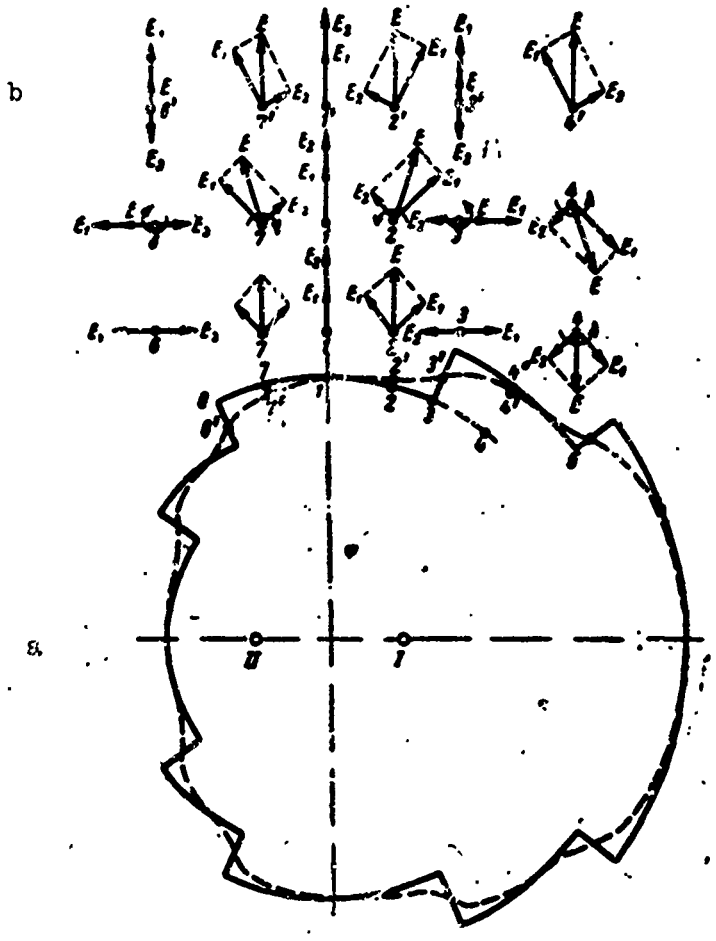


Fig. 8.6. Shape of the wave front of two sources and vector diagrams of interference at various points of the equiphase surface.

At point 1, the vectors of field strengths $E_1$ and $E_2$ and the resultant vector $E$ maintain the previous phase values. If we leave this point on a radius-$R$ sphere, then owing to the inequality of the absolute values of the vectors $E_1$ and $E_2$, the phase of the resultant field will change. At point 2, vector $E$ rotates by an angle of $\Delta\varphi$ in the direction of the larger field component. This indicates that we have moved from the equiphase surface by the distance $\Delta R = \lambda\frac{\Delta\varphi}{2\pi}$. Hence, in order to return to the previous phase value, when the vector $E$ occupies a vertical position, it is necessary that the point of observation be closer to the object (or further away from it) by a distance of $\Delta R$. In this, the vectors $E_1$ and $E_2$ change phase by identical amount – rotating by the same angle $\Delta\varphi$ and the resultant vector $E$ returns to the vertical position. Under this condition, when $E_1 \neq E_2$ the phase front is displaced to point 2' either forward or backward in relation to the previous position dependent on the relationship between $E_1$ and $E_2$.

It is not difficult to see that in this case, the phase front of the wave (dotted line in Fig. 8.6a) is an undulating surface, deviating by no more than $\lambda/2$ relative to the sphere with the center at the location point of the source with the larger field strength, namely, the front of the resultant wave is determined basically by the stronger source; the second source only slightly deforms it. The deformation is the more significant, the smaller the amplitude difference in $E_1$ and $E_2$. The largest deformation of the front occurs in areas where the fields of the sources add up in opposite phases. But the intensity of the fields for these directions diminishes. At equal amplitudes, for every value of phase, there exist two equiphase surfaces equally located relative to the first and second sources.

Continuing the previous discussion, we may explain the influence

of the relationship between the phases of the sources on the shape of the wave front. In the presence of phase shift $\varphi_0$, the equiphase line, shown in Fig. 8.6 rotates. In particular, when $\varphi_0 = \pi$, the area of the first inflection of the front is located in the direction $\psi = 0$. Similar deformation of the curve also occurs in coordinate $\psi$ because the angles $\varphi_0$ and $\psi$ determine the phase $\left(\frac{2\pi D_0}{\lambda}\sin\psi + \varphi_0\right)$ in the wave front equation (8.18) by different functions. But the general shape of the curve remains unchanged during the variation of phase shift. Equiphase surface may be formed by rotating the curve around the axis connecting the sources *I* and *II*.

For the evaluation of the probability of the error of measurement, connected with the deformation of the front, we return to a discussion of the Expression (8.21). A typical shape of the dependence of the deviation of the phase front on the angle $\psi$ is shown in Fig. 8.7.

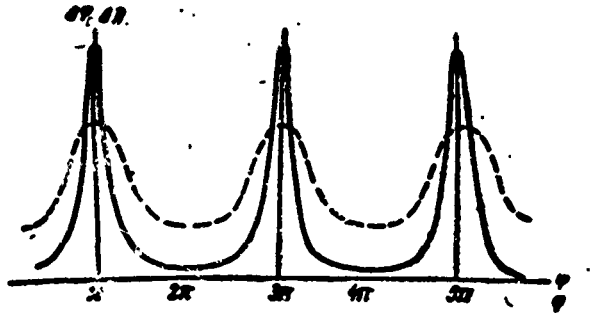

Fig. 8.7. Variation of error of phase front as a function of the orientation of the object (for solid curves, the difference of the intensity of the sources is smaller than that for the dotted lines).

For cases of practical interest, the ratio $D_0/\lambda$ has a very large value. Even for small objects measuring 20 m, at frequently employed wave length of $\lambda = 10$ cm this ratio comes to 1000. Small fluctuations in angle $\psi$ that always occur in the process of radiolocational observation lead to phase changes of many periods in the Expression (8.21). Consequently, all values of phase $\varphi$ within the limits from 0 to $2\pi$

may be considered as equally probable. Under this condition, the branch of the curve $\varphi=\varphi(\Delta D)$ is the integral law of probability distribution of $\Delta D$.

Actually, if two random quantities $\Phi$ and $\Delta D$ are mutually related by a one-to-one correspondence $\Phi=\Phi(\Delta D)$, then the probability of the values of $\varphi$ remaining within the interval $\varphi - \varphi + d\varphi$ and that of the values of $\Delta D$ within the interval $\Delta D - \Delta D + d(\Delta D)$ are equal. Expressing this probability in terms of corresponding values of probability density distributions, $W(\varphi)$ and $W(\Delta D)$, we may write $W(\varphi)d\varphi = W(\Delta D)d(\Delta D)$ or $W(\Delta D) = W(\varphi)\, d\varphi/d(\Delta D)$.

In our case, the quantity $\varphi$ is distributed evenly and for the interval of length $\pi$, the density distribution of probability consists of a constant value, equal to $W(\varphi)=\frac{1}{\pi}$.

Then,

$$W(\Delta D)=\frac{1}{\pi}\frac{d\varphi}{d(\Delta D)}. \qquad (8.24)$$

Let us find the probability with which the linear deviation of the apparent location of the object relative to its center will exceed a certain value $\Delta D$, that is, will be found within the limits $\Delta D \div \Delta D_{макс}$:

$$p(\Delta D)=\int_{\Delta D}^{\Delta D_{макс}} W(\Delta D)\, d(\Delta D)=\frac{1}{\pi}\int_{\Delta D}^{\Delta D_{макс}}\frac{d\varphi}{d(\Delta D)}d(\Delta D)=$$

$$=1-\frac{\varphi(\Delta D)}{\pi}. \qquad (8.25)$$

It can be seen that the function $\varphi(\Delta D)$, relating the value of error $\Delta D$ to the phase angle $\varphi$ in scale of $1/\pi$ represents the integral law of distribution of probability of possible deviations of the phase front. The curve of this law of distribution is the segment of the curve of the function $\varphi(\Delta D)$ within the limits from 0 to $\pi$ (Fig. 8.8). Curves are constructed for the linear deviation of the apparent position of the object $\Delta D$ relative to its actual dimension $D=D_0\cos\psi$. But, owing to

the smallness of the angular size of the target, the graph can also be used for angular deviations $\Delta\psi$ of the phase front.

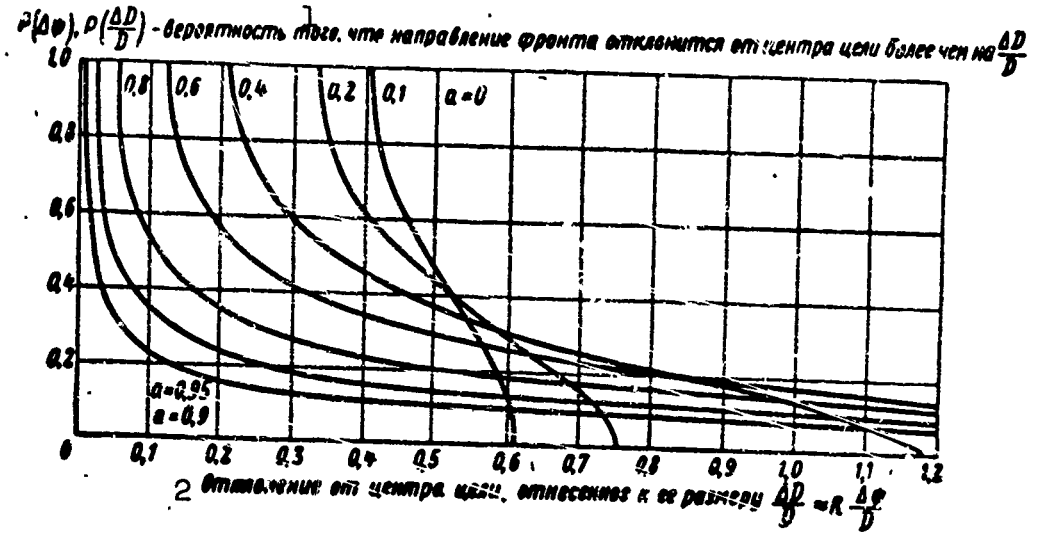


Fig. 8.8. Distribution of the probability of error of phase front at various field strength ratios ($a = E_1/E_2$) of reflecting points. 1) Probability such that the direction of the front deviates from target center by more than $\Delta D/D$; 2) deviation from the center of the object relative to its dimension $\left(a = \frac{E_1}{E_2}\right)$

From an inspection of the curves, it follows that it is impossible to measure the direction to the object with an error smaller than $\Delta D_{min}$. The probability of committing an error which would exceed the value of $\Delta D_{max}$ thus, is equal to zero. The mean value of error of phase front is equal to half of the angular measure of the object $D_0/2 \cos \psi$. This value of the error takes place in such cases when the object consists of one source – normal to wave front will pass through this source but not through the center of the target which now has no physical meaning.

Using the law of probability, $W(\Delta D)$, it is possible to determine the moments of distribution of the errors of phase front. The mean square deviations of phase front relative to the actual dimensions of the object for various values of $E_1/E_2$ consist of

TABLE 8.1

| $\frac{E_1}{E_2}$ | 0,95 | 0,9 | 0,8 | 0,6 | 0,4 | 0,2 | |
|---|---|---|---|---|---|---|---|
| $\frac{\sqrt{\Delta D}}{D}$ | 2,2 | 1,6 | 1 | 0,8 | 0,6 | 0,52 | 0,505 |

This value does not depend on the wavelength and the phases of isolated reflectors.

The conclusions made in relation to the dual point object, in a first approximation, may be extended to objects of still more complicated configuration; the physical substance of the phenomenon does not change in principle. Furthermore, analyses of dual point objects give results which agree better with practical conditions than the investigations of other complicated models of objects.

3. Effect of the Earth

An additional communications channel forming in reception of signals from a target reflected from portions of the earth or water surface may show substantial effect on the accuracy of the angular coordinates measurements. For target and radar altitudes close to the distance between them, for certain methods of measuring elevation angles, it is necessary to consider the deformation of the lobes of the diagram of visibility. Reflections from the earth, in effect equivalent to a second source of radiation, cause deformation of the phase front and lead to error in the measurement of small angles of elevation.

The effect of these factors may be sufficiently simple for analysis only in idealization when the surface of the earth is considered as a mirror reflecting plane. For actual conditions, errors of measurement of azimuth and elevation angles, dependent on the reflections

from the earth, are evaluated experimentally.

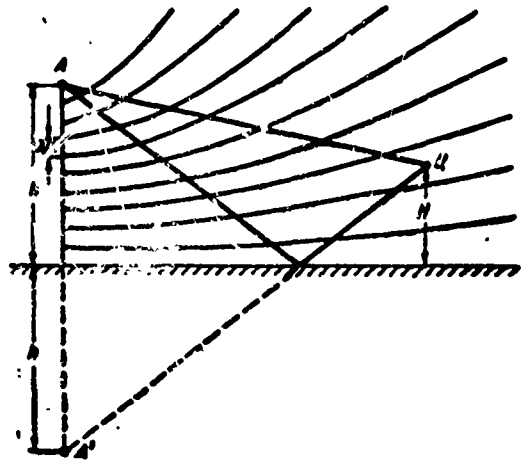

Fig. 8.9. Scheme of interference of outgoing and reflected waves at commensurable height of the object and RLS and the distance between them.

The distortion of the visibility diagram on flat surface may be calculated if the problem on the effect of the earth on radiolocational observations (see Chapter 3) is specified for cases of very small distances and large height of the antennae.

As indicated, the electromagnetic vibrations at the receiving point are the result of the interference of outgoing waves and waves reflected from the surface of the earth. Reflected waves may be considered as direct radiation of some fictitious source $A'$ (Fig. 8.9). The phase shift ($\varphi_R$), dependent on the path difference and the phase change during reflection ($\varphi_0$), makes up the quantity

$$\varphi = \varphi_R + \varphi_0 = \frac{2\pi}{\lambda} \Delta R + \varphi_0.$$

At space points for which $\varphi = 2\pi n$ ($n$ is an integer), the outgoing and reflected waves are alike in phase and the intensity of the resultant field has a maximum value.

As is well known, the geometric locus of space points for which the

difference in distance from two fictitious points – foci – remains constant takes the form of a hyperboloid of revolution. Therefore, points of vertical plane at which the resultant field has its maxima (or minima), form a family of hyperbolas with foci at the point of the location of the antenna and its mirror reflection. The number of hyperbolas corresponding to the maxima of the resultant field is equal to the number of half-waves packed in the height of the antenna, $2H/\lambda$ (Fig. 8.9).

In the far away regions of space, the distance considerably exceeding the height of the antenna, the hyperbola branches approach straightness. The resultant directional patterns considered above, which characterize the electromagnetic field in these regions, relative to the point 0 of the earth surface under the radiator where the asymptotes cut across.

Obviously, that which with the distortion of the petals of the visibility diagram should be considered in such rare cases when RLS is located at an elevation and the height of the object may be considered to be commensurate with the height of the antenna.

*Distortion of the phase front* of the reflected waves discussed above, show the effect on the measurement of the location angle if within the boundaries of the beam fall simultaneously the straight signals of the object and their reflections from the earth. Reflecting portions of the earth may be found either close to the antenna RLS or close to the object.

The first case which we saw earlier (see Fig. 8.9), is equivalent to the appearance of supplementary mirror point receiving reflected signals. By the principle of reciprocity, phase distortions occurring during the propagation and reception of the radiowave, are the same. But the straight channel through which the exposure of the object takes

place does not effect the accuracy. In principle, the source of electromagnetic vibration may be found in the object itself or through exposing it to any other points.

In the second case, the reflecting portions of the earth or water surface is located near the object such that it splits in equal strength (Fig. 8.10).

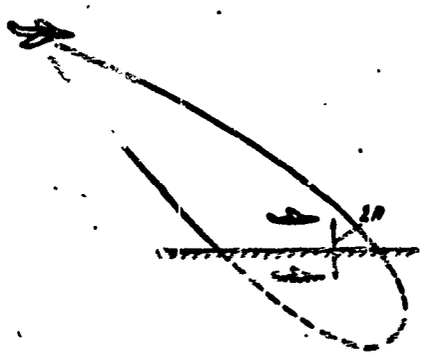

Fig. 8.10. "Splitting" of target as a result of the reflection from the earth or water surface.

The conclusions obtained earlier on the distortion of phase front may be extended to both of the cases, assuming that the distance between the sources of radiation ($D_0$) corresponds to the split height of the antenna ($h$) or object ($H$). Phase shift ($\varphi_0$) between the sources of vibration is approximately equal to the argument while the ratio of the intensity field is the modulus of coefficient of reflection $\rho$.

For very small angles of location at all forms of polarization argument, the coefficient of reflection is equal to $\pi$ while the modulus $\rho = 1$. Therefore, on the earth surface itself, the phase front is disposed horizontally (just as for identical opposite-phase sources in the direction perpendicular to their bases). In the same condition for other directions, the wave fronts remain spherical and only have deformations in the directions of minimum petals.

When the coefficient of reflection, dependent on the polarization of the waves, properties of the earth and the angle of slide, becomes smaller in units, the intensity of the mirror source diminishes. In this case, the equiphase surface is determined basically by the front of the straight waves which are distorted by the reflections from the earth. The probability of errors in the direction of the phase front may be

evaluated by Formula (8.25) but its mean square value – by the data in Table 8.1.

Thus, for example, at a wavelength of 10 cm and the angle of slide of the beam 10°, coefficient of reflection of sea water 0.95 for horizontal polarization and 0.4 for vertical. If the object lies on the surface of the sea at a height of 50 m and at a distance of 50 km from the RLS, the mean square error of the direction of phase front will be correspondingly 16' and 4' (Fig. 8.10).

*Effect of the earth in the maplitude method of measuring the angle of location* is explainable by the petal character of the resultant diagram of directionality. In order to establish the reason causing the error and evaluate its magnitude, let us examine the process of the bearing of the object by the method of maximum in the use of the interference diagrams of directionality.

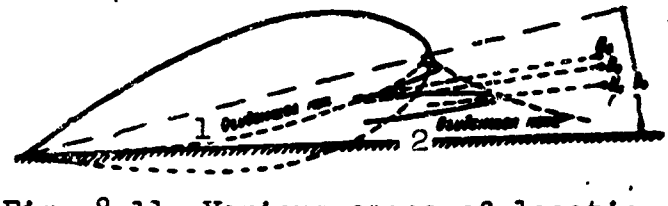


Fig. 8.11. Various cases of location of the object relative to the petal of the resultant diagram of directionality. 1) Envelope minima; 2) envelope maxima.

Striving for the maximum intensity of the signal being received, the operator of the RLS changes the angle of inclination of the antenna $\beta_a$. In this, the position of the petals of the diagrams remain unchanged since they are determined by the path difference between the straight and reflected waves and are not dependent on the direction of the antenna. If the object is located in the maxima of the petals (Fig. 8.11), the magnitude of the signal will be changed in conformity with the changed envelope maxima.

As can be seen in Fig. 8.12, the intensity of the signal in the maxima rises proportionally with the decrease of the angle $\beta_a$. Therefore, for the taking of the bearing the operator will dip the antenna downward. At the passing through of the true direction of the object ($\beta_a = \beta$), the motion of the antenna will not interrupt since the signal in the maxima continues to increase. Only for certain angles of inclination, the signal of the object starts to diminish.

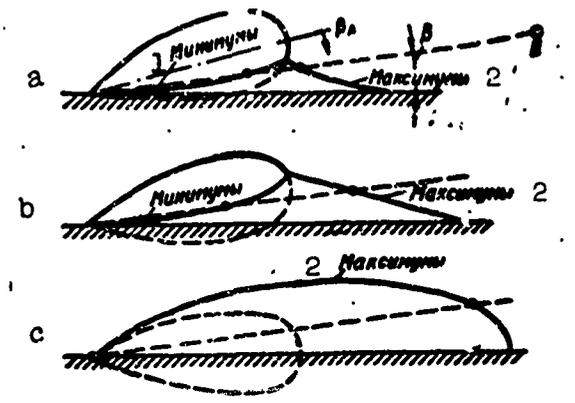


Fig. 8.12. Variations of the envelope maxima and envelope minima of the petals during the change in the inclination of the antenna. 1) Minima; 2) maxima.

In this condition, for object $Ts_1$ located in any of the maxima in the resultant diagrams of directionality, a false bearing will be taken, close to zero.

If the object is located in a minimum ($Ts_2$ in Fig. 8.11) then for an increase of intensity in the signal, the antenna should be turned upward. When the maximum of the exit diagrams passes through the direction of the object ($\beta_a = \beta$), differential signal ($E = E_1 - E_2$) continues to increase such that the straight wave ($E_1$) in the maximum region changes very slowly, while the reflected ($E_2$) continues to diminish very rapidly. Maximum value of the differential signal will be at an antenna inclination of ($\beta_a > \beta$) for which the reflected wave in the

direction of the object remains to be zero ($E = E_1$).

It is not difficult to see that in some interpoint positions (for example $Ts_3$ in Fig. 8.11) the object takes a bearing without error since the interference diagram for these directions give the same signal as the exit ones.

In this condition, transposing the object relative to the interference petals of the visibility diagram, the measured value of the angle of location fluctuates relative to the true value β. Such fluctuation of the bearing originates with reference to the direction $\beta_A = -\beta$ at a negative angle of inclination of the antenna. The boundaries within which the spread of the measured values is possible, depends on the coefficient of reflection, the width of the beam and the angle of the object location. Errors are absent when the location angle exceeds 1/4 the beam width at the zero level.

It is necessary to note that the reading with excessive results owing to the smallness of the signal in the minima of the petals, often drop out therefore, on the average, the measured values of small angles appear to be smaller than the actual values.

Using analogous conditions it is possible to follow the effect of Earth on the process of the measurement of small location angles when autotracing is used for the purpose of employing the method of amplitude comparison. For this resultant diagrams of directionality constructed in right angle coordinates for coefficient of reflection $p = 1$ are used. As an exit position of the antenna, we take the case shown in Fig. 8.13b.

Having examined the resultant diagrams of directionality for two beams formed in the free space of equal signal directions under the angle $\beta_0$, we are convinced that at the intersection of the petals there emerge many equal signal directions. Each petal gives two equisignal

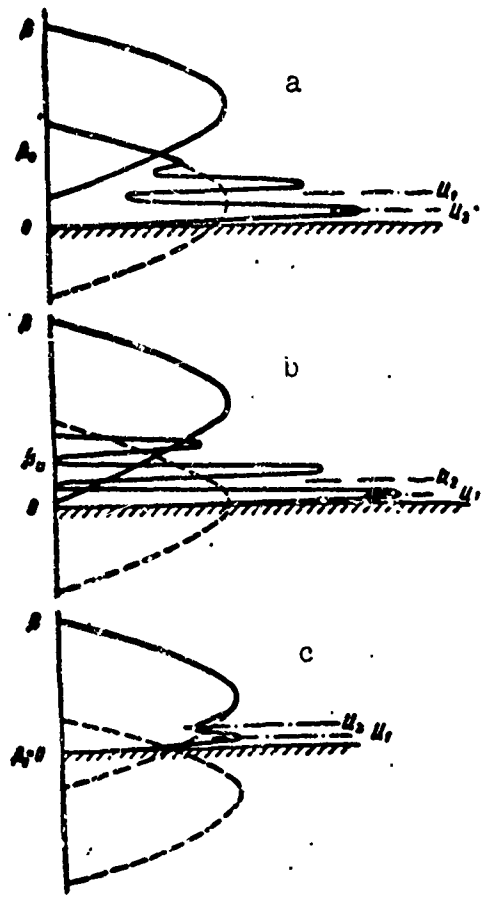


Fig. 8.13. Various cases of the location of the object relative to equal signal directions formed by petals of the diagrams of directionality.

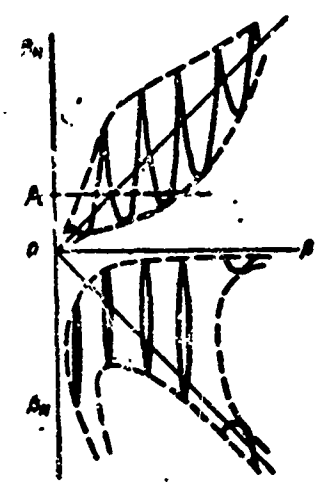

Fig. 8.14. Exemplary character of dependence between measured and true location angle during automatic location for low flying objects.

directions. For one of them, at the increase angle of location of the object in the autotracing system, signals arise by raising the antenna, in the other by lowering. But the antenna in this case, performs irregular motion which although connected with the object, in practice increases calculation.

For objects located in any of the false equisignal directions, shown in Fig. 8.13b, the autotracing system indicates a location angle $\beta_0$ corresponding to the direction of equisignal zones in free space. Namely the one and the same measurement of the magnitude of the location angle ($\beta_0$ in Fig. 8.14) may correspond to many different positions of the object. If the inclination of the antenna changes, the positions of the equisignal directions also change. Examplary character of the dependence of measured and true values of the location angle is illustrated in Fig. 8.14.

False equisignal directions may be unstable. A little mixing of the objects relative to such equisignal directions creates a signal of error, which when acting on the autotracing system further increases the discordance.

If the object is not located in the equisignal direction but in the maximum of one of the petals (point $Ts_1$ in Fig. 8.13b) then the signal of low beams surpasses that of the high beam: the autotracing system will turn the antenna downward. Without considering the complex charts of the changes of the petal diagrams, we note, that the signals may be compared at a horizontal antenna position ($\beta_0 = 0$, Fig. 8.13c) where the high and low beams coincide at all points. But, actually, equilibrium sets in at small negative angle of inclination, since the coefficient of reflection is in smaller units and the maxima of the low petals at $\beta_0 = 0$ is somewhat less than the high ones.

If in the exit condition the object is located in the minimum of

the antenna beam ($Ts_2$ in Fig. 8.13b), then there will be a signal of error turning the antenna upwards. At this, the signal in the minima of the low beam increases and at some angles of inclination of the antenna system, the object is found in the false equisignal directions.

Under this condition, at small location angles, the autotracing system achieves vibration relative to the direction to the object and its mirror reflection. The magnitude of the vibration is dependent on the angle of object location, beam width, and the coefficient of reflection just as in the method of the maximum. The error is particularly noticeable when the RLS is located on a smooth sea surface. Calculations show that for this case, at a wavelength of 10 cm and the smallest location angle, which may change with error, not exceeding 0.1°, the error is 1/2 for horizontal polarization and for vertical polarization 3/4 of the beam width at half strength.

*Effect of the earth on the measurement of the azimuth* refers to the case of low height of the radiolocational station and the object. The reason for this appears to be the local unlevelness of the ground in the region where the reflected wave is formed. For plane mirror reflecting surface this error does not exist. The calculation of this error by way of theoretical analysis is extremely difficult, therefore, we shall arrange to look at some results of experimental observations.

Figure 8.15 illustrates the effect of an average intersecting locality in the equisignal zone generated by a conical rotation of the antenna beam (antenna and reception point are located at the same height (2.5 m) and at a distance of about 1 km).

The intensity of discordance is three times the intersection at the zero level – producing three equisignal directions. One of them (the middle one) appears to be unstable. If an object is located in this direction, the autotracing system would deflect the antenna side-

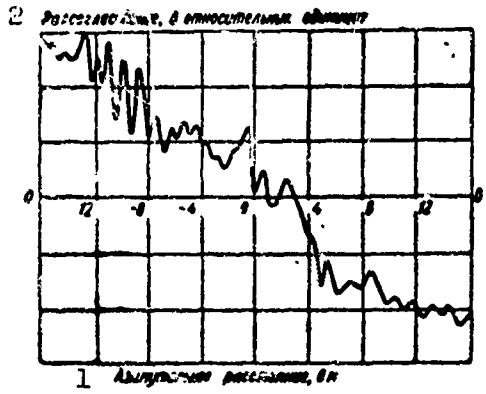


Fig. 8.15. Character of the equisignal zones in the azimuthal direction close to the surface of the earth. 1) Azimuthal distance in m; 2) discordance in relative units.

ways to one of the stable equisignal directions. The distance between the extremest stable equisignal directions determine the possible error of the system.

Approximately, errors of such magnitude arise owing to the distortion of the equisignal zones along the direction of propagation. The locations of the equisignal zones at the azimuth are dependent on the height of the point of observation. The character of this dependence is illustrated in Fig. 8.16a, where the perpendicular beams are represented on a plane as geometrical location points through which pass the equisignal directions. The formation of these points deflects to the right and the left with the change of height. Upon narrowing the antenna beam, the magnitude of the error and the probability of its appearance diminish: there is less distortion of the equisignal zones and inaccuracy occurs less frequently.

The areas of space in which considerable deviations of the equisignal directions from the center position occur are particularly concentrated in the minima of the petals dependent on the reflection from the earth. This may be explained as follows.

The coefficient of reflection from the earth, owing to the small

slide angle, is close to 1. About this, witness in part this fact, that the minima of the petals of the resultant diagrams of directionality for right and left positioned beams (Fig. 8.16b) in a majority of cases, are close to zero. Consequently, in the directions of the minima, where the straight and Earth reflected waves add up in phase – arithmetically, we obtain a typical twofold value of the force field. A small difference of the items, depending on the local unevenness of the ground, will not have substantial effect on the results. For regions of the maxima, the reflective surfaces of the earth are fully accessible.

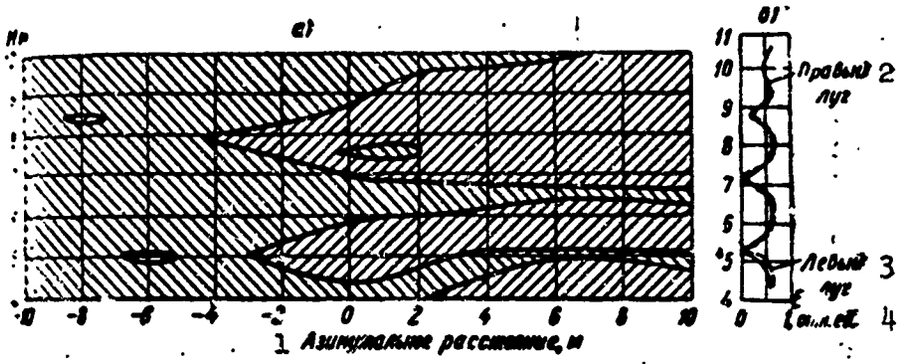


Fig. 8.16. Character of the distortion of the equisignal zone on the azimuth when height is varied: a) deviation of the equisignal zones with variations of height of the point of reception; b) variations in the intensity of the signals of right and left beams as a function of the height. 1) Azimuthal distance; 2) right beam; 3) left beam; 4) relative units.

In the directions of the minima, where the straight and reflected waves add up to a phase shift of 180°, intensity fields of almost similar values subtract. Their difference depends considerably on the condition of the area reflecting the signal of the object to the RLS.

It is well known that the small difference of two sums may be neglected; but it is, however, not permissible in subtraction. In the given case, nonhomogeneity of the location, dependent on the small difference in the reflected waves for the right and left positions of the

beam, is the reason of the large deviations from the equisignal zones. Generally deviations of the equisignal directions in the minima used to be larger in magnitude than those in the maxima of the petals.

Under this condition, anomalies of the equisignal directions – distortion, nonhomogeneity and others – arise basically in the minima regions of the petals depending on the reflection from the earth.

In conclusion of the paragraph, we note that the errors examined above, characterizing the distortion of the phase front of the waves, deformation of the trajectory of propagation and the petals of the resultant diagram, deviation from the natural amplitudes of the signals in free space, do not completely determine the errors in the measurement of the angle in question. For a judgment of the accuracy of the bearing, it is necessary to examine these problems in conjunction with the processes which do not originate directly from the radiolocational station and are dependent on the possibility of fixing the measured quantities at given noise levels.

## §8.2. POTENTIAL ACCURACY OF THE ANGULAR COORDINATES MEASUREMENTS

The analysis of potential accuracy of angular coordinates measurements and the directional resolving power may be reduced to an investigation of the frequency-time dependence, analogous to the dependence on distance obtained earlier. For this, let us examine the rotation of the antenna beam at RLS with a constant angular velocity $\Omega$ in the plane of the object (Fig. 8.17a).

The angular position of the maximum of the antenna beam $\alpha = \Omega t$ is proportional to time counted off from the moment of the intersection of the maximum with the exit zero direction. The corresponding angular position of the object $\alpha_0$, related to the momentum of passage $\tau_0$ of the maximum of the beam through the object is $\alpha_0 = \Omega\tau_0$.

For a simplification of the analysis, we assume that unmodulated

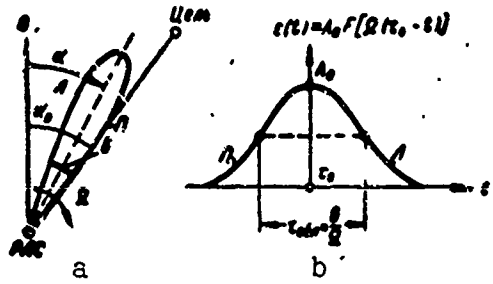


Fig. 8.17. Reception of the signal of the object during the rotation of the antenna beam: a) position of the antenna beam in the plane of the object; b) the received signal during continuous radiation.

sinusoidal signal is radiated; the effect of the actual form of the signal will be examined later. As a result, from the object, signal in the form of impulse will be received. Its envelope is measured in accordance with the forms of the diagrams of directionality of the antenna, $F(\alpha)$, while duration – time of exposure of the object $\tau_{obl} = \vartheta/\Omega$ is proportional to the width of the diagrams of directionality, $\theta$ (Fig. 8.17b).

Since the antenna beam during a rotation tc the right runs against the right side of the object (p) and goes with the object to the left (l), therefore at the beginning of the exposure a signal will be received whose amplitude corresponds to the right section of the diagrams of proportionality $F(\alpha) \equiv F(\Omega t)$, while in the end – the left section. Hence, the dependence of amplitude of the signal being received on time

$$s(t) = A_0 F[\Omega(\tau_0 - t)] \qquad (8.26)$$

appears to be mirror reflections of the diagrams of proportionality (with accuracy to the constant coefficient $A_0$). But, since the diagrams of proportionality are practically always symmetrical with respect to the maximum, the mirror reflection of the function is identical with the function itself and may be considered that the envelope of the signal being received is simply a repeat of the diagram of proportionality

of the antenna $F(\alpha)$. For this, $F(\alpha)$ is understood to be $F_E(\alpha)$ if the signal being received is straight radiation, or $F_p(\alpha)=F_E^2(\alpha)$, if the reflected signal being received is on the common receiving-transmitting antenna.

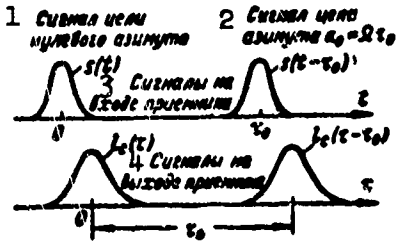


Fig. 8.18. Received signals at receiver input and output. 1) Signal of zero-azimuth target; 2) signal of target at azimuth; 3) signals at receiver input; 4) signals at receiver output.

In the receiver at RLS, mixed with the signal $s(t)$, there is a noise $n(t)$ which is Gaussian distributed as before. Thus, the envelope of the signal being received may assume this form

$$x(t)=A_0F[\Omega(\tau_0-t)]+n(t), \tag{8.27}$$

if the signal/noise ratio is sufficiently large and the second orthogonal noise may be neglected. Receivers which have been optimized for such signals have impulse characteristics of the form

$$h(t)\equiv s(-t)\equiv A_0F(\Omega t). \tag{8.28}$$

The envelope of the output signals of optimized receiver is

$$l(\tau)=\frac{2A_0}{E_0}\int_{-\infty}^{\infty}x(t)F[\Omega(t-\tau)]\,dt=l_c(\tau)+l_{\text{ш}}(\tau), \tag{8.29}$$

where, as before,

$$l_c(\tau)=\frac{2A_0^2}{E_0}\int_{-\infty}^{\infty}F[\Omega(\tau_0-t)]\,F[\Omega(t-\tau)]\,dt$$

– regular signal component

$$l_{\text{ш}}(\tau)=\frac{2A_0}{E_0}\int_{-\infty}^{\infty}n(t)\,F[\Omega(t-\tau)]\,dt$$

– incidental noise component which also distributes according to the normal law.

The maximum of the signal component $l_c(\tau)$ is reached at $\tau=\tau_0$, where time $\tau$ is counted off from the maximum of the exit signal of the object entering into the zero reading angle (Fig. 8.18). In the absence of the noise component, the moment for the approach of the maximum may be fixed as exactly as convenient. In the count-off of that moment, the position of the antenna axis is the exact value of the angular position of the object if all the remaining errors are set at zero.

The noise component $l_m(\tau)$, prevents the exact count-off of the moment of the approach of the maximum just as in the distance measurements. The moment $\hat{\tau}$ of the approach of the maximum output signal of the receiver $l(\tau)=l_c(\tau)+l_m(\tau)$ is measured with an error

$$\Delta\tau=\hat{\tau}-\tau_0,$$

which leads to the incidental error of the measurement of the angular position of the object

$$\Delta\alpha=\Omega\Delta\tau=\hat{\alpha}-\alpha_0.$$

The mean square value corresponding to angular errors

$$\sigma_\alpha=\Omega\sigma_\tau,$$

while the dispersion $\sigma_\alpha^2=\Omega^2\sigma_\tau^2$.

The potential accuracy of the count-off moment for the approach of the maximum corresponding to Formulas (7.17) and (7.18) is determined by the dispersion

$$\sigma_m^2=\frac{1}{\frac{2E_1}{E_0}\frac{\int_{-\infty}^{\infty}\left[\frac{d}{d\tau}F(\Omega\tau)\right]^2 d\tau}{\int_{-\infty}^{\infty}F^2(\Omega\tau)\,d\tau}},\quad \tau=\tau_0. \tag{8.30}$$

Multiplying the right and left portions of the formula by $\Omega^2$ we find the variance of the values of the angular positions of the object

$$\sigma^2_{\tau\text{п}} = \frac{1}{\frac{2E_s}{E_0}\frac{\int_{-\infty}^{\infty}\left[\frac{1}{\Omega}\frac{d}{d\tau}F(\Omega\tau)\right]^2 d\tau}{\int_{-\infty}^{\infty}F^2(\Omega\tau)\,d\tau}}, \quad \tau = \tau_0.$$

Reorganizing the ratio of integrals in the denominator and substituting it into the preceding formula, we finally obtain

$$\sigma^2_{\alpha\text{п}} = \frac{1}{\frac{2E_s}{E_0}\frac{\int_{-\infty}^{\infty}|F'(\alpha)|^2 d\alpha}{\int_{-\infty}^{\infty}|F(\alpha)|^2 d\alpha}}, \quad \alpha = \alpha_0, \tag{8.31}$$

where $\alpha = \Omega\tau$, while $F'(\alpha)$ – derivative of $\alpha$. The straight parentheses indicate that the diagram of directionality of the antenna is taken care by the module since in general, it may be a complex function of the angle.

The formula obtained characterizes the potential accuracy in coordinate measurements under the condition that the signal is sufficiently strong in comparison with the noise. As it follows from the formula, the potential accuracy does not depend either on the method of survey or the speed of rotation of the antenna beam $\Omega$. Consequently, it is valid and when the beam is stationary, $\Omega = 0$, the dependence of the strength of the signal on the entrance angle remains the same.

Potential accuracy is determined only by the energy ratio of signal/noise and the form of the characteristic, $F(\alpha)$ whereupon, $F(\alpha) = F_E(\alpha)$ in some cases of reception of signals of straight radiation and $F(\alpha) = F_p(\alpha) = F_E^2(\alpha)$ in cases of reception of reflected signals.

For a clarification of the physical contents of the ratio of integrals in Formula (8.31) let us compare it with Formula (8.30). For which we shall assume that signal of straight radiation is being received, $F(\alpha) = F_E(\alpha)$ and that frequency modulation of the signals in the antenna does not exist, i.e., $F(\alpha)$ is a real function.

As it follows from an analysis of formula of the form (8.30) shown in Chap.7, the root square from the ratio of integrals expresses effectively the width of the spectra of the signal

$$\Delta f_s = \frac{\sqrt{\pi}}{\tau_{обл}}, \tag{8.32}$$

if the spectra and duration of the "impulse" are taken on a defined level.

The root square from the ratio of integrals in Formula (8.31), as it was established during its derivation, is equal to the preceding ratio divided by $\Omega$, i.e. equal to the value

$$\frac{\Delta f_s}{\Omega} = \frac{\sqrt{\pi}}{\Omega \tau_{обл}} = \frac{\sqrt{\pi}}{\theta},$$

since $\tau_{обл} = \frac{\theta}{\Omega}$. But, $\theta = \frac{\lambda}{d_a}$ and $\frac{\sqrt{\pi}}{\theta} = \frac{\sqrt{\pi} d_a}{\lambda} = \frac{d_{эф}}{\lambda}$, where $d_{эф} = \sqrt{\pi} d_a$ – effective exposure of the antenna proportional to the physical exposure $d_a$ of the antenna with uniform distribution of the field. The value

$$\frac{\sqrt{\pi}}{\theta} = \frac{d_{эф}}{\lambda} \tag{8.33}$$

is called the relative effective exposure (aperture) of the antenna.

In conformity with the statement we may write

$$\left(\frac{d_{эф}}{\lambda}\right)^2 = \frac{\int_{-\infty}^{\infty} |F'(\alpha)|^2 d\alpha}{\int_{-\infty}^{\infty} |F(\alpha)|^2 d\alpha} \tag{8.34}$$

and Formula (8.31) takes the form

$$\sigma_{\alpha\alpha}^2 = \frac{1}{\frac{2E_s}{E_0}\left(\frac{d_{эф}}{\lambda}\right)^2}. \tag{8.35}$$

Under this condition, the relative exposure of the antenna, $\frac{d_{ав}}{\lambda}$ during the measurements of angular coordinates plays the same role as the width of the spectra of the signal, $\Delta f$, does in distance measurements. Increase in the relative exposure leads to an increase in the accuracy of the readings and the resolving power in angular coordinates.

As it has been shown earlier, when the pulse of the signal $\frac{2E_s}{E_0} = a^2 n$, where $a = \frac{A_0}{\sigma_ш}$ – signal/noise ratio based on the strength of one pulse, while $n$ – number of effective integrated impulse. Then from Formula (8.35) with the calculation of (8.33), we obtain

$$\sigma_{ав} = \frac{\theta}{a\sqrt{n}}, \qquad (8.36)$$

i.e., the error of the measurement of the angle is proportional to the width of the diagrams of directionality and inversely proportional to the ratio of the amplitude of the integrated signal to the effective value of noise.

This trivial and simple result may be obtained by less complex means but, Formula (8.34) gives a strict, quantitative definitude to the quantity $\theta = \frac{\lambda}{d_{ав}}$

The potential accuracy of bearing depends on whether the antenna works only for reception or simultaneously for reception and transmission. The width of the diagrams of directionality at points of half strength is, for a majority of reflecting antennae, connected with the diameter of the antenna via the relationship

$$\theta \approx 1{,}2\,\frac{\lambda}{d_a} \text{ or } d_{ав} \approx 1{,}5 d_a, \qquad (8.37)$$

or if the angle measure is in radians. When the antenna works only in reception, in Formula (8.36), the name for that quantity $\theta$ should be substituted. The deviation from the exact formula (8.34) will not be great.

For its evaluation, just as in the work on the variation of accuracy in the angle measurement on reflected signals, it is convenient to present the diagrams of directionality in the form of the bell curve.

$$F_E(\alpha)=e^{-k\left(\frac{\alpha}{\theta}\right)^2}.$$

On account of the to and fro passage of the signals, the resultant diagram of directionality for reflected signals has the form

$$F(\alpha)=F_p(\alpha)=F_E^2(\alpha)=e^{-2k\left(\frac{\alpha}{\theta}\right)^2}=e^{-k\left(\frac{\alpha}{\frac{\theta}{\sqrt{2}}}\right)^2}.$$

Consequently, in comparison with the case of the reception of straight signal when

$$F(\alpha)=F_E(\alpha)=e^{-k\left(\frac{\alpha}{\theta}\right)^2},$$

the resulting diagram of directionality is compressed в $\sqrt{2}$ times. This is in equivalent correspondence to the increase of effective exposure of the antenna. Therefore, when working on reflected signals in Formula (8.36) one must substitute

$$\theta\approx 0{,}83\frac{\lambda}{d_a} \text{ or } d_{an}\approx 2d_a. \qquad (8.38)$$

The resolving power is correspondingly increased while the effect of the lateral petals is also substantially reduced in comparison with the case of the reception of signals of straight radiation.

The above examination holds valid for cophasal antennas whose diagrams of directionality are real functions of the angle. The formulas obtained earlier (8.31), (8.34) and (8.35) however, are valid for antennas with any types of characteristics of directionality and also complex ones.

Let us pose the question: what is the optimum form of the diagrams of directionality insuring maximum accuracy when using a given size of antenna $d_a$ and a fixed signal/noise ratio?

When we were resolving the question on the selection of the form of signal insuring the highest accuracy in the measurement of distance at a given spectral width $\Delta f$, it was established that the best is the signal from two sinusoids with a frequency spread in the interval $f_d = \Delta f$ (phase method). In bearing taking, the spectral width corresponds to the relative exposure of the antenna $\frac{d_a}{\lambda}$ while the spread of frequency $f_d$ corresponds to the relative spread of the two receiving points $\frac{b_a}{\lambda}$. Therefore, it would seem that the highest accuracy of bearing during the reception of signals from two nondirectional antenna is guaranteed by the spread in the interval $b_a = d_a$. But nondirectional antennas however, do nct guarantee such signal/noise ratio as do the directional antennas therefore, the accuracy of the bearing appears low on account of the small value of the cofactors $\frac{2E_s}{E_0}$. In order to increase the value of $\frac{2E_s}{E_0}$ at the expense of directionality, it is necessary to increase the exposure of every one of the antennas so that at a given common size of the antenna, $d_a$, it is possible to attain this only by an increase of the spread $b_a$ among them. Under this condition, the phase method with the help of an antenna system of nondirectional spread does not appear to be the optimum when there is a given dimension for the antenna system. Finally, however, this question will be examined below.

We will now estimate the possibility, included in the complex diagrams of directionality, the formation of phase field in the exposure of the antenna at the expense of modulation. Modulation of the phase field in the exposure of the antenna is similar to phase (frequency) modulation inside the pulse during distance measurement, that, in principle, it permits the attainment of very nigh accuracy and resolving power in angular coordinates. At this, in the vicinity of the antenna a reactive field is formed which interacts with the

incoming waves like an imaginary internal antenna with a large effective exposure.

But, practical realization of an upward directed antenna of limited dimensions encounters serious difficulties. Significant difference of phase fields in the neighboring points of exposure leads to the appearance of compensating currents: heat loss during its flow sharply lowers the useful effect. Gain at the expense of an increase in the effective exposure of the antenna is compensated by the loss in the signal/noise ratio (operation exchange). Potential accuracy and resolving power, taking into consideration effective exposure as well as noise level, remain unchanged.* Besides, this kind of antenna is complicated in manufacturing and is unstable in operation. For these reasons, the choice of an optimum shape of characteristic directionality is at the present, still an unresolved problem.

Under certain conditions the most simple antenna manifests itself as antennas with a complex diagram of directionality. As a result, the effective exposure of such antennas exceed their physical dimensions by many times. The accuracy and resolving power in angular coordinates measurements increase many fold. We shall now switch to an examination of this case.

## §8.3. COMPRESSION OF DIAGRAMS OF DIRECTIONALITY IN COHERENT RLS OF A LATERAL FIELD OF VISION OF THE EARTH SURFACE.

Examined in Chapter 2, radiolocational stations of a lateral view possess additional advantages in comparison with stations of a circular field – a possibility of obtaining very high resolving power at the azimuth when small antenna is used at the expense of a coherent treatment of the signals being received.

In Fig. 8.19, a shows the diagram of proportionality of RLS of lateral view set up on an airplane moving straight with a velocity of

$V$ and $R$ away from the object. Lateral antenna beam will be considered as sectors (right-angled) with a small exposure angle $\theta$. We assume that the object itself radiates continuous vibration of frequency $f_0$ (wave length $\lambda$). Under this condition, the antenna works only in receiving to permit the illustration of the received results more descriptively.

In the time it takes for the signal from the object to be received at the RLS, it passes through the path $L \approx \theta R_0$, therefore, the time alone for reception (exposure) is

$$\tau_{об} = \frac{L}{V} \approx \frac{\theta R_0}{V}.$$

The radial component of the relative velocity of the object is located near the angle $\alpha$ to the direction of the maximum of the diagram of directionality.

$$V_R = -V \sin \alpha \approx -V\alpha.$$

On account of this, there arises a Doppler's frequency shift

$$F_д = -\frac{V_R}{\lambda} \approx -\frac{V\alpha}{\lambda}.$$

because $|\alpha|_{макс} = \frac{\theta}{2}$,

$$|F_д|_{макс} \approx \frac{V\theta}{2\lambda}.$$

As a result of this, we have received from the object a wide "pulse" of constant amplitude, duration $\tau_{об}$, and the frequency of which varies linearly with respect to the carrier frequency $f_0$ (Fig. 8.19b). Thanks to the relative displacement of the object, unmodulated signal, after reception becomes frequency modulated function of the angle of reception. The resulting diagram of directionality of the antenna becomes the complex function of the angle.

As it is known, such signal may be compressed with the aid of an optical (compressing) filter. The time for its completion is equal to the duration of the signal $\tau_{об}$. Since the entire deviation of fre-

quency is

$$\Delta f_{\text{д}} = 2|F_{\text{д}}|_{\text{макс}} \approx \frac{V\theta}{\lambda},$$

the signal may be compressed in the duration to the magnitude

$$\tau_c = \frac{1}{\Delta f_{\text{д}}} = \frac{\lambda}{V\theta}. \qquad (8.39)$$

In the time of the existence of the short signal $\tau_c$ RLS goes through the path

$$L_c = V\tau_c = \frac{\lambda}{\theta} = d_a. \qquad (8.40)$$

Under this condition, any two objects, located along straight parallel line paths at a separation no smaller than $L_c = d_a$ from each other, give separated signals at the output of the filter, i.e., they are resolved. The resolving angle at the azimuth is determined by the width compressed diagram of directionality

$$\theta_c = \frac{L_c}{R_0} = \frac{\lambda}{\theta R_0} = \frac{\lambda}{L}. \qquad (8.41)$$

Since in ordinary antennas, $\theta = \lambda/d_a$, therefore, the actual exposure of the hypothetical antenna forming the compressed beam

$$d_{a\text{э}} = L$$

is equal to the path going through the RLS in the time of the reception of the signal (time of exposure $\tau_{obl}$ and may reach several kilometers.

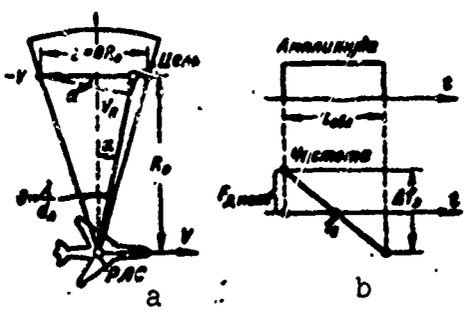


Fig.8.19. The signal being received at lateral field of vision. a) RLS transposition in the plane of the object; b) parameters of the signal being received. 1) Amplitude; 2) frequency.

The effective exposure of the antenna $d_{a\text{э}} = \sqrt{\pi}L = \sqrt{\pi}\theta R_0 = \frac{\sqrt{\pi}\lambda R_0}{d_a}$ in the given case increases with the decrease of the actual size of the antenna, $d_a$. Column of unusual results explains that transposing RLS together with the filter causes, in time, the reception of imaginary signals at virtual antenna of large dimensions.

Actually, going back to Fig. 8.20, in which from the top, the points represent the successive positions

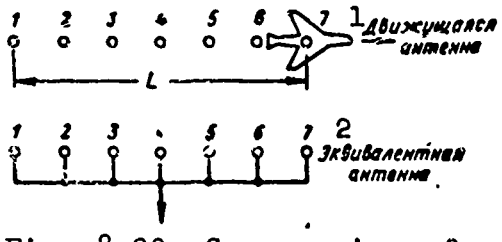


Fig. 8.20. Compression of the diagram of directionality as result of reception at an equivalent antenna of large dimensions. 1) Moving antenna; 2) equivalent antenna.

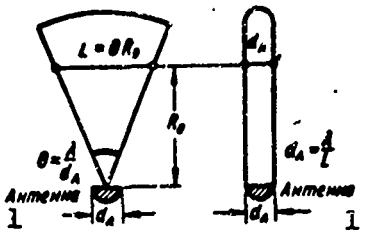


Fig. 8.21. Actual and compressed diagrams of directionality. 1) Antenna.

of the RLS of the segment $L = \theta R_0$ at the time of exposure of the object. Signals received from the object successively from various points of the interval $L$, are kept and summed up in the filter taking into account their phasal relationships. The results obtained are such that they seem as if all the signals were received simultaneously of the vibrators of the antenna depicted in the lower portion of the figure. The extension of the equivalent antenna is $d_{ab} = L$ which agrees with the results obtained earlier.

Since from the separation of the object, $R_0$ from the line, the path of actual exposure $L = \theta R_0$ increases the angular size of the compression diagram of directionality $\theta_c$ decreases while the linear dimension $L_c = \theta_c R_0 = d_a$ keeps constant (Fig. 8.21). Thanks to this, the linear dimension of the resolved segment in position is not dependent on the distance $R_0$ from the object and both small and large distances have the same clearness in the locality representation.

With the decrease in the actual exposure of the antenna $d_a$, the real diagram of directionality expands and with it, the actual exposure $L = \theta R_0$ increases and is equal to the path passing through the RLS at the time of the reception of the signal. On account of this, as we explained once before, the resolving power is increased and also

the accuracy, with reduced actual dimensions of the antenna. In reality, RLS is receiving reflected signal. In this case, the actual and effective exposures are increased by $\sqrt{2}$ as in ordinary antennas.

The actual exposure of the antenna $L = \theta R_0$ and the structure of the optimum receiver are different for different values of the distance $R_0$. This permits the resolution of unmodulated sinusoidal vibrations of the object at exposure and also at the distance $R_0$. But, the resolving power obtained at a distance (cross cut path) is considerably lower than a longitudinal path. On account of this, impulse exposure is employed.

In conclusion, we note that straight line flight and frequency exposure $f_0$ should be very strictly held. Vibrations of the phasal range of the signal in the receiving device and overload are not permissible. The opposite will lead to a decrease of the compression effect or a complete drop. Therefore, the construction of a RLS of a lateral field of view with compressed diagram of directionality is a complex technical problem.

## §8.4. MEASUREMENT OF ANGULAR COORDINATES BY THE METHOD OF ENVELOPE ANALYSIS.

The analysis of the potential accuracy of the angular coordinates measurements has indicated that the optimum receiver for angle readings of the signals received as a result of the rotation of the antenna beam in the field should, in principle, be so constructed as to be the same as in detection – in a form, in congruence with the signal of the filter, of a prominent logarithm ratio of probability. The differences lie only in the use of the results of reception: in detection, events exceeding the output signal of the receiver are fixed at some threshold level; in measurement of angular coordinates, the moment of the approach of the maximum of the output signal obtained in the

time of the exposure of the object, is fixed. The angular position of the antenna considered at this moment appears to be the angular coordinates of the object in the plane of the field of view.

The analysis of potential accuracy was conducted for continuous signals. But in the field, it is necessary to consider discontinuities, in particular, the pulse character of the signal which permits the reading of the distance simultaneously with the measurements of angular coordinates. The discrete pulse character of the exposure imposes limits on the measurement of coordinates and also on the very possibility of the construction of an actually optimum receiver.

Fig. 8.22a shows the time dependence of the amplitude of the signal being received at the input of the receiver. The envelope of the amplitude of the impulses $A_0F[\Omega(\tau_0-t)]$ repeats the characteristics of the directionality of the antenna $F(\alpha)$. The optimum receiver for this type of signal, as it follows from Chapter 6, includes the synchronized integrator. Weight factors of the synchronized integrator are determined by the amplitudes of the proper signals, i.e., by the relative values of the envelope at that moment of time when the impulse reaches the input of the receiver.

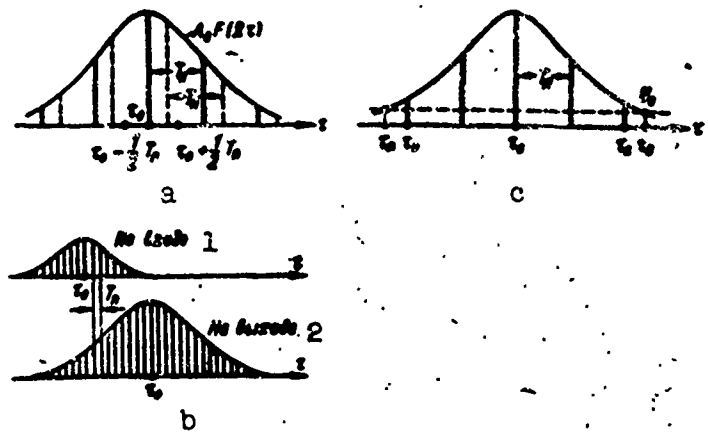


Fig. 8.22. The bearing of the object by the method of envelope analysis: a) Positions of the pulses inside the envelope; b) mutual distributions of the signals at the input and output of the integrator; c) fixed center of the packet at the beginning and end of pulse. 1) At input; 2) at output.

But, the actual positions of the pulses received in succession inside the envelope are not known. They are deeermined at random by observers of the relationship between the moment of the attainment of the maximum of the diagrams of directionality through the direction of the object and the moment close to it, of the reception of the pulse of the object. Thus, in Fig. 8.22a, the solid line indicates the pulses of the object when the moment $\tau_0$, of the attainment of the maximum through the object and the moment of reception of one of the pulses coincide while the dotted line – when there is no coincidence. Obviously, the pulse close to the moment $\tau_0$ may not lag behind it more than $\pm\frac{T_п}{2}$, while actually, the position of the pulse relative to the moment $\tau_0$ in the previous interval $\frac{T_п}{2}$, $+\frac{T_п}{2}$ can never be predicted.

The weight coefficients of the synchronized integrator of the optimum receiver may correspond only to one of the positions of the pulses within the boundaries of the stated interval. For the remaining positions, the receiver will be already not completely optimum. During detection, this circumstance does not play a significant role since it was shown that small deviations of the weight functions from the optimum show very weak effect on the signal/noise ratio.

It is somewhat a different matter with the reading of angular coordinates at the moment of attainment of maximum of the input signal of the receiver behind the time of the exposure of the object. The input signals same as the output, have a pulse character (Fig. 8.22b). The positions of the maximum pulse of the output signal, in most cases also do not coincide with the oment, $\tau_0$. The error of the reading of the moment, $\tau_0$ when the pulse is approaching it may have any value from $-\frac{T_п}{2}$ to $+\frac{T_п}{2}$. within the boundaries of the interval $T_p$, hence every value of error is equally probable.

As it was shown in Chapter 7, the mean square value of the error under this condition has the magnitude

$$\sigma_{\tau} = \frac{T_{\text{п}}}{2\sqrt{3}} \approx 0{,}3T_{\text{п}},$$

which gives the supplementary mean square error of the angle reading

$$\sigma_{\text{ш}} = \frac{\Omega T_{\text{п}}}{2\sqrt{3}} \approx 0{,}3\Omega T_{\text{п}}, \qquad (8.42)$$

where $\Omega T_{\text{p}}$ – angle of rotation of the antenna for the sending period.

Under this condition, the minimum error of the measurement of angular coordinates by the method of envelope analysis during impulse work, is

$$\sigma_{\text{ш.и}} = \sqrt{\sigma_{\text{ш}}^2 + \sigma_{\text{ш}}^2} = \sigma_{\text{ш}} K_{\text{и}},$$

where

$$K_{\text{и}} = \sqrt{1 + \frac{(\Omega T_{\text{п}})^2}{12\sigma_{\text{ш}}^2}}. \qquad (8.43)$$

– coefficient allowing for the lowering of the accuracy by the given method.

Consequently, for a reduction of the additional error of the angle measurement, it is necessary to either increase the reiterative frequency $F_{\text{п}} = \frac{1}{T_{\text{п}}}$, or decrease the velocity of the antenna rotation. Both will lead to a rise in the number of pulses in the packet $n$. With the rise in the number of pulses, the accuracy of the method approaches its potential. Therefore, the method of angle measuring by the analysis of pulse envelope may be called asymptotic optimum, i.e., optimum when $n \to \infty$.

Asymptotic optimum receiver of measurement of angular coordinates differs from detection receivers only in the form of the resolving structure.

The resolving structure may be built by two schemes. In the first scheme, the moment of attainment of the maximum of the envelope packet is fixed carefully by the input signal of the detection receiver $l(\tau)$.

In the second, the moment of passing through zero is fixed by the derivative, $l'(\tau)$, so that it is equivalent.

The first scheme is convenient in that the signals fed to it have the same form as those in the detection channel.

In Fig. 8.22b, the form of the signal at the output of the integrator of the optimum receiver is shown when noise is absent. For the reading of the moment, $\tau_0$ for this signal, it is necessary to cut the moments of intersections of the foregoing and following sections of the envelope at a certain level $U_0$ on the basis of which we obtain

$$\tau_0 = \frac{\tau_н + \tau_з}{2}. \qquad (8.44)$$

Impulse envelopes such as that do not exist in reality. They may only be imaginary. Therefore, the reading derived by the moment of intersection at the given level has its initial and final pulses correspond to the integrated signals $\tau_H$ and $\tau_K$. Since according to the reason shown earlier, the initial and final pulses are not always symmetrical with respect to the center of the packet $\tau_0$, therefore, the angle reading

$$\hat{\alpha} = \Omega \frac{\tau_н + \tau_к}{2} = \frac{\alpha_н + \alpha_к}{2}$$

derived by approximation, with admixed error is determinable by Formula (8.42).

Under this condition, for an angle reading at the output of the optimum receiver, it is necessary to install a clipping circuit and also a separating scheme of the first and last pulses of the packet which will be described some time later. The readings of the angle $\alpha_n$ and $\alpha_k$ correspond to the first and last pulses computed on the angular position of the object $\hat{\alpha}$, as half sum of these values.

Analogous method of angle reading may be used on pulse packets fed carefully from the output of the receiver to integration. It is

used in devices with binary quantized signals. In this case, the signal is weak and the effect of noise is strong: there is an ejection of the noise exceeding the level of quantization $U_0$ outside of the packet and on the other hand, some pulses inside the packet turn out to be lower than this level. The random ejection of noise may be used for the initial pulse while random disappearance of pulse for the final packet. With these pulses, after the pulses having disappeared inside the packet, they will be picked up as signals from a second object. The latter phenomenon is known as the fractional packet.

In order to eject the delivering of the false initial and fractional packets, it becomes necessary to complicate the logic of the formation of the initial and final packets, i.e., for the initial and final packets instead of using single pulses certain combinations of pulses will have to be used.

In the simplest scheme of treatment of binary quantized pulse signals, two methods of the formation of combination pulses are used: method of $K$ pulses from $n$ (binary integration) and method $K$ from $K$ (coincidence method). Generally, this logic is used for the registration of only the initial packet whereupon simultaneous with fixation, the problem of detection is also resolved. The logic of the registration of the end of the packet is generally taken care of more simply since sufficiently complex registration excludes these fractional packets in principle.

Figure 8.23 shows the circuit of the resolving arrangement of detection and measurement of the angular position of the object when using the binary quantized treatment by the coincidence method : simultaneously oscillograms indicating the voltages at the nodal points of the circuit are also shown.

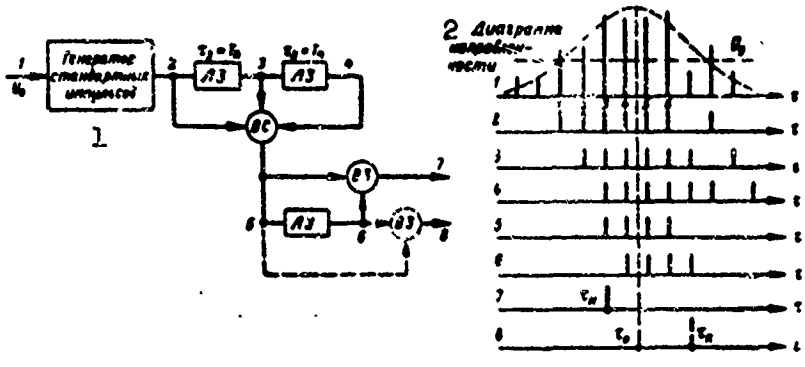

Fig. 8.23. Circuit for the determination of the center of the packet by the initial and final pulses during binary quantization. 1) Generator of standard impulses; 2) diagram of intensities.

The upper part is the ordinary circuit of detection by the coincidence method (<< three from three >>), the lower part serves as the separation of the pulses at the beginning and end of the packet. In the beginning, the third series of successive pulses, exceeding the level of quantization is received: the final packet proves to be the first passage.

The circuit for the separation of the beginning and terminal packets consists of a linear delay at the period of repetition (*LZ*) and two prohibiting valves (*VZ*): upper and lower.

The nonretarded pulses from the output of the coincidence valve (*VS*) hit the passing through input of the upper prohibiting valve while the retarded ones -- at the delay. The delay will be imposed for all nonretarded pulses except the first. As a result at the output of the upper prohibiting valve there will appear individual pulses whose time position $\tau_n$ is determined by the initial packet and the very fact of its appearance fixes the presence of the object.

The retarded impulses enter at the passage input of the lower valve while the nonretarded at the prohibiting input. As a result of this, individual pulses of the retarded series (the last) pass through

at the output of the lower prohibiting valve. The time position $\tau_k$ of these impulses correspond to the first passage in the packet of binary quantized pulses at the input.

The initial and terminal pulses obtained hit the antenna positions shown by calculation $\alpha_H$ and $\alpha_k$ in the moments $\tau_H$ and $\tau_k$. On the basis of these indications, in the long range, the angular position of the object is computed to be $\hat{\alpha}=\frac{1}{2}(\alpha_H+\alpha_k)$, whereupon the constant error of reading $\overline{\Delta\alpha}$ is compensated during the computation by corrections.

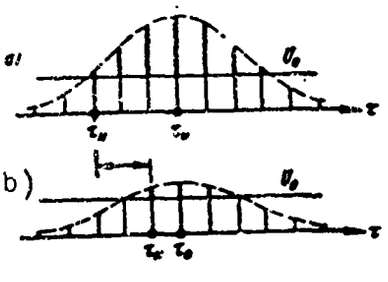


Fig. 8.24. The dependence of the position of the initial packet on the signal strength during binary quantization. a) Strong signal; b) weak signal.

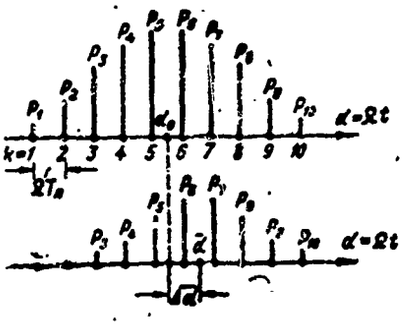


Fig. 8.25. The probability of the impulse packets exceeding the quantization level ($p_k$) and the appearance of the first pulse at the output of the coincidence valve ($P_k$).

It should be noted that the angle reading sometimes is produced only through the moment of the reading of the initial packet $\tau_H$, owing to this part of the scheme, the fixing of the terminal packet is shown in Fig. 8.23 by the dotted line. But, in this case, a systematic error appears which is dependent on the intensity of the signal: for weaker signals, the moment $\tau_H$ is closer to $\tau_0$, then for stronger signals (Fig. 8.24). If the maximum amplitude of the output signal is measured, this systematic error may be compensated during the calculations of the readings.

Fluctuating component mistake of the reading determines the

accuracy of the method. The mean square value of the error is dependent on the logic of registration of the initial and terminal packets and also on the level of quantization. There is no mathematical difficulty in the computation of this error but it is cumbersome and leads only to numbers for each concrete situation.

Let us look at the property of an example of the calculation of the error of the measurement of angle for the circuits in which the position of the object is determined by the first impulses at the output of the upper coincidence valve. Differing from the detection device, the substitution of the real pulse packet by its right-angled equivalent is not permitted in this case, since the accuracy of the measurement is determined precisely by the behavior of the envelope of pulse packets. Therefore, during calculation, it must be kept in mind that the probabilities of exceeding the threshold of the quantization of different pulses are not the same (Fig. 7.25).

The first pulse at the output of the coincidence with $K$ entrances may appear at various positions $k = 1,1,\ldots, n$. The probability of the appearance of pulses at the $k$th position under the condition that it did not appear earlier, is determined by the recurrent formula

$$P_k=(1-P_{k-1})\prod_{i=k-K+1}^{k}p_i.$$

Here the product of probabilities of the last $K$ impulses from $k$ determines the probability of the appearance of the impulses at the upper coincidence valve while the factor $(1-P_{k-1})$ fixes the fact that this pulse appears first at the $k$th position.

Under this condition, $P_k$ is the probability such that the initial pulse (pulse of the angle reading) appears at the $k$th position. The calculation of the probability $P_k$ is conducted sequentially beginning with the number $k$, at which the probability $P_{k-1}$ may be neglected with-

out any harm.

The mean value of the angle reading at the first output pulse is determined by the known formula

$$\bar{\alpha}=\sum_k \alpha_k P_k=\Omega T_n \sum_k k P_k,$$

since the angular distance between neighboring pulses is equal to $\Omega T_p$, and the value of the present angle is $\alpha_k = k\Omega T_p$. Similarly, the position of the center of the packet is $\alpha_0=\Omega T_n \sum_k k p_k$. Hence the systematic error of measurement is

$$\overline{\Delta\alpha}=\bar{\alpha}-\alpha_0=\Omega T_n \sum_k k (P_k - p_k).$$

The variance of the incidental error of the angle measurement by this method is

$$\sigma^2_{\alpha\alpha}=\sum_k (k\Omega T_n - \bar{\alpha})^2 P_k.$$

All the above formulas are valid at sufficiently large signal/noise ratio, when $\sum_k P_k \approx 1$.

The error of angle measurement at binary integration may be similarly calculated as equally weighted or unequally weighted.

Figure 8.26 shows the values of the errors of angle measurement as functions of the signal/noise ratio expressed in pulse strength for various cases. From an analysis of the diagrams, two important conclusions may be made.

Firstly, with the rise of the signal/noise ratio, the accuracy of angle measurement, taking into account only the amplitude of the pulses, approaches the accuracy of the angle reading when the phase of the angle is known. In the last case, the formulas obtained earlier characterizing the potential accuracy are valid at any signal/noise ratio. Now we may refine the conditions of applicability of these formulas introduced earlier to accuracy of angle measurement only by amplitude relationships: they give practically accurate results

when $\frac{a^2}{2} \geqslant 8$, i.e., $a \geqslant 4$

Secondly, the error of angle measurement during equalweight binary integration and the given conditions approximately doubles the error $\sigma_{an}$ calculated by the formulas given earlier. Under other conditions, this relationship changes very little. Therefore, for practical calculations, it is sufficiently reliable to assume that the lowering of the accuracy of angle measurement by the method of binary integration or by the method of coincidence may be allowed a coefficient of $K_u \approx 2$. in comparison with the potential.


Fig. 8.26. Error of angle measurement during binary integration, optimum treatment of the signal by amplitude and optimum treatment when the phase of the signal is known. 1) Equal-weight binary integration at $n = 8.p_w = 0.1$ and $K = K_{opt}$; 2) optimum treatment after amplitudinal detector; 3) optimum treatment with phase taken into consideration.

The second circuit of resolving device fixes the angular position by the moment when the derivati e from the envelope of the output (integrated) signals of the optimum receiver, $l'(\tau)$ passes through zero. This circuit is devoid of a large part of the deficiencies of the previous one, but it requires the use of synchronized integrators of special construction and their accompanying complications in comparison with the detection receivers.

It is known that when the signal is strong, the weight coefficient

$B_k$ in the synchronized integrator receiver for detection is proportional to the envelope of the signals, i.e., characteristics of directionality of the antenna $F(\alpha)$. In order to obtain the derivative from the envelope $l'(\tau)$, it is necessary that the weight coefficients, $B'_k$, it is necessary to provide channels of angle reading in which the signals total to weight coefficients of $B'_k$.

Fig. 8.27 shows an example of synchronized integrator with detection channels and angle reading, and also resolving device. The integrator works on a linear delay although it may be built with equal success by magnetic drums. For the definiteness of the number of the pulses to be totaled, five similar ones are taken. The values of the weight coefficients are shown graphically opposite every weight amplifier for specific positions of the pulses relative to the center of the packet. For all the remaining positions of the pulses within the boundaries $-\frac{T_n}{2}, +\frac{T_n}{2}$ the center packet filter deviates somewhat from the optimum so that it is immaterial if there is a sufficiently large number of pulses in the packet.

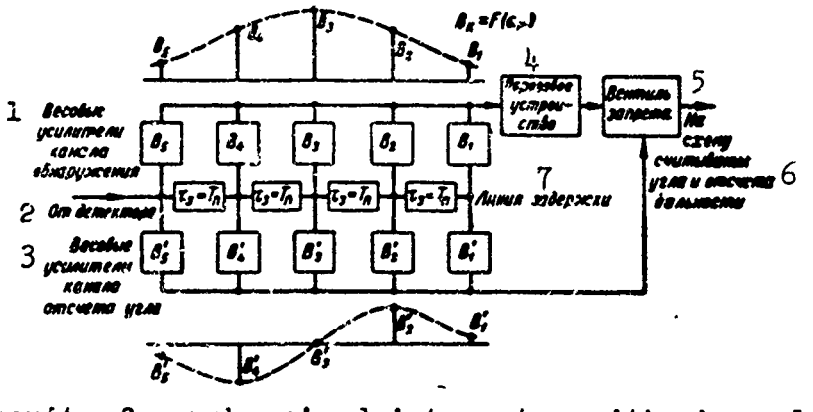


Fig. 8.27. Circuit of synchronized integrator with channel for angle reading by the method of antisymmetric wegith coefficients. 1) Weight amplifiers of channels of detection; 2) from the detector; 3) weight amplifiers for channels of angle reading; 4) cut off device; 5) prohibiting valve; 6) to schemes for the calculation of angle and reading of distance; 7) linear delay.

Totaling bars of detection channels are connected to the cut off device, at its output, appear the integrated pulses of the object which exceed the threshold of detection. From these pulses only one needs to be chosen corresponding to the center of the packet. This is carried out with the aid of the prohibiting valve controlled by the prohibiting input of the signals from the output of the angle reading channels. The prohibiting valve allows the passage only of the pulse of those detection channels at which the pulse in the angle reading channel has an amplitude of zero or close to zero (prohibiting valve opens). This moment of the coincidence with the center of the packet, is exactly the position of the maximum of the envelope.

The pulse reading obtained at the output of the valve enters into the scheme of the calculation of the angular position of the antenna in binary codes. Simultaneously, this same single pulse serves for the reading of the distance of the object and fixes the fact of its detection.

The pulse of the reading coincides in position with one of the pulses of the object therefore, it corresponds only by approximation to the center of the packet. In the results, the errors add up depending on the discrete signals, and the accuracy of the method is evaluated by Formula (8.43).

It should be noted that in the above circuit, the resolving device gives pulse of reading when and only when the pulse in the detection channel exceeds the threshold while in the channel for angle reading, it is close to the zero level. This, with the exception of the output of reading pulse when the signal inside the angle reading channel is zero, is simply because the object is absent.

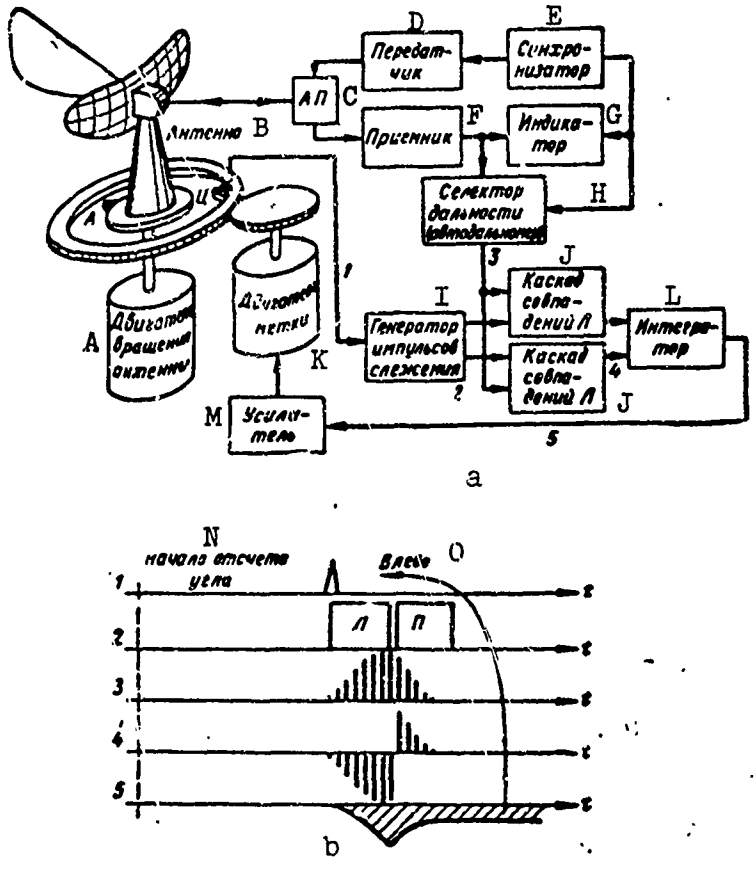


Fig. 8.28. RLS of a circular field with channels of automatic tracking of selected object by angle: a) Block diagram of RLS; b) processes in the system of autotracking by angle in a circular field. A) Antenna rotating motor; b) antenna; c) AP; D) transmitter; E) synchronizer; F) receiver; G) indicator; H) selector of distance (autodistance meter); I) generator of tracing impulses; J) coincidence cascade L; K) marking motor; L) integrator; M) amplifier; N) beginning of angle reading; O) to the left.

This is the general outline of the second circuit of the construction of the resolving system for angle reading. In the second circuit, there is also an angle discriminator built in the system of automatic tracking at the azimuth in circular or sector shape (Fig. 8.28a).

The upper part of the diagram with the antenna and its drive gears shows an ordinary RLS of circular shape. The lower part is reserved for the automatic accompaniment of selected objects.

The principle of the working of the system of tracking at the azimuth when the field of vision is circular, is shown by the oscillograms of voltages at its nodal points (Fig. 8.28b). It resembles very much

the principle of automatic tracking for distance only tracing is not carried out for one pulse but for a packet of pulses received from the object at the time of exposure in the field. The packets follow one after another with a period equal to the time of the rotation of the antenna.

Let us assume that the object is selected and the system of tracking works normally. The selection of the object is accomplished by the turning of the follower ring whose contact $T_s$ is directed in the direction of the given object. At the axis of the antenna, there is located a contact A which coincides with the focal axis of the antenna and the maximum of the diagram of directionality. By rotating the antennas, the contacts A and $T_s$ are locked and generate pulse marker *1* approximately at the moment of time when the diagram of directionality intersects the object.

Under the action of the pulse marker, special generator produces right (p) and left (l) pulse tracings *2*. These pulses appear at the inputs of the corresponding coincidence cascades. At the second input of the cascade, through the distance selector appears a packet of received pulses of Object 3. The pulses of the object which coincide with the left pulse trace appear, through the first coincidence cascade, at the integrator in negative polarity while the remaining pulses through the right in positive (pulse *4*). These pulses charge the condenser of the integrator in different polarities forming different integral effects *5*.

If the packet of pulses are shared equally between both coincidence cascades, the output voltage *5* equals zero. This will mean that contact $T_s$ is directed exactly by the azimuth of the object. When the object is displaced to the left relative to contact $T_s$ as it is shown in the drawing, then a major part of the pulses of the object will

pass through the left coincidence cascade and the output voltage of Integrator 5 will be negative. This voltage after amplification, forces the revolving marking motor which displays the ring with the contact $T_s$ in the side of the object.

Because of this, at any displacement of the object by the azimuth, there will occur an automatic transposition of the contact $T_s$ following the object. The angle of rotation of the ring with the contact $T_s$ may be either computed in the form of binary code or converted with the aid of a potentiometer into proportional angle voltage for output into computers.

In the drawing, the pulse traces are shown as right-angled. Actually, they deviate from right-angledness. The selection of the form of the pulse trace and the magnitude of the dispersion among them may be made so that the sum will be optimum, i.e., with weights proportional to the derivative from the characteristics of the directionality of the antenna.

The distance selector guarantees the delivery to the accompaniment system, only signals of single objects. Generally, it works from the autodistancemeter, accomplishing discontinuous tracing for the selected object and also for distance. Under this condition, tracing is produced for the position of the points in the surface of the field.

## §8.5. OPTIMUM PARAMETERS OF THE BEARING SYSTEM WORKING BY THE METHOD OF COMPARISON

The envelope analysis method is employed only on scanning antenna beam and only for measurement of one of the angular coordinate. The comparison method permits the bearing taking of the object by stationary as well as scanning beam whereupon two angular coordinates may be measure simultaneously.

The potential accuracy of the bearing using the method of comparison and the method of envelope is the same.

Mathematically, this is expressed by Formula (8.35) establishing the mutual relation between the minimum dispersion of the error of measurement and the antenna parameters which exist independently of the method of realization of the optimum bearing system.

From simple physical representation examined in Chapter 2, it shows that the error of bearing by the method of comparison is inversely proportional to the sharpness of the bearing ch racteristic $S$ and the signal/noise ratio $a$:

$$\sigma_{\varepsilon} \approx \frac{1}{Sa}. \qquad (8.45)$$

A comparison of Formulas (8.35) and (8.45) permits us to make the conclusion that the relative effective expcsure of the antenna $\frac{d_{ab}}{\lambda}$ introduced earlier reflects the meaning of the sharp bearing characteristic.

The sharpness $S$ characterizes the bearing sensitivity. In the system of bearing by the comparison method, it is determined by these antenna parameters which give the antenna system the sensitivity towards the angle of deviation of the object from the equisignal direction.

In the phasal system these parameters are the dispersion of the antenna $b_a$ whereupon the characteristic directionality of both antennas in the remote zones coincide. In the amplitude system, this role is played by the angle displacement $\varepsilon$ where the dispersions of reception points *1* and *2* practically do not exist (Fig. 8.29).

One may establish an amplitude-phasal system in which the points of reception are scattered in the same way as in the diagrams of proportionality. But, there is no extra eminence for this system and we shall not look at them.

At the increase of the dispersion $b_a$ or the angle displacement $\varepsilon$ to zero, the sharp bearing characteristic also strives towards zero and taking bearing by the method of comparison becomes impossible.

From the other side, for certain profile of antenna system the $b_a$ and $\varepsilon$ never reach the limits since this suppresses the signal/noise ratio $a$.

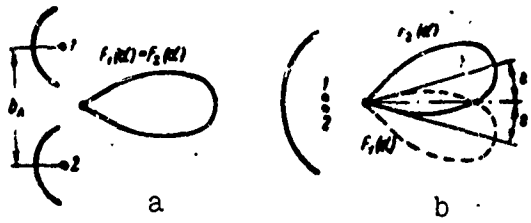

a b

Fig. 8.29. Bearing by the method of comparison: a) In phasal system owing to a dispersion of radiators at coincidence with the diagrams of directionality; b) in amplitude system owing to an angle displacement of the diagrams of directionality with coinciding radiators.

Consequently, there exist optimum values for the dispersion $b_a$ and the angle displacement $\varepsilon$, at which, the product,

$$Q = Sa$$

is a maximum while the error of bearing is minimum.

*Optimum dispersion in systems of phasal bearing.* As it follows from Formula (2.13), the sharpness of the bearing characteristic of phasal systems $S_\Phi$ obtained in Chapter 2 is proportional to the dispersion (base) of the antenna $b_a$. The signal/noise ratio $a$, is determined by the directionality of the antenna and also by the nature of its work: whether it is only receiving or both transmitting and receiving.

In the case of working with the properties of echosignal, the amplitude of the latter is proportional to the characteristic directionality of the antenna strength. Therefore, the signal/noise ratio in voltage $a$ at equisignal directions (voltage at maximum) is pro-

portional to the coefficient of directional action. The latter is proportional to the linear dimension of the exposure $d_a$ in the plane of the bearing during constant exposure in other planes.

As is seen in Fig. 8.30a, exposure is

$$d_a = 2(L - b_a),$$

where L - given profile dimension of the antenna system.

Consequently, for phasal system, the product is

$$Q_\Phi = S_\Phi a = kb_a(L - b_a),$$

where $k$ - coefficient of proportionality.

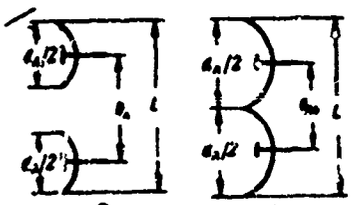

Fig. 8.30. Relationship between dispersion and exposure of the antenna at a given profile of the antenna system. a) Arbitrary dispersion; b) optimum dispersion.

As should be expected, with the increase in dispersion $b_a$, the sharpness grows $S_\Phi$ in proportion to $b_a$, and the ratio $a$, diminishes in proportion to $L - b_a$, since the increase of the dispertion $b_a$ at a given profile $L$ is possible only at the expense of a decrease in the exposure of the antenna $d_a$ and its directionality.

The product $Q_\Phi$ is maximum when the derivative $\frac{dQ_\Phi}{db_a} = 0$, that is,

$$k(L - b_{a0}) - kb_{a0} = 0,$$

from which the optimum dispersion

$$b_{a0} = \frac{L}{2} = \frac{d_a}{2}. \qquad (8.46)$$

When the dispersion is at the maximum, the reflections of the antennas close by join one another forming a complex exposure $d_a = L$ (Fig. 8.30b).

It should be noted that when dispersion is at the maximum, the condition of single valuedness of the angle reading is fulfilled within the boundaries of the solution of the diagrams of directionality $\theta$ by the output voltage of the phasal detector.

Actually, in radian measures

$$\theta = \frac{\lambda}{d_a}$$

and the maximum angle of deviation

$$|\alpha|_{макс}=\frac{\theta}{2}=\frac{\lambda}{2d_a}.$$

The maximum phase difference for narrow diagrams of directionality is

$$|\Delta\varphi|_{макс}=\frac{2\pi b_{\phi 0}}{\lambda}|\alpha|_{макс}=\frac{\pi}{2}.$$

Within the boundaries of $\pm\frac{\pi}{2}$ the output voltage of phasal detector single valuedly corresponds to the phase shift of comparable signals, therefore, the angle alpha may be considered as single valued.

In the case of the reception of signals of straight radiation, their amplitude and signal/noise ratio $a$ is proportional to the root square from the coefficient of directional action. Therefore, the product

$$Q_\phi=kb_a\sqrt{L-b_a}$$

is maximum when the dispersion

$$b_{a0}=\frac{2}{3}L=d_a.$$

It is necessary, however, to note the following circumstances. In the first place, in this case the exposure of the antenna is reduced to the value $d_a=\frac{2}{3}L$. In the second place, the optimum obtained is not very critical.

Calculations show that if dispersion is reduced to the value $b_a=\frac{L}{2}$ and exposure increases accordingly, the product $Q_\phi$ and accuracy of bearing worsens, in all, by 10%. At the same time, the resolving power increases by one half time. Therefore, just as the work in straight signals so is it with reflected signals we select expeditiously, $b_a=\frac{L}{2}$

*Optimum angle deviation in amplitude system of bearing.* In Chapter 2, we obtained formula for the bearing characteristics of the amplitude system

$$F_{ax}=\frac{F(\alpha+\varepsilon)-F(\alpha-\varepsilon)}{F(\alpha+\varepsilon)+F(\alpha-\varepsilon)}. \qquad (8.47)$$

In the numerator is written the difference and in the denominator the sum of the characteristics of the envelopes of two comparable signals. In the vicinity of the equisignal direction, the summation diagrams of directionality practically do not change while the difference is linear. Therefore, the sharpness bearing characteristic in the equisignal direction is

$$S_a = \left|\frac{dP_{пк}}{da}\right|_{a=0} = \frac{S_p}{F(a+\varepsilon)+F(a-\varepsilon)},$$

where $S_p$ – sharp differential characteristic.

The signal/noise ratio $a$ is proportional to the summation of the diagrams $F(a + \varepsilon) + F(a - \varepsilon)$. Therefore, the product

$$Q_a = S_a a = kS_p$$

determines only the sharp differential characteristic in the equisignal direction.

As it follows from Formula (2.18) obtained in Chapter 2, the sharp differential characteristic is roportional to the derivative with respect to the angle from the diagrams of directionality in the equisignal direction $F'(\varepsilon)$. Therefore, the product

$$Q_a = kF'(\varepsilon)$$

and the accuracy of the bearing in the equisignal directions is determined by the derivative from the diagram of directionality of the antennas, which increases with the increased exposure of the antenna.

Under this condition, the accuracy of the phasal system of bearing at optimum dispersion as well as the amplitude system is determined only by the relative exposure of the antenna $\frac{d_a}{\lambda}$; When construction is rationalized, the accuracy of both systems strive to potential determined by Formula (8.35). Accuracy of bearing used on practical antenna is extremely weak depending on the distribution of the field in the exposure and the forms of the characteristic directionality in strength,

which for the axial-directional antenna within the boundaries of the principal petal is approximated very well by the function of the form $e^{-ax^2}$, $\frac{\sin^2 x}{x^2}$ and $\cos^4 x$.

As it follows from the latter formula, the product $Q_a$ appears to be a function of the angle of deviation $\varepsilon$. The choice of the optimum angle of deviation at which $Q_a$ and $F'(\varepsilon)$ are maximum depends on whether the antenna works only for reception or for both reception and transmission.

In the case of reception of natural echo signal $F(\alpha)=F_p(\alpha)=F_E^2(\alpha)$. The bell curve approximating the diagram of directionality is

$$F_p(\alpha)=\exp\left[-0{,}7\left(\frac{2\alpha}{\theta}\right)^2\right].$$

Its derivative is

$$F'_p(\alpha)=-1{,}4\left(\frac{2}{\theta}\right)^2\alpha\exp\left[-0{,}7\left(\frac{2\alpha}{\theta}\right)^2\right],$$

while the product (when $\alpha = \varepsilon$) is

$$Q_a=S_a a=kF'_p(\varepsilon)=k\varepsilon\exp\left[-0{,}7\left(\frac{2\varepsilon}{\theta}\right)^2\right],$$

where $k$ – coefficients of proportionality, independent of $\alpha$ and $\varepsilon$.

For the finding of an optimum, set the derivative $\frac{dQ_a}{d\varepsilon}$ to zero, that is

$$k\exp\left[-0{,}7\left(\frac{2\varepsilon_0}{\theta}\right)^2\right]-1{,}4k\left(\frac{2\varepsilon_0}{\theta}\right)^2\exp\left[-0{,}7\left(\frac{2\varepsilon_0}{\theta}\right)^2\right]=0.$$

After simplification, we obtain

$$1{,}4\left(\frac{2\varepsilon_0}{\theta}\right)^2=1,$$

From which the optimum angle of deviation is

$$2\varepsilon_0=0{,}85\theta. \qquad (8.48)$$

In the case of antenna working only for reception $F(\alpha)=F_E(\alpha)$. There is the approximation

$$F_E(\alpha)=\exp\left[-0{,}35\left(\frac{2\alpha}{\theta}\right)^2\right],$$

$$F'_E(\alpha)=-0{,}7\left(\frac{2}{\theta}\right)^2\alpha\exp\left[-0{,}35\left(\frac{2\alpha}{\theta}\right)^2\right]$$

and

$$Q_a = k\varepsilon \exp\left[-0{,}35\left(\frac{2\varepsilon}{\theta}\right)^2\right].$$

Treating analogously as before, we obtain

$$2\varepsilon_0 = 1{,}2\theta. \qquad (8.49)$$

Consequently, in systems of bearing of lateral signals, the angle of deviation should be taken larger than working with natural echo-signals.

In the existing radiolocational stations like the monoimpulse ones as well as the single channel ones with conical rotation of the beam, the angle of deviation is taken smaller than the optimum, and do not make use of the potential possibilities of the system. The fact boils down to this: at the optimum angle of deviation, the characteristic directionalities intersect at a very low level and therefore, the strength of the signal being received (summation) in the detection channel and the distance measurement appears to be much lower than in the directional maximum. In the results, the distance of detection of the object (hold) is lowered by more than 20%.

Fig. 8.31 shows the dependence of the relative magnitude $Q_a$ and the working distance $R_{make}$ in the function from the angle of deviation for the "transmitting receiving" system. The working angle of deviation is chosen as a compromise between loss of accuracy in bearing and working distance at the detection channel in the region of points $2\varepsilon = 0.6\theta$, where both magnitudes constitutes approximately 90% from the maximum.

In recent years for monopulse RLS with antennas of special construction, it is possible to use the optimum angle without decreasing the distance for detection. The principle of their action will be examined in the following paragraph. Simultaneously, the means of over-

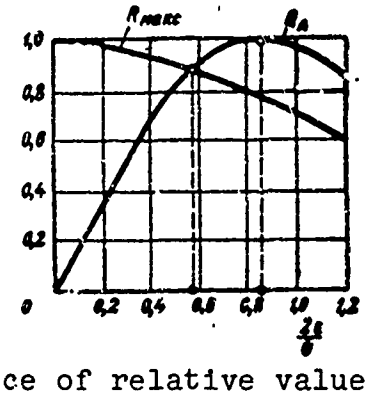


Fig. 8.31. The dependence of relative values of bearing sensitivity and working distance in the total number of channels of RLS as a function the angle of deviation.

coming other difficulties and discrepancies which come about in the use of monopulse RLS will be briefly noted

## §8.6. PRINCIPLES OF THE CONSTRUCTION OF MONOPULSE RLS, REALIZING THE POTENTIAL POSSIBILITIES OF BEARING TAKING.

One of the basic shortcomings of monopulse (multichannel) RLS is the rigid demand for the identity of channels of the receiver. Comparison of signals after amplification at identical channels gives considerable error. What is particularly bad is that in this condition the equisignal directions are fixed with the error and since the majority of bearing systems works in methods of tracing for the entire equisignal direction, these errors are extremely undesirable.

The above mentioned shortcoming – the wandering of equisignal directions – is removed completely in the summation difference monopulse RLS, in which the comparison (subtract on) of signals is carried out before amplification directly at the output of the antenna. Under this condition, the high frequency signals received are submitted to preliminary transformation which may be carried out in the amplitude bearing system as well as in the phasal system.

The amplitude monopulse RLS with the subtraction of signals be-

fore amplification will be examined below. The transformation of signals in high frequency is carried out in hybrid waveguide joints – summation difference bridge, the working principle of which is shown in Fig. 8.32.

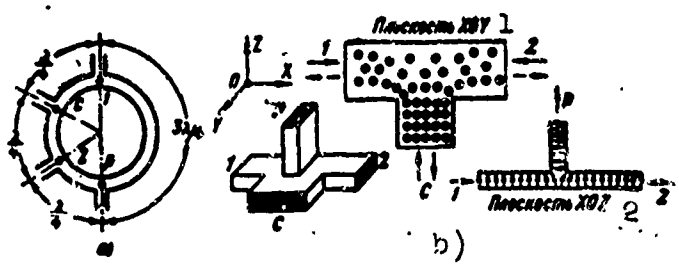


Fig. 8.32. Summation difference waveguide bridges. a) Ring bridge; b) bridge in the form of a "double T" in various projections. 1) XOY plan; 2) XOZ plane.

The ring summation difference bridge (Fig. 8.32a) has four branches in one semicircle upon which the electrical lengths of the components of the ring waveguide between these branches are all equal to the odd number $\frac{\lambda}{4}$. If cophasal high frequency signals are fed to Branches *1* and *2*, then, at the point *C* where the branches are subconnected, these two signals will add in phase since the same path goes on the ring. At the point of branch subconnection *P*, Signals *1* and *2* are added up in opposite phase, i.e., subtracted since the difference of the path is equal to $\frac{3\lambda}{4}-\frac{\lambda}{4}=\frac{\lambda}{2}$. Branches *C* and *P* are known conjunctively as summation and difference.

Signal in the difference branch has the phase of that signal whose amplitude is larger.

When Signal *1* is larger than Signal *2*, the phase of the difference signal coincides with the phase of Signal *1* at point *P*. Consequently, the difference signal in relation to Point *1* has a phase shift, proportional to $\frac{3\lambda}{4}$. The summation signal at point *C* has a phase shift relative to Point *1* (as well as relative to Point *2*) proportional to

$\frac{\lambda}{4}$. Therefore, the summation and difference signals are in opposite phase.

If Signal *2* exceeds Signal *1*, then the phase of the difference signal coincides with the phase of Signal *2* at the point *P* and the shift with respect to Point *2* is proportional to $\frac{\lambda}{4}$. The summation signal also has such a shift with respect to Point *2*. In this case, the summation and difference signals appear to be in phase.

If, however, the signal is fed to the branch *C*, then it reaches Branches *1* and *2* with the same phases and amplitude. At point *P*, signals do not fall since the path difference of the signals at the arc *C1P* and arc *C2P* is equal to $\frac{\lambda}{2}$.

The waveguide bridge of the type "double *T*" (Fig. 8.32b) has the shape of the letter *T* both in the horizontal and the vertical cross-sections, and it is from this that it gets its name. For an explanation of the principle of the action of the bridge, let us assume that strong lines of the electric field of the waveguide is in the horizontal plane directed upwards from below.

Two cophasal signals entering Branches *1* and *2* of the bridge are added up at branch *C* (plane XOY) forming a summation signal. At the branch *P* (XOZ plane) a difference signal is formed since the vectors of the electric field of Signals *1* and *2* entering the branch, have oppositely positioned directions. The direction of the vector of the difference signal changes in opposite position depending on which one of the two signals is larger. In the case of an equality of Signals *1* and *2*, the difference signal does not exist.

If a signal is fed to the branch *C*, then it is divided equally between Branches *1* and *2*, whereupon the direction of the vector of the field (i.e., phase) in both branches will be the same. At this,

no signal falls at the branch *P* since in the signal supplied, there is no horizontal component of the electric field.

It is easy to notice that by their properties both types of bridges are the same in the form of branches described. The ring bridge is more sensitive to measurement of wave length, but it is more compact since it is distributed in one plane.

Having gotten acquainted with the properties of the summation difference bridges, we shall now turn to an examination of the amplitude monopulse (multichannel) system of bearing in one plane with subtraction of signals before amplification (Fig. 8.33).

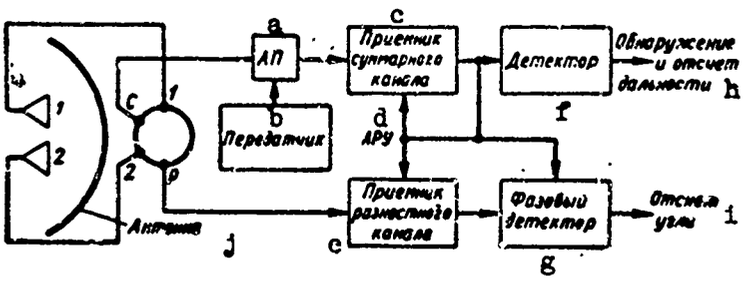


Fig. 8.33. Amplitude summation-difference bearing system in one plane. a) AP; b) transmitter; c) receiver of summation channel; d) ARU; e) receiver of difference channel; f) detector; g) phase detector; h) detection and reading of distance; i) angle reading; j) antenna.

Radiators *1* and *2* are symmetrically displaced relative to the mirror axis of the antenna, subconnected correspondingly with Branches *1* and *2* of the summation difference bridge. In so doing, their characteristic directionalities form equisignal directions toward the perpendicular to the center exposure of the antenna (Fig. 8.34a).

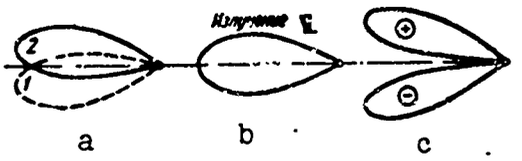


Fig. 8.34. Characteristics of summation difference systems. a) Diagrams of directionalities of two irradiators; b) summation diagram; c) difference diagram. 1) Radiation.

During the time of transmission from the transmitter through branch *C* of the waveguide bridge, high frequency vibrations are distributed equally between Branches *1* and *2* and appear at both radiators in phase.These vibrations are added up in space, forming summation characteristics of directionality (Fig. 8.34b). Vibrations from the transmitter do not appear at channel *P*.

Signals reflected from the object are received at each radiator separately. The strength of the signal received at each radiator is dependent on the position of the object relative to the equisignal directions. For example, if the object is displaced to the side of Radiator *1*, then the signal appearing in Channel *1* will be greater, and the situation is reversed when the displacement of the object is in the opposite position.

At branch *C* appears the summation signal which is received by both radiators. This signal, through the antenna switch, proceeds further to the receiver of the summation channel. The dependence of the summation signal on the direction of receiving is also characterized by the summation characteristic directionality. The face of object detection and the measurement of its distance are fixed by summation signals. Under this condition, if the branch *P* of the ring bridge is shut off and all the lower part of the scheme in Fig. 8.33 is removed, the very common one channel RLS is obtained, in which both radiator antennas act as one.

Principally, what is new in comparison with the one channel RLS, is the difference channel. If the object is not located in the equisignal direction, th n at branch *P*, a high frequency pulse will be received whose amplitude is the bigger, the bigger the displacement of the object from the equisignal directions, while the phase will be equal or opposite in position to the phase in the summation channel

(depending on the side of displacement).

If the object is displaced from the equisignal direction on the side of Radiator *1*, the phase of the difference signal is opposite in position to the phase of the summation channel; when the displacement of the object is to the side in the opposite position, the phases of the signals will be the same: in the equisignal directions, the amplitude of the difference channel is equal to zero. This dependence is a difference characteristic (Fig. 8.34b). The phase coincidence of the summation and difference signals is denoted by the plus sign and non-coincidence – by the negative sign.

It should be noted that the difference characteristic is formed only when reception is on the very receiving device. In space, its shape may only be taken mentally, in distinction from the summation characteristic which during radiation is materialized in the form of an electromagnetic field of definite intensity and may be objectively observed. Naturally, difference characteristics can never be explored from the outside by any means.

It is also necessary to note that the formation of difference signals does not take place at the expense of taking away part of the energy from the summation channel but as a result of a greater and fuller utilization of the energy received by the waves in the multichannel system. The difference signal is formed at the expense of that part of the energy of the incident waves which in ordinary one channel systems is transradiated by the antenna into space when the direction of the incident wave does not coincide with the focal axis of the antenna.*

Amplification in the receiving device of difference high frequency signal is detected with the help of phasal detectors, in which

the high frequency summation signal is delivered as a supporting voltage. From the output of the phasal detector, the error signal is suppressed in the form of pulse whose amplitude is proportional to the angle of deviation of the object from the equisignal direction, while polarity (sign) indicates the side of deviation.

It should be noted that the appearance of additional phase shift between the signals of the summation and difference channels increases only the amplitude of the difference signal in proportion to the cosine of the parasite phase shift, but does not lead to errors in the determination of the equisignal directions. Therefore, in the systems of automatic tracking of the object by means of equisignal directions the demand for stabilization and identity of phasal characteristics of the receiving channels, of the multichannel RLS is not very rigid in these aspects.

For the exclusion of the effect of the strength of the signal being received on the magnitude of the error signal, the coefficient of amplification of the receiver of the difference channel should be changed in accordance to Formula (^ 45), in inverse proportion to the intensity of the summation channel. For this purpose, the summation channel is shown in scheme ARU with the help of what the effect of any changes in the signals being received on the angle reading and the overload of the summation channel may be established in principle.

The system of the bearing of the object in two planes (Fig. 8.35) is considerably more complicated than what has been examined: in place of two, four symmetrical irradiators in the mirror exposures will be required; in place of one bridge — four; still another difference channel will have to be added. Under this condition, for a simultaneous determination of all three coordinates of the object, three receiving

channels are called for. In principle, the operation of the scheme is not different from the above.

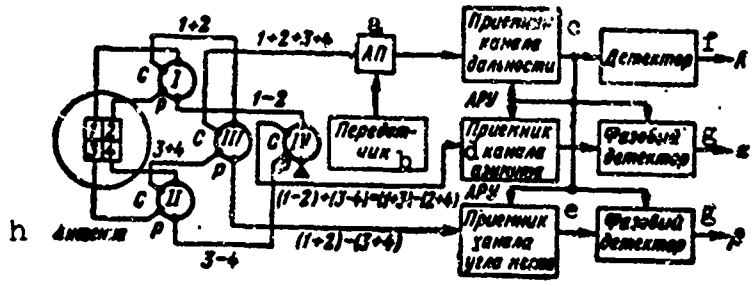


Fig. 8.35. Amplitude summation difference bearing system in two planes. a) AP; b) transmitter; c) receiver distance channel; d) receiver, azimuth channel; e) receiver angle location channel; f) detector; g) phase detector; h) antenna.

The biggest interest in the scheme being examined is the commutation system on the waveguide bridge which delivers necessary voltage to the corresponding channels. Thus, for the channels of detection and distance measurement, it is required to supply the total number of signals receivers by all the four antennas. For this, Signals *1* and *2*, *3* and *4*, are added beforehand in pairs at the two first waveguide bridges, they are totalled finally in the third ring bridge and from the bridge *C* of the third bridge fed into the receiver. High frequency transmitters are distributed, with the help of these same bridges, equally and in phase among all the four radiators.

The difference signal of the angle location receives the result of subtracting the sum of signals of Radiators *3* and *4* from the sum of the signals of Radiators *1* and *2*. For this, the sum obtained in the first two bridges is subtracted at point *P* of the third bridge and fed into the receiver of the channel of angle location.

For obtaining the difference signal at the azimuth, it requires the subtraction of the sum of signals of Radiators *2* and *4* from the sum of the signals of Radiators *1* and *3*. The operation instruction may

be accomplished somewhat differently: the differences *1–2* and *3–4* are obtained on the first two bridges and added up in branch *C* of the fourth bridge. This gives the required result since the system is linear and the calculation rule: (1 – 2) + (3 – 4) = (1 + 3) – (2 + 4) is applicable.

The difference branch of the fourth bridge (difference of the differences) is not used: it is reserved for absorbing load.

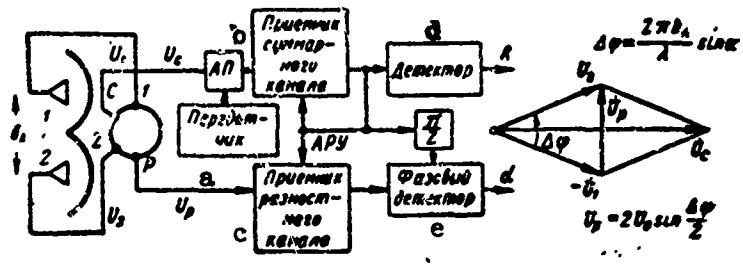


Fig. 8.36. Phasal summation difference bearing system in one plane. a) Transmitter; b) receiver summation channel; c) receiver difference channel; d) detector; e) phase detector.

Phasal summation difference bearing system is similar to the amplitude one in construction (Fig. 8.36). As can be seen from the vector diagrams, the amplitude of the difference signal

$$U_p = 2U_0 \sin\frac{\Delta\varphi}{2}$$

appears to be the function of the phase shift

$$\Delta\varphi = \frac{2\pi b_0}{\lambda}\sin\alpha,$$

dependent on the angle of deviation α. When α is small, the amplitude of difference signal

$$U_p \simeq \frac{2\pi b_0}{\lambda} U_0 \alpha$$

is proportional to the angle α same as in the amplitude bearing system.

With the change of sides of deviation (±α), the vector $\dot{U}_p$ varies in phase by π, remaining, in all cases, perpendicular to the vector of the summation signal $\dot{U}_c$. For the determination of the magnitude and

the direction of deviation, the difference signal is fed into the phase detector, the supporting voltage of which is the summation signal, displaced in phase by $\frac{\pi}{2}$. The dependence of the output voltage on the force of the signal being received is established by the help of the ARU circuit.

Under this condition, the phase summation difference system differs from the amplitude one only in the phase rotation by $\frac{\pi}{2}$ and in the antenna, the beam displacement $2\varepsilon$ is replaced by the dispersion of receiving points, $b_a$. It is possible to build an amplitude phase system having displacement and dispersion simultaneously.

Phasal summation difference bearing systems in two planes just as in the amplitude ones, have four beam antennas, four waveguide bridges and three receivers, differing from the latter only in the presence of the phase rotation of $\frac{\pi}{2}$.

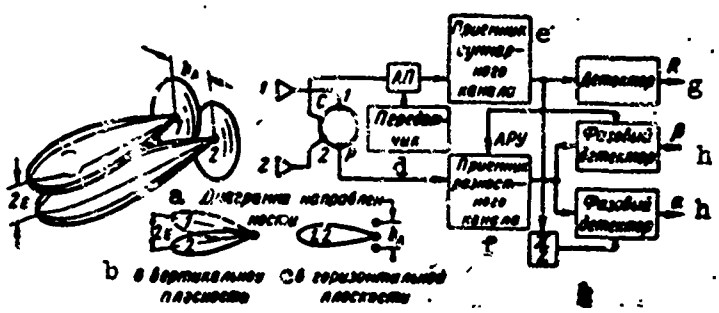


Fig. 8.37. Compound summation difference bearing system in two planes. a) Diagrams of directionality; b) in the vertical plane; c) in the horizontal plane; d) transmitter; e) receiver of summation channel; f) receiver of difference channel; g) detector; h) phase detector.

But, it is possible to construct a double beam compound summation difference bearing system in two planes having only one bridge and two receivers (Fig. 8.37). In the vertical plane the beam diverges by the angle $2\varepsilon$ in the horizontal plane the points of receiving have a dispersion of $b_a$. Under this condition, when the object deviates at the azimuth only by $\alpha$ the system works like a phasal one and has phase

shift of $\frac{\pi}{2}$, in supporting voltage. At angle location, $\beta$, the system behaves like a pure amplitude one. At a deviation of the object simultaneously by $\alpha$ and $\beta$, both the phase and amplitude channels will be in action.

The compound system distinguishes itself as ultimately simple, but its diagrams of directionality are deeply lobed, and the channels of azimuth and angle location are mutually connected.

In the multichannel bearing systems, it is practically exclusively the application of the rotating waveguide connections, since a reversal produces parasitic amplitude and phase modulations and also additional noise which suppresses the accuracy considerably. Therefore, all waveguide mixer tracts of monopulse RLS together with preliminary amplifiers generally perform as one entity with reflecting antennas.

Antenna systems of such forms have cumbersome and powerful drive gears. Borne in the focus of the mirror of the irradiator, there is considerable shading. Owing to the immense extent of the output to the irradiator, there is significant loss of power at the waveguides and a temperature variation of the electric wave brought into the phasal error.

The enumerated shortcomings are almost completely settled in the double reflecting antennas consisting of a parabolic reflector and a plane counter reflector (Fig. 8.38). The radiators irradiates the counter reflector through the aperture in the center of the reflector. Owing to this arrangement, the summation difference waveguide bridges and the mixing sections may be positioned behind the reflector and the lines of the waveguides brought to a minimum. Thanks to the counter reflector, the radiator stands artificially as if it were in the focal region of the reflector (dotted line). The dimensions of the

focal length of antennas of this type is considerably reduced in comparison with the focal length of the single reflecting antennas which have the radiator actually positioned in the focus of the reflector.

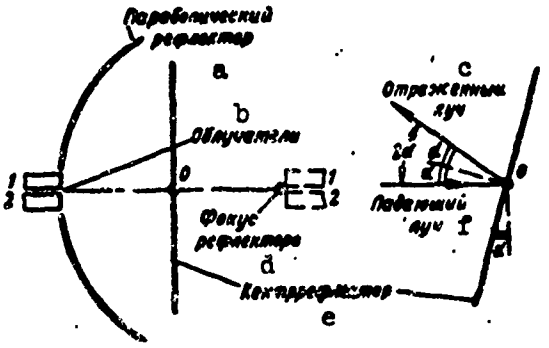


Fig. 8.38. Double reflecting antenna of monopulse RLS with plane counter reflector. a) Parabolic reflector; b) irradiators; c) beam dispersion; d) focus of the reflector; e) counter reflector; f) incident beam.

Rocking of the diagrams of directionality and equisignal directions is accomplished at the expense of the rotation of one such counter reflectors around the horizontal axis (point 0). For the rocking in two planes, the counter reflector is set on a Cardan joint. Rotating the counter reflector an angle $\alpha$ produces an inclination of the beam to an angle of $2\alpha$ as is shown in the right side of the drawing.

Thanks to this type of rocking the antenna beam, the power for the antenna drive has been considerably reduced, weight, size and inertia have all been cut down. The shortcoming of the double reflecting antennas appears to be the limiting angle of view (no bigger than $\pm 60°$) permitted by the distortion of diagrams of directionality.

The shading of the reflector by the counter reflector is accomplished with the help of systems of rotating the plane of polarization. The principle of the working of the system is explained in Fig. 8.39, where, for the simplification of the drawing, the reflectors are shown as planes.

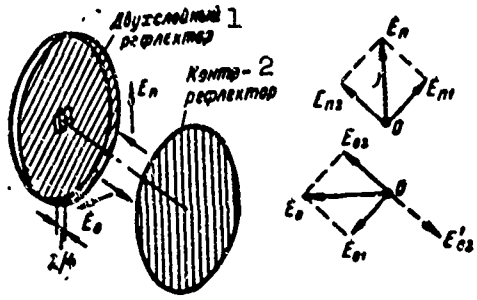


Fig. 8.39. Arrangement of shading of the reflector by the counterreflector by rotating the plane of polarization. 1) Double layered reflector; 2) counterreflector.

Counterreflectors are not made in a solid mass but in the form of metallic strips, positioned sufficiently close and embedded in disks of dielectrics, transparent to radio waves. Radiated by irradiators, vertically polarized waves are reflected from the counterreflector as from a solid mirror. Falling on the reflector, this wave (vector $\dot{E}_p$)is transformed into a horizontally polarized reflected wave (vector $\dot{E}_0$) which afterwards goes freely into the open space through the grating of the counterreflector from the vertical plane.

The rotation of the plane of polarization is accomplished by a special type of structure of the surface of the reflector consisting of two layers. The upper layer consists of a series of metallic surfaces turned at a 45° angle to the vertical. The lower layer is a solid metallic screen at a separation of thickness $\frac{\lambda}{4}$ from the upper layer of dielectrics.

The vertically polarized wave falling on the reflector $\dot{E}_p$ may be separated into two components: $\dot{E}_{p1}$ and $\dot{E}_{p2}$ the first of which is parllel to the plane of the reflector, and the second is perpendicular to it. The first component, reflecting from the plane of the reflector as from a solid screen, changes phase at 180° and forms the component

of the reflected wave $\dot{E}_{01}$. If the second component also were reflected from the same planes, it would form the component $\dot{E}'_{02}$. In so doing, the second component is perpendicular to the plane and freely approaches the metallic screen, reflecting from it and lagging behind the first component by a half wave length $(2 \cdot \frac{\lambda}{4})$. As a result, the second component of the reflected wave $\dot{E}_{02}$, experiences an additional rotation of phase by 180° (opposite in position to the vector $\dot{E}'_{02}$).

Both components add up in the space between the reflector and the counterreflector form the horizontally polarized reflected wave $\dot{E}_0$, for which the vertical plane of the counterreflector does not appear to be an obstacle.

Besides what we have examined, there are more complete double reflecting antennas, composed of parabolic reflectors and hyperbolic counterreflectors (Fig. 8.40). They receive the designation, Cassegrain's antennas – by the name of the builder of the reflecting telescope of the same construction.

During cophasal radiation from both radiators (or from all four radiators during bearing taking in two planes) the reflection from the counterreflector produces such effect as if the reflector antenna is directly irradiated by a point source, located in its focus. By the principle of reciprocity, the same will be valid for summation signal, received by all radiators.

Under this condition, in relation to the summation signal, the Cassegrain antenna behaves as a single reflecting antenna with a single point radiator in the focus. It possesses the maximum possible directional action in the direction of the maximum summation diagram (equisignal directions) at any dispersion of the radiators and

consequently at any angle of deviation ε. Therefore, the angle of deviation may be made the optimum without the lowering of the working distance of RLS by the summation channels.

Thanks to the maximum coefficient of directional action, the resolving power of angle also reaches the ultimate in distinction from other multichannel RLS or single channel RLS with conical rotation of the beam, which, at the increase of the angle of deviation, results in the widening of the solid angle of radiation and reception.

Consequently, in the multichannel RLS with Cassegrain antenna, in principle, the potential possibility is realized in the distance channel as well as in the angle channel. The actual error of angular coordinates measurements by the method of automatic tracking by direction will b evaluated in one of the following paragraphs.

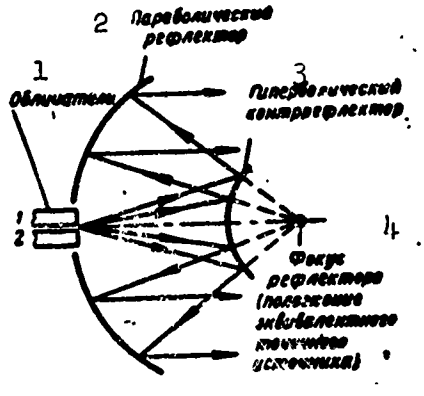


Fig. 8.40. Double reflecting Cassegrain antenna. 1) Radiators; 2) parabolic reflector; 3) hyperbolic counterreflector; 4) focus of the reflector (position of the equivalent point source).

## §8.7. AUTOMATIC TRACKING OF THE OBJECT BY DIRECTION.

Radiolocational stations with automatic tracking of the object by direction (ASN) present themselves as closed tracking systems controlled by the actions in which the object is is motion. If the direction of the antenna axis does not coincide with the line of visibility

towards the object, then an intensity error is produced in the ASN system under the action of which the antenna of RLS turns to the side to reduce the discord.

Different ASN systems differ in the methods of formulating the error signals. Below we shall examine two types of radiolocational systems of automatic tracking of the object according to direction:

1) system with conical rotation of the antenna axis;

2) single pulse ASN system.

1. Principle Of Automatic Tracking Of The Object According To Direction In RLS With Conical Rotation Of The Antenna Beam.

As it was shown in Chapter 2, in the ASN system with conical rotation of the antenna beam, the maximum of the diagrams of directionality is displaced relative to the optical axis of the antenna by a certain angle ε (Fig. 8.41). At the rotation of the radiobeam, a direction is formed at which the intensities of the receiving and radiating signals remain constant. This direction coincides with the axis of rotation of the beam, known as equisignal.

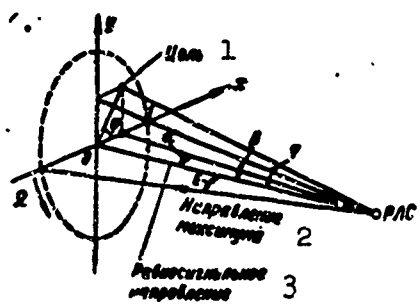


Fig. 8.41. The formation of equisignal direction. 1) Object; 2) direction of the maximum; 3) equisignal direction.

When the object is displaced from the equisignal direction, the reflected signals at the output of the receiver of the RLS appear as amplitude modulated. The envelope of the received signals is a smooth periodic function with a period $T$ equal in time to one rotation of

the antenna beam. The depth of the amplitude modulation and the form of the envelope of the pulses are dependent on the magnitude of the angle of deviation of the object $\psi$ from the equisignal direction. At small angles of deviation of the object ($\psi << 0$), the modulation is extremely close to sinusoidal. If a moment of time is selected when the maximum of the diagrams of directionality is located at the point *1*, then the envelope may be described by the expression

$$u(t) = U_0(R, \alpha_0)[1 + m\cos(\Omega t - \varphi)], \qquad (8.50)$$

where $U_0$ – amplitude of the signal being received in the equisignal direction; $\Omega$ – circular frequency of the rotation of the antenna beam; $m$ – coefficient of amplitude modulation; $\varphi$ – initial phase of the envelope, dependent on the direction of deviation of the object from the horizontal plane.

The coefficient of modulation $m$ at small angle deviations is directly proportional to the angle of discord.

$$m = \mu\psi,$$

where $\mu$ – sharp bearing characteristic.

At large deviation of the object from the equisignal direction, the modulation does not appear to be sinusoidal whereupon the most intensive higher harmonics is the second ones.

The isolation of the basic harmonics of the envelope of amplitude-modulated pulses is generally done with the help of peak detector and resonance filters built according to the frequency of the rotating antenna beam. For an increase in the coefficient of transmission of the detector and a decrease in the pulsation voltage at its output, the constant time of circuit discharge $T_p$ must be selected considerably larger than the period of the pulse sequence. But, considerable increase of $T_p$ leads to an inertness of the detector which may be said

in the negative for the quality of the process of tracking of the object. The most satisfactory results are given by the switch peak detector. The voltage at the output of such detector is regulated practically instantly and remains unchanged up to the end of a given period of the sequence of pulses. Directly before the input of the sequence of pulses, the accumulated voltage is reduced to zero and further process of charging and discharge repeats periodically. The switch detector, which appears to be practically devoid of inertness, has the maximum possible coefficient of transmission.

The spectra of the output signal of a switch detector are shown in Fig. 8.42. It presents itself as the spectra of a series of right-angled pulses with duration equal to the period of repetition. Information on the deviation of the object from the equisignal direction is contained in the component spectrum $\Omega$. For the isolation of that component generally after the detector, one installs a resonance detector the output voltage of which, designated as the error signal, may be described by the expression

$$u_{вых}(t) = U_0 m \cos(\Omega t - \varphi - \varphi_1),$$

where $\varphi_1$ – additional phase shift, generated in the circuit detector and the filter.

The amplitude of the error signal should be proportional to the depth of modulation $m$ and should not depend on the average magnitude of the signals being received, $U_0$. Only under this condition, the maintaining of the proportionality between the error signal and the magnitude of the deviation of the object from the equisignal direction is independent of the size of the object and its distance from the RLS. In order to guarantee the indicated proportionality in the ASN station with conical scanning, it is necessary to utilize automatic control of the amplification. The variable coefficient of amplifica-

tion of the receiving tract is inversely proportional to the average magnitude of the pulses. The ARU system should be sufficiently inert at the frequency Ω so that it does not produce noticeable demodulation of the error signal carrying information on the deviation of the object. At the fulfillment of this condition, the amplitude of the error voltage will only be proportional to the angle of divergence $\psi$, while phase is single valuedly determined by the direction according to the object.

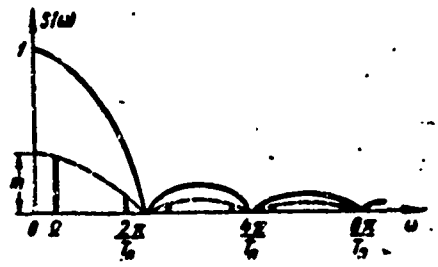

Fig. 8.42. Spectra of signals from the output of switch detector.

The error signals so obtained are used for the forming of voltages controlling the motion of the antenna in the azimuthal and angle position planes. The resolution of the error signal according to its orthogonal components, proportional to the displacement of the object at the azimuth and the angle location, is carried out with the help of two amplitude phase discriminators (detectors).

There are many different circuits of amplitude phase discriminators, but in their working principle, they all have elements, whose coefficient of amplification, $K(t)$ changes synchronously and cophase with the frequency of the supporting voltage. The passage of the error signals through the phasal discriminator increases it in equal strength according to $K(t)$.

The supporting voltages of the phasal detectors are variable sinusoidal voltages of right-angled shapes with periods equal to the time of one revolution of the antenna. The phases of the supporting voltages of the aximuth channel and the angle location channel are displaced at an angle of $90°$ from each other.

When the supporting voltage is sinuscidal, the output signals of the phase detector of the azimuth and angle location channels will be correspondingly

$$\begin{aligned} u_\alpha &= k_p U_{om} \cos(\Omega t - \varphi) \cdot U_0 \cos \Omega t = \\ &= \frac{1}{2} k_p U_0 U_{om} \cos \varphi + \frac{1}{2} k_p U_0 U_{om} \cos(2\Omega t - \varphi); \\ u_\beta &= k_p U_{om} U_0 \cos(\Omega t - \varphi) \cdot \sin \Omega t = \\ &= \frac{1}{2} k_p U_0 U_{om} \sin \varphi + \frac{1}{2} k_p U_0 U_{om} \sin(2\Omega t - \varphi), \end{aligned} \tag{8.51}$$

where $k_p$ – coefficient of transmission of the phase discriminator;

$U_0 \cos \Omega t$ – supporting voltage of the azimuth channel;

$U_0 \sin \Omega t$ – supporting voltage of the angle location channel.

Since $\cos\varphi \approx \frac{\alpha}{\psi}$, $\sin\varphi \approx \frac{\beta}{\psi}$ (Fig. 8.41) and $U_{om} \sim \psi$, the constant components of the output voltage of the phase detectors of the azimuth an angle location channels are proportional to the displacement of the object in the corresponding planes

$$\begin{aligned} u_\alpha &= k\alpha, \\ u_\beta &= k\beta. \end{aligned}$$

The larger extensions in the ASN systems with conical scanning took in fullwave phase discriminators with right-angled supporting voltage. A simplified schematic diagram of these is shown in Fig. 8.43. Supporting voltages commute by the anode circuit of the tubes of the phasal discriminator (because of this, in the literature phasal detector of this type are often designated as phase commutator). The coefficient of amplification of the cascades, collected at the tubes $L_1$ and $L_3$, varies with time according to the rules

$$\begin{aligned} k &= k_0 \quad \text{for} \quad 2n\pi \leqslant \Omega t \leqslant (2n+1)\pi; \\ k &= 0 \quad \text{for} \quad (2n+1)\pi \leqslant \Omega t \leqslant 2n\pi, \end{aligned}$$

while the coefficient of amplification of the cascades, collected at the tubes $L_2$ and $L_4$ is according to the rules

$$\begin{aligned} k &= 0 \quad \text{for} \quad 2n\pi \leqslant \Omega t \leqslant (2n+1)\pi; \\ k &= k_0 \quad \text{for} \quad (2n+1)\pi \leqslant \Omega t \leqslant 2n\pi. \end{aligned}$$

where $n = 0, 1, 2, \ldots$ – integers.

The output voltage of phase detectors of the azimuth and angle location for one period of commutation may be described in the form (Fig. 8.44).

$$u_\alpha = k_0 u_{\text{отш}}(t)\cos(\Omega t + \varphi),$$
$$u_\beta = k_0 u_{\text{отш}}(t)\sin(\Omega t + \varphi).$$

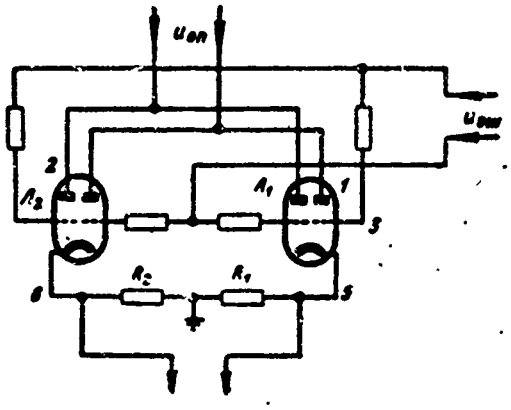

Fig. 8.43. Simplified schematic diagram of phasal discriminator.

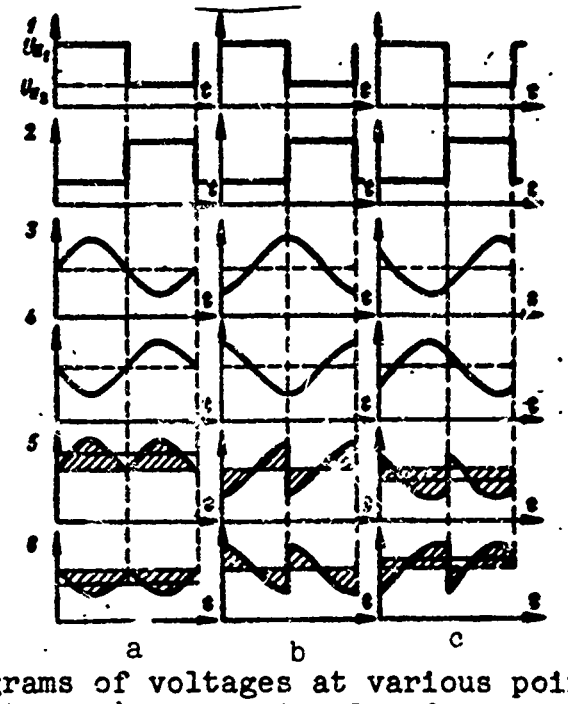


Fig. 8.44. Time disgrams of voltages at various points of the scheme of phasal discriminator: a) error signal and supporting voltage coincide in phase; b) error signal and supporting voltage displaced in phase by 90°; c) error signal and supporting voltage displaced in phase by 45°.

The error signal $u_{osh}(t)$ is a slow varying function in comparison with cos $\Omega t$ therefore, in a first approximation $u_{osh}(t)$ may be considered as constant during some fragments of time.

The constant component of the output voltage of the phase detector is proportional to the error tracking in the corresponding planes

$$u_{\alpha} = -\frac{4k_0 U_{om}}{\pi} \cos\varphi,$$

$$u_{\beta} = \frac{4k_0 U_{om}}{\pi} \sin\varphi.$$

For the isolation of useful components of the error voltages proportional to $\alpha$ and $\beta$, at the output of the phase detectors, low frequency filters are included which do not let through components containing the harmonic frequency $\Omega$. The controlled voltage from the output of the phase discriminator of each channel is amplified and led to the drive gears of the motors of the azimuth and angle location. The drive motor will turn the antenna in the side of increased angle of discord between the direction toward the object and the antenna axis. This method insures the continuous coincidence of the antenna axis with the direction toward the object with accuracy up to the error of tracking.

Let us remember that the automatic tracking of the object is only possible in the case when at the output of the detector, the error signals behave as signals from one single object. Therefore, in the RLS receiver, it is necessary to guarantee the selection of objects according to distance with the help of the ASD system.

2. Monopulse Systems Of Automatic Object Tracking.

Below, we shall examine two types of monopulse ASN systems: phasal systems of autotracking and amplitude systems of autotracking.

In the phasal monopulse ASN systems, automatic measurement of angular coordinates is accomplished by a continuous comparison

of the phase of the signals, received by the different antennas.

The equisignal directions (directions of equal phase) coincide with the symmetry axis of the antenna system.

During automatic tracking the deviation of the object from the equisignal direction is not considerable, therefore, approximately, it may be considered that the difference in phase of the signals received is proportional to the angle of deviation of the object

$$\Delta\varphi \approx \frac{2\pi b_a}{\lambda}\alpha.$$

Since in the systems, generally heterodynes are used, therefore the phasal relationship between the signals of the first and second channels is preserved even after the transformation of frequency. But, the voltage of the signals at the output of the amplifier of intermediate frequencies may have an additional phase shift on account of nonidentical amplitude phasal characteristics UPCh

$$u_1 = U_1 \sin(\omega_{пч} t + \varphi_0 + \varphi + \delta\varphi),$$
$$u_2 = U_2 \sin(\omega_{пч} t + \varphi_0),$$

where $U_{1,2}$ – amplitude of signals at the output of UPCh; $\delta\varphi$ – phase shift, dependent on the nonidentity of phasal frequency characteristics of UPCh.

Phase discriminators are often used as the sensitive elements of the systems reacting to the changes in the difference of phases of the signals being received. The constant component of the output voltage of the phase discriminator is the error signals of the ASN system

$$U_{ош} = k_д U_1 U_2 \sin(\varphi + \delta\varphi). \qquad (8.52)$$

During automatic tracking of the object the error of tracing $\varphi$ is small, consequently, it may be considered that $\sin\varphi \approx \varphi$ and $\cos\varphi \approx 1$. Under this condition, Expression (8.52) may be transformed into the following forms:

$$U_{вых} = k_p U_1 U_2 (\sin\varphi \cos\delta\varphi + \cos\varphi \sin\delta\varphi) \approx$$
$$\approx k_p U_1 U_2 \cos\delta\varphi\, \varphi + k_p U_1 U_2 \sin\delta\varphi. \qquad (8.53)$$

The first item of Expression (8.53) presents itself as the useful component of the error signal, whose magnitude is dependent on the displacement of the object from the equisignal direction and on the amplitude of the signal being received. For the exclusion of the influence of the amplitude fluctuations of the signals beings received on the magnitude of the error signal at the output of both channels of UPCh, it is necessary to install limiting devices or use circuits of automatic amplification control.

The nonidentity of the phasal frequency characteristics of the channels leads to a decrease of the useful component of the error signal (factor cos $\delta\varphi$) and the appearance of additional voltage at the output of the phase discriminator unrelated to the object in space, [second term of Expression (8.53)]. As a result of the action of the additional voltage, tracking error proportional to the value $\delta$ is produced. This error will become smaller the higher the bearing sensitivity of the system $\frac{d\varphi}{d\alpha}$.

Changes in temperature, instability of the feeding voltage and the waste frequency of the heterodyne may lead to variations in phasal delay in the UPCh channels and consequently, to the appearance of tracking error. For the elimination of the nonidentity of the channels one may use different circuits of automatic devices of phasal characteristics UPCh for special standard signals. Another way of compensating the phase frequency characteristics UPCh consists of the in period commutation of the channels so that the UPCh alternately switched to the first and second antennas. At this, the phase shift $\delta\varphi$ takes on, at time, a positive value and, at times, a negative value and in the average error signal, the magnitude of the additional

voltage will be significantly reduced.

The phase method permits the realization of automatic tracking by direction without the rotational antenna set up, since it is not connected with the use of the amplitude diagrams of directionality of the antennas. For instance, in place of the rotation of the antennas, the variation of the relative phase shift is accomplished by some other means, say, by the rotation of the axis of the phaserotator which may be constructed, then it may also determine the direction of the arrival of the reflected signal by the position of this axis. Phasal systems of autotracking of this type are generally called the interferometers. A simplified diagram of the interferometer is shown in Fig. 8.45. In distinction from the previous systems, the drive arrangement is not connected to the mechanism of the rotation of the antenna, but with the constructible phaserotator. A variation in the position of the latter leads to change of phase of the signals being received in this channel and consequently, to a change of the relative phase shift. In the capacity of the phaserotators, it is possible to use waveguide ferrite arrangement, waveguides with variable dimensions, etc.

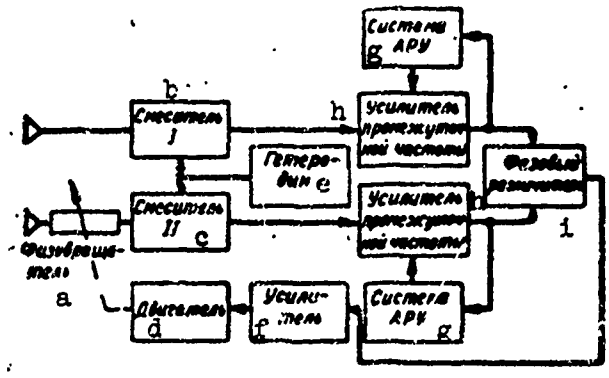


Fig. 8.45. Block diagram of interferometer. a) Phaserotator; b) mixer I; c) mixer II; d) motor; e) heterodyne; f) amplifier; g) ARU system; h) amplifier of intermediate frequency; i) phase discriminator.

Damping and linearity characteristics of both types of phase-rotator are acceptable for the problem under consideration. When the ferrite phaserotator is used the variation of phase vibrations may be accomplished by electrical methods.

When there is a displacement of the object from the equisignal direction, there appears an error signal which acting on the mechanism of rotating the phaserotator, changes the phase of the signal being received in its own channel to the time until the difference in the phases of the signals in both channels will be zero. If it is assumed that the characteristic of the phaserotator is linear, i.e., the phase shift in the phaserotator is proportional to the rotation of its axis, then the condition of the error signal equalling zero may be written as

$$k_1\psi - 2\pi\frac{d}{\lambda}a = \frac{\pi}{2}, \qquad (8.54)$$

where $k_1$ is the coefficient of transmission of the phaserotator.

From Formula (8.54) it is easy to find the angle of the rotation of the axis, at which the equisignal direction coincides with the direction of the object

$$\psi = \psi_0 + 2\pi\frac{d}{\lambda k_1}a,$$

where $\psi_0 = \frac{\pi}{2k_1}$ is the initial angle of rotation of the axis of the phase-rotator, corresponding to a phase shift of the signals in a magnitude equal to $\frac{\pi}{2}$.

With accuracy to a constant factor, the angle of rotation of the axis of the phaserotator is equal to the angle of deviation of the object from the antenna axis and consequently every direction towards the object is single-valuedly correspondent to a definite angle of rotation of the axis of the phaserotator. The merits of the tracking system of the type of the interferometer are the sufficient accuracy,

simplicity of construction and the absence of the massive structure of the following antenna and its powerful drive.

In examining the operation of the interferometers, it should, however, be remembered, that the antenna beam does not follow the track of the object, consequently, autotracking is only possible within the limits of the width of the diagrams of directionality; as soon as the object starts to move out of the beam, tracking is discontinued.

From this point of view, one should strive towards a wider diagram of directionality, but the boundaries of the spread is limited by the requirement on working distance of the systems and the necessary resolving power of the RLS.

For the increase of the zones of tracking of the interferometer when the diagram of directionality is narrow, it is necessary to move the antenna beam behind the object.

This operation may be accomplished with the help of the very phaserotator which is used for the control of the phase of the high frequency tract of the interferometer.

What we saw above was the operation of the phasal system of tracking in one plane. For the tracing of the objects in two planes, it is necessary to have one more system exactly like this.

In the amplitude monopulse systems for the determination of the direction of the object, a method of simultaneously comparing the intensities of the signals received, at the different antennas is used. If the object is located in the equisignal direction, then the signals received by both antennas are equal; if the object inclines at a certain angle $\alpha$, then at the input of the receiving part of the RLS installation, there will appear two high frequency pulses of different amplitude

$$u_1 = U(1 + \mu\alpha)\sin\omega t,$$
$$u_2 = U(1 - \mu\alpha)\sin\omega t,$$

where $\mu$ – bearing sensitivity.

At the summation-difference bridge come addition and subtraction voltages, taken from both antennas:

$$u_c = u_1 + u_2 = 2U\sin\omega t,$$
$$u_p = u_1 - u_2 = 2U\mu\sin\omega t,$$

where $u_s$ – voltage in the summation channel; $u_r$ – voltage in the difference channel.

The summation and difference voltages appear in phase for the directions of incidence of the signals, from one side and in the opposite phase from the other side.

For the isolation of the information on the side of the deviation of the object, the signals of both channels (after conversion and amplification to intermediate frequency) are compared in the phase detector. The voltage at the input of the phase detector may be written as

$$u_{np} = KU\mu\alpha\sin(\omega_{np}t + \delta\varphi),$$
$$u_{nc} = KU\sin\omega_{nc}t,$$

where $u_{pr}$ – voltage at the output of UPCh difference channel; $u_{ps}$ – voltage at the output of summation channel; $K$ – coefficient of amplification of the mixer and UPCh each of the channels; $\delta\varphi$ – phase shift, depending on the various phase characteristics of the channels.

At the output of the phase detector videopulses are formed whose magnitude is equal to

$$U_p = \frac{1}{2}K^2U^2k_p\mu\alpha\cos\delta\varphi, \qquad (8.55)$$

where $k_r$ – coefficient of transmission of the phase discriminator.

The amplitude of the pulses is proportional to the angle of deviation of the object from the antenna axis while the sign indicates

the side of deviation of the object. At the output of the phase detector, there stands a switch pulse detector lengthening the videopulses to all periods of the sequence. After the pulse detector, the constant component is isolated $U_{osh}$ whose magnitude is equal to the angle $\alpha$. The phase shift $\delta\varphi$ acts on the magnitude of the error signals depending on the nonidentity characteristics of the amplifier of intermediate frequency. The increase $\delta\varphi$ leads to a decrease of the error signals. Thus if $\delta\varphi = 60°$, then the coefficient of transmission of the system is reduced by two times while during a phase shift, approaching 90°, the operation of the ASN system becomes impossible. The error voltage from the output of the pulse detector after amplification is fed to the operating mechanism rotating the antenna installation to the side of the diminished angle $\alpha$. The coincidence with the equisignal direction with the object may be accomplished not only by mechanical but also by electrical methods, by the way of electrical deviation of the antenna beam.

In distinction from the ASN system with conical rotation of the radio beam, in monopulse systems there is no necessity to resolve the error signals into two components since the amplitude and angle location channels are not separated directly in the antenna installation. Therefore, in the monopulse system ASN, there is no error connected with the phase shift of the error signal envelope, resulting from the inertness of the pulse detector.

## §8.8. ACCURACY OF RADIOLOCATIONAL SYSTEMS OF AUTOMATIC TRACKING OF THE OBJECT BY DIRECTION.

Radiolocational station with autotracking of the object by direction consist of two closed tracing systems accomplishing the continuous measurement of the angular coordinates in two mutually perpendicular planes: azimuthal and angle location. Since both channels are iden-

tical by their actions, therefore in the future, we limit to an examination of one amplitude channel.

The total angular error of the ASN system, in view of the identity of the channels, is increased by $\sqrt{2}$ times in comparison with the error of the single channel.

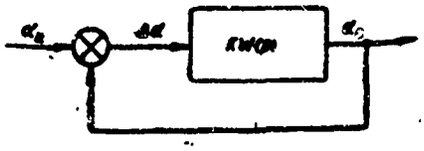

Fig. 8.46. Simplified structural circuit of the autotracking system in one plane

The structural circuit of radiolocational system of autotracking of the object in the azimuthal plane may be seen as shown in Fig. 8.46. The incident signal of the tracing system appears to be the azimuth of the object, $\alpha_{ts}$, the output – angular position of the antenna axis $\alpha_a$. The difference between the input and output signals is the error of the tracking system $\Delta\alpha$.

For the system shown in Fig. 8.46, the following basic relationships connecting the present values of $\Delta\alpha$, $\alpha_{ts}$, and $\alpha_a$ are valid:

$$\begin{aligned}
\Delta\alpha(p) &= \alpha_{ts}(p) - \alpha_a(p),\\
\alpha_a(p) &= KW(p)\,\Delta\alpha(p),\\
\alpha_a(p) &= \frac{KW(p)}{1+KW(p)}\alpha_{ts}(p) = W_z(p)\,\alpha_{ts}(p),\\
\Delta\alpha(p) &= \frac{\alpha_{ts}(p)}{1+KW(p)} = W_{\Delta\alpha}(p)\cdot\alpha_{ts}(p),
\end{aligned}$$

where $KW(p)$ – transmission function of the open system ASN; $\Delta\alpha(p)$ – image of the error of autotracking; $\alpha_{ts}(p)$ – image of the output signal (azimuth of object); $\alpha_a(p)$ – image of the output signal (azimuth of antenna axis); $W_{\Delta\alpha}(p)$ – transmission function of the system ASN; $W_z(p)$ – transmission function of the closed system.

The magnitude of the error $\Delta\alpha$ depends on the form of the transmission function of the open system and the character of the motion of the object. The values in the adjustable region may be determined very simply by resolving the transmission function of the error $W_{\Delta\alpha}(p)$ into a series in ascending powers of $p$:

$$\Delta\alpha(p) = W_{\Delta\alpha}(p) \cdot \alpha_{\text{вх}}(p) = \left(C_0 + C_1 p + \frac{C_2}{2!} p^2 + \frac{C_3}{3!} p^3 + \ldots\right) \alpha_{\text{вх}}(p), \quad (8.56)$$

where the coefficients of the series $C_0$, $C_1$, $C_2$, $C_3$, ...are computed with the help of the formula

$$C_i = \left[\frac{d^{(i)} W_{\Delta\alpha}(p)}{dp^{(i)}}\right]_{p=0}.$$

Obviously, Series (8.56) converges at $p \to 0$.

Applying Laplace transform to every term of Equality (8.56) we obtain the following series:

$$\Delta\alpha(t) = C_0 \alpha_{\text{вх}}(t) + C_1 \frac{d\alpha_{\text{вх}}}{dt} + \frac{C_2}{2!} \frac{d^2\alpha_{\text{вх}}}{dt^2} + \frac{C_3}{3!} \frac{d^3\alpha_{\text{вх}}}{dt^3} + \ldots,$$

converging at large values of $t$ and giving the possibility of determining the magnitude of error in the ASN system when the law of motion of the object is known.

The biggest effect on the magnitude of the error is, in general, indicated by the first three coefficients of the series. The smaller each one of these coefficients, the higher is the dynamic accurary of the system. The values of the coefficients of error depend on the parameters of the circuit structure of the ASN system. For systems with astatism of the $\nu$th order, all coefficients of error up to $C_{\nu-1}$ equal to zero. From this point of view, it is advantageous to increase the order of astatism of the system ASN, but, the increase of the order of astatism generally leads to construction complexities of the system. Therefore, at present time, it is more often that we encounter ASN systems with astatism of the first and second orders.

Formulas for the determination of the coefficients of error of such circuits have the following form.

1. Systems with astatism of the first order

$$C_0 = 0; \quad C_1 = \frac{1}{K}; \quad C_2 \approx \frac{T_{\text{наим}}}{K}.$$

2. Systems with astatism of the second order

$$C_0=0;\ C_1=0;\ C_2\approx\frac{2}{K},$$

where $K$ – coefficient of transmission of the open system ASN: $T_{max}$ – maximum time constant of the systems.

For guaranteeing the accuracy of tracking, it is necessary that the coefficients $C_1$ and $C_2$ were small. Consequently, the coefficient of transmission of the system should be sufficiently large. In the present ASN system, the magnitude of $K$ reaches several hundreds. The increase of $K$ when sufficient margin of stability of the system is maintained, leads to the broadening of the effective passband. In the theory of automatic control, it is demonstrated that at the optimum form of frequency characteristics of the open system and margin of stability of phase in $40 - 60°$, the effective band of the tracing system is

$$\Delta F_3\approx\frac{1\div1,5}{2\pi\sqrt{C_2}}.$$

Thus, for example, in order to obtain the necessary accuracy of the system, it is required that $C_2 = 0.01$, then the effective passband should be not less than $1.5 - 2$ hz.

In the presence of sudden maneuver of the object, the axial component part of the summation error of tracking may be error, dependent on the inertness of the system. In order to decrease the error of delay, one should strive to decrease the time of the passage process such that in its turn, the broadening of the passband of the system is demanded. The wider the $\Delta F_z$, the less time of establishing in the system and consequently, the less the dynamic error of autotracking of maneuvering objects.

For the optimum frequency characteristics the time of establishing in the system is

$$t_y \approx \frac{1{,}0 \div 2{,}5}{\Delta F_э}.$$

For example, if the condition is set that $t_u \leq 1$ sec, then the passband of the system should be not less than $1.0 - 2.5$ hz.

Under this condition, to guarantee a high accuracy of reproducing the movement of the object and a decrease in the dynamic error, dependent on the passage of the tracing system, it is necessary to broaden the zone of passage and increase its coefficient of transmission. But, the increase of the coefficient of the effective passband leads to a growth of the error of tracking, dependent on the action of the internal and external interferences.

The effect of the interferences on the accuracy of the systems of autotracking is dependent on the character of the disturbing influence and the point of its application to the system. The variance of the error may be found if the spectral density of the interference is known and the transmission of the system relative to it.

$$\sigma_\alpha^2 = \frac{1}{2\pi} \int_{-\infty}^{\infty} |\Phi_\alpha(j\omega)|^2 G_\alpha(\omega)\, d\omega,$$

where $\sigma_\alpha^2$ – variance of the error of the system; $G_\alpha(\omega)$ – spectral density of the interference; $\Phi_\alpha(j\omega)$ – transmission function of the system relative to the interference.

The form of the transmission function $\Phi_\alpha(j\omega)$ is determined by the point of application of the interference to the system. For the calculation of $\Phi_\alpha(j\omega)$ of the structural system ASN, it is convenience to express it in the form of two serially connected dynamic members (Fig. 8.47). The first one, a practically periodless member, converts the angle of deviation of the object from the axis of the antenna installation $\Delta\alpha$ into error signals $U_{ots}$. The second member characterizes

the dynamic properties of the adjustment installation.

The transmission function in relationship to interference, applied at the point *1*, as shown in Fig. 8.47, coincides with the transmission function of the closed system

$$\Phi_\alpha(j\omega)=\frac{KW(j\omega)}{1+KW(j\omega)}=\frac{K_\Pi K_\Pi W_\Pi(j\omega)}{1+K_\Pi K_\Pi W_\Pi(j\omega)}.$$

The variance of the error of the system in this case is

$$\sigma_\alpha^2=\frac{1}{2\pi}\int_{-\infty}^{\infty}\left|\frac{KW(j\omega)}{1+KW(j\omega)}\right|^2 G_\alpha(\omega)\,d\omega, \qquad (8.57)$$

where $G_\alpha(\omega)$ – spectral density of interference at the input of the ASN system.

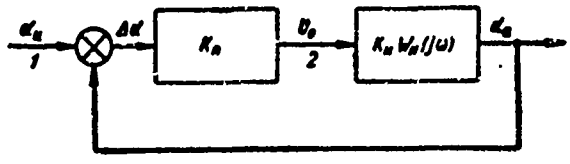


Fig. 8.47. Representation of the structural scheme of the ASN system in the form of two dynamic members in series.

Internal interference of the system is caused by the fluctuation of the error signal $U_{osh}$ at the output of the first dynamic member. The transmission function in relation to this fluctuation is described by this expression

$$\Phi_0(j\omega)=\frac{K_\Pi W_\Pi(j\omega)}{1+KW(j\omega)}. \qquad (8.58)$$

The variance of the error of tracking, dependent on the action of the internal interference may be calculated by the formula

$$\sigma_\alpha^2=\frac{1}{2\pi}\int_{-\infty}^{\infty}\left|\frac{K_\Pi W_\Pi(j\omega)}{1+KW(j\omega)}\right|^2 G_0(\omega)\,d\omega=$$
$$=\frac{1}{2\pi K_\Pi^2}\int_{-\infty}^{\infty}\left|\frac{KW(j\omega)}{1+KW(j\omega)}\right|^2 G_0(\omega)\,d\omega, \qquad (8.59)$$

where $G_0(\omega)$ – spectral density of the fluctuation of the error signal.

If the expression under the integral sign in Formulas (8.57) and (8.59) is obtained by addition, then the error determination is conveniently carried out by graphoanalytical methods, multiplying the ordinates of the curves by $G(\omega)$ and $|\Phi(j\omega)|^2$ and compute the area bounded by the resulting curves.

In a first approximation of the error of the ASN system, one may anticipate, if acceptable, that the spectral density of the interference in the passband of the system remaining at constant magnitude, is equal to the spectral density of the interference $G(0)$ at zero frequency. The fulfillment of such an approximation is substantiated in that actual systems of angular tracking of the object have sufficient narrow passbands lying within the boundaries from zero to $0.5 - 2$ hz.

Under the fulfillment of this, Formulas (8.57) and (8.59) assume the forms

$$\sigma_{\alpha}^2 = \frac{G_{\alpha}(0)}{2\pi}\int_{-\infty}^{\infty}|\Phi_{\alpha}(j\omega)|^2 d\omega, \qquad (8.60)$$

$$\sigma_{\alpha}^2 = \frac{G_0(0)}{2\pi}\int_{-\infty}^{\infty}|\Phi_0(j\omega)|^2 d\omega, \qquad (8.61)$$

where $G_{\alpha}(0)$ – spectrum density of external interference at zero frequency; $G_0(0)$ – spectral density of the fluctuation of error signals at zero frequency.

The integral from the square modulus of the transmission function, as is shown in Fig. 8.48 may be expressed through the effective passband of the system

$$\frac{1}{2\pi}\int_0^{\infty}|\Phi(j\omega)|^2 d\omega = \Delta F_{\text{э}}|\Phi(0)|^2,$$

where $\Phi(0)$ – the value of the transmission function of the system at zero frequency.

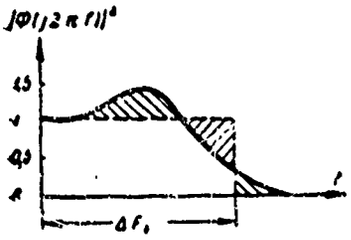


Fig. 8.48 Frequency characteristics of the closed ASN system

For astatic systems $|\Phi(0)|^2 = 1$,

therefore,

$$\frac{1}{2\pi}\int_0^\infty |\Phi(j\omega)|^2 d\omega = \Delta F_ш. \quad (8.62)$$

Substituting the value of Integral (8.62) in Formulas (8.60) and (8.61), we obtain a simple approximation expression for the determination of the incidental error of the ASN system

$$\sigma_{\alpha_1} \approx \sqrt{G_\alpha(0)\Delta F_ш}, \quad (8.63)$$

$$\sigma_{\alpha_2} \approx \frac{1}{K_ш}\sqrt{G_0(0)\Delta F_ш}, \quad (8.64)$$

where $\sigma_{\alpha_1}$ – mean square value of the error of tracking of the object, dependent on the action of the external noise; $\sigma_{\alpha_2}$ – mean square value of the error of tracking of the object, dependent on the fluctuation of voltage $U_{osh}$.

The basic sources of the incidental error of the ASN system appear to be:

– internal noise of the receiving installation;

– amplitude fluctuation of the reflected signals;

– fluctuation of the angle of incidence of the reflected signals.

1. Effect Of Internal Noise On The Receiving Installation

The character of the internal noises on the accuracy of the ASN system is the same for all types. The action of the noise leads to the appearance of fluctuation of the error signal. The component of the spectra of these fluctuations lying in the passband of the system, act on the adjustment control producing chaotic rocking of the positions of the tracing antennas. As an example, we shall evaluate the influence of the noises on the accuracy of an amplitude monopulse ASN system.

At the output of the amplifier of intermediate frequency of summation and difference channels of the system, act the high frequencies of duration $\tau_1$ and noises:

$$u_c = KU_c \sin \omega t + u_{шс}(t), \tag{8.65}$$

$$u_p = KU_c \mu \Delta\alpha \sin \omega t + u_{шр}(t), \tag{8.66}$$

where $u_s$ – voltage at the output UPCh summation channel; $u_r$ – voltage at the output UPCh difference channel; $K$ – coefficient of amplification of receiving channels (mixer of UPCh); $U_s$ – amplitude of the signal at the input of the frequency transformer; $u_{shs}$ – voltage of noises at the output of UPCh summation channel; $u_{shr}$ – voltage of noises at the output of difference channel.

The signal/noise ratio at the input of the RLS receiver, same as before, will be assumed to be sufficiently large since only under these conditions, a high accuracy of the measurement in angular coordinates is possible.

The error signal in the amplitude system is obtained by the comparison of the voltages of the summation and difference channels at the phase detector. It will be considered that the phase detector is a simple multiplier. The voltage at the output of the phase detector is

$$u_p = k_p u_c u_p = \frac{1}{2} K^2 U_c^2 k_p \mu \Delta\alpha - \frac{1}{2} K^2 U_c^2 k_p \mu \Delta\alpha \cos 2\omega t + \\ + \mu u_{шс}(t) KU_c k_p \Delta\alpha \sin \omega t + u_{шр}(t) KU_c \sin \omega t + u_{шс}(t) \cdot u_{шр}(t) \tag{8.67}$$

The first member of Formula (8.65) proves itself to be the useful signal proportional to the deviation of the object from the antenna axis. The second component of the error voltage has high frequency $2\omega$ which is suppressed by the output of the filter. The remaining three components of the error signal are interferences. At a large signal/noise ratio, ($u_{sh} \ll U_s$) and small deviation of the

object from equisignal direction ($\mu\Delta\alpha \ll 1$) the third and fifth terms in Expression (8.67) may be neglected. Under these assumptions

$$u_p \approx \frac{1}{2} K^2 U_c^2 k_\alpha \mu \Delta\alpha + u_{nc}(t) K U_c \sin\omega t.$$

As it was shown earlier, for the evaluation of the accuracy of the system, it is necessary to find the spectral density of the error signal. In the given case, the simplest way to find it is through the correlation function of the component of the interference voltage $u_r$. It will be assumed that the filter at the output of the phase discriminator does not distort from the right-angled form of the pulse signal. Then the process, happening during the flow of the pulses may be considered as continuous. The correlation function of the fluctuation of the output voltage of the phase discriminator is

$$R_p(\tau) = \overline{u_m(t)\, u_m(t+\tau) \sin\omega t \sin\omega(t+\tau)}\, k_p^2 K^2 U_c^2 = \\ = \frac{1}{2} k_p^2 K^2 U_c^2 R_{nч}(\tau) \cos\omega\tau, \qquad (8.68)$$

where $R_{pch}(\tau)$ – correlation function of noise at output of UPCh.

As it is known, $R_{pch}(\tau)$ may be described in the following form

$$R_{nч}(\tau) = r(\tau)\cos\omega\tau, \qquad (8.69)$$

where $r(\tau)$ is a slowly varying function whose nature is determined by the width and shape of the UPCh frequency characteristic.

Substituting the value $R_{pch}(\tau)$ into Formula (8.68) we obtain

$$R_p(\tau) = \frac{1}{4} k_p^2 K^2 U_c^2 r(\tau) + \frac{1}{4} k_p^2 K^2 U_c^2 r(\tau) \cos 2\omega\tau. \qquad (8.70)$$

The first term of the function $R_r(\tau)$ is determined by the low frequency component of fluctuation, lying in the passband of the tracing system. The second term is determined by the component of the error signal frequency $2\omega$, which is filtered off and does not affect the accuracy of the ASN system. Consequently,

$$R_p(\tau) \approx \frac{1}{4} k_p^2 K^2 U_c^2 r(\tau).$$

The variance of the voltage fluctuation at the output of the

phase detector is equal to the value of the correlation function when $\tau = 0$:

$$\sigma_p^2 = R_p(0) = \frac{1}{4} k_p^2 K^2 U_c^2 r(0).$$

Since $r(0)$ is the variance of the noise voltage at the output of UPCh then

$$\sigma_p^2 = \frac{1}{4} k_p^2 K^2 U_c^2 \sigma_ш^2 = \frac{1}{4} k_p^2 K^4 U_c^2 S_ш \Delta F_{пч},$$

where $\Delta F_{pch}$ – effective passband of UPCh; $S_{sh}$ – spectral density of noise at the input of UPCh.

Let us suppose that there is a switch peak detector after the phase discriminator, extending the pulses to a length equal the period of the sequence $T_p$. In a first approximation, it may be assumed that the probability characteristics of the fluctuation of the amplitude of the pulses do not change during the passage through the switch peak detector.

In this case, the process at the output of the switch detector may be looked upon as noise amplitude modulation of the 2nd kind of right-angled pulses, whose length is equal to the period of the sequence. From the theory of random processes, it is known that at noise amplitude modulation, the electrical spectra of the process have the same form as the spectra of the same pulse; while its intensity is proportional to the variance of the noise and the frequency of the repetition of the pulses:

$$G(\omega) = \frac{2}{T_п} |g(\omega)|^2 \sigma^2.$$

For the switch detector

$$g(\omega) = T_п \frac{\sin \frac{\omega T_п}{2}}{\frac{\omega T_п}{2}}.$$

Consequently, the electrical spectra of the fluctuation of the output error voltage is

$$G_0(\omega)=2\sigma_p^2 T_n\left(\frac{\sin\frac{\omega T_n}{2}}{\frac{\omega T_n}{2}}\right)^2.$$

Since the passband of the tracing system is sufficient narrow ($\Delta F_z \ll F_p = \frac{1}{T_p}$), so only the low frequency component of the spectra at near zero can produce the incidental error of the system. The spectral density of fluctuation in the regions of these frequencies is proportional to the length of the period of the sequence.

$$G_0(0)\approx 2T_n\sigma_p^2=\frac{1}{2}k_p^2K^4U_c^2T_n\Delta F_{ш}S_{ш}. \qquad (8\ 71)$$

Under this condition, the noise received by the installation may be considered as internal interference applied to the tracing system at the point 2 (Fig. 8.47) and having spectral density $G_0(0)$. In order to find the error of the tracking ASN system, it is necessary that the value $G_0(0)$ is described in Expression (8.63). After substituting, we obtain

$$\sigma_a^2=\frac{1}{2}\frac{k_p^2K^4U_c^2T_n\Delta F_{ш}S_{ш}\Delta F_э}{K_п^2}.$$

Since

$$K_п=\frac{1}{2}k_pK^2U_c^2\mu,$$

therefore the variance is

$$\sigma_a^2=\frac{T_n\Delta F_э\Delta F_{ш}S_{ш}}{\frac{U_c^2}{2}\mu^2}=\frac{1}{\mu^2}\frac{T_n\Delta F_э\Delta F_{ш}S_{ш}}{P_c}$$

or

$$\sigma_a^2=\frac{1}{\mu^2}T_n\Delta F_э\frac{P_ш}{P_c}, \qquad (8.72)$$

where $P_{ш}$ – strength of noise at the input of the RLS receiver; $P_s$ – strength of signal at the input of the RLS receiver.

Mean square value of the error of the system ASN, dependent on the action of the noise of the receiver, is increased with the increase of the period of the sequence of pulses and with the broadening of the passband of the tracking system.

If it is taken into account that at the optimum angle of dispersion of the diagram of directionality, the sharpness characteristic $\mu \approx \frac{1.4}{\theta_0}$, then Formula (8.72) may be written as

$$\sigma_\varepsilon^2 \approx \frac{\theta_0^2}{2} T_u \Delta F_\text{э} \frac{P_\text{ш}}{P_\text{с}}.$$

Approximately one may assume that the ASN system integrates the pulses during the time $T_1 = \frac{1}{\Delta F_\text{э}}$. Consequently, the number of pulses, accumulated by the tracking system is

$$N = \frac{T_1}{T_\text{и}} = \frac{1}{\Delta F_\text{э} T_\text{и}}.$$

Substituting $N$ in Formula (8.72), we obtain

$$\sigma_\varepsilon = \frac{\theta_0}{N\sqrt{a}},$$

where $a^2 = \frac{2U_\text{с}^2}{\sigma_\text{ш}^2}$.

The variance of the error is inversely proportional to the signal/noise ratio at the output of the receiver.

As a consequence of Formula (8.72), it may be considered that noises only act during the time of the receiving of useful signals, i.e., assuming the presence of ideal gating of the receiver. If there is no gating in the receiver or the length of the gating pulse is greater than the length of the pulse signal, then the variance of the error voltage fluctuation $\sigma_\text{osh}^2$ is increased on account of the effect of the ejection of noises not coinciding in time with the useful signals. The increase of $\sigma_\text{osh}^2$ leads to the rise of the errors of tracking of the ASN system. Fig. 8.49 shows a graphic dependence of tracking error on the coefficient of gating, which is understood to be the ratio

of the selected pulses to the length of the pulse of the signal. The graph indicates that the increase of the coefficient of gating may lead to a considerable rise of the errors of the tracking systems. The effect of gating is less with the increase in the signal/noise ratio.

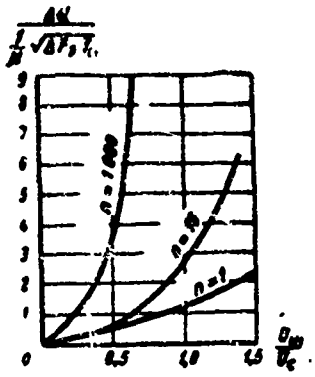

Fig. 3.49 Error of autotracking as a function of the coefficient of gating.

The above method of the determination of error, dependent on the internal noises of the receivers, may be also employed for the estimate of accuracy of phasal monopulse systems, ASN and RLS with conical rotation of the antenna beam. This same method may be used for the determination of the accuracy of the ASN system during the action of external interferences. It should be noted however, the formula obtained is valid under the condition $P_s/P_{sh} >> 1$.

2. Effects Of Amplitude Fluctuation Of The Reflected Signal

Amplitude fluctuation of the reflected signal is based on the sources of angular errors in the ASN systems with conical rotation of the antenna beam. The sensitivity of such systems to the amplitude variations of the reflected signal is demonstrated by the fact that the direction toward the object in them is determined by the comparison of the amplitudes of the signals obtained at different moments of time. In monopulse RPS, the angular coordinates are determined by the simultaneous comparison of the signals obtained from the different antennas therefore in them, in principle, the effect of amplitude pulsation may be set aside.

We shall examine now the accuracy of the ASN systems with conical rotation of the beam during tracing of the fluctuating object.

The fluctuating amplitude of the reflected signal may be expressed as

$$U = U_0\left[1 + \frac{\Delta u(t)}{U_0}\right] = U_0[1 + m(t)],$$

where $\Delta u(t)$ – fluctuation of reflected signal of average value $U_0$; $m(t)$ – coefficient of amplitude modulation, dependent on the pulsation of the signal.

Since the antenna beam rotates with the frequency $\Omega$, therefore, the envelope of reflected pulses at the output of the receiver RLS is described by the expression,

$$U = U_0[1 + m(t)][1 + \mu\Delta\psi\cos(\Omega t - \varphi)] =$$
$$= U_0[1 + m(t) + \mu\Delta\psi\cos(\Omega t - \varphi) + m(t)\mu\Delta\psi\cos(\Omega t - \varphi)].$$

After passing through the filter adjusted to the frequency $\Omega$ the constant component of the error signal is separated voltages falling on the phase detectors of the azimuth channel as well as on those of the angle location channel.

$$U_{0m}(t) = U_{0\mu}\left[\frac{m(t)}{\mu} + \Delta\psi(t)\cos(\Omega t - \varphi) + m(t)\Delta\psi(t)\cos(\Omega t - \varphi)\right].$$

The voltage at the output of the phase discriminator of the azimuth channel may be described by the expression (for simplicity, assume $\varphi = 0$

$$u_p(t) = A_1[\Delta\alpha(t) + \frac{2}{\mu}m(t)\cos\Omega t + m(t)\Delta\alpha(t) +$$
$$+ \Delta\alpha(t)\cos 2\Omega t + m(t)\Delta\alpha(t)\cos 2\Omega t],$$

where $A_1$ – coefficient, independent of time.

The voltage $u_r$, after filtration reaches the executing device, controlling the position of the antenna. Obviously, what brings about the displacement of the antenna can only be that component voltage $u_r$ in the spectra of the frequency of which there is sufficient intensity consisting of diapasons from zero to $\Delta F_z$. The useful signal, $A_1\,\Delta\alpha(t)$ characterizing the motion of the object, is a slow changing

function of time, whose frequency spectra lies practically entirely within the boundaries of the zones $\Delta F_e$. The component $A_1\ \Delta\alpha(t)\ cos\ 2\Omega t$ is suppressed by the filter of low frequency since in the system of autotracking of angular errors $\Delta\alpha(t)$ is extremely small, hence the action of the items $m(t)\Delta\alpha(t)$ and $m(t)\cdot\Delta\alpha(t)\ cos\ 2\Omega t$ are small in comparison with the action of the term $\frac{2}{\mu}\ m(t)\ cos\ \Omega t$. Consequently, in a first approximation, the expression for the error signal may be written as

$$u_p(t)=A_1\left[\Delta\alpha(t)+\frac{2}{\mu}m(t)\cos\Omega t\right].$$

The effect of the amplitude pulsation of the reflected signals leads to a condition such that the a fluctuation voltage $\frac{2}{\mu}\ m(t)\ cos\ \Omega t$ is added to the error voltage produced by the diviation of the object from the antenna axis.

This voltage may be considered as interference, applied at the point 2 (see Fig. 8.47). The error of the systems of autotracking, in this case, may be determined by Formula (8.59). The spectral density of the equivalent interference is found by its correlation function. By determining,

$$R_\text{в}(\tau)=\overline{\frac{4}{\mu^2}m(t)\,m(t+\tau)\cos\Omega t\cos\Omega(t+\tau)}\,. \qquad (8.73)$$

Since the fluctuation $m(t)$ is independent of the position of the antenna beam, therefore, the signals $m(t)\ cos\ (\Omega t+\varphi)$, differing only in phase, are equally probable. Hence Expression (8.73) may be written as

$$R_\text{в}(\tau)=\overline{\frac{4}{\mu^2}m(t)\,m(t+\tau)\cos(\Omega t+\varphi)\cos[\Omega(t+\tau)+\varphi]}\,. \qquad (8.74)$$

Averaging according to all the possible values of phase $\varphi$, we obtain

$$\frac{1}{2\pi}\int_0^{2\pi}\cos(\Omega t+\varphi)\cos\ \Omega(t+\tau)+\varphi]\,d\varphi=\frac{1}{2}\cos\Omega\tau.$$

Consequently,

$$R_a(\tau)=2R_m(\tau)\cos\Omega\tau,$$

where $R_m(\tau)$ – correlation function of amplitude fluctuation of the reflected signal.

The spectral density of interference, of the equivalent actual amplitude fluctuation, is equal to

$$G_a(\omega)=2\int_0^{\infty}R_a(\tau)\cos\omega\tau d\tau=G_m(\omega-\Omega)+G_m(\omega+\Omega), \qquad (8.75)$$

where $G_m(\omega)$ – spectral density of amplitude fluctuation of the reflected signals (Fig. 8.50 and 8.51).

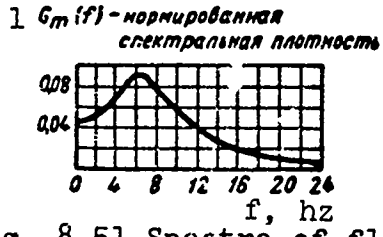


Fig. 8.51 Spectra of fluctuation of signals reflected from airplane. 1) Normalization of special density.

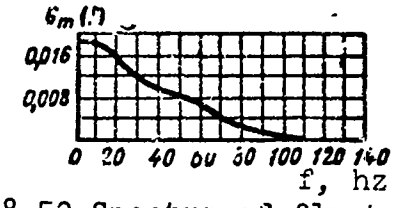


Fig. 8.52 Spectra of fluctuation of signals reflected from a ship.

The spectra of the interferences, dependent on the action of the amplitude fluctuation of the reflected signal, are equal to the sum of two spectra of amplitude fluctuation, displaced according to the frequency axis corresponding to the values $+\Omega$ and $-\Omega$. The form of the spectra of the fluctuation of error voltage is shown in Fig. 8.52. In the passband of the tracking system, the spectral density of the interferences, may be assumed with sufficient degree of accuracy, as a constant value approximately equal to $2G_m(\Omega)$. In actual ASN systems with conical rotation of the antenna beam, the autotracking error dependent on the amplitude fluctuation comes to $(1\cdot10^{-3}\div1\cdot10^{-2})°$ (see [7] to Chapter 1).

In monopulse system ASN, the fluctuation of amplitude of signals being received also may lead to errors in the measurement of angular coordinates. This is explained as follows. In any actual systems of angular tracking, errors always exist depending on the dynamic retardation of the tracking systems, the action of internal noises, etc. The presence of errors of tracking indicates that the axis of the antenna is always somewhat deviated relative to the direction towards the object and consequently, at the output of the sensitive elements of the system in any moment of time, there exist error voltages

$$u_{0m} = kU\Delta\psi,$$

where $\Delta\psi$ -- summation angular error of tracking without taking into consideration the effects of amplitude fluctuation; $U$ – amplitude of reflected signal; $k$ – coefficient of proportionality.

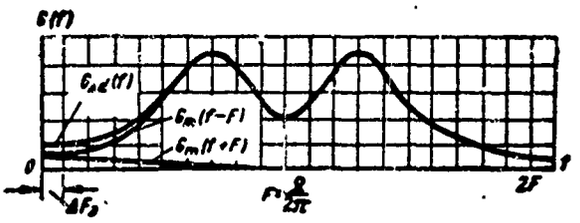


Fig. 8.52. Spectra of interferences, caused by amplitude fluctuation of the signals being received.

The amplitude fluctuation of the reflected signal leads to modulation of the error signal

$$u_{0m} = kU_0\Delta\psi + k\Delta u(t)\Delta\psi, \qquad (8.76)$$

where $\Delta u(t)$ – amplitude fluctuation of the signal reckoned relative to the mean value.

The second item in Expression (8.76) consists of the error voltage produced in the variation of the amplitude of the reflected signal. This is composed of the errors not connected with the true errors of tracking and therefore, does not carry any useful information. Besides,

in distinction fr m the errors, produced by the dynamic retardation of the tracking system, by the internal noises and by the variation of the angle of arrival of the reflected signal, the component, $k\Delta u(t)\Delta\psi$ appears to be a function of the very error of tracking and grows with its increase. Since in the voltage spectra, $k\Delta u(t)\Delta\psi$ practically always contain the component, falling in the passband of the tracking system, therefore the total error of tracking will always be increased.

For the control of the effects of the amplitude fluctuation of the reflected signal on the accuracy of autotracking, it is necessary to introduce a fast acting ARU system. The inertness of the ARU system should be such that all fluctuations whose spectra lie within the boundaries of the passband of the tracking systems, are effectively suppressed. Only under this condition, there will be practical control of the tracking errors arising from the amplitude fluctuation of the reflected signal.

3. Effects Of The Fluctuation Of The Angle Of Arrival Of The Reflected Signal

Fluctuation of the angle of arrival of the reflected signal may be considered as external interference applied to the ASN system at the point 1 (Fig. 8.47). Then, the error of the system may be computed by Formulas (8.57) and (8.60). If the width of the spectra of fluctuation, $F_{max.}$ is less than or equal to the passband of the system $\Delta F_э$ then variance of the error will be equal to the variance of the fluctuation of the position of the effective center of the reflection. However, if $F_{макс} > \Delta F_э$, then in a first approximation, the error of the system may be determined by the formula

$$\sigma_э^2 = \sigma_\theta^2 \frac{\Delta F_э}{F_{макс}},$$

where $\sigma_\theta^2$ – the variance of the fluctuation of the angle of arrival of

the reflected signal.

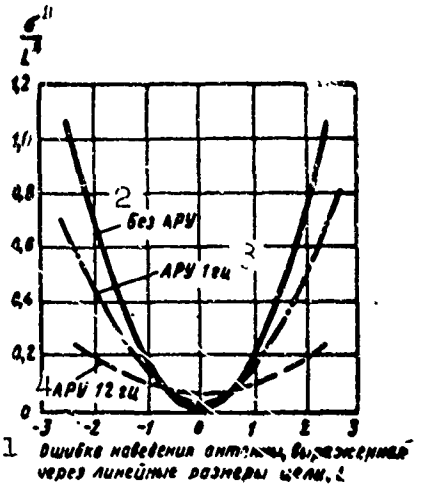


Fig. 8.53. Dependence of mean square error arising from fluctuation of the center of reflection and the amplitude of the signals on the error of induction antenna at various width of the passband of the ARU system. 1) Error of induction antenna, expressed in linear dimensions of the object $L$; 2) without ARU; 3) 1-hz ARU; 4) 12-hz ARU.

At average and large distances of the angular dimension of the object and consequently $\sigma_\theta^2$ is small. Therefore the error $\sigma_\alpha$ is also extremely small. At close distances, the fluctuation of the angle of arrival of reflected signal has considerable magnitude and the error of the ASN system dependent on these fluctuations, may prevail over all other errors.

Fig. 8.53 shows the results obtained from experiments of graphic dependence of the total error of tracking, dependent on the fluctuations of the angle of arrival of the reflected signal and the fluctuation of amplitude on the error of the induction antenna according to the object. The graph given is for ARU system with various time constants. It is interesting to note that at small angles of deviation of the antenna from the object, the errors of the system with the fast acting ARU exceed those of the inert ARU. This fact explains, in magnitude, that at small distances, the error is determined by the fluctuation of the center of reflection. As it was said previously (§8.1), at considerable deviation of the effective center of reflection from the center of the

object the amplitude of the signal being received drops. Therefore, the ARU system having boosted the amplification of the receiver during the weakening of the signal, will also amplify the error of the ARU system dependent on the fluctuation of the center of reflection. Consequently, at small distances, the cases of using the ARU system in the monopulse ASN stations may be unsuitable. For the most part, the use of the fast acting ARU will be the more effective, the larger the internal interference of the tracking system and when its equivalent passage zone is wide.

4. Total Error Of The System Of Autotracking. Besides the angular errors examined previously, in the ASN systems, other errors of tracking may also arise, dependent on the presence of zone insensitivity, gaps and friction in the mechanisms owing to the drifting of the zero of the amplifier of constant current, unbalance in the circuit of the drive amplifier and so forth. The magnitude of these errors does not depend on the character of the object nor does it depend on its distance but is determined entirely by the class of accuracy of the mechanisms used and the stability of the operation of the electric circuits.

The total error of the system of automatic tracking by direction may be determined as a mean square value of all the errors. A graph is shown in Fig. 8.34 indicating the qualitative character of the dependence of the total error on the distance of the object. It can be seen from the graph that the best tracking is obtained at average distance where the error components caused by the fluctuation of the center of reflection and the interferences of the receiver are small. Errors of the ASN systems at small distances are basically determined by the fluctuation of the angle of arrival of the reflected signal

and at maximum distance – the noises of the receiver.

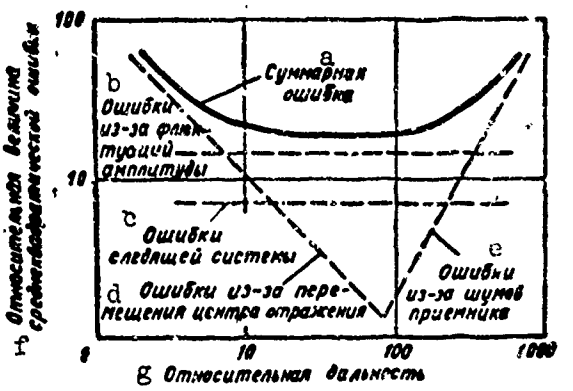


Fig. 8.54 Dependence of mean square error of the ASN system on the distance of the object. a) Total error; b) errors due to amplitude fluctuation; c) errors of the tracking system; d) errors of the shifting of the center of reflection; e) errors from the noises of the receiver; f) relative rms error; g) relative range.

## §8.9 COMPUTATION OF ANGULAR COORDINATES BY THE BINARY CODE

The representation of the angle in the form of numbers leads to the appearance of instrumental errors, dependent on the discreteness of the reading of the angle, since any position of the actual value of the angle in the boundaries of any such interval of discreteness $\Delta\alpha$ are equally probable, the mean error value of instrumental error of conversion is

$$\sigma_{\alpha\text{и}} = \frac{\Delta\alpha}{2\sqrt{3}}. \qquad (8.77)$$

The discreteness of the reading $\Delta\alpha$ should be selected such that the value $\sigma_{\alpha i}$ would be 2 to 3 times smaller than the mean square value of all the remaining errors taken together. Then, the error owing to the discreteness almost will not increase the total error. The increas of discreteness $\Delta\alpha$ in comparison with the indicated value leads to the rise of the total error; considerable decrease of the discreteness brings about unjustified increase of the number of digits and the complication of the apparatus.

In the devices of representation of the angle in binary numbers, incorrect and worn out circuits – connections, are possible. They may lead to large errors and should be unconditionally excluded.

There exist two methods the circuits of which are on the angular position of the object:

-- the calculation of the position of the axis of the antenna RLS in a certain moment of time;

– the measurement of the amplitude of the voltages in the various channels of the multichannel RLS.

Corresponding to these representations of the angular position of the object, in the form of binary codes, they lead to the operations:

– converting the angle of rotation into numbers or

– converting the voltage into numbers.

1. Converting The Angle Of Rotation Into Numbers Of The Binary Code

It is possible to convert the angle of rotation directly or indirectly into numbers. During the direct conversion, the angle of rotation is given in the form of numbers without intermediate operations. During the indirect conversion, the angle of rotation is converted, in the beginning, into time intervals or voltages proportional to the angle. Afterwards, conversion is carried out on the obtained values into numbers with the help of a circuit which we have already seen or will examine below. During the indirect conversion, there arise considerable errors, dependent on the intermediate operations.

The direct representation of the angle of rotation in the form of binary numbers may be carried out with help of converters of two forms: accumulational converter and positional converter. Below, a description of the principle of operation of these converters is introduced and the measures of preventing knockdowns are indicated.

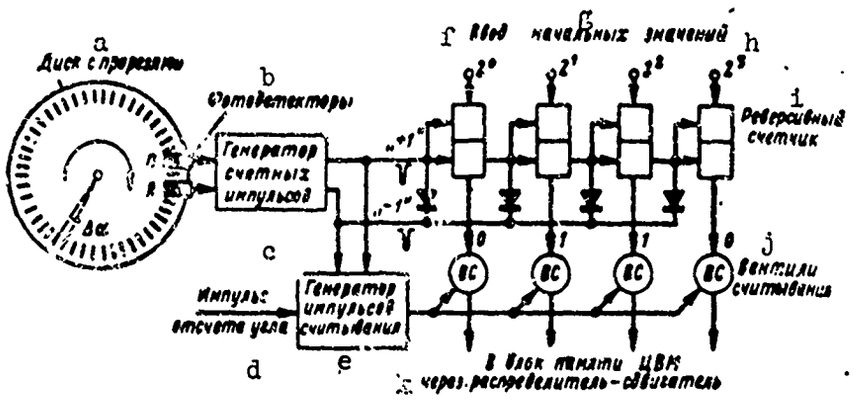


Fig. 8.55 Accumulational converter of angle of rotation into numbers. a) Disk with slits; b) photodetectors; c) generator of counting pulses; d) pulse of the angle reading; e) generator of pulses of computing; f) intake; g) initial; h) value; i) reverse counter; j) valve of computing; k) into memory block TzVM through distributor-shifter.

Accumulational converter of angle of rotation into numbers. One of the variations of the circuits of accumulational converter is depicted in Fig. 8.55. On the axis of the antenna is fixed rigidly a disk with slits distributed on its periphery with equal distance from each other. Angular displacements between the slits $\Delta\alpha$ is the discreteness of reading. On one side of the disk is located a light source, not shown in the drawing, on the other – a photodetector (photoelement) at the output of which pulse current appears every time when a sequence of lighted slits shows up opposite it. With the help of counters, the number of pulses of the photodetector is counted up

$$N_\alpha \approx \frac{\alpha}{\Delta\alpha},$$

which is proportional to the angle of rotation $\alpha$, read from a certain original direction.

In view of the fact that in general cases, the rotation of the antenna axis may take place in both sides, a reverse counter and not an ordinary counter is used. At the rotation of the antenna in the side of the increased angle, the reverse counter shows the arrival of

a series of pulses growing in units, during the rotation of the antenna in the side of the diminished angle, the counter shows a decrease. For this reverse counter, there are two inputs, addition and subtraction, on them fall the pulses "+1" and "−1" correspondingly. These pulses are produced by the generator of counting pulses: pulse "+1" at the right turn of the antenna and "−1" of the left.

In order to make the generator of counting pulses sensitive to the side of displacement, not one photodetector but two are installed. The photodetectors are mutually positioned such that their pulses follow one after the other very closely during the rotation of the disk.

During a right turn, the pulse of the photodetector *P* appears first. In the generator of counting pulses it is amplified and proceeds to the totalling input of the counter as "+1" Simultaneously, this pulse paralyses the amplifier of the pulses of the second photodetector, the pulse of which is suppressed.

At a left turn of the disk, the first pulse is the one from photodetector *L*, which after amplification, comes out as "−1" and suppresses the pulse from the right photodetector immediately following it.

With the entry of the pulse "+1" at the totalling input of the reverse counter, the processes in it goes on exactly like in the counter of distance since pulses have negative polarity and thanks to the valve, the circuit of the second input is switched off.

The computing units of the double numbers lead to the augmentation of units written in complementary codes. In the straight 4th order code, unity is written as *0001*, in reverse, as *1110* (zero and one exchange places) in the complementary code as *1111* (in the reverse code the numbers are made up of units of low digit).

Under this condition, for a decrease of the numbers written in the counter to unity it is necessary to augment the number *1111*, i.e., feed the pulse immediately to all digit counters. For this, the subtracting input of the reverse counter is closed parallel to the inputs of all triggers.

Let us show that during the entry of the negative pulse "-1" into the input of the counter, its reading is lowered to unity. Let there be an established number *0110 (6)* in the counter. With the arrival of the next "-1" pulse, the condition of all triggers simultaneously change to the opposite position and establish the number *1001*. In a very short fragment of time, at the output of the triggers $2^1$ and $2^2$ there appear transfer pulses, since in these triggers there have been a transfer from 1 to 0. The pulse of the trigger $2^1$ changes the condition of the trigger $2^2$ from 0 to 1 and thepulse of the trigger $2^2$ changes 1 to 0 in trigger $2^3$. In the counter the number *0101 (5)* is established, which also demands to be accepted.

At a lowering of the distance between the slits, the accuracy of the angle reading may be increased by the method of verniers. For this, it is necessary to install as many photodetectors as the number of times of the demand of raising the increase of the accuracy of the reading. The distances among the detectors are chosen in the same relationships to distances between the slits as the intervals between pulses of the vernier and the intervals between the counting pulses at a higher precision of distance.

With the entry of the series of counting pulses into the counter, the conversion processes start. The computed reading of the counter during the time of the conversion process may lead to itself. Therefore, the release of the readings is not originated by the pulses of the angle reading themselves entering from the RLS but by the pulses

of the computation which are generated by special generators with the intake angle reading, when the conversion process in the counter is ended. The working principle of the generator of pulses of computation is the same as in the distance converter. The computed readings of the counter enter into the memory cells of the TzVM.

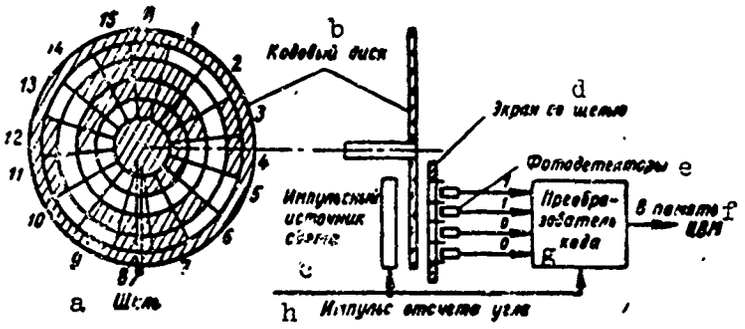


Fig. 8.56. Positional converter of the angle of rotation into numbers. a) Slot; b) code disk; c) pulse light source; d) screen with slots; e) photodetectors; f) into memory of TzVM; g) code converter; h) pulse of angle reading.

The basis of the accumulational angle converter is the reverse counter which counts only the increments of the angle positive or negative. Therefore, before the start of the operation, it is compulsory to establish in the counter the initial reading of the angle, otherwise, its reading and the readings of the angular position of the object will be incorrect. Here is its drawback.

A second drawback of the accumulational converters, – the keeping and accumulation of the errors, appearing by chance in the counters. Therefore, it is required to check its readings periodically.

A third drawback is the lengthening of the pulses entering from the photodetectors when the velocity of the rotation of the disk is close to zero that it may appear to be the reason itself.

Positional converter of the angle of rotation into numbers. The positional converters are free from the drawbacks peculiar to the

accumulational converters.

Figure 8.56 shows a schematic diagram of an optical positional converter with code disks, the principle of its operation consists of the following:

On a transparent disk fastened directly on the rotating axle of the antenna, transparent and nontransparent portions of code combinations are applied to it by photoprocesses. The code on the disk is applied in a series of stakes (digits) such that every discrete value of the angle rotation corresponds completely a definite nonrepeating combination of light and dark portion arriving opposite the slot in the screen. On one side of the disk is located an elongated pulse light source, on the other – screen with a narrow slot allowing the passage of light in the miniature photodetectors, the number of which corresponds to the number of digits. The photodetectors which are opposite the transparent portion of the disk during the moment of lighting are illuminated and produce pulses (one) while the photodetectors located opposite the nontransparent portion are not illuminated and produce nothing (0). The photodetectors optically isolate themselves so that the light current from the transparent zone of one digit does not fall on the photodetectors of the other digits.

The computation of the angle in binary code is carried out in the following manner. Let, at the moment of the arrival of angle reading pulse, a lighted and dark portion of the disk which corresponds only to that angle opposite the slot. The pulse of the angle reading, proceeding from the discriminating device of the receiver, effects the lighting of the light source. At the output of the illuminated photodetectors, flows a pulse current (one). The zeros and ones obtained from all the digits of code combinations correspond to the positions

of the antenna axis during the moment of counting and consequently, also the angle of the position of the object. The computed combinations, in principle, may be directly fed into the TzVM memory.

In doing this, the device seems considerably complex since it is necessary to prevent itself during counting when opposite the slot there is established a boundary of conversion from one number to the other. Thus, at the boundaries of the numbers *0111 (7)* and *1000 (8)* zero and one exchange places in all the four digits and may be considered as any number from zero (all zeros) to 15 (all ones).

Special codes are employed to exclude these computations in the converter - V-code and cyclic code. Before entering the intake of the TzVM, they are necessary to be converted back to normal binary code and for this a code converter is included in the diagram (see Fig. 8.56).

During the use of the V-code, on the disk the normal binary code is printed, but the computing of the numbers in all digits excepting the small ones, are carried out not by one but by two photodetectors: one computes the numbers from the front and the other from the rear. The distance between the photodetectors grows with the number of digits, as a result they form a figure in the shape of the letter V, the top of which is a single photodetector of low digit. From this, the V-code gets its name.

The use of the V-code is based on the following properties of the binary numbers: the conversion of zero to one in any digit is never accompanied by the changes of the condition in the following digits, while the conversion of one to zero always alters the condition of the following digits in the opposite position (transfer of one). Therefore, when in the given digit at the boundaries of two discrete values, the count is zero, no error happens, if in the following digit the computing is

carried out from the front while when the count is one – from the rear.

On the basis of this logic, the code converter with the help of the special circuit determines, which of the readings from the two photodetectors to be fed into the TzVM in order to exclude incorrect readings.

We shall not go into the details of the cyclic coding of binary codes (Grey's code).

Figure 8.57 shows a portion of the cyclic code combination of 16 positions of the disk. The light places correspond to the transparent portions of the disk, giving one during computation. The dark places correspond to zero. For the sake of convenience, the digits are arranged not in the form of wheels, but in the form of straight bands. Here also, for the sake of comparison, entries of the numbers in the decimal code are included as well as the cyclic and normal binary codes.

The cyclic code combinations are formed in the following way. The transparent portion of the small digits have the shape of bands occupying the length of two intervals of the angle reading and is also divided by two intervals. The transparent portions of the following digits are in the form of longer bands superimposing on every separate pair of bands of small digits. At this, exactly half of every band of a pair of small digits is overlapped.

In Fig. 8.57, it can be seen that every ensuing number of the cyclic code differs from the preceding one always only in one digit. Owing to this, errors during the counting of numbers at the boundaries of two parts cannot surpass one of the small digits in which an interchange of one to zero or vice versa takes place. Actually, let the boundaries of the positions *0100 (7)* and *1100 (8)* approach opposite the object. The photodetectors of the first three digits positively read *0*, *0*, and *1* (transition processes in these digits are absent),

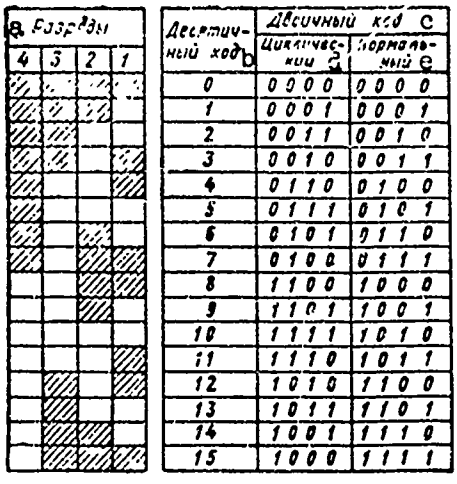


Fig. 8.57. Cyclic Binary Code (Grey Code). a) Digits; b) decimal code; c) binary code; d) cyclic; e) normal.

while the photodetector of the fourth digit may read either 0 or 1. In the first case, it will count the number *0100 (7)* and in the second *1100 (8)*. The error actually does not exceed one, although nonuniformity is observed in the older digit.

The numbers obtained in the cyclic code are fed into the computer. In principle, a converter may be built directly converting parallel cyclic code into parallel binary code. But, the scheme of conversion is obtained much simpler, if it operates with the code converter. Therefore, in the beginning a conversion of cyclic code from the parallel to the serial is conducted and then a conversion of the serial code from the cyclic into the normal binary code is made.

The conversion of parallel code into serial is accomplished in the shift registers. The shift registers look extremely simple. They consist of magnetic ferrite transformers whose residual magnetic induction may be either positive (recorded by 1) or negative (recorded by 0).

A schematic diagram of the shift register using ferrite transformers with the oscillograms of the processes on the basis of its image points are shown in Fig. 8.58. For the operation of this circuit, serial time pulses (shift pulse) are used. Let us examine this system in the example of the conversion of the number *1101*.

Before the recording of parallel code all the cores of the transformers are magnetized in the direction of C, therefore the shift pulse is continuously being entered at zero from the windings of the

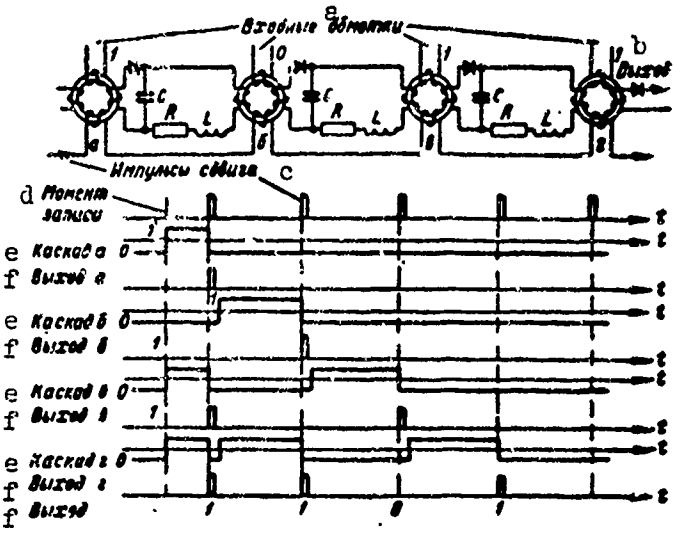


Fig. 8.58. Shift register using ferrite transformers and the processes in them. a) Input winding; b) output; c) shift pulses; d) record moment; e) cascade; f) output.

transformers and the cores being magnetized also in the direction of 0. No changes whatsoever is produced in the scheme. At the arrival of the pulse, the current from the output of the photodetectors to the corresponding input of the windings of the transformers produces a reverse magnetization in Direction 1 (cascades a, v, and g).

With the arrival of serial shift pulses, there is a reverse magnetization in the cascades a, v, and g again back in the direction of 0. At the moment of transfer to the output windings of these cascades there is a transfer of short pulses. Thanks to the diodes at the output of every transformer, there appear only positive pulses corresponding to the moment of transfer of the cores from Condition 1 into Condition 0 and the reverse action of information is prevented.

The pulses obtained in the output of the cascades a and v produce a corresponding magnetization of the cores of the cascades b and g in Direction 1. The small circuit RS and the small inductivity in the circuit of magnetization guarantee any retardation necessary in order that the magnetization of the cores by the pulses of transfer takes

place after the action of the shift pulses. This path accomplishes the shift of the number in digits one step in the direction to the output, whereupon the first one is dislodged from the register.

With the arrival of the following shift pulse, at the output of the circuit, the following 1 of Number *1101* is delivered while the transfer pulse of cascade b magnetizes the core of the cascade v in the direction of 1. The number in the register is shifted two steps whereupon two figures find themselves beyond the limits of the shift register.

The third shift pulse excites only the processes in cascade v, therefore, at the output of the circuit, there will be no pulses that correspond to zero of the serial code. The transfer pulses received in cascade v produce magnetization of the core of the next cascade in the direction of 1. In the register, the last figure remains, the remaining three find themselves beyond its boundaries.

Finally, the fourth shift pulse dislodges the last one from the shift register. At the output of the circuit, Number *1101* is shown in serial code.

The conversion of code from the cyclic to the binary is accomplished by rules which are easily established from the analysis in Fig. 8.57. They are included in the following. If the numeral of the given digit of cyclic code is preceded by an even count unit (including zero units) then that numeral is converted into the binary code without change, if the count preceding "one" is odd, the numeral changes in the opposite direction. As a consequence of this rule, it follows that the old "one" always remain unchanged, while the numeral that follows it always changes to the opposite position.

Logic circuits, converting serial cyclic code into binary according to the above rule, is illustrated in Fig. 8.59.

The circuit directs all output numerals of cyclic code into one of two channels in correspondence with them such that even or odd number of units came to the circuit before that numeral. For this, the circuit has a counter of parity in the form of a trigger and two valves of coincidence (BC) controllable from this counter and producing "sorted" numerals and also an inverter for the conversion of 0 to 1 and 1 to 0.

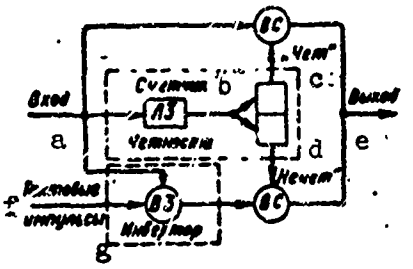


Fig. 8.59. Converter of cyclic code into normal binary code. a) Input; b) parity counter; c) "even"; d) "odd"; e) output; f) time pulses; g) inverter.

At the moment of the arrival of old ones (pulse), the counter unit is always located in the position "even," i.e., gives "high" voltage to the valve of the upper channel. Therefore, old ones pass through the upper valve without change. This same one causes the tripping of the trigger into the position "odd." A small linear delay (inductivity) is introduced into the circuit in order that the tripping of the trigger is not effected earlier than the pulse has successfully passed through the valve.

At the moment of the arrival of the second numeral, the lower coincidence valve is opened. The second numeral passes through it at the input of the circuit, having been previously changed in the inverter into the opposite position.

The inverter presents itself as a prohibiting valve (BZ), prohibiting the input pulse of the code. At the second input of the prohibiting valve, is fed the time pulse, the moment of the arrival of these pulses coincide with the time current of the cyclic code.

If the second numeral proves to be one (pulse), then it closes the prohibiting valve, not passing through coinciding with the moment

of the passing of the time pulse. At the output of the circuit in this case, the time current will be zero Almost simultaneous with this, the output pulse trips the trigger of the parity counter and the circuit is ready for the passage of the next numeral at the output of the circuit through the upper channel.

When the second numeral is zero, there is no shutting-off pulse at the input of the prohibiting valve in the inverter, and the time pulse freely passes through the prohibiting valve, and then through the coincidence valve of the lower channel to the output of the circuit. Zero at the input of the circuit is changed into one at the output. In this case, the trigger of the parity counter remains in the preceding position which will be maintained to the time when "one" enters the circuit. At the arrival of "one" which at the open lower channel becomes zero at the output of the circuit. The trigger operates anew readying the circuit for the passage of the next numeral through the upper channel, etc.

It is easy to check the regularity of this circuit, take for example converting Number 9 from cyclic code (*1101*) into binary (*1001*). The first "one" passes through without change the upper channel and also set the counter in the position "odd;" the second numeral (1) is changed into zero at the output and set the counter in the position "even;" the third numeral (0) passes through the upper channel without change, the second channel remaining open through which eventually the next 0 passes through unchanged and the fourth numeral (1).

By a special command of the counter, the "one" at the end of the transmission of the number, sets it in the position "even" readying the circuit for the passage of the next number.

The shortcoming of the positional converter of angle into number appears to be the complexity of the circuit owing to the code converter

and also the difficulty of disposing large number of digits and the photodetectors when the code disk is of limited dimensions. From this viewpoint, it is better to use code drums although the devices so built will have less compactness.

2. Conversion Of Voltage Into Numbers In Binary Code.

Among the many different forms of converters of voltage into numbers, let us examine the two circuits:

– circuit of electron commutator, and,

– circuit with intermediate conversion into time intervals.

*Electron commutator circuits.* The circuit of converting voltage into number with the help of electron commutators (Fig. 8.60) distinguishes itself by its high speed and is a typical example of the quantization of voltage by amplitude.

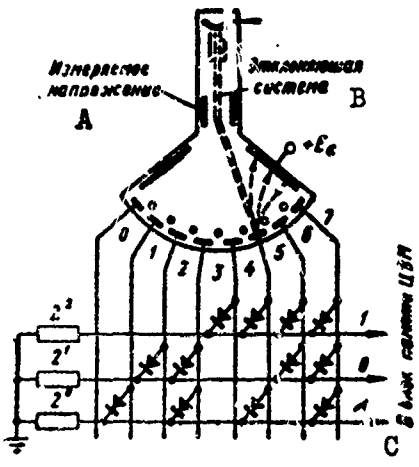


Fig. 8.60 Circuit of conversion of voltage into number by electron commutator. A) Voltage being measure; B) deflecting system; C) into the memory block of TzVM.

The voltage being measured falls on the deflecting plates of the electron commutator producing a deflected electron beam at an angle proportional to that voltage. The electron beam falling on one of the electrodes gives rise to a second electron emission, the electrode becomes positive and current flows in its circuit. The input voltage is converted into the number of that electrode in the circuit of which current flows. With the help of matrix circuits in diodes and resistances, this number is given at the output bar in binary code.

For the prevention of knockdown in the case of a fall of the electron beam on two electrodes simultaneously, the number of electrode is converted not in the common but rather in the cyclic binary code or

even by placing between the electrodes a negatively charged conductor producing complementary displacement of the electron beam to the side of one of the electrodes.

Converters of this type, when the number of electrodes is small (the order of ten) are sufficiently simple in principle and the dimensions do not exceed those of a receiving-amplifying tube of normal range. But when the number of electrodes is large, the device becomes very complicated in manufacturing.

*Circuits with intermediate conversion of voltage into time intervals.* Two types of converters use the properties of some circuits (phantasstrons, sanatrons, circuit of comparison of the growing voltage with the one being measured, etc.) producing pulses, the length of which are proportional to the voltage (pulses modulated according to length). The same measurement of voltage leads to the measurement of time interval that is already known.

The principle of conversion of voltage into pulses of corresponding duration is shown in Fig. 8.61. The voltage is measured through a period of time with the help of special pulses of inquiry (quantized by time) the frequency sequence of which should satisfy Kotelnikov's theorem on readings. In case of measurement of amplitude of pulse signals in different channels of RLS, inquiry is accomplished by the pulses of the summation channel.

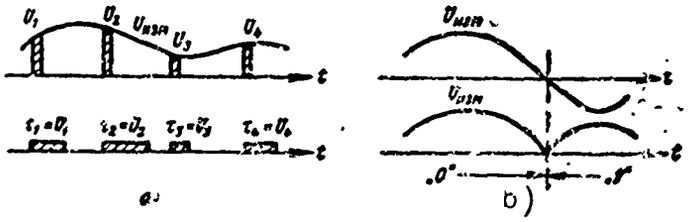

Fig. 8.61 Conversion of voltage into number. a) Conversion of amplitude of pulse readings into time intervals; b) conversion of double polar voltages into the form of amplitude and signs.

Every time with the entry of inquiry pulses, phantastron or other similar device is triggered producing gating whose amplitude is constant but the duration is proportional to the voltage being controlled. Expressed descriptively, the pulses being measured are "buried from side to side." (Fig. 8.61a).

During the measurement, negative voltages are converted beforehand into the positive by the inverter. The voltages received in the inverter are used also for the formation of one's (sign negative) in the sign digit (Fig. 8.61b).

An example of a circuit of conversion of voltage into number through the intermediate conversion into time intervals is shown in Fig. 8.62 together with oscillograms of the processes in their nodal points.

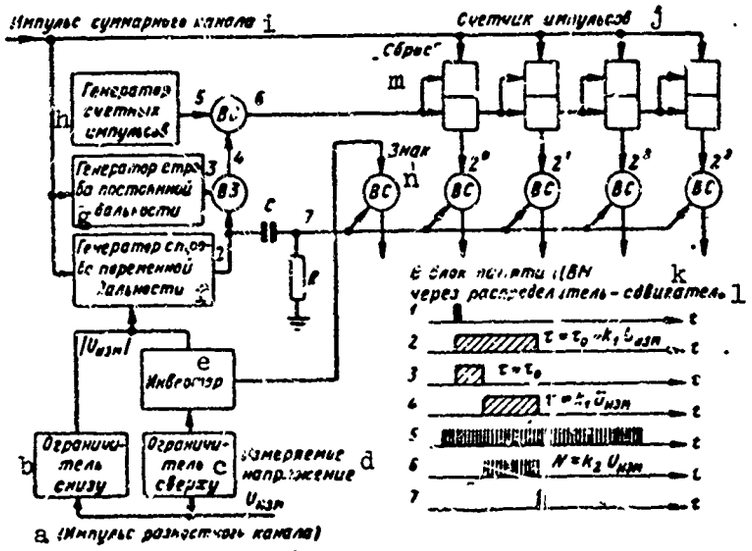


Fig. 8.62 Circuit of voltage transmission in numbers with intermediate conversion into time intervals. a) Pulse of the difference channel; b) limitor, below; c) limitor, upper; d) voltage being measured; e) inverter; f) generator of gating, variable distance; g) generator of gating, constant distance; h) counting pulse generator; i) pulse, summation channel; j) pulse counter; k) into the memory block TzVM; l) through distributor – shifter; m) "fault;" n) sign.

Inquiry pulses trigger two generators of wide gating. One generator produces gating 3, constant duration $\tau_0$. Duration of the gating 2 of the second generator is kept equal to $\tau_0$ a plus quantity proportiona. to the voltage being measured, $U_{izm}$, which is fed to the second generator. Both of these gatings fall on the prohibiting valve. From the output of the valve, the difference gating 4 of duration $\tau = k_1 U_{изм}$ is removed. This kind of method of the formation of gating of variable duration is acccomplished such that none of the real circuit may produce pulses whose durations may be smoothly changed from zero to some sufficiently large values.

Gating 4 permits the passage of count pulses 5 through the coincidence valve to the pulse counter similar to the distance register. If the counted pulse arrives with sufficiently high and stable frequency, F, then the number of pulses 6 going through the coincidence valve is $N_c = F\tau = k_1 F U_{изм} = k_2 U_{изм}$.

After this, as pulses computed by the counter, output of counts are produced in the memory cells of the TzVM through the computing valves which operate from the short pulse 7, corresponding to the tail end of the gating of variable duration.

The circuit being examined permits the measurement of positive as well as negative voltage. For this, the input is made of a double channel and in the register a special sign digit is introduced. At the input of the circuit, stand two limitors. One of them permits the passage of the positive part of the input voltage into the first channel, the second – the negative part into the second channel. In the second channel, the polarity of the negative voltage is changed to the opposite position, owing to this, to the generator of the gating of variable duration, always feeds only positive voltages $|U_{изм}|$. Besides this, when the voltage being measured is negative, the inverter feeds the voltage

to the computing valve of the sign digit, in which at computation produces one. At the positive input of voltage, the sign valve closes and produces zero.

The introduction of intermediate conversion of voltage into time intervals produces additional instrumental error, dependent on the instability of time delays. From this viewpoint, the sanatron and the comparing devices appear to be better, giving relative error of $\frac{\sigma_\tau}{\tau}=0{,}005$.

## §8.10. THE MEASUREMENT OF ANGULAR COORDINATES USING INDICATOR DEVICES

### 1. Accuracy Of Measurement Of Angular Coordinates Using Indicator Devices

When indicator devices with luminosity marks are used, the problem on the accuracy of the measurement of distance and angular coordinates are resolved mostly similarly. The error of measuring angular coordinates during the coincidence of the sight of the goniometer with the luminosity mark of the object is determined on the basis of two factors: errors, with which the operator lines up the goniometer sight with the mark of the object and the error of angle of transmission. Let us examine how can we estimate these errors.

Accuracy of the coincidence of the goniometer sight with the image of the object is determined by the size of the mark of the object on the screen of the indicator.

During coincidence, the operator positions the sight in the center of the image of the object, the permissible error for which is in the order of $0.1 - 0.2$ on the size of the object. We shall see what will be the extent of the mark of the point object on the screen of the two dimensional indicator in the direction corresponding to the angular coordinates.

According to the equation of the distance of radiolocational observations, the amplitude of the pulses of the object at the output of

the linear receiving tract changes in relation with the diagrams of directionality in power $F(\alpha)$during the rotation of the antenna

$$u_c = A\frac{F(\alpha)}{R^2}K, \qquad (8.78)$$

where $K$ – coefficient of amplification of the receiver; $A$ – constant factor.

A series of object pulses with envelope proportional to the function $F(\alpha)$, enters the controlling electrode of the tube (Fig. 8.63). The constant voltage at the controlling electrode set at the regulation of brightness, is generally lower than the threshold of unlocking the electron beam $u_0$. When the voltage of the signal reaches the level $u_0$, which we shall consider from the initial potential of the controlling electrode, the mark of the object begins to be traced out on the screen.

Lighting will be produced in the boundaries of the angle of the antenna rotation $\theta_0$ during which the pulses of the object will exceed the threshold of the limitation of the tube $u_0$. The angle $\theta_0$ we shall designate as the angle of dimension, while the corresponding beam on the screen, $(l)$ and at the location $(L = \theta_0 R)$ – tangential dimension of the image of the point object in the scale of the screen and the scale of the locality. The value $(l)$ $L$ and the tangential scale $m_t$ are connected between them by the simple relationship $l = m_t L$.

The angular dimension of the mark of the object depends on the forms of the diagrams of directionality of the antenna, the level of the limitation of the tube $u_0$, and the intensity of the reflected signals. For a given width and forms of the diagrams of directionality, the angular dimension of the image of the point object may vary within the boundaries from maximum width of the beam (at the zero level) to zero, or more exactly, to the dimensions of the diameter of the spot

being determined.

We shall examine the character of the dependence of the angular dimensions of the image on the factors determining the intensity of the sig-

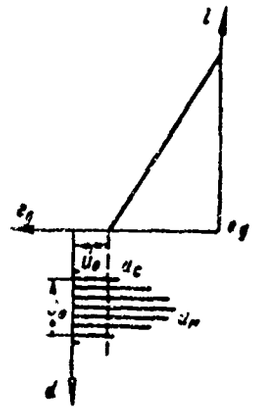

Fig. 8.63 Series of object pulses and the modulation characteristics of the tube.

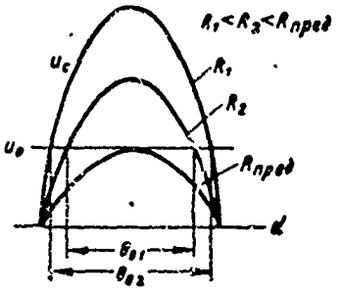

Fig. 8.64 Envelope of the pulses at the output of the receiver at various distances to the object.

nal, in particular, on the distance to the object and the amplification of the receiver. Assuming that all values besides $R$ and $F(\alpha)$ in Expression (8.78) are constant and $u_s = u_0$, we may write

$$\frac{F\left(\frac{\theta}{2}\right)}{R^2} = \text{const.} \qquad (8.79)$$

The constants may be determined for the particular case: at certain ultimate distance to the object, $R_{pred}$ (Fig. 8.64) the angular dimension of the image of the angle determined by the formula, equals zero. Expression (8.79) changes to the form

$$F_E\left(\frac{\theta_0}{2}\right) = \frac{R}{R_{пред}}, \qquad (8.80)$$

where $F_E(\alpha)$ – function expressing the diagram of directionality of the antenna according to intensity of the field.

The dependence of the dimensions of the image of the object on the distance is determined by the diagram of directionality of the antenna according to the field intensity (Fig. 8.65a). If it is assumed that in place of the function $F_e(\alpha)$ on the graph there is a distance $R$ displaced from the ultimate distance found for the given object $R_{pred}$

the angle, reckoned according to the diagram of directionality, is determined by the angular dimensions of the image of the object. According to the diagram of directionality in polar coordinates, the corresponding arc $L/R_{pred}$ determines the tangential dimensions of the mark in the scale of locality.

As it follows from Fig. 8.65a, the angular dimensions of the image of the object rise monotonously according to its proximity, from the value close to zero to the width of the diagram of directionality at the level of zero power.* The tangential dimensions of the mark of the object, $L$ in the scale of locality increases at first with the increase in distance, and afterwards, decreases according to the judgment diagram of directionality of the antenna $F_E(\alpha)$. In a similar manner, the dimensions of the mark of the object changes on the screen of the indicator with polar sweeping (Fig. 8.65b).

The dependence of the angular dimensions of the image of the object on the amplification of the receiver may be found assuming in Formula (8.78) all the values are invariable, except $F(\alpha)$ and $K$:

$$F\left(\frac{\theta_0}{2}\right)K=K_{min}. \qquad (8.81)$$

The constant coefficient $K_{min}$ may be considered as minimum amplification of the receiver, at which the image of the object appears. From Expression (8.81), it follows that with the increase in the coefficient of receiver amplification, the angular dimension of the image of the object increases from zero (at $K = K_{min}$) to the angular width of the beam at the zero level of power. The dependence, connecting the angular dimensions $\theta_0$ and the value, the reciprocal coefficient of the receiver amplification $K_{min}/K$), present itself as a function, expressing the diagram of directionality in power.

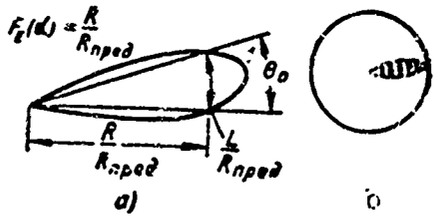

a) b)

Fig. 8.65 Tangential image size vs range. a) On terrain; b) on screen.

At a certain magnitude of the maximum amplitude of the signals and level of reading $u_0$, the angular dimensions of the mark of

the point object is roughly proportional to the width of the diagram of directionality of the antenna, θ at half power. Therefore, the tangential dimensions of the image in the scale of the locality is related to the width of the beam and the distance by the linear dependence $L = kR\theta$ ($k$ – coefficient of proportionality), which corresponds to the straight line 1 in the graph of Fig. 8.66.

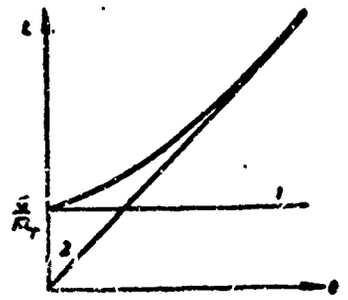


Fig. 8.66 Dependence of tangential dimensions of the image on the beam width.

Up to this moment, we have not taken into account, the dimensions of the spot, traced cut by the image of the object. If we assume that the antenna station has an infinitely narrow beam, then the tangential dimensions of the mark of the object will be equal to the diameter of the spot $l = d$. The corresponding distance to the locality $L$ may be determined through the tangential scale of the image $L = \frac{d}{m_t}$. This expression holds good also for antenna beams having final, very small width.

Under this condition for the two ultimate cases – for large and small beam width – the dependence of tangential dimensions of the image on the beam width is expressed graphically by the straight lines *1* and *2*, shown in Fig. 8.66. Similarly, this has a place in the analysis of the accuracy of the coincidence of the intensity mark according to distance. It will be assumed that in most cases, the curve of dependence $L = f(\theta)$ presents itself as a hyperbola, tangent to the straight line *1* and having the quality that line *2* is its asymptote. The analytical expression for this curve has the form

$$L = \sqrt{(kR\theta)^2 + \left(\frac{d}{m_t}\right)^2}. \qquad (8.82)$$

If we assume that in the lining up of the goniometer sight with the center of the mark, the operator is permitted an error $0.2l$, then the error of measurement corresponding to the angular coordinate consists of $0.2L/R$.

The conclusions reached relative to the point object may be applied to objects of arbitrary magnitude, but enclosing in its dimensions the cross-section of the beam.

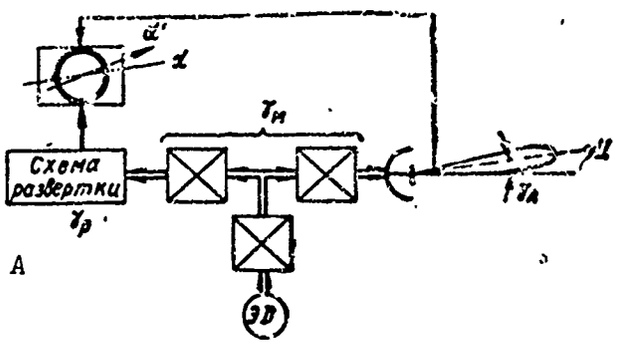


Fig. 8.67 Circuit of the angle of transmission during the measurement of the angular coordinates with the help of mechanical sights.
A) Sweeping circuit.

The error of transmission of angular coordinates in the system of the formation of the goniometer sight, in the circuit of angular sweeping, in the drive of the antenna are dependent on the errors of electromechanical devices, inaccuracy of the operation of the electron circuits or gaps in the mechanical reductors. The diagram of directionality usually seems to be somewhat asymmetry of the beam may depend on the angle of rotation and some other factors. But not all elements of the system of transmission of angular coordinates which the radiolocational stations have, influence the accuracy of measurement. Thus, for example, in one system the error of angular sweeping directly increases the error of measurement, in another it appears to be the indirect effect or it may not affect the accuracy of the measurement.

Not considering the effect of the error of concrete installations in the system of transmission of angular coordinates, we shall show only methods of approach to the problem of exposing the elements of the systems, which bring errors into the measurement of angles.

Simplified schemes of the passage of pulses in the circuits of measurement of distance may be similarly constructed as simplified circuits for the transmission of angular coordinates. Fig. 8.67 shows a convenient circuit for the case of using a mechanical goniometer sight. The signal of the object being received by the antenna beam, proceeds to the indicator, containing the mark of the object. Delays in the circuit of the passage of the signals do not have effect on the accuracy of the measurement of the angle. Therefore, high frequency elements, receivers and the indicator circuit are now shown in the figure.

We assume that the goniometer sight coincides exactly with the mark of the object. Then the position of the goniometer sight should correspond to the position of the antenna beam directed toward the object. But, in actuality, these directions do not coincide.

1. The antenna axis in ordinary cases, does not coincide with the direction of the beam. In the process of the rotation of the antenna, the angle between them may vary in magnitude and in direction.

2. Some errors are transferred to the position of the antenna system by the mechanical reductors depending principally on the geared transmission. From an examination of the schemes, it may be concluded that not all reductors of gear drives have errors but only the part of it enclosed between the antenna and the point of offtake to the sensing element of the angular sweeping. The errors of the angle of the antenna through the reductor drive and the reduction connection with the angular sweeping system have various directions. Reversing the

antenna axis, and the sensing element of the sweeper lags behind the rotation of the general axle connected with the motor. Depending on which one of the lags is larger the axis of the sensing element of the sweeper may lag behind the axis of the antenna or precede it. For radiolocational stations, that type of mechanical error of transmission is constant in magnitude during the condition when the rotation of the antenna is accomplished in one side.

3. The system of angular sweeping brings into the system defined errors. If the radially curved sweeping is accomplished by the rotation of the deflecting coil, then the error is dependent principally on the synchrono-tracing or the selsyn systems. In the case of the modulation of the sawtoothed voltage, the errors arise in the sensing element of the sweeper, for example, in selsyn-transformer, in amplifying circuits of sawtoothed currents and in deflection coils. In the right-angled sweeping of angle distance, the source of error may be the sensing element (potentiometer or selsyn transformer), and also circuits of the formation of the amplification of the deflected voltages or currents.

As a result of the above mentioned errors, the deformation of the actual sweep relative to the goniometer scale is connected with the screen. The image of the object and the angle, computed on the scale ($\alpha'$), do not correspond actually to the direction toward the object ($\alpha$), but rather to the direction

$$\alpha' = \alpha + (\gamma_a + \gamma_m + \gamma_r). \qquad (8.83)$$

The components of the error appear to be the error of angular sweeping $\gamma_r$, the error of mechanical drive $\gamma_a$ and the deviation of the antenna beam $\gamma_m$.

In the case of electron sight, the circuit of angular sweeping does not influence the accuracy of measurement directly. If the sig-

nals of the object and the pulses of the sight exist simultaneously, then their images coincide; the error of the sweeping circuit changes only the positions of their locations on the screen but cannot disturb the coincidence.

The significance of some errors, shown in Expression (8.33) do not depend on the rotation of the antenna or varies very little with the rotation. The balance of the radiolocational station may be considered as a permanent component of the total error. Balance may be fulfilled with the use of artificial objects and local objects whose angular positions relative to the radiolocational station are known. The essence of it is to compare the true angular coordinates of the object with measured values. The manufacturers of goniometer sights generally provide the tricks for the removal of errors observed in the process of balancing.

2. Resolving Power By Direction.

The question on the resolving power by direction is expeditiously considered to be applicable to the dimetric indicators with luminosity marks.

We shall assume that the antenna of a radiolocational station irradiates sequentially two objects, located at similar distance from the station. At the rotation of the antenna, the amplitude of the pulses at the output of the receiver vary, in correspondence with the diagram of directionality of the antenna in power (Fig.8.58). But, within the limits of the angles of rotation $\alpha_1 - \alpha_2$ the antenna receives the reflected signals simultaneously from both objects. In actuality, the distances of the objects can not remain strictly constant. Therefore, interference of the reflected signals will result with arbitrary coincidence of phases varying from pulse to pulse. As a result of this, within the stated limits of the angle, the antenna rotation signals at

the input of the receiver do not have a definite envelope and may change from zero to twice the value in comparison with the pulses of a single object.

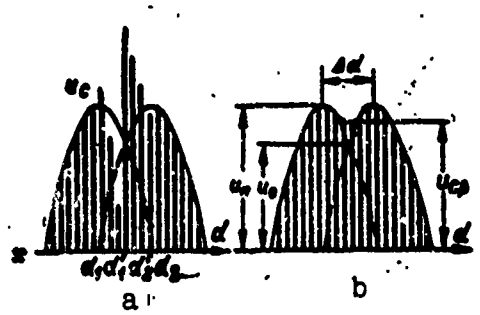


Fig. 8.68 Variation in the magnitude of two pulses of two point objects during the rotation of the antenna (a) and equivalent packet (b).

In actual conditions, scintillation is not observed at the point of the screen corresponding to the space between the two objects. This circumstance is explained by the effect of interference neutralizing the action of the pulses with random amplitudes. We shall estimate the result of this action having made the following assumptions.

1. Within the limits of the angles of rotation of the antenna $\alpha_1' - \alpha_2'$ the amplitudes of the signals of both objects remain on the average, the same (Fig. 8.68a).

2. Within these limits of rotational angles $\alpha_1' - \alpha_2'$ are much narrower than $\alpha_1 - \alpha_2$, enclosing sufficiently larger number of pulses (3-5 or more).

We shall assume that the luminosity marks are proportional to the average value of the integrated pulses. During the interference of two electromagnetic oscillations with the same values of the modulus of field intensity $E_0$, but with arbitrary phase shift $\varphi$, the modulus of the resulting vector of field intensity $E$ is equal to $2E_0\cos\frac{\varphi}{2}$. Since any phase shift between the high frequency signals are equally probable, the effect of large number of such pulses may be determined as the average value of the function $2E_0\cos\frac{\varphi}{2}$ within the limits of 0 to $\pi$, which is equal to $\frac{4}{\pi}$. Under this condition, it may be considered that the envelope of the pulses within the limits of the angles

$\alpha_1 - \alpha_2$ has a defined value corresponding to the center of this portion $u_{ср}=\frac{4}{\pi}u_0$ (Fig. 8.68b).

Assuming the modulation characteristics of the tubes to be quadractic and not taking into account the diameter of the spot, we may write the relationship between various contrasts $K$ and the corresponding voltages

$$K=\frac{u_м^2-u_{ср}^2}{u_м^2}.$$

After substituting $u_{ср}=\frac{4}{\pi}u_0$ and transformation, we get

$$\left|\frac{u_0}{u_м}\right|_0=\frac{\pi}{4}\sqrt{1-K}. \qquad (8.84)$$

Expression (8.84) permits the determination of the level of the diagrams of directionality of the antenna $\left|\frac{u_0}{u_м}\right|_0$, according to which its width is numerically equal to the angle being resolved. Thus, for example, the resolving power at various contrasts $K$ = 0.1 is determined by the width of the diagrams of directionality of the antenna in power at the level 0.75 from the maximum value. For $K$ = 0.3, we get the approximate $\left|\frac{u_0}{u_м}\right|_0\approx 0{,}65$.

Various methods of approximation of the diagrams of directionality approximately give the same relationship between angular resolving power of the radiolocational stations and the width of the diagrams of directionality of the antenna $\delta\alpha\approx 0{,}7\theta$.

Up to this point, it has been assumed that the initial voltage of the controlling electrode of the tube is set at the level of unlocking the electron beam. If a defined number of signals is introduced, then the contrast of the dip of luminosity, dependent on the two-humped curve (Fig. 8.68) increases. Consequently, the diminished luminosity of the image may be raised by various methods. But, if the objects are so close that their signal envelopes have flat tops (without dip) then not any artificial measure can permit them to be resolved. This case

corresponds to the limiting values of the angular resolving power. It is not difficult to show that the limiting value of resolving power in voltage is determined by the width of the beam at the level 0.8 from the maximum value that is approximately 0.6θ.

Under this condition, by controlling the unlocking of the tubes or the change of the intensity of the signals, the resolving power in voltage is changed in comparison with the narrow limits:

$$\delta\alpha \approx (0{,}6 \div 0{,}7)\,\theta.$$

Since linear distance corresponding to the angle δα ($\delta L = R\delta\alpha$) generally exceeds considerably the dimensions of the electron beam, (in the locality scale), therefore during the calculation of resolving power in voltage, the diameter of the spot often does not count.

If, however, the distance to the object $R$ is small, then, the dimensions of the spots do effect the resolving power. In this case, by analogy to Formula (7.112) we may write

$$\delta L = \sqrt{(R0{,}7\theta)^2 + \left(\frac{0{,}7d}{m_t}\right)^2}. \qquad (8.85)$$

where $d$ – diameter of the spot; $m_t$ – tangential scale in the given point of the screen.

The angular resolving power, taking into account the beamwidth and the diameter of the spot may be found, dividing Expression (8.85) by the distance to the objects.

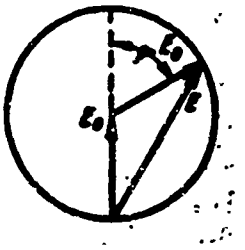


Fig. 8.69 Vector diagram of the addition of two oscillations of similar amplitude with arbitrary phase shift.

Manuscript Page No.

[Footnotes]

568 In television, similar operations are used for the improvement of the resolution of the fine details of the image and carries the designation aperture correction.

600 This fact is easily established in sharp directional antennas: at a deviation from the direction of maximum intensity, the signal being received suddenly diminishes, in the very time as the antenna surface is perpendicular to the angle of arrival and the energy taken in by it almost does not change.

665 When the intensity of the signal is large, additional illumination may be observed dependent on the lateral petals.

[Transliterated Symbols]

532 з = z = zemlya = earth

540 мин = min = minimal'nyy = minimum

540 макс = maks = maksimal'nyy = maximum

551 РЛС = RLS = radiolokatsionnaya stantsiya = radar

553 Ц = Ts = tsel' = target

560 П = P = pravyy = right-hand

560 Л = L = levyy = left-hand

560 обл = obl = oblucheniye = beaming

561 с = s = signal = signal

561 ш = sh = shum = noise

562 п = p = povtoreniye = repetition

564 э = e = effektivnyy = effective

564 обл = obl = oblucheniye = beaming, irradiation

569 д = d = dopplerov = doppler

570 м = m = modulyatsiya = modulation

570 ав = av = antenna, voobrazhayemaya = imaginary antenna

575 м = m = metod = method

576 з = z = zaderzhka = delay

576 н = n = nachal'nyy = initial

576 к = k = konechnyy = final

578 ЛЗ = LZ = liniya zaderzhka = delay line

578 ВЗ = VZ = ventil' zapreta = blocking valve

578 ВС = VS = ventil' sovpadeniya = coincidence valve

585 АП = AP = antennyy pereklyuchatel' = TR switch

591 пх = pkh = pelengatsionnaya kharakteristika = df characteristic

592 р = r = raznostnyy = differential

598 АРУ = ARU = avtomaticheskoye regulirovaniye usileniya = automatic gain control

603 с = s = summirovaniye = summation (sum)

607 п = p = polyarizovannyy = polarized

609 АСН = ASN = avtomaticheskoye soprovozhdeniye po napravlemiyu = automatic direction tracking

612 ош = osh = oshibka = error

614 р = r = razlichitel' = discriminator

618 УПЧ = UPCh = usilitel' promezhutonoy chastoty = i-f amplifier

622 п = p = promezhutochnyy = intermediate

624 з = z = zamknutyy = closed

626 э = e = effektivnyy = effective

627 у = u = ustanovleniye = settling

628 и = i = ispolnitel'noye ustroystvo = actuator

628 п = p = preobrazovatel' = converter

632 пч = pch = promezhutochnaya chastota = intermediate frequency

644 и = i = instrumental'nyy = instrumental

646 ЦВМ = TsVM = tsifrovaya vychislitel'naya mashina = digital computer

659 изм = izm = izmerennyy = measured

663 т = t = tangentsial'nyy = tangential

664 пред = pred = predel'nyy = limiting

669 р = r = razvertka = sweep

669 м = m = mekhanicheskiy = mechanical

669 а = a = antenna = antenna

671 ср = sr = seredina = center

Chapter 9

# THE DETERMINATION OF THE LOCATION OF THE OBJECT BY THE RESULT OF THE MEASUREMENT OF ITS COORDINATES

## §9.1. DETERMINATION OF THE LOCATION OF THE OBJECT WITH THE ABSENCE OF ERROR OF MEASUREMENT OF THE ORIGINAL GEOMETRIC VALUES

The position of the object may be found through three independent geometric values in space and two in a plane. These values obtained from the results of the radar measurements of the coordinates of the object should be converted such that the position of the object is characterized in a united and universal coordinate system. Such coordinate systems are the rectangular and spherical (polar) coordinates (Fig. 1.6).

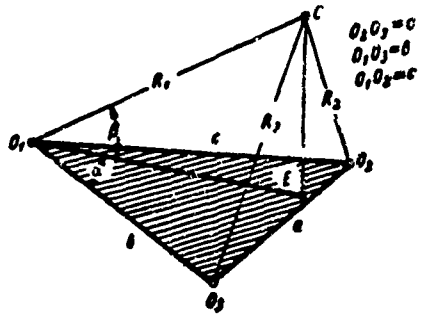


Fig. 9.1. Range finder method of location determination in space.

We shall first determine the polar coordinates of the object in planes. In the case of the application of range-finder-goniometer method, polar coordinates are measured directly.

For the range finder method (Fig. 1.6b), we have to find the conversion to the polar coordinates from an inspection of the triangle $O_1CO_2$. Set up first the polar coordinates, at the point $O_1$ and orient a polar axis $O_1L$ in the direction $O_1O_2$. Then, the radius vector of the object is equal to $R_1$ and the polar angle $\alpha$ may be found through the theorem of cosines

$$R_2^2 = R_1^2 + b^2 - 2R_1 b\cos\alpha.$$

With the use of goniometer method at known azimuthal angles, the

internal angles of the triangle $O_1CO_2$ are determined (Fig. 1.5c). The orientation of the polar system is exactly the same as obtained in Fig. 1.5b such that the polar angle of the object is equal to $\alpha'_1$, and the radius vector is determined by the theorem of cosines

$$R = O_1C = \frac{b \sin \alpha'_2}{\sin(\alpha'_1 + \alpha'_2)}.$$

We determine the polar coordinates of α and β by the known distance $R_1$; $R_2$; $R_3$ to three stations located at the points $O_1$, $O_2$ and $O_3$ (Fig. 9.1). We erect first the coordinate at the point $O_1$ and will create the reading α from the direction $O_1O_3$ in the plane $O_1O_2O_3$ and the angle reading β from the direction $O_1E$ in the plane $O_1CE$, perpendicular to $O_1O_2O_3$. If the distance between the objects is small in comparison with the radius of the earth, then it may be assumed that the triangle $O_1O_2O_3$ is located in the horizontal plane. In this case, the angle β is the location angle and angle α is entirely determined by the azimuth of the object.

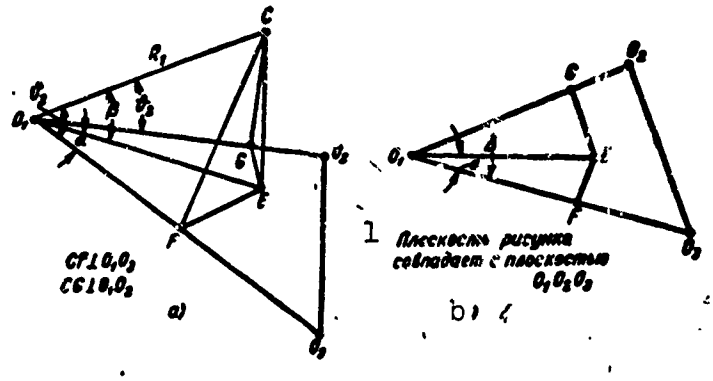


Fig. 9.2. Polar coordinates of the object: a) mutual positions of the RLS and the object; b) position of the RLS on the plane. 1) The plane of the drawing coincides with the plane $O_1O_2O_3$.

We shall look at the three sided pyramid $O_1O_2O_3C$, the basis of which is the triangle $O_1O_2O_3$.

From Fig. 9.2a, we obtain

$$\cos\theta_3 = \frac{O_1F}{O_1C} = \frac{\frac{O_1F}{O_1E}}{\frac{O_1C}{O_1E}} = \cos\alpha\cos\beta. \qquad (9.1)$$

and

$$\cos\theta_2 = \frac{O_1G}{O_1C} = \cos(\Delta - \alpha)\cos\beta, \qquad (9.2)$$

where $\Delta = \angle O_2O_1O_3 = \angle GO_1F$* (Fig. 9.2b).

The relationships (9.1) and (9.2) form the system of equations relative to α. Eliminating cos β, we find

$$\frac{\cos(\Delta-\alpha)}{\cos\alpha} = \frac{\cos\theta_2}{\cos\theta_3} = K.$$

From this expression, we obtain the equation relative to α

$$\sin\alpha\sin\Delta + \cos\alpha(\cos\Delta - K) = 0. \qquad (9.3)$$

For the solution of Eq. (9.3), divide both sides by cos α. Then

$$\operatorname{tg}\alpha\sin\Delta + \cos\Delta - K = 0$$

and, consequently,

$$\operatorname{tg}\alpha = \frac{K-\cos\Delta}{\sin\Delta} = \frac{K}{\sin\Delta} - \operatorname{ctg}\Delta.$$

If cos α = 0, then, dividing both sides of Eq. (9.3) by sin α may get similar relationship for the result cot α.

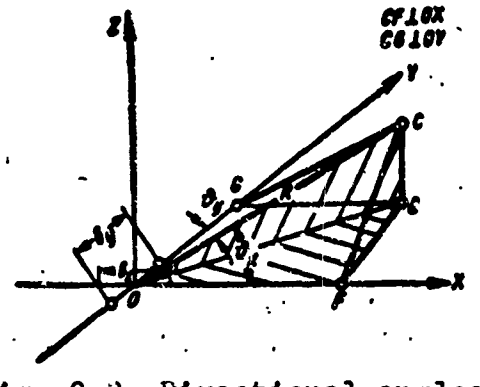


Fig. 9.3. Directional angles in space.

After the solution for α, angle β may be determined with the help of Relationship (9.1).

For the solution of the reverse problem, i.e., for the solution of $R_2$ and $R_3$ by the given polar coordinates of the object and the mutual location of RLS, we start, necessarily, with the solving of $\vartheta_2$ and $\vartheta_3$ according to the known $\alpha$ and $\beta$ using Formulas (9.1) and (9.2) (see Fig. 9.2). Afterwards, $R_2$ and $R_3$ are determined by the law of cosines

$$R_3^2 = R_1^2 + b^2 - 2R_1 b\cos\vartheta_3,$$
$$R_2^2 = R_1^2 + c^2 - 2R_1 c\cos\vartheta_2.$$

The direction toward the object may be fixed with the help of the so-called directional angles $\vartheta_x$ and $\vartheta_y$ (Fig. 9.3) The relationship connecting angles $\alpha$ and $\beta$ with the directional angles $\vartheta_x$ and $\vartheta_y$ is given in a similar manner, i.e.,

$$\cos\vartheta_x = \cos\alpha\cos\beta,\ \cos^2\beta = \cos^2\vartheta_x + \cos^2\vartheta_y.$$

We shall examine the conversion to polar coordinates of points from geometrical values very often measured with the help of the RLS. For all the remaining cases, the corresponding formulas of conversion may be conveniently done in the same manner by the use of geometrical relationships.

## §9.2. LINEAR ERRORS ON THE PLANE AND IN SPACE

The errors of measurement of geometric values are caused by the errors in the determination of the location of the object. In order to establish a connection between these errors, it is expedient to use the elements of the theory of the scalar field.

If every point in space corresponds to values determined by scalar quantities $U$, then the aggregation of these points form the scalar field. Thus, for example, we may have seen the temperature field, the pressure field, the electric field. All points in which the scalar quantities have the one and the same values are distributed over level surfaces (equipotential surfaces).

All geometric quantities also form scalar fields. In every point in space there is completely determined meaning $U$ for any geometrical value. Applied to the scalar field of geometrical quantities, the level surface forms the surface of positions.

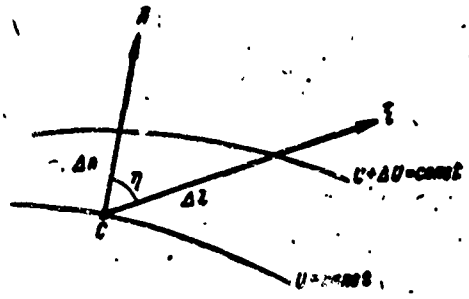


Fig. 9.4. Gradient of scalar field and linear errors.

Changes in the scalar field are characterized by vector quantities, called the gradients of the field. This quantity is designated by grad $U$. The gradient of the field is aligned according to the normal to the level surface at that point in the side of the maximum change of the scalar quantity (Fig. 9.4). The modulus of the gradient is equal to the limit of the ratio of the increment of the geometric quantity $U$ in the direction of the normal to the value of the segment of the normal $\Delta n$ when $\Delta n \to 0$ (positive direction of the normal corresponds to the increase of the geometric value).

Consequently,

$$\operatorname{grad} U = \frac{\partial U}{\partial n} \vec{n}, \qquad (9.4)$$

where $\vec{n}$ is a unit vector, directed according to the normal to the surface (lines) of position.

Under the same conditions we may consider the derivative in any direction $l$. The derivative is designated as $\partial U/\partial l$.

It can be seen from Fig. 9.4 that in the direction of the normal,

the derivative $\partial U/\partial l$ is at the maximum and in any other directions it decreases in proportion to the cosine of the angle between the normal and the direction in question.

Let the permitted error in the measurement of geometric values in the results of inaccurate measurements be $\Delta U$. Substituting the partial derivative with the final difference, we obtain

$$\Delta n = \frac{\Delta U}{|\text{grad } U|}, \tag{9.5}$$

where $|\text{grad } U|$ is the modulus of gradient of the field, and

$$\Delta n \approx \Delta l \cos(\vec{n}; \vec{l}) = \Delta l \cos \eta. \tag{9.6}$$

If a certain straight line $l$ is drawn in any arbitrary manner through the point position of the object $C$ (Fig. 9.4) then the error of measurement of the geometric value corresponds to the displacement $\Delta l$ in the direction of the introduced line. This displacement is called the linear error of the position of the object.

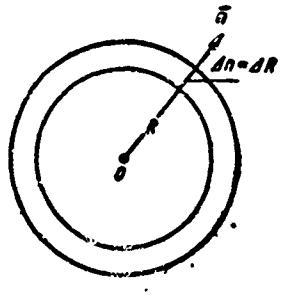


Fig. 9.5. Gradient of the field of distance.

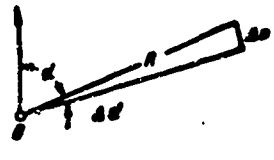


Fig. 9.6. Gradient of the field of angle.

The modulus of the field gradient permits us to establish which of the linear errors of the position of the object in the direction of the normal is the error of the measurement of geometric value leading to. The value of the vector of the gradient field gives the possibility of finding the linear error in any arbitrarily fixed direction $\vec{l}$. It is necessary to keep in mind that in correspondence with Relationships

(9.5) and (9.6), small values of the gradient leads to considerable linear error and at a deviation from the normal, the error increases.

We shall find the modulus and the directions of the gradient field for several of the lines of position on the surface. For the lines of various distances (Fig. 9.5) we obtain that the increment of distance is equal to the value of the corresponding segment of the normal, i.e., $\Delta n = \Delta R$. Under this condition $|\text{grad } R| = 1$, and the direction of the normal coincides with the radial direction. Therefore, the linear error is independent of the distance toward the object.*

We shall look now at the lines of different angles, i.e., the directions toward the object (Fig. 9.6). Normals to these lines are tangents to the circle of radius $R$. Consequently, $\Delta n = R\Delta\alpha$, i.e., $|\text{grad}\,\alpha| = \frac{1}{R}$.

Therefore, the linear error of the goniometer system is proportional to the distance toward the object.

The modulus of the gradient of the lines of constant difference of distance may be determined by the differentiation of the hyperbola equation. Thereby, it shows that

$$|\text{grad}\,R_p| = 2\sin\frac{\varphi}{2}, \qquad (9.7)$$

where $R_r = R_1 - R_2$; $\varphi$ is the angle of inclusion between the radii vectors $R_1$ and $R_3$.

If the distance to the object is considerably larger than the base $b$, then the constant difference of distance corresponds to the fixed value of the directional angle $\vartheta_x$ (Fig. 9.7). Thereby

$$|\text{grad}\,R_p| \approx |\text{grad}\,\vartheta_x| = \frac{b\sin\vartheta_x}{R}. \qquad (9.8)$$

Under this condition, the linear error produces inaccurate measurement of $\vartheta_x$, depending on the deviation of distance as well as on the directional angle. The best results are obtained in the case if

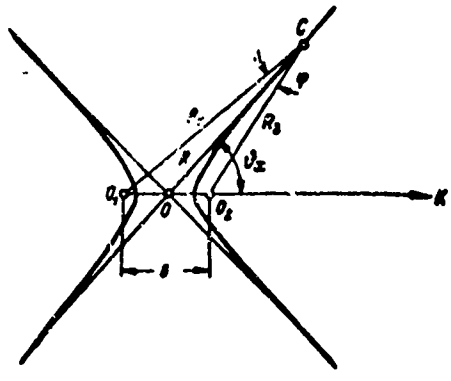


Fig. 9.7. Equal distance method of location determination.

the object is located at the normal to the base line. Errors increase with the increase of the base line, as can be seen from Formulas (9.7)-(9.8).

On the basis of what was said, the following conclusions may be made. The linear error when using the range finder method is numerically equal to the error in the measurement of range. Since this property is possessed only by the range finder systems, therefore, at a considerable distance to the object these systems appear to be more accurate. The linear error of the goniometer system is proportional to the range. The error of rangefinder-goniometer systems is dependent on the direction toward the object. The linear error of such systems is always larger than in the case of the range finder at one and the same kind of accuracy of measurement of time intervals. When the distance is larger in comparison with the base, the difference-range finder systems are degenerated into the goniometer systems. The errors obtained under this condition by the goniometer system is dependent on the direction as well as the range.

We go back now to the determination of the gradient of the field of geometric values in space. In the future we shall look at the surface of positions formed by the rotation of the lines of positions

around a certain axis. Thus, spherical and conical surfaces formed as a result of the rotation of a circle around any diameter and an inclined straight line relative to the corresponding base line. Therefore, the scalar field of geometric values on all surfaces going through the axis of rotation are all the same. Besides this, the normals to these surfaces are always intersecting the axis of rotation. Consequently, the modulus of the gradients of such fields on the planes and in space are equal among themselves.

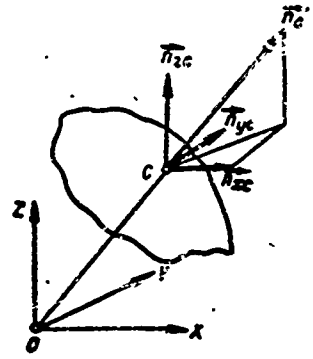


Fig. 9.8. Method of fixing the normal to the surface.

For fixing the direction normal to the surface of positions it is convenient to use the equation of the surface $F(x; y; z) = 0$ in the system of rectangular coordinates. The position of the normal is characterized by the vector $\vec{n}_c$ (Fig. 9.8), the components of which are equal to the derivatives from the function $F$ on the corresponding coordinate axis, i.e.,

$$n_{xc} = \frac{\partial F}{\partial x}, \quad n_{yc} = \frac{\partial F}{\partial y}, \quad n_{zc} = \frac{\partial F}{\partial z}, \tag{9.9}$$

where $n_{xc}$, $n_{yc}$ and $n_{zc}$ are the projections of the segments of the normals on the corresponding coordinate axes.

According to the known relationships of the vectors, the coincidence with the direction of the normal is easily determined by the an-

gles between the normal and the coordinate axes. The cosines of the directional angles of the normals are found through the following relationships:

$$\cos(\vec{n};\ \vec{x}) = \frac{\frac{\partial F}{\partial x}}{\sqrt{\left(\frac{\partial F}{\partial x}\right)^2 + \left(\frac{\partial F}{\partial y}\right)^2 + \left(\frac{\partial F}{\partial z}\right)^2}}, \qquad (9.10)$$

$$\cos(\vec{n};\ \vec{y}) = \frac{\frac{\partial F}{\partial y}}{\sqrt{\left(\frac{\partial F}{\partial x}\right)^2 + \left(\frac{\partial F}{\partial y}\right)^2 + \left(\frac{\partial F}{\partial z}\right)^2}}, \qquad (9.11)$$

$$\cos(\vec{n};\ \vec{z}) = \frac{\frac{\partial F}{\partial z}}{\sqrt{\left(\frac{\partial F}{\partial x}\right)^2 + \left(\frac{\partial F}{\partial y}\right)^2 + \left(\frac{\partial F}{\partial z}\right)^2}}. \qquad (9.12)$$

Let us look at the spherical surface of positions. The equation of the sphere of radius $R$ has the following form:

$$(x - x_1)^2 + (y - y_1)^2 + (z - z_1)^2 = R^2,$$

where $x_1$, $y_1$, $z_1$ are coordinates of the center of the sphere.

Having determined the normal $\vec{n}_R$ in accordance to Formula (9.9), we obtain the component of this vector at the point of the location of the object $(x_c;\ y_c;\ z_c)$

$$n_{xR} = x_c - x_1,\quad n_{yR} = y_c - y_1,\quad n_{zR} = z_c - z_1. \qquad (9.13)$$

We designate the vector whose components are determined by Formula (9.13) as $\vec{n_R}(x_c - x_1;\ y_c - y_1;\ z_c - z_1)$.

If, initially, the coordinates coincide with the center of the sphere, then the projections of the segments of the normals are equal to the rectangular coordinates of the points since $x_1 = y_1 = z_1 = 0$. This result is obvious since at the given angular directions the normals and the radius-vectors coincide.

We shall find the normals to the surface of mixed values of the directional angles, i.e., conical surfaces (Fig. 9.9a). With the known directional angles, $\vartheta_x$ and $\vartheta_y$, we find the equations of conical surfaces, formed at the rotation of the straight line $OC$ around the axes

$OX$ and $OY$:

$$y^2 + z^2 - \operatorname{tg}^2\vartheta_x \cdot x^2 = 0, \qquad (9.14)$$

$$x^2 + z^2 - \operatorname{tg}^2\vartheta_y \cdot y^2 = 0. \qquad (9.15)$$

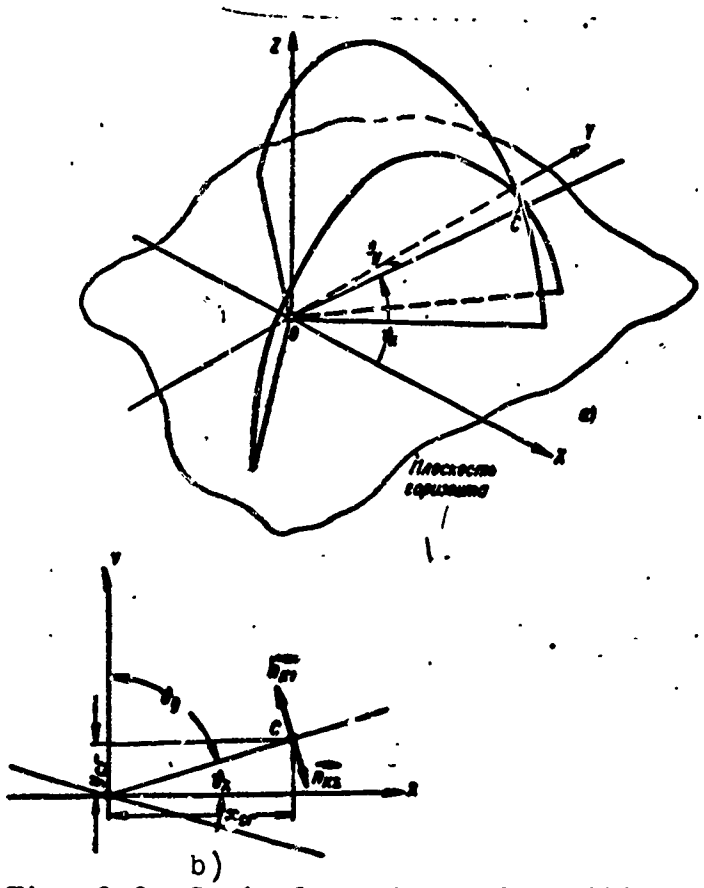


Fig. 9.9. Conical surface of positions: a) general case; b) object is located in the horizontal plane. 1) Surface of rotation.

Utilizing Formula (9.9), we find the projections of the vectors

$$\vec{n}_{k1}(-x_c \operatorname{tg}^2\vartheta_x;\ y_c;\ z_c).$$

$$\vec{n}_{k2}(x_c;\ -y_c \operatorname{tg}^2\vartheta_y;\ z_c),$$

normal to the cosines $K_1$ and $K_2$, with the axes of rotation $OX$ and $OY$.

If the object is located in the plane $XOY$ then $\vartheta_x + \vartheta_y = 90°$. Having multiplied all components by the vector $\vec{n}_{k1}$ by $\frac{1}{\operatorname{tg}^2\vartheta_x}$, we find

$$\vec{n}'_{k1}(-x_{cr};\ y_{cr} \operatorname{tg}^2\vartheta_y;\ 0),$$

$$\vec{n}'_{k2}(x_{cr};\ -y_{cr} \operatorname{tg}^2\vartheta_y;\ 0).$$

where $x_{sg}$ and $y_{sg}$ are coordinates of the object, located on the plane *XOY*.

The given vectors are located on one straight line of opposite directions. This result could also be obtained directly from geometric constructions (Fig. 9.9b).

By the use of the relationships given in the previous paragraph, the conversion of errors of measurement of geometric values into linear errors in an arbitrary direction is accomplished in this manner: first. the error in the direction of the normal is found (Formula (9.5)) and then by the angle between the normal and the direction under consideration the true error is determined by Formula (9.6).

## §9.3. ACCURACY OF THE DETERMINATION OF THE POSITION OF THE OBJECT IN PLANES

The accuracy of the determination of the position of the object in the plane is dependent on the errors of measurement of two geometric quantities, therefore the errors are necessarily considered jointly. First, we find the error of searching for the position of the object by the range finder method (Fig. 9.10). At the presence of the error of measurement of the distances $\Delta R_1$ and $\Delta R_2$ the computed position of the object corresponds to the point *C**. The error of position determination characterized by the segment *CC** depends not only on the error of measurement of the geometric quantities but also on the mutual orientation of the lines of positions in the points under consideration. As can be seen from Fig. 9.10, at the same linear error in the direction of the normal to the lines of positions, the error of position determination is dependent entirely on the angle between the lines of positions. The smallest error corresponds to the intersection of these lines at right angles, i.e., when the lines of positions are orthogonal. Error increases with the decrease of the acute angle between these given lines. In the limiting case, when the angle between

the lines of positions is zero, the error is equal to infinity, since with the use of one geometric quantity, it is never possible to determine the position of a point in a plane.

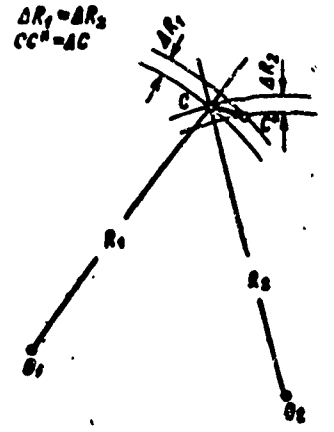

Fig. 9.10. Error of the computed position of the object by the range finder method of position determination.

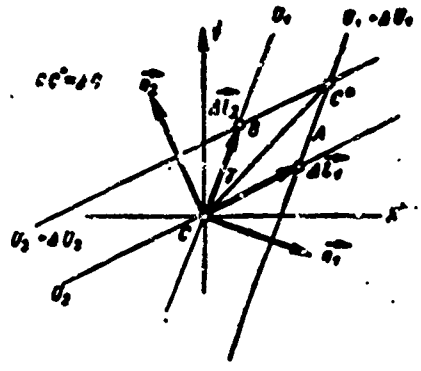

Fig. 9.11. Parallelogram of error.

Let us look at the general case of the determination of position in a plane. The error of position determination, $\Delta C$ (Fig. 9.11), is the result of the inaccurate measurement of the geometric quantities $U_1$ and $U_2$. If these errors are not great, then it may be assumed that the lines of positions $U$ = const and $U + \Delta U$ = const are parallel ($\Delta U$ is the error of measurement). Thereby, we obtain the parallelogram of error $CAC^*B$, whose sides are parallel to the position of the point un-

der consideration on the plane. The error of position determination $\vec{\Delta C}$ is equal to the sum of the vectors, determined by the sides of the parallelogram of error. The vector $\vec{\Delta l_1}$, in the direction of the tangent to the line $U_2$ = const is specified by the inaccuracy in the measurement of the quantity $U_1$. The modulus of this vector is equal to

$$\Delta l_1 = \frac{\Delta U_1}{|\operatorname{grad} U_1| \cos(\vec{n_1}; \vec{l_1})} = \frac{\Delta U_1}{|\operatorname{grad} U_1| \sin \gamma}.$$

Similarly, the vector $\vec{\Delta l_2}$ may be determined. Its modulus is equal to

$$\Delta l_2 = \frac{\Delta U_2}{|\operatorname{grad} U_2| \cos(\vec{n_2}; \vec{l_2})} = \frac{\Delta U_2}{|\operatorname{grad} U_2| \sin \gamma}.$$

In this way, the error of position determination is entirely determined by two vectors, whose magnitude and directions depend on the error of the geometric quantities, the gradients of their fields and the angle between the lines of positions.

We draw through the point of the location of the object, in an arbitrary way, the rectangular coordinates $CX'$ and $CY'$. According to the known vectors $\Delta l_1$ and $\Delta l_2$ we find their components $\Delta l_{1x}$; $\Delta l_{1y}$ and $\Delta l_{2x}$ and $\Delta l_{2y}$. The vector, characterizing the error of position determination $\Delta C$ is equal to the sum of the vectors $\Delta l_1$ and $\Delta l_2$. Therefore,

$$\Delta C_x = x' = \frac{\Delta U_1}{|\operatorname{grad} U_1| \sin \gamma} \cos(\vec{\Delta l_1}; \vec{x'}) + \frac{\Delta U_2}{|\operatorname{grad} U_2| \sin \gamma} \cos(\vec{\Delta l_2}; \vec{x'}), \tag{9.16}$$

$$\Delta C_y = y' = \frac{\Delta U_1}{|\operatorname{grad} U_1| \sin \gamma} \cos(\vec{\Delta l_1}; \vec{y'}) + \frac{\Delta U_2}{|\operatorname{grad} U_2| \sin \gamma} \cos(\vec{\Delta l_2}; \vec{y'}), \tag{9.17}$$

where $\Delta C_x$ and $\Delta C_y$ – components of the vector $\vec{\Delta C}$.

We find the probability characteristics of the components of the vector of the error $\vec{\Delta C}$. Let us assume that the errors of the measurement of geometric quantities are distributed according to the normal

law with the zero mean values corresponding to the absence of systematic errors. In this case, the combined density of the probabilities of the two random values x' and y' are described by the normal law of distribution, since these values form linear functions of two normally distributed random quantities $\Delta U_1$ and $\Delta U_2$.

The density of the probability of normal distribution of two random quantities with zero mean values may be given in the following form:

$$W(x'; y') = \frac{1}{2\pi\sigma_{x'}\sigma_{y'}\sqrt{1-\rho^2}} \times$$
$$\times \exp\left[-\frac{1}{2(1-\rho^2)}\left(\frac{x'^2}{\sigma^2_{x'}} - \frac{2\rho x' \cdot y'}{\sigma_{x'}\sigma_{y'}} + \frac{y'^2}{\sigma^2_{y'}}\right)\right], \qquad (9.18)$$

where $\sigma_x$, and $\sigma_y$, – mean square deviation x' and y'; $\rho$ – coefficient of correlation between x' and y'.

In the future, we shall assume that the errors of measurement of geometric quantities are independent. In the majority of practical cases, this assumption is valid. Thereby, the coefficient of correlation depends only on the orientation of the coordinate axes introduced $CX'$ and $CY'$.

On the basis of Formulas (9.16), (9.17) and the rule of determination of the variances of the sums of independent random values we obtain

$$\sigma^2_{x'} = \frac{\cos^2(\overrightarrow{\Delta l_1}; \overrightarrow{x'})}{|\operatorname{grad} U_1|^2 \sin^2\gamma}\sigma^2(U_1) + \frac{\cos^2(\overrightarrow{\Delta l_2}; \overrightarrow{x'})}{|\operatorname{grad} U_2|^2 \sin^2\gamma}\sigma^2(U_2),$$
$$\sigma^2_{y'} = \frac{\cos^2(\overrightarrow{\Delta l_1}; \overrightarrow{y'})}{|\operatorname{grad} U_1|^2 \sin^2\gamma}\sigma^2(U_1) + \frac{\cos^2(\overrightarrow{\Delta l_2}; \overrightarrow{y'})}{|\operatorname{grad} U_2|^2 \sin^2\gamma}\sigma^2(U_2),$$

where $\sigma^2(U)$ – variance of measurement of geometric quantity $U$.

Having crossmultiplied the right sides of Formulas (9.16) and (9.17), we obtain the average value of this product

$$\overline{(x' \cdot y')} = \frac{\cos(\overrightarrow{\Delta l_1}; \overrightarrow{x'})\cos(\overrightarrow{\Delta l_1}; \overrightarrow{y'})}{|\operatorname{grad} U_1|^2 \sin^2\gamma}\sigma^2(U_1) +$$
$$+ \frac{\cos(\overrightarrow{\Delta l_2}; \overrightarrow{x'})\cos(\overrightarrow{\Delta l_2}; \overrightarrow{y'})}{|\operatorname{grad} U_2|^2 \sin^2\gamma}\sigma^2(U_2).$$

The coefficient of correlation is determined by Expression

$$\rho=\frac{\overline{(x'y')}}{\sigma_{x'}\cdot\sigma_{y'}}. \qquad (9.19)$$

From Formula (9.18), it can be seen that the constant density of probability corresponds to the value of the expression obeying the law of exponential function. Consequently,

$$\frac{x'^2}{\sigma_{x'}^2}-\frac{2\rho x'\cdot y'}{\sigma_{x'}\sigma_{y'}}+\frac{y'^2}{\sigma_{y'}^2}=\text{const}=K^2. \qquad (9.20)$$

The relationship obtained is the equation of a curve of the second order and is precisely an ellipse which is designated the ellipse of error or ellipse of distribution.

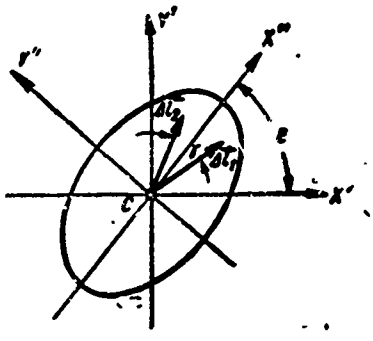

Fig. 9.12 Ellipse of distribution.

At arbitrary positions of the coordinate axes, the principal axes of the ellipse of distribution do not coincide with the coordinate axes (Fig. 912). The coefficient of correlation between x' and y' becomes zero if the coordinate axis coincides with the principal axes of the ellipse. Thereby the equation of the ellipse takes the canonical form:

$$\frac{x''^2}{a_1^2}+\frac{y''^2}{a_2^2}=1, \qquad (9.21)$$

where $\alpha_1$ and $\alpha_2$ – major and minor semi-axes of the ellipse.

The orientation of the ellipse of distribution is determined by the following formula

$$\operatorname{tg}2\varepsilon=\frac{2\rho\sigma_{x'}\cdot\sigma_{y'}}{\sigma_{x'}^2-\sigma_{y'}^2}, \qquad (9.22)$$

where $\varepsilon$ – angle between the axis $CX'$ and the major axis of the ellipse.

The tangent of the angle $\varepsilon$ corresponds to two angles displaced at 90°, i.e., Relationship (9.21) determines both principal axes of the ellipse. Thereby, the major axis of the ellipse is always located in-

side the acute angle between the lines of positions. The principal axes of the ellipse coincide with these lines when the latter intersect at right angles. If the linear mean square errors in the direction of the normals are the same $\frac{\sigma(U_1)}{|\text{grad } U_1|}=\frac{\sigma(U_2)}{|\text{grad } U_2|}$, then the principal axes of the ellipse are the bisectors of the angle between the lines of positions.

Let us combine the coordinate axes with the principal axes of the ellipse. Then the coordinates $x''$ and $y''$ are independent ($\rho = 0$). The density of the probability of two independent normally distributed random values has the following form:

$$W(x''; y'')=\frac{1}{2\pi\sigma_{x''}\cdot\sigma_{y''}}\exp\left[-\frac{1}{2}\left(\frac{x''^2}{\sigma^2_{x''}}+\frac{y''^2}{\sigma^2_{y''}}\right)\right], \qquad (9.23)$$

where $\sigma_{x''}$ and $\sigma_{y''}$ – mean square deviations of the coordinates $x''$ and $y''$.

Thereby the conversion to the mean square eviations in the new coordinate system is accomplished by the following formula:

$$\sigma^2_{x''}=\sigma^2_x\cos^2\varepsilon+\rho\sigma_{x''}\cdot\sigma_y\sin 2\varepsilon+\sigma^2_y\sin^2\varepsilon,$$
$$\sigma^2_{y''}=\sigma^2_x\sin^2\varepsilon-\rho\sigma_{x''}\cdot\sigma_y\sin 2\varepsilon+\sigma^2_y\cos^2\varepsilon.$$

We shall find the connection between the dimensions of the ellipse and the mean square deviations, $\sigma_{x''}$ and $\sigma_{y''}$. The expression

$$\frac{x''^2}{\sigma^2_{x''}}+\frac{y''^2}{\sigma^2_{y''}}=\text{const}=K^2 \qquad (9.24)$$

at different values of $K$, determines a family of ellipses the forms of which, i.e., eccentricity and orientation in the plane are the same. The dimension of the ellipse is determined by the values $\sigma_{x''}$ and $\sigma_{y''}$.

From a comparison of Formulas (9.21) and (9.23), it follows that

$$a_1=K\sigma_{x''},$$
$$a_2=K\sigma_{y''}.$$

In this way, $K$ is the coefficient of proportionality between the mean square deviation and the dimensions of the semiaxes of the ellipse.

The probability of the falling of the located position of the object inside the ellipse of distribution is determined according to the following formula

$$P_s = \int_{S(K)} \int W(x''; y'')\, dx''dy''. \qquad (9.25)$$

where $W(x''; y'')$ – density of probability (Formula 9.23); $S(K)$ – region bounded by the ellipse of error with the specified size of semiaxes.

After integration, we obtain

$$P_s = 1 - \exp\left(-\frac{K^2}{2}\right), \qquad (9.26)$$

$$K = \sqrt{-2\ln(1 - P_s)}. \qquad (9.27)$$

determined by Formula (9.25).

With the aid of Formula (9.26), the probability of the falling of the computed position of the object inside the ellipse of the specified dimensions may be found, while by Expression (9.27) the dimensions of the ellipse in which the probability of falling is fixed, may be determined. Formula (9.27) is used in these cases, when it is necessary to find the region inside of which all obtainable values with specified magnitude of probability are concentrated. For example, one may find the region inside which 95% of all the results of the determination of the position of the object are concentrated.

The probability of falling in a specified scattering the semiaxis of which is equal to $K$ average square deviations may be determined from Fig. 9.13 (curve 1).

In this way, the parameters of the ellipse of error appear to be the exhaustive characteristics of the accuracy of the position determination of a point in the plane. For a given location of the station, and at known mean square error of the measurement of the geometrical

quantities, every point in the plane corresponds to a family of ellipses of error differing only in the value of $K$. Assuming $K = 1$, we obtain the unit ellipse of error, whose semiaxes are equal to the mean square deviations in the directions of the principal axes. The unit ellipse in its turn is completely determined by the three numbers: $\sigma_x$, $\sigma_y$, and the angle $\varepsilon$. Consequently, the problem of estimating the accuracy of the position determination is resolved at the fixing of these characteristics for all the points in the plane.

In practice, the determination of the ellipse of errors is not always necessary. In a majority of cases, there exist only values of the errors of position determination. Thereby, the parameters of the distribution of the probability of the moduli of errors of location become the characteristics of accuracy. With the aid of the distribution of the probabilities of the moduli of error, one may determine the probability of finding the position of the object locating inside the circle of radius $D$ (Fig. 9.14), the center of which coincides with the true point location of the object. Analytical expressions of the above distribution may be found only for a single axis of the ellipse of error ($\sigma_{x''} = \sigma_{y''}$), i.e., when the ellipse turns into a circle. In this case, the probability of the falling inside the circle of radius $D$ is found directly by Formula (9.26). The density of probability distribution of the value $D$ may be determined, differentiating Relationship (9.26).

$$W(D) = \frac{D}{\sigma_{x'; y'}} \exp\left(-\frac{D^2}{2\sigma^2_{x'; y'}}\right).$$

In this way, the modulus of error of position determination is distributed according to the law of Rayleigh.

In the general case, when $\sigma_{x''} \neq \sigma_{y''}$, the probability of falling inside the circle, however, cannot be determined by the simple method. Therefore, the value of the error of position determination is

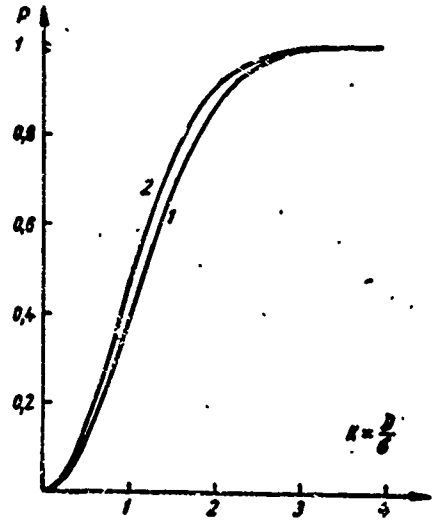

Fig. 9.13 Probability of falling into the ellipse (curve) (Curve *1*) and square of error (curve *2*).

characterized by the squares of error (Fig. 9.14) since the probability of falling of the computed position of the object inside the squares is found with the aid of the simple relationship and the areas of the squares and circles close to each other. The sides of the squares of errors are chosen to be parallel to the principal axes of the ellipse of distribution. The probability of falling in the square with side equal to $2D$ is found from the following relationships:

$$P(|x''|<D;\ |y''|<D)=$$

$$=\frac{1}{2\pi\sigma_{x''}\cdot\sigma_{y''}}\int_{-D}^{D}\int_{-D}^{D}\exp\left[-\frac{1}{2}\left(\frac{x''}{\sigma_{x''}^2}+\frac{y''}{\sigma_{y''}^2}\right)\right]dx''dy''=$$

$$=\frac{2}{\sqrt{2\pi}\sigma_{x''}}\int_{0}^{D}\exp\left(-\frac{x''^2}{2\sigma_{x''}^2}\right)dx''\cdot\frac{2}{\sqrt{2\pi}\sigma_{y''}}\int_{0}^{D}\exp\left(-\frac{y''^2}{2\sigma_{y''}^2}\right)dy''.$$

Performing a substitution of the variables of integration and assuming $r=\frac{x''}{\sigma_{x''}}$, $s=\frac{y''}{\sigma_{y''}}$, we obtain,

$$P(|x''|<D;\ |y''|<D)=\Phi\left(\frac{D}{\sigma_{x''}}\right)\Phi\left(\frac{D}{\sigma_{y''}}\right)=\Phi(K_x)\Phi(K_y), \quad (9.28)$$

where $\Phi(a)=\frac{2}{\sqrt{2\pi}}\int_{0}^{a}\exp\left(-\frac{r^2}{2}\right)dr$ is a tabulated integral.

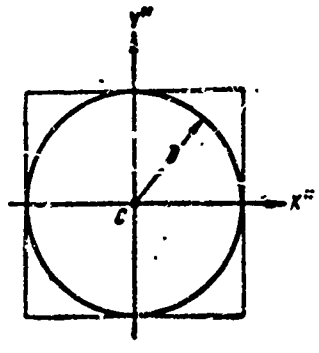

Fig. 9.14 Circle and Square of errors.

In Fig. 9.13 results are presented of the calculations for the determination of the probability of falling into the square of errors (curve *2*) and the circle inscribed in it (curve *1*). From a comparison of the curves shown, it is seen that the probabilities being examined are close to each other. Therefore, half of the side of the square of errors, $D$, the probability of falling into which is equal to a

fixed value $P$, is sufficiently complete for the determination of the modulus of errors of position determination. That value may serve as the characteristic of accuracy of the position determination of various points in the plane. Every point of the plane may be compared with the size of the half side of the square of errors. Generally, this size may well be expressed as a portion of the mean square error of measurement of any geometric quantity $d = \frac{D}{\sigma(U)}$. The aggregate of points which the value $d$ corresponds to forms the lines of position of accuracy. A family of these lines give the possibility of evaluating the accuracy of the various methods of the determination of position.

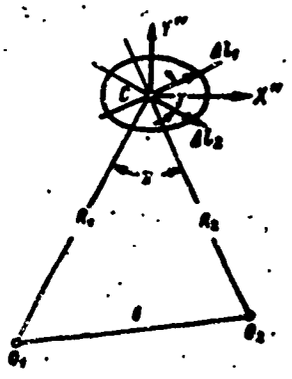

Fig. 9.15 Ellipse of error in the range finger method of position determination.

We shall find the accuracy of the position determination of the object in a plane for the previously mentioned methods.

*1) The range finder method.* We shall assume that the distance to the object is determined with the aid of two orthogonal stations, which have the same mean square error of measurement. In this assumption, the linear errors are also the same. Consequently, the principal axes of the ellipse of distribution coincide with the bisector of the angle between the lines of positions (Fig. 9.15). These angles are equal to the angles of intersection if the radius vectors are drawn from the points of the positions of the stations. The sizes of the semiaxes of the unit ellipse depend on the angle $\gamma$ and the mean square error of the measurement of distance.

We shall find the sizes of the semiaxes at the arbitary angle $\gamma$. Having determined the projections of the vectors of the linear errors $\Delta l_1$ and $\Delta l_2$ according to the axes $CX''$ and $CY''$ and converting from the

increments to the mean square errors, we obtain

$$\sigma(x'') = \frac{1}{\sqrt{2}\sin\frac{\gamma}{2}}\sigma_R, \qquad (9.29)$$

$$\sigma(y'') = \frac{1}{\sqrt{2}\cos\frac{\gamma}{2}}\sigma_R. \qquad (9.30)$$

The best results correspond to the case when the lines of position, and consequently, also the radio vectors are perpendicular. Thereby, $\sigma(x'') = \sigma(y'') = \sigma_R$.

We shall determine the lines of equal accuracy on the plane. As a measure of accuracy, we take the half of the side of the square of errors expressed as a portion of the mean square error, $d = \frac{D}{\sigma_R}$. The probability of falling in the square of errors is taken as $P = 0.6$. The error of position determination depends only on the angle between the lines of positions $\gamma$, which is equal to the angle between the radius vectors $R_1$ and $R_2$. The geometric locations of the points with the same values of $\gamma$ form a circle passing through points $O_1$ and $O_2$, therefore, only equal accuracy is indicated by the circles (Fig. 9.16). The best accuracy corresponds to the positions of the object on the circles for which the segment $O_1O_2 = b$ is the diameter. Consequently, for the necessity to obtain high accuracy at considerable distance, it is expeditious to increase the size of the base.

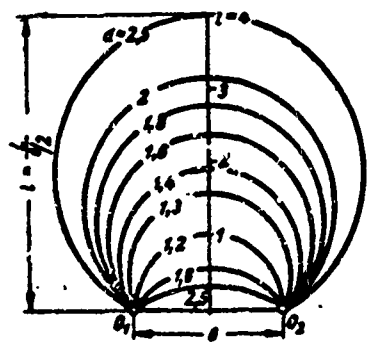


Fig. 9.16 Lines of equal accuracy using the range finder method. $L$ - segment of the perpendicular read from the center of the base.

*2) The range finder goniometer method.* With the range finder goniometer method, the lines of positions intersect at right angles. Therefore, the principal axes of the ellipse of error coincide with the lines of positions. The mean square error* in the direction of the lines of equal distance $\sigma(x'') = R\sigma(\alpha)$, and in the

direction of the lines of equal angles $\sigma(y'') = \sigma_R$. The line of equal accuracy form circles with center in the point of the location of the stations (Fig. 9.17). For the possibility of comparing with other methods, at the construction of Fig. 9.17, we assumed that the position of the object on a circle of diameter equalling to $O_1$ and $O_2$ (Fig. 9.16), corresponds to the same accuracy of the determination of position by the range finder method as well as by the range finder goniometer method.

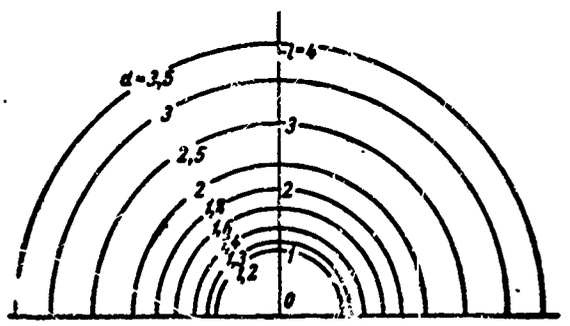


Fig. 9.17 Lines of equal accuracy using the range finder goniometer method.

*3) The goniometer method.* In the goniometer method, the accuracy of position determination depends on the angle of intersection of the radius vectors as well as on the distances to both stations. Therefore, the lines of equal accuracy have more complex shapes than in the previous cases. The character of the lines of equal accuracy is shown in Fig. 9.18. The dependence of $d$ at $P = 0.6$ on the line of segment *1*, according to Fig. 9.18 is shown in Fig. 9.19. At a calculation of that dependence, we assumed that the errors of both stations are the same. In order to compare with the methods examined earlier $\sigma(\alpha)$ is chosen with such calculations that the same accuracy of position determination for all three methods is obtained in the point of intersection of the perpendicular with the circle of the radius $\frac{b}{2}$. The size of the base is chosen in the same way as in the range finder method.

In conclusion, we may make the following remarks. When the object is located in the vicinity of the perpendicular to the base line, the highest accuracy is realized by the range finder method. But, if the deviation from the perpendicular exceeds 25 – 30°, the accuracy of position determination is lowered considerably. Therefore, in these cases, when the measuring system should be all directional, the range finder goniometer system has a substantial advantage. With the goniometer system, the accuracy of position determination is the same as the range finder system, dependent on the direction. Besides that, when the condition of the error is the same, the goniometer system is considerably greater than the rest.

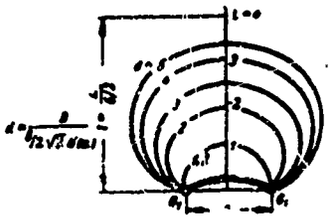

Fig. 9.18 Character of lines of equal accuracy using the goniometer method.

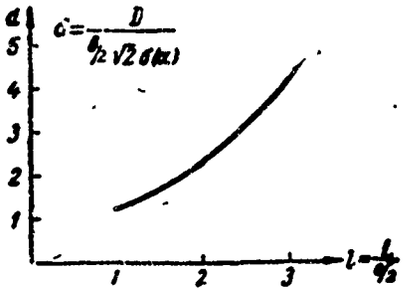


Fig. 9.19 Dependence of the error of position determination using the goniometer method on the distance to the center of the base.

## § 9.4 ACCURACY OF THE DETERMINATION OF POSITION IN SPACE.

In the searching of the accuracy of the determination of the position of the object in space, it is necessary to examine the error of measurement of three geometric quantities. The accuracy of the position determination depends on the mutual orientation of the planes of the positions and on the error in the directions of the normals to the e planes. The largest accuracy, as before, corresponds to the intersection of these normals at right angles. In the general cases, the analysis of the accuracy of the determination of the position in

space is considerably more complex than in a plane. Below, we shall examine the methods, permitting the determination of the accuracy of position determination when the object is located at any point of the space for the case of arbitrary location of the radar station.

1. Linear Error Of Position Determination

For the evaluation of the error of position determination, we examine the planes of the location of the object $C$ (Fig. 9.20). If the error of the measurement of the geometric quantity is not great, then one may substitute the surface of the position at point $C$ by the tangents of the planes, $L_1$, $L_2$, $L_3$. We find the linear error in the directions of the lines intersecting these planes. Every one of these linear errors, depend on the inaccuracy of measurement only of one geometric quantity. Thus, the intersection tangent to the planes $L_1$ and $L_3$ is determined by the straight line to which the error component is directed on account of the inaccuracy of measurement of the geometric quantity $U_2$. This error is denoted $\Delta l_2$. In the same manner, there could be assigned $\Delta l_1$ and $\Delta l_3$. Since the directional straight lines $\Delta l_1$ and $\Delta l_3$ are completely determined, so it is possible to find the corresponding moduli $\Delta l_1$; $\Delta l_2$ and $\Delta l_3$. For this it is necessary to compute the gradient of such surface positions at point $C$ and then find the angle between the normal $n_i$ and the corresponding directional lines $\Delta l_i$ .

The vectors, $\Delta l_1$; $\Delta l_2$; $\Delta l_3$ form a parallelepiped, the faces of which are the planes tangent to the surfaces of the position $U_1$; $U_2$; $U_3$ and $U_1 + \Delta U_1$; $U_2 = \Delta U_2$; $U_3 + \Delta U_3$. This parallelepiped which is analogous to the parallelogram of errors, is designated as the parallelepiped of error for the cases in space. The diagonals of the parallelepiped drawn from the point $C$ from the error of position determination in space. As can be seen in Fig. 9.20, the vector $\Delta C$

is equal to the sum of the vectors $\Delta l_1$, $\Delta l_2$ and $\Delta l_3$. In this way, the problem of finding the error of position determination leads to the determination of the vectors $\Delta l_1$; $\Delta l_2$; $\Delta l_3$ and subsequently, their sum.

We establish first coordinates at the point $C$. The coordinates of the ends of the vectors of error $\Delta\vec{C}$ may be found by the known components of the vectors parallel to $\Delta\vec{l}_1$; $\Delta\vec{l}_2$; $\Delta\vec{l}_3$.

Designate these vectors $l_1$; $l_2$; $l_3$.

We determine the direction of the vector $\vec{l}_2$. This vector belongs to the planes $L_1$ and $L_3$. Therefore, it should be perpendicular to $n_1$ and $n_3$. Consequently, its direction coincides with the directions of the vector product $\vec{n}_1 \times \vec{n}_3$ (Fig. 9.21). Using Formula (9.9), and also the rule for the finding of the components of the vector product of two vectors, we obtain

$$l_{2x} = \frac{\partial F_1}{\partial y} \cdot \frac{\partial F_3}{\partial z} - \frac{\partial F_1}{\partial z} \cdot \frac{\partial F_3}{\partial y}, \qquad (9.31)$$

$$l_{2y} = \frac{\partial F_1}{\partial z} \cdot \frac{\partial F_3}{\partial x} - \frac{\partial F_1}{\partial x} \cdot \frac{\partial F_3}{\partial z}, \qquad (9.32)$$

$$l_{2z} = \frac{\partial F_1}{\partial x} \cdot \frac{\partial F_3}{\partial y} - \frac{\partial F_1}{\partial y} \cdot \frac{\partial F_3}{\partial x}. \qquad (9.33)$$

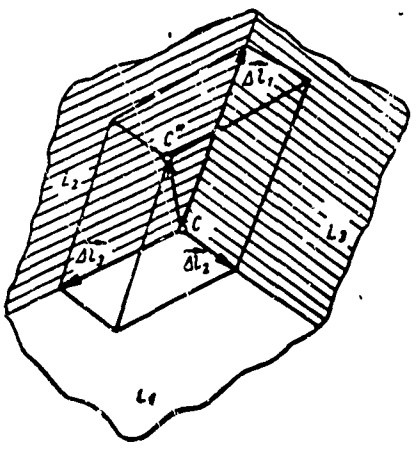


Fig. 9.20 Parallelepiped of errors. $CC^* = \overrightarrow{\Delta C}$; $\overrightarrow{\Delta C} = \overrightarrow{\Delta l_1} + \overrightarrow{\Delta l_2} + \overrightarrow{\Delta l_3}$.

Similar formulas may be found for the components of the vectors $l_1$ and $l_3$:

$$l_{1x} = \frac{\partial F_2}{\partial y} \cdot \frac{\partial F_3}{\partial z} - \frac{\partial F_2}{\partial z} \cdot \frac{\partial F_3}{\partial y}, \qquad (9.34)$$

$$l_{1y} = \frac{\partial F_2}{\partial z} \cdot \frac{\partial F_3}{\partial x} - \frac{\partial F_2}{\partial x} \cdot \frac{\partial F_3}{\partial z}, \qquad (9.35)$$

$$l_{1z} = \frac{\partial F_2}{\partial x} \cdot \frac{\partial F_3}{\partial y} - \frac{\partial F_2}{\partial y} \cdot \frac{\partial F_3}{\partial x}, \qquad (9.36)$$

$$l_{3x} = \frac{\partial F_1}{\partial y} \cdot \frac{\partial F_2}{\partial z} - \frac{\partial F_1}{\partial z} \cdot \frac{\partial F_2}{\partial y}, \qquad (9.37)$$

$$l_{3y} = \frac{\partial F_1}{\partial z} \cdot \frac{\partial F_2}{\partial x} - \frac{\partial F_1}{\partial x} \cdot \frac{\partial F_2}{\partial z}. \qquad (9.38)$$

$$l_{xz} = \frac{\partial F_1}{\partial z} \cdot \frac{\partial F_2}{\partial y} - \frac{\partial F_1}{\partial y} \cdot \frac{\partial F_2}{\partial x}. \quad (9.39)$$

By the known components, the cosines of the directional angles are found [Formulas similar to (9.10) - (9.12)].

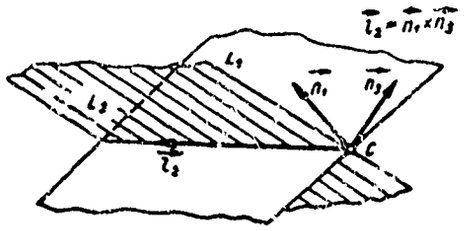


Fig. 9.21 Linear intersection of two planes $L_1$ and $L_2$.

After this, the cosines of the angles between the normals to the surface of the positions and the directional vectors $\vec{l}_1$; $\vec{l}_2$; $\vec{l}_3$

$$\cos(\vec{l}_i; \vec{n}_i) = \cos(\vec{n}_i; \vec{x})\cos(\vec{l}_i; \vec{x}) + \cos(\vec{n}_i; \vec{y})\cos(\vec{l}_i; y) + \quad (9.40)$$
$$+ \cos(\vec{n}_i; \vec{z})\cos(\vec{l}_i; \vec{z}).$$

Utilizing Formula (9.6), we find the moduli of the vectors $\Delta\vec{l}_1$; $\Delta\vec{l}_2$ and $\Delta\vec{l}_3$. Thereby,

$$\Delta l_i = \frac{\Delta U_i}{|\operatorname{grad} U_i| \cos(\vec{n}_i; \vec{l}_i)}. \quad (9.41)$$

The coordinates of the ends of the vectors of errors of position determination from an algebraic sum of the components of the vectors $\Delta\vec{l}_i$. Consequently,

$$x' = \Delta C_x = \sum_{i=1}^{3} K_{xi} \cdot \Delta U_i, \quad (9.42)$$

$$y' = \Delta C_y = \sum_{i=1}^{3} K_{yi} \cdot \Delta U_i, \quad (9.43)$$

$$z' = \Delta C_z = \sum_{i=1}^{3} K_{zi} \cdot \Delta U_i, \quad (9.44)$$

where $x'$; $y'$; $z'$ - coordinates of the ends of the vector $\Delta\vec{C}$;

$$K_{xi} = \frac{\cos(\vec{l}_i; \vec{x})}{|\operatorname{grad} U_i| \cdot \cos(\vec{n}_i; \vec{l}_i)};$$

$$K_{yi} = \frac{\cos(\vec{l}_i; \vec{y})}{|\operatorname{grad} U_i| \cdot \cos(\vec{n}_i; \vec{l}_i)};$$

$$K_{zi} = \frac{\cos(\vec{l}_i; \vec{z})}{|\operatorname{grad} U_i| \cdot \cos(\vec{n}_i; \vec{l}_i)}.$$

The relationships obtained permit us to find the linear errors in the directions of rectangular coordinate axes by the known errors of

the measurement of geometrical quantities.

2. Ellipsoid Of Errors

We switch now to the statistical characteristics of the components of the vectors of error. We assume that the errors of the measurement of geometric quantities are independent among themselves and distributed according to the normal law with zero mean value. Then the combined density of the probability of the values of the coordinates $x'$; $y'$; $z'$ describe a three dimensional normal law of distribution with zero mean value. For the specification of this distribution, it is sufficient to determine its second moments.

Similar to the corresponding formulas found in § 9.4*:

$$\sigma^2_{x'} = \sum_{i=1}^{3} K^2_{xi}\sigma^2(U_i); \tag{9.45}$$

$$\overline{x' \cdot y'} = \sum_{i=1}^{3} K_{xi} \cdot K_{yi} \cdot \sigma^2(U_i), \tag{9.46}$$

$$\overline{x' \cdot z'} = \sum_{i=1}^{3} K_{xi} \cdot K_{zi} \cdot \sigma^2(U_i). \tag{9.47}$$

$$\overline{y' \cdot z'} = \sum_{i=1}^{3} K_{yi} \cdot K_{zi} \cdot \sigma^2(U_i). \tag{9.48}$$

With the aid of these formulas, the coefficient of correlation between the values of the coordinates are determined

$$\rho(x'; y') = \frac{\overline{x' \cdot y'}}{\sigma_{x'} \cdot \sigma_{y'}}, \tag{9.49}$$

$$\rho(x'; z') = \frac{\overline{x' \cdot z'}}{\sigma_{x'} \cdot \sigma_{z'}}, \tag{9.50}$$

$$\rho(y'; z') = \frac{\overline{y' \cdot z'}}{\sigma_{y'} \cdot \sigma_{z'}}. \tag{9.51}$$

Notice that the latter formulas are valid only in the case, if the errors $\Delta U_i$ are mutually independent.

Formulas (9.49) – (9.51) allow the finding of the determinant of the coefficients of correlation which may be presented in the following form:

$$|D| = \begin{vmatrix} 1 & \rho(x'; y') & \rho(x'; z') \\ \rho(x'; y') & 1 & \rho(y'; z') \\ \rho(x'; z') & \rho(y'; z') & 1 \end{vmatrix}.$$

These characteristics obtained completely determine the density

of probability of the three dimensional normal distribution of the coordinates of the located position of the object:

$$W(x'; y'; z') = \frac{1}{\sigma_{x'}\sigma_{y'}\sigma_{z'}\sqrt{(2\pi)^3|D|}} \exp\left[-\frac{1}{2|D|}\left(\frac{D_{xx}}{\sigma_{x'}^2}x'^2 + \right.\right.$$
$$\left.\left. + \frac{D_{yy}}{\sigma_{y'}^2}y'^2 + \frac{D_{zz}}{\sigma_{z'}^2}z'^2 + \frac{2D_{xy}}{\sigma_{x'}\sigma_{y'}}x'y' + \frac{2D_{xz}}{\sigma_{x'}\sigma_{z'}}x'z' + \frac{2D_{yz}}{\sigma_{y'}\sigma_{z'}}y'z'\right)\right]. \quad (9.52)$$

where $D_{xy}$; $D_{xz}$, etc., – corresponding algebraic complement of the determinant $|D|$.

From Formula (9.52), it can be seen that the constant density of probability corresponds to the fixation of the value of the expression which obeys the law of exponential functions. Adjusting this expression to a constant value, we obtain the equation of a surface of the second order in space. In the case being examined, this surface forms the surface of an ellipsoid. This ellipsoid characterizes the distribution of the errors of position determination of the object in space and is designated as the ellipsoid of errors or the ellipsoid of distribution.

At any arbitrary location of the coordinate axes, relative to the principal axes of the ellipsoid of distribution, there are sites of correlation between the values of the coordinates. If the principal axes coincide with the coordinates, then the equation of the ellipsoid assumes the canonical form. Thereby, the values of these coordinates become independent. The combined density of the probability of the values of the coordinates may be presented in the following form:

$$W(x''; y''; z'') = \frac{1}{\sqrt{(2\pi)^3}\sigma_{x''}\sigma_{y''}\sigma_{z''}} \exp\left[-\frac{1}{2}\left(\frac{x''^2}{\sigma_{x''}^2} + \frac{y''^2}{\sigma_{y''}^2} + \frac{z''^2}{\sigma_{z''}^2}\right)\right].$$

where $\sigma_{x''}$; $\sigma_{y''}$; $\sigma_{z''}$ – mean quadratic deviation of the converted rectangular coordinates.

In this way, further problem is decided in the finding of the position of the principal axes of the ellipsoid or errors and the mean

square deviation from these axes.

3. Determination Of The Orientation Of The Principal Axes And The Mean Square Deviation In The Direction Of These Axes

We shall look at the arbitrary ellipsoid of distribution (Fig.9.22). (On the drawing a cross-section of the ellipsoid is shown, i.e., an ellipse.) Normals, drawn through various points of its surface, in the general cases, do not go through the center of symmetry of the ellipsoid, i.e., the direction of the normals and the radius vectors, drawn from the center of symmetry of the ellipsoid $C$, do not coincide. Identical directions of the normals and the radius vectors are the distinctive properties of the principal axes of the ellipsoid. Therefore, in an arbitrary system of rectangular coordinates, passing through the center of symmetry of the ellipsoid, the cosines of the directional angles of the normals and the radius vectors in the principal directions are equal among themselves. The cosines of the directional angles of the normals are proportional to the derivatives $\frac{\partial F}{\partial x}; \frac{\partial F}{\partial y}; \frac{\partial F}{\partial z}$ [Formula (9.9)] and the cosines of the radius vectors – proportional to the coordinates $x'; y'; z'$. Consequently,

$$\frac{\partial F}{\partial x}=\lambda x,\ \frac{\partial F}{\partial y}=\lambda y,\ \frac{\partial F}{\partial z}=\lambda z, \qquad (9.53)$$

where $\lambda$ – coefficient of proportionality.

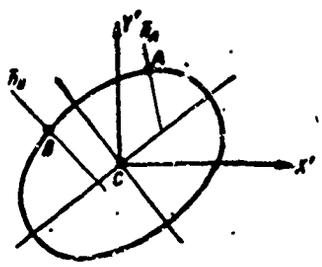


Fig. 9.22 Cross-section of the ellipsoid of distribution.

We introduce now the equations of the surface of the ellipsoid of distribution obtained on the basis of Formula (9.52) in the following

form

$$a_{11}x'^2 + a_{22}y'^2 + a_{33}z'^2 + 2a_{12}x' \cdot y' + \\ + 2a_{13}x' \cdot z' + 2a_{23}y' \cdot z' = K^2.$$

Conducting partial differentiation with respect to Relationship (9.53), we obtain

$$a_{11}x' + a_{12}y' + a_{13}z' = \lambda x', \\ a_{12}x' + a_{22}y' + a_{23}z' = \lambda y', \\ a_{13}x' + a_{23}y' + a_{33}z' = \lambda z'$$

or

$$(a_{11} - \lambda)x' + a_{12}y' + a_{13}z' = 0, \\ a_{12}x' + (a_{22} - \lambda)y' + a_{23}z' = 0, \\ a_{13}x' + a_{23}y' + (a_{33} - \lambda)z' = 0. \qquad (9.54)$$

The solution of this given system of equations determines the position of the principal axes of the ellipsoid of distribution in the arbitrary system of rectangular coordinates. The system of Equation (9.54) has a zero solution in the one and only case if the determinant of the coefficients of this system is equal to zero. Consequently, it is necessary that the condition be maintained

$$\begin{vmatrix} a_{11} - \lambda & a_{12} & a_{13} \\ a_{12} & a_{22} - \lambda & a_{23} \\ a_{13} & a_{23} & a_{33} - \lambda \end{vmatrix} = 0. \qquad (9.55)$$

Having computed the determinant (9.55), we obtain the cubic equation relative to $\lambda$, which is designated as *characteristics:*

$$\lambda^3 - (a_{11} + a_{22} + a_{33})\lambda^2 + (a_{11}a_{33} + a_{22}a_{33} + \\ + a_{11}a_{22} - a_{12}^2 - a_{13}^2 - a_{23}^2)\lambda + a_{11}a_{23}^2 + a_{22}a_{13}^2 + \qquad (9.56) \\ + a_{33}a_{12}^2 - a_{11}a_{22}a_{33} - 2a_{12}a_{13}a_{23} = 0$$

or

$$\lambda^3 + A\lambda^2 + B\lambda + C = 0.$$

The roots of this equation may be found in the following manner:

a) Determine the auxiliary values

$$p = B - \frac{A^2}{3}; \quad q = \frac{2A^3}{27} - \frac{A \cdot B}{3} + C;$$

b) find the cosine of the auxiliary angle $\varphi$

$$\cos\varphi = +\frac{3}{2}\sqrt{-\frac{3q^2}{p^3}}; \quad 0 < \varphi < \frac{\pi}{2};$$

c) determine the roots of the cubic equation according to the relationship

$$\lambda_i = \pm 2\sqrt{-\frac{p}{3}}\cos\left[\frac{\varphi}{3} + \frac{2}{3}\pi(i-1)\right] - \frac{A}{3}, \qquad (9.57)$$

where $i = 1, 2, 3$, whereupon the sign " + " stands in the case when $q < 0$, while the sign " − ", if $q > 0$.

All the roots of the cubic equation (9.56) are real.

At known values of $\lambda_1$; $\lambda_2$; and $\lambda_3$, it is not difficult to determine the direction of the principal axes in an arbitrary coordinate system $x'$; $y'$; $z'$. The cosines of the directional angles of the principal axes proportional to the values of the coordinates, are the solutions of the system of Equations (9.54).

The values of the coordinates $x'$; $y'$; $z'$ in sequence for $\lambda_1$; $\lambda_2$; and $\lambda_3$ may be found on the general formula for the solution of similar system of equations

$$x' : y' : z' = D'_{11} : D'_{12} : D'_{13}, \qquad (9.58)$$

where $D'_{11}$; $D'_{12}$; and $D'_{13}$ − corresponding algebraic complementary elements of Determinant (9.55).

For the finding of the mean square deviation in the direction of the principal axes, let us look at the canonical form of the equation of the surface of the ellipsoid

$$a^*_{11}x''^2 + a^*_{22}y''^2 + a^*_{33}z''^2 = K^2.$$

The reduced considerations on the relationship of the directions of the radius vectors and the normals remain valid in this case. Therefore,

$$\frac{\partial F}{\partial x''} = x'' \cdot a^*_{11} = \lambda x'', \quad \frac{\partial F}{\partial y''} = y'' \cdot a^*_{22} = \lambda \cdot y'';$$

$$\frac{\partial F}{\partial z''} = z'' \cdot a^*_{33} = \lambda \cdot z''.$$

From the reduced relationships, it follows that the coefficients $a_{ii}$ are equal to the roots of Cubic Equation (9.55). The equation of

the surface of the ellipsoid may be also presented in the following form:

$$\frac{x''^2}{\sigma_{x''}^2}+\frac{y''^2}{\sigma_{y''}^2}+\frac{z''^2}{\sigma_{z''}^2}=K^2, \qquad (9.59)$$

since

$$\rho(x''; y'')=\rho(x''; z'')=\rho(y''; z'')=0.$$

therefore

$$\sigma_{x''}=\sigma_{\lambda_1}=\frac{1}{\sqrt{\lambda_1}}; \quad \sigma_{y''}=\sigma_{\lambda_2}=\frac{1}{\sqrt{\lambda_2}}; \quad \sigma_{z''}=\sigma_{\lambda_3}=\frac{1}{\sqrt{\lambda_3}}.$$

In this way, the reduced method of calculation permits the determination of the mean square error by the coordinate axes and the orientation of the principal axes of the ellipsoid of distribution.

4. Sequence Of Calculations For The Determination Of The Principal Axes Of The Ellipsoid Of Distribution

For setting up the sequence of reduced calculations, we shall look at a concrete numerical example. Let us assume that the position determination of the object is determined with the aid of three range finders located at the points $O_1$, $O_2$ and $O_3$ (Fig. 9.23a). The object is located at a point having the coordinates: $R_1 = 300$ km; $\beta = 25°$; $\alpha = 15°$. The mutual positions of the stations are characterized by the following values: $O_1O_3=b=150$ км; $O_1O_2=c=350$ км, $\angle O_3O_1O_2=60°$. The mean square errors of the distance measurements for all three distances are the same ($\sigma_R = 200$ m).

1. We find the cosines of the directional angles $\vartheta_3$ and $\vartheta_1$ by Formulas (9.1) and (9.2)

$$\cos\vartheta_3=\cos 15°\cos 25°=0{,}875,$$
$$\cos\vartheta_1=\cos 45°\cos 25°=0{,}64.$$

2. We determine the deviation of the distance relative to the stations $O_2$ and $O_3$ by the theorem of cosines

$$R_2=\sqrt{R_1^2+c^2-2cR_1\cos\vartheta_2}=279 \text{ км};$$
$$R_3=\sqrt{R_1^2+b^2-2bR_1\cos\vartheta_3}=184 \text{ км}.$$

3. We compute the rectangular coordinates of the points $O_2$, $O_3$

and $C$ (in km), $O_2$ (175; 303,0); $O_3$ (150; 0; 0); $C$ (263; 70; 127).

4. We find the vectors normal to the surfaces in spherical coordinates (Fig. 9.23b; Formula 9.9) at the point of the location of the object:

$$\vec{n}_1(263;\ 70;\ 127);\ \vec{n}_2(88;\ -233;\ 127);\ \vec{n}_3(113;\ 70;\ 127).$$

5. We determine the relationship of the vectors $l_1$; $l_2$ and $l_3$, taking into account that the initial coordinates are located at the point $C$, coordinate axes parallel to the original.

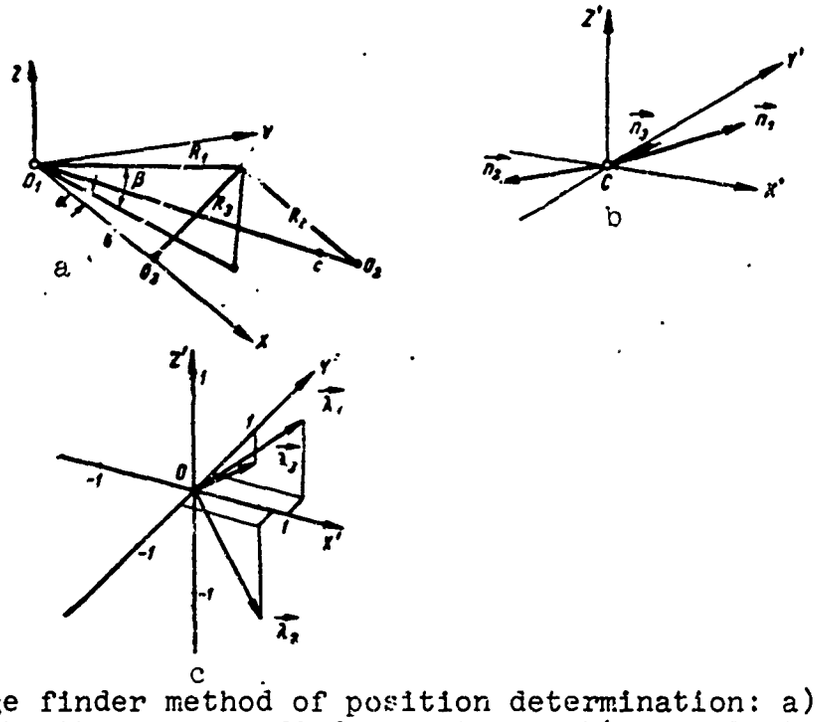


Fig. 9.23 Range finder method of position determination: a) Mutual positions of the three range finder stations; b) normals to the sphere-like surface; c) principal axes of the ellipsoid of distribution.

The calculation is carried out by Formulas (9.31) to (9.39)

$$\begin{array}{lll} l_{1x} = -3{,}85; & l_{2x} = 0; & l_{3x} = 3{,}85; \\ l_{1y} = 0{,}32; & l_{2y} = -1{,}73; & l_{3y} = -2{,}22; \\ l_{1z} = 3{,}58; & l_{2z} = 1{,}05; & l_{3z} = 6{,}75. \end{array}$$

6. We find the cosines of the directional angles between the normals and the vectors $l_i$ (Formula 9.40)

$$\cos(\vec{l}_1;\ \vec{n}_1) = -0{,}339;\ \cos(\vec{l}_2;\ \vec{n}_2) = 0{,}95;\ \cos(\vec{l}_3;\ \vec{n}_3) = -0{,}388.$$

7. We compute the momenta of the positions of the coordinates of

the ends of the vectors of errors $\Delta\vec{C}$ and the coefficients of correlation (Formula 9.44 to 9.50).

$$\sigma^2_{x'} = 6{,}17\sigma^2_R;\ \sigma^2_{y'} = 1{,}35\sigma^2_R;\ \sigma^2_{z'} = 8{,}95\sigma^2_R;$$
$$\overline{x' \cdot y'} = -1{,}257\sigma^2_R;\ \overline{x' \cdot z'} = -6{,}98\sigma^2_R;\ \overline{y' \cdot z'} = 1{,}39\sigma^2_R;$$
$$\rho(x';\ y') = -0{,}436;\ \rho(x';\ z') = -0{,}94;\ \rho(y';\ z') = 0{,}4.$$

*8.* We work out the determinant of the coefficients of correlation, compute their values and the algebraic complements of its elements

$$|D| = \begin{vmatrix} 1 & -0{,}436 & -0{,}94 \\ -0{,}436 & 1 & 0{,}4 \\ -0{,}94 & 0{,}4 & 1 \end{vmatrix} = 0{,}094,$$

$$D_{xx} = 0{,}84;\ D_{xz} = 0{,}766;\ D_{yz} = -0{,}01;\ D_{xy} = -0{,}06,\ D_{yy} = 0{,}116;$$
$$D_{zz} = 0{,}810.$$

*9.* We find the equation of the surface of the ellipsoid (Formula 9.52)

$$\frac{1}{\sigma^2_R}\left(\frac{0{,}84}{1{,}16}x'^2 + \frac{0{,}116}{0{,}254}y'^2 + \frac{0{,}810}{1{,}68}z'^2 - \frac{2 \cdot 0{,}06}{0{,}5422}x' \cdot y' + \right.$$
$$\left. + \frac{2 \cdot 0{,}766}{1{,}397}x' \cdot z' - \frac{2 \cdot 0{,}01}{0{,}6531}y' \cdot z'\right) = k^2.$$

The coefficients of this equation permits the writing of the cubic equation relative to $\lambda$.

*10.* We determine the coefficients of the characteristics equation [Formula(9.55)].*

$$\begin{vmatrix} 0{,}724\lambda & -0{,}111 & 0{,}548 \\ -0{,}111 & 0{,}457 - \lambda & -0{,}0153 \\ 0{,}548 & -0{,}0153 & 0{,}481 - \lambda \end{vmatrix} = 0.$$

*11.* We find the characteristics equation

$$\lambda^3 - 1{,}663\lambda^2 + 0{,}587\lambda - 0{,}0177 = 0.$$

*12.* We compute the roots of the characteristics equation by Formula (9.57).

$$p = -0{,}335;\ q = -0{,}0332;\ \cos\varphi = 0{,}428;\ \lambda_1 = 1{,}176;\ \lambda_2 = 0{,}0306;\ \lambda_3 = 0{,}4525.$$

*13.* We work out the system of linear equations (9.54) in sequence for $\lambda_1$; $\lambda_2$ and $\lambda_3$:

$$\lambda_1 \qquad \lambda_2$$

$$\begin{cases} -0{,}452x' - 0{,}111y' + 0{,}548z' = 0, \\ -0{,}111x' - 0{,}719y' - 0{,}0153z' = 0, \\ 0{,}548x' - 0{,}0153y' - 0{,}695z' = 0; \end{cases} \quad \begin{cases} 0{,}693x' - 0{,}111y' + 0{,}548z' = 0, \\ -0{,}111x' + 0{,}427y' - 0{,}0153z' = 0, \\ 0{,}548x' - 0{,}0153y' + 0{,}451z' = 0; \end{cases}$$

$$\lambda_3$$

$$\begin{cases} 0{,}271x' - 0{,}111y' + 0{,}548z' = 0, \\ -0{,}111x' + 0{,}0049y' - 0{,}0153z' = 0, \\ 0{,}548x' - 0{,}0153y' + 0{,}0288z' = 0. \end{cases}$$

*14.* We determine the direction of the principal axes of the ellipsoid of distribution by Formula (9.58). Each solution of Equation (9.54) determines the principal directions in the original form of coordinates, i.e., directions of the principal axes are fixed. For the fixation of the segment according to the direction of one of the obtained vector components, we set it to equal to 1 (Fig. 9.23c).

$$D'_{11} : D'_{12} \cdot D'_{13} = 0{,}499 \cdot 0{,}0853 : 0{,}395,$$

$$\vec{\lambda}_1 (1;\ 0{,}171;\ 0{,}794);$$

$$D'_{11} : D'_{12} : D'_{13} = 0{,}192 : -0{,}0415 : -0{,}232,$$

$$\vec{\lambda}_2 (0{,}827;\ -0{,}179;\ -1);$$

$$D'_{11} : D'_{12} : D'_{13} = -0{,}000093 : 0{,}005202 : -0{,}001,$$

$$\vec{\lambda}_3 (-0{,}0175;\ 1;\ -0{,}192).$$

*15.* We check the obtained results, since the principal axes are mutually perpendicular, the cosines of the angles between the directions determined by the formula similar to (9.40) should be equal to zero.

$$\cos(\vec{\lambda}_1; \vec{\lambda}_2) \approx 0, \quad \cos(\vec{\lambda}_1; \vec{\lambda}_3) \approx 0, \quad \cos(\vec{\lambda}_2; \vec{\lambda}_3) = 0{,}02.$$

Consequently, two angles equal to 90° and the third angle $\angle \vec{\lambda}_2; \vec{\lambda}_3 = 89°$, which is admissible.

*16.* We determine the mean square errors in the directions of the principal axes of the ellipsoid of distribution;

$$\sigma_{\lambda_1} = 0{,}922\sigma_R; \quad \sigma_{\lambda_2} = 5{,}72\sigma_R; \quad \sigma_{\lambda_3} = 1{,}49\sigma_R.$$

From the obtained results one can see that on account of the non-

optimum location of the stations relative to the object, the mean square errors in two axes seems to be significant.

5. Error Of Position Determination In Space

Just as the case for the position determination in a plane, every point corresponds to a family of ellipsoids of distribution, differing only in the parameter $K$ (Formula 9.59). The probability of falling into the ellipsoid of distribution, with semiaxes of which equal to $K$ – of the mean square of deviation, is determined by the following formula, found in a similar way to Formula (9.26):

$$P(K)=\Phi(K)-\frac{2K}{\sqrt{2\pi}}\exp\left(-\frac{K^2}{2}\right). \qquad (9.60)$$

The ellipsoids, whose principal semiaxes are equal to *1*, *2* and *3* mean square deviations by this axis, is characterized by the following probabilities:

$$P(1)=0{,}2;\ P(2)=0{,}74;\ P(3)=0{,}97.$$

The distribution of the moduli of errors of position determination may be found only under the condition that the mean square errors in the direction of the principal axes are the same. Thereby, the probability of the fixed values of errors of position determination are found by Formula (9.60). The parameter $K$ in this case is related to the radius of the sphere inside of which the located positions of the object are distributed with the fixed probability $P(K)$ with the mean square of errors in the direction of the principal axes. The distribution of the radii of this sphere has the name of the Maxwell distribution.

By analogy with the errors in the plane for the characteristics of the values of the errors of the position determination in the general case, the probability of the falling of the located position of

the object inside the cube is taken up. The sides of this cube are parallel to the principal axes of the ellipsoid of distribution; the center of symmetry of the cube and the ellipsoid coincide. The probability of falling inside the cube with the side $2D$ may be found by the following formula:

$$P(x'' < D;\ y'' < D;\ z' < D) = \Phi\left(\frac{D}{\sigma_{\lambda_1}}\right)\Phi\left(\frac{D}{\sigma_{\lambda_2}}\right)\Phi\left(\frac{D}{\sigma_{\lambda_3}}\right).$$

For the example given previously, we obtain that when the probability of falling into the cube is $P = 0.9$, half of the side $D$ should be equal to $10\sigma_R$. At the same time, if the normals to the spherical surfaces are mutually perpendicular, the size of the cube is $2\sigma_R$, thereby it is the same as the probability $P$.

6. Errors Of Position Determination In Space Using Various Methods

*The range finder goniometer method.* When the range finder method is used, the planes, tangent to the surfaces of positions are mutually perpendicular, (Fig. 9.24). Therefore, the principal axes of the ellipsoid of distribution coincide with normals to the surface of position, and the corresponding mean square errors are equal to the linear errors in the direction of these normals. Then,

$$\sigma_{x''} = R\cos\beta\sigma(\alpha);\ \sigma_{y''} = \sigma(R);$$
$$\sigma_{z''} = R\sigma(\beta).$$

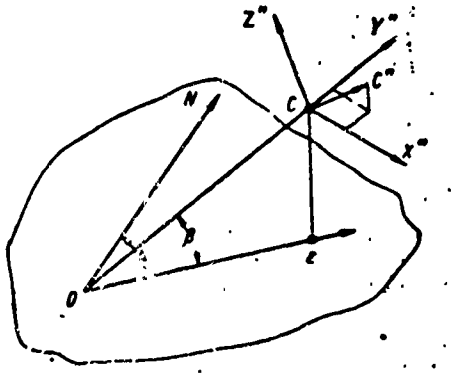


Fig. 9.24 The location of the principal axes of the ellipsoid of distribution when the range finder goniometer method is used.

Consequently, the error of position determination depends on the distance to the stations and the angle of location of the object. The geometric location points in space, characterized by the same accuracy of position determination, form a circle as a result of the intersection of

a sphere with a cone, (Figure 9.25 shows the dependence of the size of the cube of errors *(P = 0.6)* on the slope of the range for various angles.

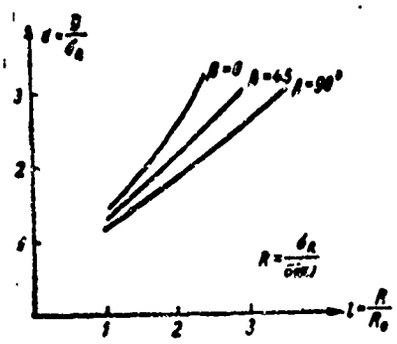


Fig. 9.25 Dependence of the magnitude of the error of location on the distance using the range finder goniometer method.

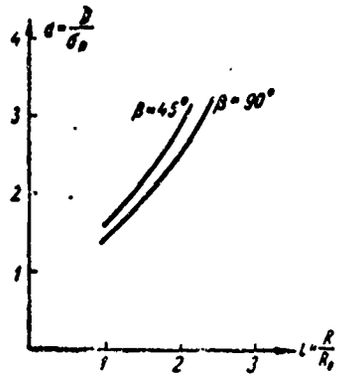


Fig. 9.26 Dependence of the magnitude of the error of location on the distance when the values of two directional angles are fixed.

$$R_0 = \frac{\sigma_R}{\sigma(\alpha)}.$$

$$R_0 = \frac{\sigma_R}{\sigma(\alpha)}.$$

*The range finder goniometer method of determination of direction with the aid of two directional angles.* Using this method, the slope of the range *(R)* and two directional angles $\vartheta_x$ and $\vartheta_y$ (Fig. 9.3). The measurement of each of these directional angles is accomplished by the reading of the various distances (from two pairs of points, located on the axes *OX* and *OY* correspondingly), to the object under the condition $b_x \ll R$; $b_y \ll R$. The object is located at the intersection of the spherical and two conical surfaces of positions. Differing from the previous method, the normal to the spherical surface is perpendicular to the normals of the other surfaces of positions. Therefore, the accuracy of position determination depends not only on the gradients of the fields of geometric quantities but also on the mutual orientation of the normals to the conical surfaces. The acute angle between these normals increases from 0 (when $\beta = 0$) to 90° (when $\beta = 90°$). At the same time,

according to Formula (9.8), the gradient of the field of fixed values of directional angles depends on the slanted distance and the angle $\delta$. Therefore, the accuracy of the position determination is lowered when $R$ increases and when the location angle $\beta$ decreases. Besides this, the highest accuracy corresponds to the position of the object in the azimuthal plane dividing in half the right angle between the base directions ($\alpha = 45°$. The curves similar to those shown in Fig. 9.25 constructed for $\beta = 45°$ and $\beta = 90°$ (Fig. 9.26) permit us to make a comparison of both methods. It seems that even in the most favorable case ($\alpha = 45°$), the accuracies of the position determination when the angles are measured using the various range finder methods are comparatively not great. But, these methods are perspective since the linear error produced during its use, may be substantially reduced when the size of the bases are $b_x$ and $b_y$ is increased (Fig. 9.8).

*The range finder method.* The error of position determination when using this method is dependent only on the accuracy of the measurement of range and the mutual orientation of the radius vectors. At a deviation from the "optimum" direction (where the radius vectors are orthogonal), the accuracy is lowered faster than the determination of location in the plane. At the same time, the method being examined is characterized by a small dependence of accuracy on the slope of the range. This method is most frequently used in systems with limited sectors of the working angles.

Manuscript Page No.

[Footnotes]

676 The angles $\vartheta_2$; $\vartheta_3$ and $\Delta$ may be found by formula for the solution of oblique angled triangles since the sides of all triangles since the sides of all triangles are known.

680 Here and further on it is to be understood that the error of measurement of geometric quantities does not depend on the coordinates of the object and at all points of space it is the same.

695 $\sigma(\alpha)$ – error of the measurement of the angle $\alpha$.

701 For obtaining $\sigma^2(y')$ and $\sigma^2(z')'$ in Formula (9.45) $K^2_{xi}$ should be replaced by $K^2_{vi}$ and $K^2_{zi}$ correspondingly.

708 All coefficients of the characteristic equations may be increased by $n$ times. Thereby, the roots of the equations increase also by the same number of times.

[Transliterated Symbols]

684 r = g = gorizontal'nyy = horizontal

Chapter 10

# DETERMINATION OF THE PATHS OF THE OBJECTS WITH THE AID OF RADIOLOCATIONAL FACILITIES

## §10.1. FEATURES OF THE DETERMINATION OF THE PATHS OF VARIOUS OBJECTS

The ultimate problem in the radiolocational measurements in most cases is the determination of all the paths of the object or parts of its sections. The path of a point object forming exhaustive space-time characteristics of the motion of the center of mass of the object, is for example, in the rectangular coordinates, being considered as a function of time:

$$x(t),\ y(t),\ z(t).$$

The path may be reproduced by a continuous observation on the object. But, at discrete measurements, it is also possible to obtain sufficiently complete data on the motion of the object. We assume for example, that with the aid of RLS a measurement of the coordinates at Points 1, 2 and 3 is to be carried out (Fig. 10.1). For simplification it will be assumed that the motion is on a plane. On the basis of the data of the measurement, a curve may be used to characterize the motion of the object. If however, besides this, the time of the stay of the object at Points 1, 2 and 3 were also specified, then the velocity of its motion will be known. Therefore, by the results of the measurements, it is possible to find the position the object is occupying between the moments of measurements and also to predict the position of the object in the ensuing moment of time.

The located position of the object is diffeent from the true one. This deviation is produced by two reasons. The first of which is included in the inaccuracy of the measurement of the true coordinates. The second reason is dependent on the incomplete correspondence between the hypotheses on the laws of motion of the object based on the results of measurement and the true characteristics of the path. At the same time, the errors of determination of the coordinates also interfere with the development of the actual law of motion.

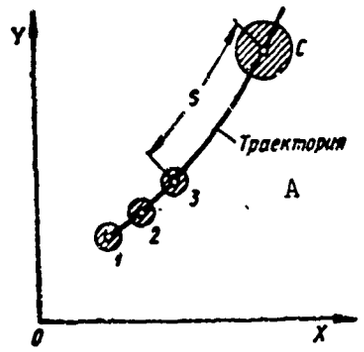


Fig. 10.1 A segment of the path of the object 1, 2, 3, observation points *C* anticipated point. *A) Path.*

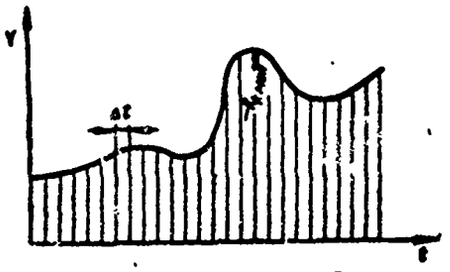


Fig. 10.2. Target rectangular coordinate as function of time.

Let us examine the error of the determination of the anticipated point of the object resulted from the deviation of the true motion form the assumed. Obviously, these errors depend on the distance between the end of the segment of observation and the anticipated point *C* (segment *S* in Fig. 10.1) and on the maneuver of the object. The maneuvering of the object in its turn is determined by its flying tactics characteristics, i.e., maximum speed of motion, maximum permissible acceleration, etc. These objects are airplanes, winged rockets and others.

Besides that, an important quality is the possibility of the control of the motion of the object. Uncontrolled objects moving under the action of natural forces do not possess maneuverability. Consequently the law of their motion may be predicted with high degree of accuracy when we have the knowledge of the characteristics of the force acting on the body being examined. To this type of objects belong the ballistic rockets, artificial earth satellites (ISZ) and cosmic rockets.

The errors of the determination of the anticipated position, being referred to also as the errors of extrapolation, are considerable

in more maneuverable objects. Therefore for the obtaining of the same accuracy in extrapolation of different objects, the radiolocational measurement of coordinates of the more maneuverable objects should be conducted with smaller errors. The obtaining of small errors is interlinked with additional energy expenditure. Consequently, at the radiolocational observation of nonmaneuverable objects the energy consumption is at the minimum.

For the establishment of the quantitative characteristics, let us look at the dependence of one of the rectangular coordinates of the object on time $y(t)$ (Fig. 10.2). The maneuverability of the object in the direction of the coordinate axis being examined is determined possibly by the curved line $y(t)$. Thus, at an uniform motion of the graph, $y(t)$ forms a straight line, at equal speed, – a parabola, etc. The maneuverability of real objects are limited by the maximum permissible acceleration. At the same time, acceleration is connected with the radius of curvature $R_k$, which is determined by the following relationship

$$R_k = \frac{(1+v_y^2)^{\frac{3}{2}}}{w_y}, \qquad (10.1)$$

where $R_k$ – radius of curvature at the arbitrary value $y(t)$; $v_y$ and $w_y$ – component velocity vectors and acceleration of the object correspondingly.

From Formula (10.1) it follows that the radius of curvature is limited below by the maximum value of the acceleration of the object. At the one and same maximum acceleration, the minimum radius of curvature is larger at the acceleration of the object, i.e., with the increase in velocity, the maneuverability becomes worse.

The maximum radius of curvature is determined by a number of parameters with the aid of which the curve being examined may be presented

in the form of an analytical expression. It is known that any continuous function determined at some interval of the values of the argument may be approximated by a polynomial with any degree of accuracy.

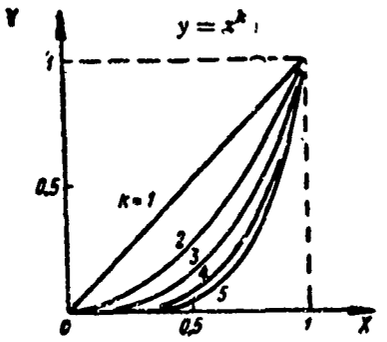


Fig. 10.3 Dependence of $y = x^k$ when $k = 1, 2, 3, 4, 5$.

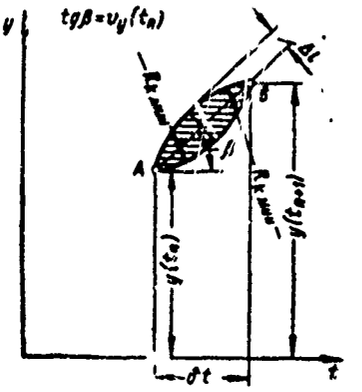


Fig. 10.4 Interval of discreteness and maximum linear error of reproduction function.

The degree of that polynomial at a given accuracy of the reproduction curve depends on the minimum radius of curvature. The stated position is explained in Fig. 10.3, on which a family of curves $y = x^k$ is shown. As one can see from the curve, the radius of curvature decreases with the increase of the index of the degree $k$. In this way, for the reproduction curve with small radius of curvature, it is necessary to have an approximating polynomial with large values of $k$.

A polynomial in the power of $k$ may be presented in the following form:

$$y = P_k(x) = C_0 + C_1 x + \ldots + C_k x^k. \qquad (10.2)$$

The combination of $k + 1$ coefficients gives the possibility of reproduction dependence $y(t)$ with specified accuracy. In the case being examined, the coefficients of the polynomial $C_i$ characterize the path completely. The numbers whose combinations permit the single-valued determination of the path are designated as the parameters of the

path. Quantitatively, these parameters are connected with the flying tactics characteristics of the object.

Let us find one of the methods of specification of the stated parameters. For which, transform Expression (10.2) by substituting

$$x = \cos t.$$

Thereby, the approximating polynomial is transformed into an even trigonometric polynomial

$$P_k(\cos t) = f_k(t) = a_0 + \sum_{i=1}^{k} a_i \cos it. \qquad (10.3)$$

From Relationship (10.3) it can be seen that the path of the object may be specified by the aid of the sum of harmonic vibrations with multiple frequencies. The largest frequency of this vibration is determined by the minimum radius of curvature $y(t)$. Consequently, $f_k(t)$ is a function with a limited spectrum. According to the theorem of Kotelnikov, such a function may be completely specified by a combination of discrete values following with equal intervals of $\Delta t$.

We shall determine the interval of discreteness at the approximation of the curve $y(t)$ with its values taken at equal intervals of time. The above mentioned values of the function $y(t)$ thereby are the parameters of the path. We find the regions of the possible values of the function between two connected readings $y(t_n)$ and $y(t_{n+1})$. Since the radius of curvature could not be smaller than its minimum value, $R_{k\ \min}$ the values of the function are distributed inside of the segment of the plane limited by the arcs of the circle of the radius $R_{k\ \min}$ (Fig. 10.4). Consequently, the maximum linear error of the reproduction function consists of $\pm\Delta l$. Having assigned the magnitude of this error, the interval of discreteness being sought may be found by way of simple geometric construction. Actually $\Delta l$ forms the altitude of the segment of the circle of the radius $R_{k\ \min}$. By the known values

of $\Delta l$ and $R_{k\ min}$, the values of the segment of $AB$ may be found which appear to be a chord of the same circle. The projection of the segment $AB$ on the horizontal axis is the necessary interval of discreteness in time

$$\Delta t = 2\sqrt{\frac{\Delta l\,(2R_{k\ мин} - \Delta l)}{1 + v^2_{y\ макс}}}. \qquad (10.4)$$

With the aid of this formula, one may find the interval of discreteness at the reproduction path with the help of series of values of rectangular coordinates taken through equal intervals of time. The error of reproduction does not exceed thereby $\Delta l$. The total number of parameters found in the above mentioned method is significant for the path of maneuverable objects. But at the determination of the total number of parameters, it must be taken into consideration that the probability of the continuous maneuvering of the object is practically equal to zero. The total number of maneuvers of the object, i.e., deviation from the forward motion, could not be significant. Therefore the quantity of parameters of path of a real object found with the consideration of the above circumstances, are relatively not large.

When the motion of the object comes under the action of a force, the laws of its variation with time and space are known, all the paths of the object are determined by six independent parameters. In truth, the law of motion of material points in the direction of the coordinate axis may be described by the differential equation of the second order

$$m\frac{d^2y}{dt^2} = F\left(y;\ \frac{dy}{dt};\ t\right),$$

where $m$ – mass of the body; $F$ – force acting on the body.

The solution of that equation is characterized by two arbitrary constants which are the parameters of the motion along the $Y$ axis.

Considering analogously when examining the motion around the other axes, we obtain that the total number of parameters is equal to six.

In this way, the total number of parameters, with whose help one may determine the path, is closely connected with the maneuvering properties of the object. In its turn, the number of parameters is an extremely important characteristic from the standpoint of the construction of the system of radiolocational observation of the object. It may be assumed under stable and equal conditions, the necessary number of coordinate measurements is proportional to the number of parameters of the path.

## §12. THE USE OF RADIOLOCATIONAL MEASUREMENTS FOR THE SEARCH OF PARAMETERS OF THE PATH

For the observation of moving objects with the aid of radiolocational facilities, the total number of coordinate measurements in many cases seem to be larger than necessary for the unambigious determination of the path. Thus, one RLS may accomplish the continuous measurement of the coordinate (during its operation in the process of automatic tracking). It is permissible that with the help of one RLS, the coordinates of the object are measured through small intervals of time $\Delta t_n$, whereupon the results of the measurement are mutually independent. As a result of the limits of the maneuverability of the object, it may be assumed that there exist some intervals of time, during which the velocity of the object is constant. We denote that time interval $-\Delta t$. If the condition $\Delta t_n \ll \Delta t$, is maintained then some measurements independent among themselves will determine the points on the path connected rigidly by functional relationships. For a well defined specification of the path, it is sufficient to locate two measurements from each coordinate in the interval, the remaining data

are superfluous. The superfluousness produced in this way is responsible for the increase in the tempo of conducting the measurement.

The superflucusness may also be obtained on account of the increase in the quantity of the measuring facilities. Observation may be carried out simultaneously by a few RLS and the data of every one of them determine the path in well defined manner. The results obtained thereby differ from one another as a result of the errors of measurements of the coordinates. The combination of all these data is superfluous.

In the presence of superfluousness, more accurate values of the parameters of the path may be obtained. The increase in accuracy comes about on account of the averaging of the results of a series of measurements. This operation carries the designation of accumulation of the parameters of path. The coordinates of the object and the parameters of the path being sought, are connected by a system of equations. When this system is solved, i.e, when the parameters are found, the equations will give the measured values of the coordinates. If there is superfluousness, then the number of equations will be larger than the unknown parameters. Solving the system of equations several times one may get series of values for every parameter. Averaging these values will lead to an increase in the resultant accuracy of the path determination.

Let us look more in detail, in what way by a series of measurement of the values of the coordinates one may find the unknown parameters of the path. Assume in the beginning that the object changes from constant velocity into $v$ by a straight direction which is known to the observer. Let us assume that a series of measurements of the distance to the object in the direction of its motion is conducted. We call the results of the measurement $y_i^*$. The measurements are

accompanied by errors, therefore in the graph $y = f(t)$ (Fig. 10.5) the value $y_i^*$ may be shown in the form of a point grouping around a straight line reflecting the true path of the object. For the determination of the straight line, it is necessary to specify two numbers. One of which is characterized by the slope of the line (velocity of the object) and the other – the position of the object at the moment of the initial reading (when $t = 0$). These numbers are the parameters of the path.

During the determination of the parameters by the results of the measurements, the condition is introduced that the sum of the squares of the deviations of the function from the measured values should be a minimum. This condition ordinarily leads to the requirement of obtaining the minimum mean square error of the determination of the parameters of the given function.

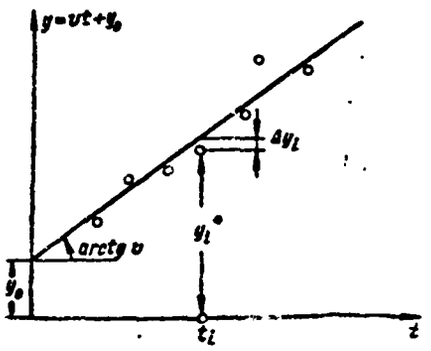


Fig. 10.5 Graph of the measured values of a linear function.

Let us examine how do we find the parameters for the case shown in the previous figure. The condition introduced may be formulated mathematically in the following form:

$$Q = \sum_{i=1}^{n} [y_i^* - (vt_i + y_0)]^2 = \min, \qquad (10.5)$$

where $v$ and $y_0$ – parameters determining the equation of the straight line in rectangular coordinates system; $n$ – number of variables.

Essentially, $Q$ is considered as a function of the parameters $v$ and $y_0$.

For the determination of the parameters $v$ and $y_0$, corresponding to the minimum values of the given amount should be found by partial derivative with respect to $v$ and $y_0$ and set them to zero. Thereby, we get the system of equations

$$\frac{\partial Q}{\partial v}=0,\ \frac{\partial Q}{\partial y_0}=0.$$

Writing the system of equations in the developed form, we obtain

$$\left.\begin{aligned} v\sum_{i=1}^{n} t_i^2 + y_0\sum_{i=1}^{n} t_i &= \sum_{i=1}^{n} y_i^{\circ} t_i, \\ v\sum_{i=1}^{n} t_i + y_0 n &= \sum_{i=1}^{n} y_i^{\circ}. \end{aligned}\right\}$$

As one can see, the equation is linear with respect to $v$ and $y_0$. The coefficients of the equation are different combination of values of the measured quantities, while the roots of the equation are the sought for parameters of the function. This method of finding the parameters is referred to as the method of the least squares.

In most general cases, the function being investigated may be presented in the form of a polynomial of the power $k$ relative to the independent variable $t$, i.e., as

$$y_0 = a_0 + a_1 t + \ldots + a_k t^k. \qquad (10.6)$$

It may be shown that the searching for the coefficients of the polynomial $a_0 \ldots a_k$ is carried out with the help of $k + 1$ linear equations with $k + 1$ unknowns. Thereby, substantially, the coefficients of the polynomial are linearly related to the values of the function $y$. The given linear equation is referred to as normal. If in place of the integral powers of $t$, there is substituted any other arbitrary function: sin $t$; $e^t$; tg $t$, etc., then the parameters $a_0$; $a_1$;...; $a_k$ as before, may be found to consist of a system of $k + 1$ linear equations.

It is necessary only that the resulting equation should be linear with respect to the unknown parameters. This limitation implies that the method of least squares may be applied to an extremely narrow class of functions. But, as it will be shown later, there are means which permit the application of the method of least squares and to arbitrary functions with the presence of some additional conditions.

In the example examined, when the resulting equation is linear, it is assumed that all the measurements may be considered as single valuedly, i.e., their errors are the same. In the selection of the parameters of the straight line, there are not as many among the measured points as it is assumed that all measurements lead to the same conditions. In practice, the measurements lead to different accuracies. The results of more accurate measurements are obviously more trustworthy. Therefore, measurements should be attached different weights — $g_i$, which should be chosen in inverse proportion to the variance of the individual measurements With this calculation, it is necessary to determine the minimum of the following expression:

$$Q=\sum_{i=1}^{n}\frac{1}{\sigma_i^2}(y_i^*-y_i)^2=\sum_{i=1}^{n}g_i(y_i^*-y_i)^2=\min, \qquad (10.7)$$

where $y_i^*$ — measured values, obtained as a result of the $i$th measurement; $y_i$ — true value of the measured random quantity; $\sigma_i^2$ — variance of the $i$th measurement.

In this way, one needs to find the values of the parameters of the function, $y_i$, which changes in a minimum sum being determined by Formula (10.7).

In many cases, the errors of measurement of the coordinates are independent and distributed according to the normal law. Then the treatment of the results of the measurements by the method of least squares leads to the obtaining of the smallest mean square error of

the determination of the path parameters in comparison with other methods.

Ordinarily, functions connecting the coordinates values measured by RLS, with the parameters of the paths are not linear with respect to the parameters. (The parameters of the path, when writing them in the ordinary form will be denoted later on by $v_j$, while the coordinates of the object by $y_i$.) Regardless of this, it is important to use the method of least squares for the solution of the given problem by the way of artificial linearization of the function being used.

In those cases where the approximate values of the parameters of the path are known, it is only necessary to calculate their magnitude. This has a place in the solving of problems of antirocket defense, when the presence of the rocket is to be specified and the depth of its trajectory is to be evaluated in the case of evaluation of ISZ, etc. Then, the function connected with the measurement of the coordinates with parameters of the trajectory $y_i = f_1(v_1 \ldots v_m)$ may be expanded into a Taylor's series relative to points which are close to the true values of the coordinates being measured. From the course of mathematical analysis, it is known that if the function is continuous and has all derivatives, then it may be expanded into a Taylor's series in the power of the increments of the values of the independent variable.

Thus, for a function of two variables, determined at the points $y_i^\circ = f_i(v_1^\circ; v_2^\circ)$, we obtain

$$y_i = f_i(v_1^* + \Delta v_1; v_2^* + \Delta v_2) = f_i(v_1^*; v_2^*) + \left(\frac{\partial f_i}{\partial v_1}\right)^* \Delta v_1 + \left(\frac{\partial f_i}{\partial v_2}\right)^* \Delta v_2 + \\ + \frac{1}{2}\left[\left(\frac{\partial^2 f_i}{\partial v_1^2}\right)^* \Delta v_1^2 + 2\left(\frac{\partial^2 f_i}{\partial v_1 \partial v_2}\right)^* \Delta v_1 \Delta v_2 + \left(\frac{\partial^2 f_i}{\partial v_2^2}\right)^* \Delta v_2^2\right] + \ldots + R_n,$$

where

$$v_1 = v_1^* + \Delta v_1;$$
$$v_2 = v_2^* + \Delta v_2;$$

$R_n$ remainder term; $\Delta v_1$ and $\Delta v_2$ – increments of the variables $v_1$ and $v_2$.

If the deviations of the parameters from their values at the selected points are not great, then it may be limited only to the first derivatives. Then in the general case of $m$ variables, we obtain

$$y_i = y_i^\circ + \left(\frac{\partial f_i}{\partial v_1}\right)^\circ \Delta v_1 + \left(\frac{\partial f_i}{\partial v_2}\right)^\circ \Delta v_2 + \ldots + \left(\frac{\partial f_i}{\partial v_m}\right)^\circ \Delta v_m. \quad (10.8)$$

From Formula (10.8), it follows that the function standing on the left hand side of the expression is linear with respect to the variable parameters $\Delta v_1; \Delta v_2; \ldots; \Delta v_m$. Therefore, as a result, the solutions found for the previous system of equations will not determine the parameters but only their increments.

For the making up of the system of equations, it is necessary to determine approximately the positions of the selected points in space. The specification of the positions of these points permits the establishing of values of the partial derivatives. Thereby, the deviation of the approximate values from the true ones should not be great since otherwise, it is impossible to be limited by the first terms of expansion in the Taylor's series.

Let us look in more detail the mathematical conversions which are necessary to carry out during the search of the values of the parameters of the trajectory. At the disposal of the observer, there are measured values of the coordinates $y_i^*$. In accordance with the general principle of the least squares, the minimum sums of the squares of deviations of the measured values from the true values are found.

Discard the indicated deviations through the approximated values of the function at the selected points $y_i^\circ$. Introduce the designation

$$l_i = y_i^* - y_i^\circ.$$

Then,

$$y_i^\circ - y_i = y_i^\circ - y_i^\circ + y_i^\circ - y_i = l_i - (y_i - y_i^\circ).$$

But $y_i$ may be computed by Formula (10.8). Thereby, we get

$$y_i - y_i^\circ = y'_{i1}\Delta v_1 + y'_{i2}\Delta v_2 + \ldots + y'_{im}\Delta v_m,$$

where

$$y'_{i1} = \left(\frac{\partial y_i}{\partial v_1}\right)^\circ; \quad y'_{i2} = \left(\frac{\partial y_i}{\partial v_2}\right)^\circ; \quad \ldots; \quad y'_{im} = \left(\frac{\partial y_i}{\partial v_m}\right)^\circ.$$

In this way we find

$$y_i^\circ - y_i = l_i - (y'_{i1}\Delta v_1 + y'_{i2}\Delta v_2 + \ldots + y'_{im}\Delta v_m).$$

Then the sum of the products of the squares of deviations of the measured quantities form the true ones according to the weight factor in analogy with Formula (10.7) may be represented in the following form

$$Q = \sum_{i=1}^{n} g_i [l_i - (y'_{i1}\Delta v_1 + y'_{i2}\Delta v_2 + \ldots + y'_{im}\Delta v_m)]^2, \qquad (10.9)$$

where $g_i$ – weighting factor, whereupon $g_i \equiv \frac{1}{\sigma_i^2}$.

It is necessary to determine the values of the increments of the parameters $\Delta v_j$ changing in minimum quantity $Q$. This may be done by computing the partial derivatives with respect to every one of the increments of the argument $\Delta v_j$ and subsequently equating them to zero. Then in the case of $m$ parameters, we obtain a system of $m$ equations. The equation being examined is linear relative to the increments of the parameters.

Let us find the structure of the indicated equations. Perform differentiation on $\Delta v_j$. The result of the differentiation after dividing by 2 may be written in the following form:

$$\sum_{i=1}^{n} g_i \cdot y'_{ij}(y'_{i1}\Delta v_1 + y'_{i2}\Delta v_2 + \ldots + y'_{im}\Delta v_m - l_i) = 0.$$

From there we get the general form of representation of the normal equations

$$\begin{aligned}
&\Delta v_1 \sum_{i=1}^{n} g_i \cdot y'^2_{i1} + \ldots + \Delta v_m \sum_{i=1}^{n} g_i \cdot y'_{i1} \cdot y'_{im} = \sum_{i=1}^{n} g_i \cdot y'_{i1} \cdot l_i, \\
&\ldots\ldots\ldots\ldots\ldots\ldots\ldots\ldots\ldots\ldots \\
&\Delta v_1 \sum_{i=1}^{n} g_i y'_{im} \cdot y'_{i1} + \ldots + \Delta v_m \sum_{i=1}^{n} g_i \cdot y'^2_{im} = \sum_{i=1}^{n} g_i \cdot y'_{im} \cdot l_i.
\end{aligned} \tag{10.10}$$

We denote the coefficients of the unknown increments of the parameters by the symbol $h_{ij}$, and the terms, standing on the right hand side by the symbol $\lambda_i$, where $i$ and $j$ — are correspondingly the number of the row and column of every coefficient [Formula (10.10)]. After this we get,

$$\begin{aligned}
&h_{11}\Delta v_1 + h_{12}\Delta v_2 + \ldots + h_{1m}\Delta v_m = \lambda_1, \\
&h_{21}\Delta v_1 + h_{22}\Delta v_2 + \ldots + h_{2m}\Delta v_m = \lambda_2, \\
&\ldots\ldots\ldots\ldots\ldots\ldots \\
&h_{m1}\Delta v_1 + h_{m2}\Delta v_2 + \ldots + h_{mm}\Delta v_m = \lambda_m.
\end{aligned} \tag{10.11}$$

Here $h_{ij} = h_{ji}$ and the total number of the various coefficients of the system of equations is equal to $\frac{m(m+1)}{2}$. Relationship (10.11) is the ordinary form of representing systems of $m$ linear equations.

In this way, the problem of computing the parameters of the trajectory leads to the solution of the system of $m$ linear equations. The actual values of the parameters are found by the method of step by step approximation. The solution of the system of linear equations (10.11) permits us to find the new oriented quantities $v_j^{o\prime} = v_j^{o} + \Delta v_j$, where $\Delta v_j$ — is the root of the system of equations. After this, differentiate again the solution of the system of equations, etc. The process of computing is discontinued when $\Delta v_j$ is smaller than some previously specified value. The number of cycles of this process is dependent on the difference $v_j^{o} - v_j$.

In this way, the method of least squares leads to the finding of the unknown parameters of the path when a combination of the measure-

ments is superfluous or at least is sufficient for the determination of these parameters. At the same time, the limitation of the application of this method is the necessity of the approximate values of these path parameters. As it was noted, this limitation fits the determination of the trajectory of the ballistic rocket and the orbit of the artificial Earth satellites. In connection with this, we shall look at the basic relationships connecting the current coordinates of such objects, being measured by RLS and the parameters of their trajectories.

## §10.3 BASIC GEOMETRIC RELATIONSHIPS OF ELLIPTIC TRAJECTORIES

It is known that the motions of the ballistic rockets and the artificial Earth satellites are accomplished only under the action of the Earth's gravitational force. Thereby, the trajectory of these objects form ellipses, located in planes passing through the Earth's center.*

As it was already demonstrated, the trajectories of the objects moving under the action of known forces are completely determined by six parameters. The parameters of the elliptic trajectory may be divided into three groups. The first group of parameters permits us to find the plane of the trajectory which is defined by two parameters. Actually the equation for any plane may be represented in the following form:

$$Ax+By+Cz+D=0. \qquad (10.12)$$

In the case being examined, the planes pass through the center of the Earth, i.e., it may be assumed $D = 0$, if the initial coordinates coincide with the center of the Earth. Then, dividing both sides of the equation (10.12) by $C$, we get

$$A_1x+B_1y+z=0.$$

In this way, the two numbers $A_1$ and $B_1$ completely determine the plane.

The second group of parameters gives the possibility of defining the trajectory in the plane. The ellipse is a curve of the second order. As it is known, for the defining of such a curve, it is necessary to have three parameters. One of them characterizes size of the ellipse. Generally, for this parameter, the size of the major semi-axis of the ellipse is used (Fig. 10.6). Then the second parameter is the eccentricity $e = \frac{c}{a}$, c with the aid of which the form of the ellipse is defined, its "oblateness" along the minor axis. The third parameter, denoted here by $\theta_0$, characterizes the orientation of the ellipse relative to the coordinate axes. The position of the ellipse in a plane is determined by the first Law of Kepler according to which the focus of the ellipse coincides with the center of the gravitational field, i.e., the center of the Earth.

It must be noted that the trajectory of ISZ forms in most cases, a closed ellipse; the trajectory of the ballistic rocket is only part of it (Fig. 10.6).

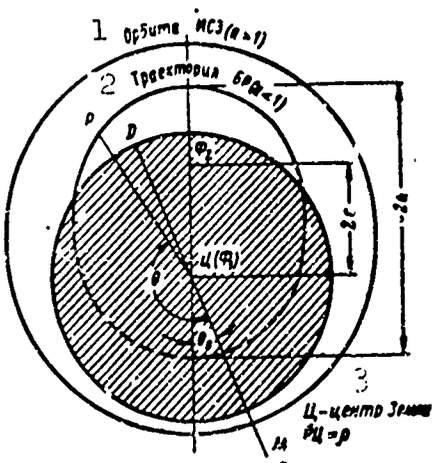


Fig. 10.6 Parameters of the ellipse $\Phi_1$ and $\Phi_2$ — foci of the ellipse. 1) Orbit of artificial Earth satellite; 2) trajectory of ballistic rocket; 3) center of Earth.

Besides the five geometric parameters for the determination of

the trajectory as indicated above, it is necessary to have a parameter connecting the position of the object with time. For this, a time is defined for the passing of the object at any characteristic point on the trajectory. The moment of the passage of the object through the bearing $t_0$ forms the sixth (time) parameter.

In the following, for the sake of simplifying the calculations, we expeditiously take the value of the equitorial radius of the Earth $R_3 = 6370$ km as the condition of unit length and for the unit of acceleration we take the magnitude $g_0$=9,81 m/sec$^2$.It may be shown that the unit velocity in this case corresponds to the first cosmic velocity, i.e., $V_0$=7910m/sec.Thereby the unit of time

$$T_0 = \frac{R_3}{V_0} = \frac{6370 \cdot 10^3}{7910} = 808 \text{ sec}$$

is determined by the duration of the flight of the imaginary object in a circular orbit along the surface of the Earth in an arc corresponding to one radian.

1. Parameters Of The Plane Of The Trajectory.

Let us examine the determination of the trajectory with the aid of RLS. Assume that the RLS is located at a point $O$ (Fig. 10.7). In general cases, this point does not lie in the plane of the trajectory.

The line CDП is formed by the intersection of the plane of trajectory with the Earth's surface. Through the point of the position of the RLS, $O$, and the center of the Earth Ts, the plane ODTs is drawn, perpendicular to the plane of the trajectory. The arc of the large circle OD formed by the intersection of the plane ODTs with the Earth's surface. The plane NOTs is the meridional plane drawn through the point of the location of the RLS. The current position of the object is denoted by the point P. The plane POTs goes through the object, the center of the Earth and the point of the location of the RLS. $R_t$ is the

projection of the current point of the trajectory on the surface of the Earth.

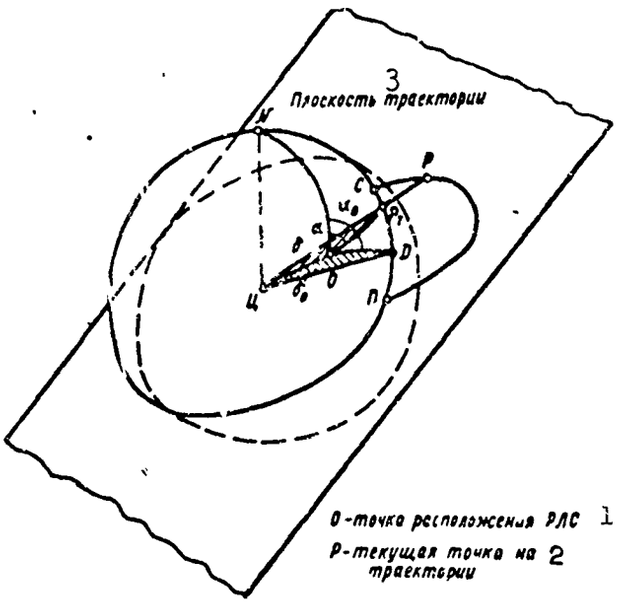


Fig. 10.7 Location of the plane of trajectory relative to the RLS. 1) Point of the location of RLS; 2) the current point on the trajectory; 3) plane of trajectory.

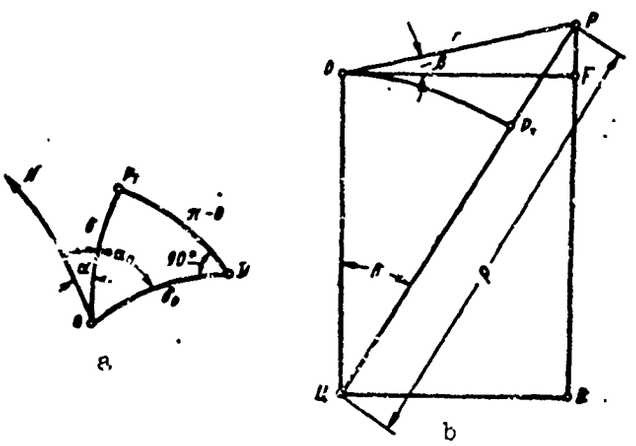


Fig. 10.8 Parameters of the plane of trajectory and the current coordinates of the object. a) Auxiliary spherical right-angled triangle; b) section of the plane going through RLS, center of the Earth (Ts) and the current point on the trajectory (P).

The position of the plane of the trajectory relative to RLS is determined by the orientation and the magnitude of the arc of the large circle OD.

The orientation of the arc is determined by the following quantities: a) The central angle $\angle OUD=\delta_0$ between the planes of the trajectory and the direction of the RLS located in the TzOD plane $\left(0\leqslant\delta_0\leqslant\frac{\pi}{2}\right)$. In the system we used, the unit of this angle is equal to the corresponding arc of the big circle on the surface of the Earth. b) The angle $\angle NOD=\alpha_0$ between the meridional plane and the normal to the plane of trajectory, i.e., the azimuthal angle perpendicular to the plane of the trajectory, drawn through the point of the location of RLS. The quantities $\delta_0$ and $\alpha_0$ are the parameters of the plane of the trajectory.

For the determination of the plane of the trajectory, one should find the position of the object with the help of the RLS at least at two points. From the points so found and the center of the Earth, the plane of the trajectory may be laid out.

Express the parameters of the plane of the projectory with the aid of the coordinates, measured by the RLS: Distance $r^*$, azimuth $\alpha$ and the location angle $\beta$. Let us look at the spherical right-angled triangle $R_TOD$ (Fig. 10.7 and 10.8).

Utilizing the relationship for spherical triangles, we obtain

$$\operatorname{tg}\delta_0=\operatorname{tg}\delta\cos(\alpha_0-\alpha). \qquad (10.13)$$

Express $\delta$ through $r$ and $\beta$. From $\Delta OPF$, located in the plane $R_TOT_Z$ (Fig. 10.8b), we find

$$\operatorname{tg}\delta=\frac{UB}{PB}=\frac{r\cos\beta}{PF+FB},\quad PF=r\sin\beta;$$

$FV = 1$ since in the unit system we adopted the radius of the Earth is 1. Then

$$\operatorname{tg}\delta=\frac{r\cos\beta}{1+r\sin\beta}.$$

Substituting the value of $tg\ \delta$ obtained into Formula (10.13), we find the equation of the plane of trajectory

$$\operatorname{tg}\delta_0 = \frac{r\cos\beta\cos(\alpha_0 - \alpha)}{1 + r\sin\beta}. \qquad (10.14)$$

This equation permits the finding of the magnitude of the central angle $\delta_0$, characterizing the departure of the RLS from the plane of the trajectory and the azimuthal angle normal to the plane of trajectory $-\alpha_0$. The value of the slope of the range, $r$, the azimuth $\alpha$ and the location angle $\beta$ measured with the help of the RLS introduced into the equation, are consequently known values. In this way, the results of the measurements of the coordinates at two points permit the building of the system of two equations (10.14) with two unknowns. Having solved this system, we find the parameters of the plane of trajectory $\alpha_0$ and $\beta_0$.

2. Determination Of The Parameters Of The Ellipse

Let us find the link between the parameters of the ellipse and the coordinates of the object. As it was noted, the orientation of the ellipse may be defined by the angle between the polar axis TsM and the principal axes drawn through the focus of the ellipse coinciding with the center of the Earth (point Ts in Fig. 10.6). The reading of the angle $\theta_0$ originated from the polar axis to the principal axis of the ellipse in the direction toward the perigee by the hour hand. The axis TsM lies on the continuation of the straight line TsD, where D is a projection point of the location of the RLS. On the plane of the trajectory (Fig. 10.7).

As it is known the equation of the ellipse in the plane of the trajectory, expressed in polar coordinates, has the form

$$\rho = \frac{a(1 - e^2)}{1 + e\cos(\vartheta - \theta_0)}, \qquad (10.15)$$

where ρ – radius vector; θ – polar angle reckoned relative to the polar axis TsM (Fig. 10.6). In the equation (10.15) the quantities $\alpha$, $e$, and $\theta_0$ are unknown parameters, ρ and θ are determined from the radiolocational measurements. Let us examine the conversion from the coordinates measured at the RLS to polar coordinates. For that, we express the slope of the range by ρ and θ. From $\Delta CPF$ and $\Delta TsPB$ (Fig. 10.8b) we obtain

$$r^2 = \rho^2 \sin^2\delta + (\rho\cos\delta - 1)^2$$

or

$$r^2 = \rho^2 + 1 - 2\rho\cos\delta. \qquad (10.16)$$

Now, we express δ through the polar angle; for which we examine the spherical right-angled triangle $OP_tD$ (see Fig. 10.7 and 10.8a). Utilizing the relationship for the cosine of the sides of the spherical right-angled triangle, we determine

$$\cos\delta = \cos\delta_0\cos(\pi - \theta) = -\cos\delta_0\cos\theta.$$

Then, substituting the obtained expression for cos δ in Formula (10.16), we obtain

$$r = \sqrt{1 + \rho^2 + 2\rho\cos\delta_0\cos\theta}. \qquad (10.17)$$

The parameter of the plane of trajectory $\delta_0$ resulted from this relationship is computed by Formula (10.14).

From the spherical triangle $POD$, we obtain also a second expression connecting the polar angle θ and the azimuth α measured by the RLS.

$$\operatorname{tg}(\pi - \theta) = \operatorname{tg}(\alpha_0 - \alpha)\cdot\sin\delta_0$$

or

$$\operatorname{tg}\theta = \operatorname{tg}(\alpha - \alpha_0)\cdot\sin\delta_0. \qquad (10.18)$$

Furthermore, it is necessary to determine the connection of the radius vector ρ with the slope of the range $r$ and the location angle

β.

From the triangles RTsB and OPF (Fig. 10.8b), we find

$$\rho^2 = r^2\cos^2\beta + (1 + r\sin\beta)^2,$$

from which

$$\rho = \sqrt{1 + r^2 + 2r\sin\beta}. \qquad (10.19)$$

Expressions (10.17), (10.18) and (10.19) permit the use of the coordinate values measured by the RLS, for the determination of the parameters of the ellipse. Besides that, with the help of these relationships, one may determine the parital derivatives from the coordinates in the parameters of the ellipse, necessary for the making up of the system of normal equations (10.10).

3. Distance Of The Flight Of Ballistic Rockets

Knowing the parameters of the trajectory $a$ and $e$, it is possible to determine the flight of the ballistic rocket, i.e., the length of the path $l$, located on the Earth's surface (Fig. 10.9).

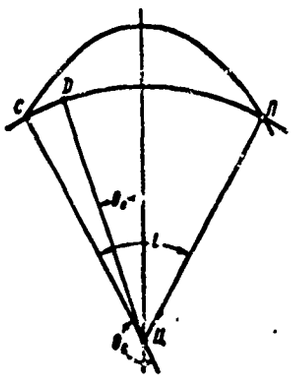


Fig. 10.9 Distance of flight of the ballistic rocket.

We determine the polar angle $\theta_c$ point of intersection of the trajectory with the surface of the Earth, taking advantage of the basic equation of the ellipse

$$\rho_c = \frac{a(1-e^2)}{1 + e\cos(\theta_c - \theta_0)}.$$

Since for the point $C$ the radius vector $\rho$ is equal to the radius of the Earth. therefore, in our unit system $\rho_c = 1$. Then

$$\cos(\theta_c - \theta_0) = \frac{a(1-e^2)-1}{e},$$

but since $\frac{l}{2} = \pi - (\theta_c - \theta_0)$, we obtain

$$\cos\frac{l}{2} = \cos[\pi - (\theta_c - \theta_0)] = \frac{1-a(1-e^2)}{e}. \qquad (10.20)$$

The expression obtained serves also for the determination of the distance of the flight $l$; it may also be considered as one of the equations determining the trajectory of the rocket. If the positions of the points of start and fall are known then $l$ is known, and the indicated expression determines some families of trajectories, since the one and the same distance corresponds to combinations of possible values of $a$ and $e$. Actually, through the points $C$ and $\Pi$ one may lead through numerous elliptic trajectories.

## §10.4 ACCURACY OF THE DETERMINATION OF THE PARAMETERS OF THE TRAJECTORY OF BALLISTIC ROCKET AND ARTIFICIAL EARTH SATELLITE

In the presence of errors of the measurement of the coordinates, there are produced errors of the determination of the parameters of the trajectory. The latter, in its turn depends not only on the errors of measurement of coordinates but also on a series of other factors. Here we are referring to: Character of the trajectory, locality of the RLS, quantity of the number of the derived measurements of coordinates, position of point of measurement on the trajectory and others.

During the projection of the system, it is necessary to find permissible errors of the measurement of coordinates guaranteeing trajectories with the required accuracy. At the same time, it is necessary to select a locality of the RLS relative to the trajectory and region of observation of the object. A direct solution of this problem seems extremely complex. Therefore, in practice, one should proceed from the

problem reversing what was indicated which may be resolved considerably easier.

When solving this problem in the capacity of original data, the accuracy of determination is specified for the coordinates of the points being measured which are found from the condition of possibility of the technical realization on the principle of the choice of the measurement of coordinates. Further, assume a known position of the location of the RLS relative to the trajectory the number of points to be measured and their positions on the trajectory. In these conditions, one may evaluate relatively simply the accuracy of the determination of the parameters of the trajectory and the coordinates of its individual points by the method of least squares.

1. Approximation Method Of The Calculation Of The Parameters Of The Trajectory.

In the evaluation of the accuracy of the trajectory parameters obtained, it is possible to simplify the solution of the stated problem. This simplification is included in a separate consideration of two equations: Equation of the plane of the trajectory in space and the equation of the ellipse in the plane of the trajectory.

In the search for the parameters of the plane of the trajectory $\alpha_0$ and $\delta_0$, it is not necessary to know the parameters of the ellipse. Therefore, the error of determination of the parameters of the plane of trajectory is independent of it however accurately the parameters of the ellipse are determined.

On the other hand, the parameters of the ellipse are dependent on $\alpha_0$ and $\delta_0$, since in the equation of the ellipse the parameters of the plane of trajectory are also involved. The fact is that the current coordinates of the object $r$, $\alpha$ and $\beta$ which characterize its position in space and consequently, are dependent on the parameters of the

ellipse as well as on the position of the plane of trajectory. Therefore, the errors of determination of the parameters of the ellipse $a$, $e$ and $\theta_0$ are also dependent on $\alpha_0$ and $\delta_0$. But this dependence in practice needs not to be taken into account. Therefore, just as in the preceding case the determination of the parameters of the ellipse is independent of the parameters of the plane of trajectory. Consequently, when finding $a$, $e$ and $\theta_0$. It is assumed that the plane of trajectory is determined without error.

On the basis of the stated evaluation, the accuracy of the determination of the trajectory may be carried out independently for the two parameters of the plane of trajectory and the three parameters of the ellipse. For this, it is sufficient to examine the system of linear equations: Of the second and third order.

The system of equations (10.10) for the determination of the parameters $\alpha_0$ and $\delta_0$ takes the form

$$\begin{cases} h'_{11}\Delta\alpha_0 + h'_{12}\Delta\delta_0 = \lambda'_1, \\ h'_{21}\Delta\alpha_0 + h_{22}\Delta\delta_0 = \lambda'_2. \end{cases}$$

We shall find the formulas determing the coefficients of the system of equations for the parameters $\alpha_0$ and $\delta_0$. Uniting the partial derivatives and the weight factors from Formula (10.11), we find

$$h'_{11} = \sum_{i=1}^{n} g_i \left(\frac{\partial y_i}{\partial \alpha_0}\right)^2, \tag{10.21}$$

$$h'_{12} = h'_{21} = \sum_{i=1}^{n} g_i \frac{\partial y_i}{\partial \alpha} \cdot \frac{\partial y_i}{\partial \delta_0}, \tag{10.22}$$

$$h'_{22} = \sum_{i=1}^{n} g_i \left(\frac{\partial y_i}{\partial \delta_0}\right)^2, \tag{10.23}$$

$$\lambda'_1 = \sum_{i=1}^{n} g_i \frac{\partial y_i}{\partial \alpha_0} l_i,$$

$$\lambda'_2 = \sum_{i=1}^{n} g_i \frac{\partial y_i}{\partial \delta_0} \cdot l_i.$$

Here $y_i$ – coordinates, measured by RLS, i.e., in the case being examined – $r$, $\alpha$ and $\beta$; $l_i$ – difference between the measured and approximation values of $r$, $\alpha$ and $\beta$.

Similarly, the system of equations for the determination of the parameters $a$, $e$ and $\theta_0$ may be written in the following manner:

$$\begin{cases} h_{11}^{*}\Delta a + h_{12}^{*}\Delta e + h_{13}^{*}\Delta\theta_0 = \lambda_1^{*}, \\ h_{21}^{*}\Delta a + h_{22}^{*}\Delta e + h_{23}^{*}\Delta\theta_0 = \lambda_2^{*}, \\ h_{31}^{*}\Delta a + h_{32}^{*}\Delta e + h_{33}^{*}\Delta\theta_0 = \lambda_3^{*}. \end{cases}$$

The coefficients of the system of equations of the third order for the finding of the parameters, $a$, $e$ and $\theta_0$ is found with the aid of the relationships

$$h_{11}^{*} = \sum_{i=1}^{n} g_i \left(\frac{\partial y_i}{\partial a}\right)^2, \tag{10.24}$$

$$h_{12}^{*} = h_{21}^{*} = \sum_{i=1}^{n} g_i \frac{\partial y_i}{\partial a} \cdot \frac{\partial y_i}{\partial e}, \tag{10.25}$$

$$h_{13}^{*} = h_{31}^{*} = \sum_{i=1}^{n} g_i \frac{\partial y_i}{\partial a} \cdot \frac{\partial y_i}{\partial \theta_0}, \tag{10.26}$$

$$h_{22} = \sum_{i=1}^{n} g_i \left(\frac{\partial y_i}{\partial e}\right)^2, \tag{10.27}$$

$$h_{23}^{*} = h_{32}^{*} = \sum_{i=1}^{n} g_i \frac{\partial y_i}{\partial e} \cdot \frac{\partial y_i}{\partial \theta_0}, \tag{10.28}$$

$$h_{33}^{*} = \sum_{i=1}^{n} g_i \left(\frac{\partial y_i}{\partial \theta_0}\right)^2, \tag{10.29}$$

$$\lambda_1^{*} = \sum_{i=1}^{n} g_i \frac{\partial y_i}{\partial a} \cdot l_i,$$

$$\lambda_2^{*} = \sum_{i=1}^{n} g_i \frac{\partial y_i}{\partial e} \cdot l_i,$$

$$\lambda_3^{*} = \sum_{i=1}^{n} g_i \frac{\partial y_i}{\partial \theta_0} \cdot l_i.$$

Having solved the above system of equations, we shall find the values of the parameters of the trajectory, which, in correspondence with the rule of the solution of system of linear equations is computed by the formulas

$$\Delta\alpha_0 = \frac{\lambda'_1 h'_{22} - \lambda'_2 \cdot h'_{12}}{|H'|}, \tag{10.30}$$

$$\Delta\delta_0 = \frac{h'_{11} \cdot \lambda'_2 - \lambda'_2 \cdot h'_{12}}{|H'|}, \tag{10.31}$$

$$\Delta a = \frac{|H''_a|}{|H''|}, \tag{10.32}$$

$$\Delta e = \frac{|H''_e|}{|H''|}, \tag{10.33}$$

$$\Delta\theta_0 = \frac{|H''_{\theta_0}|}{|H''|}, \tag{10.34}$$

where $|H'|$ and $|H''|$ – determinants of the coefficients on the system of equations of the second and third order correspondingly; $|H''_{vj}|$ – determinant, obtained by substituting the elements of the rows of the determinant $|H''|$ which are the coefficients of $\Delta_{vj}$, by the free terms of the system of equations.

In practice the increments of the parameters of the trajectory are calculated by more complex formulas taking into account the deviation of the motion from the elliptic character. But, for the determination of the accuracy of the searching of the parameters of the trajectory, it may be assumed that the computation is carried out according to Formulas (10.30) to (10.34). The errors found in this way is the same as under actual conditions.

## 2. Evaluation Of The Accuracy Of The Determination Of The Parameters Of The Trajectory

Assume at the beginning that the trajectory of an object is defined only by one parameter. Similar simplified consideration permits us to elucidate on which factors the accuracy of the searching of parameters of the trajectory is dependent. The determination of one parameter may have its place, for example, in the determination of the

radius of curvature of the orbit ISZ in the case of the known position of the plane of the orbit. Then the single parameter the determination depends on is the radius of the orbit $a$.

The condition for the finding of the unknown parameter $v$ in correspondence with the rules stated above has the form

$$Q=\sum_{i=1}^{n} g_i(l_i-y_i'\Delta v)^2=\min. \qquad (10.35)$$

In the case being examined, we obtain only one linear equation relative to the increment of the unknown parameter $\Delta v$. The minimum $Q$ is determined from the condition

$$\frac{dQ}{dv}=\sum_{i=1}^{n} g_i\left(y_i'^2\Delta v-l_iy_i'\right)=0,$$

from which

$$\Delta v=\frac{\sum_{i=1}^{n} g_i\cdot l_i\cdot y_i'}{\sum_{i=1}^{n} g_i\cdot y_i'^2}.$$

In the denominator of the expression obtained, there is a quantity independent of the results of the measurement, and in the numerator, a sum of random values $l_i$ each one of which is multiplied by the coefficient $g_iy_i'$. Assume that the results of the measurement of the coordinates are mutually independent. Then, using the formula for the searching of the variance of the sums of independent random values and taking into account that $\sigma^2(l_i)=\sigma_i^2$, we obtain

$$\sigma_v^2=\frac{\sum_{i=1}^{n} g_i^2y_i'^2\sigma_i^2}{\left(\sum_{i=1}^{n} g_i\cdot y_i'^2\right)^2}, \qquad (10.36)$$

where $\sigma_v^2$ – variance of the determination of the parameter $v$.

As it was noted that the weight factor $g_i$, is proportional to $\frac{1}{\sigma_i^2}$. The coefficient of proportionality between these quantities may have any values, which, as it is not difficult to see, does not influence the solution of the system of linear equations. Select this coeffi-

cient from the condition

$$g_i=\frac{\sigma^2}{\sigma_i^2},$$

where $\sigma^2$ – variance of the most accurate measurement of coordinate.

Thereby $g_i \leqslant 1$ and the most accurate measurement is assumed to have a weight $g = 1$. Then the relationship (10.36) may be represented as

$$\sigma_v^2=\frac{\sum_{i=1}^{n} g_i \cdot y_i'^2}{\left(\sum_{i=1}^{n} g_i \cdot y_i'^2\right)^2}\sigma^2=\frac{1}{\sum_{i=1}^{n} g_i \cdot y_i'^2}\sigma^2=\frac{1}{\sum_{i=1}^{n}\left(\frac{y_i'}{\sigma_i}\right)^2}. \qquad (10.37)$$

Assume that all measurements are conducted under one condition, i.e., $\sigma_1=\sigma_2=\ldots=\sigma_n=\sigma$ и $y_1'=y_2'=\ldots=y_n'=y'$. Then from (10.37), it follows that

$$\sigma_v=\frac{\sigma}{\sqrt{n}\cdot y'}.$$

From the relationship obtained, it can be seen that in the presence of $n$ individual measurements, the error of the determination of the parameters is decreased by $\sqrt{n}$ times in comparison with the case of one measurement of the coordinate $g$. Consequently, when the method of least square is used, actually an accumulation of the parameters of the trajectory is accomplished. The gain in accuracy is the same as for several measurements of the same coordinate.

In the same time, the resulting accuracy depends on the derivative $\frac{\partial y_i}{\partial v}=y_i'$, which determines the slope of the curve connecting the coordinates with the parameters of the trajectory. For a clarification of the effect of the quantity $\frac{\partial y_i}{\partial v}$ we shall look at a concrete example. Assume that the parameter $v$, is the size of the major semiaxis of the ellipse, $a$. A family of ellipses is shown in Fig. 10.10 differing only in the parameter whereupon the plane of the figure coincides with the plane of the trajectory. Assume that the RLS is located at the point $D$ and the measurement of the slope of the range may be carried out in Directions 1 and 2. From Figure 10.10, it is seen that in Direction 1

the one and same increment of the parameter $a$ corresponds less to the increment $r$ than in irection 2. Consequently, the derivative $\frac{\partial r}{\partial a}$ is larger when the measurement is made in the second direction:

$$\left(\frac{\partial r}{\partial a}\right)_2 > \left(\frac{\partial r}{\partial a}\right)_1.$$

At the same time, it is obvious that the choice of the second direction is more preferred since the one and the same mean square error of the measurement of distance $\sigma_r$ in the first direction leads to larger deviation of the parameter $a$. Thus, for example, if $\sigma_r$ corresponds to $\Delta a = a_2 - a_1$ in Direction 2 the same value $\sigma_r$ is produced at a smaller interval of measurement $a$.

In this way, at the determination of one parameter and in the presence of error of measurement of one coordinate, the increase in the partial derivative of $\frac{\partial y}{\partial v}$ leads to an increase in the accuracy of the sought for parameter. The indicated dependence holds as well in the presence of several parameters.

If, however, the measurement of the coordinate is not equally accurate, then during the treatment by the method of least squares, it is taken into account by the introduction of the weight factors $g_i$. The points on the trajectory should be selected in such a way that the biggest value of the derivative $\frac{\partial y}{\partial v}$ should correspond to the most accurate measurement of the coordinate.

In the general case, the determination of the trajectory in the presence of several unknown parameters, we may obtain formulas similar to Relationship (10.36). It may be shown that the variance of the determination of any parameter $v_j$ thereby may be found by the following formula:

$$\sigma_{v_j}^2 = \overline{\Delta v_j^2} = \frac{H_{jj}}{|H|}\sigma^2, \qquad (10.38)$$

where $|H|$ -- the determinant of the coefficients of the system of nor-

mal equations; $H_{jj}$ – algebraic complement of the $j$th diagonal elements of the determinant $|H|$.

Similarly, the combined moments of the distribution of the values of the parameters may be found:

$$\overline{\Delta v_q \cdot \Delta v_s} = \frac{H_{qs}}{|H|} a^2, \qquad (10.39)$$

where $\overline{\Delta v_q \cdot \Delta v_s}$ – mean value of the increments of the $q$th and $s$th parameters; $H_{qs}$ – algebraic complement of the $qs$th elements of the determinant $|H|$.

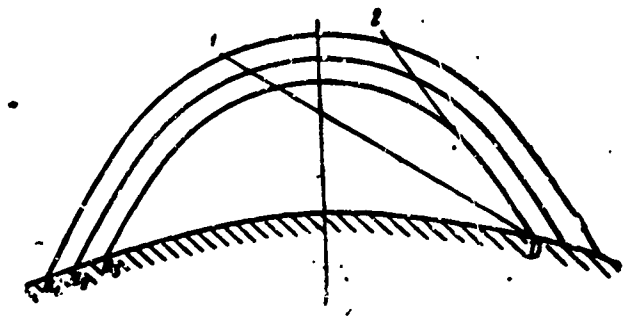

Fig. 10.10 Family of ellipses with different values of $a$.
$a_3 - a_2 = a_2 - a_1 = \Delta a$.

The quantities found by Formulas (10.38) and (10.39), permit the characterization of the distribution of the trajectories constructed of the given measurements of the coordinates. The indicated quantities are the second moments of the distribution of the probability of the deviation of the parameters from the true values. In the case being examined this distribution is normal with zero mean values and such distributions are completely characterized by the second moments. Consequently with the aid of Formulas (10.38) and (10.39) a family of trajectories (Fig. 10.11) may be found characterizing that any arbitrary computation of the trajectory will belong to this family with the defined probability $P$. This family of trajectories corresponds to several intervals of the values of the parameters of the trajectories. The

probability $P$ is characterized by the volume of the $m$-dimensional ellipsoid of distribution of the parameters of trajectories. This ellipsoid is similar to the ellipsoid of distribution in the plane ($m = 2$) and the ellipsoid of errors in space ($m = 3$) examined in Chapter 9.

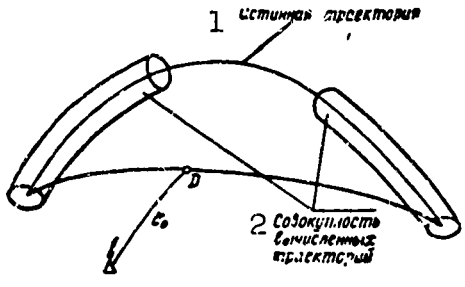


Fig. 10.11 Scatter of the computed trajectories relative to the true one. 1) The true trajectory; 2) combination of computed trajectories.

## 3. Means Of Defining The Original Data

During the analysis of the method of least squares, it was established that its application should be on known approximate values of the parameters of the trajectory and the positions of the points at which the measurements are conducted. In that case, if the assumed trajectory of the object is computed beforehand, the values of its parameter may be taken as the required approximate values.

But very often it appears that the approximate values of the parameters of the trajectory may not be defined unambiguously for example, during the solution of several problems of antirocket defense, at the considerable deviation of the orbit of the artificial Earth satellite from the calculated, etc. In these cases, the accurate determination of the trajectory of the object precedes the step of observation and the approximate finding of the parameters of the actual trajectory. At the projection of the radiolocational system it is also necessary

to define the approximate values of the parameters of the standard trajectory so that there is a possibility to estimate the accuracy of the determinations provided by the system.

Let us first look at the case of known calculated trajectory of a ballistic rocket. Obviously, there are many possible means of defining a trajectory. Thereby almost always the coordinates of the starting and falling points are known.* By the known coordinates of these points, the distance of the flight may be found with Formula (10.20). Thereby, we get an equation whose unknowns are $a$ and $e$. For the unambiguous determination of these parameters, it is necessary there is still one more equation. This equation may be written on the basis of one of the following conditions.

a) Optimum trajectory. From ballistics, it is known that for an optimum trajectory, the angle between the direction of the motion of the object and the horizontal plane at the starting point is found from the condition

$$\beta_{V_0 \text{ opt}} = \frac{\pi - l}{4}. \tag{10.40}$$

At the same time, the angle $\beta_{V_0 \text{ opt}}$ may be found from the formula

$$\rho V \cos\beta_V = \sqrt{a(1-e^2)}, \tag{10.41}$$

where $V$ – velocity of the object.

Substituting into Formula (10.41) the values of $\rho$ and $V$, corresponding to the intersection of the surface of the Earth, the trajectory of the object and taking into account Relationship (10.14), we find

$$\cos\frac{\pi - l}{4} = \sqrt{\frac{a(1-e^2)}{2-\frac{1}{a}}}. \tag{10.42}$$

Formula (10.42) may be considered as the second equation for the determination of the parameters $a$ and $e$. In this way, a system of two equations and two unknowns is obtained: Formula (10.20 and (10.42).

Excluding $a$, we obtain the quadratic equation relative to the eccentricity of the ellipse $e$. Solving it, we find

$$e=\operatorname{tg}\frac{\gamma-l}{4}.$$

At known $e$, the parameter $a$ is easily found by Formula (10.20)

$$a=\frac{1-\cos\frac{l}{2}\cdot e}{1-e^2}. \qquad (10.43)$$

b) Known height of the object at the apogee point – $h_{ap}$. From the equation of the ellipse (10.15) it follows that at the apogee point

$$a(1+e)=1+h_{ap}. \qquad (10.44)$$

Utilizing Formula (10.20), from the latter expression, we obtain

$$e=\frac{h_{ap}}{1+h_{ap}-\cos\frac{l}{2}}.$$

Afterwards, same as the preceding case, we find the parameter $a$ from Formula (10.43).

In case the trajectory being measured is not known, it is necessary to make a choice of one or several characters of the trajectory and then find $a$ and $e$ for every one of them. Ordinarily, there are conjectured regions of the start and fall which are known. It is assumed that these regions are bounded by circles of the same diameter (Fig. 10.12). If the observation of all the trajectories should be accomplished by just one RLS then obviously, the RLS should be located on the arc of the large circle, going through the center of the indicated region. The calculations of the accuracy of the determination of the parameters of the trajectory is expeditiously carried out for trajectories found in the worst conditions, i.e., at the largest distance from the RLS. The planes of similar trajectories should be tangent to the crosshatched circles, surrounding the regions of start and fall. From this condition, the distance of the flight may be defined. Further calculation is carried out for the optimum trajectory and taking into

account the measurement of the accuracy during the transformation to the nonoptimum trajectory. If the accuracy required is provided for the most unfavorable conditions, then it will not be worse for all the remaining trajectories. The parameters $a$ and $e$ and others encountered in practical cases may be found in a similar manner.

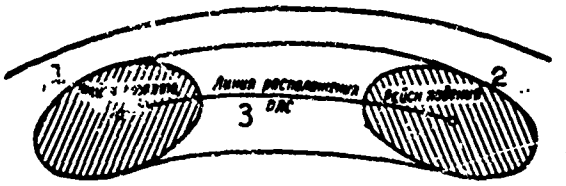


Fig. 10.12 Choice of calculated parameters of the trajectory when the regions of the start and fall are known. 1) Region of start; 2) region of fall; 3) line of RLS location.

After this, it is necessary to define the remaining parameters, i.e., $\theta_0$, $\alpha_0$ and $\delta_0$. The parameters $\theta_0$ and $\delta_0$ are determined by the location of the RLS relative to the trajectory, therefore the defining of such parameters are equivalent to the choice of the location of the RLS. The parameter $\theta_0$ characterizes the position of the projection of the point of the location of the RLS on the plane of the trajectory relative to the principal axes of the ellipse (point $D$ in Figs. 10.6 and 10.7)

The choice of the parameter $\theta_0$ is determined entirely by the assignment of the RLS. Thus, when it is necessary to prognosticate the starting point, the parameter $\theta_0$ should be chosen with such calculations that the RLS is located close to the initial segement of the trajectory. In all conditions, it is not expeditious to choose a small $\theta_0$ since then the condition of observation is worsened owing to the considerable steepness of the range in the vicinity of the apogee. At the same time, the choice of $\theta_0$ is often limited owing to the impossibility of arbitrary positioning of the RLS.

The parameter $\delta_0$ is determined by the distance of the RLS from the plane of the trajectory. In the presence of one RLS and during the observation of the only possible trajectory, i.e., assuming $\delta_0$ is equal to zero. Therefore, the choice of $\delta_0$ is determined by the possibilities of the positioning of the RLS. Thereby, the lowering of the accuracy in comparison with the case $\delta_0 = 0$ is caused mainly by the increase in the slope of the range.

The quantity $\alpha_0$ does not have any effect on the determination of the parameters of the trajectory. In reality, $\alpha_0$ characterizes the orientation of the plane of trajectory. By virtue of the spherical symmetry of the Earth, any position on the plane of trajectory is equivalent. Therefore, when calculating the accuracy, it is not necessary to define the parameter $\alpha_0$.

The furthermost problem of consideration is the choice of the point of observation for the trajectory. During the determination of the parameters of the trajectory only the automatic tracking of the object for some segments is accomplished, only the measurement of the coordinates in some points when the multibeam RLS is used (Fig. 10.13). As it was noted, the case of the automatic tracking of the object may be reduced to a measurement at a few points, which will be examined later. The calculation for a large number of points may be reduced to the calculation of just a few points (see §10.6). Therefore, during the conducting of the calculation, it is expeditiously limited to 3-5 points on the trajectory. These points should be located at equal intervals of observation.

The interval of observation is often determined in all by the maximum range of action of the RLS and the limited zones of observation of the positive location angle. The segment of the trajectory all of the point of which satisfy the condition of $r < r_{maks}$, where

$r_{maks}$ – is the maximum range of action of the RLS, may be found via making the slope of the range a function of the polar angle $r = f(\theta)$. The value $\theta$ corresponding to $r = r_{maks}$, is determined by the upper limit of the segment being observed. The lower limit is found from the condition of observation of the object under the positive location angle. The quantity $\theta$ during which $\beta = 0$ determines the lower limit of the segment of observation. After which as the limits of the segment of observation are found, the coordinates of the point of observation may be determined from the condition of equivalent filling in of the segment of the trajectory with the measured points.

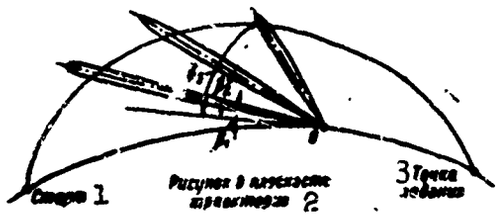

Fig. 10.13 Discrete measurement of the coordinates of the object. 1) Start; 2) drawing in plane of trajectory; 3) falling point.

It should be kept in mind that the interval of observation may also be chosen from other conditions of operation of the measuring system. In part, this interval may be chosen from the consideration guaranteeing the secrecy of the work, from the condition of the observation of the tracking of the trajectory, etc.

In this way, in the capacity of original data for calculation, four parameters $a$, $e$, $\theta_0$, $\delta_0$ and the coordinates of the points of measurement which determines the specification of the polar angle $\theta$ should be defined. Besides this, it is necessary to set the mean square error of the measurement of coordinate at all points.

4. Sequence Of Carrying Out The Calculation

On the basis of the reduced relationship, the following order of calculations of the accuracy of determination of the parameters of the trajectory may be offered

a) Determination of the necessary characteristics of the point

of observation. Radius vectors of all points are found by the following formula

$$p = \frac{a(1-e^2)}{1+e\cos(\theta-\theta_0)}.$$

The location angle is calculated in the following way

$$\beta = \arcsin\frac{-1-\rho\cos\theta\cos\delta_0}{r}.$$

The slope of the range is determined from the relationship

$$r = \sqrt{1+\rho^2+2\rho\cos\theta\cos\delta_0}.$$

Besides this, for the completion of the calculation, it is necessary to introduce auxiliary characteristics of the points of the trajectory referred to as the eccentric anomalies. With the help of these characteristics the deviation of the ellipse from the circle, its "eccentricity" at the given point, is estimated. The eccentric anomaly forms an angle read from the principal axis of the ellipse to the direction at the point of intersection of the perpendicular to the principal axis and the auxiliary circle of radius $a$ (Fig. 10.14). This angle is calculated by the formula

$$u = \arcsin\frac{\sqrt{1-e^2}\sin(\theta-\theta_0)}{1+e\cos(\theta-\theta_0)}.$$

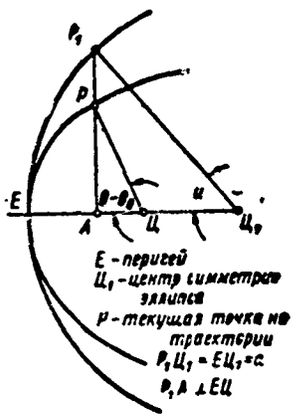


Fig. 10.14 Eccentric anomaly. 1) E – Perigee; 2) $Ts_0$ – center of symmetry of the ellipse; 3) P – current point on the trajectory.

In this way, for all the points of observation, we obtain the following characteristics



$$\begin{array}{l}\theta_1;\ \rho_1;\ r_1;\ \beta_1;\ u_1;\\ \theta_2;\ \rho_2;\ r_2;\ \beta_2;\ u_2;\\ \ldots\ldots\ldots\\ \theta_l;\ \rho_l;\ r_l;\ \beta_l;\ u_l,\end{array}$$

where $l$ – the number of points.

b) Determination of the partial derivatives. Partial derivatives may be found by the differention functions, expressing the coordinates of the object by the parameters of the trajectory. The coordinates $r$, $\alpha$ and $\beta$ are not expressed directly in the parameters of the ellipse. Therefore, these parameters are expeditiously considered as functions of the auxiliary variables, which in their turn are easily expressed as parameters of the ellipse. It is convenient for these variables to assume the polar coordinates of the points on the plane. In this way, the auxiliary variables (designated as $z_k$; $k = 1, 2$) are

$$z_1=\rho;\quad z_2=\theta.$$

The derivatives sought for may be found according to the principle of finding the partial derivative of $y_i$ from the function $z_k$.

In our case

$$\begin{array}{l}y_i=f_i(z_1;\ z_2),\\ z_k=\varphi_k(v_1;\ v_2;\ v_3),\end{array}$$

where

$$\begin{array}{l}y_1=\alpha;\quad y_2=\beta;\quad y_3=r;\\ v_1=a;\quad v_2=e;\quad v_3=\theta_0.\end{array}$$

We designate the partial derivative from the <u>ith</u> coordinate to the <u>kth</u> auxiliary parameter as $x_{ik}=\frac{\partial y_i}{\partial z_k}$, and the partial derivative from the <u>kth</u> auxiliary parameter as $v_{kj}=\frac{\partial z_k}{\partial v_j}$. Then, the general expression for the finding of the partial derivative may be written in the following form:

$$y'_{ij}=\frac{\partial y_i}{\partial v_j}=z_{i1}\cdot v_{1j}+z_{i2}\cdot v_{2j}.$$

The partial derivatives $z_{ik}$ and $v_{kj}$ may be determined by the differentiation relationships given in §10.3. The formulas obtained as a result of the differentiation are condensed in Tables 10.1 and 10.2 (see page 766). The partial derivatives from the coordinates with respect to the plane of trajectory $\frac{\partial y_i}{\partial a_0}$ and $\frac{\partial y_i}{\partial b_0}$ are determined from the equations of the planes of the trajectory. These derivatives are given in Table 10.3.

c) The determination of the weight factor $g_i$. The weight factors are found from the condition $g_i=\frac{\sigma^2}{\sigma_i^2}$ and are dimensionless quantities. Therefore, the mean square error of the measurement of angular coordinates and distance should be expressed in the same linear units as is also $\sigma^2$. As it has been noticed that is convenient for $\sigma^2$ to assume the smallest dispersion, which is natural in the majority of cases of errors of the measurement of distance. These errors are expressed in meters. The angular errors are necessary to be converted into linear by the formula

$$\sigma(\Delta s)=R_m\sigma_\alpha,$$

where $\sigma(\Delta s)$ – linear mean square error owing to the inaccurate measurement of the angle.

d) *Calculating the errors of the determination of the parameters of the trajectory.* After finding the quantities indicated above, the coefficients of the system of normal equations may be found from Relationships (10.21)–(10.29). The combination of the coefficients permits the calculation of the determinants of the system and the necessary algebraic complements. Afterwards, the variance of the determination of the parameters may be found by Formula (10.38).

Thus, for the system of equations of the second order, we find

$$|H'| = h'_{11} \cdot h'_{22} - h'^2_{12}; \quad \sigma^2_{a_0} = \frac{h'_{22}}{|H'|}\sigma^2; \tag{10.45}$$

$$H' = h'_{22}, \quad \sigma^2_{\delta_0} = \frac{h'_{11}}{|H'|}\sigma^2; \tag{10.46}$$

$$H'_{22} = h'_{11}; \quad \overline{\Delta\alpha_0 \cdot \Delta\delta_0} = -\frac{h'_{12}}{|H'|}\sigma^2. \tag{10.47}$$

Similarly, for the system of equations of the third order, we obtain

$$|H''| = h''_{11} \cdot h''_{22} \cdot h''_{33} + 2h''_{12} \cdot h''_{13} \cdot h''_{23} - \\ - (h''_{11} \cdot h''^2_{23} + h''_{22} \cdot h''^2_{13} + h''_{33} \cdot h''^2_{12}),$$

$$H''_{11} = h''_{22} \cdot h''_{33} - h''^2_{23}; \quad H''_{22} = h''_{11} \cdot h''_{33} - h''^2_{13}; \quad H''_{33} = h''_{11} \cdot h''_{22} - h''^2_{12};$$

$$\sigma^2(a) = \frac{H''_{11}}{|H''|}\sigma^2, \tag{10.48}$$

$$\sigma^2(e) = \frac{H''_{22}}{|H''|}\sigma^2, \tag{10.49}$$

$$\sigma^2(\theta_0) = \frac{H''_{33}}{|H''|}\sigma^2; \tag{10.50}$$

$$\overline{\Delta a \cdot \Delta e} = \frac{H''_{12}}{|H''|}\sigma^2; \tag{10.51}$$

$$\overline{\Delta a \cdot \Delta\theta_0} = \frac{H''_{13}}{|H''|}\sigma^2; \tag{10.52}$$

$$\overline{\Delta e \cdot \Delta\vartheta_0} = \frac{H''_{23}}{|H''|}\sigma^2. \tag{10.53}$$

The errors found of the values of the parameters of elliptic trajectory permits the calculation of the accuracy of the determination of the position of the object in any point of the trajectory which includes the point of fall of the ballistic rocket.

## §10.5 ERRORS OF PROGNOSTICATING THE POINT OF FALL OF THE BALLISTIC ROCKETS

The division of the parameters into groups obtained above is convenient also for the finding of the error of computing the point of fall. Thereby, the rectangular coordinate system is expeditiously introduced, the origin of which coincides with the true point of fall

(Fig. 10.15). One of the coordinate axes (axis PL), coincides with the line of intersection of the plane of the trajectory with the Earth's surface, while the other its perpendicular and is located in the horizontal plane (axis PN). Any deviation from the true point of fall may be represented in the form of deviation by these two axes. The deviation of the plane of trajectory, is referred to as the lateral deviation and designated as $l_n$. The deviation from the axis PL, dependent on the errors of the computed parameters of the ellipse referred to as the longitudinal deviation and designated as $l_l$.

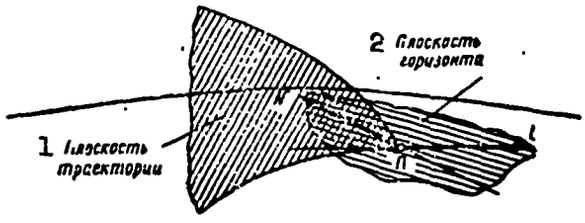


Fig. 10.15. The location of the coordinate axes during the determination of errors of finding the point of fall of ballistic rockets. 1) Plane of the trajectory; 2) horizontal plane.

It is obvious that the deviation of the coordinates of the computed point of fall from the true point is a function of the error of the determination of the parameters of the trajectory. Therefore, it is necessary to find the relationship connecting these deviations with the errors of the values of the parameters of the trajectory as found.

For the largest deviation of the point of fall, it may be considered that the connection is linear. The function, determining the lateral and longitudinal deviations in dependence of the values of the parameters is expanded into a Taylor's series and is limited by the first derivatives. This expansion should be conducted relative to the assumed position of the point of fall, computed by the approximate values of the parameters. For this, it is necessary to find the values

of the partial derivatives of the lateral and longitudinal deviations according to the parameters of the trajectory:

$$\frac{\partial l_n}{\partial \alpha_0}=S_1',\quad \frac{\partial l_n}{\partial \theta_0}=S_2',\quad \frac{\partial l_l}{\partial a}=S_1''\quad \frac{\partial l_l}{\partial e}=S_2'',\quad \frac{\partial l_l}{\partial \theta_0}=S_3''.$$

We determine at first the derivative of the lateral deviation $l_n$ according to the parameters $\alpha_0$ and $\delta_0$. Assume that errors have their places in the determination of the parameter $\alpha_0$; designate it as $\Delta\alpha_0$. Then, the measured plane of the trajectory surface is turned around by the angle $\Delta\alpha_0$ relative to the true plane (see Fig. 10.16a). Therefore, the magnitude of the lateral deviation is determined as the derivative $\Delta\alpha_0$ with respect to the distance from the point $D$. To the point of the fall (Segment $DP$ in Fig. 10.16b). In this way,

$$\Delta l_n=2\Delta\alpha_0\sin\frac{\theta_n-\pi}{2},$$

where $2\sin\frac{\theta_n-\pi}{2}$ – length of the segment $DP$; $\theta_p$ – polar angle of the point of fall. Consequently,

$$S_1'=\frac{\partial l_n}{\partial \alpha_0}\approx 2\sin\frac{\theta_n-\pi}{2}.$$

It is not difficult to see that the presence of error in the determination of the parameter $\delta_0$ leads to the lateral deviation, numerically equal to the magnitude of this error $\Delta\delta_0$. As it is seen from Fig. 10.16a, the resulting lateral deviation is equal to the difference of the deviations owing to $\Delta\alpha_0$ and $\Delta\delta_0$ at the reading $\alpha_0$ by the hour hand. Therefore, $S_2'=\frac{\partial l_n}{\partial \theta_0}=-1$. In a majority of the practical cases, the lateral deviation due to $\Delta\alpha_0$ is considerably larger than that due to $\Delta\delta_0$.

We find the derivative from longitudinal deviation by the parameters $a$, $e$ and $\theta_0$. The derivative in $a$ and $e$ may be determined by the differentiation of the relationship for the distance of the flight.

$$\cos\frac{l}{2}=-\frac{1-a(1-e^2)}{e}.$$

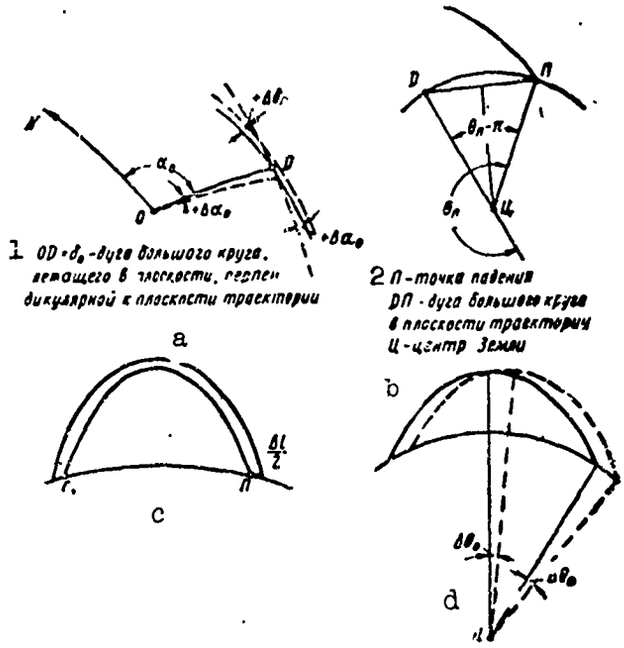


Fig. 10.16 Connection between errors of determination of the parameters of the trajectory and the deviation of the point of the fall: a) Lateral deviation; b) polar coordinates of the point of fall; c) increment of the distance of the flight; d) longitudinal deviation due to inaccurate determination of the parameter $\theta_0$. 1) $OD = \delta_0$ – arc of the large curve lying in the plane perpendicular to the plane of the trajectory; 2) $P$ – point of fall; $DP$ – arc of the great circle in plane of the trajectory; $Ts$ – center of the earth.

As can be seen from Fig. 10.16,c, the increment $\Delta l/2$ is equal to the sought for increment $\Delta I_l$. Having completed the differentiation, we find

$$S_1^* = \frac{\partial\left(\frac{l}{2}\right)}{\partial a} = \frac{\partial I_l}{\partial a} = \frac{1}{\sin\frac{l}{2}}\left(\frac{1}{e} - e\right),$$

$$S_2^* = \frac{\partial\left(\frac{l}{2}\right)}{\partial e} = \frac{\partial I_l}{\partial e} = \frac{1}{\sin\frac{l}{2}} \cdot \frac{) - a(1+e^2)}{e^2}.$$

The longitudinal deviation, caused by the inaccurate determination of the parameter $\theta_0$ is numerically equal to $\Delta\theta_0$ (Fig. 10.16, d). In this way, we obtain

$$S_3' = \frac{\partial l_l}{\partial \theta_n} = 1.$$

Now, we have all the necessary data for the finding of the variance of the lateral and longitudinal deviations.

It is obvious that the lateral deviation may be computed from the relationship

$$l_n = S_1' \Delta\alpha_0 + S_2' \Delta\delta_0.$$

The dispersion of the lateral deviation is

$$\sigma^2(l_n) = \overline{l_n^2} - (\overline{l_n})^2,$$

where $\overline{l_n^2}$ and $\overline{l_n}$ – the mean values of the corresponding magnitudes.

$$\sigma^2(l_n) = S_1'^2 \overline{\Delta\alpha_0^2} + 2S_1' \cdot S_2' \overline{\Delta\alpha_0 \cdot \Delta\delta_0} + S_2'^2 \overline{\Delta\delta_0^2} - S_1'^2 (\overline{\Delta\alpha_0})^2 -$$
$$- S_2'^2 (\overline{\Delta\delta_0})^2 = S_1'^2 \sigma_{\alpha_0}^2 + S_2'^2 \sigma_{\delta_0}^2 + 2S_1' \cdot S_2' \overline{\Delta\alpha_0 \cdot \Delta\delta_0},$$

where the mean values $\overline{\Delta\alpha}_0$ and $\overline{\Delta\delta}_0$ are equal to zero since the quantities found by the method of least squares do not have systematic errors.

Substituting the values of the partial derivatives and the moments of the determination of the parameters from Formulas (10.45)–(10.47), we obtain the calculation formula for the determination of the variance of the lateral deviations

$$\sigma^2(l_n) = \frac{\sigma^2}{|H'|}(S_1'^2 \cdot H_{11}' - 2S_1' \cdot H_{12}' + H_{22}') =$$
$$= \frac{\sigma^2}{|H'|}\left(4\sin^2\frac{\theta_n - \pi}{2} h_{22}' + 2\sin\frac{\theta_n - \pi}{2} h_{12}' + h_{11}'\right). \qquad (10.54)$$

The variance of the longitudinal deviations is found in the same manner. Thereby, it is necessary to find the sum of the derivatives all second moments with respect to the corresponding second derivatives.

Substituting in the same way as above and using Relationships (10.48)–(10.53), for the case of the longitudinal deviations, we find

$$\sigma^2(l_l) = S_1''^2 \sigma_\alpha^2 + S_2''^2 \sigma_\delta^2 + S_3''^2 \sigma_{\theta_0}^2 + 2S_1'' \cdot S_2'' \overline{\Delta\alpha \cdot \Delta\delta} +$$
$$+ 2S_1'' \cdot S_3'' \overline{\Delta\alpha \cdot \Delta\theta_0} + 2S_2'' \cdot S_3'' \overline{\Delta\delta \cdot \Delta\theta_0} = \frac{\sigma^2}{|H''|}(S_1''^2 \cdot H_{11}'' + \qquad (10.55)$$
$$+ S_2''^2 \cdot H_{22}'' + H_{33}'' + 2S_1'' \cdot S_2'' \cdot H_{12}'' + 2S_1'' \cdot H_{13}'' + 2S_2'' \cdot H_{23}'').$$

where

$$H_{12}^{*}=h_{23}^{*}\cdot h_{31}^{*}-h_{21}^{*}\cdot h_{33}^{*};\quad H_{13}^{*}=h_{21}^{*}\cdot h_{32}^{*}-h_{22}^{*}\cdot h_{31}^{*};$$
$$H_{23}^{*}=h_{12}^{*}\cdot h_{31}^{*}-h_{11}^{*}\cdot h_{23}^{*}.$$

The relationships obtained permit the determination of the mean square error of the prognostication of the point of fall according to two mutually perpendicular axes, whereupon these errors are independent. Then, in correspondence with the methods stated in Chapter 9, it is possible to determine the ellipse of distribution or the mean square error of the location in the horizontal plane.

## §10.6 EFFECT OF THE CONDITION OF OBSERVATION ON THE ACCURACY OF PROGNOSTICATION

*Effect of the character of the trajectory.* The character of the trajectory, or the form of the elliptic curve is determined by the angle between the direction of flight and the horizontal plane at the starting point $\beta_{v_0}°$. If the angle $\beta_{v_0} < \beta_{v_0\ opt}$, where $\beta_{v_0\ opt}$ – the angle under consideration for the optimum trajectory. Such trajectory is also referred to as flat (Fig. 10.17, a). From Fig. 10.17, it is seen at the same value of the error of determination of the parameters of the ellipse, the value of the longitudinal deviation is dependent on the angle $\beta_{v_0}$ increasing with the decrease of $\beta_{v_0}$. Therefore, at the conversion from the optimum trajectory to the flat one, the error of determination of the longitudinal deviation increases. The quantitative character of the trajectory is provided by the ratio $l/l_0$ where $l$ – is the factual distance, while $l_0$ – is the distance of the flight at optimum trajectory. The dependence $\frac{\sigma(l_l)}{\sigma(l_l)_{opt}}$ on this magnitude is shown in Fig. 10.17,b.

If the angle $\beta_{V_0} > \beta_{V_0 opt}$, we obtain a curved trajectory (Fig. 10.17,c). It is obvious that the mean square error of the longitudinal deviation

decreases in comparison with the case of the optimum trajectory. The dependence $\frac{\sigma(l_1)}{\sigma(l_1)_{opt}}$, similarly stated for the flat trajectory has the form shown in Fig. 10.17, d).

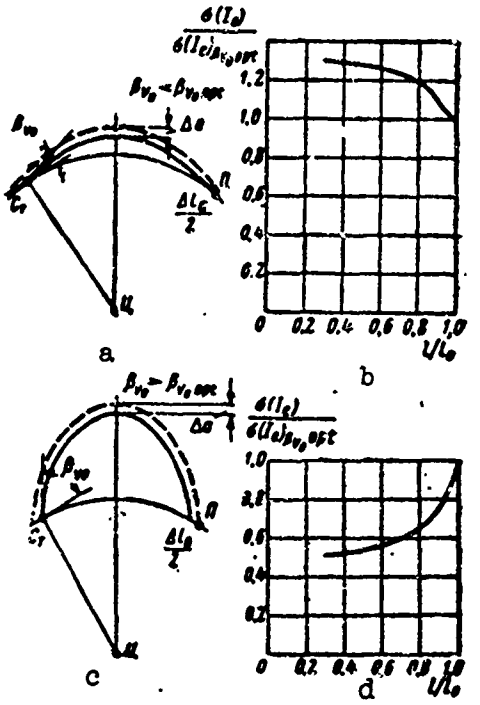


Fig. 10.17 Dependence of longitudinal deviation on the character of the trajectory. a) Flat trajectory; b) longitudinal deviation during the observation of the flat trajectories; c) curved trajectory ($\Delta l_b < \Delta l_a$); d) longitudinal deviation during the observation of the curved trajectories.

*The dependence on the values of the partial derivative.* At a defined number of points of observation, the error of lateral and longitudinal deviations changes in inverse proportion to the value of the segment of the trajectory being observed. The given condition is obviously for the case of two points. In fact the one and same error of determination of the position of the point leads to a larger deviation of the prognostication of the point than the close distance between the points found on the trajectory. During the deviation of the positions of these points from the actual computation, the trajectory is displaced to a

certain angle relative to the true one (Fig. 19.18). The linear deviation of prognosticated points satisfy the condition, $\sigma(l_{l,n}) \leq \frac{1}{\Delta\theta}$, where $\Delta\theta$ is the interval of the polar angles between the extreme observation points. Therefore the extent of the segment of observation is expeditiously increased. The dependence of the mean square error of the lateral and longitudinal deviations on the interval of the polar angles between the extreme points of observation $\Delta\theta$ is shown in Fig. 10.19 where for comparison, the curves are reduced by an inverse proportionality. From the figure, one can see that for the computed example, the error of lateral deviation rises faster than what is theoretically expected of the two point law.

*Dependence on the number of observed points.* In §10.4, it was established that the mean square error is determined by the parameters inversely proportional to the square roots from the number of derivatives of independent measurements. Similar rules are valid also for the linear errors of the prognostication of the points. Consequently, if the error of lateral and longitudinal deviations is equal to $\sigma_1$ at the presence of $n_1$ points, the corresponding error for $n_2$ points may be found from the following relationship

$$\frac{\sigma_1}{\sigma_2} = \sqrt{\frac{n_2}{n_1}}. \qquad (10.56)$$

From there one can see that at the conversion to large number of points the resulting error decreases. But, it should be noted that when the angle of the points being observed increases, the errors $\sigma(I_l)$ and $\sigma(I_n)$ strive toward zero.

Firstly, the measurement of coordinates is practically almost always associated with systematic errors. If these errors are small in comparison with the incidental ones, then Relationship (10.56) may be used. At the increase of the number of observation points, the decreas-

ed incidental errors appear to be comparable with the systematic. Therefore the indicated conversion may be carried out up to the time when the systematic errors may be neglected in comparison with the decreased incidental errors of the measurement of coordinates.

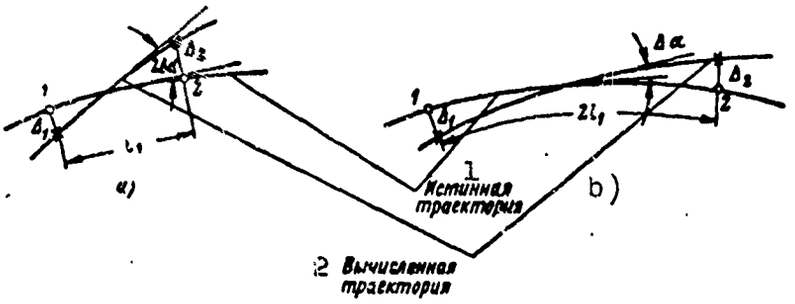


Fig. 10.18. Dependence of the deviation of the computed trajectory from the true one at a distance between the points being measured of $l_1$ *(a)* and $2l_1$ *(b)*. $\Delta_1$ and $\Delta_2$ – deviation of the position of the computed point relative to the true one($\Delta_1$ and $\Delta_2$ according to Figs. a and b are the same). 1) True trajectory; 2) computed trajectory.

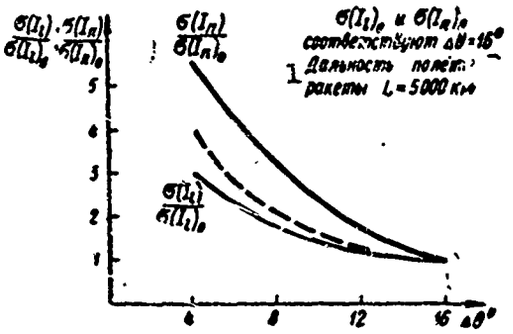


Fig. 10.19 Dependence of lateral and longitudinal errors on the segment of observation (interval of polar angles). 1) $\sigma(I_1)_\theta$ and $\sigma(I_n)_\theta$ correspond to $\Delta\theta = 16°$ distance of the flight of the rocket $L = 5000°$ *km*.

Firstly, the measurement of coordinates is practically almost always associated with systematic errors. If these errors are small in comparison with the incidental ones, then Relationship (10.56) may be used. At the increase of the number of observation points, the decreased incidental errors appear to be comparable with the systematic. Therefore the indicated conversion may be carried out up to the time when

the systematic errors may be neglected in comparison with the decreased incidental errors of the measurement of coordinates.

Secondly, the conversion of errors should be carried out only in the case if the measurement of the coordinate is statistically independent. At the same time during the decrease in the time interval between the moments of observation, individual readings may be correlated. The latter circumstance is particularly necessary to be taken into account when analysing the operation of the RLS accomplishing automatic tracking of the object. The calculation of error of the determination of parameters of the trajectory for the case of automatic tracking of the object may be conducted at the equivalent substitution of continuous observation by the discrete. Thereby, it is necessary that the interval of discreteness should be at least equal in value of the stated band pass of the system of tracking.

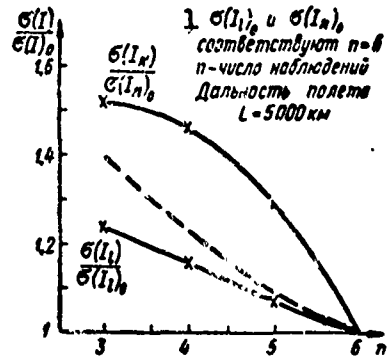


Fig. 10.20. Dependence of lateral and longitudinal deviations on the number of observations, $n$. 1) $\sigma(I_l)_o$ and $\sigma(I_n)_o$ correspond to $n = 6$ $n$ — number of observations distance of flight, $L = 5000$ km.

On the basis of the cited considerations, it is possible to establish the dependence of the errors of lateral and longitudinal deviations on the extensiveness of the interval of automatic tracking. In fact, with the increase of the interval of tracking as the value of the segment of observation so is the number of measuring points. At

joint action of both factors, it shows that $\sigma(I)$ varies in inverse proportion to the linear interval of tracking in degrees 3/2. This dependence is valid for intervals of time of tracking from 30 sec to 2.5 min (see [1] to Chapter 10).

Figure 10.20 shows the stated dependence of mean square error $\sigma(I_7)$ and $\sigma(I_n)$ on the number of points of observation. From a comparison of the indicated curve with the theoretically expected, shown in the figure in dotted line, it follows that the deviation from the assumed law is not great.

The dependence examined previously may be used for the approximate evaluation of the effect of various conditions of observation on the error of prognostication. If it is necessary to obtain accurate results, then one should for the changed condition of observation carry out anew the calculation of accuracy of prognostication by formulas of §§ 10.4 and 10.5.

TABLE 10.1

| 1 | Общее выражение. $z_{ik}=\frac{\partial y_i}{\partial z_k}$ |
|---|---|
| $z_{11}=\frac{\partial \alpha}{\partial p}=0$ | |
| $z_{21}=\frac{\partial \beta}{\partial p}=\frac{\sqrt{1-\cos^2\theta\cos^2\beta_0}}{r^2}$ | |
| $z_{31}=\frac{\partial r}{\partial p}=\frac{a(1-e^2)+[1+e\cos(\theta-\theta_0)]\cos\theta\cos\beta_0}{r[1+e\cos(\theta-\theta_0)]}$ | |
| $z_{12}=\frac{\partial \alpha}{\partial \theta}=\frac{\sin\beta_0}{1-\cos^2\theta\cos^2\beta_0}$ | |
| $z_{22}=\frac{\partial \beta}{\partial \theta}=-\frac{a(1-e^2)\sin\theta\cos\beta_0}{r^2[1+e\cos(\theta-\theta_0)]^2\sqrt{1-\cos^2\theta\cos^2\beta_0}}\times$ | $\times\{a(1-e^2)+[1+e\cos(\theta-\theta_0)]\cos\theta\cos\beta_0\}$ |
| $z_{32}=\frac{\partial r}{\partial \theta}=-\frac{a(1-e^2)\sin\theta\cos\beta_0}{r[1+e\cos(\theta-\theta_0)]}$. | |

1) General Expression

TABLE 10.2

Общее выражение: $v_{kj} = \frac{\partial z_k}{\partial v_j}$

$$v_{11} = \frac{\partial \rho}{\partial a} = \frac{1}{2\sqrt{1-e^2}\,[1 + e\cos(\theta - \theta_0)]} \times$$

$$\times \{\sqrt{1-e^2}\,[2 + e^2 - 3e^2\cos^2(\theta - \theta_0)] - 3e\,[1 + e\cos(\theta - \theta_0)]\,[\sin(\theta - \theta_0)]\,u\}$$

$$v_{21} = \frac{\partial \theta}{\partial a} = \frac{3\,[1 + e\cos(\theta - \theta_0)]}{2a\,(1-e^2)^{\frac{3}{2}}}\,\{e\sqrt{1-e^2}\sin(\theta - \theta_0) - [1 + e\cos(\theta - \theta_0)]\,u\}$$

$$v_{12} = \frac{\partial \rho}{\partial e} = -a\cos(\theta - \theta_0)$$

$$v_{22} = \frac{\partial \theta}{\partial e} = \frac{\sin(\theta - \theta_0)}{1-e^2}\,[2 + e\cos(\theta - \theta_0)]$$

$$v_{13} = \frac{\partial \rho}{\partial \theta_0} = 0$$

$$v_{23} = \frac{\partial \theta}{\partial \theta_0} = 1$$

1) General Expression

TABLE 10.3

| $\frac{\partial y_i}{\partial \alpha_0}$ | $\frac{\partial y_i}{\partial \delta_0}$ |
|---|---|
| $\frac{\partial \alpha}{\partial \alpha_0} = 1$ | $\frac{\partial \alpha}{\partial \delta_0} = -\frac{\sin\theta\cos\theta\cos\delta_0}{1 - \cos^2\theta\cos^2\delta_0}$ |
| $\frac{\partial \beta}{\partial \alpha_0} = 0$ | $\frac{\partial \beta}{\partial \delta_0} = \frac{a(1-e^2)\cos\theta\sin\delta_0}{r^2\,[1 + e\cos(\theta - \theta_0)]^2\sqrt{1 - \cos^2\theta\cos^2\delta_0}} \times$ |
| | $\times \{a(1-e^2) + [1 + e\cos(\theta - \theta_0)]\cos\theta\cos\delta_0\}$ |
| $\frac{\partial r}{\partial \alpha_0} = 0$ | $\frac{\partial r}{\partial \delta_0} = -\frac{a(1-e^2)\cos\theta\sin\delta_0}{r\,[1 + e\cos(\theta - \theta_0)]}$ |

Manu-
script
Page
No.

[Footnotes]

730 In further considerations, the rotation of the Earth is not taken into account and also other factors arising from the deviation from the elliptic trajectory. The effect of these factors on the accuracy of the parameters determined is not significant.

734 $r$ is the slope of the range $R$, expressed in polar radius of the Earth.

743 Since $l_i = y_i^* - y_i^0$, i.e., equal to the difference between the measured values of the coordinates and its approximate value which is not incidental then, $\sigma^2(l_i) = \sigma_i^2$.

748 Since only the elliptic trajectories are considered, it must be remembered that such a start is understood to be the point of intersection of the continuation of the passive part of the trajectory with the surface of the Earth. The same concerns also the point of fall of the object.

[Transliterated Symbols]

716 ИСЗ = ISZ = iskusstvennyy sputnik zemli = artificial earth satellite

717 к = k = krivizna = curvature

717 мин = min = minimal'nyy = minimum

720 макс = maks = maksimal'nyy = maximum

731 БР = BR = ballisticheskaya raketa = ballistic missile

731 Ц = Ts = tsentr = center

732 з = z = zemlya = earth

732 РЛС = RLS = radiolokatsionnaya stantsiya = radar

732 т = t = tekushchiy = current

749 ап = ap = apogey = apogee

Chapter 11

# ACTIVE INTERFERENCES AND THE METHOD OF COMBATING THEM

## §11.1 INTERFERENCES AT RADIOLOCATIONAL STATIONS

All interferences of the operation of radiolocational stations may be divided into two major groups: intentional (arranged) and natural. To the natural interferences belong the signals of the various reflections: hydrometeors, the surfaces of the Earth and the sea, various positions of objects and signals formed on account of the tremendous discharge of cosmic radiation, radiation of radiobeams on the surface of the Earth with the aid of special technical devices. Besides these two basic groups of interferences, disturbing signals entering from neighboring radiotechnical apparatus operating from the same band width may act on the radiolocational stations.

Depending on the method of forming the interferences, they may be divided into passive and active. Natural passive interferences consists of signals reflected from the clouds, rain, forest, shrubs and other local objects. Passive interferences may disguise as useful signals or create the sign of a false object.

Intentional passive interferences are created with the aid of artificial reflectors, which reradiate relatively intensively the energy of the incident radiobeams. For the creation of organized interferences, one may use dipole halfwave reflectors made of strips of foils or metallized mirrors, angular or biconical reflectors, Luneberg lenses, etc.

The dipole reflectors are used mostly for the masking of aerial objects. The degree of masking useful signal depends on the effective area of scattering of every reflector, the quantity of reflectors in unit volume and the magnitude of the reflecting volume. Various types of angular reflectors are used for the creation of false terrestial, above-water and aerial objects and for the change of the outline of terrestial objects, for example, shore lines, configuration of cities, etc. The methods of combating the passive interferences will be examined in Chapter 12.

Active interferences consist of sources of electromagnetic energy. The active natural interferences are mostly atmospheric noises, cosmic radiation, and thermal radiation radiobeams of the Earth's surface.

1. Natural Active Interferences

There are two basic forms of sources of natural active interferences: dispersed and discrete. To the dispersed interferences belong the galactic noise (Young's noise), radiation of atmospheric hydrogen and noise of the atmosphere. Discrete sources of interferences are the Sun, the Moon and radiostars.

The intensity of the external natural noises are customarily evaluated by the brightness $V$ or the temperature of brightness $T_{ya}$. By brightness is meant the current density of the energy of the noises, which is received by the ground antenna having a beam width in one steradian (it is assumed that $V$ remains constant within the limits of the diagram of directionality).

The brightness temperature $T_{ya}$ is the temperature of the absolute black surface having such brightness as the area of sky being observed. The magnitude of $T_{ya}$ is measured in degrees Kelvin. The brightness and brightness temperature are connected between them by the relation-

ship of Rayleigh-Jones

$$B = \frac{2kT_s}{\lambda^2},$$

where $k$ – Boltzmann's constant, equal to $1.38 \cdot 10^{-23}$ w/hz-degree;

$\lambda$ – wave length in $m$.

The dispersion of cosmic noises is observed at the receiving of signals from all directions but they are the most intensive in the plane of the Galactics, particularly in the direction towards its center located in the region of the constellation Sagitta. Close to the galactic center the power of the cosmic noises rises in 10–20 times in comparison with the average level of radiation of the remaining part of the Galactics.

The effective temperature of the cosmic radiation, decreases with the increase in the frequency according to the law $a/f^n$ where $n$ for most part of the radiofrequency bands lies in the limits from 2 to 2.7. At frequencies higher than 2000 Mhz the level of galactic noise becomes small and the predominant sources of external natural interferences is the natural thermal radiation of the atmosphere.

The Earth's atmosphere is composed of oxygen and water vapor, which absorbs and radiates radiobeams. The quantity of oxygen in the atmosphere is relatively constant in time and it determines the constant background noise. The quantity of water vapor and the noises produced by them vary depending on the locality and the time of the year.

The graphs characterizing the dependence of average cosmic and atmospheric noises on frequency are shown in Fig. 11.1a. The effect of the relative humidity on the intensity of the atmospheric radiation is characterized by the graphs drawn in Fig. 11.1b.

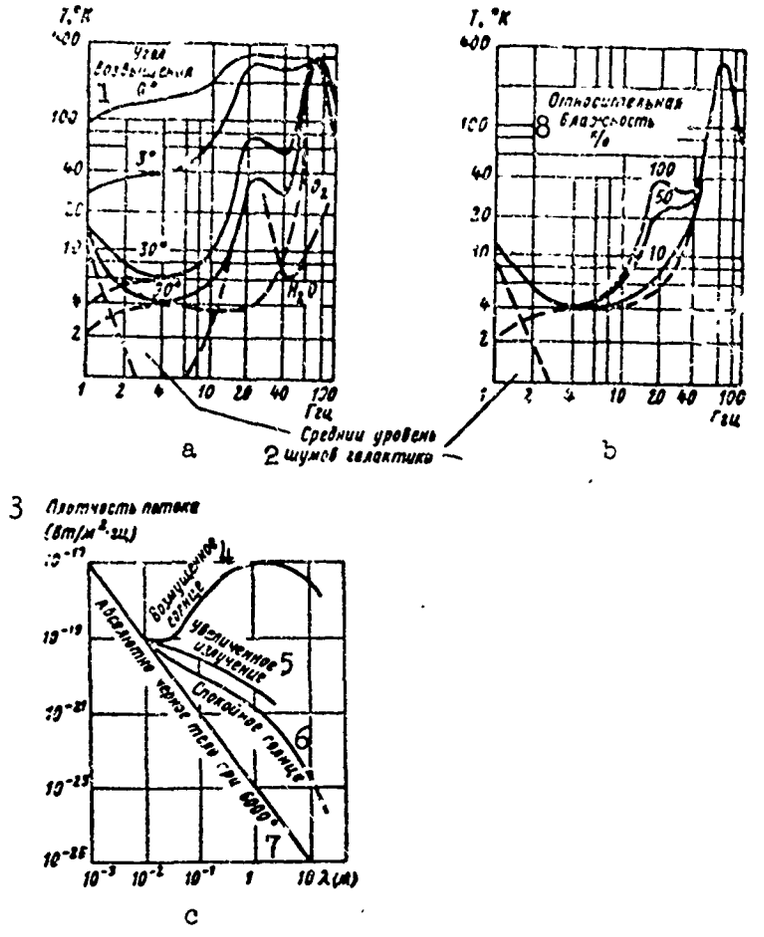


Fig. 11. 1.Characteristics of the natural active interferences: a) Temperature of the galactic and atmospheric radiations; b) dependence of noise temperature on relative humidity; c) characteristics of the radiations of the Sun. 1) Angle of elevation; 2) average level of galactic noise; 3) current density ($w/m^2$ hz); 4) disturbing Sun; 5) increased radiation; 6) quiet Sun; 7) absolute black body at *6000°*: 8) relative humidity %.

The above graphs permit the determination of the frequency band with the lowest level of natural active interferences. The lower boundary of this band is approximately equal to $(2-3)\cdot10^3$ mhz and the upper reaches $(10-15)\cdot10^3$ mhz. The average temperature of the noises in this band does not surpass 10-20°K (for an angle of elevation of the antenna arc larger than 25-30°).

To the distribution of the noise sources there also belong monochromatic radiations of the interplanetary hydrogen ($\lambda \approx 21$ cm). The intensity of this radiation exceeds considerably the power of the galactic

noise. But the radiation of hydrogen exceeds only in the fundamental frequency therefore as a source of interference for RLS working in a different wave, it has no significance.

Besides the dispersion of sources of cosmic noises there are also large quantities of sources of radiations with comparatively small angular dimensions. Such sources are called the radiostars. The most powerful radiostars are located in the galactic plane. As a rule, the current density of the radiation energy of the radiostars diminishes with the increase in frequency.

The most intensive radiostars are Cassiopeia-A, Cygnus-A and Taurus-A. The current density of the radiation of the brightest radiostar, Cassiopeia-A consists of $10^{-23}$ w/m$^2$·hz, at the frequency of 1 Ghz and approximately $6 \cdot 10^{-24}$ w/m$^2$·hz at the frequency of 10 Ghz. The noise radiation of the radiostars is not great and may be neglected in comparison with the dispersion of galactic noises even in the case of sufficiently narrow diagram of directionality of the antenna. Thus for example, at a frequency of 100 Mhz the current density of Cassiopeia-A consists of $2 \cdot 10^{-22}$ w/m$^2$·hz, while the brightness of the Galactics in the direction of the radiostars is equal to $5 \cdot 10^{-21}$ w/m$^2$·hz steradian. An antenna with effective area in A = 100 m$^2$ will receive from Cassiopeia-A the power of $2 \cdot 10^{-20}$ w hz. The beam of the antenna thereby makes a space angle of approximately 0.1 steradian and the antenna will receive radiation of the galactic background of $5 \cdot 10^{-20}$ w hz.

Among the discrete source of noise of practical effect on the operation of the radiolocational station, SVCh band, one may count the Sun and to a lesser degree the Moon. The radio frequency spectra of the solar radiation has complex characters and to a large degree de-

pends on the condition of the Sun. In the milimeter wave band, the solar radiation corresponds to the radiation of the absolute black body at 6000°K. At longer wave length, the intensity of the radiation of the quiet Sun is considerably bigger. In the band of 2–60 cm the intensity of the radiation is dependent to a very high degree on the magnitude and quantity of the solar spots. The periodicity of the appearance of the spots leads to the periodic increase of the radiowaves of the Sun.

In the metric wave band of average level, radiation remains close to constant during a significant time but there exists very strong disturbance – "noise storm" consisting of a series of sparks continuing for the duration of several hours or days whereupon the radiation at ignition possesses sharply marked circular polarization.

Solar flares produces shortlived sharp rise of the energy of radiation as in the centimeter waves as well as in the metric wave bands. The duration of such disturbance consists of a few minutes but the intensity of the radiowave in these moments of time may increase by several orders.

The characteristics of the intensity of the radiowaves of Sun is shown in Fig. 11.1c. For the sake of comparison the level of radiation of a back body at $t$ = 6000°K is also shown. The curve of the disturbed Sun characterizes the most probable level of radiation during disturbance. The maximum flare could give considerably large current of electromagnetic energy. Thus, for example, the registered flare-up had a current density of $10^{-15}$ w/m$^2$·hz.

The radiowave of the Moon has considerably less intensity and appears only in the range SVCh where the current density is approximately composed of $10^{-21}$ w/m$^2$ hz.

With the Sun and the Moon as the sources of external interferences of RLS, it should only be considered when the basic or the more intense lateral petal of the diagram of directionality of the antenna is oriented towards them. The galactic and atmospheric noises manifest themselves everywhere and they are the most serious form of natural active interferences.

For a complete account, it should be mentioned about the possible interferences from the radiations produced by gigantic discharges. The maximum radiation of atmospheric discharge lies in the long wave bands ($\lambda \approx 1$ km) but the observable magnitude could be harmonics at metric and decimetric waves. For example, on a wave of 50 cm, the current density of the radiation of lightening may reach the magnitude of $10^{-18}$ w.m$^2$ hz.

2. Active Intentional Interferences

The active intentional interferences consist of specially transmitted interferences which may be the very object after which the radiolocational observation is directed or outside of it. In the first case the interference is referred to as coincidental and in the second case – noncoincidental.

Organized active interferences: – show masking action similar to the action of internal noises of the receiver; – produce overloading of the receiver, after which during certain moments the observation of useful signals is impossible; – create signs of false object, similar in form to real objects.

Depending on whether the interferences are in the narrow or wide frequency band, one distinguishes on-target and boundary interferences. The on-target interferences refer to disturbing signals whose frequency spectra are considerably narrower than the frequency band in which

the suppressed RLS may operate. For an effective action of the RLS the transmitter of the on-target interference must have the possibility of a quick changeover to any frequency within the limits of the operating range. The boundary interferences refer to the disturbing signals whose frequency spectra embrace all frequency bands in whose boundaries it is necessary to suppress the operation of the enemy. Boundary interferences in opposite position to the on-target may suppress the operation at one stroke many radiolocational stations operating at different frequencies.

From an energetic viewpoint, the on-target interferences are more advantageous since the coefficient of the use of the transmitter of interference (the ratio of the total passband of the receiver of the suppressed RLS to the width of the frequency spectra of the interference station) for the on-target interferences is considerably higher than that of the boundary interference. But the nonproductive expenditure of power during the creation of the wide band interferences in many cases may be recovered by operative reception (no necessity in accurate tuning of the carrier frequency of the transmitter of interferences) and the possibility of simultaneous suppression of an entire group of different RLS.

The most effective action on RLS interference will be in such cases if it is created on the basis of the knowledge of the parameters of the RLS. Therefore, for the creation of the maximum effective interference it is necessary in the beginning to investigate the basic parameters of the RLS. As it is known the difficulty of investigating into the parameters of the radiolocational stations is called the secrecy of the operation of the RLS. The ability of radiolocational stations to keep their parameters during the action of interference is known as interference-immunity. The interference-immunity and the secrecy of

operation are determined by the interference protection of the radiolocational station.

The signals of interference stations may be pulsated and continuous. Pulse signals are received as a rule in the capacity of on-target interferences. Pulse interferences whose frequency sequence is equal to the short repetition frequency of the useful signals are called the synchronous interference pulses. Synchronous interferences are often completely created by retranslating the signals being received. The station of interferences receives the signals, emitted by the RLS, amplifies them, modulates, makes false informations and practically instantly re-emits accurately on the same existing frequency.

Synchronous interferences form at the indicator of the RLS one or an entire series of false moving or stable objects disinforming the recipient of the radiolocational information.

Nonsynchronous interferences are referred to as interferences, the frequency sequence of whose pulses are in an arbitrary relationship with the frequency F. Nonsynchronous interferences create on the indicator of the RLS, signs, movable in distance. The character of the motion of the false signal depends on the relationship between the frequency of the interference and the frequency of the repetition pulses of the RLS. To isolate the useful signals on the background of nonsynchronous interferences is simpler, but, when the frequency of the sequence of interference pulses is higher in comparison with $F_p$ and its variations is by a random rule, the useful signal may be masked quickly and chaotically transposed by the pulse marks.

Continuous interferences may form unattenuated, unmodulated and frequency and amplitude modulated oscillations. The continuous interferences with narrow energy spectra are received only as on-target interferences, masking the signal and producing overloading of the

receiving channels of the RLS. The continuous interferences with wide spectra, surpassing the passband of the receiver are received as on-target as well as boundary interferences.

The noise interferences having the maximum entropy possess the largest maskingaction. Such interferences may be created by direct amplification of the noise voltage or by the noise modulation of the unattenuated oscillation. The disturbing action of such interferences are similar in action to internal noises of the receiver and at high power, their interferences may cause in addition, the overloading of the receiving channels.

## §11.2 RANGE OF RADIOLOCATIONAL OBSERVATION DURING THE ACTION OF ACTIVE NOISE INTERFERENCES

The degree of suppression of the radiolocational system by the interferences of the masking type depends on the power of the interference transmitter, form of interference, distance between sources of interference and the RLS and also on whether if the interferences are coincidental or noncoincidental. Quantitatively, the effect of the interferences may be evaluated by the decrease of the working range of the RLS. If the external noise interferences are similar to the character of the internal noise of the receiver, i.e., they possess equivalent spectra and obey the normal law of distribution then the effect of the internal noises of the receiver. Since the external noises and internal noises are statistically independent therefore, the resulting power of the noises at the input of the receiver in this case is

$$P_{\text{п}} = P_{\text{ш}} + P_{\text{пр п}},$$

where $P_{sh}$ – power of the internal noises, reread at the input of the receiver. $P_{pr\ p}$ – average power of the Gaussian interferences at the input of the receiver.

If the interferences have nonhomogeneous electric spectra, then

it possesses less masking effect than noise. Therefore, the coefficient of discrimination for such interferences will be less than the coefficient of discrimination of noises, and the power of internal noises, equivalent in its action to the power of external interferences, decrease by $\xi$ times where $\xi$ is the coefficient of nonhomogeniety of the interference equal to the ratio of the coefficient of discrimination of the signals in the background to the coefficient of discrimination of the signals in the background of Gaussian noises.

In this way, if the power of the noise is known, reread at the input of the receiver and the power of the interferences being received, then in the general cases, the minimum discriminated signal in the presence of external interferences is determined by the expression

$$P_{\text{пр мин}} = m_{\text{р}} P_{\text{ш}} + m'_{\text{р}} P_{\text{пр п}} = m_{\text{р}} (P_{\text{ш}} + \xi P_{\text{пр п}}), \qquad (11.1)$$

where $\xi P_{\text{пр р}}$ – entropy power of the noises at the input of the receiver; $m'_{\text{р}}$ – coefficient of discrimination for interferences.

We determine the range of radiolocational observation for the most general case when there are noncoincidental interferences by distance as well as by direction (Fig. 11.2,b).

Under this condition, the power of interferences at the input of the receiver is determined by the expression

$$P_{\text{пр п}} = \frac{P_{\Sigma \text{п}} D_{\text{п}} A(\alpha)}{4\pi R_{\text{п}}^2}, \qquad (11.2)$$

where $P_{\Sigma \text{ п}}$ – power of radiation of the transmitter of interference into the passband of the receiver taking into account the form of the polarization field of the interference; $D_{\text{п}}$ – coefficient of directional action of the antenna of the transmitter of interference in the direction toward the RLS; $R_{\text{п}}$ – distance between RLS and transmitter of interference; $A(\alpha)$ – effective area of the antenna of RLS in the direction toward the interference station.

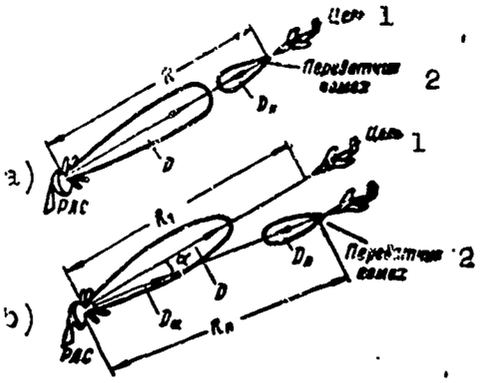

Fig. 11.2 Conclusion of the equation of range of observation in the presence of interference. a) Coincidental interference; b) noncoincidental interference. 1.) Object; 2.) transmitter of interference.

Taking into consideration that $A(\alpha)=\frac{D(\alpha)\cdot\lambda^2}{4\pi}$, where $D(\alpha)$ – coefficient of directional action of the antenna at RLS in the direction toward the station of interference, Expression (11.2) may be rewritten in the following form:

$$P_{\text{пр п}}=\frac{P_{\text{з п}}D_{\text{п}}D(\alpha)\lambda^2}{(4\pi)^2R_{\text{п}}^2}.$$

The resulting power of the noise interference at the input of the receiver of RLS is

$$P_{\text{п}}=P_{\text{ш}}+\xi P_{\text{пр п}}=P_{\text{ш}}+\xi\frac{P_{\text{з п}}D_{\text{п}}D(\alpha)\lambda^2}{(4\pi)^2R_{\text{п}}^2}. \qquad (11.3)$$

Substituting the value of $P_{\text{p}}$ in the basic equation of range of radiolocational observation, we obtain

$$R_{\text{макс p}}=\sqrt[4]{\frac{P_{\text{и}}D^2\lambda^2\sigma_{\text{ц}}}{m_{\text{p}}\cdot(4\pi)^3\left[P_{\text{ш}}+\xi\frac{P_{\text{з п}}D_{\text{п}}D(\alpha)\lambda^2}{(4\pi)^2R_{\text{п}}^2}\right]}}, \qquad (11.4)$$

where $R_{\text{maks p}}$ – range of radiolocational observation in the presence of external interference.

After several algebraic transformations, Equation (11.4) takes the form

$$R_{\text{макс п}}=\sqrt{DR_{\text{п}}}\cdot\sqrt[4]{\frac{P_{\text{и}}\sigma_{\text{ц}}}{4\pi m_{\text{p}}\left[4\pi R_{\text{п}}^2P_{\text{ш}}+\xi P_{\text{з п}}D_{\text{п}}D(\alpha)\cdot\lambda^2\right]}}.$$

The calculation of the action of the interference presents interest when the entropy power of the active interference may significantly surpass the power of the internal noises ($P_{sh} << \xi P_{pr\ p}$). Thereby, approximately it may be assumed that $P_{pr\ min} \approx m_r \xi P_{pr\ p}$) and the range of the radiolocational observation is

$$R_{макс\ п} = \sqrt{R_п} \cdot \sqrt[4]{\frac{P_\Sigma}{P_{\Sigma п}} \cdot \frac{D}{D_п} \cdot \frac{D}{D(\alpha)} \cdot \frac{\sigma_ц}{4\pi \xi m_p}}. \qquad (11.5)$$

Consequently, the range of radiolocational observation at the action of noncoincidental interferences diminishes in comparison with the range in free space by $\gamma_n$ times, where

$$\gamma_п = \frac{R_{макс}}{R_{макс\ п}} = \sqrt[4]{\frac{\xi P_{\Sigma п} D_п D(\alpha) \lambda^2}{(4\pi)^2 R_п^2 P_ш}}.$$

Interferences may diminish the range of radiolocational observation considerably since it is known that the value $R_{maks\ p}$ depends substantially on the relative locations of the diagram of directionality of the antenna of the RLS and the transmitter of interferences. The reduction of the working range of the RLS during the action of interference depends on the width of the diagram of directionality of the antenna and also on the intensity of the lateral petals. The narrower the diagram of directionality and the less the lateral petal, the less effective will be the interferences noncoincidental by direction.

The range of the radiolocational observationduring coincidental (Fig. 11.2,a) interference may be determined from the formula obtained above (11.5). Thereby, one should bear in mind that
For the case, $P_{sh} << \xi P_{pr\ p}$ the working range of the radiolocational station is

$$R_{макс\ с} = \sqrt{\frac{P_з}{P_{зш}} \cdot \frac{D}{D_п} \cdot \frac{\sigma_ц}{4\pi \xi m_p}}. \qquad (11.6)$$

The range of the radiolocational observation is reduced by $\gamma_s$ times where

$$\gamma_c = \frac{R_{макс}}{R_{макс\,п}} = \sqrt[4]{\frac{(P_{\Sigma\,т})^2 D_п^2 m_р^2 \lambda^2}{4\pi P_{пр\,min} P_Σ \sigma_ц}}.$$

When the distance to the object is less than $R_{maks\ p}$, the signal/noise ratio at the receiver input will be larger than the coefficient of discrimination and the object will be found on the background of the interferences. When $R > R_{maks\ p}$ the useful signal is lost among the interferences.

## §11.3 PROTECTIVE METHODS AGAINST ACTIVE INTERFERENCES

The most complete suppression of interferences may be accomplished on the basis of the statistical distinction between the signals and interferences. If the interferences have the normal law of distribution then its exhaustive statistical characteristics are the correlation function or the energy spectra. In this case, the maximum weakening of the interference action may be accomplished with the aid of a liner filter utilizing the distinction in the spectral composition of the signals and the interferences.

If the signals and the interferences differ in one or several parameters, then it is possible to use selection according to these parameters, i.e., to accomplish suppression based on the knowledge of the deep differences between the signals and the interferences.

For the elimination of overloading of the receiver, caused by intensive interferences, regulating amplification of various types may be used.

In this way, all methods of protection against active interferences may be subdivided into three basic types:

– optimum filtration; – selection according to determined parameters; – regulating amplification.

## 1. Optimum Filtration

The problem of the synthesis of optimum filter leads to the determination of transmission function by which at the output of the filter the ratio of the peak values of the signal to the mean square value of interference reaches a maximum magnitude. The methods of optimum filtration during the action of noise interference with equivalent spectra have been examined in Chapter 6. These methods are also applicable to the suppression of active interferences if their spectra in the passband of the receiving device are homogeneous. In the case when the interferences have nonequivalent spectra, filters optimum for white noise will not be optimum for action on these interferences. To every form of interferences, there is a corresponding optimum filter whose transmission function is determined by the character of the spectra of the interference. For the finding of the dependence of the transmission function of the optimum filters on the form of energy spectra of the noise, we shall look at the passage of the signals and interferences with arbitrary spectra through the linear filter.

Let there be the action of the summation of the signals and interferences at the input of the linear filter

$$X(t)=S(t)+n(t),$$

where $S(t)$ – signal of known form; $n(t)$ – interference forming a stationary random process whose energy spectra are $G_p(\omega)$.

Since the filter is linear, therefore its output voltage $y(t)$ may be represented in the form of two components dependent correspondingly on the action of the signal and the interference:

$$y(t)=y_c(t)+y_n(t).$$

If $K(j\omega)$ – complex frequency characteristics of the linear filter then the signal at the output of the filter has this form

$$y_c(t)=\frac{1}{2\pi}\int_{-\infty}^{\infty}K(j\omega)\,G(j\omega)\,e^{j\omega t}d\omega, \qquad (11.7)$$

where $G(j\omega)=\int_{-\infty}^{\infty}S(t)e^{-j\omega t}dt$ – the complex spectra of the signal.

Interferences form a random process, therefore, for the determination of the intensity of the interference at the output of the filter, it is possible to fulfill the theorem of Khinchin, according to which the mean square value of the interference is connected with the energy spectra by the dependence

$$\overline{y_n^2(t)}=\frac{1}{2\pi}\int_{-\infty}^{\infty}G_{n\,вых}(\omega)\,d\omega,$$

where $G_{n\,вых}(\omega)=G_n(\omega)|K(j\omega)|^2$ – energy spectra of the interferences at the output of the filter.

The signal/noise ratio (in power) at the output of the filter in a certain fixed moment of time, $t_0$ is determined by the expression

$$q=\frac{y_c^2(t)}{\overline{y_n^2(t)}}=\frac{1}{2\pi}\cdot\frac{\left|\int_{-\infty}^{\infty}G(j\omega)K(j\omega)e^{j\omega t_0}d\omega\right|^2}{\int_{-\infty}^{\infty}G_n(\omega)|K(j\omega)|^2d\omega}, \qquad (11.8)$$

where $y(t_0)$ – the value of the signal at the output of the filter at the moment $t_0$.

At given spectra of the signal and the interference, the ratio (11.8) depends only on the transmission function. The problem of finding the maximum possible signal/noise ratio and the finding of the optimum transmission function of the filter during which the quantity $q$ in a certain moment of time takes on the biggest value, may be resolved by the method of inequality of Bunyakovski-Schwarz. According to this inequality, the square of the modulus of the integral from the product of any two functions of the one and the same variable may not be larger than the product of the integral of the square of the modulus of the same function under the condition that these integrals exist:

$$\left|\int_{-\infty}^{\infty} A(j\omega)\cdot B(j\omega)\,d\omega\right|^2 \leqslant \int_{-\infty}^{\infty} |A(j\omega)|^2\,d\omega \int_{-\infty}^{\infty} |B(j\omega)|^2\,d\omega. \qquad (11.9)$$

If the functions $A(j\omega)$ and $B(j\omega)$ assume correspondingly the equalities

$$A(j\omega) = e^{j\omega t_0} K(j\omega)\sqrt{G_n(\omega)};$$
$$B(j\omega) = \frac{G(j\omega)}{\sqrt{G_n(\omega)}},$$

then according to the inequality of Bunyakovski-Schwarz, we have

$$\left|\int_{-\infty}^{\infty} e^{j\omega t_0} K(j\omega)\,G(j\omega)\,d\omega\right|^2 \leqslant \int_{-\infty}^{\infty} |K(j\omega)|^2 G_n(\omega)\,d\omega \int_{-\infty}^{\infty} \frac{|G(j\omega)|^2}{G_n(\omega)}\,d\omega$$

or

$$\frac{\left|\int_{-\infty}^{\infty} e^{j\omega t_0} K(j\omega)\,G(j\omega)\,d\omega\right|^2}{\int_{-\infty}^{\infty} |K(j\omega)|^2 G_n(\omega)\,d\omega} \leqslant \int_{-\infty}^{\infty} \frac{|G(j\omega)|^2}{G_n(\omega)}\,d\omega. \qquad (11.10)$$

Since the left part of the inequality (11.10) there is an increase in $2\pi$ times of the signal/interference ratio $q$ at the output of the filter (see Formula 11.8), therefore,

$$q \leqslant \frac{1}{2\pi}\int_{-\infty}^{\infty} \frac{|G(j\omega)|^2}{G_n(\omega)}\,d\omega. \qquad (11.11)$$

The maximum signal/interference ratio is

$$q_{\text{макс}} = \frac{1}{2\pi}\int_{-\infty}^{\infty} \frac{|G(j\omega)|^2}{G_n(\omega)}\,d\omega. \qquad (11.12)$$

It is easy to see that the inequalities (11.10) and (11.11) changes to equalities if the transmission function of the filter assumes the form

$$K(j\omega) = Ce^{-j\omega t_0}\frac{G^*(j\omega)}{G_n(\omega)}, \qquad (11.13)$$

where $C$ – arbitrary constant; $G^*(j\omega)$ – spectra, complexly conjugated with the spectra of the signal.

Filter with transmission function described by Expression (11.13) is an optimum linear filter guaranteeing the best separation of the

signals from the interferences. The amplitude frequency characteristics of the optimum filter is proportional to the ratio of the amplitude of the spectra of the signal to the energy spectra of the interferences.

$$|K_{опт}(j\omega)| = C\frac{|G(j\omega)|}{G_п(\omega)}. \qquad (11.14)$$

The optimum filter let pass the component of the frequency spectra to a larger degree the higher the amplitude of the component of the signal and the less the intensity of the interference. The ratio of signal/interference at the output of the filter is greater, the greater the spectra of the signal relative to the spectra of the interferences. At equivalent spectra $G_p(\omega)$ = const the function of transmission of the optimum filter coincides with $G^*(j\omega)$, which is also shown in Chapter 6.

As an example of finding the transmission function of the optimum filter for the case shown in Fig. 11.3,a, when the spectra of the interferences are wider than the spectra of the signal and both spectra have the bell shape:

$$|G(j\omega)|^2 = G_0^2 e^{-\frac{(\omega-\omega_0)^2}{\Delta\omega_c^2}},$$

$$G_п(\omega) = G_{п_0} e^{-\frac{(\omega-\omega_0)^2}{\Delta\omega_п^2}},$$

where $\Delta\omega_s$ – width of the spectra of the signal at the level 1/e; $\Delta\omega_p$ – width of the spectra of the interference at the level 1/e.

The amplitude frequency characteristics of the optimum filter according to (11.14) is described by the expression

$$|K_{опт}(j\omega)| = C\frac{G_0}{G_{п_0}}\exp\left\{\frac{(\omega-\omega_0)^2}{\Delta\omega_п^2} - \frac{(\omega-\omega_0)^2}{2\Delta\omega_c^2}\right\} = C\cdot\frac{G_0}{G_{п_0}}\exp\left\{-\frac{(\omega-\omega_0)^2}{2\Delta\omega_c^2}\left[1-2\left(\frac{\Delta\omega_c}{\Delta\omega_п}\right)^2\right]\right\}. \qquad (11.15)$$

As it follows from (11.15), the characteristics of the optimum filter also has the form of a Gaussian curve (11.3,a,). The signal/noise

ratio at the output of the optimum filter in correspondence with Formula (11.12) is

$$q = \frac{1}{\sqrt{2\pi}} \frac{G_0^2}{G_{n_0}} \cdot \frac{\Delta\omega_c}{\sqrt{1 - \left(\frac{\Delta\omega_c}{\Delta\omega_n}\right)^2}}. \qquad (11.16)$$

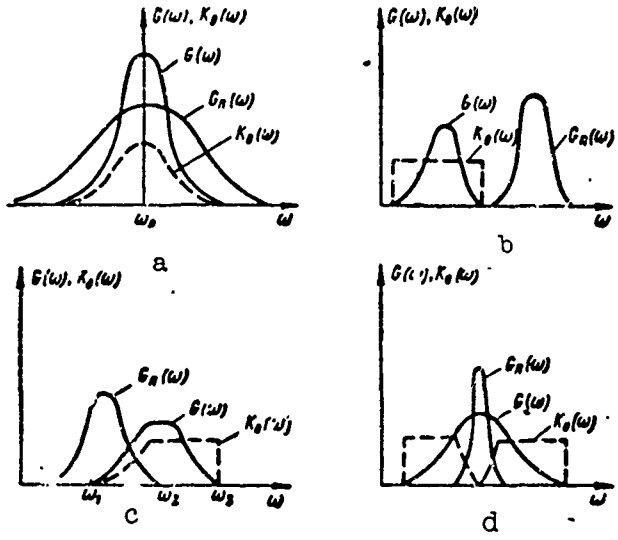


Fig. 11.3 Filtration at various relationships between the spectra of the signal and the spectra of the interference.

It should be noted that the optimum solution has meaning only when the condition that the spectra of the interference completely overlap the spectra of the signal, i.e., $\Delta\omega_p > \Delta\omega_s$. In the opposite case in correspondence with Formula (11.14), the filter should possess infinite amplification at the band of frequency where there are component spectra of the signal but no component of the spectra of the interference. But, in these cases, when the spectra of the interference only partially overlap or in general do not overlap the spectra of the signal, the optimum solution is obvious without mathematical analysis. Thus if the spectra $G(\omega)$ and do not overlap (Fig. 11.3,b), then the amplitude frequency characteristics of the optimum filter have the form

$$K(\omega) = K \text{ for } G(\omega) \neq 0,$$
$$K(\omega) = 0 \text{ for } G(\omega) = 0.$$

If the spectra $G(\omega)$ and $G_p(\omega)$ partially overlap (Fig. 11.3,c), then $K(\omega) = 0$ when $\omega < \omega_1$ and $\omega > \omega_3$; $K(\omega) = K$ when $\omega_3 > \omega > \omega_2$, and in the interval $\omega_1$—$\omega_2$ the function $K(\omega)$ monotonously rises from 0 to $K$.

Example of the use of filtration at partial overlap of the spectra of the signals and the interferences may be given, for example, the circuit of small constant time (MPV). The MPV circuit forms a differential chain (filter of high frequencies) included in the pulse RLS after the detector. The time constant of the circuit is chosen approximately equal to the duration of the working pulse. The connection of the MPV circuit practically does not have any effect on the entering of the useful pulses of the signal and weakens considerably the action of the continuous interferences with slowly changing amplitude and the pulses of the interferences of great duration.

If the interference has a narrower spectra in comparison with the spectra of the signal (Fig. 11.3,d), then the most significant weakening of the interference may be reached by the inclusion of a linear rejector filter with bands of suppression equalling in width to the spectra of the interference. Such filters may be used for the battle with the narrow band unattenuated interferences. They are relied upon to make it so that the filter will have great damping on the carrier frequency of the interferences.

In conclusion, it should be noted that the optimum linear filter is absolutely optimu, if the interference $n(t)$ has normal law of distribution, the nonlinear filter may be the absolute optimum. But, the mathematical analysis of nonlinear filtration is extremely complex and the substantial results of the investigation which could be widely

used in practice, obtain, as long as it succeeds.

2. Selection Of Radiolocational Signals

The parameters of the selection of radiolocational signals may be: carrier frequency, length and frequency of the repetition of the pulse being received, phase of high frequency reflected oscillations, amplitude of the signals and the form of polarization of the reflected electromagnetic waves.

In correspondence with these, we distinguish frequency, time, amplitude, phase and polarization selections.

All forms of selection excepting amplitude, are widely used at the present, in radiolocational installations. Amplitude selection does not find a wide application in the RLS since large dynamic range variations of useful signals and the fluctuation of magnitude of the reflected pulses may completely erase the difference in amplitude relationship between interferences and signals.

Phase selection is a particular case of time selection since the parameter of selection is the time shift between signals and interferences, which for high frequency oscillations is manifested in the phase shift between them. Phase selection is widely used in radiolocational stations with selection of two objects for the suppression of passive interferences. It will be examined in detail in the following chapter. The remaining forms of selections are described below.

*Frequency selection.* In frequency selection, various carrier frequencies of the useful signal and the interference are used. It is realized via the changeover of the high frequency tracts of the radiolocational stations.

The simplest method of accomplishing a changeover of frequency is contained in the use of two receiving transmitting channels scattered in frequency, one of which works while the other is in a readying

position for work.

The changeover of the RLS from one working wave to another may be conducted by a manual operator or automatically with the aid of a special circuit changing the level of the external interferences of the working frequency at the moment of time directly preceding the emission of the pulse of the changeover.

The methods examined possess the same drawbacks as the use of only two fixed working frequencies which are opponents in the process of operation of RLS and may easily separate or combine on-target interferences to both frequencies.

The advent of powerful pulse changeover generators SVCh and the wide band klystron generators and the tube of inverse waves permitted their use for creating perfect systems of interchangeable working frequencies in sufficiently wide range of waves.

On the basis of the use of range changeovers, two basic types of frequency changeovers may be built: tracing and synchronous tracing.

In the first case at the appearance of interference the transmitter of RLS is connected, in the connected condition it is changed over to new frequency and then connected to that frequency. After the connection of the transmitter, the system of automatic fine tuning of the receiver(APCh) produces a search for new working frequency of the transmitter, holds it and accomplishes accurate fine tuning. The advantage of such systems is the absence of connection between the changeover circuit of the transmitter and the heterodyne. Therefore, the variation of the parameters of the latter or the change of one of the generators does not require the addition regulating and the tuning systems of the APCh.

The shortcomings of the tracing systems of changeovers is that during the time of search and holding of the APCh system, there is

produced radiation of the transmitter and opponents may separate the new working frequency and create interferences like the receiver will be tuned. The elimination of this shortcoming may be done by the switching of the transmitter to the equivalent antenna to the moment of the completion of fine tuning in the receiver. But in that case, the total time of changeover of the radiolocational station may be considerable since to the time of changeover, the time of search and holding of its frequency by the APCh system is added.

The synchronous tracing method of RLS frequency changeover consists in changing the frequencies of the transmitter and the heterodyne simultaneously by jumps approximately in the same magnitude, while the inaccuracy of changeover is eliminated by an electronic APCh circuit. The shortcomings of this system are the difficulty of accurate coupling of the tuning of the transmitter and the receiver in all ranges of working frequencies and the sensitivity of the system to temperature variations (the temperature maintenance of the frequency of the changeover may be different from the maintenance of the frequency of the receiver). But, the synchronous tracing method possesses pretracing advantages, containing in the fact that it permits the considerable shortening of the time of transformation into the new working frequency, completely excluding the time for searching and holding via the application of the so-called "instant" APCh system of receiver accomplishing the fine tuning of the heterodyne during the time of the radiation of the sounding pulses.

*Time selection.* Time selection is based on the difference between useful signals and interferences in duration, repetition frequency and the time position of the pulses. On this principle, the selectors by duration and repetition frequency operate.

*The repetition-frequency pulse selector* is used for the battle with nonsynchronized pulses of the interferences. Protection of the radiolocational stations from the nonsynchronized pulses of interferences may be accomplished via feeding to the system matching unretarded reflected signals and the same signals only retarded in time, of emitted pulses of exactly equal period of repetition. Thereby, through the system of coincidence, only these signals whose periods of tracing are exactly equal to the periods of tracing of the emitted pulses will pass through.

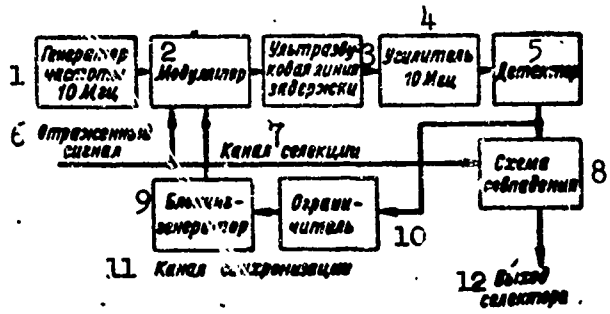


Fig. 11.4 Block diagram of the selection of the signals by the repetition of the signals by the repetition frequency. 1) Generator of frequency 10 mhz; 2) modulator; 3) ultrasonic linear delay; 4) amplifier 10 mhz; 5) detector; 6) reflected signal; 7) selection channel; 8) coincidence circuit; 9) blocking generator; 10) limitor; 11) synchronization channel; 12) output of selector.

In the selectors of this type, one may use electronic circuits of delay of pulses, oscillatory loops, tuned according to the repetition frequency of the pulses and electric or ultrasonic linear delays. The most extensively used selection circuits are those that employ ultrasonic linear delays (UZL). One of the possible functional scheme of selector with UZL is shown in Fig. 11.4. The basic element of the scheme is the ultrasonic delay. It consists of a sound transmitter with electromechanical converters of energy which is most frequently quartz plates.

Ultrasonic lines may be used for the delay of high frequency (approximately up to 15 mhz) pulses as well as video pulses. For the delay of video pulses, there are produced considerably distorted forms of the transmitted signals which may not favorably affect the operation of the coincidence circuit. Therefore in the scheme of selectors, the signals, subject to delay are first converted with the aid of special generators and modulators in high frequency pulses with frequency priming of the order of 5–15 mhz.

During the conversion of electric oscillations into ultrasonic and vice versa, and also during the passage of the ultrasonic oscillation in the linear delay considerable (to 60 db) weakening of the radiopulses takes place. The amplification of delayed pulses is accomplished by amplifiers tuned to the priming frequency.

After amplification the high frequency pulses are detected and proceed to the input of one of the coincidence circuits to the second input of which enters the reflected signals directly from the output of the videoamplifier of the receiver. If the period of the reflected signals equals exactly the magnitude of the delay in UZL, then the pulse of the current period and the delayed pulses of the preceding cycle hit the coincidence circuit simultaneously and at the output of the circuit, signal appears. Pulses having large or small repetition periods will arrive at the coincidence circuit in different moments of time, and will not pass through it.

It is obvious that when circuits of protection against nonsynchronous pulses of interference are used, it is necessary to provide highly exact equality of delay times in the UZL and the period of tracing of the emitted pulses. This requirement may be fulfilled by the use of special circuits of the formation of pulses of synchronization, in which the stabilization of the repetition period of the pulses is ac-

complished by the linear delay of the circuit of protection against interferences.

The generators of pulse stabilization may be, for example, a blocking generator with proper period of auto-oscillation, some big time delays of signals in the UZL. When the RLS is connected, the first pulse of the blocking generator proceeds to the modulator of the linear delay, having passed through that, it hit the net of blocking generators accomplishing their compulsory triggering. In this way, the second synchronizing pulse, produced by the block generator, shows a delay relative to the first one, and all the following ones – relative to the preceding ones in time, exactly equal to the time of delay of signal in the UZL. Consequently, equality of the received-signal delay time and period of tracing of the emitted pulses is automatically satisfied independent of the variations of the parameters of the UZL, caused, for example, by the fluctuating temperatures or the action of any other factors.

*Pulse selection by duration.* In the radiolocational stations, it is possible to use selectors, separating pulses whose durations:

– do not exceed a certain value; – are not less than some defined values; – are within a determined range.

For the purpose of protection against active interferences, the most extensively used selectors employ pulses of definite duration. Since pulses of durations reckoned on certain conditions, depends on the amplitude of the signal being received, therefore, the circuit of selection may only suppress these pulses of the interference which differ in duration from the useful signal no less than 1.5–2 times.

*Polarization selection.* The improvement of the observability of useful radiolocational signals on the background of interferences may be reached by the use of antennas with elliptic polarization.

The elliptic polarized waves are characterized by three parameters: the angle of spatial orientation of the ellipse of polarization, $\vartheta$, coefficient of ellipticity $k_э = \frac{a}{b}$ $(k_э < 1)$ and the direction of the rotating vector of the voltage of the electric field (Fig. 11.5,a). Elliptic polarization may be achieved by the interference of two linearly polarized orthogonal fields of the same frequency, but displaced in phase by an angle $\varphi$:

$$e_x = E_x \sin(\omega t - \varphi),$$
$$e_y = E_y \sin \omega t.$$

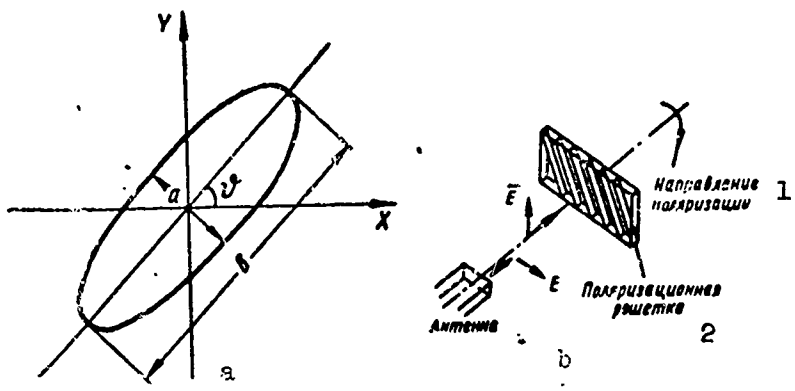


Fig. 11.5 The problem of polarization selection. a) Parameters of ellipse of polarization; b) polarization grid. 1.) Direction of polarization; 2.) polarization grid.

An example of the construction which accomplishes elliptic polarization is shown in Fig. 11.5,b. The antenna forms a special phasal rotator in the form of a grid to which the linearly polarized waves are fed. The grid is oriented in such a way that the plates form an angle of 45° with the vector of the electric field of the entering waves. In the zone of the grid, the vector is resolved into two orthogonal components, one of which is perpendicular while the other is parallel to the plates. The component perpendicular to the plates passes through the grid unchanged. The parallel component of the vector

passes through the grid with increased phasal velocity as a result of which there is a phase shift between the orthogonal components. The magnitude of the phase shift depends on the width of the grid *(d)*, the distance between the plates *(a)* and the wave length. If both components of the vector of the incident field are equal to each other and the phase shift is at an angle $(2n + 1)\pi/2$, then at the output of the grid, there will be circular polarization.

At the reception of the signals by the elliptically polarized antenna, the electromotive force, induced in it, depends on the polarization parameters of the incident field

$$E = k\left[1 \pm \frac{4k_c k_a}{(1+k_c^2)(1+k_a^2)} + \frac{(1-k_c^2)(1-k_a^2)}{(1+k_c^2)(1+k_a^2)}\cos 2\delta\right]^{\frac{1}{2}}, \qquad (11.17)$$

where $E$ – *emf*, induced in the antenna by the signals; $k$ – constant coefficient; $k_s$ – coefficient of ellipticity of the field of the signals being received ($k_c \leqslant 1$); $k_a$ – coefficient of ellipticity of the antenna (waves emitted by the receiving antenna in the region of transmission); $\delta$ -- angle between the major axes of the ellipses of polarization of the antenna and the incident waves $\left(\delta \leqslant \frac{\pi}{2}\right)$.

In Formula (11.17) the sign "+" should be taken when the field of the incident wave and the field of the emission of the receiving antenna in the region of transmission have the same direction of rotation. The sign "–" is taken in the case of opposite position rotation.

As one can see from Formula (11.17), the signal at the input of the receiver reaches a maximum value in the case of congruence of the antenna with the polarization structure of the incident wave ($k_a = k_s$, $\delta = 0$, same direction of rotation of the vectors of the electric field).

$$E_{\max} = k\left[1 + \frac{4k_c^2}{(1+k_c^2)^2} + \frac{(1-k_c^2)^2}{(1+k_c^2)^2}\right]^{\frac{1}{2}} = k\sqrt{2}.$$

At orthogonal disposition of the axes of the ellipse $\delta = \pi/2$, equal coefficients of ellipticity $k_s = k_a$ and opposite position of rotation of the vectors of the field of emission of the antenna and the field of the incident waves, a complete suppression of the signal being received is obtained $(E = 0)$. This property of the antennas of rotational polarization permits the use of them in the capacities of selectors of radiolocational signals. Emitting elliptic polarized waves and providing tuning of the antenna-waveguide tracts to the polarization parameters of the useful signals, may (at various polarization structures of signals and interferences) substantially raise the signal/interference ratio. When the powers of the fields of the signal and the interferences are the same in the exposure of the antennas, their ratio at the input of the receiver will be

$$\frac{P_c}{P_n} = \frac{2}{1 \pm \frac{4k_n k_c}{(1+k_n^2)(1+k_c^2)} + \frac{(1-k_c^2)(1-k_n^2)}{(1+k_n^2)(1+k_c^2)} \cos(\vartheta_c - \vartheta_n)}, \quad (11.18)$$

where $k_p$ – coefficient of ellipticity of the field of interference; $\vartheta_s - \vartheta_p$ – angle between the major axes of the ellipses of polarization of the signal and the interference.

The sign "–" is taken in Formula (11.18) in the case of opposite position direction of rotation of the vectors of the fields of the signal and interference.

As one can see from Formula (11.18), polarization selector permits the increase of the signal/interference ratio if the interference differs from the signal by any one of the polarization parameters. The greatest influence on the effectiveness of the selection is the difference in the direction of rotation of the vectors of the electric field whereupon, the smaller the coefficient of ellipticity differs from unity, the greater the influence. When $k_s = k_p = 1$ (circular polarization) complete suppression of interference may be accomplished only on

account of the opposite position rotation of the vectors of the fields of the signal and the interference.

Substantial effect on the effectiveness of the polarization selection is also manifested by the difference in the coefficient of ellipticity and in the spatial positions of the axes of ellipses of polarization of the signal and the interference. But, these differences may be effectively used for selection only at small values of $k_s$ and $k_p$. With the growth of $k_s$ and $k_p$, the effectiveness of selection by the coefficient of ellipticity and by the angular position of the axes drops.

In conclusion, it should be noted that at present, the emission and reception of waves with any polarization characteristics may be comparatively simply accomplished with the aid of ferrite structures.

3. Amplitude Adjustment As A Method Of Combating Interferences

The limited dynamic range of the receivers of the RLS make them extremely vulnerable to interferences of great power. We shall examine, as an illustration, the operation of the radiolocational station when it is acted upon simultaneously by useful signals and pulses of interference of great power. Thereby, it will be assumed that the carrier frequency of the interference lies within the passband of the receiver.

Depending on the relationship between the carrier frequency of the signals and the interferences, the amplitude of the high frequency resulting oscillation approaching the input of the receiving device, may be larger or smaller than the amplitude of the interferences. Therefore, the envelope of the useful signal at the output of the detector will only form positive or negative selections whose magnitude is determined by the phasal relationship between the signal and the interference in that given cycle of operation of the radiolocational stations (Fig. 11.6).

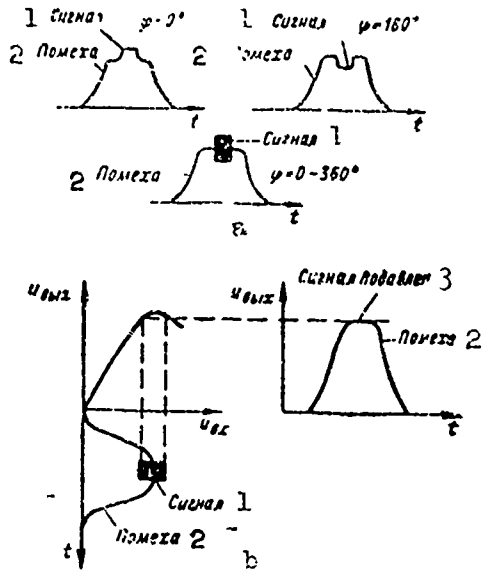


Fig. 11.6 Effect of overload of the receiver on the observability of the signals. a) Envelope of interferences and signals at the output of the detector; b) suppression of the signals during receiver overload. 1) Signal; 2) interference; 3) signal suppression.

Since the relationship of phase in every successive period of sending does not depend on the phase relationship in the preceding cycle, the relative phase between signals and interferences runs through all values within a certain segment of time and, consequently, a fluctuating useful signal on the background of intensive noise. It is obvious that if these amplitude variations of the total signals are maintained during the passage through the receiving tract, then the useful signals may be isolated on the background of interferences. But, if no special measures are taken, then the intensive interferences may produce overload of the videoamplifier or the last cascades of UPCh and fluctuation of the useful signals is lowered. The occurrence of overload excludes the possibility of uncovering the useful signals on the background of intensive interferences (Fig. 11.6,b). Similar pictures will be observed at the action of other types of interferences (unattenuated amplitude-frequency modulated oscillation, noise interferences of large

intensity, etc.)

For combating the overload in the radiolocational stations, receivers are used with special forms of amplitude characteristics (most often linear logarithmic) and circuits of fast-acting automatic adjusting amplification (BARU). Inertia circuits ARU as means of protection against interferences are not used since they may give some effects only at weak interferences, whose amplitude is small in comparison with the amplitude of useful signals. Therefore, the inert ARU system is used only for the stabilization of the coefficient of amplification of the receiver for noises in the surveying RLS or for signals of fastened objects in the stations with automatic tracking.

*Special amplitude characteristics of receivers.* For the widening of the dynamic range of the receiving tract and the elimination of overload depended on the action of the interferences, receivers with linear logarithmic amplitude characteristics are used in the radiolocational stations (Fig. 11.7). At the segment 1, (weak signal) the characteristic is linear and the output signal is proportional to the input; at segment 2 (strong signal) the increment of the output voltage decreases with the increase of the amplitude of the input signal

$$dU_{вых} = k_0 \frac{dU_{вх}}{U_{вх}}, \qquad (11.19)$$

where $k_0$ – coefficient of proportionality.

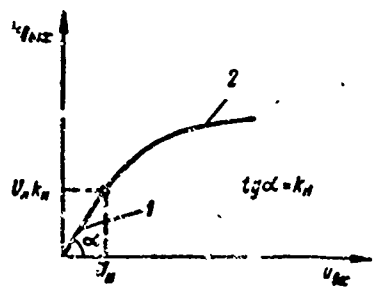


Fig. 11.7 Characteristic of UPCh with wide dynamic range.

Integrating (11.19), we obtain

$$U_{вых} = k_0 \int \frac{dU_{вх}}{U_{вх}} = \\ = k_0 \ln U_{вх} + C_0. \qquad (11.20)$$

We denote by $U_n$ and $k_n$, the input voltage and the coefficient of amplification of the receiver corresponding to the beginning of the nonlinear segment of the characteristic. Then we can write that

$$U_n k_n = k_0 \ln U_{вх} + C_0.$$

The constant of integration is

$$C_0 = U_n k_n - k_0 \ln U_{вх}.$$

In order that the amplitude characteristic of the receiver should have a smooth period from linear to nonlinear regions, it is necessary that the derivative $\frac{dU_{вых}}{dU_{вх}}$ does not have a point of discontinuity at $U_{вх} = U_n$, i.e., should fulfill the condition

$$k_0 = U_n k_n.$$

Substituting the value of $k_0$ into Formula (11.20) we obtain

$$U_{вых} = U_n k_n \left( \ln \frac{U_{вх}}{U_n} + 1 \right). \qquad (11.21)$$

For the input voltage $U_{вх} < U_n$ the amplitude characteristic is linear, and when $U_{вх} > U_n$ – logarithmic (according to the law of natural logarithm). The dynamic range of the logarithmic receiver according to the output signal consists of

$$D_{вых} = \frac{U_{вх}}{U_n k_n} = \frac{U_n k_n (\ln D + 1)}{U_n k_n} = \ln D + 1,$$

where $D = \frac{U_{вх\ макс}}{U_n}$ – dynamic range of output voltage of the receiver.

For the widening of the dynamic rangeof the receiver, the characteristic may be built according to the law of logarithm with the base $N < e$

$$U_{вых} = k_n U_n \left( b \ln \frac{U_{вх}}{U_n} + 1 \right),$$

where $b = \frac{1}{\ln N}$.

The dynamic range of the receiver in this case is

$$D_{вых} = b \ln D + 1$$

The variance of the voltage of interference at the output of the logrrithmic receiver is

$$\sigma_п^2 = \int_0^\infty [U_{вых}]^2 W(U_{вх})\, dU_{вх} - \left[\int_0^\infty U_{вых} W(U_{вх})\, dU_{вх}\right]^2, \qquad (11.22)$$

where $W(U_{vkh})$ – differential law of distribution of the envelope of interferences.

The mean square output voltage of the interferences is

$$\overline{U_{вых}^2} = \int_0^\infty [U_{вых}]^2 W(U_{вх})\, dU_{вх} = k^2 U_п^2 \int_0^\infty \left(b \ln \frac{U_{вх}}{U_п} + 1\right)^2 \times$$

$$\times W(U_{вх})\, dU_{вх} = (bk_п U_п)^2 \int_0^\infty \left(\ln \frac{e^{\frac{1}{b}}}{U_п} + \ln U_{вх}\right)^2 W(U_{вх})\, dU_{вх} =$$

$$= (bk_п U_п)^2 \left[\left(\ln \frac{e^{\frac{1}{b}}}{U_п}\right)^2 + 2 \ln \frac{e^{\frac{1}{b}}}{U_п} \int_0^\infty \ln U_{вх} W(U_{вх})\, dU_{вх} + \right. \qquad (11.23)$$

$$\left. + \int_0^\infty (\ln U_{вх})^2 W(U_{вх})\, dU_{вх}\right].$$

The mean value of the output voltage of the interferences is

$$\overline{U_{вых}} = \int_0^\infty U_{вых} W(U_{вх})\, dU_{вх} =$$

$$= bk_п U_п \left[\int_0^\infty \ln U_{вх} W(U_{вх})\, dU_{вх} + \ln \frac{e^{\frac{1}{b}}}{U_п}\right]. \qquad (11.24)$$

Substituting the values of the integrals into Formula (11.22), we obtain

$$\sigma_п^2 = \overline{U_{вых}^2} - [\overline{U_{вых}}]^2 = (bk_п U_п)^2 \times$$

$$\times \left\{\int_0^\infty (\ln U_{вх})^2 W(U_{вх})\, dU_{вх} - \left[\int_0^\infty \ln U_{вх} W(U_{вх})\, dU_{вх}\right]^2\right\}.$$

In the cases if at the input of the receiver noise interferences arrive, distributed according to the law of Rayleigh $W(U_{вх}) = \frac{U_{вх}}{\sigma^2} \exp\left(-\frac{U_{вх}^2}{2\sigma^2}\right)$.

then the variance of the output voltage is

$$\sigma_n^2 = \left\{\int_0^\infty (\ln U_{вх})^2 \frac{U_{вх}}{\sigma^2} e^{-\frac{U_{вх}^2}{2\sigma^2}} dU_{вх} - \left[\int_0^\infty \ln U_{вх} \frac{U_{вх}}{\sigma^2} e^{-\frac{U_{вх}^2}{2\sigma^2}} dU_{вх}\right]^2\right\} \times \quad (11.25)$$
$$\times (bk_и U_и)^2,$$

where $\sigma^2$ -- variance of the voltage of interferences at the input of the receiver.

For the computation of the integral in Expression (11.25), we introduce the new variable

$$z = \frac{U_{вх}^2}{2\sigma^2}.$$

Since $\sigma^2 dz = U_{вх} dU_{вх}$ and $\ln U_{вх} = \frac{1}{2} \ln 2\sigma^2 z$, then Expression (11.25) may be written as

$$\sigma_n^2 = \frac{(bk_и U_и)^2}{4} \left\{\int_0^\infty (\ln 2\sigma^2 z)^2 e^{-z} dz - \left[\int_0^\infty (\ln 2\sigma^2 z) e^{-z} dz\right]^2\right\} =$$
$$= \frac{(bk_и U_и)^2}{4} \left\{\int_0^\infty (\ln z)^2 e^{-z} dz - \left[\int_0^\infty (\ln z) e^{-z} dz\right]^2\right\}. \quad (11.26)$$

From the theory of integral transformation, it is known

$$\int_0^\infty e^{-z} \ln z dz = -C,$$
$$\int_0^\infty e^{-z} (\ln z)^2 dz = \frac{\pi^2}{6} + C, \quad (11.27)$$

where $C$ – Euler's constant.

Substituting the value of the integrals from (11.27) into Formula (11.26), we obtain

$$\sigma_n^2 = \frac{\pi^2 b^2 k_и^2 U_и^2}{24}.$$

The mean square value of the voltage of interference at the output of the receiver is

$$\sigma_n = \frac{\pi b k_и U_и}{2\sqrt{6}}. \quad (11.28)$$

The variance of the output voltage of the logarithmic receiver does not depend on the power of the input action but is determined on-

ly by the coefficient of amplification, $k_n$, the size of the linear segment of the amplitude characteristic $U_n$ and the rule of logarithmizing of the input signals *(b)*. The logarithmic characteristics generally starts from the level 20 db relative to the mean square value of the natural noises of the receiver. Here the internal noise is practically all in the logarithmic segment.

The mean value of the output voltage of the interferences, $\overline{U}_{vykh}$ grows with the increase of the power of the interferences at the input of the receiver. For the elimination of the disturbing effects of the constant component of the interferences at the output of the logarithmic receiver, it is necessary to connect the filter of high frequencies (for example, differentiating circuit after the detector). The filter suppresses the constant component and at the output of the receiver, there remain only the fluctuation of the disturbing voltage, which with adequate choice of the parameters of the logarithmic receiver may be reduced to the level of internal noises of the receiver.

There exists a few methods of obtaining logarithmic amplitude characteristics. The simplest method consists of a tube of the last cascades of UPCh placed in a hook condition at which the slope of its characteristic decreases by the exponential law with the increase of the voltage of bias.

Other methods of obtaining logarithmic characteristic of the receiving channels are based on the use of sequential detection of signals at the output of every cascade of the UPCh (Fig. 11.8). Crystal detectors work on the individual voltage, and the rectified current is accumulated according to the total resistance $R_n$. Linear attenuation is necessary for the compensation of the attenuation of radiopulses in corresponding cascades of UPCh.

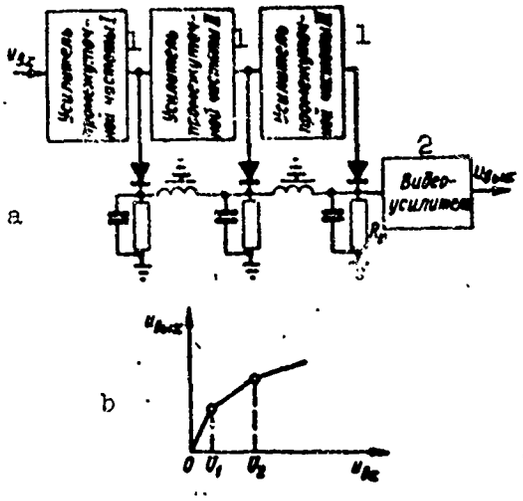


Fig. 11.8 Amplifier of intermediate frequency with logarithmic amplitude characteristics. a) Functional circuit; b) amplitude characteristics. 1) Intermediate frequency amplifier; 2) videoamplifier.

At small signals, $U_{vkh} < U_1$, the amplification takes place according to the linear law. At the amplification of signals up to the values $U_{vkh} = U_1$ in the last cascade of the UPCh saturation sets in as a result of which the velocity of the increase of the voltage $U_{vykh}$ is reduced. At the value of the signals $U_{vkh} = U_2$, saturation sets in in the second cascade and the velocity of the growth of the output voltage decreases some more since the amplification in this case takes place only at the expense of the first cascade. In this way, the amplitude characteristic of UPCh will consist of some segments of the straight line having different slopes. In real circuits, amplitude characteristics is obtained smoothly without breakoffs. Varying the relation between the coefficient of amplification of individual cascades of the UPCh, may give characteristic forms close to logarithmic.

In a number of cases for the obtaining of logarithmic amplitude characteristics methods are used based on the variation of the equivalent resistance of the load of the cascades of UPCh with the aid of nonlinear resistances shunting the output circuit. The choice of the type

of nonlinear resistance and the condition of their work may also obtain amplitude characteristics extremely close to the logarithmic.

The essential shortcomings of the logarithmic receivers are the dependence of time of attenuation of the signal $\tau_z$ on the magnitude of the input voltage of the receiver. As a result of this errors in the measurement of range may arise and the conditions of coherent treatment of the reflected signals may be upset. Therefore, in the number of cases, it is necessary to use special methods of stabilizing $\tau_z$. But, the existing methods of stabilizing the time of attenuation in logarithmic amplifiers do not permit the complete elimination of the dependence of $\tau_z$ on $U_{vkh}$.

Other shortcomings of the logarithmic amplifier are the worsening of the signal/noise ratio at the output of the receiver.

*Fast-acting automatic adjusting amplifier.* A block diagram of the BARU system is represented in Fig. 11.9,a and b. If interferences appear at the input of the cascade UPCh surpassing in amplitude by several orders of magnitude then at the output of the detector of BARU voltage is obtained which after amplification proceeds to the rectifying net of the cascade UPCh. On account of this additional [illegible] bias originating during the time of the action of the interferences, the operating point of the tube is shifted to the left. The voltage of interference at the output of the cascade UPCh suddenly decreases and the signal appears on the background of the interferences.

For the evaluation of the effectiveness of the BARU system, we shall look at its basic dynamic properties. The voltage at the output of the amplifier of intermediate frequency with BARU is described by the expression

$$u_{вых}(t) = K(u_p) \cdot u_{вх}(t), \qquad (11.29)$$

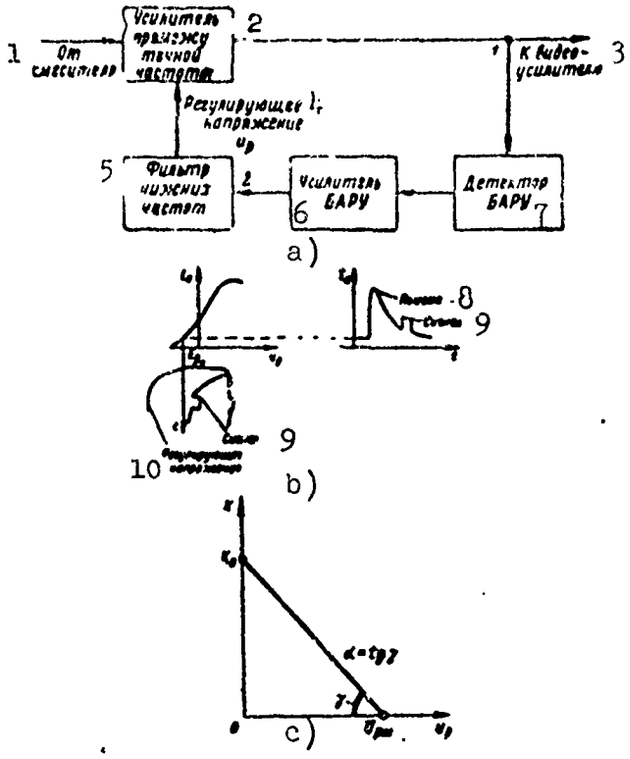


Fig. 11.9 System of fast-acting automatic adjusting amplifier. a) Block diagram; b) time diagram; c) adjusting characteristics. 1) From the mixer; 2) amplifier intermediate frequency; 3) to the videoamplifier; 4) regulating voltage; 5) filter low frequency; 6) amplifier BARU; 7) detector BARU; 8) interference; 9) signal; 10) regulating voltage.

where $K(u_r)$ – coefficient of amplification of UPCh, as a function of the adjusting voltage, $u_r$; $u_{vkh}(t)$ – voltage at the input of UPCh.

It will be assumed that in the circuit of the feedback of the BARU system, there is included an one-member $RC$ filter. In this case,

$$u_p(t)=\frac{k}{TD+1}u_{вых}(t), \qquad (11.30)$$

where $D=\frac{d}{dt}$ – operator of differentiation; $T = RC$ – time constant of the filter; $k$ – coefficient of transmission branch of the feedback (from Point 1 to Point 2 in Fig. 11.9,a).

The dependence $K(u_p)$ is approximately by the straight line

$$K(u_p)=K_0\left(1-\frac{u_p}{U_{pm}}\right)=K_0-\alpha u_p, \qquad (11.31)$$

where $K_0$ – amplification of UPCh when $u_p = 0$; $U_{rm}$ – voltage during

which the coefficient of amplification of UPCh turns to zero

$\alpha$ – slope of the adjusting characteristics (Fig. 11.9,b).

Having solved the simultaneous equations (11.29), (11.30) and (11.31), we obtain the equation describing the process in the BARU system

$$T\frac{du_{вых}}{dt}+u_{вых}[1+aku_{вх}(t)]=K_0u_{вх}(t). \qquad (11.32)$$

Let us assume that at the input of the receiver from the moment of time $t_0$ act the interferences of the type of nonmodulated and supported with amplitude equal to $U_p$ and at a certain moment $t_1$ there appears a useful signal with amplitude $U_s$. For the sake of simplicity, we shall assume that between the signals and the interferences, there is no interference action and an arithmatic addition of their envelopes takes place. The indicated conditions are equivalent to applying at time $t_0$ a disturbing influence of the type of a rapid change in the magnitude of $U_p$ to the BARU system, while at time $t_1$, the disturbance increases to $U_p + U_s$.

The equation of the BARU system during the disturbing type of rapid change is transformed into a nonhomogeneous differential equation of the first order with constant coefficients

$$T\frac{dU_{вых}}{dt}+u_{вых}[1+akU_п]=K_0U_п.$$

The solution of it for the zero initial condition ($u_p(0) = 0$) has the form:

$$u_{вых}(t)=K_0U_п\frac{1+akU_п\exp\left(-\frac{akU_пt}{T}\right)}{1+akU_п}=K_0U_с\frac{1+k_0e^{-\frac{t}{\tau}}}{1+k_0}.$$

where $k_z$ – equivalent coefficient of amplification of the BARU system;

$\tau=\frac{T}{k_z}$ – equivalent time constant of the BARU system.

The rate of the course of the conversion process is determined by the equivalent time constant $\tau$, whose magnitude decreases with the in-

crease of amplitude $U_p$. In a steady state

$$u_{вых} = \frac{K_0 U_п}{1 + k_0}, \qquad (11.33)$$

$$u_p = \frac{kK_0 U_п}{1 + k_0}. \qquad (11.34)$$

The coefficient of amplification UPCh at the end of the conversion process is

$$K_1 = \frac{u_{вых}}{U_п} = \frac{K_0}{1 + k_0}. \qquad (11.35)$$

In the moment of time $t_1$ at the input of the BARU system, the useful signals are admitted. The equation of the system during the time of action of the signal has the form

$$T \frac{du_{вых}}{dt} + u_{вых}[1 + akU_{с+п}] = K_0 U_{с+п}, \qquad (11.36)$$

where $U_{s+p}$ – total amplitude of the signals and the interferences.

The solution of this equation is

$$u_{вых}(t) = U_0 + U_1 \exp\left(-\frac{t - t_1}{\tau_1}\right), \qquad (11.37)$$

where

$$U_0 = \frac{K_0 U_{с+п}}{1 + akU_{с+п}};$$

$$\tau_1 = \frac{T}{1 + akU_{с+п}}.$$

The quantity $U_1$ is found from the initial conditions. In the moment $t = t_1$, the regulating voltage at the output of the BARU circuit is determined by Expression (11.34). This voltage supports the coefficient of amplification of UPCh equal to $K_1$. Therefore the output voltage at the moment $t = t_1$ is equal to $K_1 U_{s+p}$. Comparing the values obtained for $U_{vykh}$ with the output voltage, determined by Formula (11.37), we obtain

$$U_0 + U_1 = K_1 U_{с+п} = \frac{U_{с+п} \cdot K_0}{1 + k_0}$$

or

$$\frac{K_0}{1 + akU_{с+п}} U_{с+п} + U_1 = \frac{K_0}{1 + k_0} U_{с+п},$$

from which

$$U_1 = U_{c+n} \cdot K_0 \left[\frac{1}{1+\alpha k U_n} - \frac{1}{1+\alpha k U_{c+n}}\right] = \frac{\alpha k K_0 U_c U_{c+n}}{(1+\alpha k U_n)(1+\alpha k U_{c+n})}.$$

Taking into account that $\alpha k U_p >> 1$, we have

$$U_1 \approx \frac{U_c}{U_n} \cdot \frac{K_0}{\alpha k}. \qquad (11.38)$$

Substituting the value of $U_1$ from Formula (11.38) into the expression for the output voltage, we obtain finally

$$u_{вых}(t) = \frac{K_0}{\alpha k}\left[1 + \frac{U_c}{U_n} e^{-\frac{t-t_1}{\tau_1}}\right]. \qquad (11.39)$$

The amplitude of the useful signal decreased according to the exponential law. In the end the magnitude of the pulse signal will be

$$u_{вых}(t_1 + \tau_и) = \frac{K_0}{\alpha k}\left[1 + \frac{U_c}{U_n} e^{-\frac{\tau_и}{\tau_1}}\right].$$

Since the equivalent time constant of BARU $\tau_1 = \frac{T}{\alpha k U_{s+p}}$ decreases with increase in amplitude (see Formula 11.37), then at strong interference considerable distortion of the useful signal may take place. For the decrease of distortion, it is necessary to increase the time constant of the filter of BARU, but then in case of comparatively small interference, the system will be sufficiently inert. In practice, the ratio, $\frac{T}{\tau_1}$ generally will be equal to 3–10.

Thereby, the regulating voltage follows sufficiently exactly behind the comparatively slow variations of the input voltage of the interference and remains practically constant at quick variations of the useful signals.

It should also be noted that at large values of the interference the coefficient of amplification of BARU becomes extremely small and the increment of amplitude of the output voltage may be insignificant on account of the useful signals. Therefore, the larger the interference, the less effective the BARU system.

In order that the BARU system does not lessen the amplification of the receiver during small voltage of the interference, the initial threshold of the wearability of the system (BARU with attenuation) is often specified. If for the elimination of overload in the receiver, the variation of the coefficient of amplification of one cascade indicates to be inconstant, then automatic adjusting in two or more serially connected cascades UPCh (Fig. 11.10) is used. At comparatively small interference, only the BARU system of the final cascade works, at increased amplitude of interferences, the last cascade of BARU is connected in the beginning with the second band then to the first regulating cascade.

The BARU circuit increases the interference resistance of the radiolocational station in relationship to the interference pulses of large duration and to interferences forming unattenuated, unmodulated and amplitude frequency modulated oscillations.

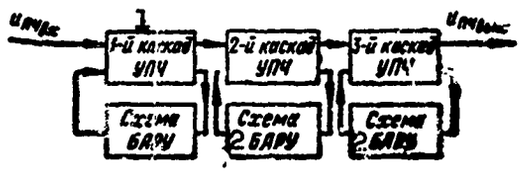


Fig. 11.10 BARU system of three UPCh cascades. 1) 1st, 2nd, 3rd, cascade UPCh; 2) BARU circuit.

Manuscript Page No. [Transliterated Symbols]

770 я = ya = yarkost' = brightness
773 РЛС = RLS = radiolokatsionnaya stantsiya = radar
773 СВЧ = SVCh = sverkhvysokaya chastota = superhigh frequency
777 п = p = povtoreniye = repetition
778 ш = sh = shum = noise
778 пр = pr = priyemnik = receiver

778 п = p = pomekha = interference

779 мин = min = minimal'nyy = minimum

779 р = r = razlichimyy = discriminated

780 макс = maks = maksimal'nyy = maximum

781 н = n = nesovmeshchennyy = noncoincidental

781 с = s = sovmeshchennyy = coincidental

783 с = s = signal = signal

784 вых = vykh = vykhod = output

786 опт = opt = optimal'nyy = optimum

788 МПВ = MPV = malaya postoyannaya vremeni = small time constant

790 АПЧ = APCh = avtomaticheskaya podstroyka chastoty = automatic frequency control

792 УЗЛ = UZL = ul'trazvukovaya liniya zaderzhki = ultrasonic delay line

795 э = e = ellipticheskost' = ellipticity

799 вх = vkh = vkhod = input

800 БАРУ = BARU = bystrodeystvuyushchaya avtomaticheskaya regulirovka usileniya = high-speed automatic gain control

800 АРУ = ARU = avtomaticheskoye regulirovaniye usileniya = automatic gain control

800 УПЧ = UPCh = usilitel' promezhutochnykh chastot = i-f amplifier

800 н = n = nelineynyy = nonlinear

801 хх = khkh = kholostoy khod = no-load

804 н = n = nagruzka = load

806 з = z = zatukhaniye = attenuation

807 р = r = reguliruyushchiy = controlling

809 э = e = effektivnyy = effective

## Chapter 12

## METHODS OF PROTECTION OF RADIOLOCATIONAL STATIONS FROM PASSIVE INTERFERENCES

### §12.1. PURPOSE OF SYSTEMS OF PROTECTION OF RLS FROM PASSIVE INTERFERENCES

The disturbing reflections from immobile or slowly moving objects are referred to as passive interferences. These objects are local subjects, surface of the seas, hydrometeors (clouds, rain, hail, snow) and metallized strips, thrown by enemies. The signals reflected from these objects may disrupt substantially the normal operation of RLS of all types: grounded ones, in the airplane, on the ship and others.

The intensity of passive interferences may surpass the 30 - 80 db level of the natural noise of the receiver. Such high level of interferences leads to the overload of the receivers and the indicators of the RLS and as a result of this, to the loss of the useful signals. Therefore, the first problem in the course of isolating the signals from the passive interferences is the prevention of overload of the receivers and the terminal arrangement of the RLS.

However, useful signals may be lost when there is no overload since to detect them on the background of a large number of various types of disturbing reflections is extremely difficult. For example, local subjects on the screen of the indicator may give reflected signals of the same type as those of the target. In this case, even the intensive signals of the target may be mixed with the signals of the local subjects found in the vicinity of the target and cannot be per-

ceived as useful signals.

The images of the local subjects on the screen of the indicator divert the attention of the operator, tiring his vision. Consequently, the image of the objects, which do not present an interest to the observer, must be removed from the screen. Sometimes, the images of the local subjects permit the operator a better orientation of the situation, and then they should be kept on the screen. But in that case, the image of the target should be given such features that it would be easy to distinguish them from the images of the local subjects. These problems are to be resolved by the systems of isolating the signals of the target on the background of the passive interference.

In the ordinary type of radiolocational stations, where no special measures of protection against passive interferences are provided, the separation of the signals of the target from the disturbing reflections is carried out by the operator. The recognition of the marks of the target on the screen of the indicator is accomplished by the trace of the target when the operator expects the regular repetition of the signals in the determined position of scanning (method of visual correlation).

But, radiolocational stations with direct observation of the signals on the screen of the indicator are characterized by substantial shortcomings:

— the holding of the images of the disturbing objects and the effectiveness of the isolation of the useful signals is low

— the resolution obtained by the operator in the presence of the object requires an additional large amount of time

— with the increase of the maximum working range of the station the spatial size of the beam grows and the contrast of the target is

lowered

Obviously, for easier selection of the signals, it is necessary to have radiolocational stations with high radial and tangential resolving powers. For example, the narrower the diagrams of directionality and the shorter the pulse in the pulse RLS, the less is the volume of the space, which corresponds to the signals entering simultaneously into the input of the receiver and the higher is the contrast of the target on the background of the disturbing reflections.

It is necessary to note that the increase in the power of the transmitter may not increase the contrast of the target since in so doing, the energies of the signals and the interferences are proportionately increased.

At the separation of the signals of moving targets from the natural noises of the receiver, the velocity of the target, as it follows from Chapter 6, does not influence in any substantial manner the effectiveness of the observation system, if the filters were adjusted only to the reception of the signals with the given Doppler shift of frequency. In distinction from noises for passive interference, it is characterized by a relatively strong correlation. Thanks to this resolving effect on the effectiveness of the observation systems, the magnitude of the radial velocity of the target begins to manifest itself. It will be shown below that at strongly correlated passive interferences and optimum velocity of the movement of the target with the help of systems constructed in the suitable way, one can succeed to weaken the interference by hundreds to a thousand times. Thereby, sufficiently good observability of the signals of the object is provided regardless that the intensity of the passive interferences may surpass the intensity of the signals by many times.

The observation of the signals in the passive interference is based on the different properties of the interference and the signals. The main reason, dependent on these differences, is the dissimilarity of the velocity of the moving object and the sources of the passive interferences. If for example, the velocity of the moving clouds of metallic strips may reach 10-15 km/hr., but the velocity of the airplane is up to 1000 km/hr. and better. As a result, the Doppler frequency shift of the signals of the target is very many times higher than that of the passive interferences and that is utilized for the observation of the signals in interferences.

For the battle with passive interferences, it is possible to use also differences in the polarization properties of the signals, reflected from the real target and the sources of the passive interferences.

Finally, the useful signals and the passive interferences differ also in statistical properties.

## §12.2. STATISTICAL PROPERTIES OF PASSIVE INTERFERENCES AND USEFUL SIGNALS

Let the radiolocational station emit monochromatic vibration of frequency $\omega_0$. Then the signal reflected from the source of passive interferences may be described as sums of signals, reflected from certain elementary reflectors within the boundaries of a permitted volume.

$$n(t)=\sum_j n_j \cdot \cos(\omega_j t-\varphi_{0j}), \qquad (12.1)$$

where $n_j$, $\omega_j$ and $\varphi_{0j}$ – amplitude, frequency, and initial phase of the signal of the *jth* reflector correspondingly; $\omega_j=\omega_0+\Omega_{rj}$ ; $\Omega_{rj}$ Doppler frequency shift of the signals of the *jth* reflector, proportional to this radial velocity.

The variations of frequency, phase or amplitude of the elementary signals which as noted in Chap.3 are always there to lead to amphitudinal and phasal fluctuations of the resulting reflected signals.

Consequently, the passive interferences should be considered as a random process.

The principal reasons for the fluctuation of passive interferences are:

— relative movements of the elementary reflectors and RLS (irregular movements of the elementary reflectors themselves, rotation of the antenna during survey of the space, movement of the RLS);

— unstable working elements of the RLS.

The movement of the elementary reflectors leads to the variation of the phase of the signals relative to the reflectors which causes the fluctuation of the resulting signals. For example, the fluctuation of the signals reflected from the clouds of dipole interferences is produced because the individual dipoles due to their differences in the velocity of falling and the local whirring action, interfere relatively each other and also relative to the RLS.

The transposition of the elementary reflectors takes place rather slowly. As a result of this, the value of the resulting reflected signal at the moment $t + \tau$ will depend on the value of the preceding moment, $t$ since during small intervals $\tau$ the distribution of the reflectors in a permitted volume is preserved to a certain degree. Therefore in distinction from the natural noises of the receiver, the passive interferences are referred to as correlated signals. If for noises at the output of UPCh of the receiving devices of the pulse RLS, the interval of correlation does not surpass the duration of the pulses, then for passive interferences it is characterized by correlation during the course of several periods or even ten periods of repetition.

The absence of necessary data on the character of the movement of the elementary reflectors makes it difficult for an analytical calcula-

tion of the energy spectra of fluctuation (correlation function) of the passive interference. Up to the present, however, there is a relative abundance of experimental materials.

It is found by experimental means that the energy spectra of the fluctuation of the signals of a multitude of reflectors depended only on the motion of the elementary reflectors (RLS immobile, antenna stopped). The envelope at the output of the detector may be approximated by the Gaussian curve

$$G(f)=e^{-\gamma\left(\frac{f}{f_0}\right)}, \qquad (12.2)$$

where $f_0$ - operating frequency of the station; $\gamma$ - parameter, depending on the type of envelope of the object and the meteorological conditions.

Dependence of a similar nature was conducted in Chap.3.

The value of the parameter $\gamma$ and the width of the spectra of fluctuation $F_{0.1}$ on the level 0.1 from the maximum when $f_0$ = 3000 Mhz and $f_0$ = 9000 Mhz are shown in Table 12.1

TABLE 12.1

| a Отражающий объект | $\gamma$ | $F_{0,1}$ ($f_0$ = 3000 Mhz) | $F_{0,1}$ ($f_0$ = 9000 Mhz) g h |
|---|---|---|---|
| b Дождевые облака . . . | $2{,}3\cdot10^{15}$ | 95 | 285 |
| c Металлизированные ленты . . . . . | $10^{16}$ | 45 | 136 |
| d Морская поверхность при ветре . . . . . | $1{,}41\cdot10^{16}$ | 38 | 115 |
| e Холмы, поросшие густым лесом, при скорости ветра 32 км/час | $2{,}3\cdot10^{17}$ | 10 | 28 |
| f Холмы, поросшие редким лесом, при тихой погоде . . . . . | $3{,}9\cdot10^{19}$ | 2,5 | 7 |

a) Reflecting object; b) rain cloud; c) metallized strips; d) sea surface in the wind; e) hills, thick forest growth at wind velocity 32 km/hr.; f) hills, thin growth, calm weather. g) hz; h) Mhz.

It is necessary to keep in mind that certainly the spectral characteristics of the passive interferences may vary within wide bounda-

ries in time and space which is particularly natural for reflections from the rain.

Depending on the characteristics of fluctuation, the sources of passive interferences may be divided into two classes. The objects of the first class form an aggregate of large numbers distributed randomly in space and are independently moving elementary reflectors. Examples of such types of reflectors are the hydrometeors, surface of the sea, metallized strips. The sources of the second type of passive interferences, besides the multitude of independently moving elementary reflectors, include immobile objects, giving reflections fixed in time (regulated signals). Examples of this type of reflectors are the surface of the earth, coverings of plant-growths.

Certainly, one can never draw a sharp line between the objects of the first class and the second class, since the character of the signals depends not only on the nature of the reflecting object but also on the velocity of the wind and the operating wave length of the RLS. For example, complex objects, whose elements are displaced by the action of the wind for no larger than 1cm may be considered as non-moving when the operating wave length is $\lambda = 10$ cm. In this case, the reflected signals will form almost a regular (non-random) function of time. But, this same object should be considered as an aggregate of randomly moving reflectors for a wave length of $\lambda = 1$ cm; during which the reflected signals will fluctuate strongly.

It has been established experimentally that the regular component of the signals reflected from hydrometeors, metallized strips is equal to zero. As a rule, the signals reflected from these objects, possess wide energy spectra of fluctuation (widebanded passive interferences). On the other hand, signals reflected from local subjects contain large values of the regular component (in comparison with the random) and

possess narrow spectra of fluctuation (narrowbanded passive interferences).

Table 3.3 introduced earlier illustrates graphically the decrease of the regular component of the signal and the increase of the intensity and width of the spectra of fluctuation with the increase in wind velocity during reflection from the Earth's surface, covered by woods.

The rotation of the antenna during the survey of the space leads to the variation of the amplitude of the elementary signals and consequently, to the fluctuation of the resulting reflected signal.

Fluctuation due to the rotation of the antenna may also be explained somewhat differently. During the rotation of the antenna, part of the elementary reflectors leave the diagrams of directionality while others enter into them. The exchange of reflectors, which are distributed in a random manner in space leads to the fluctuation. The coefficient of correlation between reflected signals $U(t_1)$ and $U(t_2)$, which correspond to the positions of the diagrams of directionality 1 and 2 (Fig. 12.1) in a first approximation may be found as

$$r_{U_1U_2} = r(\Delta\alpha) \cong 1 - \frac{\Delta\alpha}{\theta},$$

where $\theta$ - width of the diagrams of directionality; $\Delta\alpha$ - deflection angle of the diagram for the time $t_2 - t_1$.

During the deflection of the diagrams of directionality by the width of the antenna beam $\theta$ a complete exchange (renewal) of the elementary reflectors take place in the permitted volume achieving the independence of the signals $U(t_1)$ and $U(t_2)$.

Motion of the RLS similar to the motion of the elementary reflectors, produces change of phase of the elementary signals and consequently, the fluctuation of the resulting reflected signals.

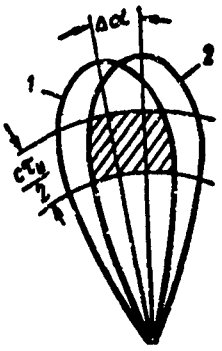

Fig.12.1 Diagrams of directionality corresponding to the time moments $t_1$ and $t_2$.

As it was shown in Chap.3, from the point of view of frequency representation, the effect of the successive of the motion of the RLS may be tracked by other means. Since the radial velocity of individual reflectors are different, so the elementary signals will have different Doppler's frequency shift. Consequently, if the RLS emits vibration of frequency $f_0$, then after reflection from a multitude of reflectors, at the input of the receiver there will appear signals occupying an entire band of frequency (spectra). The pulsations of these frequencies produce the fluctuation of the signals. Let us look at an example.

Let the RLS move in the direction of OB with a velocity of $V$ and the diagrams of directionality makes an angle $\alpha_0$ with the direction of the motion (Fig.12.2). We shall assume that the reflecting surface is an aggregate of a large number of equal sized reflectors distributed irregularly. The energy reflected from each one of these elementary reflectors is proportional to the energy of its irradiation and depends on the shape of the diagrams of directionality.

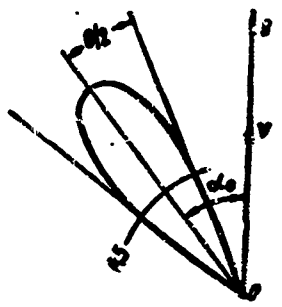

Fig.12.2 The determination of the spectra of fluctuation of the reflected signals when RLS is in motion.

The Doppler's frequency shift of the signals, reflected from the elementary reflectors with a course angle $\alpha$, is

$$F_d = \frac{2V}{\lambda}\cos\alpha. \qquad (12.3)$$

When $\alpha$ varies within small boundaries, the Doppler's frequency $F_d$ and the course angle $\alpha$ maintain between them an approximately direct proportional relationship. If the diagrams of

directionality expressed in power units is approximated by a Gaussian curve

$$U(\alpha)=e^{-2,8\left(\frac{\alpha-\alpha_0}{\theta}\right)^2},$$

where $\theta$ – the width of the diagrams at a level of 0.5 from the maximum and assuming that the diagrams are sufficiently narrow so that for the envelope of the spectra of the signals, we may write

$$S(f)=e^{-2,8\left(\frac{f-f_c}{\Delta F_д}\right)^2},$$

where $\Delta F_d$ – width of the spectra at the level 0.5 from the maximum;

$$f_c=f_0+F_{д_0};\quad F_{д_0}=\frac{2V}{\lambda}\cos\alpha_0.$$

The envelope of the spectra of the power of the signal is

$$G(f)=S^2(f)=e^{-2,8\left(\frac{f-f_c}{\Delta F'_д}\right)^2}, \qquad (12.4)$$

where

$$\Delta F'_д=\frac{\Delta F_д}{\sqrt{2}}.$$

For the determination of the value of $\Delta F_d$ from formula (12.3) we find

$$dF_д=\frac{2V}{\lambda}\sin\alpha d\alpha.$$

When the diagrams of directionality are narrow, it may be assumed $d\alpha = \theta$, $dF_d = \Delta F_d$. Consequently,

$$\Delta F_д=\frac{2V}{\lambda}\theta\cdot\sin\alpha_0. \qquad (12.5)$$

If $V$ = 800 km/hr, $\lambda$ = 3 cm, $\theta$ = 3°, $\alpha_o$ = 30°, then $\Delta F_d$ = 390 hz. The normalized correlation function corresponding to the spectra (12.4) is

$$r(\tau)=\frac{\int_0^\infty e^{-2,8\left(\frac{f-f_c}{\Delta F_\pi}\right)^2}\cdot\cos(2\pi f\tau)\,df}{\int_0^\infty e^{-2,8\left(\frac{f-f_c}{\Delta F_\pi}\right)^2}\,df}=\exp\left[-\frac{\pi^2}{2,8}(\tau\Delta F_\pi)^2\right]\cos\omega_c\tau. \tag{12.6}$$

If we substitute the value of $\Delta F_d$ = 390 hz. into the last expression then already when $\tau$ = 3 msec $r(\tau) \approx 0$, that is the values of the reflected signals of different intervals $\tau$ = 3 msec are not correlated.

A comparative evaluation of the fluctuation, depending on various reasons, shows that the fluctuation due to the motion of the RLS far surpasses the fluctuations produced by other reasons.

Instability of frequencies of probing oscillations also leads to fluctuations. As we have already noted that for the signals of the dispersed targets there is a vector sum of signals obtained from the individual reflectors within tne boundaries of permitted volume. Variations of frequency lead to the variations of phasal relationships between the elementary oscillations and consequently to the fluctuation of the resulting reflected signals. It is found that the dependence of the coefficient of correlation between the signals $U_1$ and $U_2$ corresponding to the frequencies of the probing oscillations $f$ and $f + \Delta f$, on the frequency increment $\Delta f$ has the form shown in Fig.12.3. From the curves of this figure, it follows that when $\tau_1\Delta f \ll 1$ between the signals $U_1$ and $U_2$ (their amplitudes and phases) there will be enough room for strong correlation. At the change over of the frequency of the RLS from pulse to pulse to the magnitude $\Delta f \geq 1/\tau_1$

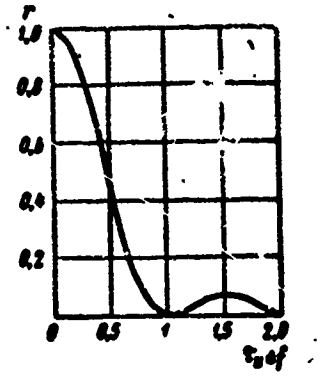


Fig.12.3 Correlation coefficient as a function of frequency change $\Delta F$.

the reflected pulses of the signals will be completely non-correlated.

Thus, we have established that the fluctuations of the passive interferences are produced from a series of independent causes. It is obvious that during the simultaneous action of a series of causes, the resulting velocity of fluctuation will be more intensive than during the action of each one of these causes by itself. It may be demonstrated that the normalized correlation function of the reflected signals during the calculation of various independent causes of fluctuation may be found as the product of the partial correlation functions*

$$r(\tau)=r_1(\tau)\,r_2(\tau)\,r_3(\tau)\,r_4(\tau),$$

where $r_1(\tau)$, $r_2(\tau)$, $r_3(\tau)$ and $r_4(\tau)$ — normalized correlation functions taking into account correspondingly the fluctuations due to motion of the elementary reflectors, the rotation of the antenna, the motion of the RLS and the instability of the frequency of the probing oscillation. In this way, the narrower every one of the partial correlation function, the narrower is the resulting correlation function and the wider is the energetic spectra of fluctuation.

We shall now write the law of probability distribution of thepassive interferences.

Let $\omega_{sr}$ be the average frequency of the energetic spectra of the passive interferences. Then expression (12.1) may be represented as

$$\begin{aligned} n(t)&=\sum_j n_j\cos(\omega_j t-\omega_{cp}t-\varphi_{0j}+\omega_{cp}t)=\\ &=X(t)\cos\omega_{cp}t-Y(t)\sin\omega_{cp}t=E(t)\sin[\omega_{cp}t+\varphi(t)], \end{aligned} \qquad (12.7)$$

where

$$\begin{aligned} X(t)&=\sum_j n_j\cdot\cos[(\omega_j-\omega_{cp})\,t-\varphi_{0j}],\\ Y(t)&=\sum_j n_j\cdot\sin[(\omega_j-\omega_{cp})\,t-\varphi_{0j}] \end{aligned} \qquad (12.8)$$

– quadrature components;

$$E(t)=\sqrt{X^2(t)+Y^2(t)},\quad \varphi(t)=\operatorname{arctg}\frac{Y(t)}{X(t)} \qquad (12.9)$$

– amplitude and phase, correspondingly of the oscillation $n(t)$.

The average frequency of the spectra of interference $\omega_{sr}$ is determined by the radial velocity $V_{Rp}$ of the motion of the sources of passive interferences as one integral object

$$\omega_{cp}=\omega_0+\Omega_{Дп},$$

where $\omega_0$ – frequency of the probing oscillation; $\Omega_{Дп}=\frac{2V_{Rп}}{c}\omega_0$ Doppler's frequency shift.

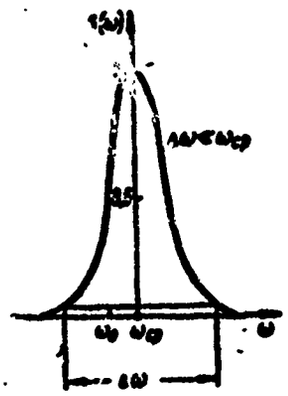

Fig.12.4 Energetic spectra of passive interferences.

It is obvious that such sources of passive interference as the local subjects, $V_{Rp}=0$, $\Omega_{dp}=0$ and $\omega_{sr}=\omega_0$.

For clouds, the dipoles $\Omega_{Дп}\neq 0$.

But, the motion of the cloud, as one complete unit, may be compensated by simple means (see §12.4) and then, also $\omega_{sr}=\omega_0$. Therefore, in the future in all cases it will be assumed that $\omega_{sr}=\omega_0$.

The frequency $\omega_j$ of the signals reflected from individual elementary reflectors in the boundaries of the permitted object, does not deviate significantly from the average frequency of the spectra $\omega_{sr}$, i.e. the width of the spectra of interference $\Delta\omega \ll \omega_{sr}$. Consequently, the passive interferences are narrowbanded interferences (Fig.12.4) Therefore, $X(t)$ and $Y(t)$ same as $E(t)$ and $\Phi(t)$ are slowly varying functions of time in comparison with $\cos\omega_{sr}t$ and $\sin\omega_{sr}t$.

Utilizing formula (12.8), we may find the autocorrelation function of the quadrature components.*

$$\left.\begin{aligned} R_X(\tau) &= \lim_{T\to\infty}\frac{1}{T}\int_{-\frac{T}{2}}^{\frac{T}{2}} X(t)\,X(t+\tau)\,dt = \\ &= \sum_j \frac{n_j^2}{2}\cos[2\pi(f_j - f_{cp})\tau], \\ R_Y(\tau) &= \lim_{T\to\infty}\frac{1}{T}\int_{-\frac{T}{2}}^{\frac{T}{2}} Y(t)\,Y(t+\tau)\,dt = \\ &= \sum_j \frac{n_j^2}{2}\cos[2\pi(f_j - f_{cp})\tau]. \end{aligned}\right| \qquad (12.10)$$

The quantity $\frac{n_j^2}{2}$ in the last expression is the power (in resistance of one ohm) of the *jth* component in the summation of (12.7). This power may be related to the frequency band $df$, adjoining the frequency $f_j$. If the energy spectra of the interference is designated by $G(f)$ then $G(f_j)\,df = \frac{n_j^2}{2}$ and expression (12.10) is rewritten in the form

$$R_X(\tau) = R_Y(\tau) = \int_0^\infty G(f)\cos[2\pi(f - f_{cp})\tau]\,df. \qquad (12.11)$$

Obviously, the variance of the quadrature components is

$$\sigma_X^2 = R_X(0) = \sigma_Y^2 = R_Y(0) = \int_0^\infty G(f)\,df = \sigma_n^2,$$

where $\sigma_n^2$ – variance of the interference $n(t)$.

The mutual correlation function is

$$R_{XY}(\tau) = -R_{YX}(\tau) = \sum_j \frac{n_j^2}{2}\sin[2\pi(f_j - f_{cp})\tau] \to$$

$$\to \int_0^\infty G(f)\sin[2\pi(f - f_{cp})\tau]\,df.$$

The spectra of interference $G(f)$ are generally symmetrical with respect to the average frequency $f_{sr}$, then

$$R_{XY}(\tau) = -R_{YX}(\tau) = 0,$$

i.e. the quadrature components of the interference are non-correlated.

As it is known that all random processes are characterized by a $N$-dimensional common density of probability of selected values.

The random functions $X(t)$ and $Y(t)$, form a weighted summation of large number of individually distributed random values, which according to the central limit theorem of the probability theory, are distributed according to the normal law. Unlike the case of non-correlated selected values examined in Chapter 6, the selected values of the passive interference are relatively strongly correlated. Assuming that the regular (non-random) component of the interference is equal to zero, for the $N$-dimensional plan of the probability functions $X(t)$ and $Y(t)$, we may write*

$$W_N(x_1, x_2, \ldots, x_n)_n = (2\pi)^{-\frac{n}{2}} |R_n|^{-\frac{1}{2}} \exp\left[-\frac{1}{2}\sum_{i,j=1}^{n} R^{ij}x_i x_j\right],$$

$$W_N(y_1, y_2, \ldots, y_n)_n = (2\pi)^{-\frac{n}{2}} |R_n|^{-\frac{1}{2}} \exp\left[-\frac{1}{2}\sum_{i,j=1}^{n} R^{ij}y_i y_j\right],$$

where $|R_n|$ – determinant of quadratic matrices $\|R_n\|$, whose elements are the correlation moments $R_{ij} = \overline{X(t_i)\cdot X(t_j)} = \overline{Y(t_i)\cdot Y(t_j)}$;

$R^{ij} = \frac{Ad(R_{ij})}{|R_n|}$ are elements of the matrices $\|R_n\|^{-1}$, reciprocal to the matrices $\|R_n\|$; $Ad(R_{ij})$ are the algebraic complements of the elements $R_{ij}$ in the determinant $|R_n|$.

From expression (12.11), it follows that

$$R_{ij} = \int_{x}^{\infty} G(f)\cos[2\pi(f - f_{cp})(t_i - t_j)]\,df, \quad i, j = 1, 2, \ldots, n.$$

In place of the correlation matrices $\|R_n\|$ it is possible to consider the nomalized correlation matrices, $\|r_n\|$, whose elements are the coefficients of correlation

$$r_{ij} = \frac{R_{ij}}{\sigma_i \cdot \sigma_j}.$$

If $\sigma_i^2 = \sigma_j^2 = \sigma^2$, then,

$$\left.\begin{aligned} |r_n| &= \frac{|R_n|}{\sigma^2}, \\ |r_n| &= \frac{|R_n|}{\sigma^{2n}}, \quad \|r_n\|^{-1} = \sigma^2 \|R_n\|^{-1}, \\ r_{ij} &= \frac{R_{ij}}{\sigma^2}, \qquad r^{ij} = R^{ij} \cdot \sigma^2, \end{aligned}\right\} \tag{12.12}$$

where $r^{ij}$ -- Elements of the matrices $\| r_n \|^{-1}$.

Since normally the distributions of the random functions $X(t)$ and $Y(t)$ do not correlate, then, they are independent. Therefore, their combined $2N$-dimensional probability density is

$$W_{2N}(x_1, y_1; \ldots; x_n, y_n) = W_N(x_1, \ldots, x_n)\, W_N(y_1, \ldots, y_n) = \\ = (2\pi)^{-n} |R_n|^{-1} \cdot \exp\left[-\frac{1}{2} \sum_{i,j=1}^{n} (R^{ij} x_i x_j - R^{ij} y_i y_j)\right]. \tag{12.13}$$

Besides the interferences on the signals, inevitably there will also be superimposed, the natural noises of the receiving devices. The addition of noises increases the power and decreases the correlation of the interferences. Since the intensity of the passive interferences, (with the exception of observation at the limiting range, when the interference becomes commensurable with the natural noises of the receiver) then the addition of noises under these conditions, is not possible to change the statistical properties of the interferences substantially.

Now, let us look at the probability properties of the useful signals. As we have already noted, the radiolocational target (airplane, ship etc.) have complex structures and may be considered as an aggregate of large number of randomly distributed sparking points. The variation of the orientation of the target relative to the RLS leads to the variations of phasal relationships between the signals, reflected from its different parts such that in their turn they produce fluctuations of the resulting reflected signals. This gives basis

to assume that the useful signals reflected from such targets like the passive interferences are random functions of time, whose values in one instant are distributed in many cases according to the normal law.

Experimental data indicate that the velocity of the fluctuation of the signals of real targets are generally not great. For example, in the centimeter wave range, the width of electric spectra of the signals is of the order of one hertz. Consequently, in the time of observation (irradiation), of the target, the reflected signal cannot change its phase substantially. Taking into account of this circumstance, and also trying to make it eady for the following analysis, it will be assumed that the useful signals are non-random functions of time

$$s(t)=A(t)\cos[(\omega_0+\Omega_д)t+\varphi_0]. \qquad (12.14)$$

$\Omega_д=\frac{2V_R}{C}\omega_0$ – Doppler's shift of the average frequency of the spectra of the signals of the moving target relative to the frequency of the probing oscillation $\omega_0$;

$V_R$ – radial velocity of the target.

Rewrite expression (12.14) in the form

$$s(t)=A_X(t)\cos\omega_0 t-A_Y(t)\cdot\sin\omega_0 t, \qquad (12.15)$$

where

$$A_X(t)=A(t)\cos(\Omega_д t+\varphi_0);$$
$$A_Y(t)=A(t)\sin(\Omega_д t+\varphi_0).$$

Then the summation of interferences (12.7) and the signals (12.15)

$$n(t)+s(t)=[X_п(t)+A_X(t)]\cos\omega_0 t-[Y_п(t)+A_Y(t)]\sin\omega_0 t$$

and the combined $2N$-dimensional law of probability distribution of the quadrature components $X=X_п+A_X$ and $Y=Y_п+A_Y$

will have the form

$$W_{2N}(x_1, y_1; \ldots; x_n, y_n)_{c+n} = (2\pi)^{-n} |R_n|^{-1} \exp \times$$
$$\times \left\{ -\frac{1}{2} \sum_{i,j=1}^{n} [R^{ij}(x_i - A_{xi})(x_j - A_{xj}) + \right. \qquad (12.16)$$
$$\left. + R^{ij}(y_i - A_{yi})(y_j - A_{yj})] \right\},$$

where

$$A_{xi} = A_x(t_i) = A_i \cos(\Omega_x t_i + \varphi_0);$$
$$A_{yj} = A_y(t_j) = A_j \sin(\Omega_x t_j + \varphi_0);$$
$$A_i = A(t_i).$$

In this way, we have obtained the multi-dimensional probability density of the interferences and the sum of the signals and the interferences.

## §12.3. OPTIMUM DETECTION OF THE RADIOLOCATIONAL SIGNALS ON THE BACKGROUND OF PASSIVE INTERFERENCES

The optimum detection of signals in passive interferences will be examined applicable to the pulse RLS.

As it is known in the pulse RLS, the optimum treatment of the data of radiolocational observations may be divided into intra-periodic (the treatment of homogeneous pulses) and inter-periodic (treatment within the boundaries of the pulse packets). The effectiveness of inter-periodic and intra-periodic treatments are different and depends on the statistical properties of the interference. If relatively strongly correlated interferences are considered then the intra-periodic treatment is less effective (this will be shown below) and the basic role is played by the inter-periodic treatment.

Let us look at the optimum rule of the inter-periodic treatment. Remember that in the case of the detection of the signals on the background of the natural noises of the receiver, the selected values of which do not correlate, these rules reduce to the integration of the

signals.

The passive interferences possess the property that all their energies concentrate in the final time intervals $\tau_{obl}$ (time of observation) and the frequency band $\Delta f$. Such functions with a large degree of accuracy according to the theorum of V.A.Kotelnikov, may be represented by an aggregate of terminal numbers of selected values of the envelope $E(t)$ and phases $\Phi(t)$: $E(t)$, $\Phi(t)$; $E(t + \tau_0)$, $\Phi(t + \tau_0)$;...; $E(t + n\tau_0)$, $\Phi(t + n\tau_0)$ measured by time intervals $\tau_0 \leqslant \frac{1}{\Delta f}$.
The total number of coordinates $E(t)$ and $\Phi(t)$, unambiguously determining the process according to the interval $\tau_{obl}$ is equal to $2\Delta f \tau_{obl}$.

In place of the values $E(t)$ and $\Phi(t)$, one may consider the quadratic components $X(t)$ and $Y(t)$, which are connected with $E(t)$ and $\Phi(t)$ by Relationship (12.9). Consequently, the expressions written earlier, (12.13) and (12.16) for the $2N$-dimensional probability densities of the quadratics $X(t)$ and $Y(t)$ will be entirely determined by the interference or the sum of the interference and the signal if only the interval between adjacent pairs of selected values $x_i$, $y_i$ and $x_{i+1}$, $y_{i+1}$ will fulfill the condition $\tau_0 \leqslant \frac{1}{\Delta f}$. The decrease of the interval between the selected values in comparison with $\frac{1}{\Delta f}$ does not guarantee the obtaining of additional information on the interferences and consequently, does not give its statistical descriptions more fully.

Since below we shall analyze the optimum rule of the inter-periodic treatment, therefore the pairs of selected values appearing in Expression (12.13) and (12.16) $x_1\ y_1, x_2, y_2; \ldots x_n, y_n$ must be considered as quadrature components of the first, second and third etc. the *Nth* pulse packet. Thereby, the treatment of the data of radiolocational observations may be considered as optimum in the case if the period

of repetition of the pulses is $T \leqslant \frac{1}{\Delta f}$. Besides this, it is assumed that the high frequency phase is the same for all pulses.

During the analysis of the optimum methods of detecting signals in passive interferences, the situation of statistical detection examined earlier in Chapter 6 is used. According to the theory, all types of optimum detections (Neumann-Pearson, ideal, etc.) compute the ratio of the probability

$$\Lambda(x_1, y_1; \ldots; x_n, y_n) = \frac{W_{2N}(x_1, y_1; \ldots; x_n, y_n)_{c+n}}{W_{2N}(x_1, y_1; \ldots; x_n, y_n)_{n}}. \qquad (12.17)$$

The difference of one detection from the other consists only in the rules of accepting the final solution with the presence or absence of the signal. The rules of accepting the solution consists of the following:

If $\Lambda(x_1, y_1; \ldots; x_n, y_n) \geq \Lambda_0$, then accept the solution on the presence of the signal,

if $\Lambda(x_1, y_1; \ldots; x_n, y_n) < \Lambda_0$, accept the solution on the absence of the signal.

The detector of Neumann-Pearson, in particular, the threshold solution $\Lambda_0$ chooses from the conditions guaranteeing a specified probability of the false detection.

1. Optimum Detection of Signals With Known Parameters

In practice, as a rule, there are no such situations when all the parameters of the signals were precisely known. The detection of signals with known parameters is considered here as a simplifying measure. Besides this, it permits, afterwards, the solution of the problem of detection of signals with unknown parameters.

Thus, the parameters of the signals are entirely known. But the signals at the input of the receiver may be present or may not be present. Analysing the data of the radiolocational observation - the

selected values $x_1, y_1; \ldots; x_n, y_n$, from either one interference (sequence of selected values, $x_{p1}, y_{p1}; \ldots; x_{pn}, y_{pn}$) or a sum of interferences and signals (sequence of the selected values $x_{p1} + A_{x1}, y_{p1} + A_{y1}; \ldots; x_{pn} + A_{xn}, y_{pn} + A_{yn}$) the receiver should decide the oscillation being received is dependent on : one interference or the sum of interferences and signals.

Utilizing Expression (12.13) and (12.16), we find the ratio of probability by the computed optimum receiver

$$\Lambda(x_1, y_1; \ldots; x_n, y_n) = \exp\left[-\frac{1}{2}\sum_{i,j=1}^{n}(R^{ij}A_{xi}A_{xj} + R^{ij}A_{yi}A_{yj})\right] \times \exp\left[\sum_{i,j=1}^{n}(R^{ij}A_{xi}x_j + R^{ij} \cdot A_{yi} \cdot y_j)\right]. \tag{12.18}$$

The logarithm of the ratio of probabilities is

$$\ln \Lambda(x_1, y_1; \ldots; x_n, y_n) = -\frac{1}{2}C_0 + \sum_{i,j=1}^{n}(R^{ij}A_{xi}x_j + R^{ij}A_{yi}y_j),$$

where

$$C_0 = \sum_{i,j=1}^{n}(R^{ij}A_{xi}A_{xj} + R^{ij}A_{yi}A_{yj}). \tag{12.19}$$

The quantity $C_0$ does not depend on the input data. The structure of the optimum receiver is determined by the function

$$\gamma = \sum_{i,j=1}^{n}(R^{ij}A_{xi}x_j + R^{ij}A_{yi}y_j). \tag{12.20}$$

From the last formula, it follows that the decision on the presence or absence of the useful signal is taken on the basis of the analysis of the data of the mutual correlation of the quadrature components $X$ and $Y$ of the input oscillation and the projections $A_x$ and $A_y$ of the apriori known useful signal.

Rewriting Expression (12.20) in the form

$$\gamma = \sum_{j=1}^{n}(B_{xj}x_j + B_{yj}y_j), \tag{12.21}$$

where

$$\left.\begin{aligned} B_{xj} &= \sum_{i=1}^{n} R^{ij} \cdot A_{xi} = \sum_{i=1}^{n} R^{ij} A_i \cos(\Omega_s t_i + \varphi_0), \\ B_{yj} &= \sum_{i=1}^{n} R^{ij} A_{yi} = \sum_{i=1}^{n} R^{ij} A_i \sin(\Omega_s t_i + \varphi_0). \end{aligned}\right\} \qquad (12.22)$$

Then the function $\gamma$ may be considered as the voltage at the output of the linear filter, determined by the combination of the weight coefficients $B_{xj}, B_{yj}$.

Expression (12.19) thereby will have the form

$$C_0 = \sum_{j=1}^{n} (B_{xj} A_{xj} + B_{yj} A_{yj}), \qquad (12.23)$$

from which it follows that the quantity $C_0$ is the useful signal (peak value) at the output of the filter.

Thus, the optimum receiver appears to be a linear receiver because the operation of forming the quantity $\gamma$ from $x_j$ and $y_j$ is linear. The receiver should separate from the input oscillations its quadrature components, $X$ and $Y$. In practice, this may be accomplished with the aid of two coherent (phasal) detectors, on which the supporting voltage is fed with a phase shift of $\pi/2$ and should be rigidly connected with the initial phase of the probing oscillation. Further, the quadrature components of the pulses $X$ and $Y$ in accordance with Formula (12.21) are subjected to conversion in the linear filter and the output voltage of the filter is compared with the threshold. The block diagram of the optimum receiver is shown in Fig.12.5

For the formation of the operation characteristics of the optimum receiver, it is necessary to find the distribution probability of the value $\gamma$.

The random value $\gamma$ forms a linear combination of normal distribution of the values $x_j$ and $y_j$ and therefore is also distributed according to the normal law.

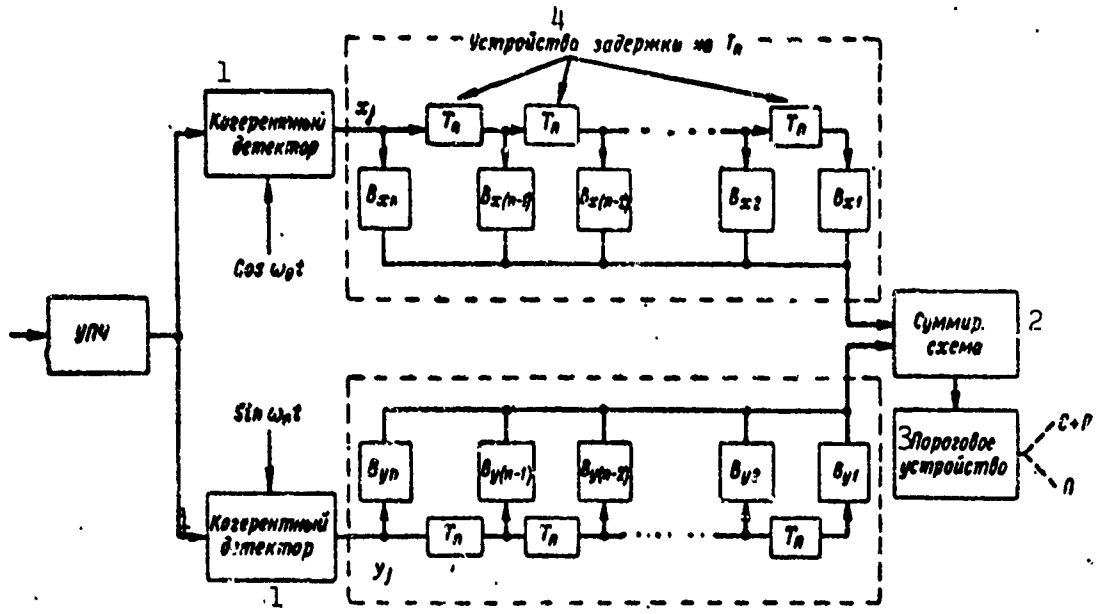


Fig.12.5. Block diagram of the optimum receiver during the detection of signals with known parameters. 1) Coherent; 2) summation circuit; 3) threshold device; 4) delay installation Tp.

The mean value of the quantity $\gamma$ under the condition of the entering of one interference ($X = X_p$, $Y = Y_p$) into the input of the receiver is equal to

$$\bar{\gamma}_n = \sum_{i,j=1}^{n} (R^{ij} \cdot A_{xi} \bar{x}_{nj} + R^{ij} \cdot A_{yi} \bar{y}_{nj}) = 0,$$

since

$$\bar{x}_{nj} = 0, \quad \bar{y}_{nj} = 0.$$

The mean square is

$$\overline{\gamma_n^2} = \overline{\left[\sum_{i,j=1}^{n} (R^{ij} A_{xi} x_{nj} + R^{ij} A_{yi} y_{nj})\right]^2} = C_0,$$

since

$$\left.\begin{aligned} \overline{\left(\sum_{i,j=1}^{n} R^{ij} A_{xi} x_{nj}\right)^2} &= \sum_{i,j=1}^{n} R^{ij} \cdot A_{xi} \cdot A_{xj}, \\ \overline{\left(\sum_{i,j=1}^{n} R^{ij} A_{yi} y_{nj}\right)^2} &= \sum_{i,j=1}^{n} R^{ij} \cdot A_{yi} \cdot A_{yj}. \end{aligned}\right\} \qquad (12.24)$$

The variance is

$$\sigma_\gamma^2 = \overline{\gamma_n^2} - (\bar{\gamma}_n)^2 = C_0.$$

Consequently, the density of the probability of the quantity $\gamma$ under the condition of the entering of an interference at the input of the receiver

$$W(\gamma)_n = \frac{1}{\sqrt{2\pi C_0}} e^{-\frac{\gamma^2}{2C_0}}. \qquad (12.25)$$

The mean value of $\gamma$ under the condition of the entering of a summation of signals and interferences at the input of the receiver ($X = X_p + A_x$; $Y = Y + A_y$) is

$$\overline{\gamma_{c+n}} = \sum_{i,j=1}^{n} (R^{ij} A_{xi} A_{xj} + R^{ij} A_{yi} A_{yj}) = C_0,$$

since

$$\overline{X} = A_X; \quad \overline{Y} = A_Y.$$

The mean square is

$$\overline{\gamma^2_{c+n}} = \overline{\left\{ \sum_{i,j=1}^{n} [R^{ij} A_{xi} (A_{xj} + x_{nj}) + R^{ij} A_{yi} (A_{yj} + y_{nj})] \right\}^2} = C_0^2 + C_0.$$

The variance is

$$\sigma^2_\gamma = \overline{\gamma^2_{c+n}} - (\overline{\gamma_{c+n}})^2 = C_0.$$

The density of the probability of the quantity $\gamma$ under the condition of the entering of a summation of signals and interferences at the input of the receiver, is

$$W(\gamma)_{c+n} = \frac{1}{\sqrt{2\pi C_0}} e^{-\frac{(\gamma - C_0)^2}{2C_0}}. \qquad (12.26)$$

The probability of the false detection and the probability of the detection of the target are equal to correspondingly

$$F = \int_{\gamma_0}^{\infty} W(\gamma)_n \, d\gamma = 0{,}5 - \Phi(\eta), \qquad (12.27)$$

$$D = \int_{\gamma_0}^{\infty} W(\gamma)_{c+n} \, d\gamma = 0{,}5 - \Phi(\eta - \sqrt{C_0}), \qquad (12.28)$$

where $\gamma_0$ – threshold solution, selected from the condition of obtaining the specified value of probability of false detection $F$;

$\eta = \frac{\gamma_0}{\sqrt{C_0}}$ - normalized value of the threshold

$\Phi(x) = \frac{1}{\sqrt{2\pi}} \int_{-\infty}^{x} e^{-\frac{t^2}{2}} dt$ - probability integral

In place of Expressions (12.27) and (12.28), we may write

$$P = 0{,}5 - \Phi\left[\Phi^{-1}(0{,}5 - F) - \sqrt{C_0}\right], \tag{12.29}$$

where $\Phi^{-1}(x)$ - function, reciprocal to the function $\Phi(x)$.

From the last formula, it can be seen that the quantity $C_0$ is an unique parameter, determing the effectiveness of the optimum receiver.

Let us show that the quantity $C_0$ is equal to double the value of the ratio of the power of the signal to the power of the interference at the output of the filter. Utilizing (12.23), we find that this ratio, same as in the case of noncorrelated Gaussian noises is

$$\frac{\frac{C_0^2}{2}}{[n(t)]^2} = \frac{\left[\sum_{i,j=1}^{n} (R^{ij}A_{xi}A_{xj} + R^{ij}A_{yi}A_{yj})\right]^2}{2\left[\sum_{i,j=1}^{n} (R^{ij}A_{xi}x_{nj} + R^{ij}A_{yi}y_{nj})\right]^2} = \frac{\left[\sum_{i,j=1}^{n} (R^{ij}A_{xi}A_{xj} + R^{ij}A_{yi}A_{yj})\right]^2}{2\left[\sum_{i,j=1}^{n} (R^{ij}A_{xi}A_{xj} + R^{ij}A_{yi}A_{yj})\right]} = \frac{C_0}{2}. \tag{12.30}$$

Converting Expression (12.19) to the form, convenient for computation

$$C_0 = \sum_{i,j=1}^{n} [R^{ij}A_iA_j \cos(\Omega_x t_i + \varphi_0)\cos(\Omega_x t_j + \varphi_0) + R^{ij}A_iA_j \sin(\Omega_x t_i + \varphi_0)\cdot\sin(\Omega_x t_j + \varphi_0)] = \sum_{i,j=1}^{n} R^{ij}A_iA_j \cos[\Omega_x(t_i - t_j)].$$

For simplification, we assume

- the diagrams of directionality are right-angled, i.e., $A_i = A_j = A$;
- the interferences are the same $(\sigma_{ni}^2 = \sigma_{nj}^2 = \sigma_n^2)$;
- the interval between the selected values (pulses) is $t_i - t_j = (i-j)\cdot T_n$.

Then the ratio of signal/interference at the output of the filter is

$$\frac{C_0}{2}=\frac{a^2}{2}\cdot\sum_{i,j=1}^{n} r^{ij}\cos[\Omega_д\cdot T_п\cdot(i-j)], \qquad (12.31)$$

where $\frac{a^2}{2}=\frac{A^2}{2\sigma_п^2}$ – ratio of the power of the signal to the average power of the interference at the input of the receiver for one pulse.

It may be shown just as in Chapter 6, that the linear optimum filters characterized by the weight conefficients $B_{xj}$ and $B_{xy}$ are concordant filters maximizing the signal/interference ratio.

In this way, the optimum receiver detecting non-random signals in the correlated interferences is made up of concordant filters and resolving devices.

Computed by Formulas (12.29) and (12.31), the curves of probability of detection for this receiver is shown in Fig. 12.6 in solid lines. The dash-point lines show the curves of probability of detection at $T_п \gg \frac{1}{\Delta f}$, when the selected values of the interference are not correlated. During the calculation the envelope of the energetic spectra of the interference was approximated by the Gauss curve

$$G(f)=ve^{-\varkappa(f-f_0)^2}, \qquad (12.32)$$

The width of the spectra of the interference $\Delta F_p$, determined by the parameter $\varkappa$, calculated at current of half strength.

Figure 12.7 shows the dependence of the threshold signal $\frac{a^2_{мин}}{2}$ corresponding to the probability of detection, $D = 0.9$, obtained on the basis of the curves in Fig. 12.6, on the value of Doppler phase increment $\varphi_д=\Omega_д T_п$ per period of repetition.

From these curves, it follows that the probability of the detection of the target depends to a large degree on the magnitude of the Doppler's increment of the phase $\varphi_D$. The variation of $\varphi_D$ from 0 to 180° (when $\Delta F_п\cdot T_п=0{,}15$) is accompanied by a decrease of the threshold

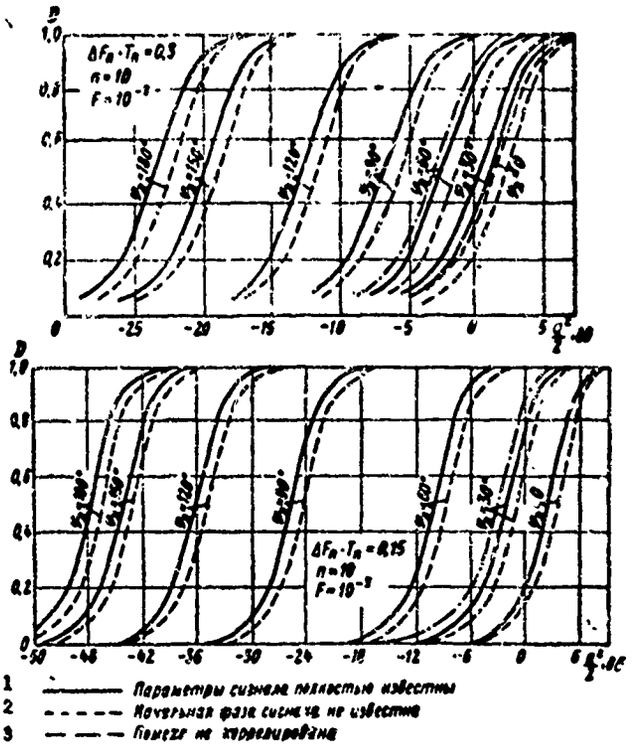


Fig. 12.6 Operation characteristics of the optimum receiver
1) Parameters of the signals completely known;
2) initial phase of the signals not known;
3) interferences not correlated.

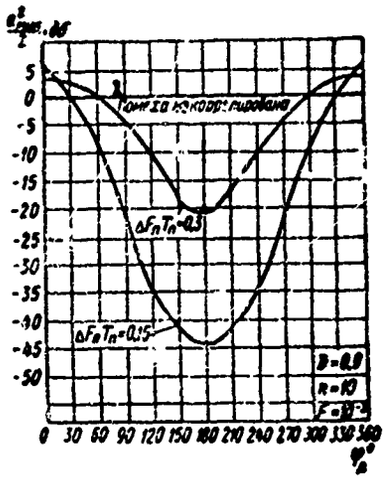


Fig. 12.7 Dependence of the threshold signal on the magnitude of Doppler increment of the phase of the signal per period of repetition
1) Interference not correlated.

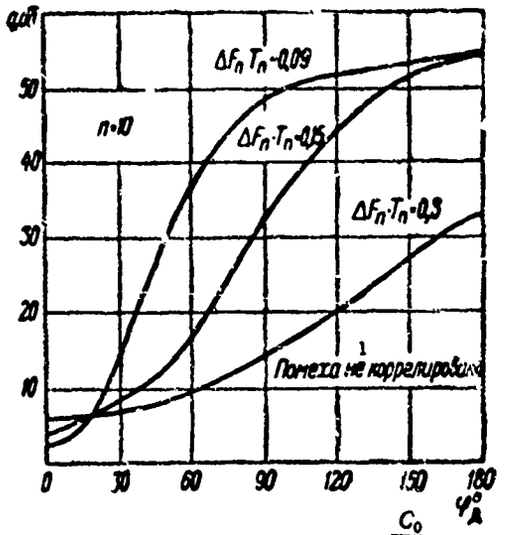


Fig. 12.8 The dependence of the quantity $q=\frac{\frac{C_0}{2}}{\frac{a^2}{2}}$ on the Doppler increment of phase per period of repetition. 1) Interferences not correlated.

signal to 50 db.

The velocity of the target corresponding to the Doppler's increment of phase $\varphi_д=\pm\pi,\ \pm3\pi,\ldots$, generally is referred to as optimum. If, however $\varphi_д=0,\ \pm2\pi,\ \pm4\pi\ldots$, then such velocities are referred to as "blind". In this way, at "blind" velocity, the effectiveness, even of the optimum receiver is not great.

The effect of the correlation of the interference may be different depending on the Doppler's effect on the phase:

– if $\varphi_д=(2\mu-1)\pi,\ \mu=0,1,2,\ldots$ when the increase in the degree of correlation of the interferences leads to the increase of the threshold sensitivity of the optimum receiver.

– if $\varphi_д=2\mu\pi$, then the increase in the degree of correlation of the interferences leads to the decrease of the threshold sensitivity In this case, the decorrelation of the interferences, for example, the change-over of the frequency at the RLS or the separation of the selected values through the interval $T_n\gg\frac{1}{\Delta f}$, may receive some gain in the

value of the threshold signal.

Figure 12.8 shows the dependence of the values $q=\frac{\frac{C_0}{2}}{\frac{a^2}{2}}$, showing by how many times the signal/interference ratio at the output of the filter is greater than that similar ratio at the input of the filter calculated by Formula (12.31) on the Doppler's variation of the phase of the signal per period of repetition. The character of this dependence also specifies the high values obtained for the threshold signals.

2. Optimum Detection of Signals With Unknown Initial Phases

As a rule, the initial phase of the signal is unknown to the observer and therefore the assumption is made that it is approximately distributed within the interval $(0.2\pi)$. The structure of the optimum receiver in this case is determined by the ratio of the probabilities averaged by the initial phase.

Transform the previous Expression (12.20) for $\gamma$ to the form

$$\begin{aligned}\gamma=\sum_{i,j=1}^{n}[R^{ij}x_jA_i(\cos\Omega_x t_i\cos\varphi_0-\sin\Omega_x t_i\sin\varphi_0)+\\+R^{ij}y_jA_i(\sin\Omega_x t_i\cos\varphi_0+\cos\Omega_x t_i\sin\varphi_0)]=\\=U\cos\varphi_0+V\sin\varphi_0=E\cos(\varphi+\varphi_0),\end{aligned}\tag{12.33}$$

where

$$\left.\begin{aligned}U=\sum_{i,j=1}^{n}(R^{ij}x_jA_i\cos\Omega_x t_i+R^{ij}y_jA_i\sin\Omega_x t_i);\\V=\sum_{i,j=1}^{n}(R^{ij}y_jA_i\cos\Omega_x t_i-R^{ij}x_jA_i\sin\Omega_x t_i);\end{aligned}\right\}\tag{12.34}$$

$$\left.\begin{aligned}E=\sqrt{U^2+V^2};\\\varphi=\operatorname{arctg}\frac{V}{U}.\end{aligned}\right\}\tag{12.35}$$

Averaging the ratios of the Probabilities (12.18) taking into account Formula (12.33) for the unknown initial phase, we get

$$\begin{aligned}\overline{\Lambda(x_1,y_1;\ldots;x_n,y_n)}=\frac{1}{2\pi}\int_0^{2\pi}e^{-\frac{1}{2}C_0+E\cos(\varphi+\varphi_0)}d\varphi_0=\\=e^{-\frac{1}{2}C_0}\cdot I_0(E),\end{aligned}\tag{12.36}$$

where $I_0$ – Bessel's function of the zero*th* order from the minimum argument.

The logarithm of the ratio of probabilities is

$$\ln \overline{\Lambda(x_1, y_1; \ldots; x_n, y_n)} = -\frac{1}{2} C_0 + \ln I_0(E). \qquad (12.37)$$

Expression (12.37) also determines the structure of the optimum receiver.

Represent (12.34) in the form

$$\left.\begin{aligned} U &= \sum_{j=1}^{n} (B_{xj} x_j + B_{yj} y_j), \\ V &= \sum_{j=1}^{n} (B_{xj} y_j - B_{yj} x_j). \end{aligned}\right\} \qquad (12.38)$$

where

$$\left.\begin{aligned} B_{xj} &= \sum_{i=1}^{n} R^{ij} A_i \cos \Omega_x t_i; \\ B_{yj} &= \sum_{i=1}^{n} R^{ij} A_i \sin \Omega_x t_i. \end{aligned}\right\} \qquad (12.39)$$

then the values $U$ and $V$ may be considered as voltages at the outputs of the linear filters characterized by the weight coefficients $B_{xj}$ and $B_{yj}$. The receiver forms the envelopes of these voltages $E = \sqrt{U^2 + V^2}$. Afterwards, $E$ (or any monotonous function of them) should be compared with the threshold for obtaining the decision on the presence or absence of the signal.

A block diagram of the optimum receiver is shown in Fig. 12.9. The receiver includes in itself the coherent detectors, concordant filters, filters similar to Fig. 12.5 and functional converters.

To calculate the operating characteristics of the optimum receiver, it is necessary to find the probability distribution law of the envelope $E$.

It is obvious that the random values $U$ and $V$, form linear combinations of normally distributed values which are also distributed according to the normal law. Similarly as it was done previously, the para-

meters of this law may be found.

Under the condition of the entering of one interference into the input of the receiver

$$\overline{U}=\overline{V}=0,\quad \sigma_U^2=\sigma_V^2=C_0,\quad \overline{UV}=0.$$

The combined density of probability of the values $U$ and $V$ is

$$W(U,\ V)_n=W(U)_n\cdot W(V)_n=\frac{1}{2\pi C_0^2}e^{-\frac{U^2+V^2}{2C_0}}.$$

Further, just as in Chapter 6, it may be shown that the density of probability of the envelopes is

$$W(E)_n=\frac{E}{C_0}\cdot e^{-\frac{E^2}{2C_0}}.$$

Under the condition of the entering of a summation of signals and interferences into the input of the receiver

$$\overline{U}=C_0\cos\varphi_0,\quad \overline{V}=C_0\sin\varphi_0,$$
$$\sigma_U^2=\sigma_V^2=C_0,\quad \overline{UV}=0,$$
$$W(U,\ V)_{c+n}=\frac{1}{2\pi C_0^2}\cdot e^{-\frac{(U-C_0\cos\varphi_0)^2+(V-C_0\sin\varphi_0)^2}{2C_0}}$$

and the density of the distribution of the envelopes is

$$W(E)_{c+n}=\frac{E}{C_0}e^{-\frac{E^2+C_0^2}{2C_0}}\cdot I_0(E).$$

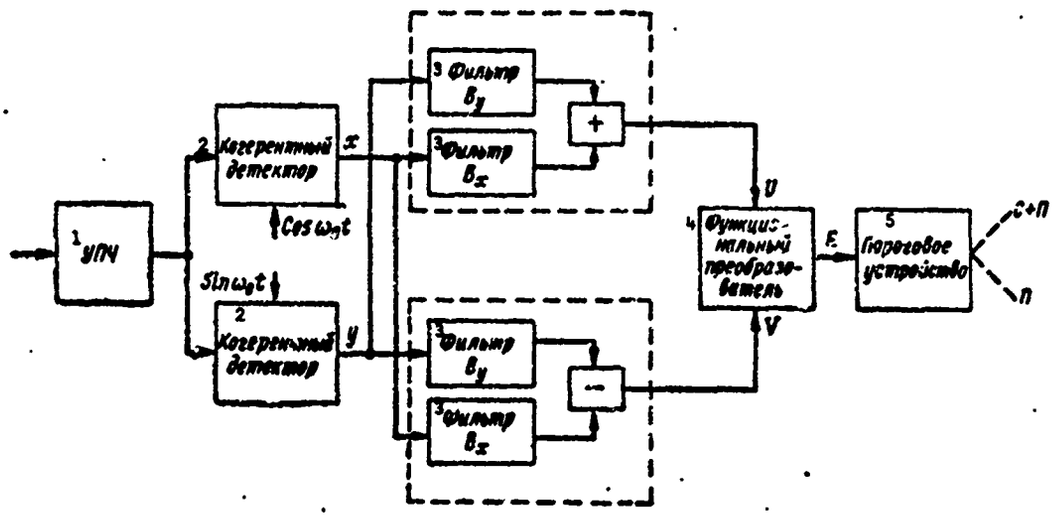

Fig.12.9 Block diagram of the optimum receiver during detection of signals with unknown initial phases. 1) UPCh; 2) coherent detectors; 3) filter; 4) functional converter; 5) threshold device.

The probability of the false detection and the probability of the detection of the target are

$$\left.\begin{aligned} F &= \int_{E_0}^{\infty} \frac{E}{C_0} e^{-\frac{E^2}{2C_0}} dE = e^{-\frac{E_0^2}{2C_0}}, \\ D &= \int_{E_0}^{\infty} \frac{E}{C_0} e^{-\frac{E^2+C_0^2}{2C_0}} \cdot I_0(E)\, dE, \end{aligned}\right\} \qquad (12.40)$$

where $E_0$ – threshold solution.

From Expression (12.40) one can see that just as in the case of known parameters, the probability of the detection of the target is determined by the unique quantity $C_0$.

By Formula (12.40) for the same condition as during the detection of signals with known phases, the curves of the probability of detection were calculated. These curves are shown in dotted lines in Fig. 12.6. From the curves, it follows, that not knowing the initial phase of the useful signals only insignificantly lowers the effectiveness of the optimum receiver. The increase in the threshold signal in comparison with the case of the completely known signals is equal to approximately 1 db at all values of the parameters, $\varphi_A = \Omega_A T_u$.

From Expression (12.39) it can be seen that the weight coefficients of the linear filters, $B_{xj}$ and $B_{yj}$ depend on the Doppler's frequency shifts of the signals $\Omega_D$ and the degree of correlation of the interferences, $R^{ij}$.

Let us examine in what way the rules of the treatment of the input signals change at the variations of the Doppler's increment of the phase $\Phi_D$ and the degree of correlation of the interferences.

For this, we transform Expression (12.35) into the form

$$E^2 = U^2 + V^2 = \left[\sum_{j=1}^{n} (B_{xj}x_j + B_{yj}y_j\right]^2 + \left[\sum_{j=1}^{n} (B_{xj}y_j - B_{yj}x_j)\right]^2 =$$

$$= \sum_{i,j=1}^{n} [(B_{xi}B_{xj} + B_{yi}B_{yj})(x_i x_j + y_i y_j) - 2(B_{xi}B_{yj} - B_{xj}B_{yi}) x_j y_i] =$$

$$= \sum_{i,j=1}^{n} \sum_{\mu,\nu=1}^{n} [R^{i\mu}R^{\nu j}A_\mu A_\nu \cos\Omega_k (t_\mu - t_\nu) x_i x_j + \tag{12.41}$$

$$+ R^{i\mu}R^{\nu j}A_\mu A_\nu \cos\Omega_k (t_\mu - t_\nu) y_i y_j -$$

$$- 2R^{i\mu}R^{\nu j}A_\mu A_\nu \sin\Omega_k (t_\mu - t_\nu) x_j y_i].$$

Assume $A_i = A_j = A$; $\sigma_{ni}^2 = \sigma_{nj}^2 = \sigma_n^2$ and designate

$$\sum_{i=1}^{n} r^{i\mu} \cdot x_i = \alpha_\mu, \qquad \sum_{j=1}^{n} r^{\nu j} \cdot x_j = \alpha_\nu,$$

$$\sum_{i=1}^{n} r^{i\mu} \cdot y_i = \beta_\mu, \qquad \sum_{j=1}^{n} r^{\nu j} \cdot y_j = \beta_\nu.$$

Then

$$E^2 = \left(\frac{A}{\sigma_n^2}\right)^2 \cdot \sum_{\mu,\nu=1}^{n} [\alpha_\mu\alpha_\nu \cos\Omega_k (t_\mu - t_\nu) + \beta_\mu\beta_\nu \cos\Omega_k (t_\mu - t_\nu) -$$

$$- 2\alpha_\mu\beta_\nu \sin\Omega_k (t_\mu - t_\nu)] = \frac{A^2}{\sigma_n^4} \left| \sum_{\nu=1}^{n} (\alpha_\nu + j\beta_\nu) e^{-j\varphi_k \nu} \right|^2, \tag{12.42}$$

where

$$j = \sqrt{-1}, \quad \varphi_k = \Omega_k T_n.$$

At "blind" velocity of the target ($\varphi_k = 0, \pm 2\pi, \ldots$)

$$E^2 = \frac{A^2}{\sigma_n^4} \left[\left(\sum_{\nu=1}^{n} \alpha_\nu\right)^2 + \left(\sum_{\nu=1}^{n} \beta_\nu\right)^2\right]. \tag{12.43}$$

If the velocity is optimum ($\varphi_k = \pm\pi, \pm 3\pi, \ldots$), then

$$E^2 = \frac{A^2}{\sigma_n^4} \left\{\left[\sum_{\nu=1}^{n} (-1)^{\nu+1} \cdot \alpha_\nu\right]^2 + \left[\sum_{\nu=1}^{n} (-1)^{\nu+1} \cdot \beta_\nu\right]^2\right\}. \tag{12.44}$$

In order to make it easy for the following analysis, we approximate the energetic spectra of the passive interferences, in distinction from Formula (12.32), by the function*

$$G(\omega) = \frac{\eta}{\Delta\omega^2 + 4(\omega - \omega_0)^2}, \tag{12.45}$$

where $\Delta\omega$ – width of the spectra at the level *0.5*;

$\eta$ – arbitrary constant.

The correlation function corresponding to this spectra is of the form

$$R_X(\tau)=R_Y(\tau)=\frac{\eta}{2\Delta\omega}\cdot e^{-\frac{\Delta\omega}{2}\cdot|\tau|}. \qquad (12.46)$$

Then the elements of the matrices $\|r_n\|$, determined by the Formulas (12.12) have the forms

$$r_{ij}=e^{-\frac{\Delta\omega}{2}|i-j|\cdot\tau_n}=r_0^{|i-j|},$$

where

$$r_0=e^{-\frac{\Delta\omega}{2}\tau_n}.$$

The optimum matrix

$$\|r_n\|^{-1}=\frac{1}{1-r_0^2}\begin{Vmatrix} 1 & -r_0 & 0 & \dots & 0 & 0 \\ -r_0 & 1+r_0^2 & -r_0 & \dots & 0 & 0 \\ 0 & -r_0 & 1+r_0^2 & \dots & 0 & 0 \\ \dots & \dots & \dots & \dots & \dots & \dots \\ \dots & \dots & \dots & \dots & \dots & \dots \\ \dots & \dots & \dots & \dots & \dots & \dots \\ 0 & 0 & 0 & \dots & 1+r_0^2 & -r_0 \\ 0 & 0 & 0 & \dots & -r_0 & 1 \end{Vmatrix}.$$

Utilizing the elements of this matrix, we find the values

$$a_1=\frac{x_1-r_0x_2}{1-r_0^2},\quad a_2=\frac{-r_0x_1+(1+r_0^2)x_2-r_0x_3}{1-r_0^2}\ \text{etc.} \qquad (12.47)$$

Similar formulas may be obtained also for $\beta_\nu$. Thereby, the signal/interference ratio at the output of the filter is

$$\frac{C_0}{2}=\frac{a^2}{2}\cdot\frac{n(1-2r_0\cos\varphi_\pi+r_0^2)-2r_0(r_0-\cos\varphi_\pi)}{1-r_0^2}. \qquad (12.48)$$

We shall analyze the case of the "blind" velocity. Taking into consideration Relationship (12.47) from Formulas (12.43) and (12.48) we obtain

$$E^2=\frac{A^2}{\sigma_n^4}\cdot\left[\left(\frac{x_1+(1-r_0)\cdot\sum_{\nu=2}^{n-1}x_\nu+x_n}{1+r_0}\right)^2+\left(\frac{y_1+(1-r_0)\cdot\sum_{\nu=2}^{n-1}y_\nu+y_n}{1+r_0}\right)^2\right],$$

$$\frac{C_0}{2}=\frac{n(1-r_0)+2r_0}{1+r_0}\cdot\frac{a^2}{2}.$$

In particular, if the selected values of the interference are not correlated ($r_0 \cong 0$). then,

$$E^2 = \frac{A^2}{\sigma_n^4}\left[\left(\sum_v x_v\right)^2 + \left(\sum_v y_v\right)^2\right],$$

i.e., the optimum receiver should create accumulations in two quadrature channels and from Envelope $E$. Thereby, the signal/interference ratio is proportional to the number of pulses in the packet

$$\frac{C_0}{2} = n \cdot \frac{a^2}{2}.$$

If the interferences are strongly correlated ($r_0 \cong 1$), then

$$E^2 = \frac{A^2}{\sigma_n^4}\left[\left(\frac{x_1 + x_n}{2}\right)^2 + \left(\frac{y_1 + y_n}{2}\right)^2\right],$$

i.e., the receiver should add up the quadratures consisting of only the first and the last pulses of the packet and form an envelope of these sums. The signal/interference ratio is $\frac{C_0}{2} = \frac{a^2}{2}$. In this way, at strongly correlated interferences and "blind" velocity, the accumulation does not lead to an increase of the observability, since both the signals as well as the interferences are increased to the same degree.

The last example shows graphically that the intraperiod treatment at strongly correlated interferences is actually very low in effectiveness. During the treatment of homogeneous pulses the coefficient of correlation between the selected values (within the boundaries of the duration of the pulses) is approximately equal to one while the Doppler's increment of phase strives toward zero. If, for example, the Doppler's frequency shift is equal to 6 khz and the duration of the pulse is 1 μsec, then $\varphi_A < \Omega_A \tau_u = 2.2°$. In this way, the treatment of one pulse can not change the signal/interference ratio.

Let us look now at the cases of optimum velocities. Substituting into Formulas (12.44) and (12.48) the values $\alpha_v$ and $\beta_v$, we obtain

$$E^2=\frac{A^2}{\sigma_n^4}\cdot\left[\left(\frac{x_1+(1+r_0)\cdot\sum_{\nu=2}^{n-1}(-1)^{\nu+1}\cdot x_\nu+(-1)^{n+1}\cdot x_n}{1-r_0}\right)^2+\right.$$
$$\left.+\left(\frac{y_1+(1+r_0)\cdot\sum_{\nu=2}^{n-1}(-1)^{\nu+1}y_\nu+(-1)^{n+1}\cdot y_n}{1-r_0}\right)^2\right],$$
$$\frac{C_0}{2}=\frac{n(1+r_0)-2r_0}{1-r_0}\cdot\frac{a^2}{2}.$$

At non-correlated selections of Interferences ($r\cong 0$)

$$E^2=\frac{A^2}{\sigma_n^4}\left[\left(\sum_{\nu=1}^{n}(-1)^{\nu+1}\cdot x_\nu\right)^2+\left(\sum_{\nu=1}^{n}(-1)^{\nu+1}\cdot y_\nu\right)^2\right],$$
$$\frac{C_0}{2}=n\cdot\frac{a^2}{2},$$

i.e., the receiver accomplishes accumulation taking into account the alternation of the phases of the signals.

If the interferences are strongly correlated ($r_0\cong 1$), then

$$E^2=\frac{A^2}{\sigma_n^4}\left[\left(\frac{x_1+2\cdot\sum_{\nu=2}^{n-1}(-1)^{\nu+1}x_\nu+(-1)^{n+1}x_n}{1-r_0}\right)^2+\right.$$
$$\left.+\left(\frac{y_1+2\cdot\sum_{\nu=2}^{n-1}(-1)^{\nu+1}y_\nu+(-1)^{n+1}y_n}{1-r_0}\right)^2\right].$$

For example, when $n=2$, and $n=3$ we will have correspondingly,

$$E_2^2=\frac{A^2}{\sigma_n^4}\left[\left(\frac{x_1-x_2}{1-r_0}\right)^2+\left(\frac{y_1-y_2}{1-r_0}\right)^2\right],$$
$$E_3^2=\frac{A^2}{\sigma_n^4}\left[\left(\frac{x_1-2x_2+x_3}{1-r_0}\right)^2+\left(\frac{y_1-2y_2+y_3}{1-r_0}\right)^2\right].$$

Consequently, the receiver accomplishes in two quadrature channels the computation of the signals of adjacent periods (intra period subtraction). Thereby, the signal/interference ratio at the output is

$$\frac{C_0}{2}=\frac{2(n-1)}{1-r_0}\cdot\frac{a^2}{2}$$

the larger, the larger is the value of $n$ and the closer is $r_0$ to unity.

The high effectiveness of the optimum receiver at strongly correlated interferences and optimum velocity of motion of the target

is explained that during these conditions there is room for the deduction of the interferences and the accumulation of the useful signals.

At present time, the intraperiod deduction, as one of the methods of selection of signals of moving targets is extensively used in practice. Therefore, in §12.4, we shall look at the problems of realization of this method.

3. Optimum Detection of Signals With Unknown Initial Phases and Doppler's Frequency Shift

The apportionment of the radial velocity (Doppler's frequency shift) is unknown in general cases, and therefore it is ordinarily assumed to be equal to some intervals. It is necessary, however, to notice that in a number of particular cases, the law of the distribution of the radial velocity may be exactly known, for example, in the case of the dispatcher RLS, when the velocity and the direction of the motion of the target are known. Besides this, the velocity of target is known in the autotracking of the target. In some systems, the information on the target may be obtained from other sources of non-radiolocational means.

In the case examined, the relationship of probabilities (12.36) must be also averaged for the unknown Doppler's frequency shift

$$\overline{\overline{\Lambda(x_1, y_1; \ldots; x_n, y_n)}} = \int \overline{\Lambda(\Omega_\Delta)} \cdot W(\Omega_\Delta)\, d\Omega_\Delta, \qquad (12.49)$$

where $W(\Omega_\Delta)$ – density of probability for the additional frequency shift of the signals.

The exact computation of Integral (12.49), by inspection does not seem to be possible. If we divide all the ranges of Doppler's frequency shift into a series of sufficiently small sub-ranges $k \cdot \Delta\Omega_\Delta$, $k = 1, 2, 3, \ldots, N$, then the approximate values of Integral (12.49) will be equal to

$$\overline{\overline{\Lambda(x_1, y_1; \ldots; x_n, y_n)}} = \sum_{k=1}^{N} \overline{\Lambda(k \cdot \Delta\Omega_\Delta)}\, W(k \cdot \Delta\Omega_\Delta).$$

The last expression may be rewritten as

$$\overline{\overline{\Lambda(x_1, y_1; \ldots; x_n, y_n)}} = \sum_{k=1}^{N} \exp\left[\ln \overline{\Lambda(k \cdot \Delta\Omega_A)}\right] \cdot W(k \cdot \Delta\Omega_A). \quad (12.50)$$

Substituting into Formula (12.50), the values $\ln \overline{\Lambda(x_1, y_1; \ldots; x_n, y_n)}$ from (12.36), we obtain

$$\overline{\overline{\Lambda(x_1, y_1; \ldots; x_n, y_n)}} = \sum_{k=1}^{N} \exp\left[-\frac{1}{2} C_0(k \cdot \Delta\Omega_A) + \ln I_0\left(E(k \cdot \Delta\Omega_A)\right)\right] \cdot W[k \cdot \Delta\Omega_A]. \quad (12.51)$$

From Fxpression (12.51), it follows that the optimum receiver detecting nonrandom signals with unknown initial phases and Doppler's frequency shifts should be composed of $N$ channels each one of which is built on its own Doppler's frequency and includes in it two coherent detectors, linear filters and functional converters. The voltage at the output of the kth channel is

$$\gamma_k = -\frac{1}{2} C_0(k \cdot \Delta\Omega_A) + \ln I_0[E(k \cdot \Delta\Omega_A)].$$

The cutput frequency of all the channels are joined exponentially with all $W(k \cdot \Delta\Omega_A)$ and the resulting voltage is checked according to the threshold.

Find the necessary number $N$, assuming that the distribution probability of the Doppler's frequency shifts is approximately according to some interval.

The voltage at the output of the kth channel $\gamma_k$ is a periodic function of the quantity $k \cdot \Delta\Omega_A T_n$, since the periodic functions $C_0[k \cdot \Delta\Omega_A \cdot T_n(\mu - \nu)]$ and $E[k \cdot \Delta\Omega_A \cdot T_n(\mu - \nu)]$, are determined by Expressions (12.31) and (12.41). Consequently, the necessary number of channels may be determined from the conditions

$$N \cdot \Delta\Omega_A \cdot T_n = 2\pi,$$

from which

$$N = \frac{2\pi}{\Delta\Omega_A \cdot T_n}.$$

For the determination of the maximum attainable frequency displacement $\Delta\Omega_D$ between channels, let us examine the structure of the spectra of the packets from $n$ coherent pulses with repetition period, $T_p$. It is known that the spectra of such a sequence of pulses have the form of combs. The width of a single "tooth" of the comb is

$$\Delta\Omega_r \cong \frac{2\pi}{nT_n}.$$

For this, in order that the useful voltage, even if in one of the summation channels of the receiver, should reach the value close to the maximum, the frequency displacement between the channels must be chosen such that $\Delta\Omega_k \leqslant \Delta\Omega_r$.

Assuming $\Delta\Omega_k = \Delta\Omega_r$, we find that $N = n$, i.e., the necessary number of channels should be equal to the number of pulses in the packet.

## §12.4 PHYSICAL BASIS OF THE DOPPLER'S METHODS OF THE SELECTION OF SIGNALS OF MOVING TARGETS (SDTz)

As it follows from the analysis indicated in §12.3, the optimum devices of detection are sufficiently complex and require apriori knowledge of the statistical properties of the interferences, which as a rule the observer does not assume in full measure. Therefore, in practice, sub-optimum devices are generally used, which are not that complex as the optimum and are relatively close in their characteristics to the optimum. In this paragraph, we shall conduct an analysis of the sub-optimum, the so-called coherent-pulse system SDTz, the basic principle of its action is the Doppler effect.

Let the transmitter RLS emit monochromatic oscillations

$$s(t) = A\cos(\omega_0 t + \varphi_0). \qquad (12.52)$$

Then from immobile objects, from one side and the objects moving, approximately in a straight line from the other side signals shall be received correspondingly

$$s_{\text{п}}(t) = A\cos\left[\omega_0\left(t - \frac{2R_0}{c}\right) + \varphi_0\right] =$$
$$= A\cos\left(\omega_0 t + \varphi_0 - \frac{2R_0}{c}\omega_0\right), \qquad (12.53)$$

$$s_{\text{д}}(t) = A\cos\left[\omega_0\left(t - \frac{2}{c}(R_0 - V_R \cdot t)\right) + \varphi_0\right] =$$
$$= A\cos\left[\omega_0\left(1 - \frac{2V_R}{c}\right)t + \frac{2R_0}{c}\omega_0 + \varphi_0\right], \qquad (12.54)$$

where $V_R$ – radial velocity of the moving object.

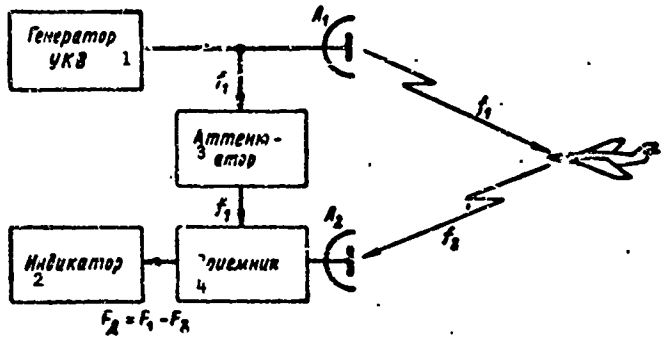


Fig. 12.10 Block diagram of the Doppler system SKTz with continuous radiation. 1) Generator UKV; 2) indicator; 3) attenuator; 4) receiver

In this way, the reflected oscillations as before, are monochromatic. But if in case of immobile objects, the reflected signal differs from the radiated only in the constant phase shift $\varphi_R = \frac{2R_0}{c}\omega_0$, then for the signals, reflected from the moving object besides the constant phase shift $\varphi_R$, it is characterized by an additional frequency displacement, $\Omega_{\text{д}} = \frac{2V_R}{c}\omega_0$. The frequency shift may be used for the detection of the signals of the moving target on the background of the reflections from immobile objects. This is realized most simply in the RLS of continuous radiation. Simultaneous with the signals reflected from the target oscillations of the transmitter also enter the receiver (Fig. 12.10). By the pulsations between the oscillations of the transmitter and reflected signals, the facts of the presence of the moving object and the determination of its radial velocity are fixed. But, as it is known, systems of continuous radiation does not give the possibility to determine directly the distance to the target. Therefore the

pulse type RLS is used.

Let the transmitter emit unlimited series of right-angled coherent radiopulses (Fig. 12.11a). The spectra of this series $S_n(f)$ is represented in Fig. 12.11b. Idealizing the operation conditions of the RLS, it will be assumed that the reflected signals are also infinite series of pulses. It is obvious that the spectra of the signals, reflected from the nonmoving objects will coincide with the spectra of the radiated oscillations. (Fig. 12.11b).

At the reflection from moving objects, the time function of the signal is deformed: it is stretched during withdrawal and compressed during approaching to the object. Consequently, the length and period of repetition are reduced at reflection from the approaching objects and increased at the reflection from the withdrawing objects. (Fig. 12.11v). Correspondingly, the spectra $S_D(f)$ of the signals reflected from the moving objects are deformed: compressed when the object is approaching (Fig. 12.11g). Every harmonic component of the spectra receives a displacement in frequency of $F_{дк}=\frac{2V_R}{c}f_к$ and a phase shift of $\Delta\varphi_к=\frac{2R_0}{c}\times 2\pi f_к$, where $f_k$ – component of the spectra. Since the displacement of each component of the spectra is proportional to its frequency, therefore all the frequency intervals of the spectra are proportionally varied by $\left(1+\frac{2V_R}{c}\right)$ times. The radial velocity of the target relative to the RLS is considered positive when it is approaching and negative when it is withdrawing from the target.

In principle, for the separation of the signals of the moving target one may use the variations of high frequency priming, the repetition frequencies of the pulses and the duration of the pulses. But, these variations are often very small and to detect them directly is extremely difficult. Practically, it is possible to use the method of pulsation to fix only the variations of the high frequency priming of

the pulses. For this, the signals reflected from moving objects are compared with the standard voltage, for example with the signals reflected from the immobile objects.

The phases of the high frequency priming pulses, reflected from moving object remain unchanged in relation to the beginning of each pulse, since the additional phase shift of the reflected components of the spectra during reflection are proportional to the frequencies of these components. But, their frequencies of repetition differ from the repetition frequencies of the pulses reflected from non-moving objects. Thanks to this during the addition of the signals of moving targets with the signals of the non-moving objects the amplitude of the summation oscillation will vary in correspondence with the phase difference of the totalled oscillation (Fig. 12.12). The variations in the amplitudes within the limits of the duration of the pulses are not great. For example, if the Doppler frequency $F_D$ = 6 *khz* and $\tau_I$ = 1 μsec then the phase difference of the signals reflected from moving and non-moving objects "creeping" in time is equal to the duration of the pulse $\varphi_д = 2\pi F_д \tau_и = 2{,}2°$. At such differences of the phases of the oscillations, the amplitudes in the limits of the duration of the pulse will be insignificant. But, the variations of the amplitudes of the pulses from period to period may be significant. Actually, the difference in phase of the signals being compared "creeping" toward the repetition period of the pulses $\varphi_д = 2\pi F_д T_п$.

In the simultaneous coherent-pulses of the SKTz systems the amplitude variations from period to period is precisely fixed by the repetition of the pulses.

All systems of selection of moving targets may be divided into systems with internal and external coherency.

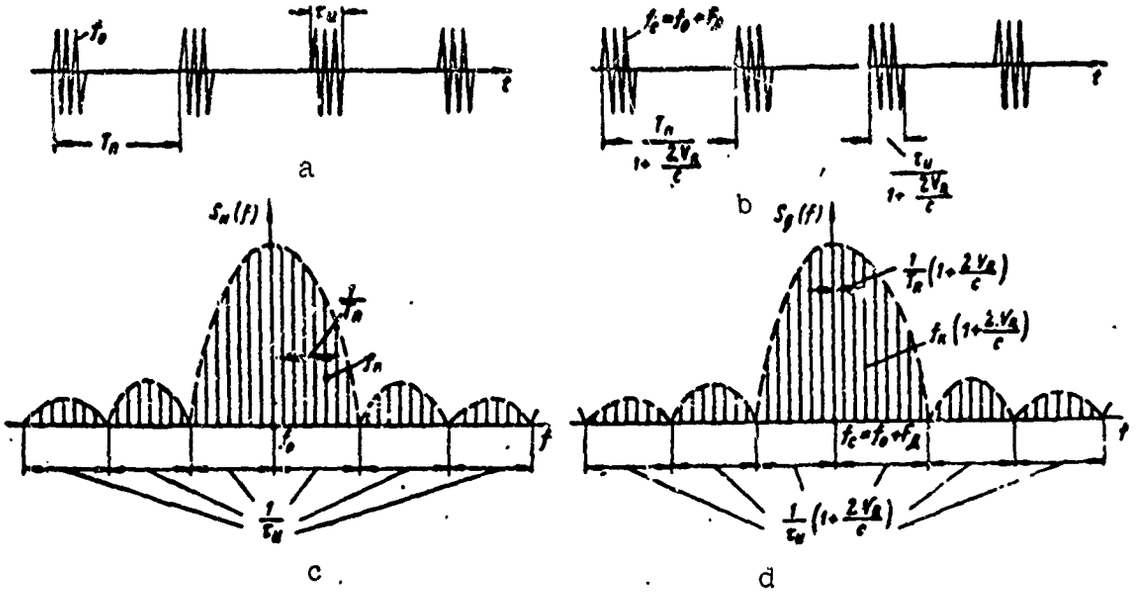


Fig. 12.11 Time and spectral characteristics of the pulses of the signals, reflected from nonmoving and moving point objects: a) infinite series of right-angled radiowaves; b) spectra of infinite series of right-angled radiowaves; c) series of pulses, reflected from moving targets; d) spectra of signals, reflected from moving targets.

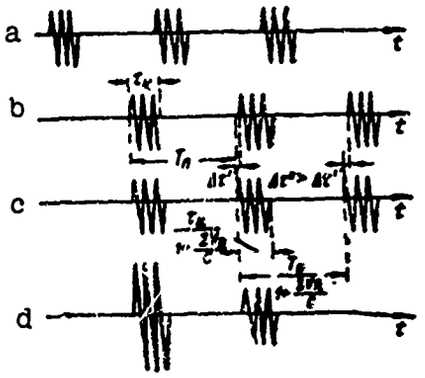


Fig. 12.12 Manifestation of Doppler's effect in pulse RLS. a) Oscillation of the transmitter; b) signals reflected from non-moving object; c) signals reflected from moving target; d) summation oscillation; $\Delta\tau$ is the displacement of the pulses of the moving target relative to the pulses of non-moving object.

1. Coherent-pulse Systems SDTz With Internal Coherency

In these systems the oscillations emitted from the same radiolocational station are used as the calibrating oscillations with which the reflected signals are compared.

Two methods of obtaining the calibrating oscillations may be pointed out depending on the principle of construction of the RLS. If the transmitting arrangement forms a generator with an internal excitation (triod, spanned klystron, and others) then the calibrating oscillations is obtained by the increase of the frequencies of the highly stabilized specified generator. An exemplary block diagram of a coherent-pulse RLS of the similar type in the centimeter wave range is represented in Fig. 12.13. The working principle of these SDTz systems will be understood from an examination of other systems described below. Here we will only note that klystron of low power is used for the amplification of oscillation of the specified generator to the level, providing normal operation of powerful output klystrons.

If a magnetron or other similar devices were used in the capacity of a high frequency generator of the transmitter then the obtaining of the calibrating oscillation is complicated in that in the time of reception of reflected signals, the transmitter does not generate. In this case, oscillations of a special, so-called coherent heterodyne is used as calibrating oscillations. These oscillations are rigidly synchronized in phase with the oscillations of the transmitter so that the difference in phase between these two oscillations are maintained constant in each period of the sending of pulses. That type of oscillation is referred to as coherent.

Coherent heterodyne may operate either in the system of continuous generation or in the pulse system. In the latter case the duration of the pulse should surpass the time of recovery of the reflected

signals from the maximum working range of the station.

According to the method of obtaining the coherent voltage and the reflected signals compared with it, the systems with internal coherency may be classified by the following features:

- the direction of the phasal synchronization (transmitter synchronizes the coherent heterodyne or vice versa);

- frequency of synchronization (at what frequency is synchronization accomplished - at the frequency of the transmitter or at the intermediate frequency);

- frequency of the comparison oscillation (at what frequency is the comparison of the reflected oscillation with the coherent conducted - at high frequency or at intermediate).

The phasing of the magnetron transmitter to be coherent to the generator is hardly expeditious since the latter should possess considerable power to contradict the requirement of guaranteeing high stabilization of frequency. The phasing of coherent heterodyne transmitter to the high frequency is linked with considerable difficulty since for the guaranteeing of high stability of frequency of the oscillation, the circuit of the heterodyne should have a high quality factor.

The most extensively used circuits in the centimeter wave are those in which the phasing of coherent heterodyne and the comparison of the coherent and reflected oscillations are conducted at the intermediate frequency. The block diagram of such a RLS and the oscillograms clarifying its operation are shown in Fig. 12.14.

For an analysis of the operation of the circuit, combine the initial reading of the time with the moment of the emission of the first probing pulse when the target is located at a distance $R_0$ from the radiolocational station.

Pulses of the synchronizer *(1)* trigger the modulator, rectifying

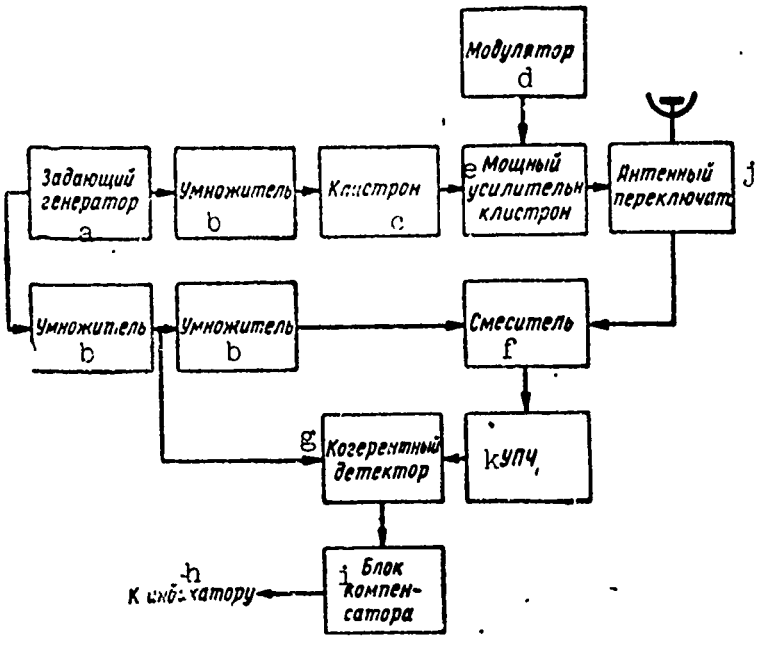


Fig. 12.13 Block diagram of coherent-pulse RLS with internal coherency a) Fixing generator; b) multiplier; c) klystron; d) modulator; e) power amplifier klystron;f) mixer; g) coherent detector; h) to indicator; i) block compensator; j) antenna switch; k) UPCh.

the megnetron generator. The high frequency pulses of the transmitter (3) enter through the antenna switch into the antenna. We record the pulses of the magnetron emitted in the *n*th period of repetition in the form

$$u_м = U_м \cdot \sin(\omega_м \cdot t_n - \varphi_{мn}), \quad 0 \leqslant t_n \leqslant \tau_и,$$

where $t_n$ – the current time, read from the beginning of the *n*th period of repetition.

$\varphi_{mn}$ – initial phase of the oscillation of the magnetron in the *n*th pulse.

Then the reflected signal at the input of the receiver in the *n*th period of repetition is

$$u_c = U_c \cdot \sin[\omega_м (t_n - \tau) - \varphi_{мn}], \quad \tau \leqslant t_n \leqslant \tau + \tau_и, \qquad (12.55)$$

where $\tau$ – time of diffusion of the signals from the radiolocational station to the target and back.

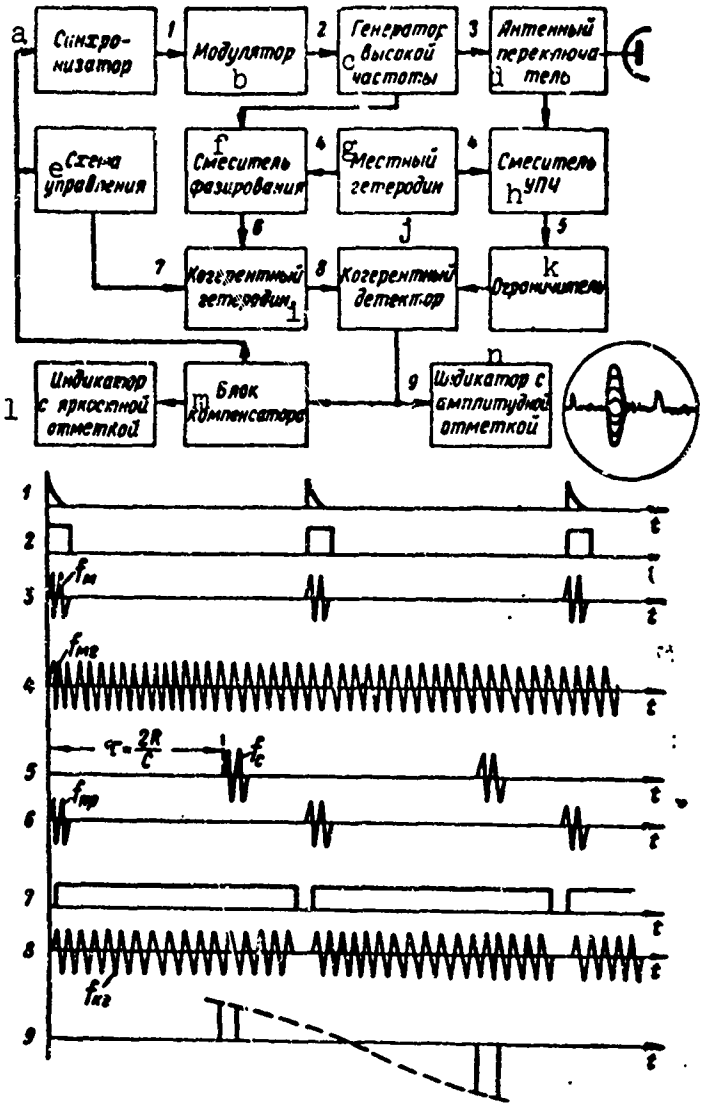


Fig. 12.14 Block diagram of coherent - pulse RLS with internal coherency and time diagrams, clarifying its operation. a) Synchronizer; b) modulator; c) generator of high frequency; d) antenna switch; e) rectifying circuit; f) mixer of phasing; g) local heterodyne; h) mixer UPCh; i) coherent heterodyne; j) coherent detector; k) limitor; l) indicator with luminous marks; m) block compensator; n) indicator with amplitude markings.

For non-moving objects $\tau=\frac{2R_0}{c}$ is a constant value. In the case of moving targets, the time is

$$\tau=\frac{2}{c}[R_0-V_R[t_n+(n-1)\cdot T_n]]. \qquad (12.56)$$

Substituting the value of τ from Formula (12.56) into Expression (12.55), we get $u_c=U_c\sin[\omega_c t_n+\Omega_д(n-1)T_n-\varphi_R-\varphi_{нн}];\ \tau\leqslant t_n\leqslant\tau+\tau_и$, (12.57)

where

$$\omega_c = \omega_м\left(1 + \frac{2V_R}{c}\right) = \omega_м + \Omega_д;$$

$$\Omega_д = \frac{2V_R}{c}\omega_м;$$

$$\varphi_R = \frac{2R_0}{c}\omega_м.$$

The oscillations of the heterodyne *(4)*, operating in the system of continuous generation, corresponding to the *n*th period of repetition of the pulses are

$$u_{мг} = U_{мг} \cdot \sin(\omega_{мг} t_n - \varphi_{мг\,n}),$$

where $\varphi_{мг\,n}$ – phase of the oscillations of the local heterodyne in the beginning of the *n*th period of repetition of the pulses.

As a result of the mixing of the frequency of the reflected signals and the heterodyne at the output of the mixer, (UPCh), signals of intermediate frequencies are formed *(5)*

$$u_{спр} = U_{спр} \cdot \sin[(\omega_c - \omega_{мг})\, t_n + \Omega_д (n-1)\, T_n - \varphi_R - \varphi_{мп} + \varphi_{мг\,n}],$$

$$\tau \leqslant t_n \leqslant \tau + \tau_и.$$

The pulses of the transmitter *(3)* enter also into the input of mixer of phasing, where they are transformed into pulses of intermediate frequencies *(6)*. These pulses are used for the phasal synchronization of coherent heterodynes operating at intermediate frequency. In every period of repetition, in the current time interval of equal duration of pulses, the coherent heterodynes are phase to the transmitter. In the process of phasing the frequency and phase of the oscillation of the coherent heterodyne is equal to the frequency and phase of the phasing pulse. After the completion of the process of phasing the frequency of the oscillations of the coherent heterodyne is restored to the natural frequency of the oscillation $\omega_{kg}$, but the phase of the oscillation of the coherent heterodyne $\varphi_{kg\,n}$ now is closely connected with the initial phase of the transmitter, $\varphi_{mn}$, even though

it is not equal to it. This route guarantees the coherence of the oscillations of the transmitter and the coherent heterodyne. Consequently, taking into account the phasing of the voltage of the coherent heterodyne may be written in the form

$$u_{кг} = U_{кг} \cdot \sin(\omega_{кг} t_n - \varphi_{кг\,n}), \quad t_y \leqslant t_n \leqslant T_n,$$

where $t_y$ – time from the moment of introduction of phasing pulses to the final establishment of oscillations of the natural frequency referred to as the time of the establishment of the process of phasing.

The length of the time of generation of the coherent heterodyne surpasses the time of the retardation of the reflected signals arriving from a maximum range. Before the arrival of every subsequent phasing pulse, for the restoration to the original conditions, the coherent heterodyne is locked by a rectifying circuit at 20-50 μsec. The pulse of the rectifying circuit *(7)* hits the coherent heterodyne somewhat later than the moment of the arrival of the phasing pulses *(6)*. In this case the phasing pulse remains overcome only by the voltage of the fluctuation of noises at the oscillational circuit of the heterodyne. Thanks to this, the expected phasing of the latter is insured.

The reflected signals and the coherent voltage *(8)* are fed to the coherent detector. For the compressing of the dynamic range of the reflected signals and also for the elimination of the parasitic modulation of the signals of non-moving objects as a result of the rotation of the antenna during a survey of the space, amplitude limitors are placed in front of the coherent detectors. The voltage at the output of the coherent detector (to the filter) is

$$u'_{сд} = u_{с\,пр} \cdot u_{кг} = U_{сд} \{\cos[(\omega_с - \omega_{мг} - \omega_{кг}) t_n + \\ + \Omega_д (n-1) \cdot T_п - \varphi_R - \varphi_\phi] + \cos[(\omega_с - \omega_{мг} + \omega_{кг}) t_n + \\ + \Omega_д (n-1) \cdot T_п - \varphi_R - \varphi'_\phi]\}, \quad \tau \leqslant t_n \leqslant \tau + \tau_и,$$

where

$$U_{\text{сд}} = \frac{1}{2} U_{\text{с пр}} U_{\text{кг}};$$

$$\varphi_{\phi} = \varphi_{\text{мп}} - \varphi_{\text{мг}\,n} - \varphi_{\text{кг}\,n};$$

$$\varphi'_{\phi} = \varphi_{\text{мп}} - \varphi_{\text{мг}\,n} + \varphi_{\text{кг}\,n}.$$

After the filter of low frequency there will be signals

$$u_{\text{сд}} = U_{\text{сд}} \cos[(\omega_{\text{с}} - \omega_{\text{мг}} - \omega_{\text{кг}}) t_n + \Omega_{\text{д}} (n-1) T_{\text{п}} - \varphi_R - \varphi_{\phi}],$$
$$\tau \leqslant t_n \leqslant \tau + \tau_{\text{и}}.$$

At the reflection from the non-moving objects $\Omega_{\text{д}} = 0$, $\omega_{\text{с}} = \omega_{\text{м}}$ and the signal at the output of the coherent detector has the form

$$u_{\text{сд}} = U_{\text{сд}} \cdot \cos[(\omega_{\text{м}} - \omega_{\text{мг}} - \omega_{\text{кг}}) t_n - \varphi_R - \varphi_{\phi}]. \qquad (12.58)$$

If the frequency of the magnetron, local and coherent heterodyne are absolutely stable, then the quantity $\varphi_f$, referred to as the parameter of phasing, will remain constant from period to period of repetition of pulses. Then, as can be seen from Expression (12.58), at the absence of disarrangement ($\Delta\omega_{\text{кг}} = \omega_{\text{м}} - \omega_{\text{мг}} - \omega_{\text{кг}} = \omega_{\phi} - \omega_{\text{кг}} = 0$) videosignals of non-moving objects will have constant amplitude, determined by the distance to the object $R_0$ and the parameter of phasing $\varphi_f$.

In the presence of moving targets, the envelope of videopulses *(9)* varies according to the sinusoidal law with frequencies of Doppler's pulsation

$$u_{\text{сд}} = U_{\text{сд}} \cdot \cos[\Omega_{\text{д}} t_n + \Omega_{\text{д}} (n-1) T_{\text{п}} - \varphi_{\text{к}} - \varphi_{\phi}]. \qquad (12.59)$$

The variation of the amplitude of the videopulses can take place from period to period as well as within the limits of one pulse. If now the output voltage of the coherent detector fall on the indicator with amplitude markings, then the markings of the moving targets will appear crosshatched while at the same time the markings of the non-moving objects will not have such hatchings (see Fig. 12.14). This difference in form of the markings is used by the operator for the separation of signals of moving targets from the background of re-

flections from nonmoving objects. These SDTz systems are known as the comparing systems.

Compensation of the signals of nonmoving objects. On the indicators with luminous markings, the varying as well as the amplitude unchanged videopulses give markings of almost the same brightness. Consequently, if the videopulses from the output of the coherent detector fall directly on the indicator with the luminous markings, then to distinguish the moving targets from the nonmoving objects will be extremely difficult. Therefore in the RLS with indicators of the luminous type, a method of compensation of the signals of the moving and the slowly moving objects (compensation system SDTz) is used. The videopulses from the output of the coherent detector enter the input of the compensating device in which via the intraperiod subtraction of signals the suppression of the pulses with unchanged amplitude is accomplished and also the isolation of the pulses whose amplitude changes from period to period.

The compensating device may be made of linear delays or electrostatic memory tubes. Let us examine the operation of the compensating device, made of ultrasonic linear delays (UZL) (Fig. 12.15). For the accomplishment of intraperiodic subtraction in the compensating device the signals enter the two channels directly and "delayed," and then the two subtraction circuits are compared producing the difference signal. In the delayed channel an ultrasonic line is included accomplishing the delay of the pulses for the period of repetition. Therefore, the series of pulses at the output of the direct and "delayed" channels show a displacement of one relative to the other by a period of repetition.

For the undistorted transmission of videopulses of the receiver through the ultrasonic line of delay, the latter is transformed into

high frequency pulses with a maintained rule of the variation of the envelope. This transformation is accomplished by auxiliary modulators made up of generator of oscillation of frequency $f_1$ and a modulating amplifier.

We shall find the voltage at the output of the compensating device

$$u_к = K_0 [u_{сд(n-1)} - u_{сд\,n}],$$

where $K_0$ – amplification of the direct and delayed channels; $u_{сд\,n}$ and $u_{сд(n-1)}$ – voltage of the two adjacent videopulses at the output of the receiver.

On the basis of Expression (12.59)

$$u_{сд(n-1)} = U_{сд} \cos [\Omega_д t_n + \Omega_д (n-1) T_п - \varphi],$$
$$u_{сд\,n} = U_{сд} \cos [\Omega_д t_n + \Omega_д n T_п - \varphi].$$

Taking $K_0 = 1$, we find

$$u_к = 2U_{сд} \sin \left(\frac{\Omega_д T_п}{2}\right) \cdot \sin \left[\Omega_д t_n + \Omega_д \cdot T_п \left(n - \frac{1}{2}\right) - \varphi\right]. \quad (12.60)$$

From Formula (12.60), it is seen that for the nonmoving objects the difference signal is equal to zero, at the same time for the moving targets, it differs from zero. This signal is also used for getting the luminous markings of the moving object on the screen of the indicator.

The pulses at the output of the subtraction circuit may be positive as well as negative. For the obtaining of luminous markings on the screen of the indicator, the bipolar pulses are transformed into unipolar with the aid of the full-wave videodetector.

For the guaranteeing of good compensation signals of nonmoving objects, it is necessary to provide strict equality between the total time of delay of the signals $T_{zad}$ and the period of repetition $T_p$. The variation of the period of repetition or the time of delay leads to the relative displacement of the signals being compared and the

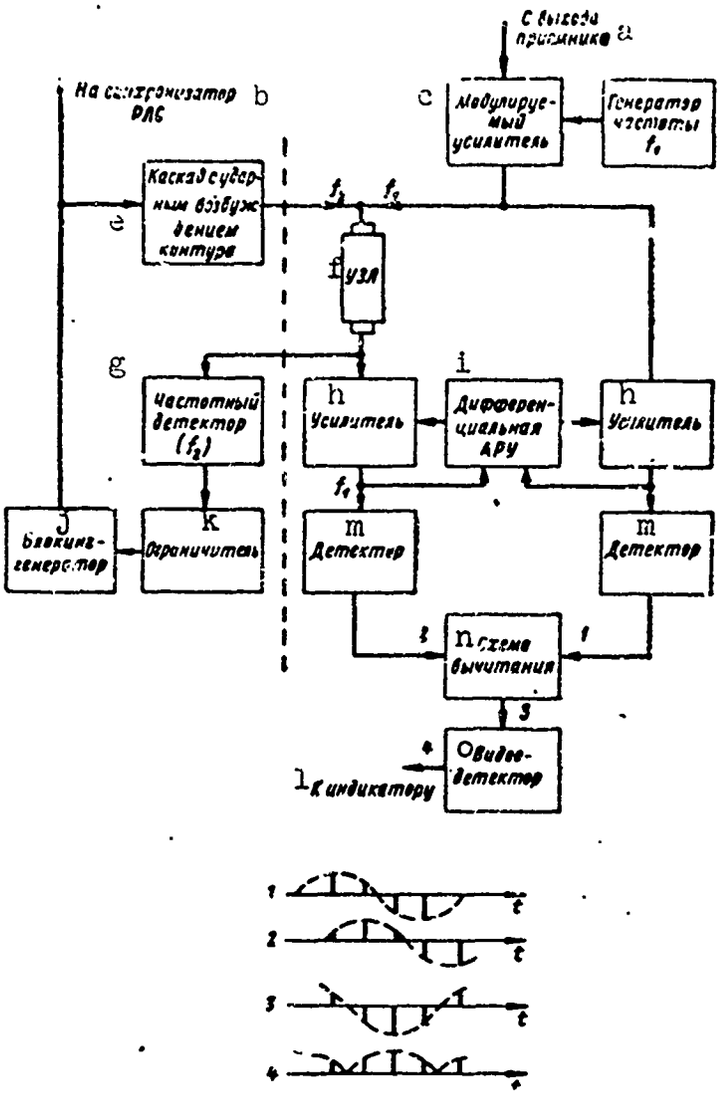


Fig. 12.15 Block diagram of the compensating device and time diagram showing its operation. a) From the output of the receiver; b) to the synchronizer RLS; c) modulated amplifier; d) generator of frequency $f_1$; e) cascade with shock excitation circuit; f) UZL; g) frequency detector ($f_2$); i) differential ARU; j) blocking generator; k) limitor; l) to the indicator; m) detector; n) subtraction circuit; o) video detector.

appearance of uncompensated residues.

In the process of the operation, the time of delay may be varied, since the velocity of the propagation of the ultrasonic wave in the sound transmitter is dependent on the temperature of the surrounding medium. One of the methods of maintaining equality between the time of delay and the period of repetition is the method of the formation of

synchronizing pulse stations with the aid of the same UZL, which is used for the delay of output signals of the receiver. For this purpose, in the compensator there are synchronization circuits (Fig. 12.15), including cascades with shock excitation circuits at frequency $f_2$, frequency detector, limitor and blocking generator. The frequency $f_2$ differs somewhat (as far as the passband of the UZL permits) from the priming frequency of the signals of the pulses, $f_1$.

The operation of the synchronization circuit is included in the following.

The blocking generator has characteristic generation period, somewhat surpassing the time of delay in UZL. The pulses of the generator hit the cascade with the shock excitation circuit. From the output of this cascade, radiowaves with carrying frequency $f_2$ enter the UZL, where they are delayed by the time $T_{zad} = T_p$, detected by the frequency detector and after limitation hit the blocking generator anew for the synchronization of the latter. The frequency detector is tuned in such a way that synchronized pulses with frequency $f_2$ are produced and the pulses of the compensation channel whose priming frequency $f_1 \neq f_2$ are suppressed. Thanks to this the possibility of the untimely triggering of the blocking generator by the reflected signals is excluded. The pulses of the blocking generator trigger the synchronizer of the transmitter and the circuit of rectifying the coherent heterodyne.

Notice, besides the frequency principle of the division of channels and compensation examined above, amplitude selection of the signals may also be used.

The effectiveness of the suppression of the signals of nonmoving objects depends to a large degree also on the identity of the frequency character of the direct and delayed channels and the constancy of their coefficients of amplification. The equality of the coeffi-

cients of amplification is provided with the aid of the differential APU, automatically regulating the magnitude of the voltage of displacement at the grid of the amplifier tubes in such a way that at the absence of moving targets the voltage at the output of the circuit of subtraction is equal to zero.

Let us examine briefly the operation of the compensation device achieved by electrostatic memory tubes. The electric signals from the output of the receiver are recorded at the target of the electrostatic memory tube and maintained for a duration of time equal to the period of repetition of the pulses. In the following period of repetition, the reflected signals are taken into acccunt and compared by the circuit of subtraction with the signals being received. In this arrangement, the operation of the electrostatic memory tube performs only the function of recording.

More complete electrostatic memory tubes with barrier grids which may accomplish at the same time the recording and compensation.

At a certain cycle, let the target of the electrostatic memory tube with barrier grids composed of potential relays record the output signals of the receiver $U_1$. During the second cycle of recording, when the magnitude of the signals $U_2$ at the output of the receiver will be different, the potential relays correspond to the new signals. At the repeated recording in every point of the target there results an overcharge from the old potential to the new. The current of the overcharge of the target is proportional to the difference between the voltages $U_1-U_2$ of the output signals in the first and second cycles of recording. Flowing past the resisting charge in the target of the collector, this current is composed of a voltage proportional to the difference of the output signals in the adjacent cycles of recording.

In the operation of the compensating device of the electrostatic

memory tube, the equality $T_{zad} = T_p$ is maintained all the time automatically and any special measure of equalizing $T_{zad} = T_p$ is not required.

Let us examine the operation of the block compensator originated from the spectral representation.

As it has already been noticed that during the reflection from nonmoving objects, the videopulses at the output of the coherent detector have constant amplitude. It may be shown that the amplitude spectra of unlimited series of right-angled unmodulated videopulses with amplitude $U_0$, duration $\tau_i$ and period of repetition $T_p$, have the form (Fig. 12.16 a)

$$S(\omega) = A_0 \cdot \sum_{k=0}^{\infty} \frac{\sin \frac{k\omega\tau_u}{2}}{\frac{k\omega\tau_u}{2}}, \qquad (12.61)$$

where

$$A_0 = \frac{2U_0\tau_u}{T_u};$$

$$\omega = \frac{2\pi}{T_u}.$$

In this way, the spectra of the videopulses of nonmoving objects consist of constant components and harmonic frequencies of repetition (Fig. 12.16 b).

At the reflection from the moving targets the videopulses at the output of the coherent detector shows modulated frequencies of Doppler pulsation $\Omega_d$ (Fig. 12.16 c). The rule of the variation of the envelope of the amplitude of the pulses may be written in the form $U = U_0 \cdot \cos \Omega_d t$.

The amplitude spectra in this case will be

$$S(\omega) = \frac{A_0}{2} \cdot \sum_{k=0}^{\infty} \left\{ \frac{\sin\left[(k\omega + \Omega_d)\frac{\tau_u}{2}\right]}{(k\omega + \Omega_d)\cdot\frac{\tau_u}{2}} + \frac{\sin\left[(k\omega - \Omega_d)\cdot\frac{\tau_u}{2}\right]}{(k\omega - \Omega_d)\cdot\frac{\tau_u}{2}} \right\}. \qquad (12.62)$$

Consequently, the spectra of the videopulses of the moving targets is composed of the component Doppler's frequency $\Omega_d$ and the lateral fre-

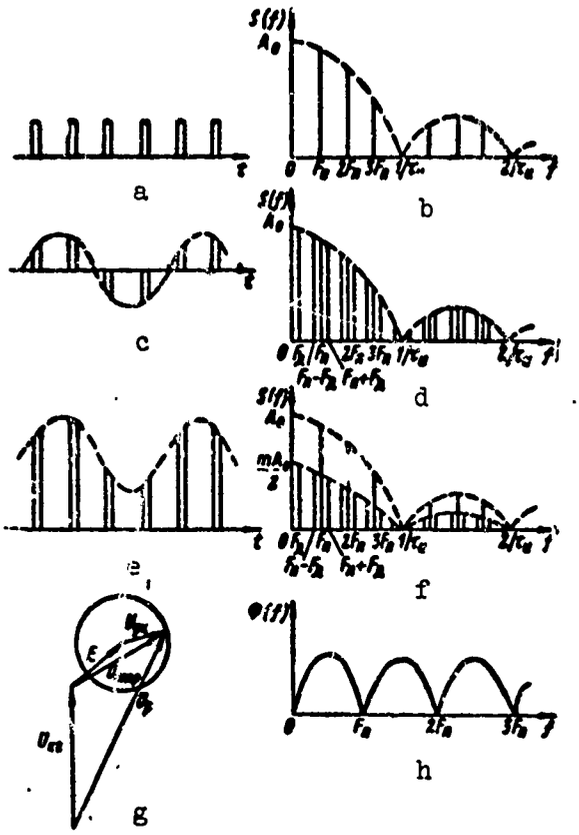

Fig. 12.16. Reflected signals of nonmoving objects and moving targets and the spectra corresponding to them. a) Pulses of the nonmoving objects at the output of the phase detector; b) spectra of the series of pulses a; c) pulses of the moving targets at the output of the phase detector; d) spectra of the series of pulses c; e) pulses of the moving targets, located on the background of local subjects, at the output of the phase detector; f) spectra of the series of pulses e; g) vector diagram of the signals entering the phase detector: $U_{kg}$ – oscillation of the coherent heterodyne; $E$ – signal, reflected from the local subjects; $U_{dtg}$ – signal reflected from moving target; $U_{otr}$ – summation reflected signal; $U_r$ – resultant signal; z – frequency characteristics of the compensating device. h) oscillation of the coherent heterodyne.

quencies of modulation $k\omega-\dot{\Omega}_a$ and $k\omega+\dot{\Omega}_a$ (Fig. 12.16 d).

If the moving target is located on the background of local subjects (Fig. 12.16 g), then under the condition, $E \gg U_{dt}$ the videopulses at the output of the coherent detector will be already not bipolar but unipolar (Fig. 12.16 e). The rule of variation of the envelope of the amplitude of the videopulses has the form

$$U = U_0(1 + m \cdot \sin \Omega_a t).$$

The amplitude spectra of this series is (Fig. 12.16 f)

$$S(\omega)=A_0\cdot\sum_{k=0}^{\infty}\frac{\sin\frac{k\omega\tau_{\text{и}}}{2}}{\frac{k\omega\tau_{\text{и}}}{2}}+$$

$$+\frac{mA_0}{2}\sum_{k=0}^{\infty}\left\{\frac{\sin\left[(k\omega+\Omega_{\text{д}})\cdot\frac{\tau_{\text{и}}}{2}\right]}{(k\omega+\Omega_{\text{д}})\frac{\tau_{\text{и}}}{2}}+\frac{\sin\left[(k\omega-\Omega_{\text{д}})\frac{\tau_{\text{и}}}{2}\right]}{(k\omega-\Omega_{\text{д}})\frac{\tau_{\text{и}}}{2}}\right\}. \qquad (12.63)$$

From a comparison of Expressions (12.61), (12.62) and (12.63) it can be seen that the spectral component of the signals of moving targets and non-moving objects are located at different points on the axis of frequency. Consequently, for the separation of the signals of the moving targets it is necessary to place after the coherent detector a filter which would suppress the components of the spectra, short repetition frequencies and let pass all remaining frequencies. The circuit of intraperiod subtraction does have such a filter.

Let us find the frequency characteristics of the circuit of intraperiod subtraction

$$\Phi(j\omega)=\frac{\dot{U}_{\text{вых}}}{\dot{U}_{\text{вх}}}=\frac{\dot{U}_{\text{вх}}-\dot{U}_{\text{вх}}\Phi_1(j\omega)}{\dot{U}_{\text{вх}}}=1-\Phi_1(j\omega),$$

where $\dot{U}_{\text{вх}}$ and $\dot{U}_{\text{вых}}$ – complex amplitudes at correspondingly the input and the output of the subtraction circuit. $\Phi_1(j\omega)$ – transmission function of the delay channel.

The delay of the pulses is accomplished at the period of repetition. Consequently, one may write $\Phi_1(j\omega)=e^{-j\omega T_{\text{п}}}$. Then

$$\Phi(j\omega)=1-e^{-j\omega T_{\text{п}}}$$

and

$$\Phi(\omega)=2\sin(\pi fT_{\text{п}}).$$

As one can see from Fig. 12.16 m, the frequency characteristics of the compensating device are such that the component of the spectra, short frequency of repetition are suppressed.

Some types of sources of passive interferences, those, like the

rain clouds, metallized strips, are disturbed by the action of the wind as a single object, i.e., they have regular component velocities. Thereby, the videopulses of interference will be modulated by the frequency of Doppler's pulsation, as a result of which at the output of the compensating device there will be room for the uncompensated residual interferences. For the separation of uncompensated residues, the compensation of the moving sources of interferences is carried out. For this with the aid of the so-called wind compensation device the frequency of the coherent detector is changed as much as the frequency of the signal reflected from the moving sources of interferences is changed. As a result of this, the phase of the interference relative to the coherent oscillation will remain constant from period to period and the quality of the compensation of interference is improved.

2. Coherent - Pulse Systems SDTz With External Coherency

In the SDTz systems with external coherency in the capacity of calibrating oscillation, signals, reflected from nonmoving objects located at the same distance from the RLS as the moving target, are used.

If it is assumed that the relative positions of the elementary reflectors of the nonmoving object remain unchanged with the current time, then the signals of a multitude of reflectors would have characters of a regular function of time, and the nonmoving objects themselves would be ideal sources of calibrating oscillation. Actually, this signal fluctuates, such that the effectiveness of the selection of the signals of the moving objects is lowered. The lower the velocity of fluctuation of the signals of the multitude of reflectors in comparison with $\frac{1}{T_n}$, the higher will be the quality of the selection of signals of moving targets.

Signal, reflected from moving point target, is described by Expression (12.57). As a result of the addition of the signals, those reflected from the sources of passive Interferences (12.7) and the moving targets (see Fig. 12.17 a), there is a pulsation at the input of the receiver. If these pulsations are fed to the linear detector of envelopes, then, the voltage at the output of the detector in the nth period of repetition will be

$$U_{\text{д}} = \sqrt{E^2 + U_c^2 + 2EU_c \cos\psi}, \qquad (12.64)$$

where $\psi = \Omega_{\text{д}} t_n + \dot{\Omega}_{\text{д}}(n-1)T_n - \varphi_R - \varphi_{\text{мп}} + \varphi$ – angle between the vectors of the interferences and the useful signals; $E$ and $\varphi$ – envelope and the phase of the interferences.

From Formula (12.64), it follows that at the output of the detector, the amplitude of the videopulses of the moving targets located on the background of local subjects, varies with the frequency of the Doppler pulsations. (See Fig. 12.17 b).

The simplest way using the SDTz system with external coherency is the observation of the characters of the pulses on the indicator with amplitude markings. If the moving target is located on the background of local subjects, then the top of the pulses appears to be cross-hatched (Fig. 12.17 c), which is also shown by moving targets.

More effective indication is provided by the use of compensating devices similar to those in the systems of SDTz with internal coherency. The compensation of the signals of nonmoving objects in the SDTz system with external coherency is illustrated in Fig. 12.17 d, in which the spectra of the infinite series of videopulses, modulated by the frequency of the Doppler pulsation, and the frequency characteristics of the compensating device are shown.

In the SDTz system with external coherency, as a rule, receiver with logarithmic amplitude characteristics is used. As shown in

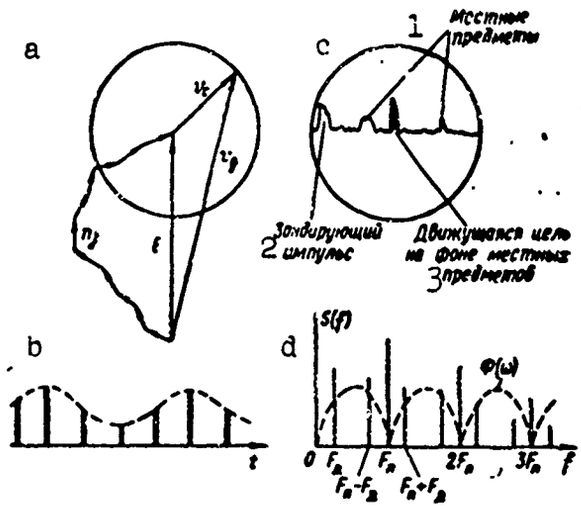


Fig. 12.17 Working principle of the coherent-pulse SDTz system with external coherency. a) Vector diagram of signals at the input of the coherent detector; b) series of pulses at the output of the detector of envelope; c) image of signals of nonmoving objects and moving targets on the screen of the indicator with amplitude markings; d) spectra of series of pulses b and the frequency characteristics of the compensating device. 1) Local subjects; 2) moving targets on the background of local subjects; 3) probing pulses.

Chapter 11, the logarithmic characteristics, compressing the fluctuation of the input signals, permit the maintenance of the amplitude difference at the output of the receiver, which is principally necessary for the operation of the SDTz system with external coherency examined above.

3. Selection of the Moving Target During the Motion of the Radiolocational Station

If the radiolocational station is found in motion, then the nonmoving objects relative to it in the general cases, do not exist altogether and the problem of the selection of useful signals have, in this case some peculiarities.

Let us examine, for example, airplane radiolocational station with SDTz. From Fig. 12.18, one can see that the radial velocity $V_R$ of certain nonmoving object $O$ on the Earth's surface depends on the course angle $\alpha$ as well as on the location angle $\beta$.

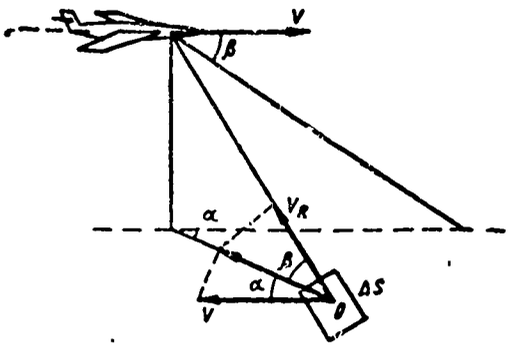


Fig. 12.18. The calculation of radial velocity of the approach of the airplane and a portion of the Earth's surface.

For the suppression of the signals of the object 0, compensation of the natural motion of the RLS is necessary. The compensati. e motion is accomplished in the same way as the compensation of the wind, -- changing the frequencies of the oscillations of the coherent heterodyne to an amount equal to the Doppler's frequency shift of the reflected signals

$$F_{\text{д}} = \frac{2V \cos\alpha \cos\beta}{\lambda}.$$

The accurate compensation of the natural motion of the RLS may be accomplished for any point sequentially of the exposed surface. If we consider however the aggregate of elementary reflectors within the limits of the permitted area $\Delta S$, the radial velocities of whic are different, then to accomplish compen sation of all these reflectors does not seem possible. As a result of this, complete suppression of the signals reflected from the Earth's surface is never attained.

In the radiolocational stations established on moving objects, in principle SDTz systems with internal coherency as well as SDTz systems with external coherency may be used.

The use of the SDTz system with internal coherency on moving objects is linked with considerable difficulties. These difficulties are produced in the first place, by the necessity to have devices on the

airplane to compensate its own velocity. Since the radial velocities of the elements of the Earth's surface depends not only on the course angle but also on the angle of the location of the target, therefore the corresponding device of compensation becomes complicated. In the second place, for the stabilization of the operation of the high frequency generator of the SDTz system with internal coherency presents rigid requirements, which are extremely difficult to meet on an airplane.

One may use more successfully the SDTz system with external coherency on moving objects. In these systems, the requirements for the stability of the operation of the high frequency generators are less rigid. There is no coherent heterodyne and it is not required to compensate for its own velocity. But, the SDTz systems with external coherency and compensation of signals of non-moving objects have one serious shortcoming. If the moving target is found outside of the background of disturbing reflections or this background is small then there will not be any pulsation. Thereby, all pulses at the output of the detector will have constant amplitude and the output signal of the compensating device becomes equal to zero. Therefore it is necessary that measures are provided permitting the release from the above mentioned shortcoming of the system with external coherency.

## § 12.5. EFFECTIVENESS OF THE COHERENT-PULSE SYSTEM SDTz

The fluctuation of passive interferences leads to the appearance of uncompensated residues at the output of the compensating device, which worsens the quality of the selection of signals of the moving targets. The uncompensated residues produced from each one of the reasons enumerated earlier, are statistically independent. Therefore, the resultant power of the fluctuation is equal to the sum of the

powers of fluctuations caused by each of the reasons individually.

The degree of suppression of interference in compensating devices is well characterized by the so-called coefficient of suppression, which is understood to be the ratio of the powers at the input and output circuits of the intraperiod subtraction.

Let us evaluate the magnitude of the uncompensated residue, caused by every one of the reasons individually, in the example of the system SDTz with external coherency.

1. The Evaluation of the Magnitude of Uncompensated Residue Taking Into Account the Motion of Elementary Reflectors

Due to the motion of the elementary reflectors, the series of pulses at the output of the detector of envelope change in amplitude in a random manner. The normalized correlation function of such series of pulses may be represented in the form of the product

$$r(\tau)=r(\delta+\nu T_n)=r_{or}(\nu T_n)\cdot r_{\phi}(\delta), \qquad (12.65)$$

where $\tau=\delta+\nu T_n$ – argument, represented in the form of a sum of discrete parts $\nu T_n$, $\nu=0, 1, 2, \ldots$ and the continuous parts $\delta(0\leqslant\delta\leqslant T_n)$;

$r_{or}(\nu T_n)$ – normalized correlation function of the envelope of the series of pulses determined for the discreet values of the argument, $\nu T_n$;

$r_{\phi}(\delta)=\dfrac{\int_{-\infty}^{\infty}s(t)s(t+\delta)dt}{\int_{-\infty}^{\infty}s^2(t)dt}$ – normalized correlation function, determined by the form of the pulses.

Examine the coefficient of suppression of interferences. The constant component of the voltage at the output of the detector may be excluded from the analysis since it does not pass through the compensating device. Therefore, it remains only to investigate the passage of the voltage of fluctuation.

Let us denote the voltage of fluctuation at the input of the compensating device by $U_{вх}(t)$. Then, the voltage at the output is $U_{вых}(t)=U_{вх}(t)-U_{вх}(t-T_{зад})$. The correlation function of the output voltage

is

$$R_{вых}(\tau)=\overline{U_{вых}(t)\cdot U_{вых}(t+\tau)}=2R_{вх}(\tau)-$$
$$-R_{вх}(\tau-T_{зад})-R_{вх}(\tau+T_{зад}), \qquad (12.66)$$

where $R_{вх}(\tau)=\overline{U_{вх}(t)U_{вх}(t+\tau)}$.

Assuming in Formula (12.66) $\tau = 0$, we find the average power of the fluctuation at the output of the compensating device is

$$\overline{U^2_{вых}}=2[R_{вх}(0)-R_{вх}(T_{зад})].$$

since

$$R_{вх}(T_{зад})=r_{вх}(T_{зад})\cdot R_{вх}(0),$$

where $r_{вх}(T_{зад})$ – coefficient of correlation of the input voltage then

$$\overline{U^2_{вых}}=2[1-r_{вх}(T_{зад})]\cdot\overline{U^2_{вх}}.$$

The coefficient of suppression of interferences is

$$L=\frac{\overline{U^2_{вх}}}{\overline{U^2_{вых}}}=\frac{0{,}5}{1-r_{вх}(T_{зад})}.$$

Consequently, at strongly correlated interferences $[r_{вх}(T_{зад})\cong 1]$ $L\to\infty$; at weak correlation $[r_{вх}(T_{зад})\cong 0]$ suppression is absent.

Substituting the value $r_{vkh}$ from Formula (12.65) in to the expression for coefficient of suppression, we get

$$L=\frac{0{,}5}{1-r_{от}(T_п)\cdot r_ф(\delta)}. \qquad (12.67)$$

If the period of the sequence of the pulses is exactly equal to the time of delay in the line ($T_п=T_{зад}$), then in the last formula, it is necessary, obviously to set $\delta=0$, $r_ф(\delta)=1$ and then

$$L=\frac{0{,}5}{1-r_{от}(T_п)}. \qquad (12.68)$$

The energetic spectra of the fluctuation of the interferences at the output of the detector of envelopes is determined by Expression (12.2). The correlation function corresponding to this spectra is

$$r_{от}(\tau)=\exp\left[-\left(\frac{\pi f_0\tau}{\gamma}\right)^2\right].$$

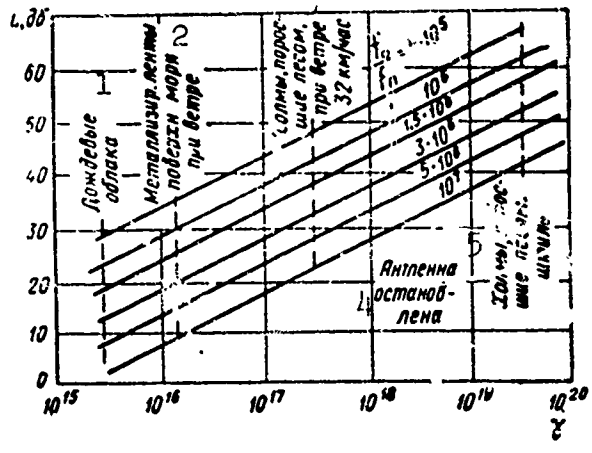


Fig. 12.19. Dependence of the coefficient of suppression on the ratio $f_0/F_p$ for various types of multitude of reflectors. 1) Rain clouds; 2) metallized strips, surface of the sea in the wind; 3) hills with plant growth in the wind 32/km/hr; 4) antenna stopped; 5) hills with plant growth, calm.

Consequently,

$$L = \frac{0{,}5}{1 - \exp\left[-\left(\frac{\pi f_0 T_n}{\gamma}\right)^2\right]}. \qquad (12.69)$$

From Eq. (12.69), one can see that the coefficient of suppression decreases with the shortening of the wave length and the decrease of the frequency of repetition of the pulses.

In correspondence with Formula (12.69) curves of the dependence of the coefficient of suppression on the ratio $\frac{f_0}{F_n}$ for various objects characterized by the parameter γ are constructed in Fig. 12.19. From the curves, it follows, in particular that in the centimeter wave range $\left[\frac{f_0}{F_n} \approx (0{,}5 \div 1)\,10^7\right]$ the coefficient of suppression of the reflections from moving objects hardly ever gets to be larger than 10 db. It is estimated experimentally that in many cases the reflection from the rain in the installations of the SDTz almost is not weakened.

2. Evaluation of the Uncompensated Residue Caused by the Rotation of the Antenna

At reflection from isolated nonmoving objects, the envelope of the signals at the input of the receiver will vary in correspondence

with the diagrams of directionality of the antenna in power (Fig. 12.20 a). The maximum variation of magnitude of the reflected signal per period of repetition will be in points where the diagrams of directionality have the largest slope.

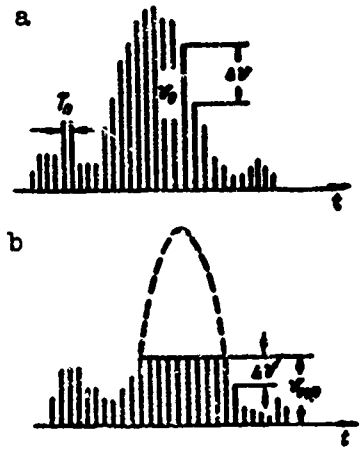


Fig. 12.20. Variation of signals reflected from isolated objects during the rotation of the antenna. a) At the output of the linear receiver; b) at the output of receiver with limits.

If we approximate the diagrams of directionality in power with the Gaussian curve

$$U(\alpha)=U_0 e^{-2,8\left(\frac{\alpha}{\theta}\right)^2},$$

where $\theta$ – width of the diagram at Level 0.5, then the abscissa of the point of the largest slope may be found from condition

$$\frac{d^2U(\alpha)}{d\alpha^2}=$$

$$=-\frac{5,6}{\theta^2}U_0 e^{-2,8\left(\frac{\alpha}{\theta}\right)^2}\cdot\left[1-\frac{5,6}{\theta^2}\right]=0,$$

from which we get

$$|\alpha|_{MK}=\frac{\theta}{\sqrt{5,6}}.$$

We find the tangent of the angle of inclination tangent to the curve at the point $\alpha=|\alpha|_{MK}$

$$\left|\frac{dU(\alpha)}{d\alpha}\right|_{\alpha=|\alpha|_{MK}}=\frac{5,6\alpha}{\theta^2}U_0\cdot e^{-2,8\left(\frac{\alpha}{\theta}\right)^2}\Big|_{\alpha=|\alpha|_{MK}}=\frac{1,4}{\theta}U_0.$$

Then the quantity,

$$\frac{\Delta U}{U_0} = \frac{b}{n_0}\left|\frac{dU(\alpha)}{d\alpha}\right|_{\alpha=|\alpha|_{MX}} = \frac{1,4}{n_0}, \qquad (12.70)$$

where $n_0$ – number of pulses, arriving in the width of the diagrams of directionality at the level of half the power value.

If the receiver has linear amplitude characteristics, then Expression (12.70) will also be characterized by the magnitude of the uncompensated residues of the interference. For example, at a width of the diagram of directionality of $\theta = 3^\circ$, the velocity of the rotation of the antenna 6 rpm and the frequency of repetition of the pulses $F_p$ = 400 pulses/sec, the number of pulses $n_0$ = 33 and the value of the remaining signal $\frac{\Delta U}{U_0} = 4,3\%$, or the coefficient of suppression is

$$L = 10 \lg \left(\frac{U_0}{\Delta U}\right)^2 = 27,5 \text{ db}.$$

Applying the limitations of the signals it is possible the lower the value of the uncompensated residues caused by the rotation of the antenna considerably. (Fig. 12.20 b).

Let us find the magnitude of the remaining signals during the reflection from a multitude of reflectors. It will be assumed that the relative positions of the individual reflectors in time equal to the period of repetition, remain substantially unchanged. Then during the rotation of the antenna there will be room only for the variation of amplitude corresponding to the elementary signals, the phasal relationships remain unchanged. The amplitude variations of the elementary signals lead to the fluctuation of the resulting signals. Therefore, if the vector $\vec{u}_n$ (Fig. 12.21) represents the signal of a multitude of reflectors in the *n*th period of repetition of the pulses, then in the $(n+1)$th period, the signal will be represented by another vector, $\vec{u}_{n+1}$. The various vectors $\vec{u} = \vec{u}_n - \vec{u}_{n+1}$ characterize the change of the resulting signal per period of repetition.

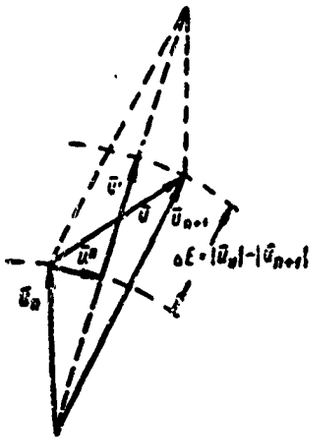

Fig. 12.21. Vector diagram of signals reflected from a multitude of reflectors during the rotation of the antenna.

The mean square value of the different vectors is

$$u_{\Sigma} = \sqrt{k \int [U(\alpha + \Delta\alpha) - U(\alpha)]^2 d\alpha},$$

where $\Delta\alpha = \frac{\theta}{n_0}$ – angle of rotation of the antenna in the time between two pulses; $k$ – coefficient of proportionality.

Substituting the function $U(\alpha+\Delta\alpha)$ into the form of a Taylor's series and limiting to two terms of the series, we obtain

$$u_{\Sigma} = \sqrt{k \int [U(\alpha) + U'(\alpha)\Delta\alpha - U(\alpha)]^2 d\alpha} = \frac{\theta}{n_0} \sqrt{k \int [U'(\alpha)]^2 d\alpha}.$$

Separate the vector of difference $\vec{u}$ into two components, one of which, $(\vec{u'})$ is found in phase with the vector of the sum of vectors $\vec{u}_n$ and $\vec{u}_{n+1}$ and characterizes the variation of amplitude, and the other, $(\vec{u''})$ – in quadrature with it and characterizes the phases of the resulting oscillation. The elementary components of the signal, as a result of the irregular distribution of the reflectors in the permitted volume, are statistically independent. Therefore, one may write, that the mean square value is

$$u'_{\Sigma} = u''_{\Sigma} = \frac{u_{\Sigma}}{\sqrt{2}} = \frac{\theta}{\sqrt{2} \cdot n_0} \cdot \sqrt{k \int [U'(\alpha)]^2 d\alpha}.$$

Thus we have found the mean square value of the difference vectors $u_{\Sigma}$. The finding of the difference vectors corresponds to the

subtraction of signals in the KPCh channel. We are however, interested in the magnitude of the signal at the output of the block of compensation. If we assume the detector of envelope of the receiver to the linear then this value is equal to the difference of the envelopes of two adjacent pulses, $\Delta E$ (Fig. 12.21).

Between the values of the vectors $\vec{u}_n$ and $\vec{u}_{n+1}$ there is room for the signal of correlation, since when the antenna is rotated an angle of $\Delta\alpha$, corresponding to the period of repetition of the pulses, part of the permitted volume common for the first and second positions of the diagrams, is sufficiently large. Therefore, the variations of the vector $\vec{u}_n$ per period $T_p$ cannot be significant, i.e., the value of the vector $u$ is generally small. Thereby, the level of mean square value of the difference of the envelopes $\Delta E_д$ is approximately equal to the mean square value of the value $u'_д$, component $u'$ of the difference vectors

$$\Delta E_д \cong u'_д = \frac{\theta}{\sqrt{2}\cdot n_0}\sqrt{k\int [U'(\alpha)]^2 d\alpha}. \qquad (12.71)$$

The mean square value of the voltage of fluctuation before subtraction is

$$E_д = \sqrt{k\int [U(\alpha)]^2 d\alpha}. \qquad (12.72)$$

On the basis of Formulas (12.71) and (12.72), we find the coefficient of suppression

$$L = \left(\frac{E_д}{\Delta E_д}\right)^2 = \left[\frac{\sqrt{2}\cdot n_0}{\theta}\cdot\sqrt{\frac{\int [U(\alpha)]^2 d\alpha}{\int [U'(\alpha)]^2 d\alpha}}\right]^2.$$

For the approximation assumed earlier of the diagram of directionality, we get after integration,

$$L \cong n_0^2. \qquad (12.73)$$

The dependence of the coefficient of suppression on the number of pulses, arriving at the diagram of directionality computed by Formula

(12.73) is shown in Fig. 12.22. As should be expected, the bigger the number of pulses arriving at the diagram of directionality, the less is the remaining signal.

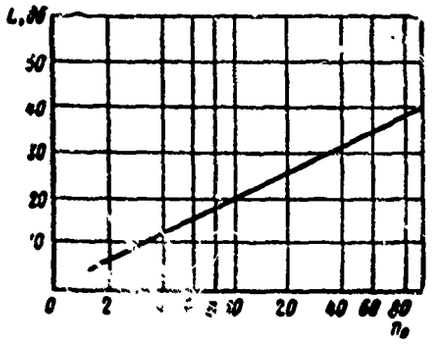


Fig. 12.22. The dependence of the coefficient of suppression on the number of pulses at the diagram of directionality.

A comparison of the curves of Fig. 12.19 and 12.22 shows that in the RLS of the third decacentimeter wave range $\left[\frac{f_0}{F_п} \cong (0{,}5 \div 1)\,10^7\right]$ the fluctuation of the reflections from metallized strips and rain produced by the motion of the elementary reflectors prevail over the fluctuations caused by the rotation of the antenna. In the RLS of decimeter wave range, $\left[\frac{f_0}{F_п} \cong (1{,}5 \div 3)\,10^6\right]$ these fluctuations are approximately equal. During reflection from hills covered with woods, in the condition of a slight wind, the fluctuation due to antenna rotation prevails over the fluctuations caused by the motion of the reflectors in the centimeter wave range as well as in the decimeter range.

3. Evaluation of the Magnitude of Remaining Signals Caused by the Motion of the RLS

The energetic spectra of the fluctuation of the interferences produced by the motion of the RLS (in the plane of the target), is determined by Expression (12.4). The normalized correlation function corresponding to this spectra is

$$r(\tau) = r_1(\tau)\cos\omega_c\tau, \qquad (12.6$$

where

$$r_1(\tau)=\exp\left[-\frac{(\pi\cdot\tau\cdot\Delta F_д')^2}{2,5}\right]. \qquad (12.74)$$

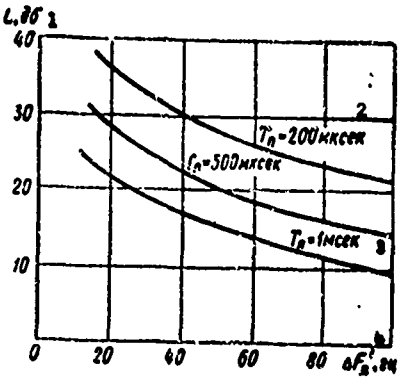


Fig. 12.23. Suppression coefficient as a function of spectral width of signal reflected from a plural reflector and of pulse repetition period. 1) db; 2) μsec; 3) msec; 4) hz.

Knowing the coefficient of correlation $r(\tau)$ of the process at the input of the detector, we may find the coefficient of correlation of the low frequency components of the fluctuation at the output of the detector $\rho(\tau)$.

For linear detector of envelopes

$$\rho(\tau)=\frac{\overline{S_н(t)\cdot S_н(t+\tau)}}{\overline{S_н^2(t)}}=r_1^2(\tau), \qquad (12.75)$$

where $S_н$ - low frequency component of the fluctuation at the output of the detector.

Substituting the value of coefficient of Correlation (12.75) into Formula (12.69), we find the coefficient of suppression

$$L=\frac{0,5}{1-\exp\left[-7,2(T_п\Delta F_д')^2\right]}. \qquad (12.76)$$

From Expressions (12.5) and (12.76), it follows that the wider the diagram of directionality and the bigger the course angle $\alpha_0$, the wider is the band of frequency and the smaller is the coefficient of suppression. With the increase of the period of repetition, the coefficient of suppression also decreases. According to Formula (12.76), the graphs in Fig. 12.23 are constructed illustrating the dependence of the coefficient of suppression on the quantity $\Delta F_д'$ at various values of $T_д$. Let us look at an example: $V=360$ km/hour, $\alpha_0=30°$, $\theta=2,8°$, $\lambda=3$ *см*. Thereby, $\Delta F_д'=115$ hz and the coefficient of suppression at $T_п=1$ msec is equal to L = 8 db.

If the RLS is installed on an airplane, then the fluctuation of the signal depends not only on the azimuthal angle but also on the angle of inclination of the antenna. The magnitude of the uncompensated residue in this case grows still higher. Calculations show that the

motion of the RLS is the deciding factor, determing the magnitude of the uncompensated residues. The motions of the elementary reflectors and the rotation of the antenna in the case of an airplane RLS may often be neglected.

4. Operational Characteristics of the Coherent-Pulse System SDTz

The coefficient of suppression of interferences characterizes the quality of the operations of the SDTz system only from one side; showing, in what degree the interference is weakened, it never does tell us about the passage of the signals themselves. It is obvious, however, that if the selector of the moving target will suppress in equal degrees the interferences as well as the useful signals then such a selector is useless.

Let us examine some specific features of the SDTz system with compensation, stipulated by the intraperiod subtraction of the signals. For this we rewrite the expression determining the amplitude of the signals at the output of the compensating device [see Formula(12.60)]:

$$U_{\text{вых}} = 2U_{\text{вх}} \sin\left(\frac{1}{2}\Omega_{\text{д}} T_{\text{п}}\right). \qquad (12.77)$$

From this expression we see that in the case of the optimum velocity, when $\Omega_{\text{д}} = \frac{(2\mu-1)\pi}{T_{\text{п}}}$, $\mu = 0, \pm 1, \pm 2, \ldots$, adjacent pulses have equal amplitudes, but opposite position polarity and the voltage at the output of the compensating device reach a maximum value.

At "blind" velocity, when $\Omega_{\text{д}} = \frac{2\pi\mu}{T_{\text{п}}}$, all pulses have the same amplitude and polarity and therefore the voltage at the output circuit of subtraction is equal to zero. Under these conditions, the target cannot be detected. In this way, the observability of the signals of the moving targets on the background of passive interferences depends not only on the magnitude and velocity of the fluctuation of the interferences but also on the radial velocity of the targets.

The presence of blind velocity is the essential shortcoming of the coherent-pulse system with intraperiod subtraction of signals. At the autotracking of the target and in all the other cases, when the velocity of the target is known, the period of repetition of the pulses, $T_p$ and the frequency of the coherent voltage $f_{kg}$ vary, then the velocity of the target may be made optimum while that of the interference, 'blind'. Thereby, the best condition of the observation of the useful signals is guaranteed (accumulation of signals and deduction of interferences).

During the operation of the RLS in the regime of survey, the velocity of the targets as a rule is not known. In this case for the decrease of the probability of letting pass the target having blind velocity it is necessary to have in the receiver a series of channels tuned to the receiving of signals with different Doppler's frequency shift. Another way of solving this problem -- the variation of the frequencies of the period of repetition of the pulses at the presence of an one-channel receiver.

Up to this time, it has been assumed that the useful signal forms a nonrandom function of time (nonfluctuating signal). Actually, the signals of real targets do fluctuate and this circumstance noticeably effects the condition of their detection.

Complete objective evaluation of the effectiveness of the SDTz system, considering the velocity of the fluctuation of the interferences as well as the velocity of fluctuation and magnitude of the Doppler's frequency shift of the useful signal may be done only with the aid of the operational characteristics (RKhP).

The calculation of the operational characteristics of the coherent-pulse system SDTz is extremely unwieldy and it will not be examined here. We shall look only at the completed results considering

as an example the operational characteristics of the receiver, whose block diagram is represented in Fig. 12.14, for the case of the detection of the fluctuating useful signals on the background of passive interferences with different velocities of fluctuation.* These characteristics, shown in Fig. 12.24, are calculated for the following conditions:

– no limits in the receiver;

– the useful signals and the interferences are distributed according to the normal law with zero mean value, i.e., regular components of the useful signals and the interferences are equal to zero;

– the energetic spectra of the fluctuation of the useful signals and the interferences are described by the Gaussian curve;

– the diagram of directionality of the antenna is rightangled;

– the Doppler's phase increments of the signals per period of repetition are taken as "blind" $(\varphi_A = \Omega_A T_n = \pm 2\pi\mu,\ \mu = 0, 1, 2, \ldots)$ and optimum $(\varphi_A = (2\mu - 1)\pi)$.

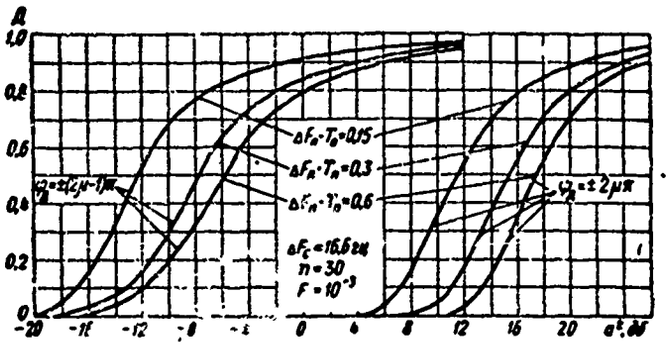


Fig. 12.24. Operational characteristics of the SDTz system with internal coherency: $\Delta F_p$ *and* $\Delta F_s$ – width of the energetic spectra of fluctuation of interferences and useful signals correspondingly (at the level 0.5); $n$ – number of pulses in the packet; $q^2 = \sigma_c^2/\sigma_n^2$ – ratio of the power of the signal to the power of the interference at the input of the receiver; $F$ – probability of false detection.

From the curves of Fig. 12.24 we see that during the detection of the signals of the moving targets, the quantity $\varphi_d$ plays an extremely essential role: the variation of $\varphi_d$ from 180° to 0° leads to the rise of the threshold signal to 20 db. It is necessary, however, to notice that the target cannot move with "blind" velocity for a long time. The quantity $\varphi_d$ depends on the radial velocity of the target and it does not remain constant when the direction of the motion of the target does not coincide with the direction toward the RLS. Besides this, the absolute value of the velocity of the target is subject to fluctuation. If for example, the velocity of the target is equal to 720 km/hr varies by 2%, then at $\lambda=10$ *см* and $T_n=3$ msec, parameter $\varphi d$ varies by 26°. This leads to a better observability of the target if it moved before this with "blind" velocity and was badly discerned on the background of interferences.

From an examination of the operational characteristics it follows that the probability of detecting the target at blind velocity is not equal to zero. This is explained by the fluctuations of the useful signals. The growth of the probability of the detection with the increase in the ratio of the power of the signals to the power of the interference $a^2$ in the region of large probability takes place slowly, which is also explained by the fluctuations of the useful signals.

As it should be noticed, with the increase of the velocity of the fluctuation of the interferences, the magnitude of the threshold signal increases. With wide band passive interferences, the effectiveness of the coherent-pulse receiver with the intraperiod subtraction is not great. Therefore there is interest to present a comparison of evaluation of the effectiveness of this type of receiver and the classical receiver carrying out the accumulation of the signals after the detector of the envelopes, the operational characteristics of which is

shown in Fig. 12.25. From the curves of Figures 12.24 and 12.25 the dependence of the magnitude of the threshold signal $a^2_{мин}$ on the width of the energetic spectra of the fluctuations of the interference $\Delta F_п$ is calculated for the coherent receiver with intraperiod subtraction and also for the ordinary receiver with the detector of envelopes and integrator. This dependence for the probability of detection $D = 0.9$ is shown in Fig. 12.26. From the curves of the figures, one can see that even in the case of optimum velocity of the motion of the target at $\Delta F_п \cdot T_п > 0{,}36$ the coherent receiver for the level shown in the figure is less effective than the ordinary receiver.

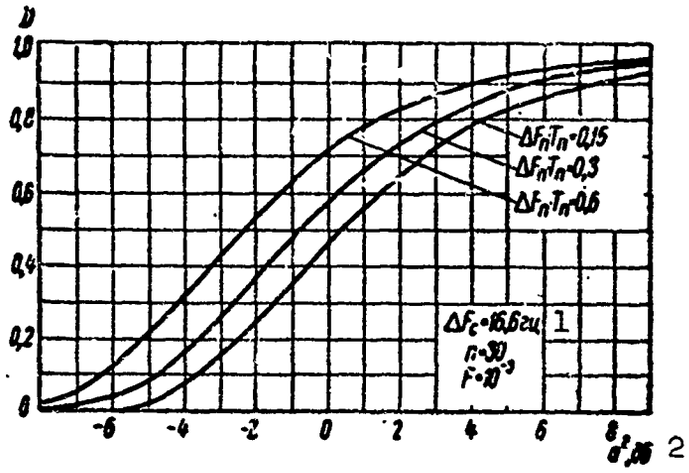


Fig. 12.25. Operational characteristics of the receiver carrying out accumulation of signals after the detector of envelopes. 1) hz; 2) db.

In conclusion, it is necessary to indicate that the coherent-pulse method with the intraperiod subtraction is the only one of the possible methods of selection of signals of moving targets against the background of passive interferences. Experience of exploitation shows that regardless of the relative width of the practical reception, the indicated method is not the best.

Other methods have been proposed for the detection of the signals

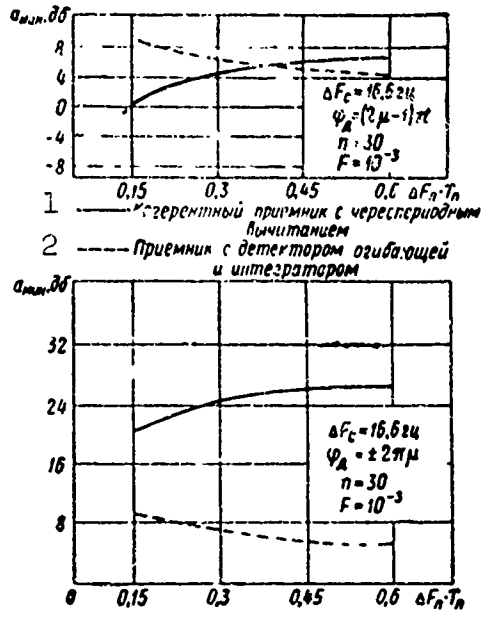


Fig. 12.26. Dependence of the threshold signal on the width of the spectra of the fluctuation of the interference. 1) Coherent receiver with intraperiod subtraction; 2) receiver with detector of envelope and integrator.

in passive interferences, in particular, double, triple and even $(n - 1)$ -tuple compensation ($n$ – the number of pulses in the packet of reflected signals). The methods of multiple compensation are more effective than intraperiod subtraction, but they as well as other suboptimum methods which we have not examined here are far from fully realizing the potential possibility of the detection of the signals in passive interferences. This possibility is only realized when the method of optimum reception is used.

## 5. Sensitivity of the Receivers of the Coherent-Pulse SDTz System with Internal Coherency

Let us examine the effectiveness of the receiver with the detector and the intraperiod subtraction in the case of the detection of signals against the background of natural noises of the receiver.

The average value of the amplitude of the videopulse signal after compensation and the change of polarity of the negative pulses to the

opposite position is equal to

$$|U_к|_{ср} = 2U_{сд}|\sin(\pi \cdot F_д \cdot T_п)| \cdot \frac{1}{T_д}\int_0^{T_д}|\sin(2\pi F_д t)|\,dt = \\ = \frac{4}{\pi} \cdot U_{сд}|\sin(\pi F_д T_п)|, \tag{12.78}$$

where $T_д = \frac{1}{F_д}$ – period of Doppler's frequency.

Form (12.78) it follows that at the optimum velocity of the target ($\sin \pi F_д T_п = 1$) the average value of the amplitude of the signals at the output of the coherent-pulse receiver is $\frac{4}{\pi} = 1{,}27$ times greater than the amplitude of the signals at the output of the receiving device of an ordinary RLS. At "blind" velocity ($\sin \pi F_д T_п = 0$) the signal at the output of the coherent receiver is equal to zero.

The noise level of the receiving-indicator tract of the coherent-pulse RLS with compensation and that of the ordinary RLS are approximately the same. Actually, the compensating device increases the noise voltage by a factor $\sqrt{2}$, since the noise voltages in the direct and delayed channels are statistically independent.

But the coherent detector, having suppressed the quadrature component and allowing the phasal component of the input signal pass without change raises the signal/noise ratio by $\sqrt{2}$ times.

Consequently, the sensitivity of the receiver of the coherent-pulse RLS with compensation is a function of the radial velocity (Fig. 12.27).

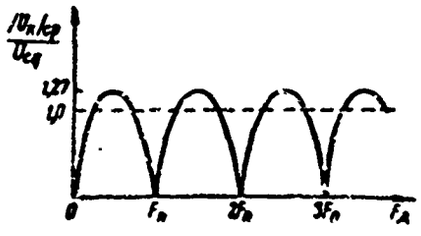


Fig. 12.27. The dependence of the sensitivity of the receiver of the coherent-pulse RLS with intraperiod subtraction of signals on the radial velocity of the target.

It is necessary to note that also at the "blind" velocity the signal at the output of the coherent receiver is not equal to zero. This is explained by the fluctuation of the useful signals. If it is further assumed that all the values of the velocity of the target are approximately distributed in some intervals, then by a first approximation, it may be assumed that the sensitivity of the receiver of the coherent-pulse RLS on the average is equal to the sensitivity of the ordinary RLS.

## § 12.6. STABILITY REQUIREMENT OF THE OPERATION OF THE ELEMENTS OF THE SDTz SYSTEM

It is necessary to have in view two circumstances when discussing the basis of the requirement of stabilization of the operation of the elements of the RLS system.

From one side, the stability should be sufficiently high such that the uncompensated residues of the interference are not substantially increased and the quality of the selection of the signals of the moving target is not worsened. From the other side, very high stability is not expeditious since then the uncompensated residue is not substantially reduced while the construction of the RLS is sharply more complicated. From an analysis of the graphs of Figs. (12.19) and (12.22), one can see that the coefficients of suppression of fluctuation produced by the motion of the elementary reflectors and the rotation of the antenna cannot somehow significantly surpass 30 db. Consequently, even at the absolute stability of the operation of the elements, the coefficient of suppression is limited to the order of magnitude of about 30 db and lower. If the RLS is installed on a moving object, then to the residual signal caused by the wind and the rotation of the antenna, there are added the residual signals due to the change of position of the antenna and the coefficient of suppression becomes

still smaller.

It is assumed that at coefficient of Suppression 28-30 db good observability of the signals of the moving target on the screen of the indicator is guaranteed. The value $L=28\div30\ дб$ corresponds to the ratio of the voltages at the output and the input of the block compensator $\frac{\Delta U}{U}=0{,}04\div0{,}03$. This value of the ratio is generally used as the starting point for the basis of requirement of the stability of operation of the elements of the RLS.

1. Requirement of the Stability of Operation of High Frequency Generators in the SDTz Systems with Internal Coherency

Since in the SDTz systems with intraperiod subtraction, the phase variation of the reflected signals is fixed per period of repetition, therefore the magnitude of the reflected signal at the output of the subtraction circuit will be determined by the stability of the frequency of the transmitter of the local and coherent heterodynes during the course of that period.

The variation of the frequency of any of these generators or all of them together will lead to the appearance of a parasitic phase difference between the reflected signals and the coherent voltages. If it is assumed that the variation of frequencies of any generator takes place according to the linear rule that is equivalent approximately to the variation of the distance between the RLS and the target then the signals of the nonmoving objects will never differ from those of the moving target. There will not be a full suppression of the signals of the nonmoving objects.

The amplitude of the videopulses at the output of the balanced phasal (coherent) detector, very often used in practice, is determined by the expression

$$U_{\text{в}}=U_0\left(\cos\frac{\psi}{2}-\sin\frac{\psi}{2}\right),\quad 0\leqslant\psi\leqslant180^\circ,$$
$$U_{\text{в}}=U_0\left(\sin\frac{\psi}{2}-\cos\frac{\psi}{2}\right),\quad 180^\circ\leqslant\psi\leqslant360^\circ, \tag{12.79}$$

where $U_0 = k_A U_c$;

$k_d$ – coefficient of transmission of the detector;

$U_s$ – amplitude of the signal at the input of the detector;

$\psi$ – phase difference of the reflected signal and the coherent voltage.

It is obvious that the summation of the phase differences is

$$\Delta\phi = \Delta\phi_n + \Delta\phi_{мг} + \Delta\phi_{кг},$$

where $\Delta\phi_n$, $\Delta\phi_{мг}$ and $\Delta\phi_{кг}$ variations of phase of the transmitter, local and coherent heterodynes correspondingly.

If it is assumed that the frequencies of the generators vary according to the linear rule then the corresponding variation of phases per period of sending will equal to*

$$\left.\begin{aligned} \Delta\phi_n &= \frac{d\omega_n}{dt} T_n \tau_n, \\ \Delta\phi_{мг} &= \frac{d\omega_{мг}}{dt} T_n \tau, \\ \Delta\phi_{кг} &= \frac{d\omega_{кг}}{dt} T_n \tau. \end{aligned}\right\} \qquad (12.80)$$

On the basis of the requirement of stability of the frequency of every generator individually it is necessary to take into account that the time of delay is $\tau \gg \tau_n$. Consequently, the most rigid requirement needs to be imposed on the absolute stability of the local and coherent heterodynes. Since the local heterodyne operates on a significantly much higher frequency than the coherent one (high frequency and intermediate frequency correspondingly), therefore, when their absolute instability is the same, considerably more rigid requirement should be imposed on the individual instability of the local heterodynes. Besides this, it needs to be taken into account the fact that the higher the stability of the coherent heterodyne, the more difficult is its phas-

ing. Therefore, it is necessary to demand the same absolute stability from both heterodynes $\Delta\psi_{мг} = \Delta\psi_{кг}$.

Since $\tau_и \ll \tau$, therefore, the absolute instability of the transmitter shows considerably less effect on the variation of the phase $\psi$. Consequently, less stringent requirements may be imposed on the absolute instability of the transmitter, the more powerful the transmitter in the pulse system, the stability requirements of which would be significantly harder than the less powerful heterodyne. Therefore, it may be accepted that the phase variation due to the maintenance frequency of the transmitter may be the same as the maintenance frequency of the heterodynes, i.e.,

$$\Delta\psi_и = \Delta\psi_{мг} = \Delta\psi_{кг} = \Delta\psi_0.$$

The variation of the phases of the oscillations of the transmitter, local and heterodyne, takes place by a first approximation, independently of each other. In the worst case, the phases of all the three generators change in such a way that there are room for the arithmatic addition of the individual phase shifts. In the other extreme case, the phasal variation will compensate each other.

Based on this, we will assume that the resulting variation of phases is equal to, on the average.

$$\Delta\psi = \sqrt{\Delta\psi_и^2 + \Delta\psi_{мг}^2 + \Delta\psi_{кг}^2} = \sqrt{3} \cdot \Delta\psi_0. \qquad (12.81)$$

From Formula (12.79), we find the relative variation of amplitude of the videopulses when the variation of phase is at the magnitude of $\Delta\psi$.

$$\left|\frac{\Delta U}{U_0}\right| = \frac{1}{2}\left(\cos\frac{\psi}{2} + \sin\frac{\psi}{2}\right)\Delta\psi, \quad 0 \leqslant \psi \leqslant 360°.$$

The maximum value $\left|\frac{\Delta U}{U_0}\right|_{макс} = \frac{\Delta\psi}{\sqrt{2}}$ will be when $\psi = 90°$, from which

$$\Delta\psi = \sqrt{2} \cdot \left|\frac{\Delta U}{U_0}\right|_{макс}. \qquad (12.82)$$

Equating the right hand sides of Formulas (12.82) and (12.81), we find the maximum permissible phase variation

$$\Delta\psi_{0\text{доп}} \cong \left|\frac{\Delta U}{U_0}\right|_{\text{макс доп}}.$$

From Relationship (12.80), assuming in correspondence with the earlier statement $\left|\frac{\Delta U}{U_0}\right|_{\text{макс доп}} = 0{,}03$, for the permissible velocity of the maintenance frequency of the heterodyne, we find

$$\left.\begin{aligned} \frac{d\omega_{\text{п}}}{dt} &\cong \frac{0{,}03}{T_{\text{п}}\tau_{\text{и}}}, \\ \frac{d\omega_{\text{мг}}}{dt} &\cong \frac{0{,}03}{T_{\text{п}}\tau}, \\ \frac{d\omega_{\text{кг}}}{dt} &\cong \frac{0{,}03}{T_{\text{п}}\tau}. \end{aligned}\right\} \qquad (12.83)$$

The permissible absolute maintenance frequency per period of repetition (short duration instability) correspondingly will be

$$\Delta f_{\text{п}} = \frac{0{,}03}{2\pi\tau_{\text{и}}}; \quad \Delta f_{\text{мг}} = \Delta f_{\text{кг}} = \frac{0{,}03}{2\pi\tau}.$$

From the last formula we see that the permissible maintenance frequency for the local and coherent heterodynes depends on the distance to the target.

As an example, in Table (12.2) the permissible velocities of the maintenance frequency, absolute and relative to the instability per period of repetition for the transmitter, local and coherent heterodyne are shown: $\tau_{\text{и}} = 0.5\,\mu\text{sec}$, $T_{\text{п}} = 500\,\mu\text{sec}$, $\tau = 300\ \mu\text{sec}$ ($R = 45$ км), $f_0 = 10\,000$ Mhz, $f_{\text{кг}} = 30$ Mhz.

TABLE 12.2

| 1 Местный гетеродин | 2 Когерентный гетеродин | 3 Передатчик |
|---|---|---|
| 32 khz/s<br>16 hz<br>$10^{-9}$ | 32 khz/s<br>16 hz<br>$0{,}5\cdot10^{-6}$ | 20 Mhz/s<br>10 khz<br>$10^{-6}$ |

1) Local heterodyne; 2) coherent heterodyne; 3) transmitter.

The requirement of short duration stability $10^{-6}$ for the transmitter and the coherent heterodyne is not too rigid and may be easily relaxed in practice. The short duration stability, $10^{-9}$ for the local heterodyne is reached with great difficulty.

The variation of the amplitude of the signals, reflected from the nonmoving object happens not only at the maintenance frequency but

also during its variation according to the length of the emitted pulses. The maintenance frequency of the transmitter, within the limits of the duration of the pulse, leads to the variation of the phase difference of reflected signals and the coherent oscillation in the beginning and the end of the pulses. This produces variations of form and even the polarity of the videopulses. Since the maintenance frequency arises independently of the period to period repetition, therefore at the output of the compensating device there appears residual signal.

As it is known, the output voltage of the phase detector varies from zero to the maximum value during the variation of $\psi$ to $90°$. If it is required that within the limits of the pulses no more than four intervals should be included then we may write

$$\tau_{\text{и}}\Delta\omega_{\text{д}} \leqslant \frac{\pi}{2},$$

or

$$\Delta f_{\text{д}} \leqslant \frac{1}{4\tau_{\text{и}}}.$$

If for example, $\tau_N = 0.5$ μsec then the permissible absolute maintenance frequency of the transmitter during the course of the duration of the pulse is $\Delta f_D = 500$ kilocycle.

Let us look now at the requirement on the stab-lity of the frequency of the transmitter from the viewpoint of the fluctuation of the signals, reflected from a multitude of reflectors and caused by the instability of the probing oscillation. As it was shown in §12.2, the fluctuation of the reflected signal due to the variation of the frequency of the transmitter is not significant in such case if Actually it is ordinarily required that $\tau_{\text{и}} \cdot \Delta f \ll 1$ and then the permissible maintenance frequency of the transmitter from pulse to pulse is $\tau_{\text{и}} \cdot \Delta f \leqslant 0{,}05$,

$$\Delta f \leqslant \frac{0{,}05}{\tau_{\text{и}}}.$$

We shall determine finally the required stability of the generators from the viewpoint of dependability of the phasing of the coherent heterodyne. We shall use $\Delta f_{\phi\,макс}=|f_п-f_{кг}|-f_{кг}$ to designate the maximum derangement of the phasing pulse relative to the frequency of the coherent heterodyne at which phasing is still possible.

If no measures were taken in the RLS for the stabilization of the frequency of the transmitter, then as a rule, the tuning of $\Delta f_\phi$ is determined on the base of the maintenance frequency of the transmitter. In such cases, the inequality should be fulfilled

$$|\Delta f_п|_{макс} \leqslant |\Delta f_\phi|_{макс}.$$

Since the pulse phasing is dependably accomplished when the relative derangement is of the order of 5% $\left(\frac{\Delta f_{\phi\,макс}}{f_{кг}} \leqslant 0{,}05\right)$ therefore,

$$\Delta f_{п\,доп} \leqslant 0{,}05 f_{кг}.$$

2. <u>Requirements For The Stability Of The Operations Of High Frequency Generators In The SDT$_z$ Systems With External Coherency</u>.

In these systems the magnitude of the uncompensated residues will dpend on the stability of the frequency and the amplitude characteristics of the local heterodyne.

Since the phase of the reflected signals in the receiver does not fluctuate, therefore the special measure for the stabilization of the local heterodyne is not undertaken. The requirements for the local heterodyne is not undertaken. The requirements for the local heterodyne in the sense of maintenance frequency in this case are determined by the parameters of the APCh system as well as in general t RLS.

The variation of the frequency of the transmitter produces the fluctuation of the signals of the dispersed reflecters. As it has been shown before, the permissible maintenance frequency of the transmitter per period of repetition of the pulses should not exceed in order of magnitude of

$$\Delta f \leqslant \frac{0{,}05}{\tau_и}.$$

The fluctuation of frequency and amplitude of the oscillation of the transmitter is produced by the variations of the load and the instability of the operation of the modulator. The magnetron is generally used in the capacity of the transmitting device in present day RLS of the centimeter wave range. The velocity of the maintenance frequency of the magnetron in the process of the operation of the RLS is the bigger, the shorter the wave length and the faster the rotation of the antennas. The most favorable condition in the sense of the maintenance frequency is in the case of the airplane RLS where the operational frequencies are relatively high and the antennas are rotating at a great speed and are shielded by deflectors. In these stations, the velocity of the frequency variation of the magnetron may reach hundreds and even a thousand megahertz in a second.

It is necessary to keep in mind that there is still the fact that fast variation of the frequencies of the magnetron produces distortion of the forms of the frequency spectra of the pulses whereupon the harmful effect of this distortion on the operation of the station cannot be lessened by the use of the system of fine tuning the frequency of the receiver.

For the increase in the stability of the operation of the magnetron, measures should be taken by guaranteeing its separation from the linear transmission. For this purpose one may use, for example, filters, which not bringing in any noticeable weakening of the transmission energy in the antenna, practically fully absorbs the reflected waves.

The decrease of the fluctuation of the output power of the magnetron is attained by the stabilization or the voltage of the modulator, or the current of the magnetron.

3. Requirements For The Stability Of The Time Delay, The Period Of Repetition And The Duration Of The Pulse.

The variation $T_{zad}$ or $T_p$ and also $T_i$ leads to the appearance of uncompensated residues at the output of the circuit of subtraction, since as this takes place, the precise coincidence of the pulses of the direct and delayed channels at the output of the circuit of subtraction is destroyed.

The effect of the instability of $T_{zad}$ or $T_p$ as before, may be estimated by the coefficient of Suppression (12.67), it is necessary only to set $r_{or}(T_n)=1$. Then, the coefficient of suppression as a function of the mutual displacement of the pulses is

$$L(\delta)=\frac{0,5}{1-r_\phi(\delta)}.$$

If we take the form of the pulses as right-angled,

$$U(t)=\begin{cases} U_0, & -\frac{\tau_u}{2}\leqslant t\leqslant\frac{\tau_u}{2}, \\ 0 \text{ for all other values of } t \end{cases}$$

then,

$$r_\phi(\delta)=1-\frac{|\delta|}{\tau_u}$$

and the coefficient of suppression is

$$L(\delta)=\frac{\tau_u}{2|\delta|}. \qquad (12.84)$$

Assigning in (12.84) the accepted value of $L(\delta)$, we may find the maximum permissible value of $T_{zad}$ or $T_p$.

Similarly the requirement for the stability of the duration of the pulses may be estimated.

## § 12.7 POLARIZATION SELECTION OF USEFUL SIGNALS

The observability of the useful signals against the background of the disturbing reflections from hydrometeors and metallized strips may be improved if probing oscillation with circular polarization is used.

In general cases, the power of the signals being received reflected from defined objects, changes dependent on the form of the polarization of the oscillation being emitted. For real objects, small in comparison with the size of the reflecting volume, there is always polarization at which the intensity of the reflected signal is maximum and conversely, polarization at which the intensity is maximum.

If the probing oscillations have the circular polarization, then the waves, reflected from the real targets, for example, airplane, as a result of the asymmetry of the latter, will be elliptically polarized. Rain drops have almost spherical shapes, acting like symmetrical reflectors for any polarization. Therefore being reflected from the rain, the waves also will have circular polarization. But, the direction of the rotation of the vector of the electric field changes to the opposite direction upon reflection from the rain. If, for example, the vector of the electric field of the wave being emitted is, relative to the direction of the propagation, rotated clockwise, then the vector of the reflected waves relative to the direction of propagation will be rotated counter clockwise.

As noticed in Chapter *11*, one of the devices permitting the acceptance of waves of circular polarization, is the phase rotator in the form of a quarter wave grid, placed in front of the antenna exposure (See Fig. *11.5*). In passing through such a grid linearly polarized probing waves obtain at the output waves with circular polarization and the vector of the electric field is rotated for example, clockwise. If the wave being received has circular polarization and the vector of the electric field is rotated counter clockwise, then at the output of the grid the wave will become again linearly polarized. But the plane of polarization of the reflected wave will be perpendicular to the plane of polarization of the inci-

of the incident waves. Wave with such linear polarization cannot pass through the waveguide tract of the RLS.

Consequently, waves reflected from rain having circular polarization, oppositely positioned to the direction of the rotation of the vector of the electric field, will be suppressed in the system. Elliptically polarized waves of real targets will have, at the output of the grid, components of vertical as well as horizontal polarization and therefore, part of the power of the reflected signals falls in the receiver of the radiolocational stations.

Experimental investigations show that when circular polarization is used in the RLS of centimeter range signals reflected from the rain, are weakened to *6-8* db, reflected from snow – to *10-15* db. It is interesting to note that for the reflection from non-moving objects, whose polarization differs from circular is weakened not in excess of *4-8* db.

When circular polarization is used, not only the disturbing reflections are suppressed but the useful signals are also weakened by *6-8* db. Therefore, the system should be completed in such a manner that when disturbing reflections are absent it may be converted from waves of circular polarization into linearly polarized waves.

The earth shows substantial effect on the magnitude of the suppression of the disturbing reflections. If part of the energy of the waves reflected from the rain falls on the earth and afterwards reflected from it and enters through the antenna, then this wave will not be suppressed and enters the input of the receiver of the RLS. This is explained by the change of direction of polarization when reflected from the earth. The effect of the earth depends on the diagram of directionality, the angle of inclination of the axis of the antenna and on the coefficient of reflection of the surface coverings.

Manuscript Page No.

[Footnotes]

823 See book by L.A. Vainshtein (Weinstein) and V.D. Zubakov "Isolation of signals from the background of random interferences." Publisher "Soviet Radio," 1960.

824 In the interval of observation, the interference is considered as a stationary random process.

826 More details on the normal random processes are found for example in the book by B.R. Levine "Theory of random processes and their applications in radio technology." Publisher "Soviet Radio," 1962.

844 Such approximation agrees sufficiently well with actual practice.

880 During the calculation of RKhP it was proposed that in place of the indicator an integrator and a threshold device are used.

893 In so doing the variation of frequency in the course of the duration of the pulse is negligible.

[Transliterated Symbols]

812 РЛС = RLS = radiolokatsionnaya stantsiya = radar
815 д = d = dopplerov = doppler
816 УПЧ = UPCh = usilitel' promezhutochnykh chastot = i-f amplifier
821 с = s = spektr = spectrum; signal = signal
822 и = i = impul's = pulse
823 ср = sr = sredniy = average
824 п = p = pomekha = interference
830 обл = obl = oblucheniye = beaming
834 Вх = Vkh = vkhod = input
837 мин = min = minimal'nyy = minimum

850 г = g = grebenka = comb

850 СДЦ = SDTz = selektsiya dvizhuyushchikhsya tseley = moving-target selection

851 УКВ = UKV = ul'trakorotkaya volna = ultrashort wave

857 м = m = magnetron = magnetron

859 мг = mg = mestnyy geterodin = local oscillator

859 пр = pr = promezhutochnyy = intermediate

859 кг = kg = kogerentnyy geterodin = coherent heterodyne

860 у = u = ustanovleniye = settling

860 д = d = detektor = detector

860 ф = f = fil'tr = filter

862 УЗЛ = UZL = ul'trazvukovaya liniya zaderzhki = ultrasonic delay line

863 п = p = povtoreniye = repetition

863 зад = zad = zaderzhka = delay

864 АРУ = ARU = avtomaticheskaya regulirovka usileniya = AGC

868 дц = dts = dvizhuyushchaya tsel' = moving target

868 отр = otr = otrazhennyy = reflected

868 р = r = rezul'tiruyushchiy = resultant

869 вх = vkh = vkhod = input

869 вых = vykh = vykhod = output

875 ог = og = ogibayushchaya = envelope

878 мк = mk = maksimal'naya krutizna = maximum slope

882 дб = db = detsibel = decibels

883 н = n = nizkochastotnyy = low-frequency

885 РХП = RKhP = rabochaya kharakteristika priyemnika = receiver operating characteristic

893 д = d = detektor = detector

894 макс = maks= maksimal'nyy = maximum

895 доп = dop = dopustimyy = permissible

897 Ф = f = faziruyushchiy = phasing

897 АПЧ = APCh = avtomaticheskaya podstroyka chastoty = automatic frequency control

## Chapter 13

## PASSIVE RADIOLOCATION

### §13.1. PHYSICAL BASIS OF PASSIVE RADIOLOCATIONAL OBSERVATION AND SOME AREAS OF ITS APPLICATION

In the passive radiolocational observation of the locations of various objects or the reliefs of the locations, these positions are determined by the reception of electromagnetic vibrations emitted by these same objects being observed. In the last few years, it has been established that the objects, depending on the temperatures, emit electromagnetic waves not only in the frequency of the infrared but also in the longer wave lengths close to the centimeter waves. The electromagnetic radiations of various substances dependent on the temperature of the regime, are known ordinarily as the thermal radiowaves and are utilized for their passive detection and position definition.

In connection with the development of rocket technology, it has been made clear that during the launching of a ballistic rocket, sufficiently intensive electromagnetic waves have been observed. At large distances (to *8000-10,000 km*) the high frequency components of the spectra are absorbed by atmospheric diffusion, while the low frequency (below *30* kilohertz) may be received and used for the determination of the moment and position of the launching of the ballistic rockets and the tracing behind its trajectory (when the engine is working).

It is assumed that during the launching of a ballistic rocket, its accelerated motion, intensive ionization and vibration of the molecules of the gases take place on account of the high temperatures

and the velocity of the escape of the jet exhaust of the rocket engine. The vibration process of the ionized molecules is accompanied by radiations of electromagnetic waves. The intensity of the long wave radiation increases on account of the fact that the jet of strong-ionized gases dragging behind the rocket provides a highly effective antenna of very low radiofrequency. Besides, this, same ionized "tail" forms a conducting layer for the discharge of the vertical component of the electromagnetic field of the earth, accompanied by additional radiations of electromagnetic waves.

Electromagnetic vibrations of still lower frequency are formed by nuclear explosions. Their reception permits the assured registration of the location and the measurement of the strength of the nuclear explosion.

The reason of the appearance of the ultra low frequency electromagnetic vibration during a nuclear explosion is the process of intensive generation of electrically charged elementary particles possessing gigantic kinetic energy. Appearing during the atomic explosion, the strongly ionized clouds create condit on for the discharge of the vertical field of the earth. Thereby, the unsettled process of the type of lightning discharge is developed accompanied by the radiation of electromagnetic vibrations.*

The intensity of the radiation of nuclear explosion is mostly close to a frequency of 30 hertz and quickly diminishes to a frequency amounting at the maximum of *0.1%* of *1* kilohertz. In spite of that, the level of signals even at frequencies of *10-20* kilohertz is sufficient for them to be received at a range of several thousands of kilometers.

Thus, at the present, from the purpose of passive radiodetection and position defining we may use:

- electromagnetic oscillations, formed by thermal radiations of various objects;

- electromagnetic oscillation, produced by strong aerodynamic disturbances and processes of intensive ionization.

Passive radiolocation is developed in the last few years mainly for the solution of problems of navigation of airplanes and ships at the geodesic and astronomical investigations etc. To the largest degree, it is developed and verified by the numerous experiments of reception of thermal radiowaves of objects in the centimeter wave range and the attention paid to it in a wide range of publications.

Passive radiolocation station (PRLS) is a non-radiating system (insofar there is no transmitter) and therefore, possesses high secrecy, since its operational frequency cannot be determined by the enemy using techniques of reconnoitering. PRLS may detect objects that are not contrasted in radiolocational relationships. Besides this, PRLS requires very much less energy and have relatively small weight and bulk.

With the aid of airplane stations, passive radiolocation has succeeded to receive extremely good reproduction of reliefs of localities and a number of objects on them whose radiations differ in intensity from the signals of the surrounding background (Fig. *13.1a*).

The survey of localities is accomplished by the needle shaped antenna beam which is intermixed in direction by the perpendicular course of the carrier of the PRLS (Fig. *13.1b*). Plate scanning of several bands is provided by the motion of the carrier. In this way, the survey of the locality goes "line by line." In so doing, the velocity of the intermixing of the antenna beam should coincide with the motion of the carrier of the apparatus.

The signals being received is reproduced on an electrobeam indicator of direction. The brightness of the image on the screen of the indicator depends on the temperature contrast of the objects.

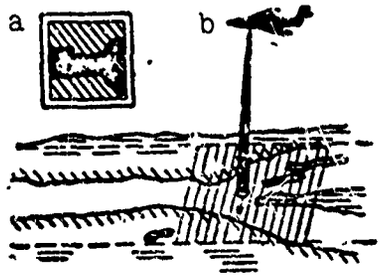


Fig. 13.1. Survey of locality by an airplane PRLS: *a)* image on the screen of the indicator; *b)* survey of locality.

The scale of the image obtained is unknown, since the passive radiolocation system does not directly determine the distance to the objects. The thermal radiowave is continuous in time and therefore it is impossible to register the time of the propaganda of the electromagnetic wave from the object to the PRLS. Because of this, the scale of the image is established by the juxtaposition with geographical charts or by the method of bearing taking on the objects: the distance to them is determined by the known height of the flight and the angle of tilt of the diagrams of directionality of the antennas.

The capability of the PRLS to react with the temperature contrast, depending on the differences in the intensity of their thermal radiowaves, may be used for the leading of the guided missiles along the borders between water surface and dry land in the detection of the course of the ships passing through by their dead water current which has much higher temperature in comparison with the surrounding water, and in a number of other cases.

## §13.2. BASIC CHARACTERISTICS OF THE COURSES OF THERMAL RADIOWAVES.

Spectral distribution of radiations. The best sources of thermal radiation waves in the centimeter and millimeter range is the absolute black body.

The spectral distribution of thermal radiation of the absolute

black body for the radio frequency range is given by the Law of Rayleigh-Jeans determining the power of the radiation from unit surface of the black body in an unit solid angle in the frequency band of 1 hertz:

$$p=\frac{2}{\lambda^2}\cdot kT^\circ, \qquad (13.1)$$

where $P$ – spectral density of the power of radiation volt/cm$^2$·hz;

$\lambda$ – wave length cm;

$k = 1.37 \times 10^{-23}$ watt/cm$^2$·degree (Boltzmann's constant);

$T^\circ$ – absolute temperature

From the law of Rayleigh (13.01), one can see that the spectral density of the radiation depends sharply on the wave length decreasing with the increase of the latter.

*Radiating capability of bodies.* In the radiowave range, the absolute b ack body possesses the best radiating capability in the frequency of the centimeter waves. Therefore this is used as a standard with which the levels of the energy radiated by any other bodies is compared under the same conditions.

The radiating capability ε denotes the ratio of the power of radiation $P_{\varepsilon T}$ of the given body in the specified frequency band at temperature $T^\circ$ to the power of radiation $P_{\varepsilon}$ of the absolute black body at the same temperature and in the same frequency band, i.e.

$$\varepsilon=\frac{P_{\varepsilon T}}{P_{\varepsilon}}. \qquad (13.2)$$

The quantity ε is always smaller than unity, since the maximum radiation is given by the absolute black body. If, for example, the radiating capability of a body is equal to 45%, then it radiates in the given frequency bank only 45% of the energy which would be radiated by the absolute black body under the same conditions.

*Reflecting capability of bodies.* All real objects not only radi-

but they also reflect the energy from other surrounding media incident on them. The level of this energy depends on the magnitude of the reflecting capabilities of various bodies. The reflecting capability of the object, $\varkappa$ is related to the radiating capability $\varepsilon$ by the simple relationship

$$\varkappa = 1 - \varepsilon, \qquad (13.3)$$

which is a result of the law of conservation of energy.

*Equivalent and apparent temperature of bodies.* Rayleigh's law and the data on the determination of radiating capabilities of objects permit us to characterize their temperature equivalent to the radiation of the absolute black body. The temperature level so obtained of real bodies is referred to as equivalent.

From Expressions (13.1) and (13.2) it follows that the equivalent temperature $T_э^\circ$ of any body is equal to its absolute physical temperature $T^\circ$ multiplied by the radiating capability $\varepsilon$, i.e.,

$$T_э^\circ = \varepsilon T^\circ. \qquad (13.4)$$

For example, water at the temperature 300°K and radiating capability of 45% behaves like an absolute black body with temperature 0.45 x 300°K = 135°K. Consequently, water has an equivalent temperature of 135°K, which is completely determined by the level of radiating energy.

The high frequency energy, entering from any object is dependent not only on the thermal radiation but also on the reflection of the energy incident upon it from the outer space. The level of the reflected energy may be characterized by some absolute black body temperature giving the same value of the radiated energy and the equivalent temperature produced by the external medium $T^\circ_{э\,ср}$ multiplied by the reflecting capability of the object $\varkappa$ according to Formula (13.3).

Let, for example, the equivalent temperature of the external medium be $T^{\circ}_{э.ср}=50^{\circ}$K. The reflecting capability of the body is 55% and consequently the energy of the external medium reflected from the body will be equivalent to the radiation of the absolute black body with temperature $50^{\circ}\text{K}\times 0{,}55=27{,}5^{\circ}$K.

The total amount of energy may also be characterized by some temperature of the absolute black body, at which the latter gives the same amount of radiation energy. This temperature we use, is designated as "apparent" temperature of the object, $T^{\circ}_{каж}$ It, in correspondence with the description, is determined by the relationship

$$T^{\circ}_{каж}=T^{\circ}_{э.об}+T_{э.ср}\cdot\varkappa, \qquad (13.5)$$

where $T^{\circ}_{э.об}$ — equivalent temperature of the object.

As an example, we shall determine the apparent temperature of water. Earlier it has been calculated that its equivalent temperature is $T^{\circ}_{э}=135^{\circ}$K. Besides this, it was established that water reflects energy, equivalent to the radiation of the absolute black body with temperature $27.5^{\circ}$K. Consequently, its apparent temperature consists of $135 + 27.5 + 162.5^{\circ}$K.

*Temperature contrast of objects.* By temperature contrast, we mean the difference of their apparent temperature. In the presence of temperature contrast, the objects are distinguished by the intensity of the entering radiations.

Temperature contrast exists at the same absolute temperature of the objects. For example, the radiating capability of the earth's surface is *90%* while the reflecting capability is *10%*. For water surface, these values are correspondingly equal to *45%* and *55%*. Consequently, the apparent temperature of the surface of the earth is higher than that of water; the latter is as if "colder." As a result, according

to the level of the total radiation of the earth surface and water, they may be distinguished.

This possibility is illustrated by the curve of the difference of apparent temperature in Fig. 13.2, obtained by recording the intensity of the radiation of the earth's surface and water with the help of an airplane PRLS.

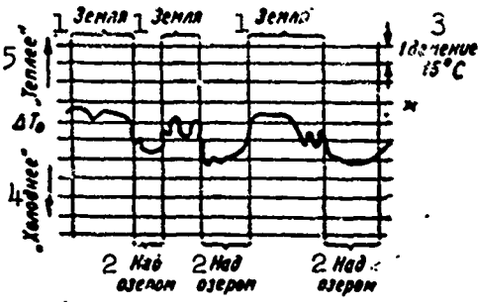


Fig. 13.2. Curve of the difference of apparent temperature of the earth's surface and water.
1) Earth; 2) over a lake; 3) 1 division, 15°C 4) "cold;" 5) "warm."

As a final register of the PRLS, the self-recording device was used. The useful signal at the output of the receiver activated the pen of a strip recorder which allows a continuous recording of the profile of the apparent temperatures of the objects being observed.

Note that the temperature contrast may even be there at the same equivalent temperature of the objects. This is valid in such cases, if the objects have different reflecting properties.

## §13.3. OPTIMUM TREATMENT OF THE SIGNALS OF THERMAL RADIOWAVES.

The thermal radiowaves are signals $s(t)$ for the receiving devices of the passive radiolocational stations. They are similar in their structure and statistical properties to the natural fluctuations of the noises of the receiver $n(t)$. This circumstance makes it difficult for the separation and determination of the parameters of the weak signals on the background of the noises since its actual shape is not known.

The problem of isolation of the useful information from the background of noises is resolved in the basis of the theory of statistical

testing hypothesis. The latter permits us to get recommendations for the synthesis of the optimum devices for the treatment of useful signals.

*The detection of fluctuation signals.* The optimum procedure of the treatment of the signals for the solution of the problem of detection may be determined on the basis of the criteria of the ratio of probabilities (Chapter 6).

The signals of thermal radiowaves being received are extremely close in statistical properties to the normal stationary random process. The detection of fluctuation signals is carried out on the background of noises with similar probability characteristics. Their additive mixture $x(t) = s(t) + n(t)$ will also be random normal processes with summation variance.

In this way, the single physical characteristic of the presence of the signals of thermal radiowaves is the increase of the variance. In the presence of the signals it is equal to the sum of $\sigma_c^2 + \sigma_{ш}^2$ of the variances of the signals and the natural noises, while in the case of their absence, it is simply $\sigma_{ш}^2$.

The statistical properties of the thermal radiowaves and the natural noises noted above permit us to determine the probability function in the absence and also in the presence of the signals.

$$L(x_1, x_2, \ldots, x_n; 0) = \frac{1}{(2\pi \cdot \sigma_{ш}^2)^{\frac{n}{2}}} \cdot \exp\left(-\frac{1}{2\sigma_{ш}^2} \cdot \sum_{i=1}^{n} x_i^2\right), \quad (13.6)$$

$$L(x_1, x_2, \ldots, x_n; s) = \frac{1}{[2\pi \cdot (\sigma_c^2 + \sigma_{ш}^2)]^{\frac{n}{2}}} \times \exp\left(-\frac{1}{2(\sigma_c^2 + \sigma_{ш}^2)} \cdot \sum_{i=1}^{n} x_i^2\right). \quad (13.7)$$

Expressions (13.6) and (13.7) permit us to create the ratio of probabilities

$$\Lambda(x_1, x_2, \ldots, x_n) = \left(\frac{\sigma_{ш}^2}{\sigma_c^2 + \sigma_{ш}^2}\right)^{\frac{n}{2}} \cdot \exp\left[\frac{\sigma_c^2}{2\sigma_{ш}^2(\sigma_{ш}^2 + \sigma_c^2)} \cdot \sum_{i=1}^{n} x_i^2\right]. \quad (13.8)$$

The solution on the presence of the signals is obtained in the cases, if the ratio of Probabilities (13.8) surpasses some threshold value $\Lambda_0$ or the logarithm of the ratio of probabilities satisfying the condition

$$\ln \Lambda(x_1, x_2, \ldots, x_n) = \frac{n}{2} \cdot \ln \frac{\sigma_m^2}{\sigma_m^2 + \sigma_c^2} + \\ + \frac{\sigma_c^2}{2\sigma_m^2(\sigma_m^2 + \sigma_c^2)} \cdot \sum_{i=1}^{n} x_i^2 \geqslant \ln \Lambda_0. \tag{13.9}$$

Performing transformation on Inequality (13.9), we obtain the condition for the detection of the signals of thermal radiowaves

$$\frac{1}{\sigma_m^2} \cdot \sum_{i=1}^{n} x_i^2 \geqslant \frac{2(\sigma_m^2 + \sigma_c^2)}{\sigma_m^2} \cdot \ln \left[ \Lambda_0 \cdot \left( \frac{\sigma_m^2 + \sigma_c^2}{\sigma_m^2} \right)^{\frac{n}{2}} \right] = \lambda_0. \tag{13.10}$$

It is known (§6.2), that

$$\frac{1}{\sigma_m^2} \cdot \sum_{i=1}^{n} x_i^2 = \frac{2F_m}{\sigma_m^2} \int_0^T x^2(t)\, dt = \frac{2}{E_0} \int_0^T x^2(t)\, dt, \tag{13.11}$$

where $F_m$ – the highest frequency of the spectra of the signals in the receiving target; $E_0 = \frac{\sigma_m^2}{F_m}$ – spectral density of the noise.

Therefore, the optimum procedure of detection, satisfying Condition (13.10) consists in the completion of the quadratic detection and integration. More precisely, (13.11) tells about the summation of the squares of the sum of signals and noises. On account of this, it is possible to reach maximum sensitivity independent of the site of performing the treatment of the signals according to high frequency or videofrequency.

Another way of the optimum treatment of the signals, $s(t)$ of the thermal radiowaves may be pointed out. Let the reception be carried out in two channels with independent noises $n_1(t)$ and $n_2(t)$. In each channel, there will be corresponding signals

$$x_1(t) = s(t) + n_1(t)$$

and

$$x_2(t)=s(t)+n_2(t), \tag{13.12}$$

which afterwards is compared by the determination of the extent of their mutual correlation

$$q=\int_0^T x_1(t)\cdot x_2(t)\,dt. \tag{13.13}$$

The execution of Operation (13.13) is equivalently fulfilled by the optimum procedure of the treatment of the signals given in Expression (13.11).

Actually,

$$\int_0^T x^2(t)\,dt=\int_0^T s^2(t)\,dt+2\int_0^T s(t)\cdot n(t)\,dt+\int_0^T n^2(t)\,dt. \tag{13.14}$$

The first integral is the energy of the signals, accumulated in the time of integration $T$; the second integral is equal to zero since the signal $s(t)$ and the internal noise $n(t)$ are independent*; the third integral characterizes the energy of the noise. In this way, the only substantial operation in the execution of the optimum procedure is the finding of the first integral in Expression (13.14) i.e., the accumulation of energy of the useful signals.

From the other side, the completion of the procedure of the treatment in correspondence with Expression (13.13) is determined equivalently by the following integrals:

$$\begin{aligned}\int_0^T x_1(t)\,x_2(t)\,dt&=\int_0^T [s(t)+n_1(t)]\cdot[s(t)+n_2(t)]\,dt=\\&=\int_0^T s^2(t)\,dt+\int_0^T s(t)\cdot n_1(t)\,dt+\\&+\int_0^T s(t)\cdot n_2(t)\,dt+\int_0^T n_1(t)\cdot n_2(t)\,dt.\end{aligned} \tag{13.15}$$

The last three integrals strive to zero at the increase of $T$, since the corresponding values are mutually independent. The first integral as can be seen determines the only substantial operation co-

inciding with the optimum Procedure (13.14) recommending to carry out the accumulation of the energy of the useful signals.

Consequently, from the position of the optimum treatment of the signals according to the threshold (detection), the procedures given by Expressions (13.11) and (13.13) are the same. In both cases, it is necessary to carry out the one and the same operation – accumulation of energy. The quality of the treatment is determined by the time of reception and the time of integration. The longer the time of integration, the more sensitive is the receiving tract to weak signals of thermal radiowaves.

*The evaluation of the parameters of thermal radiowaves.* The objects giving thermal radiowaves may be different one from the other in the power of the signals entering the receiver of the PRLS. The power of the fluctuating signals is characterized by its variance. Carrying out an evaluation of the variance may determine the intensity of the radiation of the different objects at the point of reception and also accomplished their identification.

In order to determine the evaluation of the variance $\hat{\sigma}_c^2$ at the maximum probability, it is necessary to find such values $\sigma_c^2=\hat{\sigma}_c^2$, at which the probability Function (13.7) is at the maximum. The condition of the maximum is given by the probability equation

$$\frac{\partial}{\partial \sigma_c^2} \cdot L(x_1, x_2, \ldots, x_n; s)\Big|_{\sigma_c^2=\hat{\sigma}_c^2}=0. \qquad (13.16)$$

Then the probability function has a maximum at $\sigma_c^2=\hat{\sigma}_c^2$.

Utilizing Expression (13.7) for the probability function and conducting the necessary computation in correspondence with the probability Equation (13.16), it is possible to obtain

$$\left(\sigma_m^2+\hat{\sigma}_c^2\right)=\frac{1}{n}\cdot\sum_{i=1}^{n}x_i^2$$

or

$$\hat{\sigma}_c^2 = \frac{1}{n} \cdot \sum_{i=1}^{n} x_i^2 - \sigma_{ш}^2. \qquad (13.17)$$

When treating continuous values of the signals, the evaluation of its variance will be obviously

$$\hat{\sigma}_c^2 = \frac{1}{T} \int_0^T x^2(t)\, dt - \sigma_{ш}^2. \qquad (13.18)$$

In this way, the optimum procedure of the evaluation of the variance of the useful signals is included in the calculation of the difference between the accumulated values of the energy of the signals $x(t)=s(t)+n(t)$ and the power of the natural noises $\sigma_ш^2$ of the treatment installation.

The comparison of Expression (13.18), giving the optimum procedure for the evaluation of the variance, with Expressions (13.14) and (13.15), uncovering the meaning of the optimum treatment during detection, permit us to draw the conclusion that in both cases, it is necessary to conduct just one and the same operation -- the accumulation of the energy of the useful signals. Therefore, the devices of treatment which realizes the recommendation of optimum Procedure (13.18) for the evaluation of the variance, are also optimum for the purpose of detection.

## §13.14. RECEIVER OF THERMAL RADIOWAVES.

The realization of the recommendations from Expressions (13.18), (13.13) and (13.11) permit us to synthesize circuits of receivers of thermal radiowaves which are optimum for detection as well as for the evaluation of intensity (variance) of the useful signal.

The receiver of thermal radiations, realizing Procedures (13.13) is referred to as correlational.

The receiver with the aid of which Operation (13.11) is carried

out is referred to as compensational.

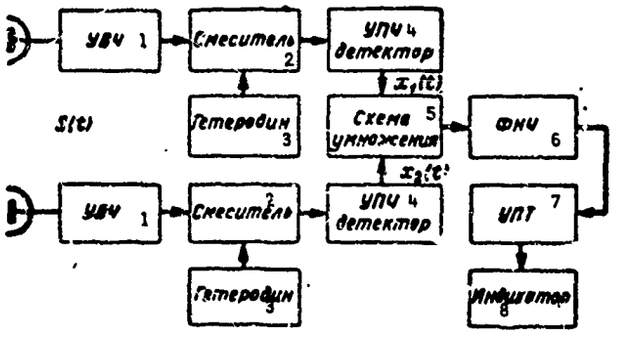


Fig. 13.3. Block diagram of correlational receiver of thermal radiowaves. 1) UVCh; 2) mixer; 3) heterodyne; 4) UPCh detector; 5) multiplying circuit; 6) FNCh; 7) UPT; 8) indicator

*Compensational receiver.* A block diagram of the correlational receiver of thermal radiowaves is represented in Fig. 13.3 The reception is carried out in two independent channels with stabilized amplification.

The input signal $s(t)$ in the presence of general antennas should be suppressed at each receiving channel by uncoupling devices for the exclusion of the entry of the natural noise of one receiving tract into the input of the other. The difference of channels is most commonly achieved by the use of two different antennas.

If superheterodyne receivers were used, then the local heterodyne should be synchronized. General heterodynes are never used because the noises natural to them would fall on both of the receiving channels and would be received as signals.

After the detection of the signals in each of the independent receiving tracts, their mutual comparison is conducted with the aid of the multiplier and the filter of low frequency (FNCh), forming the correlator.

The noises of the receivers are not correlated, whereas the signal voltages are strongly correlated. As a result at the output of the circuit of the multiplier, there will be a constant juxtaposition at the beginning of the signals and the fluctuation component of the natural noises of the receiving channels. The components received are integrated by the filter of low frequency with a very narrow passband

for the separation of the useful component which is suppressed by the amplifier of constant current (UPT). The signal from the output of the latter guarantees the operation of the indicator device, for example, to be used for the modulation of the brightness of the indicator direction.

*Compensational receiver of thermal radiowaves.* The compensational receiver realizes the recommendations set forth in Expressions (13.11) and (13.18) for optimum operation. Its block diagram is shown in Fig. 13.4. The input signal $s(t)$ of the thermal radiowaves passes through the low noise receiving tract to the compensating device. The compensation is conducted at the same part of the constant voltage, which is proportional to the variance of the natural fluctuation of the noises of the receiver.

The filter of low frequency separates the component of constant voltage which is fed to the indicator installation. As an indicator, electronic beam indicators may be used or self recorders.

In actual conditions, the parameters of the receiving tract is subjected to slow fluctuational variations. Particularly significant is the fluctuation of the coefficient of amplification which leads to the slow variation of the constant voltage dependent on the useful signals and the natural noises. As a result, the compensating voltage established at a certain moment will appear as ineffective at other moments. The same condition of optimum reception will not be maintained.

Partial elimination of the effect of the fluctuation of the coefficient of amplification of the receiving tract is achieved by the variation of the output voltage in short time intervals. During the course of these intermediate times, the coefficient of amplification is substantially unchanged. Similar principle is used as the basis

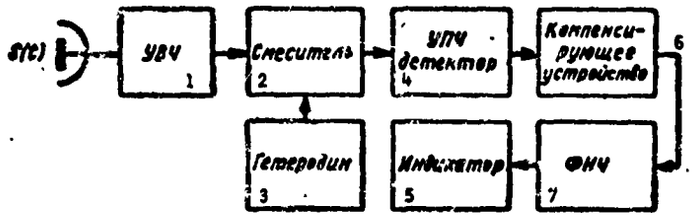


Fig. 13.4. Block diagram of compensational receiver of thermal radiowaves. 1) UVCh; 2) mixer; 3) heterodyne; 4) UPch detector; 5) indicator; 6) compensating device 7) FNCh.

of the operation of the modulational receiver.

*Modulational receiver of thermal radiowaves.* A typical block diagram of modulational receiver is illustrated in Fig. 13.5 while the forms of the signals in various chains are represented in time diagrams in Fig. 13.6.

The natural electromagnetic radiations of the objects of the centimeter or millimeter wave range are received by the antenna as useful signals, $s(t)$ (Fig. 13.6a) and enter the modulator of input signals. Ordinarily modulators are slit sections in right angled wave guides in which an absorbing plate – the modulator proper, driven by an electric motor – is inserted.

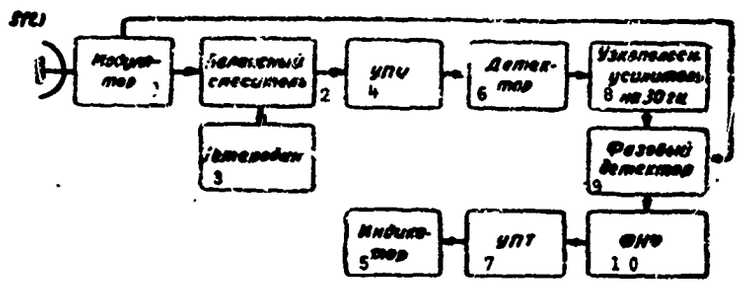


Fig. 13.5. Block diagram of modulational receiver of thermal radiowaves. 1) Modulator; 2) balanced mixer; 3) heterodyne; 4) UPCh; 5) indicator; 6) detector; 7) UPT; 8) narrow band amplifier at 30 hz; 9) phase detector; 10) FNCh.

The velocity of the turning of the plates composes of, for example, 30 revolutions/sec, which leads to the modulation of the output signals of the modulator, right-angled or sinusoidal oscillations of a frecuency of 30 hz. (Fig. 13.6b). The character of the envelope of modulation is determined by the form of the rotating plates.

The output signal of the modulator is transformed in frequency (Fig. 13.6c) and amplified by the wideband UPCh. The voltage at the output of the detector (Fig. 13.6d) contains the component, which

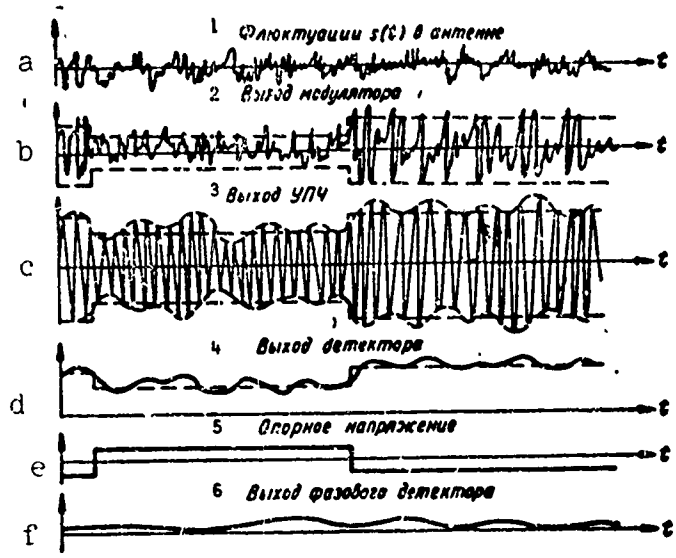


Fig. 13.6. Time diagrams of the voltage in the elements of the modulational receiver. 1) Fluctuations of $s(t)$ in antenna; 2) output of modulator; 3) output of UPCh; 4) output of detector; 5) supporting voltage; 6) output of phase detector.

varies in cycle with modulation (periodic component) and the noise component. The periodic component is filtered off and is amplified by the narrowband amplifier, tuned to the frequency of the modulation.

Afterwards, demodulation is carried out in the double cycle phase detector in which the supporting voltage enters (Fig. 13.6e) from the drive systems of the modulator. The periodic component gives at the output a constant component (Fig. 13.6f) while the spectra of the juxtaposing noise is displaced in the region of zero frequency.

Further treatment of the useful signal is carried out as in the correlational reception: the signals are integrated by the filter of low frequency with the narrow passband and are fed to the amplifier of constant current whose output controls the operation of the indicator device.

In the modulational receiver, as it is not difficult to notice the comparison of the useful signal and the natural noises is conducted in the subsequent time interval determined by the law of modulation. As a result, the useful signal is completely not used during the course of reception that leads to the decrease of the characteristics of the modulated reception in comparison with the optimum treatment.

## §13.5. SENSITIVITY OF THE RECEIVERS OF THERMAL RADIOWAVES.

The operational characteristics of the receiver (RKhP) realizing the optimum rules of detection of fluctuation signals (13.10), are represented by families of curves, which reflect the dependence of the probability of detection $D$ on the magnitude of the level of probability of false alarm $F$ under various values of the ratio of signal noise, $\frac{q_c}{\sigma_ш}$. Outwardly, the RKhP for the case of treatment of fluctuation signals does not differ from the operational characteristics shown in Fig. 6.5.

The calculation formulas for the probability of false alarm $F$ and the probability of detection $D$ may be found taking into account the rule of Dection (13.10). It is obvious that the probability of false alarm has a probability of occurrence, which is constituted such that

$$\frac{1}{\sigma_ш^2}\cdot\sum_{i=1}^{n}x_i^2\geqslant\lambda_0 \qquad (13.19)$$

in the absence of the signal, i.e.,

$$F=P\left\{\frac{1}{\sigma_ш^2}\cdot\sum_{i=1}^{n}x_i^2\geqslant\lambda_0\right\}\Big|_{q_c=0}. \qquad (13.20)$$

Similarly, the probability of detection is

$$D=P\left\{\frac{1}{\sigma_ш^2}\cdot\sum_{i=1}^{n}x_i^2\geqslant\lambda_0\right\}\Big|_{q_c\neq 0} \qquad (13.21)$$

under the condition that there is signal at the input.

For the determination of the probabilities $D$ and $F$, it is necessary to know the density of the distribution of the probability values

$$z=\frac{1}{\sigma_ш^2}\cdot\sum_{i=1}^{n}x_i^2. \qquad (13.22)$$

In the theory of probability, it is proved that similar sums of independent normal random values are distributed according to a law called the CHI$^2$ -- distribution ("chi"—square distribution):

$$W_n(z)=\begin{cases}\dfrac{1}{2^{\frac{n}{2}}\cdot\Gamma\left(\frac{n}{2}\right)}\cdot z^{\frac{n}{2}-1}\cdot e^{\frac{z}{2}}, & z\geqslant 0\\ 0, & z<0\end{cases} \qquad (13.23)$$

Here the symbol $\Gamma(x)$ refers to gamma-function.

The shape of the curves of CHI$^2$-distribution are shown in Fig. 13.7 for several values of $n$. At $n\leqslant 2$ the curves monotonously decreases; at $n>2$ they are close to the curve of normal distribution.

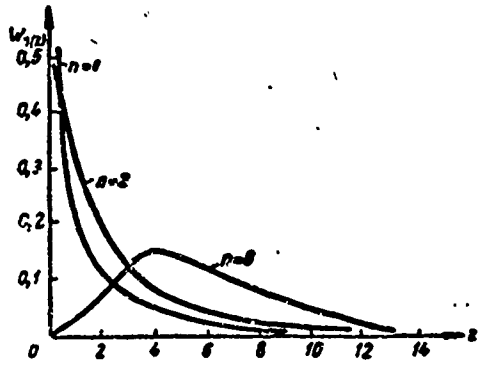


Fig. 13.7 CHI$^2$-distribution.

The quantity $z$ as it follows from Expression (13.22), obeys the law of distribution $W_n(z)$, since in the presence of the signal as well as in its absence, the value $x_i$ obeys the normal law. Therefore, the probability of false alarm $F$ and the probability of detection $D$ in correspondence with (13.20) and (13.21) are formally computed by the one and same formula

$$\int_{\lambda_0}^{\infty} W_n(z)\,dz.$$

But $\lambda_0$ in the presence of the signal $(\sigma_c\neq 0)$ has the value $\lambda_0=\lambda_{oc}$, while in its absence $(\sigma_c=0)$, $\lambda_0=\lambda_{om}$.

Consequently, the probability of detection is

$$D=\int_{\lambda_{oc}}^{\infty} W_n(z)\,dz \qquad (13.24)$$

and is computed under the condition that the signal is present at $(\sigma_c\neq 0)$. In correspondence with Expression (13.10) for this case

$$\lambda_{oc}=\frac{2(\sigma_{\text{ш}}^2+\sigma_c^2)}{\sigma_{\text{ш}}^2}\cdot\ln\left[A_0\cdot\left(\frac{\sigma_{\text{ш}}^2+\sigma_c^2}{\sigma_{\text{ш}}^2}\right)^{\frac{n}{2}}\right]. \qquad (13.25)$$

The probability of false alarm

$$F=\int_{\lambda_{\text{ош}}}^{\infty} W_n(z)\,dz \qquad (13.26)$$

is found under the condition of the absence of the signal ($\sigma_c=0$), i.e.,

$$\lambda_{\text{ош}}=2\ln A_0. \qquad (13.27)$$

The Integrals (13.24) and (13.26) are expressed by an incomplete gamma-function, which is determined by the equality

$$\int_0^y e^{-t}\cdot t^x\cdot dt=\Gamma(1+x;\ y).$$

Therefore the probability of detection is

$$D=1-\frac{\Gamma\left(\frac{n}{2};\ \frac{\lambda_{0c}}{2}\right)}{\Gamma\left(\frac{n}{2}\right)}, \qquad (13.28)$$

while the probability of false alarm is

$$F=1-\frac{\Gamma\left(\frac{n}{2};\ \ln A_0\right)}{\Gamma\left(\frac{n}{2}\right)}. \qquad (13.29)$$

The Expressions (13.28) and (13.29) permit us to calculate RKhP).

At fixed values of the probability of false alarm $F$ the probability of detection $D$ will be bigger, the bigger the ratio of signal/noise $\frac{\sigma_c}{\sigma_{\text{ш}}}$, as this follows from Expression (13.28) and (13.25).

Concrete values of $D$ and $F$ are assigned by tactical considerations. For a guarantee of reception of the magnitude $D$, the signal/noise ratio $\frac{\sigma_c}{\sigma_{\text{ш}}}$ should be somewhat bigger than the minimum value $\frac{\sigma_{c\,\text{мин}}}{\sigma_{\text{ш}}}$, i.e., the useful signal should surpass the determined necessary minimum value $P_{\text{пр мин}}=\sigma^2_{c\,\text{мин}}$.

The magnitude of the minimum necessary signal $P_{\text{пр мин}}$, providing the required value of probability of detection $D$ at a defined level of false alarm $F$ is generally used as the quantitative characteristics of the sensitivity of the receiving tract.

The output signal $P_{пр\,мин}$ corresponds to the determined value of the signal/noise ratio $n_p$ at the output of the integrating filter (FNCh) of the receivers of the thermal radiowaves. Therefore the sensitivity of the receivers of thermal radiowaves is quantitatively estimated by the magnitude of the minimum power of the signal at the input $P_{пр\,мин}$, necessary for the obtaining of the required signal/noise ratio $n_p$ at the output of the filter of low frequency (FNCh in Fig.13.3, 13.4, 13.5).

*Sensitivity of the correlational and compensational receivers.* The correlational and compensational receivers of thermal radiowaves realize the optimum procedure of the treatment of signals. Therefore their sensitivity are the same and below we shall carry out its calculation for the correlational receiver only.

The determination of the magnitude of the minimum necessary signal $P_{пр\,мин}$ at the input of the receiver is related to the signal/noise ratio found at the output of FNCh (Fig. 13.3). For this, in the following we shall calculate the spectra of the signal and noise at the out put of the linear and non-linear elements of the receiving tract.

The spectral components of the signal and the noise pass through the narrow band linear high frequency tracts with right-angled frequency characteristic of width $\Delta f = \frac{\Delta\omega}{2\pi}$, symmetrical with respect to the operating frequency $\omega_0$ and the nonlinear element – correlator formed by the multiplier circuit and FNCh with the passband $\Delta F = \frac{\Delta\Omega}{2\pi}$.

The spectra of the signal and noise at the output of the linear element with frequency characteristic $K(\omega)$ are found by the known energetic spectra of the input process $G_{вх}(\omega)$ according to the formula

$$G_{вых}(\omega) = G_{вх}(\omega) \cdot K^2(\omega). \qquad (13.30)$$

Expression (13.3) permits subsequently the calculation of the spectral components of the signal and noise after passing through the

linear elements of the correlational receiver.

Some difficulties of a computing nature are encountered at the determination of the energetic spectra of the signal and noise after the passage through the nonlinear elements. The known transformation

$$R(\tau)=\frac{1}{2\pi}\cdot\int_0^{\infty}G(\omega)\cdot\cos\omega\tau\cdot d\omega. \qquad (13.31)$$

is used hereby between the functions of the correlational process $R(\tau)$ and its energetic spectra $G(\omega)$. A reverse transformation, according to the energetic spectra of the process $G(\omega)$ permits us to find its correlation function

$$G(\omega)=4\int_0^{\infty}R(\tau)\cdot\cos\omega\tau\cdot d\tau \qquad (13.31a)$$

The multiplication circuit conducts linear transformation of the form

$$y(t)=k\cdot x_1(t)\cdot x_2(t), \qquad (13.32)$$

i.e., the output signal $y(t)$ is proportional to the product of the input signals $x_1(t)=s(t)+n_1(t)$ and $x_2(t)=s(t)+n_2(t)$ of each receiving tract. Therefore at the output of the multiplication circuit there is, in the presence of signals, a random process

$$y(t)=k\,[s^2(t)+s(t)\,[n_1(t)+n_2(t)]+n_1(t)\cdot n_2(t)]. \qquad (13.33)$$

The calculation of the autocorrelation function $T(\tau)$ of the process $y(t)$ is conducted by the averaging of the products $y(t)\cdot y(t+\tau)$. i.e.,

$$R(\tau)=\overline{y(t)\cdot y(t+\tau)}, \qquad (13.34)$$

and connect, as is seen from Expressions (13.3-) and (13.34), with the determined average value of the products $\overline{s^2(t)\cdot s^2(t+\tau)}$ and $\overline{n(t)\cdot n(t+\tau)}$ correspondingly for the first ($n_1$) and the second ($n_2$) receiving channels. Their calculation on the basis of the general rule of finding the average value require the knowledge of the two dimensional laws of distribution for signal and noise.

The two dimensional law of the distribution of signal $W(s; s_\tau)$ and noise $W(n; n_\tau)$is normal and given by the expression

$$W(s; s_\tau)=\frac{1}{2\pi\cdot\sigma_c\sqrt{1-r_c^2}}\cdot\exp\left[-\frac{s^2+s_\tau^2-2s\cdot s_\tau\cdot r_c}{2\sigma_c^2\cdot(1-r_c^2)}\right], \qquad (13.35)$$

$$W(n; n_\tau)=\frac{1}{2\pi\cdot\sigma_{sh}\sqrt{1-r_{sh}^2}}\cdot\exp\left[-\frac{n^2+n_\tau^2-2n\cdot n_\tau\cdot r_{sh}}{2\sigma_{sh}^2(1-r_{sh}^2)}\right],$$

in which $r_s$ and $r_{sh}$ – coefficients of correlation for signal and noise and for the simplicity of writing, they are designated $s(t)=s$; $s(t+\tau)=s_\tau$; $n(t)=n$; $n(t+\tau)=n_\tau$.

The fluctuations of noise and signal of thermal radiowaves are statistically similar, therefore $r_c=r_{sh}$. The coefficient of correlation is by definition the ratio of the correlation function $R(\tau)$ to its value at $\tau = 0$.

$$r(\tau)=\frac{R(\tau)}{R(0)}. \qquad (13.36)$$

Utilizing Expressions (13.31a) and (13.36) according to known spectra for signal and noise, it is not difficult to find the coefficient of correlation of random processes after the passage through the narrow band $(\omega_0 \gg \Delta\omega)$ of the linear system with right-angled frequency symmetrical with respect to the central frequency $\omega_0$ and width characteristic $\Delta\omega$.

$$r_c=r_{sh}=\frac{\sin\frac{\Delta\omega\tau}{2}}{\frac{\Delta\omega\tau}{2}}\cdot\cos\omega_0\tau. \qquad (13.37)$$

The final expression for the correlation function at the input of FNCh (13.34) after the completion of the intermediate calculations and the exclusion of the corresponding double frequencies $(2\omega_0)$ has the form

$$R(\tau)=k^2\sigma_c^4+\frac{k^2}{2}\left[2\sigma_c^4+\sigma_c^2(\sigma_{sh_1}^2+\sigma_{sh_2}^2)+\sigma_{sh_1}^2\cdot\sigma_{sh_2}^2\right]\times \times\frac{\sin^2\pi\cdot\Delta f\cdot\tau}{\pi^2\cdot\Delta f^2\cdot\tau^2}. \qquad (13.38)$$

The first term

$$R_c(\tau) = k^2 \cdot \sigma_c^4 \qquad (13.39)$$

determines the spectral component of the signal at the input of the FNCh. The second term in Expression (13.38)

$$R_{ш}(\tau) = \frac{k^2}{2} \cdot \left[2\sigma_c^4 + \sigma_c^2(\sigma_{ш_1}^2 + \sigma_{ш_2}^2) + \sigma_{ш_1}^2 \cdot \sigma_{ш_2}^2\right] \cdot \frac{\sin^2\pi \cdot \Delta f \cdot \tau}{\pi^2 \cdot \Delta f^2 \cdot \tau^2} \qquad (13.40)$$

specifies the noise spectral component at the input of the FNCh.

In correspondence with Transformation (13.31), the spectral density of the power of the signal at the input of FNCh is

$$G_c(\omega) = 4 \cdot \int_0^{\infty} R_c(\tau) \cdot \cos\omega\tau \cdot d\tau$$

or taking into consideration, Expression (13.39)

$$G_c(\omega) = 4 \cdot \int_0^{\infty} k^2 \cdot \sigma_c^4 \cdot \cos\omega\tau \cdot d\tau = 2k^2 \cdot \sigma_c^4 \cdot \delta(\omega), \qquad (13.41)$$

where $\delta(\omega) = 2 \cdot \int_0^{\infty} \cos\omega\tau \cdot d\tau$ is delta-function.

The power of the signal at the input of FNCh with passband $\Delta F$ is determined by the known spectral density of the signal at its input

$$P_c = \int_0^{2\pi\Delta F} 2k^2 \cdot \sigma_c^4 \cdot \delta(\omega) \cdot d\omega = k^2 \cdot \sigma_c^4. \qquad (13.42)$$

Similarly, the spectral density of noise at the input of FNCh may be found by the known "noise" component $R_{sh}(\tau)$ of the correlation function

$$G_{ш}(\omega) = 4 \cdot \int_0^{\infty} \frac{k^2}{2} \cdot \left[2\sigma_c^4 + \sigma_c^2 \cdot (\sigma_{ш_1}^2 + \sigma_{ш_2}^2) + \sigma_{ш_1}^2 \cdot \sigma_{ш_2}^2\right] \times$$

$$\times \frac{\sin^2\pi \cdot \Delta f \cdot \tau}{(\pi \cdot \Delta f \cdot \tau)^2} \cdot d\tau$$

or after taking the last integral, we have

$$G_{ш}(f) = \left[2\sigma_c^4 + \sigma_c^2 \cdot (\sigma_{ш_1}^2 + \sigma_{ш_2}^2) + \sigma_{ш_1}^2 \sigma_{ш_2}^2\right] \cdot \frac{k^2}{\Delta f}. \qquad (13.43)$$

Since the frequency band FNCh $\Delta F \ll \Delta f$, therefore the power of noise at its output may be calculated by the formula

$$P_{ш} = G_{ш}(f) \cdot \Delta F, \qquad (13.44)$$

approximately, it may be assumed that the power of the noise is equal-

ly distributed in the frequency band $\Delta F$. Consequently, the power of the noise at the output of FNCh is

$$P_{ш} = [2\sigma_c^4 + \sigma_c^2 \cdot (\sigma_{ш_1}^2 + \sigma_{ш_2}^2) + \sigma_{ш_1}^2 \cdot \sigma_{ш_3}^2] \cdot \frac{k^2 \cdot \Delta F}{\Delta f}. \qquad (13.45)$$

Expressions (13.42) and (13.45) permits us to find the signal/noise ratio at the output of FNCh

$$\frac{P_c}{P_{ш}} = \frac{\sigma_c^4}{2\sigma_c^4 + \sigma_c^2(\sigma_{ш_1}^2 + \sigma_{ш_2}^2) + \sigma_{ш_1}^2 \cdot \sigma_{ш_3}^2} \cdot \frac{\Delta f}{\Delta F}. \qquad (13.46)$$

For the most interesting case of weak signals $\sigma_c^2 \ll \sigma_{ш}^2$; besides this, let us assume $\sigma_{ш_1}^2 = \sigma_{ш_2}^2 = \sigma_{ш}^2$. Therefore, the ratio

$$\frac{P_c}{P_{ш}} = \frac{\sigma_c^4}{\sigma_{ш}^4} \cdot \frac{\Delta f}{\Delta F}. \qquad (13.47)$$

By definition, the magnitude of the minimum necessary power determining quantitatively the sensitivity of the receiver is found from the conditions obtained at the output of FNCh, the signal/noise ratio is equal to $n_p$. Consequently,

$$P_{пр\ мин} = \sigma_{с\ мин}^2 = \sigma_{ш}^2 \cdot \sqrt{\frac{\Delta F}{\Delta f}} \cdot n_p \qquad (13.48)$$

or taking into account that the power of the noises $P_{sh}$ is equal to $\sigma_{ш}^2$,

$$P_{пр\ мин} = P_{ш} \sqrt{\frac{\Delta F}{\Delta f}} n_p. \qquad (13.49)$$

The time constant $\tau_\Phi$ of the receivers of thermal radiowaves defines the magnitude, the reciprocal of the width of the passband $\Delta F$ of the integrating filter, i.e.,

$$\tau_\Phi = \frac{1}{\Delta F}. \qquad (13.50)$$

The time constant defines the fast acting channel. Taking into account Expression (13.50) the minimum necessary power at the input of the optimum receiver of thermal radiowaves is

$$P_{пр\ мин} = n_p \cdot \frac{P_{ш}}{\sqrt{\tau_\Phi \cdot \Delta f}}. \qquad (13.51)$$

It is seen that the sensitivity may increase, decreasing the natural

noise $P_{sh}$ and increasing the frequency band by the high frequency $\Delta f$ and the time constant of the receiver $\tau_{\Phi}$.

*Sensitivity of modulational receiver.* Modulational receiver of thermal radiowaves, whose block diagram is shown in Fig. 13.5, is not optimum since owing to the modulation, the useful signal is not utilized during the course of all the receiving time. Therefore, its sensitivity is in principle lower than the correlational and compensational receivers of thermal radiowaves.

The minimum necessary signal for the modulational receiver is determined by methods similar to what was used above. In carrying out the calculation, it should be assumed that the characteristic transformation of the nonlinear elements of the receiving tract has the following form

$$x(t)=k\cdot y^2(t) \tag{13.52}$$

for the detector of the receiver also

$$W(t)=V(t)\cdot \sin 2\pi qt \tag{13.53}$$

for the phase detector. In the last expression $q$ – frequency of modulation of the input signal.

In the cases of weak signals $\sigma_c^2 \ll \sigma_{ш}^2$ the signal/noise ratio at the output of FNCh are equal

$$\frac{P_c}{P_{ш}}=\frac{1}{32}\cdot\left(\frac{\sigma_c}{\sigma_{ш}}\right)^4\cdot\frac{\Delta f}{\Delta F}\cdot \tag{13.54}$$

Therefore, the magnitude of the maximum necessary power at the input of the receiver

$$P_{пр\ мин}=\sigma^2_{c\ мин}=4\sqrt{2}\cdot\sigma^2_{ш}\sqrt{\frac{\Delta F}{\Delta f}}\cdot n_p \tag{13.55}$$

or in the designations used earlier

$$P_{пр\ мин}=4\sqrt{2}\cdot\frac{P_{ш}}{\sqrt{\tau_{\Phi}\cdot\Delta f}}\cdot n_p. \tag{13.56}$$

Expressions (13.51) and (13.56) follow on the fact that the sensitivity of the modulational receiver is $4\sqrt{2}$ times lower than that of

the optimum receivers of thermal radiowaves even though qualitatively the character of the dependence of the magnitude of minimum necessary power on the basic parameters of the receiving tract remains as before.

For the minimum necessary power at the input of the receiver of thermal radiowaves the general expression

$$P_{\text{пр мин}}=\zeta\cdot\frac{P_{\text{ш}}}{\sqrt{\tau_{\phi}\cdot\Delta f}}\cdot n_{p}, \qquad (13.56)$$

may be written where $\zeta=1,0$ for correlational and compensational receivers and $\zeta=4\sqrt{2}$ for modulational reception.

The presence of obvious advantages in the sensitivity for the optimum receivers does not predetermine their preference in use. It is necessary to take into account also the degree of complexity of the technical realization and the conditions of exploitation. For example, for the correlational receiver, an extremely difficult problem is the stabilization of the amplification of the two receiving tracts – in the presence of two channels, two different ARU are necessary, providing identity of their amplitudinal characteristics.

*Methods of raising the sensitivity of the receivers of thermal radiowaves.* Expressions (13.51) and (13.56) permit the establishment of a route to raise the sensitivity of the receivers of thermal radiowaves. It is seen that the minimum detectable power of the signal $P_{\text{пр мин}}$ is directly proportional to the power of the natural noises of the receiver and inversely proportional to the root square of the passband for high frequency and the time constant of the integrating elements.

The first method of reducing $P_{\text{пр мин}}$ consists of the decrease of the passband of the integrating filter. But, in so doing, the time constant of the receiver is increased such that it may seem unattainable for the use of passive radiolocation systems on a high velocity flying apparatus. Airborne PRLS with high time constants do not guaran-

tee the observation of quickly varying thermal reliefs of locality and objects.

The second method of raising the sensitivity is based on the simultaneous (or different) decrease of the power of the natural noise of the receiver and the widening of the passband for high frequency. Perspective devices for the solution of this problem are high frequency amplifiers for LBV, parametric and quantum mechanical amplifiers possessing uniquely low coefficient of noise at wide passband frequency.

## §13.6. WORKING RANGE AND DISTINGUISHABILITY OF OBJECTS DURING PASSIVE DETECTION BY THERMAL RADIOWAVES.

The working range and the distinguishability of objects are the basic tactic characteristics of passive radiolocational stations. The principal physical parameters determining these characteristics are correspondingly the apparent temperatures of the objects and the difference of the apparent temperatures.

*Working range.* The range of the detection of the sources of thermal radiowaves is determined by the sensitivity of the receiver and the magnitude of the power entering into its input.

Let us carry out the calculations of the levels of power of the thermal radiowaves of the objects at the input of the receiving device under the following assumptions:

1. The power of thermal radiowave of unit area of the object with surface $S_1$ constant for all directions.

2. Receiving antenna with effective surface $A$ removed from the radiator with the surface $S_1$ at a distance of $R$. The surface of the radiator and the exposure of the antenna are perpendicular to the line joining their axes.

3. The distance $R$ is sufficiently great. Therefore the effective

surface $A$ of the receiving antenna is "visible" from every element of the surface $S_1$ of the radiator at the one and the same spatial angle $\Omega = \frac{A}{R^2}$.

Utilizing Rayleigh's Law (13.1), giving the magnitude of power radiating from an unit surface of the object in an unit solid angle and a frequency band of 1 hz, one may determine the full power of the radiowave from the surface $S_1$ in the solid angle $\Omega$:

$$P_1 = p \cdot S_1 \cdot \frac{A}{R^2} = \frac{2kT_1^\circ}{\lambda^2} \cdot \frac{S_1 A}{R^2}. \qquad (13.57)$$

Here $T_1^\circ$ – apparent temperature of the object. If the band of the receiver is $\Delta f$, then the full power of the useful signal at its input will be

$$P_{пр} = \frac{S_1 \cdot A}{R^2} \cdot 2k \cdot T_1^\circ \cdot \frac{\Delta f}{\lambda^2}. \qquad (13.58)$$

Ordinary antenna system receives electromagnetic oscillations only of a certain polarization. On account of this, on the average of only half the entering power will be received inasmuch the different forms of polarization are equally probable (for a majority of cases).

We shall calculate also the connection between the effective surface of the antenna $A$ with the coefficient of directional action in the principal direction $D$. As a result of Expression (13.58) for the power, entering the input of the receiving device, transformed into the form

$$P_{пр} = \frac{D \cdot S_1}{4\pi R^2} \cdot k \cdot T_1^\circ \cdot \Delta f. \qquad (13.59)$$

If $P_{пр}$ exceeds the minimum necessary power at the input of the receiver, then the object will be detected. Therefore, the maximum range of the detection of the sources of thermal radiowave without considering the attenuation of the electromagnetic wave in the atmosphere.

$$R_{макс} = \sqrt{kT_{и}^{\circ} \cdot \Delta f \cdot \frac{D \cdot S_{и}}{4\pi \cdot P_{пр\,мин}}}. \qquad (13.60)$$

The quantity $P_{пр\,мин}$ is determined by Expression (13.56a) which, taking into consideration, that $P_{ш} = NkT^{\circ} \cdot \Delta f$, may be written as

$$P_{пр\,мин} = n_{р} kT^{\circ} \cdot N \cdot \zeta \cdot \sqrt{\frac{\Delta f}{\tau_{ф}}}, \qquad (13.61)$$

where $N$ – the coefficient of noise of the receiver, and $T^{\circ}$ is the absolute temperature which generally is assumed to be around 300°K. Therefore Expression (13.60) may be transformed

$$R_{макс} = \sqrt[4]{\tau_{ф}\Delta f} \sqrt{\frac{T_{и}^{\circ}}{n_{р}NT^{\circ}} \frac{DS_{и}}{4\pi\zeta}} \qquad (13.62)$$

or replacing $D$ with the effective surface $A$,

$$R_{макс} = \sqrt[4]{\tau_{ф}\Delta f} \sqrt{\frac{T_{и}^{\circ}}{n_{р}NT^{\circ}} \frac{AS_{и}}{\Omega^{2}}}. \qquad (13.63)$$

From Expressions (13.62) and (13.63), one may establish the degree of the effects of various parameters on the range of detection of passive radiolocational observation. In particular, one can see that the range of detection is increased with the increase in the passband frequency, time constant and the relative drop of temperature of the radiator and the receiver.

From the equations of range (13.62) and (13.63), it also follows that for a workable amplification of high frequencies, it is necessary in the first place to reduce their noise coefficient and then take measures for the widening of the band $\Delta f$, since $N$ strongly influences the range of detection.

In conclusion, by Formula (13.62) we shall estimate the working range of the PRLS at the following conditions:

1) The passband for high frequency $\Delta f = 50$ Mhz the noise coefficient $N = 1.5$. There are receiving tracts with modern parametric amplifiers which need no cooling and have similar characteristics.

2) Time constant of correlational receiver, $\tau_ф = 3{,}2$ sec, necessary signal/noise ratio $n_p = 1{,}5$; antenna has a coefficient of directional action $D = 15{,}000$.

3) The object of detection has a surface of $S_ц = 15$ м² and apparent temperature of $T_ц^\circ = 300°$K. The working range is 10 km, i.e., the PRLS concedes in working radius to the ordinary radiolocational station at the present state of technology.

*Distinguishability of objects during passive detection.* With the aid of airplane stations passive radiolocation has succeeded to get extremely good reproductions of the relief of localities (Fig. 13.8). The image of the locality on the screen of the indicator of the PRLS is referred to as the radiometric chart.

The differences in the targets and objects are detected in the passive radiolocational stations by various factors, among which the principal ones are:

– The difference of apparent temperature of the objects;

– the angle of sliding of the antenna beam, the formation of the axis of the diagrams of directionality of the antenna and the perpendicular to the surface of the objectives;

– type of polarization of the electromagnetic waves, being received by the antenna;

– width of the diagrams of directionality of the antenna;

– sensitivity of the receiver of thermal radiowaves.

The decisive factor determining the distinguishability of the objects which cannot be controlled is the difference in the apparent temperature. Below, results are cited of the measurement of difference of apparent temperature of some objects obtained at the operation in the centimeter wave range:

- snow covered earth and buildings - 10°K.
- damp earth and automobile - 12°K.
- dry and damp earth - 19°K.
- snow covered and damp earth - 41°K.

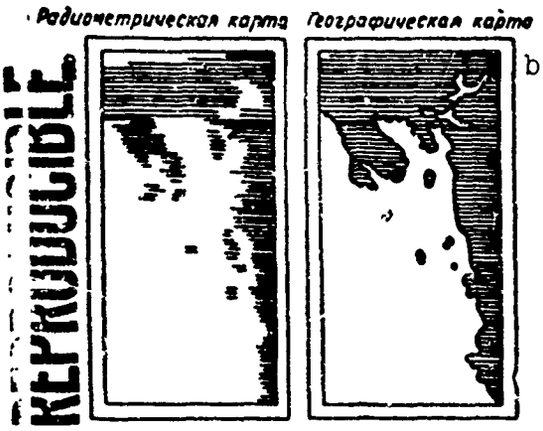


Fig. 13.8. Image of the locality on the screen of the indicator of PRLS. a) Radiometrical chart; b) geographical chart.

The effect of the type of polarization of the antenna is most strongly expressed at large angle of sliding and disappears when the maximum of the diagrams of directionality is perpendicular to the surface of the object. For example, the surface of water with absolute temperature 293°K has an apparent temperature of 160°K, if the angle of sliding is 90°, independent of the polarization of the antenna. At an angle of sliding of 30° and vertical polarization, the apparent temperature of water is 280°K, but when using antenna of horizontal polarization, its apparent temperature again becomes 1 0°K.

The best condition for distinguishing asphalt landing strip from the surrounding grass covering will be when the maximum of the diagrams of directionality forms a small angle with the surface of asphalt while the polarization of the antenna is horizontal. In this case, the asphalt will appear to be more "cold," than the ground growth, which seems to be "warm." From the other side, grass maintains the same apparent temperature at any angle of sliding and type of polarization. Asphalt, however, has the same temperature regardless of the angle of sliding at the vertical polarization of the antenna; at horizontal polarization, its apparent temperature rapidly decreases with the increase of the angle of sliding. Therefore, for distinguishing the smooth metallic objects (for example, flying objects), located on

asphalt cover, the antenna should have vertical polarization, since metals radiate weakly, practically under any conditions while asphalt radiates more intensively vertically polarized electromagnetic waves.

The effects of the width of the diagrams of directionality of the antenna on the apparent temperature of the objects are expressed in the following way. If the width of the diagrams of directionality exceeds the angular size of the object then its apparent temperature in percentage ratios will be that much lower as the angular size of the object differs from the width of the diagrams of directionality of the antenna. Therefore, in principle, passive radiolocational systems for the survey of localities should possess possibly higher resolving power i.e., have extremely narrow diagrams of directionality. On the road to the realization of such diagrams of directionality, some well known difficulties are encountered: constructionally unacceptable bulk of the antenna or in trying to raise the operational frequency, an increase in the damping of the thermal wave in the atmosphere.

## §13.7. PASSIVE DETECTION OF SOURCES OF LONGWAVE RADIATIONS.

The ultra low frequency radiowaves *(15-30 khz)* originating from lightning discharges, the exhaust of ballistic rockets and nuclear explosions may be used for their passive detection.

On the range of detection, basically one talks about the condition of propagation of the ultra long waves.

The principal essential features which determine the character of the propagation of the long electromagnetic waves are included in the following:

1) The long waves bend very well around the earth's surface which lead to the propagation of straight (earth) waves to an extremely large distance.

2) The propagation of long waves takes place in the space of a spherical waveguide formed by the surface of the earth and the ionosphere. It is established that the absorption of energy is minimum in the *10-30 khz* range and consists of not more than 1-2 db at *1000 km*.

3) On long waves, one almost does not speak about roughness or non-uniformity of the earth's surface, which permits us to consider it as uniform in the calculation of the field intensity at the point of reception.

It is experimentally established that the intensity of the electrical field, in dependence on the distance $R$ to the radiating source at the frequency range of *10-30 khz*, is characterized by the curve in Fig. 13.9. The field intensity varies in dependence on the conditions in some areas, the shape of the curves *AB* and *CD*. Since the source of the radiowave is the operating engine of the rocket, therefore, as seen in the graph, even at a distance of up to *10,000 km*, the field strength is sufficient for the reception of the signals originated from the exhaust.

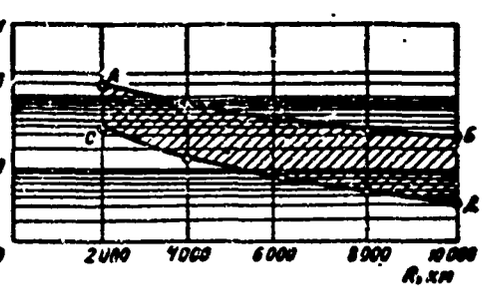


Fig. 13.9. Graph of dependence of the intensity of electric field $E$, on the distance $R$ for the frequency *10-13 khz*.

The propagation of the cylindrical earth (straight) waves of the ultra low frequency range in the space of the wave guide is illustrated in Fig. 13.10. As a result of a great number of experiments, a formula was proposed for the calculation of the field intensity $E$ created by the source of long wave radiowaves at a distance of $R$ to the point of reception:

$$E = \frac{300\sqrt{P_\Sigma}}{R} \cdot \sqrt{\frac{\delta}{\sin\delta}} \cdot e^{-\frac{0{,}0015R}{\sqrt{\lambda}}} \left[\frac{мв}{м}\right], \qquad (13.64)$$

where $P_\Sigma$ – power of the source kilovolt; $R$ and $\lambda$ – correspondingly

distance and wave length, km; $\vartheta$ – heliocentric angle.

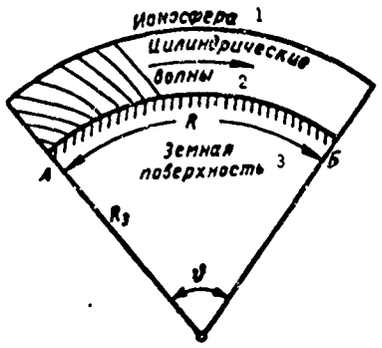


Fig. 13.10. The spread of the electromagnetic wave, frequency *10-30 khz* in the space of the waveguide. 1) Ionosphere; 2) cylindrical waves; 3) earth's surface.

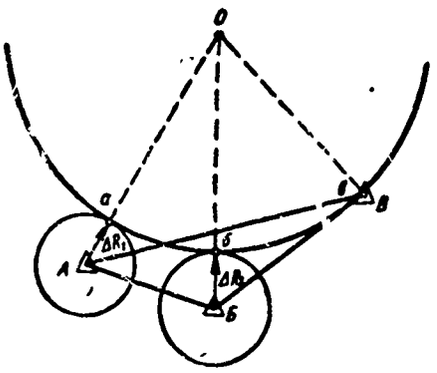


Fig. 13.11. Determination of the location of the source of radiowave.

Expression (13.64) allows us to carry out the oriented calculation, in particular, to evaluate the strength of radiation, existing at the location of the exhaust of the rocket or the conducting of a nuclear explosion.

For the determination of the source of the long wave radiation three receiving stations, A, B and C are used, spaced at some distance apart. The magnitude of the spacing of the receiving points determines the base of the system AB and BC. The registration of the time of the arrival of the signal in the receiving stations is carried out. From them it is possible to determine the difference in the distances of the points A, B and C from the course of the radiowave. Consequently, the location is determined by the exact intersection of two hyperbolic lines of position. All necessary calculations are generally conducted with the help of digital computers.

The principle of the operation may be elucidated by Fig. 13.11. Let the time of reception of the radiosignal at station A be $t_A$ and station B and C – $t_B$ and $t_C$ correspondingly. Let us also suppose that the signal arrives first at station C. It is easy to determine the

difference in the time of arrival of the radiosignals: at station A, the signal arrives with a delay of $\Delta t_{AB} = t_A - t_B$, and at station B with a delay of $\Delta t_{БВ} = t_Б - t_B$. Multiplying $\Delta t_{AC}$ and $\Delta t_{BC}$ by the velocity $S$ of the propagation of the electromagnetic wave we find the difference of distance

$$\Delta R_{AB} = c \cdot \Delta t_{AB}$$

and

$$\Delta R_{БВ} = c \cdot \Delta t_{БВ}, \qquad (13.65)$$

which determines the location of the source of the radiowave.

Actually, we draw circles of radii $\Delta R_{AC}$ and $\Delta R_{BC}$ correspondingly with centers at A and B. The course of the signal should be found in the center of the circle, passing through the point of the location of the station C and tangent to the circles drawn earlier at the points a and b, since the electromagnetic wave arrives at the points a, b, and c in one and the same time.

The accuracy of the location determination depends principally on the magnitude of the base, errors in the registration of the difference of the time of arrival of the signal and the condition of propagation. Generally, for an increase in the accuracy, the base AB and BC are set at large values in a few hundred kilometers and more, but then there will be strong effects on the accuracy arising from the difference in the condition of propagation of the electromagnetic wave from the source to the receiving stations and the differences in the parameters of the soil at the place of their location. Therefore, a system is adopted of three receiving stations with small bases, which permit the determination of the direction to the source of Radiowave (Fig. 13.12). If there is a second of the same system sufficiently far from the first, then it is possible to determine the location of the source.

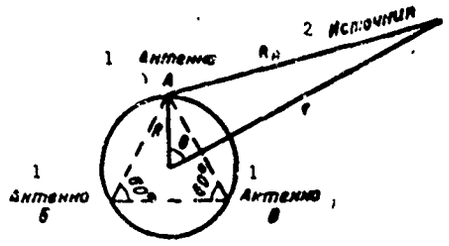


Fig. 13.12. Geometry of the system of bearing taking. 1) Antenna; 2) source.

Three antennas of the receiving system are positioned on the corners of an equilateral triangle, as it is shown in Fig. 13.12. The distances from the source of the signal to every one of the antennas in the notations used are

$$R_A = \sqrt{R^2 + r^2 - 2rR\cos\theta},$$
$$R_Б = \sqrt{R^2 + r^2 - 2rR\cos(120° + \theta)},$$
$$R_B = \sqrt{R^2 + r^2 - 2rR\cos(120° - \theta)}. \qquad (13.66)$$

For each pair of the antennas one may find the relative time of delay, which is proportional to the difference in distance from these antennas to the course of the signal

$$\Delta t_{BA} = \frac{R_B - R_A}{c},$$
$$\Delta t_{БВ} = \frac{R_Б - R_B}{c}, \qquad (13.67)$$
$$\Delta t_{БА} = \frac{R_Б - R_A}{c}.$$

Expressions (13.66) and (13.67) permit us to construct what is so called a polar diagram of time of delay of the signal for neighboring pairs of Antennas (Fig. 13.13). In the construction of the diagram, the length of the base $(R\sqrt{3})$ is taken as unity. The exact meaning of these distances and the form of the diagram itself depend, obviously, on the ratio $\frac{r}{R}$. Under the condition $r >> R$ the form of the polar diagram of the time of delay of the signal practically does not depend on the distance $r$ to the source of radiation. At $\frac{r}{R} = 10$ the values shown in Fig. 13.13 differ from the exact values not more than 0.5%.

Ordinarily, the condition $r << R$ is fulfilled with sufficiently large delay. Therefore, by the difference in the time of the arrival of the signal, one may judge the azimuth of the source of radiation as it is seen from the polar diagrams of the delay of the signals.

The accuracy of the determination of the azimuth depends on the errors of the fixing of the difference of the time of arrival of the signal at the neighboring antennas. Since the distances between the antennas are small in comparison with the long wave (ordinarily the base is taken as 1/10 – 1/3 of the length of the wave), therefore, the differences in the time of delay for each pair of antennas are also small. Thus the accuracy of the determination of the corresponding time differences should be sufficiently high, in order to obtain acceptable accuracy of the measurement of the aximuth of the source of long wave radioradiations.

The system examined for the determination of the location of the source of long wave radiation finds application for the solution of problems of weather forecasting. Stations with scattered receiving points permit us to take extremely accurate radiobearing of stormy areas and hurricanes. Broad possibilities of the long wave systems lead us to suggest that they will gain extremely extensive applications for the solution of many problems.

In conclusion, it should be noted that the objects of passive radiolocational observations may be also radiolocational devices operating in other frequency ranges.

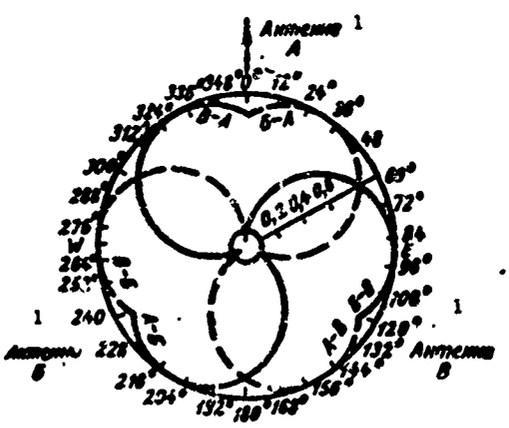


Fig. 13.13. Polar diagram of time delay. 1) Antenna.

Manuscript Page No.

[Footnotes]

904 See book by B.A. Malyshkin entitled "Passivnaya radiolokatsiya" [Passive Radar], Voyenizdat 1961

913 For sufficiently large averaging time T.

[Transliterated Symbols]

905 ПРЛС = PRLS = passivnaya radiolokatsionnaya stantsiya = passive radar

908 э = e = ekvivalentnyy = equivalent

908 ср = sr = sreda = medium, environment

909 каж = kazh = kazhushchiysya = apparent

909 об = ob = ob"yekt = object

912 м = m = maksimal'nyy = maximum

912 ш = sh = shum = noise

914 с = s = signal = signal

916 УВЧ = UVCh = usilitel' vysokoy chastoty = r-f amplifier

916 УПЧ = UPCh = usilitel' promezhutochnykh chastot = i-f amplifier

916 ФНЧ = FNCh = fil'tr nizkikh chastot = low-frequency filter

916 УПТ = UPT = usilitel' postoyannogo toka = d-c amplifier

922 ош = osh = oshibka = error

922 мин = min = minimal'nyy = minimum

922 пр = pr = priyemnik = receiver

923 вых = vykh = vykhod = output

923 вх = vkh = vkhod = input

930 ЛБВ = LBV = lampa begushchey volny = traveling-wave tube

930 и = i = izluchatel' = radiator

936 мкв/м = microvolts/meter

## REFERENCES

### To Chapter 1


1. Aleksandrov, S.G., Fedorov, R.Ye. Sovetskiye sputniki i kosmicheskiye korabli [Soviet Satellites and Spacecraft]. Izd-vo AN SSSR, 1961.

2. Astashenkov, P.T. Radioelektronika v upravlenii snaryadami [Radioelectronics in Missile Guidance]. Voyenizdat, 1960.

3. Bakulev, P.A. Radiolokatsionnyye metody selektsii dvizhushchikhsya tseley [Radar Methods of Selection of Moving Targets]. Oborongiz, 1958.

4. Bardzhes, Dzh. Budushcheye radiolokatsii [Future Radar]. Zarubezhnaya radioelektronika, 1961, No. 2.

5. Barton, D. Perspektivy ispol'zovaniya impul'snykh RLS na raketnykh poligonakh dlya izmereniya v kosmose [Prospects for the Use of Pulse Radars at Rocket Proving Grounds for Measurements in Space]. Zarubezhnaya radioelektronika, 1962, No. 7.

6. Belotserkovskiy, G.B. Radiolokatsionnyye ustroystva [Radar Devices]. Oborongiz, 1961.

7. Bogomolov, A.F. Osnovy radiolokatsii [Fundamentals of Radar]. Izd-vo "Sovetskoye radio," 1954.

8. Bol'shaya Sovetskaya Entsiklopediya [Great Soviet Encyclopedia, 2nd edition, Vol. 35, 1955, pages 520-531.

9. "Bor'ba s vrazheskoy radiolokatsiyey" [Countermeasures Against Enemy Radar], translated from the English. Izd-vo "Sovetskoye radio," 1946.

10. Brenev, I.V., Shchegolev, Ye.Ya. Radionavigatsiya i radiolokatsiya [Radio Navigation and Radar]. In collection entitled: "60 let radio" [60 Years of Radio]. Svyaz'izdat, 1955.

11. Bukhanovskiy, I.L. Plavaniye v stesnennykh vodakh s pomoshch'yu sudovogo radiolokatora [Navigation in Narrow Waterways with the Aid of Shipboard Radar]. Izd-vo "Morskoy transport," 1956.

12. Varaksin, Ya.G. Radioelektronika v voyennom dele [Radioelectronics in War]. Voyenizdat, 1958.

13. Vodop'yanov, F.A. Radiolokatsiya [Radar]. Gosplanizdat, 1947.

14. Getlend, K.U. Razvitiye upravlyayemykh snaryadov [Development of Guided Missiles]. Translated from the English, Izd-vo inostrannoy literatury, 1956.

15. Gorin, B.Sh. Indikatory dal'nosti [Range Indicators]. Voyenizdat, 1957.

16. Grover, D. Universal'naya samoletnaya radiolokatsionnaya stantsiya [A Universal Airborne Radar]. Voprosy radiolokatsionnoy tekhniki, 1958, No. 3.

17. Dzhigit, I.S. Razvitiye radarnoy tekhniki radiolokatsii v SShA [Development of Radar Location Techniques in the USA]. Amerikanskaya tekhnika i promyshlennost', 1945, No. 11.

18. Billington, Koul and Lemb. Zashchita ot mezhkontinental'nykh ballisticheskikh snaryadov [Defense Against Intercontinental Ballistic Missiles]. Voprosy raketnoy tekhniki, 1957, No. 3.

19. Zibert, V. Obshchiye zakonomernosti obnaruzheniya tseley pri pomoshchi radiolokatsii [General Relationships in Target Detection with Radar]. Voprosy radiolokatsionnoy tekhniki, 1957, No. 5.

20. "Impul'snyye radionavigatsionnyye ustroystva" [Pulse Radio Navigation Devices], translated from the English. Voyenizdat, 1955.

21. "Issledovaniya oblakov s pomosh'yu radiolokatsionnykh stantsiy" [Study of Clouds with Radar]. Voprosy radiolokatsionnoy tekhniki, 1955, No. 5.

22. Katrona, D. et al. Radiolokatsionnaya stantsiya s vysokoy razreshayushchey sposobnost'yu dlya nablyudeniya za polem boya [Radar with High Resolution for Observation of the Battlefield]. Zarubezhnaya radioelektronika, 1961, No. 12.

23. Klass, P. Poluavtomaticheskaya sistema obnaruzheniya i navedeniya [A Semiautomatic Detection and Homing System]. Voprosy radiolokatsionnoy tekhniki, 1957, No. 1.

24. Klass, P. Infrakrasnaya tekhnika osparivayet monopoliyu radiolokatsii [Infrared Breaks the Monopoly of Radar]. Voprosy radiolokatsionnoy tekhniki, 1958, No. 2.

25. Kelli, Ye. Radiolokatsionnoye izmereniye dal'nosti, skorosti i uskoreniya [Radar Measurements of Range, Speed and Acceleration]. Zarubezhnaya radioelektronika, 1962, No. 2.

26. Korostelev, A.A. Avtomaticheskoye izmereniye koordinat [Automatic Coordinate Measurements]. Voyenizdat, 1961.

27. Kruks, Dzh. Radiotekhnicheskaya sistema soprovozhdeniya, upravleniya i svyazi s dal'nost'yu deystviya do 400 mln. km [A Radar System for Tracking, Control and Communication with

an Effective Range of up to 400 Million Kilometers]. Zarubezhnaya radioelektronika, 1962, No. 6.

28. "Kratkiye osnovy radiolokatsii" [An Outline of the Fundamentals of Radar], translated by A.Ya. Breytbart. Izd-vo "Sovetskoye radio," 1951.

29. Lovell, B. and Klegg, Dzh. Radioastronomiya [Radio Astronomy], translated from the English, edited by V.V. [illegible]kevich. Izd-vo inostrannoy literatury, 1953.

30. Lokk, A.S. Upravleniye snaryadami [Missile Guidance], translated from the English by G.V. Korenev. Gostekhizdat, 1957.

31. Lykov, I.A. Koordinaty, opredelyayemyye radiolokatorom [Coordinates that Can be Determined by Radar]. Voyenizdat, 1957.

32. Mayorov, F.V. Elektronnyye vychislitel'nyye mashiny ikh primeneniye [Electronic Computers and Their Application]. Voyenizdat, 1959.

33. Mel'nik, Yu.A. Samoletnyye radiolokatsionnyye bombopritsely i radiolokatsionnyye stantsii perekhvata [Aircraft Radar Bombsights and Radar Interception Stations]. Voyenizdat, 1954.

34. Merril, G. Issledovaniye operatsiy [Operations Research], translated from the English. Izd-vo inostrannoy literatury, 1959.

35. Morz, F.M., Kimbel, D.Ye. Metody issledovaniya operatsiy [Operations Research Methods]. Izd-vo "Sovetskoye radio," 1956.

36. "Nadezhnost' nazemnogo radioelektronnogo oborudovaniya" [Reliability of Ground Electronic Equipment], translated from the English, edited by N.M. Shuleykin. Izd-vo "Sovetskoye radio," 1957.

37. "Nazemnyye amerikanskiye i angliyskiye radiolokatsionnyye stantsii" [American and British Ground Radars]. Voyenizdat, 1947.

38. "Osnovy radiolokatsionnoy tekhniki" [Fundamentals of Radar], Vols. 1 and 2, translated from the English, edited by B.F. Vysotskiy. Oborongiz, 1949.

39. Petrov, V.P., Sochivko, A.A. Upravleniye raketami [Rocket Guidance]. Voyenizdat, 1963.

40. Penroz and Boulding. Printsipy i tekhnika radiolokatsii [Principles and Engineering of Radar], translated from the English. Voyenizdat, 1956.

41. "Printsipy radiolokatsii" [Principles of Radar], Parts 1 and 2, translated from the English, edited by L.Yu. Blyumberg and R.I. Perets. Izd-vo "Sovetskoye radio," 1949.

42. Radar, translated from the English. Izd-vo "Sovetskoye radio," 1946.

43. "Radiolokatsionnaya voyna" [Radar Warfare], translated from the English. Izd-vo "Sovetskoye radio," 1946.

44. "Radiolokatsiya na more" [Radar at Sea], translated from the English. Izd-vo inostrannoy literatury, 1959.

45. "Radiolokatsionnaya tekhnika" [Radar Engineering], Parts I and II, translated from the English by A.I. Batrakov et al. Izd-vo "Sovetskoye radio," 1949.

46. "Reaktivnoye oruzhiye kapitalisticheskikh stran, po materialam zarubezhnoy pechati" [Rocket Weapons of the Capitalistic Countries, According to Data Published in the Foreign Press]. Voyenizdat, 1957.

47. Rerikh, K. Obnaruzheniye raket radiolokatsionnymi stantsiyami sverkhdal'nego deystviya [Detection of Rockets by Superlong-Range Radar]. Radiotekhnika i elektronika za rubezhom, 1959, No. 2.

48. Saybel', A.G. Osnovy teorii tochnosti radiotekhnicheskikh metodov mestoopredeleniya [Fundamentals of the Theory of Accuracy of Radio Location Methods]. Oborongiz, 1958.

49. Saybel', A.G. Osnovy radiolokatsii [Fundamentals of Radar]. Izd-vo "Sovetskoye radio," 1961.

50. Sardzhent, R. Obnaruzheniye dvizhushcheysya tseli impul'sno-dopplerovskim metodom [Detection of a Moving Target by the Doppler Pulse Method]. Voprosy radiolokatsionnoy tekhniki, 1955, No. 2.

51. Sivers, A.P. Radiolokatsionnyye priyemniki [Radar Receivers]. Izd-vo "Sovetskoye radio," 1959.

52. Sivers, A.P., Suslov, N.A. Osnovy radiolokatsii [Fundamentals of Radar]. Izd-vo "Sovetskoye radio," 1956.

53. "Sistema dal'nego obnaruzheniya i slezheniya za ballisticheskimi mezhkontinental'nymi raketami BMEWS" [The BMEWS System for Long-Range Detection and Tracking of Intercontinental Ballistic Rockets]. Zarubezhnaya radioelektronika, 1961, No. 1.

54. Siforov, V.I. Radioelektronika v issledovaniyakh kosmosa [Radioelectronics in Space Research]. Izd-vo "Znaniye," 1960.

55. Smirnov, G.D., Gorbachev, V.P. Radiolokatsionnyye sistemy s aktivnym otvetom [Radar Systems with Active Response]. Voyenizdat, 1962.

56. Solodyazhnikov, N.N. Radiolokatsiya [Radar]. Gosenergoizdat, 1956.

57. Sytina, N.V. Avtonomnyye dopplerovskiye radionavigatsionnyye pribory [Autonomous Doppler Radio Navigation Instruments]. Izd-vo "Sovetskoye radio," 1957.

58. Tarasenko, F.P. Sravneniye metodov radiolokatsionnogo priyema s tochki zreniya informatsii [Comparison of Radar Reception Methods from the Standpoint of Information]. Radiotekhnika, 1959, No. 7.

59. "Tekhnika radiolokatsii" [Radar Engineering], Parts I and II, translated from the English. Voyenizdat, 1949.

60. Tiberio, U. Umen'sheniye dal'nosti deystviya radiolokatsionnoy stantsii pod vliyaniyem vneshnego generatora shuma [Decrease in Effective Range of Radar under the Influence of an External Noise Generator]. Voprosy radiolokatsionnoy tekhniki, 1955, No. 3.

61. Traskii, K.A. Radiolokatsionnaya tekhnika i yeye primeneniye [Radar and Its Application]. Voyenizdat, 1956.

62. Trofimov, K.N. Radiolokatsiya [Radar]. Voyenizdat, 1957.

63. Chayt, F. Razrabotka samoletnoy apparatury dlya predotvrashcheniya stolknoveniy v vozdukhe, udobnoy v eksplutatsii [Development of an Easy-to-Operate Airborne Anticollision Radar]. Voprosy radiolokatsionnoy tekhniki, 1958, No. 2.

64. "Upravleniye snaryadami s pomoshch'yu radiolokatsionnykh stantsiy" [Use of Radar Stations to Guide Missiles]. Voprosy radiolokatsionnoy tekhniki, 1956, No. 4.

65. Frolkip, V.T. Indikatornyye ustroystva [Indicator Devices]. Oborongiz, 1956.

66. Kharris, K.Ye. Nekotoryye voprosy postroyeniya obzornykh radiolokatsionnykh sistem s aktivnym otvetom [Certain Problems in the Construction of Scanning Radars with Active Response]. Izd-vo "Sovetskoye radio," 1957.

67. Kholakhan, D. Radiolokatsionnyy pritsel [The Radar Sight]. Voprosy radiolokatsionnoy tekhniki, 1957, No. 4.

68. Kholakhan, D. Rol' teorii informatsii v konstruirovanii novykh radiolokatsionnykh sistem [The Role of Information Theory in the Design of New Radar Systems]. Radiotekhnika i elektronika za rubezhom, 1959, No. 3.

## To Chapter 2

1. Bakulev, P.A. Radiolokatsionnyye metody selektsii dvizhushchikhsya tseley [Radar Methods for Selection of Moving Targets]. Oborongiz, 1959.

2. Bogomolov, A.F. Osnovy radiolokatsii [Fundamentals of Radar]. Izd-vo "Sovetskoye radio," 1954.

3. Vinitskiy, A.S. Ocherk osnov radiolokatsii pri nepreryvnom izluchenii radiovolny [An Outline of the Fundamentals of Continuous-Wave Radar]. Izd-vo "Sovetskoye radio," 1961.

4. Korostelev, A.A. Avtomaticheskoye izmereniye koordinat [Automatic Coordinates Measurement]. Voyenizdat, 1961.

5. Lykov, I.A. Koordinaty, opredelyayemyye radiolokatorom [Coordinates that can be Determined with Radar]. Voyenizdat, 1957.

6. "Printsipy radiolokatsii" [Principles of Radar], Parts I and II, translated from the English, edited by L.Yu. Blyumberg and R.I. Perets, Izd-vo "Sovetskoye radio," 1949.

7. "Radiolokatsionnaya tekhnika" [Radar Engineering], Parts I and II, translated from the English. Izd-vo "Sovetskoye radio," 1949.

8. Saybel', A.G. Osnovy radiolokatsii [Fundamentals of Radar]. Izd-vo "Sovetskoye radio," 1961.

9. Sivers, A.P., Suslov, N.A., Metel'skiy, V.I. Osnovy radiolokatsii [Fundamentals of Radar]. Sudpromgiz, 1959.

10. Stepanov, B.M. Radiolokatsionnyy obzor [Radar Scanning]. Voyenizdat, 1959.

## To Chapter 3

1. Arenberg, A.G. Rasprostraneniye detsimetrovykh i santimetrovykh voln [Propagation of Decimenter and Centimeter Waves]. Izd-vo "Sovetskoye radio," 1957.

2. Bogomolov, A.F. Osnovy radiolokatsii [Fundamentals of Radar]. Izd-vo "Sovetskoye radio," 1954.

3. Brisk, Kh. Effektivnyye radiolokatsionnyye ploshchadi rasseyaniya konusov razlichnykh razmerov v napravlenii s vershiny [Effective Radar Scattering Areas of Cones of Various Sizes in the Direction of the Vertex]. Radiotekhnika i elektronika za rubezhom, 1959, No. 5.

4. Broun, I. Ekho-signaly ot luny [Echo Signals from the Moon]. Voprosy radiolokatsionnoy tekhniki, 1957, No. 5.

5. Vinitskiy, A.S. Ocherk osnov radiolokatsii pri nepreryvnom izluchenii radiovoln [An Outline of the Fundamentals of Continuous-Wave Radar]. Izd-vo "Sovetskoye radio," 1961.

6. Golev, K.V. Raschet dal'nosti deystviya radiolokatsionnykh stantsiy [Calculation of the Range of Radars]. Izd-vo "Sovetskoye radio," 1963.

7. Gorelik, G.S. Kolebaniya i volny [Vibrations and Waves]. Fizmatgiz, 1959.

8. Dann, Dzh. et al. Vliyaniye flyuktuatsiy ekho-signala na rabotu radiolokatsionnykh stantsiy soprovozhdeniya tseli [Influence of Echo Signal Fluctuations on Performance of Target Tracking Radars]. Radiotekhnika i elektronika za rubezhom, 1959, No. 6.

9. Dolukhanov, M.P. Dal'neye rasprostraneniye ul'trakorotkikh voln [Long-Range Propagation of Ultrashort Waves]. Svyaz'izdat, 1962.

10. Kato, I. Veroyatnost' poyavleniya radiolokatsionnykh otrazheniy ot osadkov nad rayonami proizvol'nykh razmerov [Probability of Appearance of Radar Reflections from Precipitation over Regions of Arbitrary Extent], 1957, No. 6.

11. Katsin, M. Mekhanizm radiolokatsionnogo otrazheniya ot poverkhnosti morya [Mechanism of Radar Reflection from the Surface of the Sea]. Voprosy radiolokatsionnoy tekhniki, 1957, No. 6.

12. Levin, B.R. Teoriya sluchaynykh protsessov i yeye primeneniye v radiotekhnike [Theory of Random Processes and its Application in Radar]. Izd-vo "Sovetskoye radio," 1960.

13. "Maksimal'naya dal'nost' deystviya radiolokatsionnoy stantsii" [Maximum Effective Range of Radar], translated from the English, edited by B.F. Vysotskiy. Izd-vo "Sovetskoye radio," 1947.

14. Peresada, V.P. Radiolokatsionnaya vidimost' morskikh ob"yektov [Radar Visibility of Objects at Sea]. Sudpromgiz, 1961.

15. Piyk, V. Teoriya radiolokatsionnykh otrazheniy ot zemnoy poverkhnosti [Theory of Radar Reflection from the Surface of the Earth]. Zarubezhnaya radioelektronika, 1960, No. 3.

16. Piters, R. Ustanovka dlya izmereniya kharakteristik radiolokatsionnykh tseley [Device for Measurement of the Characteristics of Radar Targets]. Voprosy radiolokatsionnoy tekhniki, 1952, No 4.

17. Plank, V. Otrazheniya ot atmosfery -- istochnik lozhnykh radiolokatsionnykh signalov [Reflection from the Atmosphere, a Source of Spurious Radar Signals]. Radiotekhnika i elektronika za rubezhom, 1959, No. 2.

18. "Radiolokatsionnaya tekhnika" [Radar Engineering], Part I, translated from the English by A.D. Batrakov et al. Izd-vo "Sovetskoye radio," 1949.

19. "Rasprostraneniye ul'trakorotkikh voln" [Propagation of Ultrashort Waves], translated from the English, edited by P.A. Shilleiov. Izd-vo "Sovetskoye radio," 1954.

20. Robertson, S. Otrazhayushchiye ob"yekty dlya samoletnogo radiolokatora na santimetrovykh volnakh [Reflecting Object for Centimeter-Wave Airborne Radars]. Voprosy radiolokatsionnoy

tekhniki, 1951, No. 1.

21. Rols, D. Izmereniye otrazhayushchey poverkhnosti na modelyakh [Measurements of Reflecting Surface on Models]. Voprosy radiolokatsionnoy tekhniki, 1954, No. 6.

22. Saybel', A.G. Osnovy radiolokatsii [Fundamentals of Radar]. Izd-vo "Sovetskoye radio," 1961.

23. Sivers, A.P., Suslov, N.A., Metel'skiy, V.I. Osnovy radiolokatsii [Fundamentals of Radar]. Sudpromgiz, 1959.

24. Teylor, R. Izmereniya radiolokatsionnykh otrazheniy ot zemnoy poverkhnosti na chastotakh 10; 15,5 i 35 Ggts [Measurements of Radar Reflections from the Ground at Frequencies of 10, 15.5 and 35 Ghz]. Zarubezhnaya radioelektronika, 1960, No. 3.

25. Khuker, Dzh. Kipans, A. Otrazheniye radiolokatsionnykh signalov ot atmosfernykh obrazovaniy [Reflection of Radar Signals from Atmospheric Formations]. Voprosy radiolokatsionnoy tekhniki, 1951, No. 2.

26. Shtyuber, N. Primeneniye iskusstvennykh otrazhayushchikh ob"yektov v radiolokatsii [Use of Reflecting Artifacts in Radar]. Voprosy radiolokatsionnoy tekhniki, 1951, No. 1.

27. Eshpman, V. et al. Otrazhennyye radiolokatsionnyye signaly ot solntsa [Reflection of Radar Signals from the Sun]. Zarubezhnaya radioelektronika, 1960, No. 6.

## To Chapter 4

1. Arenberg, A.G. Rasprostraneniye detsimetrovykh i santimetrovykh voln [Propagation of Decimeter and Centimeter Waves]. Izd-vo "Sovetskoye radio," 1957.

2. Basgang, Dzh. et al. Yedinyy metod otsenki dal'nosti deystviya radiolokatsionnykh stantsiy nepreryvnogo izlucheniya, impul'snogo izlucheniya i impul'sno-dopplerovskogo tipa [A Single Method for Estimating the Effective Range of Continuous-Wave, Pulsed and Doppler-Pulsed Radars]. Zarubezhnaya radioelektronika, 1960, No. 5.

3. Belkina, M.G. Tablitsy dlya vychisleniya elektromagnitnogo polya v oblasti teni dlya razlichnykh pochv [Tables for Calculation of the Electromagnetic Field in the Shadow Region for Various Soils]. Izd-vo "Sovetskoye radio," 1954.

4. Bogomolov, A.F. Osnovy radiolokatsii [Fundamentals of Radar]. Izd-vo "Sovetskoye radio," 1954.

5. Vvedenskiy, B.A., Arenberg, A.G. Voprosy rasprostraneniya UKV [Problems of Ultrashort-Wave Propagation]. Part I. Izd-vo "Sovetskoye radio," 1948.

6. Veysbrod, S., Anderson, L. Metody rascheta refraktsii v troposfere i ionosfere [Methods for Calculating Refraction in

the Troposphere and Ionosphere]. Zarubezhnaya radioelektronika, 1960, No. 6.

7. Vinitskiy, A.S. Ocherk osnov radiolokatsii pri nepreryvnom izluchenii radiovoln [Outline of the Fundamentals of Continuous-Wave Radar]. Izd-vo "Sovetskoye radio," 1961.

8. Vysotskiy, B.F., Kharybin, A.Ye. Radiolokatsionnyye ustroystva [Radar Devices], Part I. Oborongiz, 1960.

9. Gol'dshteyn, L.D., Zernov, N.V. Elektromagnitnyye polya i volny [Electromagnetic Field and Waves]. Izd-vo "Sovetskoye radio," 1956.

10. Golev, K.V. Raschet dal'nosti deystviya radiolokatsionnykh stantsiy [Calculating the Effective Range of Radar Stations]. Izd-vo "Sovetskoye radio," 1963.

11. Grim, Kh. Shumovaya temperatura vkhodnykh tsepey radiolokatsionnykh sistem [Noise Temperature of Radar-System Input Circuits]. Zarubezhnaya radioelektronika, 1960, No. 8.

12. Dolukhanov, M.P. Rasprostraneniye radiovoln [Propagation of Radio Waves]. Svyaz'izdat, 1951.

13. Dolukhanov, M.P. Rasprostraneniye radiovoln [Propagation of Radio Waves]. Svyaz'izdat, 1960.

14. "Maksimal'naya dal'nost' deystviya radiolokatsionnoy stantsii" [Maximum Effective Range of Radar], translated from the English, edited by B.F. Vysotskiy. Izd-vo "Sovetskoye radio," 1947.

15. Millman, G. Vliyaniye atmosfery na rasprostraneniye metrovykh i detsimetrovykh voln [Influence of the Atmosphere on Propagation of Meter and Decimeter Waves]. Radiotekhnika i elektronika za rubezhom, 1959, No. 2.

16. "Radiolokatsionnaya tekhnika" [Radar Engineering], Parts I and II, translated from the English by A.D. Batrakov et al. Izd-vo "Sovetskoye radio," 1949.

17. Rakov, V.I. Indikatornyye ustroystva radiolokatsionnykh stantsiy [Indicator Devices in Radars]. Sudpromgiz, 1962.

18. "Rasprostraneniye ul'trakorotkikh voln" [Propagation of Ultrashort Waves], translated from the English, edited by B.A. Shillerov. Izd-vo "Sovetskoye radio," 1954.

19. Rerikh, K. Obnaruzheniye raket radiolokatsionnymi stantsiyami sverkhdal'nego deystviya [Detection of Rockets by Ultralong-Range Radars]. Radiotekhnika i elektronika za rubezhom, 1959, No. 2.

20. Sabranskiy, R. Issledovaniye povyshennoy dal'nosti deystviya radiolokatsionnoy stantsii, raspolozhennoy nad vodoy [An Investigation of the Increase in the Range of a Radar Situated

over Water]. Radiotekhnika i elektronika za rubezhom, 1959, No. 1.

21. Sivers, A.P., Suslov, N.A., Metel'skiy, V.I. Osnovy radiolokatsii [Fundamentals of Radar]. Sudpromgiz, 1959.

22. Siforov, V.I. Radiopriyemniki sverkhvysokikh chastot [Superhigh-Frequency Radio Receivers]. Voyenizdat, 1955.

23. Smirnov, G.D., Gorbachev, V.P. Radiolokatsionnyye sistemy s aktivnym otvetom [Radar Systems with Active Response]. Voyenizdat, 1962.

24. Stivens, S. Nadezhnyye granitsy dal'nosti deystviya radiolokatsionnoy stantsii dal'nego obnaruzheniya [Reliable Operating-Range Limits for Long-Range Radars]. Voprosy radiolokatsionnoy tekhniki, 1958, No. 3.

25. Tetel'baum, S.I. Osnovnyye sootnosheniya pri radiolokatsii [Basic Relationships for Radar]. Radiotekhnika, 1947, No. 2.

26. Khodkina, Kh., La Plent, O. Ukhudsheniye kharakteristik radiolokatsionnoy stantsii v tumane i dozhde [Deterioration of Radar-Installation Characteristics in Fog and Rain]. Radiotekhnika i elektronika za rubezhom, 1959, No. 6.

27. Kholl, U. Raschet dal'nosti deystviya impul'snoy radiolokatsionnoy stantsii [Calculation of the Effective Range of a Pulse Radar]. Voprosy radiolokatsionnoy tekhniki, 1956, No. 6.

28. Kholl, U. Obobshchennoye uravneniye radiolokatsii dlya sopostavleniya kharakteristik RLS razlichnykh tipov [A Generalized Radar Equation for Clocking the Characteristics of Various Types of Radars]. Zarubezhnaya radioelektronika, 1963, No. 4.

29. Chernyy, F.B. Rasprostraneniye radiovoln [Propagation of Radio Waves]. Izd-vo "Sovetskoye radio," 1962.

30. Yang, L. Tochnyy raschet dal'nosti deystviya radiolokatsionnoy stantsii [Precision Calculation of the Effective Range of a Radar]. Radiotekhnika i elektronika za rubezhom, 1959, No. 5.

31. Shirman, Ya.D., Golikov, V.N. Osnovy teorii obnaruzheniya radiolokatsionnykh signalov i izmereniya ikh parametrov [Fundamentals of the Theory of Detection of Radar Signals and Measurement of Their Parameters]. Izd-vo "Sovetskoye radio," 1963.

## To Chapter 5

1. Bleyk, L. Effektivnoye chislo impul'sov na shirinu diagrammy napravlennosti RLS, vedushchikh obzor prostranstva [Effective Number of Pulses on Width of Radar Directional Pattern in Space Scanning]. Voprosy radiolokatsionnoy tekhniki, 1953, No. 6.

2. Bunimovich, V.I. Flyuktuatsionnyye protsessy v radiopriyemnykh ustroystvakh [Fluctuation Processes in Radio Receiving Devices]. Izd-vo "Sovetskoye radio," 1951.

3. Kaplan, S. and Sakroll, R. Statisticheskiye svoistva shumov i ikh vliyaniye na dal'nost' radiolokatsionnogo obnaruzheniya [Statistical Properties of Noise and Their Influence on the Range of Radar Detection]. Voprosy radiolokatsionnoy tekhniki, 1952, No. 1.

4. Klyuyev, N.F. Obnaruzheniye impul'snykh signalov posredstvom nakopiteley diskretnogo deystviya [Detection of Pulse Signals by Means of Intermittent Accumulators]. Izd-vo "Sovetskoye radio," 1963.

5. Levin, B.R. Teoriya sluchaynykh protsessov i yeye primeneniye v radiotekhnike [Theory of Random Processes and its Application in Radio]. Izd-vo "Sovetskoye radio," 1960.

6. "Porogovyye signaly" [Threshold Signals], translated from the English, edited by Sivers, A.P. Izd-vo "Sovetskoye radio," 1952.

7. Rays, S. Teoriya flyuktuatsionnykh shumov [Theory of Fluctuation Noise]. In collection entitled: "Teoriya peredachi elektricheskikh signalov pri nalichii pomekh" [Theory of Electrical Signal Transmission in the Presence of Noise]. Izd-vo inostrannoy literatury, 1953.

8. Rakov, V.I. Indikatornyye ustroystva radiolokatsionnykh stantsiy [Indicator Devices of Radars]. Sudpromgiz, 1962.

9. Saybel', A.G. Osnovy radiolokatsii [Fundamentals of Radar]. Izd-vo "Sovetskoye radio," 1961.

To Chapter 6

1. Basharinov, A.Ye., Fleyshman, B.S. Metody posledovatel'nogo analiza i ikh prilozheniya [Methods of Sequential Analysis and Their Application]. Izd-vo "Sovetskoye radio," 1962.

2. Journal of the Optical Society of America, Vol. 43, No. 12, 1953.

3. Vaynshteyn, L.A., Zubakov, V.D. Vydeleniye signalov na fone sluchaynykh pomekh [Isolation of Signals Against a Background of Random Noise]. Izd-vo "Sovetskoye radio," 1960.

4. Vudvord, F.M. Teoriya veroyatnostey i teoriya informatsii s primeneniyami v radiolokatsii [Probability Theory and Information Theory, with Applications in Radar]. Izd-vo "Sovetskoye radio," 1955.

5. Geratevol'. Kontrasty yarkosti i porogi obnaruzheniya tseli na ekranakh indikatorov radiolokatsionnykh stantsiy [Brightness Contrasts and Target-Detection Threshold on the Display Screens of Radars]. Voprosy radiolokatsionnoy tekhniki, 1956, No. 5.

6. Golev, K.V. Raschet dal'nosti deystviya radiolokatsionnykh stantsiy [Calculation of the Effective Range of Radars]. Izd-vo "Sovetskoye radio," 1963.

7. Griffits. Obnaruzheniye impul'snykh signalov v shume. Vliyaniye ploshchadi pyatna signala na vizual'noye obnaruzheniye [Detection of Pulse Signals in Noise. Influence of Signal-Spot Area on Visual Detection]. Voprosy radiolokatsionnoy tekhniki, 1957, No. 6 (42).

8. Gutkin, L.S. Teoriya optimal'nykh metodov priyema pri flyuktuatsionnykh pomekhakh [Theory of Optimum ethods of Reception in the Presence of Fluctuation Noise]. Gosenergoizdat, 1961.

9. Dinnin, G., Rid, I. Issledovaniya obnaruzheniya i lokatsii signalov pri pomoshchi schetchikov [Investigations of Detection and Location of Signals Using Counters]. In collection entitled: "Priyem signalov pri nalichii shuma" [Reception of Signals in the Presence of Noise]. Izd-vo inostrannoy literatury, 1960.

10. Zibert, V. Obshchiye zakonomernosti obnaruzheniya tseley pri pomoshchi radiolokatsii [General Relationships in the Detection of Targets Using Radar]. Voprosy radiolokatsionnoy tekhniki, 1957, No. 5.

11. Klyuyev, N.F. Obnaruzheniye impul'snykh signalov s pomoshch'yu nakopiteley diskretnogo deystviya [Detection of Pulse Signals by Means of Intermittent Accumulator]. Izd-vo "Sovetskoye radio," 1963.

12. Knol', M. and Keyzan, B. Elektronno-luchevyye trubki s nakopleniyem zaryadov [Electron-Beam Tubes with Charge Accumulation]. Gosenergoizdat, 1955.

13. Korostelev, A.A. Avtomaticheskoye izmereniye koordinat [Automatic Coordinate Measurements]. Voyenizdat, 1961.

14. Kotel'nikov, V.A. Teoriya potentsial'noy pomekhoustoychivosti [Theory of Potential Noiseproofness]. Gosenergoizdat, 1956.

15. Lebedev, V.V. O diskretnom predstavlenii signala, organichennogo vo vremeni [Discrete Representation of a Time-Limited Signal]. Radioelektronika, 1961, No. 1.

16. Makfarlan, A. Analiz grebenchatykh fil'trov [Analysis of Comb Filters]. Zarubezhnaya radioelektronika, 1960, No. 10.

17. Markus, M., Sverling, P. Posledovatel'noye obnaruzheniye v radiolokatore so mnogimi elementami razresheniya [Sequential Detection in a Radar with Numerous Decision Elements]. Zarubezhnaya radioelektronika, 1963, No. 3.

18. "Otsenka kachestva izobrazheniya na ekranakh elektronno-luchevykh trubok" [Evaluation of Image Quality on Electron Beam Tube Screens] "Teli-tekh," March 1953, page 88, condensed translation of article in Vestnik informatsii, 1953,

No. 15. Izd-vo "Sovetskoye radio."

19. Piterson, V., Berdsal, T., Foks, V. Teoriya obnaruzheniya signalov [Theory of Signal Detection]. In collection entitled "Teoriya informatsii i yeye prilozheniya" [Information Theory and its Application]. Fizmatgiz, 1959.

20. "Porogovyye signaly" [Special Signals], translated from the English, edited by Sivers, A.P. Izd-vo "Sovetskoye radio," 1952.

21. Sergovantsev, B.V. Peredacha radiolokatsionnogo izobrazheniya [Transmission of the Radar Image]. Izd-vo "Sovetskoye radio," 1957.

22. Taker. Obnaruzheniye impul'snykh signalov v shume. Korrelyatsiya mezhdu sledami pri vizual'nom nablyudenii [Detection of Pulse Signals in Noise. Correlation Between Traces in Visual Observation]. Voprosy radiolokatsionnoy tekhniki, 1957, No. 6 (42).

23. Fal'kovich, S.Ye. Priyem radiolokatsionnykh signalov na fone flyuktuatsionnykh pomekh [Reception of Radar Signals Against a Background of Fluctuation Noise]. Izd-vo "Sovetskoye radio," 1961.

24. Kharrington, D.V. Issledovaniye obnaruzheniya povtoryayushchikhsya impul'snykh signalov v shume pri pomoshchi dvoichnogo nakopleniya [Investigation of Detection of Recurrent Pulse Signals in Noise Using a Binary Accumulator]. In collection entitled: "Priyem signalov pri nalichii shuma" [Reception of Signals in the Presence of Noise]. Izd-vo inostrannoy literatury, 1960.

25. Kholakhan, D. Rol' teorii informatsii v proyektirovanii novykh radiolokatsionnykh sistem [The Role of Information Theory in the Design of New Radar Systems]. Radiotekhnika i elektronika za rubezhom, 1959, No. 3.

26. Kholakhan, D. Sovremennoye sostoyaniye radiolokatsii [The Contemporary State of Radar]. Radiotekhnika i elektronika za rubezhom, 1959, No. 4.

27. Kholl, U. Obobshchennoye uravneniye radiolokatsii dlya sopostavleniya kharakteristik RLS razlichnykh tipov [Generalized Radar Equation for Plotting the Characteristics of Various Types of Radars]. Zarubezhnaya radioelektronika, 1963, No. 4.

28. Shvarts, L. Printsipy umen'sheniya shumov v kanalakh svyazi [Principles of Noise Reduction in Communications Channels]. Voprosy radiolokatsionnoy tekhniki, 1958, No. 1.

29. Shkol'nik, M. Obnaruzheniye impul'snykh signalov v shumakh [Detection of Pulsed Signals in Noise]. Voprosy radiolokatsionnoy tekhniki, 1958, No. 3 (45).

30. "Elektronno-luchevyye trubki i indikatory" [Electron-Beam Tubes and Indicators], Parts 1 and 2, translated from the English, edited by A.Ya. Breytbart. Izd-vo "Sovetskoye radio," 1949.

31. Yang, L. Tochnyy raschet dal'nosti deystviya radiolokatsionnoy stantsii [Precision Calculation of Effective Radar Range]. Radiotekhnika i elektronika za rubezhom, 1959, No. 5.

32. Shirman, Ya.D., Golikov, V.N. Osnovy teorii obnaruzheniya radiolokatsionnykh signalov i izmereniya ikh parametrov [Fundamentals of the Theory of Detection of Radar Signals and Measurement of Their Parameters]. Izd-vo "Sovetskoye radio," 1963.

## To Chapter 7

1. Barton, D. Perspektivy ispol'zovaniya impul'snykh RLS na raketnykh poligonakh dlya izmereniya v kosmose [Prospects for the Use of Pulse Radars at Rocket Launching Areas for Measurements in Outer Space]. Zarubezhnaya radioelektronika, 1962, No. 7.

2. Vudvord, F.M. Teoriya veroyatnostey i teoriya informatsii s primeneniyami v radiolokatsii [Probability Theory and Information Theory with Applications in Radar]. Izd-vo "Sovetskoye radio," 1955.

3. Gardner, F. Fil'tr dopplerovskoy chastoty s polosoy propuskaniya 1 gts [Doppler-Frequency Filter with a 1-hz Passband]. Zarubezhnaya radioelektronika, 1960, No. 8.

4. Gerrak, R. et al. Opredeleniye razreshayushchey sposobnosti na indikatore krugovogo obzora [Determination of Resolution on a Circular-Scan Indicator]. Nauchno-tekhnicheskiy otdel obobshcheniy i informatsii [Scientific and Technical Department for Generalization and Information], translation No. 1620, 1959.

5. Zibert, V. Obshchiye zakonomernosti obnaruzheniya tseley pri pomoshchi radiolokatsii [General Relationships in Target Detection by Radar]. Voprosy radiolokatsionnoy tekhniki, 1957, No. 5.

6. Kelli, Ye. Radiolokatsionnoye izmereniye dal'nosti, skorosti i uskoreniya [Radar Measurement of Range, Speed and Acceleration]. Zarubezhnaya radioelektronika, 1962, No. 2.

7. Korostelev, A.A. Avtomaticheskoye izmereniye koordinat [Automatic Coordinate Measurements]. Voyenizdat, 1961.

8. Kotel'nikov, V.A. Teoriya potentsial'noy pomekhoustoychivosti [Theory of Potential Noiseproofness]. Gosenergoizdat, 1956.

9. Krivitskiy, B.Kh. Avtomaticheskiye sistemy radiotekhnicheskikh ustroystv [Automatic Systems in Radio Engineering Devices]. Gosenergoizdat, 1962.

10. Kruks, Dzh. Radiotekhnicheskaya sistema soprovozhdeniya, upravleniya i svyazi s dal'nost'yu deystviya do 400 mln. km [A Radar System for Tracking, Control and Communication with Effective Range of up to 400 Million Kilometers]. Zarubezhnaya radioelektronika, 1962, No. 6.

11. Kuk. Povysheniye effektivnosti radiolokatsionnykh ustroystv za schet szhatiya impul'sa [Improving the Effectiveness of Radars by Pulse Compression]. Zarubezhnaya radioelektronika, 1960, No. 10.

12. "Lampovyye skhemy dlya izmereniya vremeni" [Tube Circuits for the Measurement of Time], Parts 1 and 2, translated from the English, edited by A.Ya. Breytbart. Izd-vo "Sovetskoye radio," 1952.

13. Mityashev, B.N. Opredeleniye vremennogo polozheniya impul'sov pri nalichii pomekh [Determination of the Time Position of Pulses in the Presence of Noise]. Izd-vo "Sovetskoye radio," 1962.

14. Pen, U. Tochnost' vosproizvedeniya pri obrabotke radiolokatsionnykh signalov [Precision of Reproduction in the Processing of Radar Signals]. Zarubezhnaya radioelektronika, 1963, No. 4.

15. "Avtomaticheskoye upravleniye i vychislitel'naya tekhnika" [Automatic Control and Computer Technique], edited by V.V. Solodovnikov. Mashgiz, 1958.

16. Priyemnaya apparatura sistemy "Mikrolok" [Receiving Apparatus of the "Microlock" System]. Zarubezhnaya radioelektronika, 1960, No. 4.

17. Saybel', A.G. Osnovy radiolokatsii [Fundamentals of Radar]. Izd-vo "Sovetskoye radio," 1961.

18. Fal'kovich, S.Ye. Priyem radiolokatsionnykh signalov na fone flyuktuatsionnykh pomekh [Reception of Radar Signals Against a Background of Fluctuation Noise]. Izd-vo "Sovetskoye radio," 1961.

19. Kholakhan, D. Rol' teorii informatsii v proyektirovanii novykh radiolokatsionnykh sistem [The Role of Information Theory in the Design of New Radar Systems]. Radiotekhnika i elektronika za rubezhom, 1959, No. 3.

20. Kholakhan, D. Sovremennoye sostoyaniye radiolokatsii [The Contemporary State of Radar]. Radiotekhnika i elektronika za rubezhom, 1959, No. 4.

21. Kholl, U. Obobshchennoye uravneniye radiolokatsii dlya sopostavleniya kharakteristik RLS razlichnykh tipov [Generalized Radar Equation for Plotting the Charcteristics of Various Types of Radars]. Zarubezhnaya radioelektronika, 1963, No. 4.

22. Chernyy, F.B. Rasprostraneniye radiovoln [Propagation of Radio Waves]. Izd-vo "Sovetskoye radio," 1962.

23. Shcnukin, A.N. Dinamicheskiye i flyuktuatsionnyye oshibki upravlyayemykh ob"yektov [Dynamic and Fluctuation Errors of Controlled Systems]. Izd-vo "Sovetskoye radio," 1961.

24. Shirman, Ya.D., Golikov, V.N. Osnovy teorii obnaruzheniya radiolokatsionnykh signalov i izmereniya ikh parametrov [Fundamentals of the Theory of Detection of Radar Signals and Measurement of Their Parameters]. Izd-vo "Sovetskoye radio," 1963.

## To Chapter 8

1. Barton, D. Perspektivy ispol'zovaniya impul'snykh RLS na raketnykh poligonakh dlya izmereniya v kosmose [Prospects for the Use of Pulse Radars at Rocket Launching Areas for Measurements in Outer Space]. Zarubezhnaya radioelektronika, 1962, No. 7.

2. Bernstey, R. Issledovaniye uglovoy tochnosti radiolokatora [An Investigation of Radar Angle Error]. In collection entitled: "Priyem signalov pri nalichii shuma" [Reception of Signals in the Presence of Noise]. Izd-vo inostrannoy literatury, 1960.

3. Vysotskiy, B.F., Kharybin, A.Ye. Radiolokatsionnyye ustroystva [Radar Devices]. Oborongiz, 1962.

4. Gutkin, L.S. Printsipy radioupravleniya bespilotnymi ob"yektami [Principles of Radio Control of Pilotless Aircraft]. Izd-vo "Sovetskoye radio," 1958.

5. Katrona, D. et al. Radiolokatsionnaya stantsiya s vysokoy razreshayushchey sposobnost'yu dlya nablyudeniya za polem boya [A High-Resolution Radar for Observation of the Battlefield]. Zarubezhnaya radioelektronika, 1962, No. 12.

6. Katrona, D. Kholl, U. Sravneniye razlichnykh sposobov dostizheniya vysokoy azimutal'noy razreshayushchey sposobnosti [Comparison of Various Methods for Securing High Resolution in Azimuth]. Zarubezhnaya radioelektronika, 1962, No. 2.

7. Korostelev, A.A. Avtomaticheskoye izmereniye koordinat [Automatic Coordinate Measurement]. Voyenizdat, 1961.

8. Kotel'nikov, V.A. Teoriya potentsial'noy pomekhoustoychivosti [Theory of Potential Noiseproofness]. Gosenergoizdat, 1956.

9. Krivitskiy, B.Kh. Avtomaticheskiye sistemy radiotekhnicheskikh ustroystv [Automatic Systems in Radio Engineering Devices]. Gosenergoizdat, 1962.

10. Levin, A. Interferometr dlya radionavedeniya upravlyayemykh snaryadov [An Interferometer for Radio Homing of Guided Missiles]. Zarubezhnaya radioelektronika, 1958, No. 7.

11. Mayorov, F.V. Elektronnyye vychislitel'nyye mashiny i ikh primeneniye [Electronic Computers and Their Application]. Voyenizdat, 1959.

12. Milman. Vliyaniye atmosfery na rasprostraneniye metrovykh i detsimetrovykh radiovoln [Influence of the Atmosphere on the Propagation of Meter and Decimeter Waves]. Radiotekhnika i elektronika za rubezhom, 1959, No. 2.

13. "Avtomaticheskoye upravleniye i vychislitel'naya tekhnika" [Automatic Control and Computer Technique], edited by V.V. Solodovnikov. Mashgiz, 1958.

14. Rodo, D.R. Vvedeniye v monoimpul'snuyu radiolokatsiyu [Introduction to Monopulse Radar]. Izd-vo "Sovetskoye radio," 1960.

15. Saybel', A.G. Osnovy radiolokatsii [Fundamentals of Radar]. Izd-vo "Sovetskoye radio," 1961.

16. Tipugin, V.N., Veytsel', V.A. Radioupravleniye [Radio Control]. Izd-vo "Sovetskoye radio," 1962.

17. Fal'kovich, S.Ye. Priyem radiolokatsionnykh signalov na fone flyuktuatsionnykh pomekh [Reception of Radar Signals Against a Background of Fluctuation Noise]. Izd-vo "Sovetskoye radio," 1961.

18. Kheymiller, R. Teoriya i raschet diagrammy napravlennosti sintezirovannykh antennykh reshetok [Theory and Calculation of Directivity Patterns for Synthesized Antenna Arrays]. Zarubezhnaya radioelektronika, 1963, No. 2.

19. Khellgren, G. Voprosy teorii monoimpul'snoy radiolokatsii [Problems of Monopulse Radar Theory]. Zarubezhnaya radioelektronika, 1962, No. 12; 1963, No. 1.

20. Kholakhan, D. Rol' teorii informatsii v proyektirovanii novykh radiolokatsionnykh sistem [Role of Information Theory in the Design of New Radar Systems]. Radiotekhnika i elektronika za rubezhom, 1959, No. 3.

21. Kholakhan, D. Sovremennoye sostoyaniye radiolokatsii [The Contemporary State of Radar]. Radiotekhnika i elektronika za rubezhom, 1959, No. 4.

22. Kholl, U. Obobshchennoye uravneniye radiolokatsii dlya sopostavleniya kharakteristik RLS razlichnykh tipov [Generalized Radar Equation for Plotting the Characteristics of Various Types of Radars]. Zarubezhnaya radioelektronika, 1963, No. 4.

23. Chernyy, B.F. Rasprostraneniye radiovoln [Propagation of Radio Waves]. Izd-vo "Sovetskoye radio," 1962.

24. Shchukin, A.N. Dinamicheskiye i flyuktuatsionnyye oshibki upravlyayemykh ob"yektov [Dynamic and Fluctuation Errors of

Controlled System]. Izd-vo "Sovetskoye radio," 1961.

To Chapter 9

1. Saybel', A.G. Osnovy radiolokatsii [Fundamentals of Radar]. Izd-vo "Sovetskoye radio," 1961.

2. Yefimov, N.V. Kratkiy kurs analiticheskoy geometrii [A Brief Course in Analytical Geometry]. Fizmatgiz, 1958.

3. Venttsel', Ye.S. Teoriya veroyatnostey [Probability Theory]. Fizmatgiz, 1962.

4. Astaf'yev, G.P., Shebshayevich, V.S., Yurkov, Yu.A. Radionavigatsionnyye ustroystva i sistemy [Radio Navigation Devices and Systems]. Izd-vo "Sovetskoye radio," 1958.

5. Levin, B.R. Teoriya sluchaynykh protsessov i yeye primeneniye v radiotekhnike [Theory of Random Processes and its Application in Radio]. Izd-vo "Sovetskoye radio," 1960.

6. Yanke, Ye. and Emde, F. Tablitsy funktsiy s formulami i krivymi [Tables of Functions with Formulas and Curves]. Fizmatgiz, 1959.

To Chapter 10

1. Shapiro, I.I. Raschet trayektoriy ballisticheskikh snaryadov po dannym radiolokatsionnykh nablyudeniy [Calculation of Ballistic-Missile Trajectories from Data of Radar Observations]. Izd-vo inostrannoy literatury, 1961.

2. Kramer, G. Matematicheskiye metody statistiki [Mathematical Methods of Statistics]. Gostekhizdat, 1956.

3. Van der Varden. Matematicheskaya statistika [Mathematical Statistics]. Izd-vo inostrannoy literatury, 1960.

4. Linnik, Yu.V. Metod naimen'shikh kvadratov i osnovy matematiko-statisticheskoy teorii obrabotki nablyudeniy [The Method of Least Squares and the Foundations of the Mathematical-Statistical Theory of Observational-Data Processing]. Fizmatgiz, 1962.

5. Pogorelov, D.A. Teoriya keplerovykh dvizheniy letatel'nykh apparatov [Theory of Keplerian Motions of Aircraft]. Fizmatgiz, 1961.

6. Barton, D. Perspektivy ispol'zovaniya impul'snykh RLS na raketnykh poligonakh dlya izmereniya v kosmose [Prospects for the use of Pulse Radars at Rocket Launching Areas for Measurements in Outer Space]. Zarubezhnaya radioelektronika, 1962, No. 7.

7. Aleksandrov, S.G., Fedorov, R.Ye. Sovetskiye sputniki i kosmicheskiye korabli [Soviet Satellites and Space Crafts]. Izd-vo AN SSSR. 1961.

8. Kotel'nikov, V.A. et al. Ispol'zovaniye effekta Dopplera dlya opredeleniya parametrov orbity ISZ [Utilization of the Doppler Effect to Determine the Parameters of Satellite Orbits]. In collection entitled: "Iskusstvennyye sputniki Zemli" [Artificial Earth Satellites], No. 1, izd. AN SSSR, 1962.

9. Eneyev, T.M., Platonov, A.K., Kazakova, R.K. Opredeleniye parametrov orbity iskusstvennogo sputnika po dannym nazemnykh izmereniy [Determination of Satellite Orbit Parameters from Data Measured on the Ground]. In collection entitled: "Iskusstvennyye sputniki Zemli," No. 4, izd. AN SSSR.

10. Kantor, A.V. Apparatura i metody izmereniy pri ispytaniyakh raket [Apparatus and Methods of Measurements in Rocket Tests]. Oborongiz, 1963.

11. "Upravleniye poletom kosmicheskikh apparatov" [Guidance of Spacecraft], translated from the English. Izd-vo inostrannoy literatury, 1963.

12. "Elektronnyye metody kontrolya trayektoriy kosmicheskikh apparatov" [Electronic Measurements for Observing the Trajectories of Spacecraft], translated from the English. Izd-vo inostrannoy literatury, 1963.

## To Chapter 11

1. "Antenny ellipticheskoy polyarizatsiy" [Elliptical Polarization Antennas]. Collected translations. Izd-vo "Sovetskoye radio," 1961.

2. Belkin, M.A. Ob avtomaticheskoy stabilizatsii usileniya pri priyeme impul'snykh signalov [Automatic Stabilization of Gain in Reception of Pulse Signals]. Radiotekhnika, 1948. No. 3.

3. Bychkov, S.I., Burenin, N.I., Safarov, R.T. Stabilizatsiya chastoty generatorov SVCh [Frequency Stabilization of Superhigh-Frequency Generators]. Izd-vo "Sovetskoye radio," 1962.

4. Vaynshteyn, L.A., Zubakov, V.D. Vydeleniye signalov na fone sluchaynykh pomekh [Isolation of Signals Against a Background of Random Noise]. Izd-vo "Sovetskoye radio," 1960.

5. Volkov, V.M. Logarifmicheskiye usiliteli [Logarithmic Amplifiers]. Gostekhizdat, Kiev, 1962.

6. Grimm, Kh. Osnovnyye kharakteristiki vneshnego shuma [Basic Characteristics of Extraneous Noise]. Zarubezhnaya radioelektronika, 1960, No. 6.

7. Drabkin, A.L., Zuzenko, V.L. Antenno-fidernyye ustroystva [Antenna Feeder Devices]. Izd-vo "Sovetskoye radio," 1961.

8. Kovit, B. et al. Metody i tekhnika radioprotivodeystviya i bor'ba s nimi [Methods and Technique of Radio Countermeasures and Countercountermeasures]. Zarubezhnaya radioelektronika,

1960, No. 11.

9. Krivitskiy, B.Kh. Avtomaticheskiye sistemy radiotekhnicheskikh ustroystv [Automatic Systems in Radio Devices]. Gosenergoizdat, 1962.

10. "Nekotoryye primeneniya ferritov v antenno-fidernoy tekhnike" [Certain Applications of Ferrites in Antenna Feeders]. In collection of translations edited by A.L. Mikaelyan. Izd-vo "Sovetskoye radio," 1958.

11. Tartakovskiy, G.P. Dinamika sistem avtomaticheskoy regulirovki usileniya [Dynamics of Automatic Gain Control Systems]. Gosenergoizdat, 1957.

12. Forvard, R., Rigi, F. Vliyaniye vneshnikh shumov na pokazateli radiolokatsionnoy stantsii [Influence of Extraneous Noise on Performance Data of a Radar]. Zarubezhnaya radioelektronika, 1961, No. 7.

13. Chayt, V. Unichtozheniye otrazheniy ot dozhdya s pomoshch'yu krugovoy polyarizatsii [Elimination of Raindrop Reflection by Circular Polarization]. Voprosy radiolokatsionnoy tekhniki, 1954, No. 5.

14. Khoggdi et al. Vliyaniye dozhdya i vodyanykh parov na shumy neba v santimetrovom diapazone voln [Influence of Rain and Water Vapor on Sky Noise in the Centimeter-Wave Band]. Zarubezhnaya radioelektronika, 1962, No. 12.

15. Gutkin, L.S. Teoriya optimal'nykh metodov radiopriyema pri flyuktuatsionnykh pomekhakh [Theory of Optimum Radio Reception Methods in the Presence of Fluctuation Noise]. Gosenergoizdat, 1961.

## To Chapter 12

1. Vaynshteyn, L.A., Zubakov, V.D. Vydeleniye signalov na fone sluchaynykh pomekh [Isolation of Signals Against a Background of Random Noise]. Izd-vo "Sovetskoye radio," 1960.

2. Fal'kovich, S.Ye. Priyem radiolokatsionnykh signalov na fone flyuktuatsionnykh pomekh [Reception of Radar Signals Against a Background of Fluctuation Noise]. Izd-vo "Sovetskoye radio," 1961.

3. Bakulev, P.A. Radiolokatsionnyye metody selektsii dvizhushchikhsya tseley [Radar Methods for the Selection of Moving Targets]. Oborongiz, 1958.

4. Barlow, E.J. Doppler Radar. Proc. of the IRE, 1949, Vol. 37, No. 4.

5. Grizetti, Santa, Kirkpatrik. Vliyaniye flyuktuatsiy i obzora prostranstva na podavleniye otrazheniy ot mestnykh predmetov v radiolokatorakh s indikatorami dvizhushchikhsya tseley [Influence of Fluctuations and Space Scanning on Suppression of

Signals from Local Objects in Radars with Moving-Target Indicators]. Voprosy radiolokatsionnoy tekhniki, 1956, No. 3 (33).

6. Dzhordzh, M. Flyuktuatsii signalov samoletnoy radiolokatsionnoy stantsii, otrazhennykh ot zemli [Fluctuations of Airborne Radar Signals Reflected from the Ground]. Voprosy radiolokatsionnoy tekhniki, 1953, No. 5 (17).

7. Krandel, V. Turniketnyy polyarizator dlya podavleniya otrazheniy ot dozhdya [A Tourniquet Polarizer for Suppression of Rain Reflections]. Voprosy radiolokatsionnoy tekhniki, 1955, No. 5.

8. Chayt, V. Unichtozheniye otrazheniy ot dozhdya s pomoshch'yu krugovoy polyarizatsii [Elimination of Reflection from Rain by Means of Circular Polarization]. Voprosy radiolokatsionnoy tekhniki, 1954, No. 5.

## To Chapter 13

1. Al'pert, Ya.L. O rasprostranenii elektromagnitnykh voln nizkoy chastoty nad zemnoy poverkhnost'yu [Propagation of Low-Frequency Electromagnetic Waves Above the Earth's Surface]. Izd-vo AN SSSR, 1955.

2. Levin, B.R. Teoriya sluchaynykh protsessov i yeye primeneniye v radiotekhnike [Theory of Random Processes and its Application in Radio]. Izd-vo "Sovetskoye radio," 1960.

3. Malyshkin, Ye.A. Passivnaya radiolokatsiya [Passive Radar]. Voyenizdat, 1961.

4. Klass, R. Passivnaya radiolokatsiya [Passive Radar]. Vestnik informatsii, 1957, No. 3.

5. Khefli, Linfil'd, Devis. Sistema *E*-φ dlya radiopelengovaniya na sverkhdlinnykh volnakh [An *E*-φ System for Radio Direction Finding at Superlong Wavelengths]. Zarubezhnaya radioelektronika, 1962, No. 3.